

DOT/FAA/AR-96/81,II

Office of Aviation Research
Washington, D.C. 20591

Proceedings of the FAA International Conference on Aircraft Inflight Icing, Volume II

Working Group Papers

August 1996

Final Report

This document is available to the U.S. public
through the National Technical Information
Service, Springfield, Virginia 22161.

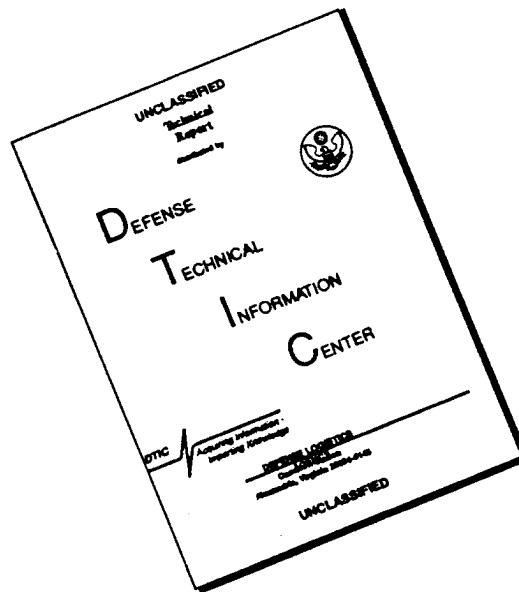
19961018 126



DTIC QUALITY INSPECTED 3

U.S. Department of Transportation
Federal Aviation Administration

DISCLAIMER NOTICE



THIS DOCUMENT IS BEST QUALITY AVAILABLE. THE COPY FURNISHED TO DTIC CONTAINED A SIGNIFICANT NUMBER OF PAGES WHICH DO NOT REPRODUCE LEGIBLY.

NOTICE

This document is disseminated under the sponsorship of the U.S. Department of Transportation in the interest of information exchange. The United States Government assumes no liability for the contents or use thereof. The United States Government does not endorse products or manufacturers. Trade or manufacturer's names appear herein solely because they are considered essential to the objective of this report.

1. Report No. DOT/FAA/AR-96/81,II	2. Government Accession No.	3. Recipient's Catalog No.	
4. Title and Subtitle PROCEEDINGS OF THE FAA INTERNATIONAL CONFERENCE ON AIRCRAFT INFLIGHT ICING, VOLUME II WORKING GROUP PAPERS		5. Report Date August 1996	
		6. Performing Organization Code	
7. Author(s) Contributing authors of the FAA International Conference on Aircraft Inflight Icing		8. Performing Organization Report No. DOT/FAA/AR-96/81,II	
9. Performing Organization Name and Address Systems Resource Management, Inc. 10400 Connecticut Avenue, Suite 507 Kensington, MD 20895		10. Work Unit No. (TRIS)	
		11. Contract or Grant No.	
12. Sponsoring Agency Name and Address U.S. Department of Transportation Federal Aviation Administration Office of Aviation Research Washington, DC 20591		13. Type of Report and Period Covered Conference proceedings: May 6-8, 1996	
		14. Sponsoring Agency Code	
15. Supplementary Notes Compiled and edited by Dr. James Riley and Ms. Barbara Horn, FAA William J. Hughes Technical Center			
16. Abstract <p>The FAA International Conference on Aircraft Inflight Icing, held on May 6-8, 1996, in Springfield, Virginia, was attended by over 400 participants from the U.S. and nineteen foreign countries. The conference included a review of major aspects of airworthiness when operating in icing conditions. It consisted of an opening plenary session, five working group sessions addressing (1) Icing Environmental Characterization, (2) Ice Protection and Ice Detection, (3) Forecasting and Avoidance, (4) Requirements for and Means of Compliance in Icing Conditions (Including Icing Simulation Methods), (5) Operational Regulations and Training Requirements, and a closing plenary session. One of the primary areas of concern at the conference was icing due to supercooled large droplets (SLD).</p> <p>Volume I of the conference proceedings covers presentations of the speakers at the opening plenary session and the reports of the co-chairs of the working groups at the closing plenary session.</p> <p>Volume II of the conference proceedings is a compendium of technical papers presented in the various working groups.</p>			
17. Key Words Aircraft inflight icing, Supercooled large droplets (SLD), Icing simulation methods, Icing forecasting, Ice protection, Ice detection		18. Distribution Statement This document is available to the public through the National Technical Information Service (NTIS), Springfield, Virginia 22161.	
19. Security Classif. (of this report) Unclassified	20. Security Classif. (of this page) Unclassified	21. No. of Pages 558	22. Price

FAA INTERNATIONAL CONFERENCE ON AIRCRAFT INFLIGHT ICING

Technical Papers

EXECUTIVE SUMMARY

ix

I. ICING ENVIRONMENTAL CHARACTERIZATION

George A. Isaac, Industry Co-Chair

Richard K. Jeck, FAA Co-Chair

Analysis of Aircraft Icing Environments Associated with Supercooled Drizzle

1

Stewart G. Cober, Atmospheric Environment Service

George A. Isaac, Atmospheric Environment Service

J. Walter Strapp, Atmospheric Environment Service

Dave Marcotte, Institute for Aerospace Research, National Research Council

Freezing Drizzle Encountered by a Research Aircraft Over the Park Range in Colorado

13

R. Paul Lawson, SPEC Incorporated

Marcia K. Politovich, National Center for Atmospheric Research

In Situ Measurements of Aircraft Icing

23

Jeffrey Stith, University of North Dakota

Michael Poellot, University of North Dakota

Cedric Grainger, University of North Dakota

Ronald Rinehart, University of North Dakota

Roger Tilbury, University of North Dakota

Ryan Zerr, University of North Dakota

Supercooled Large Droplet Distributions in the Natural Environment and Comparison to Artificial Drizzle From the Air Force Water Spray Tanker

33

Russell Ashenden, University of Wyoming

John D. Marwitz, University of Wyoming

A Canadian Climatology of Freezing Precipitation and a Detailed Study Using Data from St. John's, Newfoundland

45

J.W. Strapp, Atmospheric Environment Service

R.A. Stuart, Weather Reset House

G.A. Isaac, Atmospheric Environment Service

Representative Values of Icing-Related Variables Aloft in Freezing Rain and Freezing Drizzle	57
<i>Richard K. Jack, FAA William J. Hughes Technical Center</i>	
Comparison of Two Data Processing Techniques for Optical Array Probes	69
<i>Ray Hobbs, Aeromet, Inc.</i>	
<i>Brian Morrison, Aeromet, Inc.</i>	
<i>Russell Ashenden, University of Wyoming</i>	
<i>Robert F. Ide, NASA Lewis Research Center</i>	
Comparison of Liquid Water Content Measurement Techniques in an Icing Wind Tunnel	91
<i>Robert F. Ide, NASA Lewis Research Center</i>	
On the Accuracy of PMS Optical Array Probes	105
<i>A.V. Korolev, Atmospheric Environment Service</i>	
<i>J.W. Strapp, Atmospheric Environment Service</i>	
<i>G.A. Isaac, Atmospheric Environment Service</i>	
Some Instrumentation Effects on Airborne Measurements of the Drop Size Distribution in Freezing Drizzle	115
<i>R. Paul Lawson, SPEC Incorporated</i>	
<i>A.V. Korolev, Atmospheric Environment Service</i>	
<i>T. Huang, SPEC Incorporated</i>	
<i>L.J. Angus, SPEC Incorporated</i>	
<i>K.A. Weaver, SPEC Incorporated</i>	
<i>J. Walter Strapp, Atmospheric Environment Service</i>	
<i>George A. Isaac, Atmospheric Environment Service</i>	
<i>Stewart G. Cober, Atmospheric Environment Service</i>	
The NRC Convair-580 Research Aircraft: Configuration in the Canadian Freezing Drizzle Experiment	125
<i>Dave L. Marcotte, Flight Research Laboratory, National Research Council</i>	
<i>J. Walter Strapp, Atmospheric Environment Service</i>	
<i>Stewart G. Cober, Atmospheric Environment Service</i>	
<i>George A. Isaac, Atmospheric Environment Service</i>	

II. ICE PROTECTION AND ICE DETECTION

David Sweet, Industry Co-Chair
Charles Masters, FAA Co-Chair

An Operational Perspective on Ice Detection and Protection Systems Research and Development	137
<i>Joe Bracken, USA Air Line Pilots Association</i>	
<i>Steve Green, USA Air Line Pilots Association</i>	
<i>Jim Bettcher, USA Air Line Pilots Association</i>	
<i>Steve Erickson, USA Air Line Pilots Association</i>	

An Impedance-Based Sensor Technology for Accessing Airframe Icing	149
<i>David C. Parkins, Innovative Dynamics Inc.</i> <i>Jack Edmonds, Innovative Dynamics Inc.</i>	
Ultrasonic Detection of Large Droplets Ice Accretions	161
<i>Michel Le Pimpec, Inter technique</i>	
Super-Cooled, Large Drop (SLD) Ice Formation Detection	169
<i>D.B. Sweet, B.F. Goodrich Ice Protection Systems</i> <i>A.D. Reich, B.F. Goodrich Aerospace R&D</i>	
Remote Detection and Avoidance of Inflight Icing	179
<i>Charles C. Ryerson, U.S. Army Corps of Engineers</i>	
Application of New Electrothermal Systems on Aircraft for Extended Ice Protection	191
<i>Porter J. Perkins, Consultant, Aircraft Icing</i> <i>G.P. Buzz Lynch, Aerospace Safety Technologies, Inc.</i>	
Low Adhesion Surfaces for Ice Protection	215
<i>James T. Hindel, B.F. Goodrich Aerospace</i> <i>Richard L. Rauckhorts, III, B.F. Goodrich Aerospace</i>	
Ice Protection System for a New Commuter Aircraft	229
<i>F. Averous, AERAZUR</i>	
Use of Flush-Mounted Smart Skin Ice Sensors for the Detection/Exit Criteria	241
<i>Philip Zollinger, Vibro-Meter SA</i>	
Overview of Experimental Water Droplet Impingement Research and Future Aviation Community Requirements, Including SLD Experimental Data	257
<i>Michael Papadakis, Wichita State University</i> <i>Colin S. Bidwell, NASA Lewis Research Center</i>	
An Eulerian Approach to Ice Droplets Impingement Calculations	275
<i>Y. Bourgault, Concordia University</i> <i>W.G. Habashi, Concordia University</i> <i>J. Dompierre, Concordia University</i> <i>G. Chevalier, Concordia University</i> <i>W. DiBartolomeo, Pratt & Whitney Canada</i>	
The Formation of an Ice Ridge Beyond Protected Regions	285
<i>Kamel Al-Khalil, Ph.D. Cox and Company</i>	

III. FORECASTING AND AVOIDANCE

Marcia Politovich, Industry Co-Chair

Myron Clark, FAA Co-Chair

**In-Flight Icing – The Critical Need for Improved
Forecasts and Indexing of the Hazard** 297

Dan Stack, USA Air Line Pilots Association

**A Forecast and Verification Experiment
for Supercooled Large Drops (SLD)** 301

John Marwitz, University of Wyoming

**A Comparison of a Physically-Based
Aircraft Icing Forecast Algorithm
With Currently-Used Automated
Algorithms Using SSM/I Retrievals** 307

Andre Tremblay, Atmospheric Environment Service

Stewart Cober, Atmospheric Environment Service

Anna Glazer, Atmospheric Environment Service

George Isaac, Atmospheric Environment Service

**Verification of In-Flight Icing Forecasts:
Methods and Issues** 319

Barbara G. Brown, National Center for Atmospheric Research

**Differentiation of Freezing Drizzle
From Ice Hydrometeors and Freezing
Rain with Dual-Polarization Radar** 331

Roger F. Reinking, NOAA

Sergey Y. Matrosov, CIRES

Brooks E. Matner, NOAA

Robert A. Kropfli, NOAA

**Measurements of Supercooled Liquid Water
and Applications to Aircraft Inflight Icing** 339

Geoffrey E. Hill, Atek Data Corporation

**The Stovepipe Algorithm: Identifying
Locations Where Supercooled Large Droplets
Are Likely to Exist** 353

Ben C. Bernstein, National Center for Atmospheric Research

**Aircraft Icing Detection Using Satellite Data
and Weather Forecast Model Results** 365

Jothiram Vivekanandan, National Center for Atmospheric Research

Gregory Thompson, Naval Research Laboratory

Thomas F. Lee, Naval Research Laboratory

A Meteorologically-Based Icing Severity Index 375

Marcia K. Politovich, National Center for Atmospheric Research

Gregory Thompson, National Center for Atmospheric Research

IV: REQUIREMENTS FOR AND MEANS OF COMPLIANCE IN ICING CONDITIONS (INCLUDING ICING SIMULATION METHODS)

Thomas Bond, NASA Co-Chair

Eric Parelton, JAA Co-Chair

John P. Dow, Sr., FAA Co-Chair

**Aerodynamics of Supercooled-Large-Droplet
Ice Accretions and the Effect on Aircraft Control** 387

Michael B. Bragg, University of Illinois at Urbana-Champaign

**Effect of Icing on Aerodynamic
Characteristics of Aircraft with Unswept
Wings and Ensuring their Flight Safety** 401

G.T. Andreev

S.Ya. Naumov

Yu.M. Rogozhkin

Yu.F. Shelyukhin

**JAA Certification Policy NPA 25F-219
Flight in Icing Conditions Acceptable Handling
Characteristics and Performance Effects** 413

Eric Parelton, JAA (DGAC-France)

**A Review of Certification for Flight in
Icing Conditions and Recommendations
for Necessary Improvements** 437

Jim Bettcher, USA Air Line Pilots Association

Steve Green, USA Air Line Pilots Association

Steve Erickson, USA Air Line Pilots Association

Joe Bracken, USA Air Line Pilots Association

**EURICE: A European Research on aircraft
Ice Certification** 447

A. Amendola, Centro Italiano Ricerche Aerospaziali

G. Mingione, Centro Italiano Ricerche Aerospaziali

**Flight in Icing Conditions: International
Standardization of Certification Requirements
for Transport Category Airplanes** 459

Colin S. Fender, FAA

David J. Kotker, Boeing Commercial Airplane Group

**The NASA Lewis Icing Research Tunnel:
Testing and Data Acquisition** 469

Thomas B. Irvine, NASA Lewis Research Center

David N. Anderson, NASA Lewis Research Center

A Study of Large Droplet Ice Accretion in the NASA Lewis IRT at Near-Freezing Conditions; Part 2	485
<i>Harold E. Addy, Jr., NASA Lewis Research Center</i>	
<i>Dean R. Miller, NASA Lewis Research Center</i>	
<i>Robert F. Ide, Army Research Laboratories/NASA Lewis Research Center</i>	
Large Scale Icing Tests in the ONERA S1MA Wind Tunnel: Current Capabilities and New Studies to Generate Large Supercooled Droplets	499
<i>F. Chapin, O.N.E.R.A. Modane-Avrieux Test Center</i>	
<i>J. Prieur, O.N.E.R.A. Chatillon Center</i>	
The Effect of Altitude on Icing Tunnel Airfoil Icing Simulation	511
<i>Myron M. Oleskiw, National Research Council, Canada</i>	
<i>Fabrizio De Gregorio, CIRA Wind Tunnel Department, Italy</i>	
<i>Biagio Esposito, CIRA Wind Tunnel department, Italy</i>	
Survey of Ice Accretions Formed in Freezing Drizzle Under Natural Icing and Simulated Icing Behind the United States Air Force Tanker and in the NASA-Lewis Icing Research Tunnel	521
<i>Porter J. Perkins, Consultant, Aircraft Icing</i>	
<i>John P. Dow, Sr., FAA</i>	
<i>Dave Sweet, B.F. Goodrich Aerospace</i>	
Aircraft Icing Due to Supercooled Large Droplets	533
<i>M.T. Brahimi, Ecole Polytechnique de Montreal</i>	
<i>P. Tran, Ecole Polytechnique de Montreal</i>	
<i>F. Tezok, Bombardier Inc./Canadair</i>	
<i>I. Paraschivoiu, Ecole Polytechnique de Montreal</i>	
Computational Simulation of Large Droplet Icing	545
<i>William B. Wright, NYMA, Inc.</i>	
<i>Mark G. Potapczuk, NASA Lewis Research Center</i>	

**V. OPERATIONAL REGULATIONS
AND TRAINING REQUIREMENTS**
Robert Brayton, Industry Co-Chair
Katherine Hakala, FAA Co-Chair

Flight into Freezing Rain/Drizzle: A General Aviation/Business Jet Manufacturer's Perspective	557
<i>S. Heathman, Cessna Aircraft Company</i>	
<i>R. Rice, Cessna Aircraft Company</i>	
<i>D. Wariner, Cessna Aircraft Company</i>	
<i>S. Woodson, Cessna Aircraft Company</i>	

Some Observations on Design, Certification, and Training for Operation of Aircraft in Icing Situations <i>C.P. (Pete) Hellsten, Aeronautical and Marine Consultant</i>	565
Difficulties in the Operation of Aircraft in Icing Conditions <i>Steve Erickson, USA Air Line Pilots Association</i> <i>Steve Green, USA Air Line Pilots Association</i> <i>Jim Bettcher, USA Air Line Pilots Association</i> <i>Joe Bracken, USA Air Line Pilots Association</i>	575
Aircraft Icing: The Dispatcher's Role in Forecasting and Avoidance <i>Steve Horton, Airline Dispatchers Federation</i>	585
Presentation by Air Transport Association of Canada <i>Jack Squires, Air Transport Association of Canada</i>	587

VI. APPENDIX OF ADDITIONAL PAPERS SUBMITTED AT THE CONFERENCE

Executive Summary

The FAA International Conference on Aircraft Inflight Icing, held on May 6-8, 1996, in Springfield, Virginia, was attended by over 400 participants from the U.S. and 19 foreign countries. The conference was an integral part of the third phase of the response of the Federal Aviation Administration (FAA) to an accident of a transport category aircraft in October 1994. The goal of this phase is to review current certification requirements, applicable operating regulations, and forecast methodologies associated with aircraft icing under varying environmental conditions. The conference included a review of major aspects of airworthiness when operating in icing conditions to determine if changes or modifications should be made to provide an increased level of safety.

One of the primary areas of concern at the conference was icing due to supercooled large droplets (SLD) (or other icing conditions outside of the FAA icing certification envelope described in Appendix C of Part 25 of the Federal Aviation Regulations).

The conference began with a plenary session on May 6 during which presentations were given by representatives of the FAA, the Joint Airworthiness Authorities, foreign airworthiness authorities, and national organizations concerned with flight safety.

The attendees met in working groups from mid-afternoon on May 6 to noon on May 8. The titles of the working groups were: Icing Environmental Characterization, Ice Protection and Ice Detection, Forecasting and Avoidance, Requirements for and Means of Compliance in Icing Conditions (Including Icing Simulation Methods), and Operational Regulations and Training Requirements.

The working groups began with technical presentations intended to provide a survey of the state of the art and knowledge for the respective groups. The technical presentations were followed by discussions resulting in recommendations for short-term actions in areas such as operations, training, and education and for long-term efforts such as research, development, and rulemaking.

The conference closed with a plenary session on the afternoon of May 8, which was devoted to reports by the working groups and closing remarks by

Anthony Broderick, FAA Associate Administrator for Regulation and Certification.

Volume I of the conference proceedings covers the plenary sessions. Speakers at the opening plenary session submitted written text to accompany their presentations, and these are reproduced in this volume. This is followed by the reports of the co-chairs of the working groups, Administrator Broderick's closing remarks, and a roster of registrants for the conference. The recommendations in the working group reports will be evaluated in the preparation of an FAA inflight icing plan with specific actions and milestones.

Volume II of the conference proceedings is a compendium of technical papers presented in the various working groups. All papers included were either received in response to a "call for papers" or were invited papers of special interest to the conference. In addition, the FAA working group co-chairs had the prerogative of granting time for brief presentations in response to requests made directly to them. In some cases, the FAA co-chairs asked that the papers accompanying these brief presentations be included in Volume II. These papers can be found in the appendix at the end of Volume II.

Section I

Icing Environmental Characterization

George A. Isaac, Industry Co-Chair

Richard K. Jeck, Federal Aviation Administration Co-Chair

ANALYSIS OF AIRCRAFT ICING ENVIRONMENTS ASSOCIATED WITH SUPERCOOLED DRIZZLE

Stewart G. Cober¹, George A. Isaac¹, J. Walter Strapp¹,
and Dave Marcotte²

1. Cloud Physics Research Division, Atmospheric Environment Service
2. Institute for Aerospace Research, National Research Council

ABSTRACT

Measurements of the aircraft icing environments associated with cloud regions with supercooled drizzle have been obtained from twelve research flights conducted as part of the Canadian Freezing Drizzle Experiment. Several instruments were used to make measurements of hydrometeor concentrations and diameters from 0.13 to 6400 μm , which has allowed quantification of the droplet spectra. Cloud droplet median volume diameter, liquid water content, and other parameters of the spectra are used to characterize the icing environment, and comparisons are made to the FAR 25-C icing curves. The data include measurements of droplet median volume diameters up to 950 μm , liquid water contents up to 0.44 g m^{-3} , and minimum temperatures of -10°C . Approximately 20% of the data were associated with the classical drizzle formation mechanism of ice crystals melting and subsequently supercooling, while 80% of the measurements were associated with drizzle which grew through a condensation-collision-coalescence process.

1. INTRODUCTION

Ground based observations of freezing precipitation are common along the Canadian east coast during the winter (McKay and Thomson 1969). Strapp et al. (1996) found that St. John's Newfoundland had the highest frequency of freezing precipitation in Canada, receiving 103 hours of freezing drizzle and 51 hours of freezing rain per year. Freezing drizzle peaks in February and March when it is observed for 30 hours per month, representing 4% of the total hours. Therefore, it was not surprising that in-flight measurements of supercooled drizzle drops were made on four research flights during the Second Canadian Atlantic Storms Program (CASP II), which was conducted during January to March 1992 (Stewart 1991), and based out of St. John's. During two of the four encounters, the icing on the research aircraft appeared sufficient to cause the pilots to modify the flight path to exit from the icing region. One of these cases is described by Cober et al. (1996) where the drizzle formation region was a thick stratiform cloud which formed in an area of frontal uplifting. Cloud base was at 3150 m (-7.5°C) and cloud top was at 4200 m (-11°C), and drizzle drops up to 500 μm in diameter were observed at cloud base. The average supercooled liquid water content was 0.1 g m^{-3} with a cloud droplet median volume diameter of 50 μm . The drizzle drops had formed through a condensation collision coalescence process. While the

hazards to aircraft associated with supercooled drizzle have long been recognised (Lewis 1951), few in-flight measurements have been reported (Sand et al. 1984, Politovich 1989). Analysis of the CASP II cases pointed to significant uncertainties in both our understanding of the microphysics associated with the formation of supercooled drizzle, and our abilities to forecast it.

To obtain a better understanding of the mesoscale and microscale physics associated with the development of supercooled drizzle, and to attempt to provide additional data for quantifying the corresponding aircraft icing environments, the Canadian Freezing Drizzle Experiment (CFDE) was conducted during March 1995, based out of St. John's. An additional objective was the improvement of numerical forecasts of aircraft icing from supercooled drizzle. CFDE comprised 12 research flights into regions of North Atlantic storms where supercooled drizzle was forming. Approximately 10-12 hours of in-flight measurements were obtained from cloud regions where drops greater than 50 μm were measured. Preliminary analysis of the icing environments associated with supercooled drizzle are reported here. The data are compared to the U.S. Federal Aviation Administration Regulation 25 Appendix C curves (FAR 25-C).

2. AIRCRAFT AND INSTRUMENTATION

The research aircraft for CASP II and CFDE was a Convair-580 operated by the Institute for Aerospace Research of the National Research Council. The aircraft was fully instrumented for cloud microphysics measurements. Instrumentation used during CASP II is described by Cober et al. (1995), while a brief description of the instrumentation used during CFDE is presented below. Marcotte et al. (1996) provide additional details of the research aircraft.

Instrumentation used in this investigation included the following: King liquid water probe (King et al. 1978) which was accurate to $\pm 0.02 \text{ g m}^{-3}$ for liquid water content (LWC) less than 0.2 g m^{-3} ; Nevzorov liquid water and total water (ice plus liquid) probes (Korolev et al. 1996a) which were accurate to $\pm 10\%$; two Rosemount temperature probes and a reverse flow temperature probe which measured temperature to within $\pm 1^\circ\text{C}$; Cambridge dewpoint hygrometer which measured dew point to within $\pm 2^\circ\text{C}$; Rosemount 871FA221B icing detector; and a Rosemount 858 gust probe for measuring 3-dimensional winds and gusts. Instruments used for measuring hydrometeor spectra over specific diameter ranges included the following: PCASP 100x (Passive Cavity Aerosol Spectrometer Probe) which measured aerosol concentrations and sizes in the 0.13 to 3 μm range; two FSSP 100x (Forward Scattering Spectrometer Probe) which measured droplet concentrations and sizes in the ranges 3 to 45 μm and 5 to 95 μm respectively; 2DC mono 25-800 μm , 2DC grey 25-1600 μm and 2DP mono 200-6400 μm probes which measured 2-dimensional images of hydrometeor shapes and concentrations in their respective size ranges; and 1DC 20-300 μm and 1D 260 10-640 μm probes which measured 1-dimensional lengths and concentrations of hydrometeors. In addition, there were other instruments (see Marcotte et al. 1996), however they have

not been used in this analysis. The instruments collectively covered the entire range of hydrometeors from 0.13 to 6400 μm , thereby including aerosol particles greater than 0.13 μm , cloud droplets, drizzle drops, rain drops and ice particles.

Calibration of the King probes and FSSPs have been described by Cober et al. (1995) while the accuracy of the Nevzorov probes have been described by Korolev et al. (1996a). In the absence of ice crystals, these instruments provided three simultaneous measurements of the cloud LWC, which usually agreed within 15%. The King probe and Nevzorov LWC probe tended to underestimate the LWC associated with drops greater than 50 μm in diameter (Biter et al. 1987), however the design of the Nevzorov total water content (TWC) probe minimizes this effect (Korolev et al. 1996a). Therefore the Nevzorov TWC probe is believed to give a better measurement of LWC when drops larger than 50 μm are present. Calibration of the FSSP probes is discussed by Cober et al. (1995), and these instruments are believed capable of providing concentration measurements within $\pm 20\%$.

Depth of field uncertainties associated with the 25 to 150 μm channels of the 2DC mono probe causes significant uncertainty in the concentrations measured in these channels, particularly in the channels below 100 μm . In addition, the 2D probes are known to size some droplets incorrectly (Joe and List 1987, Korolev et al. 1991, Korolev et al. 1996b). Specifically, particles smaller than 100 μm are poorly sized, while those greater than 100 μm may be over sized by up to approximately 125 μm . Consequently, measurements from the first 4 channels of the 2DC were ignored in this analysis. Drops larger than 125 μm were considered to be systematically sized within 2 bins (50 μm), and any error associated with this will tend towards overestimating the sizes of the droplet distribution. For these reasons, data from between 2 and 8 channels from the 2DP, 2DG, 1DC and 1D 260 were similarly discounted. Droplet images from 2D instruments were measured with 2D analysis software following the centre-in technique of Heymsfield and Parrish (1978). Particles were accepted if their box-area ratios were greater than 0.6 and box-axis ratios were between 1.0 and 1.6. In addition cloud regions with recognizable ice crystals on the 2D imagery were removed from the data set to minimize the possibility of analyzing ice crystals as liquid droplets.

Ice build up on the instruments can have a significant effect on their measurements. The majority of the instruments are heated to avoid this problem, and several probes were modified to augment the icing protection. The data from each instrument were examined for indications of ice build up, and data were discounted when such indications were found.

3. ANALYSIS AND DISCUSSION

Cloud regions with supercooled drizzle were identified by visually examining the 2D imagery. There is a clear distinction between cloud which is predominantly glaciated and cloud which is predominantly supercooled, and cloud regions in which ice crystals were observed were not included in the analysis reported here. The data were averaged over 300 s intervals, which corresponded to horizontal distances of approximately 30 km. This allows direct comparison with the FAR 25-C icing curves for continuous icing which are based on a horizontal extent of 17.6 n mi (33 km). There were 185 data points, of which 38 were assessed as having ice crystals which might contaminate the 2D analysis (i.e. ice crystals could possibly be interpreted as droplets by the 2D software and would bias the calculations of median volume diameter). For the remaining 147 data points, data from the FSSP, 2D and 1D probes were combined together to calculate an integrated spectra, from which characteristics of the complete drop spectra could be determined. Drop concentration and LWC spectra from four examples are shown in Fig. 1.

Figure 1a shows the number concentration and LWC spectra associated with rain at -3.1°C which formed below a melting layer. The average LWC was 0.07 g m^{-3} with a droplet concentration of 6 cm^{-3} and a median volume diameter (MVD) of $520\text{ }\mu\text{m}$. The largest drop size measured was 2 mm in diameter. The mass distribution in Fig. 1a shows peaks around $40\text{ }\mu\text{m}$, 0.5 mm and 1.5 mm , which are consistent with the high MVD. A drizzle spectra at -9°C which formed through collision coalescence in a thick stratiform deck is shown in Fig 1b. The average LWC was 0.16 g m^{-3} with a droplet concentration of 86 cm^{-3} and a MVD of $174\text{ }\mu\text{m}$. Drops to $600\text{ }\mu\text{m}$ were measured at cloud base and a distinct mass peak can be seen at $300\text{--}400\text{ }\mu\text{m}$ in Fig 1b. Figure 1c shows drizzle spectra observed in a region of high LWC. The temperature was -1.8°C with an average LWC of 0.37 g m^{-3} , droplet concentration of 85 cm^{-3} and MVD of $26\text{ }\mu\text{m}$. Drizzle drops to $250\text{ }\mu\text{m}$ were measured on the 2DC. A final example is shown in Fig. 1d, which shows a hydrometeor spectra at -2.5°C . The average LWC was 0.11 g m^{-3} with a droplet concentration of 72 cm^{-3} . The MVD was $25\text{ }\mu\text{m}$, although drops up to $600\text{ }\mu\text{m}$ were observed.

Data from each instrument channel are shown in Fig. 1, although data from channels which were discounted for reasons discussed in Section 2 are not shown. Similarly, channels with less than 10 particle counts over the averaging interval are also not shown and were not used in the analysis. The 1DC and 1D 260 data were not used in the integrations shown in Fig. 1, although they are shown for comparison.

A comparison of the LWC measured with the Nevzorov LWC probe and King probe is shown in Fig. 2a. These instruments agreed within $\pm 15\%$. The Nevzorov LWC and Nevzorov TWC measurements are compared in Fig 2b. The TWC was often higher than the LWC because of the reduced response of the LWC probes to drops larger than $50\text{ }\mu\text{m}$ (Biter et al. 1987). Figure 2c shows the Nevzorov TWC versus the LWC calculated from the integrated spectra. Since cloud regions with ice particles have been screened from the data, the TWC measurement represents a LWC measurement. While

uncertainties in the FSSP and 2D measurements cause the integrated LWC to be only accurate to $\pm 50\%$ (Baumgardner 1983), the agreement in Fig. 2c is much better, and gives confidence in both the TWC measurement and integrated spectra measurements. When a significant proportion of the hydrometeor mass is incorporated in drizzle sized drops, the MVD calculations are particularly sensitive to the measurements from the 2DC. As discussed in Section 2, the errors associated with 2DC measurements can be considerable (Korolev et al. 1996b), because of its tendency to oversize drops. Figure 2d shows the calculated LWC versus the Nevzorov TWC for only the 34 data points where the MVD was calculated to be greater than $40\text{ }\mu\text{m}$ (the limit of the FAR 25-C curves). While error estimates have not been calculated for these data, Fig. 2d indicates a fairly good agreement between the calculated LWC and the measured TWC, and gives some confidence in the measurements of the hydrometeor spectra.

The MVD was calculated for each integrated spectra, and the MVD and LWC for each point are shown in Fig. 3a compared to the FAR 25-C curves for 0 and -10°C . The coolest temperature observed during CFDE for a data point shown in Fig. 3 is -10°C . Figure 3b shows the same data compared to the icing envelopes of Newton (1978). The Newton (1978) curves characterize icing in terms of a rate of accumulation, and most of the CFDE data was characterized as being between light and moderate in intensity. However, the Newton curves do not account for factors such as the location where the ice forms, or the shape of the ice accretion, both of which are different for icing associated with drizzle, than for icing from cloud droplets. Figure 3a also shows the drizzle formation mechanism for each point, while Fig. 3b identifies data that were observed at temperatures warmer and cooler than -4°C . Eighty percent of the 147 measurements were associated with drizzle formed through a condensation-collision-coalescence (non-classical) process, while 20% were associated with a melting and subsequent supercooling (classical) process.

In general the average LWC varied between 0.05 and 0.2 g m^{-3} when the MVD was greater than $40\text{ }\mu\text{m}$. There were 26 observations with LWC greater than 0.2 g m^{-3} , all of which had MVDs smaller than $30\text{ }\mu\text{m}$, and none of which exceeded the FAR 25-C 0°C curve. Thirty four of the data points had MVDs greater than $40\text{ }\mu\text{m}$ and 8 points had MVDs greater than $500\text{ }\mu\text{m}$. The maximum MVD measured was $950\text{ }\mu\text{m}$ which occurred when the aircraft flew through a freezing rain region below cloud base. All observations of MVDs larger than $250\text{ }\mu\text{m}$ were made in regions where the drizzle formed through a classical process. Measurements of LWC from icing associated with large supercooled drops have been reported by Politovich (1989) for 14 research flights. Most of the flights were made in the Sierra Nevada in northern California, with one flight in northern Arizona and one near Amarillo Texas. Politovich (1989) reported LWCs between 0.05 and 0.36 g m^{-3} , with an average of 0.15 to 0.2 g m^{-3} , which are quite similar to those presented here. Recently, Rasmussen et al. (1995) presented an example of supercooled drizzle which formed in a shallow upslope cloud in Colorado. The LWC was 0.25 g m^{-3} , and $200\text{ }\mu\text{m}$ drops formed through a condensation collision coalescence process at -10°C . These values are also similar to several of the cases reported here.

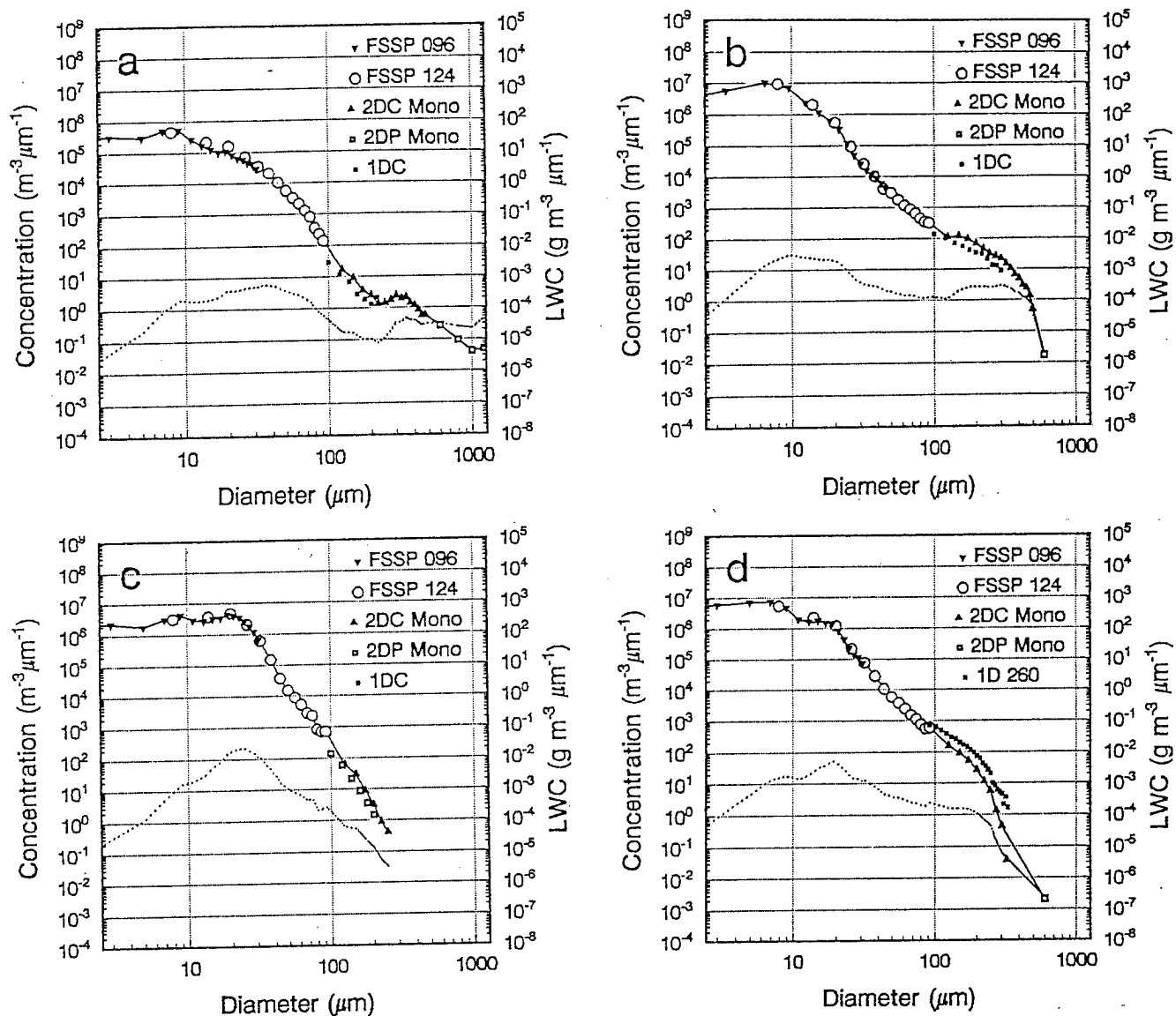


Fig. 1. Normalized drop spectra for concentration (solid curve and left axis scale) and LWC (dotted curve and right axis scale) for four cases during CFDE. a) 10 March 1995 from 1715 to 1720 UTC; b) 09 March 1995 from 1835 to 1840 UTC; c) 09 March 1995 from 1710 to 1715 UTC; and d) 15 March 1995 from 1940 to 1945 UTC. The FSSP 096, FSSP 124, 2DC mono and 2DP mono instruments were used to determine an integrated spectra which could then be used to determine characteristics such as MVD. The 1DC and 1D 260 data were not used for this analysis, and are shown only for comparison.

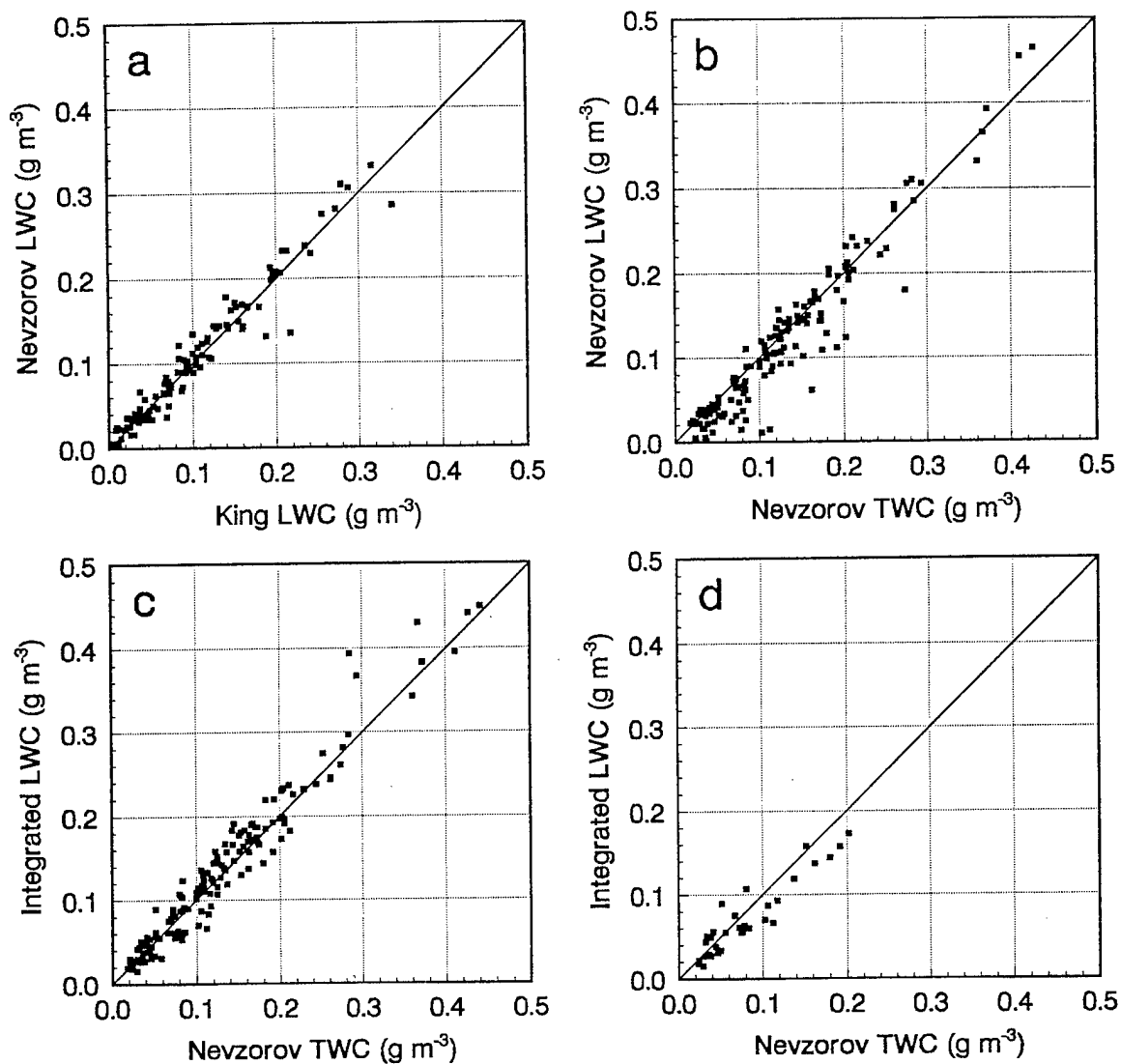


Fig. 2. Comparison of LWC measurements. a) King LWC probe versus Nevzorov LWC probe; b) Nevzorov TWC probe versus Nevzorov LWC probe; c) Nevzorov TWC probe versus calculated LWC using the integrated drop spectra; and d) Nevzorov TWC probe versus calculated LWC for cases where the calculated MVD exceeded $40 \mu\text{m}$. The solid lines represent 1:1 fits.

With only 147 data points, it is difficult to draw 0.1 percentile curves on Fig. 3 for comparison with the FAR 25-C curves. It is unlikely that the data in Fig. 3 represent the most extreme icing conditions which can occur from supercooled drizzle. Regardless, in terms of certifying aircraft for flight into regions with supercooled drizzle, Fig. 3 does reflect the minimum limits for icing environments in winter storms over the North Atlantic. Since little data has been previously published, this represents an improvement in current attempts to define the worst case icing environments. While the synoptic conditions in the storms reported by Politovich (1989) and Rasmussen et al. (1995) are quite different than those in east coast winter storms, the microphysics processes likely have similarities, and similar LWCs might be expected. Therefore the measurements of LWC and MVD taken during CFDE may be applicable to a larger area of North America than just over the Atlantic coast.

The percentiles for LWCs incorporated in drops between specific size ranges are listed in Table 1 following Jeck (1996). The LWC incorporated in drops larger than 50 μm in diameter averaged 0.02 g m^{-3} , although the maximum value observed was 0.11 g m^{-3} . Pruppacher and Klett (1978) indicated that concentrations of drops greater than 40 μm should exceed a few per litre in order for a collision coalescence growth mechanism to be initiated. Table 1 shows that the concentrations averaged 62 L^{-1} for drops greater than 50 μm , which is consistent with Pruppacher and Klett (1978), and with the observation that 80% of the CFDE data formed through a condensation collision coalescence process. As suggested by Jeck (1996), the data in Table 1 may prove useful in the design of certification studies and in tanker simulations.

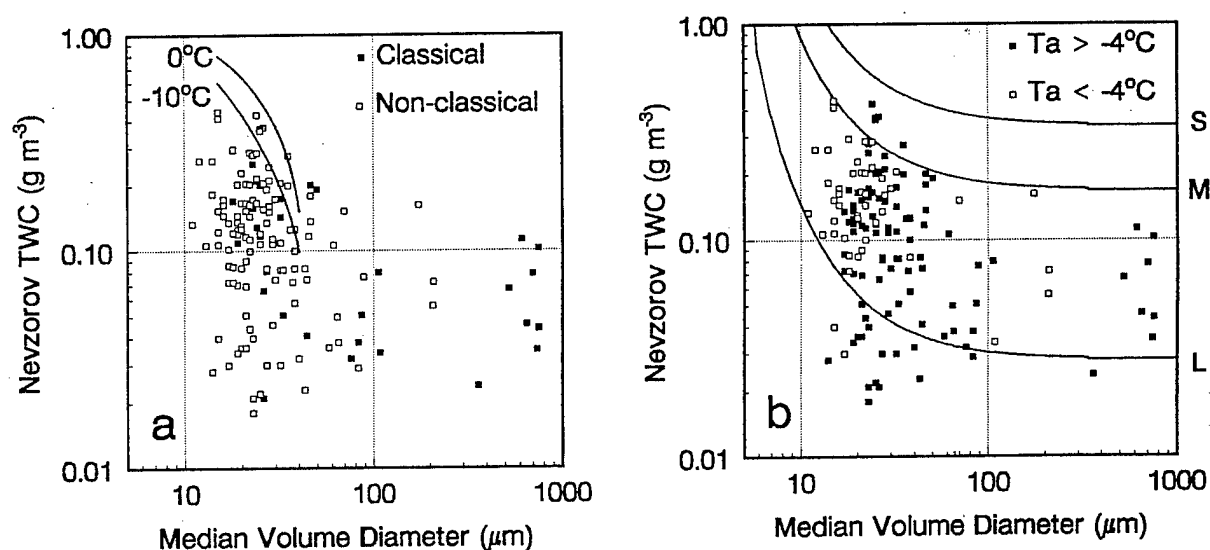


Fig. 3. Comparison of MVD-LWC points measured in CFDE to a) the FAR 25-C curves for 0 and -10°C ; and b) the icing intensity curves of Newton (1978). Newton's curves refer to rates of accumulation of 12, 6 and $1 \text{ g cm}^{-2} \text{ hr}^{-1}$ which correspond to severe (S), moderate (M), and light (L) icing respectively. The CFDE data are distinguished by a) formation mechanism (classical versus non-classical) and b) temperature (less than -4°C versus greater than -4°C).

Table 1. Percentiles for LWC in g m^{-3} and drop concentration in L^{-1} for the 147 CFDE data points over specific diameter ranges.

Range μm	Average g m^{-3}	25% g m^{-3}	50% g m^{-3}	75% g m^{-3}	90% g m^{-3}	99% g m^{-3}
1-50	0.11	0.024	0.089	0.16	0.23	0.43
> 50	0.021	0.002	0.010	0.032	0.055	0.11
51-100	0.008	0.0013	0.0042	0.013	0.021	0.034
101-200	0.0039	0	0.00042	0.0048	0.015	0.026
201-300	0.0022	0	0.00011	0.0018	0.0063	0.028
301-400	0.0013	0	0	0.00082	0.0040	0.023
401-500	0.00072	0	0	0.00070	0.0030	0.0065
501-1000	0.0019	0	0	0.00053	0.0087	0.020
Range μm	Average L^{-1}	25% L^{-1}	50% L^{-1}	75% L^{-1}	90% L^{-1}	99% L^{-1}
1-50	57954	7234	32569	84651	140880	337220
> 50	62	11	40	100	151	295
51-100	59	12	35	87	136	296
101-200	3.1	0	0.35	4.2	11	21
201-300	0.31	0	0.016	0.22	0.89	3.6
301-400	0.064	0	0	0.040	0.18	1.1
401-500	0.016	0	0	0.015	0.063	0.15
501-1000	0.012	0	0	0.0070	0.050	0.13

4. CONCLUSIONS AND FUTURE WORK

Measurements of aircraft icing environments associated with cloud regions with supercooled drizzle have been made during 12 flights in the Canadian Freezing Drizzle Experiment. The average LWC was 0.12 g m^{-3} , with a maximum of 0.44 g m^{-3} . Drops greater than $50 \text{ }\mu\text{m}$ in diameter had average concentrations of 62 L^{-1} , and an average LWC of 0.02 g m^{-3} . The liquid water contents of cloud regions with median volume diameters larger than $40 \text{ }\mu\text{m}$ ranged from 0.05 to 0.2 g m^{-3} . Comparisons to the icing curves of FAR 25-C, showed that 34 of the 147 data points were outside the FAR 25-C curves.

Future work will focus on continued quality control of the data, and in particular on correction of the 2D data (Korolev et al. 1996b). Detailed error analysis will be conducted with an aim of quantifying the errors associated with each data point shown in Fig. 3. Comparisons will be made with other reports of supercooled drizzle in order to compare the microphysics mechanisms, and attempts will be made to link the data to other microphysical parameters such as wind shear (Pobanz et al. 1994).

5. ACKNOWLEDGEMENTS

This work was funded by the Canadian National Search and Rescue Secretariat, the Institute of Aerospace Research (IAR) of the National Research Council of Canada, the Atmospheric Environment Service (AES) and Transport Canada. The authors would like to thank the pilots of IAR for their support in flying in difficult icing conditions, and the technicians of AES for their support in keeping the instruments operational and calibrated.

6. REFERENCES

- Baumgardner, D., 1983: An analysis and comparison of five water droplet measuring instruments. *J. Climate Appl. Meteor.*, **22**, 891-910.
- Biter, C.J., J.E. Dye, D. Huffman, and W.D. King, 1987: The drop-size response of the CSIRO liquid water probe. *J. Atmos. Oceanic. Technol.*, **4**, 359-367.
- Cober, S.G., J.W. Strapp, and G.A. Isaac, 1996: An example of supercooled drizzle droplets formed through a collision-coalescence process. Accepted by *J. Appl. Meteor.*
- Cober, S.G., G.A. Isaac, and J.W. Strapp, 1995: Aircraft icing measurements in east coast winter storms. *J. Appl. Meteor.*, **34**, 88-100.
- Heymsfield, A.J., and J.L. Parrish, 1978: A computational technique for increasing the effective sampling volume of the PMS two-dimensional particle size spectrometer. *J. Appl. Meteor.*, **17**, 1566-1572.
- Jeck, R.K., 1996: Representative values of icing-related variables aloft in freezing rain and freezing drizzle. *34th Aerospace Sci. Meeting*, Reno Nevada, 15-18 January 1996.

- Joe, P., and R. List, 1987: Testing and performance of two-dimensional optical array spectrometers with greyscale. *J. Atmos. Oceanic. Technol.*, **4**, 139-150.
- King, W.D., D.A. Parkin, and R.J. Handsworth, 1978: A hot wire liquid water device having fully calculable response characteristics. *J. Appl. Meteor.*, **17**, 1809-1813.
- Korolev, A.V., J.W. Strapp, and A.N. Nevzorov, 1996a: On the accuracy of Nevzorov airborne hot wire LWC/TWC probe. *Proceedings of 12th Intl. Conf. Clouds and Precipitation*, Zurich, Switzerland, August 19-23 1996.
- Korolev, A.V., J.W. Strapp, and G.A. Isaac, 1996b: On the accuracy of PMS optical array probes. *Proceedings of the FAA Intl. Conf. on Aircraft Inflight Icing*, Springfield, Virginia, May 6-8, 1996.
- Korolev, A.V., S.V. Kuznetsov, Y.E. Makarov, and V.S. Novikov, 1991: Evaluation of measurements of particle size and sample area from optical array probes. *J. Atmos. Oceanic. Technol.*, **8**, 514-522.
- Lewis, W., 1951: Meteorological aspects of aircraft icing. *Compendium of Meteorology*. Amer. Meteor. Soc., Edited by T. F. Malone, Waverly Press Inc., 1197-1203.
- Marcotte, D.L., J.W. Strapp, S.G. Cober, and G.A. Isaac, 1996: The NRC Convair-580 research aircraft: Configuration in the Canadian Freezing Drizzle Experiment. *Proceedings of the FAA Intl. Conf. on Aircraft Inflight Icing*, Springfield, Virginia, May 6-8, 1996.
- McKay, G.A., and H.A. Thompson, 1969: Estimating the hazard of ice accretion in Canada from climatological data. *J. Appl. Meteor.*, **8**, 927-935.
- Newton, D.W., 1978: An integrated approach to the problem of aircraft icing. *J. Aircraft*, **15**, 374-380.
- Pobanz, B.M., J.D. Marwitz, and M.K. Politovich, 1994: Conditions associated with large-drop regions. *J. Appl. Meteor.*, **33**, 1366-1372.
- Politovich, M.K., 1989: Aircraft icing caused by large supercooled droplets. *J. Appl. Meteor.*, **28**, 856-868.
- Pruppacher, H.R., and J.D. Klett, 1978: *Microphysics of Clouds and Precipitation*. Reidel, 714 pp.
- Rasmussen, R.M., B.C. Bernstein, M. Murakami, G. Stossmeister, and J. Reisner, 1995: The 1990 Valentine's Day arctic outbreak. Part 1: Mesoscale and microscale structure and evolution of a Colorado front range shallow upslope cloud. *J. Appl. Meteor.*, **34**, 1481-1511.
- Sand, W.R., W.A. Cooper, M.K. Politovich, and D.L. Veal, 1984: Icing conditions encountered by a research aircraft. *J. Climate Appl. Meteor.*, **23**, 1427-1440.
- Stewart, R.E., 1991: Canadian Atlantic Storms Program: Progress and plans of the meteorological component. *Bull. Amer. Meteor. Soc.*, **72**, 364-371.
- Strapp, J.W., R.A. Stuart, and G.A. Isaac, 1996: A Canadian climatology of freezing precipitation, and a detailed study using data from St. John's, Newfoundland. *Proceedings of the FAA Intl. Conf. on Aircraft Inflight Icing*, Springfield, Virginia, May 6-8, 1996.

FREEZING DRIZZLE ENCOUNTERED BY A RESEARCH AIRCRAFT OVER THE PARK RANGE IN COLORADO

R. Paul. Lawson
SPEC Incorporated
Boulder, Colorado, USA

Marcia K. Politovich
National Center for Atmospheric Research*
Boulder, Colorado, USA

1. Introduction

The crash of a commuter aircraft in October 1994 generated renewed interest in the potential problems of turboprop aircraft flying in freezing drizzle. This stimulated new research using icing wind tunnels and numerical simulations (for example, see Miller et al. 1996 and Ashenden et al. 1996). However, published results of performance degradation of turboprop research aircraft in natural freezing drizzle are scarce. The most comprehensive investigations in freezing drizzle are based on the University of Wyoming (UW) Beechcraft Super King Air B-200T (Cooper et al. 1984; Sand et al. 1984; Politovich 1989; Pobanz et al. 1994; Politovich 1996). Additional results of some effects of icing on the performance of the NASA Lewis Twin Otter research aircraft are found in Ranaudo et al. (1984). The German DLR has also performed extensive research in natural icing conditions using a piston-driven DO-28 research aircraft (Hoffman and Roth 1989; Hoffman 1990)

Most of the published performance data collected in freezing drizzle by the UW B-

200T are at temperatures warmer than -10°C . In this paper we present comparative data collected in freezing drizzle at -15°C by a Piper Cheyenne II (PA-YE II) turboprop research aircraft.

2. COSE III Field Experiment

In the winter of 1981-1982, Colorado State University (CSU) conducted an intensive field program near Steamboat Springs, Colorado. The third Colorado Orographic Seeding Experiment (COSE III) focused on understanding the structure of both shallow and deep orographic storms over the Park Range. Data were collected using a vertically-pointing K_a -band radar, a scanning microwave radiometer, two special radiosondes, a network of surface observations and the PA-YE II research aircraft instrumented and operated by Colorado International Corporation (CIC). The surface and aircraft instrumentation are described by Rauber (1985), who also describes in detail the microphysical characteristics of several of the storms that were studied.

* The National Center for Atmospheric Research is Sponsored by the National Science Foundation.



Figure 1. Photograph of the CIC Piper Cheyenne II (PA-YE II) turboprop research aircraft used in the CSU COSE III field program. The PMS FSSP and 2D-C probes are mounted on struts protruding from the right side of the nose. The other microphysical and state parameter instrumentation is on the strut extending from the left side of the nose. An ice crystal decelerator is mounted on top of the fuselage.

3. Research Aircraft

The PA-YE II research aircraft was equipped with Particle Measuring Systems (PMS) FSSP, 2D-C (Knollenberg 1981), a Johnson-Williams (J-W) hot-wire liquid water content (LWC) device (Strapp and Schemenauer 1982), ice crystal decelerator and other standard meteorological instrumentation. A photograph of the aircraft is shown in **Figure 1**. The aircraft typically made spiral descents and ascents through the storms, starting about 60 km upwind of the Park Range and extending 20 km downwind of the ridgeline. The COSE III field program was not designed for making measurements of aircraft performance in icing conditions; however, significant airframe icing was encountered in shallow (~2 km deep) orographic storms during three missions (Raubert 1985). In one case, 5 January 1982, the

aircraft flew in freezing drizzle for 15 min and then made a spiral ascent while carrying the ice accumulated in the freezing drizzle. The freezing drizzle encounter and subsequent climb present an opportunity to compare the climb performance with another similar occasion when the aircraft was not encumbered by accreted ice.

4. Icing Encounter on 5 January 1982

The cloud system of 5 January 1982 underwent an extreme transition at about 1445 UTC (0745 local time).¹ A deep synoptic storm system overran the shallow orographic cloud during the course of the research flight. As seen in **Figure 2**, cloud top observed by the vertically-pointing

¹ Unless otherwise noted, all times cited in this paper are UTC.

radar rose rapidly from about 4.5 km (-15°C) at 1445 to 7 km (-30°C) at 1500. **Figure 2** also shows that between 1415 and 1500 the integrated cloud liquid water measured by the microwave radiometer fell rapidly and snow observed at the ground increased sharply. These observations support a scenario where a shallow orographic cloud containing supercooled liquid water was overrun by a deeper storm containing mostly ice crystals.

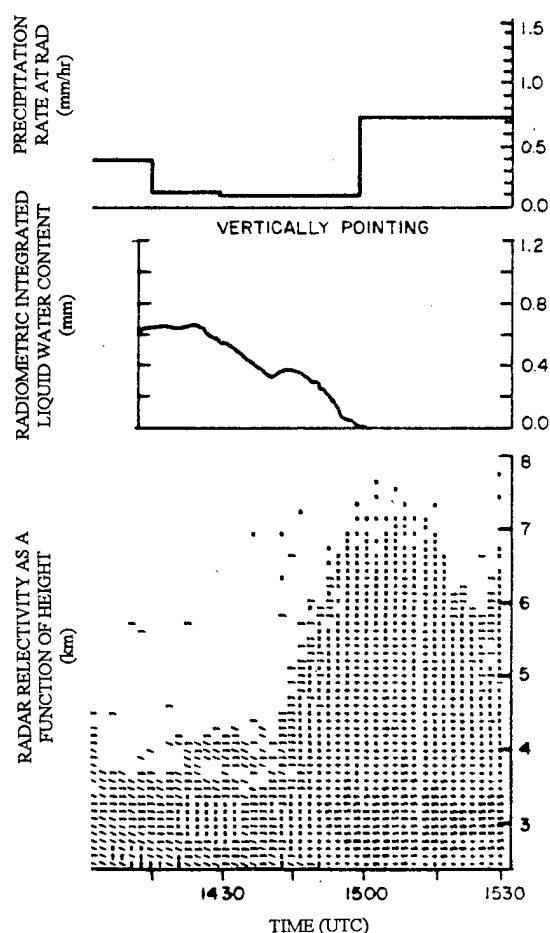


Figure 2. Vertical profiles of (bottom) K_a band radar reflectivity estimate of cloud top, (middle) integrated liquid water from microwave radiometer and (top) precipitation rate measured on the ground at the radar site (from Rauber 1985).

Rauber (1985), based on his study of five shallow orographic storms during COSE III, found that just upwind of the ridge line near cloud top was the preferred location for supercooled liquid cloud water. **Figure 3** shows a profile view of the flight track of the PA-YE II. Based on the information in **Figures 2** and **3**, it can be seen that the aircraft flew between 4.3-4.7 km just below cloud top, from upwind to a position about 10 km downwind of the ridge line of the Park Range. Prior to 1436, the drop size spectra measured by the FSSP and 2D-C were confined to drops with diameters $< 30 \mu\text{m}$ and the J-W and FSSP LWC were $< 0.05 \text{ g m}^{-3}$. From 1436-1450 the drop spectra broadened dramatically, the MVD based on the FSSP data increased from $15 \mu\text{m}$ to about $25 \mu\text{m}$, the J-W LWC increased by $0.1\text{-}0.4 \text{ g m}^{-3}$ and drops up to about $400 \mu\text{m}$ in diameter were observed by the 2D-C probe.

The origin of the freezing drizzle drops on 5 January is not clear. Measurements from the special radiosondes launched during the case study did not show evidence of wind shear at cloud top that would support the large drop generation criteria established by Pobanz et al. (1994). It is interesting to note, however, that the FSSP drop concentrations were unusually low, ranging from about $10 - 40 \text{ cm}^{-3}$ in the large drop region.

Relatively broader cloud drop distributions are generally associated with relatively low cloud condensation nuclei (CCN) concentrations (Pruppacher and Klett 1978). Rauber (1985) notes that the COSE III drop concentrations were unusually low compared with typical continental values and attributes this to four possible environmental factors: 1)

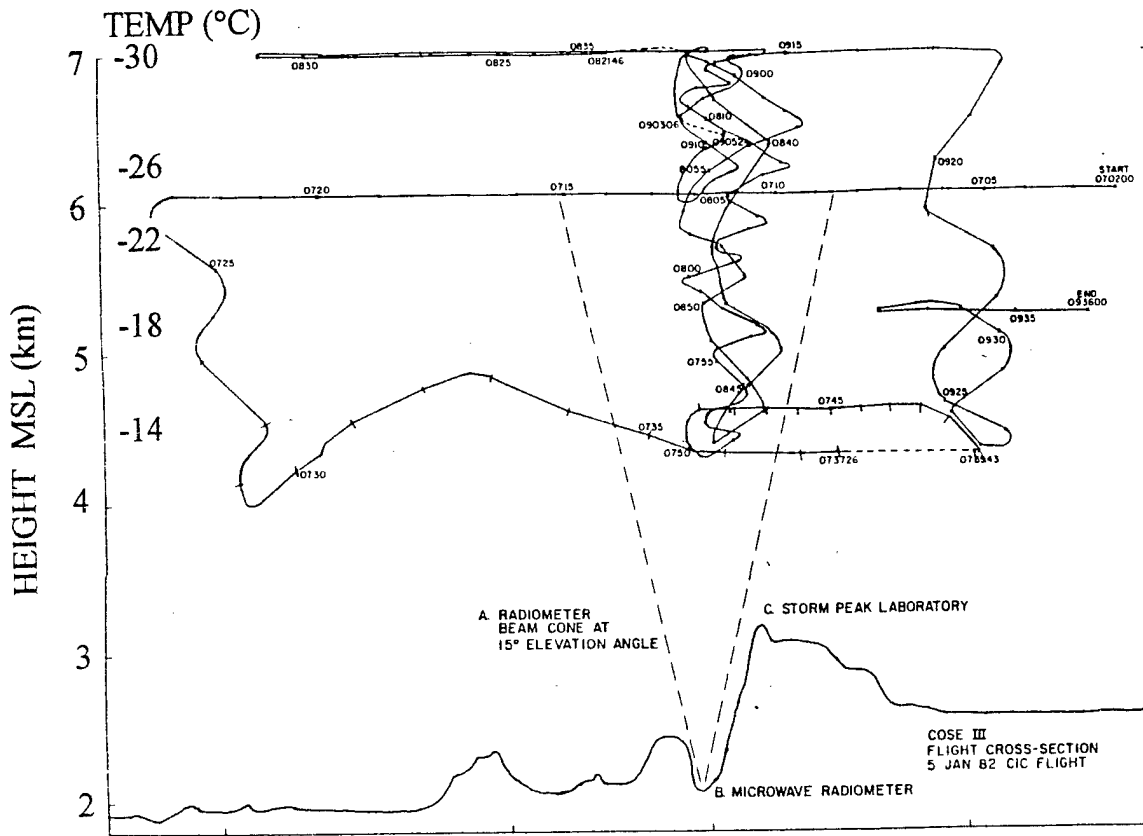


Figure 3. Vertical profile of the flight track of the PA-YE II research aircraft during the COSE III case study on 5 January 1982. Note that times shown are in MST (from Rauber 1985).

Stable layers occur frequently over the region in the winter and this limits mixing between boundary layer and mid-level cloud layers. This inhibits the rate at which CCN are resupplied to the cloud system. 2) The large amount of snow cover over the region limits interaction with the surface, restricting the supply of CCN. 3) The upwind region is relatively free of anthropogenic sources of CCN. 4) Scavenging of CCN can occur in cloud systems developing over upwind mountain ranges.

Cober et al. 1995 observed freezing drizzle in the Canadian Maritimes at -8°C in a shallow cloud system with a cloud top temperature of -10°C . They reported cloud microphysical conditions (FSSP

concentration $< 50 \text{ cm}^{-3}$, $\text{MVD}=25 \text{ }\mu\text{m}$, $\text{LWC} < 0.2 \text{ g m}^{-3}$ and 2D drops up to $500 \text{ }\mu\text{m}$) which are nearly identical to the conditions observed in the 5 January 1982 COSE III case. Cober et al. (1995) attributed the formation of freezing drizzle to a collision-coalescence process.

Figure 4 shows examples of the FSSP drop distributions before and during the freezing drizzle encounter on 5 January. For purposes of comparison, **Figure 5** shows 2D-C images of freezing drizzle drops observed on 5 January and during a 26 February 1982 icing encounter over the Sierra Nevada mountains (Sand et al. 1984; Cooper et al. 1984). The MVD calculated from FSSP measurements (on the $2\text{-}30 \text{ }\mu\text{m}$ range) reported by Sand et al.

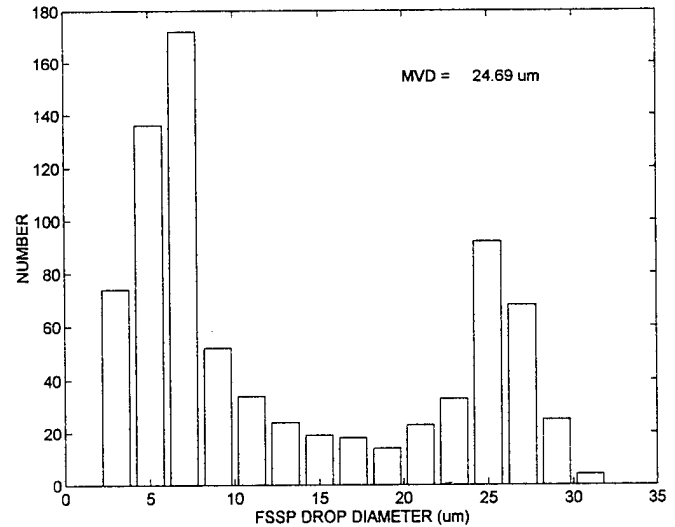
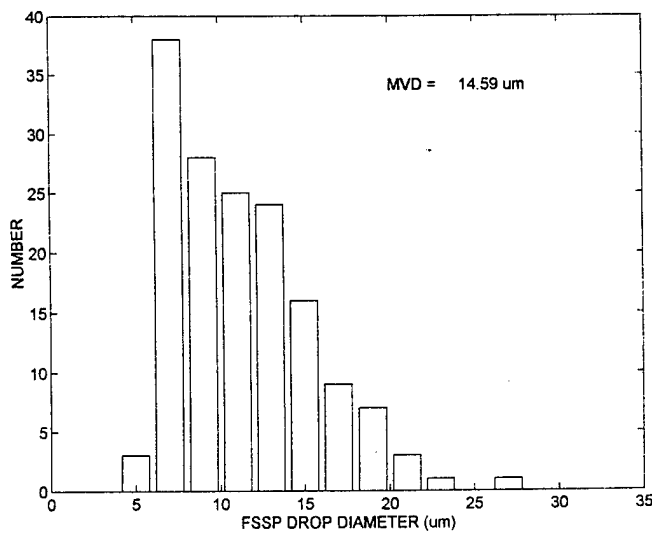


Figure 4. Examples of FSSP drop size distribution and median volume diameter (MVD) observed by the PA-YE II research aircraft in the COSE III project (left) before entering freezing drizzle on 5 January 1982 at 143615 and (right) during the freezing drizzle encounter at 144419.

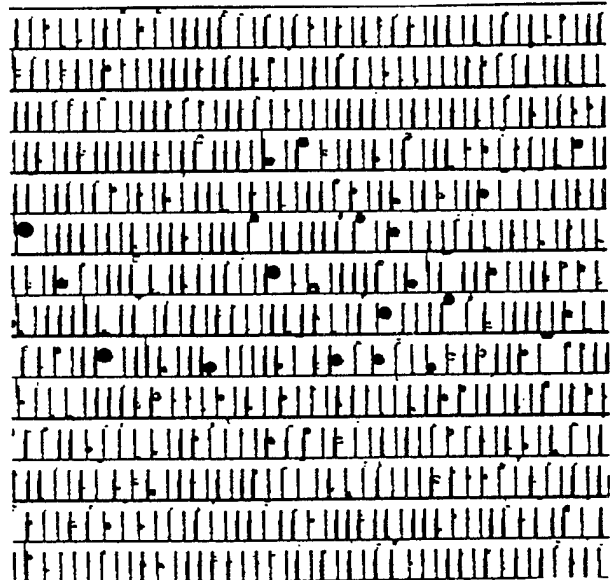
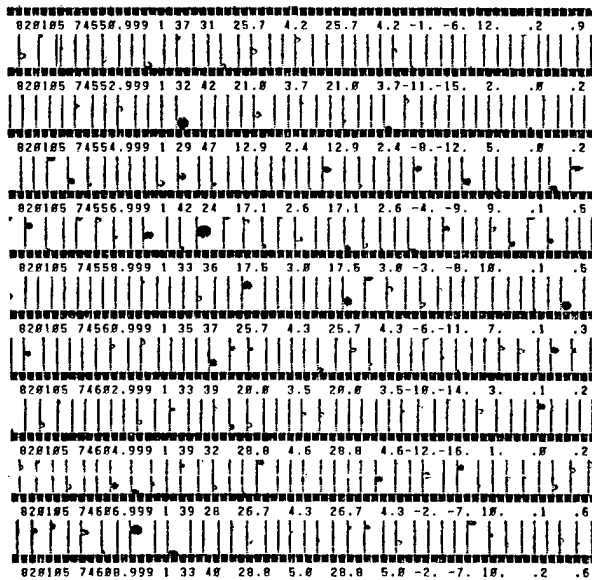


Figure 5. Examples of 2D-C images observed in freezing drizzle by (left) a PA-YE II research aircraft over Steamboat Springs at about 1446 on 5 January 1982 and (right) a B-200T research aircraft upwind of the Sierra Nevada Mountains on 26 February. The length of the vertical lines is 800 μm (images on the right are from Sand et al. 1984).

(1984) for the 26 February encounter was $\sim 18 \mu\text{m}$, while the MVD for the same FSSP size range during the 5 January encounter was $\sim 25 \mu\text{m}$. When the 2D-C data are incorporated into the calculation, the MVD for the 5 January case is $163 \mu\text{m}$

and for 26 February it is $94 \mu\text{m}$.² The FSSP MVD measurements and the 2D-C data in Figures 4 & 5 indicate that the PA-

² The difference in MVD between the two cases is not visually apparent in Figure 5 and may be the result of different averaging times and image processing software.

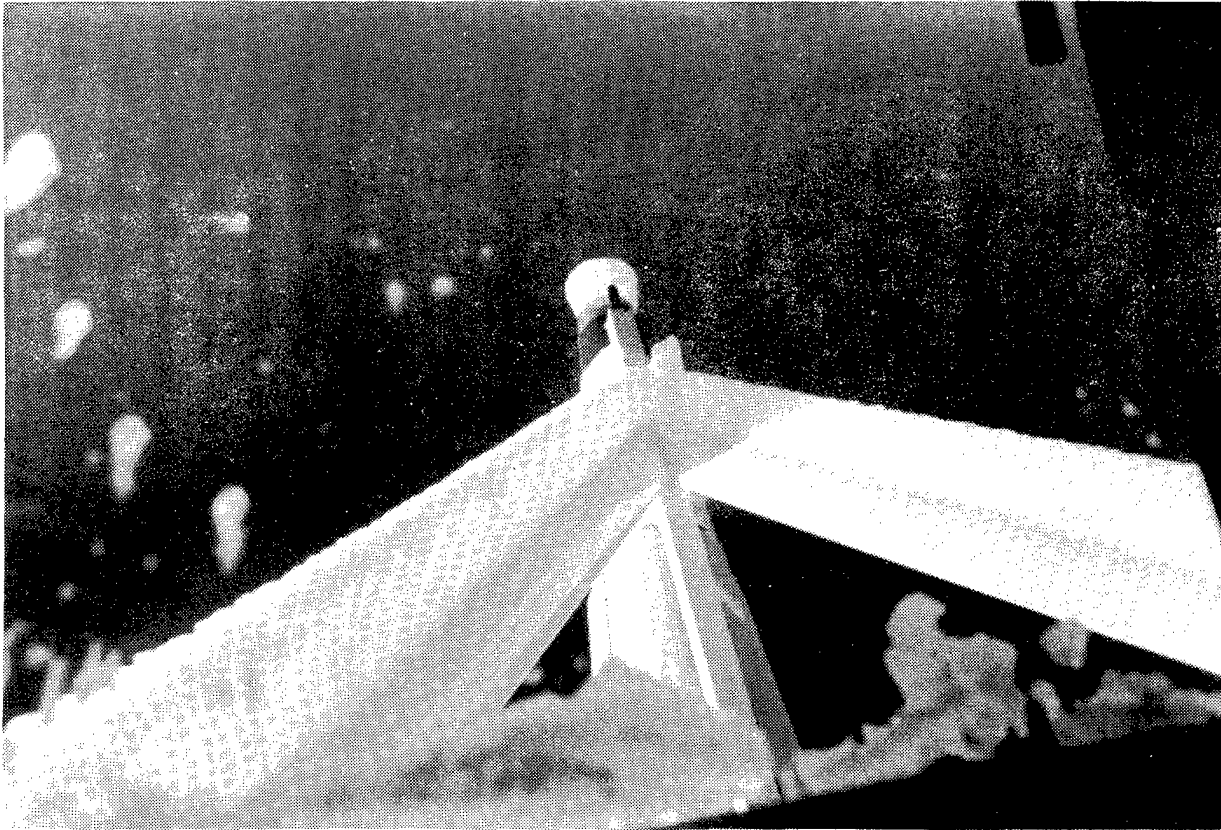


Figure 6. Photograph showing ice accumulation on the struts of the ice crystal decelerator of the PA-YE II research aircraft after a freezing drizzle encounter from 1436-1450 on 5 January 1982.

YE II research aircraft encountered a region of freezing drizzle from 1436-1450 on 5 January 1982.

As shown in **Figure 3**, the PA-YE II aircraft started a spiral ascent to (the new) cloud top at 7 km immediately following the freezing drizzle encounter. **Figure 6** shows a photograph taken after the aircraft exited through the top of cloud. The ice accreted on the struts of the decelerator (see **Figure 1** for reference) shows a build up of about 3-4 cm. It is difficult to tell from the photograph, but the accumulation appears to be mostly rime mixed with possibly a small amount of clear ice.

The spiral ascent on 5 January can be used to gauge the relative degradation in climb performance of the aircraft after the

freezing drizzle encounter. An analogous spiral ascent was analyzed to determine the climb performance of the PA-YE II under conditions when it was unaffected by accreted ice. The aircraft power settings were not recorded by the data acquisition system, however, a maximum allowable continuous climb rate was routinely executed during the COSE spiral ascents. Rauber (1985) shows a spiral ascent from 4 - 6 km during the period 0856-0905 on 18 December 1981 when the aircraft was at the same weight (due to fuel burn) as the ascent on 5 January. The overall rate of climb was 2.2 m s^{-1} on 18 December compared with 1.2 m s^{-1} on 5 January after the 15-min encounter in freezing drizzle.

Using the relative climb rates as an indicator, the PA-YE II experienced about a 45% decrease in climb performance after the freezing drizzle encounter on 5 January. In comparison, using performance curves from Cooper et al. (1984), approximately 70-90% ($7-9 \text{ m s}^{-1}$) of climb performance was lost during the 26 February 1982 encounter with freezing drizzle at 3 km upwind of the Sierra Nevada Mountains.

In both cases, the cloud microphysical conditions were very comparable. The 2D-C images shown in **Figure 5** are very similar. The potential ice accumulation on 5 January was estimated from LWC and true airspeed measurements to be $\sim 2.5 \text{ g cm}^{-2}$ and Sand et al. (1984) computed $\sim 3 \text{ g cm}^{-2}$ for the 26 February case. Assuming an ice density of 0.8 g cm^{-3} , this translates to an ice thickness of 3.1 cm on the PA-YE II, which is in general agreement with **Figure 6**.

The main meteorological difference is that the environmental temperature was -9°C (-4°C total temperature) for the 26 February case over the Sierra Nevada's and it was -15°C (-10°C total temperature) during the 5 January COSE III encounter over the Park Range. Recent investigations of freezing drizzle with MVD's of 40, 99 and $160 \text{ }\mu\text{m}$ were reported by Miller et al. (1996). Using the NASA Lewis icing research tunnel (IRT), they found that the characteristics of ice accretion were very sensitive to total temperature. However, the coldest total temperature investigated by Miller et al. (1996) was -2.2°C . Previous work by Olsen et al. (1984) in the IRT has shown that, at an airspeed of 94 m s^{-1} , MVD of $20 \text{ }\mu\text{m}$ and 1.05 g m^{-3} LWC, the shape of the ice formation is more irregular at -12.2°C than at -16.6°C .

5. Summary and Discussion

During the COSE III project, a Piper Cheyenne II (PA-YE II) research aircraft encountered freezing drizzle ($40 - 400 \text{ }\mu\text{m}$) drops near the top of a shallow orographic storm over the Park Range near Steamboat Springs, Colorado. The encounter occurred from 1436-1450 UTC on 5 January 1982 at about 4.5 km where the environmental temperature was -15°C . Photographs show that 3-4 cm of ice accreted on unprotected surfaces of the aircraft. This observation agrees well with the $0.1 \rightarrow 0.4 \text{ g m}^{-3}$ LWC and 15 min icing duration measurements used to predict the $\sim 2.5 \text{ g cm}^{-2}$ potential ice accumulation.

Shortly after the icing incident, the aircraft climbed 2.5 km through an ice crystal cloud (that had rapidly advected into the area). Compared with a similar climb on another COSE III mission when the aircraft was not affected by accreted ice, the PA-YE II lost about 45% of its climb performance due to the freezing drizzle encounter. Based on data presented in Sand et al. (1984) and Cooper et al. (1984), an encounter of the same duration by the UW B-200T in very similar microphysical conditions, but at an environmental temperature of -9°C , resulted in a loss in climb performance of about 70-90%.

As mentioned in the Introduction, the German DLR has conducted icing research for several years using their high-wing, piston driven DO-28 aircraft. Hoffman (1990) shows measurements using an FSSP, J-W and 2D-C probe where the DO-28 flew in freezing drizzle at about -3 to -5°C for up to 30 min. The cloud

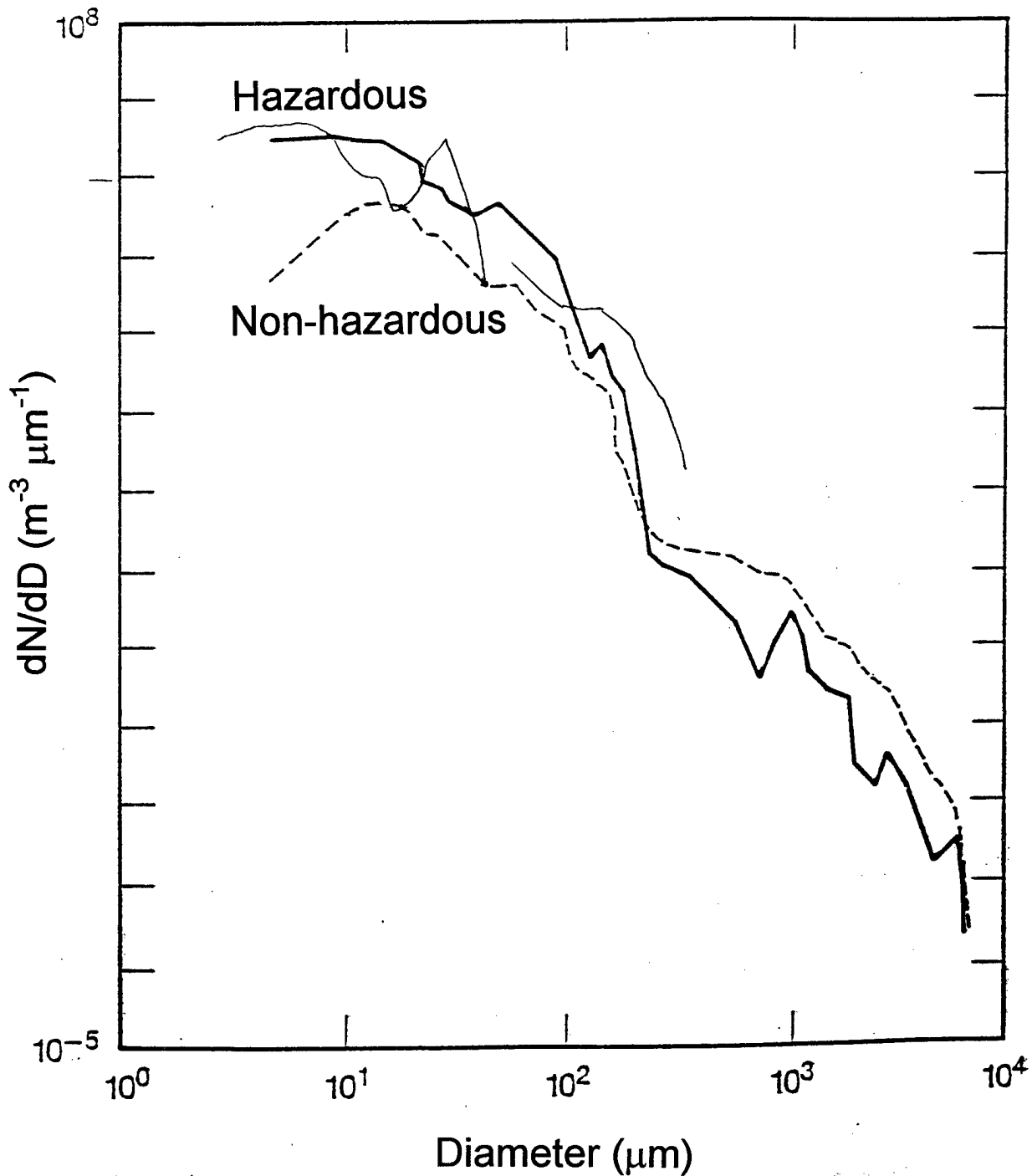


Figure 7. Graph showing drop size distributions using FSSP and 2D-C measurements determined by Politovich (1989) for hazardous (heavy line) and non-hazardous (dashed line) conditions and drop size distribution (thin solid line) for icing encounter in the COSE III project from 1436-1450 on 5 January 1982.

microphysical conditions (except for the warmer temperature) appeared to be similar to those reported during the encounters described in this paper. Video

cameras recorded accreted ice up to 30 cm aft of the DO-28 boots, which extend back 30 cm. These measurements suggest that the DO-28, even with its (relatively less-

powerful) piston engines, may be well-suited to handle freezing drizzle conditions. Bragg (1996) examined the available data concerning the relative performance ability of airfoils in icing and concludes that there is not enough research to know if some airfoils are more susceptible to ice accretion than others.

The difference in apparent performance degradation of the B-200T compared with the PA-YE II in very similar microphysical conditions, but different temperatures, can be attributed to (at least) three factors. 1) The colder temperature of the PA-YE II encounter probably favors a more regular ice formation with less runback and less performance degradation. 2) The PA-YE II and B-200T have different wings and the B-200T has a retrofitted spar strap. Thus, the B-200T wing may be more adversely affected by freezing drizzle encounters than the PA-YE II. This second factor is, of course, speculation, since there is no evidence to directly support or refute this possibility. 3) The third possibility is that, since a rigorous measurement uncertainty analysis was not conducted (and may not be possible), the composite measurement errors in these cases may exceed the ability to draw quantitative conclusions.

For the J-W liquid water contents of 0.1-0.4 g m⁻³, the icing conditions encountered on 5 January fall into the light to (top of the) moderate category established by Politovich (1996). The representative value of 0.22 g m⁻³ used for the potential accumulation places the encounter in the lower end of the moderate category. **Figure 7** shows plots of the hazardous and non-hazardous hydrometeor size distributions from Politovich (1989), along with the 5 January spectrum. Although the

5 January spectrum more closely resembles the hazardous spectrum, the degradation in performance of the airplane was not as great as in the King Air hazardous encounters. At this time we cannot determine whether this is due to differences in aircraft type, in the temperatures encountered, or in subtle differences in the microphysical measurements.

Acknowledgments: This research is (in part) sponsored by the National Science Foundation through an Interagency Agreement response to requirements and funding by the Federal Aviation Administration's Aviation Weather Development Program. The views expressed are those of the authors and do not necessarily represent the official policy or position of the U.S. Government.

References

- Ashenden, R., W. Lindberg, and J. Marwitz, 1996: Two-dimensional NACA 23012 airfoil performance degradation by super cooled cloud, drizzle, and rain drop icing. AIAA 96-0870. Presented at the 34th Aerospace Sciences Meeting and Exhibit, 15-18 Jan., 1996, Reno, Nevada.
- Bragg, M. B., 1996: Aircraft aerodynamic effects due to large droplet ice accretions. AIAA 96-0932. Presented at the 34th Aerospace Sciences Meeting and Exhibit, January 15-18, 1996, Reno, Nevada.
- Cober, S. G., G. A. Isaac, and J. W. Strapp, 1995: Aircraft icing measurements in east coast winter storms. *J. Appl. Meteor.*, **34**, 88-100.
- Cooper, W.A., W.R. Sand, M.K. Politovich, and D.L. Veal, 1984:

- Effects of icing on performance of a research airplane. *J. Aircraft*, **21**, 708-715.
- Hoffman, H. and R. Roth, 1989: Cloudphysical parameters in dependence on height above cloud base in different clouds. *Meteorol. Atmos. Phys.* **41**, 247-254.
- Hoffman, H. E., 1990: The analysis of three icing flight with various ice accretion structures when reaching icing degree severe. ICAS 17th Congress of the International Council of the Aeronautical Sciences, September 9-14, 1990, Stockholm, Sweden.
- Knollenberg, R. G., 1981. Techniques for probing cloud microstructure. In: *Clouds, Their Formation Optical Properties and Effects*. Eds: P. V. Hobbs and A. Deepak. Academic Press, New York. 15-92.
- Miller, D. R., H. E. Addy, Jr., and R. F. Ide, 1996: A study of large droplet ice accretions in the NASA-Lewis IRT at near-freezing conditions. AIAA 96-0934. Presented at the 34 Aerospace Sciences Meeting and Exhibit, January 15-18, 1996, Reno, Nevada.
- Olsen, W., R. J. Shaw, and J. Newton, 1984: Ice shapes and the resulting drag increase for a NACA 0012 airfoil. NASA TM-83556.
- Politovich, M.K., 1989: Aircraft icing caused by large supercooled droplets. *J. Appl. Meteor.*, **28**, 856-868.
- Politovich, M.K., 1996: The effect of icing on a research aircraft and evaluation of severity indices. *J. Aircraft*, in press.
- Pobanz, B.M., J.D. Marwitz and M.K. Politovich, 1994: Conditions associated with large-drop regions. *J. Appl. Meteor.*, **33**, 1366-1372.
- Pruppacher, H.R., and J.D. Klett, 1978: *Microphysics of Clouds and Precipitation*, D. Reidel Publishing Company, 707 pp.
- Ranaudo, R. J., K. L. Mikkelsen and R. C. McKnight, 1984: Performance degradation of a typical twin engine commuter type aircraft in measured natural icing conditions. AIAA 84-0179. Presented at the 22nd Aerospace Sciences Meeting, January 9-12, 1984, Reno, Nevada.
- Rauber, R. M., 1985: Physical structure of Northern Colorado River Basin cloud systems. Ph.D. Thesis Colorado State University. Also available as: Dept. Atmos. Science, Paper No. 390, 362 pp.
- Sand, W.R., W. A. Cooper, M.K. Politovich and D. L. Veal, 1984: Icing conditions encountered by a research aircraft. *J. Clim. Appl. Meteor.*, **23**, 1427-1440.
- Strapp, J. W., and R. S. Schemenauer, 1982: Calibrations of Johnson-Williams liquid water meters in a high-speed icing tunnel. *J. Appl. Meteor.*, **21**, 98-108.

IN SITU MEASUREMENTS OF AIRCRAFT ICING

Jeffrey Stith, Michael Poellot, Cedric Grainger, Ronald Rinehart,
Roger Tilbury and Ryan Zerr

University of North Dakota
Box 9006, University Station
Grand Forks, ND 58202-9006

1. INTRODUCTION

Airborne measurements of hydrometeor size spectra, air motions, and meteorological parameters have been made in a variety of icing conditions using the University of North Dakota (UND) Citation research aircraft. We will present highlights from some of the major icing cases that we have encountered. In particular, we will show results from a significant icing event with supercooled large drops and we compare these with results obtained in freezing rain. Finally, for freezing rain and ice pellet observations, we show how the depth of the freezing and melting layers are related to the type of precipitation encountered on the ground.

Aircraft data were collected by the UND Citation research aircraft. It carries a number of standard instruments for wind and microphysical measurements. These include a inertial navigation-gust probe system for wind and turbulence, a cooled-mirror dewpoint sensor (EG&G model 137), an NCAR-type reverse-flow temperature sensor, A Rosemount ice detector, Particle Measuring Systems (PMS) probes (2DC, 1DC, 1DP, FSSP) for cloud particle size spectra, and a Johnson-Williams liquid water sensor. PMS data processing methods are described in Arnott et al., (1994).

2. MEASUREMENTS IN FREEZING DRIZZLE

During the winter of 1987-1988, the University of North Dakota Citation aircraft was operated in the Denver, Colorado area to assist in the development of a NEXRAD icing algorithm. On January 31, 1988 (local date), the Citation flew two research missions in a shallow orographic cloud system during which moderate to severe icing conditions were encountered. These conditions were due to the presence of large supercooled droplets which created significant ice accumulations on the aircraft leading edges and upper and lower wing surfaces. The meteorological conditions, cloud microphysical characteristics and resultant aircraft icing from the second mission will be described in the following sections.

2.1 Meteorological Conditions

On the synoptic scale, the North American continent was being influenced by a broad, high amplitude long wave upper trough. On the back side of the trough, a strong surface high pressure system centered over Alberta, Canada, was pushing Arctic air southward through the plains. This cold air was pushed up against the lee side of the Rocky Mountains in Colorado by the

easterly anti-cyclonic flow at low levels. The mid- and upper-level flow around the bottom of the long wave trough over Colorado was from the west and relatively warm producing an inversion over the top of the cold air. An short wave embedded in this flow passed over eastern Colorado around 00Z on February 1. Although the moisture content of the low-level air mass was limited, the upslope lifting of the air was sufficient to produce a shallow cloud less than 800 meters thick. The upslope lifting was enhanced for a while by the approaching short wave.

This cloud layer was maintained from approximately 13Z on the 31st to 15Z on the 1st until the upslope flow weakened. Ground based radiometers measured integrated liquid water values of up to 0.5 mm during much of this time, which led to persistent icing conditions. A controlling factor in the length of this episode is the fact that there was no overlying cloud precipitating ice crystals into the supercooled upslope stratus. Some snow fall was induced by the passage of the short wave, causing the Citation to divert to Grand Junction, CO, for landing at the conclusion of the first mission. However, the upslope flow provided a continuous source of liquid water which was not significantly depleted by the snow. With the exception of the snow areas, the cloud was not detectable by ground-based 5 cm weather radar.

2.2 Cloud Microphysical Characteristics

On its return from Grand Junction for the second mission, the Citation descended into the top of the upslope cloud at 0406 UTC. For the

next hour, north-south oriented legs were flown in cloud at 2160 m and 2300 m (7000' and 7500'). Corresponding temperatures were -8.3 °C and -9.5 °C, respectively. Cloud and liquid water sensors included PMS FSSP, 1D-C, 2D-C and 1D-P probes, a J-W liquid water content meter, and a Rosemount ice detector. Due to the prolonged exposure to the strong icing conditions, the probe data are not continuously available. There were times when the sampling apertures on the PMS probes iced over.

The most remarkable and hazardous character of this cloud was the presence of many large supercooled water drops. According to Pobanz, et al. (1994) large drops are those with diameters greater than 30 μm and large drop regions are defined as meeting at least one of the following criteria:

- 1) FSSP concentration $\geq 5 \text{ cm}^{-3}$ for drops with diameter $> 22 \mu\text{m}$;
- 2) 1D-C concentration $\geq 5 \text{ L}^{-1}$ for particles with diameter $> 75 \mu\text{m}$;
- 3) distinguishable drops on the 2D images.

Figure 1 shows a composite particle spectrum from the FSSP, 1D-C and 2D-C probes, with the particle images from the 2D-C probe in Fig. 2. All three criteria for large drop regions are met: large FSSP drop concentration = 23 cm^{-3} ; large 1D-C particle concentration = 88 L^{-1} ; and 2D images showing the presence of liquid water drops. In addition, the Rosemount ice detector was cycling regularly at a rate of about 2 times per minute, indicating that the particles were liquid, not ice.

Pobanz et al. (1994) suggested that the mixing caused by shear-induced

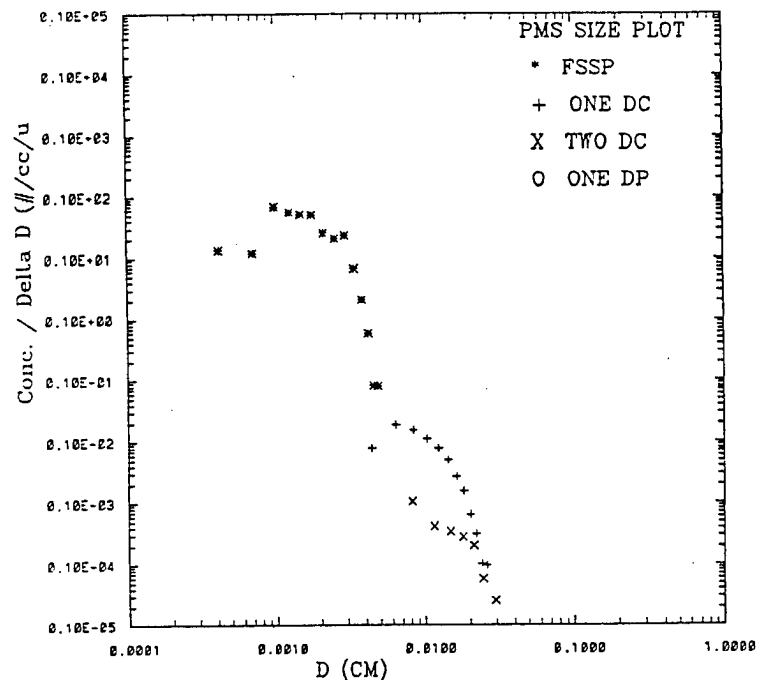


Figure 1. Composite size distribution in a drizzle region on January 31, 1988.

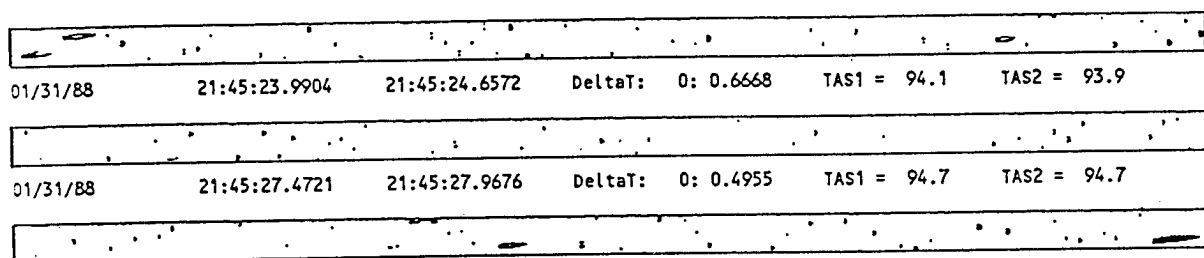


Figure 2. Images from the PMS 2DC probe in the drizzle region shown in Fig. 1.

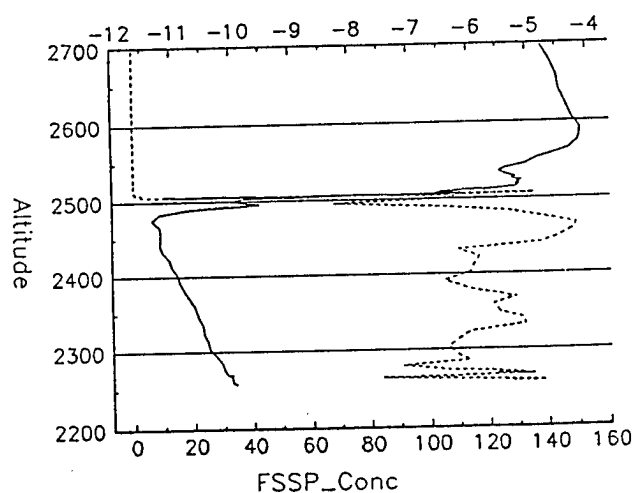


Figure 3. Profile of Temperature (°C) and Droplet concentration (per cc) through the drizzle region ion January 31, 1988.

turbulence might lead to the formation of large drops. The cloud top was found beneath a strong inversion (7°C) formed by the relatively warm overlying westerly air flow. The shear magnitude was 0.06 s^{-1} . The bulk Richardson number calculated from the wind shear through the cloud top layer was 0.7, which is in the range where shear-induced turbulence and Kelvin-Helmholtz billows are possible.

2.3. Aircraft observations

The ice buildup on the Citation could best be described as continuous moderate icing, with occasional severe mixed and clear icing. The de-icing boots were activated six times during the time in cloud. A post-flight inspection found ice accumulations of 2-4 inches or more on the non-protected parts of the airframe and on the research probes. This amount of ice is consistent with FSSP-measured liquid water contents of $0.3\text{-}0.4\text{ g m}^{-3}$. An intensity of severe was ascribed to the icing conditions because the flight had to be terminated due to ice accumulation on the aircraft Pitot tubes. Both the pilot and co-pilot tubes became obstructed, causing the airspeed indications to become unreliable. Backup airspeed readings were available from the onboard research Pitot systems which remained ice-free.

The pattern of ice accumulation on the airframe was indicative of large drop conditions. Ice accumulations were found along side the fuselage aft of the nose for several feet in the form of globules extending forward into the airstream. Similar accumulations were found on the underside of the wings back to about mid-chord. There was also a

significant amount of runback and refreeze evident on the top and underside of the wing aft of the anti-iced inboard leading edge section. This part of the wing is electrically heated. This process formed an ice bluff or ridge approximately one inch high.

Despite the dramatic accumulations of ice on various parts of the airframe and appendages, the pilot reported no abnormal handling characteristics. Additional power was required to maintain altitude and airspeed over that required for a clean airplane; however, the plane did not feel sluggish. Higher than normal airspeed was maintained through to the landing flare, but when power was pulled, there was no stall or rapid settling tendency.

3. MEASUREMENTS IN FREEZING RAIN

3.1 Size Distribution Measurements

Measurements from the UND Citation in freezing rain conditions have been made on March 17, 1987, January 17, 1990, January 19, 1990, February 1, 1990, and February 14, 1990. Most of these cases also have simultaneous Doppler radar data available from the UND 5 cm Doppler radar.

The best documented are those reported by Prater and Borho (1992), which occurred on 1 February, 1990 and on 14 February, 1990. The 14 February case was part of a large system that was further documented by Martner et al. (1993). Both cases were caused by overrunning of warm air over large regions of cold air associated with cold or stationary fronts. In contrast to the

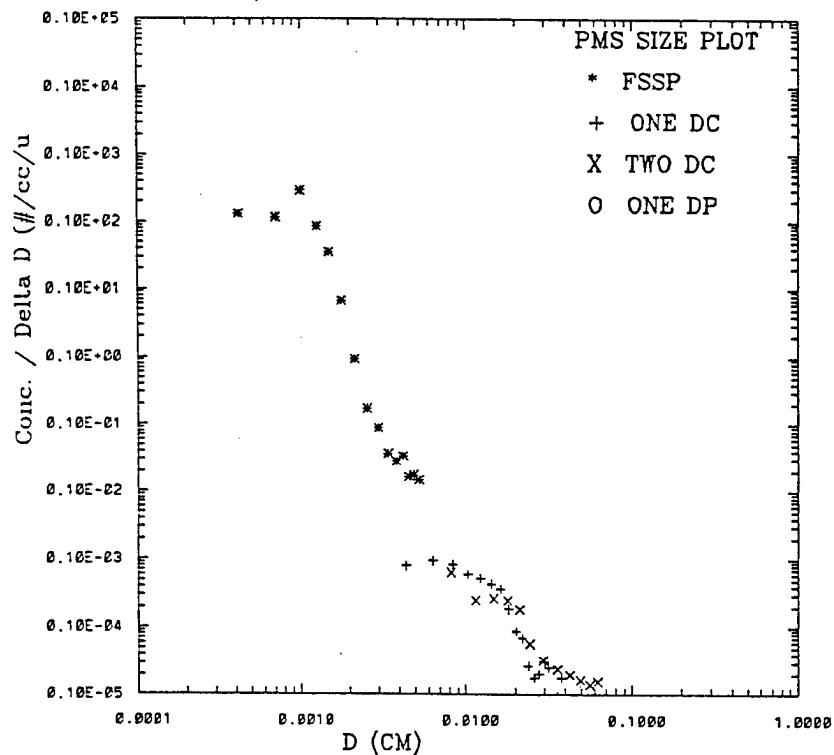


Figure 4. Size distribution of hydrometeors in the refreezing layer of a freezing rain event on 14 February, 1990.

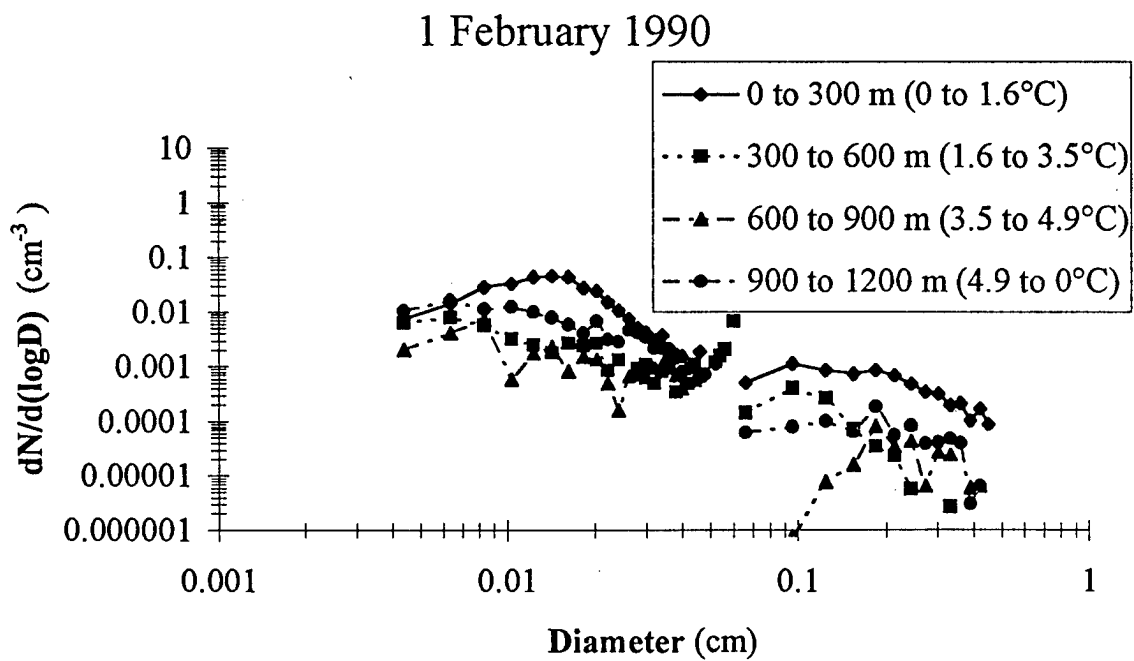


Figure 5. Size distribution in various regions of the melting layer on 1 February, 1990.

freezing drizzle case, freezing rain exhibited lower concentrations of droplets in the 20 to 200 μm sizes, and higher concentrations above about 200 microns (Fig. 4).

The evolution of the particle size distributions through the melting layer is given in Figs. 5 and 6. A shift to lower concentrations is observed as particles melt. The size distributions in the melting regions on 1 February and 14 February are rather similar just below the 0 degree level. The 14 February distributions show a regular pattern of a shift to lower concentrations as the particles melt. A similar pattern overall is seen in the 1 February data, but there is more variation in the data, which may reflect horizontal variability in the cloud.

3.2 Precipitation Type and Sounding Characteristics

In the case of both freezing rain and ice pellet formation, hydrometeors melt in the warm layer then descend into sub-freezing temperatures. If they subsequently freeze before hitting the ground, ice pellets are formed. If not, freezing rain occurs. One likely factor in ice pellet formation is incomplete melting of the original ice particle in the warm layer. When a partially melted hydrometeor descends into the lower freezing layer refreezing should be rapid in comparison to a completely melted hydrometeor, due to the action of the immersed ice as a nucleus for further ice growth. Consequently, the depth of the melting layer, should play a critical role in determining whether ice pellets or freezing rain is formed. To examine this process, data from 34 soundings were examined from a variety of locations (Table 1).

The results are presented in Figs 7 and 8. For these data the depth of the melting layer and the maximum temperature was somewhat better as a discriminator of the presence of freezing rain than the depth of the refreezing layer and the minimum temperature, but the influence of both layers is clearly evident in the data.

4. SUMMARY

We have shown a few of the features of the in situ data that we have collected in large droplet and freezing rain conditions. Additional data that are available include Doppler radar measurements, wind and turbulence data, and aircraft performance data.

For the cases we have examined, freezing rain exhibited lower concentrations of droplets in the 20 to 200 μm sizes, and higher concentrations above about 200 microns than were found in the freezing drizzle case. In addition, the presence of freezing rain is distinguished from ice pellets by parameters that can be determined from sounding information. We are presently developing comparisons between the observed melting effects on the hydrometeor size distribution and that predicted by theoretical models of melting. It is hoped that these results will help in better forecasting the types and sizes of supercooled hydrometeors that are likely to be encountered by aircraft.

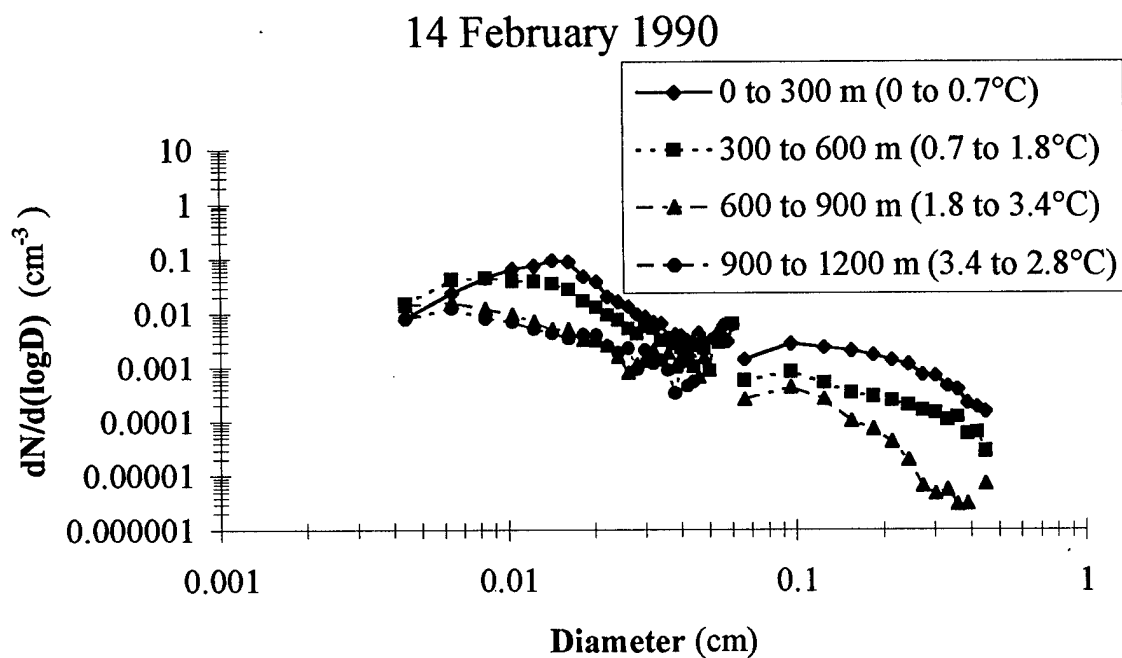


Figure 6. As in Fig. 5, except for 14 February, 1990.

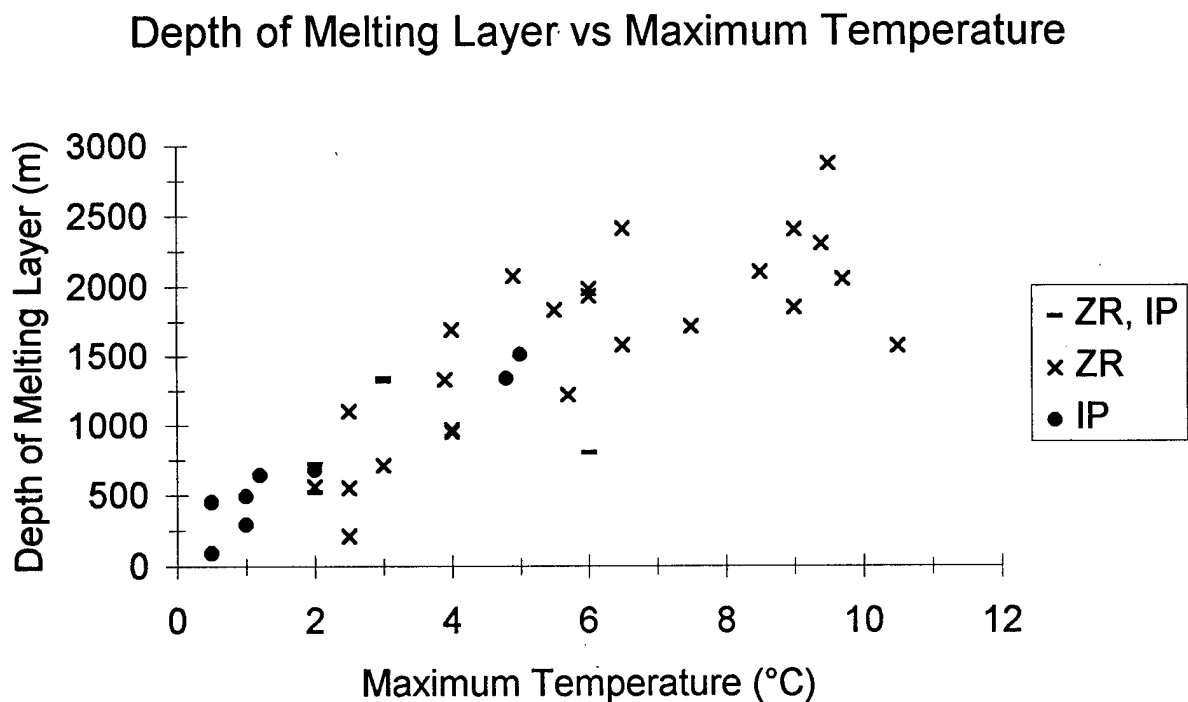


Figure 7. Depth of the melting layer vs Maximum Temperature for the soundings listed in Table 1.

Table 1. Sounding derived values for various freezing rain and ice pellet events. UND (1) refers to data obtained from the University of North Dakota Cessna Citation II instrumented aircraft and UND (2) refers to data obtained from the University of North Dakota C-band Doppler radar. Abbreviations used are: freezing rain (ZR), freezing drizzle (ZL), ice pellets (IP), snow (S), freezing rain with thunder (TZR), and snow showers (SW).

Date	Time	Location	Source	Precip	T _s	T _{max}	T _{min}	H _{max}	H _{min}
	(UTC)				(°C)	(°C)	(°C)	(m, AGL)	(m, AGL)
11 Dec 94	0000	BUF	NWS	ZR-S-IP-	-0.3	2.0	-4.0	1360	740
19 Dec 95	1200	PIT	NWS	ZR-S-IP-	-2.9	3.0	-5.5	1240	440
14 Nov 95	1200	YXE	AES	ZR-S-	-6.1	6.0	-6.0	280	0
9 Nov 95	1900	GFK	UND (2)	ZR-IP-	-1.7	3.0	-3.0	1080	150
10 Jan 96	2130	GFK	UND (2)	ZR-IP-	-0.6	2.0	-2.5	530	210
6 Dec 94	1200	TOP	NWS	ZR-	-1.1	6.5	-4.5	1730	570
7 Jan 95	0000	GSO	NWS	ZR-	-1.7	9.5	-2.0	610	120
27 Jan 95	1200	STC	NWS	ZR-	-4.7	2.5	-6.0	1790	190
15 Feb 95	0000	TOP	NWS	ZR-	-0.3	9.0	-5.0	1790	810
27 Feb 95	1200	BUF	NWS	ZR-	-7.5	2.0	-7.5	690	0
14 Nov 95	1200	GGW	NWS	ZR-	0.0	6.5	0.0	330	0
24 Nov 95	1200	BIS	NWS	ZR-	-2.5	10.5	-3.0	380	310
9 Dec 95	1200	SLE	NWS	ZR-	-0.7	8.5	-4.0	1180	340
14 Dec 95	0000	PIT	NWS	ZR-	-2.7	2.5	-4.0	1640	200
14 Dec 95	1200	BUF	NWS	ZR-	-0.7	6.0	-1.5	1070	180
1 Feb 96	1200	JAN	NWS	ZR-	-1.7	9.7	-6.0	1280	560
2 Feb 96	1200	GSO	NWS	ZR-	-1.9	4.9	-4.7	900	420
1 Feb 90	2300	MKC	UND (1)	ZR	-0.3	5.7	-5.9	1020	710
14 Feb 90	2000	MKC	UND (1)	ZR	-2.9	3.9	-7.9	1590	740
7 Jan 95	1200	ALB	NWS	ZR	-0.7	4.0	-2.0	580	180
14 Jan 95	1200	CAR	NWS	ZL-	-2.1	7.5	-6.0	1040	280
17 Jan 95	1200	PIT	NWS	ZL-	-1.1	6.0	-4.5	2220	570
20 Jan 95	1200	CAR	NWS	ZL-	-1.9	9.0	-4.0	1870	380
14 Feb 95	1200	LRK	NWS	ZL-	-3.9	5.5	-4.0	1610	200
28 Feb 95	0000	ALB	NWS	ZL-	-3.5	4.0	-6.0	1090	560
2 Feb 96	0000	SHV	NWS	TZR-	-2.3	9.4	-6.6	1730	720
28 Feb 95	1200	BUF	NWS	SW-IP-	-2.9	1.0	-5.5	840	370
21 Jan 95	1200	CAR	NWS	S-IP-	-1.7	2.0	-6.5	1220	810
14 Dec 95	0000	GRB	NWS	S-IP-	-4.1	0.5	-8.5	1390	720
12 Jan 95	0000	SSM	NWS	IP-	-6.9	0.5	-9.0	1400	250
15 Dec 95	0000	ALB	NWS	IP-	-5.1	1.0	-6.5	1570	500
7 Jan 96	1200	GSO	NWS	IP-	-6.9	5.0	-10.0	1280	380
2 Feb 96	0000	BNA	NWS	IP-	-3.7	1.2	-10.0	1900	1060
2 Feb 96	1200	SHV	NWS	IP-	-3.3	4.8	-8.3	1690	720

Depth of Refreezing Layer vs Minimum Temperature

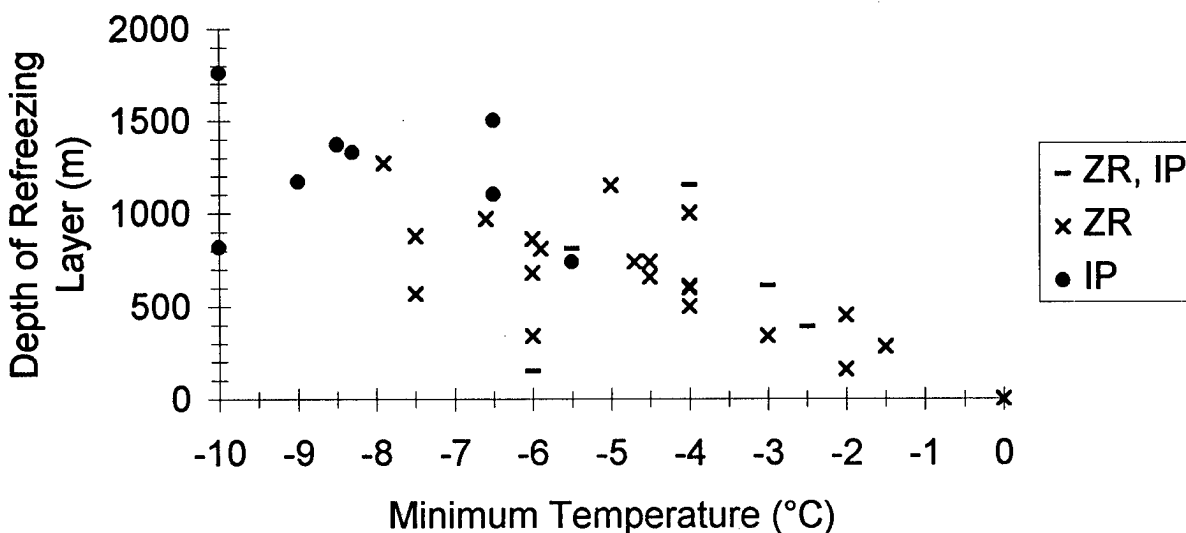


Figure 8 Depth of the refreezing layer vs the minimum temperature of the layer for the sounding data in Table 1.

ACKNOWLEDGMENTS

Most of the data that were presented were collected under support from Contract DFTA 01-87-C-0019, with the Federal Aviation Administration. Thanks are due to several field crew members in collecting these data.

REFERENCES

Arnott, W.P., Y. Dong, J. Hallett, and M. Poellot, 1994: Role of small ice crystals in radiative properties of cirrus: A case study, FIRE II, November 22, 1991. *J. Geophys. Res.*, **99**, 1371-1381.

Martner, B. E., J. B. Snider, F. J. Zamora, G. P. Byrd, T. A. Niziol, and P. I. Joe, 1993: A remote-

sensing view of a freezing-rain storm, *Mon. Weather Rev.*, **121**, 2562-2577.

Pobanz, B.M., J.D. Marwitz, and M.K. Politovich, 1994: Conditions associated with large-drop regions. *J. Appl. Meteor.*, **33**, 1366-1372

Prater, E. T. and Borho, A. A., 1992: Doppler radar wind and reflectivity signatures with overrunning and freezing-rain episodes: Preliminary results. *J. Appl. Meteor.*, **31**, 1350-1358.

SUPERCOOLED LARGE DROPLET DISTRIBUTIONS IN THE NATURAL ENVIRONMENT AND COMPARISON TO ARTIFICIAL DRIZZLE FROM THE AIR FORCE WATER SPRAY TANKER

Russell Ashenden* and John D. Marwitz†

Department of Atmospheric Science
University of Wyoming, Laramie, WY 82071

ABSTRACT

Aircraft icing that results from super cooled drizzle drops (SCDD) can be extremely hazardous to general aviation and many commuter aircraft. Encounters with these drizzle drops (40 - 400 μ m diameter) by the Wyoming King Air B200T research aircraft have forced the aircraft to descend to de-ice after as little as 5 minutes. These drizzle drops freeze as moderate feathers and glaze nodules at or just beyond the deicing equipment. These feathers tend to form on small imperfections on the wing and fuselage such as seams and rivets. The accreted ice results in a substantial increase in drag, a substantial increase in stall speed, and a moderate decrease in lift. The possibility that SCDD contributed to the ATR-72 crash near Roselawn, Indiana the night of 31 October 94 has raised the awareness in the aviation community of the hazards of aircraft icing by SCDD. With this awareness will, undoubtedly, come increased research and evaluations corresponding to the drizzle conditions. One method of aircraft evaluation in the SCDD conditions is artificial icing utilizing the USAF Water Spray Tanker at Edwards Air Force Base. The artificial cloud distributions produced by the tanker have been compared to natural cloud distributions obtained by the Wyoming King Air. This paper presents supercooled cloud and large droplet distributions measured with the King Air. In addition, a background and description of the water spray tanker are provided, along with the favorable results of the droplet mass distribution comparisons to the natural environment.

BACKGROUND

Governing Regulation for Aircraft Certification

Aircraft anti/de-icing systems are typically designed for a droplet range specified by the Federal Aviation Administration (FAA) and other certifying agencies. The current FAA Federal Aviation Regulations, Part 25, Appendix C Icing Envelopes in Figure 1 show that the maximum evaluated droplet Median Volumetric Diameter

(MVD) is 50 microns. The Appendix C envelopes are used as certification standards and are referenced by FAR parts 23.1419 and 25.1419. These envelopes (developed in the late 1940s) represent a majority of the icing clouds encountered by aircraft; however, a low percentage of icing clouds contain drizzle and rain drop sizes (termed supercooled large drops). These conditions are rare, but they can be extremely hazardous for aircraft.

Drizzle Research at Wyoming

Aircraft icing that results from super cooled drizzle drops (SCDD) can be extremely hazardous to general aviation and many commuter aircraft. Encounters with these drizzle drops (40 - 400 μ m diameter by Byers 1974; Marwitz et al. 1995) by the Wyoming King Air B200T have forced the aircraft to descend to de-ice after as little as 5 minutes. The Wyoming King Air is instrumented to measure drop size distributions, liquid water content, ambient temperature, engine torque and other aircraft parameters to allow for the determination of aircraft performance in a measured icing condition. The Wyoming King Air has encountered roughly 30 super cooled drizzle and rain size drop conditions since 1982. These drizzle drops freeze as moderate feathers and glaze nodules at or just beyond the deicing equipment. The feathers and nodules are typically 1 to 15 mm in length. They tend to form on small imperfections on the wing and fuselage such as seams and rivets. The accreted ice results in a substantial increase in drag, a substantial increase in stall speed, and a moderate decrease in lift (Cooper et al. 1984).

Aircraft ice accretion is dependent on many variables such as liquid water content, drop diameter, ambient temperature, airspeed, angle of attack, shape of the object (airfoil), and the time spent in the icing condition. Many of these variables are interdependent, that is, the airfoil collection efficiency is dependent on the size of the drops and the shape of the airfoil. The size of the

* Graduate Student at UW, Former USAF/AFFTC Aircraft Icing Engineer

† Professor, University of Wyoming

drops also determines the impingement limits, that is, how far back from the leading edge the drops hit the object such as a propeller spinner or airfoil. This impingement limit increases in percent chord from the leading edge as the relative sizes of the drops increase. The bigger the drops, the farther back on the object the ice will accrete. This effect can best be seen on cockpit side windows, prop-spinners, and wing leading edges.

Visual cues for drizzle drop induced icing can be determined during artificial aircraft icing evaluations. Flight crews can then be trained to recognize SCDD conditions and take appropriate evasive action. Utilizing the USAF Water Spray Tanker is one proven method of evaluating aircraft in artificial SCDD conditions where these visual cues can be readily obtained. In addition, evaluating aircraft in artificial SCDD conditions is recommended due to the risks involved with evaluating aircraft in natural SCDD conditions. These risks are due to full aircraft icing exposure and the difficulty in evading the natural conditions.

ATR-72 Artificial Icing Evaluation

An artificial icing evaluation of the ATR-72 was completed in December 94 at Edwards Air Force Base utilizing the water spray tanker. The program was conducted as part of a Special Certification Review by the FAA and the DGAC (French equivalent of the FAA) and the investigation into the crash of American Eagle Flight 4184 near Roselawn, Indiana the night of 31 October 94. The tests were designed to examine both the upper limits of the certification envelope at temperatures just below freezing and the icing characteristics of SCDD not currently covered by the FAA FAR, Part 25-C.

These tests required the USAF water spray tanker to produce conditions consistent with SCDD conditions. Based on recent research at Wyoming (Pobanz et al. 1994) it was argued by a group of scientists (Marwitz et al. 1995) that SCDD were probably present in the ATR-72 holding pattern prior to the crash. In order to simulate the natural SCDD conditions, the USAF tanker test team referred to the SCDD distributions obtained from the Wyoming King Air. The spray tanker system was then modified to provide an artificial SCDD cloud consistent with those measured in the natural environment.

USAF WATER SPRAY TANKER DESCRIPTION

General

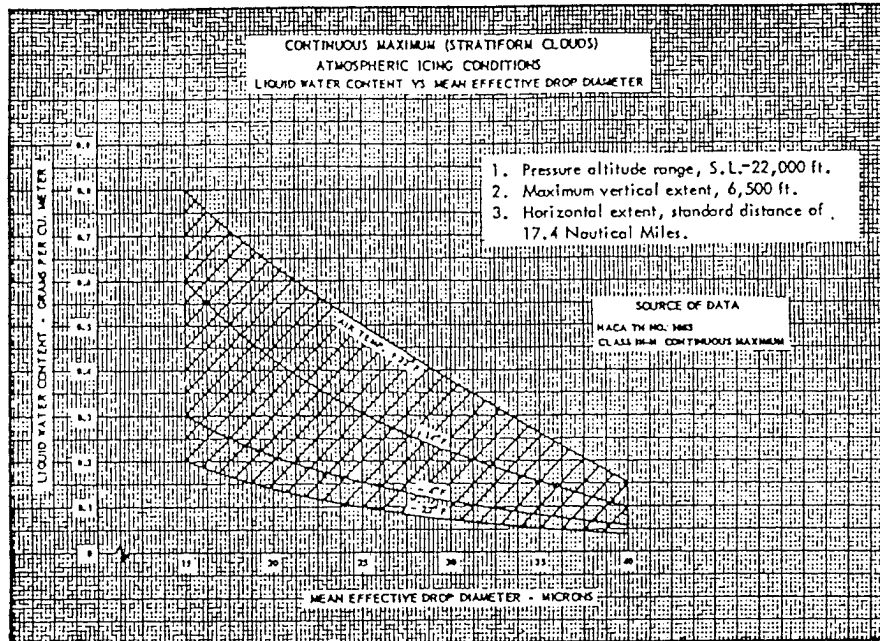
The USAF has used a modified NKC-135A tanker aircraft since the late 1950's for aerial icing and rain testing. This testing is conducted to assure that Department of Defense weapon systems have the capability to operate to design specifications in icing and rain atmospheric conditions. The NKC-135A S/N 55-3128 tanker aircraft (Figure 2), is modified for aerial refueling as well as water spray for icing and rain tests. Water spray or aerial refueling missions are ground selectable, and the tanker capabilities in the water spray configuration are 150 to 335 KIAS and up to 40K Ft pressure altitude.

Artificial Icing and Rain Test History

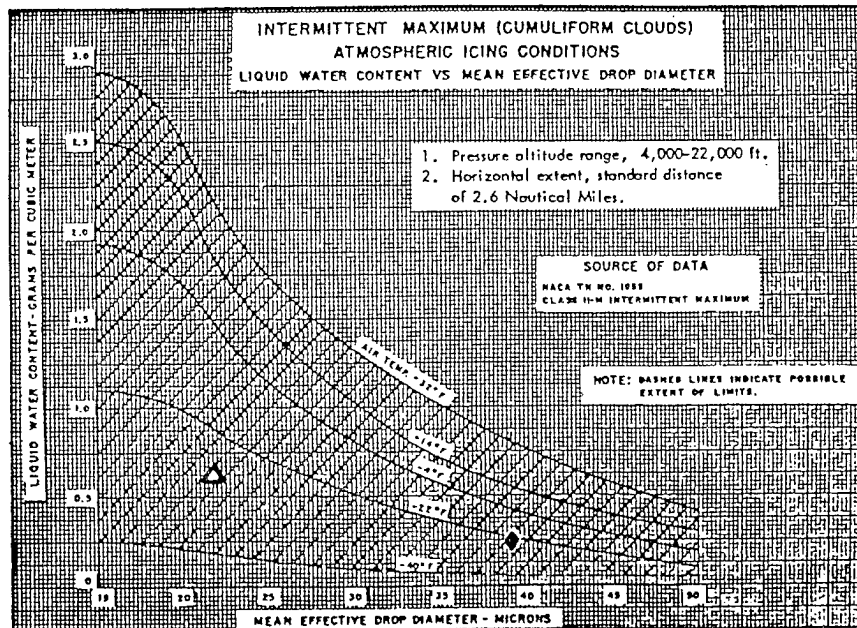
The US Air Force modified NKC-135A has been used to test an extensive selection of aircraft and missiles. These include: B-58, AV-8, F-111, A-7D, Concorde, DC-8, T-38, C-130, C-5, B-52, F-14, EA-6B, F-15, F-4, A-10, E-3A, F-16, F-18, Canadair Cl-601, Boeing 737 and 757, KC-135R, Piaggio Avanti P180, B-1B, HU-25A, AGM-109, AGM-129, C-27A, C-17, B-2, V-22, MU-2B-60, and the ATR-72.

Spray System

The water spray system consists of a water delivery system, bleed air for spray atomization and anti-icing, and a modified refueling boom with a nozzle array to deliver the spray cloud. Engine bleed air is used to prevent the water system from freezing - the effects of which would either prevent water spray and/or cause accumulation of large chunks of ice which, during testing, could pose a catastrophic hazard to the test aircraft. Bleed air is tapped from the sixteenth stage of the two inboard J-57 engines. 2,000 gallons of demineralized water are contained in the modified forward body fuel tank (Figure 2). The spray system water is routed through a flow meter, flow control valve, purge valve, and finally through the boom to the nozzle array. The circular icing array consists of a manifold and icing nozzle elements. Bleed air is routed through the boom (around the water line) down to the air feeder tubes in the manifold, which in turn distributes air to the nozzle elements for water atomization and for heating to prevent nozzle freezing.



Continuous Maximum



Intermittent Maximum

Figure 1. FAA, Federal Air Regulations, Part 25, Appendix C. The points denoted by a Δ and \diamond correspond to tanker conditions (a: 0.61 g/m^3 , $22 \mu\text{m}$) and (b: 0.29 g/m^3 , $38 \mu\text{m}$) in Figure 8, respectively.

Tanker Cloud Calibration

Cloud calibrations are performed with an instrumented Learjet. The instrumentation consists of three Particle Measurement Systems (PMS)

probes, a Johnson and William's Liquid Water Content (LWC) probe, ambient air temperature, dew point, and airspeed. The Optical Array Probes (OAP), and Forward Scattering Spectrometer Probes (FSSP) are used to measure drop size and

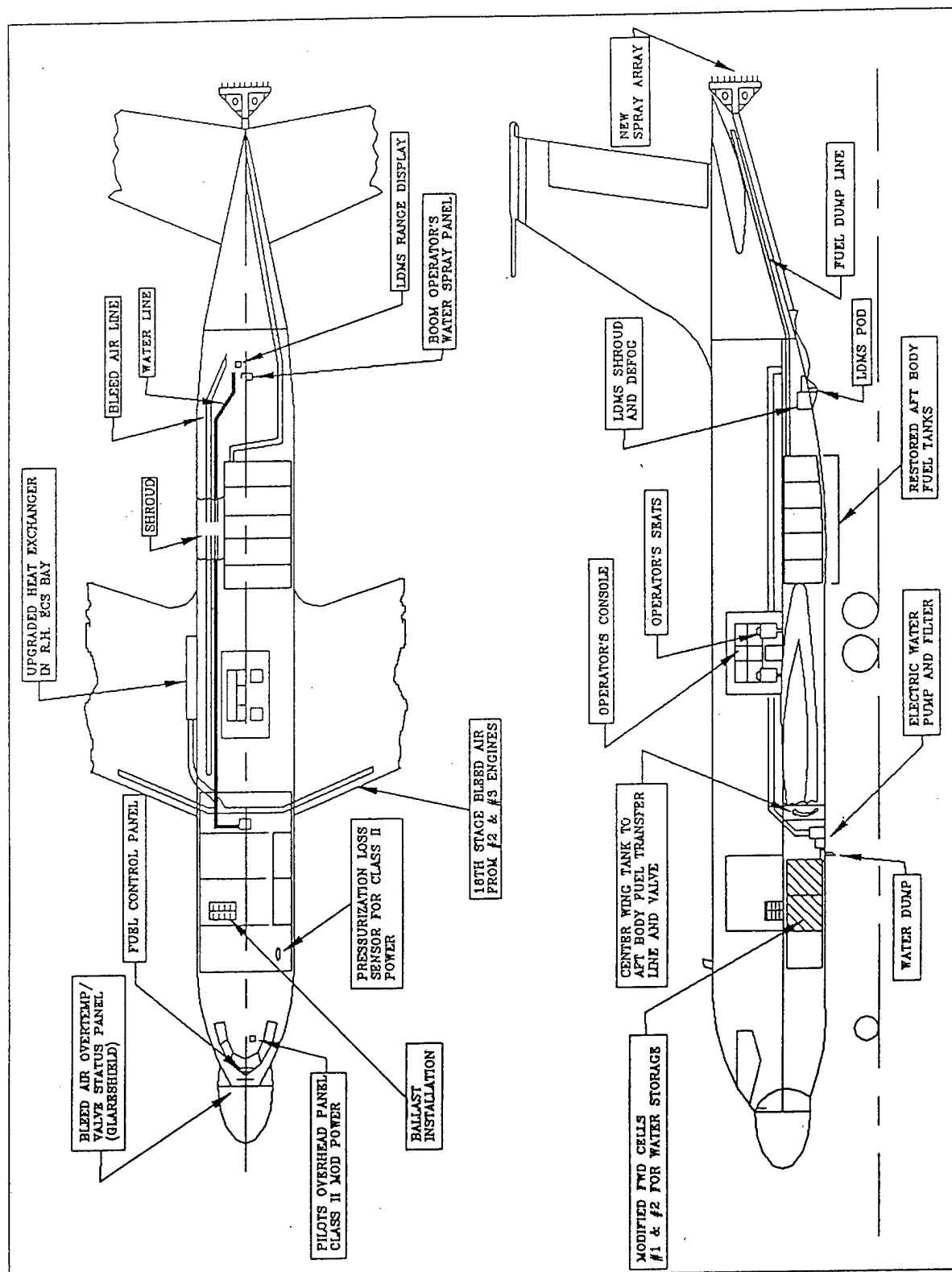


Figure 2. NKC-135A S/N 55-3128 Tanker Aircraft

LWC. The tanker spray drop size distributions are obtained by plotting the mass concentrations versus drop diameters from the three PMS probes. These probes, with plotting ranges, are as follows:

Probe	UW King Air	Aeromet Learjet
FSSP-100	3 to 45 μm	3 to 45 μm
OAP 1D-C	12.5 to 187.5 μm	90 to 300 μm
OAP 2D-C	25 to 800 μm	325 to 800 μm

The raw data obtained by the PMS probes were processed using two techniques. The processing technique used for the Wyoming King Air data is described in several references including PMS manuals, Cerni (1983), and Knollenberg (1970). The processing techniques used for the Aeromet Learjet (tanker distributions) and the Wyoming King Air data are similar except for additional OAP corrections described by Baumgardner (1987) and Hobbs (1995) for the Learjet. The corrections implemented by Hobbs and Baumgardner account for the higher airspeeds when measuring the tanker distributions (~ 100 m/s). Without these corrections the OAPs undersample the hydrometeors at these higher airspeeds. These corrections are not used in the Wyoming OAP processing since the airspeeds are lower (~ 80 m/s) and the first 3 and 4 bins of the 1DC and 2DC probes, respectively are ignored.

The tanker Laser Distance Measuring System (LDMS) is used to provide separation distance between the spray array and the spectrometer probes or the test aircraft. The cloud shape for the USAF spray tanker was obtained using calibration sweep data. Horizontal sweep data indicated a relatively homogeneous cloud of LWC while vertical sweep data indicated a maximum LWC and MVD just below the cloud center due to gravitational effects (Figure 3). By using photographs obtained from the Learjet during calibration, the visible cloud size was measured by comparing it to the known size of the Learjet. The cloud diameter varied from 4.0 to 8.25 feet depending on the separation distance from the icing array.

NATURAL DISTRIBUTIONS

Natural liquid Hydrometeor distributions are shown in Figures 4 through 7. With the exception of Figures 5 and 6, the raw data used to produce these distributions have been processed utilizing a circle-fit routine to remove ice particles from the 2D data.

Due to funding constraints, this processing technique was not utilized for the California Sierra data. The images were reviewed manually to reduce the chance of ice contamination for these cases shown in Figures 5 and 6. Mass concentrations ($\text{g}/\text{m}^3/\mu\text{m}$) have been plotted with drop diameter (μm). The data points labeled with an [o] are from the FSSP, [+] from the 1D-C, and [*] from the 2D-C probes. The symbols not connected by a line show the cumulative mass used to determine the volumetric diameters. The total liquid water content is determined by integrating the liquid water in non-overlapped channels.

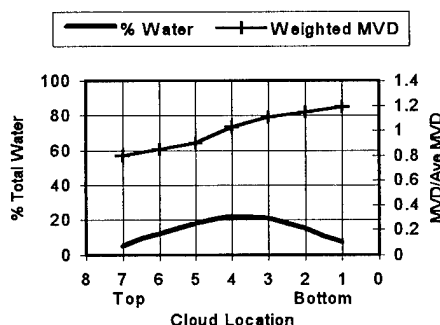


Figure 3. Tanker Cloud Vertical Profile

For comparison, an 80% Volumetric Diameter (80VD) parameter is used in Figures 4 through 7. The determination of the 80VD is shown in Figure 4 where the cumulative mass and 80% lines intersect. The 80VD is a more appropriate measure of the hazardous hydrometeor diameters when considering aircraft icing as compared to the standard (50%) MVD. The 80VD parameter includes the drizzle-sized drops which may cause dramatic aircraft performance degradation as discussed earlier. The significance of this parameter is demonstrated in Figure 6 where the MVD is 25 μm and signifies cloud drops. The 80VD is 65 μm which better correlates with the high performance degradation experienced by the King Air while obtaining this distribution. Another example of the advantages of the 80VD parameter is shown in Figure 9 where the King Air standard MVD is 31 μm ; however the 80VD is 122 μm due to the drizzle-sized hydrometeors, and again the measuring aircraft experienced high performance degradation.

Figures 4 through 7 represent supercooled cloud, drizzle, drizzle, and freezing rain distributions, respectively. Included with these figures are hydrometeor two-dimensional images from the

2D - C Optical Array Probe. The height of each bar represents 800 μm for reference. These images allow for a visual comparison of the relative sizes of the hydrometeors and facilitates determining the phase the hydrometeors (ice or liquid).

DISTRIBUTION COMPARISON

FAA FAR Part 25-C

Two tanker distributions for conditions within the current FAA FAR, Part 25-C icing envelopes are provided in Figure 8 for comparison. These conditions have been added to Figure 1 for the corresponding LWC and MVD. A natural distribution obtained by the King Air is overlaid on Figure 8 for comparison. Note the lower concentration of large drops in both the natural and tanker distributions. It should be noted that the Appendix C envelopes do not represent actual physical relationships between LWC, MVD and temperature, but combinations for the highest probability for occurrence. Every combination of these variables are possible in nature and should be considered for certification of transport, utility, and commuter categories (Parts 25.1419 & 23.1419).

Artificial and Natural SCDD Distributions

Drizzle drop distributions produced by the Air Force Water Spray Tanker and natural distributions obtained by the Wyoming King Air are shown in Figures 9 and 10. The distributions are illustrated by again plotting liquid water content per unit size ($\text{g}/\text{m}^3/\mu\text{m}$) versus drop diameter on log/log scale. A comparison of the artificial distributions produced by the tanker to those measured in the natural environment by the King Air show favorable results. The natural distributions appear to be bi-modal with peak mass concentrations around 20 μm and between 100 and 180 μm . The mode of the artificial tanker cloud is difficult to determine with the available data; however, the distributions appear to be mono-modal. The absence of a peak near the 100 μm diameter in the tanker distributions compared to the natural distributions may be an instrumentation artifact due to undersampling. The 80VD ranges from 195 to 200 μm and 122 to 147 μm for the tanker and natural distributions, respectively. The 20 μm mode in the tanker distributions was probably suppressed because of evaporation. The artificial cloud is typically produced in a dry atmosphere and the small drops evaporate very fast.

A bi-modal characteristic appears in the natural distributions and may be present in the tanker artificial distributions. This bi-modal characteristic may be an instrumentation artifact or it may be real. The Learjet and the King Air instrumentation are similar. In the overlap drop size region between the FSSP and 1D-C and 2D-C (20 to 45 μm) the FSSP statistically undersamples because of the small sample volume and the 1D-C and 2D-C physically undersamples because of poor response to small particles. Classical coalescence growth theory (Pruppacher and Klett 1978) shows that a bi-modal distribution is normal in nature. Both bi-modal and mono-modal distributions are present in the atmosphere depending upon the processes at work. There is no apparent reason for a bi-modal distribution in the artificial cloud and the bi-modal distribution in the natural cloud is a result of natural cloud processes and/or instrumentation artifact. The fact that the mode of the artificial distributions can not be determined with the available data should not directly factor into the comparison of the artificial and natural distributions. When considering aircraft ice accretion it is the relative location of the peak concentrations and the 80VD parameter that is important when comparing the distributions.

A linear regression line is used in the tanker data processing to account for the probe overlap region discussed above. This regression line (50 - 90 μm) was used to estimate dN/dD and $\text{d}(\text{LWC})/\text{dD}$ where data were not accurately measured. This regression line fit is described by Hobbs (1995) and is shown in Figures 8 through 10.

Mass-weighted tanker and natural SCDD distributions without FSSP data are shown in Figure 11 for comparison. SCDD distributions from the Optical Array Probes (1DC, 2DC) may be a more appropriate method since the drizzle drop envelope ranges from 40 to 400 μm . Two natural and two tanker distributions are illustrated in Figure 11. In order to cover the same size spectrum, the natural distributions contain both 1DC and 2DC data while the tanker distributions contain only 1DC data.

The USAF Water Spray Tanker is a viable and important tool in the evaluation of aircraft icing in SCDD and the FAA FAR Part 25-C conditions based on the close agreement of the, tanker produced, artificial droplet distributions to that of

the natural distributions presented and discussed herein.

CONCLUSIONS

Aircraft icing that results from SCDD is extremely hazardous to general aviation and many commuter aircraft. The accreted ice results in a substantial increase in drag, a substantial increase in stall speed, and a moderate decrease in lift. Visual cues for drizzle drop induced icing can be determined during aircraft icing evaluations. Utilizing the USAF Water Spray Tanker is one proven method of evaluating aircraft in artificial SCDD conditions where these visual cues can be readily obtained while minimizing the risk to the flight test crew. These results indicate that the USAF Water Spray Tanker is a viable and important tool for the evaluation of aircraft in SCDD and FAA FAR Part 25-C icing conditions. This conclusion is based on the favorable comparison of the tanker and the natural cloud droplet distributions presented herein.

In addition, as demonstrated in the provided distributions, the 80VD is a more appropriate measure of the hazardous hydrometeor diameters when considering aircraft icing as compared to the standard (50%) MVD. The 80VD parameter includes the drizzle-sized drops which may cause dramatic aircraft performance degradation.

Finally, the current FAA FAR, Part 25-C Icing Envelopes do not adequately characterize the natural environment. The current maximum droplet MVD allowed is 50 microns. Drizzle-sized drops (40 to 400 μm) should be incorporated into the FAA FAR, Part 25-C Icing Envelopes based on the SCDD data obtained by the Wyoming King Air and the apparent aircraft hazard due to these conditions.

RECOMMENDATION

Expand the icing envelopes contained in the FAA FAR, Part 25 Appendix C to include the super cooled drizzle drop distributions (40 to 400 μm). The current envelopes do not represent physical relationships between LWC, MVD and temperature, and every combination of these variables must be considered during certification; however, the highest probability of SCDD occurrence is for temperatures near freezing and low liquid water contents.

ACKNOWLEDGMENTS

Contributions to this paper from the University of Wyoming was funded by NSF-ATM/9308409 and the Wyoming King Air was provided through cooperative agreement between UW and NSF/ATM-9019603 and ATM-9319141. The author would like to also acknowledge Mr. Sean W. Hamilton, USAF/AFFTC/412 TS for the tanker distributions.

REFERENCES:

- Baumgardner, D., 1987: Corrections for the Response Time of Particle Measuring Probes. Preprints of the 6th Symposium on Meteor. Obs. and Instrumentation, New Orleans, Jan 12-16, pp 148-151.
- Byers, H., 1974: General Meteorology, 4th edition, McGraw Hill Inc, pp 461.
- Cerni, T. A., 1983: Determination of the Size and Concentration of Cloud Drops with an FSSP. *J. Climate Appl. Meteor.*, 22, 1346-1355.
- Cooper, W.A., W.R. Sand, M.K. Politovich and D.L. Veal, 1984: Effects of Icing on Performance of a Research Airplane. *Journal of Aircraft*, 21, 708-715.
- Hobbs, R., B. Morrison, D. Baumgardner, 1995: Processing Data from Particle Measuring Probes for Icing Certification. Presented at the American Helicopter Society/SAE International Icing Symposium, Montreal, Canada, Sept 18-21, 1995.
- Knollenberg, R. G., 1970: The Optical Array: An Alternative to Scattering or Extinction for Airborne Particle Size Determination, *J. Appl. Meteor.*, 9, 86-103.
- Marwitz, J., M. Politovich, B. Bernstein, F. Ralph, P. Neiman, and R. Ashenden, 1995: Meteorological Conditions Associated with the ATR-72 Aircraft Accident Near Roselawn, Indiana On 31 October 1994. Presented at the American Helicopter Society/SAE International Icing Symposium, Montreal, Canada, Sept 18-21, 1995.
- Pobanz, B.M., J.D. Marwitz and M.K. Politovich, 1994: Conditions Associated with Large-Drop Regions. *J. Appl. Meteor.*, 33, 1366-1372.
- Pruppacher, H.R. and J.D. Klett, 1978: Microphysics of Clouds and Precipitation, 1st edition, D. Reidel, pp.714.

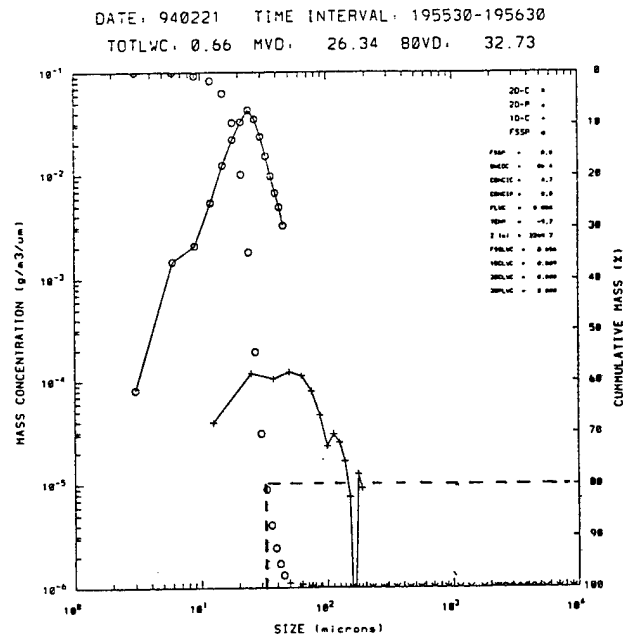


Figure 4. Mass-weighted natural supercooled cloud distribution. The distribution was obtained on 940221 along the front range of the Colorado Rocky Mountains with an LWC: 0.66 g/m^3 , MVD: 26 μm , and 80VD: 33 μm . The [o] symbols represent the data from the FSSP and the [+] symbols represent the data from the 1D-C. The [o] symbols not connected with a line represents the cumulative mass. The line intersecting this cumulative mass at 80 percent signifies the determination of the 80VD. The first 3 bins of the 1-DC have been ignored in the statistics due to probe undersampling. 2D-C hydrometeor images are not provide due to their small size.

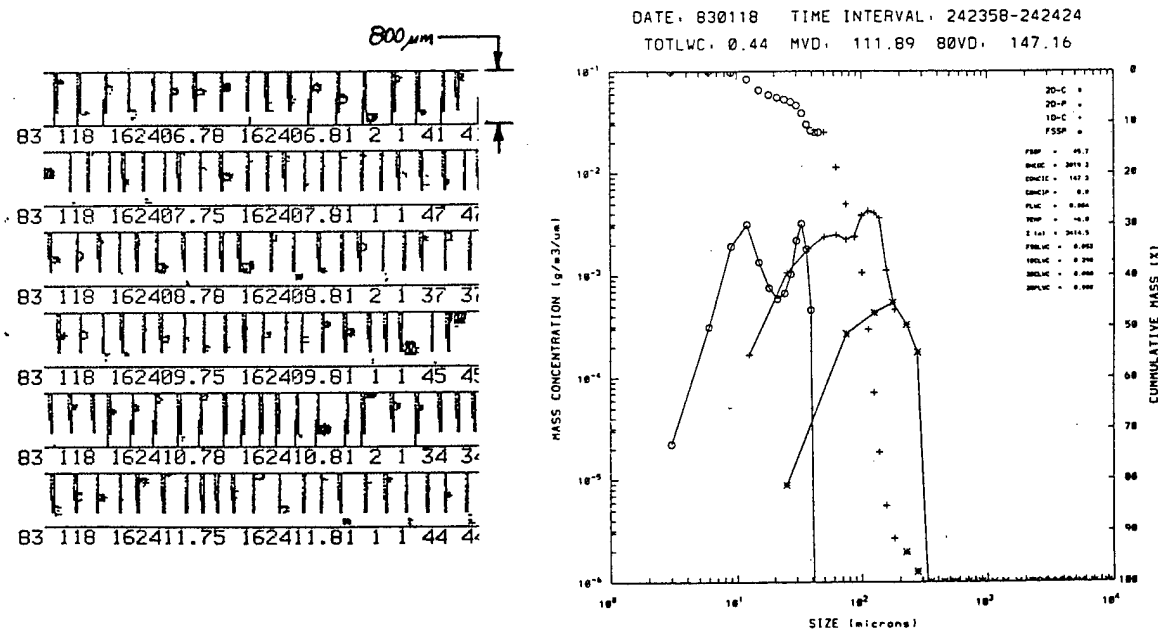


Figure 5. Mass-weighted natural freezing drizzle distribution. The distribution was obtained on 830118 above the California Sierra Nevada Mountains with an LWC: 0.44 g/m^3 , MVD: 112 μm , and 80VD: 147 μm . The [o] symbols represent the data from the FSSP, the [+] symbols represent the data from the 1D-C, and the [*] symbols represent the data from the 2D-C. The first 3 and 4 bins of the 1-DC and 2D-C, respectively have been ignored in the statistics due to probe undersampling. 2D-C hydrometeor images for the same period are provided. The height of the image bar represents 800 microns.

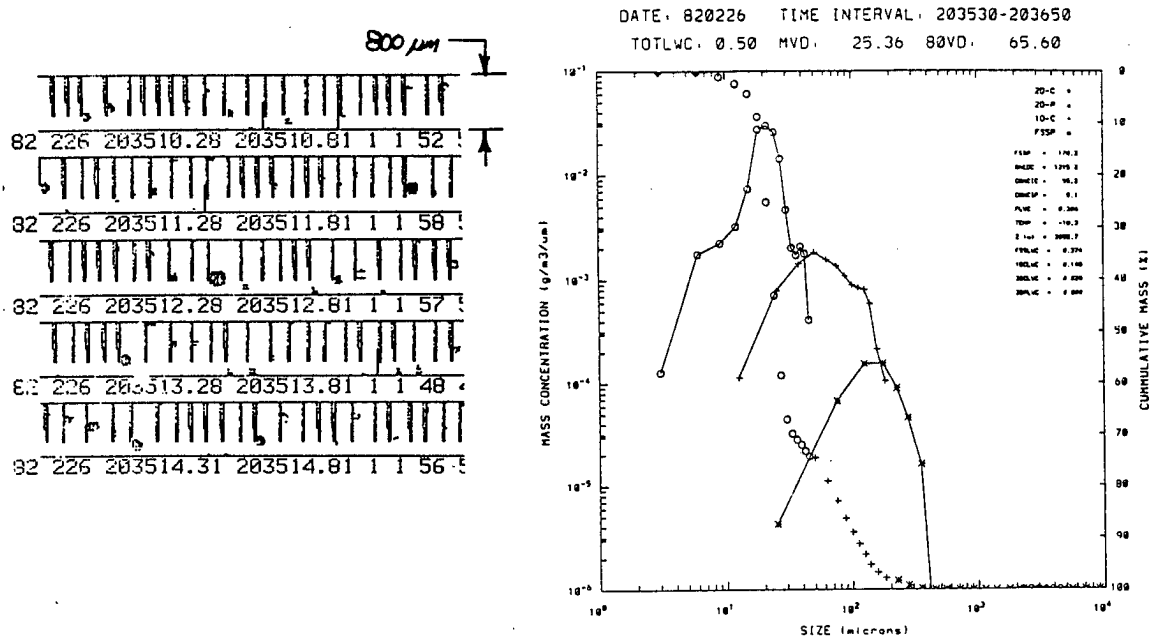


Figure 6. Mass-weighted natural freezing drizzle distribution. The distribution was obtained on 820226 above the California Sierra Nevada Mountains with an LWC: $0.50 \text{ g}/\text{m}^3$, MVD: $25 \mu\text{m}$, and 80VD: $66 \mu\text{m}$. The [o] symbols represent the data from the FSSP, the [+] symbols represent the data from the 1D-C, and the [*] symbols represent the data from the 2D-C probe. The first 3 and 4 bins of the 1-DC and 2D-C, respectively have been ignored in the statistics due to probe undersampling. 2D-C hydrometeor images for the same period are provided. The height of the image bar represents 800 microns.

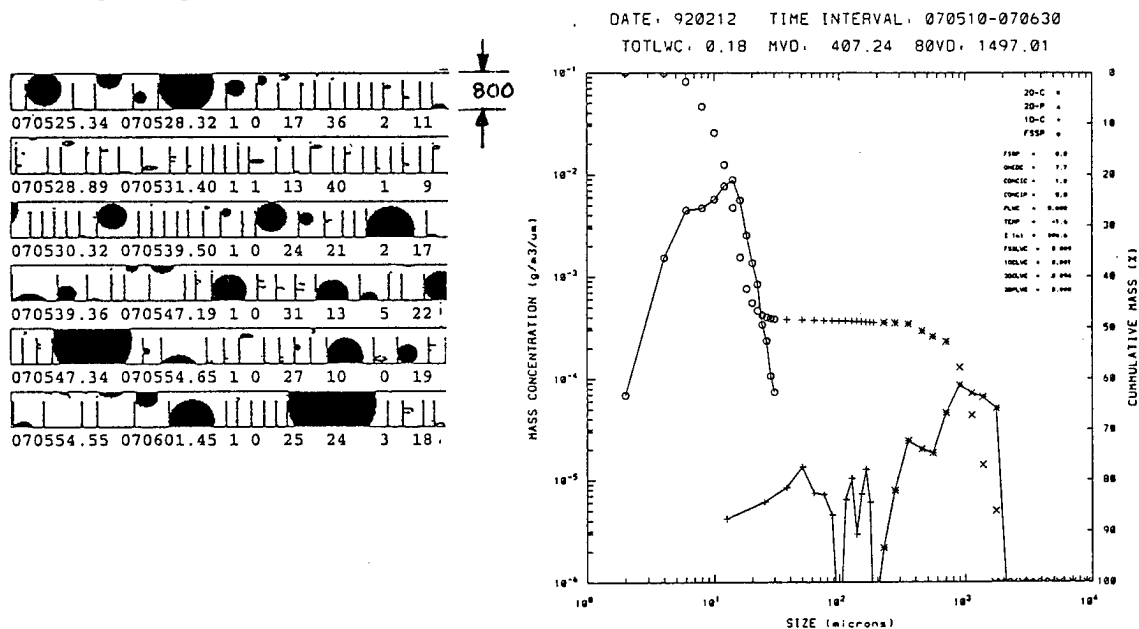


Figure 7. Mass-weighted natural freezing rain distribution. The distribution was obtained on 920212 over northern Kansas with an LWC: $0.18 \text{ g}/\text{m}^3$, MVD: $407 \mu\text{m}$, and 80VD: $1497 \mu\text{m}$. The [o] symbols represent the data from the FSSP, the [+] symbols represent the data from the 1D-C, and the [*] symbols represent the data from the 2D-C probe. The first 3 and 4 bins of the 1-DC and 2D-C, respectively have been ignored in the statistics due to probe undersampling. 2D-C hydrometeor images for the same period are provided. The height of the image bar represents 800 microns.

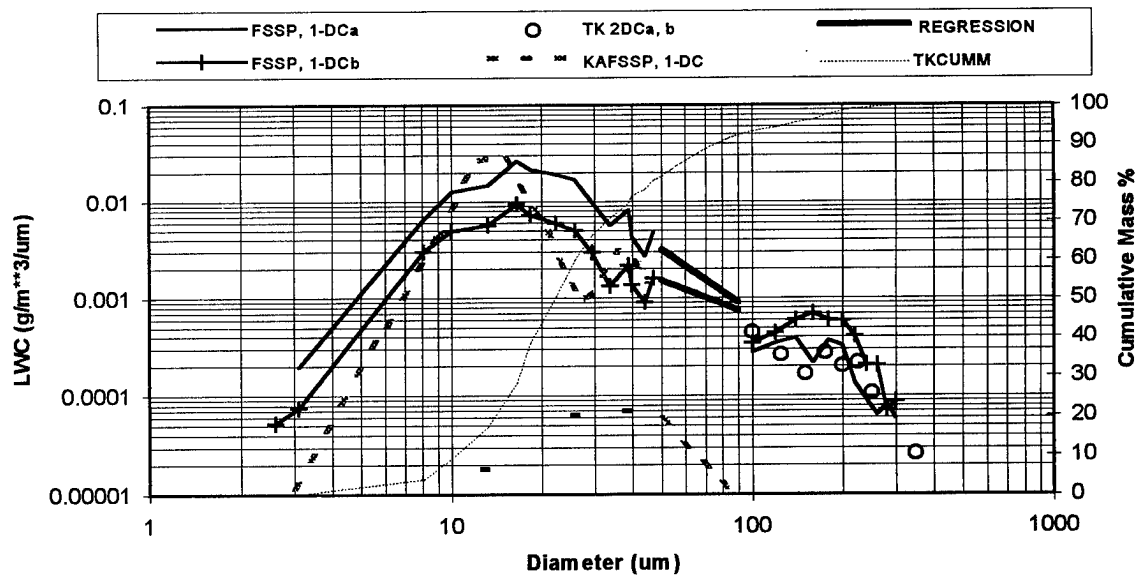


Figure 8. Mass-weighted tanker and natural distributions for FAA FAR, Part 25, Appendix C conditions. The solid lines indicate tanker distributions and the heavy-dash line indicates a natural distribution. Tanker distribution (a) was obtained on 941219 at 234616 UTC with LWC: 0.61 g/m^3 , MVD: $22 \text{ } \mu\text{m}$, and 80VD: $47 \text{ } \mu\text{m}$. Tanker distribution (b) was obtained on 941219 at 234719 UTC with LWC: 0.29 g/m^3 , MVD: $38 \text{ } \mu\text{m}$, and 80VD: $140 \text{ } \mu\text{m}$. The thin-dotted line indicates the cumulative mass for tanker distribution (a). The natural distribution was obtained by the King Air on 940307 at 225344 UTC with LWC: 0.28 g/m^3 , MVD: $17 \text{ } \mu\text{m}$, and 80VD: $23 \text{ } \mu\text{m}$. The tanker points have been marked on Figure 1 for comparison. The heavy-solid line indicates the linear regression from Hobbs (1995).

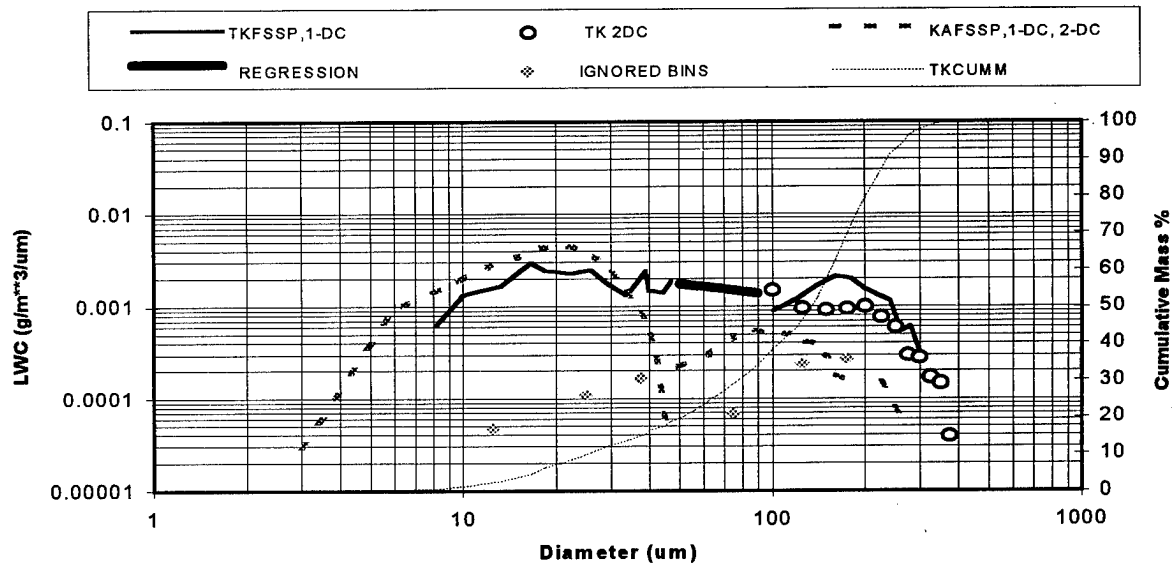


Figure 9. Mass-weighted tanker and natural SCDD distributions. The solid lines indicate the tanker distribution and the heavy-dash lines indicate the natural distribution obtained by the King Air. The tanker distribution was obtained on 941218 at 190609 UTC with LWC: 0.41 g/m^3 , MVD: $140 \text{ } \mu\text{m}$, and 80VD: $200 \text{ } \mu\text{m}$. The King Air Distribution was obtained on 940307 at 241440 UTC with LWC: 0.15 g/m^3 , MVD: $31 \text{ } \mu\text{m}$, and 80VD: $122.2 \text{ } \mu\text{m}$. The thin-dotted line indicates the cumulative mass for the tanker distribution. The heavy-solid line indicates the linear regression from Hobbs (1995). The first 3 and 4 bins of the 1-DC and 2-DC, respectively, have been ignored in the statistics due to probe undersampling (diamond labels).

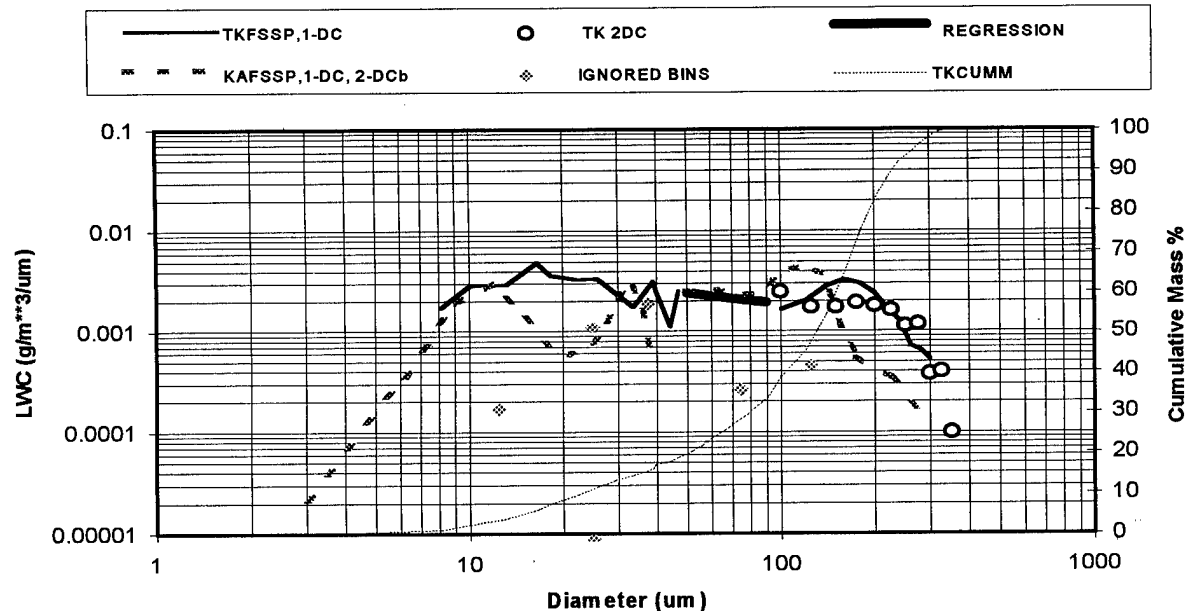


Figure 10. Mass-weighted tanker and natural SCDD distributions. The solid lines indicate the tanker distribution and the heavy-dash lines indicate the natural distribution obtained by the King Air. The tanker distribution was obtained on 941219 at 174039 UTC with LWC: 0.61 g/m^3 , MVD: $140 \text{ } \mu\text{m}$, and 80VD: $195 \text{ } \mu\text{m}$. The King Air Distribution was obtained on 830118 at 242358 UTC with LWC: 0.44 g/m^3 , MVD: $112 \text{ } \mu\text{m}$, and 80VD: $146.7 \text{ } \mu\text{m}$. The thin-dotted line indicates the cumulative mass for the tanker distribution. The heavy-solid line indicates the linear regression from Hobbs (1995).

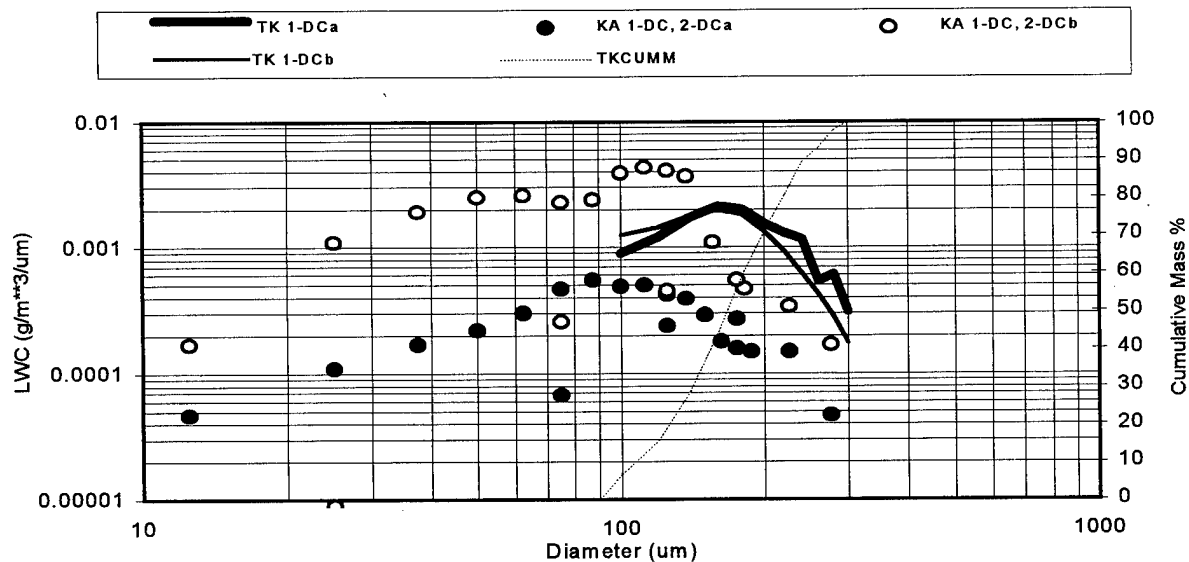


Figure 11. Mass-weighted tanker and natural SCDD distributions without FSSP data. The solid lines indicate the tanker distribution and the circles indicate natural distributions obtained by the King Air. Tanker distribution (a) was obtained on 941218 at 190609 UTC with 1-DC LWC: 0.27 g/m^3 , MVD: $180 \text{ } \mu\text{m}$, and 80VD: $219 \text{ } \mu\text{m}$. Tanker distribution (b) was obtained on 941216 at 190609 UTC with 1-DC LWC: 0.24 g/m^3 , MVD: $160 \text{ } \mu\text{m}$, and 80VD: $200 \text{ } \mu\text{m}$. King Air Distribution (a) was obtained on 940307 at 241440 UTC with 1-DC and 2-DC LWC: 0.06 g/m^3 , MVD: $123 \text{ } \mu\text{m}$, and 80VD: $183 \text{ } \mu\text{m}$. King Air Distribution (b) was obtained on 830118 at 242358 UTC with 1-DC and 2-DC LWC: 0.39 g/m^3 , MVD: $118 \text{ } \mu\text{m}$, and 80VD: $151 \text{ } \mu\text{m}$. The thin-dotted line indicates the cumulative mass for tanker distribution (a).

A CANADIAN CLIMATOLOGY OF FREEZING PRECIPITATION, AND A DETAILED STUDY USING DATA FROM ST. JOHN'S, NEWFOUNDLAND

J. W. Strapp¹, R. A. Stuart², and G.A. Isaac¹

**¹Atmospheric Environment Service,
Downsview, Ont. M3H 5T4**

**²Weather Research House,
Willowdale, Ont.**

Abstract:

A climatology of freezing precipitation (FP) for North America has been compiled using 30 years of observations from the Canadian network and already compiled US data. Areas of maximum FP are linked to regional influences. A detailed study of FP at St. John's, the location of highest frequency of FP in North America, shows that ZI is more frequent than Zr. Most Zr cases result from a classical melting layer aloft, but most ZI cases result from non-classical situations with no melting layer. In contrast, most of the FP at the continental station at Maniwaki results from the classical mechanism. Analysis of radiosonde data reveals that non-classical ZI in St. John's most frequently arises from relatively thick stratus decks, and ZI-altitude probabilities are discussed. Non-classical FP formation mechanisms are common in Canadian clouds, and are most likely explained by condensation and/or coalescence drop growth mechanisms.

Introduction:

Freezing precipitation (FP) is a natural hazard to society, seriously impacting the public through adverse effects on the transportation, communication, energy, and agricultural sectors. The effects on aviation have been most recently underscored by the possible links of freezing drizzle to the fatal accident of an ATR-72 near Roselawn Indiana in the fall of 1995. Reports of FP occur in Canada from at least one station every month of the year. Frequencies of FP in the Canadian Atlantic provinces are the highest in North America, and perhaps the world. This article examines FP distributions in North America, and provides detailed information on the vertical structure of clouds which produce freezing rain (Zr) and freezing drizzle (ZI) in St. John's Newfoundland, the location of maximum frequency of FP in North America.

A Climatology of Freezing Precipitation:

McKay and Thompson (1969) have provided a Canadian climatology of yearly total FP (Zr and ZI) using data from 160 hourly observing stations across Canada, for the 10 year period of 1957-1966. In this study a 30 year record from 1961-1990 from 137 Canadian hourly observing stations has been compiled and analysed for monthly distributions of FP. The yearly Zr+ZI isopleths from McKay and Thompson are similar to those found in this study,

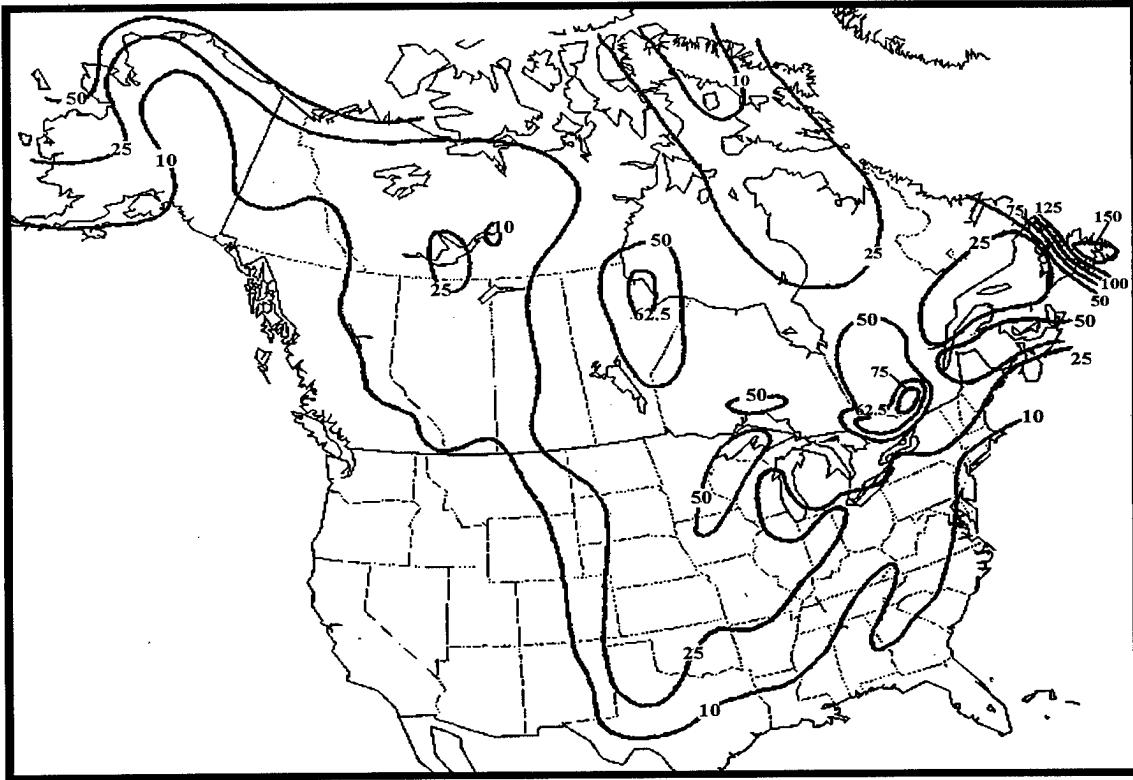


Figure 1: Isopleths of the number of hours per year of freezing precipitation in North America. USA data (excluding Alaska) from Vilcans (1989).

although there are some significant difference particularly around the Great Lakes. It is assumed that the differences are due at least in part to the larger data set collected for the current study.

Figure 1 contains the yearly distribution of Zr+Zl for North America. Data for the USA (excluding Alaska) have been extracted from Vilcans(1989). Canadian and Alaskan data were processed by the Atmospheric Environment Service for this study. A fairly good overlap was found at the Canada-USA border when combining the data, although some subjective interpretation was necessary near the Great Lakes due to the relatively large variation in this region. The data display relatively low frequencies for most of the western part of the continent. There are four general regions of maxima in Canada: the Beaufort Sea area, the western side of Hudson Bay, the east side of the Great Lakes and the Atlantic provinces, especially eastern Newfoundland. The Beaufort Sea area maximum occurs in October and in May, at the time the sea freezes in fall and thaws in spring. Most of the FP is in the form of Zl, and it is postulated that during this transition season low level stratus and salt water temperatures below 0 C contribute to this maximum. A similar scenario is proposed for the Hudson Bay maximum, which occurs in May and November, again when the sea ice melts and freezes. The maxima tend to be found in coastal stations, and Zl is most frequently observed when the wind is onshore. The third maximum is found in the area near the Quebec-Ontario border east of the Great Lakes ; North Bay, Ottawa, Mirabel, and

St. Agathe all receive more than 60 hours of FP per year, with St. Agathe receiving 85 hours per year. Frequency peaks in the month of November in this region. The final and strongest maximum is found in Atlantic Canada, and especially the east coast of Newfoundland. At St. John's, 154 hours per year of FP are observed, the highest in North America. Values peak in the month of March, when the ice flow originating in the Davis Strait is off the coast. Upper air stations at Inuvik ($68^{\circ}18'N, 133^{\circ}29'W$), Maniwaki ($46^{\circ}23'N, 75^{\circ}58'W$), and St. John's ($47^{\circ}37'N, 52^{\circ}44'W$) provide vertical temperature structure data from 3 of these four maxima, and this information during FP events will be examined later.

Maxima in FP in the USA are found at coastal stations in northern Alaska, and to the southwest of the Great Lakes, both of the order of 60 hours per year.

Classical and non-classical freezing precipitation:

The mechanism of formation of FP most commonly recognized by weather forecasters involves frozen precipitation melting and falling through an elevated warm layer, and then supercooling as rain or drizzle in a sub-zero surface layer ('classical' method). FP can occasionally also occur when rain or drizzle above $0^{\circ}C$ contacts a sub-zero surface, although this study found few cases by this mechanism. A less commonly known route for FP formation involves the development of rain or drizzle by a diffusional growth and coalescence of small cloud droplets, which we term here 'non-classical' FP. In this case precipitation drops can form and supercool without going through the ice phase. This process has in the past been termed the 'warm rain process', since it is usually associated with warm clouds. Classical FP is handled reasonably well by numerical weather prediction (NWP) models. Non-classical FP is simply not handled by NWP models, since the microphysical factors leading to its formation are complicated and at present poorly understood. In some regions however, local human skill at forecasting non-classical events based on experience is quite good. It is nevertheless important to address the shortcomings of NWPs in this area.

Non-classical FP has been suggested or inferred in many articles in the literature, but the most comprehensive study of the regional scale of the phenomenon has been accomplished by Bocchieri(1980) and Huffman and Norman(1988). The latter study found that for 48 US continental radiosonde stations, 30% of the total FP measurements were observed with no melting layer aloft (i.e. non-classical). Aircraft in-situ measurements documenting cases where supercooled drizzle developed from non-classical processes were made as early as the late 50s (Singleton; 1960), although perhaps more convincing data with imaging particle probes have appeared in more recent years (e.g. Polotovitch, 1989; Cober et al., 1996). It is now clearly known and observed that this mechanism exists in nature and accounts for a large percentage of total FP measured at the surface.

The frequencies of classical and non-classical Zr/Zl in Canada:

In order to examine the relative importance of classical and non-classical Zr and Zl in Canada, a detailed investigation of upper air observations during FP events was undertaken for St. John's, Newfoundland, Inuvik, NWT, and Maniwaki, which are located in the Atlantic, Beaufort Sea, and Great Lakes Zr/Zl maxima. The Maniwaki yearly FP (25 hours) is much lower than surrounding stations (it lies within the 62.5 hours per year isopleth in

Table 1: Frequencies of freezing precipitation at three Canadian stations, and characterization of Zl and Zr formation mechanism.

Station	hrs/yr	%Zr	%Zl	% no warm layer	% total non-classical
St. John's	154	33	67	42	64
Inuvik	26	15	85	53	72
Maniwaki	25	60	40	35	38

Fig. 1, and has been disregarded for this figure as an outlier). Nevertheless, twenty two years of observations were analysed from 1971 to 1992. Each individual radiosonde was examined by eye to determine whether the sounding fit into a classical or a non-classical type. In Table 1 the results are summarized for the three stations. In St. John's, most of the FP hours are Zl. In 46% of the observations, no warm layer was observed aloft (non-classical). There are also some cases of warm layers above cloud (i.e. the entire layer from the surface to cloud top is below 0 C), and many cases where the region at the top of the cloud is above 0 C, but the lower part of the cloud is below 0 C. In both of these latter cases there is no classical melting layer for frozen precipitation, and Zr or Zl develops from a condensation and/or coalescence process. The final column in the table shows that an additional 18% of the cases fall into this category, with a total of 64% of the FP cases arising from an inferred condensation and/or coalescence, or non-classical process. These are the cases which are currently not handled by NWP models. It is also evident that a higher proportion of the FP hours are found for non-classical FP, compared to the average calculated for USA stations by Huffman and Norman(1988). Although Inuvik observes less than 20% of the FP hours of St. John's, a higher percentage (85%) are due to Zl, 53% have no warm layer aloft, and 72% are inferred to be a result of condensation and/or coalescence, the highest of the 3 stations. The location of Maniwaki is more representative of continental airmasses, and provides somewhat different results. Here Zl hours dominate (60%), and FP is more commonly by classical mechanisms. Only 35% of the FP hours exhibit no warm layer aloft, and in only 38% of the cases can a condensation and/or coalescence process be inferred. Therefore these results suggest that the Canadian Great Lakes maximum is not dominated by non-classical FP, but more by classical FP events. These frequencies are closer to those reported by Huffman and Norman(1988) for the USA.

Jeck(1996) has performed a similar radiosonde analysis on 8 stations in continental USA, and has defined essentially the same radiosonde temperature structure types as this study. That study found soundings of classical FP in the minority in all 8 stations, varying from 40% at JFK airport in New York to 0% at Denver. The results of this study for Maniwaki indicate a higher percentage of classical FP than any of the stations described by Jeck(1996), although local effects at Maniwaki may be an issue.

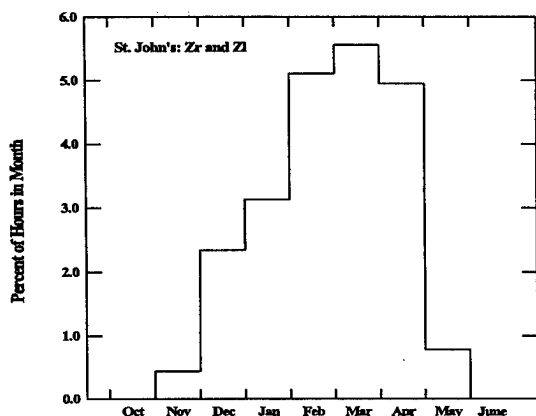


Figure 2: Percentage of hours with freezing precipitation in each month at St. John's; 1961-1990.

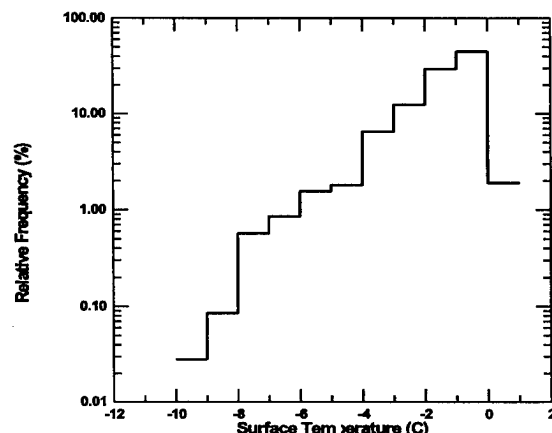


Figure 3: Relative Frequency of freezing precipitation observations vs. Surface temperature, St. John's, 1961-1990

A detailed study freezing precipitation at St. John's:

Figure 2 displays FP frequency by month for St. John's, Newfoundland. It is seen that FP peaks sharply in the March, coincident with the advance of the sea-ice pack off the east coast. Figure 3 displays the frequency of FP as a function of surface temperature. It is evident that the observations drop off sharply below 0 C, and the vast majority of the observations are between 0 and -2 C. Figure 4 displays the frequency of FP as a function of time of day. It is apparent that FP frequency peaks before sunrise and minimizes in the middle of the day. These figures indicate that FP is strongly dependent of factors affecting the surface temperature. When the sea ice is off the coast, water temperatures drop below 0 C, and thus modify surface temperatures to similar sub-freezing values. For coastal regions with conditions favourable for the formation of drizzle, this sea surface temperature forcing will tend to result in ZI instead of simply drizzle. Diurnal temperature trends due to solar heating perhaps raise temperatures at mid day, creating the cycle observed. This scenario may account for the high ZI observations near ocean freezeup at both Inuvik and St. John's.

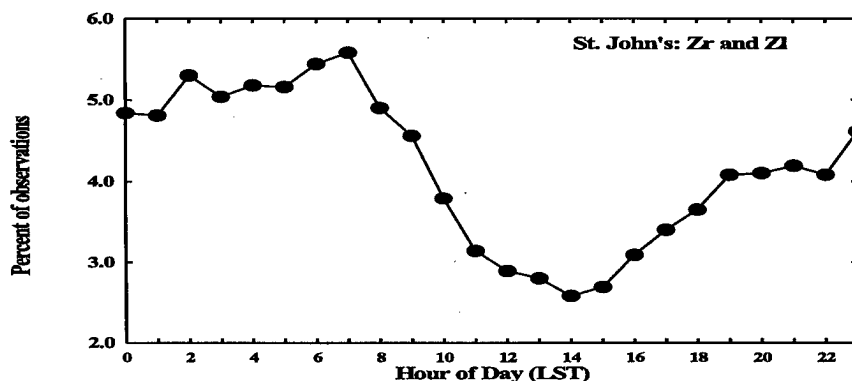


Figure 4: Percentage of freezing precipitation observations as a function of hour of day, St. John's 1961-1990.

Figure 5 contain typical soundings observed during classical Zr, classical ZI, non-classical Zr and non-classical ZI events. Note that in the classical cases, a warm melting layer overriding the sub-zero surface layer is observed. In the two cases shown the supercooled zone is restricted to below 2100' and 4240' respectively. The cases of non classical Zr and ZI show less deep clouds, with an often observed deep dry layer above cloud top, also noted by Huffman and Norman(1988). The entire cloud is supercooled, and the supercooled layers are deeper (7300' and 5600') than in the classical cases. Therefore although the FP is

Figures 5: Typical skew-T temperature profiles during surface freezing precipitation events in St. John's

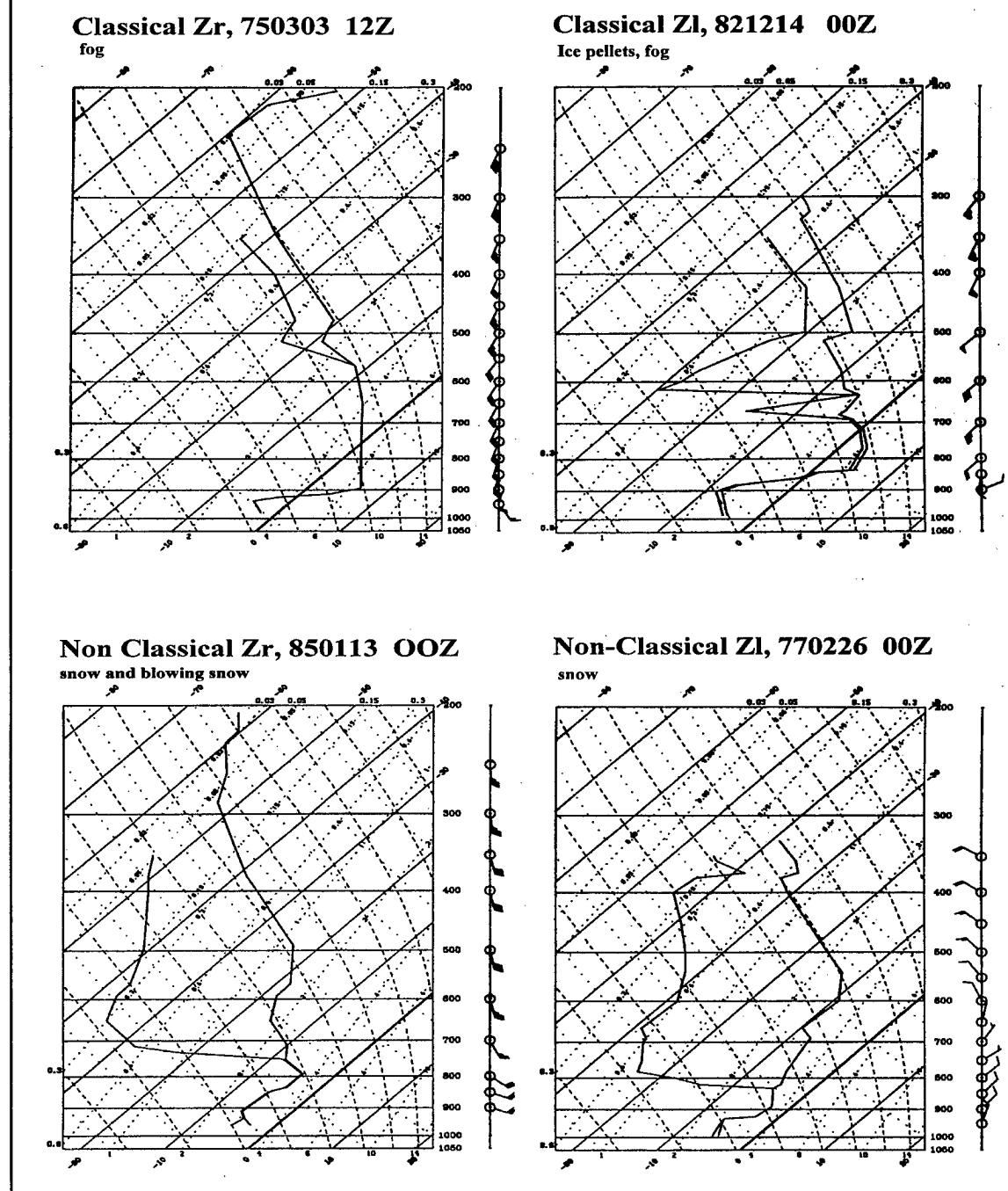
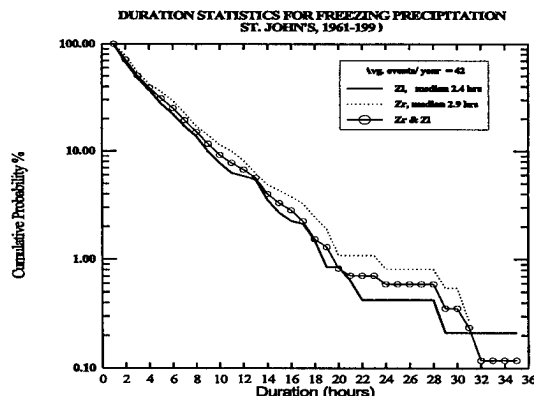


Table 2: Details on the temperature structure of soundings observed in cases of surface freezing precipitation at St. John's.

	classical	all-cold (non-classical)	warm above cloud (non-classical)	warm cloud top (non-classical)	no upper air data	total non-classical
ZI	15%	57%	2%	24%	2%	83%
Zr	74%	8%	1%	9%	0%	18%
Zr+ZI	36%	42%	2%	20%	1%	64%

Figure 6: Cumulative probabilities of freezing precipitation duration for St. John's, 1961-1990.



usually less intense in non-classical cases, it tends to occupy a deeper region of cloud. Note that freezing rain actually can occur from a completely cold cloud, as shown in the non-classical Zr case of Fig. 5. The cloud was approximately 7300' deep, with temperatures varying between -3 and -6 C.

A more detailed breakdown of the data from Table 1 for St. John's is given in Table 2. Four main categories of temperature profiles observed in the data and noted earlier are described in more detail as follows: (1) the entire atmosphere, including cloud, is below 0 C (non-classical 'all-cold'), (2) a melting layer is present below an ice-saturated layer, and above a surface cold layer (classical) (3) a warm layer exists but is clearly above cloud (non-classical 'warm above cloud'), and (4) a warm layer is observed at the top part of the cloud, but there is no sub-zero in-cloud layer aloft to required for nucleation and growth of ice particles (non-classical 'warm top'). From a total of 295 hourly observations of FP at St. John's at radiosonde release times, roughly 69% of the hours are ZI observations, and 31% are Zr. On a percentage basis, non-classical mechanisms account for 83% of the ZI observations, and 18% of the Zr cases. Therefore non-classical mechanisms are dominant in clouds producing ZI, and secondary in clouds producing Zr, but a surprisingly high percent of Zr cases can be attributed to non-classical mechanisms.

St. John's duration statistics:

Statistics on the duration of FP are summarized in Figure 6. On average, approximately 42 FP episodes are observed per year in St. John's. Although the distributions of duration are skewed to single one hour observations for both Zr and ZI, rare occasions of freezing drizzle and rain for up to 35 and 31 consecutive hours respectively have been observed. The median ZI and Zr durations are 2.4 and 2.9 hours respectively. Approximately 25% of the Zr or ZI cases exceed ~ 5 hours.

Cloud statistics estimated from radiosonde:

It is possible to estimate certain cloud properties for FP events, assuming that cloud boundaries can be defined by relative humidity thresholds. As observed in Figure 5, cloud tops and bases can be reasonably estimated from the relative humidity profiles in the 2 non-

Table 3: Statistics on the heights and depths of the lowest cloud layers for non-classical surface ZI in St. John's. Layer boundaries are defined by relative humidities exceeding 95%.

CLOUD LAYER STATISTIC	ALL COLD			WARM TOP		
	Min	Max	Median	Min	Max	Median
Base alt. (Kft)	.45	3.78	.45	.45	.75	.45
Top alt. (Kft)	.97	17.99	5.51	.71	8.24	3.82
Depth (Kft)	.51	17.5	4.81	.25	7.78	3.37
Min. Temp °C	-18.1	-1.6	-7.3	-8.1	0.1	-2.0
Max Temp °C	-10.1	0.0	-1.5	0.0	9.6	3.0
number of clouds	117	117	117	49	49	49

classical cases. The classical cases are more ambiguous however, and in general cloud top is often difficult to estimate due to the quite deep ice saturated layers at the tops of these soundings. The data set thus have been examined here only for the case of non-classical ZI. Statistics on the lowest cloud layer during each non-classical surface ZI event are given in Table 3. Cloud boundaries are defined here by relative humidities greater than or equal to 95% (this was found by visual inspection to be the most appropriate value so as not to eliminate clouds with an instrument relative humidity bias). The events are divided into 'all-cold', and 'warm-top' categories, as described earlier. In both these cases drizzle development is likely by a condensation and/or coalescence mechanism. Examining the statistics, it is evident that these cloud are relatively thick, with median depths of 4810' and 3370' m for 'all-cold' and 'warm-top' clouds respectively. Not surprisingly, cloud bases are usually very low. The 'warm-top' temperature statistics reveal that ZI often occurs when elevated warm layers are present in cloud, without subzero in-cloud layers aloft. Table 3 also shows that temperatures as high as 9 C are observed in clouds with ZI at the base. This is an important characteristic of some of these clouds ; a warm layer at the top of the cloud suppresses the formation of ice and allows a fairly deep layer to form and potentially exist for long periods. In deep layers with more conventional temperature profiles, temperatures at cloud top drop to levels at which ice nucleation is efficient, creating a ice precipitation mechanism which develops at the expense of liquid water. Figure 7 displays a histogram of the minimum in-cloud temperatures for 'all-cold' ZI soundings. The distribution has a fairly sharp cutoff at approximately -14 C, perhaps indicative of a temperature threshold at which ice begins to form very efficiently, glaciating clouds and inhibiting drizzle formation.

It is also possible to estimate from radiosonde data the probability of cloud as a function of height above ground during surface ZI. These probabilities are shown in Figure 8 for non-classical ZI events. For 'all-cold' events, the probabilities maximize near the surface (~83%

at 1000'), are approximately 60% at 4000', and drop below 10% at 9000'. Since the probability of non-classical surface ZI in March in St. John's is ~3.7%, it also follows that in non-classical ZI surface events, cloud defined by a relative humidity > 95% (and possibly ZI) was present at 4000' in ~ 2% of the total hours in March.

The probabilities noted above are arguably inaccurate due to a number of factors. The definition of cloud boundaries by relative humidity thresholds does not necessarily define areas of liquid water and drizzle, although the sharp demarcations often observed at cloud top are similar to those observed during the Canadian Freezing Drizzle experiment during airborne studies of stratus decks where significant LWC and drizzle were observed throughout the entire high relative humidity layer. This factor would tend to imply that Figure 8 overestimates true probabilities. On the other hand, it is also almost certain that ZI exists aloft which does not reach the ground (e.g. Cober et al.,1996 describes a likely case). Furthermore, hourly probabilities at St. John's underestimate the scale sampled by an aircraft in transit, since it covers a much larger atmospheric distance in one hour than is advected over St. John's in the same period. The latter factors tend to indicate that Figure 8 probabilities are underestimates of the probabilities to be expected by aircraft in flight. Without corroborating evidence from aircraft studies, the accuracy of radiosonde derived cloud statistics is unknown, and further work is needed in this area.

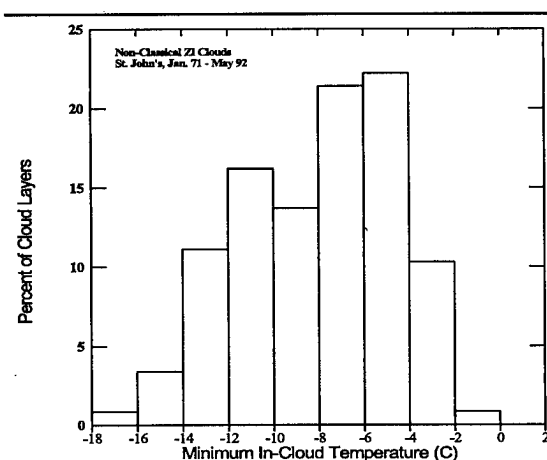


Figure 7: Percentages of cloud layers with minimum in-cloud temperatures as shown; for 'all-cold' non-classical ZI, St. John's Jan 71 - May 92

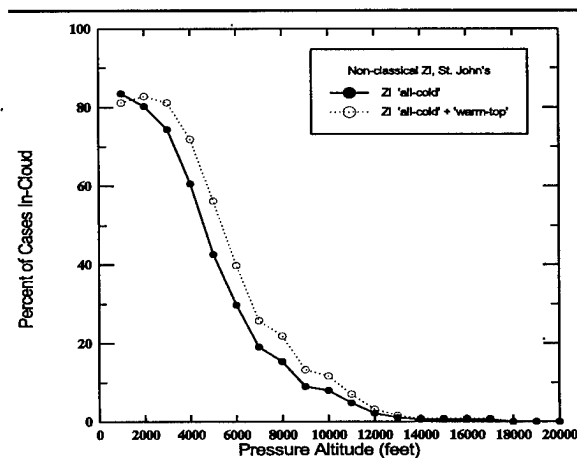


Figure 8: Percentages of cases of non-classical ZI at the surface in which the first cloud layer extends to the noted 1000' pressure altitude interval; St. John's Jan 71 - May 92.

Conclusions:

A climatology of the frequency of FP over North America reveals a strong maximum in the vicinity of St. John's Newfoundland, and other maxima near the Great Lakes, Hudson's Bay, and the Beaufort Sea. Local effects strongly affect the frequencies, as observed by the factor of 6 gradient across the island of Newfoundland. Coastal areas at the higher latitudes tend to be associated with higher frequencies especially of ZI, and maxima tend to coincide with periods of freezeup and thaw, or periods when sea-ice is present. It is postulated that sub-zero

sea temperatures favour the development of low level stratus with sub zero surface temperatures, and thereby ZI if other conditions are favourable.

Examination of radiosonde data for St. John's Newfoundland reveals that ~83% of the ZI cases can be interpreted as having formed from a condensation and/or coalescence process, instead of the more commonly accepted classical case of melting in an elevated warm tongue and falling into a subzero surface layer. This proportion is roughly reversed in the case of Zr, but it is found that Zr can also result without a warm layer aloft. Overall, 64% of FP cases (Zr and ZI) in St. John's were interpreted as non-classical cases. Radiosonde data also provided some insights into the type of clouds producing non-classical drizzle. Using relative humidity thresholds to define cloud boundaries revealed a median cloud base essentially at the surface, with a fairly large median depth of ~1500 m. Approximately 30 % of the non-classical ZI cases are found to have warm layers in cloud with no sub-zero in-cloud layer aloft. It is thought that this could be an important factor in creating favourable conditions for ZI formation, since ice nucleation and growth is suppressed by the warm top temperatures. Radiosonde derived rough probabilities of non-classical ZI for March at St. John's were estimated at 3%, 2%, and 0.4% for 1000', 4000', and 9000' respectively.

Comparison of St. John's radiosonde results to Inuvik, NWT reveals some similarities between these two coastal stations. Both show most ZI originating from non-classical soundings. Both show maxima in ZI frequencies during the periods of coldest sea-surface temperatures. In contrast, only 38% of the cases at the continental station at Maniwaki are non-classical, closer to the findings for continental USA stations by Huffman and Norman(1988), but much lower than values found by Jeck(1996) for 8 continental stations east of the US Rocky Mountains.

Non-classical FP mechanisms are found to be very active in Canadian clouds, particularly in the region of St. John's, where the highest ZI and Zr frequencies in North America are found. This substantiates earlier work by other authors, but is not a commonly recognized fact. Modeling of non-classical FP for improved forecasts may prove to be a difficult task, since physical schemes may need to incorporate many atmospheric parameters which are not currently available from standard network data.

Acknowledgements:

This work was funded by the Canadian National Search and Rescue Secretariat. The authors wish to thank Dr. Richard Jeck for his help in locating USA FP data.

References:

- Bocchieri, J.R., 1980: The objective use of upper air soundings to specify precipitation type. *Mon. Wea. Rev.*, **108**,596-603.
- Cober, S.G., J.W. Strapp, and G.A. Isaac, 1996: An example of supercooled drizzle droplets formed through a collision coalescence process. Accepted to *J. Appl. Meteor.*

Jeck, R., 1996: Representative values of icing-related variables aloft in freezing rain and freezing drizzle. *Proc. FAA Intl. Conf. On Aircraft Inflight Icing*. (this issue).

Huffman, G.J., and G.A. Norman, 1988: The supercooled warm rain process and the specification of freezing precipitation. *Mon. Wea. Rev.*, **116**, 2172-2182.

McKay, G.A., and H.A. Thompson, 1969: Estimating the hazard of ice accretion in Canada from climatological data. *J. Appl. Meteor.*, **8**, 927-935.

Polotovitch, M.K., 1989: Aircraft icing caused by large supercooled droplets. *J. Appl. Meteor.*, **28**, 856-868.

Singleton, F., 1960: Aircraft Observations of rain and drizzle from layer clouds. *Quart. J. R. Met. Soc.*, **80**, 195-204.

Vilcans, J., 1989: Climatological study to determine the impact of icing on the low level Windshear Alert System. Tech. Report DOT-TSC-FAA-89-3 (Vols. 1 and 2), U.S. Dept. Of Transportation, Transportation Systems Center, Cambridge. MA 02142.

REPRESENTATIVE VALUES OF ICING-RELATED VARIABLES ALOFT IN FREEZING RAIN AND FREEZING DRIZZLE

Richard K. Jeck
FAA William J. Hughes Technical Center
Atlantic City, New Jersey 08405
U.S.A.

Abstract

Radiosonde and surface observations in freezing rain (ZR) and freezing drizzle (ZL), and a limited number of aircraft measurements in ZR, have been examined for information on the magnitude and altitude dependence of meteorological variables associated with aircraft icing in these conditions. The variables include temperature aloft, humidity (clouds), and windshear from the radiosondes; surface temperatures, ceiling heights, precipitation type and amount from the surface observations; and temperature, dropsize, rainwater concentration, and icing rate from the instrumented aircraft. These and other data are used here to arrive at tentative maximum and representative values of these variables. Finally, a new convention establishing standard dropsize intervals is proposed for ZL and ZR. This simplifies the reporting and comparison of data, overcomes the inadequacy of median volume diameter (MVD) for use with these wide dropsize distributions, and can serve as a useful way to "characterize" ZR and ZL conditions for possible test or design requirements.

Summary of the Results

An important recent study³ was the compilation of ZR and ZL occurrences and durations at a hundred or so airports in the United States over a 25 year period from about 1962 to 1987. Eighteen of the airports were also at or near the launch sites for twice-daily radiosondes. Although the original study was based only on surface weather reports, the author fortunately obtained the dates and times of occurrence of the ZR and ZL conditions at each airport. This allowed an easy retrieval of archived surface observations and radiosonde data for use in the present study. More than 700 radiosonde ascents were identified in this way,

where ZR or ZL was present at the time of the ascent. These data are currently being analyzed to give previously unavailable statistics on conditions *above* the surface during freezing rain and freezing drizzle. In particular, the depths and extreme temperatures in the freezing layers and warm layers aloft are revealed by the radiosondes. Cloud layers can also be deduced from the onboard humidity sensor.

The following results are extracted from a more complete report by the same title¹.

Most ZR or ZL occurrences reported at the surface are accompanied by low ceilings. The ratio of ZR to ZL differs markedly among some sites; but overall, ZL is reported for about 60% of the cases compared to 40% for ZR. Assuming that the observers have correctly distinguished ZL from ZR, this indicates that drizzle is more common than previously thought, at least in low ceiling conditions involving freezing precipitation. Table 2 gives some preliminary results showing the variations in the type of freezing precipitation and accompanying vertical temperature profiles at different locations in the United States.

From the radiosonde data it is found that ZR conditions can extend up to 7000 Ft above ground level (AGL) at some locations, and temperatures can range down to -11°C. Table 3 shows the range of temperatures aloft and the range of vertical extents recorded at several locations.

Aircraft measurements¹² have documented ZL up to 12,500 Ft AGL at temperatures down to -11°C.

As a result of the crash near Roselawn, Indiana in October, 1994, the radiosonde data used for this report have been searched for evidence of cloud layers aloft that could produce "elevated" freezing drizzle similar to that suspected of causing the accident.

Adequately deep, supercooled cloud layers in the 5000 Ft to 17,000 Ft AGL altitude range are inferred in about 30% of the cases, but there is no direct evidence from the radiosondes about how many of these cloud layers may be producing ZL.

From the few available passes of an instrumented aircraft² in ZR conditions at several locations, rainwater concentrations (RWC) of 0.1 to 0.3 g/m³ were documented along with typical RMVD's (raindrop median volume diameters) of about 1 mm. These are consistent with other indirect estimates for these variables. Onboard ice detectors registered icing rates up to 15 mm/hr (5/8 inch/hr). This means that during a 15 minute approach and landing sequence, an aircraft could accumulate up to 4 mm (5/32 inch) of glaze ice on the airframe in the observed ZR conditions.

Only small amounts of data on drizzle dropsizes and drizzle water concentrations (DWC) are available so far in the literature. These suggest representative DWC's of about 0.1 g/m³ distributed over the drizzle-drop size range of 50-500 μ m. Maximum DWC's have been reported up to 0.3 g/m³ or more in clouds.

Inflight Measurements of Freezing Rain. The University of North Dakota (UND) cloud physics research aircraft, a Cessna "Citation", has been flown into conventional, low-altitude, freezing rain conditions about a dozen times during winter research projects. Three of those encounters, two near Kansas City, MO and one near Grand Forks, ND have valuable data² on droplet size, water concentration, and icing rate in ZR. The encounters occurred during routine takeoff and landing phases of flight, since the ZR was confined to low levels.

Figure 1 shows the computed RWC's and MVD's for one of these cases, and Table 1 lists pertinent results for all of the encounters. These were the only ZR dropsizes measurements available for this report. Some interesting conclusions from two of the cases are the following:

◆ Although the surface air temperature was -1°C or -2°C, the temperature decreased to as much as -8°C at the coldest point in the ZR layer, which was from 3000 Ft to 4000 Ft deep in these cases.

◆ Ice accumulation on the ice detector starts within 6 seconds after descending into the top of the subfreezing layer.

◆ During about 30 minutes of level flight in ZR at 2200 Ft AGL (and -6°C), the Rosemount ice detector registered an accumulation of at least 9 mm of ice (0.7 inch/hour). The flight crew had to increase fuel consumption by 60% (from 500 lbs/hr to 800 lbs/hr on each side) to maintain the un-iced performance level.

◆ The aircraft spent about 16 minutes in the ZR layer during approach and landing, during which time the Rosemount ice detector registered about 4mm (1/6-inch) of ice accretion.

◆ A 1000 to 2000 Ft deep supercooled cloud layer with LWC up to 0.3 g/m³ may form a low ceiling in the cold air during ZR conditions. This can add to the ice accretion from the ZR itself.

◆ The fastest ice accretion appears to occur where the temperature is lowest in the freezing rain layer.

Droplet Sizes

By convention, drizzle drops are taken to be less than 0.5 mm in diameter. Larger drops are considered raindrops. The largest dropsizes for either rain or drizzle depends on the circumstances of the droplet formation and how the drops evolve during their fall.

Freezing rain results from snowflakes melting in a layer of warm air aloft and then falling into a layer of subfreezing air near the ground. The largest raindrop size depends on the maximum size of the melting snowflakes and on the amount of evaporation the drops undergo during their fall to the height at which they are measured. They may also grow somewhat by collision with other, smaller droplets if they fall through a layer of cloud on the way down. The complete raindrop size distribution is generally a continuum extending from the largest available size down into the drizzle size range. If enough evaporation takes place during their fall, the rain drops could all be shrunk into the drizzle size range by the time they reach the ground. In any case, the size (and RWC) distribution can change with altitude. They can also change horizontally (or over periods of minutes at a given location) in response to

variable amounts of snow aloft. A snow shower aloft can result in a shower of larger or more plentiful freezing rain drops below.

Drizzle usually forms by an in-cloud process known as collision and coalescence. Contrary to the melting process for rain, drizzle drops have to *grow* by the gradual collection of mostly smaller cloud droplets as the drizzle drops descend through the cloud(s). The maximum dropsize is therefore limited in part by the depth of the cloud. Observation shows that drizzle drops are usually no larger than about 0.5 mm (500 μm), and that the number of droplets decreases as the size increases toward 0.5 mm. That is, the greatest number of drizzle droplets are in the smaller sizes.

It is known that two mechanisms can enhance drizzle production by promoting the quick and continual growth of ordinary droplets into the 30 μm range where they can start to fall, thereby beginning the collision and coalescence process. One such mechanism is the presence of relatively large (10 μm or so) microscopic salt particles in the air where the cloud is forming. This happens frequently in oceanic coastal areas where whitecaps and surf spray inject saltwater droplets into the air. The smaller droplets evaporate and leave a residual aerosol of microscopic salt particles. This can be easily seen as a whitish haze all along the beach zone. Cloud droplets always form on submicron hygroscopic particles (called cloud condensation nuclei) anyway, but the presence of unusually large nuclei is known to result in unusually large cloud droplets. This is why drizzle is more often observed under low cloud conditions in coastal areas than anywhere else. But large salt nuclei seldom reach very far inland or rise to the vicinity of the 10,000 Ft (3 km) level where the elevated freezing drizzle clouds are occurring like those that are suspected of being responsible for the Roselawn, Indiana accident in October, 1994. Therefore, some other mechanism must be at least occasionally active inland and at the altitudes of interest, in order for large numbers and sizes of drizzle drops to be present.

The other drizzle catalyst is thought to be turbulence. Almeida⁴ and others have shown theoretically that sufficiently intense in-cloud turbulence can promote the growth of droplets into the 30 μm size and enhance the subsequent collision and coalescence of these droplets into drizzle⁵. This suggests that large droplets can be expected to occur widely,

geographically. Warm fronts and turbulence are common, and indeed drizzle is sometimes recorded at surface observing sites in association with warm front arrivals in the winter. Thus, there are some statistics available for drizzle at the surface, but it is not known how often it occurs at aircraft holding altitudes of 5000 Ft to 15,000 Ft, AGL, for example.

Based on some numerical simulations and on comparisons with experimental evidence, Pobanz et al. (Ref. 6) have postulated some minimum wind shear (turbulence) conditions that must be met in order for drizzle to be promoted in cloud layers. Specifically, they propose that a definite windshear layer must be present at the top of the cloud layer, and that the windshear strength be at least 0.02 m/sec per meter of height. In addition, the bulk Richardson number (Ri) computed across the shear layer must be less than unity. The bulk Richardson number is taken as a measure of the wind shear-induced mixing, and $Ri < 1.0$ is sufficient to maintain turbulence.

The radiosonde data used for this report have been examined for any elevated, turbulent, supercooled cloud layers that meet the Pobanz, Marwitz, and Politovich requirements⁶. Although about a third of these radiosonde observations indicate the presence of supercooled cloud layers covering part of the altitude interval between 5000 Ft (1.5 km) and 15,000 Ft (4.5 km), the proposed windshear and Richardson number requirements are seldom met. This suggests that although significant aircraft icing from ordinary supercooled clouds may be present in these layers, only rarely are conditions right for the enhanced formation of elevated freezing drizzle, according to the requirements of Pobanz et al. One case where the proposed windshear requirements appear to be met is shown in Figure 2.

Displaying the Data

Because the droplet concentration changes so rapidly with droplet size, it is usually desirable to divide the overall size range into many narrow sub-intervals, in order to accurately display the variation. Modern, electro-optical, droplet sizing probes do this by automatically tallying the number of droplets detected in each of 15 or more narrow size intervals. A typical graphical presentation of the results often looks like that shown in Figure 3. Because of the wide range in both dropsize and droplet numbers over the size

range, logarithmic scales are often used to compress the scales to fit a single page and to preserve the detail in both the small dropsizes and the low droplet concentrations. In addition, in order to make the results universally comparable (independent of the probe), it is necessary to plot the number of droplets per unit volume of air *per unit size interval* (i.e., per μm or per mm) instead of simply the number of droplets detected in each arbitrary size interval. While these conventions are often necessary for accurate scientific depiction and unambiguous use of the data, they obviously add considerable complication to the matter. For one thing, it is difficult to quickly assess the significance of the differences between two or more sets of results. For example, what is the significance of the difference between the curves beyond $100\ \mu\text{m}$ in Figure 3?

In order to avoid these complications and to simplify the interpretation of dropsizes and water concentration data, the median volume diameter (MVD) has been traditionally used as a single variable substitute to represent conventional cloud droplet distributions for aircraft icing purposes. The MVD conveniently indicates the dropsizes which divides the water concentration in half. That is, by definition, half of the available water in the droplet population is contained in droplets smaller than the MVD and half is contained in larger droplets. But the MVD is known to be unsatisfactory for wide dropsizes distributions because it gives no information about what the largest dropsizes are.

A Standard Dropsizes-Interval Scheme. This method of distributing DWC or RWC with dropsizes, introduced here, has some attractive features. Basically, for research purposes at least, the idea is to establish the convention of reporting all drizzle and freezing rain dropsizes data in terms of DWC or RWC amounts in a few, standard, dropsizes intervals. This is illustrated in Table 4. Five dropsizes intervals will span the ZL or ZR droplet size range with sufficient resolution for aircraft icing purposes. Reported ZL or ZR encounters can then be easily compared as shown in the table.

This scheme has the simplicity needed for compiling and comparing diverse measurements of DWC or RWC in ZL or ZR conditions. It is convenient for routine dropsizes measurements because it allows the use of any dropsizes probe(s) that cover the necessary dropsizes range. It also compromises between the difficult task of trying to compare dropsizes distribution

curves plotted on a log-log scale, and the simpler but inadequate usage of a single variable like MVD which gives no clue about the actual dropsizes distribution.

In addition, once a minimum test spray requirement has been decided upon, it can be expressed in the same manner.

This makes the method suitable for wet wind tunnel operators or spray rig operators too. The spray nozzles can be adjusted to approximate the desired amount of DWC or RWC in each of the standard size intervals. Test crews then need only document the DWC or RWC amounts they achieved in each of the fixed size intervals. A glance will quickly tell whether the amounts meet, exceed, or fall below the specified (required) amounts.

For computer modeling of ice accretion, a few, fixed dropsizes are more suitable and realistic than a simple MVD too.

Other variables, such as the MVD, can still be included as supplementary indicators. But the proposed scheme establishes the standard dropsizes intervals as the primary means for reporting data and possibly for specifying test and design requirements.

It is important to remember that dropsizes distributions for ZR generally extend down into the ZL range ($50\text{-}500\ \mu\text{m}$ diameter). This means that up to ten standard size intervals may be needed to describe some ZR events. An analyses (not shown) of the available ZR data indicates that anywhere from zero to fifty percent of the RWC can be contained in the drizzle portion of the size spectrum. Typically, however, the drizzle size range contains 10% to 25% of the observed RWC in ZR conditions.

The number of standard size intervals may be eventually reduced if research shows that DWC or RWC distributions can be replaced by a few, stock, Langmuir-like distributions, or if it is found that dropsizes is not important above some value. But for the time being, a scheme like this is needed to facilitate a common approach for the accumulation and analysis of data.

Representative Values of All Variables

Very limited amounts of data are presently available for variables associated with ZR and ZL conditions aloft. The most important variables include RWC or DWC, air temperature, dropsize, and vertical extent, at least. For interim test or guidance purposes, representative or average values and the extreme values are needed. At the moment, extreme values can only be estimated, but representative values are easily obtainable from the data in this study and elsewhere. Proposed values are given in Table 5.

References

1. Jeck, R.K., 1995: **"Representative Values of Icing-Related Variables Aloft in Freezing Rain and Freezing Drizzle"**, Technical Note DOT/FAA/AR-TN95/119, FAA Tech Center, Atlantic City, NJ 08405.
2. University of North Dakota, Dept. of Aerospace Sciences, private communication of data.
3. Vilcans, J., 1989: **"Climatological Study to Determine the Impact of Icing on the Low Level Windshear Alert System"**, Technical Report DOT-TSC-FAA-89-3 (2 Vols.), U.S. Department of Transportation, Transportation Systems Center, Cambridge, Massachusetts 02142.
4. Almeida, F.C., 1979: **"The Effects of Small-Scale Turbulent Motions on the Growth of a Cloud Droplet Spectrum"**, *J. Atmos. Sci.*, **36**, 1557-1563.
5. Khain, A.P., and Pinsky, M.B., 1995: **"Drop Inertia and Its Contribution to Turbulent Coalescence in Convective Clouds"**, *J. Atmos. Sci.*, **52**, 196-206.
6. Pobanz, B.M., Marwitz, J.D., and Politovich, M.K., 1994: **"Conditions Associated with Large-Drop Regions"**, *J. Appl. Meteor.*, **33**, 1366-1372.
7. Ashenden, R., and Marwitz, J., 1996: **"A Comparison of the Air Force Water Spray Tanker Artificial Drizzle Cloud Distributions to the Natural Environment"**, paper no. AIAA 96-0632, 34th Aerospace Sciences Meeting, Reno, Nevada.
8. Mills-Hicks, C.J., and Mansfield, D.A., **"The Climatology of Freezing rain in the British Isles Based on Radiosonde Station Records"**, *Met. O. (P)*

Special Investigations Technical Memorandum No. 1 (199), Meteorological Office, London Road, Bracknell, Berkshire, RG12 2SZ.

9. Lewis, W., and Perkins, P.J., 1958: **"A Flight Evaluation and Analysis of the Effect of Icing Conditions on the ZPG-2 Airship"**, Technical Note No. 4220, National Advisory Committee for Aeronautics, Lewis Flight Propulsion Laboratory, Cleveland, Ohio.

10. **"Hourly Precipitation Data (New England)"**, Vols. 5-7 (1955-1957), U.S. Department of Commerce, U.S. Weather Bureau.

11. Politovich, M.K., 1989: **"Aircraft Icing Caused by Large Supercooled Droplets"**, *J. Appl. Meteorology*, **28**, 856-868.

12. Cober, S.G, Isaac, G.A., and Strapp, J.W., 1995: **"Aircraft Icing Measurements in East Coast Winter Storms"**, *J. Appl. Meteor.*, **34**, 88-100.

13. University of Wyoming, Atmospheric Sciences Dept., private communication of data.

Acknowledgement

The author is indebted to colleague Dr. James T. Riley at the FAA Technical Center for help in processing and analyzing the freezing rain flight data from UND.

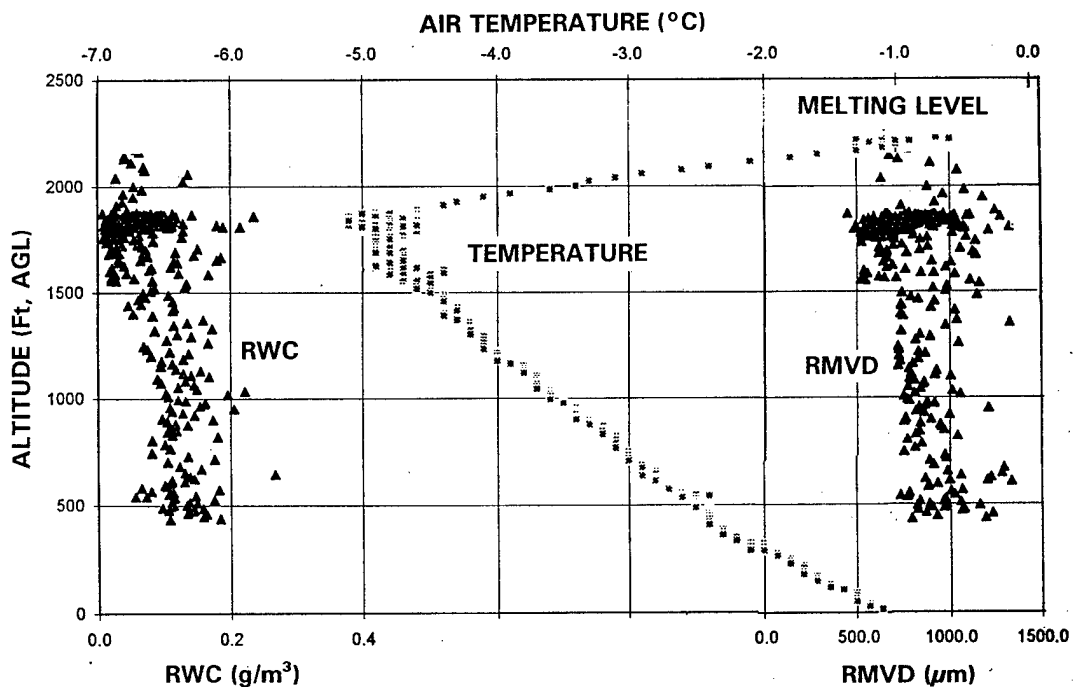


FIGURE 1. FREEZING RAIN AT KANSAS CITY, FEB. 1, 1990 (Ref. 2).

TABLE 1. AVAILABLE FREEZING RAIN DATA FROM THE UNIVERSITY OF NORTH DAKOTA INSTRUMENTED AIRCRAFT (Ref. 2).

<u>Date</u>	<u>Loc</u>	<u>Flight Phase</u>	<u>AGL Altitude</u> (1000's Ft)	<u>IDP Probe</u>		<u>Temp</u> (°C)
				<u>LWC</u> (g/m ³)	<u>MVD</u> (mm)	
3-17-87	GFK	Takeoff	0 - 4	0.1 avg.	1-1.3	0 to -2
3-17-87	GFK	Climb out	3 - 4	0.1-0.2	1-1.5	0 to -4
3-17-87	GFK	Climb out	3 - 4	0 - 0.1	0.9-1.3	0 to -4
1-19-90	MKC	Landing	0 - 1.4	0.1-0.3	1-1.5	0 to -4
1-19-90	MKC	Landing	0.5 - 2	0.3 avg.	1-1.3	0 to -4
2-01-90	MKC	Takeoff	0 - 2.5	0.1-0.2	1-1.3	0 to -6
2-01-90	MKC	Landing	0 - 2.5	0.1-0.2	0.7-1.2	0 to -5
2-14-90	MKC	Takeoff	0 - 4	0.1-0.3	0.8-1.5	0 to -8

TABLE 2. STATISTICS ON TYPE OF FREEZING PRECIPITATION AND ACCOMPANYING VERTICAL TEMPERATURE PROFILES AT SELECTED LOCATIONS. (Listed in order of decreasing frequency of ZR and increasing frequency of ZL at the locations.)

Location	Precipitation Type ¹			Temperature Structure Types ²			
	ZR (%)	ZL (%)	+IP (%)	A (%)	B (%)	C (%)	Other (%)
IAD	84	5	11	21	47	0	32
BUF	53	47	21	32	32	36	0
PIA	47	53	21	26	32	37	5
JFK	30	40	60	40	30	30	0
MAF	26	74	5	11	68	21	0
GRB	21	79	31	11	16	68	5
CHI	20	80	20	30	40	30	0
DEN	0	100	50	0	17	83	0

¹ Note: These columns distinguish between freezing rain (ZR) and freezing drizzle (ZL), and list the percentage of cases where one or the other was reported in the surface observations at or near the release time of the radiosonde balloon. The column headed "+IP" gives the percentage of cases in which light snow or ice pellets were reported along with, or instead of ZR or ZL.

² Definitions of the temperature profile types.

Code	Explanation
A	Classic textbook case of ZR (cold surface layer overrun by warm layer aloft, snowing cloud above warm layer, with melting layer (and snow cloud base) at the 0°C crossing at top of warm layer).
B	Classic textbook temperature profile as above, but precipitation apparently originating in the low cloud layer---i.e., the upper cloud layer is absent or is not precipitating (not extending down to the 0°C level at the top of the warm layer).
C	Cold layer only---no warm layer present; ZL apparently forming by "warm rain" or coalescence process.

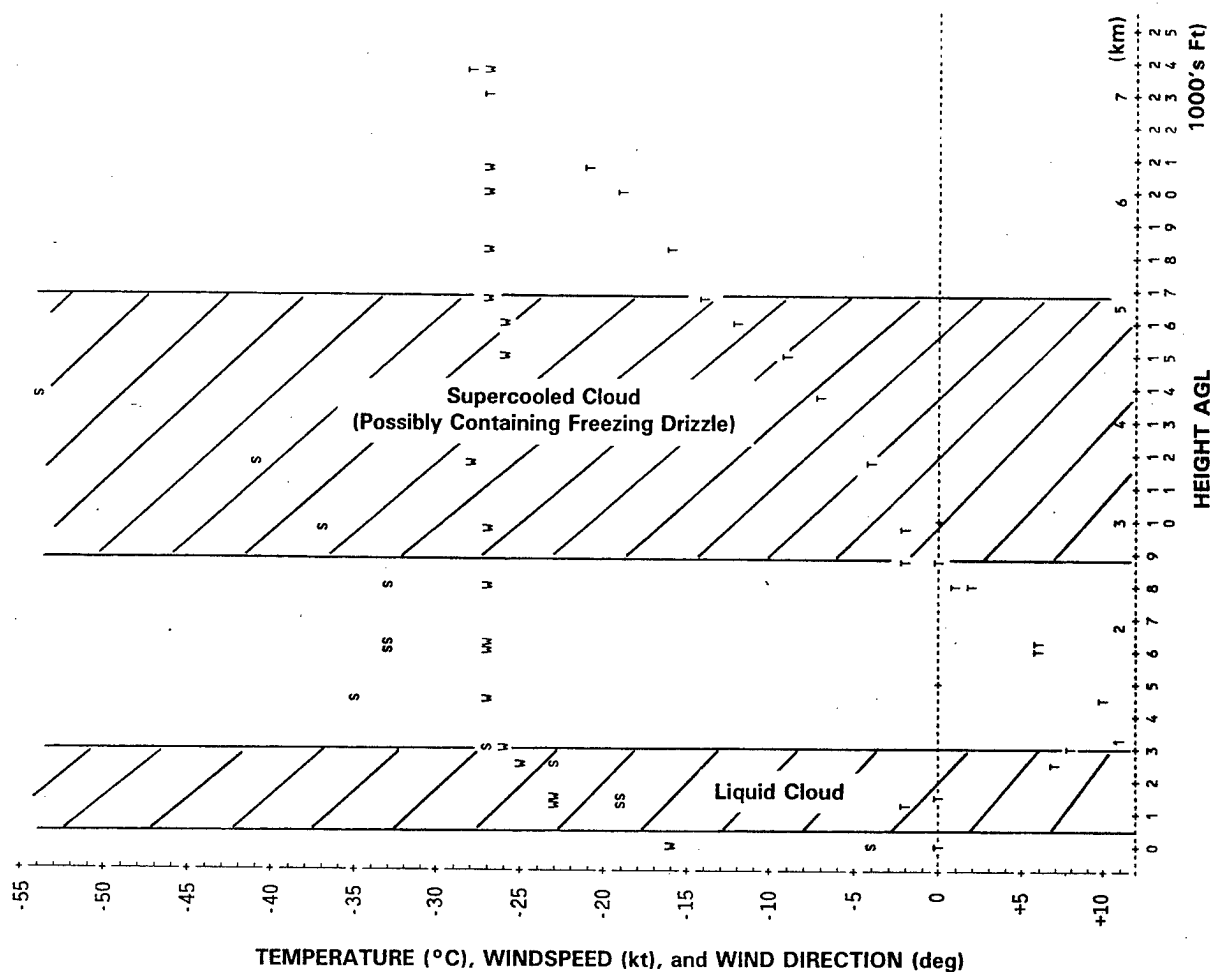


FIGURE 2. EXAMPLE OF MID-LEVEL CLOUD LAYER THAT MAY CONTAIN FREEZING DRIZZLE. Freezing drizzle and freezing rain were reported at the surface. Windshear and turbulence may be creating "large drops" (i.e., freezing drizzle) in the upper cloud layer at temperatures down to -15°C ! (Cloud layers were inferred from radiosonde humidity data (not shown). Case is for Washington, DC (IAD), Jan. 14, 1971.) The horizontal scale is used to display: Temperature (T) from $+10^{\circ}\text{C}$ to -55°C ; Windspeed (S) from 0 to 55 kt; Wind Direction (W) from 0 to 360 degrees.

TABLE 3. TEMPERATURES AND DEPTHS OF THE FREEZING RAIN OR FREEZING DRIZZLE LAYERS FROM RADIOSONDE MEASUREMENTS AT SELECTED LOCATIONS.

Location	Layer Temperatures (°C)				Layer Depths (Ft)			
	Lowest Recorded	Average Lowest	Lowest in		Overall		Max. when topped by:	
			ZR	ZL	Max.	Avg.	Warm Layer	Cloud Top
IAD	-8.3	-3.8	-7.6	-8.3	4800	3060	4090	4800
BUF	-15.7	-5.7	-6.1	-15.7	9900	4110	3600	9900
PIA	-11.8	-6.2	-11.1	-11.8	11400	4130	3950	11400
JFK	-11.0	-5.1	-3.5	-11.0	11800	5150	5150	11800
MAF	-10.4	-6.5	-10.4	-10.3	8200	3075	4350	8200
GRB	-13.4	-7.9	-9.6	-13.4	10900	5920	6900	10900
CHI	-7.3	-4.0	-4.0	-7.3	9500	3390	2455	9500
DEN	-14.1	-9.0	-	-14.1	8200	4225	3100	6900

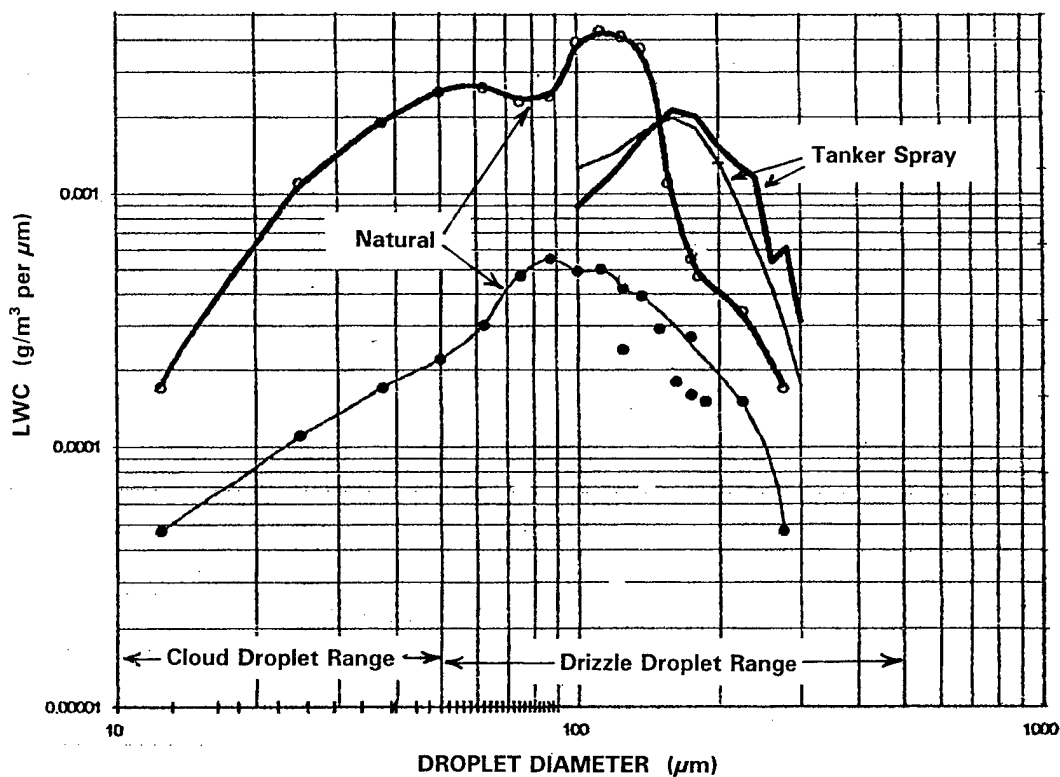


FIGURE 3. EXAMPLES OF NATURAL CLOUD AND DRIZZLE DROPSIZE DISTRIBUTIONS COMPARED TO TANKER SPRAY. Small droplet component not shown for tanker spray (Ref. 7).

Rule: Show or Specify LWC in Five Standardized Dropsizes Intervals
over an Appropriate Dropsizes Range.

Advantages:

- ◆ Easy to use and understand.
- ◆ Easy to specify test or design requirements: e.g., meet or exceed specified minimum LWC's for each size interval.
- ◆ Easy to compare measurements and requirements.
- ◆ Avoids the ambiguity of MVD or other single-number characterizations.
- ◆ Independent of any particular droplet probe.

Examples for Data Reporting, using the proposed scheme:

(The droplet concentrations are optional and are shown here for illustration purposes.)

TABLE 4. PROPOSED LWC vs DROPSIZE REPORTING SCHEME FOR DRIZZLE AND FREEZING RAIN.

Drizzle

PROPOSED STANDARD SIZE INTERVALS	Canada AES (3-14-92)		U. Wyoming (3-8-94)		USAF Tanker (12-18-94)	
	CONC (no./ltr)	DWC (g/m ³)	CONC (no./ltr)	DWC (g/m ³)	CONC (no./ltr)	DWC (g/m ³)
50 - 100 μ m	-	-	120	0.021	360	0.065
0.1 - 0.2 mm	1.7	0.003	20	0.035	100	0.173
0.2 - 0.3 mm	1.4	0.010	1.2	0.010	11	0.093
0.3 - 0.4 mm	0.6	0.012	0	0	0.4	0.009
0.4 - 0.5 mm	0.08	<u>0.003</u>	0	<u>0</u>	0	<u>0</u>
Total LWC's:		0.028		0.066		0.34

Freezing Rain

PROPOSED STANDARD SIZE INTERVALS	Univ. North Dakota (2-14-90)	
	CONC (no./ltr)	RWC (g/m ³)
0.5 - 1 mm	0.4	0.069
1 - 1.5 mm	0.03	0.036
1.5 - 2 mm	0.01	0.035
2 - 3 mm	0.002	0.012
3 - 4 mm	0.000	<u>0.000</u>
Total LWC's:		0.15

TABLE 5. REPRESENTATIVE VALUES OF VARIABLES IN FREEZING RAIN AND DRIZZLE.

-----Freezing Rain-----				
Variable	Known or Estimated Range	Representative Value	Source of Data	
RWC (g/m ³)	0 to 0.3	0.15	a,b,c,d	
Dropsiz (mm)	0.25 to 4 dia.	(see below)	a,c,d	
Temperature (°C)	0 to -12	-2 (at ground level) -7 (at 3300 Ft AGL)	b,d d	
Altitude (AGL): Ft. km	0 to 6900 0 to 2	0 to 3300 0 to 1	a,d a,d	
Exposure: Use representative time below 7000 Ft AGL during approach.				
-----Representative LWC Distribution vs. Dropsiz----- (in the freezing rain dropsiz range only)				
Dropsiz Interval (mm):	0.5 - 1	1 - 1.5	1.5 - 2	2 - 3
Droplets per liter:	0.4	0.03	0.01	0.002
Incremental RWC (g/m ³):	0.07	0.04	0.03	0.01

-----Freezing Drizzle-----					
Variable	Known or Estimated Range	Representative Value	Source of Data		
DWC (g/m ³)	0 to <0.3	0.08	e,d		
Dropsiz (μm)	50 to 500 dia.	(see below)	f,d		
Temperature (°C)	0 to -15	-2 (at ground level) -2 to -10 (at 3-5 km AGL)	d d		
Altitude (AGL) Ft. km	0 to 17,000 0 to 5	0 to 15,000 0 to 4	d d		
Exposure: Use holding time.					
-----Representative LWC Distribution vs. Dropsiz----- (in the drizzle dropsiz range only):					
Dropsiz Interval (μm):	50-100	100-200	200-300	300-400	400-500
Droplets per liter:	120	20	1.2	0.6	0.08
Incremental DWC (g/m ³):	0.021	0.035	0.010	0.012	0.003

Sources of Data:

- a = Ref. 13, 25 (British Isles)
- b = Ref. 1, 27 (New England region of U.S.A.)
- c = Ref. 26 (central U.S.A.)
- d = present study (central and eastern U.S.A.)
- e = Ref. 5
- f = Ref. 14, 31

COMPARISON OF TWO DATA PROCESSING TECHNIQUES FOR OPTICAL ARRAY PROBES

by

Ray Hobbs and Brian Morrison
Aeromet, Inc., Tulsa OK

Russell Ashenden
University of Wyoming, Laramie WY

Robert Ide
NASA Lewis Research Center, Cleveland OH

Abstract

The liquid water content (LWC) and median volume diameter (MVD) are parameters used in aircraft icing tests and are primarily derived from measurements made with a Forward Scattering Spectrometer Probe (FSSP) and Optical Array Probes (OAPs)¹. Data from OAPs can be reduced in more than one way and the technique used to reduce the data can affect the derived LWC and MVD values. Two methods are described for reducing OAP data; one method is given in the manufacturer's manuals and is referred to as the *PMS processing technique* and the other is based on Baumgardner (1987) and is referred to as the *NCAR processing technique*. For comparison, three different drop size distributions are examined using these two techniques; these were produced by, an icing wind tunnel, an airborne water spray array, and natural clouds. The results are compared and the accuracies of each technique for determining the LWC and MVD are discussed.

Introduction

Recently, there has been interest in accurately measuring the drop size distribution in freezing drizzle, a potentially hazardous flight condition. Two frequently derived parameters from a drop size distribution are the liquid water content (LWC) and the median volume diameter (MVD). Drop size distributions can be measured with an FSSP, and OAPs such as a one-dimensional cloud (1D-C) probe and a two-dimensional cloud (2D-C) probe.

The methods used to reduce the OAP data affect the values of the LWC and MVD. Two processing techniques are compared: one technique is given in the Particle Measuring Systems Inc. (PMS) manuals (e.g., PMS, 1985) which is based on Knollenberg (1970) and is referred to as the *PMS processing technique*. The other technique is based on Baumgardner (1987) and is referred to as the *NCAR processing technique*.

¹ These probes are manufactured by Particle Measuring Systems (PMS), Inc., Boulder Co.

The purpose of this work is to examine these two processing techniques and give an assessment of which produces more reasonable values of LWC and MVD. The reasonableness is determined by which technique gives a better fit of the OAP data with the FSSP data where the two probe ranges overlap. Three data sets are processed to investigate their generality. These data include: an example of a cloud produced by the NACA Lewis icing tunnel, an icing cloud produced the U. S. Air Force NKC-135A water spray tanker and measured by Aeromet's Learjet, and two natural freezing drizzle clouds measured by the University of Wyoming's King Air.

Determining the Drop Size Distribution

Figure 1 is a diagrammatic view showing how the OAP detects and sizes drops. Drops are sized as they traverse a laser beam and shadow a photodiode array. Drop diameters are determined by the number of photodiodes occulted.

The drop concentration (N_i) for a given drop diameter (D_i) measured using an OAP is given by.

$$N_i = \frac{n_i}{V_i} = \frac{n_i}{DOF_i \cdot w_i \cdot s \cdot \Delta t} \quad 1$$

where n_i is the number of drops in a given size bin (i) having an average diameter of D_i , and V_i is the sample volume. The sample volume (V_i) is determined by the probe's depth-of-field (DOF_i) over which the particle can be accurately sized, the effective optical array width (w_i)², the sampling speed (s) of the probe³, and the time interval over which the sample was taken (Δt). The DOF_i is a function of D_i .

Of the parameters in Equation 1, determining the value of the DOF_i presents the most difficulty. Herein lies one of the differences between the PMS and NCAR processing techniques. We will focus on the DOF_i calculation.

PMS Processing Technique

Steps in processing OAP data using the PMS processing technique include determining:

1. The mean drop diameter for each size bin (D_i)⁴,
2. The depth-of-field (DOF_i) for each D_i ,
3. The effective array width (w_i).

² The effective array width (w_i) has the notation EAW in the PMS manuals.

³ This is taken as the true airspeed (TAS).

⁴ The size bin for the 1D-C probe is the number of photodiodes occulted. This is also the case for a 2D-C probe when the data are processed like a 1D-C probe.

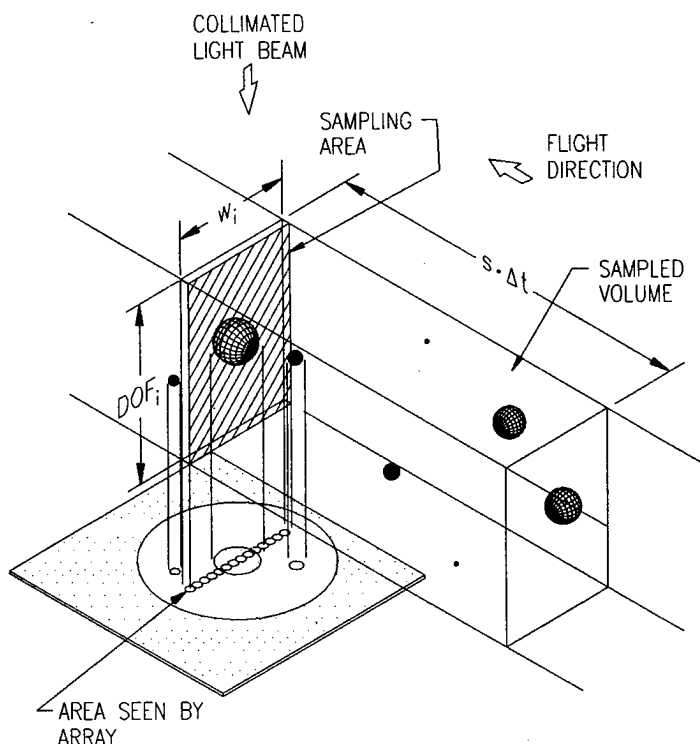


Figure 1 Diagrammatic View of the Optical Array Probe (OAP) Detecting and Sizing Drops.

Symbols shown include the depth-of-field (DOF_i), the array width (w_i), and the length of the sample which is the product of sampling speed and the time interval over which the sample was taken ($s \cdot \Delta t$) [figure taken from PMS (1985)].

A spreadsheet is given in **Table 1** detailing the steps for processing the data using this technique⁵. For example, columns C and E in **Table 1** give the drop size range (normalized to the bin spacing) for the 1D-C (OAP-200X) and column F gives the mean drop diameter (D_i , μm).

The mean drop diameter is determined by the average of the smallest and largest drop size placed in that bin and is used to calculate DOF_i and the liquid water content per bin (LWC_i), and.

The DOF is given by Knollenberg (1970) as:

$$DOF = \frac{Zr^2}{\lambda} \quad 2$$

⁵ The spreadsheet enables the details of the calculations to be followed. It is from the NKC-135A tanker distribution sampled on 960418. The values of dN/dD (Column R) are plotted in Figure 5 and $dLWC/dD$ in Figure 6.

Table 1: PMS Processing Technique - Tanker Distribution

	A	B	C	D	E	F	G	H	I	J	K	L
1	1D-C	Nominal				Average	Size	Drop		Probability		Width
2	Diodes	Diameter	non-	dimensional	diameter	Diameter	Interval	Count		Correction	Corrected	of Field
3	Occulted	D (μ m)	LO	Average	HI	(D _i)	(δ D _i)	(n _i)	DOF _i	Factor	DOF _i	24
4	(i)	20	(i)	(i)	(i)	μ m	mm		mm		mm	Diodes
5												
6	1	20	0.710	1.205	1.700	24.1	19.8	59	1.45	0.26	0.38	22
7	2	40	1.700	2.195	2.690	43.9	19.8	346	4.82	0.62	2.99	21
8	3	60	2.690	3.185	3.680	63.7	19.8	589	10.14	0.89	9.03	20
9	4	80	3.680	4.175	4.670	83.5	19.8	834	17.43	1.00	17.43	19
10	5	100	4.670	5.165	5.660	103.3	19.8	799	26.68	1.00	26.68	18
11	6	120	5.660	6.150	6.640	123.0	19.6	614	37.82	1.00	37.82	17
12	7	140	6.640	7.130	7.620	142.6	19.6	447	50.84	1.00	50.84	16
13	8	160	7.620	8.115	8.610	162.3	19.8	300	61.00	1.00	61.00	15
14	9	180	8.610	9.105	9.600	182.1	19.8	144	61.00	1.00	61.00	14
15	10	200	9.600	10.095	10.590	201.9	19.8	75	61.00	1.00	61.00	13
16	11	220	10.590	11.075	11.560	221.5	19.4	47	61.00	1.00	61.00	12
17	12	240	11.560	12.055	12.550	241.1	19.8	21	61.00	1.00	61.00	11
18	13	260	12.550	13.040	13.530	260.8	19.6	16	61.00	1.00	61.00	10
19	14	280	13.530	14.025	14.520	280.5	19.8	6	61.00	1.00	61.00	9
20	15	300	14.520	15.010	15.500	300.2	19.6	5	61.00	1.00	61.00	8
21								Total				
22	Date	960418	Time Int.	19:03:30	19:03:38	Δt (s)=	7.4	4302				

	M	P	Q	R	S	T	U	V	W
1	Width	Sample	Concen-				0.1688		HI
2	of Field	Volume	tration				SUM	Acc.	Diameter
3	(w _i)	(V _i)	(N _i)	dN/dD	d(LWC)/dD	LWC _i	LWC	Fraction	(D _i)
4	mm	m ³	m ⁻³	m ⁻⁴	g m ⁻³ μ m ⁻¹	g/m ³	g/m ³	of LWC	μ m
5									
6	0.44	1.31E-04	4.50E+05	2.27E+10	1.67E-04	0.0033			34.0
7	0.42	9.90E-04	3.50E+05	1.77E+10	7.82E-04	0.0155			53.8
8	0.40	2.85E-03	2.07E+05	1.04E+10	1.41E-03	0.0280			73.6
9	0.38	5.22E-03	1.60E+05	8.06E+09	2.46E-03	0.0487	0.2175	0.384	93.4
10	0.36	7.58E-03	1.05E+05	5.33E+09	3.07E-03	0.0609	0.2783	0.491	113.2
11	0.34	1.01E-02	6.05E+04	3.09E+09	3.01E-03	0.0590	0.3373	0.595	132.8
12	0.32	1.28E-02	3.48E+04	1.78E+09	2.70E-03	0.0529	0.3902	0.689	152.4
13	0.30	1.44E-02	2.08E+04	1.05E+09	2.35E-03	0.0465	0.4367	0.771	172.2
14	0.28	1.35E-02	1.07E+04	5.40E+08	1.71E-03	0.0338	0.4705	0.830	192.0
15	0.26	1.25E-02	5.99E+03	3.03E+08	1.30E-03	0.0258	0.4963	0.876	211.8
16	0.24	1.15E-02	4.07E+03	2.10E+08	1.19E-03	0.0232	0.5195	0.917	231.2
17	0.22	1.06E-02	1.98E+03	1.00E+08	7.35E-04	0.0146	0.5340	0.942	251.0
18	0.20	9.62E-03	1.66E+03	8.48E+07	7.88E-04	0.0154	0.5495	0.970	270.6
19	0.18	8.66E-03	6.93E+02	3.50E+07	4.04E-04	0.0080	0.5575	0.984	290.4
20	0.16	7.70E-03	6.49E+02	3.31E+07	4.69E-04	0.0092	0.5667	1.000	310.0
21									
22					LWC =	0.3979	MVD =	114.9	

where r is the drop radius, λ is the laser wavelength, and Z is a factor dependent on the amount of light intensity reduction required for the photodiode array to detect the presence of a drop. For a coherent laser light source with a 60% reduction in light intensity, Z was found to be approximately 6. For the 1D-C probe a 67% reduction in the light intensity is required for the probe to detect to drop. However, after the drop is detected, the probe sizes the drop using a 50% reduction in light intensity. The 2D-C requires a 50% reduction in light intensity to initially detect and subsequently size a drop⁶.

⁶ In Knollenberg (1970) the threshold level required for drop detection by the photodiode array is expressed as a percentage of the maximum shadowing that can occur. For example, a 40% threshold is equivalent to a 60% loss in the unobstructed light intensity on the photodiode array.

From the OAP manuals (e.g.: PMS, 1985), the depth-of-field for both the 1D-C and 2D-C probes is given as:

$$\text{DOF} = 10 \bullet r^2 \quad 3$$

where the drop radius r and the DOF are in μm . **Figure 2** shows the DOF as a function of D . The DOF is also limited by the physical distance between the arms of the probe (approximately 61 mm).

Arranging Equation 4 in the same form as Equation 3 for $\lambda = 0.6328 \mu\text{m}$ (the wavelength of the He-Ne laser used in the OAPs) gives:

$$\text{DOF} = \frac{6.328 \bullet r^2}{\lambda} \quad 4$$

The value of Z recommended in the PMS OAP manuals for determining DOF is approximately 5% greater than given in Knollenberg (1970).

The value of the DOF as a function of mean drop diameter is given in **Table 1**, Column I. For the 1D-C probe, PMS uses a probability correction factor to adjust the value of the DOF for the first three bin sizes (Column J). This factor is multiplied by the value of the DOF determined from Equation 4 to obtain the corrected value of the DOF (Column K)⁷.

The effective array width, w_i , is given in PMS (1985) as:

$$w_i = (n_e - 1 - i) \bullet l_e \quad 5$$

where n_e is the number of photodiodes in the array (24 for the OAP-200X probe used in **Table 1**), i is the number of photodiodes occulted (column A), and l_e is the resolution of the probe (20 μm for the probe used in this example). Column M lists the effective array width in mm.

The DOF_i and w_i , along with the sampling speed (s) and sample time interval (Δt), enable calculation of the sample volume (V_i) for each drop diameter (D_i) (**Table 1**, Column P). Using the drop counts for each bin (Column H) and V_i the drop concentration (N_i) is determined using Equation 1 (Column Q). The liquid water content for each bin (LWC_i) is determined using:

$$\text{LWC}_i = \frac{\rho\pi}{6} N_i D_i^3 \quad (\text{Column T}) \quad 6$$

⁷ Knollenberg, J. K. (private communication, April 1996) recommends that the probability correction factor be applied to processing the 2D-C data, however, not all the 2D-C manuals have this correction applied to the DOFs (e.g.: PMS, 1984).

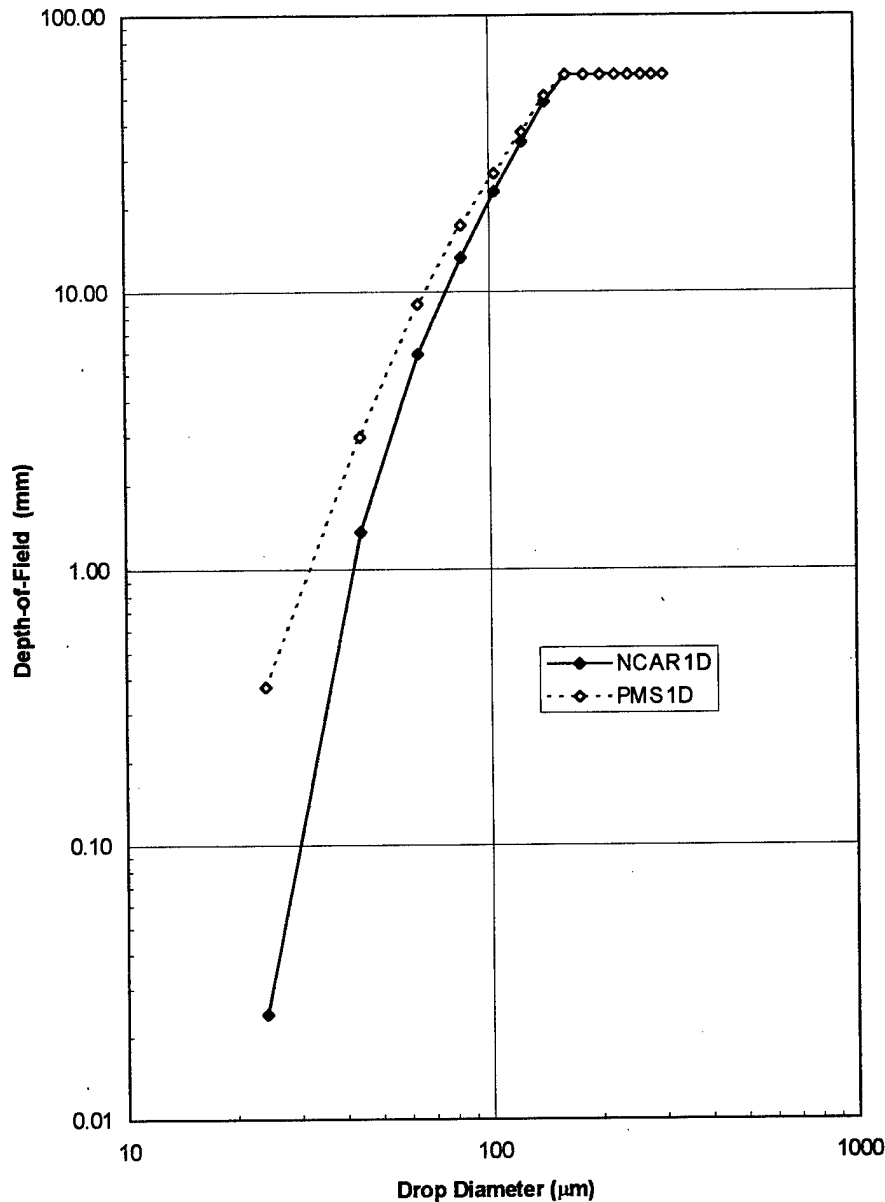


Figure 2 Depth-of-Field (DOFi) versus Drop Diameter for the 1D-C (OAP-200X).
 The “◇” symbol is for DOF_i calculated using the PMS processing technique and the “◆” symbol is for DOF_i calculated using the NCAR processing technique ($TAS = 106.6$ m/s, $\tau = 0.35$ μs, $C = 0.5$).

where ρ is the density of water. The total LWC is given by summing Equation 6 over i^8 . The MVD is determined from the cumulative LWC and is the diameter where the cumulative LWC is equal to the half of the total LWC.

⁸ This equation assumes that there is no overlap or gap in the measured drop size distribution using the FSSP or OAPs. If there is, the effect on the LWC needs to be taken into account.

NCAR Processing Technique

Baumgardner (1987) introduced three processing techniques for reducing the data from the OAPs. These included:

1. Correcting the depth-of-field (DOF_i) for the response time (τ) of the OAP electronics,
2. Accounting for how the amount of light intensity reduction for particle detection affects the DOF_i ,
3. Correcting for undersizing the drop due to the discrete nature of the photodiode array.

Each of these techniques can result in a large change in the calculated drop concentration (N_i) and thus a large change in the LWC. Applying all three techniques can cause more than a factor of two increase in the LWC as compared to using the PMS processing technique (Hobbs and Morrison, 1995).

Correcting the DOF for τ has resulted in improving the agreement between the FSSP, 1D-C and 2D-C. This technique is described in detail and the effect on the application of the other two techniques is discussed. A spreadsheet with processed values from OAP-200X data using the NCAR technique for correcting the DOF for the response time (τ) is given in **Table 2**.

Baumgardner (1987) found from experiment that Z in Equation 2 can be empirically determined using the following expression:

$$Z = 30.46 - 0.628F + 0.003246F^2 \quad (\text{Table 2, Column L}) \quad 7$$

where F is given by:

$$F = \frac{100 \cdot C}{1 - e^{-f}} \quad (\text{Column K}) \quad 8$$

where C is the light intensity reduction required for the probe to detect a drop⁹ and f is the ratio of the transit time of a drop crossing the array (t_i) to the response time of the probe (τ) and is given by:

$$f = \frac{t_i}{\tau} \quad (\text{Column I}) \quad 9$$

The transit time (t_i) for the image of the drop to cross the array is¹⁰:

$$t_i = \frac{D_i}{s} \quad (\text{Column G}) \quad 10$$

⁹ Nominal values of C are 0.67 for those OAPs with a secondary threshold (e.g., OAP-200X) and 0.5 for those having a single threshold (e.g., OAP 2D-C). However, for this study a value of 0.5 is used for both the 1D-C and 2D-C.

¹⁰ This assumes the photodiode in the array is infinitely small.

where D_i is the diameter of the drop (column B) and s is the sampling speed. The transit time (t_i) represents a characteristic time the photodiode array is occulted. τ is the time it takes for a signal to reach $1 - e^{-1}$ (or 63.2 %) of its final value and needs to be measured for each probe.

Table 2 NCAR Processing Technique - Tanker Distribution

	A	B	C	D	E	G	H	I	J	K	L	M
1	1D-C	Nominal	Size	Drop	Drop	Transit	Ratio	$\tau =$	C =			
2	Dioles	Size (D)	Interval	Radius	Counts	Time	$t_i/\tau =$	0.35	0.50			
3	Occulted	Dia (μm)	(d Di)	(r_i)	(n_i)	(t_i)	f	FRAC	FRC	F	Z	Z
4	(i)	20	mm	mm		μs						
5												
6	1	24.1	19.8	0.0121	59	0.23	0.65	0.4758	1.00	100.00	0.1200	0.1058
7	2	43.9	19.8	0.0220	346	0.41	1.18	0.6917	0.72	72.29	2.0254	1.7863
8	3	63.7	19.8	0.0319	589	0.60	1.71	0.8186	0.61	61.08	4.2127	3.7154
9	4	83.5	19.8	0.0418	834	0.78	2.24	0.8933	0.56	55.97	5.4793	4.8325
10	5	103.3	19.8	0.0517	799	0.97	2.77	0.9373	0.53	53.35	6.1958	5.4644
11	6	123.0	19.6	0.0615	614	1.15	3.30	0.9630	0.52	51.92	6.6040	5.8244
12	7	142.6	19.6	0.0713	447	1.34	3.82	0.9781	0.51	51.12	6.8397	6.0323
13	8	162.3	19.8	0.0812	300	1.52	4.35	0.9871	0.51	50.65	6.9780	6.1543
14	9	182.1	19.8	0.0911	144	1.71	4.88	0.9924	0.50	50.38	7.0594	6.2261
15	10	201.9	19.8	0.1010	75	1.89	5.41	0.9955	0.50	50.22	7.1071	6.2681
16	11	221.5	19.4	0.1108	47	2.08	5.94	0.9974	0.50	50.13	7.1349	6.2926
17	12	241.1	19.8	0.1206	21	2.26	6.46	0.9984	0.50	50.08	7.1513	6.3071
18	13	260.8	19.6	0.1304	16	2.45	6.99	0.9991	0.50	50.05	7.1610	6.3157
19	14	280.5	19.8	0.1403	6	2.63	7.52	0.9995	0.50	50.03	7.1668	6.3207
20	15	300.2	19.6	0.1501	5	2.82	8.05	0.9997	0.50	50.02	7.1701	6.3237
21					Total							
22					4302							
23												
24	Date =	960418	Time Int =	19:03:30	19:03:38							
25		TAS(m/s)	106.60	Δt (s) =	7.4							

	N	O	P	R	U	V	W	Y	Z	AA	AB	AC
1					Sample	Concen-				0.1439		HI
2		DOF	PMS	EAW	Volume	tration				SUM	Acc.	Diameter
3	DOF	(d)	DOF	(w_i)	(V_i)	(N_i)	dN/dD	d(LWC)/dD	LWC _i	LWC	Fraction	(Di)
4	mm	mm	mm	mm	m ³	m ³	m ⁴	g m ⁻³ μm^{-1}	g/m ³	g/m ³	of LWC	mm
5												
6	0.02	0.02	0.38	0.44	8.427E-06	7.001E+06	3.536E+11	2.591E-03	0.0513			34.0
7	1.36	1.36	2.99	0.42	4.505E-04	7.680E+05	3.879E+10	1.718E-03	0.0340			53.8
8	5.95	5.95	9.03	0.40	1.879E-03	3.135E+05	1.583E+10	2.143E-03	0.0424			73.6
9	13.31	13.31	17.43	0.38	3.989E-03	2.091E+05	1.056E+10	3.218E-03	0.0637	0.2077	0.362	93.4
10	23.03	23.03	26.68	0.36	6.541E-03	1.222E+05	6.169E+09	3.561E-03	0.0705	0.2782	0.484	113.2
11	34.81	34.81	37.82	0.34	9.335E-03	6.577E+04	3.356E+09	3.270E-03	0.0641	0.3422	0.596	132.8
12	48.45	48.45	50.84	0.32	1.223E-02	3.655E+04	1.865E+09	2.831E-03	0.0555	0.3977	0.693	152.4
13	64.03	61.00	61.00	0.30	1.444E-02	2.078E+04	1.050E+09	2.349E-03	0.0465	0.4443	0.774	172.2
14	81.55	61.00	61.00	0.28	1.347E-02	1.069E+04	5.398E+08	1.707E-03	0.0338	0.4780	0.832	192.0
15	100.93	61.00	61.00	0.26	1.251E-02	5.995E+03	3.028E+08	1.305E-03	0.0258	0.5039	0.877	211.8
16	121.95	61.00	61.00	0.24	1.155E-02	4.070E+03	2.098E+08	1.194E-03	0.0232	0.5270	0.918	231.2
17	144.82	61.00	61.00	0.22	1.059E-02	1.984E+03	1.002E+08	7.352E-04	0.0146	0.5416	0.943	251.0
18	169.68	61.00	61.00	0.20	9.624E-03	1.663E+03	8.482E+07	7.878E-04	0.0154	0.5570	0.970	270.6
19	196.44	61.00	61.00	0.18	8.661E-03	6.927E+02	3.499E+07	4.043E-04	0.0080	0.5650	0.984	290.4
20	225.11	61.00	61.00	0.16	7.699E-03	6.494E+02	3.313E+07	4.694E-04	0.0092	0.5742	1.000	310.0
21												
22										MVD =	116.0	

To compare the NCAR and PMS techniques only for the effect of accounting for the response time (τ) of the probes, the value of Z in Equation 7 is given the value of 6.328 when $C = 0.5$ and $\tau = 0$. This constant (6.328) is that given in Equation 4 for the PMS technique. This allows the two techniques to have the same DOFs for large drops or at

slow sampling speeds, when the response time of the probe does not have a significant effect on the DOF.

For $C = 0.5$ and $\tau = 0$, the value of F is 50 in Equation 8 and from Equation 7, $Z = 7.175$. The modified value of Z is designated by Z' and is given by:

$$Z' = Z \cdot \frac{6.328}{7.175} \quad (\text{Column M}) \quad 11$$

Z' is used in Equation 3 to determine the DOF for the NCAR processing technique. Using Equation 11 in 7 forces the DOF for the NCAR technique to be the same as the DOF for the PMS technique for large drops or slow sampling speeds. This is a reasonable correction to Z because there was much scatter ($\sim 20\%$) in the data used in determining the coefficients in Equation 7.

Data Examples

The purpose of processing three different data sets is to see if correcting for the time response of the OAPs using the NCAR processing techniques improves the agreement between the FSSP and OAPs¹¹. The techniques are processed as follows:

PMS processing technique:

1. The average drop diameters that are used for the OAPs (both 1D-C and 2D-C) are those given in the PMS OAP manuals (e.g., PMS, 1984 and 1985).
2. The probability correction factor for the smallest three bins is applied to calculating the DOF for the 1D-C but not for the 2D-C.

NCAR processing technique:

1. The response time (τ) used in Equation 9 for processing the data from the three 1D-Cs is set to $0.35 \mu\text{s}$ ¹².
2. The value of the threshold detection (C) used in Equation 8 is set to 0.5 for both 1D-C and 2D-C probes. This is the nominal value for the 2D-C but is used for the 1D-C to enable both probes to have the same DOFs as recommended by PMS¹³. There are two reasons for doing this; measured values of τ and C for the probes used in this study are

¹¹ It needs to be pointed out that the NCAR technique as described by Baumgardner (1987) has three distinct processing algorithms and by only using one algorithm may not be using the NCAR technique as intended.

¹² The value of τ estimated from Figure 1 in Knollenberg (1995) for the Aeromet OAP (S/N 735-0678-09) was $0.3 \mu\text{s}$ but a value of $0.35 \mu\text{s}$ gives a slightly better fit of the drop size distributions between the FSSP and the 1D-C for the tanker spray plume. This value is used for the NASA and Wyoming 1D-C probes.

¹³ John Knollenberg (private communication) and PMS (1994 and 1995).

not available and only the response time correction is being investigated in the NCAR processing technique and therefore we want the drop size distribution to be the same for large drop when processed with either method.

3. The average drop diameters for the 1D-C and 2D-C are calculated the same as for the PMS processing technique and the counts in any measured bin are processed for that bin size¹⁴.

The data will be presented as follows: 1) NASA Icing Tunnel, 2) U. S. NKC-135A spray plume, and 3) Wyoming's natural cloud data. The order is from the most controlled conditions where the drop size distribution should be easily understood to a natural condition which can have much complexity.

Icing Tunnel Distribution

The first example is an icing cloud produced in the NASA Lewis Icing Tunnel. The drop size distribution was measured with the FSSP and 1D-C. **Figure 3** shows the relationship between drop concentration per unit size interval (dN/dD) and drop diameter (D). Three curves are shown and are designated as follows: FSSP (\square), 1D-C processed using the PMS technique (\diamond) and NCAR technique (\blacklozenge).

The 1D-C underestimates the concentration (dN/dD) using the PMS technique (\diamond) as compared to the FSSP concentration (\square) where their sizes overlap. For drop diameters less than 100 μm there appears to be a "roll off" in the calculated 1D-C concentration.

There is good agreement of dN/dD values between the FSSP and 1D-C using the NCAR technique (\blacklozenge). This indicates that correcting for the response time improves the agreement between these two probes which implies that the accuracy of the OAP is improved.

Figure 4 shows the relationship between the liquid water content per unit size interval ($dLWC/dD$) and D for the three curves presented in **Figure 3**. The NCAR processing technique did not show a significant decrease in $dLWC/dD$ in the 1D-C for drop diameters less than 100 μm . As a result the liquid water content (LWC) from the NCAR processing technique is higher (approximately 7%) than that calculated using the PMS technique (**Table 3**). The median volume diameter (MVD) for the NCAR technique is smaller (approximately 8%) than calculated from the PMS technique because of the increase in $dLWC/dD$ between 40 and 100 μm ¹⁵.

¹⁴ Baumgardner (1987) recommends shifting the counts up one bin to correct for undersizing. This causes an increase in the LWC and MVD calculated from the OAPs.

¹⁵ The LWC is larger using the NCAR technique compared to the PMS technique because of the increase in $dLWC/dD$, however the effect on the value of the MVD is dependent on the shape of the

Table 3: Summary of the Calculated Values of LWC and MVD for Three Examples: NASA Lewis Icing Tunnel, U. S. Air Force NKC-135A Spray Tanker, and natural clouds, one with a small MVD and one with a large MVD (freezing drizzle).

Data	Tech.	LWC ¹⁶	MVD	FSSP	1D-C
Icing Tunnel	PMS	0.59	102	2-47	55.2-458
Icing Tunnel	NCAR	0.63	94	2-41	40.4-458
Tanker	PMS	0.56	115	5-77	73.6-310
Tanker	NCAR	0.60	116	5-65	73.6-310
Natural Cloud (small MVD)	PMS	0.19	25.8	2-44	46-194
Natural Cloud (small MVD)	NCAR	0.20	26.4	2-44	46-194
Natural Cloud (large MVD) ¹⁷	PMS	0.43	106	2-38	46-300
Natural Cloud (large MVD)	NCAR	0.49	98	2-35	33.6-300

Water Spray Tanker Distribution

The second example is an artificial cloud produced by the U. S. Air Force NKC-135A Tanker. This cloud was generated to simulate freezing drizzle. **Figure 5** shows the relationship between dN/dD and D . Five curves are shown and are designated as follows: FSSP (\square), 1D-C processed using the PMS technique (\diamond) and NCAR technique (\blacklozenge) and 2D-C processed using the PMS technique (\circ) and the NCAR technique (\bullet). In addition, dashed lines designate PMS processing and solid lines designate NCAR processing.

The processing technique that gives the more accurate results will be determined by the best continuous agreement between the FSSP size range (6 to 95 μm) and the OAP size range (1D-C: 24.1 to 300.2 μm , and the 2D-C: 30.1 to 750 μm ¹⁸). It is assumed that the drop size distribution (dN/dD versus dD) produced by the Tanker is strictly monotonically decreasing with increasing drop diameter.

For the 1D-C there is an underestimation of the concentration (dN/dD) using the PMS technique (\diamond) as compared with the FSSP concentration (\square) where the sizes overlap. For drop diameters less than 100 μm there appears to be a distinct "roll off" in the calculated 1D-C concentration. There is good agreement between dN/dD from the FSSP and 1D-C using the NCAR technique (\blacklozenge). As in the icing tunnel case, this indicates that correcting for the response time improves the accuracy of the calculation.

drop size distribution. When the MVD is small (<50 μm) the MVD is increased using the NCAR technique whereas when the MVD is large (> 100 μm) the calculated MVD is decreased.

¹⁶ Minor corrections are applied to the LWC to account for either gaps or overlaps in the FSSP and 1D-C drop size distribution in calculating the LWC. However, the MVD is not corrected for this effect.

¹⁷ The water content measured with the 2D-C is used both for the PMS and NCAR technique in calculating the LWC and MVD.

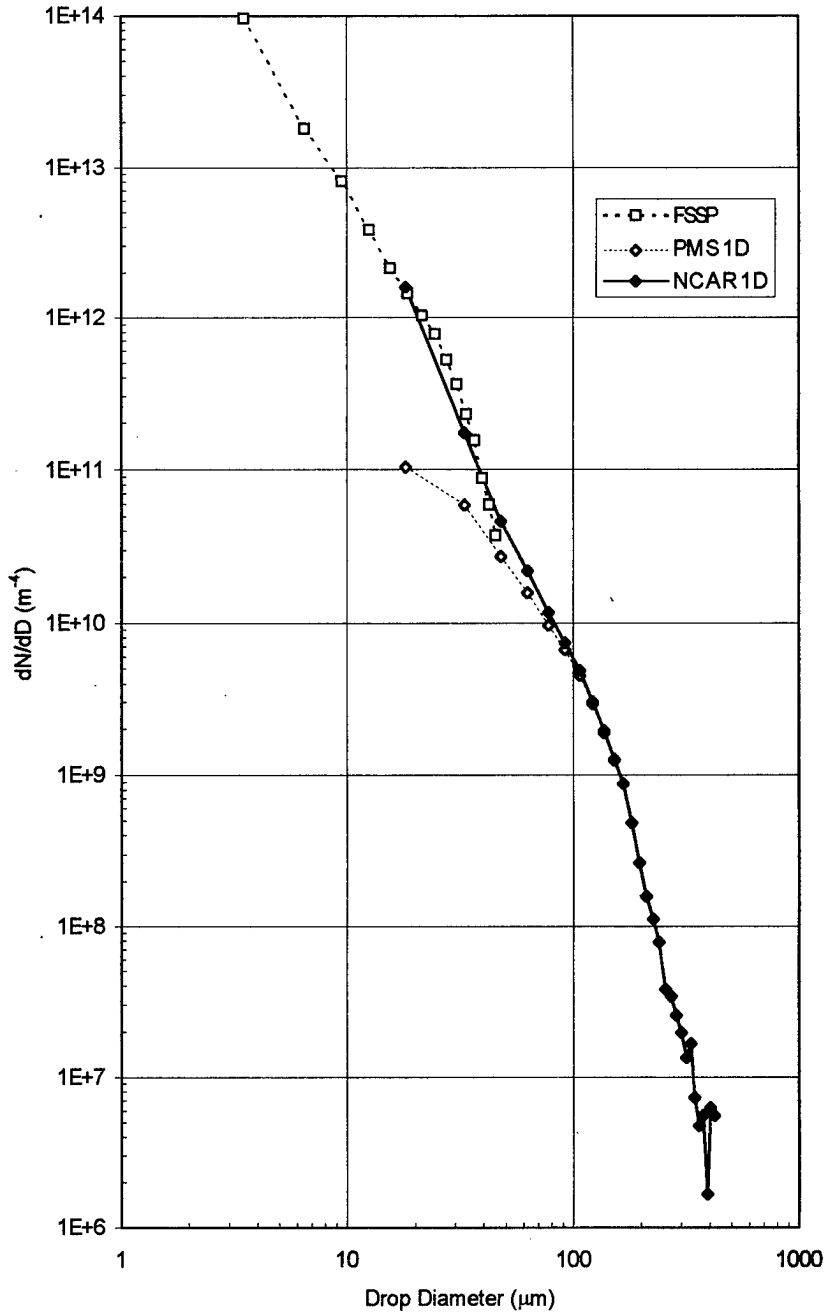


Figure 3 dN/dD versus D produced from the NASA Lewis Icing Tunnel.

Five curves are shown and are designated as follows: FSSP (\square), 1D-C processed using the PMS technique (\diamond) and NCAR technique (\blacklozenge). In addition, dashed lines designate PMS processing and solid lines designate NCAR processing.

¹⁸ This is the maximum size usable from the 2D-C when processed like a 1D-C, that is the drop diameter is determined by the number of photodiodes shadowed.

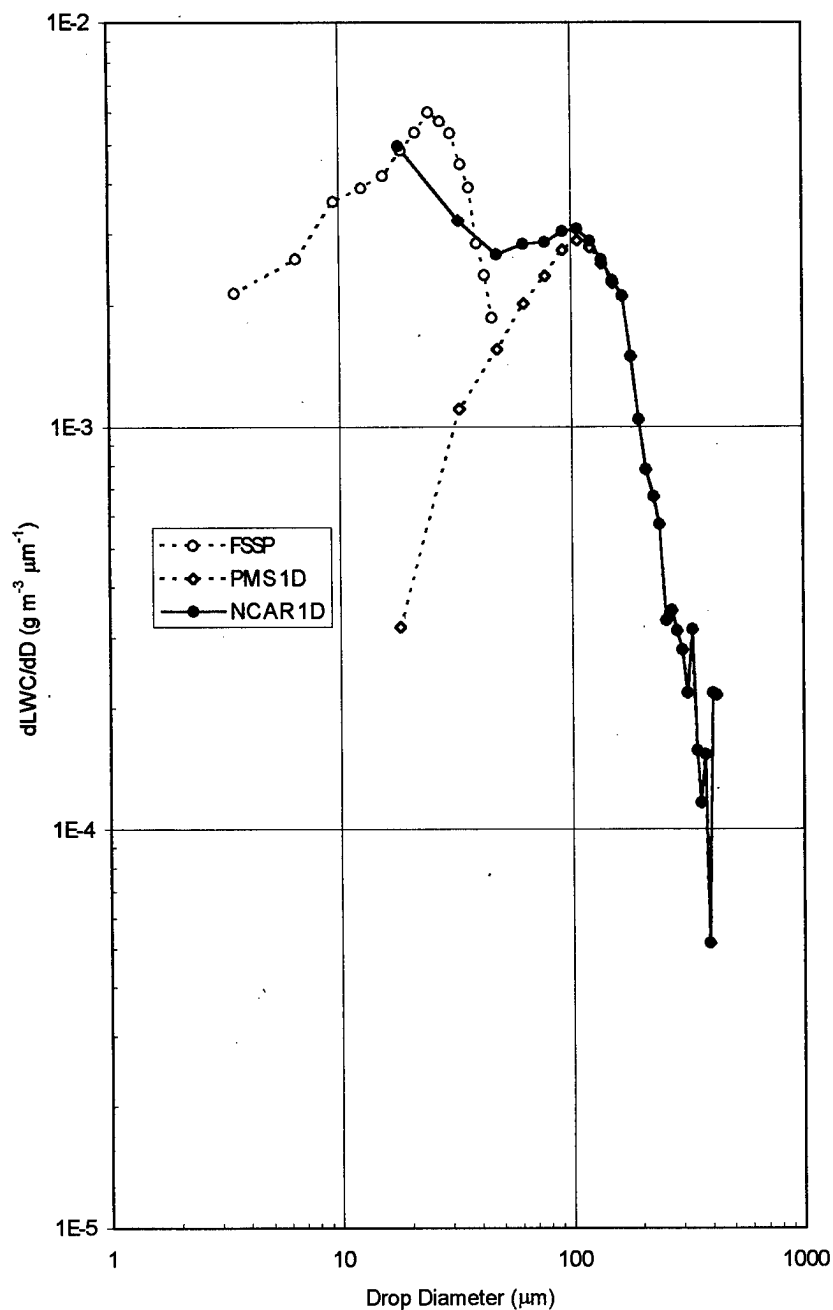


Figure 4 dLWC/dD versus D produced from the NASA Lewis Icing Tunnel.
Five curves are shown and are designated as follows: FSSP (\square), 1D-C processed using the PMS technique (\diamond) and NCAR technique (\blacklozenge). In addition, dashed lines designate PMS processing and solid lines designate NCAR processing.

The 2D-C concentrations calculated from the PMS technique¹⁹ (\circ) are greater than the FSSP and 1D-C (NCAR technique) for diameters less than 125 μm ²⁰. However, the slope

¹⁹ N.B., the probability correction factor is set to 1 for the first three bin sizes.

of the distribution follows that of the FSSP. Also, the PMS 2D-C concentration does not “roll off” like the PMS 1D-C concentration. The PMS 2D-C concentration being greater than the FSSP concentration could be a result of the 2D-C data being taken closer to the spray array than the FSSP and 1D-C data. The measured small drop concentration is sensitive to distance behind the spray array because of droplet evaporation. This explanation is supported by the observation that the 1D-C and 2D-C concentrations are in good agreement for the larger drop sizes (diameters $> 150 \mu\text{m}$).

A partial explanation of the PMS 2D-C concentration not “rolling off” like the 1D-C concentration may be a result of the two probes having different DOFs for small drops. The 2D-C has a lower threshold of drop detection (50%) than that initially required to trigger the 1D-C (67%) and therefore the 2D-C has a larger DOF than the 1D-C for these smaller drop sizes. However, the DOFs given in the PMS manuals for these two probes are the same for the same drop diameters and if the calculated DOFs for the 2D-C are applied to the 1D-C, the 1D-C concentration could be underestimated.

The 2D-C concentration for small diameter drops determined from the NCAR technique is higher than that from the PMS technique, as is expected. However, it is not in as good agreement with the FSSP and NCAR 1D-C concentrations as are the PMS technique²¹.

Figure 6 shows the relationship between the liquid water content per unit size interval ($d\text{LWC}/dD$) and drop diameter (D) for the five curves presented in **Figure 5**. The liquid water content (LWC) and median volume diameter (MVD) for the drop size distribution from 5 to $310 \mu\text{m}$ is presented in **Table 3** from the distribution using the FSSP and 1D-C processed using both techniques. For this case the calculated LWC is 7 % greater using the NCAR technique and there is only $1 \mu\text{m}$ difference in the MVDs.

Natural Cloud Distribution

Two distributions from natural clouds are presented that were measured with the University of Wyoming’s King Air. One distribution has a moderately small MVD of approximately $26 \mu\text{m}$ and LWC of approximately 0.2 g/m^3 which falls within Appendix C of Federal Aviation Regulation Part 25, but has the presence of large drops around $100 \mu\text{m}$ in diameter which could pose an ice accretion problem to aircraft. The other

²⁰ Before drawing any conclusions it needs to be pointed out that the 2D-C measurements are not taken simultaneously with the FSSP and 1D-C measurements. The spray plume is approximately 2 to 3 m in diameter. The 2D-C is mounted in the Learjet tip tank and the FSSP and 1D-C are mounted mid-span under the wing (Hobbs et al., 1995).

²¹ If the value of C used in Equation 8 is reduced to 0.37 which is 0.75 ($0.5/0.67$) of its original value the agreement between the small drop concentration between the 1D-C and 2D-C improves markedly when processed by the NCAR technique. That curve is not presented because we are only examining the effect of response time (τ) on the calculated concentrations. If the NCAR technique were being implemented according to Baumgardner (1987) C should be set to 0.5 for a 2D-C and 0.67 for the 1D-C.

distribution is broad, with a moderately high LWC of approximately 0.45 g/m^3 and a high MVD of approximately $100 \text{ }\mu\text{m}$. This distribution is discussed by Ashenden and Marwitz (1996).

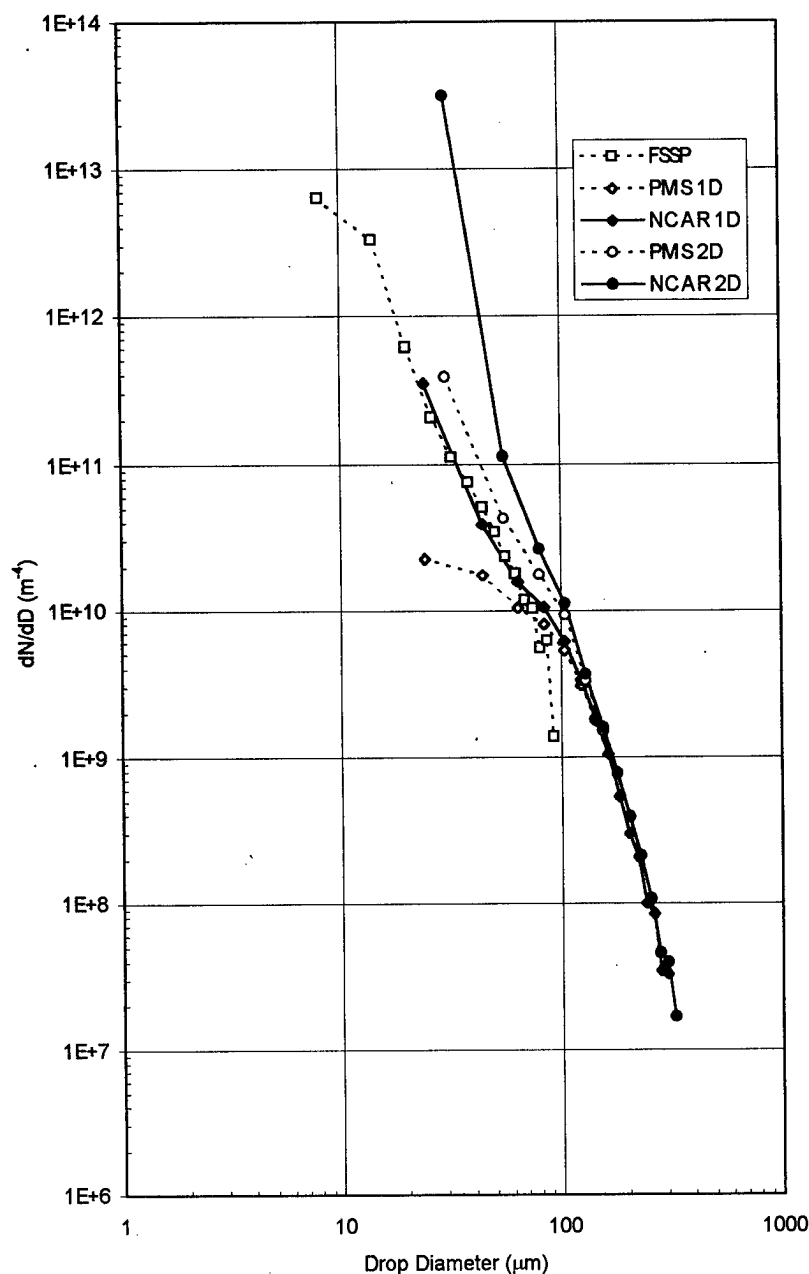


Figure 5 dN/dD versus D produced from the NKC-135A Tanker.

Five curves are shown and are designated as follows: FSSP (\square), 1D-C processed using the PMS technique (\diamond) and NCAR technique (\blacklozenge) and 2D-C processed using the PMS technique (\circ) and the NCAR technique (\bullet). In addition, dashed lines designate PMS processing and solid lines designate NCAR processing. The data were collected on 960418, the FSSP and 1D-C data were collected between 19:03:30.70 and 19:03:38.10 UTC and the 2D-C data were collected between 19:07:32.27 and 19:07:42.87 UTC.

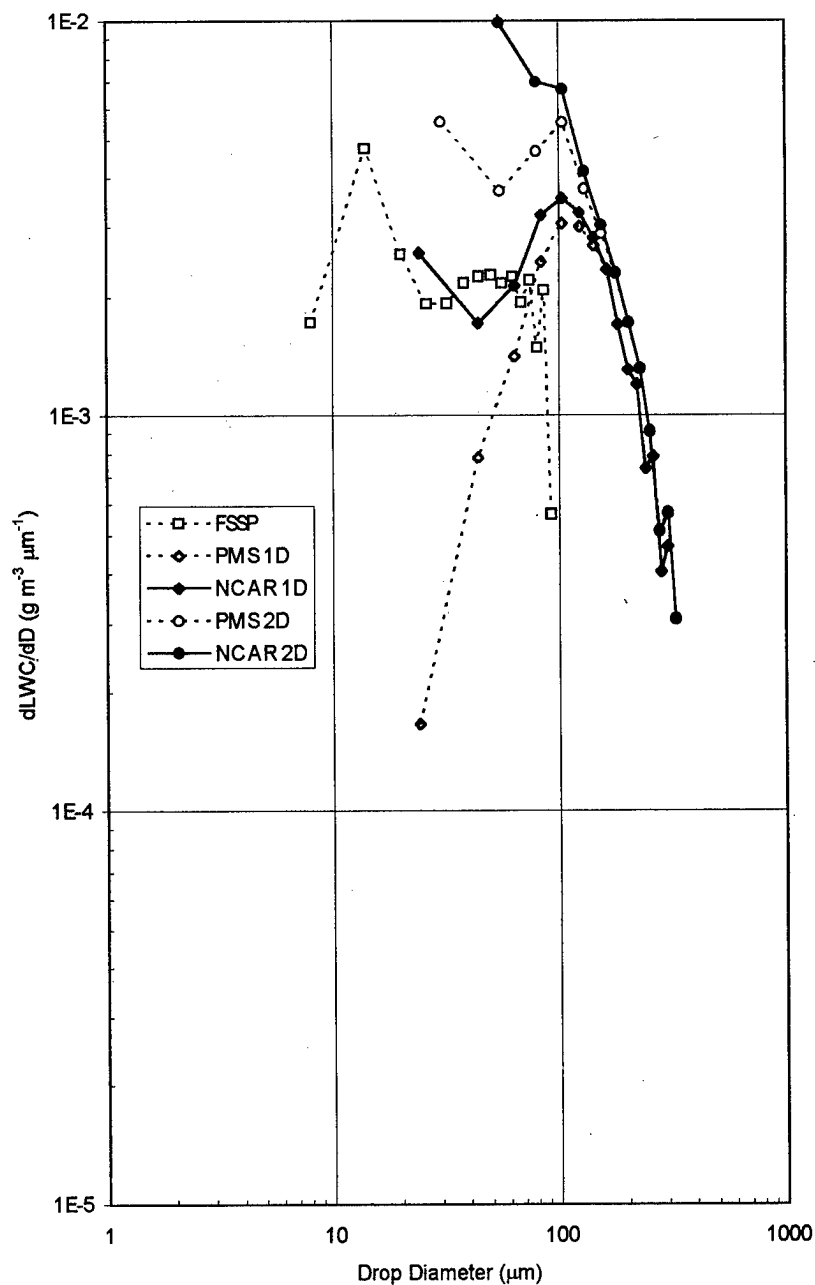


Figure 6 dLWC/dD versus D produced from the NKC-135A Tanker.

Five curves are shown and are designated as follows: FSSP (\square), 1D-C processed using the PMS technique (\diamond) and NCAR technique (\blacklozenge) and 2D-C processed using the PMS technique (\circ) and the NCAR technique (\bullet). In addition, dashed lines designate PMS processing and solid lines designate NCAR processing.

From **Figure 7** there is an underestimation of the 1D-C concentration (dN/dD) using the PMS technique (\diamond) as compared to the FSSP concentration (\square) where their sizes overlap but there is better agreement between dN/dD between the FSSP and 1D-C using the NCAR technique (\blacklozenge).

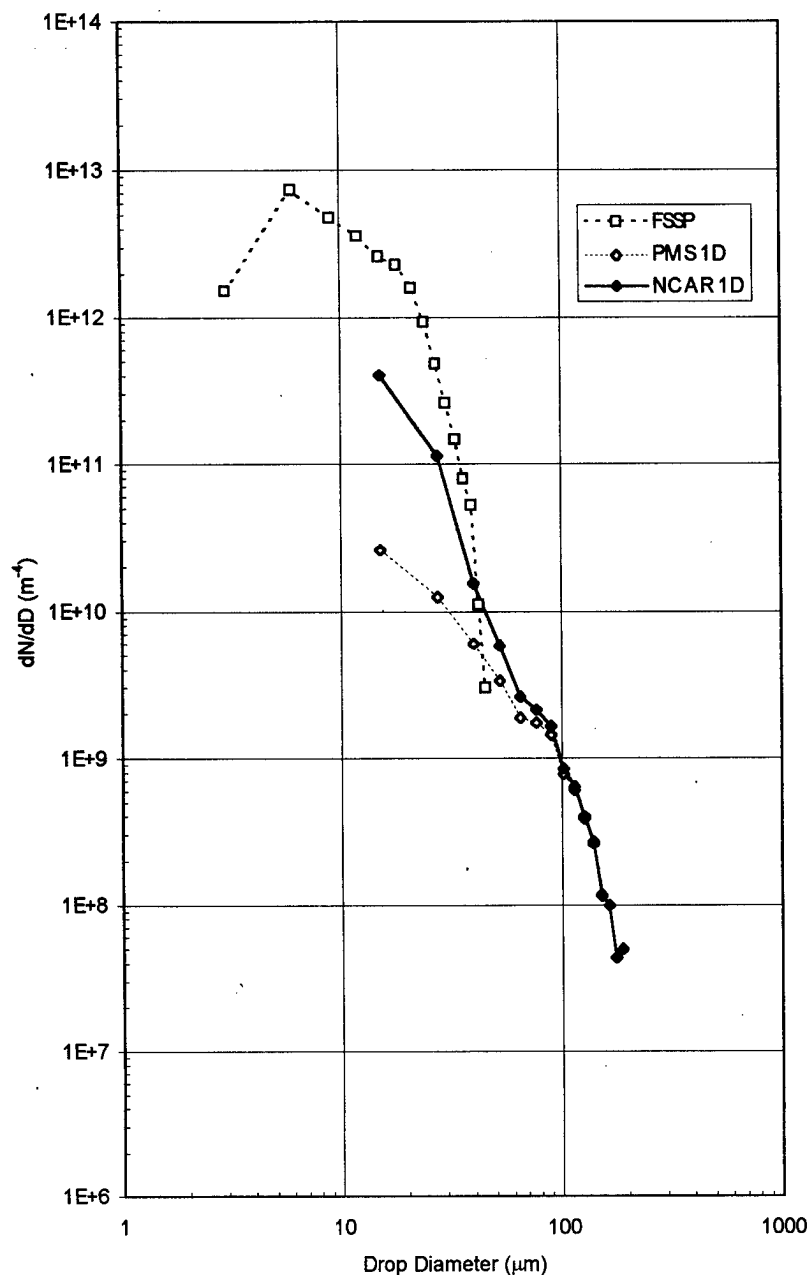


Figure 7 dN/dD versus D produced from Natural Cloud (small MVD).

Five curves are shown and are designated as follows: FSSP (\square), 1D-C processed using the PMS technique (\diamond) and NCAR technique (\blacklozenge) and 2D-C processed using the PMS technique (\circ) and the NCAR technique (\bullet). In addition, dashed lines designate PMS processing and solid lines designate NCAR processing. The data were collected on 940308 between 24:15:27 and 24:15:50 UTC.

Figure 8 shows the relationship between the liquid water content per unit size interval ($dLWC/dD$) and D for the three curves presented in **Figure 7**. The NCAR technique calculated more LWC between approximately 46 and 95 μm than the PMS processing

technique. However, this does not significantly affect the overall LWC or change the MVD much (**Table 3 - Natural Cloud (small MVD)**).

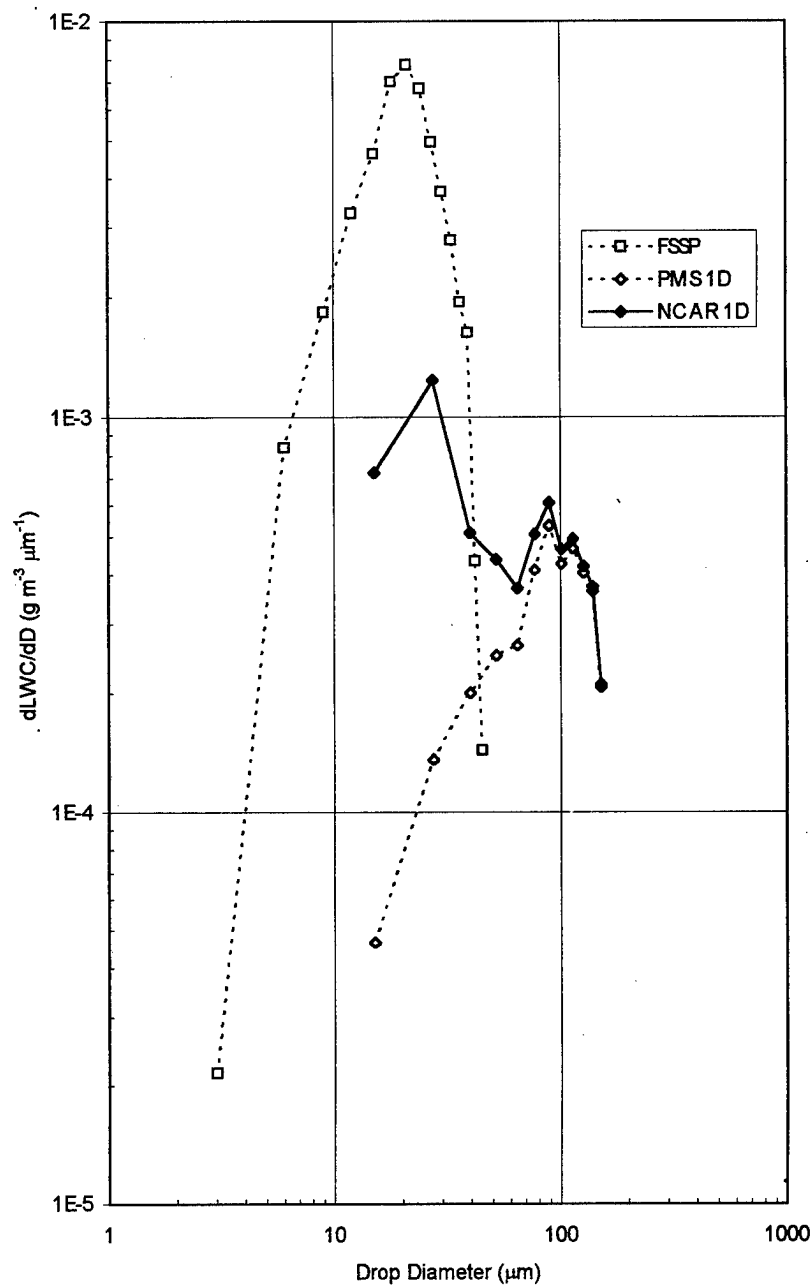


Figure 8 dLWC/dD versus D produced from Natural Cloud (small MVD).

Five curves are shown and are designated as follows: FSSP (\square), 1D-C processed using the PMS technique (\diamond) and NCAR technique (\blacklozenge) and 2D-C processed using the PMS technique (\circ) and the NCAR technique (\bullet). In addition, dashed lines designate PMS processing and solid lines designate NCAR processing.

Figure 9 shows dN/dD versus dD for a natural cloud having a large MVD. For this example, the characteristic “roll off” of the 1D-C data processing using the PMS method

is apparent, but the values of dN/dD do not show this when the data are processed using the NCAR technique. However, it is not clear from the FSSP which processing of the 1D-C really is best, but based on the previous three examples it is argued that the NCAR technique should also give the more accurate results in this freezing drizzle case.

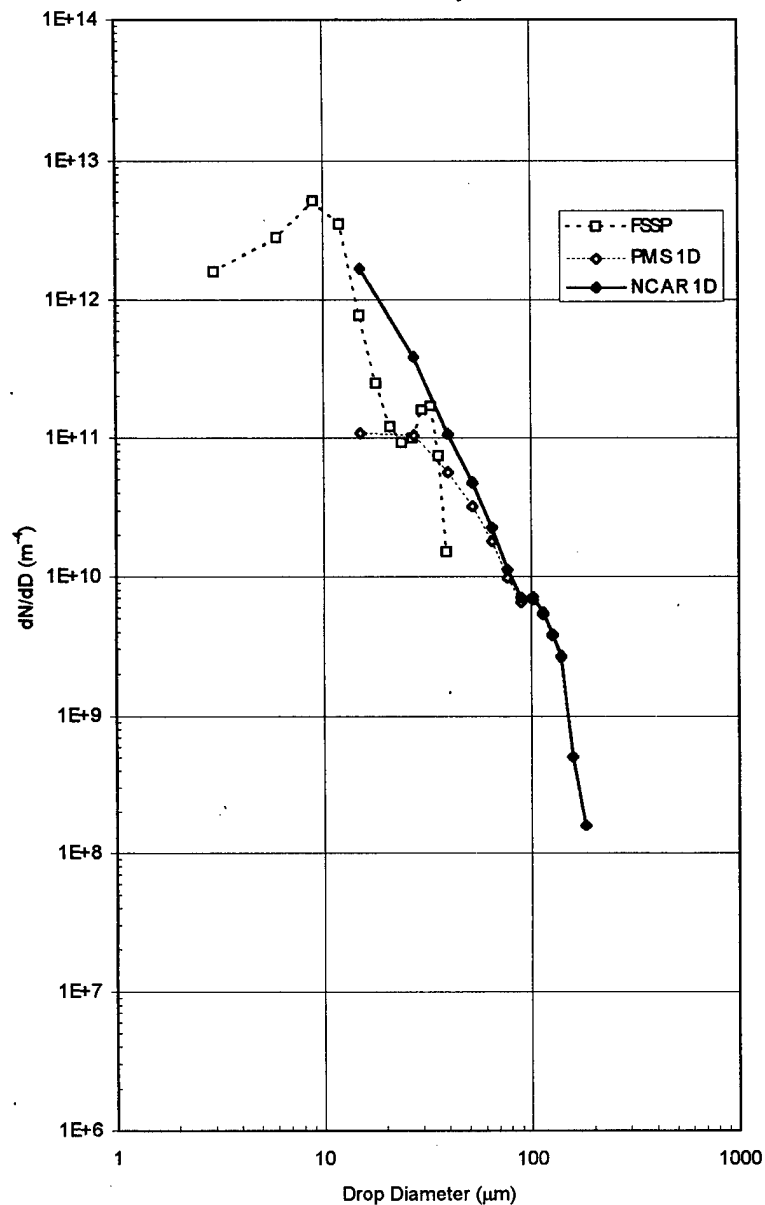


Figure 9 dN/dD versus D produced from Natural Cloud (large MVD).
Five curves are shown and are designated as follows: FSSP (\square), 1D-C processed using the PMS technique (\diamond) and NCAR technique (\blacklozenge) and 2D-C processed using the PMS technique (\circ) and the NCAR technique (\bullet). In addition, dashed lines designate PMS processing and solid lines designate NCAR processing. The data were collected on 930118 between 24:23:58 and 24:24:24 UTC.

Using the NCAR results as a likely description of this distribution, **Figure 10** suggests that there is less structure in the dLWC/dD distribution than from the FSSP and 1D-C processed using the PMS method. From **Table 3** using the NCAR technique as compared to the PMS technique, the LWC increases by 14% and the MVD decreases by 8%. In addition to these changes in LWC and MVD the NCAR technique may give a better characterization of this natural freezing drizzle event.

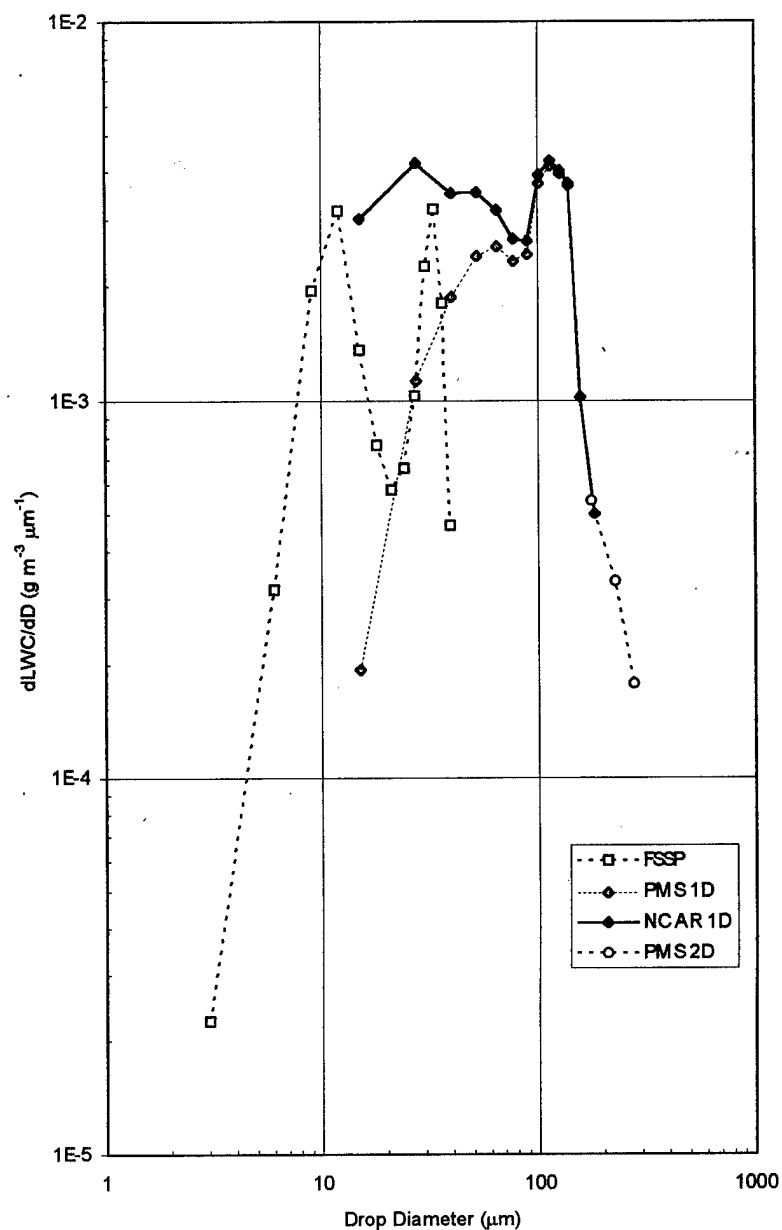


Figure 10 dLWC/dD versus D produced from Natural Cloud (large MVD).

Five curves are shown and are designated as follows: FSSP (\square), 1D-C processed using the PMS technique (\diamond) and NCAR technique (\blacklozenge) and 2D-C processed using the PMS technique (\circ) and the NCAR technique (\bullet). In addition, dashed lines designate PMS processing and solid lines designate NCAR processing.

Conclusion

Accounting for the response time (τ) of the OAPs improves the agreement between them and the FSSP where their sizes overlap. Therefore the derived LWC and MVD using the response time algorithm from the NCAR technique should improve the accuracy of these calculations. Also, more accurate calculation of the DOF for the smaller sizes of the OAPs should improve understanding of the freezing drizzle drop size distribution (Fig 10).

Acknowledgments

We thank members of the 412th Operational Group of the U. S. Air Force at Edwards AFB for their support of the field programs. We especially thank Mr. Sean Hamilton, Lead Refueling and Icing and Rain Engineer, for his logistic support during the field program. We thank Lt Col David J. Eichhorn, Commander of the 452nd Flight Test Squadron and his pilots for their precision formation flying during data collection.

We thank Mr. John Knollenberg of Particle Measuring Systems for helpful information about the 1D-C and 2D-C probes and Dr. Darrel Baumgardner of NCAR for details about the NCAR processing technique.

The data processing techniques were implemented on a program sponsored by the Department of the Air Force, Contract F04611-94-D-0105.

References

- Ashenden, Russell A. and John D. Marwitz, 1996: A comparison of the Air Force water spray tanker artificial drizzle cloud distributions to the natural environment", 34th Aerospace Sciences Meeting and Exhibits, AIAA 96-0632, January 15-18, 1996, Reno, NV, 9 pp.
- Baumgardner, D., 1987: Corrections for the response time of particle measuring probes. Preprints of the 6th Symposium on Meteor. Obs. and Instrumentation, New Orleans, 12-16 January, pp 148-151.
- Hobbs, Ray, Brian Morrison, and Darrel Baumgardner, 1995: Processing data from particle measuring probes for icing certification, American Helicopter Society/Society of Automotive Engineers International Icing Symposium Proceedings, September 18-21, 1995, Montreal, 12 pp.
- Knollenberg, Robert G., 1970: The optical array: An alternative to scattering or extinction for airborne particle size determination, *J. Appl. Meteor.*, 9, 86-103.
- Knollenberg, John, 1995: OAPs containing failing UDT 32 element arrays, PMS Service Bulletin No. 09/95, 4 pp.
- PMS, 1984: Optical array probe PMS Model OAP-2D2-C, operating manual, November 1984, Particle Measuring Systems, Inc., Boulder, CO.
- PMS, 1985: Optical array cloud droplet spectrometer probe, PMS model OAP-260X, operating and servicing manual, July 1985, Particle Measuring Systems, Inc., Boulder, CO.

COMPARISON OF LIQUID WATER CONTENT MEASUREMENT TECHNIQUES IN AN ICING WIND TUNNEL

Robert F. Ide
Vehicle Propulsion Directorate
Army Research Laboratory
Lewis Research Center
Cleveland, Ohio

ABSTRACT

This paper compares the results of liquid water content measurements by various means in an icing wind tunnel. The techniques/instrument results are from the icing blade, the single rotating cylinder, the Johnson-Williams and CSIRO-King hot-wire probes, and the liquid water content calculated from the combined droplet distributions of two droplet sizing probes - the Forward Scattering Spectrometer probe and the Optical Array probe.

A large range of icing conditions was used for this study. The liquid water content range is from 0.1 to 1.25 g/m³ and the median volumetric droplet diameters range from approximately 10 to 200 μm . Not all of the techniques listed above were used over this whole range of conditions. The hot-wire probes were used when the median volumetric droplet diameter was between 10 and 40 μm . The icing blade, rotating cylinder and droplet sizing probes were used between 15 and 200 μm .

This study shows the degree of agreement between the various methods. It reveals a large disagreement between the droplet sizing probe results and the other methods. The implications and possible causes of the disagreement are discussed. Recommendations for additional investigations to resolve disagreements are included.

INTRODUCTION

Liquid water content (LWC) along with airspeed, air temperature and to a lesser extent water droplet size is one of the important parameters that effects icing on aircraft. It effects the rate of ice accretion on the aircraft, the type of icing (i.e. rime, glaze, or mixed) and whether there will be water runback that might freeze aft of protected areas. LWC therefore has a large impact on an aircraft's potential loss of performance in an icing encounter.

There are many ways that the LWC of icing clouds has been measured. The early icing cloud characterization work in the 1940's and early 1950's employed the rotating multicylinder technique (ref 1) which was used to measure both the liquid water content and the droplet size. The results of this work were used in large part to establish the current FAA aircraft icing certification criteria. Since that time other methods of measuring LWC have been developed. These methods fall into three categories based on the basic principle of operation: ice accretion methods, hot-wire methods and droplet sizing/counting methods.

This report compares results of LWC measurements made in an icing wind tunnel using several methods. The methods are the icing blade, a single rotating cylinder, two hot-wire instruments and a pair of droplet sizing instruments.

DESCRIPTION OF TEST FACILITY

Testing was conducted in the NASA-Lewis Icing Research Tunnel. A plan view of the tunnel is shown in figure 1. The icing tunnel is a closed-loop refrigerated design with a test section that is 6 feet high by 9 feet wide (1.8 x 2.7 m). It has a spray system containing approximately 95 air-assist type spray nozzles installed in eight horizontal spraybars. The tunnel is capable of running at airspeeds of 50 to 400 mph (22 to 179 m/s) at temperatures down to -40°F (-40°C). It can produce clouds of supercooled water over an LWC range from approximately 0.1 to greater than 3.0 g/m³ although this range is airspeed dependent. Two different spray nozzles, called Standard and ModI, are used to produce this LWC range. The normal range of cloud droplet sizes is from median volumetric diameters (MVD)¹ of 10 to 40 μm. The MVD capability of the tunnel has recently been extended to 190 μm in response to the interest in performing icing tests at large droplet conditions.

The relative humidity in the test section of the IRT is very near and sometimes above saturation, depending on airspeed. After the tunnel has been humidified by the first spray the dew point at the spray location is less than 7°F (3.9°C) below the air temperature. As the air passes through the 14:1 contraction it speeds up resulting in a decrease in the static air temperature. Above 200 mph (89 m/s) the test section air is saturated, even assuming none of the water from the spray is evaporated. At all airspeeds the test section relative humidity is greater than 75%. This high relative humidity reduces droplet evaporation and results in very repeatable spray

¹MVD is defined as the diameter at which an equal volume of water is contained in droplets with diameters smaller (and larger) than this value.

conditions in the test section.

All tests reported here were conducted in the center of the tunnel to avoid questions about the spacial variations in the LWC of the cloud effecting the results.

DESCRIPTION OF MEASUREMENT TECHNIQUES

ICING BLADE

The icing blade is a very simple device. It consists of a piece of aluminum which is 6 inches long, 0.125 inches wide and 0.75 inches thick. The blade is placed behind a shield in the center of the tunnel. After the desired spray condition has been established the shield is raised, exposing the 6 inch by 0.125 inch face of the blade to the cloud for a predetermined time. The appropriate exposure time results in an ice accretion which is less than 0.2 inches thick. The icing blade was used at a temperature of 0°F (-18°C) to ensure that rime icing occurred thereby minimizing the width of the ice. The LWC of the cloud is determined by the following equation:

$$LWC = \frac{C * \rho_{ice} * \Delta S}{E_b * V * t} \quad (1)$$

where:

C	is a constant
ρ_{ice}	is the density of ice
ΔS	is the ice thickness on the blade
E_b	is the blade collection efficiency
V	is the airspeed
t	is the exposure time

The ice density is assumed to be a constant, $\rho_{ice} = 0.88$. The collection efficiency of the blade, which is a function of the airspeed and the droplet size, was calculated using the FWG two-dimensional trajectory code (ref. 2). This code uses a Hess-Smith panel code for the flowfield prediction and a C.W. Gear stiff equation scheme to integrate particle trajectories.

ROTATING CYLINDER

The rotating cylinder used for this testing was 1.5 inches in diameter and was six feet high. It was rotated at approximately 60 rpm. All testing was performed at a temperature of 0°F (-18°C) to eliminate the possibility of water run-off. The tunnel spray system was turned on for a predetermined time and the resulting iced diameter of the cylinder was then measured. Equation (1) was used to calculate LWC. The exposure time was divided by two since one-half of the cylinder is always exposed to the cloud.

HOT-WIRE LWC INSTRUMENTS

The Johnson-Williams (J-W) instrument, also known as a Cloud Technology probe, uses two wires in a balanced bridge circuit. The main sensing wire is mounted perpendicular to the airstream and is heated at a constant voltage to a temperature above the boiling point of water. Cloud droplets impinging on the wire are evaporate, causing the wire to cool and its electrical resistance to decrease. This change in resistance causes an imbalance in the bridge circuit; the degree of imbalance is related to the LWC. The second wire is mounted parallel to the airstream and is shielded from droplet impingement. This wire is connected to the opposite side of the bridge and compensates for small changes in air temperature, air density and speed.

The CSIRO-King instrument employs a sensor composed of three wire coils wound around a small hollow tube. The slave coils on each side of the master coil are connected in series and minimize the longitudinal heat conduction from the master coil. The sensor element is 0.19 cm in diameter and 2.3 inches long. Unlike the J-W instrument the CSIRO-King is a constant temperature device. The total heat transfer rate from the coil is determined from the power required to keep the sensor coil at a constant temperature. This heat transfer rate is composed of the "dry" term which is a function of airspeed, air density and air temperature and a "wet" term which is a function of airspeed and LWC.

DROPLET SIZING PROBES

There are two instruments which are commonly used to measure cloud water droplet sizes in flight programs and some icing facilities. They are the Forward Scattering Spectrometer Probe (FSSP) and the Optical Array Probe (OAP)². The FSSP is used to measure the smaller droplets in the range of 2 - 47 μm and the OAP used in this study measures droplets in the range of 15 to 450 μm .

The FSSP determines droplet diameter by measuring the intensity of light scattered in the near-forward direction when the droplet passes through a focused laser beam. It is assumed that only one droplet is within the depth of field of the probe optics at a time. Each measured droplet is then classified into one of fifteen bins, which for a range of 2 - 47 μm means each bin is 3 μm wide. The standard corrections for "activity" and "ratio of total counts to total strobes" as described in the instrument manufacturer's manual (ref 3) are applied in calculations of number density and LWC.

The OAP determines droplet diameter by measuring the diameter of a shadow of the particle formed as it passes through a collimated laser beam. The shadow is expanded by optical lenses and projected on a linear photodiode array. The droplet diameter is determined from the number of diodes shadowed and the magnification of the system. The OAP used in this study has 30 bins, each bin having a width of 15 μm . As in the FSSP it is assumed that only one droplet is

²The FSSP and OAP are manufactured by Particle Measuring Systems, Inc. of Boulder, Colorado.

within the probe's depth of field at a time. The standard calculations for sample area for each bin as contained in the manufacturer's manual (ref 4) were used in calculations of number density and LWC.

In order to average out any fluctuations in the cloud and to obtain a good statistical sample of droplets, particularly for the larger droplets measured by the OAP, each cloud measurement is made for a duration of 100 seconds.

LWC is calculated from the combined droplet distributions of the FSSP and OAP using the following equation:

$$LWC = \frac{\rho * \pi}{6} * \Sigma \frac{N_i * d_i^3}{SA_i * V * t} \quad (2)$$

where:

ρ	is the density of water
N_i	is the number of particles in the bin
d_i	is the mid-bin diameter
SA_i	is the sample area for the bin
V	is the airspeed
t	is the total sample time

For the FSSP the sample area, SA_i , is the same for each bin. The sample area is a function of bin number (or droplet diameter) in the OAP.

ICING TUNNEL CALIBRATION

The LWC calibration of the icing tunnel is established by making measurements of numerous spray conditions over the full operating range of the tunnel using the icing blade technique. This covers an airspeed range from 50 to 350 mph and a droplet size (MVD) range from 10 to 40 μm . Water spray settings also cover the complete range of atomizing air pressures and water flow rates. It should be noted that all data are taken at an air temperature of 0° F to assure that the water droplets freeze on impact with the blade. The blade results are then used to establish an equation which accounts for the interplay of these variables. The equation takes the form:

$$LWC = A * \left(\frac{V}{150}\right)^x * \left(\frac{P_{air}}{40}\right)^y * \frac{\sqrt{dP}}{V} \quad (3)$$

where

A , x and y	are constants
V	is tunnel airspeed
P_{air}	is the spray nozzle air pressure
dP	is the nozzle water pressure minus the air pressure

Figure 2 shows a comparison of the icing blade measurements to the tunnel calibration, that is the above equation. It can be seen that the majority of the data is well within the $\pm 10\%$ agreement lines. This plot is typical of the agreement to be expected from the tunnel as demonstrated by the twice-yearly calibration checks.

COMPARISON OF OTHER LWC INSTRUMENTS/TECHNIQUES

HOT-WIRE LWC INSTRUMENTS

Figure 3 shows a comparison of the LWC measured by the Johnson-Williams hot-wire instrument to the tunnel calibration. This data was obtained over an airspeed range of 75 to 250 mph, a droplet size (MVD) range of 10 to 40 μm and air temperatures of 20 and 30° F. It shows that the majority of the J-W results are within $\pm 0.1 \text{ g/m}^3$ of the tunnel values. No trends due to airspeed or droplet size were evident in the data and are therefore not presented here.

Figure 4 shows a comparison of the CSIRO-King hot-wire results to the tunnel calibration. The data on this plot were obtained over an airspeed range of 75 to 250 mph, a droplet size range of 10 to 40 μm , and a temperature range of -15 to 40° F. This instrument's results show good agreement with the tunnel calibration. Only a small percentage of the data are outside the $\pm 0.1 \text{ g/m}^3$ band. This plot also demonstrates that there is no apparent effect of temperature on the tunnel LWC. This is an important piece of information since the LWC calibration of the tunnel was developed using the icing blade at a single air temperature of 0° F. As with the J-W, no trends due to airspeed or droplet size were evident in the data from this test.

ICING BLADE AND ROTATING CYLINDER

To date five large droplet (i.e. $\text{MVD} > 40 \mu\text{m}$) conditions have been established in the tunnel. They have nominal droplet size (MVD) values of 56, 99, 117, 160 and 190 μm . For these large droplet clouds it was initially felt that the icing blade normally used for tunnel LWC calibrations might not be appropriate since its surface area is so small. Therefore the initial measurements of LWC for large droplet conditions were made with the 1.5 inch diameter rotating cylinder. The icing blade was then used to measure the LWC of these clouds as a source of comparison to the rotating cylinder measurements. Figure 5 shows the results of this comparison between the rotating cylinder and icing blade measured LWC. It can be seen that there is reasonable agreement between the two methods. Only two points are significantly outside the $\pm 0.1 \text{ g/m}^3$ band. Figure 6 shows the same data, this time plotting the difference in the measured LWC versus the nominal droplet size. It can be seen that reasonable agreement exists until the MVD exceeds 160 μm . At this droplet size it is possible that the larger droplets of the distribution are breaking up and splashing off the surface of the icing blade. The vertically adjacent points at 99, 160 and 190 μm are repeat runs with the rotating cylinder and serve to demonstrate the excellent repeatability of the tunnel sprays in terms of LWC.

DROPLET SIZING INSTRUMENTS

The droplet size (MVD) calibration of the icing tunnel is established by making hundreds of measurements of droplet distributions of different spray nozzle air and water pressure settings. Measurements are made with the Forward Scattering Spectrometer Probe (FSSP) and the Optical Array Probe (OAP). The LWC can be calculated from these droplet distributions as previously described. Figure 7 shows a comparison of the calculated LWC from these instruments to the icing tunnel LWC as determined by the icing blade for MVD's less than 50 μm and the rotating cylinder for MVD's greater than 50 μm . None of the calculated LWC values from the droplet sizing instruments are within the $\pm 0.1 \text{ g/m}^3$ bands of agreement. All LWC values from the droplet sizing instruments are significantly greater than the actual LWC. Figure 8 shows the ratio of the FSSP plus OAP LWC to the tunnel LWC plotted against droplet size. The plot shows that the ratio of LWC is between 1.5 for the smaller droplet cases and 2.5 for some of the larger droplet size cases. It should be noted that for the smallest MVD of 15 μm all of the calculated LWC comes from the FSSP. As the MVD increases more of the LWC is contained within the range of the OAP. Figure 8 demonstrates that the LWC discrepancy is caused by both the FSSP and the OAP.

In the legend of figures 7 and 8 symbols are shown to differentiate between "half spraybars" and "all spraybars". In the half spraybar cases even numbered spraybars were turned off in order to reduce the droplet number density and hence the FSSP "activity" level (ref. 5). All spraybars means that all eight spraybars were spraying. Measurements made during the half-spraybar tests did show a significant decrease in measured number density and FSSP activity but as can be seen in figure 8 the ratio of the LWC calculated from the FSSP and OAP compared to the tunnel LWC did not change significantly. In fact, for the larger droplet sizes, the LWC ratio is higher for the half-spraybar cases.

DISCUSSION OF MAJOR RESULTS

It has been shown that most techniques of measuring LWC agreed well in the NASA-Lewis Icing Research Tunnel, at least within the range of "normal" droplet sizes of 10 to 40 μm as defined by the FAA's FAR Part 25, Appendix C envelopes. It was also shown that good agreement was achieved between the rotating cylinder and the icing blade measured LWC values for the larger droplet sprays with MVD's of 56 to 190 μm .

The major finding in this work is that, at least in the tunnel environment, the calculated LWC from the droplet distributions measured by the FSSP and OAP severely overestimate the LWC. The LWC was overestimated by 50% for MVD's up to 60 μm and 100% to 150% for higher MVD's. The most probable reason for this overestimation of LWC is oversizing by the droplet sizing instruments. This oversizing could be caused by either spectral broadening or coincidence errors or both. Spectral broadening is caused by a droplet being sized differently depending on where it passes through the sample volume or in the case of the FSSP, by noise - either electronic or optical. Coincidence errors result when more than one droplet is in the sample volume at the same time. These sizing errors would effect both the LWC and the MVD calculated from the instruments. Table 1 contains a listing of droplet sizes (diameters) and the

measured size for the LWC to be overestimated by 50%, 100% and 150% is was shown to be the case in figure 8. The table illustrates that in at least some cases the oversizing would have to be very significant.

CONCLUSIONS

1. Good agreement was shown between the LWC derived from icing blade technique and two hot-wire LWC instruments for $10 < \text{MVD} < 40 \text{ } \mu\text{m}$.
2. Good agreement was shown between the LWC derived from the icing blade and the rotating cylinder techniques for $15 < \text{MVD} < 160 \text{ } \mu\text{m}$.
3. The LWC calculated from the droplet distributions measured by the FSSP and OAP severely overestimated the actual LWC.

RECOMMENDATIONS

1. The accuracy of the hot-wire LWC instruments to clouds with MVD's greater than $40 \text{ } \mu\text{m}$ should be investigated.
2. The cause of the overestimation of LWC by the FSSP and OAP should be investigated.

REFERENCES

1. Brun, R.J., Lewis, W., Perkins, P.J., and Serafini, J.S., "Impingement of Cloud Droplets on a Cylinder and Procedure for Measuring Liquid-Water Content and Droplet Sizes in Supercooled Clouds by Rotating Multicylinder Method", NACA Rep. 1215, 1955.
2. Frost, W., "Two-Dimensional Particle Trajectory Computer Program," Interim Report for Contract NAS3-22448, March, 1982.
3. "Forward Scattering Spectrometer Probe Operating and Servicing Manual", PMS Model FSSP-100, Particle Measuring Systems, Inc., 1855 South 57th Street, Boulder, Co. 80301. 1991
4. "Optical Array Cloud Droplet Spectrometer Probe Operating Manual", PMS Model OAP-230X, Particle Measuring Systems, Inc., 1855 South 57th Street, Boulder, Co. 80301. 1991
5. Hovenac, E. A. and Ide, R. F., "Performance of the Forward Scattering Spectrometer Probe in NASA's Icing Research Tunnel", NASA TM101381, AIAA-89-0769, 1989

TABLE 1

DROPLET DIAMETER	MEASURED DROPLET DIAMETER IF LWC WERE OVERESTIMATED BY:		
	50%	100%	150%
10	11.4	12.6	13.6
20	22.9	25.2	27.1
40	45.8	50.4	54.3
50	57.2	63.0	67.9
100	114.5	126.0	135.7
200	228.9	252.0	271.4

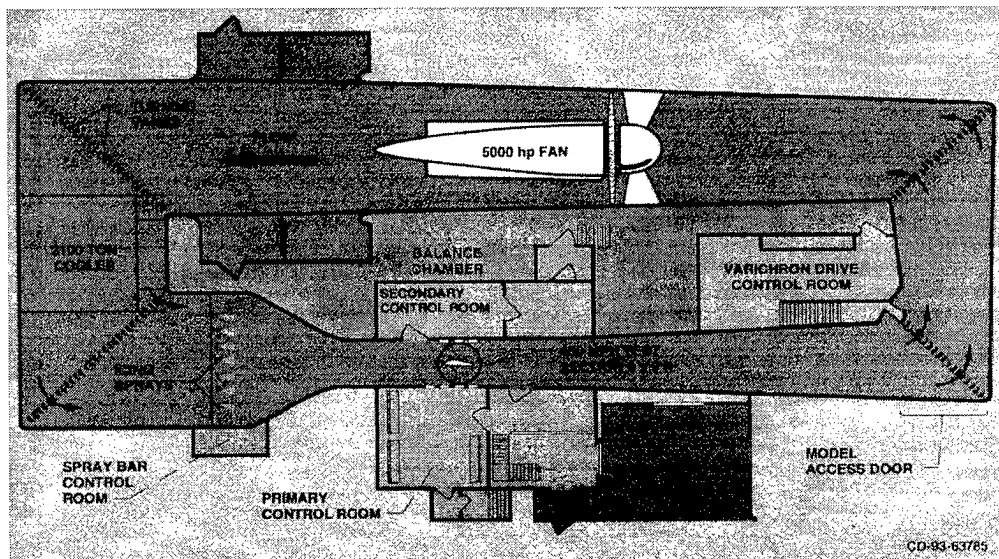


Figure 1. Plan view of the NASA-Lewis Icing Research Tunnel

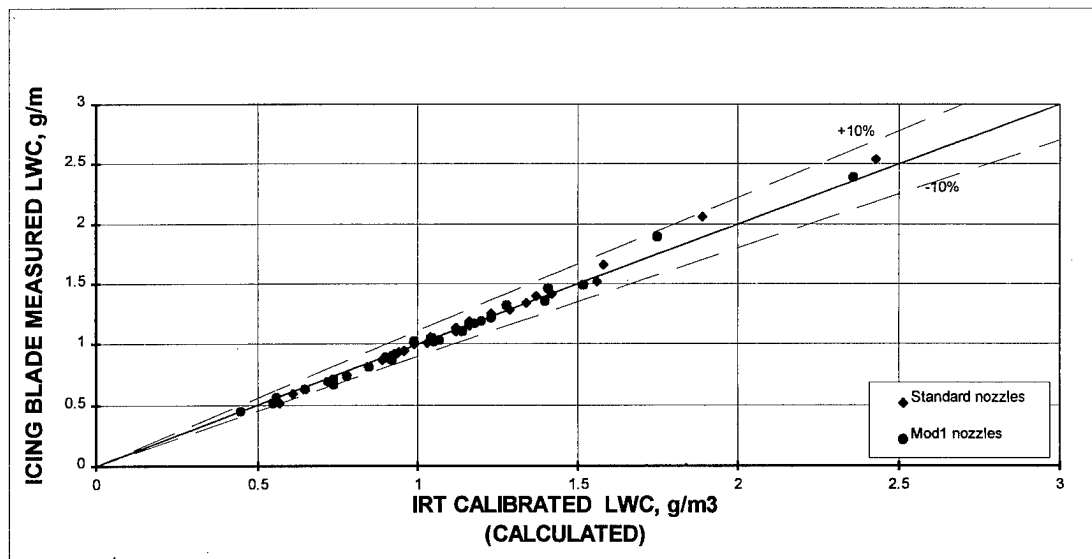


Figure 2. Comparison of icing blade measured LWC to icing tunnel calculated LWC for $50 < \text{Airspeed} < 350$ mph, $14 < \text{MVD} < 40$ μm , Temp=0 F.

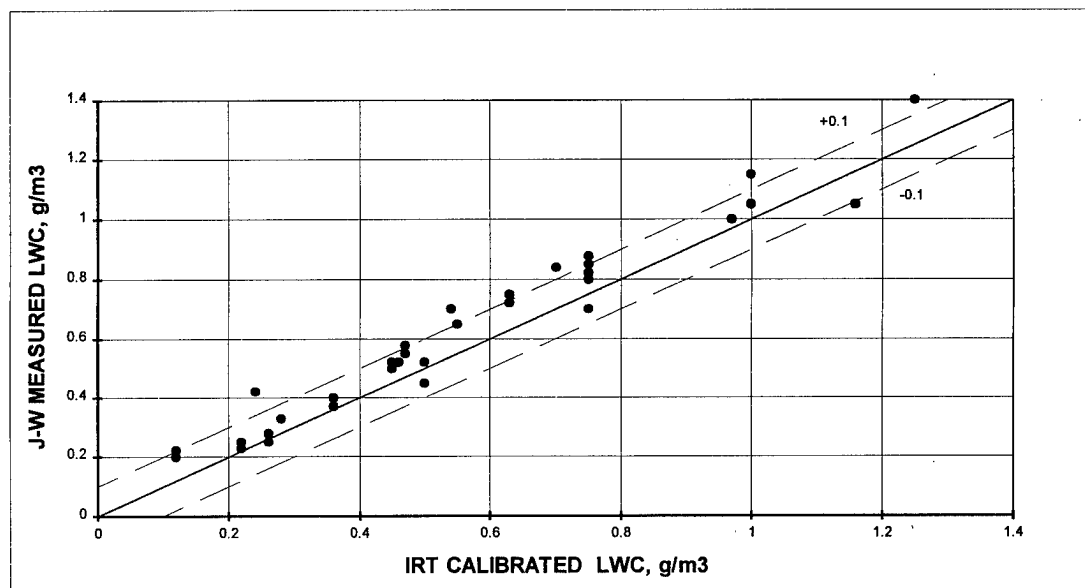


Figure 3. Comparison of Johnson-Williams measured LWC to IRT calibrated LWC for $75 < \text{Airspeed} < 250$, $10 < \text{MVD} < 40$ μm , Temp=20, 30 F.

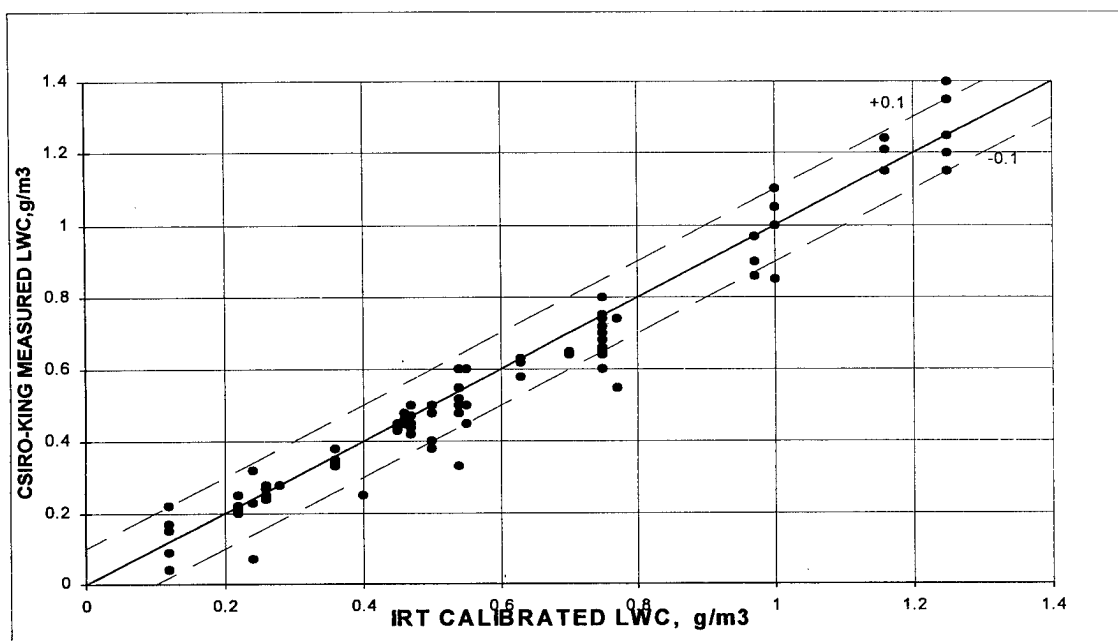


Figure 4. Comparison of CSIRO-King measured LWC to IRT calibrated LWC for $75 < \text{Airspeed} < 250$ mph, $10 < \text{MVD} < 40$ μm , $-15 < \text{Temp} < 40$ F.

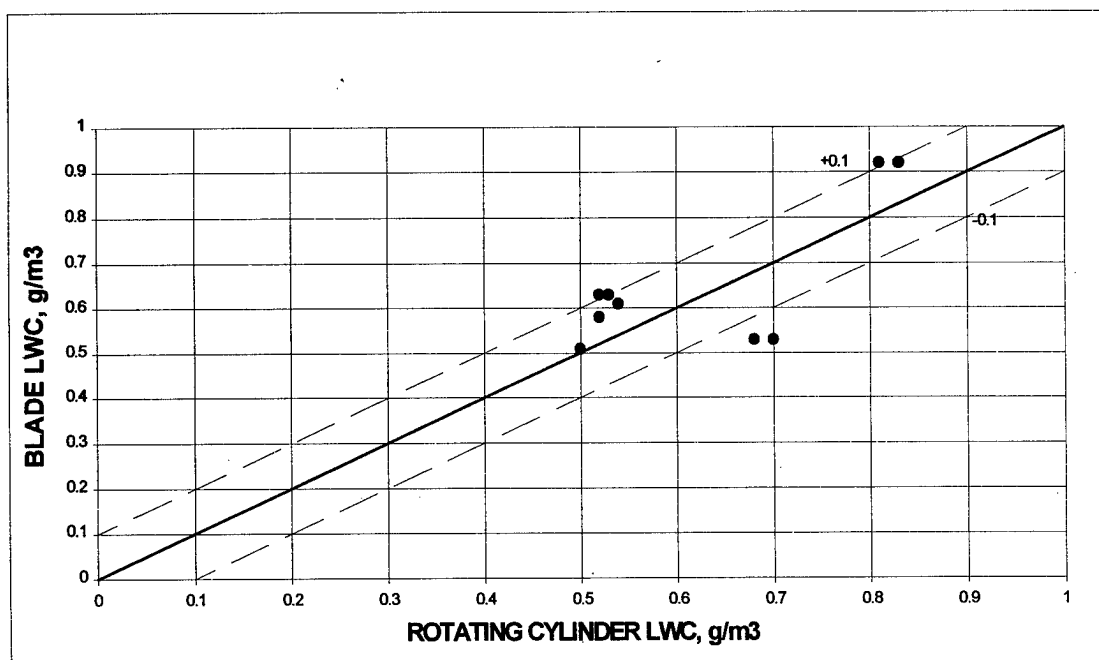


Figure 5. Comparison of the icing blade measured LWC to the rotating cylinder LWC for droplet sizes (MVD) up to 190 μm .

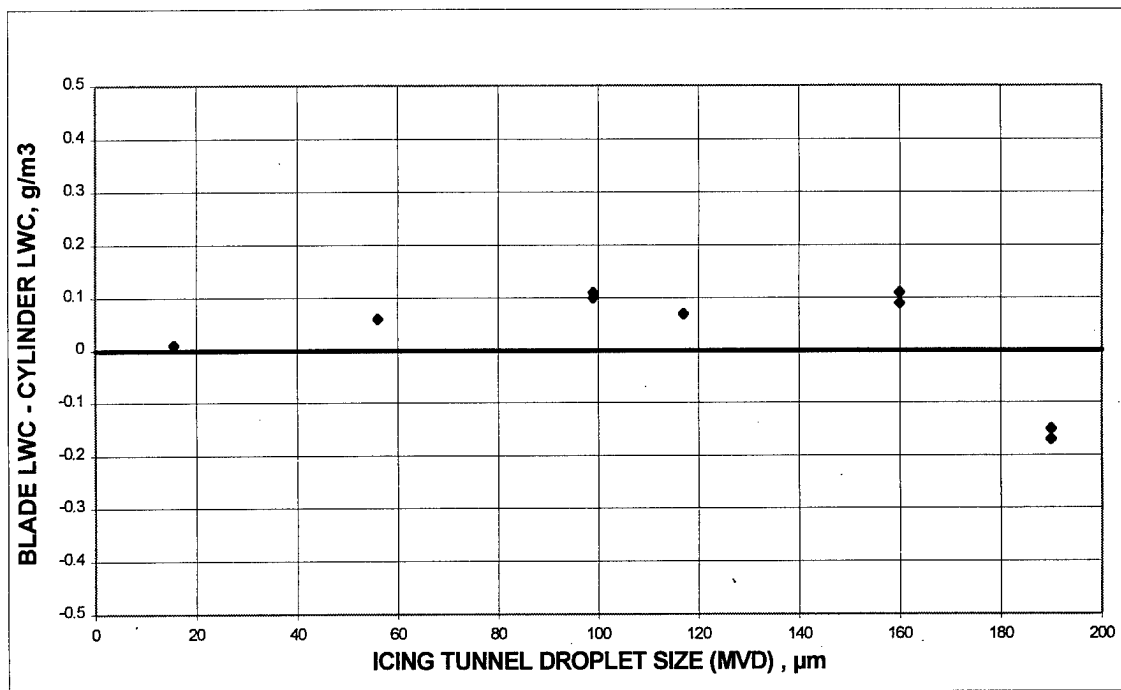


Figure 6. Icing blade measured LWC minus the rotating cylinder LWC for a range of droplet sizes (MVD) from 15 to 190 μm .

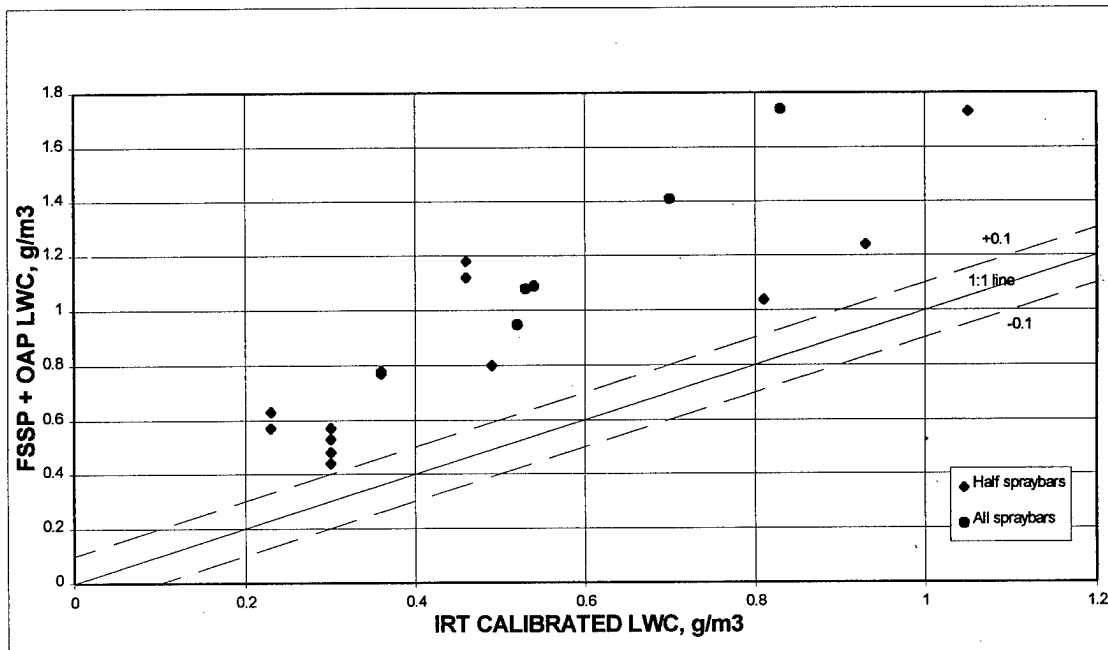


Figure 7. Comparison of the LWC calculated from the FSSP and OAP plotted against the icing tunnel LWC for airspeeds of 150 and 195 mph.

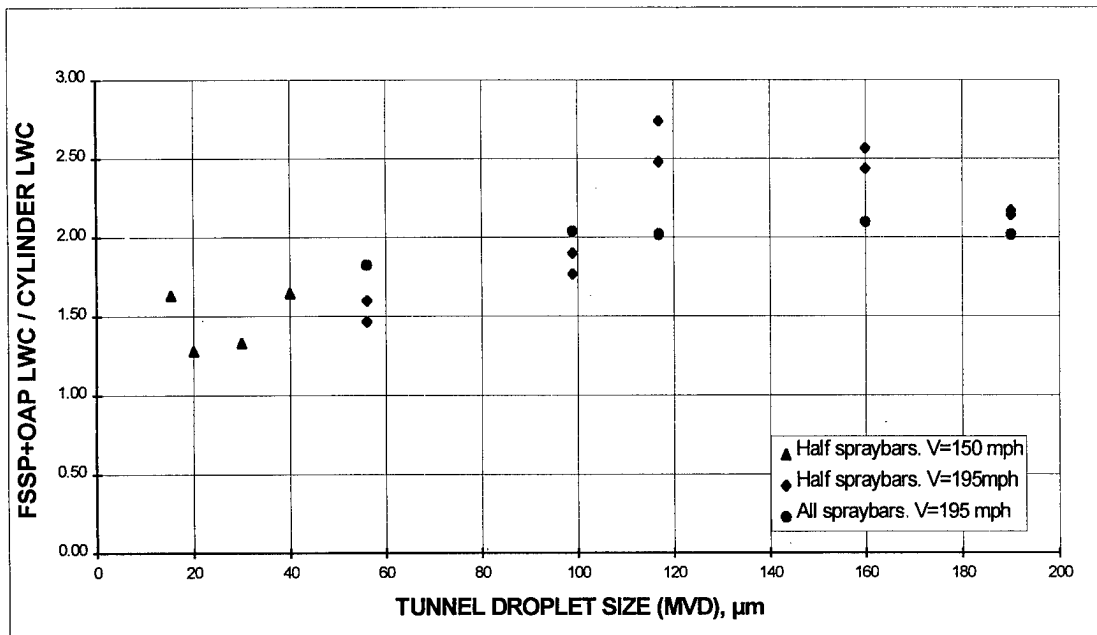


Figure 8. Ratio of the FSSP plus OAP LWC to the icing tunnel LWC plotted against droplet size (MVD).

ON THE ACCURACY OF PMS OPTICAL ARRAY PROBES

Korolev A. V., J. W. Strapp, and G. A. Isaac

Cloud Physics Research Division
Atmospheric Environment Service
Downsview, Ontario, Canada, M3H 5T4

Abstract

This paper considers the theory of diffraction image formation of spherical particles and peculiarities of particle sizing by a discrete photodiode array. The diffraction images of spherical water droplets are approximated by Kichhoff-Fresnel diffraction on an opaque disc. It is shown that OAPs lead to both oversizing and undersizing for droplets less than 100 μm in diameter, and oversizing of droplets greater than 100 μm . The errors in droplet sizing for OAPs increase with decreasing size. The discrete manner of particle image registration also leads to losses of particles with sizes less than 100 μm . For the ideal case with zero photodiode response time, the losses reach 70% for 25 μm droplets. A non-zero response time will increase these losses. These findings help explain the problems in the overlap region of the FSSP and OAP droplet spectra. A variety of calculated digital images for OAP-2D-C and OAP-2D grey are presented. Spherical and nonspherical particles can be confidently distinguished for images having more than 10x10 pixels. Different methods of particle image sizing are discussed. Several methods of size retrieval of individual droplets and droplet ensembles are suggested. Correction algorithms for these effects have been derived, and distortion and correction retrieval matrices have been calculated. Several examples of actual and measured size distributions are presented.

1. Introduction

Optical Array Probes (OAP) designed by PMS Inc. in the early 70s have been used intensively for measurements of cloud particles with sizes larger 50 μm . These are currently the main instruments used for airborne studies of drizzle and precipitation formation. Since the development of OAPs there have been a number of limited studies related to the accuracy of particle sizing. Laboratory calibrations reported by Heymsfield and Baumgardner (1985) and Joe and List (1987) showed that the measured particle size varies with the distance from the object plane. The dependence of measured particle size on its distance from the object plane was found to be nonmonotonous and dependent on particle size. A theoretical explanation of these results was given by Korolev et al. (1991). Based on laboratory studies, the authors showed that diffraction images of transparent spheres (glass beads and water droplets) are well approximated by Fresnel diffraction by an opaque disc. A good agreement between the theoretically predicted droplet size as a

function of a distance from the object plane and that found from laboratory measurements were obtained in this work. To date corrections for this type of OAP oversizing have not been commonly applied by research groups.

The present work is an evolution of the work initiated by Korolev et al. (1991). The formation of discrete digital images of spherical particles are simulated based on Kichhoff-Fresnel diffraction by an opaque disc. This work addresses measurement problems related to counting losses, depth-of-field, particle sizing. Several possible retrieval algorithms are suggested.

The results obtained can be applied for PMS OAPs for low airspeed (< 20 m/s), since the influence of response time was not taken into account. Response time mainly affects the first few channels of OAPs, and future work must also consider this issue. The current results are, however, useful for processing data of different probes with digital registration of particle images (Lawson and Cormack 1995) or new designs of similar probes, and also provides

first order corrections of OAPs, especially for larger particles.

2. Theory of formation of diffraction images by spherical particles.

2.1 Fresnel diffraction by an opaque disc.

An approximation of diffraction on transparent water droplets by Fresnel diffraction by an opaque disc is based on the two following assumptions (Korolev et al. 1991). First, spherical water droplets in visible light are known to be short-focus collecting lenses with a focal length approximately equal to their radii. Thus, we can neglect the refracted component of light and consider water droplets as an opaque spheres in the analysis of their images at distances larger then ten radii. Second, it is assumed that the diffraction by an opaque sphere can be approximated by that of an opaque disc.

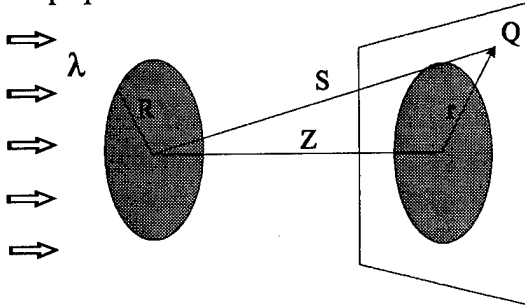


Figure 1. The calculation of Fresnel diffraction on an opaque disc.

Diffraction by an opaque disc may be calculated using Fresnel-Kirchhoff theory (Born and Wolf 1968). Suppose a plane wave is incident on an opaque disc with radius R (Fig.1). The amplitude of a diffracted light at point Q following Babinet's principle can be presented as

$$U(Q) = U_a(Q) + U_b(Q) \quad (1)$$

where

$$U_a(Q) = \begin{cases} \exp(ikZ) & \text{if } r > R \\ 0 & \text{if } r \leq R \end{cases} \quad (2)$$

$$U_b(Q) = -\frac{1}{4\pi} \int_0^{2\pi} \frac{\exp(ikZ)(R^2 - Rr \cos \alpha)}{Z(S - Z)} d\alpha \quad (3)$$

where $k=2\pi/\lambda$, λ is the wavelength, Z is the distance between the disc and its image; r is the distance from the center of the image to point Q ; and S can be found as $S = (Z^2 + R^2 + r^2 - 2Rr \cos \alpha)^{1/2}$

Using (1), (2) and (3) the intensity of a diffraction image will be

$$I(Q) = |U(Q)|^2 \quad (4)$$

The analysis of equations (1)-(4) yields the following important results:

1. The diffraction image can be presented as a function of only one dimensionless variable

$$Z_d = \frac{\lambda|Z|}{R^2}.$$

2. Two droplets with different diameters give

$$\text{the same diffraction image if } \frac{|Z_1|}{R_1^2} = \frac{|Z_2|}{R_2^2}.$$

3. The diffraction image does not depend on the sign of Z , i.e. on both sides of the object plane, the diffraction image will be the same.

2.2 Universal Z_d - R_d diagram

Figure 2 shows the isolines of intensity levels in Z_d - R_d coordinates for the Fresnel-Kirchhoff diffraction by an opaque disc, here $R_d=r/R$ is the dimensionless distance from the center of the image. In this paper the following convention is used: 0% level is totally dark, 100% level is unshadowed illumination. It is seen from Figure 2 how the shadow levels change with an increase of Z_d , i.e. deviation from the object plane. The peripheral part of the image with $r/R > 1$ contains zones with illumination brighter than the background illumination. In these zones the intensity may exceed 130%. On the other hand the central zone with $r/R \sim 0$ has a bright zone with maximum intensity equal to 100% (Poisson spot). The light intensity of the darkest zone in the diffraction image decreases with the distance from the object plane. For example the image has no zones with intensity less than

25%, 50% and 75% for droplets with $Z_d > 3.68$, $Z_d > 8.18$, and $Z_d > 21$, respectively. Figure 3 shows the shadow level versus the distance Z_d $_{max}$, such that for all $Z_d > Z_d$ $_{max}$ this level of shadow does not exist in the diffraction image.

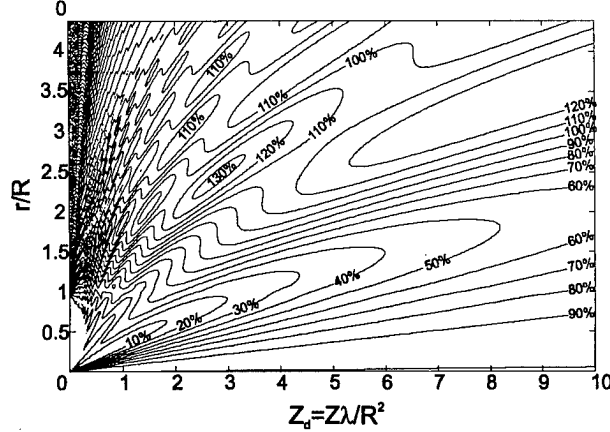


Figure 2 Universal Z_d - R_d diagram

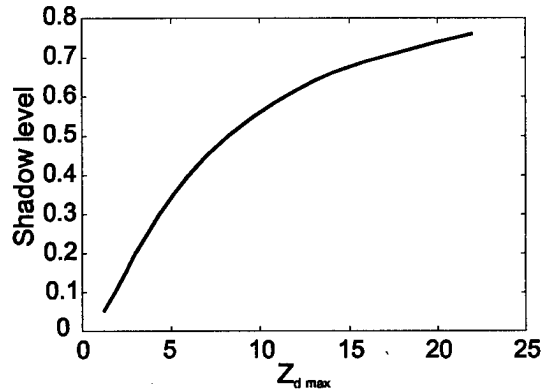


Figure 3. Dependence of shadow level on the distance from the object plane Z_d $_{max}$ where this level still exist.

2.3 Depth-of-field

Depth-of-field Z_{DoF} in OAPs is defined as the maximum distance of the particle from the object plane where the particle image can trigger at least one photodiode in the array. In other words, the particle image at distances $Z > Z_{DoF}$ has zones with the intensities lower than the triggering level of the probe. For OAP-2DC and OAP-200X these levels are 50% and 33%, respectively.

Based on Figure 4 the depth-of-field can be calculated as

$$Z_{DoF} = 2 \frac{Z_{dmax} R^2}{\lambda} \quad (5)$$

Equation 5 shows that the depth-of-field continuously increases with increasing particle size. However, for large particles Z_{DoF} is limited mechanically by the distance between the probe arms, which is equal to $Z_{asp} = 61$ mm. Figure 4 presents the depth-of-field versus droplet size for different level of shadow thresholds. It is seen that for droplets larger 100 μ m the depth-of-field is defined by the probe arms Z_{asp} for an OAP-2DC. For OAP-2Dgrey which uses three shadow levels (25%, 50% and 75%) the depth-of-field is different for different shadow levels.

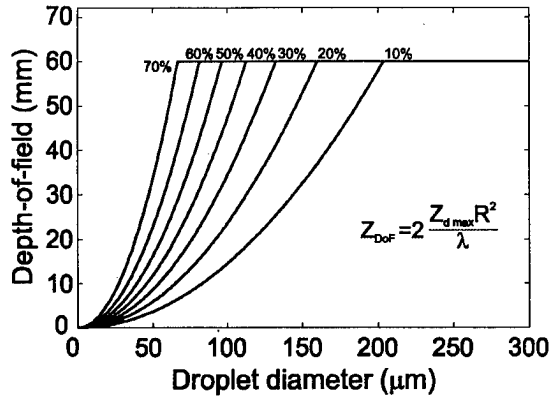


Figure 4. Depth-of-field at different shadow levels.

3. Ideal digital images

Figure 5 shows the changes of ideal digital droplet images at different distances from the object plane. The first two columns show the smooth distribution of light intensity in the diffraction image and the last two show the digital images at grey levels 25%-50%-75%-100% (OAP-2Dgrey) and 50%-100% (OAP-2DC), respectively. The external diameter of the image at 50% level has some oscillations for $Z_d < 2$. One such sharp change in the image size is seen on Figure 5 when Z_d changes from 1.9 to 2.0. For $Z_d > 2$ the droplet image size monotonously increases with the distance from the object plane. Note that the digital image may consist of several concentric rings. Such rings are observed at 25% and 50% shadow levels at $Z_d \sim 1$ and $Z_d \sim 1.9$, respectively. The size of the central (Poisson) spot monotonously increases away from the object plane.

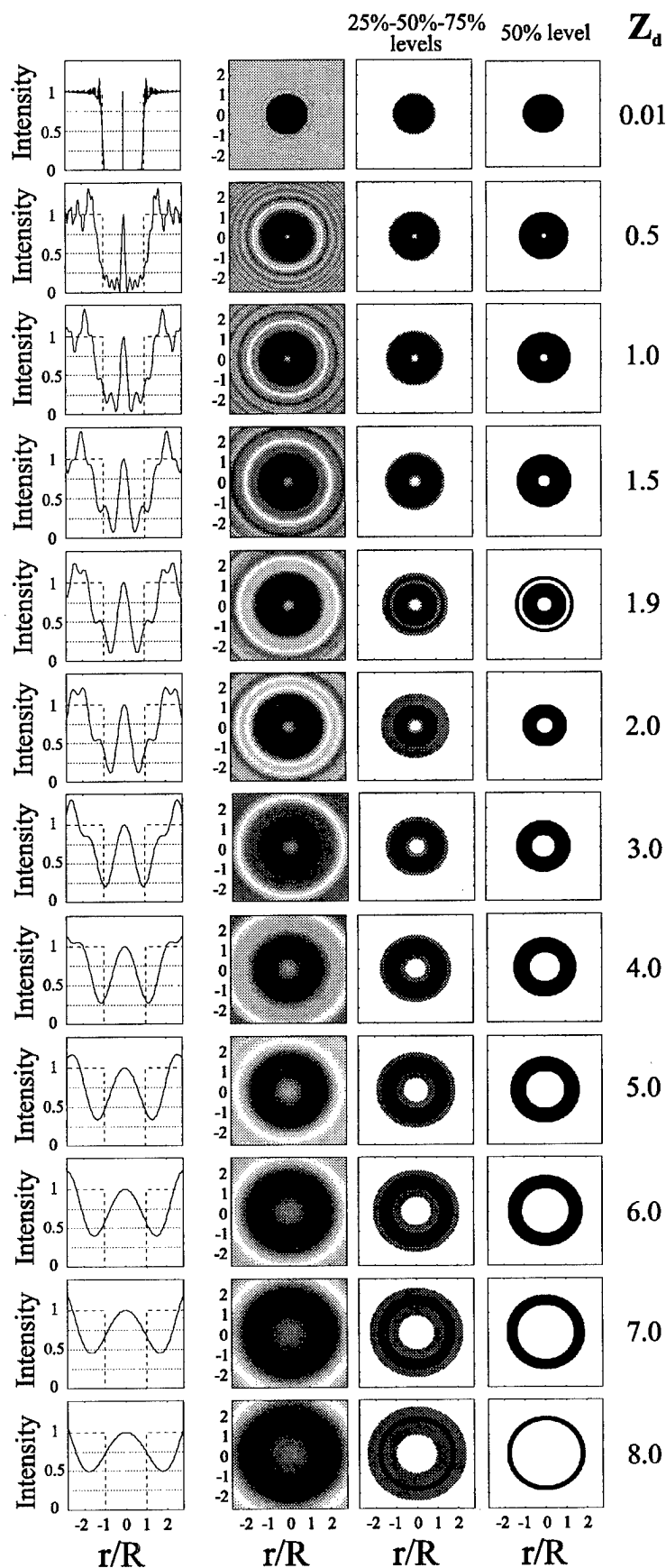


Figure 5. Smooth and digital diffraction images of a spherical particle.

4. Discrete images

4.1 Shape of discrete images

The OAPs register not ideal digital images but discrete images. The quality of the image depends on the probe resolution. The resolution in the direction perpendicular to the axis of photodiode array (X-direction) is defined by the sampling frequency (slice rate). Along the axis of the photodiode array (Y-direction) the resolution is defined by the magnification of the optical system and the distance between photodiodes. In order to get the proper particle image aspect ratio, the slice rate should be proportional to the airspeed. The registered image also depends on the shape and size of each photodiode, since the light intensity of the diffraction image is integrated over its area. The effect of a photodiode shape is important especially for small particles, when the photodiode size becomes comparable with the size of the particle.

Since the position of the particle in space is random, the time the particle enters the sample volume of the probe and its position in the Y-direction will be also random values. Figure 6 shows possible discrete images resulting from the particle image covering two photodiodes. Depending on the position with respect to the photodiodes and the timing of the first slice, the particle image may trigger from one to four elements.

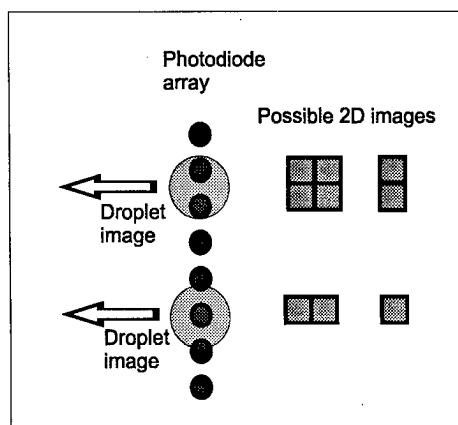


Figure 6. Formation of digital images in OAPs.

Thus, the same particle at the same distance from the object plane may produce different discrete images.

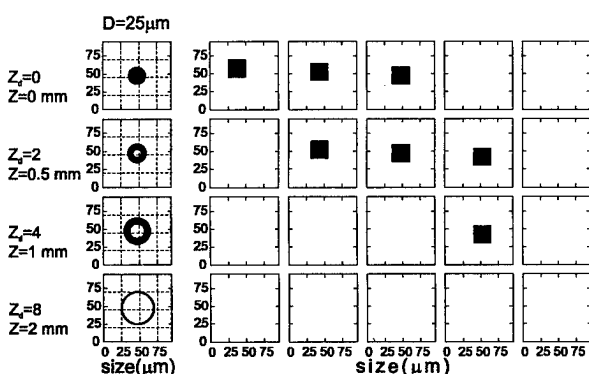


Figure 7. Calculated discrete images of a 25 μm droplet at different distances from the object plane at 50% shadow level. The original digital images are shown on the left. Dashed lines denotes the photodiode grid.

Figures 7, 8, 9 and 10 demonstrate discrete images for particles 25 μm , 50 μm , 100 μm , 200 μm , respectively, at different distances from the object plane. The left column on Figures 7-10 shows the ideal digital images. The dashed line grid denotes the imaginary photodiode grid producing the discrete images shown on the right. For the calculation of the digital image, the integration of the intensity distribution of the diffraction images was performed over the area which occupies two third of each cell. The difference between discrete images is produced by a 5 μm shift of an original diffraction image in both X and Y

directions with respect to the photodiode grid. It is seen that small variation in space positioning of a droplet may lead to large changes in a discrete image.

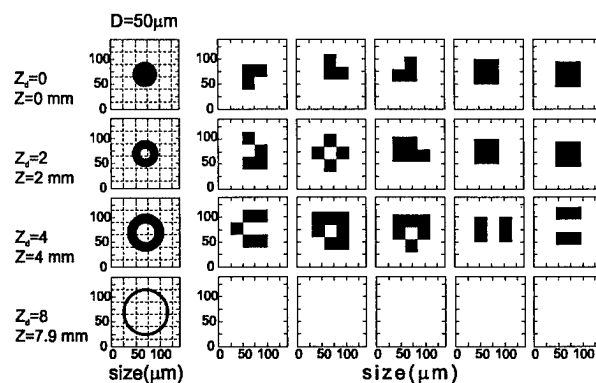


Figure 8. Same as on Fig. 7. Droplet diameter is 50 μm .

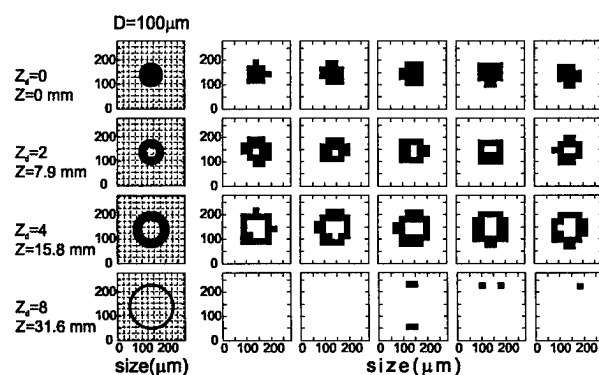


Figure 9. Same as on Fig. 7. Droplet diameter is 100 μm .

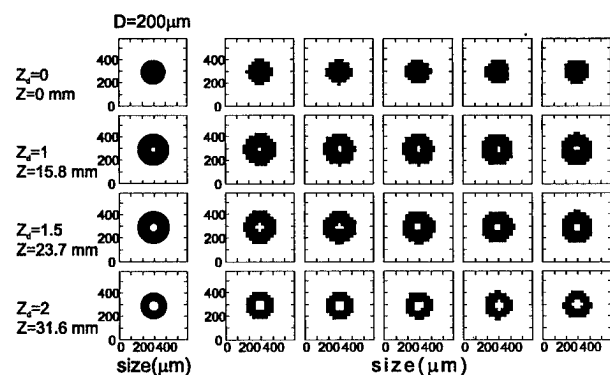


Figure 10. Same as on Fig. 7. Droplet diameter is 200 μm .

Another important point is that a particle cannot be recognized as a sphere until the image is at least 10 pixels in size. Thus, we can confidently distinguish between droplets and ice particles (spheres and nonshperes) starting

from 250 μm particles at 25 μm resolution (OAP-2DC).

Figure 11 presents an example of 2D images of drizzle measured by an OAP-2DC installed on NRC Convair-580. One can see that the measured images have many similar features to the calculated theoretically images of Figure 8-10.

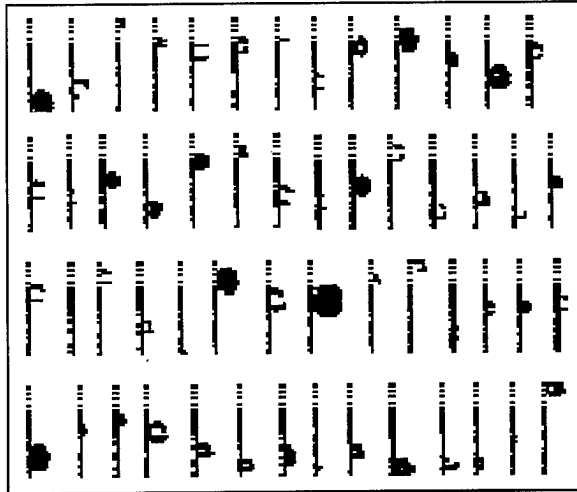


Figure 11 Measured OAP-2DC drizzle images at 25 μm resolution. Canadian Freezing Drizzle Project, Newfoundland, 17:40, 9 March 1995.

4.2 Losses

Figures 7-10 shows that droplets up to 100 μm may produce "empty" images within the depth-of-field for the OAP-2DC. This occurs because after integration over the area of a photodiode the resulting intensity is higher than the triggering level, even though the image has zones with the intensity below the triggering level. This leads to the losses of parts of images which are theoretically supposed to be counted. The probability of these "blank" images increases towards the edge of depth-of-field. Figure 12 shows calculated percentage of counting losses versus droplet size. The smaller the particle the larger the losses. For 25 μm droplets, the losses may reach about 70%. This leads to the reduction of the effective sample area and the sample area should be calculated as

$$S = N \Delta Y Z_{\text{eff}} \quad (6)$$

where $Z_{\text{eff}} = \int_{-Z_{\text{DoF}}/2}^{Z_{\text{DoF}}/2} P(z) dz$ is the effective depth-of-field; $P(z)$ is the probability of the counting the particle versus the distance from the object plane.

Particles with sizes smaller than the probe resolution can initialize an image registration. For example droplets starting from 15 μm may trigger the photodiode if the image intersects the photodiode through its center. Note that these calculations were performed for ideal zero response time, and can be applied only for the very slow velocities ($U < 20 \text{ m/s}$). In reality the OAP electronics have a finite response time, that may essentially increase the losses of small particles at aircraft velocities ($U \sim 70-150 \text{ m/s}$).

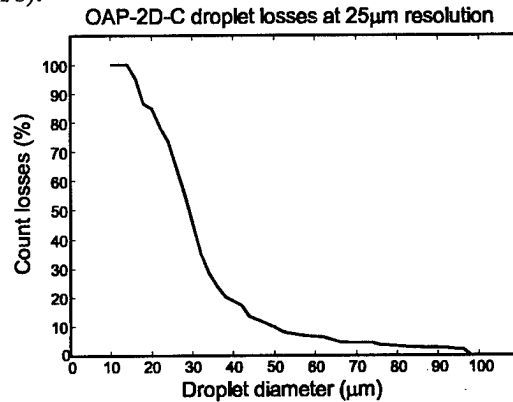


Figure 12. Calculated counting losses versus droplet diameter.

5. Sizing of 2D images

5.1 Definition of droplet sizes from digital images

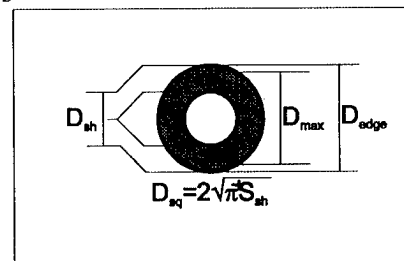


Figure 13

The size of a droplet image can be defined in several different ways. Figure 13 shows some possible definitions of droplet sizes. D_{edge} is a size defined as the distance between two edge shadowed pixels. D_{sh} corresponds to a number

of shadowed pixels in the slice having maximum distance between the edge shadowed pixels. D_{max} is a size corresponding to maximum number of shadowed pixels in a slice. $D_{sq} = 2\pi\sqrt{S_{sh}}$ is an area equivalent size, where S_{sh} is total area corresponding to all shadowed pixels.

5.2 Dependence of droplet size on distance from the object plane

Figure 13 shows the dependence of measured size on distance from the object plane for different size definitions at different shadow levels. Both D_{edge} and D_{sq} at shadow level 50% (Fig. 14ab) oversize droplets for almost all distances. The error in sizing for D_{edge} may reach 90%. The definition D_{sq} is more accurate for droplet sizing; the maximum error in oversizing reaches only 40%. The definition D_{sh} mostly leads to undersizing of droplets.

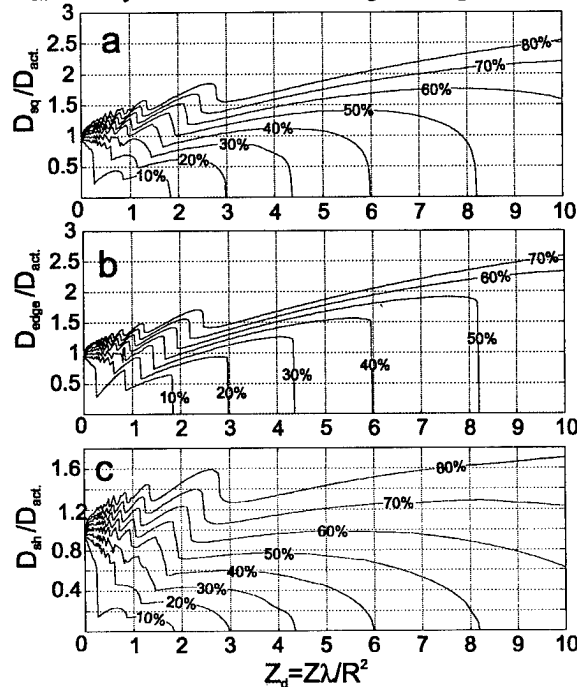


Figure 14 Dependence of measured droplet size on distance from the object plane for different size definitions at different shadow levels.

6. Retrieval of individual images

There are two basic approaches to the correcting of measured OAP's particle sizes. The first approach is based on processing each image and introducing corrections for each individual particle. The output of such

processing is a corrected size of each individual particle. The second version of retrieval is based on a statistical approach, which can be applied to large ensembles of images. The output of this processing is a corrected size distribution of an ensemble of particles but not individual ones. Each approach has its own advantages and disadvantages, and the choice depends on the problem. For example, the statistical approach cannot be used for cases with statistically insignificant sets of images. In such situations, it is better to use the retrieval of individual images. However, algorithms using a statistical approach are much faster than the retrieval of individual images. Furthermore the individual image approach is not effective to small images.

The individual particle retrieval is based on the fact that the diffraction image of a spherical particle is a function of two independent parameters: the actual particle size D and the distance from the object plane Z . So, the measured droplet size can be represented as $D_{meas} = DF(Z_d(D, Z))$. Thus, in order to find D , we have to solve a system of two equations

$$\begin{aligned} D_{meas1} &= DF_1(Z_d(D, Z)) \\ D_{meas2} &= DF_2(Z_d(D, Z)) \end{aligned} \quad (7)$$

where D_{meas1} , D_{meas2} are two different measured sizes of the same image; F_1 , F_2 are known functions obtained from theoretical calculations or laboratory measurements. The choice of D_{meas1} and D_{meas2} is to some extent arbitrary and depends on the type of OAP. It could be sizes measured at two different shadow levels (in the case OAP-2Dgrey), or sizes measured using two different definitions of droplet size at the same shadow level (see sect. 5.1), or any other possible measured size of a diffraction image.

Since F_1 and F_2 are nonlinear functions, the system (7) may have multiple solutions. This problem can be solved in two different manners. First, one or two new equations could be added to system (7) to reduce the number of solutions. Second, a pair of measured parameters D_{meas1} , D_{meas2} could be found that gives a unique solution of (7).

There are several possible well behaved pairs of measured sizes D_{meas1} , D_{meas2} that could be used for retrieval. For an OAP-2D imaging at the 50% shadow level, the ratio of the central spot size D_{spot} to the size D_{edge} (see sect. 5.1) can be used. Figure 15a shows that the dependence of the ratio D_{spot}/D_{edge} on Z_d is a monotonic function. Thus the ratio D_{spot}/D_{edge} obtained from measurements immediately yields Z_d . Knowing Z_d , $F_1(Z_d)$ and $F_2(Z_d)$ we can find the actual size D . Another possible ratio that can be used is $(D_{sq}/D_{edge})^2$. Figure 15b shows that the dependence of $(D_{sq}/D_{edge})^2$ on Z_d is also monotonic.

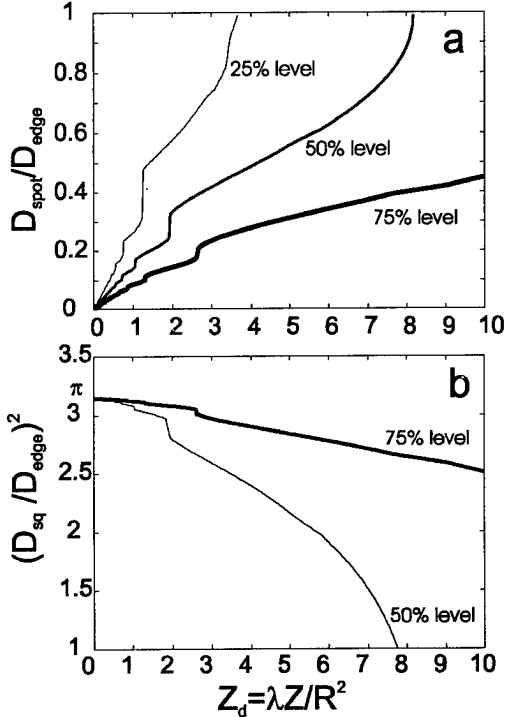


Figure 15 Measurable OAPs ratios, which are possible to use for retrieval of the size of individual images.

7. Retrieval of ensembles of images

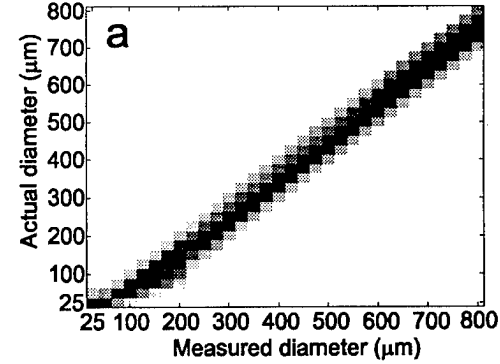
The retrieval of ensembles of images requires finding a function Φ that provides $f_m(D) = \Phi(f_o(D))$, where $f_m(D)$ and $f_o(D)$ are the measured and the actual particle size distributions, respectively. If the function Φ is known, the actual size distribution can be found as $f_o(D) = \Phi^*(f_m(D))$, where Φ^* is the inverse of Φ . Since OAPs have discrete registration of images, the function Φ will be represented by a square matrix M , where each line is a response

of a probe to one discrete bin size. Thus the actual size spectrum can be found by

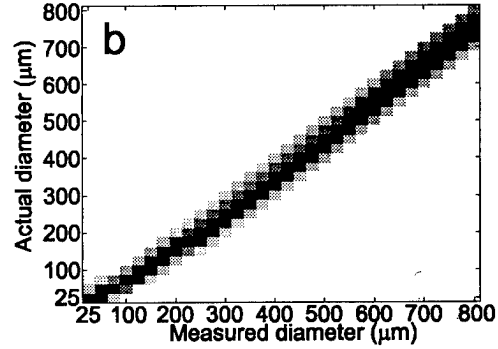
$$\bar{N}_0 = M^{-1} \bar{N}_m \quad (8)$$

where \bar{N}_0 and \bar{N}_m are the vectors of actual and measured size distributions; M^{-1} is an inverse matrix of the measured distortions of true discrete sizes by the probe.

max distance between edge shadowed pixels



max number of shadowed pixels



squareroot of shadowed pixels

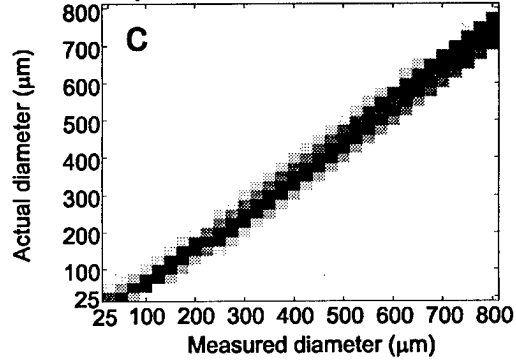


Figure 16 Distortion matrices for different definitions of measured size. The grey shade indicates the probability of an expected measured droplet size.

Figure 16 shows distortion matrices M calculated for three different definitions of droplet size D_{edge} , D_{sq} and D_{sq} . The grey shade indicates the probability a particle will be

counted in this size bin, i.e. the darker the grey the higher is the probability. These matrices were calculated with a size step of 2 μm and steps in X and Y directions of 5 μm . It is seen that droplets with sizes less than 100 μm can both be undersized and oversized. Droplets with size larger than 100 μm can be only oversized. The maximum error for these droplets is approximately constant and equal to 125 μm . The matrices M presented on Figure 16 are well defined and can be easily inverted.

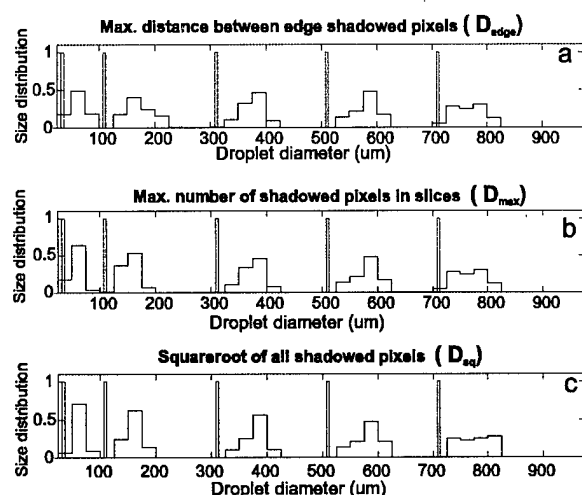


Figure 17. Response of OAP-2DC (solid lines) to monodisperse size distributions (dashed lines) for different definitions of measured droplet size.

Figure 17 shows the response of OAP-2DC (solid lines) to monodisperse size distributions (dashed lines). Droplets of 100 μm may be measured as 25 μm or 200 μm . For 300 μm droplets the expected measured size ranges from 300 μm to 425 μm . The comparisons of probe response for different definitions of droplet size shows that D_{edge} yields the largest error in sizing of small particles. The sizing of large particles is approximately equivalent for the other suggested definitions.

8. Discussion and conclusions

Kichhoff-Fresnel diffraction by an opaque disc was used for analysis of sizing inaccuracy of OAP 2D-images. The errors in droplet sizing for OAPs increase with decreasing size. For 100 μm true diameter, the expected measured sizes will be from 0 to 200 μm . For 500 μm

true diameter, the corresponding expected measured sizes will be from 500 μm to 625 μm . The discrete manner of particle image registration also leads to losses of particles with sizes less than 100 μm . For the ideal case with zero photodiode response time, the losses reach 70% for 25 μm droplets. A non-zero response time will increase these losses. These findings help explain the problems in the overlap region of the FSSP and OAP droplet spectra. A variety of calculated digital images for OAP-2D-C and OAP-2D grey are presented. Spherical and nonspherical particles can be confidently distinguished for images having more than 10x10 pixels. Calculated images are compared to examples of real images from clouds. Different methods of particle image sizing are discussed. Droplet size is better deduced from the maximum number of shadowed pixels in one of the image slices or from equivalent area size. Different methods of size retrieval of individual droplets and droplet ensembles are discussed. Correction algorithms for these effects have been derived, and distortion and correction retrieval matrices have been calculated. Future work must also incorporate the effect of non-zero time response to complete the OAP-2D size spectrum correction algorithm.

REFERENCES

- Born M., and D. S. Wolf, 1968: *Principles of Optics*. Fourth Edition, Pergamon Press, Oxford, p 808
- Heymsfield A. and D. Baumgardner, 1985: Summary of a Workshop on Processing of 2D Probe Data. *Bull. Amer. Meteor. Soc.*, **66**, 437-440.
- Joe P., and R. List, 1987: Testing and performance of two-dimensional Optical Array Spectrometer with greyscale. *J. Atmos. Ocean. Techn.*, **4**, 139-150
- Korolev A.V., S. V. Kuznetsov, Yu. E. Makarov and V. S. Novikov, 1991: Evaluations of measurements of Particle size and sample area from optical array probes. *J. Atmos. Ocean. Tech.*, **8**, 514-522.
- Lawson R. P., and R. H. Cormack, 1995: Theoretical design and preliminary tests of two new particle spectrometers for cloud microphysics research. *Atmos. Research*, **35**, 315-348.

SOME INSTRUMENTATION EFFECTS ON AIRBORNE MEASUREMENTS OF THE DROP SIZE DISTRIBUTION IN FREEZING DRIZZLE

R. Paul. Lawson*, A. V. Korolev[†], T. Huang*, L. J. Angus*, K. A. Weaver*,
J. W. Strapp[†], G. A. Isaac[†], S. G. Cober[†]

* SPEC Incorporated, Boulder, Colorado, USA.

[†] Atmospheric Environment Service, Downsview, Ontario, Canada.

1. Introduction

There is a significant potential icing hazard to general aviation and commuter aircraft flying in freezing drizzle (Cooper et al. 1984; Politovich 1989; Politovich 1996; Ashenden et al. 1996). Following the crash of a commuter aircraft enroute from Indianapolis to Chicago on 31 October 1994, awareness of this hazard has gained international attention (for example, see the *New York Times*, March 4, 1995).

The Canadian Freezing Drizzle Experiment (CFDE) field program conducted near St. Johns, Newfoundland in March 1995 focused on improving our understanding of the meteorology associated with freezing drizzle and making improved in situ observations (Isaac et al. 1996). A Convair 580 research aircraft operated by the National Research Council (NRC) and the Atmospheric Environment Service (AES) of Canada was extensively equipped with microphysical instrumentation. The instrumentation on the Convair 580 included a new optical imaging probe with 3.7 μm size resolution that makes digital images of particles from about 10 μm to 2 mm in diameter. The new probe uses digital holography to reconstruct in-focus images from in-line holograms (Lawson and Cormack 1995; Lawson 1995, Lawson et al. 1996).

New data collected in freezing drizzle during the CFDE support theoretical calculations (Korolev et al. 1991, 1996) and recent laboratory work (Reuter and Bakan 1996) showing that size measurements of drops up to about 200 μm diameter using the PMS 2D-C imaging probe (Knollenberg 1981) can be overestimated by nearly a factor of two. A statistical correction applied to the 2D-C data (Korolev et al. 1996) can improve the measurements somewhat, but cannot correct for all of the measurement deficiencies of the older imaging probes. In this paper, we compare measurements in freezing drizzle using the new digital holographic probe, the Particle Measuring Systems (PMS) 2D-C, 1D-260X and FSSP¹ probes. The recent statistical corrections to the 2D-C probe applied by Korolev et al. (1996) are presented. Some instrumentation effects on calculation of median volume diameter (MVD) are also discussed.

2. 2D-C Measurements

Korolev et al. (1991) present theoretical arguments and laboratory measurements which suggest that the PMS 2D-C can overestimate by up to 80% the size of spherical objects up to about 200 μm in

¹ Two FSSP probes were installed on the Convair 580, one has a size range from 2-31 μm and the other with a range from 5-95 μm .

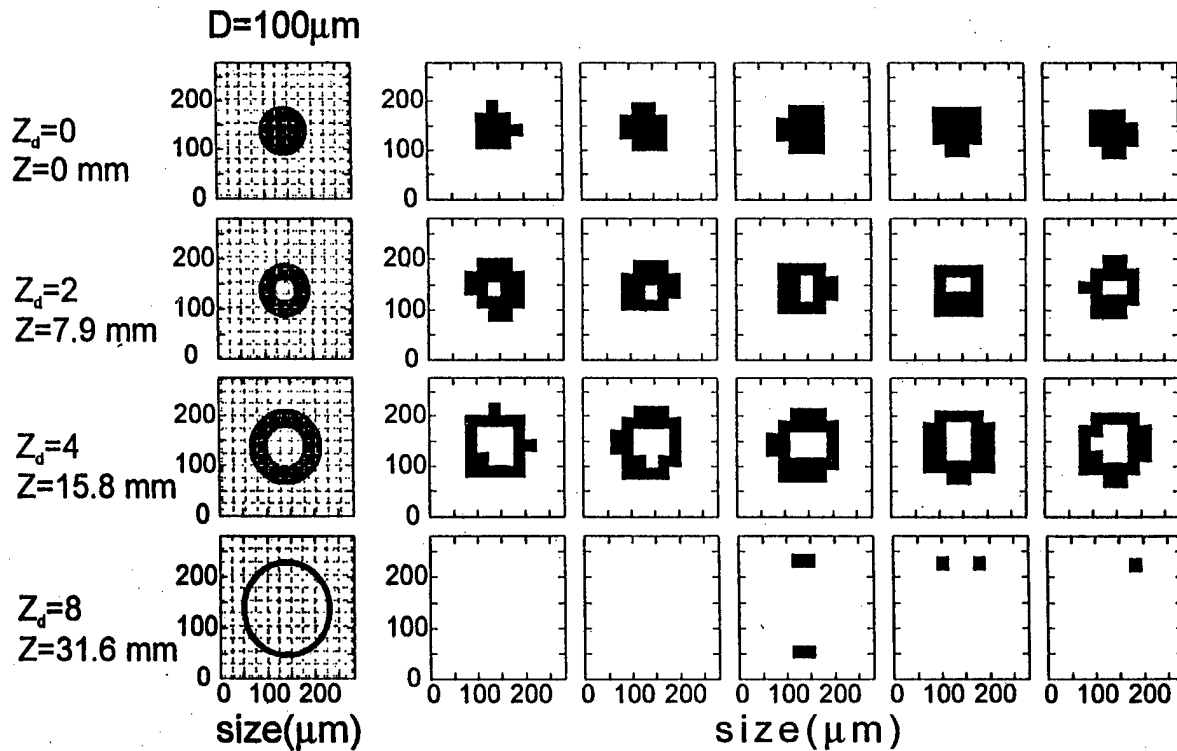


Figure 1. Korolev numerical simulations of Fresnel diffraction of a 100 μm spherical particle. Patterns on the left are for 1-bit shadow images with infinitely small pixels and on the right as seen by the PMS 2D-C with 25 μm pixels resolution. Moving down the figure, the patterns vary as a function of distance from the focal plane.

diameter. Recently, Korolev et al. (1996) and Reuter and Bakan (1996) have strengthened both the theoretical and laboratory results. Basically, the 2D-C measurement problems stem from two inadequacies: 1) the probe provides only a one-bit digitization of the shadow size, so particles that are from about $3 \rightarrow 8 \ r^2/\lambda$ (where r is radius and λ is the wavelength of laser light) are mis-sized by about $20 \rightarrow 80\%$ and 2) at aircraft (100 m s^{-1}) speeds, the probe electronics detect only a fraction of the particles that are $< \sim 150 \mu\text{m}$ in diameter.

Figure 1 shows examples of numerical simulations of Fresnel diffraction of 100 μm diameter spherical particles seen by the PMS 2D-C probe as a function of distance ($Z=Z_d \ r^2/\lambda$) from the focal plane. The

simulation on the left shows the diffraction pattern with infinite size resolution and on the right with 25 μm pixels. The numerical simulations show that the 100 μm particles are oversized as Z_d increases until about $Z_d = 8$ where they are missed all together or severely undersized. The patterns in **Figure 1** only take into account the pixel size and thresholding inadequacies of the 2D-C probe and not latency in the electronics. Recent laboratory tests at the GKSS in Geesthacht, Germany by two of the authors (AVK and JWS) suggest that the number of particles with diameters $< 150 \mu\text{m}$ that are missed or undersized increases dramatically with particle velocity.

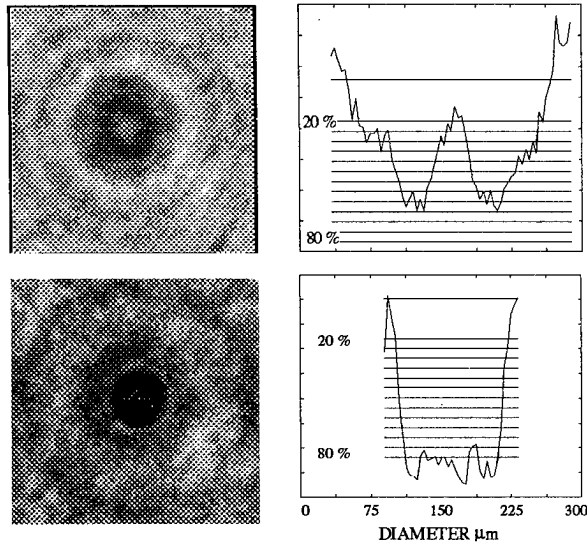


Figure 2. Example of (top) digital hologram of 100 μm bead taken at $Z_d=4$ and cross-section with shadow intensity labeled at 20% and 80%, and (bottom) image and shadow cross-section of bead after digital holographic processing.

3. Holographic Measurements

Lawson and Cormack (1995) describe the measurement technique of the digital holographic probe in detail. Here we give a brief overview of the instrument used in the CFDE. Interruption of the beam from an upstream laser diode triggers another laser diode which is pulsed for 30 ns to cast a Fresnel diffraction (shadow) pattern of the particle on a 512 x 512 solid state camera. The shadow pattern, actually an in-line (Gabor 1949) hologram, is computer-processed by numerically propagating the particle through the sample volume until the best in-focus image is obtained. An example of the numerical process is depicted in **Figure 2**. The first panel in the figure shows the 256 grey-level (8 bit) hologram and a cross section of shadow depth of a $100 \pm 1\sigma = 4.2 \mu\text{m}$ glass bead that is $Z=13.5 \text{ mm}$ ($4 r^2/\lambda$) from the focal plane. Casting the Fresnel equation in terms of Fourier transforms,

the image was propagated through the sample volume in 0.5 mm steps until the best in-focus image was found. The second panel in **Figure 2** shows the result of propagating the image and the cross section of the resulting shadow. The processed size of the drop, 103 μm , is determined by thresholding the propagated image at the 65% (of full shadow) level.²

The holographic sizing technique is compute intensive and requires some operator interaction to select and process the holograms. In order to increase processing speed, an alternative processing technique was developed which uses a software neural net to size spherical particles. A cross-section of the hologram with shadow widths at thirteen thresholds ranging from 20 \rightarrow 80% of shadow depth is feed into the neural net algorithm. The neural net was first trained using polystyrene beads and water drops generated by a TSI 3450 drop generator and then tested on another data set.

Figure 3 shows laboratory measurements using both the holographic technique and the neural net algorithm for various diameter polystyrene beads and 45 μm water drops produced by the TSI device. The manufacturers' standard deviations in diameters of the actual size distributions of the beads and drops differs for different sizes, but is on the order of 4%. Both the holographic and neural net algorithms produced good results; the RMS sizing errors over the range of

² By thresholding the original hologram (the top left image in **Figure 2**) in a way analogous to the processing done in the PMS 2D-C probe (i.e., sizing the particle by measuring the width of the shadow at the 50% level), the bead 100 μm bead is measured to be 125 μm in diameter, which is in good agreement with the theoretical simulation shown in **Figure 1**.

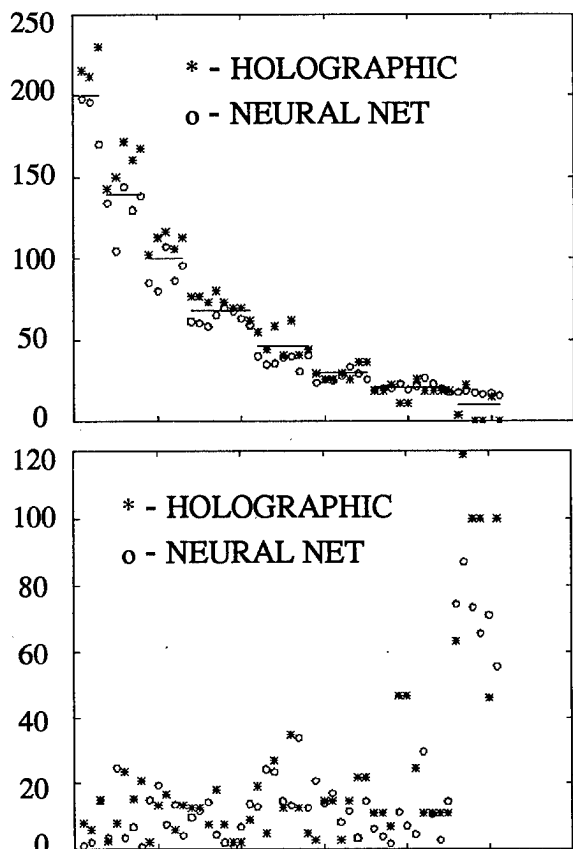


Figure 3. Top graph shows results of holographic (*) and neural net (o) sizing measurements where solid horizontal lines represent (from left) 200, 139, 100, 68, 30, 20, 10 μm beads and 45 μm diameter drops. Bottom graph plots sizing error on the vertical axis versus particle diameters which register with the horizontal lines on the top graph.

diameters from 30 \rightarrow 200 μm is 11% for the neural net algorithm and 12% for the holographic technique. The RMS error increases for both techniques to about 35% at diameters $< 30 \mu\text{m}$. The neural net approach takes less computer time and facilitates data processing.

The holographic data from the CFDE were processed using a hybrid approach. Holograms where the drops were noisy or far out of focus (say, $Z > 20 r^2/\lambda$) were flagged and processed using the full holographic algorithm while the bulk of

the drops were processed using the neural net algorithm. Periodic comparisons between the holographic and neural net techniques provided a quality check. The measurement of particle concentration using the holographic probe involves corrections for probe activity and dead time. These corrections are currently being refined.

4. Measurements in Freezing Drizzle

The numerical simulations of Fresnel diffraction for discretized pixels shown in **Figure 1** were used as a basis to develop a technique to statistically correct the PMS 2D-C measurements. The details of the technique are given in Korolev et al. (1996). **Figure 4** shows the theoretical results of the Korolev statistical corrections as a function of particle size, without the effects of particle speed, mentioned above, and instrument noise.

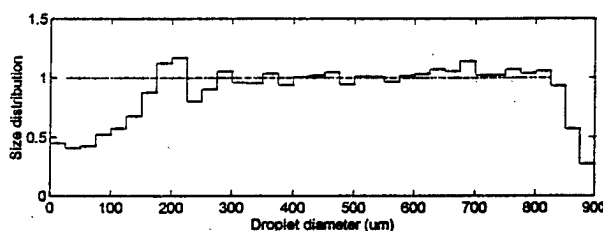


Figure 4. Theoretical results using the Korolev statistical correction scheme for the 2D-C probe. Size distribution on the vertical axis is the normalized number concentration of drops versus drop diameter. Dashed line is actual concentration.

Simultaneous measurements from the 2D-C and the new digital holographic probe were made in freezing drizzle during the CFDE. Both probes have a sample volume on the order of 4 l s^{-1} at 100 m s^{-1} . **Figure 5** shows a comparison of drop size distributions from the two probes along

with the Korolev theoretical correction. The measurements were made on 15 March 1995 near cloud top from 1943 - 1947 UTC in a region which appeared to form via the coalescence freezing drizzle process (Cober et al. 1995; Isaac et al. 1996). The 2D-C data suggest that drops with diameters out to 350 μm were observed, while the holographic probe measured drops only as large as 225 μm . The apparent oversizing in the 150 \rightarrow 350 μm range by the 2D-C is in general agreement with the Korolev theoretical correction, also shown in Figure 5. The agreement in the overall shape of the holographic and corrected 2D-C distributions is very good. The large (artificial) tail seen in the uncorrected 2D-C measurements is shifted to smaller sizes by the correction scheme.

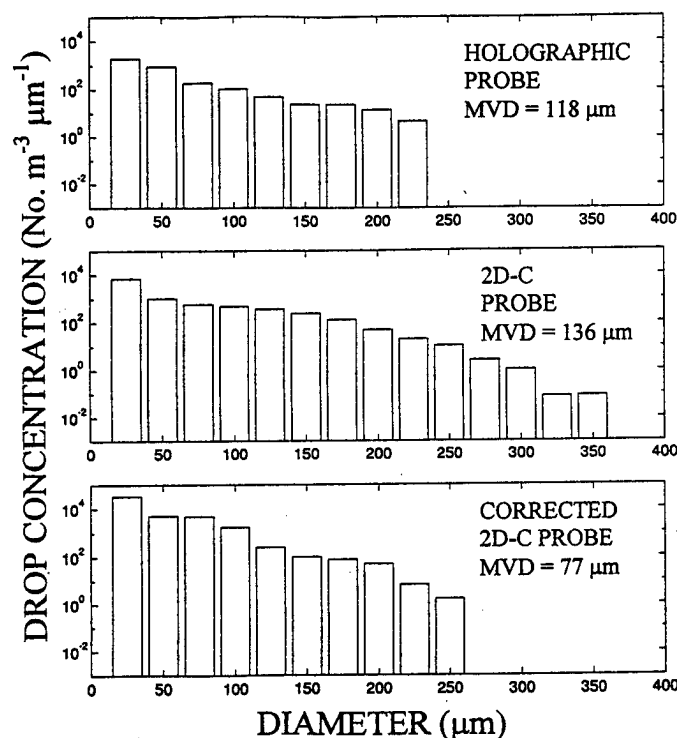


Figure 5. Comparison of digital holographic, uncorrected and corrected 2D-C measurements collected in freezing drizzle from 1943-1947 UTC on 15 March 1995.

Values of the median volume diameter (MVD), a quantity commonly used in icing studies, are also shown on the individual drop spectra plots shown in Figure 5. The MVD computed from the uncorrected 2D-C size distribution is 136 μm while the MVD computed from the holographic measurements is 118 μm . The increase in MVD reflects the apparent oversizing of the larger drops by the 2D-C. The large "tail" of the drop size distribution is important for computing icing severity (Politovich 1989, 1996).

The MVD of the Korolev corrected 2D-C distribution shown in Figure 5 has been reduced from the uncorrected value of 136 μm to 77 μm , which is 41 μm less than the holographic measurements. This is mostly due to the shifting of particles to smaller size bins, which as shown in Figure 4, may not be applicable to particles <150 μm because several of the particles go undetected.

The computation of MVD for the 1943-1947 UTC freezing-drizzle drop spectra shown in Figure 5 is sensitive to the instrumentation used as well as the relative distribution of liquid water. Cober et al. (1996) shows that, for 12 CFDE flights, only about 20% of the LWC was found in drops > 50 μm . When an order of magnitude or more of the LWC is found in drops < 50 μm , the MVD is not particularly sensitive to the drop size measurements in the 50 \rightarrow 300 μm range. However, when the LWC is more evenly balanced, the measurements in the large drop range can strongly influence the MVD.

The LWC measured from 1943-1947 by the CSIRO probe (King 1978),

TABLE 1

Measurements of LWC and MVD for the 1943-1947 UTC encounter in freezing drizzle. FSSP₁ has a size range of 3-21 μm and FSSP₂ is 5-95 μm . 2D-C_{AR} has artifacts rejected and 2D-C_{ALL} has no artifacts rejected. Other nomenclature is explained in the text.

Probe	LWC (g m^{-3})	Probe Combination	MVD (μm)	\int LWC
FSSP ₁	0.04	FSSP ₁ + FSSP ₂ + 2D-C _{AR}	40	0.08
FSSP ₂	0.06	FSSP ₁ + FSSP ₂ + 2D-C _{ALL}	74	0.09
CSIRO	0.07	FSSP ₁ + FSSP ₂ + 260X	112	0.12
Nevzorov	0.07	FSSP ₁ + Holographic	62	0.09
Nevzorov _{Total}	0.08			

Nevzorov probe, (Korolev 1996)³ and FSSP probe(s) are shown in Table 1 along with MVD calculated using some different combinations of instruments and processing techniques. The calibration and accuracy of the AES PMS probes are discussed in Cober et al. (1995). The LWC measurements all contain some degree of uncertainty, perhaps 0.01 to 0.02 g m^{-3} at these low values of LWC. Therefore, it is not possible to rigorously determine the percentage of LWC that is contained in drops $> 50 \mu\text{m}$, however, the measurements suggest that it is on the order of 50%. Using the technique discussed in Cober et al. (1996) to combine the measurements from the FSSP probe(s), PMS 2D-C and 1D-260X probes, a combined drop size distribution was generated and the MVD's were calculated from the results. The FSSP measurements from 3-29 μm were combined with the holographic probe data.

Table 1 shows that in the freezing drizzle encountered from 1943-1947, the

values of MVD calculated using the FSSP probes, plus various combinations of imaging probes, ranges from 40 \rightarrow 112 μm . This demonstrates the sensitivity of the calculation of MVD to probe measurement uncertainty when about half of the LWC is in drops $> 50 \mu\text{m}$. The best MVD agreement with the FSSP₁ + Holographic measurements is found using the FSSP₁ + FSSP₂ + 2D-C (without artifact rejection and without including the 2D-C channels from 25 - 100 μm). Visual inspection of the 2D-C images showed no streakers and obvious artifacts, so in this case, the artifact rejection criteria may have been removing images of actual drops.

As shown in Figure 4, the 2D-C is predicted to significantly undercount particles $< \sim 150 \mu\text{m}$, even without airspeed effects. Preliminary results of laboratory tests with a spinning disk rotating at aircraft speeds at the GKSS suggest that a substantial percentage of particles are undersized and missed all together in the 50 \rightarrow 150 μm size range. Figure 6 shows measurements taken in freezing drizzle on

³ The Nevzorov probe provides a measure of both the cloud drop and the total (including the larger drop portion of) liquid water content.

15 March from 1938-1939 and 1939-1941 UTC. The MVD determined from the holographic probe alone is about $40\text{ }\mu\text{m}$ in both time periods, smaller than for 1943-1947.

The size distributions measured by the 2D-C in Figure 6 are grossly different than the holographic measurements. During these time periods, the cloud LWC measured by the CSIRO, Nevzorov and FSSP probes was on the order of 0.4 g m^{-3} . The integrated LWC from the drop spectra in Figure 6 is on the order of a few hundredths of a g m^{-3} , so contributions to MVD from the larger drops are minor. The MVD calculated for these time periods is $\sim 21\text{ }\mu\text{m}$, regardless of whether the 2D-C with or without artifact rejection, 1D-260X, or holographic probe is used for measuring the larger part of the drop size distribution.

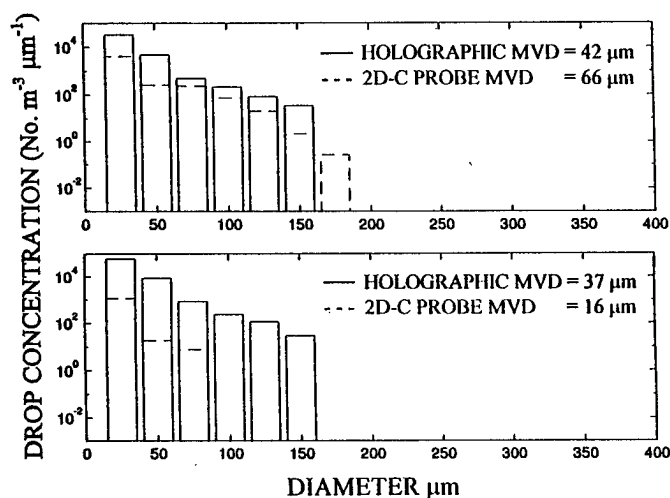


Figure 6. Comparison of 2D-C and digital holographic measurements collected in freezing drizzle from (top) 1939-1941 UTC and (bottom) 1938-1939 UTC on 15 March 1995.

5. Summary and Discussion

Measurements made in freezing drizzle of drop size distribution and LWC from

some selected portions of the Canadian Freezing Drizzle Experiment (CFDE) are discussed. Measurements from a new airborne instrument, a digital holographic imaging probe with $3.7\text{ }\mu\text{m}$ pixel size resolution, are compared with the standard PMS probes. Numerical simulations, laboratory and flight data indicate that the PMS 2D-C probe can create an artificial "tail" in the drop size distribution of freezing drizzle. The new digital holographic probe does not create the artificial tail in the drop size distribution. Korolev's theoretical corrections applied to the 2D-C data can statistically correct for the artificial tail in the $150 \rightarrow 350\text{ }\mu\text{m}$ region; however, due to effects of airspeed and noisy data, corrections to 2D-C measurements in the $25 \rightarrow 150\text{ }\mu\text{m}$ do not appear to be straightforward at this time.

The drop median volume diameter (MVD) was computed for two different regions containing large drops. One region contained low ($\sim 0.1\text{ g m}^{-3}$) LWC with about half of the LWC found in drops $> 50\text{ }\mu\text{m}$. MVD was calculated by combining in an eclectic way the measurements from various probes with different measurement size ranges. In the region where the mass of drops was approximately evenly balanced between small and large drops, the MVD calculation was very sensitive to the probe used to image the larger drops. The measured values of MVD in this region ranged from $40 \rightarrow 112\text{ }\mu\text{m}$, depending on the instrumentation. The best MVD agreement with the FSSP₁ + Holographic measurements is found using the FSSP₁ + FSSP₂ + 2D-C (without artifact rejection and without including the 2D-C channels from $25 - 100\text{ }\mu\text{m}$). In the second region, the LWC was much higher, about 0.4 g m^{-3} , and $< \sim 5\%$ of the LWC was found in drops $> 50\text{ }\mu\text{m}$. In this

region, MVD $\approx 21 \mu\text{m}$ and was insensitive to the probe used to image the larger drops.

The recent icing severity index suggested by Politovich (1996) incorporates LWC, temperature, MVD and the ratio of MVD to $15 \mu\text{m}$ drops. She notes that icing severity in situations with $\text{LWC} < 0.1 \text{ g m}^{-3}$ is generally low. Inaccuracies measuring the larger drops will influence the MVD when drops $> \sim 50 \mu\text{m}$ comprise a significant fraction of the total LWC. This implies that the large-drop portion of the distribution needs to contain $\text{LWC} > \sim 0.1 \text{ g m}^{-3}$ and be a small fraction of the total LWC for MVD measurement inaccuracies to be negligible. In these situations, the small-drop portion of the LWC will probably be large enough to flag a moderate to severe icing condition anyway (see Politovich 1996). However, a parameter that includes directly the LWC contained in drops $> \sim 50 \mu\text{m}$ may better quantify regions of freezing drizzle that could present icing hazards to commuter and general aviation aircraft.

Acknowledgments. This work was partially supported by NSF Grant No. DMI9322818, NASA Contract No. NAS1-19591 and funding from Transport Canada.

7. REFERENCES

- Ashenden, R., W. Lindberg, and J. Marwitz, 1996: Two-dimensional NACA 23012 airfoil performance degradation by super cooled cloud, drizzle, and rain drop icing. AIAA 96-0870. Presented at the 34th Aerospace Sciences Meeting and Exhibit, 15-18 Jan., 1996, Reno, Nevada.
- Cober, S. G., G. A. Isaac, and J. W. Strapp, 1995: Aircraft icing measurements in east coast winter storms. *J. Appl. Meteor.*, **34**, 88-100.
- Cober, S. G., G. A. Isaac and J. W. Strapp, 1996: Aircraft icing from supercooled drizzle. To be Presented at the 12th Inter. Conf. on Clouds and Precip., 19-23 August, 1996, Zurich, Switzerland.
- Cooper, W.A., W.R. Sand, M.K. Politovich, and D.L. Veal, 1984: Effects of icing on performance of a research airplane. *J. Aircraft*, **21**, 708-715.
- Gabor, D., 1949: Microscopy by reconstructed wave-fronts. *Proc. Roy. Soc.*, **A197**, 454-487.
- Isaac, G. A., A. Korolev, J. W. Strapp, S. G. Cober, A. Tremblay, and R. A. Stuart, 1996: Freezing drizzle formation mechanisms. 12th International Conference on Clouds and Precipitation, 19-23 Aug., 1996, Zurich, Switzerland.
- Knight, C.A., 1979: Observations of the Morphology of Melting Snow. *J. Atmos. Sci.*, **36**, 1123-1130.
- Knollenberg, R. G., 1981. Techniques for probing cloud microstructure. In: Clouds, Their Formation Optical Properties and Effects. Eds: P. V. Hobbs and A. Deepak. Academic Press, New York. 15-92.
- Korolev, A. V., S. V. Kuznetsov, Y. E. Makarov, and V. S. Novikov, 1991: Evaluation of measurements of particle size and sample area from optical array probes. *J. Atmos. Oceanic Technol.*, **8**, 514-522.
- Korolev, A. V., J. W. Strapp, and A. N. Nevzorov, 1996: On the accuracy of the Nevzorov airborne hot wire

- LWC/TWC probe. To be Presented at the 12th Inter. Conf. on Clouds and Precip., 19-23 August, 1996, Zurich, Switzerland.
- Korolev, A. V., J. W. Strapp, and G. A. Isaac, 1996: To be presented at the FAA International Conference on Aircraft Inflight Icing, 6-8 May, 1996, Springfield, Virginia.
- Lawson, R. P., 1995: Digital holographic measurements of cloud particles. Reprint from: AMS Conference on Cloud Physics, 15-20 Jan., 1995, Dallas, Texas.
- Lawson, R. P. and R. H. Cormack, 1995: Theoretical design and preliminary tests of two new particle spectrometers for cloud microphysics research. *Atmos. Res.*, 35, 315-348.
- Lawson, R. P., A. V. Korolev, T. Huang, L. J. Angus, K. A. Weaver, J. W. Strapp, G. A. Isaac, S. G. Cober, 1996: Improved airborne measurements of the drop size distribution in freezing drizzle. To be Presented at the 12 Inter. Conf. on Clouds and Precip., 19-23 August, 1996, Zurich, Switzerland.
- Politovich, M.K., 1989: Aircraft icing caused by large supercooled droplets. *J. Appl. Meteor.*, 28, 856-868.
- Politovich, M.K., 1996: The effect of icing on a research aircraft and evaluation of severity indices. *J. Aircraft*, in press.
- Reuter, A. and S. Bakan, 1996: Improvements of cloud particle sizing with a 2D-grey probe. Submitted to: *J. Atmos. Oceanic Technol.*

THE NRC CONVAIR-580 RESEARCH AIRCRAFT: CONFIGURATION IN THE CANADIAN FREEZING DRIZZLE EXPERIMENT

Dave L. Marcotte (1), J. Walter Strapp (2), Stewart G. Cober (2), George A. Isaac (2)

1. Flight Research Laboratory
Institute for Aerospace Research
National Research Council
Ottawa, Canada, K1A 0R6

2. Cloud Physics Research Division
Atmospheric Environment Service
Downsview, Ontario, Canada

ABSTRACT

The National Research Council of Canada's (NRC) Convair-580 was the aircraft used in the Canadian Freezing Drizzle Experiment, during March, 1995. The aircraft was instrumented with systems to: make cloud physics and atmospheric state measurements, measure and observe ice accretion on the aircraft directly, and characterise the aircraft response to flight in freezing precipitation. The project was conducted from a base at St. John's, Newfoundland and most flights were conducted within 350 nm of the base. The project-specific cloud physics instrumentation was chosen to provide accurate estimation of the hydrometeor spectra from aerosol size to 6.4 mm, and accurate measurements of liquid and total water content. The aircraft response to atmospheric conditions was characterised by monitoring engine parameters and flight conditions including air-flow angles and airspeed. Direct observations of icing conditions were recorded by video cameras mounted in wingtip pods, by a system designed to measure ice thickness directly, by an icing accretion rod and a by commercial ice accretion sensor. The results from the Canadian Freezing Drizzle Experiment include more than 150 cases, each of up to 5 minute exposure to cloud conditions where droplets greater than 50 μm existed.

INTRODUCTION

The Convair 580, operated by the National Research Council of Canada (NRC), is configured as a multi-purpose research aircraft and is used for such diverse activities as aeromagnetic systems research, synthetic aperture radar development and atmospheric research. This latter role has been developed since 1992, when a strategic partnership with Canada's Atmospheric Environment Service (AES) was arranged after many years of ad-hoc collaboration involving other aircraft in the NRC fleet. The Convair was the aircraft used for in-flight measurements during the Canadian Freezing Drizzle Experiment (CFDE) conducted from St. John's, Newfoundland between March 2 and March 22 1995. Figure 1 is a photo of the aircraft in the CFDE configuration.

Aircraft equipped for flight research in natural icing have been operated by various groups, including the University of Wyoming (Politovich and Sand, 1981), the US

National Centre for Atmospheric Research, and NASA (Reinmann et al., 1989). In Europe, the Commission of the European Communities is proposing a multi-year project in aircraft icing, that will include atmospheric characterisation studies with research aircraft (Minigione, G., 1995 - personal communication).

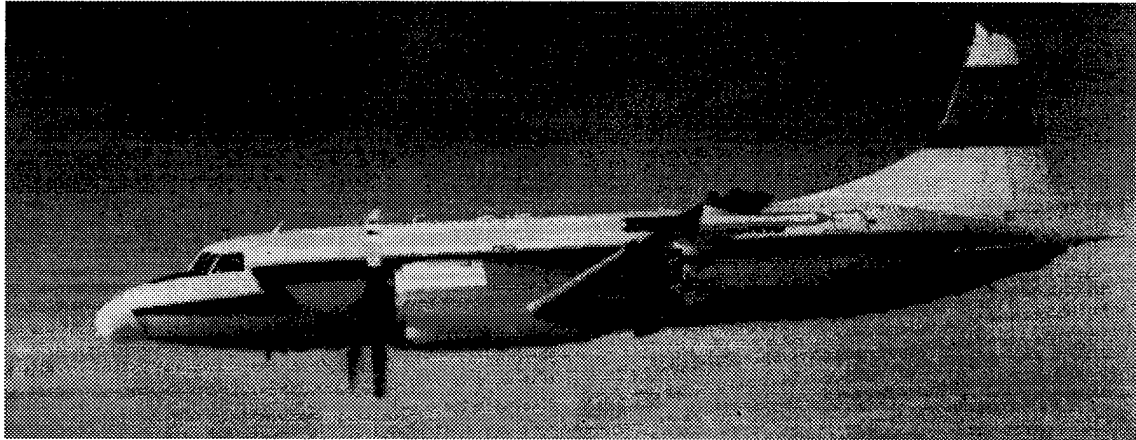


Figure 1. The NRC Convair-580. The long wingtip boom held the laser (see text) and video cameras for recording ice accretion on the ice rod and for the laser system. Underwing pylons held up to four PMS probes each.

For the CFDE, the Convair was equipped with systems for atmospheric characterisation, for the direct observation of icing on the aircraft, and for characterising the response of the aircraft to freezing precipitation. Since the principle objectives of this project involved atmospheric characterisation, in order to improve icing forecasts and to document the formation mechanisms for freezing precipitation, most attention was paid to the systems for making atmospheric state and microphysical measurements. An array of optical imaging probes was used to measure cloud water droplets and aerosol-sized particles. Liquid water content, static temperature and humidity were each measured by redundant systems. Total water content was also measured by a separate system. The resulting data set is comprehensive by virtue of our success in locating regions of freezing precipitation, as well as the complete instrumentation suite that was carried. This paper describes the systems on the aircraft and is meant to complement other papers in this series that deal in more detail with the results of the CFDE.

CFDE DESCRIPTION AND OBJECTIVES

The project was initiated in the spring of 1994 as an effort to investigate the mechanisms for the formation of freezing precipitation, especially freezing drizzle. It followed an earlier project, the Second Canadian Atlantic Storms Program (CASP II), which included objectives related to aircraft icing. During CASP-II, there were four occasions in which freezing drizzle was encountered. In all four cases drizzle formed through a 'non-classical' collision coalescence process, rather than the 'classical mechanism' of melting and refreezing (Cober et al, 1995). The main microphysical objectives of the CFDE were then to ascertain the differences between classical and non-classical freezing

precipitation, and to improve the understanding of the formation mechanisms of Supercooled Large Drops (SLD) generally. The overall objective was to reduce the danger to aircraft, either through better forecasts or avoidance based on better physical understanding.

Twelve research flights took place between March 2 and March 22, 1995, and were preferentially directed at targets that we anticipated would be productive regions for encountering freezing precipitation. Eleven of the twelve flights encountered freezing precipitation. The majority (approximately 60%) of the freezing precipitation encounters were of the non-classical type - formed without a warm layer aloft. Most flights were targeted to stratiform clouds over the ocean, although approximately 10% of the 60 flight-hours occurred over land. Data analysis, conducted to date, indicates that approximately 10-12 hours were spent in cloud regions which contained drizzle droplets greater than 50 μm (Cober et al., 1996). Figure 2 is a composite track plot of the 12 research flights.

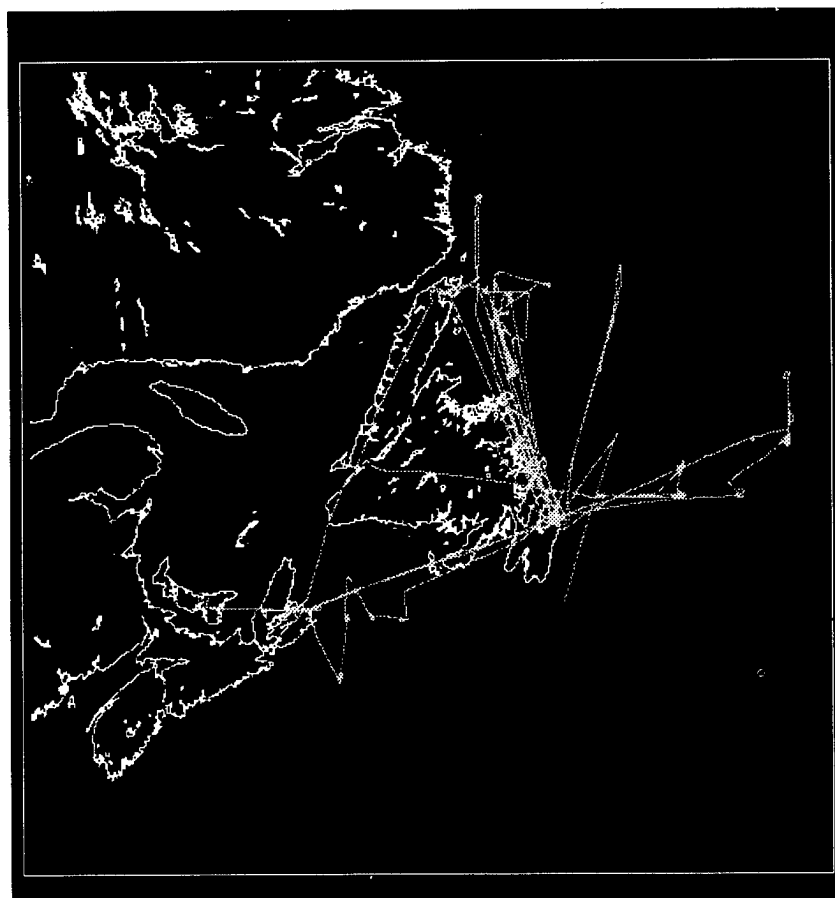


Figure 2. Composite tracks of the 12 research flights flown from St. John's, Newfoundland in the 1995 CFDE.

The selection of the base of operations for the project resulted from a climatological study showing that eastern Newfoundland receives a mean of 154 hours a year of freezing

precipitation, with 103 hours of this falling as freezing drizzle. For comparison, most of the Great Lakes region experiences a mean annual occurrence of less than 50 hours of freezing precipitation (Strapp et al., 1996).

THE AIRCRAFT FACILITY

As shown in Figure 1, the Convair-580 is a twin engine turbo-prop, thoroughly modified from its original role as a corporate aircraft. In typical configurations, in which the aircraft carries 900 kg of project specific instrumentation, we have a *useable endurance* of as much as 5 hours with a full complement of flight and research crew and with fuel reserves for an alternate airfield. The aircraft is certified for operation in light icing conditions, when the anti-icing systems are functioning (Convair Flight Manual, 1970). The baseline capabilities of the facility are summarised in Table 1.

Table 1: Capabilities of Convair-580

LENGTH/HEIGHT (m)	25.6 / 9.3
SPAN (m)	32.1
MAX. T/O WEIGHT (kg)	26,400
CEILING - (feet)	25,000
PAYLOAD * (kg)	1900
RANGE** (nm)	1200
ENDURANCE** (hrs)	6.5
CRUISE SPEED - TAS (kts)	270

* Typical values with full project installations and crew.

**Actual values depend on mission profile, distance to alternates, etc.

OPERATING PROCEDURES FOR FLIGHT IN ICING CONDITIONS

The Convair Flight Manual specifies that, with the anti-icing systems operating, the aircraft is limited to operations in light icing. By definition light icing conditions include flight operations where the use of anti-icing equipment prevent ice accumulation. Our approach during CFDE was to enter regions of suspected icing conditions from regions where icing did not occur, and to always have an escape route planned. The decision to exit or remain in the icing condition was made solely on whether or not the aircraft's anti-icing systems could cope with the conditions. Regions of severe icing conditions if found, would not be returned to intentionally and, if inadvertently encountered, were exited.

Since it was not the primary objective of the CFDE to document the performance degradation of the aircraft in icing conditions, there was little temptation to intentionally accrete ice to the aircraft, for example by porpoising, at cloud top.

SYSTEMS FOR ATMOSPHERIC CHARACTERISATION

The aircraft is outfitted with underwing pylons that provide sites for 8 PMS-type canisters, although we can operate with as many as 12, with additional sites on each wingtip and with two fuselage mounted probes. The pylons were designed so that the combined aerodynamic effects of the wing, instrument canister and pylon would not induce break-up of droplets of up to 5 mm diameter at typical operating conditions. This droplet stability analysis fixed some of the design parameters of the pylon (spanwise mounting location, length and thickness) and also determined the ideal mounting location for imaging probes that are designed to image larger droplets, for example the PMS 2D-C and 2D-P. In the project under discussion, droplets as large as several mm were not anticipated; nevertheless the underwing PMS sites were expected to give reliable droplet statistics, since sorting and droplet break-up would be minimised.

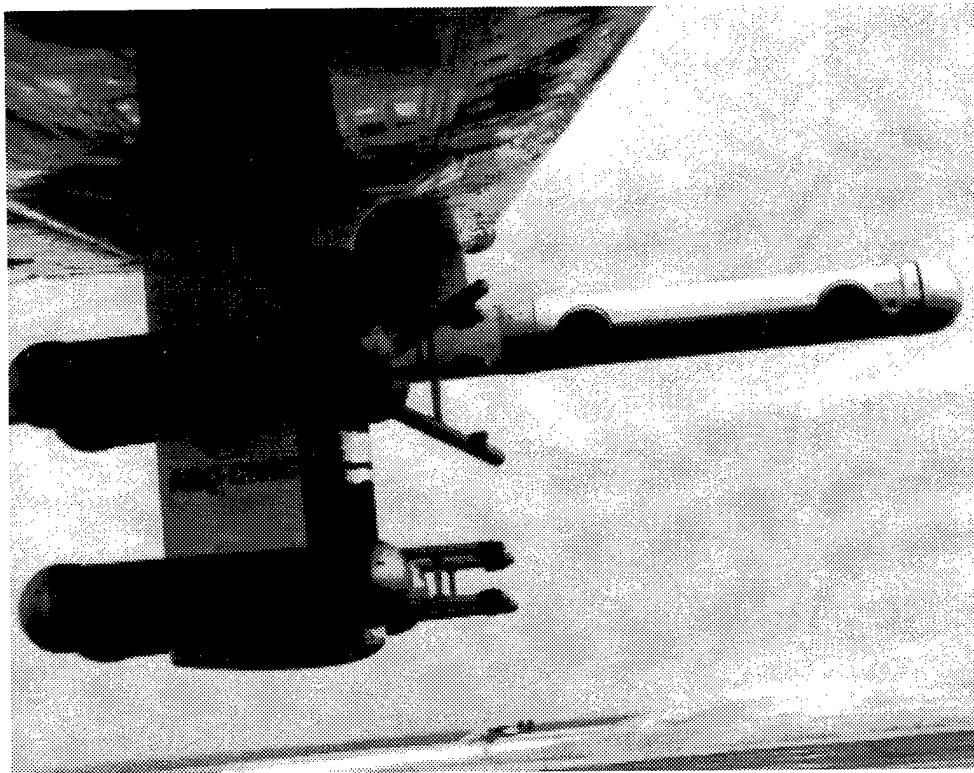


Figure 3. Photo along the port wing. The 2D-P probe is located in a region where a droplet stability analysis indicates large droplets are not subject to break-up. The extended wingtip boom held two cameras and a laser for measuring the thickness of glaze ice build-up on the pylon leading edge, which could be electrothermally de-iced.

During the CFDE, seven underwing pylon sites were occupied by PMS probes. These were: a PCASP-100x 0.13-3 μm aerosol probe, FSSP-100x 3-45 μm probe, FSSP-100x 5-95 μm probe, 2DC mono 25-800 μm probe, 2DC grey 25-1600 μm , 2DP mono 200-6400 μm probe, 1DC 20-300 μm probe and a 1D260 10-640 μm probe. Not all probes were in operation for all flights. The probe data were recorded asynchronously to Exabyte tape by a SEA model 200 DAS.

A prototype probe, based on a digital holographic camera not subject to the particle size range limitations of the other optical probes, was mounted on the starboard wingtip boom for flights occurring in the second half of the field campaign. The probe uses a new technique for making measurements throughout the range 10-2000 μm (Lawson et al., 1996).

A complete tabulated instrumentation list is presented in Table 2.

Liquid and total water content measurements were made by 2 King probes accurate to within $\pm 0.02 \text{ gm}^{-3}$ for $\text{LWC} < 0.2 \text{ gm}^{-3}$ and a Nevzorev liquid and total water probe for which accuracy of $\pm 10\%$ is claimed (Korolev et al., 1996). Static and dynamic air temperature were measured by three temperature probes, one of which was collocated with the liquid water probes (Figure 4). The other two temperature probes, a reverse flow and a standard Rosemount total temperature probe, are mounted under the port wing.

The three liquid water probes, and one of the temperature probes are positioned in a cluster surrounding a pitot-static head on a boom mounted under the starboard wing, extending approximately 23 cm forward of the leading edge of the wing. The instruments are in a region of upwash, being forward and under the wing, and, so, the 'air-speed' measured by the local pitot-static probe is used for correcting data from the probes located here.

Humidity measurements were made by two instruments, a dewpoint/frostpoint hygrometer and a Cambridge Systems dewpoint hygrometer, each mounted on the fuselage.

Three-axis gust velocities and the airflow angles were measured by a Rosemount 858 five-hole probe, which was housed in a PMS-type canister mounted on the starboard underwing pylon.

Special attention was paid to selecting an instrument complement appropriate for drizzle measurements, since the 50-200 μm size range is a particular problem for optical probes and hot wire devices. Particularly, the extended range FSSP-100, the 1D-260X and the holographic camera probe were chosen to provide coverage in this size range. The holographic camera, described by Lawson et al., (1996) offers the possibility of high resolution (approximately 2 μm) images which can be mathematically re-focused for optimal sizing accuracy. Finally a Nevzorev LWC/TWC device provides hot wire LWCs

to an accuracy of 10%. The TWC device has a high collection efficiency for drizzle sized droplets and thus does not suffer from the underestimates in this size range unlike conventional hot wire devices.

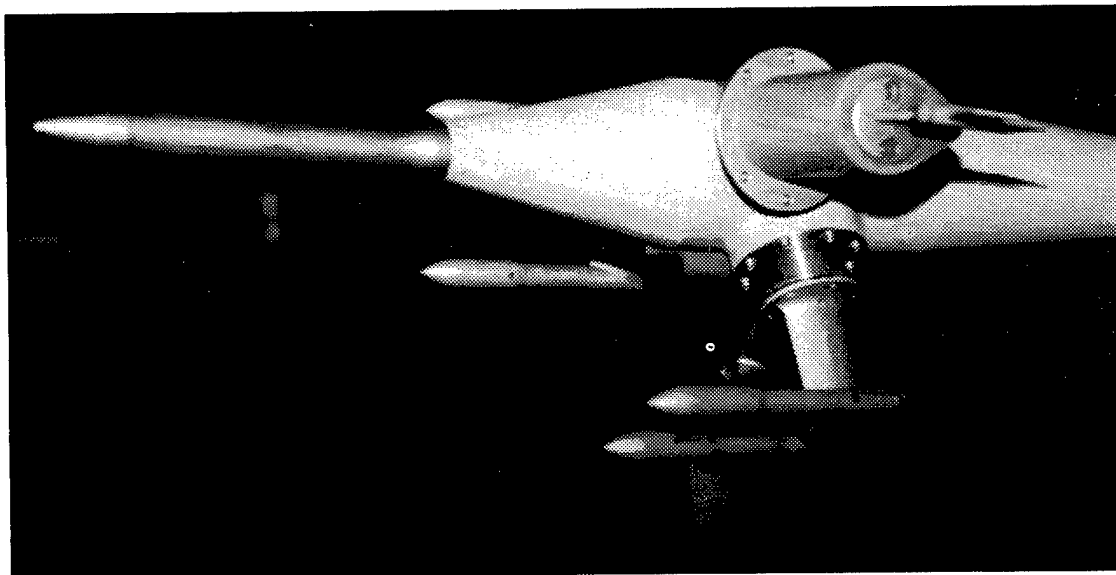


Figure 4. Starboard underwing boom site for King probes, Nevzorev probe and a Rosemount total temperature probe. Local airspeed is measured by the pitot-static probe on the front end of the boom.

SYSTEMS FOR ICE ACCRETION OBSERVATION AND MEASUREMENT

The aircraft was equipped with four systems for measuring ice accretion, as well as a video camera for observing ice build-up on the starboard pylon. Icing rate was measured by a Rosemount icing rate meter, mounted under the starboard wing immediately forward of the flap. This instrument uses magnetostriction to drive a 6mm diameter rod at a natural frequency of 40 KHz. When the small diameter rod with its high collection efficiency ices up, the frequency of oscillation decreases to some preset trip limit, at which point it is electrically deiced. Icing rate or severity is determined by the heater cycle rate.

A prototype laser-based system was used for determining the thickness of any glaze ice accumulation at a preset spot on the port pylon. The system makes use of the refractive property of ice to measure the thickness of non-opaque ice wherever the laser was directed (Gagnon and Marcotte, 1995). For this purpose, a laser was installed in the port wingtip boom and a video camera, also installed in the port boom, was focused on the laser image.

On the outboard side of the port pylon, an icing accumulation rod was mounted. This is a 12 cm long rod with a 2.54 cm diameter. At the base is an annular ring marked at 0.5 cm intervals, providing a scale to measure ice accumulation. The rod was electrothermally

heated from a control within the aircraft, in order to shed accumulated ice between encounters.

An embedded icing sensor, manufactured by Instrumar Ltd., was mounted on the underside of the horizontal stabiliser. This instrument was meant to provide a means of recognising the presence of run-back icing. The instrument determines ice thickness by measuring the impedance of the contaminant that covers the sensor head. The sensor was mounted 57 cm from the leading edge, where the chord length of the stabiliser is 2.4 m.

Observations of ice build-up were made by a video camera mounted in the starboard wingtip boom, which provided a wide angle image of the entire pylon, and much of the underside of the starboard wing. This video image, and the ones from the cameras mounted on the port side, were passed through a sequencer and then recorded by a single VCR.

SYSTEMS FOR CHARACTERISING AIRCRAFT RESPONSE

An attempt was made to measure the engine parameters and flight conditions in order to correlate aircraft response to the atmospheric conditions that it was subject to. Most of these measurements are facility based, or have since become part of our standard suite of parameters always recorded on the aircraft. These parameters include: true and indicated airspeed, angle of attack and sideslip, roll, pitch and yaw attitudes, three-axis accelerations, true heading, groundspeed and position and the engine parameters of fuel flow, shaft horsepower and Turbine Inlet Temperature.

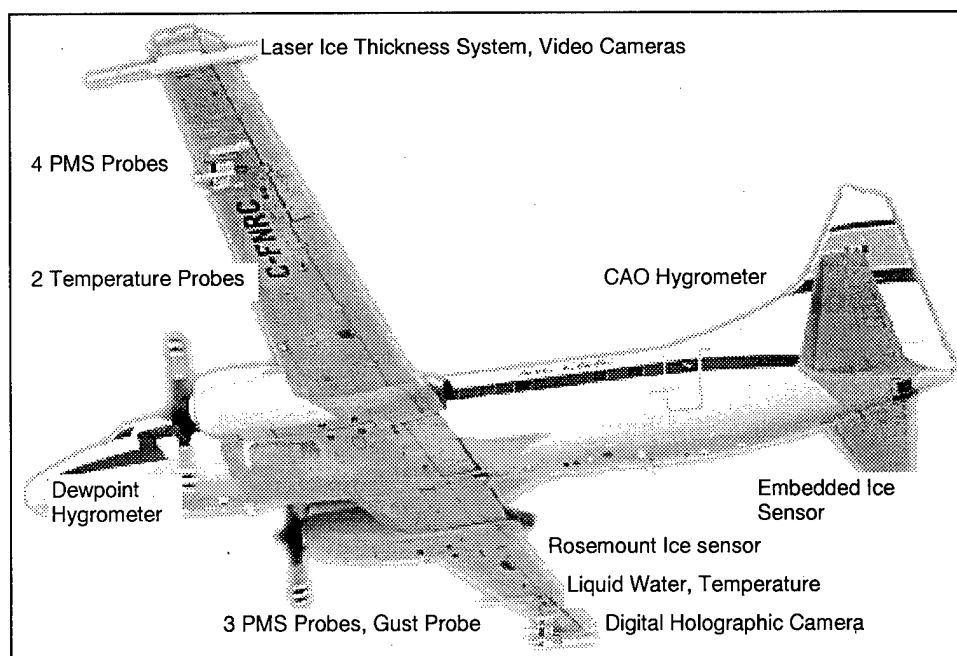


Figure 5. Drawing of C-FNRC showing location of instruments for the CFDE.

Table 2. Instrumentation List

Category	Measurement	Instrument
Atmospheric State	Temperature	Rosemount temperature probe (deiced)
	Temperature	Rosemount fast response temperature probe (deiced)
	Temperature	Reverse flow (NCAR design)
	Dewpoint	Cambridge (chilled mirror) hygrometer
	Dewpoint /frostpoint	CAO hygrometer
	Surface temperature	Barnes PRT-5
	3 axis winds	Rosemount 858 on starboard pylon
Cloud Microphysics	Droplet liquid water	PMS King probe (long version)
	Droplet liquid water	PMS King probe (short version)
	Droplet liquid water	Nevzorev LWC probe
	Total water content and phase ratio	Nevzorev TWC/LWC probe
	Aerosol spectrum (0.1-3 μm)	PMS PCASP-100X probe
	Aerosol spectrum (0.3-20 μm)	PMS FSSP 300 probe
	Droplet spectrum (2-30 μm)	PMS FSSP 100 probe
	Droplet spectrum (5-95 μm)	PMS FSSP 100 probe
	Small cloud particles and droplet spectrum tail (70-300 μm , and 10-600 μm)	PMS 1D-C probe
	Droplet/ice spectrum and 3D particle (5-2000 μm)	PMS 1D 260X probe
	Cloud particle spectrum and images (25-800 μm)	SPEC holographic probe
	Cloud particle spectrum and images (25-1600 μm)	PMS 2D-C mono probe
	Precipitation spectrum and images (200-6400 μm)	PMS 2D-C grey probe
	Cloud precipitation collectors	PMS 2D-P (mono) probe
Ice Accretion	Icing rate	NRC-AES design, heated, deployable
	Icing rate	Rosemount icing rate meter
	Ice thickness and properties	Instrumar microwave detector
	Ice accretion	Airbus certification rod and video camera
	Ice thickness	NRC laser system and video camera
Aircraft State / Performance	Ice accretion	Starboard wingtip boom video camera
	Altitude	
	Altitude	Bendix radar altimeter
	Altitude (pressure)	TRT radar altimeter
	Airspeed (true, indicated)	Digiquartz static pressure on fuselage
	Position	Pitot under wing, static pressure on fuselage
	Attitude, accelerations, heading, ground speed	GPS, LTN-91 Inertial Navigation System
	3-axis speeds wrt to ground	LTN-91 Inertial Navigation System
	Fuel flow	GPS
	Shaft horsepower	Engine instruments
	Turbine inlet temperature	Engine instruments

CONCLUSIONS

Aircraft-based measurements were made for the Canadian Freezing Drizzle Experiment in March 1995, by the Atmospheric Environment Service and the National Research Council of Canada. During the experiment 10-12 hours of data from cloud regions containing drizzle droplets greater than 50 μm were collected. The freezing precipitation was found most often in stratus clouds. Measurements were made from the NRC Convair-580 which had been outfitted with instrumentation for measuring cloud physics, atmospheric state parameters, ice accretion and aircraft state parameters. Special attention was paid to selecting instruments appropriate for drizzle measurements

ACKNOWLEDGEMENTS

The project was conducted by NRC and AES and funded by AES, NRC the Canadian National Search and Rescue Secretariat and Transport Canada.

REFERENCES

- Cober, S.G., J.W. Strapp, G.A. Isaac, 1995: A case of freezing drizzle formed through a collision coalescence process. Pre-prints, Cloud Physics Conference, Amer. Meteor. Soc., Texas, January 1995.
- Cober, S. G., G. A. Isaac, J. W. Strapp, and D L. Marcotte, 1996: Analysis of aircraft icing environments associated with supercooled drizzle droplets. Proceedings of FAA International Conference on Aircraft Inflight Icing, Springfield, Va., May, 1996.
- Gagnon, R.E. and D.L. Marcotte, 1995: Icing thickness measurements from an airfoil and model helicopter rotor using a new remote technique. Proceedings International Icing Symposium, Montreal, Sept., 1995.
- Korolev, A.V., J.W. Strapp and A.N. Nevzorev, 1996: On the accuracy of Nevzorev airborne hot wire LWC/TWC probe. Proceedings of 12th Intl. Conf. Clouds and Precipitation Zurich, Aug., 1996.
- Lawson, R. P., A.V. Korolev, T. Huang, L.J. Angus, K.A. Weaver, J.W. Strapp, G.A. Isaac, S.G. Cober, 1996: Improved airborne measurements of the drop size distribution in freezing drizzle. Proceedings of 12th Intl. Conf. Clouds and Precipitation, Zurich, Aug., 1996.
- Politovich, M.K. and W.R. Sand, 1981: Measurement of natural aircraft icing conditions. AIAA Aircraft Systems and Technology Conference, Dayton, August 1981.

Reinmann, J.J., R.J. Shaw, R.J. Ranaudo, 1989: NASA's program on icing research and technology. Symposium on Flight in Adverse Environmental Conditions, Gol, Norway, May 1989.

Strapp, J.W., G.A. Isaac and R.A. Stuart, 1996: Canadian climatology of freezing precipitation, and a detailed study using data from St. John's, Newfoundland. Proceedings of FAA International Conference on Aircraft Inflight Icing , Springfield, Va., May, 1996.

Section II

Ice Protection and Ice Detection

David Sweet, Industry Co-Chair

Charles Masters, Federal Aviation Administration Co-Chair

AN OPERATIONAL PERSPECTIVE ON ICE DETECTION AND PROTECTION SYSTEMS RESEARCH AND DEVELOPMENT

Joe Bracken, Steve Green,
Jim Bettcher, Steve Erickson
USA Air Line Pilots Association
Inflight Icing Certification Project Team

ABSTRACT

Presently, there is no requirement for manufacturers to provide a means for the pilot to determine whether the aircraft is operating in an environment which is outside of the certification envelope. Further, there is no requirement to provide ice detection systems which monitor critical areas of the airframe, such as the horizontal stabilizer or the area forward of the aileron. Current ice detection systems assume the ice accretion and its effects to be more or less homogeneous, when in fact a given set of icing parameters may have a wide range of effects, depending on which location on the airframe is examined.

There is a need to investigate the possibilities of developing a form of predictive ice detection. This would allow airlines and the flightcrews to respond to an icing threat prior to entering the threat environment.

In order for pilots to conduct operations in the modern air traffic environment while exposed to icing conditions, there is also an urgent need for both reactive detection of the exceedance environment as well as reactive detection of ice accretions in critical areas of the airframe.

Energy efficient ice protection enhancements must be considered as a means of protecting primary control surfaces from the aerodynamic effects of supercooled large droplet and/or runback accretions.

This paper will focus primarily on the area of inflight icing prediction, detection and protection.

PAST PERCEPTIONS

On October 31, 1994 an aircraft accident occurred over Roselawn, Indiana. The aviation community is very much aware of the details of that particular accident and the focus of the investigation to date. The investigation, almost immediately after the accident, began to focus on the meteorological conditions present that afternoon and their effects on the aircraft.

Was the accident crew aware that now-tested Side Window Icing visual cue was indicative of an Appendix C exceedance encounter? No. Was the accident crew of that flight experiencing Side Window Icing? Analysis done of the meteorological conditions at the time indicate that they may have been. Was the accident crew experiencing icing conditions that they should have deemed "severe"? Cockpit discussions prior to the upset indicate that the crew did not sense any severe icing conditions. Did the accident crew have any reason to believe that their aircraft may be operating in a meteorological condition that it had never been certificated for? No.

The industry has certainly learned a considerable amount since October 1994.

For one specific series of aircraft, the ATR-42/72, there is now a tested and, to that extent, valid indicator of an Appendix C exceedance encounter (hereafter referred to as 'exceedance conditions' or an 'exceedance encounter', these terms will pertain to meteorological conditions beyond the current FAR Part 25, Appendix C certification criteria). Also, industry now understands that icing caused by freezing drizzle, freezing rain and/or some severities of clear icing or the clear component of mixed icing may appear benign to a flight crew while impinging and building aft of the protected surfaces of an aircraft. However, in spite of what has been learned to date, actions by industry still fall far short of what is necessary to ensure the safe operation of aircraft in meteorological conditions which are difficult, if not impossible, to predict or identify.

In addition, the industry must be willing to treat Appendix C icing conditions as a "nominal" environment; that being a condition that can be expected to be encountered on a rather routine basis. The nominal icing environment should not result in handling and performance characteristics that are substantially less than that expected of a dry wing. Industry must then address exceedance conditions; or those atmospheric conditions which exist, but are difficult to predict and are challenging in terms of recognition and safe operation.

MINIMIZING THE EXPOSURE & MAXIMIZING THE PREDICTABILITY

A. Exceedance Encounter Probabilities

The aviation industry is currently (and has historically been) basing design considerations on a probability of encountering an exceedance icing condition of 1×10^{-3} , or 1 chance in a 1000¹. We must accept this probability as a valid assessment in terms of encountering such conditions. However ALPA feels that this number is unacceptably high and must be controlled in such a way to avoid a condition that has the potential of resulting in a catastrophic event.

FAR Part 25.1309 describes the requirements for aircraft equipment, systems and installations. 25.1309(b)(1) and 25.1309(b)(2) state:

"(1) The occurrence of any failure condition which would prevent the continued safe flight and landing of the airplane is extremely improbable, and

(2) The occurrence of any other failure conditions which would reduce the capability of the airplane or the ability of the crew to cope with adverse operating conditions is improbable."

Advisory circular 25.1309-1A² defines "improbable" and "extremely improbable" as:

"(2) Improbable failure conditions are those having a probability on the order of 1×10^{-5} or less, but greater than on the order of 1×10^{-9} ,

(3) Extremely Improbable failure conditions are those having a probability on the order of 1×10^{-9} or less."

These probabilities are specified in order to define the acceptable risk of system or equipment failure. A loss of control due to structural icing should be considered an extremely improbable event. Once the 10^{-3} probability has been encountered, or exceedance conditions are being experienced, industry presumes that the flight crew will provide the remaining actions necessary to insure that a loss of control is "extremely improbable". Yet the flight crew; 1) has no means of detecting entry into the exceedance environment, and 2) no assurance of adequate handling characteristics for the period of time required to depart the exceedance environment. Thus, for all practical purposes, the probability of a catastrophic event due to an encounter with the exceedance environment cannot be specified, and thus has not been adequately protected against to the degree established by such rules as 25.1309.

No one disagrees that with the coming of the regional airlines, and the necessity to provide short leg, frequent service between relatively close locations, the turboprop aircraft is susceptible to frequent operation at altitudes containing icing conditions.

The Regional Airline Association (RAA) has implemented an Unusual Icing Reporting program which is intended to provide aircraft manufacturers, regulatory authorities, pilot representative groups and research institutions information concerning

encounters with unusual icing conditions. A database of these reports will be used to further study the icing phenomena and develop better weather forecasting techniques. It is ALPA's understanding that, to date, input to the RAA program has been minimal, quite possibly due to several limiting criteria for submitting a report (e.g. Reporting forms kept in airlines Chief Pilot office which makes submitting a report cumbersome and precludes pilot anonymity, and the program requests only "unusual" icing reports which is a subjective judgment by the flightcrew).

Certainly, several products could result from this icing reporting program; frequency of reports, location of reports, frequency vs. location of reports, prominent geographical locations conducive to such icing reports, as well as a rough estimate of probability of an exceedance encounter. With proper handling of the data, several key products could be obtained prior to the next significant icing season which would help minimize the exposure of aircraft to potential exceedance conditions.

The Air Line Pilots Association has developed and conducted a simple exceedance icing survey over the past several months. The data used in the survey was requested of all ATR-42/72 pilots flying for three ALPA regional airlines. The survey asked for the number of side window icing encounters over the past 17 months as well as the geographic location in which the aircraft was being operated at the time of the encounter. Although a limited amount of data was requested, the survey arrived at several significant conclusions. A more detailed report on the results of the

survey has been prepared by Mr. Steve Green. Copies can be made available upon request.

B. Predictive Ice Detection

First and foremost is the need for reliable forecasting / prediction of exceedance environmental conditions. This information can then be provided to dispatchers and flightcrews to preclude encountering such conditions. This can be done through Predictive Ice Detection methods. If the exposure can be minimized or negated in total, less emphasis and concern need be placed on Reactive Detection methods.

Conversations with the National Center for Atmospheric Research (NCAR) indicate that there are several short-term efforts underway in the areas of Ground-Based Predictive Ice Detection and Large Droplet Icing Forecasting. NCAR also has several long-term programs in place that will not be available for several years. This paper will attempt to highlight the short-term.

NCAR has been providing Freezing Precipitation Aloft information to the Aviation Weather Center (AWC) in Kansas City. The AWC is then providing this information in any icing AIRMETS that are issued. This program has been in place since January of this year. The Freezing Precipitation Aloft information is arrived at through freezing drizzle, freezing rain or ice pellet surface and weather station reports and then compared with a numerical model taking temperature and relative humidity into account. The output is a 3-dimensional depiction of where freezing precipitation is expected to occur. This product offers

a highly conservative forecast covering a broad area. A validation of the end product will be conducted using pilot reports.

As a by-product of the RAA program mentioned earlier, NCAR is attempting to evaluate icing conditions aloft by comparing pilot reports of 'unusual icing' with the actual weather occurring at the time of the report. To date, it is ALPA's understanding that response to the RAA program has been minimal and is providing NCAR with little information for analysis.

An effort underway by the National Oceanic and Atmospheric Association (NOAA) is the Differential Attenuating Radar. This system operates under the concept that the attenuation of a beam of microwave energy is directly proportional to the amount of liquid water along its path. This attenuation, for a given amount of liquid, increases with decreasing wavelength. With this being true, the differential attenuation between two wavelengths may be used for measuring spatial distribution of liquid within a cloud by simultaneously transmitting two radar frequencies along the same path. Specific wavelengths are chosen as the baseline indicative of Supercooled Liquid Water (SLW)³. It is envisioned that this may eventually be used as a "Look-Ahead" system installed on aircraft. Testing is ongoing.

There was also a project underway to analyze icing conditions aloft through the use of satellite imagery in an attempt to isolate and identify SLW environments. This program is currently on hold due to funding shortfalls.

There is certainly a great deal of research presently in progress in the area of large droplet icing forecasting and prediction with even more planned for the future. Industry must encourage further research in these areas to preclude any intentional aircraft operations in exceedance icing conditions. Perhaps with additional research, over time the icing envelope referred to as Appendix C could be expanded, thus allowing future aircraft to be certificated for operations in such large droplet icing conditions.

MAXIMIZING THE RECOGNITION AND MINIMIZING THE ERROR

A. More Specific Visual Cues

In the absence of current and reliable Predictive Ice Detection equipment, pilots must rely on in-flight visual cues to indicate to them that they are encountering an exceedance environment. It has been written recently that *"...Pilots of turboprop aircraft are confident in their ability to detect the onset of in-flight icing conditions through the use of visual cues."*⁴ Let's briefly take a look at this statement a little more closely to determine the overall validity in today's industry.

For decades, pilots have been using inflight icing visual cues such as windshield wiper ice, window frame ice and propeller spinner ice as indicators of the magnitude and severity of icing conditions being encountered. Until recently, however, pilots felt that this was just "ice", and could easily identify when their aircraft could no longer handle these conditions. But now we have further refined the classification of "ice" to 'within Certification' and

'outside Certification' conditions. And we've seen how benign 'outside certification' icing may appear and how hazardous it can become.

First, how does industry determine which of the above age-old visual cues represent Certification criteria icing and which does not? Second, once we've determined which is which, how do we inform the pilots of this? And third, once we've informed the pilots, how do we make them understand that what they felt may have been benign before, may now be extremely hazardous?

As mentioned earlier, subsequent to the accident in Roselawn, Indiana, ATR embarked on a significant effort to primarily; 1) Determine whether their aircraft exhibited any adverse performance and/or handling qualities after exposure to exceedance icing conditions and 2) identify specific exceedance icing cues which could be utilized by flight crews to determine when such conditions were being experienced. Conclusions were determined for both efforts.

Specific to this paper, a very definite exceedance icing visual cue was determined. This very aircraft specific icing cue has been termed "Side Window Icing". It is characterized on this particular aircraft as *"dispersed granular ice pattern, spanning the entire height of either side window, covering all or part of the window from front to back."*⁵ Although only tested in conditions capable of being generated by the USAF NKC-135 Icing Tanker, this visual cue has been taught by companies and used by flightcrews for approximately fourteen

(14) months now with relatively good results.

In January of this year, the FAA issued seventeen (17) proposed Airworthiness Directives (AD) covering all or a majority of the scheduled passenger turboprop fleet. In the area of exceedance visual icing cues, each proposed AD recommended Airplane Flight Manual (AFM) language revisions that cited the visual cues indicative of a freezing rain or freezing drizzle encounter as "*--Unusually extensive ice accreted on the airframe in areas not normally observed to collect ice, -- Accumulation of ice on the upper surface (for low-wing airplanes) or lower surface (for high-wing airplanes) of the wing aft of the protected area, -- Accumulation of ice on the propeller spinner farther back than normally observed.*"

The differences between the exceedance cues identified through **testing** for the ATR aircraft and the cues **recommended** for the 17 aircraft covered in the proposed AD's in January are substantial and serious. The exceedance icing cues identified for the ATR aircraft are specific to that aircraft and are based on flight testing in very specific flight conditions and icing cloud physics.

By the FAA's own admission, "*Since turbopropeller-powered airplanes are more likely to operate at low altitudes and to make more frequent landings, they are more likely to encounter icing conditions that are outside the icing envelope.*"⁶ Therefore, providing such generic visual cues as "*...unusually extensive ice accreted on the airframe in*

areas not normally observed to collect ice..." or "*...accumulation of ice on the propeller spinner farther back than normally observed...*" are inadequate for aircraft types that frequently operate in and encounter such conditions. Ice accretions at these locations for flight crews of these particular aircraft may not be deemed unusual or farther back than normal. If visual cues are going to be provided to flight crews as exceedance icing encounter indicators, they must be more specific and dependent upon aircraft type.

Naturally, all visual cues provided are also subject to the flight crews ability to see and identify that cue. Flights conducted at night or in IFR conditions, or both, may make the recognition of cues some distance away from the cockpit (e.g. propeller spinners or wing surfaces) more difficult at the very least, if not impossible.

Therefore, in the absence of a requirement for Reactive Detection Equipment, a well thought-out test plan must be generated and very detailed testing must be conducted to identify visual cues specific to each individual aircraft. These specific visual cues must identify accretion locations and degree of coverage which characterize exceedance conditions.

B. Reactive Detection of Exceedance Environment / Ice Accretions

It has also been written that "*...For turboprop aircraft, existing in-flight ice detection systems are regarded by pilots and aircraft manufacturers as being of limited value.*"⁷ Let's now take a look

at this statement to determine its validity in today's industry.

As mentioned earlier, for decades, pilots have been using inflight icing visual cues such as windshield wiper ice, window frame ice and/or propeller spinner ice as indicators of the magnitude and severity of icing conditions being encountered. But these visual cues may be specific to a particular aircraft type and are certainly dependent upon the meteorological conditions being encountered and the configuration the aircraft is being operated in (at least as far as we can tell at the time due to the limited testing conducted by industry).

Because of the subjectivity and variability of these icing cues, not to mention the absence of good data on the icing environment beyond Appendix C, industry must push forward and strongly encourage and bolster research in the area of Reactive Ice Detectors. In the event an inadvertent encounter with exceedance icing occurs which does not provide an adequate or recognizable visual cue to the flight crew, a Reactive Ice Detector is the only other means available. This Detector must provide the flight crew with a conservative assessment of the conditions being encountered and provide that information in a timely manner to provide an adequate margin to exit those conditions.

There are several means in which exceedance icing conditions may be encountered in nature; an exceedance in Liquid Water Content (LWC), an exceedance in Mean Volumetric Diameter (MVD), or both. An exceedance in LWC, with non-exceedance MVD's will result in rapid

accretion rates on the protected surfaces of an aircraft. On the other hand, exceedance MVD's and non-exceedance LWC's will result in aft of protected surface impingement. (Appendix C can be exceeded if the MVD value is higher than that specified for the LWC/temperature conditions. Recent research into bimodal mass distributions, however, may render the MVD term meaningless with regard to supercooled large droplet environments. It may be possible to encounter significant concentrations of large droplets while the aggregate MVD remains within Appendix C.

Presently, several devices are being researched and tested that will provide a detection means for the above conditions. Without endorsing any single item, ALPA will attempt to highlight a few of the products currently on the market.

In 1965, Vibro-meter pioneered the use of a piezoelectric based technology for an airborne engine vibration monitoring system. This technology has been transferred to use as an ice detection device. This particular method of ice detection is based upon the principle that the resonant frequency of a body will alter with changes in mass or stiffness. By flush mounting such a resonating sensor diaphragm, ice can be detected. As ice accretes on the diaphragm, the diaphragm becomes stiff and increases in mass. This induces an increase in resonant frequency. Liquid accretions (e.g. rain, deicing fluid, etc.) increases mass without increasing stiffness, thus lowering the resonant frequency. Therefore, a clear discrimination between ice and liquid can be ensured. This

system was tested on the ATR aircraft during the second series of Edwards AFB testing in March of 1995 with very promising results. Proper placement of such a sensor could provide flightcrews with a clear indication of an exceedance encounter and aft-of-protected-surface impingement. A similar system has been tested on an MD-80 aircraft for on-ground ice detection.

The same sensor mentioned above, in conjunction with minor software adjustments, provides the capability to determine accretion rates on particular surfaces of an aircraft. This could then provide information to flightcrews when their aircraft, or a specific surface of that aircraft, is experiencing high accretion rates, indicative of high LWC.

Intertechnique of France also manufactures a flush mounted, ultrasonic ice detection system that was successfully tested on an ATR aircraft at Edwards Air Force Base in March of 1995. This particular system is capable of providing to the flightcrew a measurement of the actual amount of ice and the rate of accretion that is present on a particular sensor. Intertechnique's goal is to have an improved system with smaller sensors ready for airframe testing by Fall of this year.

The Intertechnique and Vibro-meter systems could also, by placing a sensor within the booted area, provide the capability of automatic anti-ice/de-ice operation when ice accretions reach a pre-determined thickness. Testing is continuing on both company's systems, while systems are ready for flight testing by operators or manufacturers.

The Rosemont System installed on all ATR aircraft is also an oscillatory device to detect ice accretions. The probe is exposed to the slipstream and is electrically oscillated at a prescribed frequency. As ice accumulates, the probe mass increases which causes decreased frequency. When the probe frequency reaches a predetermined level, an ice detection warning is triggered. During the accident flight and subsequent testing, this particular device was effective in identifying ice accretions and providing an aural notification to the flightcrew, however, it is unclear whether this particular system is capable of discriminating between nominal and exceedance icing environments.

The Marinvent Corporation, in conjunction with BFGoodrich Aerospace, has taken a different approach to Reactive Detection. They have developed a system that senses the actual condition of the airflow of an aircraft surface as it is affected by contaminants. This system is designed to *"provide accurate stall warning plus the expanded capability of detecting the presence and effect of any lift-reducing contamination such as ice, snow, slush or insects..."*⁸ The system is intended to provide warning to the flight crew when accretions exceed certified levels. The system has been tested in wind tunnel, heavy rain facilities and flight tests. Recent flight tests on ATR aircraft have achieved acceptable results, however further testing and aircraft fitting is required.

Naturally, the use of remote detectors to alert the cockpit crew to ice accretion is highly dependent upon the placement of the sensor to provide accurate detection.

Because of the unique extended lines of impingement of supercooled large droplets, a sensor mounted aft of normal ice accretion areas may be fairly accurate in detecting these conditions. The current application of most detectors is to alert the cockpit to the accretion of ice on the airframe without regard to location, type, or quantity. Current sensors are generally used as a backup to the primary method of pilot visual cues.

It is obvious that In-Flight Ice Detection technology is not only a reality, but it is currently available for testing and use. If ice detector manufacturers are willing to provide the means, industry should make a serious and relatively inexpensive effort to remove some of the guesswork from exceedance icing visual detection. This means providing a real-time mechanical detection and indication to flightcrews.

MINIMIZING THE EFFECTS ON THE AIRFRAME

A. Energy Efficient Ice Protection Enhancements.

FAR 25.1419 describes the requirements for Ice Protection systems on transport category aircraft. The provisions under this particular regulation makes no provision or distinction regarding the status of the aircraft surface being protected subsequent to the activation of the equipment. In other words, there is no requirement for the protected surface or surface of concern (i.e. wing, tailplane, engine inlet, etc.) to be back to a dry-air state after activation of the ice protection system. Paragraph (a) simply states: *"(a) An analysis must be performed to establish that the ice*

protection for the various components of the airplane is adequate, taking into account the various airplane operational configurations..."

Evaporative systems found on large transport category aircraft (turbojets) are clearly at an advantage in terms of having adequate engine bleed air available to completely clean the surface of the wing, minimizing the effects of residual ice on the airframe. The smaller, less powerful turboprop aircraft, which have no excess bleed air available to incorporate an evaporative system, therefore must rely predominately on pneumatic systems to clear ice from the critical areas of the airframe.

Historically, pneumatic systems were considered adequate in removing accreted ice, thus allowing the safe operation of the aircraft in icing conditions. For Appendix C conditions, this is true. However, we now know that once the aircraft exceeds "nominal" Appendix C icing conditions, the possibility exists to either form an ice ridge at the aft limit of the pneumatic system due to its activation or actually build a ridge which is unaffected by the activation of the pneumatic system. With regard to totally evaporative systems, performance in exceedance conditions has not been well tested or documented.

In December of 1994, ATR conducted its first series of Icing Tanker tests at Edwards Air Force Base. The objectives of these tests were three-fold, one of which was the:

- *"testing various coatings, paints and other chemicals reputed by their manufacturers to be "ice-phobic,"*

*i.e. they are supposed to help prevent ice adhesion."*⁹

One result of the testing concluded that "ice phobic" coatings were ineffective in preventing ice accretions.

In addition, it was discovered that the aircraft:

- *"accretes ice in certain test conditions exceeding FAR Part 25 maximum continuous conditions within and beyond the active area of the de-ice boots...develops a jagged, spanwise ridge of ice at the upper edge of the boot (8% chord at flaps 0, 9% chord at flaps 15) and trailing back to approximately 14% chord with decreasing thickness..."*¹⁰

So, how does industry avoid a situation such as this during line flying; that being encountering an environmental condition that poses the threat of accreting ice on a lifting surface beyond the protected area? Currently, the capability exists to: a) Provide a means of Predictive Detection, either ground or satellite based, or on-board the aircraft, which could preclude putting an aircraft into an environment which has the potential of building ice at the aft limit or beyond of a de-ice system, b) Provide a means of Reactive Detection that would provide the flightcrew with immediate identification of such an environment and afford the flightcrew adequate warning to exit said condition prior to any adverse ice accretions, or c) Install a system on the aircraft that would preclude adverse ice formations on critical areas of the airframe.

Since extending pneumatic boots over the entire airframe, or at least over critical areas of the airframe is neither cost effective nor practical, other means must be researched. At present, ALPA is aware of only a few evaporative systems installed on turboprop aircraft; all of which are installed on older vintage models. The evaporative system to which I am referring would be similar to turbojet operations which use engine bleed air to remove ice accretions in critical areas of the airframe.

An interesting system was tested in May of 1994 at the NASA Lewis Icing Tunnel facility in Cleveland, Ohio. The system was designed by Aerospace Safety Technologies, Incorporated (ASTI) of Nevada. This "No-Ice" system is effectively a heater blanket which is bonded directly to the necessary airframe surface and can be used in the anti-ice and/or de-ice mode. The "blanket" is an extremely low weight system which requires minimal power to operate, well within single engine power availability. During icing tunnel testing, the system was effective in removing ice accretions over its entire surface. Results of those particular tests showed real value. Currently, this system is being tested on a prototype air carrier turboprop aircraft and is exhibiting promising results. The blanket is located under the aft portion of the installed de-icing boot and has been shown to remove any ice ridges or residual ice on the surface.

Since a large number of aircraft have excess electrical power available over that required by the above system, ASTI is conducting laboratory experiments on a system that uses a higher voltage. This allows the blanket to require less current

to operate and fewer wires to be effective. The system can be operated on AC or DC current and by having the capability to modify the voltage requirements, allows the operator to tailor a system specifically for their aircraft. This higher voltage system is currently being tested on a Lear aircraft. Several other manufacturers have noted strong interest in this particular de-ice system.

CONCLUSION

In conclusion, ALPA has attempted to highlight several key areas that must be addressed in the aviation industry; those being Predictive Ice Detection (forecasting), Reactive Ice Detection (on-board systems), Aircraft specific exceedance icing visual cues, and energy efficient aircraft ice protection. We have also attempted to include a brief discussion of the systems that ALPA is presently aware of and their status.

Although not discussed in great detail within the body of this paper, the need for the systems discussed is an industry wide concern. The events that have brought the aviation community to this point concerning in-flight icing detection and protection evolved, not from a single event, but from several spanning many years. Several other aircraft types have experienced icing related incidents and/or accidents that expand the scope of these efforts beyond one specific aircraft model. It must be understood that a tailplane icing/stall event is no different than that experienced over Roselawn, Indiana. Furthermore, considering the impossibility of visually inspecting a tailplane surface, as well as upper surfaces of high wing aircraft, the need

for the systems described are even more necessary.

Predictive Ice Detection is a reality and efforts are underway to increase the capability to provide additional and extensive information to weather services, airlines and ultimately flight crews.

Reactive Ice Detection equipment is not only a reality, it is now available for testing and use.

A specific exceedance icing visual cue is only available for one aircraft type. Until one or both of the aforementioned systems are available for use on aircraft, a clearly defined test plan must be generated and implemented to determine aircraft specific cues for all other aircraft.

Energy Efficient Ice Protection Enhancements are minimal in number, but promising technology is currently available.

Any of the above systems, or a combination of several or all, would remove the subjectivity presently required in pilot judgment when assessing the severity of environmental icing conditions.

The Bottom Line and Immediate Goal:

- ✈ ALPA would like to see no future certification of aircraft under part 25.1419 unless an approved Reactive Detection System is installed and operational. This Reactive Detection System should have the capability to annunciate to the flightcrew any Appendix C exceedance encounter.

- ➔ ALPA would also like to see, for current certificated aircraft, a retroactive requirement for aircraft specific visual cues be required. These visual cues will be derived through flight testing to a clearly defined test plan in exceedance conditions or the equivalent.

REFERENCES

1 Aircraft Icing Handbook, DOT/FAA/CT-88/8-1, FAA Technical Center, Atlantic City International Airport, N.J. 08405, Chapter V, Section 1.1.4 Evaluation Criteria, March 1991.

2 U.S. Department of Transportation, Federal Aviation Administration, Advisory Circular AC No. 25.1309-1A, System Design and Analysis, June 21, 1988.

3 B.E. Martner, R.A. Kropfil, L.E. Ash, J.B. Snider, Progress Report on Analysis of Differential Attenuation Radar Data Obtained During WISP-91, Wave Propagation Laboratory, October 1991, NOAA Technical Memorandum ERL WPL-215.

4 CAA Paper 95007, Ice Detection for Turboprop Aircraft, P.M. Render, L.R. Jenkinson, R.E. Caves, D.E. Pitfield, Loughborough University of Technology.

5 ATR Icing Conditions Procedures, Version 1.0, ATR

6 Docket No. 96-NM-18-AD, Airworthiness Directives; Dornier Model 328-100 Series Airplanes, Notice of Proposed Rulemaking, Federal Register January 25, 1996.

7 CAA Paper 95007, Ice Detection for Turboprop Aircraft, P.M. Render, L.R. Jenkinson, R.E. Caves, D.E. Pitfield, Loughborough University of Technology.

8 BFGoodrich Aerospace Brochure, Jet Electronics and Technology, Inc.

9 National Transportation Safety Board, Washington, D.C., Icing Tanker Factual Report, Docket no. SA-512, Exhibit no. 13B.

10 National Transportation Safety Board, Washington, D.C., Icing Tanker Factual Report, Docket no. SA-512, Exhibit no. 13B.

AN IMPEDANCE-BASED SENSOR TECHNOLOGY FOR ACCESSING AIRFRAME ICING

David C. Parkins and Jack Edmonds

Innovative Dynamics Inc.

244 Langmuir Labs

Ithaca, NY 14850

(607) 257-0533

Abstract

Development efforts at Innovative Dynamics Inc. (IDI) have produced an impedance based sensing technology for assessing airframe icing. This technology utilizes a sensor that provides a large area measure and is therefore uniquely suitable for the super-cooled large droplet (SLD) application where runback ice forms beyond the protected region of the wing. A proprietary method has been developed to detect ice thickness as well as differentiate between ice, water, and deicing fluid. The 'patch' sensors are approximately 0.010" thick, suitable for conforming to complex surfaces and are easy to retrofit to aircraft in the field. IDI has developed a prototype ice thickness sensor under a two year program sponsored by NASA Lewis. Commercialization and certification of the sensor has continued under contract with BFGoodrich Corporation.

IDI has also begun an effort to develop a low-cost version of this sensor for general aviation aircraft as well as for unmanned air vehicles (UAV) that indicates the initial onset of icing. UAVs in particular are vulnerable to icing threats due to the use of laminar flow airfoils that are very sensitive to ice formation. With increasing demands being made on UAVs to achieve higher altitude and longer endurance, the need exists for a reliable system to detect the onset of ice accretion for use in closed loop deicing, making a return to base decision, or detouring the flight path to a less hazardous route. The IOI system is a simple, low cost, low power, and light weight system that meets the need for these UAVs. Three pre-production Icing Onset Indicators (IOI) have recently been installed on the Predator UAV for field use and evaluation in Bosnia. This system is directly applicable to the SLD problem. This paper will address the sensor design and include tunnel as well as flight test data from the current IOI system.

Presented at the FAA International Conference on Aircraft Inflight Icing, Springfield, VA, May 6-8, 1996.

Introduction

Since the early attempts at flying across the Atlantic, aircraft and aviators have had to address some very real concerns about weather. While aviation was still in its infancy, the early mail pilots encountered rain, snow, ice, thunderstorms and all the other myriad of weather phenomena. As transportation by air became more commonplace, the expectations of the flying public grew. Fortunately as these expectation grew so did the capabilities of our aircraft, pilots, and air traffic control system. The public expects to arrive at their destination safely, economically, and on time. To aid in the pursuit of these goals we as an industry have devised precision landing systems, ground based radar, air based radar, and other tools of the trade that 60 years ago were unheard of.

The vast majority of winter flights in the United States have to consider the possibility of in-flight icing. The common forms of this phenomena are easily recognized if the pilots attention is drawn to them. On October 31, 1994 an ATR-72 went down in Roselawn, Indiana. This incident was attributed to SLD icing. During the subsequent investigation it became apparent that SLD phenomena is difficult or impossible to directly observe from many cockpits; typically another visual cue must be determined and used. Even in those aircraft where upper flight surfaces can be easily viewed, these atmospheric conditions could just as easily look like light rain to the pilot. While no aircraft is certified for flight into freezing rain or drizzle, these particular conditions are insidious because of the difficulty in assessing them. SLD icing is characterized by an ice formation aft of the protected portion of the wing. This spanwise formation forms a forward facing feature that affects the flow downstream of the ice formation. This flow produces time varying control forces in the aileron that can make an aircraft confusing or difficult to fly. This combined with the extensive use of autopilots can surprise the pilot when the autopilot is disconnected during approach.

A point type sensor might be considered to assess such a phenomena except that portions of the ice formation tend to break off. A spanwise ice formation covering approximately 30% span upstream of the ailerons may cause control problems. A point type sensor is impractical because there is no guarantee where this 30% span section of ice will be. Additionally, flow measuring devices suffer from the same limitations because the location of this turbulent flow can vary. Thin film 'patch' sensors as shown in Figure 1 may be a more viable approach for sensing ice formations over a statistically significant span of the wing. A proprietary method has been developed at IDI to detect ice thickness as well as differentiate between ice, water, and deicing fluid¹. Icing tunnel tests performed at BFGoodrich have demonstrated that such a sensing concept is viable for SLD². This sensor is easy to retrofit to an existing fleet as well as easy to integrate into a new airframe.

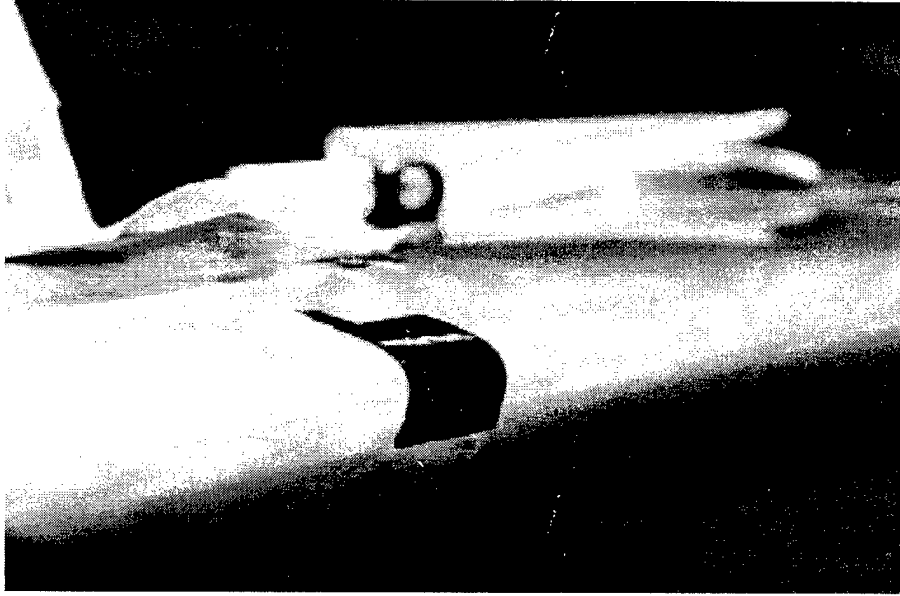


Figure 1. Ice sensor patch installed on UAV wing.

Sensor Fundamentals

An impedance-based ice sensor is formed by two electrodes. The ice-water-air mixture above the sensor acts as the dielectric material in the electric field path between the electrodes. If the electrodes are encased in a non-conductive (good dielectric) material, there are additional parallel and series capacitance elements that contribute to the measurement result. In the following discussion, we consider the parallel capacitor-resistor model of Figure 2 that represents the icing volume.

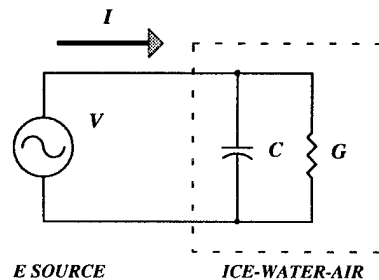


Figure 2. Simple capacitance sensor model.

In the most basic implementation, a known AC voltage V is impressed across the electrodes and the current I is measured. Due to the presence of the reactive element C , a phase difference between V and I exists. The measured admittance is

$$Y = I/V = j\omega\epsilon^*\xi \quad (1)$$

where ω is the radial frequency, ϵ^* is the complex permittivity of the dielectric (ice-water-air mixture), and ξ is a geometric factor. For the well known case of a simple parallel plate capacitor, $\xi = A/d$, the area of one plate is divided by the separation between the plates.

It is computationally convenient to use relative permittivity $\kappa^* = \epsilon^* \epsilon_0$ where

ϵ_0 is the permittivity of free space = $10^{-9}/36\pi$ farads per meter, and

$\epsilon^* = \epsilon_0(\epsilon' - j\epsilon'') = \epsilon_0(\kappa' - j\kappa'')$, a dimensionless value.

Equation (1) becomes

$$Y = 2\pi f \epsilon_0 \xi \kappa^* = 2\pi f \epsilon_0 \xi (j\kappa' + \kappa'') = G + jB \quad (2)$$

which relates the dielectric material properties to the measurement parameters of conductance G and susceptance B . Note that $B = 2\pi f C$ and $C = \epsilon_0 \kappa' \xi$. Although κ' is usually referred to as the *dielectric constant*¹, it is frequency dependent and can be considered constant only over certain frequencies which are determined by the properties of the dielectric material. This frequency dependence can be exploited to differentiate between materials (ice and water in our case) and to estimate temperature.

In the simplified model of Eq. (2), we see that ξ equally affects the conductance and capacitance components of admittance. As a further extension, the magnitude of the admittance $|Y|$ is also equally affected. Thus, there is no apparent physical basis for preferring one of these measures over the others for the determination of ξ and ultimately, ice thickness.

Because of the geometric configuration of practical ice sensors and the complexity of the ice formation, ξ is not as easily derived from the electrode geometry. Intuitively, one can develop a first order approximation by unfolding a parallel plate capacitor until both plates lay in the same plane as illustrated in Figure 3. The thicker field lines indicate the region affecting the sensor output the most.

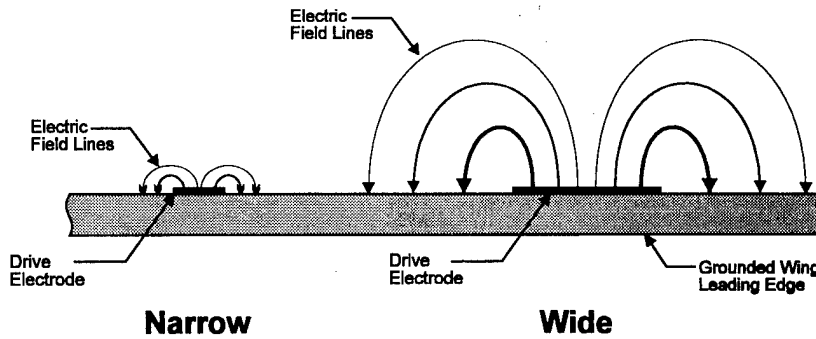


Figure 3. Cross-sectional view of a narrower and wider sensor showing their respective electric field lines (not to scale).

Length l is fixed by the length of the sensor elements in the direction normal to the paper. Width w and separation d are determined by the electrode dimensions and spacing. If, for the moment, we make one additional assumption - - the ice-water mixture dominates the dielectric contribution - - we see that w grows from zero to some maximum value as ice accumulates on the sensor while d grows much less dramatically. Thus, ice thickness

¹ Note that κ' is often denoted by ϵ_r .

which now corresponds to w can be inferred from ξ up to a limiting value determined by the measurable extent of the electric field region. As a practical matter, the material constants κ' and σ vary with the porosity of the ice, its liquid water content, the presence of pollutants, and the temperature, even at a fixed sensor operating frequency. The Weinstein³ algorithm is an attempt to eliminate the influence of these variations on the measurement result through the use of two sensors, one with a small limiting w value (called the *Type 1* sensor), the other (*Type 2* sensor) with a limiting w value greater than the desired ice thickness threshold. By taking the ratio of the two measurements

$$\frac{Y_2}{Y_1} = \frac{\xi_2 \omega \epsilon_0 \kappa^*}{\xi_1 \omega \epsilon_0 \kappa^*} = \frac{\xi_2}{\xi_1} \quad (3)$$

one can estimate the thickness of the ice as a multiple of the reference thickness defined by the limiting value (*saturation* point) of the Type 1 sensor, see Figure 4.

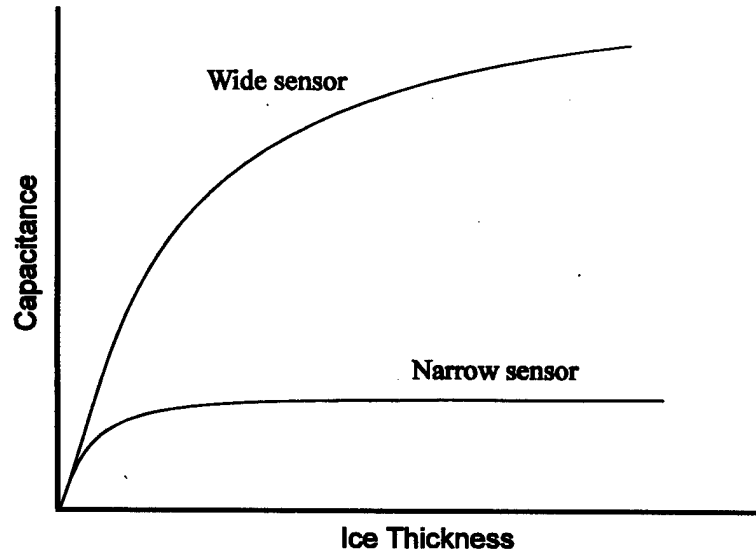


Figure 4. Typical capacitance versus ice thickness curves for narrow and wide sensors.

The relationship, however, is approximately linear for thickness' small in comparison to the electrode separation, with reduced effect of w on ξ until a peak value for ξ is reached, whereupon ξ begins to decrease. The general trend is followed even for wet ice, although not as faithfully as for rime ice due to variations in κ^* caused by water capture and freezing cycles in the ice pack.

The sensor design can be tailored toward specific performance requirements. The narrower sensor provides greater initial sensitivity while it is insensitive at greater thickness. The wide sensor provides more uniform sensitivity to a greater thickness of ice at the cost of initial sensitivity.

System Description

The system is comprised of an ice detector and a signal conditioning/processing box, see Figure 5. The sensor is a 'patch' type sensor that measures the change in impedance over an area approximately 2" cord by 4" span. The size of the patch is dictated by such design

constraints as electronics sensitivity, electronics cost, noise susceptibility, and the statistical nature of ice formation and removal. The electronics package is powered by 24 VDC aircraft power drawing less than 0.3 amperes. The electronics package has two functional elements: signal conditioning and signal interpretation. The output of the electronics package are two discrete output signals. These signals indicate when the sensor is covered with an adequate amount of ice and when system failure occurs. Ice impedance data will also be stored in future systems.

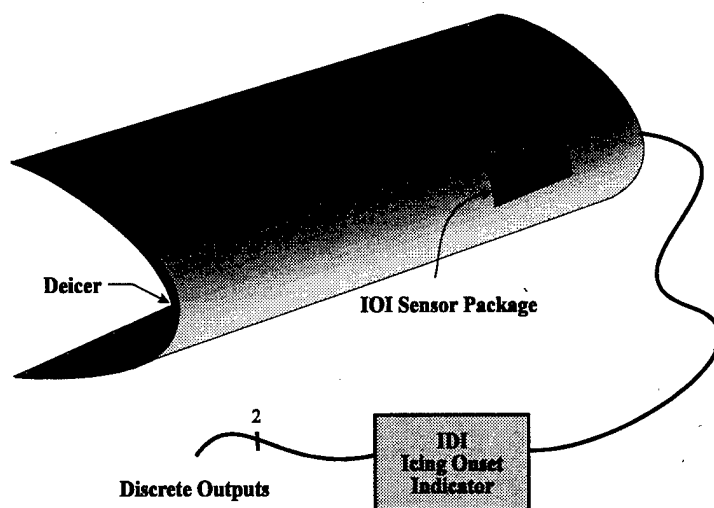


Figure 5. Icing Onset Indicator system drawing.

Icing Wind Tunnel Test Results

During the development of the system, IDI performed a series of icing wind tunnel tests carried out at Canadian National Research Council's tunnel and NASA Lewis. Presented here are typical tunnel data for the IOI sensor. This data is for 20 micron MVD, 0.6 g/m³ LWC, and an AOA of 0 degrees. Various angles of attack were used, and as long as the ice forms over more than 20% of the cord dimension of the sensor, the signal is more than adequate for detecting ice.

Figure 6 shows the capacitance component of the impedance response under very cold rime conditions. This condition is the most difficult to detect. The change in capacitance is the smallest and during subsequent ice accumulation, the capacitance decreases to a level only 11 picofarads greater than the clear air condition of 6 picofarads. Under these conditions, the cordwise extent of the ice is smallest and the dielectric properties of the ice are the lowest. The sensor output peaks at roughly 0.016" of ice. The fast and steep reaction to the ice formation that occurs roughly 20 seconds into the run is typical of this type of sensor. The initial response to ice forming on the surface is immediate and the ice detection threshold can be crossed within seconds of encountering ice at typical accumulation rates. Figure 7 shows another rime encounter with a change in capacitance of 39 picofarads between the clear air response and saturation. This change in capacitance at saturation is typical for uniform rime ice morphology.

Response of Ice Sensor in NASA IRT: Test Run 41

V=180 mph, AOA=0 deg, D=20 microns, T=-20 degF, LWC=0.6g/m³

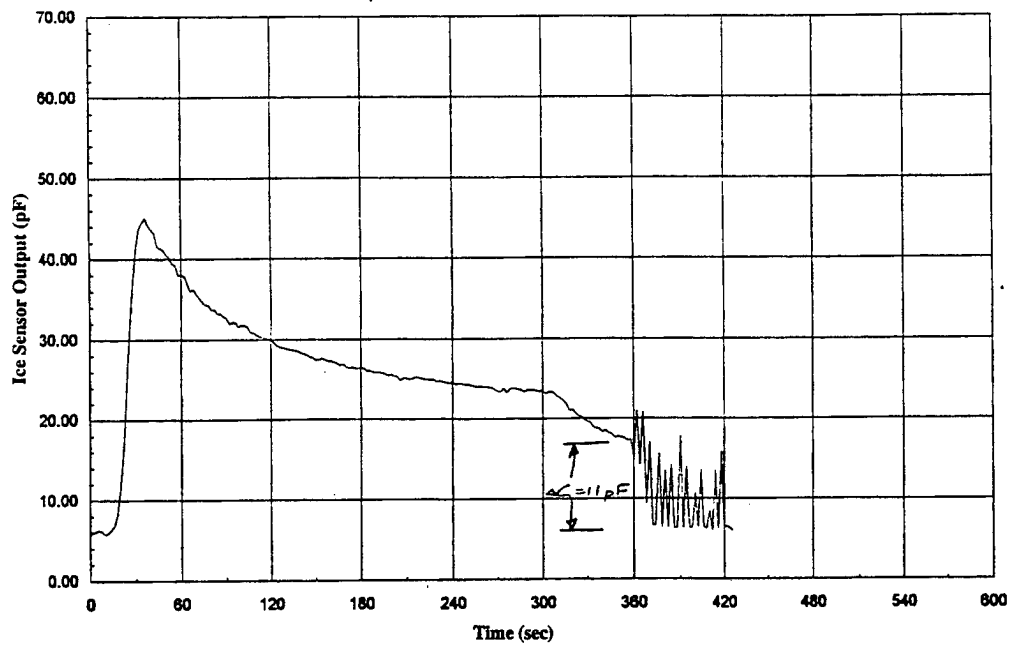


Figure 6. IOI sensor response for very cold rime condition.

Response of Ice Sensor in NASA IRT: Test Run 40

V=125 mph, AOA=0 deg, D=20 microns, T=0 degF, LWC=0.6g/m³

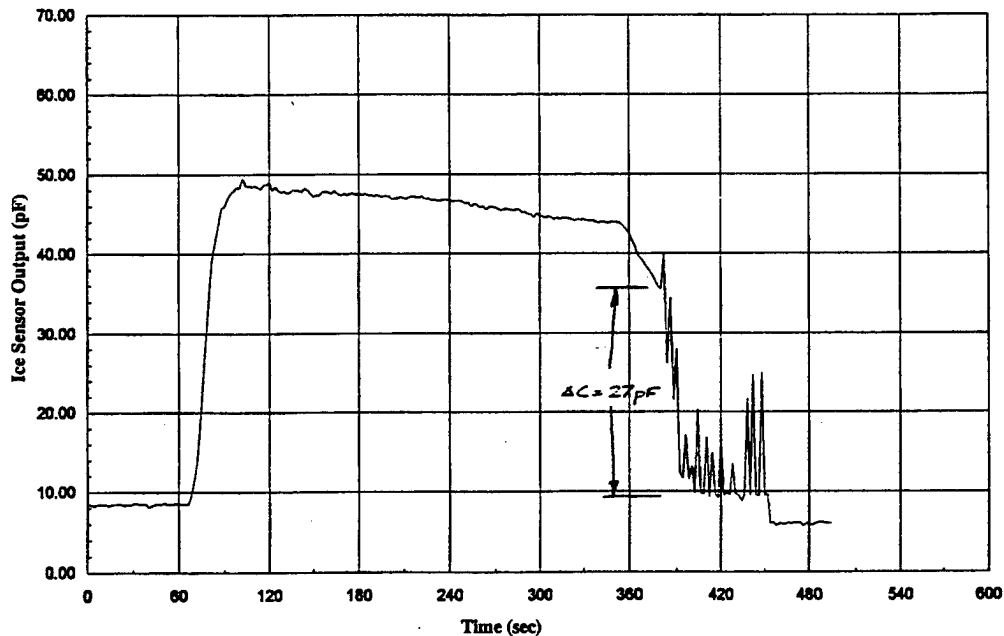


Figure 7. IOI sensor response for cold rime.

Figure 8 is representative of a glaze ice condition. The change in capacitance is greater for the glaze ice condition, and we don't see the type of distinct saturation shown in the

earlier plots. The lack of a distinct saturation is attributed to the changing morphology of the ice formation as ice is accumulating. Since the sensor signal is most sensitive to the ice immediately above the sensor, any freeze-out or change in the morphology of this ice can change the signal more than changes due to ice accumulation. While the data presented above resembles that of a point sensor, it must be remembered that the IOI sensor output is a volumetric integration of the material properties of the ice in the sensor's electric field. This integration comes at no additional cost other than that of the material for the sensor.

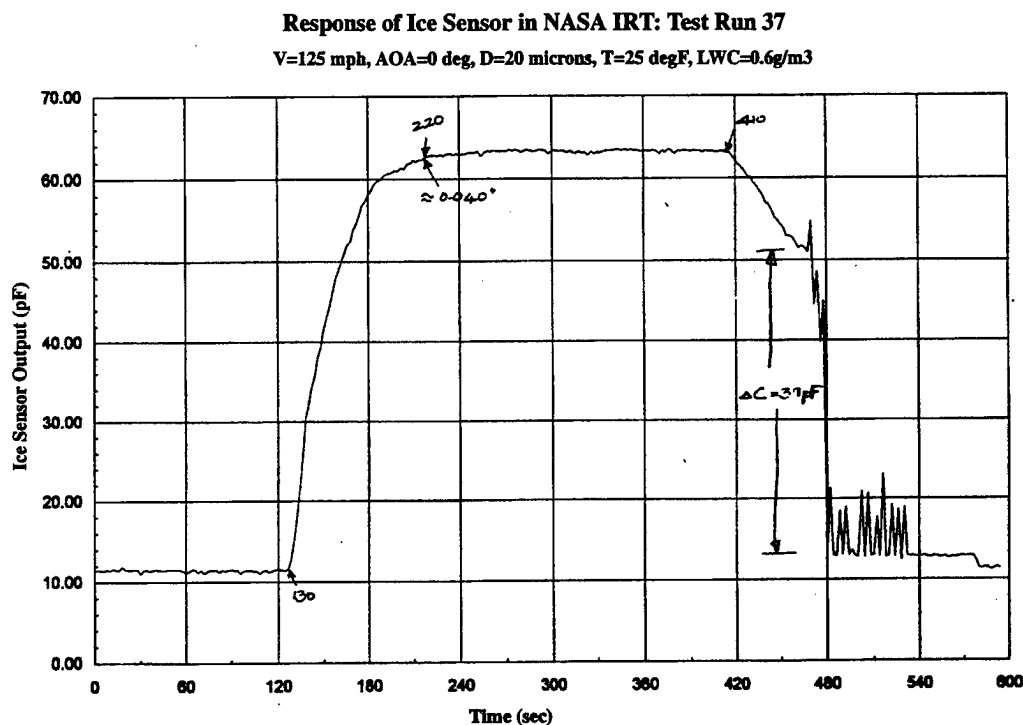


Figure 8. IOI sensor response for warm glaze.

Flight Test Results

During the spring of 1995, IDI began certification testing of its IOI general aviation ice detector on IDI's Icing Testbed shown in Figure 9. The testbed aircraft is a Piper Malibu (PA46-310P) equipped with an IDI developed modular data acquisition package. The package includes a dedicated data acquisition computer, two video cameras, OAT, airspeed, altimeter, Rosemount Ice Detector⁴, Johnson-Williams LWC meter, and a wing surface thermocouple.

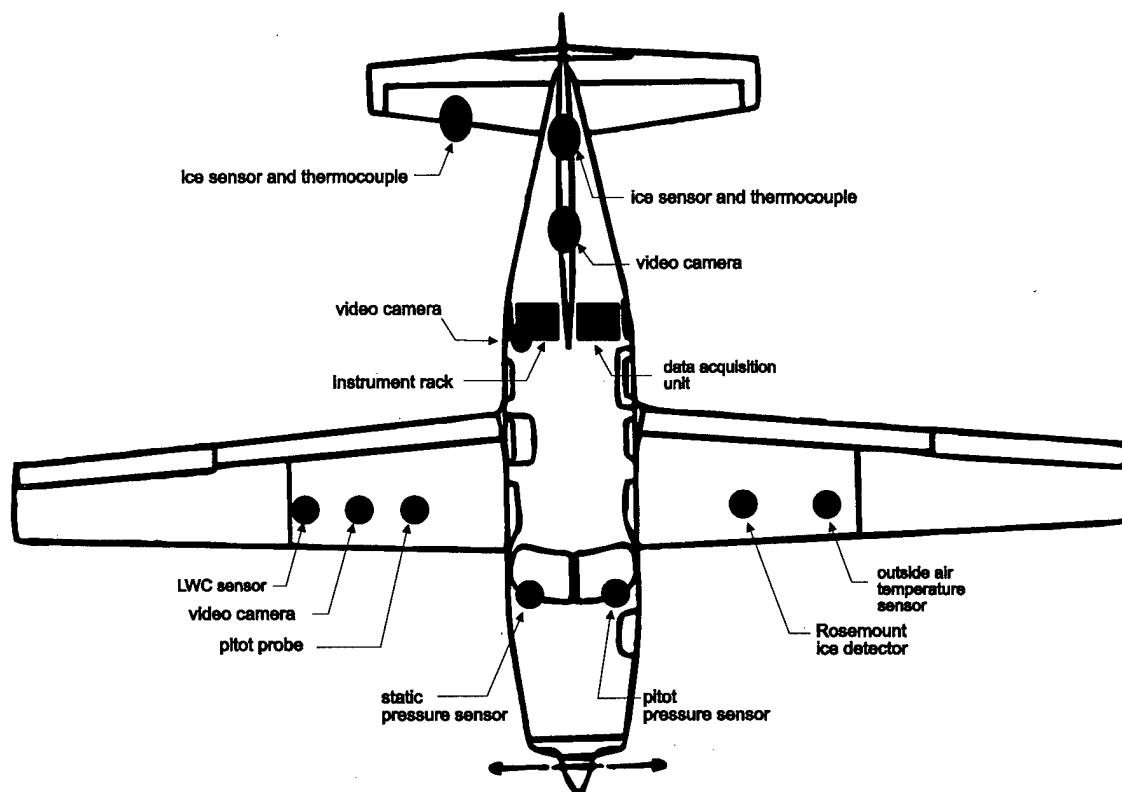


Figure 9. IDI Icing Flight Testbed configuration.

The sensors tested were approximately 0.5" by 1.5". During FAA observed testing, it was discovered that the system would indicate ice at an accumulation smaller than could be visibly confirmed by the pilot. These encounters were verified by OAT, LWC, and Rosemount Ice Detector readings. The system was later re-calibrated to allow a thicker accumulation of ice before indicating an icing encounter to the pilot, henceforth consistent with existing visual cues on the PA-46 aircraft. Typical flight data using the patch sensors are depicted in Figure 10. Shown are analog output data from narrow and wide sensors along with LWC readings. Test results were consistent with tunnel data. FAA certification is expected next year.

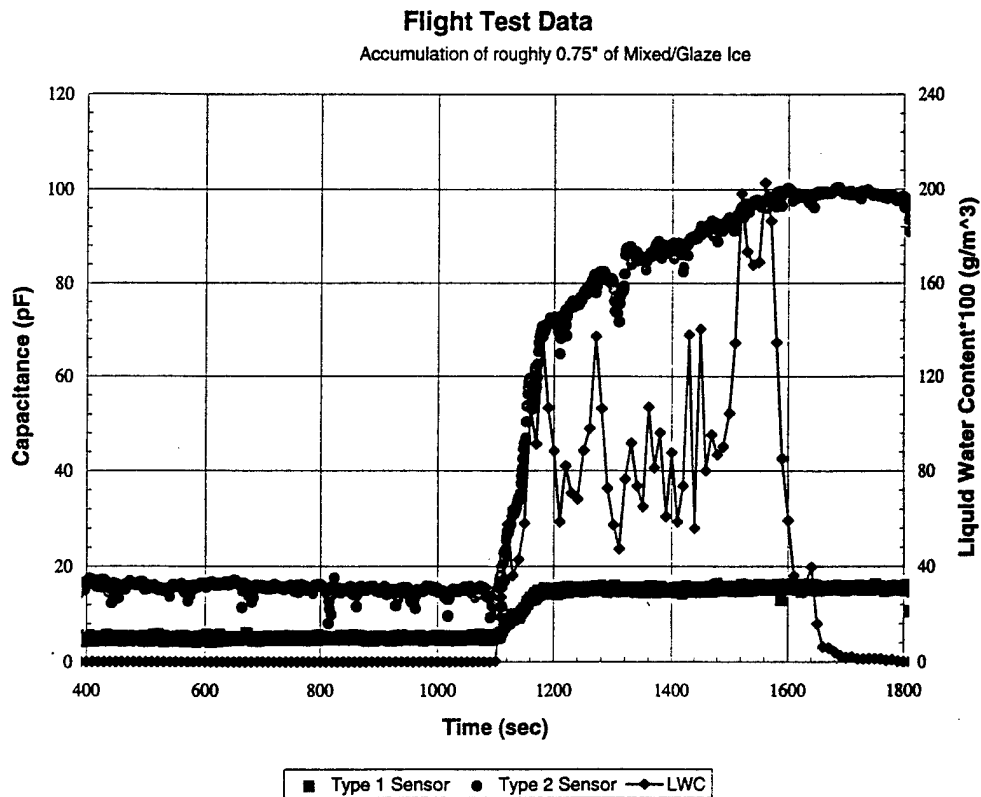


Figure 10. Patch sensor response in mixed/glaze icing conditions.

Sensor Evolution to Accommodate SLD Conditions

To be beneficial to the pilot, an SLD sensor needs to be sensitive to any ice formation aft of the protected region of the wing. The critical unprotected region is approximately 5% cord in width. The aileron snatch phenomena associated with the ATR-72 accident suggests that sensing upstream of the ailerons is critical both for determining the existence of ice and its potential effect on the handling of the aircraft. Unfortunately as the SLD ice forms, portions of the ice pack break off making point type sensing impractical. Testing has demonstrated that an SLD formation approximately 30% aileron span in length and upstream of the ailerons can create significant changes in control forces. A sensor must have a high initial sensitivity for early notification of the pilot and an insensitivity to the spontaneous shedding of spanwise portions of the ice formation covering up to 60% of the sensor. A sensor needs to measure ice accumulation over a span at least 36" long in a wing with a 120" span aileron. An SLD sensor would be located aft of the wing ice protection system and upstream of the ailerons. The sensing area would extend approximately 5% in the cordwise direction and extend 4 feet in the spanwise direction. This sensor would provide high initial sensitivity to ice formation, 0.015" or less, while sensing over an area large enough to overcome error from partial shedding of the SLD ice formation.

Integrated Ice Management System

The impedance based ice sensing technology is currently being incorporated into an Integrated Ice Management System (IIMS), see Figure 11. This system combines an SLD sensor, an ice thickness sensor, and autopilot load sensors. This combination of sensors is used to provide early indication of an icing encounter, to actively drive the deicing or anti-icing equipment, to alert the pilot of SLD conditions, and to assess autopilot loads to determine if the potential for aileron snatch exists. The IIMS reduces pilot workload by integrating the control of deicing equipment into a closed loop system. Additionally, it provides monitoring of the autopilot effort, icing onset, and icing aft of the protected area of the deicers. A display indicating a high autopilot workload will alert the pilot to degrading handling that might otherwise be noticed if the pilot were hand flying the aircraft.

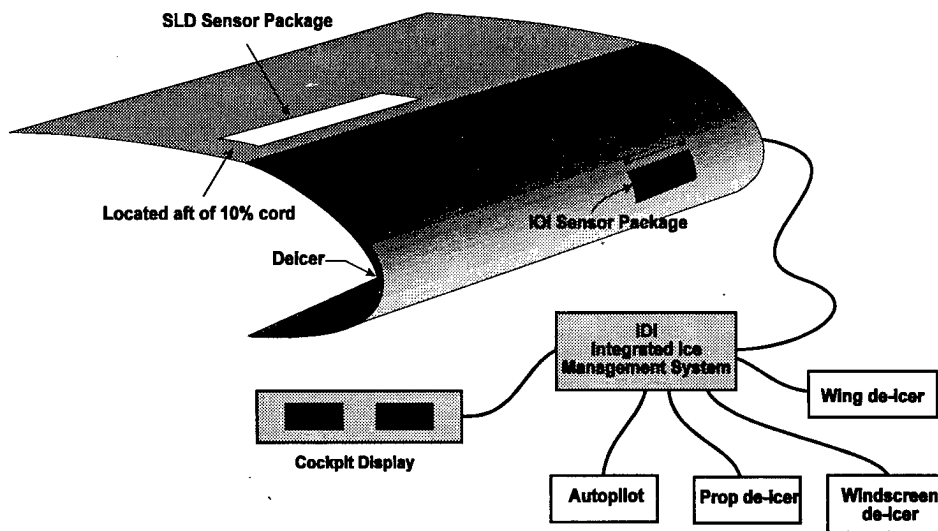


Figure 11. Integrated Ice Management System.

Conclusions

The impedance sensor technology demonstrated on the leading edge for icing onset detection is uniquely capable of assessing SLD formations over a statistically significant region of the upper wing surface. A proposed SLD sensor would be located upstream of the ailerons. This sensor would provide a signal that integrates the material properties of the ice over the span of the ice formation. Partial shedding of the SLD ice formation would not mislead the system. The sensor could be attached with an adhesive to the wing such that the thickness of the sensor provides no aerodynamic penalty. A combination of these thin film sensors located at strategic points on the aircraft could provide key information to an advanced icing management system.

Acknowledgments

A number of others have made contributions and provided assistance during this effort. These include from IDI, Dr. D. Pruzan, A. Khatkhate, R. Catarella, M. Bartos, and G. Codner and from BFGoodrich, D. Sweet and A. Reich. Additionally invaluable support has been provided by NASA Lewis under the SBIR program, and by A. Reehorst in particular.

Bibliography

- ¹ Gerardi, J.J., G. A. Hickman, A. A. Khatkhate, and D. A. Pruzan (Innovative Dynamics Inc.), "Apparatus for Measuring Ice Profiles", Patent No. 5,398,547, May 1995.
- ² Sweet, D.B., and A. D. Reich, 1996. "Super-Cooled, Large Drop (SLD) Ice Formation Detection", 34th Aerospace Sciences Meeting, Reno, NV.
- ³ Weinstein L. M., 1988. "Ice Detector", Patent No. 4,766,369.
- ⁴ Rosemount Aerospace ice sensor Model 0871FA211B..

ULTRASONIC DETECTION OF LARGE DROPLETS ICE ACCRETIONS

Michel LE PIMPEC
Research and Data Processing Manager

INTERTECHNIQUE, Plaisir, France

ABSTRACT :

Effects of SLD icing on the critical surfaces have been shown as being very hazardous situation for which the pilot must be alerted. Current alert systems based on a direct vision of icing in the cockpit vicinity may be advantageously replaced by ultrasonic ice detection systems. Such a system can monitor SLD icing accretion directly on the critical surfaces.

INTERTECHNIQUE has proven the ability of this technology to work correctly in artificial and natural conditions and is currently developping a certifiable system promised for the end of 1996.

I - NECESSITY OF DETECTING SLD ICE ACCRETION

A lot of work has been done about the SLD ice accretion phenomena since the Roselawn accident which has been the starting point of all these investigations. Many people have worked and continue to work on this subject which is far to be entirely completed. It is clear that, today, we do not have a full understanding of the mechanisms implied in SLD ice accretion. We need to learn more and this conference will greatly help us in this way.

However, as of today, we know some interesting and global characteristics about SLD icing. For example :

- SLD icing is due to large droplets and when occurring leads to ice accretion very different from the well known Appendix C icing,
- SLD ice accretion may be formed aft the protected areas resulting, in some cases, in the inefficiency of the deicing system,
- SLD icing is mostly known as a small ice wall buildup at some distance from the leading edge. However different SLD icing shapes have been reported including complete extrados icing or intrados icing,
- SLD icing occur in specific and very local climatic conditions which means that it may appear, and disappear, very rapidly.

These characteristics show that SLD icing is a very hazardous phenomena. Its suddenness and, under certain conditions, the impossibility to de-ice the aircraft are the most serious points.

Given these elements, it is clear that we MUST alert the pilot about such a hazardous situation when it occurs. This clearly means that we need to provide to the crew a mean to know whether or not the aircraft is being accreting SLD icing.

II - CURRENT MEANS FOR DETECTION OF SLD ICE ACCRETION

The SLD icing phenomena has begun to be known and investigated only 18 months ago. Of course existing equipment was not certified nor designed to handle this "new" issue of icing. But, meanwhile, aircraft had to fly and it was necessary to provide some empirical, but as efficient as possible, means to detect the SLD icing situation.

The most popular mean is probably the "visual cues". It has been noticed during the SLD tests that in that case, specific icing shapes (cues) appear in the cockpit vicinity. Monitoring these cues is a way.

A derivative may also be provided by lighted devices located under the lateral windshields. Such devices look differently when they are iced.

Detecting modifications of the return effort in the broom-stick is a way to be alerted about the first aerodynamical effects of SLD icing on the aircraft.

These means provide temporary solutions for detecting the SLD accretions and the fact that they exist is a good thing. However :

- they are empirical,
- they depend on the type of aircraft,
- the visual means require an intentional action from the pilot,
- recognizing visual cues needs a special training,
- the visual means do not permit to monitor the critical surfaces,
- the return effort method more alerts on the fact that the aircraft is now in a difficult situation.

From the above we can conclude that there is certainly a need for better SLD ice detection systems.

III - IDEAL MEANS FOR DETECTION OF SLD ICE ACCRETION

Should we have to design the ideal SLD ice accretion system, the main features to retain would be :

- The system must monitor the critical surfaces where the SLD icing provides hazardous behaviour of the aircraft. Critical surfaces such ailerons may also be monitored.

- The pilot does not have to pay special attention to the SLD icing detection system. The system has to keep him informed about the situation whilst minimizing the intentional pilot attention.
- The SLD ice detection sensitivity has to be high in order to detect SLD icing as soon as it appears. This will give time to the pilot for taking the appropriate actions.
- Giving information derivated from the ice thickness and/or growth speed may be of a great interest to appreciate the severity of icing and then modulate the appropriate actions.
- A discrimination between Appendix C icing and SLD icing is necessary because of the different actions to be taken in each case.

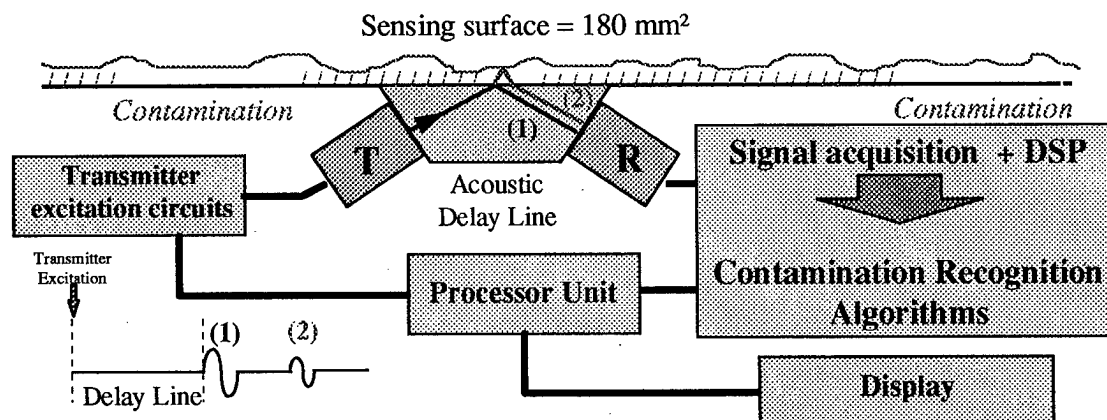
IV - USING ULTRASONIC TECHNIQUES FOR DETECTING SLD ICE ACCRETION

INTERTECHNIQUE has been working for many years on ultrasonic technology and has applied it to a variety of applications including fuel gauging system, ice and ground contamination detection.

Based on this large background INTERTECHNIQUE propose to use the system described below to detect SLD ice accretions.

Theory of operations

Let us consider the following sensor, flush mounted to a critical surface to be monitored.



Let us consider first a clean surface. An ultrasonic transducer provides an acoustic pulse to an acoustic delay line. This pulse propagates thru the delay line and reflects on the test surface towards a receiving transducer. This is the path (1) on the figure.

Now, if the surface is covered with a contaminant, we observe that a part of the incoming acoustic energy propagates inside the contaminant layer and is also reflected towards the receiving transducer. This is the path (2) on the figure.

In fact, the reflection characteristics of an acoustic wave on a contaminant are very dependant on the contaminant nature and, more precisely, is determined by the acoustic impedance of this contaminant, the acoustic impedance of a material being defined by the product of its density and of the velocity of sound in this material.

The interesting thing is that air, liquid water and ice have very different acoustic impedances, thus providing different kinds of reflection on the test surface. Moreover, it can be demonstrated that, if the acoustic impedance of the acoustic delay line is intermediate between the acoustic impedance of ice and the acoustic impedance of liquid water, then the wave (2) has an opposite phase from one case to the other. This property of the system guarantees that no confusion can be made at any time between liquid water and ice. Other critical choices such as frequency of the acoustic waves have been made to ensure that the system can handle a wide variety of ice.

The receiving transducer collects a wave which is the sum of (1) and (2) and transmits the resulting signal to a data processing unit using DSP algorithms. The result of the computation is an information about the contaminant nature and thickness. This information can be communicated to the pilot in different forms, from the simplest solution, a red light activated when the contaminant is ice with a thickness greater than a prespecified threshold, to the activation of complex data charts on EICAS for example.

Potential / Benefits

The above described system is able to detect an ice layer as soon as its thickness reaches 0.15 mm which is very thin.

Of course, due to the acoustic impedance principle used, no confusion between ice and liquid contamination can occur.

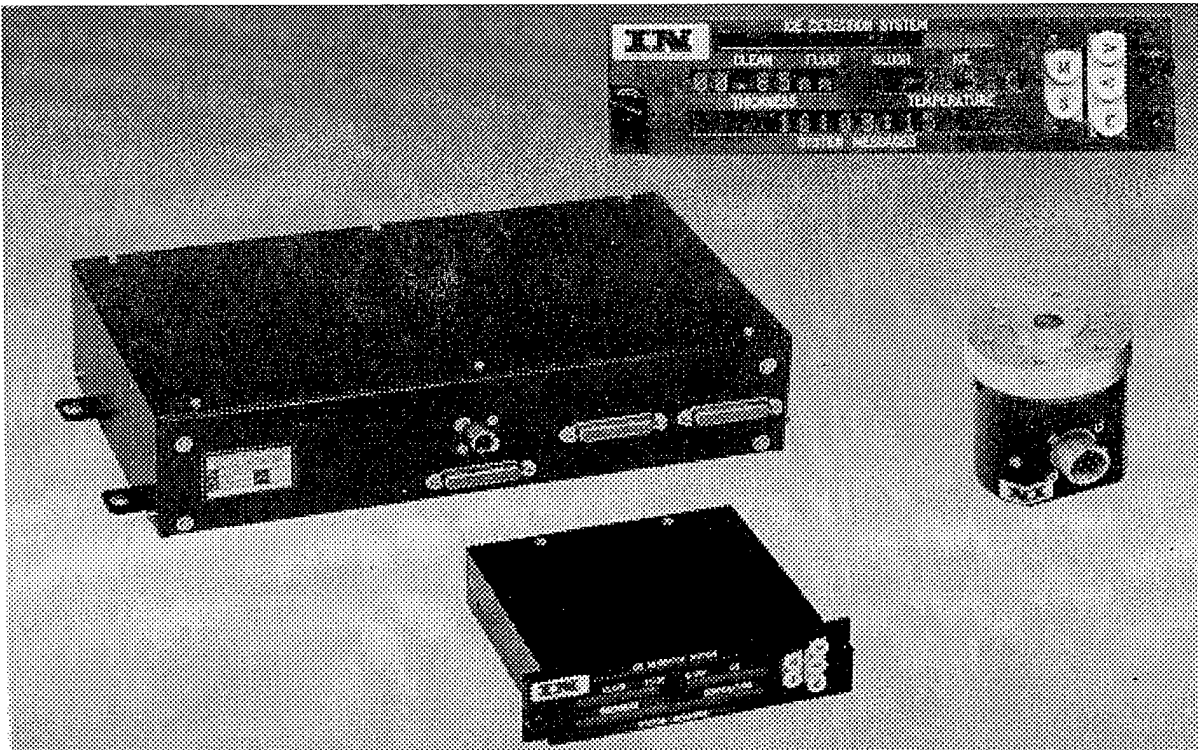
Alerting the pilot about a hazardous SLD icing situation can be made simply by comparing the accretion thickness to a threshold but one can also take the growth speed of this accretion into account. This growth speed is simply a smoothed first derivative of the thickness.

Multiple sensor systems are highly recommended in order to monitor different areas on the critical surfaces and/or different critical surfaces including the empennage. The system can monitor up to eight different locations

Last but not least, the system has provision to be used also on ground. Of course it can serve as an ice detection system before deicing but also, it will be able to monitor the protective liquids and give the associated holdover time.

Photos

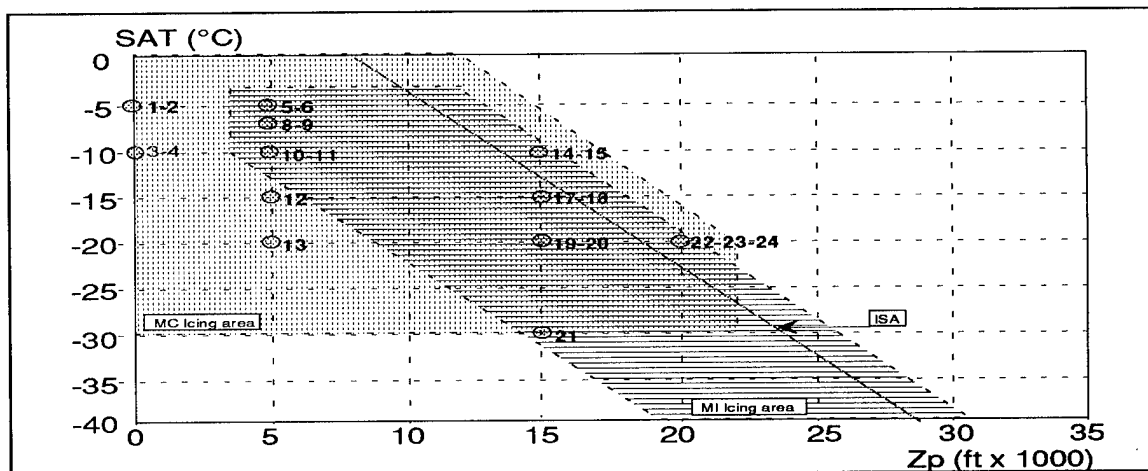
The hereafter photos show the experimental system which has been used until now. It comprises a calculator (the largest black box), several sensors and a verbose display providing complete information including the nature of the contaminant, its thickness and temperature, plus system messages.



Icing tunnel tests

Many preliminary tests have been made at INTERTECHNIQUE facilities using a specific climatic chamber with trimmable spraying elements producing different kinds of ice on a test surface in which were integrated two sensors..

An extensive test campaign for validating the technology has been conducted at the CEPr, Saclay, France. During that campaign, a lot of point covering the Appendix C domain have been covered resulting in testing a wide variety of ice accretion.



ICE DETECTION RATE : 100 %
FALSE ALARM RATE : 0 %

The results were totally successful. Ice detection occurred for all the icing situations showing the possibility of the system to handle all kinds of ice. In no icing situations no false alarm occurred at any time. This excellence is a direct consequence of the efficiency of the ultrasonic technology.

Flight tests

In March 1995, a flight test campaign was conducted at Edwards AFB with an ATR72 flying behind a spraying tanker. INTERTECHNIQUE participated to the test, providing a sensor and a system on the aircraft and demonstrated the ability of detecting ice accretion from the tanker spraying.

Current status

INTERTECHNIQUE has fully proven the concept of using ultrasonic technology for detecting various icing conditions in icing tunnel and even in flight during SLD icing tests.

Taking profit from all this background, INTERTECHNIQUE is yet developing a certifiable system able to work in SLD icing conditions and having provisions for ground icing.

This system will comprise a reduced size calculator and will handle three groups of bussed sensors (threes per wing and two for the empennage).

First units will be available for evaluation by the end of 1996.

V - CONCLUSIONS

Flying with SLD icing conditions has been established as being a very hazardous situation for which the pilot must be alerted as soon as SLD ice accretion begins.

Current means of alert/detection exist but require a special pilot attention and being empirical, they cannot be considered as fully compliant with the basic requirements for such a system.

It has been proven by INTERTECHNIQUE that ultrasonic technology has a great potential for achieving efficient SLD icing detection systems.

Extensive tests have conducted to the decision of developing a certifiable system which will be ready by the end of 1996.

VI - CONTACT POINT

Should you need any additional information, please contact :

Michel J. LE PIMPEC
Research and Data Processing Manager
INTERTECHNIQUE
BP1
78374 PLAISIR CEDEX
FRANCE

Phone : 33 1 30 54 80 39
Fax : 33 1 30 54 83 01
Email : 101317.2201@compuserve.com

SUPER-COOLED, LARGE DROP (SLD) ICE FORMATION DETECTION

**D. B. Sweet
B.F. Goodrich Ice Protection systems
Uniontown, Oh**

and

**A. D. Reich
B.F. Goodrich Aerospace R&D
Brecksville, OH**

**FAA
INTERNATIONAL CONFERENCE ON
AIRCRAFT INFLIGHT ICING**

May 6-8, 1996/Springfield, Virginia

ABSTRACT

An impedance based detection method has been developed for large area detection of the presence of ice formations on airfoil surfaces. The technique is applicable for detecting the run back ice formed from super-cooled, large droplets (SLD) which form a ridge like structure beyond the zone protected by deicing devices. The detector consists of an array of parallel electrodes deployed over the zone where ice ridges form. The electrodes are composed of electrical conducting elements fabricated with standard processing used in the fabrication of pneumatic deicers. The electrodes are driven with an audio frequency signal source and the conduction current through the ice layer is amplified and compared to a fixed reference voltage. These are non-microprocessor, analog functions implemented with easily obtained active and passive components. The output is typically a warning light which turns on when the ice layer exceeds a selected thickness that can be in the low range from .025 to .110 inch. Investigations were performed showing that the method does not respond to a water layer that does not freeze. The sensor detects thin ice formations under icing tunnel conditions using high conductivity spray water to simulate cloud moisture. Finally, the sensor monitors local ice growth and ice loss (both cohesive and adhesive) during long periods of SLD exposure.

INTRODUCTION

SLD, in the 60-150 micron diameter range, produces ice formations beyond expected impingement limits. This has been identified as a possible cause of the ATR-72 crash near Roselawn, Indiana on Oct. 31, 1994. The SLD ice formation that forms has been observed in icing tunnels and has been simulated behind the Air Force KC-135 tanker. It is believed that the ice build up does not form quickly. Hence, a sensitive ice detector can provide enough warning time for the crew to take evasive action. This strategy has been implemented to date with local, or "spot" sensors. However, the SLD ice formation is not continuous spanwise and also varies chordwise with changes in the accretion temperature and angle of attack. Complete or at least extended surveillance of the accretion zone aft of the ice protection system would require the use of more than one "spot" sensor. This introduces additional hardware as well as added installation expense. The impedance sensor reported here provides affordable detection over extended areas where SLD accretion occurs.

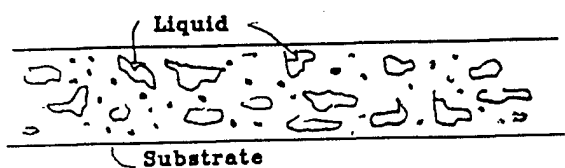
ICE PROPERTY FUNDAMENTALS

A number of different types of sensing principles have been employed for detecting the presence (and thickness) of ice. These include inertial techniques^{1,2}, ultrasonic and related sound propagation effects³, microwaves⁴, and capacitance^{5,6}. The sensor in this study uses a total impedance measurement as shown in Fig. 2 and 3. In general, noise sources arise from the

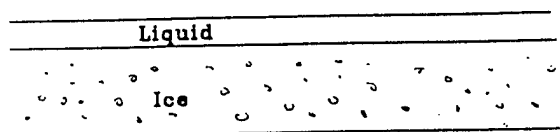
nonuniformity and variability of the ice formation. This is the reality common to all approaches. These noise sources will be reviewed here, but the impact and details of the noise effects on the other approaches are outside of this study. Attention here will be restricted to the noise effects seen in the impedance measurement.

Significant ice nonuniformity arises across the icing envelope involving a range of temperatures, LWC, drop size and air velocity. For example, a glaze-rime transition plane has been suggested⁷ as a means of identification of two zones with differing physical ice properties. It is reasonable to expect that these two zones will have changing density and bond strengths which introduce inertial and acoustical "noise" and different conductivity levels which generate an electrical noise term. The problem goes beyond the glaze-rime variability within the ice "phase". More serious is the larger dimensional scale involving solid (ice), liquid (water) and gas (air) domains in the ice formation. The air phase of interest here is not the finely distributed volume fraction characteristic of the decreasing density of the rime structure. Instead, it occurs when a fracture has occurred within the ice formation or from debonding of the formation over a portion of the ice-substrate interface. Additional configurations of air separation between the solid, air phase are possible.

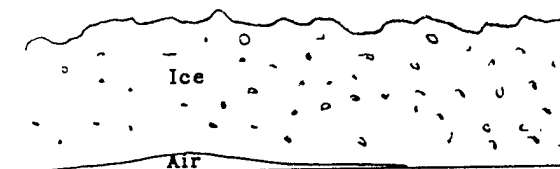
Four situations are shown in Fig. 1 which summarize the nonuniformity problem. Typically, the water component will have a conductivity at least two orders higher than ice and the air is an insulating dielectric. In 1-A the liquid water is dispersed as a discontinuous phase of "macro-particles" in the ice structure. In 1-B the water phase is shown as a continuous, more or less planar phase. This is a glaze condition and the water layer thickness is a maximum at the stagnation line and decreases at locations along the chord where the ice horn is formed. These possibilities are usually encountered at higher temperatures and high LWC when the refrigeration capacity provided by forced convection heat transfer is not able to completely freeze the impinging drops⁸. This is always the condition with the large drop ice formations under warm conditions which are of interest in this session. Fig. 1-C shows a thin air film present due to partial ice fracture. This can occur as debonding on or near the active surface of a portion of a deicer after an inflation cycle. It may also occur at certain locations and under certain accretion conditions due to thermal expansion. Finally, 1-D shows an ice formation at near freezing temperatures, at high LWC and at a positive angle of attack. The main ridge forms behind and usually adjacent to the trailing edge of the deicer boot. The ridge is thought to deflect the air flow, allowing the formation of the fragile looking, needlelike structures. High impedance has been observed in the needle zone suggesting that the needles grow as isolated dendrites on the otherwise bare airfoil surface. At very high LWC, water can be visually observed flowing over and through very rough looking SLD ice formations. This



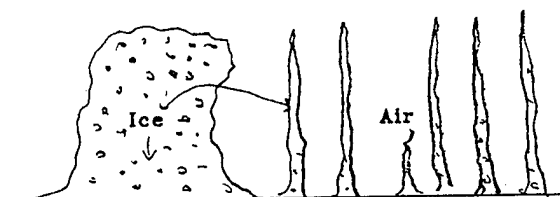
A. Distributed Water Phase



B. Continuous Water Phase



C. Air Void--Due to Cohesive or Adhesive Debonding



D. Needle Formation (Behind Ridge in Large Droplet Icing)

Fig. 1 WATER (UNFROZEN) AND AIR NON-UNIFORMITY DETECTOR NOISE SOURCES

situation is best approximated by Fig. 1-B. Although added detail would add realism, the simplification expressed in Fig. 1-B assists our understanding. In essence, the channels of liquid are formed parallel to, but not necessarily in contact with, the electrode surface. In addition to this simplified picture of the nonuniformity, the variability in the conductivity of both the water and the ice needs to be understood. The spray water used in icing tunnels is usually de-ionized and has a conductivity in the $10 \text{ (micro-ohm cm.)}^{-1}$ range. This is relatively pure and non-conducting, resulting in impedance that is primarily capacitive. However, water droplets in natural icing nucleate on foreign particles^{9,10} resulting in water conductivity increases of a factor of 10 to 30^{11} . Tap water, for example has an electrical

conductivity of about $350\text{--}400 \text{ (micro-ohm*cm.)}^{-1}$. For these reasons, icing tunnel evaluation of sensor performance needs to be performed over the range of spray water conductivities ranging from de-ionized to tap water.

Finally, ice formed from water over this range of impurity may result in variable ice conductivity. Hobbs addresses this issue with a comprehensive, yet concise review¹² of the electrical properties of ice. He reminds us that the primary carriers are protons rather than electrons. He discusses data showing that ice can be "doped" to provide either negative or positive charged, majority carriers. Finally, ice junctions, formed from suitably doped materials, perform rectification. These are semi-conductor properties and it is attractive to consider expressing these characteristics of ice in terms of the standard band theory used to classify and understand most solid materials^{13,14}. In any case, Hobbs describes doping experiments using both acids and bases. At small concentrations, the conductivity of ice increases linearly or as the square root of the doping concentration. The addition of certain, other dopants were found to have little effect upon conductivity.

The studies performed with the impedance sensor used different spray water conductivities by either mixing tap water with de-ionized water or by simply bypassing one or more of the purification stages used to condition the icing tunnel spray water. Though crude and poorly characterized, this can be viewed as a method for "tap water" doping the accreted ice. The dopants are probably dominated by the usual metal salts rather than well defined acids or bases. In any case, our doping studies did not show a significant effect on the conductivity of the ice phase. This means in practice that the conductivity difference between the water and the ice shown in Fig. 1-A and 1-b increase with increasing water conductivity. But at any water conductivity, the big problem is the high nonuniformity of the ice formation when water (liquid) is present.

These considerations, in terms of Fig. 1, mean that the impedance measurement of a uniform ice formation is capacitive and noise free. That is, the ice thickness inferred from a capacity measurement will be little effected by the conductivity level of the impact water droplets. But when the water phase begins to appear, as in Fig. 1-A or 1-B, significant output signal changes occur. The impedance drops dramatically and becomes resistive in the audio frequency range used with this sensor. However, the effect of an increasing water volume fraction is not additive. Consider an increasing volume fraction of highly conducting "particles" in Fig. 1-A. At some point the particles statistically come into contact^{15,16}, opening highly conducting paths which short circuit the lower conducting ice. Hence the observed electrode impedance dramatically decreases at some intermediate volume fraction of the water phase. In the case of Fig. 1-B the impedance is also non-linear, but in a different way. These effects will be discussed in more detail in connection with

Fig. 4. The presence of the air film shown in Fig. 1-C and D also may influence the measured impedance. An air void opens the conducting path, changing the impedance from resistance to capacitive reactance. When the electrode-ice separation width is small, C is large and the reactance can be small. Hence, the void may not produce a large jump in impedance. Fortunately, the air films caused by thermal expansion are infrequent and usually form in high curvature regions near the stagnation line. In the case of 1-D the needles were found to be electrically isolated and spanwise electrodes under the needles (but not under the ridge) did not detect the presence of ice (as a decrease in electrode impedance.)

The high conductivity of contaminated water compared to ice raises the possibility of an additional noise source. That is, does a wet surface at a temperature above the freezing point have enough conductance to produce a false signal? This source of noise was studied by recording the sensor output in an icing tunnel at high LWC starting at a temperature above freezing. As the tunnel temperature was lowered an ice build up was eventually observed. Though not easily anticipated, the sensor output remained negligible until the ice began to build up. This suggests that the water layer must be extremely thin. The ice build up apparently introduces an effective increase in cross section of the current path between the electrodes which is greater than the effect of the lower conductivity of ice compared to water. The high temperature data included in the experimental sections that follow partially illustrate the dominance of geometry effects compared to the intrinsic conductivity changes between water and ice.

SENSOR DESIGN DESCRIPTION

The essential concept of the impedance sensor¹⁷ is shown in Fig. 2. The geometry consists of flat electrodes 1 and 2 of width w and separation, b . The coordinates x and y locate a field point in the region above the plane of the electrode surfaces. When a potential difference, $V_2 - V_1$, is applied between the electrodes the potential at x, y is established from Laplace's equation¹⁸ in the form

$$\frac{\partial^2 V}{\partial x^2} + \frac{\partial^2 V}{\partial y^2} = 0$$

and the field components, E_x and E_y are given by

$$E_x = -\frac{\partial V}{\partial x}, \quad E_y = -\frac{\partial V}{\partial y}.$$

The potential, $V(x, y)$, describes either a non conducting medium (with no bound charges) or a conducting medium over the

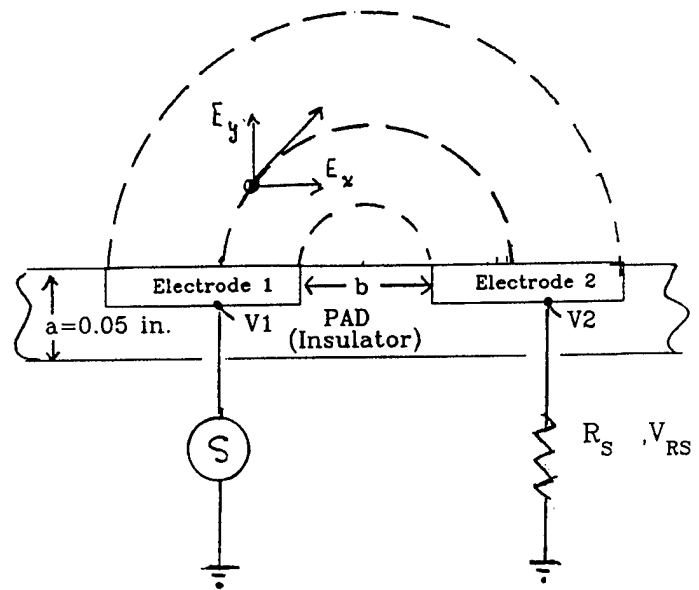


Fig. 2 SENSOR CROSS-SECTION SHOWING ELECTRODE-FIELD RELATIONSHIP

electrodes. This elementary result from electrodynamics means that the resultant field lines are defined by the electrode geometry independent of the conductivity level of the medium. The practical case as shown in Fig. 1, involves dramatic non-uniformity. This idealized picture in Fig. 2 is still useful for showing how the electrode geometry controls the field penetration into the medium. Closely spaced electrodes at a particular b will become insensitive to increases in the ice thickness for $y > b$. An additional electrode is needed to measure ice thickness. However, the configuration shown in Fig. 2 is enough to detect the presence of ice. As will be shown, this simple electrode pair also measures relative changes in SLD ice during an extended encounter.

The highest sensitivity is reached at smallest b , although design compromises enter. As b is decreased, a larger number of electrode pairs are needed to cover a given area. More importantly, the construction sets a lower limit on b . The electrodes are made of highly conducting urethane while the pad is insulating urethane. The leakage increases with decreasing b and progressively degrades the sensor sensitivity. This is a non-trivial material and processing issue, which lies beyond the scope of this study. The bottom line is that the electrode spacing in the design is typically in the order of 0.1 inch which meets both the low leakage and high sensitivity requirements.

The functions carried out by the electronic circuit is summarized in Fig. 3. The signal source is connected to the drive electrode, D. The current is returned through the return electrode, R, through a sensing resistor, R_s . The voltage, V_{RS} , developed across R_s , is amplified in A and is peak detected and compared

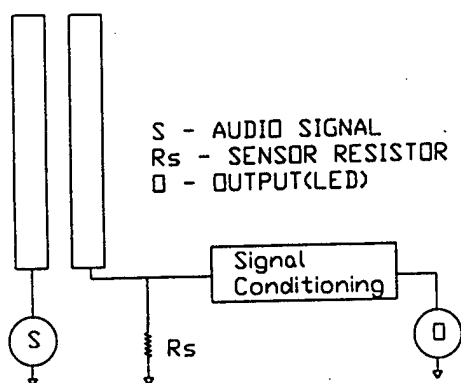


Fig. 3 DETECTORS CIRCUIT OVERVIEW

a reference voltage, V_{ref} . When the amplified voltage exceeds the threshold, the warning light, L, turns on. Most of these requirements are satisfied with low cost operational amplifiers. However, the high ice impedance confronting the circuit requires a careful design.

Typical outputs from the circuit are illustrated in Fig. 4. As the

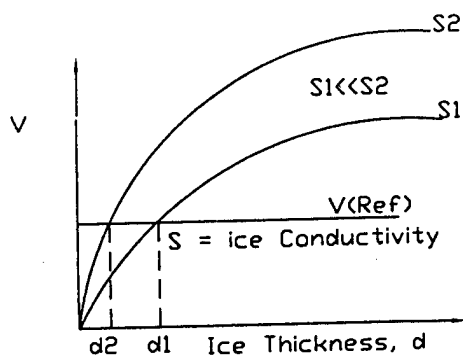


Fig. 4 DETECTOR RESPONSE

thickness of the ice layer builds up (see Fig. 2) the current increases across the electrodes in Fig. 3 and V increases as shown in Fig. 4. The voltage increases linearly at first and at large d becomes constant. The two curves correspond to two conductivity levels with $S_2 > S_1$. It is apparent that the voltages reach the reference level, V_{Ref} with $d_2 < d_1$. This represents an error range which can be minimized by raising the gain of the signal conditioner in Fig. 3 to handle the lowest expected ice conductivity. To be successful, this strategy requires that the various sources of noise be sufficiently low. The sensor error trend arising from the water channel flow pictured in Fig. 1-B

can now be described. As Fig. 3 shows, the sensor voltage reading across R_s tends to increase and then become constant as the ice thickness builds. Consider next a floating water layer over the ice in Fig. 13-B. Almost all the voltage will be generated in the path to the floating water layer, with a negligible voltage drop from the path from drive to return in the water layer. Hence, the impedance will increase with a decrease in output voltage as the ice layer thickness increases. This is the opposite trend shown in Fig. 4 for a homogenous ice layer. This inversion in the response trend was verified in tunnel tests with wet ice formations.

ICING TUNNEL TEST RESULTS

The electrode designs were implemented with arrays of electrodes formed into 0.050" patches covering an area of 4"x5". The patches were installed on a NACA 23012 air foil section in the IRT (Icing Research Tunnel) at NASA Lewis. The geometry of the installation is shown in Fig. 5. Pneumatic ice protection

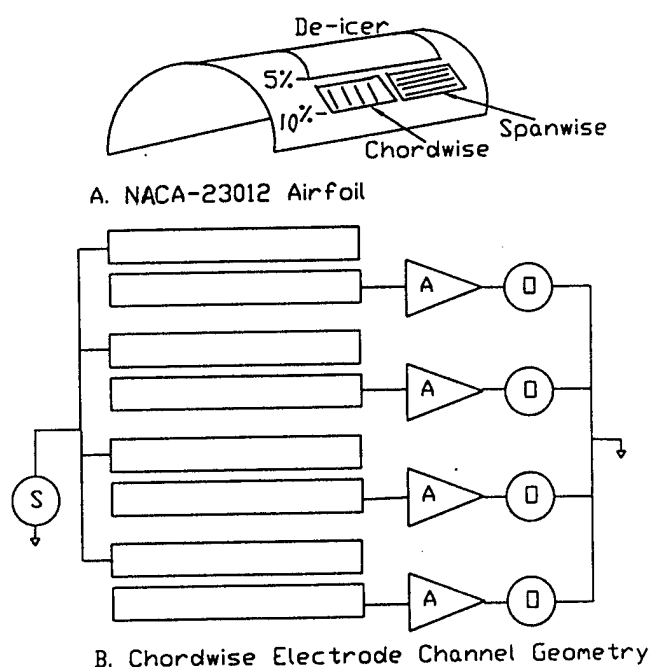


Fig. 5 SENSOR LOCATION ON AIRFOIL SECTION

was provided with active deicer tubes mounted out to about 5% chord as shown in Fig. 5A. The large droplet icing ridges occur adjacent and beyond 5% chord. The figure shows both a spanwise and chord-wise sensor array deployed in the large droplet icing zone. Fig. 5B shows the circuit scale up with four channels that duplicates the functions shown in Fig. 3. The four drive electrodes are supplied in parallel, but the returns are directed into four separate return channels. The four lights detect the presence of ice in the local regions covered by the electrode

pairs. A separate set of channels was provided for the second pad. The simplicity of the channels made this the preferred approach compared to feeding the output into a single channel with multiplexing circuitry.

The test matrix was designed with the total air temperature and the angle of attack (AOA) as the principal variables. The constants were the air speed (V_a) at 195 mph, liquid water content (LWC) of 0.8 grns/M³ and drop diameter (MVD)=160 microns. The operating point distribution is shown in Fig. 6.

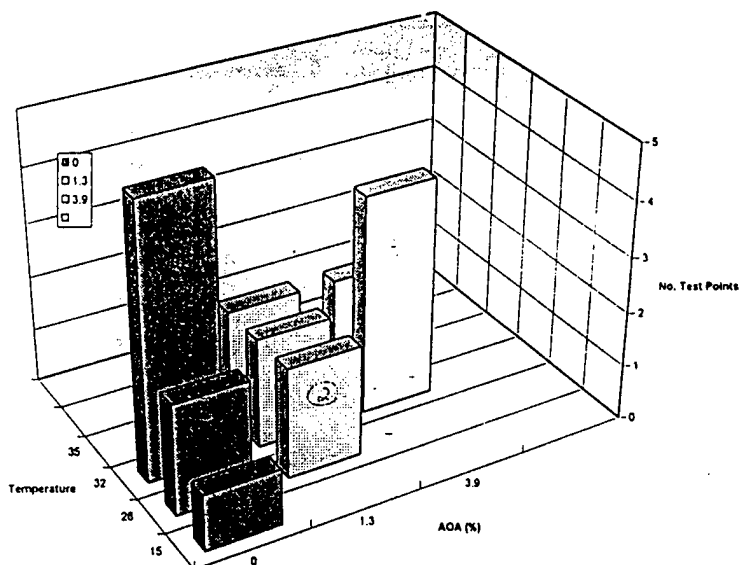


Fig. 6 TEST CONDITION MATRIX

More than half of all of the points were performed at 32 deg. All of these tests generated ice formations over the sensor pads, including the one test point at 15 deg. F. It is acknowledged that a LWC of 0.8, an MVD of 160 microns at 15 deg. would be rare and unexpected in nature. Typically, the tests were paired. The first was run for 21 minutes with the boots cycled at 3 minute intervals. Then the test was repeated and terminated when the sensor light turned on. This was almost always before one minute and always before the boot was inflated.

The test results demonstrated that the ice ridge shifts location, depending upon the test conditions. Both the span and chordwise orientations gave useful signals provided that the ice formation bridged the electrodes, even at a small, local region of the array. In some cases the ice ridge formed extremely close to the trailing edge of the deicer with an ice formation as shown in Fig. 1-D. In these cases the needle structure made up part of the bridge path for the forward most electrode pair, and the ice was not detected. Even for these difficult cases the ends of the chordwise electrode pairs were bridged and useful results were obtained. Typical results are shown in Fig. 7 for $T=32$ deg. and an AOA of zero deg. This is the more routine case when the ridge forms

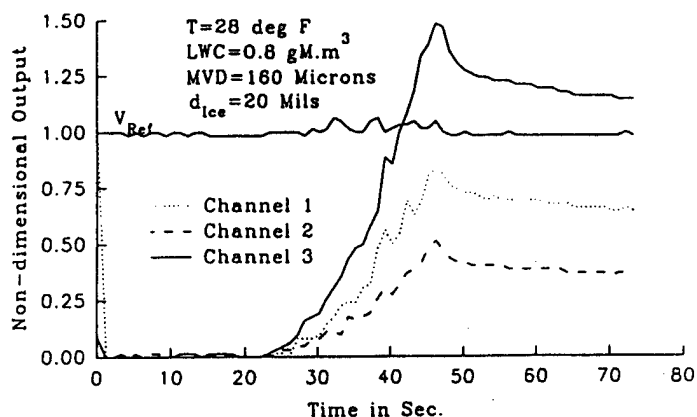


Fig. 7 ICE PRESENCE DETERMINATION, $AOA=0^\circ$

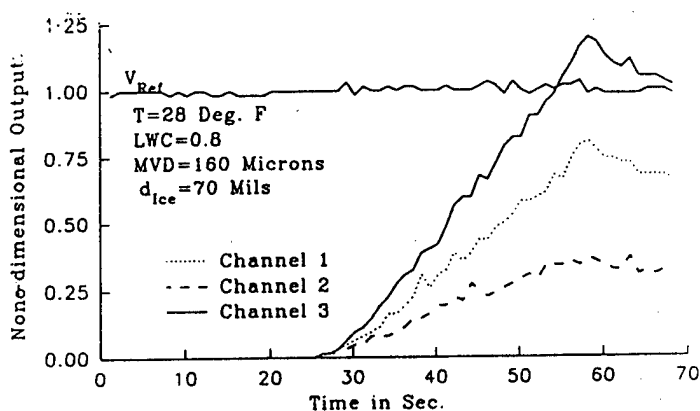


Fig. 8 ICE PRESENCE DETERMINATION, $AOA=1.3^\circ$

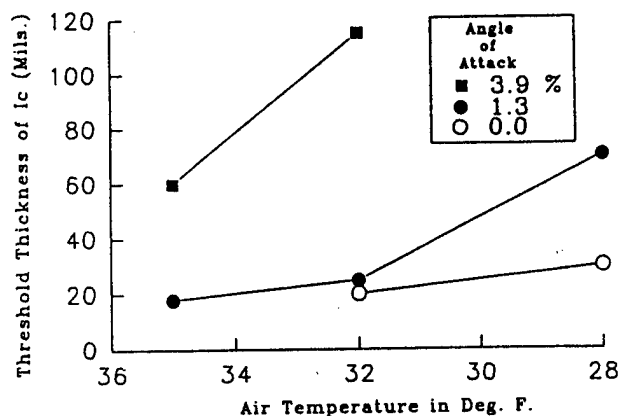


Fig. 9 THRESHOLD THICKNESS OF ICE OVER CHORD-WISE ORIENTED ELECTRODES

farther aft, providing full electrode coverage with the higher conductance, dense ice. The ice is detected within the first minute of icing at a thickness of 20 mils. In Fig. 8 the temperature is decreased to 28 deg. F and the ridge moves forward. The same

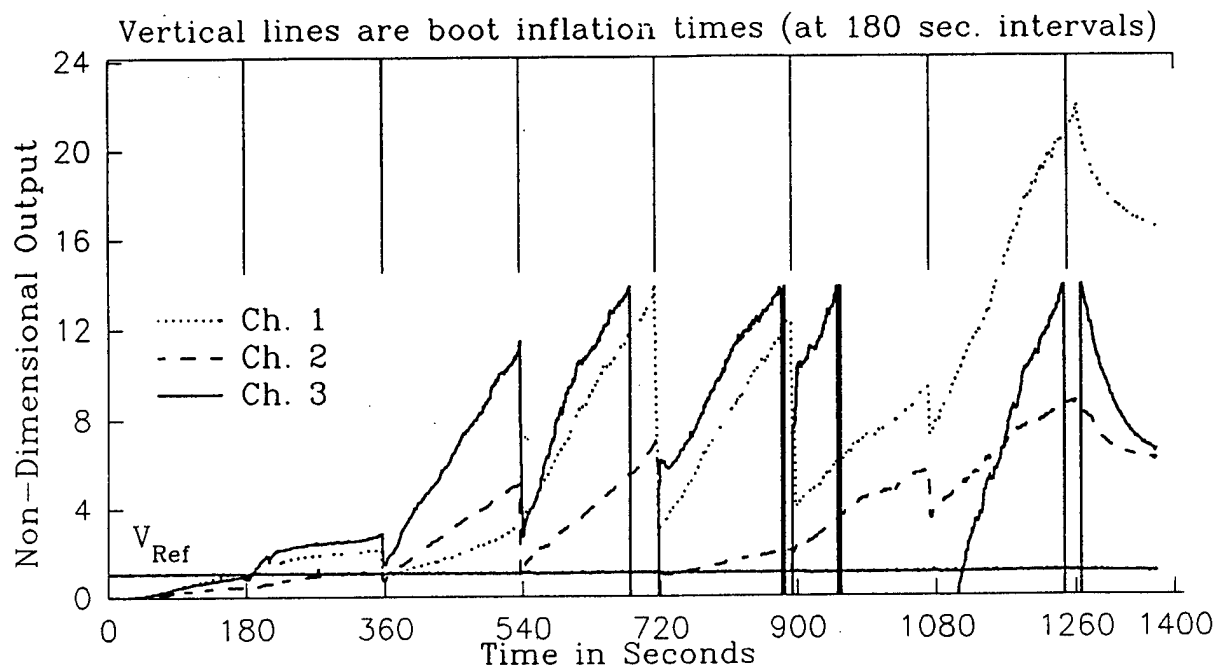


Fig. 10 PARTIAL AND COMPLETE ICE LOSS EVENTS COMPARED TO BOOT INFLATION TIMES
 $\{T=32^{\circ}\text{F}, \text{AOA}=3.9^{\circ}, \text{LWC}=0.8, \text{MVD}=160 \text{ Microns}, V=185 \text{ mph}\}$

channel crossed the threshold first at about 52 seconds at a thickness of 70 mils. The spray was turned off at 58 seconds, shortly after the first light turned on. Beyond this point the response began to decrease due to freeze out of the water phase..

Considerable attention was given so that the sensor output begins when the spray was first turned on. Hence, the data shown in Fig. 7 and 8 start out quite wet, at least at the highest temperatures in the test matrix. Both curves show little response during the first 20 or 30 seconds. This is offered as evidence that the sensor is very insensitive to the presence of water only on the electrode surfaces.

Fig. 9 shows a summary of the detector results for the chordwise sensor. The curves show an increasing ice thickness threshold with decreasing temperature and increasing AOA. These trends may be related to the following factors. First, the ice conductivity decreases as a function of temperature. This is due in small part because the ice phase has a temperature dependence. The major effect, however, is the decrease in the water content in the ice as shown either in Fig. 1A or 1B. These effects upon the response were illustrated in Fig. 2. The forward movement of the ridge with decreasing temperature and increasing AOA may also be a factor. This may decrease the amount of electrode bridging and may also be related to the increase in the high impedance needle structures that form aft of the ridge under these conditions. The detector response from runs lasting beyond the first crossing provides additional

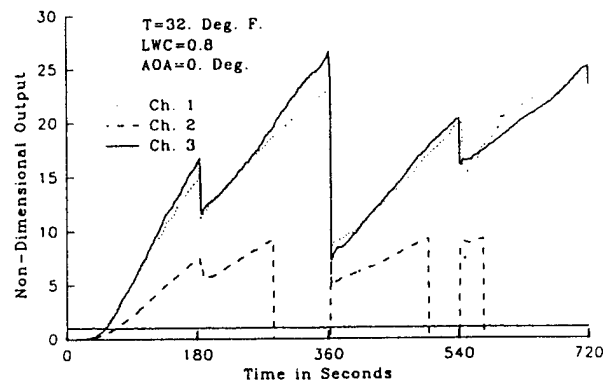
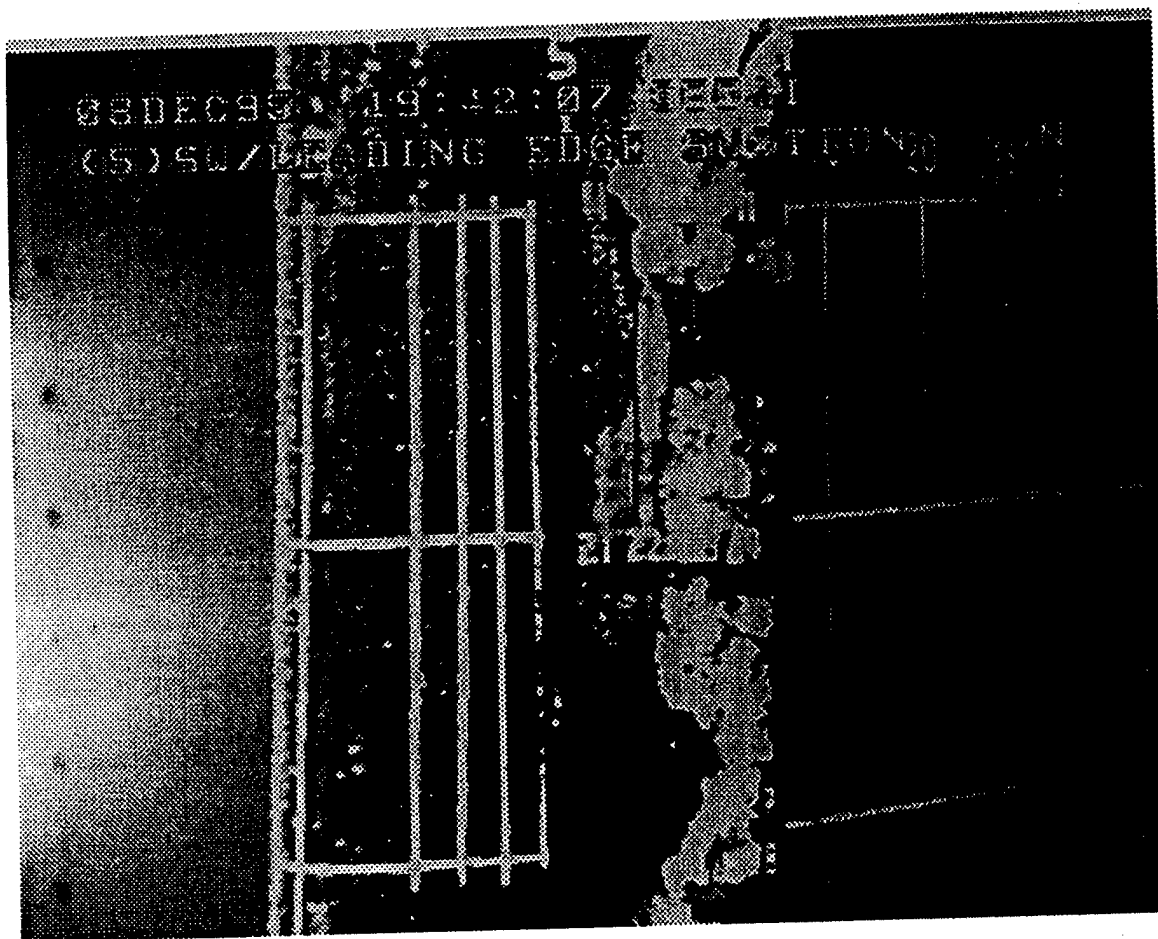


Fig. 11 RESPONSE SUGGESTING COMPLETE ICE REMOVAL FROM AREA NEAR CHANNEL 2 ELECTRODES

information about the progress of the large droplet accretions in the zone behind the normal impingement limits. The output response for a 21 minute case at an AOA of 3.9° is shown in Fig. 10 and a 12 minute run at 0° is shown in Fig. 11. These are "warm" test conditions (32 deg. F) at the standard LWC of 0.8 gm/M³, 160 micron MVD and 185 mph. The cycle time of the deicer is indicated in Fig. 10 by the values entered along the x-axis and by the upper, vertical bars. The three channels show roughly similar positive slopes. This is interpreted as a measure of the increasing thickness of the SLD ice growth. The almost periodic, stepwise decreases are interpreted as partial ice removal and in a few cases, complete



loss of ice over the corresponding electrode pair. The ice growth appears to grow very slowly for the first six minutes with only small ice losses at the first deicer cycles (at 180 and 360 sec.). Beyond this time the growth is rapid and the ice loss is usually large. An inspection shows that the channels register either a slope change or a discontinuity during each deicer cycle, except for the first inflation at 180 sec. Only channel 3 shows ice loss between cycles, one before the inflation at 720 sec. and the second after 900 sec. Except for these two, all of the slope changes and discontinuities occur only at the inflation times. This is repeated for the channel in Fig. 11 indicated by the solid line. This strong coupling is interesting because the ice being monitored is located on the sensor pad which is, at best, only adjacent to the last inflation tube. This could be partly rationalized for Fig. 10 because the ice structure moves forward with increasing AOA, which was set at the highest value of 3.9° during this run. But, in Fig. 11, the AOA is 0° , which should move the ice structure away from the aft tube. The 32° temperature should also move the structure further aft in both runs. Finally, the negative jump in Fig. 10 after the inflation at 900 sec. and the last negative jump in Fig. 11 do not have a positive, jump. These cases may indicate a true adhesive event

which removes all of the ice over the electrode. This is confirmed in Fig. 10 on channel 3 by the gradual slope starting shortly after the inflation at 1080 seconds. Fig. 12 is a photo of the ice formation after a run showing the complete removal of a small spanwise segment. While this does not match the specific cases tested in Fig. 10 or 11, it does illustrate the frequently observed, local ice removal in support of the above interpretation.

Fig. 10 and 11 illustrate some of the monitoring capability of the ice sensor. Generally speaking, the output changes appear to track the build up and loss of ice. With added interpretation of the ongoing behavior of the signal output, the ice-air nonuniformity (illustrated in Fig. 1-C), can be identified. The result is a significant step towards residual ice detection and monitoring. This has applications that go beyond the SLD application discussed here. The pads, being only 0.050 in. thick, can be placed in most locations where monitoring is desired. The electrodes can also be built into the active tubes. Hence, the results shown in Fig. 10 and 11 can be anticipated for the ice on the active surfaces as well. These figures also offer clues about some of the forces that are controlling the thickness of the

evolving SLD ice formations. The self shedding between inflations indicates that the convective forces from the air flow can produce cohesive failure of variable, spanwise segments of the formation. The deicer inflation effects apparently work in tandem with the air flow. The ice particles shed by the active deicer may impact the SLD formation producing cohesive fracture. Secondly, the crack propagation and related stresses may generate voids and ultimately adhesive debonding. In summary, the impedance detector is doing more than detecting the presence of the SLD ice. It is also helping us understand the failure mechanisms that may eventually provide a means of protection.

CONCLUSIONS

1. A parallel electrode based impedance sensor has been developed which detects the presence of ice formations from large droplets at high LWC icing conditions.
2. The sensor output was observed to signal the presence of ice at thicknesses in the .025 to 0.11 inch range, depending upon the accretion temperature and angle of attack. The changes in thickness thresholds were shown to increase as the ice ridge moved forward with decreasing temperature and increase in angle of attack.
3. In addition to providing early warning of the ice ridge build up, the sensor also monitors the progress of formation, for example, over the time periods of exposure prior to landing. The sensor output indicates self shedding at times that are sometimes coincident with and at other times independent of deicer boot inflation times. In most locations along the monitored zone the ridge appears to reach an average steady state thickness with a fluctuating build up-self shed sequence.
4. The sensor design provides the following, practical advantages:
 - (a), Electrode pair orientation in spanwise or chordwise directions for providing large area coverage of the airfoil surface.
 - b), Very thin elastomeric, electrode and pad design (0.05 in.) permits both passive applications, as reported here, as well as direct integration into the deicer construction.

ACKNOWLEDGEMENTS

A number of others have made contributions and provided assistance during this development. These include R. Rauckhorst and R. Wallace at Ice Protection Systems (IPS), M. Herold, BFG/Tremco R&D and D. Pruzan, Inovative Dynamics Co.

BIBLIOGRAPHY

1. Rosemount Aerospace ice sensor Model 0871M1.
2. Floyd M. D., "A Piezoelectric Ice Sensor For Aviation Applications", Sensors, May, 1990
3. Hansman J. R., Measurement of Ice Accretion Using Ultrasonic Pulse-Echo Techniques", J. Aircraft, 22,6,530, 1985
4. Magenheim, B. and Rocks, J. K. "Development and Test of a Microwave Ice Detection Measurement Instrument (MIAMI)." NASA CR-3598, 1982.
5. Weinstein L. M. "Ice Detector, Patent No. 4,766,369, 1988
6. Gerardi, J. J., Hickman, G. A., Khatkhate, A. A., Pruzan, D. A., "Apparatus for Measuring Ice Distribution Profiles", Patent No. 5,398,547, May, 1995.
7. Reich A. D. "Ice Property/Structure Variations Across the Glaze/Rime Transition", AIAA-92-0296, Paper presented at the 30th Aerospace Sciences Meeting, Reno Nevada, Jan. 6-9, 1992.
8. Ref. 7, Fig. 1
9. R. Dorys, P. Demott, E. Hindman and D. Feng, "The Significance of Snow Crystals and Mountain-Surface Riming to the Removal of Atmospheric Trace Constituents from Cold Clouds", in Precipitation Scavenging, Dry Deposition and Resuspension, Ed. Pruppacher, et al., Elsevier Science Publishing Co. Inc.
10. G. Raynor, and J. Hayes, "Differential Rain and Snow Scavenging Efficiency Implied by Ionic Concentration Differences in Winter Precipitation", in Precipitation Scavenging, Dry Deposition, and Resuspension, Ed. Pruppacher, et al., Elsevier Science Publishing Co. Inc.
11. H. Johnson and B. Vonnegut, "Apparatus for Measurements of the Electrical Conductivity of Rainwater with High Resolution in Space and Time", J. Appl. Meteorology, 30 (1220), 1991
12. Hobbs, P. V., Ice Physics, (Clarendon Press, Oxford, 1974), Chap. 2
13. Band structure theory of solids provides a useful basis for dealing with the electrical and thermal properties of most solid materials. Based upon the review by Hobbs

(Ref. 12), it appears this has not been fully developed or utilized in describing the electrical transport properties of ice. Since ice conduction is via protons and not electrons, ice may be unique. Nonetheless, many of the experimental findings as well as theoretical treatments reviewed by Hobbs show close analogies with other materials. At the most general and elementary level, for example, band structure considerations permit the classification of materials as either metals, semi-metals, semiconductors or insulators. Most of these classes appear to be relevant for understanding the electrical behavior of ice. The only point here is that additional attention to the band structure-transport relationships would be helpful even for something as practical as the development of an impedance sensor for ice. The following example is a case in point. On p. 169 the Seebeck coefficient (or thermoelectric power) in ice may arise from different mobilities of the positive and negative carriers diffusing in a temperature gradient. If this results in changes in the carrier concentrations at the different temperatures a voltage would be generated. Related to this, Hobbs shows the Seebeck coefficient in the 2-3 millivolt/Deg. C with a change of sign at an intrinsic doping range of 10^{14} cm⁻³ carriers. The conductivity range is plotted for up to 10^{19} carriers, which is the range for heavily doped semiconductors. From a band structure standpoint it is extremely unlikely that the difference in the majority and minority carrier mobility can generate a fairly constant Seebeck effect across this wide concentration range. Hobbs reviews a second approach which uses the diffusion of the majority carriers down the temperature gradient as the source of the thermal voltage. This is the standard approach which has been satisfactory for many materials. Chap 12 and 13 in Ref. 14 review both elementary and formal treatments using thermal diffusion. A similar calculation by Brooks for ice was reviewed by Hobbs. It is also interesting that this calculation led to the definition of a electro-chemical potential for the conducting system. In band theory terminology this potential is identified as the Fermi level.

14. Reich, A. D. Transport Theory in Solid Structures. Unpublished Manuscript, Available on request.
15. V. I. Odeevskii, Zhur. Tekh. Fiz. 21, 667 (1951) [Translation: W. Garston]
16. Airapetiants, C. F., Zhur. Tekh. Fiz. 27, 478(1957). [Translation: Soviet Phys. 3, 1935(1958)]
17. Patent Pending
18. Panofsky, W. K., Classical Electricity and Magnetism. (Addison-Wesley Publishing Co., Inc., Cambridge, Mass., 1955.)

REMOTE DETECTION AND AVOIDANCE OF INFLIGHT ICING

Charles C. Ryerson
Cold Regions Research and Engineering Laboratory
U.S. Army Corps of Engineers
Hanover, NH 03755-1290

ABSTRACT

Icing forecasts are not sufficiently accurate to prevent all icing mishaps. Remote detection of icing potential ahead of aircraft may allow avoidance and escape from icing encounters. Remote detection is intended to identify and assess icing potential ahead of an aircraft, with regard to aircraft type and airspeed, and provide guidance for avoidance in a manner similar to current wind shear and thunderstorm avoidance systems. Remote detection requires mapping of temperature and cloud liquid water magnitude by droplet size in the flight path ahead of the aircraft. Two promising technologies include multiple field-of-view lidar and differential attenuation radar. Both technologies have had limited testing. The advantage of radar is its ability to penetrate clouds and measure liquid water, and lidar is able to detect cloud droplet size spectra. Several other potential technologies, and the potential and problems of icing prediction detection, are assessed.

INTRODUCTION AND BACKGROUND:

Two strategies allow aircraft to contend with airframe icing. One strategy is abatement to prevent deterioration of airworthiness by anti-icing or deicing. The second strategy is to prevent or minimize icing by either avoiding icing when in flight, or by not flying. Avoidance is the principal reason for icing forecasting because, by knowing where icing is occurring and knowing its intensity, operators can judge whether their craft can cope with the accretions expected.

Unfortunately, neither strategy works perfectly. Deicing and anti-icing systems often fail to keep critical airframe components sufficiently free of ice, and icing forecasts lack sufficient precision for enroute avoidance. If anti-icing and deicing equipment could maintain airworthiness in the most severe icing conditions with minimal weight, space and power penalties, then icing avoidance would be unnecessary.

Some aircraft must fly even when icing intensities beyond aircraft capabilities are possible. Search and rescue and medevac flights, military flights during conflict, and unmanned aerial vehicles (UAVs) may be required to fly in icing. Some aircraft, such as charter flights in remote areas, may fly without the benefit of specific icing forecasts and find ice quite by chance. And, unforecast increases in icing severity endanger all aircraft.

Aircraft need a system to warn of icing conditions in the flight path as do existing weather avoidance avionics for wind shear and thunderstorms. Such a capability will allow aircraft to avoid icing conditions and to seek routes of least icing exposure. This can be accomplished by either seeking paths of low icing intensity, or the shortest route through ice of any intensity. Though more difficult to achieve, aircraft that inadvertently enter icing also need a method of seeking expeditious escape.

Thus a capability is needed for advising pilots of icing potential in the flight path ahead of aircraft, and recommending actions to minimize icing exposure. Icing potential may be assessed by sensing weather parameters in the flight path that will cause ice to accrete on aircraft components. These parameters should include at least atmospheric liquid water content, drop size distribution and temperature. This remotely sensed information is then

microprocessor-analyzed onboard and is supplied in a form most useful to the pilot. The ultimate goal is to provide information that will allow the pilot to efficiently minimize airframe icing and still fly the airplane. The concept of such a system is not new and has been proposed by others (Siquig 1993, Sand and Kropfli 1991, Fournier 1993).

The U.S. Army Corps of Engineers Cold Regions Research and Engineering Laboratory (CRREL) has developed a Small Business Innovative Research Program (SBIR) Request for Proposals (RFP) to develop an onboard remote sensing icing avoidance system. Prior to submitting the SBIR RFP, CRREL assessed the potential utilization and technology of such a system. This report reviews the need for an onboard icing avoidance system, proposes potential system operating characteristics and surveys candidate sensing technologies.

NEED FOR ONBOARD ICING AVOIDANCE:

Icing Forecasts:

Current icing forecast techniques do not provide adequate resolution for icing avoidance, and is one reason onboard icing avoidance capability is needed. This forecast inadequacy is due to problems with general weather forecasting, and icing forecasts themselves. One problem is the availability of data to generate weather forecasts. Upper air soundings are widely spaced in the continental United States, with each representing about 90,000 km², and observations are made only twice daily. Curry and Liu (1992) found 56% of icing encounters to be within cloud masses with areas of less than 46 km², about 0.05% of the areal spacing of upper air soundings.

Another problem is the large grid spacing of global forecast models. For example, the Air Force Global Spectral Model has a grid size of 2.5° latitude and longitude (Knapp 1996). Continental models, such as the National Weather Service Nested Grid Model and Eta Model, have finer resolutions, with grids of 80 km or less. However, they are still generally synoptic scale models. Icing is often a mesoscale or sub-mesoscale phenomenon that is strongly influenced by even relatively small topographic features.

Spatial-temporal resolution and topography are improved by predicting icing with mesoscale models, such as the National Weather Service's Rapid Update Cycle with a soon-to-be-operational 40-km-resolution and one-hour-update cycle (Benjamin et al. 1995), and the Army's Battlescale Forecast Model with a 10-km resolution (Knapp 1996). However, even with improved spatial resolution, intense icing events are often very localized and may be missed. Also, these mesoscale models are still fed with a coarse data net, and cannot process large areas because of their fine net size.

Often icing is forecast to occur within a large region, and yet icing occurs only within a small portion of the forecast area (Curry and Liu 1992, Green 1995). At other times icing occurs outside of areas for which it is forecast. Errors in forecasted icing rate are also common. As a result, icing of various types and intensities are forecast to occur within relatively large areas, yet during the time that the forecast is valid, icing may occur within only a small portion of the forecast area.

Icing forecast techniques need improvement. The physical processes of supercooled liquid water formation, large supercooled liquid droplet formation, entrainment and glaciation are not fully understood and thus cannot be modeled with accuracy, especially from standard meteorological parameters. Some models attempting to simulate liquid water and droplet size spectra have been largely abandoned, such as the Smith-Feddes model. As a result, there has been a return to more reliable empirical models. For

example, Cornell et al. (1995) compared three empirical forecast techniques used by the Air Force and Navy with 9693 icing pilot reports. The Air Force RAOB technique performed best, with 67% of type forecasts and 42% of intensity forecasts agreeing with pilot reports. However, all of the algorithms failed to forecast clear and mixed icing in stable conditions.

Several other tests of either current or experimental icing forecast models by the National Center for Atmospheric Research, the National Aviation Weather Advisory Unit and the Air Force, indicate that improvement is needed for reliable operational use on the national or local scale (Brown et al. 1995, Thompson et al. 1995, Coffey 1996). Most of these schemes are based upon temperature ranges and dew point depressions, and often a stability term. Some can be operated strictly from radiosondes, whereas others are fed from numerical forecast models (Knapp 1992). All have been compared to pilot reports. However, it is unlikely that forecasting will improve significantly until reliable methods are available to operationally calculate cloud liquid water and drop spectra, and satellite imagery is used to improve spatial resolution of icing forecasts by eliminating cloud-free areas (Thompson et al. 1995, Lef et al. 1994).

Overall, current forecasting techniques, though improving in quality primarily because of increased capabilities and resolution of numerical forecast models, will not provide adequate icing avoidance in the foreseeable future.

Incidents and Accidents:

In-flight incidents and accidents indicate a need for onboard icing avoidance systems. CRREL has focused on the need for icing avoidance in the military (Ryerson et al. 1995). The perceived need for onboard icing avoidance in the military varies. In general, a system would extend operating conditions for all-weather helicopters and fixed-wing attack aircraft and improve safety and military readiness.

Army:

In-flight icing is not generally considered a problem in the Army because most missions are flown in warm climates, missions are not flown if ice is predicted, and icing is so infrequent that readiness is little affected. However, about 9% of Army medevac flights are canceled due to icing in Alaska, and medevac commanders give icing avoidance a high priority.

Navy:

Mayer et al. (1984) found about 525 icing-related mishaps in the Navy between 1964 and 1984, with about 70% due to in-flight problems, and nearly all due to foreign object damage. Accident reports in recent years suggest that the Navy has had fewer icing problems, with more reports of hail impact damage than airframe ice accretion problems. However, Lef et al. (1994) state that the Navy is concerned about the icing threat to carrier-launched aircraft, and that helicopter icing accidents are not infrequent.

Air Force and Coast Guard:

Anecdotal evidence from discussions with pilots indicates that Air Force fixed-wing aircraft experience icing problems. The Coast Guard reports no problems with icing despite their search and rescue and enforcement missions. They do not fly if icing is forecast.

General Military Issues:

Other military issues with remote detection of icing include weight, power and cost. Whereas some military aircraft have an abundance of space and power, others are at their capacity in both regards, and if a new avionics package is added others must be removed. However, not having an avoidance capability also causes weight penalties. In 1986, the Army indicated that icing forecasts were about 50% accurate—and ice is usually over-forecast in area and intensity. Over-forecasting reduces aircraft payload and range because more fuel is required. Cost of new avionics packages is also a major problem. Since icing occurs less than 5% of the time in most parts of the world, it is easy to place other spending priorities higher than icing avoidance.

Unmanned Aerial Vehicles:

Military and civilian UAVs are special cases in need of icing avoidance systems. UAVs, especially high altitude long endurance UAVs, must autonomously seek a route through icing conditions (Siquig 1993). UAVs may also be required to avoid icing on low altitude, short duration missions, but also may simply be grounded due to ice. This occurred with the Predator UAV this winter in Bosnia (Anon 1995). Onboard weather-sensing systems would be coupled with autonomous controls to allow UAVs to avoid or minimize icing, which impacts them more severely than conventional aircraft because of their low power and high efficiency airfoils.

General Aviation:

There is considerable evidence that ice avoidance systems will also aid general aviation, though size, power and cost are again issues. Aircraft flying at 400 kts or greater, which includes most jets, generally do not have icing problems (Taylor 1986). However, jets on approach and departure, 300 kt turboprops, piston aircraft and helicopters are all susceptible. Turboprops fly exclusively at lower altitudes and are thus exposed to ice for extended periods. Jets in long holding patterns with dirty wing configurations may also be particularly susceptible to icing. Piston-driven aircraft, principally light aircraft, are rarely equipped with deicing equipment, with only some twins having icing capability. Helicopters are probably the most threatened of all aircraft because of their unique aerodynamics and mission requirements.

Fortunately, transport category aircraft are not often lost to icing, though there may be incidents, as occurred to ATRs prior to the Roselawn accident (Engelberg and Bryant 1995). However, private general aviation does not fare as well. The popular pilot press carries many reports of private general aviation icing incidents and accidents. Between 40 and 60 private general aviation accidents annually are attributed to in-flight structural icing, about 50% of which are fatal (AVEMCO 1983, Taylor 1986). Though about 50% of these are visual flight rule (VFR) pilots in instrument meteorological conditions (IMC), a pilot training problem, many of the accidents may be preventable with onboard icing avoidance (Bertorelli 1992). Even a VFR pilot may be able to avoid the most serious of icing conditions, freezing drizzle or rain, with onboard icing avoidance capability. An instrument flight rule (IFR) pilot could avoid icing within IMC, or at least avoid conditions that tax aircraft ice removal systems.

As in the military, civilian helicopters are probably the most threatened by icing. Low altitude missions in icing weather, such as servicing offshore oil rigs and search and rescue, make helicopters particularly vulnerable. Also, their limited altitude capability, low speeds, rotating components and generally low power reserves make them more susceptible to ice than are fixed-wing aircraft (Manningham 1991). However, helicopters'

low speed and maneuverability may be an asset if equipped with an icing avoidance system because they have more flexible course and altitude changing capability than fixed-wing aircraft. Only one commercial helicopter is icing certified, the Super Puma (AHS 1995).

ON-BOARD ICING AVOIDANCE SYSTEM OPERATING CHARACTERISTICS:

An autonomous icing avoidance system would scan continuously ahead, above and below, and perhaps behind, an in-flight aircraft for potential icing conditions. If icing potential is detected, the system, considering weather conditions, aircraft aerodynamics and ice previously accreted on the aircraft, advises the pilot how to avoid icing. Advice may apply to course direction, altitude or speed of flight or to changes in aircraft configuration such as raising flaps and activating anti-icing/deicing equipment.

An icing avoidance system must continuously monitor the atmosphere for conditions conducive to icing. Meteorologically, icing potential is governed primarily by atmospheric liquid water content, drop size and temperature.

Liquid Water Content:

Liquid water content is generally considered the most important icing parameter if temperatures are below freezing and droplets are smaller than about 80 μm . Ideally, liquid water should be sensed from a minimum of 0.02 g m^{-3} to near 2.0 g m^{-3} , covering nearly all liquid water contents likely encountered within clouds. Cooper et al. (1982) found that over 99% of liquid water measurements in clouds during summer and winter and in continental and coastal areas were less than 1.0 g m^{-3} , though higher values can occur near the tops of cumulus clouds in summer icing conditions. Liquid water content typically does not exceed 1.0 g m^{-3} even in a 25 mm hr^{-1} rainfall (AFGL 1985). A low minimum liquid water content sensing capability is also required because an aircraft can gradually accrete small amounts of ice at low liquid water contents that cumulatively could be dangerous, especially if areas of greater liquid water are subsequently entered.

Drop Size Distribution:

Sensing of liquid water content and temperature alone would probably allow detection of the majority of hazardous icing, but perhaps not the most dangerous situations. Since the Roselawn accident in 1994, supercooled large drops (SLD) have been recognized as a more serious hazard than previously considered because SLD are difficult to forecast and they runback aft of ice protection systems before freezing. SLD, ranging from about 40 μm to 400–500 μm , may occur in areas of relatively low liquid water content (Politovich 1989, Coffey 1995), yet their impact on aerodynamics is large. Since the Roselawn accident, droplet size sensing has added importance. As a result, the most capable icing avoidance system should detect drop sizes through three orders of magnitude, from a minimum of about 4 μm to at least 4000 μm (Willis and Tattelman 1989).

Temperature:

Icing is generally avoided if temperatures are warmer than 0°C. Air or droplet temperature must be sensed in the same space in the flight path as water parameters. Temperatures should be sensed from about +20°C to about -40°C. In theory, supercooled liquid water does not occur below -40°C, and supercooled drops are not a practical problem below about -25°C. Temperatures above 0°C must be sensed to predict melt rates or changes in aerodynamics from melt, runback and possible refreezing during altitude changes. Temperatures to -40°C should be sensed because airfoil surfaces are

warmed by aerodynamic heating. Most critical is the accuracy of temperature measurement because of its effects, with liquid water content and drop size, on ice type and density, and ice shape on leading edges (Wright 1995). Temperature must also be sensed above and below the flight path because, within a given distance, temperature typically changes more rapidly in the vertical than in the horizontal, which may provide more rapid escape from icing.

In addition to the types of parameters sensed scan rate, resolution, range, aircraft condition and the pilot interface are critical.

Scan Rate:

For a practical implementation a sensor must rapidly "paint" an image of the atmospheric volume ahead to allow sufficient time for pilot-initiated avoidance of an icing threat. Scan rate is a function of scan volume, aircraft speed and cloud liquid water structure. Complex liquid water structure, large scan volume and high aircraft speed demand higher scan rates.

Scan Resolution:

Scanning volumetric resolution should be based on the dimensions and structure of liquid water concentration. Resolution is also tied to scan rate, with higher scan rates allowing lower resolution. Resolution on the order of magnitude of the aircraft dimensions, or finer, may be most desirable for close-in, low speed navigation through regions of high icing potential. For general in-flight guidance, lower-resolution sensing may be adequate.

Scan Range:

Sensing range must be at least 10 nm to allow time for avoidance maneuvering. This provides two minutes of warning for 300 kt fixed-wing aircraft, and more time for helicopters. Larger scan distances provide more warning time. The primary value of larger scan distances is the greater opportunity allowed to view completely through an area of icing potential and determine the amount of exposure. This is important for route finding because ice accretion is a product of icing rate and exposure time (Jeck 1994, Cooper et al. 1982). Inability to sense completely through icing limits avoidance options, and may limit an aircraft to turning back along its original route to avoid icing. Though scan distances of 50 nm and more are preferable (Curry and Liu 1992), 10 nm is more practical for instrument development. Greater distances may be achievable at a later time.

Aircraft Condition:

Because icing potential includes the aircraft, the condition of the aircraft must be considered when analyzing icing potential. This is distinct from icing forecasting where the intensity of icing forecast must be independent of aircraft type (Air Weather Service 1980). The aircraft influences the amount, type and shape of ice that forms on its surfaces, and the location of ice formation (Hansman 1989). These factors are controlled by the aircraft's design, skin temperature, deicing and anti-icing equipment, and its flight attitude such as speed, angle of attack and configuration. Also, the amount of ice residing on critical airfoil surfaces, and thus aerodynamics, perhaps as expressed by engine torque, are considerations. All of these factors must be analyzed with the weather conditions to determine whether an aircraft has the ability to penetrate a region of icing potential.

Pilot Interface:

Pilots should be advised by a visual display or audible signal that allows rapid and positive response. Only useful advisory information should be provided to the pilot, not raw liquid water content or drop-size distributions. The pilot needs to know how to change course to avoid or minimize icing, and what the potential impact of action, or no action, is on aerodynamics. Overall, the system should decrease pilot workload, and preserve airworthiness.

Ideally, an icing avoidance system should be integrated with wind shear and thunderstorm weather avoidance avionics. This would reduce space, cost, weight, maintenance, and ultimately reduce pilot workload by requiring attention to be paid to only one display for multiple warning modes. The ultimate goal may be a system that, at the pilot's discretion, flies the aircraft around icing without pilot intervention. Thus, it could be an intelligent autopilot and perform similarly to UAV guidance systems.

CANDIDATE TECHNOLOGIES:

One technology is unlikely to sense all of the variables necessary to determine icing potential ahead of an aircraft. Fusion of several technologies may be necessary. Westwater and Kropfli (1989) review several methods of remotely sensing icing conditions.

Ideal characteristics of sensors for an icing avoidance system include capabilities to measure atmospheric liquid water content, drop size spectra, temperature, and to make measurements at a high scan rate, high resolution and long range. Also, it may be necessary to discriminate ice from liquid particles. Potential technologies include radar, lidar, radiometers and radio acoustic sounding (RASS).

Radar:

The most promising radar technologies are in the short, microwave wavelengths most capable of detecting cloud droplets and precipitation. Liao and Sassen (1994) demonstrate the capability of using K_a -band radar for determining liquid water in clouds.

Martner et al. (1991) demonstrated the use of a dual X(3.2 cm)– K_a (0.87 cm) band radar system to measure cloud liquid water contents in WISP91. They were able to range-resolve liquid water contents from 0.2–0.6 g m⁻³ to a distance of about 15 km.

Sand and Kropfli (1991) have patented an airborne system consisting of a dual X-band and K_a -band scanning radar for remote detection of atmospheric liquid water to 50 km. X-band and K_a -band radar signals exhibit different attenuation characteristics in volumes of atmospheric liquid water and similar characteristics when transmitted through a volume of ice crystals. Comparison of backscatter from the two radar bands results in a determination of the likelihood of liquid water. The system has not yet flown nor has it been constructed as an integrated prototype.

Fournier (1993) also proposes a dual X– K_a -band radar as a terminal aviation weather sensing system to estimate cloud parameters at distances from 20 to 30 km. He indicates that the radar would be capable of estimating, through differential attenuation, cloud type, visibility, wind fields, median drop diameters, ice versus liquid water content and light and moderate precipitation.

Kropfli et al. (1995) use 8-mm wavelength doppler radar to measure liquid water in marine stratus clouds. They also state that 8-mm radar has advantages over shorter wavelength radar, or lidar, because it can penetrate optically thick clouds, high liquid water content areas and light precipitation. It is compromised by heavy precipitation.

Lhermitte (1987, 1988) has experimented with the shortest wavelength radar useful for cloud measurements, 3.2 mm W-band. He proposes that the use of three doppler radar bands, W, K_a and X, could jointly provide the size distribution of raindrops. It is not clear whether drop sizes as small as 400 μm could be characterized, however.

Lidar:

Lidar has promise, but also has several potential liabilities. Eberhard (1993) demonstrated analytically that cloud drop radius can be measured with a 10.6 μm wavelength CO₂ laser.

Hutt et al. (1994, Bissonnette and Hutt 1995) have used the backscattered power from a 1.06 μm pulsed multiple field of view (MFOV) lidar to characterize cloud, fog, and aerosols. The system measures the backscatter from a central beam, and multiscattered return signal intensity at three or more coaxial fields of view. These measurements are fit to a multiple scattering lidar equation, which provides a scattering coefficient and a droplet effective radius. From this, and an assumed gamma drop size distribution, liquid water content and extinction coefficients are computed. Cloud parameters such as range-resolved droplet size distribution (1–25 μm), liquid water content and extinction coefficients have been made at ranges to 1000 m.

Lidar has several problems, however. For MFOV lidar, cloud extinction coefficients must be large enough to provide a multiscattered return signal, yet not so large as to prevent penetration into the cloud. All lidars are compromised by large extinction coefficients in dense clouds where moderate-to-heavy icing conditions may occur. Also, certain laser wavelengths, such as 1.06 μm , are not eye-safe. However, at eye-safe wavelengths the MFOV feature is less efficient.

Radiometers:

Considerable work has been done with microwave radiometers measuring temperature profiles and liquid water content. Kropfli et al. (1995) argue that droplet characteristic size and drop concentration can be determined with microwave radiometers. Fotino et al. (1986) used integrated liquid water measurements from 20.6 and 31.65 GHz, and temperature profiles measured from four frequencies from 52.85 to 58.80 GHz, to estimate icing conditions (Hogg et al. 1983). The radiometers were ground-based, viewing vertically through the atmosphere. Radiometer-estimated icing conditions were successfully compared to icing pilot reports.

Others have also applied radiometer measurements to aircraft icing problems including Gary (1983), Curry and Liu (1992), Lef et al. (1994) and Lawyer (1995). Except for Hogg et al. (1983), nearly all radiometer work has involved vertical soundings of liquid water and temperature. Horizontal, or nearly so, microwave soundings of liquid water may provide useful integrated values. Though the distance over which the integration occurs is unknown, horizontal measurements may indicate whether flight on a given heading is practical. Horizontal measurements of temperature may also be integrated, unlike vertical radiometer temperature soundings that are height discriminated by optical thickness and frequency (Elachi 1987). Some theory does suggest, however, that horizontal passive

microwave measurements of temperature and liquid water may be discriminated by distance.

Among satellite radiometer methods that may be applicable to aircraft is MODIS (Moderate Resolution Imaging Spectrometer), to be launched on EOS (King et al. 1992). MODIS utilizes radiometers operating in 36 channels from 0.659 to 14.235 μm . Among the variables that may be obtained are droplet-effective radius to about 25 to 35 μm over spatial resolutions of 250 to 1000 m. Tests of the instrument were made from a NASA aircraft.

Radio Acoustic Sounding:

RASS may also possibly measure temperature from an aircraft. RASS has been used successfully to obtain vertical temperature profiles from the surface to 9 km and even to the stratosphere, and can be extremely accurate (May et al. 1988, May et al. 1989, Matuura et al. 1986). However, it has not apparently been tested from a moving platform and is sensitive to wind speed.

There is no integrated system currently capable of satisfactorily sensing icing potential from an aircraft, though elements of such a system exist. A compact, lightweight, low-power and economical system is needed. Detection of liquid water vs. frozen water is possible with varying precision from radar, lidar and radiometers, and may be necessary depending upon the technology used. More difficult is the problem of determining if liquid water is supercooled. There does not appear to be an instrument capable of providing range-gated temperatures of atmospheric volumes.

EFFECTS OF ON-BOARD ICING AVOIDANCE ON AVIATION:

Onboard icing avoidance will both enhance operation of the national airspace system, and cause complications. It also may change procedures for certification of aircraft for flight in known or forecasted icing.

The capability of detecting and escaping icing may allow aircraft to fly in icing weather not currently considered safe or legal for flight. For example, icing often occurs in only a portion of areas forecasted for icing due to the coarseness of forecasts. As a result, an aircraft certified for light icing may be allowed to fly in an area forecasted for light-to-moderate icing if the moderate icing is expected to cover limited areas and can be avoided. Such an ability would allow reduced departure and arrival delays, reduced airport congestion as a result of reduced delays, and overall better on-time performance for operators. Operational costs of shutdowns or flight cancellations due to icing may also be reduced (AHS 1995).

However, to be most effective, aircraft should have the ability to change heading and altitude without permission from air traffic control. In some icing conditions changes of altitude may be more effective than changes in heading. This complicates separation, especially in congested terminal areas. This is less of a problem for helicopters on search and rescue or serving offshore facilities in low traffic density regions.

Procedures for certifying aircraft may also be changed if they are equipped with icing avoidance systems. Equipped aircraft may be certified to fly in conditions now considered illegal, pending further research into the spatial patterns of icing and thus the probability of avoidance or escape.

CONCLUSIONS:

Future research will facilitate and manage development of a prototype instrument through the Department of Defense SBIR program. Thus, it will foster development of a product that will sense icing potential ahead of an aircraft and provide meaningful guidance to pilots. This development, if fundable proposals are received, should begin in 1997. The intent is for the developer to produce a marketable product.

Other research should occur concurrently with instrument development. The spatial patterns of icing on sub-kilometer to tens-of-kilometers scale and its relationship to synoptic and mesoscale weather is poorly understood. The ability to avoid icing is a function of its spatial distribution. Large cloud masses that are homogeneous with respect to icing are difficult to avoid. Such research may specify the synoptic weather conditions within which onboard icing avoidance may be most effective.

Icing avoidance system signals need to be integrated with ice accretion and aerodynamics models and onboard ice detectors to predict iced-aircraft performance. Iced aircraft performance may be the most desirable information to provide pilots because it predicts effects upon airworthiness if the aircraft is allowed to ice. Such models would be run onboard using explicit liquid water content, drop size spectra and temperature information extracted from the sensors in addition to aircraft performance information. Onboard icing models similar to NASA's LEWICE would require modification for specific aircraft. This could evolve into an intelligent interface advising pilots how to change aircraft configuration and performance if icing cannot be avoided.

Finally, methods of detecting temperature with range do not appear as well developed as techniques for measuring liquid water. More research is needed in this area.

Though in-flight icing avoidance would improve flight safety, it is not the ultimate solution to the airframe icing problem. It does not improve the ability of an aircraft to fly within icing, nor does it improve airworthiness of ice-covered aircraft. It does, however, provide opportunities to fly because of the current quality of icing forecasts and the ephemeral spatial and temporal nature of ice. Thus, icing avoidance is a stopgap. The ideal solution is to develop aircraft that are totally unaffected by icing, and have the same freedom to fly within ice as within clear, dry air.

REFERENCES:

- AFGL, 1985, *Handbook of Geophysics and the Space Environment*. Air Force Geophysics Laboratory, Hanscom AFB, MA.
- AHS, 1995, *Tape transcription of International Icing Symposium '95 Workshop*, American Helicopter Society, Montreal.
- Air Weather Service, 1980, *Forecaster's Guide to Aircraft Icing*. AWS/TR-80/001. Scott AFB, IL.
- Anon, 1995, "Army Approves Requirements Document for Unmanned Tactical Vehicles." *Inside the Army*, Nov. 20, p. 6.
- AVEMCO, 1983, "ICE: As Unwelcome a Sight There Is." *AVEMCO Pilot Bulletin*, Flying Safety Update No. 60.
- Benjamin, S., G. Grell, K. Brundage, T. Smith, J. Brown, T. Smirnova and Z. Yang, 1995, "The Next Version of the Rapid Update Cycle—RUC II." In *Proceedings of the Sixth Conference on Aviation Weather Systems*, American Meteorological Society, Dallas, TX, pp. 57–61.
- Bertorelli, P., 1992, "Icing: Assessing the Risk." *IFR*, November, pp. 6–9.

- Bissonnette, L. and D. Hutt, 1995, "Lidar Remote Sensing of Cloud and Fog Properties." *European Symposium on Optics for Environmental and Public Safety*, Munich, June 19–23 1995, Proceedings # 2506, paper # 62.
- Brown, B., R. Bullock, G. Thompson and R. Bruintjes, 1995, "WISP94 Real-Time Icing Prediction and Evaluation Program (WRIPEP): Statistical Issues and Forecast Evaluation Results." In *Sixth Conference on Aviation Weather Systems*, American Meteorological Society, Dallas, pp. 207–212.
- Coffey, R., 1995, "Big Fat Drops of Ice." *IFR*, October, pp. 6–8.
- Coffey, R., 1996, "Neural Net Icing Forecasts." *IFR*, February, pp. 6–9.
- Cooper, W., M. Politovich and W. Sand, 1982, *Nature of Icing Conditions Encountered During Meteorological Research*. Unpublished contract report, Martin, Pringle, Oliver, Triplett and Wallace, Wichita, Kansas.
- Cornell, D., C. Donahue and C. Keith, 1995, *A Comparison of Aircraft Icing Forecast Models*. U.S. Air Force Combat Climatology Center, Scott AFB, IL, AFCCC/TN-95/004, 33 p.
- Curry, J. and G. Liu, 1992, Assessment of Aircraft Icing Potential Using Satellite Data, *Journal of Applied Meteorology*, Vol. 31, pp. 605–621.
- Eberhard, W., 1993, "CO₂ Lidar Technique for Observing Characteristic Drop Size in Water Clouds." *IEEE Transactions on Geoscience and Remote Sensing*, Vol. 31, pp. 56–63.
- Elachi, C., 1987, *Introduction to the Physics and Techniques of Remote Sensing*. John Wiley & Sons, New York, 413 p.
- Engelberg, S. and A. Bryant, 1995, "Lost Chances in Making a Commuter Plane Safer." *New York Times*, 26 February, pp. 1, 24–25.
- Fotino, P., J. Schroeder and M. Decker, 1986, "Ground-Based Detection of Aircraft Icing Conditions Using Microwave Radiometers." *IEEE Transactions in Geoscience and Remote Sensing*, Vol. GE-24, pp. 975–982.
- Fournier, G., 1993, "Transport Canada Proposed R&D Program for the Development of a Multi-Parameter Dual X-K_a Band Doppler Radar for Aviation Meteorology Applications." In *Proceedings of the Fifth International Conference on Aviation Weather Systems*, American Meteorological Society, Vienna, VA, pp. 146–147.
- Gary, B., 1983, *Microwave Monitoring of Aviation Icing Clouds*. Report AFGL-TR-83-0271, Air Force Geophysics Laboratory, Hanscom Field, MA, 22 p.
- Green, S., 1995, personal communication, Burlington, VT.
- Hansman, J. Jr., 1989 "The Influence of Ice Accretion Physics on the Forecasting of Aircraft Icing Conditions." In *Third International Conference on the Aviation Weather System*, American Meteorological Society, Anaheim, CA, pp. 154–158.
- Hogg, D., F. Guiraud, J. Snider, M. Decker and E. Westwater, 1983, "A Steerable Dual-Channel Microwave Radiometer for Measurement of Water Vapor and Liquid in the Troposphere." *Journal of Climate and Applied Meteorology*, Vol. 22, pp. 789–806.
- Hutt, D., L. Bissonnette and L. Durand, 1994, "Multiple Field of View Lidar Returns from Atmospheric Aerosols." *Applied Optics*, Vol. 33, no. 12, pp. 2338–2348.
- Jeck, R., 1994, *Other Ways to Characterize the Icing Atmosphere*. Presented at the American Institute of Aeronautics and Astronautics, 32nd Aerospace Sciences Meeting, Reno, NV, 6 p.
- King, M., Y. Kaufman, W. Meinel and D. Tanre, 1992, "Remote Sensing of Cloud, Aerosol, and Water Vapor Properties from the Moderate Resolution Imaging Spectrometer (MODIS)." *IEEE Transactions on Geoscience and Remote Sensing*, Vol. 30, pp. 2–27.
- Knapp, D., 1992, *Verification Report: Comparison of Various Icing Analysis and Forecast Techniques*. Internal report, AFGWC/DOA, 10 p.
- Knapp, D., 1996, personal communication, White Sands, NM.

- Kropfli, R., S. Matrosov, T. Uttal, B. Orr, A. Frisch, K. Clark, B. Bartram, R. Reinking, J. Snider and B. Martner, 1995, "Cloud Physics Studies with 8-mm Wavelength Radar." *Atmospheric Research*, Vol. 35, pp. 299-313.
- Lawyer, D., 1995, *Exploratory Study of an Icing Index from Satellite Remote Sensing of Cloud Liquid Water Over Land*. Colorado State University Masters Thesis, 111 p.
- Lef, T., J. Clark and S. Swadley, 1994, "Potential Applications of the SSM/I Cloud Liquid Water Parameter to the Estimation of Marine Aircraft Icing." *Weather and Forecasting*, Vol. 9, pp. 173-182.
- Lhermitte, R., 1987, "A 94-GHz Doppler Radar for Cloud Observations." *Journal of Atmospheric and Oceanic Technology*, Vol. 4, pp. 36-48.
- Lhermitte, R., 1988, "Observation of Rain at Vertical Incidence with a 94-GHz Doppler Radar: An Insight on Mie Scattering." *Geophysical Research Letters*, Vol. 15, pp. 1125-1128.
- Liao, L. and K. Sassen, 1994, "Investigation of Relationships Between Ka-Band Radar Reflectivity and Ice and Liquid Water Contents." *Atmospheric Research*, Vol. 34, pp. 231-248.
- Manningham, D., 1991, "Rime and Reason." *Business and Commercial Aviation*, pp. 82-85.
- Martner, B., R. Kropfli, L. Ash and J. Snider, 1991, *Progress Report on Analysis of Differential Attenuation Radar Obtained During WISP-91*. NOAA Technical Memorandum ERL WPL-215, 43 p.
- Matuura, N., Y. Masuda, H. Inuki, S. Kato, S. Fukao, T. Sato and T. Tsuda, 1986, "Radio Acoustic Measurement of Temperature Profile in the Troposphere and Stratosphere." *Nature*, Vol. 323, pp. 426-428.
- May, P., K. Moran and R. Strauch, 1989, "The Accuracy of RASS Temperature Measurements." *Journal of Applied Meteorology*, Vol. 28, pp. 1329-1335.
- May, P., R. Strauch and K. Moran, 1988, "The Altitude Coverage of Temperature Measurements Using RASS With Wind Profiler Radars." *Geophysical Research Letters*, Vol. 15, pp. 1381-1384.
- Mayer, P., R. Jeck and P. Drake, 1984, *An Analysis of Icing-Related Mishaps on U.S. Navy Aircraft from 1964 to 1984*. Navy Research Lab Memorandum Report 5418, 13 p.
- Politovich, M., 1989, "Aircraft Icing Caused by Large Supercooled Droplets." *Journal of Applied Meteorology*, Vol. 28, pp. 856-868.
- Ryerson, C., N. Yankielun, and J. Clark, 1995, *Remote Sensing Aircraft Icing Sensor - An Assessment*. unpublished CRREL In-House Laboratory Independent Research report, 2 p.
- Sand, W. and Kropfli, R., 1991, Icing Hazard Detection for Aircraft, United States Patent 5,028,929, July 2, 1991.
- Siquig, R., 1993, *Weather and Unmanned Aerial Vehicles*. Naval Research Laboratory report NRL/MR/75432-93-7206, 77 p.
- Taylor, R., 1986, *Aviation Weather*. Belvoir Publications, Inc., Greenwich, CT, 240 p.
- Thompson, G., R. Brintjes and B. Brown, 1995, "A Comprehensive Icing Prediction and Evaluation Program." In *Sixth Conference on Aviation Weather Systems*, American Meteorological Society, Dallas, pp. 243-248.
- Westwater, E. and R. Kropfli, 1989, *Remote Sensing Techniques of the Wave Propagation Laboratory for the Measurement of Supercooled Liquid Water: Applications to Aircraft Icing*. NOAA Technical Memorandum ERL WPL-163. NOAA Environmental Research Laboratories, 28 p.
- Willis, P. and P. Tattelman, 1989, "Drop-Size Distributions Associated with Intense Rainfall." *Journal of Applied Meteorology*, Vol. 28, pp. 3-15.
- Wright, W., 1995, "Capabilities of LEWICE 1.6 and Comparison with Experimental Data." In *Proceedings, International Icing Symposium '95, American Helicopter Society*, Montreal, pp. 349-361.

APPLICATION OF NEW ELECTROTHERMAL SYSTEMS ON AIRCRAFT FOR EXTENDED ICE PROTECTION

BY

**PORTER J. PERKINS
CONSULTANT, AIRCRAFT ICING
ROCKY RIVER, OHIO**

**G. P. BUZZ LYNCH
PROGRAMS MANAGER
AEROSPACE SAFETY TECHNOLOGIES, INC.
MINDEN, NV**

FOR

**PRESENTATION AT FAA INTERNATIONAL
CONFERENCE ON AIRCRAFT INFLIGHT ICING
MAY 6 - 8, 1996**

Abstract

Icing wind tunnel testing has demonstrated that added ice protection needed for particular icing conditions is easily achieved by installing a new lightweight electrothermal system on critical surfaces where ice is not effectively removed by existing pneumatic boots, or other leading edge ice protection systems.

This paper describes a complete supplemental system as installed on an aircraft surface. This includes application of the heater laminate to the surface, power sequencing concepts, over-

temperature controls, and other safety features.

Several features of this new electrothermal ice protection system provide a much superior aircraft installation than previous electrothermal systems. Compared to all other designs used in the past, this new technology has the advantages of:

1. A much lighter installed weight;
2. Aerodynamic surfaces unaffected by installation on the surface;
3. Heater component close to the outer surface providing rapid

temperature rise to the icing surface;

4. Uniform distribution of heat over the applied surface;
5. Lower electrical power required for anti-icing or de-icing because of uniform heat distribution near the protected surface;
6. Easily applied retro-fit to aircraft with existing leading edge protection;
7. Safe operation if localized damage occurs - does not affect overall operation of the electrothermal panels.

Introduction

New technology has been needed in the field of aircraft ice protection to achieve safe flight without the penalties of excessive weight and energy requirements. Recent advances in airfoil designs now being used on turboprop aircraft (laminar flow, high wing loading, thin cross-sections, and small leading edge radii), have created airfoils more sensitive to ice contamination than earlier designs. Hot gas available from jet powered aircraft essentially solved the icing problem over forty years ago for that type of aircraft, but this technique is not practical for modern turboprops where sufficient jet bleed air required for ice protection is not economically available. Thus, these type aircraft have had to rely on long standing pneumatic boots that proved adequate for older airfoils.

This paper describes the design, testing and aircraft installation of a new electrothermal conductive

matrix laminate only .012-inch thick applied in a new role for electrothermal ice protection. Recent in-flight icing incidents involving turboprop aircraft with advanced airfoil designs have created a need for this unique design of ice protection. Investigations into these incidents have determined that ice accretions forming aft of the protection limits of the pneumatic boots have seriously deteriorated the aerodynamic performance of the airfoils and associated control surfaces. Thus, a very immediate application exists for this new technology ice protection. It is applied beyond the chordwise limit of the existing pneumatic boots as supplemental ice protection.










Ice accretions beyond the pneumatic boots occurs both on the wing and on the horizontal stabilizer during an encounter having droplet sizes that exceed the normal impingement protected range (freezing drizzle) and/or an encounter near freezing. At temperatures close to freezing, droplets striking around the leading edge do not freeze because of kinetic heating of the surface. However, the surface temperature decreases back from the leading edge and will go below freezing causing ice to form from liquid runback. This ice formation can grow rapidly creating a ridge of ice from the runback and can further grow from direct droplet impingement. Such an ice ridge can cause airflow separation stalling the airfoil at an angle of attack less than the normal stall

or ribbons reduce the effectiveness of the heat energy applied to the surface. Also, damage to the individual wires or ribbons eliminates heat to the damaged area and cannot be easily repaired.

Conductive Matrix Laminate

This new technology uses a matrix of a large number of very small conductive fibers embedded in a thin and flexible sheet. Electrical conductivity is provided by nickel-coated carbon fibers which provide heat when a voltage is applied. This commercially available matrix was originally developed for use as a shielding material against Radio Magnetic Interference (RMI) and Electro Magnetic Interference (EMI) for security sensitive U. S. government facilities.

Application of the conductive matrix material to a surface to be heated requires a laminate (Figure 1 below)

	PAINTE
	FINAL PRIMER
	VINYL ESTER RESIN
	"E" GLASS LAMINATE
	NO-ICE™ LAYER(S)
	"E" GLASS LAMINATE
	VINYL ESTER RESIN
	MIL SPEC EPOXY PRIMER
	AIRCRAFT SURFACE

consisting of: preparing the surface, followed by a coat of vinyl ester resin (.001" thick), a layer of "E" glass laminate (.004" thick), then the conductive material (.002" thick), and finally outer protection material and finish paint. This entire "heater blanket" shown in figure 1 is only .012"-.015" thick. Also embedded on the "E" glass are the foil type electrical connectors. One pound of the installed No-IceTM heater laminate will cover 500 square feet of surface to be heated. Thus, application on an airfoil surface results in practically no weight penalty but with a highly efficient heated surface. Because of the very large numbers of conductive fibers, local damage does not render other sections of the heated area ineffective as would be the case if a wire were broken in a conventional heater. In fact, the local temperature becomes slightly warmer in the area of the damage.

Because of the very thin nature of the installed heater blanket, aerodynamic surfaces are essentially unaffected. Efficient airfoils (e. g. designs for laminar flow including laminar flow control) can be covered with this electrothermal ice protection without compromising the design performance.

A Practical Solution For Protection From Freezing Drizzle

Ice formations caused by the impingement of large droplets (freezing drizzle) and/or runback formations aft of the normally ice

protected surfaces have resulted in serious aircraft performance losses. Recognition of this problem has imposed operational restrictions when the condition is known by the flight crew. A more practical solution to the problem, however, is to prevent the adverse ice accretion from forming. This can be accomplished by applying an easily installed electrothermal ice protection system as a retrofit to aircraft with existing leading-edge ice protection systems. Thus, the concept of using the electrothermal conductive matrix laminate as supplemental ice protection behind the pneumatic boots has been designed and tested. Such a concept can be described as a hybrid ice protection system.

Ice Tunnel Test Description

For convenience and expediency, when tests were conducted in the NASA-Lewis Icing Research Tunnel, an existing full scale (78 inch chord) airfoil previously tested in the tunnel for other purposes was used (Figure 2). A conventional pneumatic deicing boot was installed on the leading edge. It extended to 10 percent chord on both sides, however, the active part of the boot extended to only 7 percent chord. To prevent ice from forming in this unprotected area (from 7 to 10 percent chord), the conductive matrix heater was installed under the boot at this location and extended aft to about 30 percent of the chord. With the objective to obtain design data for this

A Hybrid Pneumatic-Electrothermal System

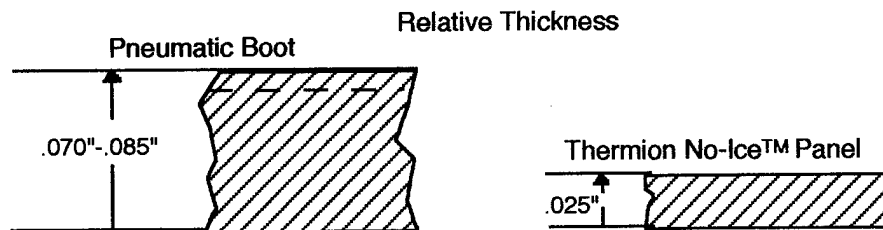
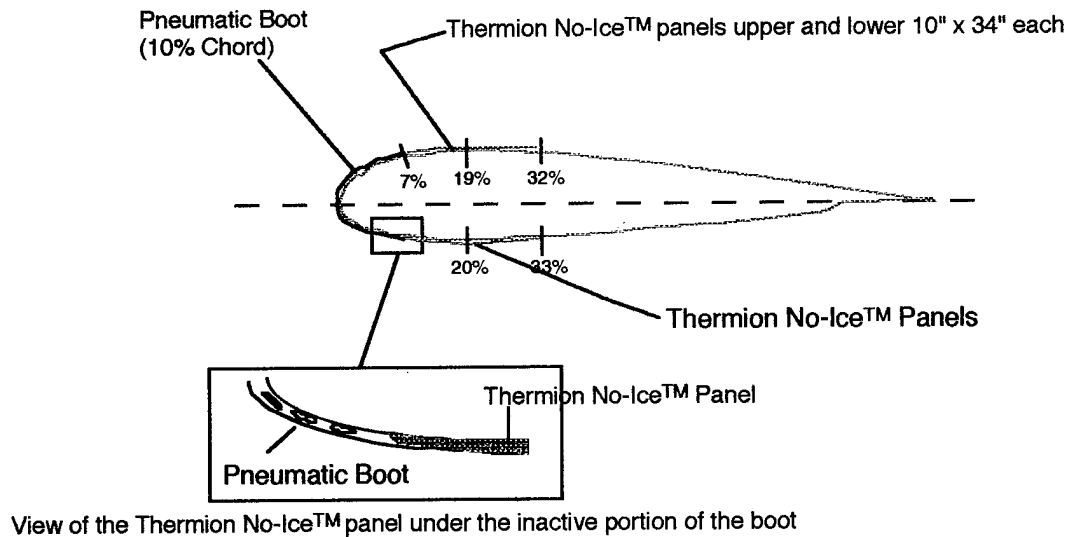


Figure 2

supplemental ice protection concept, but not necessarily for a specific aircraft installation, the conductive matrix laminate was installed in two separate heater panels on both the top and bottom surfaces. This provided independent control of the power in two sections in the chordwise direction on both surfaces. A sketch of the pneumatic boot and the electrothermal panels mounted on the surfaces of the wing is shown in Figure 3. The primary objective of the tunnel tests was to determine the minimum electrical power densities (watts per square

inch) required for the two modes of ice protection, deicing and anti-icing. In the anti-icing mode, both the "running wet" and the evaporative modes were evaluated.

Instrumentation

Power to each of the heater panels was controlled by a variable voltage 110 volt AC power transformer. Power density in watts per square inch was determined by measuring volts and amperage. Ice accretion removal (deicing) or prevention (anti-icing) was observed and recorded by several

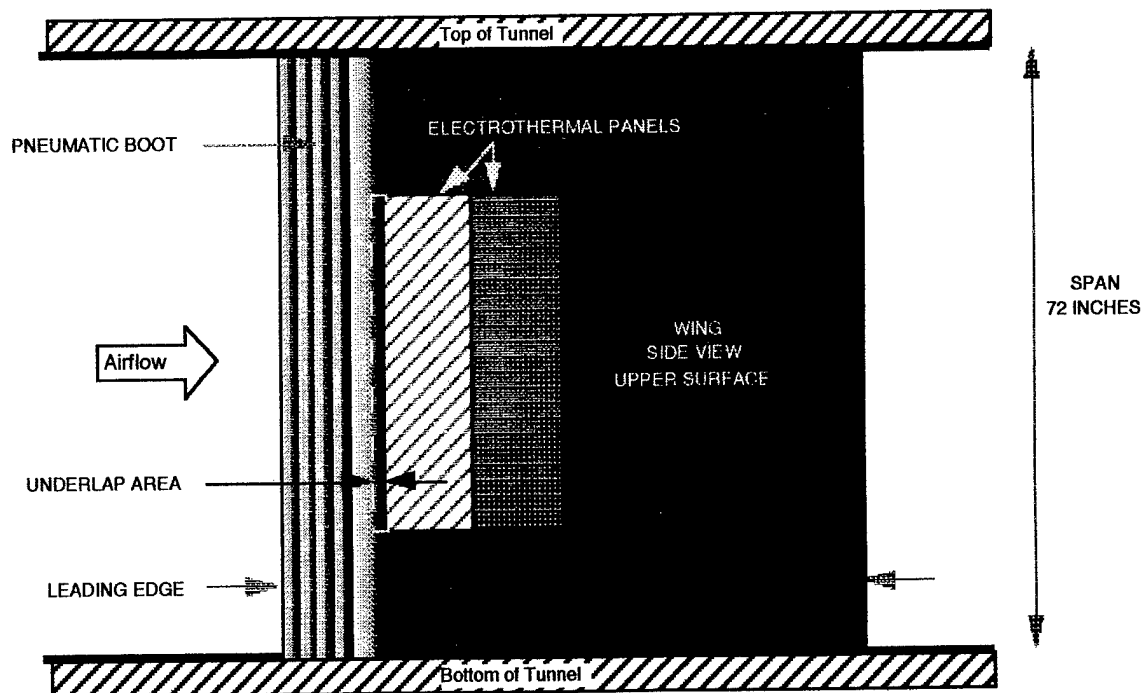


Figure 3

video cameras with time notations for reference. Surface temperatures on the airfoil were remotely measured by an infrared camera.

Wind tunnel airflow parameters that were recorded included airspeed measured in the test section and total air temperature measured upstream of the test section in the low velocity area ahead of the contraction section. Static air temperature (SAT) was calculated by assuming an adiabatic expansion of the air as it accelerates through the contraction.

Icing of the wing was produced by a water spray system of air atomizing nozzles located upstream in the low velocity section of the tunnel. Previous calibrations of the spray

cloud were used to set water droplet sizes and water content based on measured water and air pressure at the nozzles. All tests were run at 190 microns diameter (MVD) droplet size and 0.6 grams per cubic meter liquid water content.

Test Results and Discussion

Both the deicing and anti-icing capabilities of the supplemental ice protection design (hybrid electrothermal and pneumatic) were evaluated during over 70 test runs. Power densities required for quick ice shedding (deicing) and for preventing ice forming (anti-icing) at various air temperatures were the primary variables during the testing.

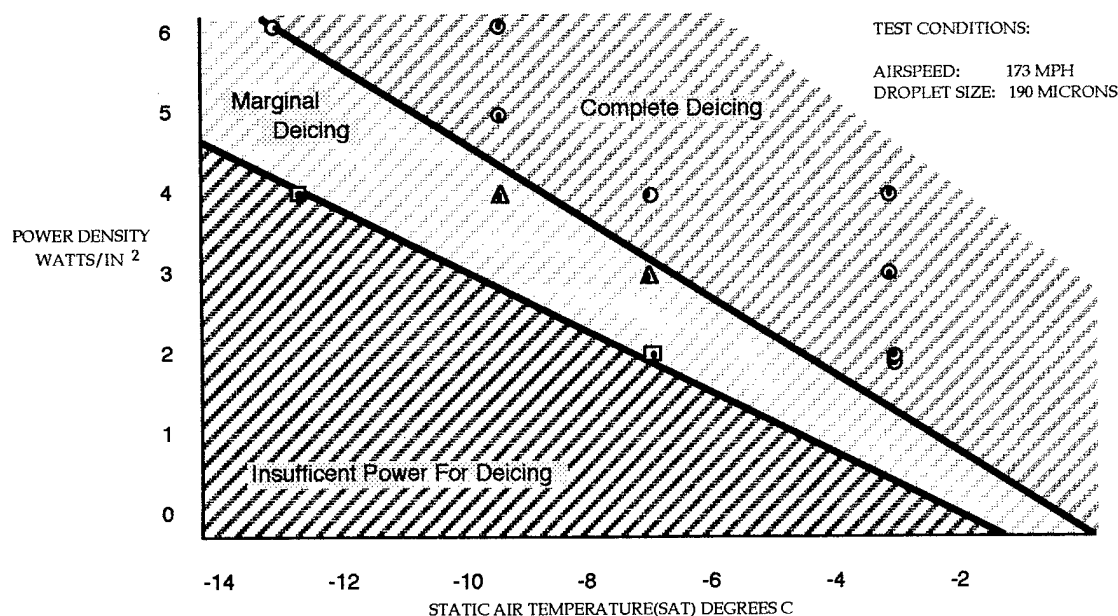


Figure 4

Results of deicing by the electrothermal panels under and aft of the pneumatic boots are shown in Figure 4 where power densities for deicing are plotted against the static air temperature (SAT) in the tunnel. Airspeed was held at 173 MPH which gave a total air temperature rise of 5.4° above the SAT. Deicing of the ridge of ice formed by runback and impingement aft of the boots was successful at static temperatures of 28° F. (-3.3° C), 19° F. (-7.2° C), 15° F. (-9.4° C), and 9° F. (-12.8° C). It is particularly interesting to note that at a SAT of -3° C deicing was accomplished in about one half minute at a power density to the heater of 2 watts per square inch. This included clearing the ice from the area of the inactive portion of the boot. As the power density was increased up to 4 watts per square inch, the time to deice decreased. At a SAT of -7° C, 4 watts per

square inch deiced the surface completely in about one minute or less. At 3 watts per square inch the deicing was somewhat marginal leaving small areas with residual ice. However, this is a common occurrence for pneumatic boots. At a SAT of -9.4° C. it required 5 watts per square inch for complete deicing and 4 watts per square was marginal. A power density of 6 watts per square inch deiced the heated area at a SAT of almost -13° C. (9° F). It was interesting to note that at temperatures near freezing (-3° C) where most of the runback and large droplet icing occurs in natural icing, less than 2 watts per square inch cleared the electrothermal protected area. A unique feature of the testing was the remote measurement of wing surface temperatures using an AGEMA infrared camera. Images during the heater activation showed a very uniform surface

temperature distribution over the heated area (a variation of less than 2° C.). Also, of significance was the rapid temperature rise when deice power was applied. This fast increase in surface temperature uniformly distributed, produces quick deicing with practically no amount of runback from the melting ice.

A graph illustrating the operation of the heater during a deicing cycle is shown in Figure 5.

Displayed on this graph, (1) the maximum temperature in the heated area of the upstream panel, (2) the local (spot) temperature on the center of the upstream panel, (3) the local temperature on the overlap of the panel and the boot,

and (4) the local temperature in the center of the boot. Note that the heat was on for about one minute (17.392 to 17.450 seconds on the timeline). At the start, the surface temperature rose about 50° in 20 seconds which provided the quick deicing.

Results of operating the electrothermal section in the continuous heating (anti-icing) mode disclosed that very little power is required to keep ice from forming but without completely evaporating impinging water (running wet). At the -3° C. SAT only 0.75 watts per square inch were required. At the -13° C. SAT only 4.0 watts per square inch provided an ice free surface.

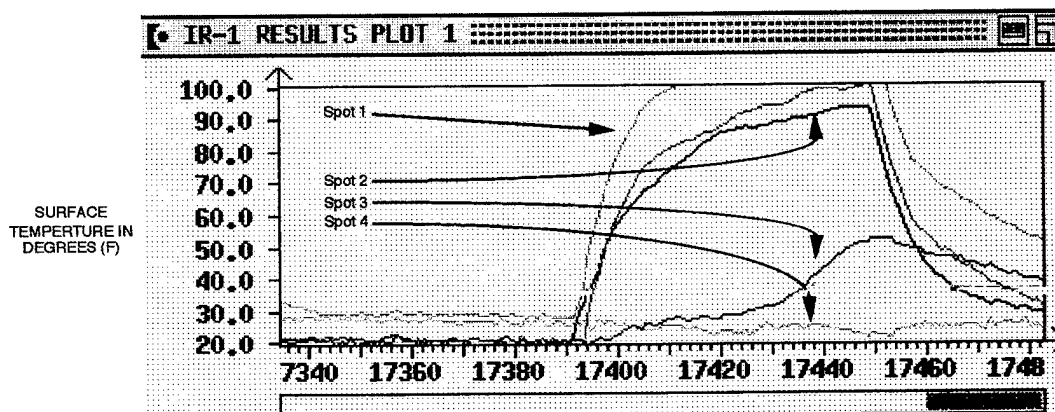


Figure 5

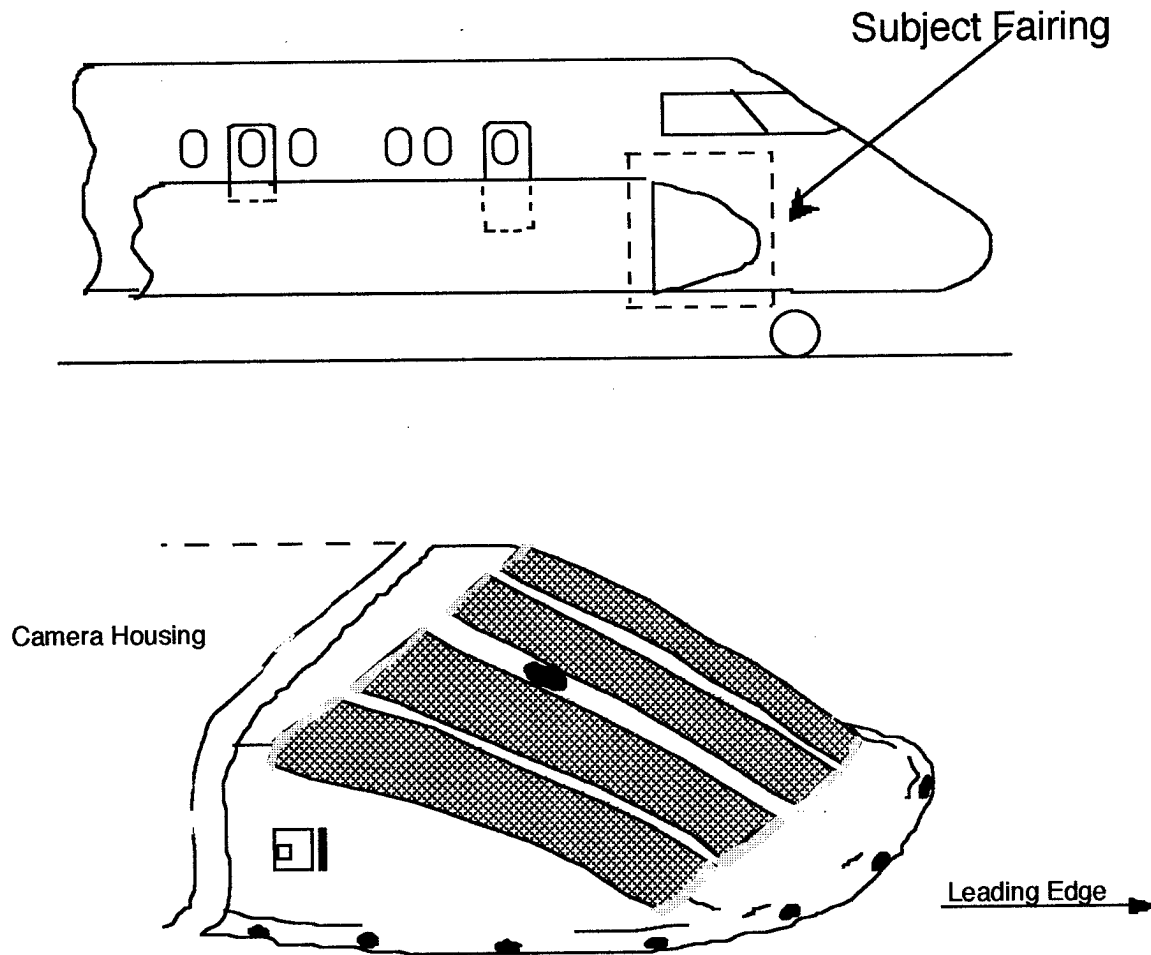


Figure 6

Installation on Aircraft

A recent application of No-Ice™ for ice protection on a USAF E-9 aircraft external pod fairing is shown on Figure 6. The system consists of : (1) the heater panels configured to cover the appropriate area to be deiced and designed for a power density adequate for the anti-ice or de-ice task; (2) temperature sensors and relays to monitor and protect the system; and, (3) a controller unit that sequences the panels if necessary

and monitors the desired temperatures as well as performing fault monitoring.

Figure 7 shows a simple schematic for this control system.

The system consists of a Programmable Logic Computer (PLC), temperature sensors, fault monitoring circuits, sequence control of individual panels and over/under temperature control using thermocouples and relays.

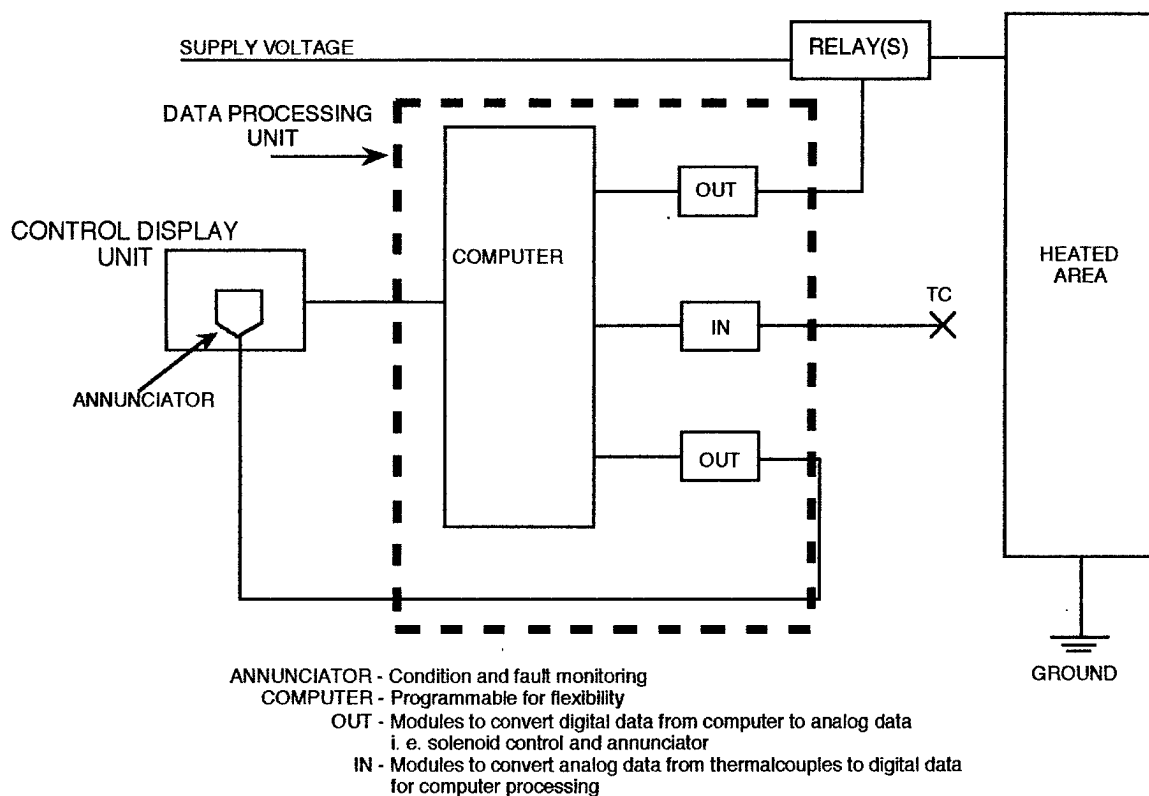


Figure 7

The PLC operation and procedures are as follows: (1) when the system is turned on the PLC will automatically perform a self test, then engage the four panel solenoids and light the annunciators, indicating power to the four panels. (2) the PLC controls power to the panels by opening and closing solenoids. Two thermocouples per panel provide temperature and fault monitoring feedback to the PLC.

The entire system works in harmony and is only "on" when needed. In this case the system operates as a sequenced anti-ice system, fully automatic but monitored by the pilot through the annunciator panel.

Comparison to Previous Electrothermal Ice Protection

Several areas of past concern with electrothermal heaters have been minimized with the new Thermion No-Ice™ system. The first area is damage tolerance. The Thermion nickel coated carbon fiber mat has thousands of strands that carry the electrical load producing heat. The fibers are not a single path that are vulnerable due to stress, vibration, or physical abuse. Rather, the fibers make up a homogeneous mat that can withstand localized damage of holes, cracks or even a major portion eliminated. Each of these situations can cause some reduction in the heat pattern but does not cause the heater to fail.

Improved areas such as lightness of weight and better aerodynamic qualities due to thinness of the laminate (.012-.015 inch) are obvious. The key to Thermion No-Ice™ power reduction is the efficient use of the heat. This is possible because of two factors. These are; uniform heating due to the homogeneous mat, and second, the closeness of the heater to the surface where the heat is required to melt the ice. In essence, neither case requires the heater mat to heat other areas of structure (or surface) while placing the heat next to the ice. Thus less power is required to do the same job of melting or preventing ice formation.

Conclusions

Ice protection behind the conventional pneumatic boots has been successfully demonstrated using a new design of a very lightweight electrothermal conductive matrix laminate. Full scale tests in the NASA Icing Research Wind Tunnel revealed fast deicing at low power densities (less than 2 watts per square inch at -3° C., and only 6 watts per square inch at -13° C.).

This new electrothermal design can be effectively applied as a practical solution for ice formations aft of the normally protected surfaces. These ice formations result from impingement of large droplets and/or water runback when the surface temperatures around the leading edge are above freezing. Such conditions have caused serious aerodynamic performance

losses particularly with airfoil designs now existing on many aircraft.

This new technology of supplemental ice protection is easily applied to aircraft with existing leading edge ice protection. Only one pound of the electrothermal laminate can cover 500 square feet of surface to be heated. With the heater element close to the surface (total thickness only .012 - .015 inch thick), a very fast surface temperature rise results and quick deicing is achieved. Application on an airfoil has no affect on the aerodynamic surfaces and results in almost no weight penalty for the aircraft. Localized damage does not affect overall operation. Durability and long cycle life have been demonstrated.

References

U. S. Patent No. 5344696,
Electrically conductive laminate for temperature control of aircraft surfaces.

Canadian Patent No. 20744787,
Electrically conductive laminate for temperature control of aircraft surfaces.

European Patent No. 0521003
Electrically conductive laminate for temperature control of aircraft surfaces.

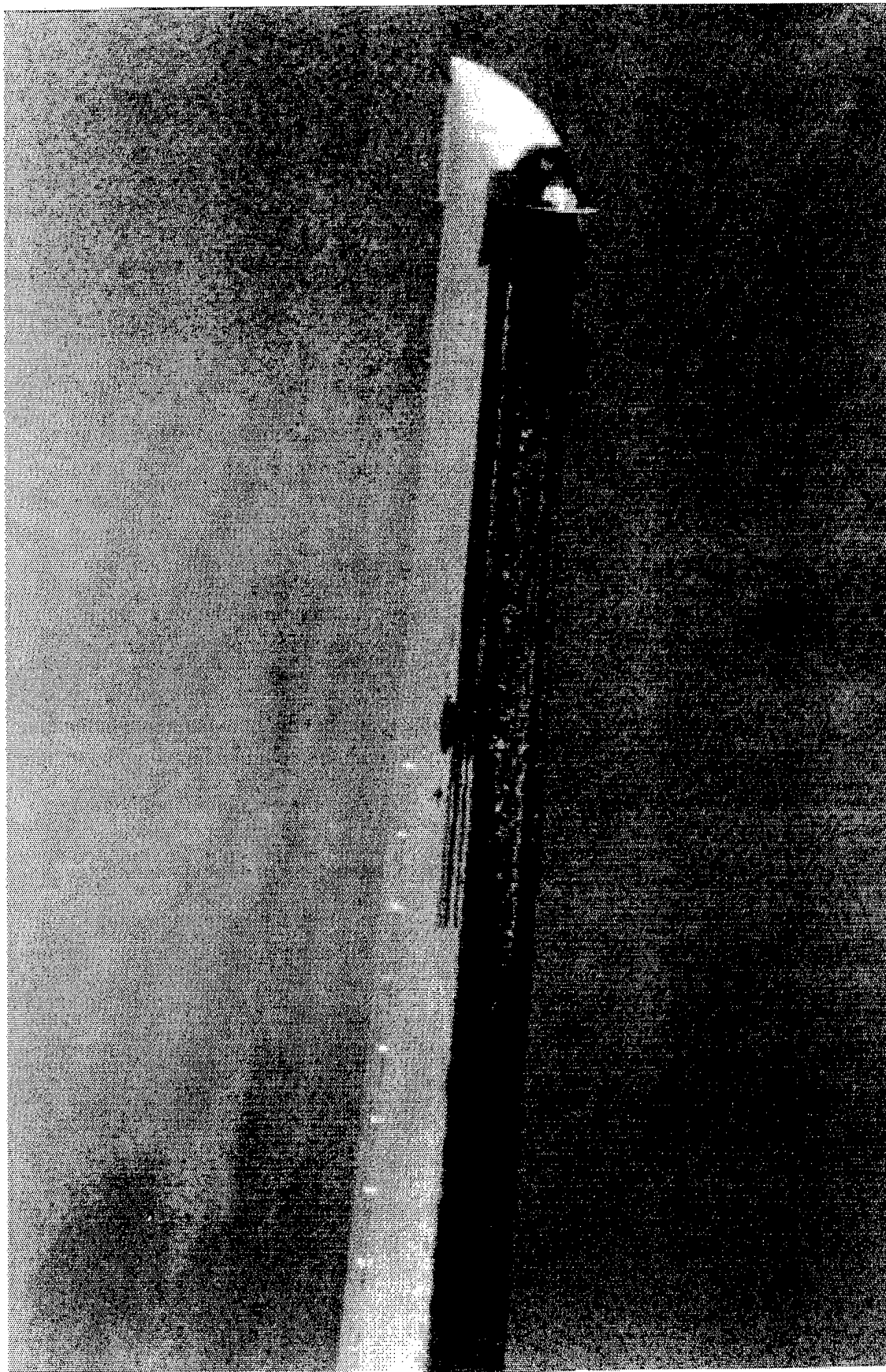


Figure 1(a)
Results of Icing at TAT of $+2.7^{\circ}\text{C}$ to $+3.7^{\circ}\text{C}$

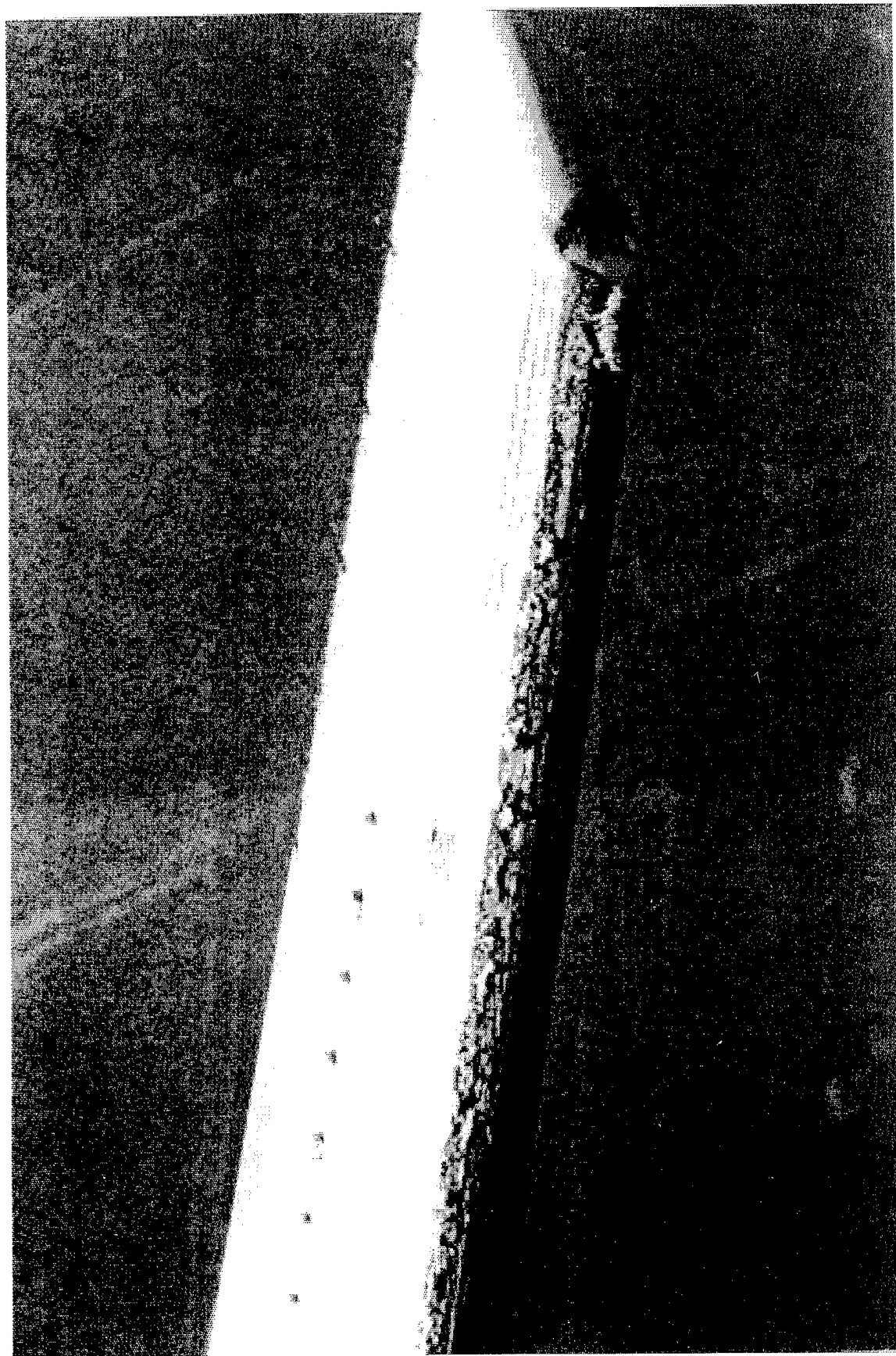


Figure 1(b)
Ice Formations After 20 Minutes Behind Tanker



Figure 1(c)
Close-up of Fig. 1(b) Ice Formation
Showing Jagged Nature of the Ice Estimated to be $\frac{3}{4}$ in. High

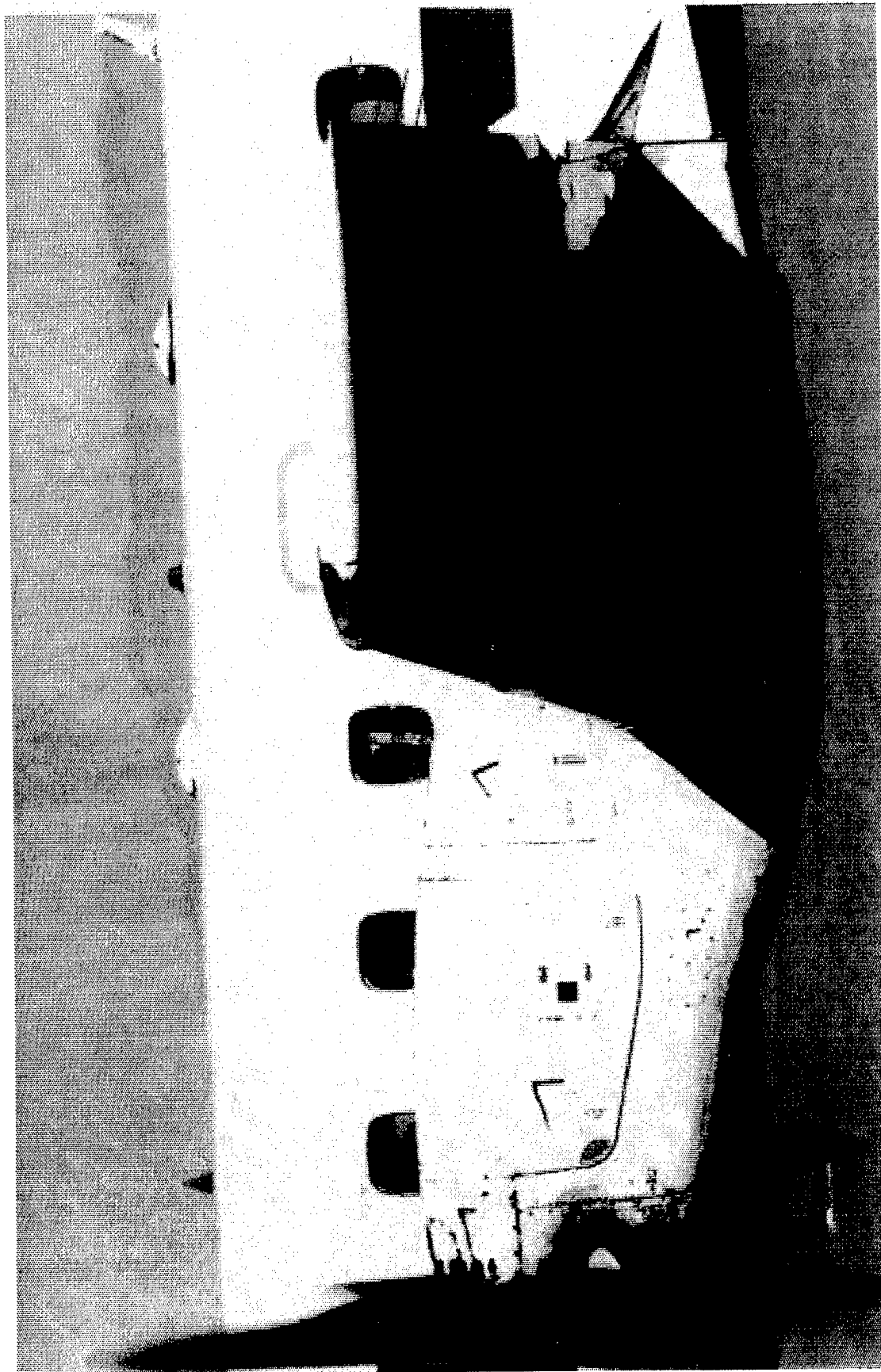


Figure 1(d)
Chordwise Extent of Ice on Pressure Side
of Wing from Behind the Tanker



Figure 1(e)
Large Ridge of Ice Formed in Line with Test Aircraft Prop Wash

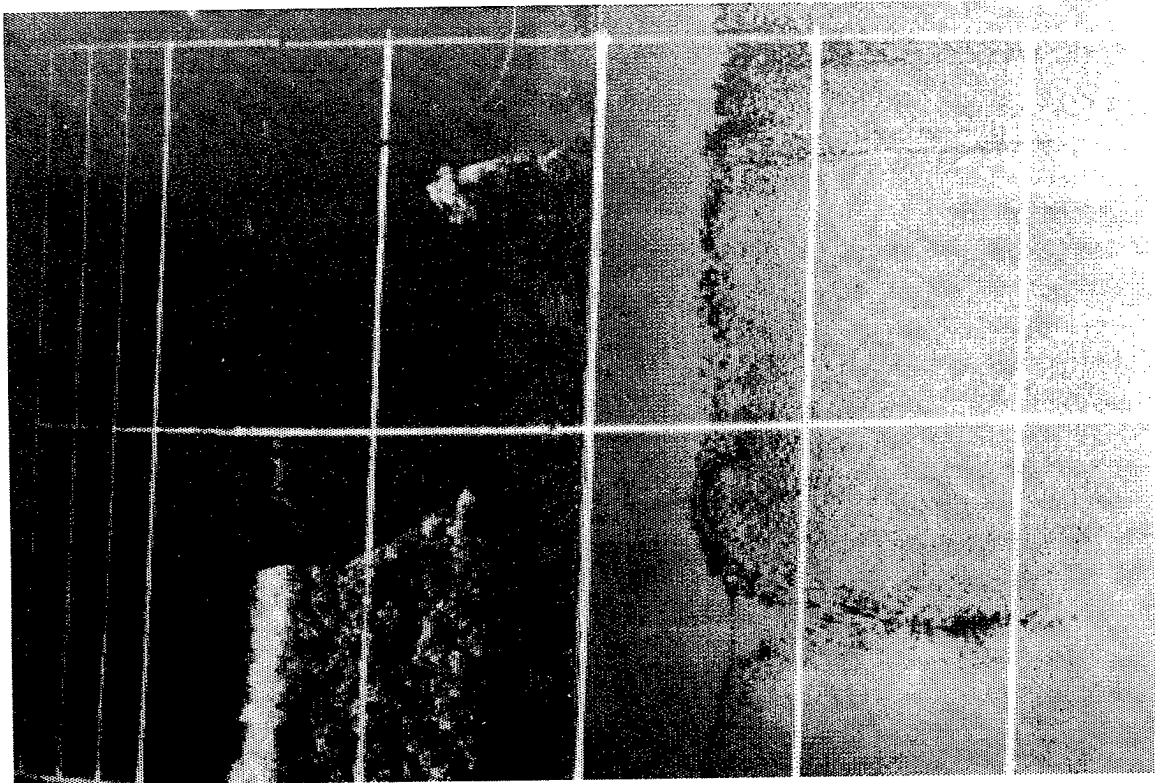


Figure 2(a)

Figures 2(a & b)
Ice formations on the IRT mounted airfoil
at a temperature near freezing (suction side)

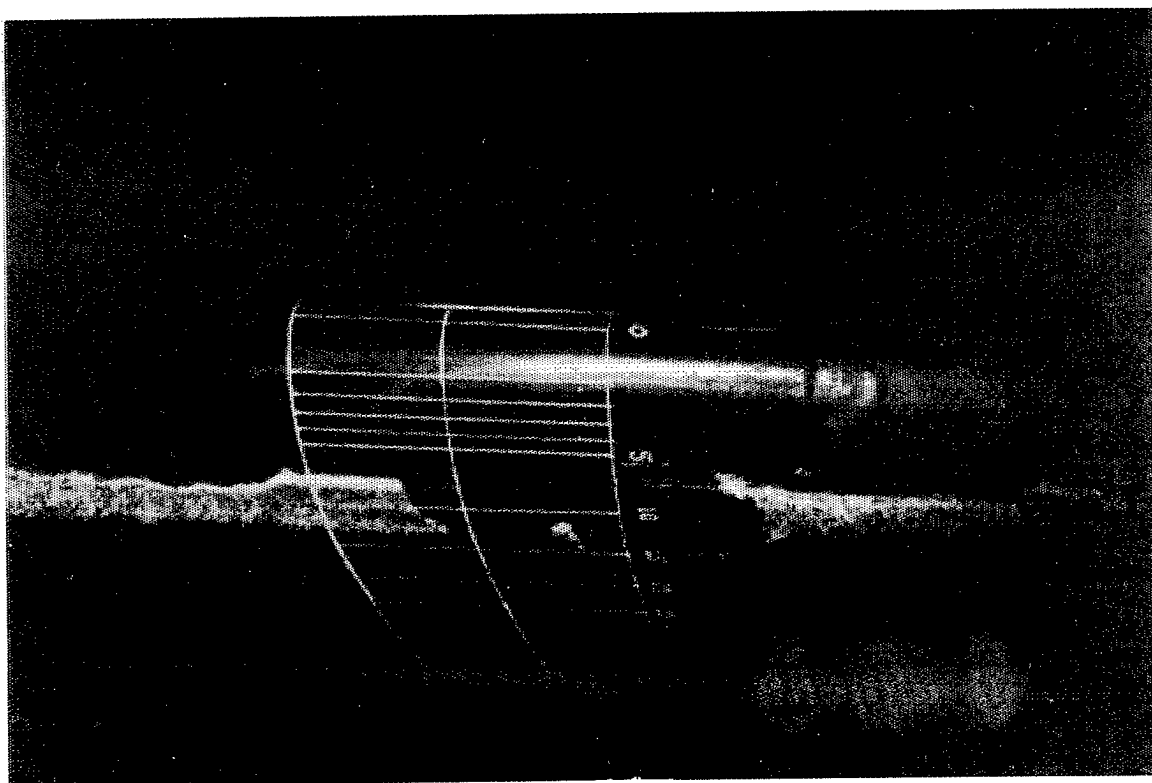


Figure 2(b)
207

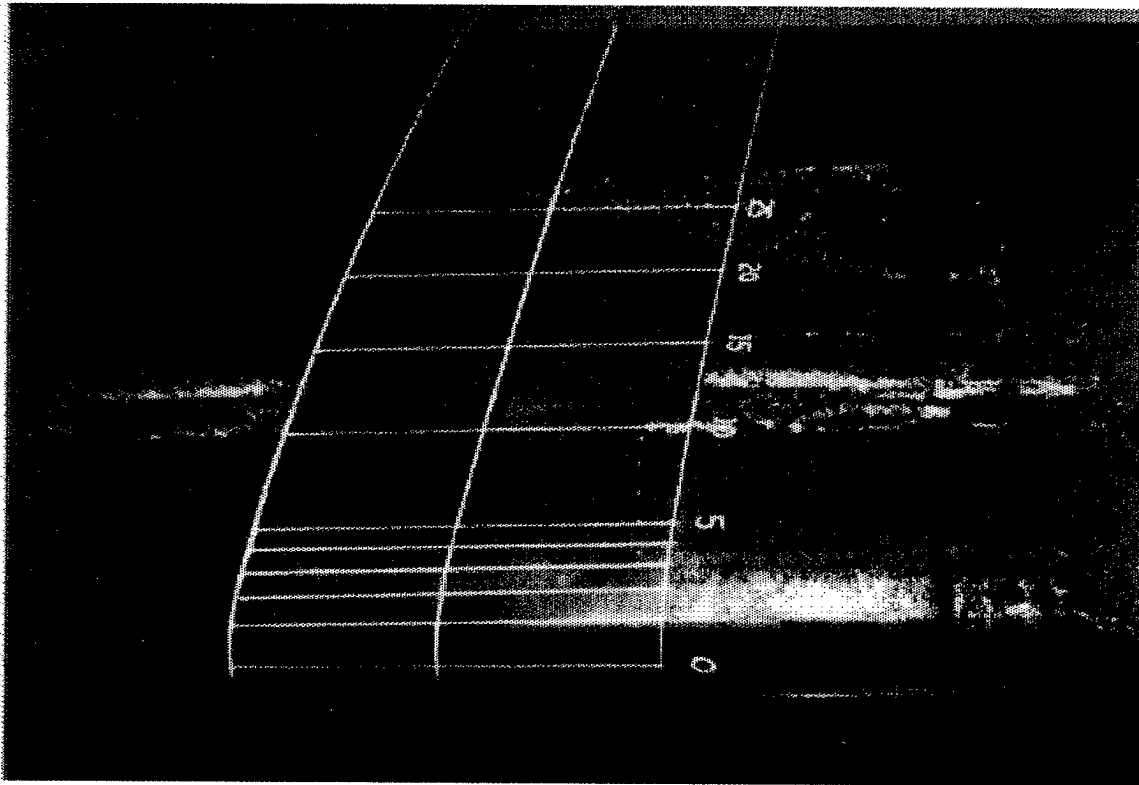


Figure 2(c)

Figures 2(c & d)
Same Test as Figures 2(a & b)
Showing Ice on Pressure Side

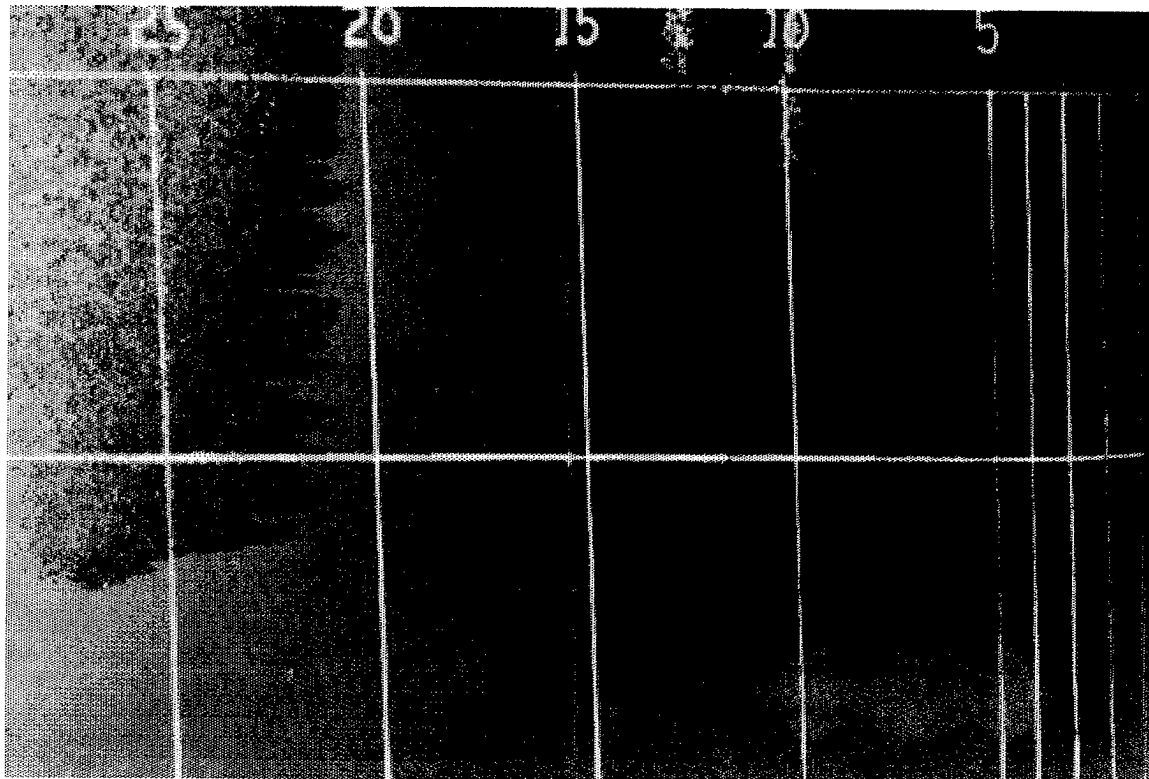


Figure 2(d)
208

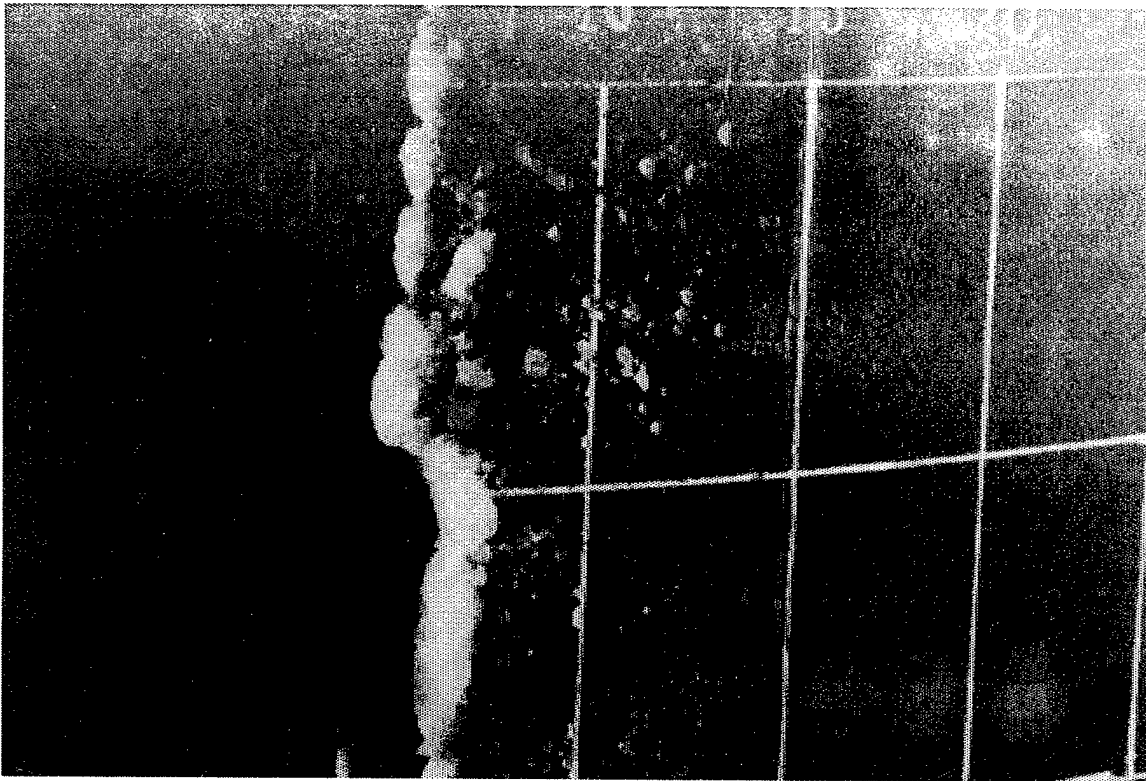


Figure 2(e)

2(e & f)
Ice Formation on the IRT Mounted Airfoil
At a Temperature of 28°F (Suction Side of Airfoil)

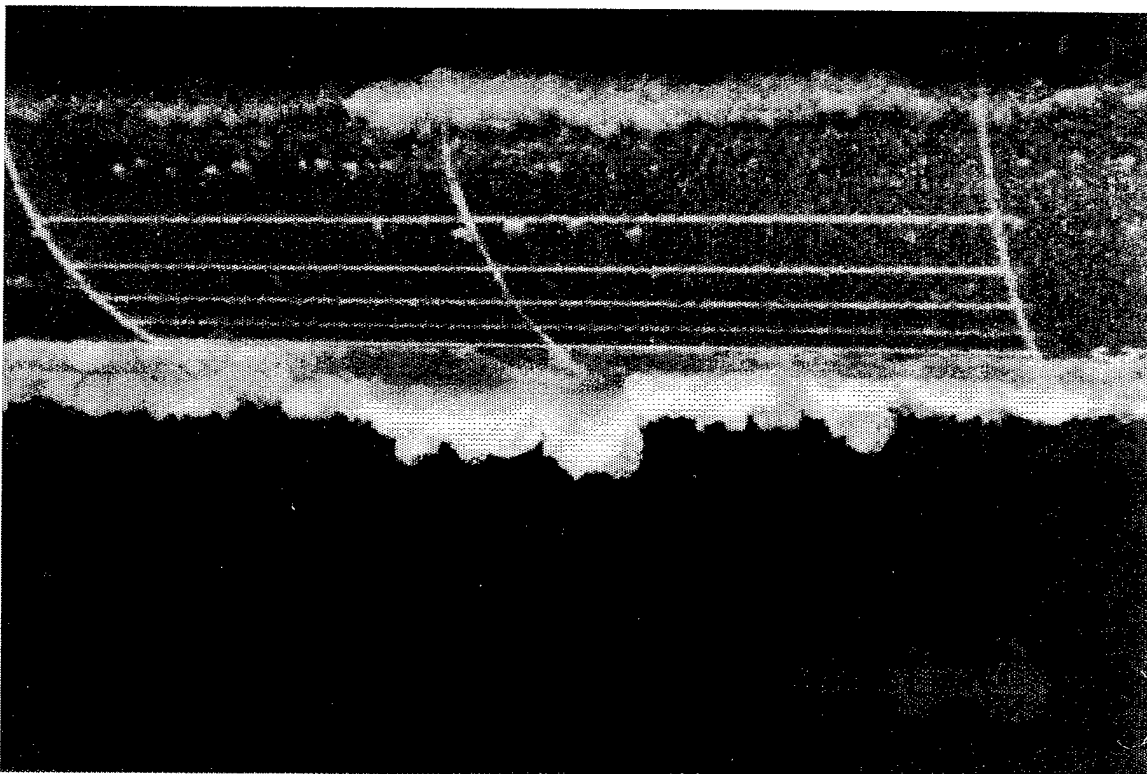


Figure 2(f)

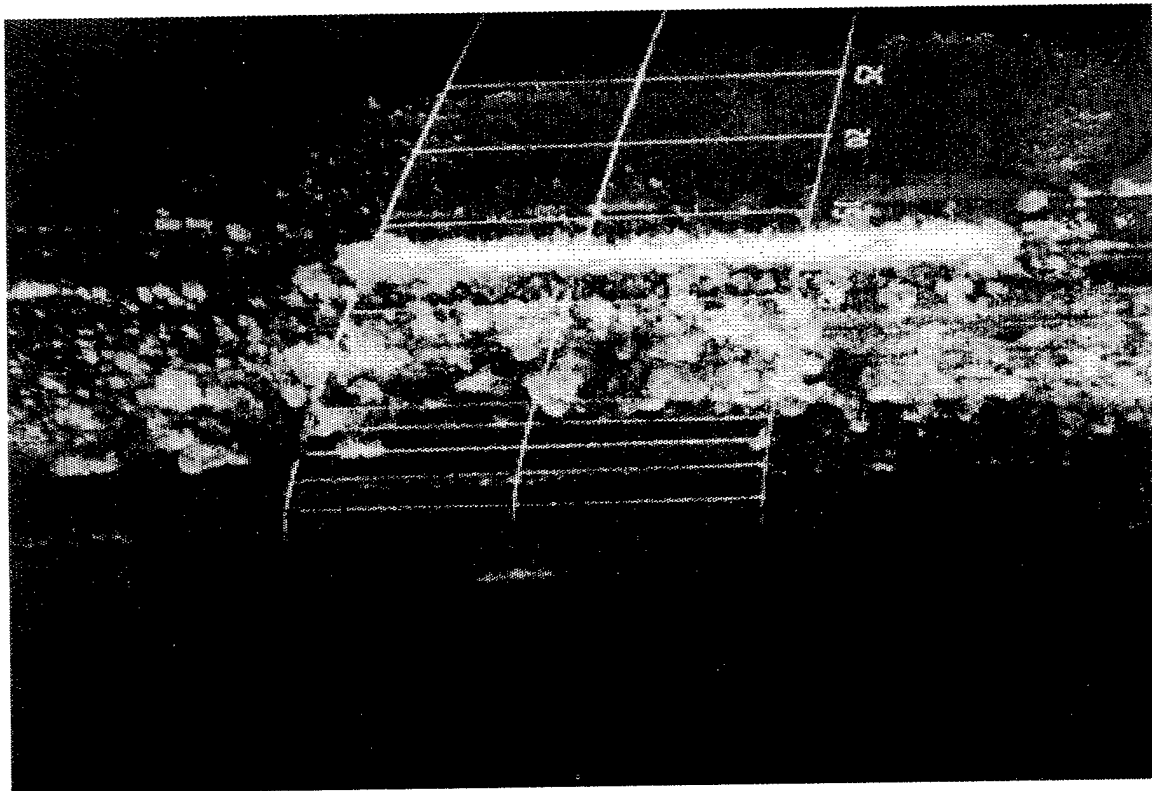


Figure 2(g)
Ice Formation Ridge on the IRT Mounted Airfoil
Pressure Side at 28°F Total Temperature

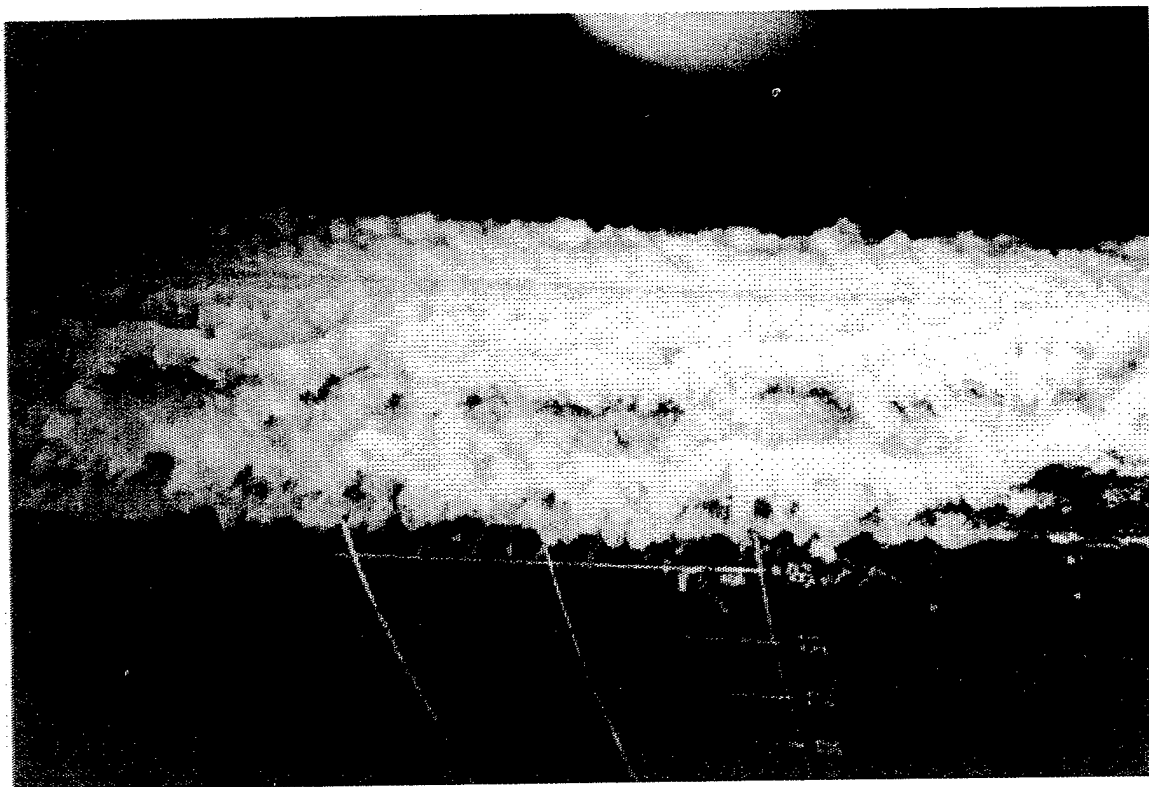


Figure 2(h)
Ice Formation on the IRT Mounted Airfoil
Without De-Icer Activation for 21 Minutes of Icing

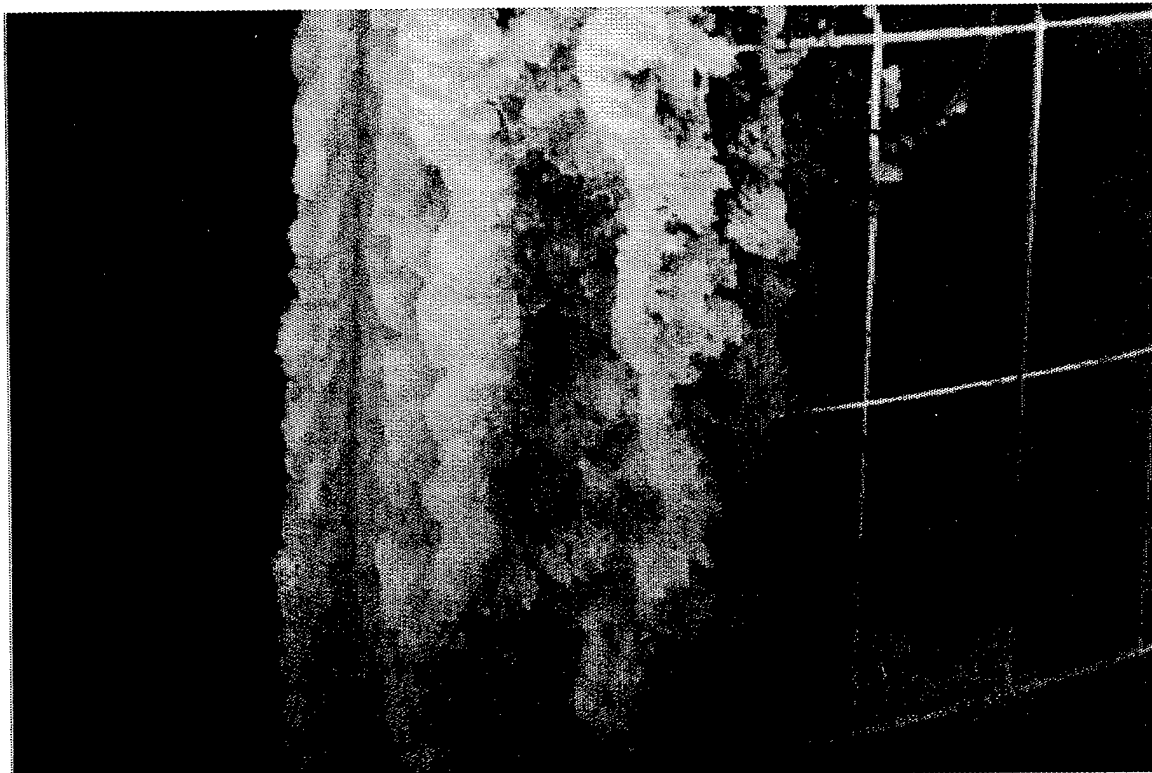


Figure 2(j)
Close-up of Ice Formation Shown in Figure 2(h)

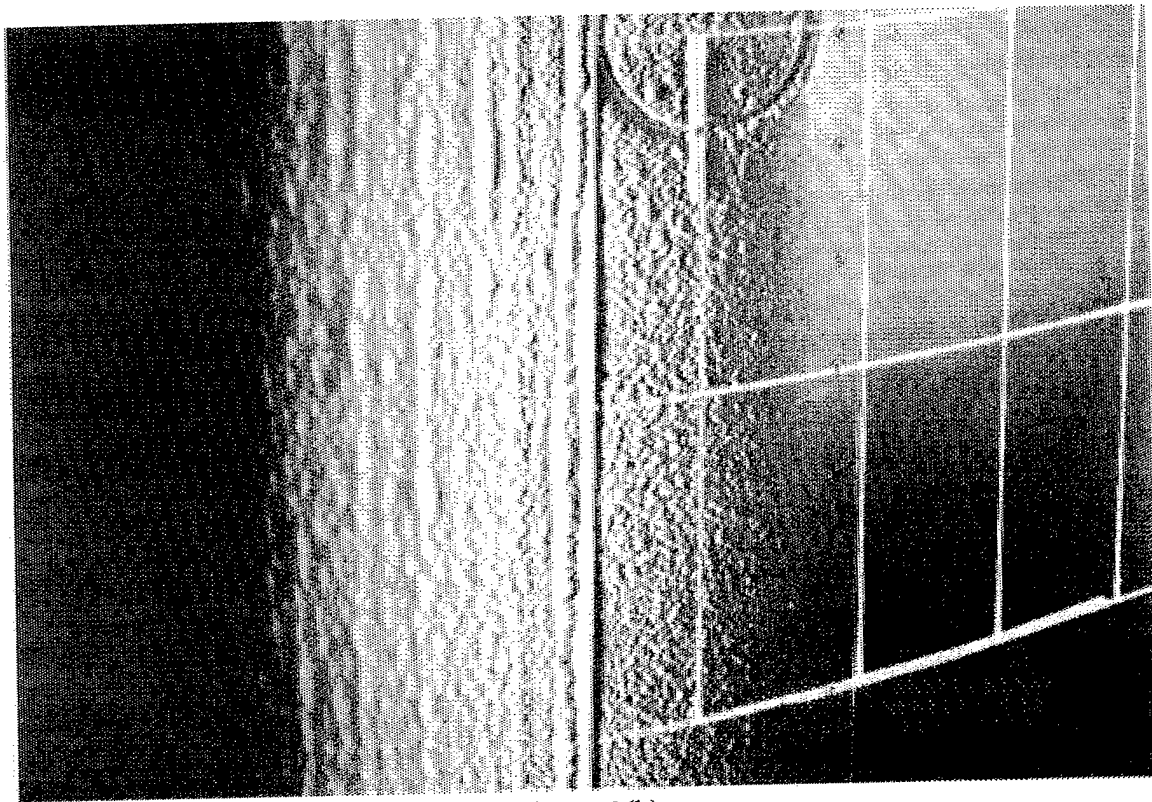


Figure 2(k)

Figures 2(k & l)
 Droplet Impingement Limit Test at 0°F on the
 IRT Mounted Airfoil. Suction Side Limit of 13% Chord

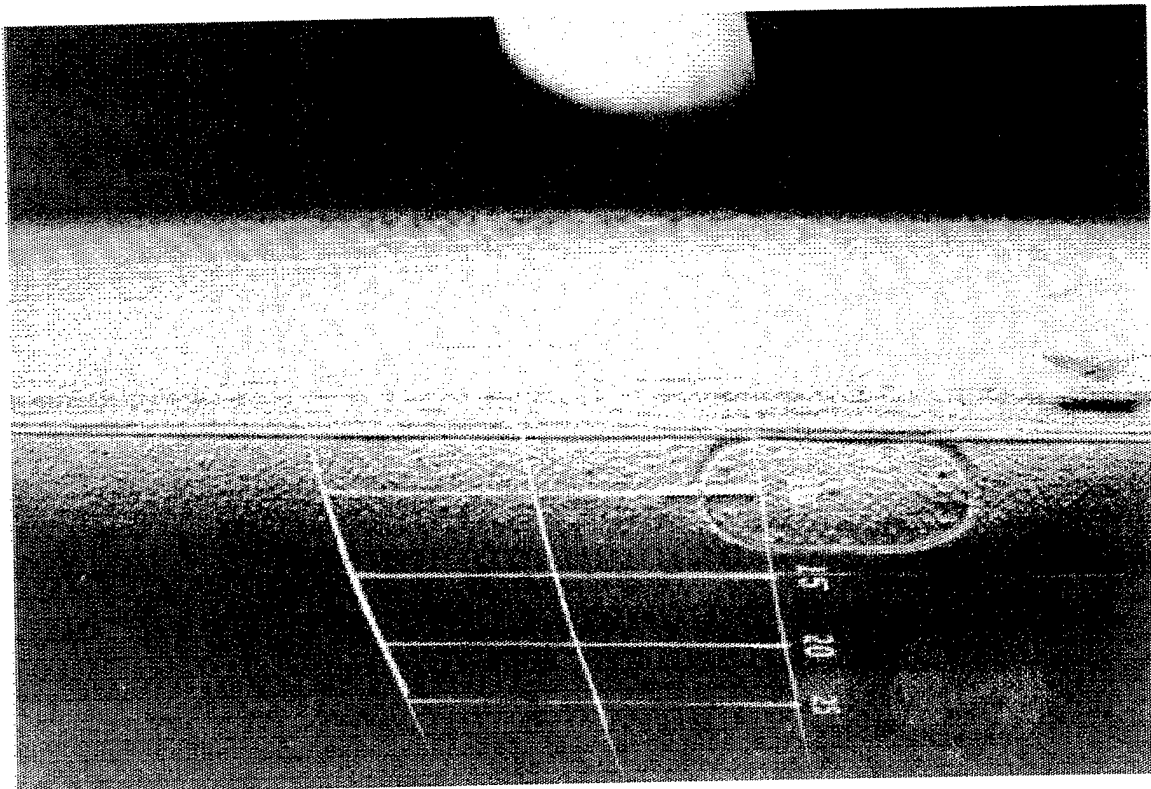
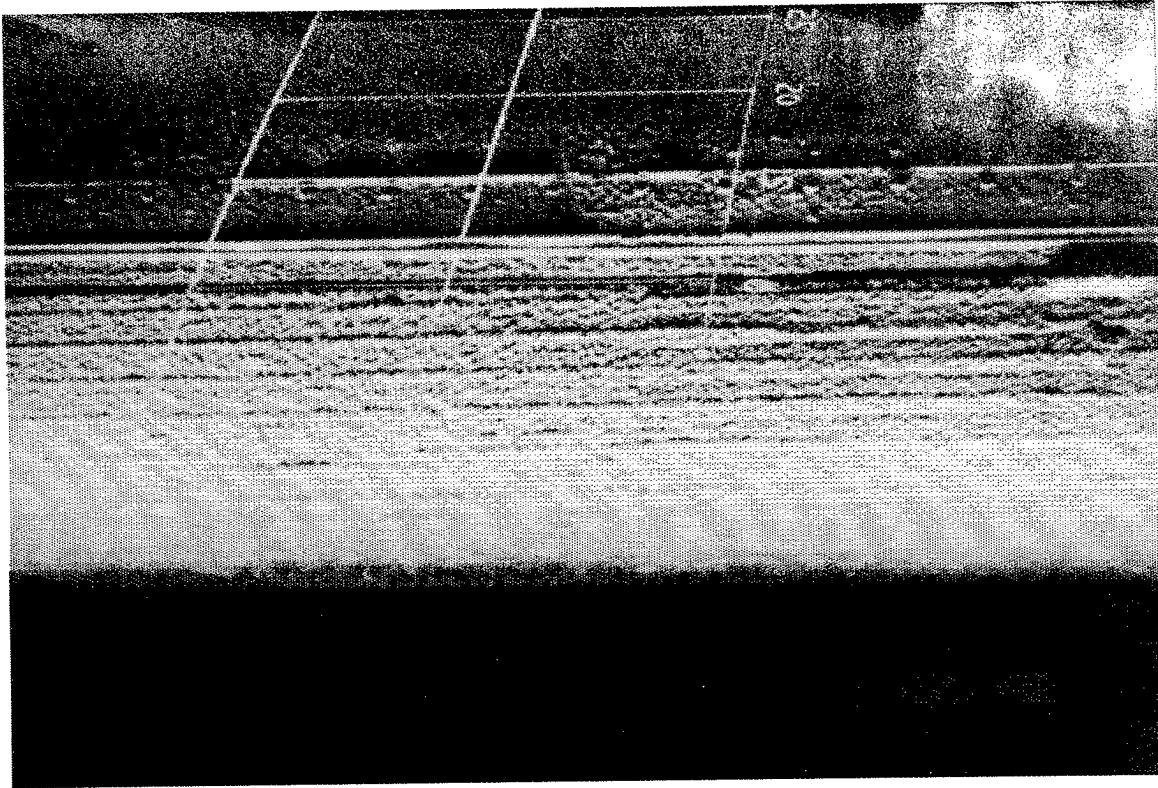
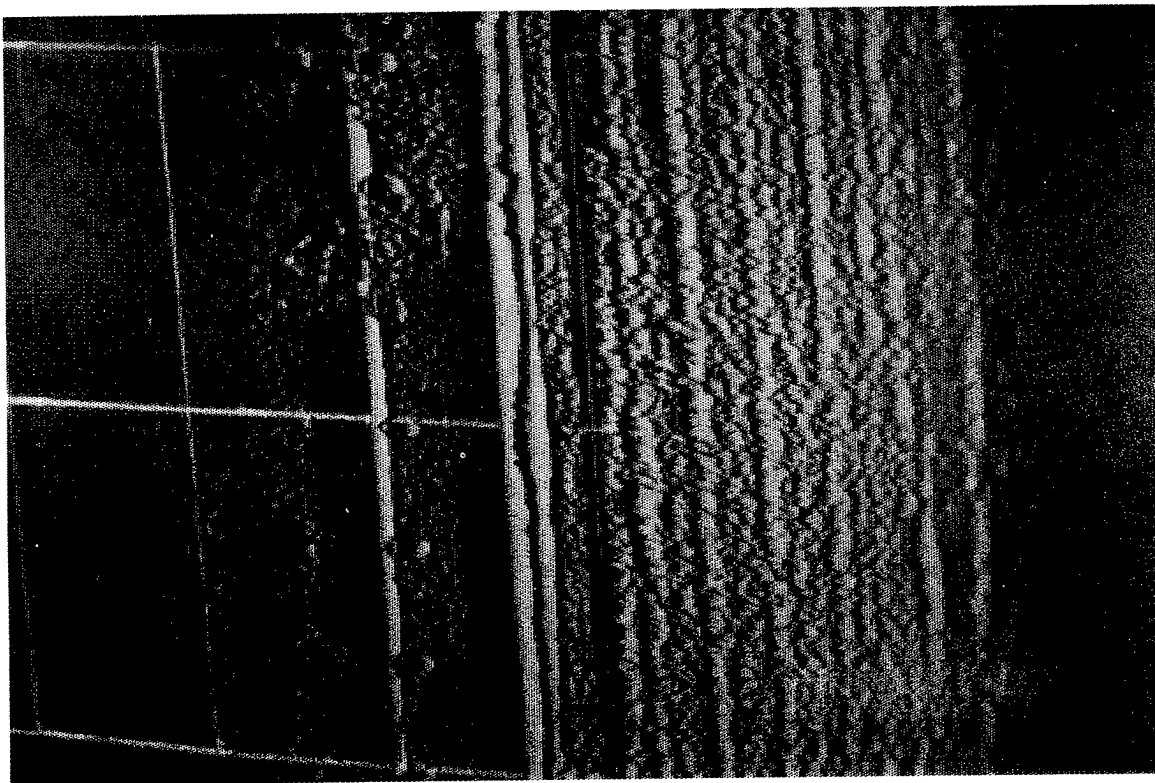


Figure 2(l)



2(m)

Figures 2(m & n)
Same Test as Figure 2(k & l) showing
Impingement Limit of 21% on the Pressure Side



2(n)
213

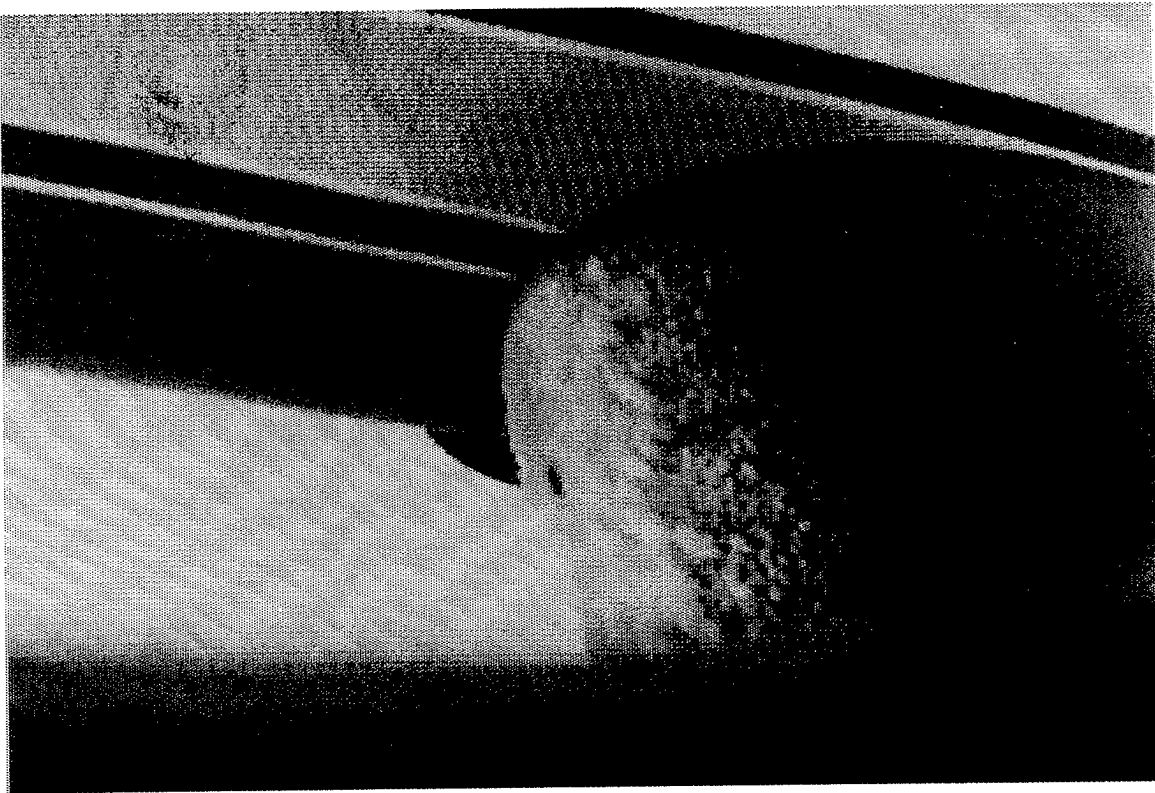


Figure 3(a)
Right Wing Between Fuselage & Nacelle
Natural SLD Encounter

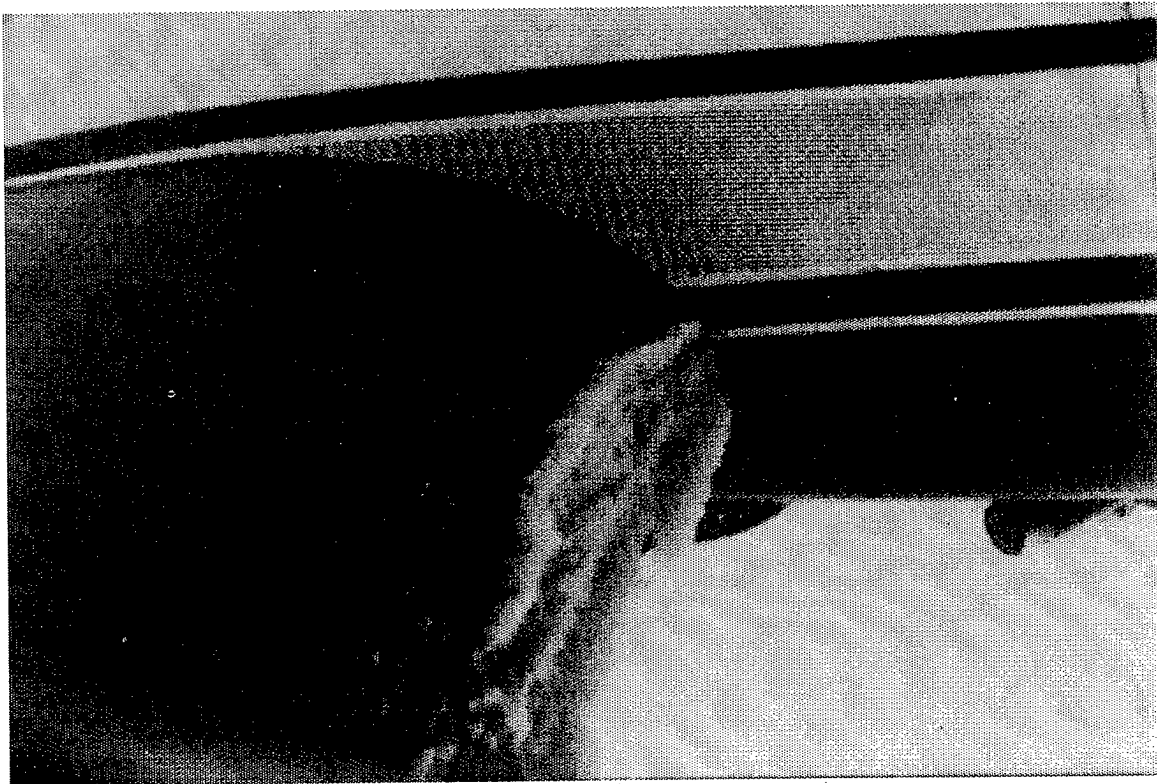


Figure 3(b)
Left wing Between Fuselage and Nacelle
Natural SLD Encounter

LOW ADHESION SURFACES FOR

ICE PROTECTION

BY

JAMES T. HINDEL

BFGOODRICH AEROSPACE

ICE PROTECTION SYSTEMS DIVISION

UNIONTOWN, OH

RICHARD L. RAUCKHORST, III

BFGOODRICH AEROSPACE

ICE PROTECTION SYSTEMS DIVISION

UNIONTOWN, OH

ABSTRACT

This paper presents some unique applications of a pneumatic de-icer and improved capabilities to remove ice more effectively. The first application is geared toward Super-cooled Large Droplet (SLD) conditions which can cause ice formation beyond typical ice protected coverage. The SLD de-icer designs consist of 1) additional low deflection tubes, either spanwise or chordwise in orientation, with a low adhesion surface ply; 2) a low adhesion coating applied to a non-inflatable area aft of the tube coverage, and 3) a low adhesion coating applied to the additional spanwise or chordwise tubes. A low adhesion coating in addition to low deflection tubes can eliminate the concern of ice attachment beyond the typical expected limits. The second application is an improved performance de-icer (IPD) that combines smaller tubes, higher inflation pressure and a low adhesion surface ply. The improved performance de-icer effectively removes ice at much thinner and cleaner levels than a conventional pneumatic de-icer.

INTRODUCTION

Current airfoils are being designed to provide higher baselines of aerodynamic performance, but which in turn, are somewhat more susceptible to performance degradation due to ice accretion. An atmospheric phenomenon called "Super-cooled Large Droplets" has recently been discovered which causes ice to form aft of typical ice protected coverage. A new de-icer design, along with low adhesion materials have been developed to address these concerns.

SLD De-Icer

BFGoodrich Ice Protection Systems has evaluated several methods for removing the ice ridge that can develop aft of the typical coverage (20-50 micron diameter droplets) due to the Super-cooled Large Droplets (60-300 micron diameter). The methods include an extension to the normal de-icer (typically 6-8% chord on the upper surface) to approximately 10-12% coverage. The extension could consist simply of a non-inflatable area with a low adhesion coating (Figure 1), de-icer tubes in either spanwise (Figure 2) or chordwise (Figure 3) direction with an integral surface ply of low adhesion material, or a combination.

Low Adhesion Coating

Testing was completed at the NASA-Lewis Icing Research Tunnel (IRT) for a typical aircraft wing section. The testing was a parametric study to evaluate SLD conditions through tunnel testing and modeling. BFGoodrich provided a test de-icer for use in the IRT (Figure 4). A flat pattern of the de-icer is shown in (Figure 5). The testing proved that an ice ridge of a thickness one inch or greater at various angles of attack could form beyond the de-icer during tunnel runs (Figure 6). The NASA Lewis Research Center IRT droplet diameter was 160 microns. A low adhesion coating, approximately 2-3 mils thick, was then applied to the de-icer aft of the active tubes and onto the wing surface, or approximately 25% chord coverage. Although ice still formed aft of the de-icer, self-shedding occurred at less than the one inch threshold of ice thickness (Figure 7). The corresponding test of this figure was performed at 0.0° angle of attack to allow ice formations on the upper and lower surface. Again, the ice formed on both surfaces, but the upper surface exhibited self-shedding at less than the one inch threshold (Figure 8).

Ice adhesion testing has also been performed at the BFG Research and Development laboratory located in Brecksville, Ohio on a variety of aircraft surfaces. These results provide an understanding of ice adhesion to various aircraft materials. The following table compares various materials and shows measured average adhesion values.

Ice Adhesion Values on Aircraft Surfaces		
Material	No. of Test Points	Avg. Adhesion Value
Aircraft Aluminum	20	125psi
Std. Pneumatic De-Icer Erosion Ply	20	83psi
Low Adhesion Surface Ply	74	29psi
Low Adhesion Coating	40	32psi

Additional Tube Coverage With Low Adhesion Coating

The extended non-inflatable area can also be designed to include inflatable tubes. The tubes could be oriented in either the spanwise (Figure 2) or chordwise (Figure 3) direction. By applying the low adhesion coating over the inflatable area, the tubes can be smaller, .38 to .50 inch, than the more typical 1.0 inch size tubes. This minimizes the increase in air volume required to inflate the de-icers, which could have an effect on the pneumatic flow valve requirements. The smaller tubes and associated tube height would also reduce the aerodynamic drag when the de-icers are inflated as compared to the typical de-icer tube size of .75-1.0 inch in this area.

Improved Performance De-Icer (IPD)

The pneumatic de-icer is an outgrowth of BFGoodrich's research in the 1920's to develop a coating that prevents the formation of in-flight ice on wings of airplanes. The first of a continuing series of de-icer patent applications was made in 1930.

Although the specific design, materials and mode of operation has substantially changed in today's de-icer, the original principle is still used. The pneumatic de-icer removes accumulated ice mechanically, through air pressure inflation of normally flat de-icing tubes.

The Improved Performance De-Icer (IPD) system provides a means of removing thinner ice than the standard pneumatic de-icer. The pneumatic de-icer has already proven its value through its low power requirements and system simplicity. IPD is a continuation of BFGoodrich's effort to provide a Pneumatic De-Icing system which will meet and exceed the needs of our customers well into the future.

IPD Overview

The IPD is a thin elastomer/fabric blanket, containing two to four 0.75 to 1.0 inch wide inflatable tubes at the leading edge, and a series of 0.5 to 0.75 inch wide tubes aft of the leading edge that break and remove ice when inflated (Figure 9). The de-icer is designed so that the de-icing or "inflatable" tubes cover the complete area to be protected.

The de-icer consists of several layers of elastomers and fabrics. The outer surface layer is comprised of weather-resistant elastomers, chosen for good rain erosion resistance as well as slow weathering. Directly beneath is a natural rubber layer, whose resilience aids in the expulsion of air after the de-icing tube is inflated. The outer surface and natural rubber layers are bonded to a stretchable fabric layer to form the outer tube wall, which when inflated flexes to remove ice (Figure 10).

The opposite wall of the tube is formed by sewing the stretchable fabric to non-stretchable fabric, which is bonded to another elastomer layer that forms the installation surface for bonding the de-icer to an airfoil. Other materials are added to form a pneumatic seal of the ends and edges of the de-icing tubes. An autoclave cure is used to fuse these layers into a relatively thin, smooth blanket. The de-icer is designed with internal venting, which permits all tubes in a de-icer to be inflated and deflated through an air connection normally located within the de-icing tube area and on the installation side of the de-icer when it projects through a mating hole in the airfoil outer skin.

De-icing occurs when the tubes are inflated using 24-30 psig air pressure. This is a higher operating pressure than the standard pneumatic de-icer which typically uses 18-22 psig. The smaller size tubes, higher pressure, shorter inflation time and low adhesion surface ply are what give the IPD the capability to remove thinner ice. The IPD consistently removes ice to a 0.1 inch ice thickness versus a 0.25 inch to 0.50 inch ice thickness threshold for a standard pneumatic de-icer. Figure 11 is a typical icing run in the BFGoodrich tunnel for an IPD de-icer operated at 30 psig. The test shows gradual build-up of ice up to 0.1 inch and complete ice removal. An Optical Measurement Device was used to trigger the system when an ice thickness of 0.1 inch is achieved at the leading edge. Figure 12 demonstrates a typical "Estane" surfaced de-icer operated at 18 psig. The graph depicts several cycles, with the system again started by the Optical Measurement Device. As seen in Figure 12, complete ice removal did not occur until approximately 0.25 inch of ice was achieved.

CONCLUSION

Two conclusions can be drawn from the preceding paragraphs. The first conclusion is that a pneumatic de-icer which offers a low power, low cost technology can be improved in its capability to effectively remove ice in thinner layers. The improved performance is achieved with smaller tubes, higher operating pressure and a BFGoodrich proprietary low adhesion surface ply. The second conclusion is that a BFGoodrich proprietary low adhesion coating, when applied chordwise aft of de-icer tubes, has shown effective removal of SLD ice ridges. The IPD would require little to no modification to existing pneumatic hardware components.

ACKNOWLEDGMENTS

Contributions to this document by the following individuals are greatly appreciated by the authors:

Mr. Harold Addy, Jr.: NASA Lewis Research Center

Mr. Peter Brown: BFGoodrich Ice Protection Systems Division

Mr. Alan Fahrner : BFGoodrich Ice Protection Systems Division

Mr. Marc Holyfield : BFGoodrich Ice Protection Systems Division

Mr. Dean Miller : NASA Lewis Research Center

Dr. Allen Reich: BFGoodrich Aerospace Research & Development

Mr. David Sweet: BFGoodrich Ice Protection Systems Division

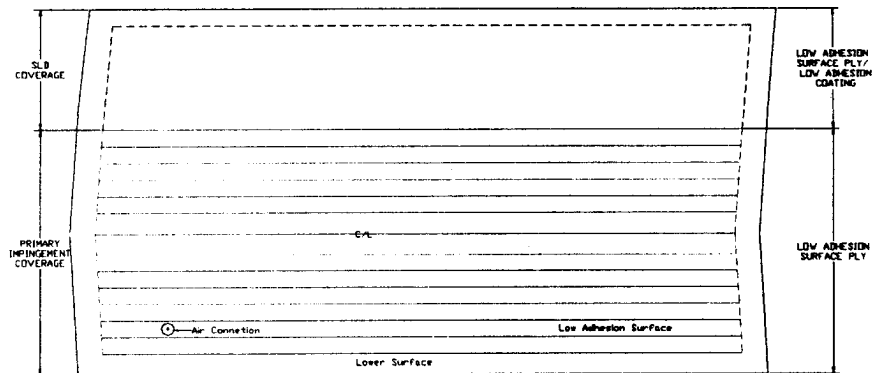


Figure 1
Flat Pattern De-Icer With Additional Non-Inflatable Coverage

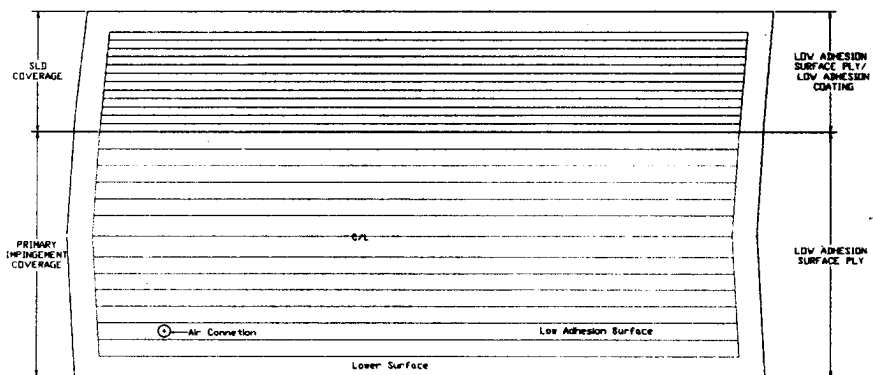


Figure 2
Flat Pattern - Additional coverage With Spanwise Tubes

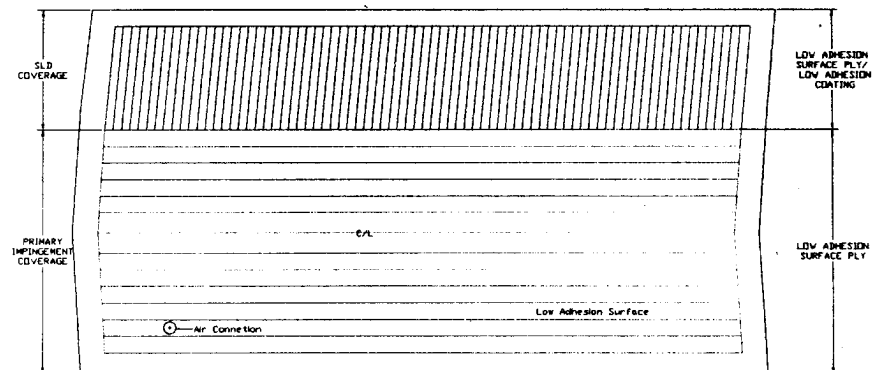


Figure 3
Flat Pattern - Additional Coverage With Chordwise Tubes



Figure 4
Icing Model Installation at NASA Lewis Icing Research Center IRT

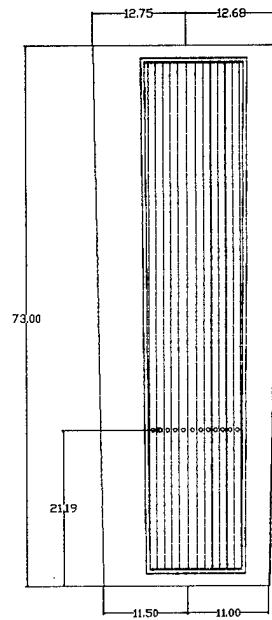


Figure 5
Flat Pattern of Test De-Icer for IRT Testing

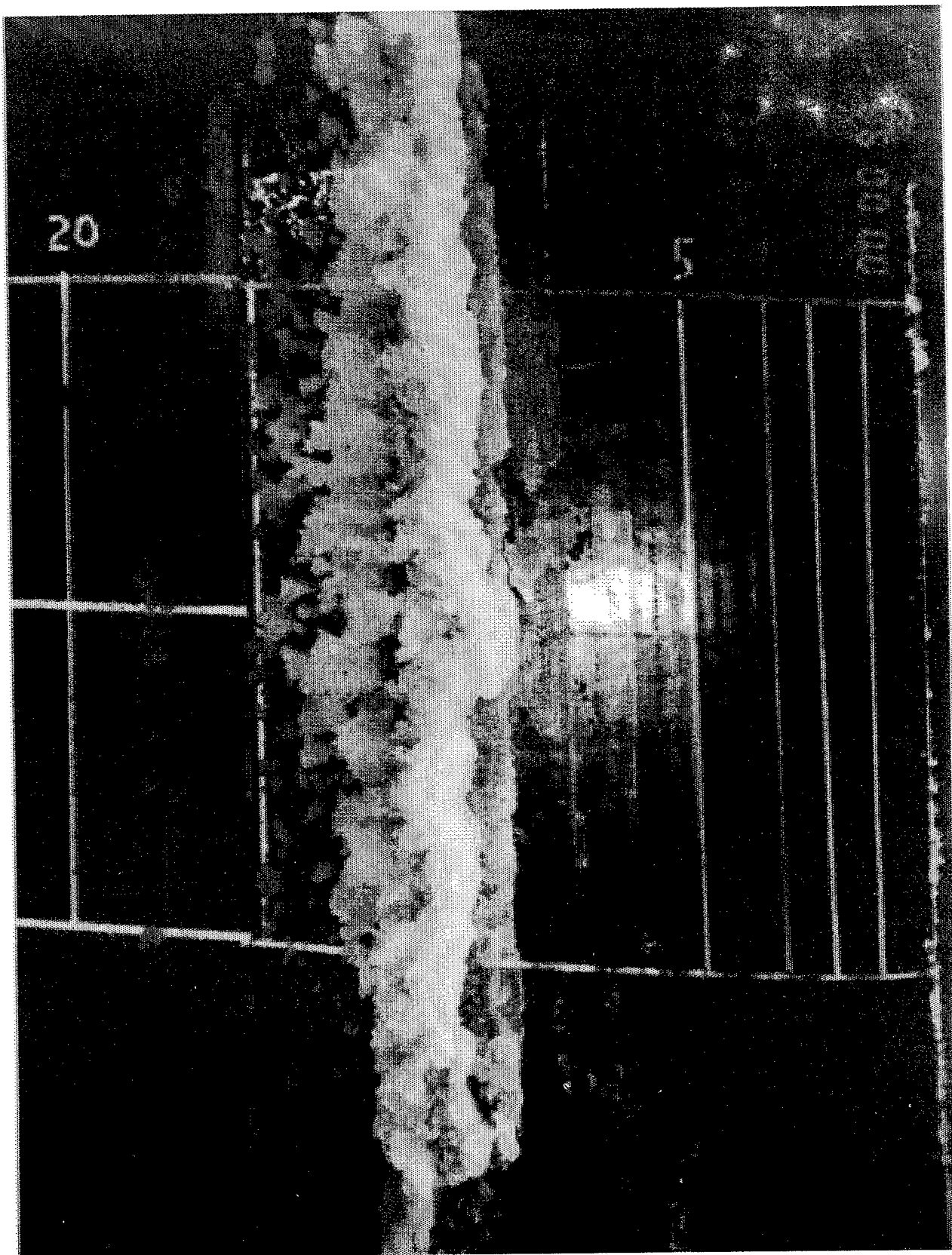


Figure 6
Ice Ridge Formation Aft of Protected Area (Pressure Side)



Figure 7
Ice Ridge Formation After Application of Low Adhesion Coating (Suction Side)

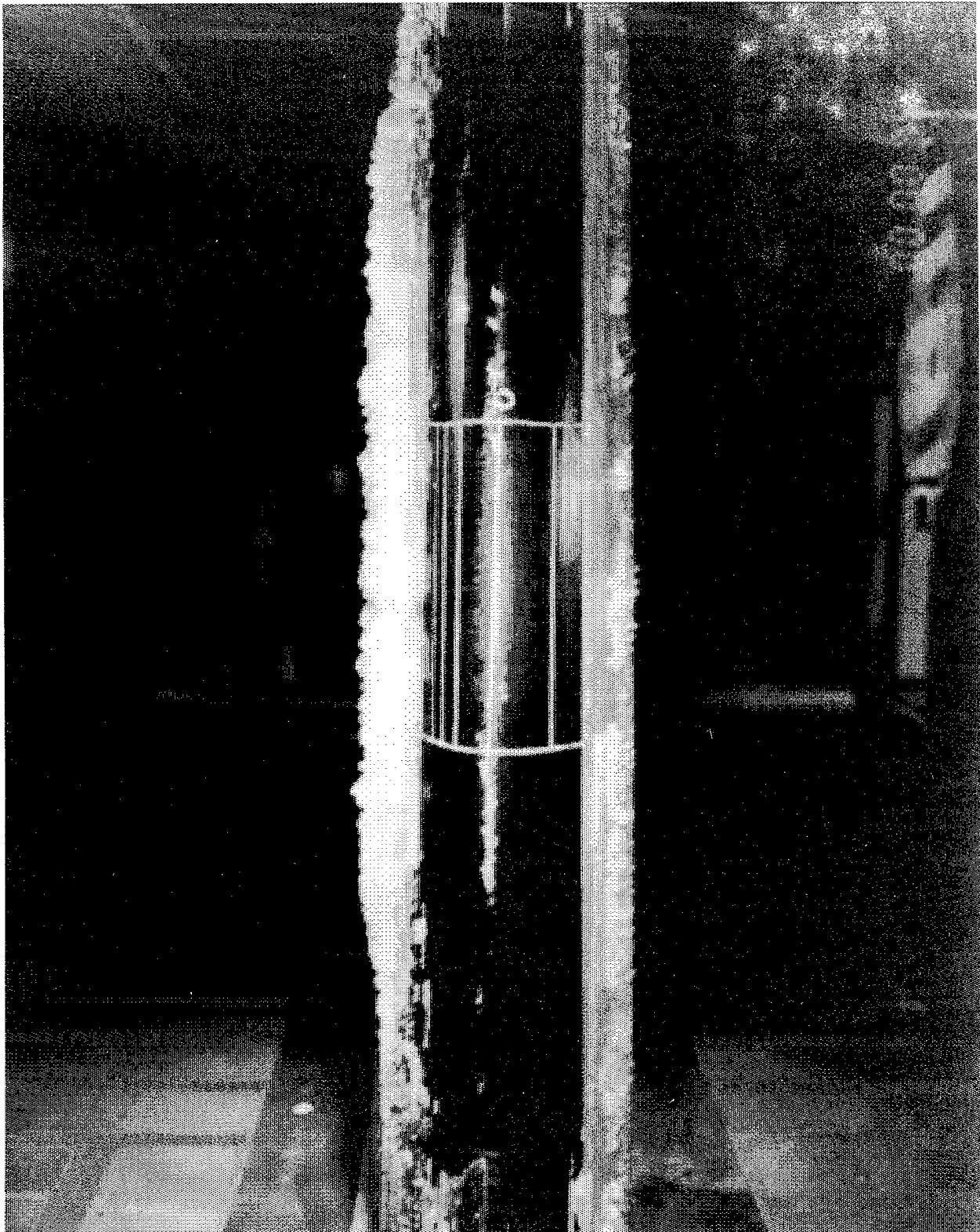


Figure 8
Frontal View of Test Model
Pressure Side No Low Adhesion Coating
Suction Side Low Adhesion Coating

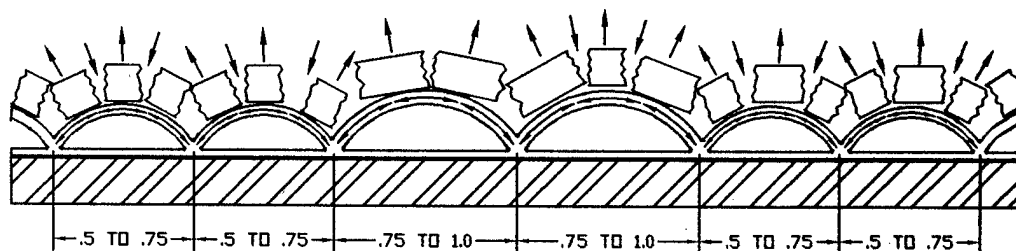


Figure 9

Inflated De-Icing Tube Cross Section

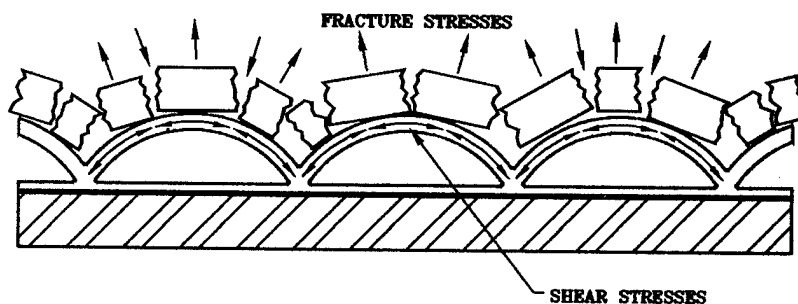
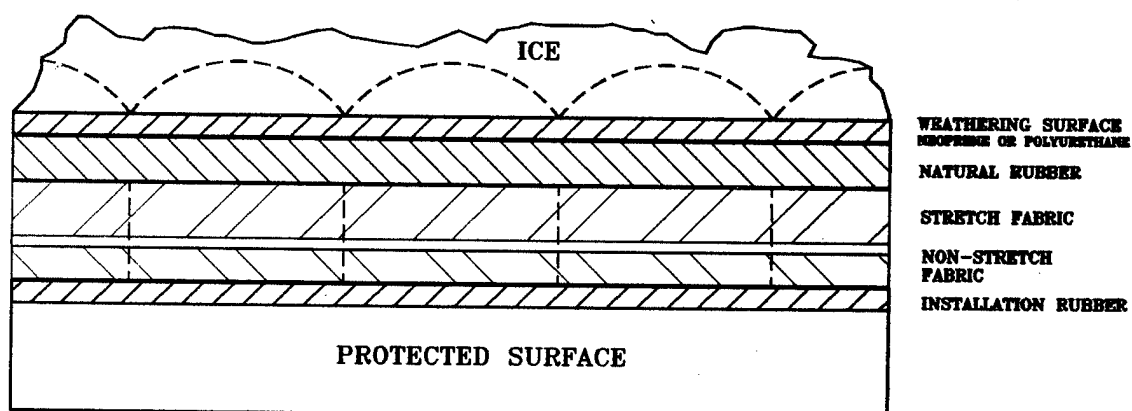


Figure 10

Pneumatic De-Icer Construction

TEST CONDITIONS
IMPROVED PNEU. DE-ICER

TEMP.	LWC	MVD	VEL.	AOA
-22°F	.15 G/M ³	20.1	165	0

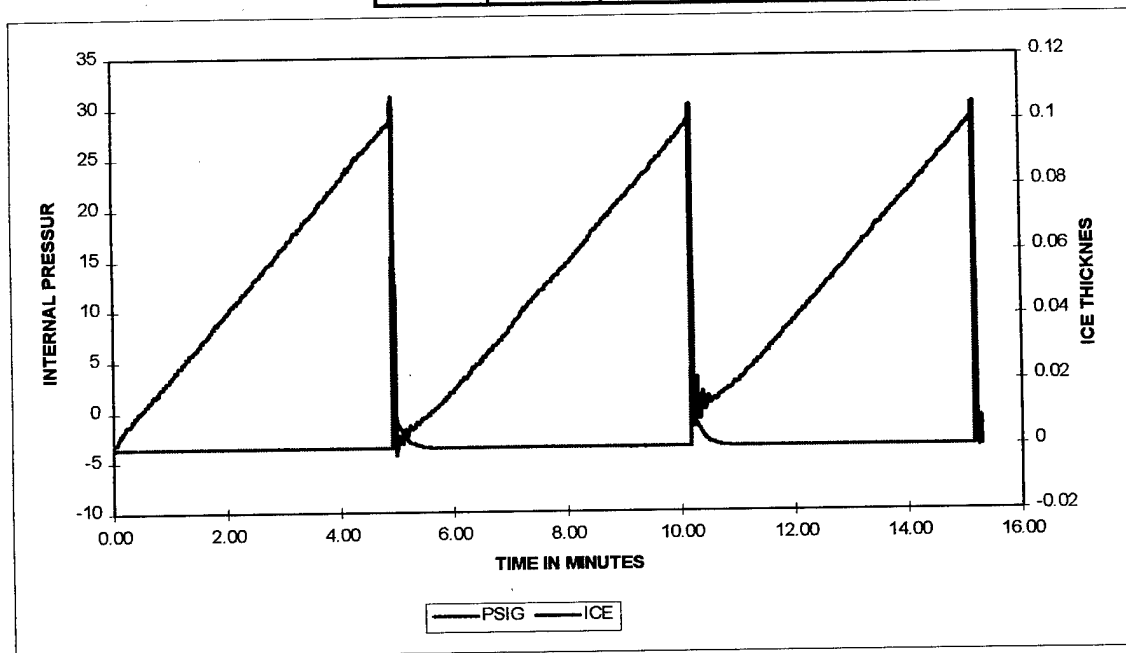


Figure 11
Icing Wind Tunnel Results of Improved Pneumatic De-Icer at 30 psig

TEST CONDITIONS:
STANDARD PDI

TEMP.	LWC	MVD	VEL.	AOA	PDI PRESS.
-22°F	.15 G/M ³	20.1	165	0	18

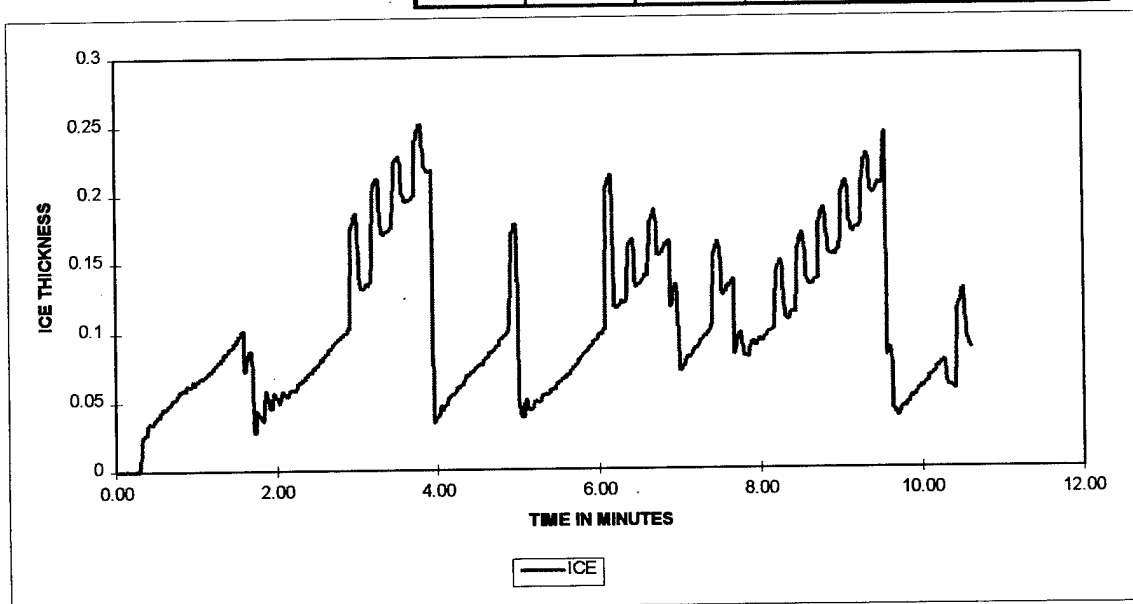


Figure 12
Icing Wind Tunnel Results of Standard Pneumatic De-Icer at 18 psig

Ice Protection System for a New Commuter Aircraft

Paper presented by F. AVEROUS, AERAZUR (France)

ABSTRACT :

Pneumatic deicing systems have been used for more than 50 years and a vast operational experience has been gained. This type of system remains, in the opinion of the writer, the best and most cost effective system for protecting commuter aircraft against inflight icing.

Recent developments in control and ice detection systems ensure that this technology can cope with the currently debated issues of tailplane icing and large droplets icing conditions.

The paper outlines a proposed deicing system incorporating flush ice detectors embedded in the boots, allowing monitoring ice build-up and shedding as well as full automatic activation of the deicing function.

Installation of similar detection devices on flying surfaces aft of the area protected by boots allows warning of the aircrew of entering icing conditions outside of those addressed in current Appendix "C", allowing initiation of flight maneuvers to exit a potentially dangerous situation.

ICE PROTECTION SYSTEM FOR A NEW COMMUTER AIRCRAFT

Paper presented by F. AVEROUS, AERAZUR (France)

1- Pneumatic deicing systems :

Pneumatic deicing systems, usually known as boots for the more visible parts, have been routinely used for more than 50 years to protect aircraft against inflight icing.

They were almost universally used before the apparition of the jet airliners, when different flight profiles and availability of bleed-air gave a new life to hot-air anti-icing of flying surfaces, a system tried earlier, using gasoline burners and fans, but abandoned after numerous inflight fires. The drawbacks of hot-air deicing (especially high energy demands) were found tolerable during the limited duration of anti-icing system actuation on jets.

Present-day commuters, whose flight profiles are similar to that of the piston-engined airliners of the 50's, with cruise altitudes mostly between 10 and 20 000 ft, need systems allowing constant use if necessary, under tolerable economical conditions. For this very reason, they are relying almost universally on the pneumatic deicing technology.

Typically, an aircraft is protected by a combination of different techniques : usually a pneumatic deicing system is used for the airframe and possibly the engine inlets, with electrothermal heating protecting small areas like probes, control horns, windscreens and propeller blades (see Fig 1).

A "conventional" deicing system (Fig 2) consists of boots installed on the leading edges of the airfoils, a pneumatic circuit with distribution valves supplying the boots with compressed air (typically 20 PSI), when actuated, and providing vacuum to ensure compliance with desired airfoil shape when not actuated, ancillary devices to ensure a proper supply of air (pressure regulators, check valves, water separators, drains, etc....) and a control and monitoring device, controlling the valves and checking for proper operation through pressure switches. Compressed air can be bled from the engines (solution universally adopted on turboprops) or generated by dedicated compressors (solution currently limited to piston-engined general aviation aircraft). Vacuum is generated

by venturis fed with compressed air (if bleed-air is used for the system) or by vacuum pumps (in fact the mechanical compressors used backwards).

Ice shedding is achieved by the inflation of tubes in the deicers, simultaneously increasing the girth of the airfoil to induce ice cracking and modifying the shape, resulting in loosening of the bond of the ice to the airfoil. Ice is actually shed by the airflow around the airfoil.

2- Pneumatic deicing systems pros and cons :

As a matter of facts, pneumatic deicing systems enjoy marked advantages compared to other systems :

- unequaled flight experience accumulated, literally hundred of millions of flight hours,
- low installation and negligible operating costs, without specific logistic requirements,
- simple and rugged systems, familiar to A&P mechanics around the world,
- moderate maintenance costs (typically < 10 USD / flight hour),
- environmentally friendly system (no polluting chemicals used, negligible energy consumption, hence no additional emissions).

More relevant to military uses are the absence of unwanted infrared signature and the compatibility with "Stealth" technologies..

These advantages explain the continued popularity of the system, including a trend to expand its use to other aircraft, including jets and military aircraft.

It can also be noted that pneumatic deicers are gaining popularity for air intakes deicing (ATR and DASH 8 families, DO 328).

3- Recent questions raised :

Most currently operating systems have been designed according to US Appendix "C" of FAR 23 and 25 or equivalent national regulations. These rules basically define a flight profile and atmospheric conditions that the aircraft has to be able to cope with.

In the last five years or so, concerns have surfaced within the aviation community about the efficiency of present deicing systems in "marginal" conditions and more specifically two issues have been addressed and have been the subject of FAA meetings :

- tailplane icing, eventually resulting in a possible loss of aircraft control,
- large droplets icing situation, resulting in ice accretion outside of the area covered for situations within Appendix "C", with potential for "runback" still aggravating the situation.

These issues are in fact not specifically addressing shortcomings of pneumatic deicing systems, since most other systems would be similarly affected.

One contributing factor to the problems encountered in recent years may be the basic design of the recent commuter aircraft :

- quasi-universal use of unpowered flight controls on commuters, with the resulting risk of abnormal control loads arising from the disruption of normal airflow around the airfoils, up to the point of impossibility for the aircrew to counter control forces,
- increase of aircraft performance, together with a decrease in size of tail surfaces, combined with the use of inverted high lift airfoils to compensate for the lower area, use of very efficient flaps system to allow acceptable landing speeds with smaller wing areas as well as the introduction of so-called "modern" airfoils, that in some cases seem more sensitive to surface pollution than more conventional airfoils. These design tendencies result in lower controllability margins in extreme situations.

Other contributing factors may be :

- the congestion of US air traffic, resulting in long holding periods both on-ground (ground icing problems) and in-flight (tending to expose aircraft for extended periods to local meteorological conditions that may be worse than the average on the flight path, as for the Roselawn accident),
- the reluctance to cancel or delay flights in a very competitive airline environment.

4- Recent studies at AERAZUR :

Extensive studies have been initiated at AERAZUR to explore these problem areas and define solutions. These studies have covered both basic studies to understand the phenomenon encountered and possible cures, as well as improvements to the present pneumatic deicers systems and alternate designs like medium pressure pneumatic, improved electrothermal and electro expulsive deicing systems.

Although alternate systems may offer very promising solutions for future aircraft, it has been found that relatively minor modifications of the present pneumatic systems provided an acceptable answer to the problems of tailplane icing and large droplets icing, available at short notice and readily applicable to existing aircraft.

The solutions are based on a progressive transition from the present "dumb" system to a progressively "smarter" system, by incorporating recent advances in ice detection and system control technologies to improve efficiency of the ice shedding and warn the crew of exceeding design limitations.

Currently operational systems rely on detection by the aircrew of the onset of an icing situation, relying on clues like Outside Air Temperature, airframe element visible ice accretion (e.g. windshield wiper arm...), or in the best case ice detection by an icing probe installed on the airframe. The deicing system is then switched "On" and inflates the boots at regular intervals (eventually with two hand-selectable periods between consecutive inflation cycles).

4-1 Tailplane icing :

It should first be noted that on modern aircraft, direct detection of ice accretion as well as visual monitoring of effective ice shedding on the tail surfaces is outright impossible. On some aircraft, the engine nacelles and even the wing are not observable from the flight deck.

FAA has proposed a flight test condition to prove that adequate control margins remain with ice shapes simulated on the tailplane (the so-called "Og pushover"), but, in our opinion, the solution should rather rely on an effective and reliably monitored tailplane deicing system, to allow retaining full tailplane efficiency even in icing conditions, and, as a consequence, no short-field performance limitations.

Our analysis showed first the necessity of an improvement in the detection of ice accretion. We figured that, if we could design a detection system that could be installed flush in a boot :

- we would achieve detection of ice accretion on the airfoil itself and not in an unrelated position, suppressing all doubts about correlation, leading edge radius, etc....
- by measurement of the actual accreted thickness, we could trigger boot actuation at the optimum point for best shedding efficiency,
- if we managed to have the detection device cleaned solely by the boot actuation, we would have a fault-free monitoring of the effective ice shedding and clearing of ice from the airfoil.

As a supplementary benefit, outputs from the detectors could be used to control automatically the actuation of the boots, either individually or by implementation of an "OR" function globally, resulting in more efficient shedding and a sizable maintenance cost saving by avoiding unnecessary cycling of the boots. Automatic actuation would, in our opinion, enhance operational safety, particularly for small aircraft where a single pilot flying IMC conditions in terminal areas may have a high workload, inducing insufficient awareness of airframe icing situation. This opens, on the other side, interesting Certification Issues that would have to be clarified during detailed System Design.

Further, the possibility of measuring the rate of ice accretion with these sensors leaves open the possibility of informing the crew about the "severity" of the icing situation.

This solution has been implemented in cooperation with the Swiss company "VIBROMETER", who has developed a flush sensor with the necessary sensitivity and precision. Splitting the sensing unit itself and the signal processor offered an acceptable solution, pricewise, because the sensing unit that had to be bonded into the boot for best results. A sketch of such a system is shown in Fig. 3. It should be noted that several sensors may be needed, placed at different chord locations on the airfoil and on the aircraft, depending on the flight conditions and most critical case for the considered airfoil.

Windtunnel tests have been completed and have proved the feasibility and effectiveness of the system. Flight tests in natural icing conditions are scheduled for next winter season.

4-2 Large droplets icing problem :

This problem was emphasized after the Roselawn crash on October 31st 1994. A commuter aircraft flew an holding pattern in conditions that were reconstructed as presenting a freezing drizzle situation, where droplets may have been as big as 400 μm in diameter, against 40 μm maximum in Appendix "C". This unfortunate situation ultimately resulted in loss of control and a fatal crash.

This kind of situation had been suspected for a long time, but it was the first time that an elaborate flight recorder installation allowed reconstitution of the chain of events and subsequent satisfactory reproduction in flight tests behind an icing tanker.

To summarize the problem, larger droplets diameter results, due to the far greater weight/area ratio (a 400 μm droplet is 1 000 times heavier than a 40 μm droplet) in totally different accretion patterns, resulting in ice built-up outside the presently protected areas. This accretion could cause control difficulties or even such a drag increase and lift loss that the aircraft can simply not maintain level flight.

To give an example, wing boots usually cover the front 6-8 % of the wing chord. In large droplets flight tests, accretion has been observed up to 20 %-25 % of the chord ! An aggravating phenomenon may result from the fact that these large droplets situations are often encountered at ambient temperatures around freezing. The influence of kinetic heating and temperature may result in droplets melting on impact, flowing back and refreezing ("runback" effect), resulting in ice build-up on an even greater airfoil area.

The first solution that comes to mind is increasing the area protected by the boots. This results in an immediate gain in margins for the aircraft encountering large droplet icing, especially since accretion rate does not seem to be very high (1 mm/mn ?). This gives the crew more time to detect the situation and alter the flight conditions to exit this potentially dangerous situation. This should not however be considered as a solution covering all possible icing situations, and should not result in overconfidence by the pilots.

It must be emphasized that this solution is ultimately self-defeating, since the suspected meteorological conditions outside Appendix "C" have not been clearly quantified and are not likely to be in the near future, since we are addressing statistically infrequent situations, and progressively less frequent with worsening precipitation parameters.

Computer simulations show that extreme situations can result in extensive accretion areas, reaching 30 % of the chord or even the entire aircraft...

It is clear that increasing the protected area up to protecting the entire aircraft is not a practical proposition, for all sorts of reasons : cost, weight penalty, power consumption for thermal systems.... This stands true for purely pneumatic systems as well as hybrid systems, incorporating for example electrothermal elements behind the boots.

We strongly doubt that a reasonable deicing system could be developed that would allow an aircraft to fly without restrictions in ANY situation that could be encountered in the real world.

In this perspective, we consider that the way to go may well be to design a system covering the present Appendix "C", which, after all, has been proven by experience to cover most icing situations, including eventually some designs provisions to improve margins, like wider coverage for outer wings boots.

Large droplets icing conditions can be detected very efficiently and simply by installing flush icing sensors behind the after edge of a normally dimensioned pneumatic boot (see sketch Fig. 4). The detection of ice accretion behind the "normal" limit of 6-8 % of chord would be a sure hint that the aircraft has entered conditions outside of the certification envelope, allowing the crew ample time to initiate maneuvers to leave the dangerous area. The same type of detector used for in-boot installation is well adapted for that warning role.

Such a system has been developed and is currently being prepared for flight testing (in real airline use) in the near future.

5- Proposed system and summary :

At AERAZUR we are convinced that the pneumatic deicing system remains, for the foreseeable future, the best and most effective solution for inflight ice protection for General Aviation and Commuter turboprop aircraft.

The problems associated with tailplane icing and large droplets icing encounters can be successfully addressed by incorporating recent advances in icing detection technology, by incorporating flush ice sensors in the boots themselves and on the airfoil surface aft of the boot area.

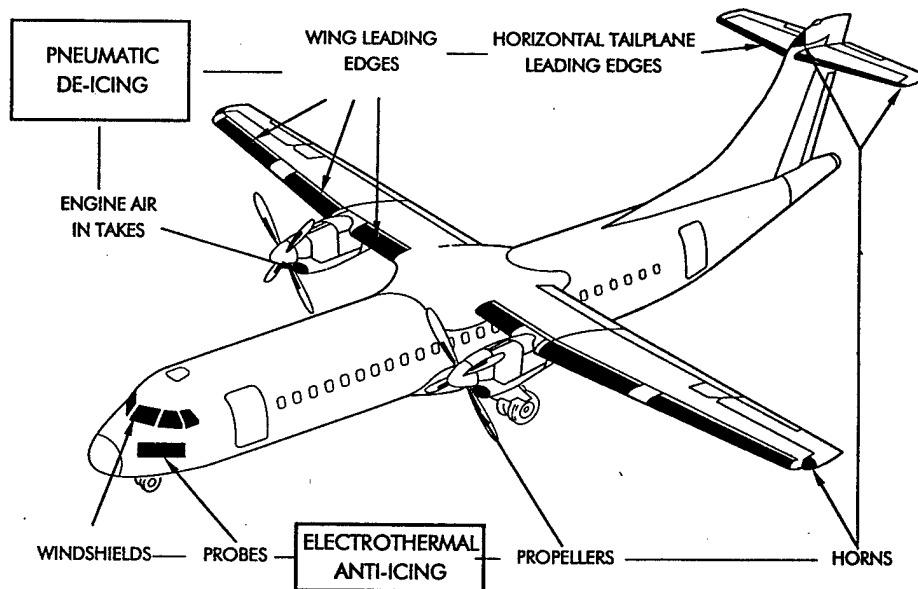
Such a system would effectively detect the onset of ice build-up on the airfoil, trigger the deicing at the most favorable moment and monitor effective deicing, as well as advising the crew of entering an area where icing conditions prevail for which the aircraft was not certificated.

An option for automatic actuation of the deicing system could be offered, further easing the workload imposed on pilots.

The cost increase would be limited compared to the advantages offered, especially if incorporated into a new design from scratch.

We are convinced that the installation of one or both of these systems would result in a significant contribution to increasing the safety of operations in icing conditions.

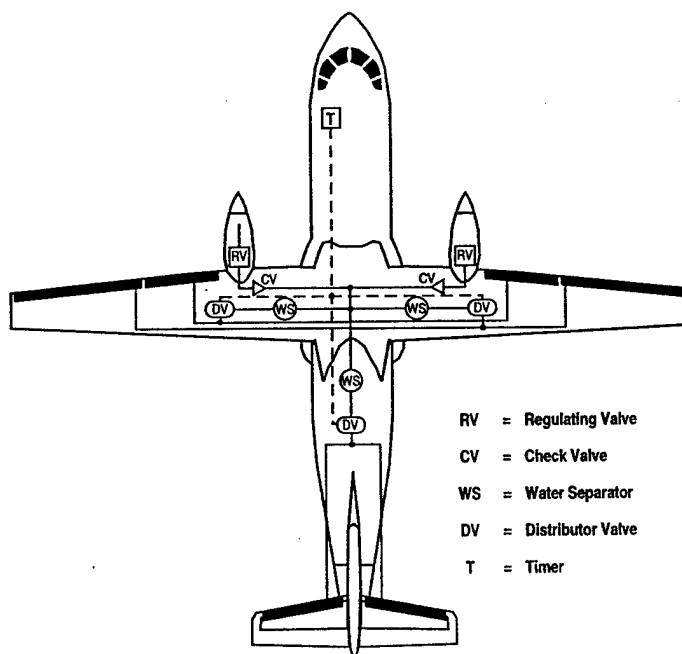
TYPICAL COMMUTER AIRCRAFT ICE PROTECTION SYSTEM



FAA Meeting on Inflight Icing May 1996

AERAZUR Presentation Figure 1

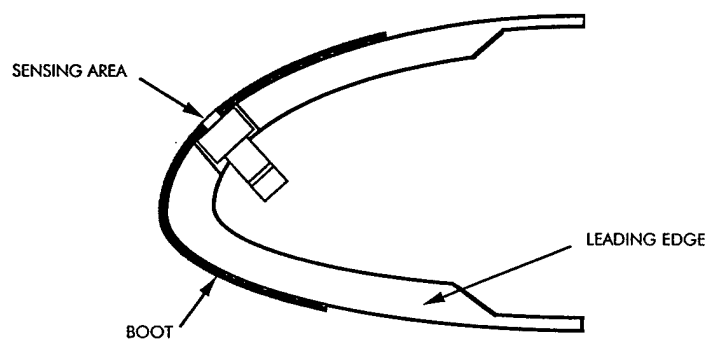
"Conventional" Pneumatic Deicing System



FAA Meeting on Inflight Icing, May 1996

AERAZUR Presentation Fig. 2

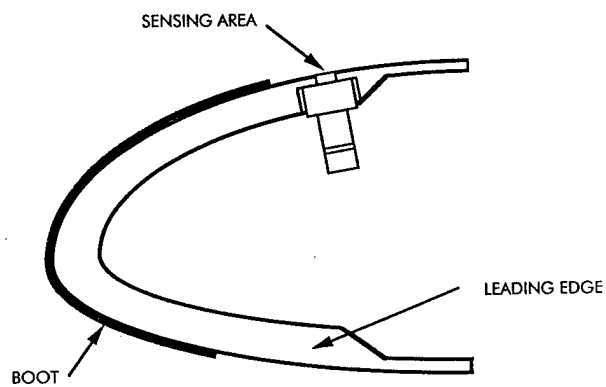
FLUSH IN BOOT ICING SENSOR (PRINCIPLE)



FAA Meeting on Inflight Icing, May 1996

AERAZUR Presentation Fig. 3

LARGE DROPLETS ICING SENSOR (PRINCIPLE)



FAA Meeting on Inflight Icing, May 1996

AERAZUR Presentation Fig. 4

USE OF FLUSH-MOUNTED SMART SKIN ICE SENSORS FOR THE DETECTION/EXIT CRITERIA

Philip Zollinger

Vibro-Meter SA
Route de Moncor 4
1701 Fribourg
SWITZERLAND

ABSTRACT

"I hear pilots saying all the time 'We need help. We need equipment. We need stuff to tell us. We've got iced up tail planes. We've got iced up wings in the night', that sort of thing"¹

Ice has always been a major hazard in aviation. With the Roselawn accident in October 1994 one more problem has come to the forefront: Supercooled Large Droplets (SLD).

The present FAA certification requirements do not take the danger of SLD into account. The existence of such droplets changes the shape of ice-build-up in a way which may exceed the active part of the installed ice protection system. A similar situation exists with tailplane icing², as the ice accretion on the tailplane is often faster than on the wings and may thus exceed the effectiveness of the ice protection system, or may result in ice accretion on the tail without ice accretion on the wing.

The ice detector probe, which has been the only ice detection technology used on FAR 25 Transport category aircraft until now, offers no help. It can only inform the pilot that there are icing conditions. It cannot tell where the ice is accumulating nor how fast the ice build-up is.

What is required is a technology which can detect the limits of ice protection and assess the performance of the ice protection devices.

The Smart Skin Ice Detection System developed by Vibro-Meter presents a cost-effective, simple and reliable solution. Based on certified technology it has undergone several tests including in-flight testing in conditions with SLD. All cases of ice build-up beyond the protected area were detected.

A completely qualified system is now available. In-service evaluation will take place in the near future on a major turbo-prop aircraft.

The same technology is used in the In-Boot Ice Detection System developed jointly with Aératur, and is designed to control and monitor the effectiveness Ice Protection System, using a closed loop system.

¹ Ken WALPER, Transport Canada, from the International Icing Symposium held in Montreal in September 1995

² First International Tailplane Icing Workshop was held in 1991 at the NASA Lewis Research Centre

INTRODUCTION

This paper concentrates on the in-flight icing issue and the main emphasis is on the detection criteria with the objective of providing the pilot with reliable information in time for him to take the necessary measures.

The effect of in-flight icing on the aircraft forms part of the certification procedure. This is much less true for the on-ground scenario, which is covered by the "Clean Aircraft Concept" and therefore shall not be discussed within this paper, as the only common feature is the word ICE.

ICE AND AVIATION

Aircraft in-flight icing is one of the major hazards in aviation. Ice on the airframe decreases lift and increases drag and stalling speed. Therefore aircraft are equipped with anti-/de-icing equipment to ensure safe flight within the certification envelope as defined by the FAR standards.

The accumulation of ice on control surfaces affects the controllability of the aircraft and ice accretion on specific sensors (such as angle of attack sensors) can result in unreliable information.

In-flight icing has been or is suspected to be the cause of many accidents. Over 60 of these accidents are considered to have resulted from tailplane icing.

With the accident at Roselawn in October 1994 a new and serious problem has surfaced: Supercooled Large Droplets (SLD).

SUPERCOOLED LARGE DROPLETS (SLD)

The analysis of the Roselawn accident resulted in new meteorological findings. At an altitude of around 10'000 ft droplets of up to 400 μm were found.³ These are now generally referenced as SLD.

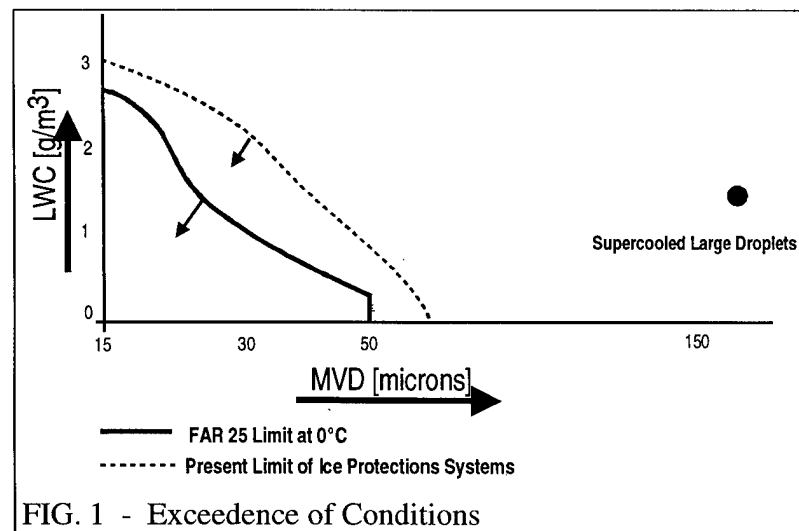
This meteorological situation has been confirmed. Since becoming aware of this phenomenon following the accident at Roselawn, those involved in meteorological research have repeatedly observed it. In the past it was generally thought that this condition could not exist above 2000 ft, where such droplets were thought to precipitate out, or to appear only in mountain regions, according to Prof. Maverick (University of Wyoming). However, this condition may even be encountered at altitudes above 10'000 ft, which encompasses the cruising altitude of many aircraft.

The major concern is that these droplets are far larger than the certification requirements for transport category type aircraft, which are defined at max. 50 μm (maximum

³ Roselawn accident happened at 10'000 ft at around 175 knts (Source Commuter World, Issue April-May 1995)

intermittent over 2.6 nm^4 or at max. $40 \text{ }\mu\text{m}$ (maximum continuous over 17 nm^5). The certification exceedence is shown graphically in Figure 1.

As is shown later, the Medium Volume Diameter (MVD) of the droplets has a major effect on the shape of the ice accretion. As SLD are significantly larger than average droplets, the certification exceedence has major consequences for the present safety of aircraft operations, as no aircraft to date are certified to fly in the conditions which were prevailing during the accident at Roselawn in October 1994.



SLD must therefore be considered as a very probable threat to the aviation world today and this phenomenon must be taken into account by future certification requirements..

TAILPLANE ICING

The tailplane icing problem is characterised by ice accretion on the tailplane, which causes ice-induced stalls, known as ice contaminated tailplane stall, leading to accidents^{6 7}.

The tailplane, being a smaller airfoil, is a more efficient ice collector than the wing. The difference in the ice accretion rate is even greater the higher the liquid water content (LWC). Reports indicate that the accretion rate on the tailplane may be 3 to 6 times faster than on the wing. Further cases exist where there was ice accretion on the tailplane without any ice accretion on the wing.

On aircraft with no ice protection system this may result in ice contaminated tailplane stalls without the pilot having the possibility to react, as there may be no ice seen on the wing. On aircraft equipped with an ice protection system the latter may no longer be effective and thus may also result in an ice contaminated tailplane stall. The ineffectiveness of the ice protection system may be due to the fact that the ice accretion rate on the tail is too high or that the system is not switched on or not onto the appropriate cycling speed, as the pilot controls the de-icing cycling upon visual observation of the wing. Remember on almost all aircraft the tailplane cannot be seen from the cockpit.

⁴ FAR 25 Appendix C Figure 4

⁵ FAR 25 Appendix C Figure 1

⁶ Accidents reported have occurred with 3/16" to 1" thick ice on the tailplane leading edge.

⁷ Accidents occurred mainly between 800 and 2000 ft

This issue is of concern to pilots, as the operating speed of the ice protection system based on boots is selected manually upon visual observation of the wing, which may drastically differ from the actual situation on the tail.

The first FAA Tailplane Icing Workshop was held in 1991, others followed in 1993 and 1994. One directive formulated at these workshops concerned the implementation of ice detectors: "Speed up the implementation of ice detector technology as a practical solution to ice contaminated tailplane stall"⁸. However, to date no in-service aircraft is mounted with built-in ice detectors in the tailplane to monitor the ice accretion. Unless manufacturers are mandated to install such systems, it is very unlikely that they will ever be installed.

PARAMETERS AFFECTING ICE ACCRETION

Significant icing occurs only in clouds or in precipitation composed of supercooled water droplets.

The amount and rate of icing depends on a number of meteorological and aerodynamic factors, including temperature, the median volume diameter (MVD) of the droplets, the amount of liquid water content (LWC) in the path of the aircraft, the fraction of liquid water collected by the aircraft (collection efficiency), the amount of aerodynamic heating and the exposure time. Collection efficiency depends on the size of the aircraft component involved, airspeed, droplet size (MVD) and the angle of attack.

Parameters Affecting Ice Accretion

- Temperature
- Median Volume Diameter (MVD)
- Liquid Water Content (LWC)
- Collection Efficiency
 - Size of Aircraft Component
 - Droplet Size
 - Airspeed
 - Angle of Attack of Aircraft
- Aerodynamic heating
- Exposure Time

These are the main parameters which have to be taken into account for the simulations done to define the ice protection limits.

The temperature range is known and the most critical temperature for ice accretion is towards 0°C, as a result of runback. This is due to the fact that the time for freezing takes longer, the nearer the airfoil is to 0°C.

The range of speed of the aircraft is known for a specific aircraft as well as the range of the angle of attack. With respect to speed, icing coverage will be greater the higher the speed.

The only factors which are uncertain are LWC and MVD.

⁸ Tailplane icing workshop recommendations

As shown in simulations, LWC affects the speed of accretion only, whereas the actual surface of the ice on the aircraft remains the same. Figure 2 shows the accretion of ice on the airfoil at two different LWC values for the same exposure time. As can be seen in the figure, the impingement limit⁹ is not affected. An exceedance of the FAR requirements with respect to LWC could therefore mean that the ice protection system cannot cope with the severe situation, although the coverage is

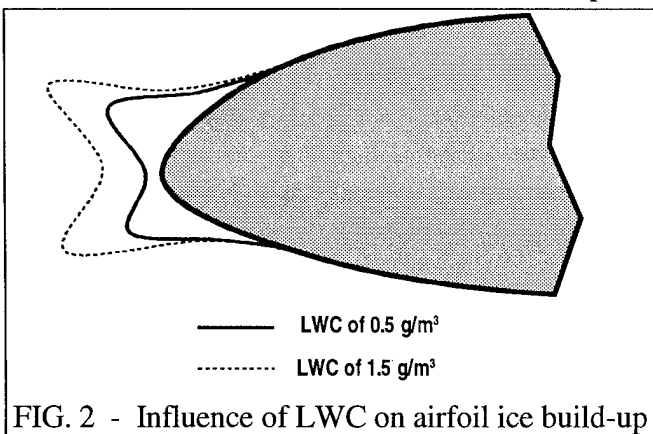


FIG. 2 - Influence of LWC on airfoil ice build-up

sufficient.¹⁰

It is however MVD, which has a major impact on the impingement limit, as has been demonstrated by simulations and flight tests and is shown in figure 3. This is based on the fact that large droplets are more likely to collide with an object moving through air as opposed to following the flow lines around the object. Further, the larger the droplets, the longer the freezing time and therefore the more runback.

This explains the effect of the SLD phenomenon. As SLD are significantly larger droplets than defined under FAR Appendix C, they result in an increased ice coverage on the airfoil with respect

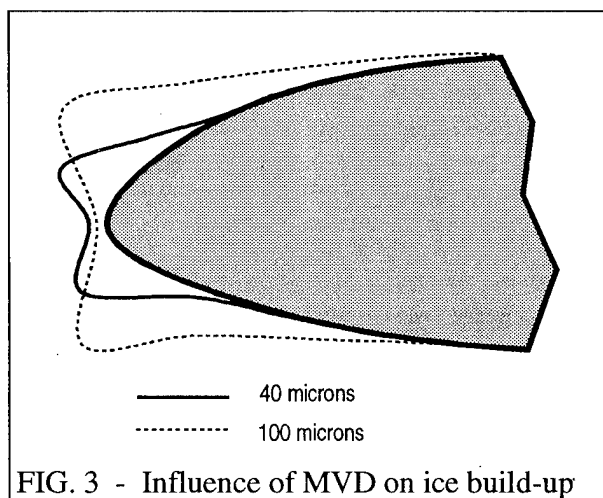


FIG. 3 - Influence of MVD on ice build-up

to the chord. Ice accretion may thus stretch beyond the active area of the ice protection system of the aircraft, certified to current certification limits. Such an ice accretion will not be removed until the saturated air temperature rises above 0°C and may cause uncontrollable performance problems, due to ridges. As we are all aware, this has led to accidents.

PRESENT CERTIFICATION REQUIREMENTS

The required aircraft ice protection is defined according to the manufacturers' specification, which reflects the certification requirements, as defined by the Federal Aviation Authority in the applicable FAR Appendix C. At present, flight into known freezing drizzle or freezing rain is banned for all aircraft.

⁹ Limit of ice accretion on airfoil

¹⁰ This is generally referred to as the SEVERITY of the icing condition as such severity is directly linked with icing rate or LWC

Transport category aircraft must be capable of safe operation in conditions defined under FAR 25, Appendix C, that is, operating an aircraft under defined continuous and intermittent maximum icing conditions.

The definition of ice protection during the design phase is done using simulation codes (ONERA, LEWICE, ...) and aerodynamic performance simulation. The designs are tested according to FAR, which include in-flight icing tests. The protection is based on various proven de-icing and anti-icing technologies in order to meet the certification requirements in the most practical and cost effective way.

The present in-flight certification requirements are limited to ice protection and do not include ice detection. This is the reason why today most aircraft still rely on pilot decision to activate the ice protection system and as such it is the pilot's responsibility based on visual observation.

PRESENT IN-FLIGHT ICE DETECTION

Currently, only Ice Detector Probe type equipment (refer to Figure 4) are used on some FAR 25 Transport Category Aircraft as in-flight ice detection systems. Many aircraft do not have any ice detection systems at all, relying on visual detection by the crew only. This is also true for the turbo-prop aircraft, whose flight envelope is the most sensitive with respect to icing in general, as well as SLD and tailplane icing, due to their long exposure time in the icing environment during a normal flight.

Ice detector probes are designed to give an "ice-detected" signal as long as the aircraft flies in icing conditions. This signal will remain active as long as the aircraft is in icing conditions and will extinguish when this is no longer true. The ice detector probes have a "finger" which is exposed to the free stream airflow. They have an in-built de-icing capability, which is designed to de-ice the probe once ice has been detected and to allow re-accumulation so as to continue to confirm the icing environment. When no re-confirmation is given, the signal resets and thus extinguishes in the cockpit.

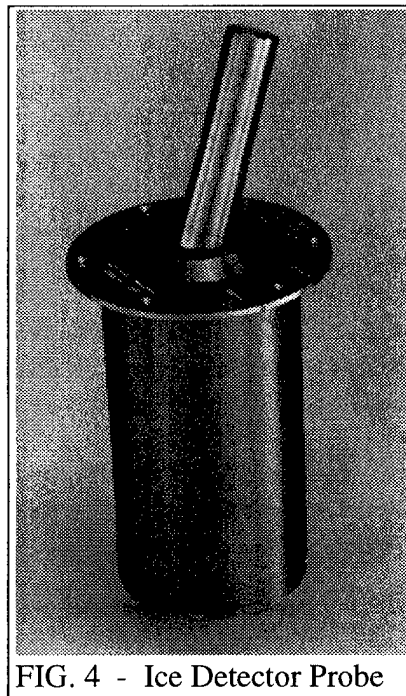


FIG. 4 - Ice Detector Probe

Certain ice detector probes have a severity output. This severity indication is to date purely based on a counter of the internal de-icing cycles and when a given number is reached within a given time then this severity signal will be activated.¹¹ As the ice accretion rate is measured based on the number of de-icing cycles, the severity indication

¹¹ This philosophy is based on a technology used for ice detector probes for over 20 years, which cannot measure the icing rate on the probe directly

may produce misleading results: de-icing will take longer, the worse the conditions are and therefore the severity signal will take longer to activate.¹²

Furthermore, even an Ice Detector Probe with a reliable severity signal would be unable to indicate whether the accretion of ice extends beyond the active zone of the ice protection system (SLD-scenario) and/or whether the ice protection system is working effectively (tailplane scenario)

In general, the pilot uses the ice detector probe information (if available) on an advisory basis to control the on/off of the ice protection system. However he has no feed back about the performance of the system and therefore the pilot must take the correct functioning for granted. As can be seen by accidents due to SLD or tailplane stall, such an assumption may be wrong. This is also true for the automatic system (primary control) used for anti-ice system which are based on an open loop control, using ice detector probes. As the ice detector probes are remotely located from the actual aircraft surface instead of being flush mounted and integrated into the ice protection system, and as they are not anti-iced by the ice protection system, there is no system monitoring potential. Such a primary system activates/deactivates the anti-ice protection system automatically and as such replaces the pilot switch and the pilot action. This philosophy, based on ice detector probes for the control, cannot be applied to de-icing systems, which require a certain ice accumulation to be effective and as such require integral sensors to control the system activation.

The Ice Detector Probe can only be used to indicate to the pilot that the aircraft is flying in icing conditions. The Ice Detector Probe cannot indicate whether the accretion goes beyond the protected area¹³ or whether the ice protection system is effective¹⁴. This limited application of the Ice Detector Probe philosophy was fatal for the accident at Roselawn: An Ice Detector Probe was installed on that aircraft.

Therefore, the present ice detection technology is unable to solve the problems involving SLD and tailplane icing.

THE PROBLEM

The problem can be divided into three aspects :

Certification gap: Due to the gap between the actual icing environment - SLD and tailplane icing - and the current certification requirements, the presently certified aircraft cannot assure a safe flight in all icing conditions.

Technology: The present ice detection technology is not sufficient, as it supplies no information on the performance of the ice protection system, no information on the actual

¹² Although technology exists (refer to figure 4), which could include direct icing rate measurement due to the specific unique measuring principle used in the Vibro-Meter ice detector probe

¹³ Supercooled Large Droplets problem

¹⁴ Tailplane Icing problem

situation on the tailplane and no information on the accretion of ice beyond the active zone of the ice protection system. Therefore, new technical solutions must be found.

Implementation: Aircraft manufactures are only likely to apply the current FAR standards and specific advisory directives, in order to remain competitive and to avoid the possibility of having to retrofit whole fleets. Therefore, clear action by the authorities is required if the new technology is to be implemented on future aircraft.

POSSIBLE SOLUTIONS

As has been shown, the present ice detection technology (Ice Detector Probe) is unable to provide a complete or even adequate solution to the icing problem.

The following options are available at present¹⁵:

1. Change of certification requirements
2. Visual detection of limits of ice protections
3. Detection of limit of ice protection by on-board equipment

CHANGE OF CERTIFICATION REQUIREMENTS

Theoretically, the certification requirements could be changed to reflect the new meteorological findings. However, to date, real maximum icing values for simulation and evaluation are not known and the impact on the design of the aircraft is substantial. This impact, as experienced by the author, suggest it will not be technically feasible given the economical constraints of today's aircraft manufacturers.

Furthermore, even if such a solution were technically feasible, all test installations (wind tunnels, simulation etc.) would need to be re-equipped and re-qualified to meet the changed specifications and this would entail a long implementation time, estimated to be several years at the minimum. A solution is, however, required now. The operators are flying their aircraft today in conditions which exceed the certification requirements of the subject aircraft and are presently relying fully on pilots being able to recognise any adverse situations. This is not acceptable for the operators and has been recognised as a problem by the FAA, who initiated this International Workshop.

VISUAL DETECTION OF LIMITS OF ICE PROTECTION

The FAA has decided to take the conservative approach which has the smallest impact on the actual cost of implementation and operation.¹⁶

ATR has defined the pilot side-window¹⁷ as the visual cue for SLD. This was a result of simulated SLD conditions behind the tanker aircraft at Edwards AFB, with max. 200 μm

¹⁵ The meteorological now-/forecasting is not considered as a short term solution by the author

¹⁶ According to Air Cosmos (Issue No. 1549, Friday 19. Jan 1996) this will imply no less than 20 regulations

droplets. But can this approach based on visual detection be justified? Does it fulfil all requirements? Can the pilots have full confidence in visual cues? The following concerns arise, according to the author:

- Visual cues do not provide a clear and unambiguous signal
- Visual detection based on cues depends on human recognition of the risk
- Visual cues cannot cover the icing rate criteria
- Visual cues do not necessarily reflect the airfoil of importance
- Visual cues cannot cover the tailplane issue
- Visual detection requires visibility which often may be impaired in icing conditions
- Visual detection makes the pilot responsible for the detection
- Visual detection gives no indication on the effectiveness of the ice protection system

The visual detection option relocates the responsibility for safe flight in icing conditions into the cockpit and onto the shoulders of the crew - away from the regulators and the manufacturers. The main factor thus remains with the pilot, who still has no assurance that the ice protection system is performing as required for a continued safe flight.

As a result visual detection is not considered an adequate solution by the author as an answer to the in-flight icing problems of SLD and tailplane.

DETECTION OF LIMIT OF ICE PROTECTION SYSTEM BY ON-BOARD EQUIPMENT

The problem of tailplane icing and of SLD exists and needs to be treated now. The optimum solution of changing certification requirements remains a valid approach, so long as the necessary detection technology to identify these changed certification requirements does not exist. But it does exist.

Therefore, the best solution, in terms of cost, practicality and speed of implementation is to identify the problem: to install a system on-board that will detect and indicate clearly to the pilot that the accretion rate has grown beyond the protected areas of the ice protection system (SLD-Scenario) or that the ice protection system is no longer effective or that ice is accreting on the tailplane (tailplane scenario).

As has been discussed the present technology - the ice detector probe is not able to furnish the necessary information.

Nor is visual detection an adequate answer.

¹⁷ Please note that the pilot side window of the ATR aircraft is not heated

A. DETECTION OF ICE ACCRETION BEYOND THE LIMIT OF THE PROTECTED AREA

Technology that indicates to the pilot that the impingement limit has been reached is available and has been proven to be effective on several occasions, including during the in-flight SLD icing tests at Edwards AFB.

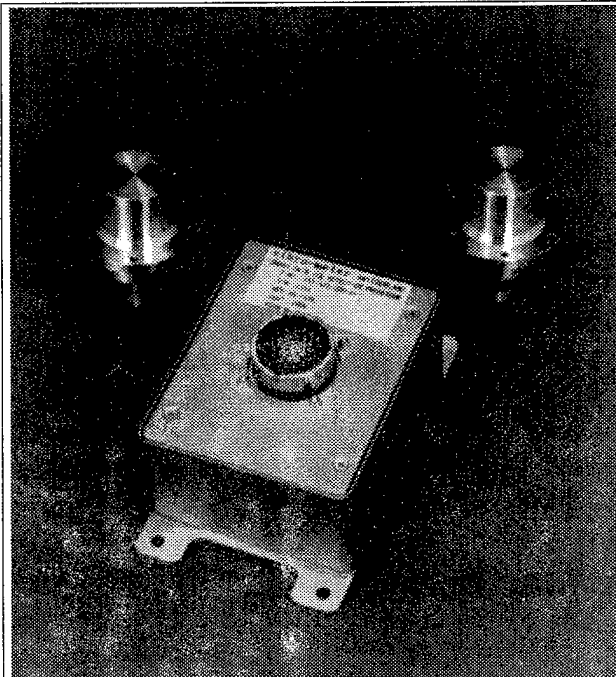


FIG. 5 - Vibro-Meter
Smart Skin Ice Detection System

Such a system is the SMART SKIN ICE DETECTION SYSTEM from Vibro-Meter and is shown in figure 5 (Refer also to figure 7).

The prototype system has been flight tested during in-flight tests behind a tanker. The results obtained on the Vibro-Meter System were eight (8) detected situations out of eight (8), which had ice accretion behind the boots, out of a total of nine (9) tests flown in simulated conditions with supercooled large droplets beyond the FAR 25 Appendix C requirements. This is a 100% detection success rate. One test did not result in ice accumulation beyond the active zone of the boots. This system exhibited superior performance to all other systems under evaluation in all cases.

The system is based on two sensors mounted on the upper wing at the surface at the upper limit of the activation zone of the ice protection, i.e. the boots for that particular aircraft.

The philosophy of the ice detection system installed on the ATR aircraft during the Edwards tests in March 1995 explains clearly the value of such a system.: "The threshold we had set on the ice detector was one millimetre, about 7%, normally the limit of the active part of the boot. The time to reach one millimetre, ... , is around 2 to 3 minutes at the maximum, and the time to get the thickness for which the ridge could effect the aileron is around 15 to 17 minutes."¹⁸

In the mean time a qualified prototype system is available. The system is being flight tested and is due for In-Service Evaluation by various operators.

¹⁸ Didier Caihol, Aérospatiale, from the proceedings of the International Icing Symposium held in Montreal in September 1995. The 7% is with respect to wing chord.

B. ICE PROTECTION ACTIVE ZONE PERFORMANCE MONITORING

Vibro-Meter is working together with Aératur on an In-Boot Ice Detection System development. The design objective of this system is to automatically control the de-icing cycle and to monitor the effectiveness of the de-icing by measuring ice accretion directly on the boot surface. The flush mounted ice sensors are integrated into the active zone of the boots and are de-iced by the boot-activation. The result of wind tunnel tests, showing

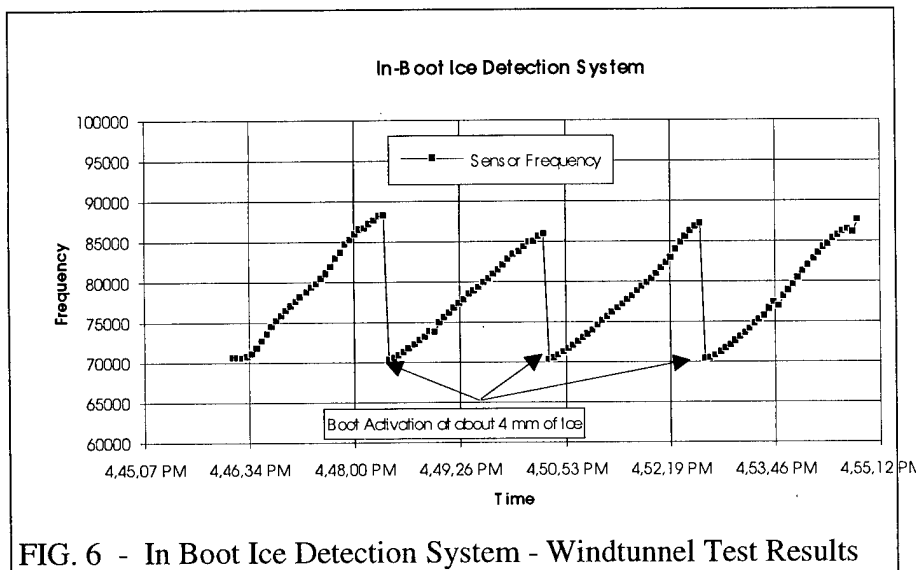


FIG. 6 - In Boot Ice Detection System - Windtunnel Test Results

ice accretion as a function of time measured by the integrated sensors, is shown in figure 6. The ice accretion is measured directly by the sensor and reflects the ice stiffness (thickness). When a certain stiffness is reached the boot is activated. The boot activation de-ices the sensor as can be seen clearly in the figure. The tests were done at T_{sat}^{19} : -10°C , MVD: $20\text{ }\mu\text{m}$ and LWC: 0.9 g/m^3 . These results show clearly that ice accretion rate can be measured, too.

The In-Boot Ice Detection System will not only automate the de-icing control, but will also reduce pilot work load resulting in safer operation. It will also optimise boot activation, as the boots will only be activated when necessary, which will result in minimal direct maintenance costs, as the boot life is to a large extent dependent on the activation cycles.

The system concept of the In-Boot Ice Detection System covers and includes the exceedence criteria. The pilot will be made aware of a situation in which the ice protection is no longer effective. The same philosophy is also being promoted for Anti-Icing System Design in order to attain a closed-loop system.

The advantageous features of the design are given below:

- Sensor shall measure ice accretion on the active zone of the boot
- Sensor shall be de-iced by the boot activation
- Sensor shall be an integral part of the boot
- Sensor integration shall not affect MTBF of boot

¹⁹ Saturated air temperature

An integration of such a sensor is given in figure 7, showing a NACA 0012 airfoil for

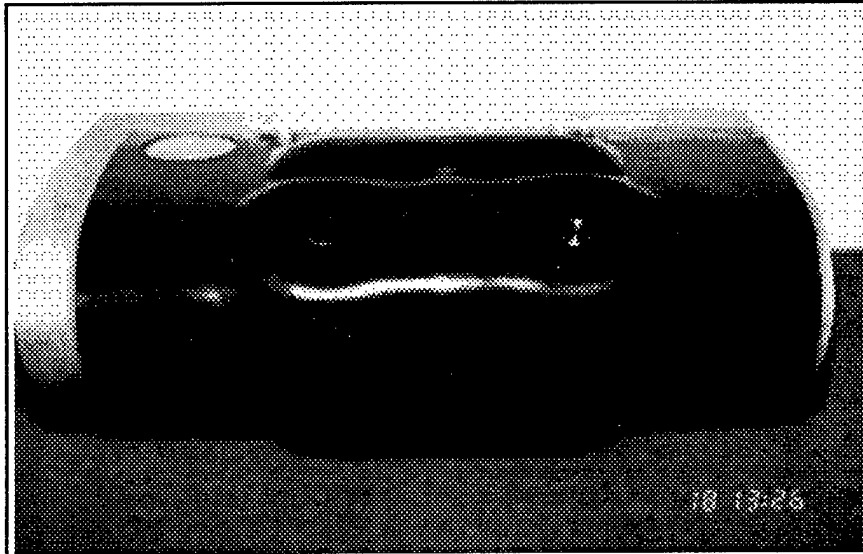


FIG. 7 - Airfoil with In-Boot Sensor and Smart Skin Sensor

laboratory tests. This profile includes a Smart Skin Ice Sensor towards the back at the left and an In-Boot Ice Sensor towards the front at the right.

THE DETECTION TECHNOLOGY

The Vibro-Meter ice sensor detection technology is based on a simple physical system - the mass-spring system. The sensor operating principle is given in Figure 8. The sensor measures directly the physical parameters, based on the principle that the resonant frequency of a solid body will alter with a change in mass and stiffness. Ice is detected using a continuously vibrating sensor diaphragm which is forced into oscillation at its resonant frequency by a piezo-electric material. The resonant frequency is ultrasonic and the maximum oscillation amplitude is very small (under 1 micrometer) so that there are effectively no moving parts.

Ice accretion on the sensor diaphragm increases its stiffness and mass. As the increase in stiffness is the dominant feature it induces an increase in resonant frequency. Water or liquid contaminants increase the mass without increasing the stiffness and thus decreases the resonant frequency. A clear discrimination is therefore ensured.

No contaminant is known other than ice which increases the frequency and as such no false alarms have ever been experienced.

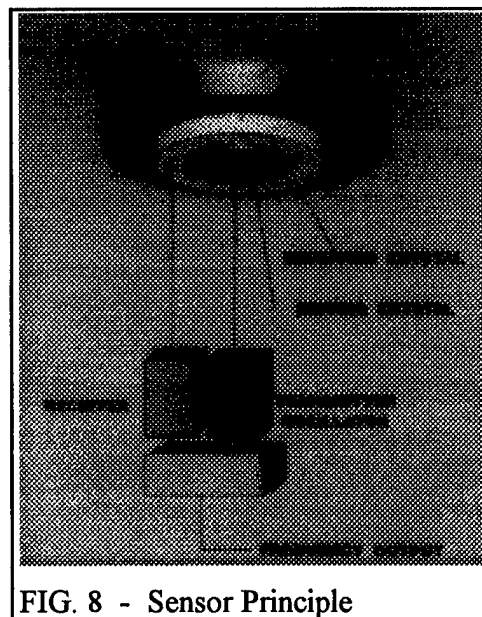


FIG. 8 - Sensor Principle

The principle has not only been validated by practical and experimental experience. It is also FAA certified, and in-service as standard fit on the MD-80 series aircraft for On-Ground Clear Ice detection²⁰. The sensor has also been modelled for computer simulation using an infinite-element model. The results of the correlation between the experimental and the simulated data can be seen in Figure 9²¹. The x-axis zero is the sensor resonant frequency when it is clean, whereas the y-axis is the measurement of ice (positive) and water (negative) in mm.

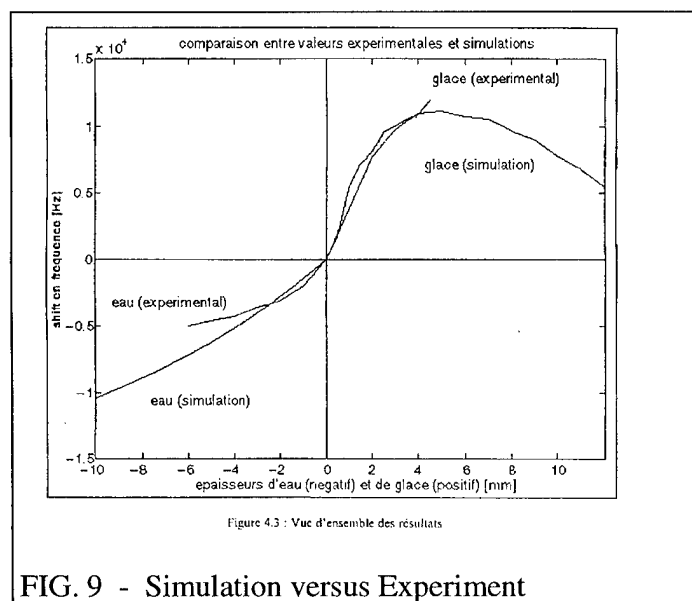


FIG. 9 - Simulation versus Experiment

airfoil or as used for our ice detector probe, into the "finger" exposed to the airflow. As the illustration show the diaphragm may be curved, convex or concave, in order to fit the airframe shape. (refer to figure 4 or figure 10).

The following are further features of the Vibro-Meter ice detection technology, which are maintained thanks to extensive experience and continuous research and development:

- proven high reliability of the sensor of over 100'000 hours experienced
- processing requiring no software
- total system weight of less than 1.5 kg (typical new system with 2 sensors)
- simple double wiring between sensor and processor



FIG. 10 - Curved Ice Sensor

²⁰ The Vibro-Meter Ice FOD Alert System based on two flush mounted sensors installed on the upper surface on the wing to detect clear ice during on-ground operation is standard fit on the MD-80 aircraft since 1990.

²¹ The table is in French (Glacé = Ice; Eau = Water)

EXPERIENCE

For over 30 years Vibro-Meter has gained experience of applying piezo-electric based sensor technology for accelerometers, used mainly for the vibration monitoring and analysis on turbo-jet engines, turbo-propeller and rotor-blades. The same baseline knowledge led in the mid-eighties, to the first flush mounted ice sensor design. This resulted indirectly on the vibration analysis domain skill for which Vibro-Meter is the world leader in engine vibration monitoring.

Such experience has allowed Vibro-Meter to develop an ice sensor which is reliable, light and simple. The hazard of icing has induced Vibro-Meter to constantly seek for optimal solutions to cover the problems encountered. Vibro-Meter has been working in the aerospace icing field for over 10 years now and has constantly invested in the Research&Development of systems to resolve icing detection problems.

The Vibro-Meter ice detection technology is standard fit on the MD-80 aircraft. Further, Vibro-Meter ice sensors have undergone various successful flight tests. Among the numerous flight tests, including a variety on turbo-propeller aircraft, a flush mounted ice sensor was also installed in the engine cowl of the Boeing B-747-400 (refer to Figure 11) during certification testing. It was used to calibrate the ice detector probe. The flush mounted sensor detected ice accretion which was not detected by the ice detector probe!

The latest flight tests conducted during the Edward's Program in March 1995 resulted in a feasible application of the system. The flight tests highlighted the superiority of the system and the reliability of the detection principle with all cases detected during the flight tests. The system is ready.

Further, from the experience gained in the Aerospace field, Vibro-Meter Instrumentation Division is marketing a Road and Runway Contamination Detection System for winter operations based on the same principle.

CONCLUSION

The problem of SLD and tailplane icing exists. Both are a major hazard for aircraft operations, as current certification requirements do not cover such conditions.

A change to the aircraft design certification requirements does not address the urgency of these problems, and does not appear to be feasible in the near future. Visual detection does not represent an appropriate answer.

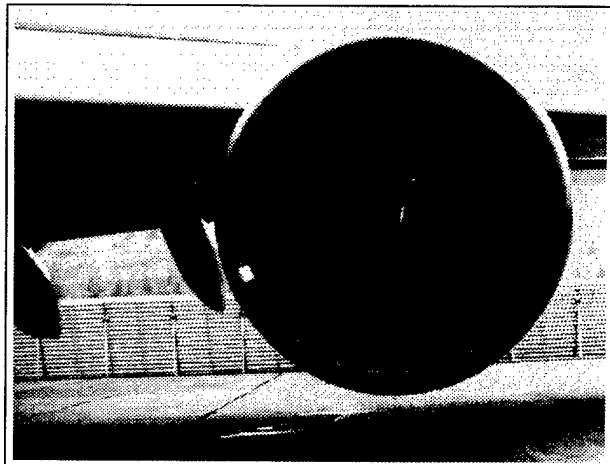


Figure. 11 - BOEING 747-400 with sensor

A feasible and reliable solution is ice detection technology that can detect ice accretion at the location of interest and that can indicate to the pilot that the ice protection system is no longer effective. Such technology is available.

The Smart Skin Ice Detection System is a cost effective, light weight, proven, reliable system to meet the detection/exit criteria for the Supercooled Large Droplets issue. The following quote strengthens the need for such equipment:

"... That's where I think the detectors that are presently available can do the job without necessary qualifying whether it's Appendix C or not. They're just going to tell me I'm outside of my protected area"²²

and the following which shows that the accident at Roselawn could have been prevented:

"... In fact, for this accident to happen, it happened very fast after the aircraft had accreted about one inch of ice behind the deicers. That means that the detectors at that location would have given a warning 15 minutes or 18 minutes before the problem, and just telling that we have to do something to get out of here. ... If you had such a warning system, you would have had some indication a long time before the accident happened. ..." ²³

The In-Boot Ice Detection System is designed to control and monitor the effectiveness of the ice protection system and will detect the tailplane scenario.

The following summarises the answers discussed:

DETECTION OF ICING CONDITIONS (FAR APPENDIX C)

- The answer. The ice detector probe

MONITORING PERFORMANCE (DETECTION/EXIT CRITERIA)

Detection of the limits of ice protection (SLD)

- The answer: The Smart Skin Ice Sensors

Active ice protection zone performance monitoring (Tailplane)

- The answer: In-Boot Sensors or Smart Skin Ice Sensors depending on ice protection

It is time to move.

²² Steve GREEN, Air Line Pilots Association of the United States, from the proceedings of the International Icing Symposium held in Montreal in September 1995

²³ Unidentified Aérospatiale Speaker, from the proceedings of the International Icing Symposium held in Montreal in September 1995

OVERVIEW OF EXPERIMENTAL WATER DROPLET IMPINGEMENT RESEARCH AND FUTURE AVIATION COMMUNITY REQUIREMENTS, INCLUDING SLD EXPERIMENTAL DATA

Michael Papadakis
Associate Professor, Department of Aerospace Engineering
Wichita State University, Wichita, KS 67260

Colin S. Bidwell
Icing Technology Branch, NASA Lewis Research Center
Cleveland, OH 44135

Abstract

A major concern in the design of ice protection systems for aircraft surfaces is the extent and amount of water impingement. The impingement characteristics of aerodynamic surfaces have been historically determined experimentally but in recent years a number of computer codes have been developed capable of predicting the impingement characteristics of aircraft. Validation of trajectory computer codes for icing analysis requires experimental water droplet impingement data for a wide range of aircraft geometries as well as flow and icing conditions.

This paper provides a brief overview of experimental water droplet impingement research starting with the early efforts of NACA in the 1950's. Experimental methods used and a summary of test geometries and conditions are provided. Future research is outlined based on the results of a recent industry survey. Experimental and computational issues related to droplet impingement are discussed.

Introduction

Aircraft flying at subsonic speeds through clouds below 8000 meters can be subject to ice formation on critical aerodynamic surfaces. This can lead to deterioration of aerodynamic performance and handling qualities of the aircraft. Ice accretion results from small supercooled droplets (droplets cooled below freezing), usually 5 to 50 microns in diameter, which can freeze upon impact with the aircraft surface. Ice protection systems are employed on aircraft to protect them from the adverse effects of ice accretion.

Basically, ice protection systems can be classified as either deicing or anti-icing. Deicing involves the periodic removal of a layer of ice by mechanical, thermal or chemical means. Deicing systems typically have low energy requirements; however, periodic ice-removal results in higher aerodynamic penalties. Anti-icing involves the prevention of ice formation on the protected area at all times by using thermal energy or Freezing Point Depressant. These methods minimize aerodynamic losses but either require large amounts of energy or substantial weight penalty. The choice between anti-icing and deicing techniques depends upon the component geometry and its function as well as upon energy requirements.

The design of ice protection systems requires knowledge of the extent of water impingement as well as local and total droplet impingement intensities in order to evaluate the necessary energy requirements. Furthermore, this information is also required for the validation of trajectory computer codes which are an important part of aircraft ice accretion analyses. These computer codes are used by industry as a cost effective tool for evaluating icing protection requirements of aircraft components and to assist in the testing and certification of ice protection systems. Thus, experimental water droplet impingement characteristics on aircraft surfaces are essential to the development and certification of ice protection systems.

The first extensive water droplet impingement database was developed by NACA in the 1950's for two-dimensional cylinders, airfoils, several bodies of revolution and a supersonic inlet (Refs. 1-5). These geometries were tested by NACA personnel using a dye-tracer technique. In 1984 a research program was initiated to further expand and update the experimental water droplet impingement database and to provide much needed impingement data for aircraft inlets and modern wing sections. This program was sponsored by NASA Lewis in Cleveland, Ohio and the FAA Technical Center in Atlantic City, New Jersey. Work was performed by researchers at Wichita State University and Boeing Military Airplanes. The research program was divided into six phases and it was successfully completed in 1993.

Recently, a peer review of NASA Lewis icing research activities and results from an industry survey have indicated that additional water droplet impingement data including large droplet impingement are required for a wide range of modern aircraft geometries ranging from multi-element airfoils to aircraft tails, engine inlets, s-ducts, propellers, to radomes. The large droplet impingement data were requested in response to a recent commuter aircraft icing related accident which has raised the question of the effect of ice accretion due to Supercooled Large Droplets (SLD) on aircraft performance and handling characteristics (Ref. 6 and 7). Preliminary studies of the effect of SLD on the ice accretion characteristics of a full-scale Twin-Otter wing section were reported in Ref. 8. Icing tests conducted with large droplets of 99 and 160 microns MVD demonstrated that an ice ridge formed after the active portion of the deicer boot. Potential adverse effects due to this ice ridge formation on the aerodynamic characteristics of aircraft are presented in Ref. 9 and include large losses in lift, increases in drag and pitching moment and in severe cases aileron hinge moment reversal and aileron snatch.

Currently, the Federal Aviation Administration (FAA) is examining the possibility of adding large droplet icing conditions to the icing certification envelope for aircraft certified under Appendix C of FAR Part 25 as well as applicable FAR Part 23 rules (Ref. 10). If large droplets are included in the icing certification envelope the icing community will have a need for large droplet experimental impingement data. This is because water impingement data for large MVDs is very limited. Thus, extensive research is required to address the experimental and computational issues of large droplet impingement and ice accretion.

The objectives of this paper are: to review experimental water droplet impingement research starting with the efforts of NACA personnel in the 1950's, to address future research efforts for the modernization and expansion of the water droplet impingement database including large droplet impingement data, and to discuss issues related to the validation of current computer trajectory codes. For this paper large droplet icing clouds are defined as clouds with MVDs in the range 50 to 400 microns.

Early Impingement Work Conducted by NACA (1955-1958)

A dye-tracer technique for measuring local impingement efficiency on aircraft aerodynamic surfaces was developed by NACA in the 1950's (Ref. 1). In this technique, water containing a small amount of water-soluble dye was injected in the form of droplets into the air stream ahead of the body by means of spray nozzles. The surface of the body was covered with an absorbent material upon which the dyed water impinged and was absorbed. At the point of impact and droplet absorption, a permanent dye deposit (dye trace) was obtained. The impingement limits were obtained directly from the rearmost dye trace on the absorbent material.

The data analysis consisted of removing the dyed blotter strips from the body and punching out small segments of the blotter material for the determination of local impingement characteristics. The dye was dissolved out of each segment in a known quantity of water. The weight of dye in this solution was determined by the amount of light of a suitable wavelength transmitted through the solution by use of a calibrated colorimeter (colorimetric analysis). The weight of water which impinged at any surface location per unit time was determined from the weight of dye collected per unit area and from knowledge of the original concentration of the dye in the water droplets.

The liquid water content in the cloud was determined using an aspirating device (Refs. 1,2). This device consisted essentially of a tube which sucked in the approaching air and cloud droplets at the free stream velocity (inlet velocity ratio 1) so that both the air streamlines and droplets entered the tube along straight-line paths. The dyed droplets were deposited on a filter mounted within the tube, leaving a dye trace which could be analyzed using colorimetric analysis. The droplet size distribution was determined by comparing experimental local impingement rates on cylinders of different sizes with theoretical predictions of droplet trajectories and impingement points using a differential analyzer.

Between 1955 and 1958 NACA personnel developed a water droplet impingement database for a wide range of cylinders, airfoils sections, bodies of revolution and a supersonic inlet. Table 1 provides a selected list of test geometries and conditions used by NACA personnel for water droplet impingement testing. For most test configurations, the NACA method was sufficiently accurate. The error in evaluating maximum local impingement efficiency varied from 10 to 25 percent (Refs. 1,2). The major limitations of the NACA method included reduced spatial resolution and a laborious and time consuming process for reducing the experimental data. In addition, the uncertainty in measuring the LWC and MVD values of the spray clouds used in the impingement tests was considerable.

WSU/Boeing/NASA/FAA Impingement Research (1984-1993)

The database developed by NACA was limited in scope and in particular was confined to geometries of interest to the aviation community in the 1950's. In addition, three dimensional impingement data were limited to bodies of revolution. Thus, in 1984 NASA and FAA sponsored a new research program to expand the impingement data-base. During this research program an experimental method, similar to the one used in the early 1950's by NACA researchers was developed for measuring local impingement efficiency (Ref. 11). A new method for extracting the impingement data from the blotter strips was also developed. In this method the amount of dye trace on a blotter strip obtained in a given time interval was converted into local impingement efficiency distribution using a laser reflectance method.

To generate the required spray clouds for the impingement tests a twelve nozzle spray system was fabricated. This system was designed to have a very fast on/off response because the spray duration had to be very short (approximately 2-4 sec) to avoid saturation of the blotter paper. For the laser reflectance method to be accurate the dye penetration into the blotter paper had to be kept to a minimum.

To extract the impingement data from the dyed blotter strips the blotter strips were illuminated with a He-Ne laser and the laser light reflected from the blotter was measured using a silicon photodetector. Spatial variations in the concentration of dye on the blotter strips were related to the amount of measured reflected laser light from the blotter surface with the use of a calibration curve (Ref. 11). Low reflectance values corresponded to large dye mass per unit area of the blotter paper while large reflectance values corresponded to low dye mass and therefore low water impingement. Preliminary tests showed that the laser reflectance method was significantly more efficient than the method of colorimetric analysis used in the 1950's by NACA personnel.

The large number of blotter strips obtained from the wind tunnel tests were reduced by an automated processing system which was designed and manufactured during the course of the research program. Briefly, the system consisted of a laser reflectometer and a digital data acquisition system. The laser reflectometer converted dye distribution on the blotter strip into reflectance and then into local impingement efficiency using specially designed software (Ref. 11).

To determine the local impingement efficiency distribution on the surface of a body the local water impingement rate obtained with the laser reflectance method was normalized with the liquid water content (LWC) of the spray cloud. The LWC was obtained with a device called the "reference collector" which was designed to have a collection efficiency close to 1. LWC measurements were made at several locations within the test area to minimize the effect of cloud non-uniformity on the experimental data.

Preliminary impingement tests were conducted in the NASA Lewis Icing Research Tunnel (IRT) in June of 1985 to verify the experimental procedure and the data reduction method.

During these tests impingement data were obtained for a two inch diameter cylinder, a four inch diameter cylinder and a NACA 652-015 airfoil section. The new impingement data were found to be in very good correlation with analytical data and with experimental data obtained in the 1950's.

The first series of impingement tests were conducted in September of 1985 in the NASA IRT for a period of four weeks. The geometries tested included a four inch cylinder, a NACA 652-015, an MS(1)-0317 supercritical airfoil, three simulated ice shapes, an axisymmetric engine inlet model and a Boeing 737-300 engine inlet model. Details of the configurations tested are given in Table 2. The second and final series of impingement tests were performed in the IRT facility during April of 1989 and lasted for approximately four weeks. The geometries tested during this phase of the research program included two simulated ice shapes, a Natural Laminar Flow airfoil section NLF(1)-0414F, an infinite span 30 degree swept MS(1)-0317 wing, a finite span 30 degree swept NACA 0012 wing, and a Boeing 737-300 engine inlet model. Details of the test geometries and conditions are given in Table 3. The experimental impingement data obtained during these tests can be found in Refs. 11,12. During the last phase of this research program significant improvements were made to the data acquisition system used to store and analyze the impingement results. In summary, the water droplet impingement research program conducted between 1984 and 1993 was very successful and considerably expanded the impingement database.

Research Program to Modernize the Impingement Database

Current and Future Research Activities

In response to the recommendations made by its industry peers the NASA Lewis Icing Technology Branch initiated a new research program in August of 1995 to modernize and expand the experimental water droplet impingement database for aircraft surfaces. A grant was awarded to Wichita State University to develop a test matrix which will address the industry requirements, to improve the experimental and data reduction methods and to begin development of the required impingement database.

Industry Survey

During Phase I (August 7, 1995 - March 9, 1996) of this new research program an industry survey was conducted to identify test geometries and conditions to be considered for the next series of water droplet impingement. Participants of this survey were invited to attend a workshop at NASA Lewis on December 8, 1995, to discuss concerns, experimental tasks, priorities, test models and test conditions and to help define a test matrix for the first series of the new impingement tests to be conducted in 1997.

A total of 54 surveys were sent out. The survey participants were chosen from a database kept by the NASA Lewis Icing Branch of all known icing related persons. Surveys were sent to anyone that was remotely interested in the goals of this program. About 50% of the surveys were received back. Table 4 shows a summary of the survey participants by group. Table 5 shows the participation by company. Table 6 shows the types of

geometries requested by group. As could be imagined from the diversity of the surveyed groups the number and type of geometries and test conditions were diverse. Geometries requested ranged from wings, inlets, S-ducts to radomes. Conditions specified included drop sizes from 15-4,000 microns, airspeeds from 0-500 mph, a wide range of angles of attack and inlet mass flows. Table 7 provides a summary of models, test conditions, and test priority given by the survey participants broken down by geometry class.

In general, the survey participants desired data for impingement limits, impingement efficiency, and total impingement. The overall importance of impingement data as rated by the respondents and typical usage of these data are summarized in Table 8.

Experimental Method for Future Impingement Tests

Future impingement tests will be conducted in the NASA Lewis Icing Research Tunnel (IRT) facility described in Ref. 13. The choice of this wind tunnel facility is based on availability, size of test section, availability of a suction system for simulating inlet and S-duct flows, force and pressure instrumentation, spray facilities, and experience with nozzle location for obtaining a uniform cloud. Three entries are currently planned to test approximately 20 to 24 test geometries for a wide range of test conditions.

The dye tracer technique described in Ref. 11 will be used with an improved spray system that will permit more precise control of the water droplet spray parameters. Pressure transducers will be added to both the air and water lines connected to each nozzle in order to monitor the performance of the system during each test. In addition, a flow meter will be added to the main dyed water supply line to monitor the volume flow rate during each spray. The spray system will be controlled by a Personal Computer (PC) which will activate the solenoid valves controlling the air and water flow. Software will be developed to store and process all spray system parameters recorded during each test.

The Standard IRT nozzles used during the 1985 and 1989 impingement tests will be replaced by the IRT Mod-1 nozzles which are capable of generating clouds with MVDs in the range 9-190 microns (Ref. 14). In addition, the Mod-1 nozzles have a lower flow rate than the Standard nozzles and this will permit longer spray times than those used in previous tests (Ref. 15). The droplet distribution, MVDs and LWC of the spray clouds generated by the twelve nozzles of the spray system will be measured at various spanwise locations in the IRT test section by NASA personnel. These measurements will be more representative of the cloud characteristics than the single nozzle measurements used during the 1985 and 1989 impingement tests. Currently, droplet clouds with MVDs of 12, 20 and 160 microns are being considered for the next series of impingement tests which will be conducted in 1997.

The collector mechanism which was developed during the 1984-1993 research effort will be used, along with a new collector device, to measure the local LWC required for reducing the impingement data. The collector impingement efficiency will be determined for the new MVD sizes using computer codes. The new collector device will be capable of providing a more detailed distribution of the local LWC variation within the test area of

interest. This new device will be a grid consisting of beams with the same cross section and size as the original collector mechanism and will span the entire impingement area (2 ft wide by 3 ft high).

A New Automated Data Reduction System

The automated laser reflectometer used in the 1980's will be replaced with a new automated data reduction system. The main objective in developing a new automated data reduction system is to significantly reduce the time it takes to analyze the data. This will permit evaluation of the experimental results immediately after an impingement test and it will allow for corrective action to be taken if any discrepancies are observed in the data.

The new automated data reduction system will make use of a modified reflectance method based on a CCD camera and it is anticipated that it will be an order of magnitude faster than the laser reflectometer in extracting impingement data from the dyed blotter strips. Early tests conducted at Wichita State University using an 8-bit Cohu 4080 CCD camera with a Dipex frame grabber in the fall of 1992 showed that such a system can be used to analyze experimental water droplet impingement data. However, it was determined that a system with resolution higher than 8-bits was required for accurate data analysis. Recently, Bragg et. al (Ref. 16) developed a method based on a 14-bit CCD camera which was used to accurately extract impingement data from dyed blotter strips. This demonstrates the viability of CCD cameras for reducing impingement data.

Tentative Test Matrix for 1997 Impingement Tests.

A preliminary test matrix for the 1997 impingement tests was developed based on an industry survey and a workshop held at NASA Lewis on December 8 of 1996. Note that the test matrix includes test conditions with large droplets of MVD 160 microns. This matrix (see Table 9) will be distributed to all survey participants by June of 1996 for further input so that a final test matrix can be developed. Test models and conditions were selected based on priorities gleaned from the industry survey and the workshop. Another factor considered in selecting the test models was model availability. The test matrix includes one test model used in the previous tests to provide sufficient reference points for validating the new experimental data. From Table 9 approximately 295 runs will be needed to complete the first series of impingement tests. The estimated wind tunnel time required for the installation of the spray system, installation of test models, aerodynamic data acquisition, and to complete the impingement tests is 35 - 40 days (approximately 7 to 8 weeks). Over 3500 blotter strips will be produced during these impingement tests.

Computational Issues Related to Droplet Impingement

The use of analytical tools has become very popular for the design and certification of deicing systems in the last several years. The popularity increase is due to the cost effectiveness of the tools, the proliferation of fast, low cost computers and the increased acceptance of the codes. At the heart of all of these methods is a trajectory code. Trajectory codes have three basic elements: a flow code, a trajectory integration scheme,

and a collection efficiency calculation scheme. Many trajectory codes are available to calculate the collection efficiency for 2-dimensional and 3-dimensional geometries (Ref. 17-26). These codes have similar trajectory integration and collection efficiency routines. The main difference between these codes is the way in which the flowfield is computed. The flow codes can be panel codes, structured and unstructured grid based Euler, full-potential or Navier-Stokes codes. When properly validated and used these tools can provide large cost savings in the design and certification of aircraft.

The validation issue is a complex one for the trajectory codes. Theoretically if a tool has the correct model, it has been debugged properly, and if favorable agreement has been shown for several points then that code should be validated and should be able to be used with complete confidence if used properly within its design envelope. In reality though favorable agreement is expected for a large amount of data throughout the design envelop. The analytical tools are only validated for conditions and geometries for which favorable agreement has been previously shown. Before the codes can be used for new geometries and conditions, experimental data must be generated and favorable agreement must be shown. This philosophy is due in part to cynicism and in part to conservatism. It has been said that research is 98% failure and in the realm of flight safety failure is not acceptable, hence tools must be continuously checked and reevaluated for new conditions and configurations. This system is not the most cost effective but it does err on the side of conservatism. The above definition of validation in essence obviates the problem. Many conditions must be met to prove validation none of which are easy to meet. The proper model must be employed. The code must be free of bugs. This can be difficult for codes approaching 30,000 lines. Favorable agreement must be shown with the data. How does one define favorable. The code must be used properly. This can be troublesome with new users who are not familiar with the tool. The code must be used within the design envelope of the tool. It is difficult sometimes to tell exactly where a tool is appropriate and where it is not appropriate and engineers want engineering solutions. Because all of these questions cannot be answered for an analytical tool a more conservative approach is taken wherein a tool is only considered validated for a range of geometries and conditions for which positive comparison has been shown. The tool can only be used with confidence for those geometries and conditions which are sufficiently similar to those for which previous validation has been shown. As the size of the validated range increases the code gains wider acceptance.

For trajectory codes validation data comes in the form of flowfield and collection efficiency information. The flowfield data is used to validate the flow code while the collection efficiency data is used to validate the trajectory code. The flowfield code validation is a separate issue and is usually handled during assimilation with the trajectory code. The validation of the trajectory code is done for the most part by showing favorable agreement with collection efficiency data.

The main problem in validating trajectory codes using experimental impingement data is defining favorable agreement. The evaluation process is at best subjective for two reasons. It is hard to generate an exact experimental curve because the impingement data

is statistical in nature and because only a small number of samples are taken (3-5) for each test condition. Additionally, the insensitivity of the method to small amounts of dye makes the exact determination of impingement limits difficult. Figure 1 shows a typical collection efficiency comparison between prediction and experiment. In judging the quality of the comparisons the following criteria are used:

- a) general shape of curve,
- b) the analytical curve position within the repeatability band,
- c) the location and size of the maximum collection efficiency and
- d) agreement with the impingement limits.

In general, trajectory codes have shown good agreement with the current experimental data-base for these criteria with the exception of impingement limits. The codes tend to overpredict the impingement limits. This is good from a safety standpoint where one wants to err on the side of conservatism but bad from a design standpoint where one would like to minimize system cost. The problem of overpredicting the impingement limits is compounded by the fact that previous design methods which used the experimental data have a good safety record and that the experimental impingement limits agree well with experimental icing limit data which is the main driver in designing and certifying an ice protection system. The agreement in the limits between the two experimental methods is probably because both methods involve measuring deposition generated from the same spray system. This also suggests a reason for the difference and a way to rectify the problem. Trajectory codes predict impingement limits while the two experimental methods measure icing limits. It may be that the codes are predicting the impingement limit accurately but that there is so little water accumulation near the impingement limit that it is not discernible in the impingement tests or in the icing tests. If the trajectory codes could be used to generate icing limits instead of impingement limits then the comparison to experiment would be more favorable. If one were to use the trajectory data to generate ice shapes (for a typical condition) and calculate the icing limit (say by some minimum ice thickness) and compare this icing limit to the experimental data then maybe the comparisons would be more reasonable. This method would produce icing limits more consistent with the experimental data and more consistent with the designers wishes (i.e. icing limit not impingement limit) and allow for a more optimal design. Figure 2 depicts such a type of calculation and the associated improvement in comparison with the experimental data.

Recently the applicability of trajectory codes to the large droplet regime (50-400 μm) has been questioned. For large droplets and large droplet Reynolds numbers flattening and breakup can occur. Breakup is a very large droplet problem ($\sim 3000 \mu\text{m}$) well outside of the large drop size range considered here. Droplet flattening can occur for droplet Reynolds numbers greater than 90. The flattening can result in a deviation from the standard spherical droplet drag correlations used in many trajectory codes. Codes such as that of Norment (Ref. 17), LEWICE3D (Ref. 19) and LEWICE (Ref. 25) incorporate correlations for droplet Reynolds Numbers greater than 90. Studies have shown that droplet flattening has no large effect on the droplet drag coefficient for droplet diameters

less than 1 mm with droplet Reynolds numbers less than 1000 (Ref. 27-31). This suggests that the flattening is not a factor for the range of droplet sizes considered here.

Summary

Experimental water droplet impingement data are important to the development and certification of aircraft ice protection systems. In this paper a brief summary of experimental impingement research conducted since the 1950's was presented. The majority of the experimental water impingement data available today were obtained by NACA personnel between 1950 and 1958 and by WSU/Boeing researchers in the 1984 to 1993 time period. Recently a peer review of NASA Lewis icing research efforts has indicated that additional impingement data are needed. Results from an industry survey conducted in the Fall of 1995 show that additional experimental impingement data are needed for a wide range of geometries and test conditions. Furthermore, industry members discussed the need for developing large water droplet impingement data. Impingement data for MVDs ranging from 15 to 4,000 microns were requested. A preliminary test matrix for the first series of impingement tests to be conducted in 1997 developed from the survey results and from discussions with industry members during a recent workshop at NASA Lewis was presented. Proposed modifications to the experimental and data reduction methods for conducting the next series of impingement tests which will include large droplet spray clouds with median volumetric diameter of 160 microns were discussed. Issues related to droplet impingement prediction by the use of trajectory codes and trajectory code validation with experimental impingement data were presented.

References

1. Von Glahn, U., Gelder, T.F., and Smyers, W.H. Jr, "A Dye Tracer Technique for Experimentally Obtaining Impingement Characteristics of Arbitrary Bodies and a Method for Determining Droplet Size Distribution," NACA TN 3338, March 1955.
2. Gelder, T.F., and Smyers, W.H. Jr, and Von Glahn, U., "Experimental Droplet Impingement on Several Two-Dimensional Airfoils with Thickness Ratios of 6 to 16 percent," NACA TN 3839, December 1956.
3. Lewis, J.O., and Ruggeri, R.S., "Experimental Droplet Impingement on Four Bodies of Revolution," NACA TN 3587, 1957.
4. Lewis, James P., Ruggeri, Robert S., "Experimental Droplet Impingement on four bodies of revolution", NACA TN 4092, December 1955.
5. Gelder, T.F., "Droplet Impingement and Ingestion by Supersonic Nose Inlet in Subsonic Tunnel Conditions," NACA TN 4268, May 1958.

6. Phillips, E.H. "ATR42/72 Review Focuses on Icing," Aviation Week and Space Technology, November 14, 1994.
7. Phillips, E.H. "FAA Lifts Icing Ban on ATR Flights," Aviation Week and Space Technology, June 5, 1995.
8. Miller, D.R., Addy, H.E., and Ide, R.F, "A Study of Large Droplet Ice Accretions in the NASA-Lewis IRT at Near-Freezing Conditions, AIAA Paper 96-0934, 34th Aerospace Sciences Meeting and Exhibit, Reno, NV., January 15-18, 1996.
9. Bragg, M.B., "Aircraft Aerodynamic Effects due to Large Droplet Ice Accretions," AIAA Paper 96-0932, 34th Aerospace Sciences Meeting and Exhibit, Reno, NV., January 15-18, 1996.
10. Phillips, E.H. "FAA Urges retention of NKC-135A for Icing Tests," Aviation Week and Space Technology, May 15, 1995.
11. Papadakis, M., Elangovan, R., Freund, G.A., Jr., Breer, M., Zumwalt, G.W. and Whitmer, L., "An Experimental Method for Measuring Water Droplet Impingement Efficiency on Two- and Three-Dimensional Bodies," NASA CR 4257, DOT/FAA/CT-87/22, November 1989.
12. Papadakis, M, Breer, M.D., Craig, N, and Liu, X, "Experimental Water Droplet Impingement Data on Airfoils, Simulated Ice Shapes, an Engine Inlet and a Finite Wing," NASA CR 4636, DOT/FAA/CT-TN93/18, December 1994.
13. Soeder, R.H. and Andracchio, C.R., " NASA Lewis Icing Research Tunnel User Manual," NASA TM 102319, June 1990.
14. Ide, R.F, private communication, April 16, 1996
15. Ide, R.F., "Liquid Water Content and Droplet Size Calibration of the NASA Lewis Icing Research Tunnel," AIAA Paper 90-0669, 28th Aerospace Sciences Meeting and Exhibit, Reno, NV., January 8-11, 1990.
16. Bragg, M.B., Sweet, D., Waples, T., and Shick, R. " An Experimental Method for Water Droplet Impingement Measurement," Proceedings of the American Helicopter Society/Society of Automotive Engineers, International Icing Symposium, Montreal Canada, September 18-21, 1995.
17. Norment, H.G., "Calculation of Water Drop Trajectories To and About Three-Dimensional Lifting Bodies," NACA CR 3935, Oct. 1985.
18. Kim, J.J., "Particle Trajectory Computation on a 3-Dimensional Engine Inlet," NASA CR 175023, Jan. 1986.

19. Bidwell, C.S., and Potapczuk, M.G., "Users Manual for the NASA Lewis Three-Dimensional Ice Accretion Code (LEWICE3D)," NASA TM 105974, Dec. 1993.
20. Ruff, G.A., Berkowitz, B.M., "Users Manual for the NASA Lewis Ice Accretion Code," NASA CR 185129, May 1990.
21. Potapczuk, M.G., "LEWICE/E: An Euler Based Ice Accretion Code," NASA TM 105389, Jan 1992.
22. Caruso, S.M. "Development of an Unstructured Mesh/Navier-Stokes Method for Aerodynamics of Aircraft with Ice Accretions," AIAA Paper 90-0758, Jan. 1990.
23. Craig, N., Vu., S, Breer, M., "3-D Particle Trajectory Analysis (PTA) Code - Users Manual," Internal Document.
24. Nathman, J.K., "Ice Particle Trajectory and Ice Accretion Program, Users Manual, Version 2.0," Internal Document, December 1992.
25. Wright, W.B., "Users Manual for the Improved NASA Lewis Ice Accretion Code LEWICE 1.6," NASA CR 198355, June 1995.
26. Wells, S.L., and Bragg, M.B., "A Computational Method for Calculating Droplet Trajectories Including the Effects of Wind Tunnel Walls," AIAA 92-0642, January, 1992.
27. Davies, C.N., "Definitive Equations for the Fluid Resistance of Spheres," Proc. Phys. Soc. London, Vol. 57, 1945 pp. 259-270.
28. Beard, K.V., "Terminal Velocity and Shape of Cloud and Precipitation Drops Aloft," J. Atm. Sci., Vol. 33, 1976, p. 851.
29. Beard, K. and Pruppacher, H.R., "A Determination of the Terminal Velocity and Drag of Small Water Drops by Means of a Wind Tunnel," J. of the Atmospheric Sci., Vol. 26, pp 1066-1072, 1969.
30. Gunn, R. and Kinzer, G.D., "The Terminal Velocity of Fall for Water Droplets in Stagnant Air," J. Meteor., Vol. 6, 1949, pp. 243-248.
31. LeClair, B.P., Hamielec, A.E., Pruppacher, H.R. and Hall, W.D., "A Theoretical and Experimental Study of the Internal Circulation in Water Drops Falling at Terminal Velocity in Air," J. of the Atmospheric Sci., Vol. 29, pp 728-740, May 1972.

Table 1: Test geometries and conditions for NACA impingement tests

NACA TN #	Geometry	MVD (μm)	α (deg.)	V_∞ (mph)
3338	Cylinders (Diam. = 2,4 and 6 inches, Span = 1 ft)	7.6, 12, 14.8	0	175
4092	Spheres (diam 5.92 , 18 inch)	11.5, 12.7, 16.7-18.6	0, 3, 6	181
4092	Ellipsoids (minor axis 30 and 20 inch) with fineness ratios of 2.5 and 3.0	11.5, 12.7, 16.7-18.6	0, 3, 6	181
4092	Conical (30°) with 18.93 inch base radius-RPMs = 0,600, 800, 1200	11.5, 12.7, 16.7-18.6	0, 3, 6	181
3564	NACA 0011, 87 inch chord, 6 foot span	22-59	0 to 9.3	175 - 275
3839	Joukowski 0015, NACA: 651-206, 652-206, 651-212, 652-212, 632-015, 652-216 chord lengths: 13-96 inches	11.5, 16.7, 18.6	0 to 12	175
4151	NACA 65A004 (unswept) 19 inch cord, 42 inch span,		11	275
4155	NACA 65A004 , 6 ft chord, 42 inch span removable L.E., flap angle: -15 to 15°	11-19	0 to 12	125 - 276
4268	Supersonic inlet with - conical center body	11.5, 16.7, 19.4	0 to 4.2	179

Table 2: Test matrix for 1985 impingement tests (all tests were conducted at a freestream speed of 165 mph, each test condition was repeated 2-3 times, Ref. 11)

Geometry	MVD (μm)	α (deg.)	Mass Flow lbm/sec
Cylinder (2, 4 inches in diameter)	16, 20	0	NA
NACA 65 ₂ 015 airfoil (13 inch chord)	16, 20	0, 8	NA
MS(1)-317 airfoil (36 inch chord)	16, 20	0, 8	NA
Rime Ice Shape	20	0	NA
Small Glaze Ice Shape	20	0	NA
Large Glaze Ice Shape	20	0	NA
Axisymmetric Engine Inlet	16, 20	0, 15	17, 23
Boeing 737 Engine Inlet	16, 20	0, 15	17, 23

Table 3: Test matrix for 1989 impingement tests (all tests were conducted at a freestream speed of 165-173 mph, each test condition was repeated 5 times, Ref. 12)

Geometry	MVD (μm)	α (deg.)	Mass Flow lbm/sec
Small Glaze Ice Shape	20	0	NA
Large Glaze Ice Shape	20	0	NA
NLF(1)-414 airfoil (36 inch chord)	16, 20	0, 8	NA
MS(1)-317 airfoil, 30 deg. infinite swept wing (36 inch chord)	16, 20	0, 8	NA
NACA 0012, 30 deg. swept finite wing, (15 inch chord)	16, 20	0, 8	NA
Boeing 737 Engine Inlet	16, 20	0, 15	17, 23

Table 4 - Survey Participants by Group.

ORGANIZATION	CUSTOMERS SURVEYED	SURVEYS SENT	NUMBER OF RESPONDENTS
1. Large Aircraft Manufacturers	2	13	10
2. Business Jet Manufacturers	4	7	6
3. Small Aircraft Manufacturers	3	3	1
4. Helicopter Companies	4	4	2
5. Aircraft Engine/Inlets	6	7	5
6. Military Aircraft Companies	4	4	1
7. Icing Systems Companies	2	3	0
8. Government Research Centers	4	4	0
9. FAA/Universities/Other	9	9	5
Total	38	54	29 (54%)

Table 5. - Survey Participants by Company.

AIRCRAFT COMPANIES	ENGINE AND INLET COMPANIES
Boeing Commercial Airplane Co.- Seattle (8)	Allison Engine Company (2)
Boeing Commercial Airplane Co.- Wichita (1)	GE Aircraft Engines (1)
McDonnell Douglas Aerospace-Long Beach (1)	Rohr, Inc. (1)
Lockheed Martin Aeronautical Systems (1)	OTHER COMPANIES
Cessna Aerospace Corporation (2)	AlliedSignal Aerospace (1)
Gulfstream Aerospace Corporation (1)	Chrysler Technologies Airborne Systems (2)
Learjet, Inc. (2)	Key Industries Corporation (1)
The New Piper Aircraft, Inc. (1)	FAA/UNIVERSITIES
HELICOPTER COMPANIES	FAA Technical Center - Atlantic City (1)
Bell Helicopter Textron, Inc. (1)	Univ. of Illinois at Urbana-Champaign (1)
Sikorsky Aircraft Corporation (1)	

Table 6. - Geometry Requested by Group.

ORGANIZATION	AIRFOIL SECTIONS	WINGS	TAILS	INLETS S-DUCTS	PROPS	OTHER
Large Aircraft Manufacturers	3/5/2	4/1/0/D	1/HV	2/0/1/2c		
Business Jet Manufacturers	1/2/1	3/0/1	2			I
Small Aircraft Manufacturers		5/0/0	1	1/0/1		
Helicopter Companies	3/1/1					
Aircraft Engine/Inlet Comp.				5/4/1/1c		II
Military Aircraft Companies				1/0/1		
FAA	1/2/0	2/0/0	1			
Universities	1/2/0				1	III
Other	1/0/1			1/1/1		IV
Total (Approx. 80 models)	10/12/5	14/1/1/D	5/HV	10/5/5/3c	1	

Airfoil Sections: Single/Multi-element/With Ice Shapes; **Wings:** Single/Multi-element/With Ice Shapes/Delta Wings; **Tails:** HV - Horizontal & Vertical; **Inlets S-Ducts:** Inlet/S-duct/With Ice Shapes/Cascade Configurations; **I** - Windshields, **II** - Spinners, Center bodies, **III** - Droplet Trajectories, **IV** - Radomes, Antennas, Appendages.

Table 7: Summary of industry survey results

1. LARGE AIRCRAFT MANUFACTURERS: MULTI-ELEMENT WINGS

PRIORITY	TYPE OF GEOMETRY AND SPECIFIC MODEL IF KNOWN	TEST CONDITIONS V_{∞} (mph), α (deg.), MVD (μm), m (lbm/s)
H	Multi-element airfoil with full scale openings between main foil & LE & TE (5 element 737 model)	170 mph, ($\alpha_{\text{main}}=0,10$), (16, 20 μm)
H	Multi-element airfoil (3 element MDC model)	$M_{\infty} \approx 0.2$, -4 to 16°, 10-30 μm
H	Multi-element airfoils/737/MCD Multi-element wings with simulated ice shapes	Low speed, -10 to 20°, range of modified inertia param. (k_0) to ensure validity to full scale
M	Multi-element airfoil/TBD	0°, 4°, 8°, 12°, 16,20, 100 μm
M	Multi-element airfoils-wing	250-275 kts, -5 to 10°, 15- 20 μm

2. LARGE AIRCRAFT MANUFACTURERS: SINGLE-ELEMENT WINGS

H	Single Element airfoil/modern section	Low speed to $M=.55$, 0 to 10°, range of modified inertia param. (k_0) to ensure validity to full scale
H	Airfoils with various leading edge radii	300 mph, 0 to 10°, 20 to 40 μm
H	Single element wings with simulated ice shapes	Low speed, -10 to 20°, range of modified inertia param. (k_0) to ensure validity to full scale
H	Finite span wing with swept leading edge	300 mph, 0 to 10°, 20 to 40 μm
H	Airfoils with simple control surfaces	150 to 170 mph, 0 to 10°, 20 to 150 μm
M	Single element airfoils/wing	250-275 kts, -5 to 10°, 15- 20 μm

3. LARGE AIRCRAFT MANUFACTURERS: TAILS

H	Aircraft tail/horizontal with modern sections	Low speed to Mach .55, 5 to -10°, range of modified inertia param. (k_0) to ensure validity to full scale
M	Single element airfoils (tail)	250-275 kts., -1 to 4°, 15-20 μm
M	Aircraft tail configuration (Horiz. & Vertical)	300 mph, 0 to 10°, 20 to 40 μm

4. LARGE AIRCRAFT MANUFACTURERS: INLETS

M	Engine inlet Engine inlet with simulated ice shapes Turbofan model in cascade configuration	Low speed to Mach .55, 0 to 10°, range of modified inertia param. (k_0) to ensure validity to full scale
M	Engine inlets (3D)	250-275 kts, 0 to 5°, 15-20 μm , Inlet capture area ratio ~0.4 to 1.0

5. BUSINESS JET MANUFACTURERS: TAILS

H	Finite span 25° swept tail (64A008)	170 mph, 0 to 12°, (20, 200, 400 μm)
H	Finite span wing with simulated ice shapes (NACA 64A009 Typ. $AR=5$, $\lambda=0.4$, $\Delta c/4=30^\circ$)	120-150 kts, 0° to stall
H	Single Element airfoil with simulated ice shape (NACA 64A009 Typical)	120-150 kts, 0° to stall
M	Airfoils with simple control services / Rep tailplane with elevator TBD	(0°, 4°, 8°, 12°), (16,20, 100 μm)
M	Tail airfoil 64A008	170 mph, 0 to 12°, (20, 200, 400 μm)

Table 7: Summary of industry survey results (continued)

6. BUSINESS JET MANUFACTURERS: WINGS /OTHER

PRIORITY	TYPE OF GEOMETRY AND SPECIFIC MODEL IF KNOWN	TEST CONDITIONS V_{∞} (mph), α (deg.), MVD (μm), m (lbm/s)
H	Full-scale Learjet airfoil, Learjet airfoil with full-scale L.E., half-scale chord & flap	Duplicate icing conditions from modern airfoil program
H	Finite span with 30° swept leading edge (NACA 0012 wing tip)	(0°, 4°, 8°, 12°), (16,20, 100 μm)
H	Swept wings	200-cruise & holding, <200-descent - α sweep
H	Large drops, indicators LSD, windshields	40 to 1,000 μm
M	Single element airfoils	To 200 ktas, 0-10°, 20 μm
M	Single element airfoils with glaze ice shape	
M	Airfoil with simple control surface	120-150 kts., 0° to stall, 20 to 40 μm
M	Airfoil with fowler flap deflected 0° to 40°	120-150 kts, 0° to stall, 20 to 40 μm
M	Finite span wing (tapered)	
L	High Lift	climb < 150 kts, descent

7. SMALL AIRCRAFT MANUFACTURERS: WINGS /TAILS /INLETS

H	652415, Finite Span w/ Straight T.E.	160 mph, 180 mph, 0 to 6°, 16, 20, 50 μm
H	Infinite span wing with 30° swept leading edge (MS(1)-0317)	(0°, 4°, 8°, 12°), (16,20, 100 μm)
H	Single element airfoil (NLF(1)-0414F)	(0°, 4°, 8°, 12°), (16,20, 100 μm)
H	NACA 0009 & NACA 0010 Aircraft Tail Configurations	160 mph, 10°, (16, 20, 50 μm) 180 mph, 0°, (16, 20, 50 μm)
H	Symmetric Engine Nacelle Engine Inlets, Simulated Shapes	160 mph, -8 to 8°, (16, 20, 50 μm), 1-3 kg/s 180 mph, -8 to 8°, (16, 20, 50 μm),
M	NACA 23016, NACA 23009, tapered wing	190 mph, 0 to 10°, (16, 20, 50 μm) 150 mph, 0 to 10°, (16, 20, 50 μm)
M	631A212, tapered wing	140 mph, 0 to 10°, (16, 20, 50 μm) 210 mph, -4 to 4°, (16, 20, 50 μm)
M	64A010 & NACA 0012, Aircraft Tail Configurations	190 mph, -4 to 4°, (16, 20, 50 μm) 150 mph, -4 to 4°, (16, 20, 50 μm)

8. HELICOPTER COMPANIES: WINGS

H	Single element airfoils	700 ft/sec, $\pm 25^\circ$, 30 μm
H	Single element rotorcraft airfoil (SC2110)	150 mph, 300 mph, -2 to 15°, 15, 30 μm
H	Airfoils with simple control surfaces	225 mph, 0 to 10°, 55 μm
H	Airfoils with simple control surfaces & simulated ice shapes	225 mph, -10 to 10°, 55 μm
M	Single Element rotorcraft airfoil (SSC-A09)	150 mph, 300 mph, -2 to 15°, 15, 30 μm

9. AIRCRAFT ENGINE COMPANIES: S-DUCTS

H	Gooseneck or S duct	0-400 mph
H	S-Duct	100 mph, (0 \pm 10) deg., 20 μm , (0-12) lbm/s
H	S-duct (turbo prop inlet)	Flow Mach no.=0.3, 0.4, 20 μm
M	S ducts & turboprop, turbojet (727)	To 200 ktas, 0-5°, 20 μm , IVR 8-1.2
M	Water droplet impingement at face of engine with F/A-18E/F Inlet or B-2 S-duct inlet	150 mph, 0, 18-20 μm , 45 to 150 lbm/s

Table 7: Summary of industry survey results (concluded)

10. AIRCRAFT ENGINE COMPANIES: INLETS

PRIORITY	TYPE OF GEOMETRY AND SPECIFIC MODEL IF KNOWN	TEST CONDITIONS V_{∞} (mph), α (deg.), MVD (μm), m (lbm/s)
H	Turbofan engine inlets	Free stream Mach no.=0.4-0.6, large droplets 1000 μm -4000 μm , Altitude 10K to 20K
M	Axisymmetric NACA nacelle contour with different highlighted throat radius ratio with simulated internal flow	0-560 mph, 15-40 μm
M	Engine inlet	0-300 mph, (0 \pm 15 deg.), 20 μm , (10-40 lbm/s)
M	Engine inlet	to 200 ktas, 0-5°, 20 μm , IVR 8-1.2
M	Engine Inlets with Ice Shapes	

11. AIRCRAFT ENGINE COMPANIES: OTHER

H	Inlet Particle Separator	100 mph, (0 \pm 10) deg., 20 μm , (0-12) lbm/sec
H	Turbofan model in cascade configuration	170 mph, 2 α 's, (16, 20 μm)
H	Cascade with different solidity & aspect ratios	TBD
?	Engine centerbody/spinner shapes: conical, elliptical, double conical	0-200 mph

12. MILITARY AIRCRAFT COMPANIES: INLETS

M	Sharp leading edge inlets with simulated ice shapes, Straight leading edge (F-15) & swept leading edge \approx 12° sweep angle	185 mph, 0-15° α , 0° β , 15 to 30 μm , LWC 0.1-0.8 g/m ³
---	--	--

13. OTHER

H	Radomes	200 mph, 0 to 10°, 20 μm
H	Validate trajectory codes for large droplet case	
H	Special geometry with large velocity and pressure gradients	100-300 mph, 20-500 μm
H	Semispan cropped delta wing w/ sharp, round, deflected L.E.	$M_{\infty} \approx 0.4$, (2,8,10 deg.), 25 μm
H	Full span cropped delta wing w/ sharp, round, deflected L.E.	$M_{\infty} \approx 0.4$, (2,8,10 deg.), 25 μm
H	Propeller Sections, Clark 4 or 16 series	Near max tunnel speed, 0 to 10°, 20, 40 μm
M	Antennas	200 mph, 0 to 10°, 20 μm
L	Appendages	200 mph, 0 to 10°, 20 μm

Table 8: Importance and usage of impingement data

Importance of Impingement Data		Usage of Impingement Data	
High-	75% of respondents (15 out of 20)	Code Validation	14/20
Medium-	25% of respondents (5 out of 20)	Design	5/20
Low-	0% of respondents (0 out of 20)	Certification	2/20
		Other	3/20

Table 9: Tentative Test Matrix for 1997 Impingement Tests

Test Model	α (deg.)	MVD μm	Capture Area Ratio	Test Repeats	Blotters per Run	Total Test Runs	Total Blotters
1. Douglas (3 element) Flap Nested (2 configs)	0, 8	12, 20, 160	NA	5	6	45	370
2. NLF(1)-0414 Airfoil	0, 8	12, 20	NA	5	2	20	40
3. Horizontal Tail	0, 8	12, 20, 160	NA	5	2	25	50
4. Helicopter Wing	0, 10	12, 20	NA	5	2	20	40
5. S-Duct	0, 10	12, 20, 160	1, 0.75 or 0.5	5	14	45	630
6. Radome	0	12, 20, 160	NA	5	8	15	120
7. Uniformity Tests	0	12,20,160	NA	70	30	70	2100
8. Collector Mechanism	2-loc.	12, 20, 160	NA	5	30	9	270
Totals						295	3570

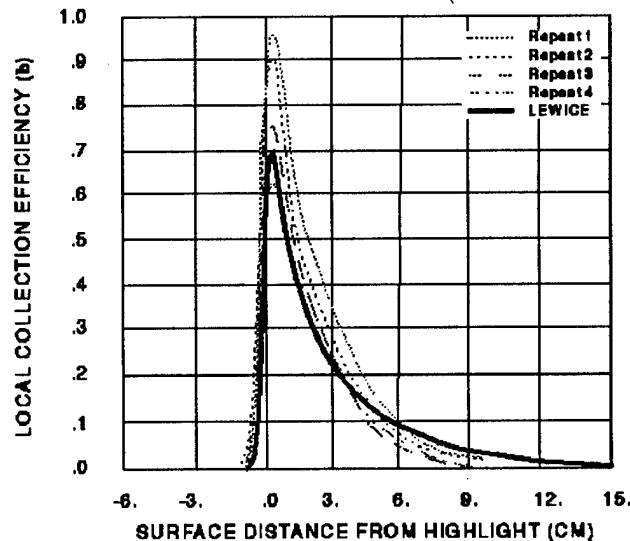


Fig. 1 Comparison of experimental (Repeat 1-4) and computational (LEWICE) impingement efficiency distributions.

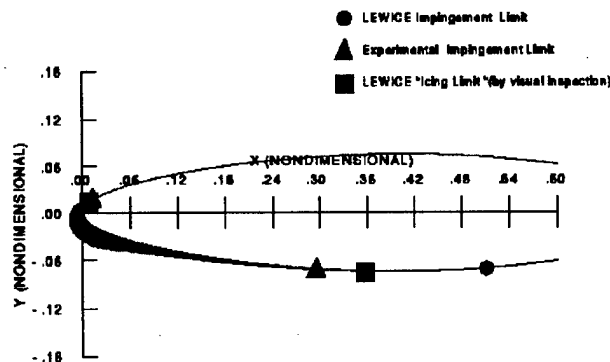


Fig. 2 Comparison of experimental and computational impingement limits.

An Eulerian Approach to Ice Droplets Impingement Calculations

Y. Bourgault, W. G. Habashi, J. Dompierre, G. Chevalier
In-Flight Icing Consortium*, CFD Laboratory,
Department of Mechanical Engineering, Concordia University,
Montreal, Qc, Canada, H3G 1M8

W. DiBartolomeo
Pratt & Whitney Canada,
1000 Marie-Victorin,
Longueuil, Qc, Canada, J4G 1A1

May 4, 1996

Abstract

To compute droplets impingement on airfoils, an Eulerian model for air flows containing water droplets is proposed as an alternative to the traditional Lagrangian particle tracking approach. Appropriate boundary conditions are presented for the droplets equations. Some finite element formulations are proposed to solve the droplets problem, based on conservative and non-conservative forms of the equations and using different stabilization terms. Numerical results on single and multi-elements airfoils, for droplets of mean volume diameter, as well as for a Langmuir distribution of diameters, are presented.

1 Introduction

The CFD Lab of Concordia University is spearheading a Consortium for the numerical simulation of In-Flight Icing phenomena, its main objectives being an integrated approach to the analysis of ice accretion, performance degradation due to ice, as well as de-icing and anti-icing heat transfer optimization. The Consortium includes meteorologists, aircraft and engine manufacturers, flight simulation companies and pilots.

The simulation of aerodynamic performance and of ice accretion has been traditionally based on inviscid Panel or Euler flow computations for the air and on Lagrangian particle-tracking techniques for the droplets impingement, as can be seen in the NASA Lewice [17] and ONERA codes [10]. In our effort, we prefer to solve the compressible Navier-Stokes equations, thus fully and directly accounting for the influence of the viscous effects on the degradation of performance. Furthermore, to compute ice accretion on airfoils, we propose an Eulerian model for air flows containing water droplets, as an alternative to the traditional Lagrangian particle tracking approach. This is thought to be more suitable for use with a field solver such as a finite element one. Droplets velocity and volume fraction of water have to be computed only at the nodes where the air flow variables are known, so no particles have to be tracked as they go through the mesh as in a Lagrangian approach. The net flux of water at the airfoil surface may also be recovered directly, while an averaging process would be needed with the Lagrangian one after impacting particles have been detected. In 3-D, such an averaging process is far from being evident to define and code, giving a clear advantage to the Eulerian approach.

Droplets two-phase flows have already been computed in an Eulerian manner a number of times in

*This research is supported by a NSERC Strategic Grant and a Quebec-US Collaboration Grant.

the past (see [7, 8, 9] and references therein). To our knowledge though, only one attempt has been made to use the Eulerian approach for droplets impingement [18]. In that paper, the objective was also to predict the flux of water on the leading edge of an airfoil, although the technique was only applied to flows around a cylinder. A spatial marching scheme was used to solve the droplets equations, the main drawback being that complex configurations with recirculating flows are difficult to handle with such a scheme. With such a limitation, one of the advantage of the Eulerian approach to droplets impingement is totally missed: the possibility to compute droplets impingement on multi-element airfoils in an automatic way, without a painful determination of launching areas for droplets to impact on each airfoil element, as needed with the Lagrangian approach.

It is the purpose of the present paper to show the well-posedness and the efficiency of the Eulerian model for impinging droplets. Thus, comparisons of numerical and experimental results are made, some of them using a distribution of droplet diameters instead of the mean volume diameter (MVD). Numerical results on a multi-element airfoil are also presented. Meanwhile, comments on some of the most up-to-date techniques used for viscous flow computations will be made, in particular mesh adaptation.

2 Flow Field Computations

A complete characterisation of airfoil performance must account for the viscous forces if both lift and drag have to be recovered. The resolution of the full compressible Navier-Stokes equations, combined with appropriate turbulence models, is the most promising avenue for such performance simulation. Internal and external flows could then be computed with the same code, providing the opportunity for aircraft and engine designers to integrate their efforts in simulating performance degradation due to ice. Moreover, by solving the Navier-Stokes equations, heat transfer would then be computed in a natural and almost automatic way, even in complex icing situations.

Among the technologies available today for the solution of the Navier-Stokes equations, the Finite Element Method (FEM) is considered one of the

most versatile. This numerical method can be applied to all sort of equations, e.g. those of fluids and structures, on all sort of geometries. For example, once a finite element Navier-Stokes solver has been coded, it can be used on single and multi-element airfoils, without any modifications.

In the present study, different FE solvers were used to compute the air flow. The flow field solvers were kept independent of the droplet solver, simply to allow more flexibility in the choice of these solvers. So, we did numerous computations using a NS solver on triangular meshes [2, 3], but also using Euler solvers on quadrilateral [1] and triangular [14] meshes.

The choice of one or another flow FE solver is no more that critical, as a very efficient remesher was used to obtain a mesh over which a mesh-independent and solver-independent solution of the Euler or NS equations can be computed [20]. Here, *mesh-independence* is to be understood as the independence of the final mesh and solution from the mesh used to initiate the adaptation process. Otherwise, the accuracy of any numerical solution is highly dependent upon the mesh used, not only in terms of the size of the elements but also with respect to the orientation and aspect ratio of the elements. Anisotropic flow structures, such as shock waves and boundary layers, ask for *anisotropic* elements. The second derivative of the local Mach number is then used to control the amplitude and the direction of the numerical solution error, hence the size and the orientation of the elements, over the mesh. The present adaptation library computes iteratively a mesh adapted to the test case, starting with a generic mesh.

To illustrate the evolution of the mesh during the solver/remesher iterations, Fig. 1 shows the initial, second and final meshes for a subsonic flow over a NACA0012 airfoil. Figure 2 shows the Mach contours of the solutions for the meshes of Fig. 1. One should note how close the solutions fit to the meshes. The whole adaptative process appears to be convergent, as can be seen in Fig. 3. While improving the mesh at each adaptation step, the C_f curves get closer and closer to the final one.

These techniques are applied to an iced NACA0012 airfoil. The shape of the glaze ice is inspired from those in [6]. Zoom on the leading

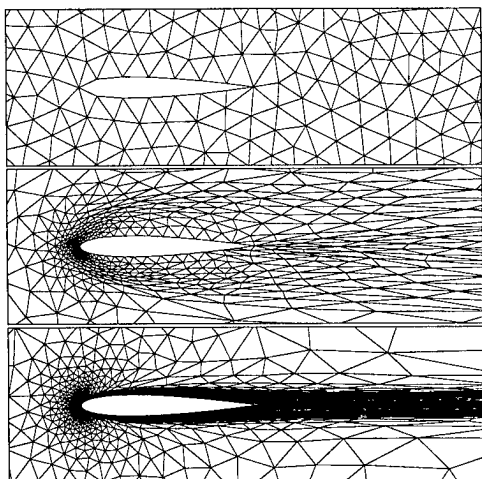


Figure 1: Initial mesh (top), second adapted mesh (middle) and final adapted mesh (bottom) for a viscous flow at $Ma=0.236$, $Re=8000$, $AOA=0.0$.

edge of the mesh and flow field shown on Fig. 4 demonstrate the power and the flexibility of this CFD technology.

3 Eulerian Droplets Model

The classical compressible Navier-Stokes equations are at the basis of the air flow computations, but an inviscid flow solver may be used as well, as the flow and droplets solvers are kept independent. No modification of the Navier-Stokes equations is needed although droplets are present, because the loading, i.e. the ratio of the bulk density of the droplets over the bulk density of the air, is of the order of 10^{-3} in icing conditions. It is generally agreed that a loading smaller than 0.1 is well modeled by a one-way coupling [7].

Using the Eulerian approach for the droplets, one tries to recover a volume fraction of water α and a velocity field \mathbf{u} . The variables $\alpha(x, t)$ and $\mathbf{u}(x, t)$ are mean values of the ratio of the volume occupied by water over the total volume of the fluid element and of the droplets velocity over the element, given a small fluid element around any specific location x in space at time t . The continuum hypothesis remains valid for the droplets phase as long as the fluid element contains enough droplets, let's say 10^4 for a fluctuation below 1% in volume fraction [7]. For typical icing conditions, i.e. for a MVD equal to $20\mu\text{m}$

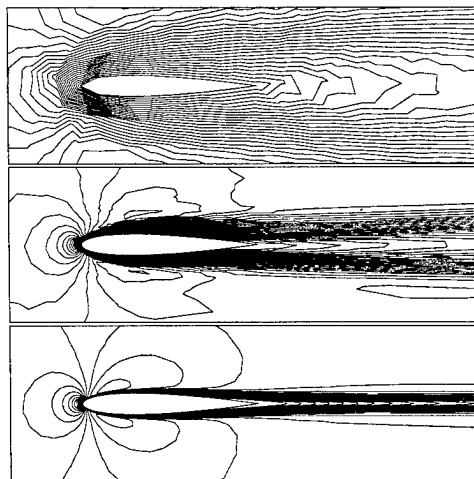


Figure 2: Initial solution (top), second adapted solution (middle) and final adapted solution (bottom) corresponding to the meshes of the Fig. 1, for a viscous flow at $Ma=0.236$, $Re=8000$, $AOA=0.0$.

and a liquid water content (LWC) equal to 1g/m^3 , the length scale of the 1% fluctuation fluid element should be of the order of 1cm.

A number of phenomena and forces may be considered while modeling air-droplets flows, but the following assumptions are sensible in icing conditions:

- the droplets are spherical without any deformation or breaking;
- no droplets collision, coalescence or splashing;
- no heat and mass exchange between the droplets and the surrounding air;
- turbulence effects on the droplets are neglected;
- the only forces acting on the droplets are due to air drag, gravity and buoyancy.

The first two assumptions rest on the fact that icing droplets are small (1–100 microns range) and the icing droplets flow should be considered dilute with a volume fraction around 10^{-6} . The gravity and buoyancy forces are kept in the model, even if they are three orders of magnitude lower than the drag force for typical flight applications. These forces would be important for the simulation of de-icing fluid contamination by rain and snow during ground operation. Among the forces on droplets neglected, one

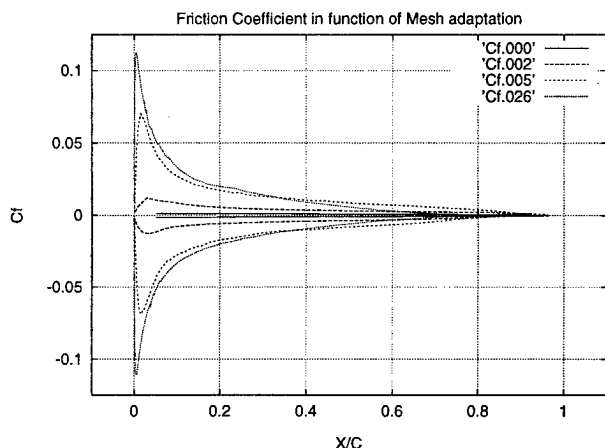


Figure 3: Evolution of the C_f curves with the solver-remesher iterations for a viscous flow at $Ma= 0.236$, $Re= 8000$, $AOA= 0.0$.

may notice the effect induced by the unsteadiness of the flow around a droplet and the air pressure gradient in the vicinity of the droplet.

The continuity and momentum droplets equations are written, using non-dimensional variables, as

$$\frac{\partial \alpha}{\partial t} + \nabla \cdot (\alpha \mathbf{u}) = 0, \quad (1)$$

$$\frac{\partial \mathbf{u}}{\partial t} + \mathbf{u} \cdot \nabla \mathbf{u} = \frac{C_D Re_d}{24K} (\mathbf{u}_a - \mathbf{u}) + \left(1 - \frac{\rho_a}{\rho}\right) \frac{1}{Fr^2} \mathbf{g} \quad (2)$$

where

\mathbf{u}_a = non-dimensionalized velocity of air,

ρ = density of water, ρ_a = density of air,

d is the droplet diameter,

$Re_d = \frac{\rho d U_\infty |\mathbf{u}_a - \mathbf{u}|}{\mu}$ is the droplet Reynolds number,

$K = \frac{\rho d^2 U_\infty}{18 L \mu}$ is an inertia parameter,

$C_D = \frac{24}{Re_d} (1 + 0.15 Re_d^{0.687})$, $Re_d \leq 1000$, is the drag coefficient for spherical droplets,

$Fr = \frac{U_\infty}{\sqrt{L g_0}}$ is the Froude number.

The last term on the right-hand-side of the momentum equations accounts for gravity and buoyancy effects. The system (1)–(2) models the evolution

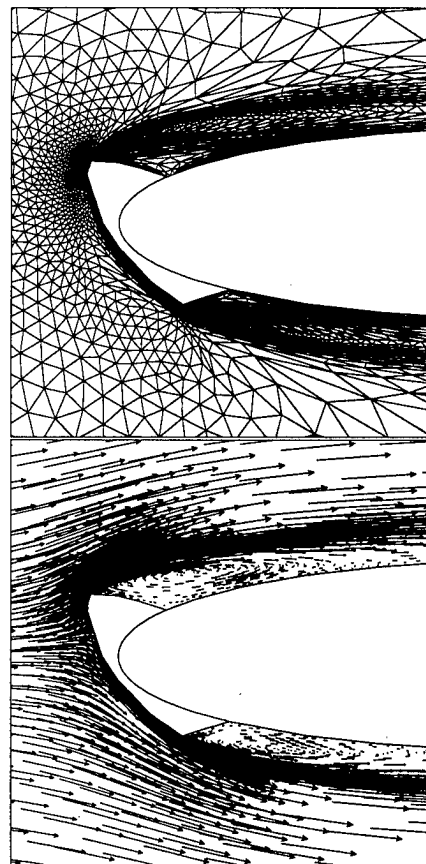


Figure 4: Mesh and flowfield on the leading edge for an iced NACA0012 and for a viscous flow at $Ma= 0.236$, $Re= 8000$, $AOA= 0.0$.

of droplets having the same given diameter, usually chosen equal to the mean volume diameter (MVD) of the size distribution. The handling of multiple droplet sizes will be shown below by duplicating the number of equations solved, using the above system once for each class of diameters.

For icing computations, the solution is smooth everywhere except near the contact discontinuity between the non-shadowed and shadowed area besides the suction surface of the airfoil. In the non-shadowed area, the solution presents small departures from the cloud characteristics. On the opposite, the droplets are removed or washed out from the shadowed area, the airfoil being a screen for incoming droplets on the pressure surface. The solution discontinuity is apparent only on the volume fraction α and the droplets velocity field \mathbf{u} is parallel to the contact discontinuity, as is usual for such discontinuity. Such features of the solution allow the

use of the non-conservative form of the momentum equation, without compromising accuracy compared to the conservative form. Moreover, the use of the non-conservative form gives a more efficient code in terms of convergence behavior of the nonlinear iterative solver. The details concerning the conservative form of the droplets equations can be found in [8, 9, 21].

The system (1)–(2) is easily amenable, after linearization, to a stability analysis, similar to those in [12], to determine where boundary conditions are needed. This stability analysis reveals that a boundary condition should be imposed on the inflow boundary for every variable and that no boundary condition is needed on slip or outflow boundaries. Here, slip, inflow and outflow boundaries are defined with respect to the droplets velocity field. In other words, boundary conditions are needed on boundaries with incoming characteristics, the direction of which being controlled by the droplets velocity \mathbf{u} . The inflow outer boundary obviously requires boundary conditions. No boundary condition is needed on the airfoil surface or on the outflow outer boundary.

An initial solution ensuring the physical meaning of the final one is given by $\alpha = 1$ and $\mathbf{u} = (\cos(AOA), \sin(AOA))$ everywhere except near the airfoil surface, where both variables are forced to zero. Here AOA stands for the angle of attack of the airfoil.

4 Computational Methods for the Droplets Model

We compared different strategies for the numerical resolution of the droplets equations, the main features of which are:

- standard Galerkin FEM on triangular meshes;
- use of the conservative or non-conservative forms of the droplets equations, the simplest one being the system (1)–(2);
- a stabilization term was added to removed possible oscillations in the solution of the volume fraction α ; this could for example be a classical artificial viscosity or a streamline upwinding (SUPG) term [11];
- a Newton-GMRES algorithm was used to solve the nonlinear system of equations (see [5]).

For an introduction to the finite element method, see [16, 23].

Given a triangulation of the domain Ω and the space V_h of continuous piecewise linear elements, the volume fraction $\alpha^n \in V_h$ and the droplets velocity $\mathbf{u}^n \in V_h^2$ at time t^n are solutions of

$$\int_{\Omega} \left[\frac{\alpha^n - \alpha^{n-1}}{k} + \nabla \cdot (\alpha^n \mathbf{u}^n) \right] \varphi \, dx + a_{\alpha}(\alpha^n, \varphi) = 0, \quad (3)$$

$$\int_{\Omega} \left[\frac{\mathbf{u}^n - \mathbf{u}^{n-1}}{k} + \mathbf{u}^n \cdot \nabla \mathbf{u}^n \right] \cdot \psi \, dx + a_u(\mathbf{u}^n, \psi) = \int_{\Omega} \mathbf{f} \cdot \psi \, dx \quad (4)$$

for all $\varphi \in V_h$, $\psi \in V_h^2$. Here, \mathbf{f} stands for the drag and gravity forces on the droplets, thus depends on \mathbf{u} and \mathbf{u}_a . The expressions $a_{\alpha}(\cdot, \cdot)$ and $a_u(\cdot, \cdot)$ are the stabilization terms mentioned above, the details of which being given in [4]. The following boundary conditions are imposed node by node on the inflow outer boundary:

$$\alpha^n = 1 \quad \text{and} \quad \mathbf{u}^n = (\cos(AOA), \sin(AOA)). \quad (5)$$

The FEM has been presented for the non-conservative form (1)–(2), but it is not difficult to write down the scheme for the conservative form.

It is mainly the volume fraction that requires some extra stabilization, as the velocity suffers little numerical instabilities (see Fig. 5). The oscillations on the volume fraction are mainly due to the nonlinear convective nature of the Eulerian droplets model. Figure 6 shows the improvement on the volume fraction obtained with SUPG terms.

As far as the appropriate way to write the droplets system is concerned, no obvious difference was observed between the solutions obtained with the conservative and non-conservative forms of the equations, except for lower computing times using the non-conservative form. Hence, the FEM based on the non-conservative form (1)–(2) of the droplets equations and on the SUPG stabilization term appears to be the winner, in terms of computing time,

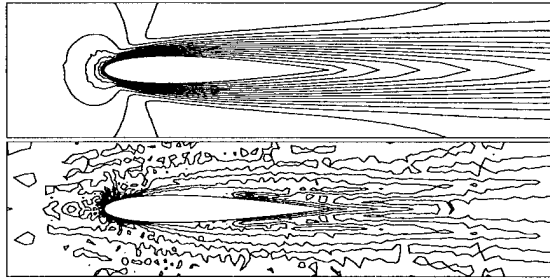


Figure 5: Numerical solution without stabilization term: Horizontal component of droplets velocity (top) Volume fraction of water (bottom) (Air speed 165m/s, AOA= 0.0, MVD=20 μ m, LWC=1g/m³)

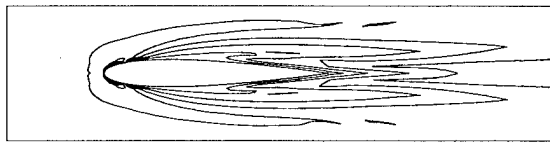


Figure 6: Volume fraction with a SUPG stabilization term (Air speed 165m/s, AOA= 0.0, MVD= 20 μ m, LWC=1g/m³)

simplicity of coding and quality of the numerical solutions.

An important parameter which controls the accretion of ice on an airfoil is the local collection efficiency β , i.e. the normalized flux of water on the airfoil's surface. To compute the collection efficiency with the Lagrangian particle tracking, one must determine if a droplet impacts the airfoil or not along its trajectory, compute the impact point for droplets within the impingement limit which is not known in advance, and then evaluate the distance between neighboring droplets. This strategy becomes cumbersome to implement for multi-element airfoils [22] and even more so in 3-D [10].

Within the Eulerian approach, the collection efficiency is computed on every edge (face in 3-D) belonging to the airfoil surface using

$$\beta = -\alpha \mathbf{u} \cdot \mathbf{n}.$$

The water flux m_w at the airfoil surface would then be

$$m_w = \text{LWC } U_\infty \beta.$$

Some special attention is required for the computation of the normal \mathbf{n} to the airfoil surface, but apart from that, the recovery of the collection efficiency

can be coded in less than 100 lines in 2-D and the code handles multi-element airfoils the same way as single element ones. Actually, we compute the normal \mathbf{n} and the collection efficiency β at the center of every edge on the airfoil. It should be noted that the presence of one or another stabilization term, even of no one at all, has almost no effect on the collection efficiencies recovered.

5 Results and Comparisons

First, numerical results on a NACA0012 single element airfoil are presented. Comparisons with experiments, based on a NASA series of wind tunnel tests [17], are also reported. Computations using a Langmuir distribution of droplet sizes are shown to improve the accuracy of the collection efficiency near the impingement limits. Finally, numerical results on a multi-element airfoil are given.

5.1 NACA0012 airfoil

A typical output of the Eulerian droplet code is the volume fraction, as in Fig. 6, and the droplets velocity field, as in Fig. 7. In the latter figure, a clear difference is observed on the leading edge where the air stops on the airfoil surface, while the droplets hit the surface with a strictly positive speed. Here, the air speed is 80m/s (Ma= 0.236), the angle of attack 0°, the droplet mean volume diameter 16 μ m and the LWC is equal to 1g/m³.

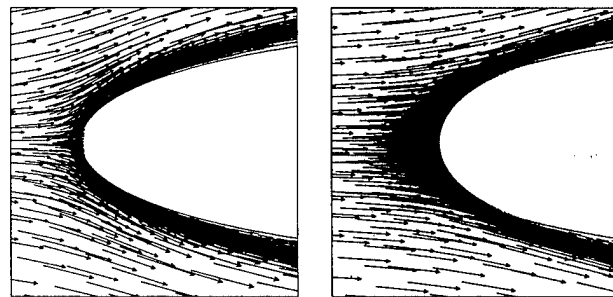


Figure 7: Air velocity (left) and water droplets velocity (right) (Ma= 0.236, Re= 8000, AOA= 0.0, MVD= 16 μ m, LWC=1g/m³)

A Lagrangian particle tracking code usually computes droplets trajectories and uses them to calculate the collection efficiency. With an Eulerian code,

even if the trajectories are useless for computing the collection efficiency, they can be recovered in the steady case by plotting the streamlines of the droplets velocity field with any flow visualization package. The trajectories shown on Fig. 8 have been computed in that manner, using the droplets velocity field of Fig. 7.

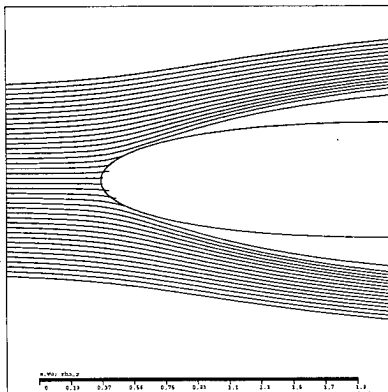


Figure 8: Droplets trajectories

In Fig. 9, the collection efficiency for test case of Fig. 6 are plotted against the arc length s of the airfoil. The technique for collection efficiency recovery explained above has been used. Two numerical results are shown, one combines an Euler flow computation with a droplets solution, the other a laminar Navier-Stokes solution at $Re = 8000$, again with an Eulerian droplets computation. The agreement with experimental results is quite good in both cases. The gap between the collection efficiency curve for the Navier-Stokes flow and the one for the Euler flow is due to the large thickness of the boundary layer in the laminar regime. A turbulent Navier-Stokes solution at the experimental Reynolds number of 1.6×10^6 would reduce the gap between the two curves and will be the next step in our research.

Droplets clouds, however, usually present themselves with a distribution of droplet diameters instead of with droplets of the same size. The Langmuir D distribution, as given in Table 1 for a MVD of $16\mu m$, is a typical one for an icing cloud [13, 17]. Figure 10 compares the collection efficiency for monodisperse droplets of MVD and for droplets with a Langmuir D distribution of diameters. Impingement limits are more accurately predicted with polydisperse droplets. The maximum value of the collection efficiency is larger for the monodisperse

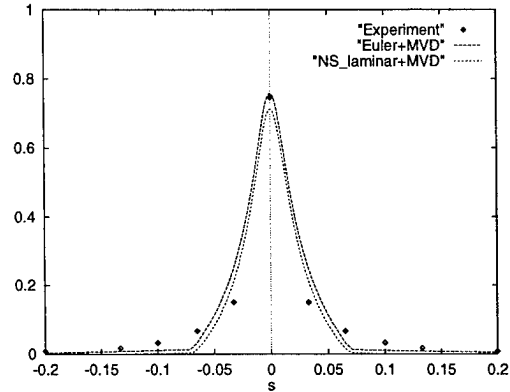


Figure 9: Local collection efficiency β as a function of the arc length s (in inches) of the airfoil ($AOA=0^\circ$)

Table 1: Langmuir D distribution of droplet diameters for a MVD of $16\mu m$

Percentage LWC	Ratio of Diameters	Droplet Diameter (μm)
0.05	0.31	5.0
0.10	0.52	8.3
0.20	0.71	11.4
0.30	1.00	16.0
0.20	1.37	21.9
0.10	1.74	27.8
0.05	2.22	35.5

droplets.

The results for a second test case with an angle of attack (air speed $80m/s$, $AOA = 8^\circ$, $MVD = 16\mu m$, $LWC = 1g/m^3$) are shown in Fig. 11. The agreement between experimental and numerical results is quite good. Again the boundary layer thickness for the laminar NS flow ($Re = 8000$) should account for the reduced local collection efficiency when compared to the inviscid Euler flow.

5.2 Multi-element airfoil

Numerical results are now presented for a four-element airfoil taken from [15, 19], whose leading edge slat is at 45° , the first trailing flap at 25° and the second flap at 51.2° . The droplets diameter is $20\mu m$ and the air velocity $94m/s$, with a 0° angle of attack. The initial mesh and the final one given by the adaptive library are shown on Fig. 12. The final mesh

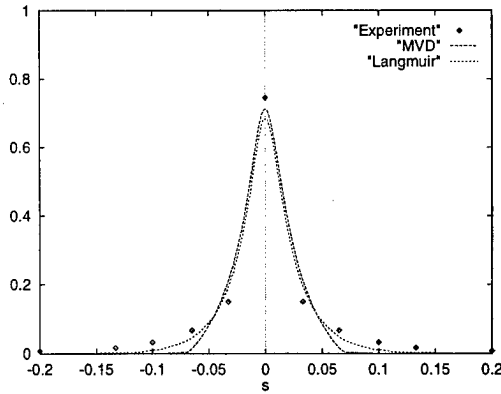


Figure 10: Collection efficiency β for MVD droplets or a Langmuir D distribution of droplets

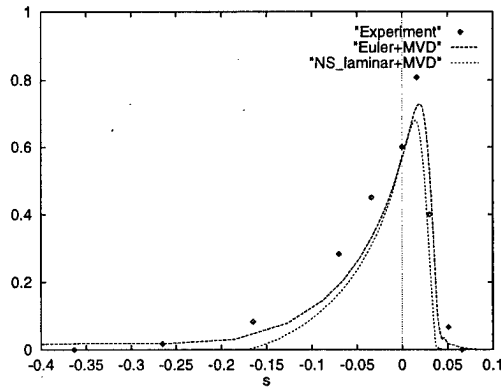


Figure 11: Collection efficiency β as a function of the arc length s (in inches) of the airfoil ($\text{AOA}=8^\circ$)

has been adapted to the air flow but is also used for the droplet computations. As can be seen on this figure, not much effort has been put on the initial mesh, the adaptative library improving it tremendously.

Multi-element airfoils are typical configurations where viscous effects may have a strong impact on the flow. For example, the Fig. 13 shows the huge difference between an inviscid flow and a laminar viscous one at Re equal to 5000. An unsteady vortex appears besides the slat in the viscous case. An impact of the viscous forces in this particular example is the upward displacement of the stagnation point when compared to the inviscid one. The displacement of the stagnation point clearly has an effect on the position of the impingement area on the slat, as can be seen in Fig. 14. Similar differences have been observed on the flaps and the main element between the inviscid and viscous flows. These comments are

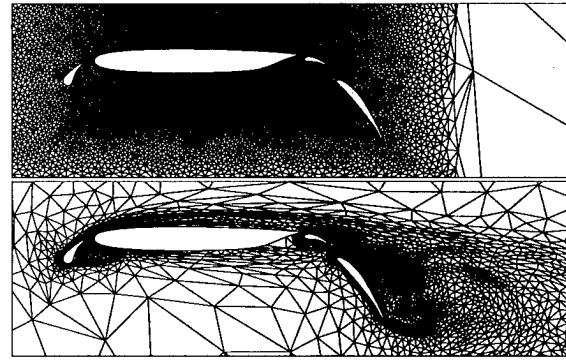


Figure 12: Initial (top) and adapted (bottom) meshes for the multi-element airfoil

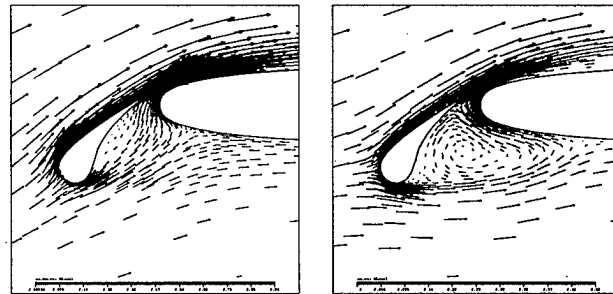


Figure 13: Inviscid flow (left) Viscous flow at $\text{Re}=5000$ over the slat (right) ($\text{Ma}=0.3$, $\text{AOA}=0.0$)

confirmed by the Fig. 15–18, where the local collection efficiency β is plotted along each element of the airfoil in the upward normal direction. Of course, all these preliminary results on droplets impingement with laminar NS flows have to be confirmed for turbulent NS ones.

The following comments have to be made concerning the computing strategy for the viscous flow multi-element airfoil example. Provided the air flow is steady, one can freeze the air variables and let the droplets' solver reach a steady-state. But, for unsteady air flows with moving vortices, a stronger coupling of the air and droplets solver is needed. Using the strategy for steady flows in this latter case, the frozen vortices would centrifuge the droplets, creating an endless accumulation of water at the periphery of these vortices. To prevent this type of divergent behavior, one should alternate between the air and droplets solvers in order to move the vortices and prevent the over-accumulation of water.

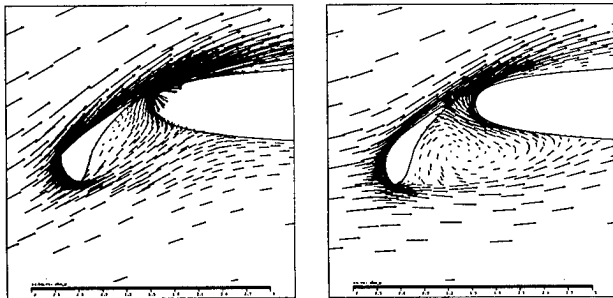


Figure 14: Droplets velocity over the slat in the inviscid case (left) and the viscous case (right) ($Ma=0.3$, $AOA=0.0$, $MVD=20\mu m$, $LWC=1.05g/m^3$)

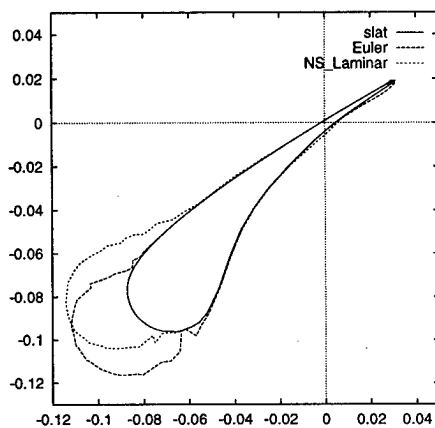


Figure 15: Local collection efficiency β plotted along the slat

6 Conclusion

The Eulerian approach proposed for the computation of droplets impingement has been shown to be feasible, efficient and accurate. Moreover, the generality and the simplicity of the method makes it a promising tool for computing impingement on multi-element airfoils and on 3-D aircraft components. The implementation of a 3-D droplets Eulerian code is under way. These encouraging results will soon be completed on with turbulent and 3-D flow computa-

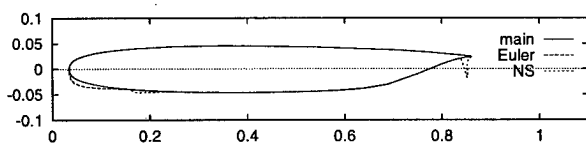


Figure 16: Local collection efficiency β plotted along the main element

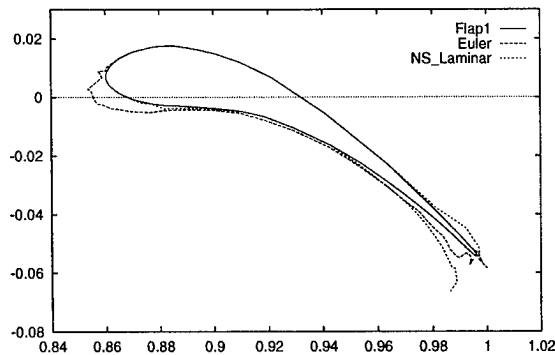


Figure 17: Local collection efficiency β plotted along the first flap

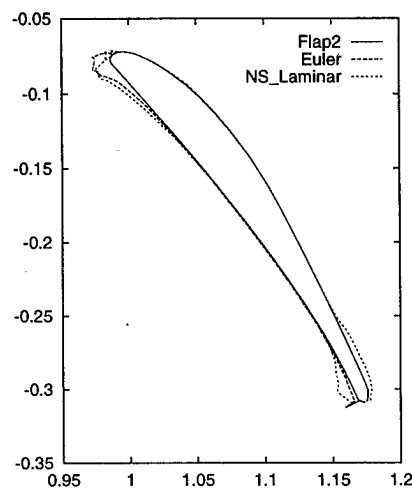


Figure 18: Local collection efficiency β plotted along the second flap

tions with the latest FE flow solver currently under development at the CFD Lab.

References

- [1] G.S. Baruzzi. *A Second Order Finite Element Method for the Solution of the Transonic Euler and Navier-Stokes Equations*. PhD thesis, Concordia University, Montreal, 1995.
- [2] S. Boivin and M. Fortin. A new artificial viscosity method for compressible viscous flow simulations by FEM. *Comp. Fluid Dyn.*, 1:25-41, 1993.
- [3] Y. Bourgault. *Méthode d'éléments finis en mécanique des fluides, Conservation et autres*

- propriétés. PhD thesis, Université Laval, Québec, 1996.
- [4] Y. Bourgault, W. G. Habashi, J. Dompierre, G. S. Baruzzi, and G. Chevalier. An Eulerian computational approach to ice droplets impingement. In *Third ECCOMAS Computational Fluid Dynamics Conference*, Paris, September 1996. GAMNI/SMIAI, CNRS, INRIA.
 - [5] P. Brown and Y. Saad. Hybrid Krylov methods for nonlinear systems of equations. Technical Report UCRL-97645, Lawrence Livermore National Laboratory, November 1987.
 - [6] S. C. Caruso. NEARICE: An unstructured mesh Navier-Stokes-based ice accretion prediction model. In *NASA-Industry Workshop on Aircraft Icing*, Cleveland, Ohio, July 1993. NASA Lewis Research Center.
 - [7] C.T. Crowe. Review-Numerical models for dilute gas-particle flows. *Trans. ASME, J. Fluids Engin.*, 104:297-303, 1982.
 - [8] F. Durst, D. Milojevic, and B. Schonung. Eulerian and Lagrangian predictions of particulate two-phase flows: A numerical study. *Appl. Math. Modelling*, 8:101-115, 1984.
 - [9] M. Hallman, M. Scheurlen, and S. Wittig. Computation of turbulent evaporating sprays: Eulerian versus Lagrangian approach. *J. Engin. Gas Turbines and Power*, 117:112-119, 1995.
 - [10] T. Hedde. *Modélisation tridimensionnelle des dépôts de givre sur les voilures d'aéronefs*. PhD thesis, Université Blaise Pascal, 1992.
 - [11] T.J.R. Hughes and M. Mallet. A new finite element formulation for computational fluid dynamics : III The generalized streamline operator for multidimensional advective-diffusive systems. *Comput. Methods Appl. Mech. Engrg.*, 58:305-328, 1986.
 - [12] H.O. Kreiss and J. Lorenz. *Initial-Boundary Value Problems and the Navier-Stokes Equations*. Academic Press, 1989.
 - [13] I. Langmuir and K.B. Blodgett. A mathematical investigation of water droplet trajectories. Technical Report 5418, US Army Air Forces, 1946.
 - [14] B. Mohammadi. Fluid dynamics computation with NSC2KE: An user-guide release 1.0. Technical Report RT-0164, INRIA, 1994.
 - [15] E. Omar, T. Zierten, M. Hahn, E. Szpiro, and A. Mahal. Two dimensional wind tunnel test of a NASA supercritical airfoil with various high-lift systems. Technical Report CR-2215, Vol.2, NASA, 1973.
 - [16] J. N. Reddy. *An Introduction to the Finite Element Method*. McGraw-Hill, 1993.
 - [17] G.A. Ruff and B.M. Berkowitz. Users manual for the NASA Lewis ice accretion prediction code (LEWICE). Technical Report 185129, NASA, 1990.
 - [18] J.N. Scott, W.L. Hankey, F.J. Giessler, and T.P. Gielda. Navier-Stokes solution to the flowfield over ice accretion shapes. *J. Aircraft*, 25:710-716, 1988.
 - [19] P. Tran, M. T. Brahimi, F. Tezok, and I. Paraschivoiu. Numerical simulation of ice accretion on multiple element configurations. AIAA paper 96-0869, January 1996.
 - [20] M.-G. Vallet, J. Dompierre, Y. Bourgault, M. Fortin, and W. G. Habashi. Coupling flow solvers and grid through an edge-based adaptive grid method. In *ASME Fluids Engineering Conference*, San Diego, CA, July 1996.
 - [21] G.B. Wallis. *One-dimensional Two-phase Flow*. McGraw-Hill, 1969.
 - [22] W.B. Wright and C.S. Bidwell. Additional improvements to the NASA Lewis ice accretion code LEWICE. AIAA paper 95-0752, January 1995.
 - [23] O. C. Zienkiewicz and R. L. Taylor. *The Finite Element Method*, vols. 1 and 2. McGraw-Hill, 1989 and 1991.

THE FORMATION OF AN ICE RIDGE BEYOND PROTECTED REGIONS

Kamel Al-Khalil, Ph.D.
Engineering Scientist
Cox & Company, Inc.
200 Varick Street, New York, NY 10014

ABSTRACT

The accident of an ATR-72 regional aircraft has been attributed by many scientists to the existence of large droplets in the flying atmosphere. The present study considers the effect of other parameters and conditions that could produce undesired frozen ice beyond a "normally" protected airfoil surface. Particularly, the effect of temperature on thermally and mechanically protected airfoils, and surface runback water refreeze will be addressed. A few example cases and experimental data are illustrated to examine different scenarios of ridge formation.

I. INTRODUCTION

Since the accident of an ATR-72 regional aircraft on October 31, 1994 near Roselawn, Indiana, there has been a great deal of interest in the issues surrounding Supercooled Large Droplets (SLD). The FAA has played a lead role in the scientific investigation using the NASA Lewis Icing Research Tunnel (IRT) to some extent, and the US Air Force icing tanker aircraft (KC-135) to a greater extent. The existence of large droplets in the flying atmosphere has been suspected to be a main cause behind the accident. Large droplets generally impinge on a greater percentage of an airfoil Leading Edge (LE) than do smaller droplets. The direct impingement area can extend beyond the ice protected regions as a result of their relatively high momentum.

A pneumatic boot system was used in the case of the ATR-72. Cycling the boot would clear the LE from the gross ice contamination up to the limits of the actively protected region. Downstream, the ice would remain on the surface and form a spanwise ridge.

Several experimental studies have been conducted recently to examine the effect of an ice ridge buildup on the aerodynamic performance of an airfoil. Among the researchers are Bragg [1] and Ashenden et al. [2]. The common conclusion was a drastic reduction in the maximum lift, the angle of attack margin-to-stall, as well as a possible hinge moment reversal on control surfaces downstream of the ridge. The level of performance reduction varies between one aircraft airfoil design and another. The majority of these studies assumed that the ridge formation was a result of direct impingement of large droplets on the surface. Regardless of that assumption and the source of the ice ridge formation, the conclusion still stands correct. There exist several possible reasons that can be attributed to an ice ridge formation on an aircraft LE surface. These are discussed in the following sections.

II. THE EXCEEDANCE ENVIRONMENT

The range of Mean Volume droplet Diameter (MVD) in the icing envelope extends to 40 microns as shown in Appendix C of the FAR Part 25. Recent and previous evidence show that this envelope needs to be reconsidered to include larger droplets that exist in freezing rain and freezing drizzle environments. An extension to this envelope may be considered to include an additional zone of larger droplets referred to as the "exceedance environment". Apparently, freezing rain (500 to 5000 microns) may be excluded from consideration since its precipitation on an aircraft surface tends to form a more or less uniform glaze ice layer as opposed to ice ridges and forward facing steps. Consequently, only freezing drizzle conditions (50 to 400 microns) are considered here.

The amount of data available on freezing rain (ZR) and freezing drizzle (ZL) is very limited. Recently, Richard Jeck, FAA Technical Center, was able to compile occurrences and durations of ZR and ZL at many airports in the US over the last 25 years [3]. His results for ZL are summarized in Table 1. These representative values were meant to be for interim test and guidance purposes where the most important variables are: Outside Air Temperature (OAT), Drop Size, and Liquid Water Content (LWC).

Table 1: Representative Values of Variables in Freezing Drizzle [3].

Variable	Known or Estimated Range	Representative Value
LWC (g/m ³)	0 to <0.3	0.08
Drop Size (μm)	50 to 500 dia.	See below
Temperature	0 to -15 (°C) 32 to 5 (°F)	-2 °C (at ground level) -2 to -15 °C (at 3-5 km AGL)
Altitude AGL	0 to 17,000 Ft 0 to 5 km	0 to 15,000 Ft 0 to 4 km

Representative LWC Distribution vs. Drop Size for ZL Range Only					
Drop Size Interval (μm)	50 - 100	100 - 200	200 - 300	300 - 400	400 - 500
Incremental LWC (g/m ³)	0.021	0.035	0.010	0.012	0.003

Inspection of the data in Table 1 suggests that the LWC is relatively low in the case of large droplets. The impingement limits extend further downstream in the case of large droplets than in the case of small droplets. However, the impingement efficiency near those locations is low. At the low temperature regime, the droplets normally freeze in place upon impingement. Considering an exposure time as high as 30 minutes, the accreted ice near the boot limits may be near 0.25 inch which in many cases is not very detrimental. A near-freezing temperature is required to force a larger mass of runback downstream and create a larger ridge upon freezing. At this temperature, a cloud with an MVD of 40 microns at high LWC can produce such a ridge buildup.

III. ICE RIDGE FORMATION SCENARIOS

The ATR involved in the accident was outfitted with a pneumatic boot ice protection system. However, rather than to restrict this analysis to that particular situation, the discussion that follows on the formation process of an ice ridge will span a broader picture to cover other possibilities. This includes mechanical de-icing systems as well as thermal de-icing and anti-icing systems. The effect of ambient temperature on these systems will also be addressed.

The following are possible scenarios for an ice ridge formation:

- Direct impingement of large droplets at cold and near freezing temperatures may extend beyond, for example, a pneumatically protected LE surface. Once the boots are activated, the ice within the active zone is broken and shed. The ice past the active zone remains on the surface and forms a ridge. Other systems will behave in a similar manner in this situation.
- Surface water may run back from the direct impingement zone to the downstream regions beyond the boots and freeze when the ambient static temperature is close to freezing and LWC is high.
- Runback water resulting from a running-wet system will freeze in place at cold ambient temperatures when the heat supply is diminished below the required amount.
- Runback water resulting from insufficient heating of a thermal evaporative system will also freeze past the protected regions.
- Direct impingement of moderate to large droplets on a small ridge of ice that may have formed on the surface during a short encounter to a SLD environment, or due to runback refreeze at warm temperatures, can also promote a ridge formation. Extended periods of exposure to the icing environment could lead to the buildup of a large spanwise ice ridge.

These issues will be considered in this paper. The findings may trigger the need to reconsider the traditional practice of limiting ice protection to the direct impingement regions.

The effect of near freezing temperature is very significant as will be discussed in a later section. A select number of experimental results obtained in the NASA LeRC Icing Research Tunnel will be illustrated and discussed.

IV. DISCUSSION OF VARIOUS ICE PROTECTION SYSTEMS

The maximum ice thickness that can be tolerated on the LE is a function of the airfoil geometry and its aerodynamic sensitivity to the different types and thicknesses of ice along the chordwise direction. The existence of ice on the LE decreases the airfoil maximum lift and the angle-of-attack margin to stall. The flow over the surface can be disrupted by the ice shape on the low pressure side of the airfoil (i.e., upper surface of wings or lower surface of horizontal tail stabilizers). This causes a reduction in pressure on downstream surfaces such as ailerons in the case of wings, and elevators in the case of horizontal stabilizers. The result is a reversed hinge moment on control surfaces, not necessarily total loss of lift, which could lead to an uncontrolled roll of the aircraft to one side or the other, or to ICTS (Ice Contaminated Tailplane Stall).

IV.1 Direct Droplet Impingement:

The phenomena suspected in the ATR accident due to ice remaining on the surface aft of the protected region following ice shedding events has already been discussed. The formation of even a small ridge downstream of an unprotected zone for any of the reasons discussed earlier and in the following paragraphs can pose a serious problem. At some point in time, the ridge height becomes greater than the boundary layer thickness, changes the airfoil shape locally, and becomes a direct impingement site for moderate to large droplets. At this point, the local heat transfer coefficient at the tip of the ridge -- the "ice feather"-- is very high. Therefore, there is a greater potential for the runback to freeze rather than to run back or shed from the surface.

In many situations, this problem is self remedied: the ridge grows sufficiently large that the shear and moment forces induced by the free stream break the ridge near its root and shed it off the surface. This leaves the airfoil with a much smaller ridge that will grow again with time while the aircraft is still exposed to an icing environment. The process repeats itself assuming the lifting surface is still under control and maintains enough lift to stay aloft.

IV.2 Running-Wet Anti-icing Systems:

A running wet system will always lead to runback refreeze. The size of the resulting ridge will depend mostly on the ambient temperature, the LWC and, as well, the time of exposure to the icing environment. In a warm ambient temperature (only a few degrees below freezing) the runback freezes in the form of rivulets that extend several inches, thus resulting in a smaller overall thickness. In cold conditions, the runback usually freezes within less than one inch resulting in a greater growth rate of the ridge height. Therefore, running-wet anti-icing systems suffer in colder temperatures.

Figures 1 and 2 illustrate these facts. The model is a NACA 0012 airfoil, 6 ft span and 36 inches chord. The LE has a electro-thermal ice protection system consisting of seven heater bands symmetrically located around the highlift. Surface temperature was controlled to 40 °F. The total temperature in Figs. 1&2 was 20 °F and 0 °F, respectively. Notice that

the runback in the colder condition spreads 1.25 inches only. This formed a ridge that continued to grow while exposed to the icing environment. In many situations, this ridge became large enough, about 1 inch, that aerodynamic forces broke it. The ridge height was noted to increase faster in the colder condition due to the shorter spread distance of runback. Again, this phenomena was enhanced at higher air speeds due to the higher rate of cooling (higher heat transfer coefficients).

IV.3 Evaporative Anti-icing Systems:

Generally speaking, evaporative systems require high power to function properly due to the high latent heat of vaporization of water. This power is a strong function of LWC as opposed to temperature in the case of running-wet systems. A full power may not be available at all times, for example, during approach if a bleed air system is used as a result of the decrease in engine speed. If available power is insufficient for total evaporative performance, a running-wet situation may result as discussed above. Some runback is expected to flow past the heated zone and freeze downstream. A similar problem could arise during multiple exposures to Intermittent Maximum cloud (high LWC), or during an inadvertent encounter to an icing environment. When the runback is thick enough, it is possible that direct impingement may occur downstream and form a ridge. Additionally, when flying through high LWC of snow, ice crystals, or mixed conditions, the power requirements increase to account for the latent heat of fusion.

IV.4 Electro-thermal De-icing Systems:

Electro-thermal de-icing systems exhibit the same problem as running-wet anti-icing systems. They result in smaller amounts of runback refreeze, however. An electro-thermal de-icing system will always result in frozen runback beyond the last heater band. A good design will minimize the amount of runback, but it cannot be eliminated. Therefore, an exposure time limit to an icing environment could be imposed on an aircraft equipped with such a system. A longer de-icing cycle time results in less runback refreeze but causes a larger ice thickness to accrete on the LE of lifting surfaces. Again, the frozen runback past the last heater band could grow large enough and become a direct impingement accretion site.

V. LARGE DROPLET EXPERIMENTAL STUDIES AT THE NASA IRT

Several studies have been conducted at the NASA Lewis Research Center since the Fall of 1994 to address the problem of large droplets [4] and [5]. The work done consisted of examining the effect of large droplet accretion on a 3 foot chord MS-317 airfoil at warm conditions in response to a request from the National Transportation Safety Board (NTSB) and the Federal Aviation Administration (FAA). Some of these results are shown in Fig. 3.

The effect of MVD was investigated at a relatively constant LWC of 0.5 g/m^3 . Close interpretation of the results suggests that large MVD droplet size distribution does not seem to be more detrimental than small droplet size. It is the relatively high LWC and the near-

freezing temperature that promotes the shift in the ridge location by a large percentage with a change of as low as 1 °F. This is more clear in the case of 56 micron MVD in Fig. 3 (note that the vertical and horizontal hashed areas represent a total temperature of 35.2 °F and 34.2 °F, respectively).

Currently available information [3] suggest that the LWC is relatively low in the case of large droplets. Consequently less icing severity would have been obtained during the IRT tunnel tests. It is believed that the thin layer of ice in the region of 15 to 33% of the chord on the upper surface, for MVD = 190 μm , is a result of direct impingement and not runback from upstream locations. The water surface tension forces are larger than the local aerodynamic forces at the far downstream locations where the boundary layer is thick. Therefore, the surface water drops that coalesce remain stationary and freeze thereafter. The leading edge region seems cleaner for the largest MVD case. One of the reasons is the sliding and shedding of accreted ice lumps at the warm conditions. Another possible reason may be more splashing phenomena in the case of large droplets as presented by Wright [6]. The effect of large droplets as illustrated in those results does not seem to be very significant on the accumulated ice.

Moreover, the local temperature associated with the ATR accident is suspected to be close to -2 °C [7]. This was the temperature at which the icing tanker tests were conducted to reproduce the accident conditions. Those test showed that large droplets cause ice to accrete on side windows in the cockpit. To the best of this author's knowledge, pilots flying in the vicinity of the accident region did not report any ice formation on side windows. One pilot flying on American Eagle airline reported [8]: "while the boots were clean, a ridge of ice between 1/4"-1/2" thick had formed on the top of the wing just aft of the boot. No ice was visible anywhere else on the airframe." The description of this flight encounter does not indicate the possibility of the existence of large droplets.

It is hypothesized that the ice ridge could have been formed from frozen runback water that extends past the boot zone as a result of the near-freezing ambient temperature. At the 15 degrees flap position, the main wing element is at a negative angle of attack. Consequently, the upper surface (low-pressure side) is exposed to direct droplet impingement further downstream. The combination of this with warm ambient conditions and a 40 micron MVD (upper limit of the FAR 25-C) is probably enough to cause runback refreeze past the boot region.

A second near freezing large droplet test followed in May, 1995 in the NASA Lewis IRT. The model tested was a full scale wing section of the Twin Otter with the flap in a stowed position. The model was also fitted with a pneumatic de-icing system. Test conditions were as follows:

Case 1: MVD = 190 μm , LWC = 0.5 g/m³, T_{TOT} = 32°F, V = 173 mph, AOA = 0

Case 2: MVD = 40 μm , LWC = 1.0 g/m³, T_{TOT} = 32°F, V = 173 mph, AOA = 0

Following those tests, NASA distributed a Video tape of some of the findings. The de-icer

boot was cycled every three minutes, with a final cycle when the spray was turned off. The measured ice thickness averaged about 0.7" on the upper surface and 0.5" on the lower surface for Case 1. The corresponding thicknesses for Case 2 were 0.4" and 0.4", respectively. The 190 micron case showed a distinct ice ridge at the end of the active boot zone. The 40 micron case had a similar but less distinctive ridge. Clearly, during the test, the effect of temperature was very significant when operating at near freezing temperature. Even a one degree F change in the temperature substantially affected the ice accretion shapes. Also, at the warmer conditions, the ridge moved further back.

The effect of temperature on the ice accretion was further studied in the IRT in the Fall of 1995 [9]. The test matrix included droplets of size 165 microns down to 40 microns. Test section air speeds were in the range of 125 to 195 mph. Total temperatures up to 35 °F were investigated.

The test article was the same 77.25" chord Twin Otter wing section. The LE was outfitted with a full span pneumatic de-icer boot extending to 10% chord on the suction surface, and to 11% chord on the pressure surface (the active boot zone is slightly less). Among the parametric studies conducted, the effect of the total temperature on the ridge formation was investigated. An ice ridge was observed to move further downstream at the warmer conditions, even beyond the already extended boot zone. Similarly, a clear liquid water zone was observed near the stagnation area. The warmer the temperature, the wider was that the zone. Had the current model been outfitted with a pneumatic boot to cover only 5 to 6% of the wing, serious problems would have arisen at the warm conditions as a result of runback refreeze.

An ice ridge was observed to form near the end of the active boot region when the boot was cycled at 3 minute intervals. This was the case when large droplets impinged on the surface regardless of the ambient temperature. A case of 40 microns drop size was tested at 163 mph, and 30 °F total temperature. An ice ridge was observed to form at the 5% chord location on the upper surface. This could be attributed to runback and to the ineffectiveness of the boot near the end of the active region. In most cases, the ice ridge height varied from 0.5" to as much as 1.25". In another attempt to prove that the droplets impinging on the model are supercooled, NASA repeated some of the cases at water temperature supply to the nozzles ranging from as low as 55 °F to as high as 180 °F. The accreted ice shapes were observed to be consistent within test repeatability margins.

In summary, the temperature effects on the formation of surface ice were found to be a large function of static temperature as opposed to the total temperature. This is due to the enhanced heat loss from the runback water to the local free stream as a result of evaporation. Also, the feather growth in the downstream regions was observed to occur normal to the surface at the warm temperature conditions, and into the flow direction at the cold temperatures. The clear (glaze) feathers forming in warm conditions looked very strange as they stood like nails normal to the surface. It is unclear that such a phenomena would occur during natural icing conditions. Not enough flight data is available where the ice physics has been observed in sufficient detail.

VI. CONCLUDING REMARKS

Freezing drizzle and freezing rain environments are recognized flight hazards and must be addressed. The ATR controversy revolved around the wing, and no apparent consideration was given to the tail, even though the latter is known to collect more ice and to be a serious element in the control of the aircraft. The subject of ICTS needs to be given a similar consideration and study as well.

There exist other conditions which promote hazardous situations and must not be overshadowed by the focus on SLD. Near freezing static temperature and a high LWC environment are apparently key elements in ice ridge formation.

The considered extension to the current FAR envelope in Part 25-C is a large step taken by the FAA. The existence of an SLD condition at the time of the ATR-72 accident had not been proven to be an absolute evidence. Before including SLD as part of the certification process, it must be proven that SLD could occur at near freezing static ambient temperatures and at relatively high LWC. Moreover, the effect of runback refreeze at near freezing static temperatures must be explored with droplet size 40 micron MVD (current maximum in the FAR envelope). It seems that the Russian authorities recommend using higher LWC values than what is listed in the FAR 25-C. This may be one way of modifying the envelope. Finally, a more thorough flight test program must be organized on an international effort level to assess the SLD atmosphere.

ACKNOWLEDGMENTS

The author would like to acknowledge the work performed at the NASA LeRC, and the cooperation and willingness of the NASA engineers involved in the project to discuss the IRT tests in particular, and the whole problem evolving around large droplets in general.

REFERENCES

1. Bragg, M., "Aircraft Aerodynamic Effects Due to Large Droplet Ice Accretions," 34th Aerospace Sciences Meeting and Exhibit, Jan. 15-18, 1996, AIAA Paper 96-0932.
2. Ashenden, W., Lindberg, W., and Marwitz, J., "Two-Dimensional NACA 23012 Airfoil Performance Degradation by Super Cooled Cloud, Drizzle, and Rain Drop Icing," 34th Aerospace Sciences Meeting and Exhibit, Jan. 15-18, 1996, AIAA Paper 96-0870.
3. Jeck, R., "Representative Values of Icing-Related Variables Aloft in Freezing Rain and Freezing Drizzle," 34th Aerospace Sciences Meeting and Exhibit, Jan. 15-18, 1996, AIAA Paper 96-0930.
4. Bond, T, and Ratvasky, T., Presentation at the SAE Subcommittee AC-9C Meeting No. 22 on Aircraft Icing Technology, Seattle, WA, April 25, 1995.

5. Bond, T, Irvine, T., Potapczuk, M., and Ratvasky, T., "LeRC Near-Freezing/Large Droplet Icing Research," FAA Phase II Meeting on super Cooled Large Droplet Icing Meeting, Crystal City, VA, June 22, 1995.
6. Wright, W., "Capabilities of LEWICE 1.6 and Comparison with Experimental Data," AHS International Icing Symposium, Montreal, Canada, Sept. 18-21, 1995.
7. "FREEZING DRIZZLE Towards a Better Knowledge and a Better Protection," Avion De Transport Regional, Issue 1, Nov. 5, 1995.
8. American Eagle Flight Operations Debrief, Nov. 1, 1994. Flight#: 4204; Flight date: 10/31/94; Departed: ORD; Landed: SBN; Aircraft#: 407.
9. Miller, D.R, and Addy, H.E., Jr., "A Study of Large Droplet Ice Accretions in the NASA-Lewis IRT at Near-Freezing Conditions," 34th Aerospace Sciences Meeting and Exhibit, Jan. 15-18, 1996, AIAA Paper 96-0934.

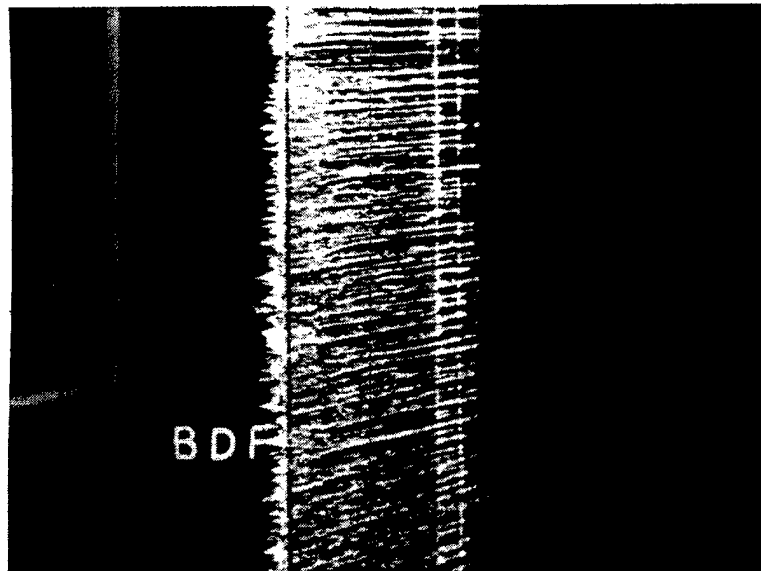


Figure 1: Running wet anti-icing system at 20 °F (freezing runback extent \approx 7 in)

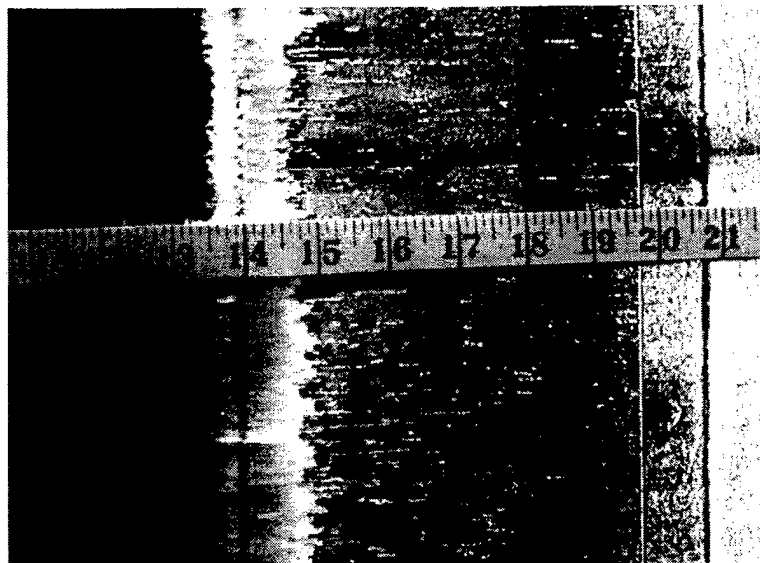


Figure 2: Running wet anti-icing system at 0 °F (freezing runback extent \approx 1.25 in)

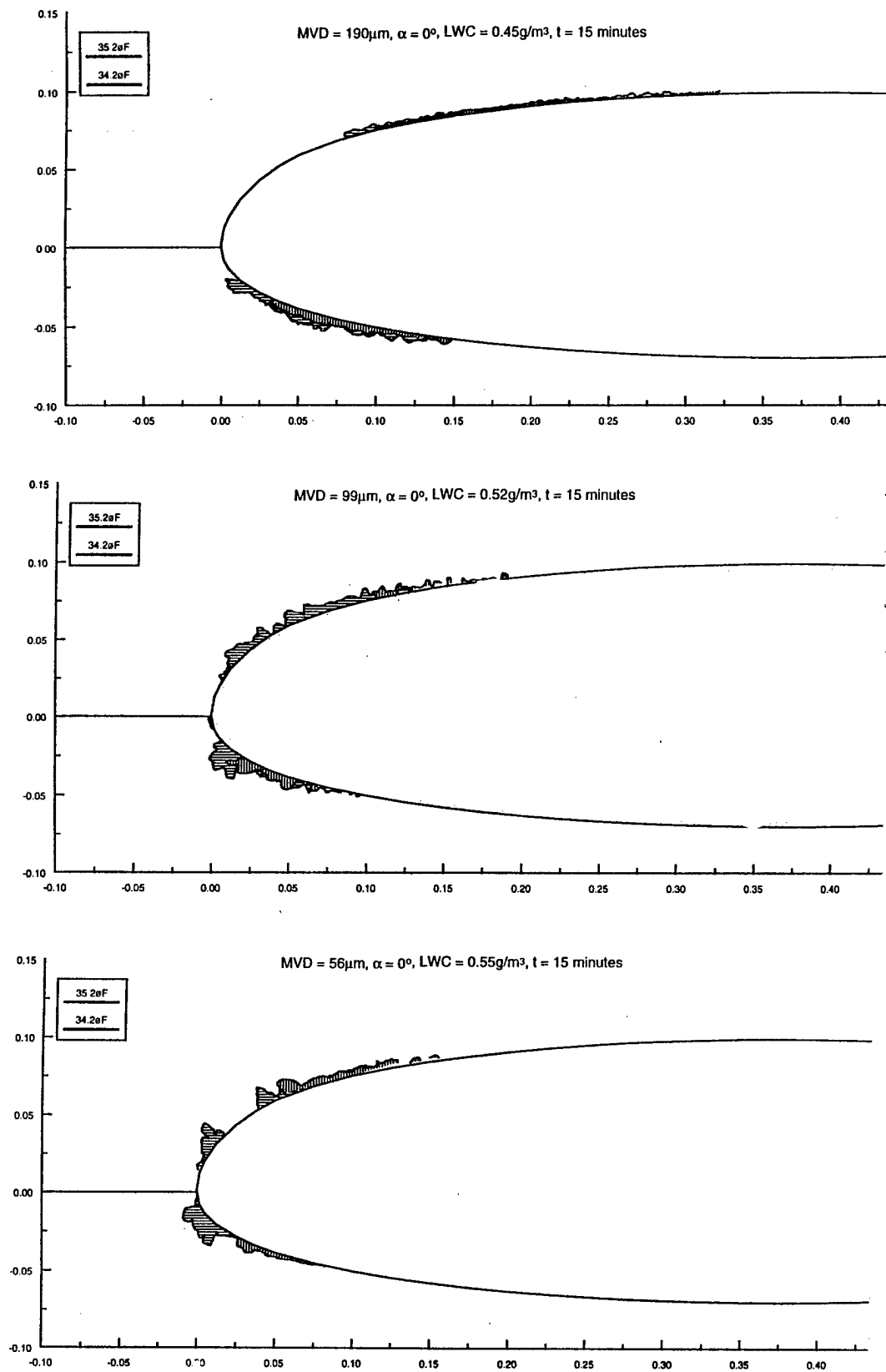


Figure 3: Effect of drop size on ice formation at near freezing temperatures [4].

Section III

Forecasting and Avoidance

Marcia Politovich, Industry Co-Chair

Myron Clark, Federal Aviation Administration Co-Chair

IN-FLIGHT ICING - THE CRITICAL NEED FOR IMPROVED FORECASTS AND INDEXING OF THE HAZARD

Dan Stack
USA Air Line Pilots Association

ABSTRACT

The development of an objective icing index to codify the threat or hazard of in-flight icing is essential. This index is but one part of a strategic approach to dealing with the operational aspects of icing in-flight. Other elements, certainly not lesser in terms of need, include the improved modeling and algorithms necessary for greater spatial and temporal accuracy in forecasting. There is an immediate need to go beyond a PIREP (Pilot Report) as an indication that the in-flight icing threat is present in an area. There are presently operational several systems, satellite mounted, ground based, and perhaps even aircraft-borne, that could be brought together to achieve more accurate forecasts. It is essential that the work and research in this field be continued and made operational as soon as possible. When possible, the technology for an on-board predictive ice detection system should be put on transport category aircraft and existing detection systems, if possible, be upgraded to predictive capabilities.

BACKGROUND

For the most part, experience in aviation has given the pilot a basis from which to make operational judgments on real as well as potential threats (as well as the lack of those threats) to safely conduct a flight through an area. As with anything else, the more insidious the situation is, the greater

the total threat becomes. We usually react to surprises in unpredictable ways. An offshoot to these unpredictable actions is the current trend of implementing unusual attitude training in the flight simulator syllabus. An obvious extension of windshear, microburst and stall recovery training: All are events into which we would never knowingly or willingly choose to submit our aircraft, passengers or ourselves.

The words hazard and threat imply that the phenomena is known, forecast, predicted. With exposure and experience, the pilot has come to believe that the phenomena can be circumvented, avoided, or even operated in with due precaution or with modified procedures. The reality of this type of experience is really a false sense of security, much like operating near a thunderstorm or gust front and managing to complete the segment without incident or accident. Schedules and economics have made this type of exposure a fact of life in the present-day world of commercial aviation. As pilots, controllers and dispatchers, we have come to expect that present technologies will provide the margins required to prevent us from personally becoming statistics and the subjects of a National Transportation Safety Board investigation. Indeed, present technologies have contributed significantly to safety in the world of aviation as well as benefited the general public. The Terminal Doppler Weather Radar (TDWR), Next Generation Radar (NexRad - WSR-88D), Low Level Wind Shear Alert System (LLWAS) have all been developed to aid in providing sufficient warning for microburst, gust front shear, tornadic activity, even flood warnings. The hardware and software created and tested for these systems has, at times, come on line in relatively short

order, especially when the needs were obvious. Frequently, the basic concept and the resulting technology have created additional benefits and products. The Integrated Terminal Weather Information System (ITWIS) is one such usable product having grown out of the TDWR and data link technologies.

ICING - THE THREAT

It is unfortunate that progress in aviation safety too often has come about because of an accident. Because of the Aviation Safety Summit brought forward by Secretary Pena and Director Hinson, the industry has another opportunity to provide for a greater margin of safety in day-to-day operations. It has been determined that the primary cause of the Simmons 4184 Roselawn, Indiana ATR-42 crash was the accretion of ice on the control surfaces and wings beyond the ability of the aircraft to carry it. The resulting loss of lift as well as controllability put the flight into a situation from which safe recovery became virtually impossible. The inadvertent operation in a severe icing environment for even a short period, can quickly place an aircraft in an environment which is significantly beyond its normal design. This is a part of the problem.

Last June, at the Phase II Aircraft Icing Conference hosted by the FAA in Washington, D. C., the question was raised as to whether or not the certification process adequately addressed an aircraft's ability to safely operate in icing environment. Should the process be changed in the Federal Air Regulations (FARs) Part 25 Appendix C so as to demonstrate an aircraft's Ultimate Ability to operate in the most adverse environment? There was, and is, obvious

resistance on the part of the manufacturers as well as the FAA to accept the fact that a change to the certification regulations should be made especially for "now unknown" threats. Present regulations do not call for the demonstration of how much ice an aircraft can carry before it falls out of the sky. Rather than this type of dynamic, destructive testing, they have preferred to demonstrate methods of defense (i.e. engine heat, deicing boots or hot wings and leading edges, ice-detector probes that may automatically turn on engine and/or wing heat). Then again, there is always the dictum to a pilot that you never operate an aircraft in severe icing, but if you do, you must leave the area immediately - unless its too late.

Present day operations are constantly driven by economic as well as time constraints. Even light aircraft operations frequently find the pilot in a situation where he would rather be somewhere else. I recall being in mid-Atlantic a February night and relaying a position report for a Cessna ferrying from Gander to Shannon. He was asking for advice on guard frequency (121.5) - he was at 5,000 feet, six and a half hours from either airport. The engine was running a bit rough, in the clouds and bumpy, and the outside air temperature was right at freezing. He thought that there might be some ice on the aircraft and was hoping for the OAT to warm up, as forecast. He was not sure of the best combination of mixture control and alternate air to help the engine run smoother as well as conserve fuel. The bottom line was that he did not want to become a statistic. This was not an enjoyable way to build flight time but, in the long run, I am sure it became valuable experience for the pilot when dealing with icing conditions in flight.

FORECASTS

With all-weather flying, often the first indication that there is a threat to a safe and comfortable ride is when a pilot makes a PIREP (Pilot Report) to the area traffic controller as well as to other pilots on the same frequency. These could be for low level wind shear, turbulence, and in-flight icing. As often as not, the PIREPS serve to validate, even invalidate forecasted phenomena. By their very nature, PIREPS are a direct reflection of the personal experience and observations of the individual pilot. It is because of this subjectivity that the need exists to create a less biased method of categorization of threat. Turbulence as well as in-flight icing could be indexed in such a manner. Such indices for area and altitude could be and should be a forecast product.

With fairly unanimous agreement, the presence of supercooled large water droplets (SLD) poses the greatest possibility for airframe and control icing. It also seems that the very size of these droplets would make them and the environments which support SLDs detectable with present technologies (NexRAD, TDWR, Satellite, Lidar and Profilers). It should be possible to fine-tune the algorithms for more enhanced forecasting, both spatially as well as temporally. We do it with both snow and rain precipitation in a surface environment in near-real time predictability. Serious icing research has been ongoing for more than forty years. There has been some ongoing research in the United States, Canada, and the United Kingdom, and progress has been made. Unfortunately, the cost of this research makes it one of

many items subjected to reductions due to the budget crunch.

Recent papers on inflight icing (Politovitch & Rasmussen) & (Mailhot, Tremblay et al) clearly state the need to be able to identify areas containing Supercooled Large Droplets (SLD's) - The areas of greatest threat. There appears to be a direct correlation of icing with major synoptic events. It also is quite likely that certain geographic areas are more prone to severe icing than others.

Understandably, the goals of science and technology are to make things as specific and perfect as possible. In forecasting, this would be to maximize the "hits" (correct) while minimizing the "misses." While it is important to seek these levels of success in forecasting, I would suggest that implementing the present levels of science now is much more operationally sound than waiting for perfection of the system and risking another Roselawn.

CONCLUSION

I believe the problems are quite clear and that the solutions are available. I would like to put forth four challenges to the industry in general - including the scientists, manufacturers, regulatory agencies, and operators - dealing with the hazard of inflight icing.

I. Validate and refine the modeling to create forecasts spatially and temporally accurate, easily understood as to degree of threat.

II. When necessary, willingly adjust operations when the threat warrants.

III. Create a clearly defined Icing Index to reflect an aircraft's ability to deal with this hazard in the enroute environment.

IV. On transport category aircraft, certificated for "all-weather" operations, install onboard ice detectors on critical surfaces capable of detecting impinged areas. This type of unit would provide the critical warning needed to deal with the threat or to exit an area of threat inadvertently entered or unforecasted.

ACKNOWLEDGMENTS

I would like to thank the following for their support and assistance on this project; Dr. Wayne Sand, the folks at National Center for Atmospheric Research (NCAR), the Engineering and Air Safety staff as well as the pilot volunteers of the Air Line Pilots Assoc.

REFERENCES

1. Politovitch, M & Rasmussen, R. 1995: Freezing Drizzle and Rain: Significant Issues in Forecasting. FAA Transport Airplane Directorate Docket No. 95-NM-01-AD
2. Tremblay, A., Mailhot, J., et al 1996: Intercomparison of Mesoscale Forecasts of Aircraft Icing, AMS Journal of Weather and Forecasting, March, 1996

A FORECAST AND VERIFICATION EXPERIMENT FOR SUPERCOOLED LARGE DROPS (SLD)

by

John Marwitz
University of Wyoming

ABSTRACT

On 31 Oct. 94 an ATR72 commuter aircraft crashed near Roselawn IN. Using data from the modernized National Weather Service, an analysis was performed (Marwitz et al. 1996) based on the concept that supercooled drizzle drops are related to wind shear (Pobanz et al. 1994). This analysis concluded that supercooled drizzle drops were likely present.

A new definition of ZL and ZR is proposed based on their formation processes. Specifically, ZL forms from an enhanced coalescence process related to wind shear and ZR forms from melted snowflakes. Justifications for redefining ZL and ZR are as follows:

- * Flight in ZL is more hazardous than in ZR or small drops,
- * The new definitions of ZL and ZR will likely result in similar drop sizes to the present definitions of ZL and ZR,
- * Discriminating between the new ZLs and ZRs is possible with the modernized NWS technology.

The forecasts of supercooled large drops (SLD) will be made based on the concepts that ZL forms from an enhanced coalescence process related to wind shear and ZR forms from melted snowflakes. Verification of the forecasts will be made by flying an instrumented research aircraft through these regions. A number of piggy-back experiments relating to aircraft icing will also be conducted.

INTRODUCTION

On 31 Oct. 94, an ATR72 commuter aircraft crashed southeast of Chicago near Roselawn, Indiana. Sixty-eight people were killed. Scientists at NCAR, UW and NOAA analyzed in detail the weather data associated with this accident. The objective was to apply the concept of super cooled drizzle drops related to wind shear as presented by Pobanz et al. (1994), using information from the modernized National Weather Service technology to infer the icing conditions associated with the accident. From the GOES infrared satellite data the cloud top temperatures (CTT) were -10[degree]C to -15[degree]C. The new NEXRAD radar at Lockport IL indicated that the reflectivity was about 10 dBZ and that there was no bright band through the 0[degree]C level in the accident area. The Winchester IL wind profiler, the Rapid Update Cycle model outputs, and MM-5 model outputs each indicated

that substantial vertical wind shear was present in the area that the ATR72 had been held by ATC enroute to Chicago. The weather data, therefore, was consistent with previous findings that related warm cloud tops and wind shear to freezing drizzle aloft. These results were provided to the NTSB (Politovich et al. 1995) as part of the accident investigation and a revised version of this analysis (Marwitz et al. 1996) has been accepted for publication.

The first documented encounter with super cooled drizzle drops (SCDD) by an instrumented aircraft occurred with the Wyoming King Air in 1982. This encounter occurred during a weather modification research project over the Sierra Nevada in Central California. The characteristics of the SCDD and the effect on the performance of the aircraft were described by Cooper et al. (1984) and by Sand et al. (1984). The effect of SCDD on performance by the King Air is primarily a major increase in the coefficient of drag, a major increase in the stall speed, and a minor decrease in the coefficient of lift. Additional encounters with SCDD in the Front Range of CO/WY, over the Sierra Nevada, Northern AZ, and near Amarillo TX were published by Politovich (1989). Our first encounter with freezing rain (ZR) occurred in 1992 while studying severe winter storms near MKC. The second encounter occurred in 1994 during similar studies near OKC. In both cases there was minimal performance degradation. These two ZR cases were described by Thomas and Marwitz (1995) and will be described in detail by Thomas (1995) and by Ashenden (1996).

SLDs lie outside of the so-called "icing envelopes" included in the FAA/FAR, Part 25, Appendix C (Dow, 1995). SLD includes SCDD, freezing drizzle (ZL), and freezing rain (ZR). Sizes for SCDD (Marwitz et al. 1996) are 40-400 microns in diameter. The size interval for SCDD was selected based on our experience that these drop sizes cause the greatest performance degradation on the Wyoming King Air. ZL and ZR are defined in the Glossary of Meteorology (Huschle 1959) based on the estimated drop sizes and rainfall rates as follows:

Freezing rain: Rain that falls in liquid form but freezes upon impact to form a coating of glaze upon the ground and on exposed objects. While the temperature of the ground surface and glazed objects initially must be near or below freezing (0[degree]C), it is necessary that the water drops be supercooled before striking. Rain drops have diameters > 500 microns.

Freezing drizzle: Drizzle that falls in liquid form but freezes upon impact to form a coating of glaze. Drizzle drops have diameters of 200 to 500 microns.

Drizzle is classified from 'very light', comprised of scattered drops that do not completely wet the surface, regardless of duration, to 'light', to 'moderate' to 'heavy', the rate of fall equals or exceeds 0.02 inch per hour.

NEW DEFINITIONS OF ZL AND ZR IN TERMS OF FORMATION

A new definition of ZL and ZR has been proposed in terms of the processes of formation of these weather phenomena (Thomas 1996). The weather conditions associated with SCDD, ZL, and ZR have been described. Then, the procedure was described whereby one can identify which phenomenon is occurring using the new observation systems being installed by the National Weather Service under their modernization program.

Pobanz et al. (1994) has established a strong statistical relationship between the presence of SCDD in stratiform clouds and wind shear near the tops of these clouds when the CTTs are warmer than -10°C to -15°C . If the CTT is colder than -10°C to -15°C , the cloud will be glaciated and, hence, contain no liquid water. The conditions associated with SCDD were reported as follows:

- * Cloud top temperatures are warmer than -15°C , (otherwise, the cloud will be glaciated)
- * The Richardson number at cloud top is < 1

Celik and Marwitz (1996) have provided a physical basis to the statistical relation that vertical wind shear is related to SCDD in stratiform clouds. Specifically, Celik and Marwitz (1996) have shown that Ostwald Rippening is enhanced when a cloud parcel experiences a series of slow updrafts and rapid downdrafts. Ostwald Rippening occurs because the equilibrium saturation vapor pressure over small drops exceeds the equilibrium saturation vapor pressure over large drops. Consequently, small drops will evaporate and the vapor will diffuse to the large drops. The Ostwald Rippening process is accelerated when a cloud parcel experiences an asymmetric oscillation. Asymmetric oscillations occur when vertical wind shear produces internal gravity waves.

The sounding beneath the SCDD can be either warmer or colder than 0°C . If the sounding is warmer than 0°C beneath the SCDD, there will not be a bright band because the drizzle drops are already liquid and obviously, do not melt. If the sounding is colder than 0°C beneath the SCDD, then ZL is occurring. This new definition of ZL implies that the drizzle drops originate from wind shear and that the cloud is colder than 0°C at all levels. Since the cloud is colder than 0°C , a melting layer and a bright band is not present. From an aircraft icing point of view, ZL from wind shear is an extremely hazardous icing condition because ZL drops cause much greater aircraft performance degradation than either small cloud droplets or ZR drops and the only evasive action available to the pilot is to climb above the cloud. If the pilot fails to recognize the hazard in time, the aircraft may not have sufficient excess power to climb.

The new definition of ZR states that ZR drops originate when snowflakes fall from an upper cloud layer which is colder than 0[degree]C into a middle layer which is warmer than 0[degree]C, and finally into a surface layer which is again colder than 0[degree]C. A bright band will appear on radar or wind profiler when the snowflakes begin to melt. When the raindrops fall into the surface layer and do not refreeze, they become super cooled rain drops or ZR. The ZR drops freeze upon contact with the ground, trees, or airplanes. If the ZR drops refreeze during fall through the cold surface layer, the resulting hydrometeors are ice pellets.

There are a number of reasons why it is appropriate to redefine ZL and ZR at this time. The first reason is that several recent climatological studies indicate that many soundings in the vicinity of reports of ZL do not display a 0 [degree]C level. These soundings were everywhere colder than 0[degree]C (Young 1978, Bocchieri 1980, and Huffman and Norman 1988). These climatology studies may have underestimated the percent of ZL from wind shear because:

- * The reported ZL may have originated as ZR (from melting snowflakes), but evaporated to ZL sizes during the last few hundred meters of fall below cloud base and
- * The observer may have underestimated the drop sizes and reported ZL based on a light rainfall rate when, in fact ZR was occurring.

A second reason is that ZL is much more hazardous to aviation than ZR. A third reason is that the processes of formation of ZL and ZR (by the new definitions) are uniquely different. Lastly, it is likely that the same drop sizes will occur with the new definitions of ZL and ZR as with the present definitions. We propose to discriminate between ZL and ZR based on the presence of a bright band using the WSR88D radar and/or wind profilers. If no bright band exists when freezing precipitation is occurring, then report ZL, otherwise report ZR.

FORECAST PROCEDURE

The forecast procedure for SCDD and ZL will be exactly the same as used in analyzing the meteorology associated with the ATR72 crash on 31 Oct. 94. Specifically, the available model outputs (including RUC, ETA, and MM-5) will be examined for predictions of conditions conducive for SCDD and ZL. In the nowcast mode the CTTs and wind shear will be determined from the available soundings, the new GOES-I/M satellites (GOES-8 and GOES-9 are presently on line), the wind profiler data, the NEXRAD/WSR88D radar. If the CTT is warmer than -15[degree]C to -10[degree]C and significant wind shear is present near cloud top, then SCDD will be forecasted/nowcasted for those levels colder than 0 [degree]C. If the whole sounding is colder than 0[degree]C and there are no indications of a bright band, then ZL will be forecasted/nowcasted.

The forecast procedure for ZR will be to examine the available model outputs using vertical cross sections for predictions of a folded 0[degree]C isotherm with a cold cloud (colder than -10[degree]C) above the upper 0[degree]C level. In nowcast mode, the soundings, satellite, and radar data will be examined for indications of CTT colder than -10[degree]C to -15[degree]C and the radar and wind profiler data will be examined for indications of a bright band. If a cold cloud and a bright band are present when freezing precipitation is occurring, then ZR will be forecasted/nowcasted.

VERIFICATION PROCEDURE

The verification procedure will be to direct an instrumented research aircraft into as many clouds as possible forecasted/nowcasted to contain SCDD, ZL, and ZR. Penetrations of these areas will be conducted with extreme caution.

PIGGY-BACK EXPERIMENTS

While the forecast/nowcast and verification experiment will have first priority, this experiment will provide unique opportunities to obtain additional valuable information on SLD environments as well as on aircraft response to flight in those environments. These will be treated as "targets of opportunity" and will be conducted as weather conditions permit. Listed below are some possible piggy-back experiments which we plan to conduct.

Icing Documentation: A concentrated effort will be made to obtain high quality documentation of the structure and location of icing on the aircraft as a function of drop size distributions and temperature. We will also document the performance degradation and possible effects on handling of the aircraft caused by the ice. This work will be useful for comparisons with numerical icing simulation models such as LEWICE to determine accuracy of calculated droplet impingement limits.

Development and effect of ice ridges: The development of ice ridges on the airfoil is a relatively rare occurrence, and is a function of angle of attack, temperature, liquid water content and droplet size distribution. When these ridges form aft of the deicing boots the effect on aircraft performance can be extreme.

Freezing nucleus measurements: The temperature at which ZL and ZR refreeze to become ice pellets (IP) can vary from around -5[degree]C to -12[degree]C. The refreezing temperature must be a function of properties of the condensation/freezing ice nuclei contained in the ZL and ZR drops. These ice nuclei most likely became part of the drops during their formation. UW has extensive experience in developing and interpreting drop freezing experiments, which are

well suited for this application. Uncontaminated airborne samples of liquid water will be collected and stored during flight in ZL and ZR, using techniques already found successful in previous experiments. The samples will be tested using drop-freezing equipment available at UW. This research was funded by an NSF grant to the Univ. of Wyo. (ATM-9308409)

References

- Ashenden, R, 1996: MS thesis, Univ. of Wyo. (in progress).
- Bocchieri, J, 1980: *Mon Wea Rev*, 108, 596-603.
- Celik, F and J Marwitz, 1996: Submitted to *J. of the Atmos Sci.*
- Cooper, W, et al., 1984: *J. Aircraft*, 21, 708-715.
- Huffman, G and G Norman, 1988: *Mon Wea Rev*, 116, 2172-2182.
- Marwitz, J, et al., 1996: Submitted to *Bull. of the Amer Met Soc.*
- Pobanz, B, et al., 1994: *J. Appl. Meteor.*, 33, 1366-1372.
- Politovich, M, 1989: *J. Appl. Meteor.*, 28, 856-868.
- Politovich, M, et al., 1995: Paper prepared for NTSB and FAA, 9 pp.
- Sand, W, et al., 1984: *J. Clim. Appl. Meteor.*, 23, 1427-1440.
- Thomas, M, 1996: MS thesis, Univ. of Wyo. (in progress)
- Young, W, 1978: MS thesis, Texas A&M Univ., 123 pp.

A comparison of a physically-based aircraft icing forecast algorithm with currently-used automated algorithms using SSM/I retrievals.

André Tremblay(1), Stewart Cober(2), Anna Glazer(1) and George Isaac(2)

Cloud Physics Research Division
Atmospheric Environment Service
2121 Trans Canada Highway
(1) Dorval, Québec, CANADA, H9P 1J3
(2) Downsview, Ontario, CANADA, M3H 5T4

Introduction

The use of numerical weather model output to generate forecasts of significant weather for aviation has grown through the years. Current methods to predict aircraft icing are typically diagnostics which use criteria for the dew point depression, temperature and vertical motion to delineate icing regions. These procedures are based mostly on the criteria suggested by Appleman (1954), or by Schultz and Politovich (1992) and are used as predictors for supercooled liquid water (SLW). Recently, Tremblay *et al.* (1995) proposed an alternative technique to forecast the occurrence of supercooled clouds based on a prognostic cloud scheme that can provide the cloud liquid water content. Recent studies have emphasized the importance of this parameter in the development of reliable aircraft icing forecast techniques that embody the crucial cloud physics processes (Modica *et al.*, 1994).

In this paper, mesoscale forecasts of icing, for a few east coast Canadian winter storms, produced with different aircraft icing algorithms, will be discussed. These forecasts will be next intercompared using a satellite-based verification technique. It will be shown that currently-used automated algorithms give incorrect distributions of icing events with temperature and systematically include glaciated clouds in icing forecasts. This problem is eliminated when the scheme of Tremblay *et al.* is used. The evaluation of the accuracy of the Canadian icing forecasting system will be presented for the different icing algorithms. An intercomparison of ATR-72 crash case forecasts produced with the various icing schemes will be briefly outlined.

Aircraft icing forecast schemes

Direct output of meteorological models are still currently used to generate forecasts of aircraft icing (see Schultz and Politovich, 1992 and references therein). Typically a diagnostic forecast of icing is produced using criteria for the dew point depression, temperature and upward vertical motion. These parameters are tested at each grid point to verify if certain critical conditions are met.

The U.S. Air Force Global Weather Central, in their automated icing forecast program (Mansur, 1984), uses criteria based on results from an aircraft icing survey. The criteria for the presence of icing at any altitude are: temperatures between 0 and -16 °C, upward vertical motion greater than -0.2 Pa s⁻¹, and the dew point depression less than a certain threshold.

Such an indicator for aircraft icing was first suggested by Appleman (1954). From frost-point theory and aircraft icing reports, Appleman concluded that when temperature was plotted against dew point as in Fig. 1, observations of fog or cloud lying between the lines $T = T_d$ (saturation line) and $T = 0.8T_d$ (Appleman line) represented cases of SLW, and icing was highly probable.

Appleman verified this conclusion with only a relatively small sample (49 cases) of weather reconnaissance observations and his conclusion was validated with a considerably larger sample of data (5,483 observations in sub-freezing stratiform clouds) by AWS (1980). Since these comparisons did not consider non-icing events, the results can only suggest that the Appleman criterion [hereafter referred as APP] may be a *necessary* condition to observe icing events. Unfortunately, it was not possible to demonstrate from these observations that this criterion is a *sufficient* condition for the occurrence of icing.

Using a database of icing reports over the continental United States and numerical model output, Schultz and Politovich (1992) identified temperature and relative humidity criteria for two icing threat classes. Class I utilized temperatures extended from 0 to -20°C and relative humidity greater than 50% which encompassed 87% of icing reports in the database. Class II [hereafter referred as the Schultz and Politovich standard algorithm or SPS] was more restrictive, with a temperature range of -2 to -15°C and relative humidity greater than 65%, which included only 71% of the icing reports.

By evaluating the relative importance of the various microphysical processes involved in the production of SLW, Tremblay *et al.* (1995) showed that the conditions for the existence of SLW can be inferred by comparing production rate of supersaturation with respect to water (wG) with its depletion rate ($SDEP$), as illustrated in Fig. 2.

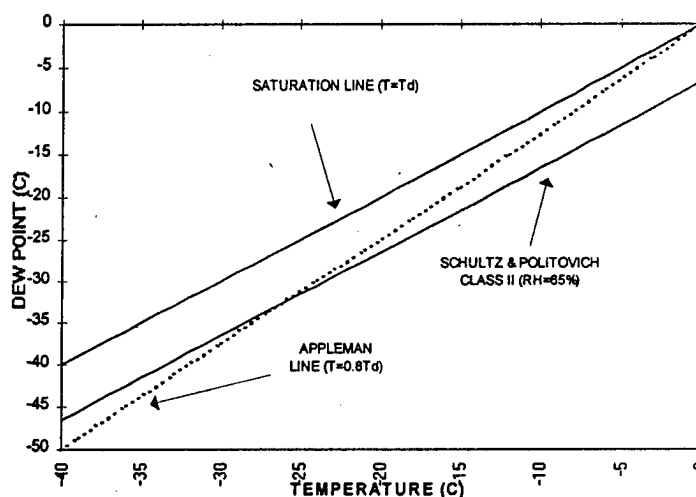


Figure 1: Dew point vs. temperature diagram showing icing occurrence according to Schultz and Politovich (1992) class II and Appleman (1954) schemes. Icing is predicted for regions between the saturation line and the Appleman line or for regions between the saturation line and the RH = 65% line for the Schultz and Politovich scheme

With temperature as an independent variable at constant pressure, Fig. 2 shows an ensemble of functions wG indexed by vertical velocity, and an ensemble of functions $SDEP$ indexed by snow content. By fixing temperature (-15°C), pressure (700 mb) and vertical velocity (0.10 m s^{-1}), giving a specific value of wG , the point X in this figure is obtained. The proposed criterion states that for all $SDEP$ points on isotherm -15°C located below X, there is a possibility of existence of SLW. These points correspond to a snow content lower than 0.06 g m^{-3} . For all the points above X, corresponding to a snow content greater than 0.06 g m^{-3} , an ice cloud exists. Alternatively, the point X may also be interpreted as characterizing fixed conditions of temperature (-15°C) and snow content (0.06 g m^{-3}), giving a specific value of $SDEP$. In this manner, the criterion predicts a possibility of existence of SLW for vertical velocities exceeding 0.10 m s^{-1} (above point X) and ice cloud for vertical velocities less than 0.10 m s^{-1} (below point X).

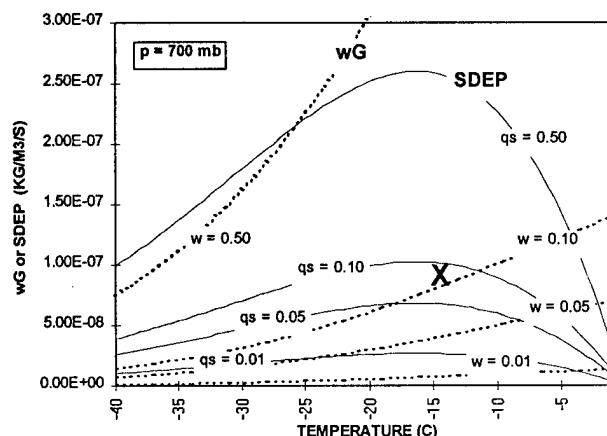


Figure 2: A diagram illustrating the determination of supercooled liquid water at a given point as a function of temperature ($^{\circ}\text{C}$), vertical velocity w (m s^{-1}), and snow content q_s (g m^{-3}), for 700 mb pressure level. The wG and $SDEP$ curves are shown for a few selected values of w and q_s , however, an ensemble of curves is implied.

The above technique can easily be combined with mesoscale prognostic cloud schemes such as the one proposed by Sundqvist *et al.* (1989), to generate aircraft icing forecasts. In this scheme, all hydrometeors are combined within a single variable m , which is calculated explicitly from a continuity equation.

Comparison methodology

To provide a framework for validation, comparison and optimization of the various icing prediction schemes, several numerical mesoscale simulations were performed with the RFE model (Mailhot *et al.*, 1995) for selected North Atlantic winter storms observed during CASP II. An important feature of the model is the use of an explicit treatment of condensation and clouds, based on Sundqvist *et al.* (1989). This formulation explicitly treats the cloud content as a prognostic variable, which allowed the application of the cloud microphysics icing forecast scheme of Tremblay *et al.* (1995) [hereafter referred as the T95 scheme].

To evaluate the accuracy of any icing scheme, one should ideally know the distribution of SLW in the atmosphere. Such information is rarely available and direct validation is a difficult task. In this study, SSM/I retrievals of the vertically integrated liquid water, satellite infrared measurements, and analyses from the Canadian Meteorological Centre were used to obtain a diagnostic of the SLW distribution in the horizontal. At a given horizontal point, SLW was inferred if the cloud top temperature was less than 0°C , SSM/I retrievals of LWP (computed from algorithms given in Petty, 1990; Petty and Katsaros, 1990) exceeded 0.3 kg m^{-2} , and the SSM/I signals were assessed as not being significantly influenced by ice crystal scattering.

Such a retrieval procedure is based on vertically integrated values and gives the horizontal distribution of SLW events. Thus, this technique can be used only within a two-dimensional framework to evaluate the accuracy of the forecast system for positioning SLW events in the

horizontal. Strictly, a three-dimensional forecast verification can be done from a direct comparison between model output and research aircraft measurements, such as in T95, however, this approach is limited due to the relatively small size of the dataset. In principle, using a PIREPs dataset for forecast verification allows a three-dimensional validation, but the non-systematic and biased nature of these observations causes problems (Brown *et al.*, 1995).

The schemes outlined above (APP, SPS and T95) produce yes/no categorical forecasts on the three-dimensional grid of the weather prediction model. In order to insure a consistent comparison with SSM/I retrievals, these three-dimensional forecasts were collapsed to two dimensions by identifying horizontal points where a SLW forecast existed somewhere in the vertical. The signal detection theory (SDT) (Mason, 1982) is a verification procedure applicable to two-state categorical weather elements, such as in the present case. With the SDT, the forecast skill can be evaluated from the probability of detection (*POD*) and the probability of false detection (*POFD*). The *POD* can be described as the number of correct SLW forecasts divided by the total number of SLW observations. Conversely, the *POFD* is the number of erroneous SLW forecasts divided by the total number of non-SLW observations. A perfect forecast is described by $POD = 1$ and $POFD = 0$.

A straightforward application of these specific statistical parameters to icing forecast schemes may yield to incorrect evaluations as discussed in Tremblay *et al.* (1996) and a different approach is proposed. For each point with a SLW observation (as retrieved from SSM/I), the distance d to the nearest forecast is calculated. Let $N_1(d)$ represent the distribution of these distances (the number of SLW observations where d is within the interval d and $d + \delta d$). Next, for each point where SLW is not detected, the distance d to the nearest non-SLW forecast is also calculated. Alternatively, let $N_0(d)$ represent the distribution of these distances.

The skill of forecasts can be discussed in term of the cumulative relative frequency functions of these distributions $f_0(d)$ and $f_1(d)$. The function $f_1(d)$ can be interpreted as the *POD* within a circle of radius d of the observations, and $1 - f_1(d)$ as the probability of misses (*POM*) [fraction of missed events lying outside of the validation circle]. Equivalently, $f_0(d)$ represents the fraction of correct forecasts of non-SLW events within the validation circle. In other words, it can be called the probability of correct null forecasts (*POCN*). Within this framework, $1 - f_0(d)$ delineates the *POFD* and the SDT is a particular case obtained as $d \rightarrow 0$.

Results

For validation, 18 icing mesoscale forecasts were produced with the RFE model. These cases encompassed fundamental aspects of winter storms, including warm frontal regions, low pressure areas, cold fronts and warm sector clouds. These are regions where the most severe icing was expected to be found, and should provide a strong background for comparison of the three icing forecast schemes.

To match SSM/I retrievals, each forecast was mapped on a 25 km (latitude-longitude) grid and was evaluated with the verification technique outlined above. Results are presented in Fig. 3. The two diagrams in the figure show the frequency functions $f_1(d)$ and $f_0(d)$ for each forecast in the data set. To help in the visualization of the results, the frequency functions are represented with a stacked bar format. The distance d was classified with 25 km bins that were close to the nominal resolution of the SSM/I at 37 GHz. In the figure, only distances ≤ 100 km ($2 \cdot \Delta x$ for model forecasts) are represented; forecasts with $d > 100$ km were considered to have missed their target. Those forecasts enclosed within the first bin [$f_1(0)$ and $f_0(0)$], were hits, and those within $f_1(100)$ and $f_0(100)$ were accurate at a $2 \cdot \Delta x$ level. Illustrating the extremes found in these situations, the model had $f_1(0) = 0.9$ for the forecast L but $f_1(0) = 0.05$ for the forecast G.

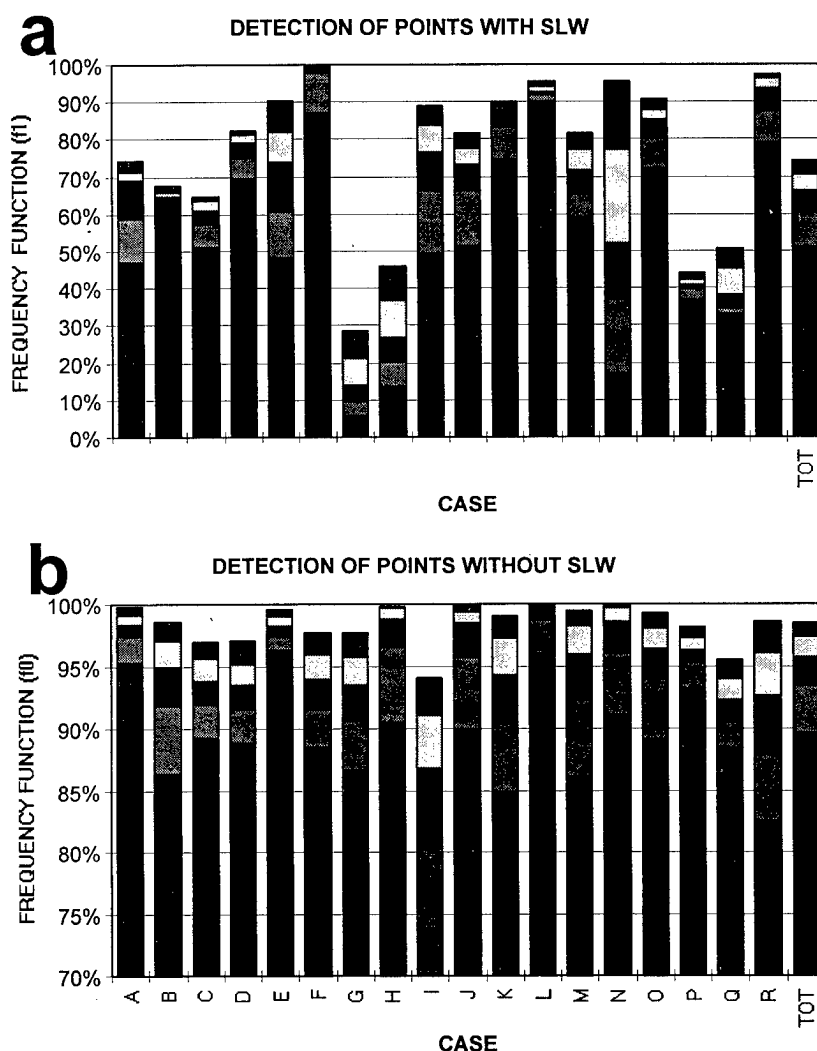


Figure 3: The frequency functions $f_1(d)$ for SLW events (panel a), and $f_0(d)$ for non-SLW events (panel b) for each forecasts in the data set, displayed with 25 km bins stacked bar format (shading corresponds to $d = 0, 25, 50, 75$ and 100 km). The category labeled TOT represents the entire data set.

Alternatively, the model had a fair degree of success in detecting non-SLW events. For example, the forecast showed $f_0(0) = 0.95$ and $f_0(100) = 0.99$ for case A, but for case I, which was a bad forecast for non-SLW events, $f_0(0) = 0.70$ and $f_0(100) = 0.94$. In these diagrams, the category labeled **TOT** represents the same calculation for all data points. Overall, about 50% of SLW events were detected at their right location, 65% within a $1 \cdot \Delta x$ distance and 75% within a $2 \cdot \Delta x$ distance. Roughly 25% of SLW events were absolutely missed ($d > 100$ km) by the forecasting system. About 90% of the non-SLW events were forecasted at their right location and about 1% of these events were not forecasted within the $2 \cdot \Delta x$ accuracy, as shown in Fig. 3b.

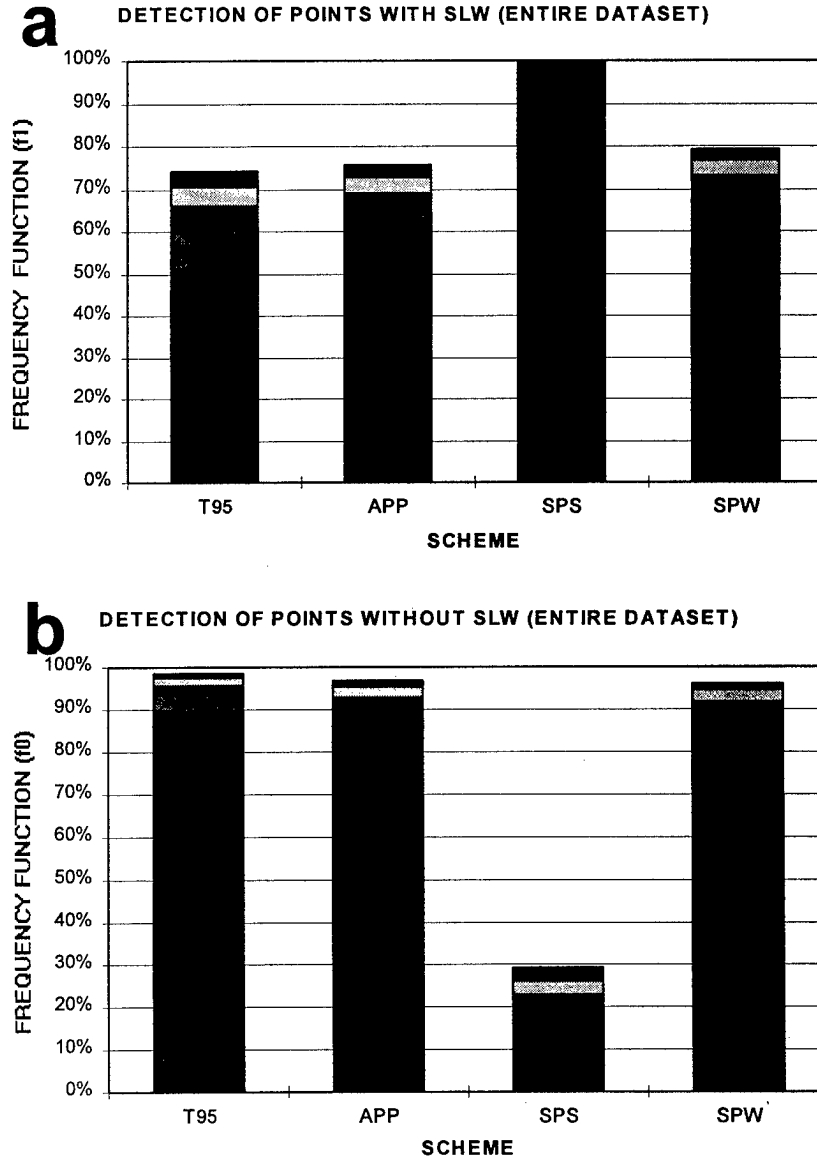


Figure 4: The frequency functions $f_1(d)$ (panel a) and f_0 (panel b) as in Fig. 7 for the entire data set and for the four forecast schemes

To examine, in detail, the behavior of the different SLW schemes, Fig. 4 depicts the frequency functions calculated for the entire data set using four different SLW forecast algorithms. To insure a consistent comparison, the APP and SPS criteria were applied within the same temperature interval $-20^{\circ}\text{C} \leq T \leq 0^{\circ}\text{C}$. The SPW scheme was identical to the SPS scheme but used the APP condition for vertical motion (i.e., $\omega \leq -0.2$ Pa/s). Figures 4a and 4b show that the forecast performances are seriously impaired when d decreases, for each SLW algorithm. For example, for $d = 0$, f_i falls below 0.60, which is close to the number of expected correct forecasts due purely to chance. This suggests that the system does not produce reliable point forecasts ($d = 0$). However, as indicated by the values of f_o and f_i displayed in figure 4, it generates useful predictions within 100 km accuracy. Figure 4b demonstrates that the SPS scheme systematically flagged most of the mesoscale domain for aircraft icing, as indicated by the low value of $f_o(100) = 0.30$, implying its uselessness in the present context. However, if the SPS scheme is modified for vertical velocity (SPW), dramatic improvement occurs and $f_o(100)$ increases to about 0.95.

Figure 4a shows that T95 ($f_i(100) = 0.745$), APP ($f_i(100) = 0.755$) and SPW ($f_i(100) = 0.790$) schemes have about the same accuracy for detecting the vertically integrated SLW signal. This relatively weak dependence of f_i with respect to the forecasting technique used, suggests that the quality of the SLW forecast was strongly related to model accuracy in predicting vertical velocity, temperature, moisture and cloud content. Since there was 8822 SLW events in the dataset, these values of f_i imply that T95 has missed 2250 of these events, APP 2161 and SPW 1853.

Figure 4b, indicates that $f_o(100) = 0.987$ for T95, $f_o(100) = 0.952$ for SPW and $f_o(100) = 0.963$ for APP. This implies a *POFD* of 0.013 for T95, 0.048 for SPW, and 0.037 for APP. Since there was 74784 non-SLW observations in the dataset, the T95 scheme had erroneously flagged as SLW 972 data points. Equivalently, the SPW scheme erroneously flagged 3589 data points. Thus SPW had issued a number of false detections greater by a factor of 3.7 with respect to T95. The performance of APP was superior to SPW with a total number of false detections of 2804. As a comparison, T95 missed 397 more events than SPW, but removed false alarms at 2617 points.

From the above discussion, it can be established that T95 had issued 7544 yes-forecasts, SPW 10558 and APP 9465. This implies that T95 tends to slightly *underforecast* the SLW extent (8822 observed events), while SPW and APP tend to slightly *overforecast* the SLW signal. Another useful statistical evaluator for forecasts comparisons is the frequency of hits (*FOH*). This parameter is defined as proportion of yes-forecasts matched by a yes-observation. Its complement is the false alarm ratio (*FAR*) defined as the proportion of yes-forecasts contraindicated by a no-observation. It can be easily showed that $FOH = 0.871$ for T95, 0.660 for SPW, 0.704 for APP. This correspond to $FAR = 0.129$ for T95, 0.340 for SPW and 0.296 for APP. Thus, according this statistical evaluator, 87% of SLW forecasts issued by T95 were correct. This number falls to 70% for APP and to 66% for SPW. This discussion is summarized in Table 1.

d = 100					
Estimator	Description	T95	SPW	APP	SPS
POD	Probability of Detection	0.74	0.79	0.76	1.00
FOM	Frequency of Misses	0.26	0.21	0.24	0.00
POCN	Probability of Correct Null Forecasts	0.99	0.95	0.96	0.29
POFD	Probability of False Detection	0.01	0.05	0.04	0.71
FOH	Frequency of Hits	0.87	0.66	0.70	0.14
FAR	False Alarm Ratio	0.13	0.34	0.30	0.86

d = 0					
Estimator	Description	T95	SPW	APP	SPS
POD	Probability of Detection	0.52	0.59	0.56	0.98
FOM	Frequency of Misses	0.48	0.41	0.44	0.02
POCN	Probability of Correct Null Forecasts	0.90	0.82	0.84	0.16
POFD	Probability of False Detection	0.10	0.18	0.16	0.85
FOH	Frequency of Hits	0.37	0.28	0.30	0.12
FAR	False Alarm Ratio	0.63	0.72	0.70	0.88

Table 1. Summary statistics.

The high number of false detections of the APP, SPS and SPW schemes was likely related to the oversimplified cloud microphysics embodied in the construction of these algorithms. As discussed above, the physical principles underlying these icing forecast procedures may result in an erroneous distribution of SLW with temperature, implying that glaciated and supercooled clouds were not discriminated correctly. Glaciated clouds may also have significantly contributed to the SLW horizontal hits of these procedures (Fig. 4a), emphasizing the need to discuss the vertical structure of the forecasts. Since the atmosphere is thermally stratified in the vertical the distribution of SLW forecasts with temperature gives indirect information about their vertical structure and reveals their physical consistence. This is illustrated in Fig. 5 which displays the distribution of all predicted SLW events on the three-dimensional model grid, with respect to temperature (for the 18 cases). The T95 scheme has generated a sharp distribution of SLW events decreasing with colder temperature. On the other hand, both SPS and SPW schemes generated relatively flat distributions with respect to temperature. This result suggests that the probability of an ice encounter is independent of temperature and contradicts observations. The APP scheme had a clear tendency to generate a decreasing frequency of SLW events with increasing temperature. In fact, such a tendency is just the reverse of observations, and this non-physical behavior classifies the APP scheme as an inadequate forecasting tool for aircraft icing. As indicated in the diagrams of Fig. 5, the total number of forecasted SLW points is strongly dependent on the algorithm used. For example, the SPS scheme generated 10 times the number of SLW events compared with the T95 scheme, showing the high rate of false alarms characterizing this scheme. The SPW scheme generated approximately 2 times the number obtained from the T95 scheme. Figure 5 shows that colder temperatures contribute to this difference, suggesting that the SPW scheme issued icing forecasts within cold clouds classified as being glaciated by the T95 scheme.

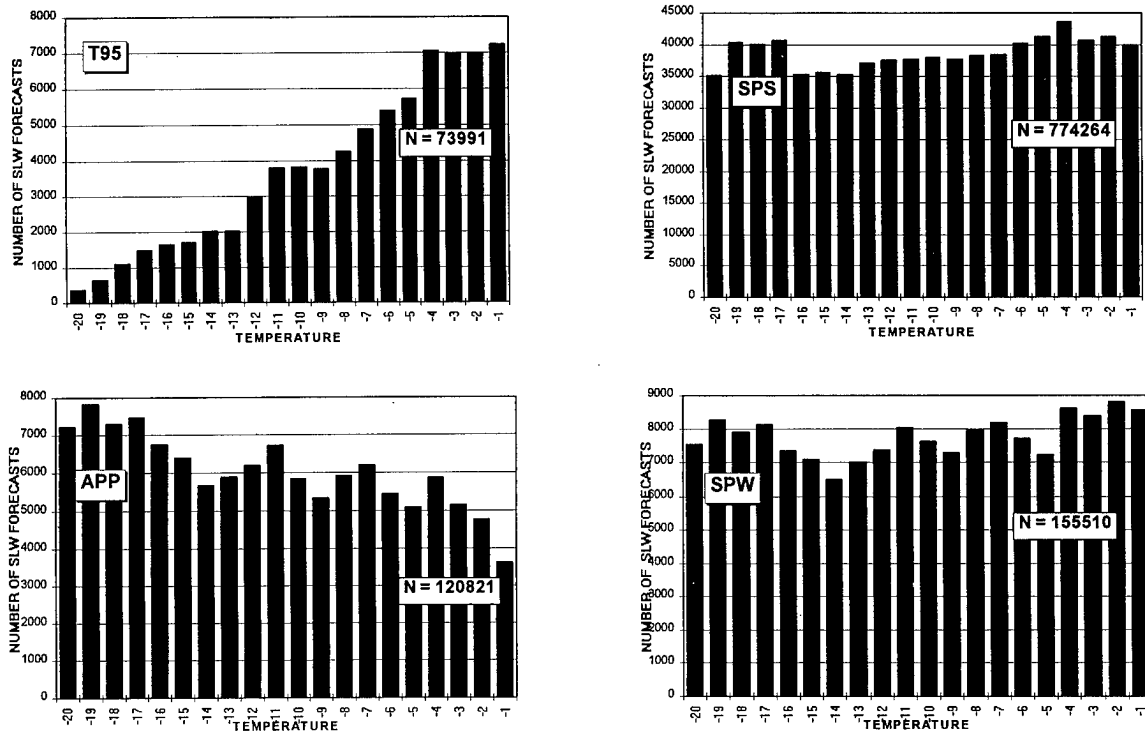


Figure 5: Distribution of the number of forecasted icing events on the three-dimensional model grid with respect to temperature, for the 4 schemes. The total number of forecasts is also reported in each diagram.

As an example, Fig. 6 depicts icing forecasts over the continental US (a 40 km grid was used). This map is valid on 21 UTC 31 Oct. 1994, one hour before the ATR-72 aircraft accident near Roselawn, Indiana

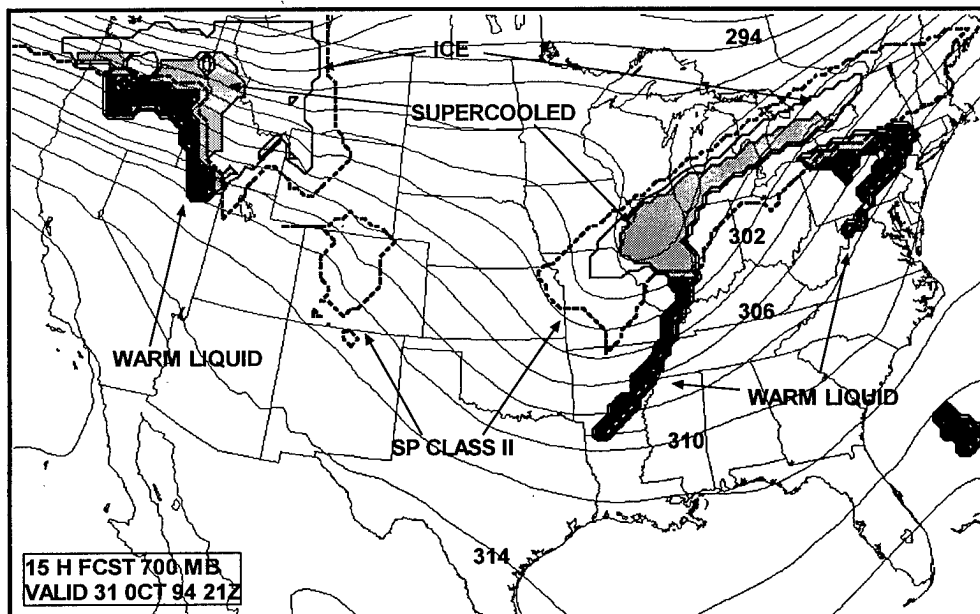


Fig. 6: 700 mb icing forecasts valid 21 UTC Oct. 31 1994 using SPS and T95

(Politovich *et al.*, 1995). The figure shows that T95 has successfully identified the icing threat zone near the crash localization. However, the aeral coverage of the T95 icing is considerably less than for the SPS algorithm.

Conclusions

In this paper, the accuracy of three aircraft icing (or equivalently SLW) forecast schemes were evaluated. From integrations of the Canadian RFE model with an explicit cloud scheme, a data set of mesoscale icing forecasts, representative of typical east coast Canadian winter storms, was constructed. The forecasts were evaluated by comparison with SLW distributions derived from satellite data.

It was argued, and subsequently demonstrated from numerical integrations, that the forecast procedures of Appleman (1954) and Schultz and Politovich (1992) resulted in erroneous distributions of SLW events as a function of temperature. The Schultz and Politovich (1992) forecast scheme yielded a flat distribution of SLW frequency with respect to temperature. For the Appleman (1954) procedure, the frequency of icing forecasts decreased as temperature increased. These contradict measurements and imply that glaciated clouds were systematically included in SLW forecasts resulting in a large number of false detections. Therefore the operational use of these schemes is questionable.

The procedure of Tremblay *et al.* (1995) was found to give a realistic distribution, with the number of SLW events sharply decreasing as temperature decreases. This distribution is consistent with atmospheric conditions and suggests that the basic cloud physics embodied in the derivation of the Tremblay *et al.* (1995) scheme is fairly well representative of microphysical processes found in natural clouds. This resulted in the total number of SLW forecasts (on the three-dimensional model grid) decreasing by a factor of 2 when compared to the Appleman scheme, and by a factor of 10 with respect to the Schultz and Politovich (1992) scheme.

In order to provide a verification of SLW forecasts, a retrieval technique for the SLW, based on infrared satellite imagery, microwave data from the SSM/I DMSP satellites, and weather analyses was suggested. A SLW retrieval, matching each numerical icing forecast was then generated and used with a validation procedure based on the signal detection theory to evaluate the accuracy of forecasts.

The Tremblay *et al.* (1995) icing forecast system detected, with a perfect precision (i.e. at the right location), 50% of the model grid points where a SLW signal is retrieved from satellite analyses. However, 65% of the signal can be detected within one grid length Δx (50 km, in the present study) and 75% within a $2\Delta x$ range. The 25% of the forecasts outside the validation circle of radius $2\Delta x$ were considered as missed events. The false alarm rate was rather low with about 99% of non-SLW events detected by the system within a $2\Delta x$ range (100 km). This number of false alarms was roughly equivalent to 13% of the observations of SLW. It was also established that T95 forecasts had a false alarm ratio of 13% while APP and SPW forecasts had FARs of 30% and 34% respectively. This outlines the limit of operational applicability of the forecasting system and should be used as a guideline to properly educate potential users. The Tremblay *et al.* (1995) scheme represents a significant improvement in accuracy over existing schemes and should be considered as a good first guess for aviation forecasts.

Acknowledgments. This work was funded by the Canadian National Search and Rescue Secretariat. Funding for the field project was also provided by the Institute for Aerospace Research (IAR) of the National Research Council of Canada, Boeing Commercial Airplane Group and Airbus Industrie.

References

- Air Weather Service, 1980: Forecasting guide on aircraft icing. AWS Tech. Rep. AWS/TR-80/001, U.S. Air Force, Scott AFB, IL, 55 pp. [INTIS AD-A085 490/1]. 105-39, 41 pp.
- Appleman H., 1954: Design of a cloud-phase chart. *Bull. Amer. Met. Soc.*, 35, 223-225.
- Brown B., R. Bullock, G. Thompson, and R. Brientjes, 1995: WISP94 real-time icing prediction and evaluation program (WIREP): Statistical issues and forecast verification results. Preprints, 6th Intl. Conf. on Aviation Weather Systems, Dallas, TX, 15-20 Jan, AMS, 207-212.
- Mailhot J., R. Sarrazin, B. Bilodeau, N. Brunet, A. Methot, G. Pellerin, C. Chouinard, L. Garand, C. Girard, and R. Hogues, 1995: Changes to the Canadian regional forecast system. *Atmos. Ocean*, 33, 55-80.
- Modica G.D., D.W. Johnson, and R.M. Rasmussen, 1994: Application of an explicit microphysics mesoscale model to a regional icing event. *J. Appl. Meteor.*, 33, 53-64.
- Petty G.W., 1990: On the response of the Special Sensor Microwave/Imager for atmospheric parameters retrievals. 291 pp..
- Petty G.W., and K.B. Katsaros, 1990: New geophysical algorithms for the Special Sensor Microwave Imager. Fifth Int. Conf. on Satellite Meteorology and Oceanography, London, Amer. Met. Soc., 247-251.
- Politovich M.K., B.C. Bernstein, F.M. Ralph, P.J. Neiman, J.D. Marwitz and R. Ashenden, 1995: Meteorological conditions associated with the ATR-72 aircraft accident near Roselawn, Indiana on 31 October 1994. Proc. International Icing Symposium, Montreal Canada. Amer. Helicopter Soc.
- Schultz P., and M. Politovich, 1992: Toward the improvement of aircraft icing forecasts for the continental United States. *Wea. and Forecasting*, 7, 491-500.
- Sundqvist H., E. Berge, and J.E. Krisjansson, 1989: Condensation and cloud parameterization studies with a mesoscale numerical weather prediction model. *Mon. Wea. Rev.*, 117, 1641-1657.
- Tremblay A., A. Glazer, W. Szyrmer, G. Isaac, and I. Zawadzki, 1995: Forecasting of supercooled clouds. *Mon. Wea. Rev.*, 123, 2098-2113.
- Tremblay A., S. Cober, A. Glazer, G.T. Isaac and J. Mailhot, 1996: An intercomparison of mesoscale aircraft icing using SSM/I retrievals. *Wea. Forecasting*, 11, 66-77.

VERIFICATION OF IN-FLIGHT ICING FORECASTS: METHODS AND ISSUES

Barbara G. Brown

Research Applications Program
National Center for Atmospheric Research
Boulder, Colorado

Abstract

Verification of icing forecasts is a difficult process due to characteristics of the data available for use in the verification process. Characteristics of pilot reports (PIREPs), which are frequently used for such studies, are described, and implications of these characteristics for icing forecast verification are investigated. Several approaches that have been applied for the verification of icing forecasts are described and compared.

1. Introduction

Statistical verification of icing forecasting techniques is a critical part of their development. By evaluating forecast products throughout the development process, deficiencies in the algorithms can be identified, and improvements can be made. Verification also provides important data for users of the forecasts, who need objective information about the quality (e.g., accuracy) of the forecasts for making decisions.

Unfortunately, evaluation of in-flight icing forecasts is not straightforward, primarily due to the limited nature of the data available for verification analyses. Frequently, pilot reports (PIREPs) are the best data available for this task. However, PIREPs are not systematic in time or space, and they contain a number of inherent biases (e.g., the highest frequencies of PIREPs are in high-traffic regions) which make them a difficult dataset to use for this purpose.

One important consequence of these characteristics is the inability to estimate the false alarm ratio (FAR) using standard verification approaches, which forces reliance on other measures of overwarning. Characteristics of the PIREPs also have implications for the reliability and representativeness of the verification statistics. Forecasting and detection techniques focused on specific types of icing (e.g., severe conditions; supercooled large droplets) are even more difficult to evaluate.

The primary purpose of this paper is to describe and compare methods that have been developed and applied to verify in-flight icing forecasts. These methods are considered in Section 4, following discussions of PIREP characteristics in Section 2 and verification methods in Section 3. Implications and recommendations are summarized in Sections 5 and 6, respectively.

2. Icing verification data

The ideal data for verification of icing forecasts would be *an objective, systematic measurement of icing on aircraft at a specified set of times and locations (in three dimensions)*. Some physically based measurements, derived from radar or satellite data, are currently becoming available (e.g., Lee and Cook, 1995; Tremblay et al., 1996) and eventually may meet many of these criteria. However, until recently these

measurements have not had widespread coverage; they generally are two-dimensional; and they are subject to interpretation and the effects of parameterization. In addition, their relationship to icing on an airplane is not necessarily straightforward. Moreover, *estimates from such measurement systems themselves require extensive verification.*

Thus, PIREPs typically are the measurement chosen for verification of icing forecasts. One major advantage of PIREPs is that they are a *direct measurement of the actual forecast event*: that is, whether current meteorological conditions are conducive to the formation of ice on the frame and wings of an airplane.

While PIREPs may be a *direct* measurement of icing, they also have numerous disadvantages for use as verification data: they are non-systematic, haphazard, subjective, and biased, at least to some degree. Characteristics of PIREPs and some of the difficulties involved in using them for verification studies have been discussed previously by Brown et al. (1993, 1995); Kelsch and Wharton (1996); Schultz and Politovich (1992); and Schwartz (1996). Much of the rest of this paper is concerned with the use of PIREPs for verification. Thus, PIREP characteristics and their implications are considered here in some detail.

Spatial and temporal distributions of icing PIREPs generally represent flight patterns for the day-of-week, time-of-day, and altitude, as previously shown by Schultz and Politovich (1992). For instance, air traffic normally is heavier during mid-week than on weekends. Correspondingly, more PIREPs are received on weekdays. Most flights occur during day-light hours, and the same is true of PIREPs, as shown in Fig. 1. In fact, 95% of the icing PIREPs in February and March 1990-1996

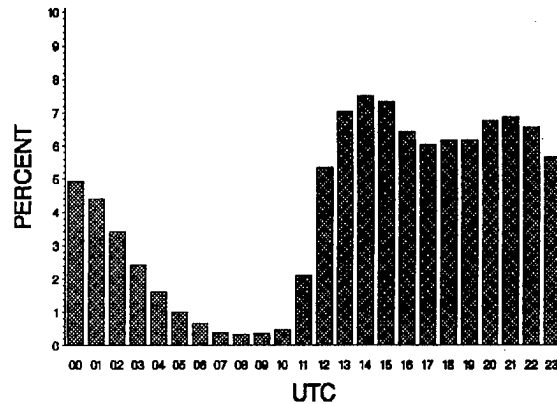


FIGURE 1. Relative frequencies of PIREPs by time of day (February and March, 1990-1996).

occurred between 1200 and 0400 UTC, roughly corresponding to day-light hours in the United States.

PIREPs also are not evenly distributed across the country, as illustrated in Fig. 2. This map suggests that PIREPs are clumped over larger urban population centers (e.g., the Northeast corridor, Denver, Salt Lake City, Seattle). Moreover, some areas of the country (e.g., most of Nevada) have very few or no PIREPs.

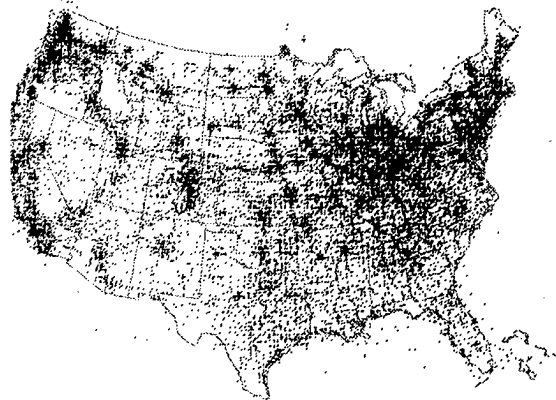


FIGURE 2. Locations of all icing PIREPs, March, 1990-1996.

Of most concern for verification is the *non-systematic nature* of PIREPs. In particular, icing observations are not made at the same set of locations and times every day. In most weather forecast verification studies, an observation is available to

match every forecast (or a specified subset of forecasts) every day. For example, a precipitation forecast concerns the accumulation of liquid in a rain gauge at a specific location; precipitation is collected in the gauge for the specified period of time, and the total amount collected is used to verify the forecast. Thus, for precipitation, the comparison of forecast to observation is relatively straightforward. In contrast, the locations and times of PIREPs are determined by many factors (e.g., flight patterns), as described earlier. Hence, PIREPs are not available for the same set of locations/forecasts and times every day.

The non-systematic nature of PIREPs also means that the distribution of PIREPs between Yes and No values is unlikely to represent the "true" distribution of icing conditions. No PIREPs are very limited in frequency because pilots are not required to report "No-icing" conditions. In contrast, pilots *are* required to report icing (i.e., to make a Yes report) whenever it is experienced. The resulting distribution of PIREPs over-estimates the relative frequency of icing. Specifically, if actual icing conditions could be observed at all points on a grid across the continental United States, a much larger proportion of the grid-point observations typically would be No than would be Yes. In contrast, only about 25% of the icing PIREPs are for "No icing." Thus, PIREPs do not adequately sample the No icing regions.

It also is important to note that while PIREPs are not a *systematic* measure, they also are not *random*. For example, as noted earlier, PIREP locations and times are strongly related to flight patterns. Thus, PIREPs cannot be treated as a random sample of grid points, which also has implications for their use as verification data.

3. Verification issues

This section is a general discussion of verification methods and measures. The discussion is illustrated with a simple, artificial, forecast verification example.

3.1 Grid-based verification

In the typical forecast verification situation described in the previous section (i.e., for precipitation), in which each forecast has a matching observation, some standard approaches and measures can be applied to the verification analysis. These approaches and measures are illustrated in this section using Fig. 3 and Table 1.

Fig. 3 shows a hypothetical icing forecast on a grid (Fig. 3b) for which the actual icing region (Fig. 3a) is known. Thus, in this case each of the 100 Yes/No forecast grid boxes has a matching Yes/No observation. (For the moment, ignore the PIREP points scattered around the grid). The grid overlap plot (Fig. 3c) shows that some of the forecast and actual icing grid points overlap, and some do not. Counts of these 100 forecast/observed Yes/Yes, Yes/No, No/Yes, and No/No pairs from Fig. 3c can be summarized in a contingency table like Table 1a. The resulting counts associated with the Fig. 3c grid are shown in Table 1b.

From the counts in Tables 1a and 1b, a number of standard verification measures can be computed. These measures include the probability of detection (POD) and false alarm ratio (FAR), which are defined as

$$\text{POD} = \frac{a}{a + c}, \quad (1)$$

and

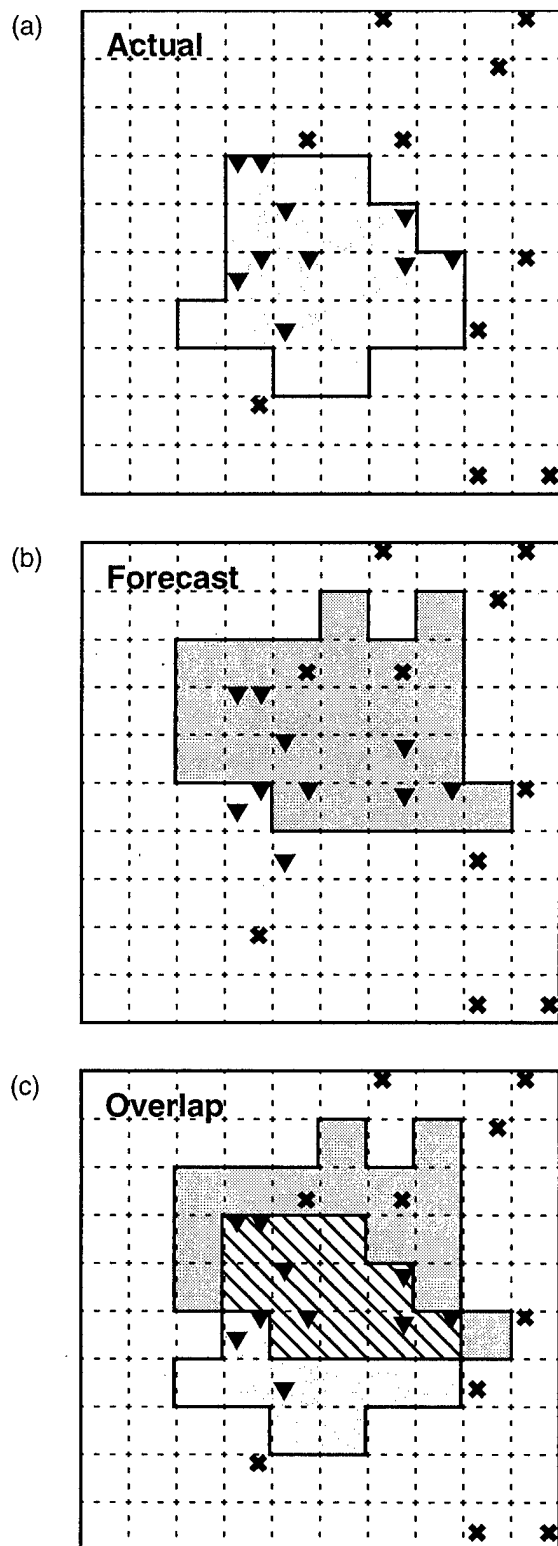


FIGURE 3. Artificial (a) actual ("true") and (b) forecast icing regions, with Yes PIREPs (inverted triangles) and No PIREPs (X's) randomly assigned to grid squares. Part (c) shows overlap (hatched region) between actual and forecast icing regions.

TABLE 1. Frequencies of forecast/observation pairs (a) in general; (b) for grid-based verification of a hypothetical forecast, using "actual" icing grid in Fig. 3; (c) for verification based on hypothetical PIREPs in Fig. 3; and (d) for alternative verification based on PIREPs in Fig. 3.

	Observed		
Forecast	Yes	No	Total
<i>(a) General</i>			
Yes	a	b	a+b
No	c	d	c+d
Total	a+c	b+d	a+b+c+d
<i>(b) Grid-based</i>			
Yes	11	14	25
No	9	66	75
Total	20	80	100
<i>(c) PIREP-based</i>			
Yes	7	2	9
No	3	8	11
Total	10	10	20
<i>(d) Alternate PIREP-based</i>			
Yes	6	19	25
No	2	73	75
Total	8	92	100

$$\text{FAR} = \frac{b}{a+b} \quad (2)$$

POD is the proportion of Yes observations that are correctly forecast to have icing; FAR is the proportion of Yes forecasts that are incorrect. POD and FAR range between 0 and 1; perfect forecasts would be characterized by $\text{POD} = 1$ and $\text{FAR} = 0$. Another statistic of interest is the Bias, defined as

$$\text{Bias} = \frac{a+b}{a+c} \quad (3)$$

or the ratio of the number of Yes forecasts to the number of Yes observations. This measure indicates whether the icing region

is overforecast (Bias > 1) or underforecast (Bias < 1) overall.

Row (a) of Table 2 shows the values of these three statistics computed for the grid-based forecasts and observations represented by the counts in Table 1b. These statistical measures represent the "True" verification statistics for the hypothetical forecast. In particular, as measured by the actual icing grid, 55% of the Yes grid points also have a Yes forecast; 56% of the Yes forecasts are not associated with actual icing; and the size of the forecast icing region is 125% of the size of the actual icing region (i.e., the forecast region is larger than the actual icing region).

TABLE 2. Verification results for icing forecast shown in Fig. 3 using (a) grid-based observations of actual icing region; (b) PIREPs; and (c) alternative use of PIREPs.

	Method	POD	FAR	Bias
(a)	Grid	0.55	0.56	1.25
(b)	PIREP	0.70	0.22	0.90
(c)	Alt. PIREP	0.75	0.76	3.12

3.2 PIREP-based verification

To demonstrate the effects of basing the verification statistics on PIREP data, a set of artificial PIREPs were added to the grid in Fig. 3. For this example, 10 Yes PIREPs and 10 No PIREPs were randomly assigned to the actual icing and no-icing regions in Fig. 3a (note that No PIREPs were only assigned to the actual No-icing region, and Yes PIREPs were only assigned to the Yes-icing region). By counting the PIREP/forecast pairs in Fig. 3b, the numbers in Table 1c are obtained; these counts lead to the POD, FAR, and Bias estimates shown in row (b) of Table 2. Note that the POD estimated by the PIREPs (0.70) is too large, and the FAR value (0.22) is much too small. Moreover, the Bias estimate (0.90) indicates that the

forecast is an *underforecast* rather than an *overforecast*, as is the actual case.

An alternative method of using PIREPs for verification is occasionally implemented [e.g., see Reap (1996) for an application to turbulence forecasting]. This method assumes that if a PIREP is not associated with a grid point, then there is no icing at that grid point. This method allows verification at all grid points. However, the assumption of no icing whenever there are no PIREPs is unrealistic (e.g., due to the spatial distribution of PIREPs). Using this alternative method, the counts in Table 1d are obtained from Fig. 3, and the verification statistics in row (c) of Table 2 are computed. With this method, POD and FAR (0.75 and 0.76, respectively) are both over-estimated, and Bias (3.12) is drastically over-estimated.

To obtain a broader view of the PIREP results, the single simulation experiment represented by the PIREPs in Fig. 3 was repeated 25 times. For each of the 25 "trials," PIREPs were randomly assigned to the forecast/actual icing grid in Fig. 3 and the verification statistics were computed. Median (i.e., 0.50th percentile) values of the 25 POD, FAR, and Bias values are shown in Table 3. Note that the grid-based statistics were the same for every trial.

TABLE 3. Median values of verification statistics for 25 random PIREP experiments based on the grid in Fig. 3, with statistics computed using (a) grid-based observations of actual icing region; (b) PIREPs; and (c) alternative use of PIREPs.

Method		Median		
		POD	FAR	Bias
(a)	Grid	0.55	0.56	1.25
(b)	PIREP	0.50	0.22	0.60
(c)	Alt. PIREP	0.50	0.84	3.12

Results in Table 3 for the 25 experiments are quite similar to those shown in Table 2 for one trial, with the exception of the results for POD. In particular, both PIREP methods, *on average*, are able to estimate POD with relatively little error (though the POD values exhibit large errors in specific cases). In contrast, both methods provide incorrect overall estimates of both FAR and Bias, with the basic PIREP method greatly *underestimating* both FAR and Bias, and the alternative PIREP method greatly *overestimating* both measures.

An approach involving random sampling of the grid by not requiring a specified distribution of Yes/No PIREPs, was also applied to the Fig. 3 grid. Results of that test (not shown here) indicate that random sampling would provide good estimates of the verification statistics. See Brown and Murphy (1996) for more details on these results.

It should be noted that the PIREP-based results for FAR and Bias in this example are closer to the true values than is likely to occur in the "real world," due to the relatively large number of No PIREPs that were assigned to the grid. Specifically, 50% of the PIREPs in this example were No PIREPs, whereas in actual PIREP datasets, the No reports constitute a much smaller fraction (20-25%) of the total. Thus, for this example, a larger fraction of the No Icing grid points were sampled than is typically the case, and the FAR values are more representative of the actual icing grid.

Results of this little experiment illustrate the fact that the alternative PIREP-based method is inappropriate and leads to incorrect results. Moreover, even with the standard PIREP approach, *FAR and Bias cannot be correctly estimated from current*

PIREP datasets, using traditional methods. In addition, as noted earlier, POD can and should be interpreted as *the proportion of observed (Yes) icing reports that were correctly forecasted*, rather than in the strict sense implied by the word "probability." This proportion can be reasonably estimated using the PIREP data, because it is *observation-based*, in contrast to FAR, which is *forecast-based*. It is important to note use of the word "PIREPs" rather than "icing events" in the definition of POD: PIREPs and their frequencies cannot be assumed to represent the frequencies and characteristics of all icing events, since not all icing regions are observed and/or reported by pilots (e.g., many icing regions are avoided).

Thus, POD values based on PIREPs should be interpreted very carefully, due to the PIREPs' non-systematic nature. In fact, *a POD value from traditional icing verification analyses should not be treated in an absolute sense as representing the "true" POD associated with an algorithm or a model.* Instead, it can be used to great advantage in a relative sense, such as for comparing the detection rates of different forecasting algorithms.

4. Icing verification approaches

This section summarizes various approaches that actually have been used for icing forecast verification. These approaches include case studies and grid-based methods, as well as a few PIREP-based approaches.

4.1 Case studies

Case studies provide a focused form of verification of forecasting methods. However, they typically are very limited in spatial and temporal extent, and may not be representative of conditions in general.

Thus, they provide guidance for development of forecasting methods, but do not provide definitive information about the performance of forecasting algorithms. Broader methods are required to obtain a true forecast verification.

4.2 *Grid-based approaches*

The grid-based approach described in Section 3.1 can be applied when verification data are available at all or a specified subset of forecast grid points. Such a situation would exist if a physically-based measurement that is related to icing (e.g., derived from satellite or radar observations) were available. In that case, it is straightforward to estimate POD, FAR, and Bias, as well as other statistics that summarize the counts shown in Table 1a [see Doswell et al. (1990), Schaefer (1990), Stanski et al. (1989), or Wilks (1995) for a description of other statistics].

Tremblay et al. (1996) propose a modified grid-based approach in which the verification statistics are estimated as a function of the distance from a forecast grid point to the closest matching observation. The goal of this approach is to compensate for situations in which a very bad forecast (e.g., a “false alarm” region located far from the actual icing region) achieves the same verification scores as a more reasonable forecast (e.g., a forecast region that is only slightly offset in location from the actual icing region). The method developed and applied by Tremblay et al. computes verification statistics for varying distances from the forecast grid point. As would be expected, the statistics improve with increased distance.

For their verification, Tremblay et al. (1996) compute a POD-type statistic plus a measure based on a statistic called the Probability of Correct Null (POCN). This

statistic also has been called the Probability of Detection of No observations (POD-No), and has been used in PIREP-based verification studies (Brown et al., 1995). POCN is defined as

$$\text{POCN} = \text{POD-No} = \frac{d}{b + d} \quad (4)$$

and can be interpreted as *the proportion of No observations that are correctly forecast to have no icing*. Tremblay et al. compute the POCN rather than the FAR so all their verification statistics are from the “users’ point of view.”

4.3 *PIREP-based POD/Area approach*

The PIREP-based approach (i.e., Section 3.2) relies on POD as a measure of the ability of a forecast to identify PIREP locations. Because FAR cannot be estimated using basic PIREP datasets, it is necessary to develop an alternative measure of overforecasting. POD alone is not a sufficient verification measure for comparing two algorithms (Ehrendorfer and Murphy, 1988). An alternative measure suggested and applied by Brown et al. (1995) is the Impacted Area of the forecast; that is, the areal extent of the icing forecast region.

For three-dimensional gridded forecasts (e.g., based on the output of numerical weather prediction models), Impacted Area is the total area of surface grid points for which icing is forecast at any model level. A related variable, Impacted Volume, can also be computed. This variable is the sum of the volumes of all grid points (at all levels) with a “Yes” forecast.

The plot in Figure 4 demonstrates why Impacted Area is a reasonable verification measure. In this figure, the forecast region from Fig. 3 is shown along with a set of artificial Yes PIREPs. Two forecasts

are shown: Forecast 1 has an areal extent of 25 grid boxes (i.e., Forecast 1 covers 25% of the total area) and encloses 70% of the PIREPs. Naively, one might say, "I can improve that forecast easily by moving the forecast box out," and thus create Forecast 2. Forecast 2 now encloses *all* of the PIREPs, but it also covers 64% of the total area, including a large area with no PIREPs and probably no icing. Thus, Forecast 2 *has* increased POD, but it also covers a much larger area.

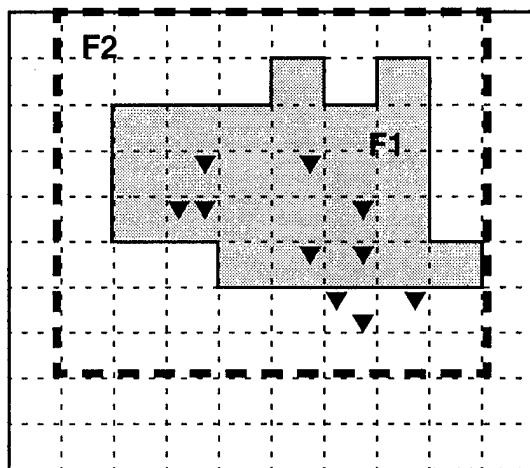


FIGURE 4. Hypothetical icing forecasts F1 (shaded) and F2 (dashed outline), with artificial "Yes" PIREPs overlaid.

The use of Area and Volume as verification measures implies that the goal of the forecasting system is to maintain a high POD while simultaneously minimizing the Area impacted by the forecast. This goal is reasonable from an aviation viewpoint, since it is undesirable to overforecast regions of icing and unnecessarily limit access to them by aircraft.

When POD and FAR are the basic verification measures, a trade-off typically exists between having a high POD and a low FAR. Specifically, it usually is difficult to increase POD without simultaneously increasing FAR. Similarly, a trade-off exists between POD and Area/Volume for

the PIREP-based verification of icing: it is difficult to increase POD without simultaneously increasing the impacted Area and Volume. This trade-off is illustrated in Fig. 5, which is a plot of POD vs. Area for several components of the RAP icing algorithm, which are treated here as individual algorithms (see Thompson et al., 1995, 1996 for a description of this algorithm).

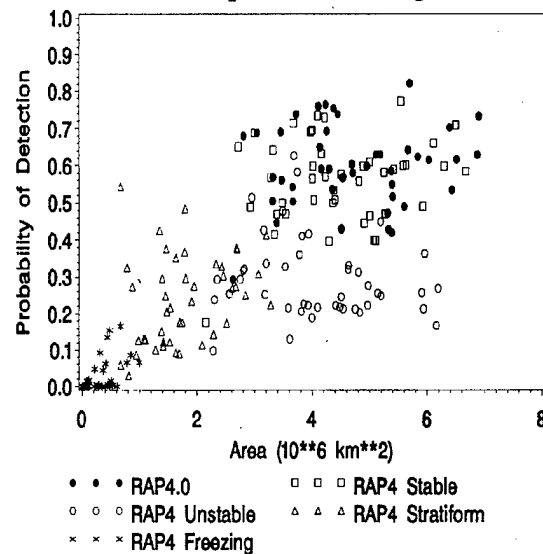


FIGURE 5. Scatter plot of daily values of POD vs. Area for components of the RAP icing algorithm, based on experimental model output from the Eta model; 18-hr forecasts issued at 0000 UTC, 1 Jan to 28 March 1995.

Some of the algorithm components in Fig. 5 have high POD and large Area; others have low POD and small Area. Some components (e.g., the "Stratiform" component) seem more able than others to "buy" larger amounts of POD for smaller amounts of Area. For example, the stratiform algorithm (triangles) has comparable POD values to the Unstable algorithm (circles) but smaller Area values.

This ability, to attain greater amounts of POD for smaller Area or Volume amounts, can be evaluated using simple measures of "Area Efficiency (AE)" and "Volume Efficiency (VE)," defined as

$$AE = \frac{POD}{Area} \quad (5)$$

and

$$VE = \frac{POD}{Volume} \quad (6)$$

(Brown et al., 1996). These efficiency measures can be interpreted as "POD per unit Area" and "POD per unit Volume," respectively. They provide supplementary information regarding the quality of the forecast, but are not sufficient verification by themselves (e.g., without other basic information such as POD). For example, it frequently is the case that algorithms with the highest efficiency values also have very small POD values.

4.4 PIREP-based "Cities" approach

The "Cities" approach represents a combination of grid-based and PIREP-based methods. It is designed to use PIREPs to define a systematic icing measurement at certain locations, by making use of the fact that PIREPs are more frequent in the vicinity of major airports. This approach is described and applied in Brown et al. (1993, 1994), respectively.

The Cities approach is based on the critical assumption that *icing conditions will always be reported (a Yes observation) if they exist in the regions around major cities. Thus, if icing is not reported in the region, icing conditions can be assumed to not exist (a No observation)*. Hence, every forecast for a city region has a corresponding observation. Observations and forecasts are assigned to a city by examining grid points and PIREPs within a specified radius (e.g., 60 km) of the city.

With an accumulation of forecasts and observations over a period of time, the standard grid-based verification statistics

(e.g., POD, FAR, Bias) can be computed. Figure 6 shows an example of a Cities-based verification of the RAP icing algorithm (Thompson et al., 1995) for April 1995, for Denver. Fig. 6 includes both POD and FAR as a function of altitude (for three layers); the values at the 0 altitude level represent the statistics achieved when the entire column above Denver is verified as a whole. As shown in Fig. 6, the POD values for the entire column and for the lower layers are very large for this case. FAR values, however, indicate a large amount of overforecasting: about half the time that icing was forecast in the Denver region during this period, it was not reported by pilots.

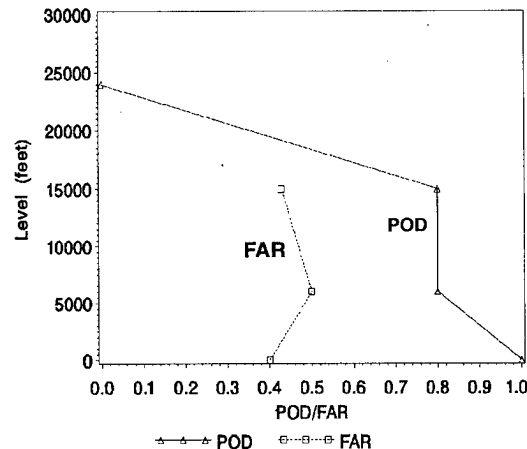


FIGURE 6. Denver Cities-based verification results for three layers (Low, Medium, High) plus the entire column (0 level), for the RAP algorithm, April 1995, with Rapid Update Cycle (RUC; Benjamin et al., 1994) model output for 6-hr forecasts issued at 1200 UTC. Points are plotted at the center level of each layer.

The Cities approach has many advantages, particularly because it allows direct estimation of FAR based on pilots' experiences. However, uncertainty remains regarding whether the assumptions on which it is based are always valid. A concerted data collection effort would provide a better basis for applying this approach.

4.5 Other considerations

Two other factors that should be considered in the process of verifying icing forecasts are (i) stratification of the results according to time of year, region, icing severity and type, and possibly weather regime; and (ii) examination of day-to-day variability in the verification statistics. With regard to stratifications, it is important for both algorithm developers and users to know how the verification results vary according to these various factors. For example, an algorithm may be quite accurate in one part of the continent (e.g., in coastal regions) but perform very poorly in other (e.g., drier) regions. Some algorithms may be particularly good at identifying locations of severe icing reports but less capable at identification of milder conditions.

Day-to-day variability in the performance of an algorithm also is important information for both the algorithm developer and the user of the forecasts. If an algorithm does well on some days but not others, the developer may seek to understand why and to make improvements. In an operational setting, it is important to know how well a forecast algorithm performs on a day-to-day basis. Moreover, for comparing algorithms, differences in performance may appear in the daily statistics that are not apparent in the overall results. For example, two algorithms may have the same *overall* POD value, but one may have very *low* POD values on 20% of the days and very *high* values on other days. In this case, it might be optimal to select the algorithm with less day-to-day variability.

Fig. 7 provides an example of one way to display and compare daily values of the verification statistics for several algorithms. In this figure, POD values for two versions of the RAP algorithm (RAP3 and

RAP4) and a model-based estimate of cloud liquid water (CLW2) are illustrated using box plots. These plots summarize and compare the distributions of POD values. The box plots in Fig. 7 indicate that the POD values for the RAP3 algorithm and for CLW are quite similar, whereas the box for the RAP4 algorithm is somewhat lower than the other two. Note also that although the median values are all around 0.60 to 0.70, the POD values range as high as 0.90 and as low as 0.30 for this set of daily forecasts.

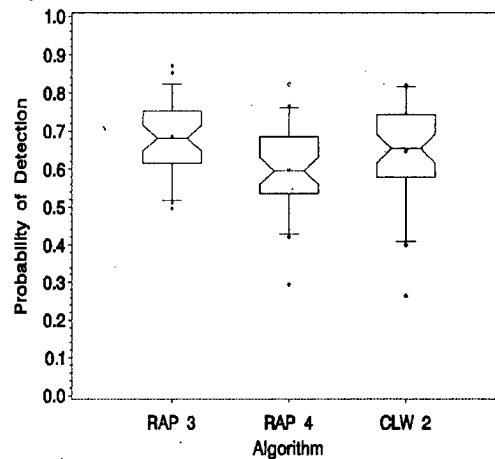


FIGURE 7. Box plots of distributions of daily POD values for three icing algorithms, based on 18-hr forecasts from an experimental version of the Eta model issued at 0000 UTC, 1 Jan to 28 March 1995. For each plot, the line in the center of the box is the median value; top and bottom of the box are the 0.75th and 0.25th quantile values; and endpoints of the lines extending up and down from the box represent the 0.95th and 0.05th quantiles (i.e., 5% of the observations are greater than the 0.95th quantile and 5% are smaller than the 0.05th quantile).

5. Implications

Verification of icing forecasts clearly is not a simple or straightforward task. Advances in verification approaches are limited by characteristics of the available verification data. However, despite these difficult issues, verification of icing forecasts is still possible, especially when performed in a comparative rather than

absolute sense. That is, current data do not allow conclusions about the "absolute" quality of an algorithm, but they do allow us to say that "algorithm A consistently outperforms algorithm B." Moreover, alternative methods are available to compensate for the inability to estimate FAR.

Unfortunately characteristics of the verification data do limit what can be accomplished with regard to forecasting icing severity and developing probability forecasts. It is broadly believed that reported icing severity is strongly dependent on several non-meteorological factors, including pilot experience and aircraft type. Such unreliable and inconsistent verification data makes it difficult to develop algorithms to predict icing severity. With regard to developing probabilistic forecasts, it would be necessary to obtain some form of systematic observational dataset in order to have appropriate relative frequencies and observations of the No-icing situations. With more complete and reliable observations, the Cities approach could be applied to this task.

6. Recommendations

The most important recommendation to result from this research is a strong urge to the aviation community to support and enhance the collection of adequate icing verification data. This improved data collection could occur at many levels, including the following: (i) stressing to all pilots the importance of icing reports; (ii) encouraging pilots to report *all* icing events encountered, as well as routinely including an icing report (even/especially if negative) when reporting other phenomena (e.g., turbulence, sky cover); (iii) making airlines' "in-house" icing reports available to the research community; (iv) enhancing and modernizing the systems

for collecting and distributing PIREPs; (v) developing a systematic icing reporting project that would involve a select set of pilots and/or cities; (vi) developing ongoing cooperative programs with the National Weather Service's Center Weather Service Units to collect supplemental PIREPs; and, finally, (vii) collecting a complete set of verification data as part of a research/field experiment, with the data to be used for verification of both icing forecasts and new radar/satellite based icing detection methods.

Costs of these efforts would be minimal in comparison to the benefits they would provide in terms of development of a useful and meaningful icing forecasting system. Until comprehensive and "clean" datasets are obtained, it will be difficult or impossible to develop reliable forecasting systems that will meet many of the desired capabilities (e.g., probability forecasts; forecasts of severity).

Acknowledgments

The National Center for Atmospheric Research is sponsored by the National Science Foundation. This research is sponsored by the National Science Foundation through an Interagency Agreement in response to requirements and funding by the Federal Aviation Administration's Aviation Weather Development Program. The views expressed are those of the authors and do not necessarily represent the official policy or position of the U.S. government. The author expresses deep appreciation to Randy Bullock, Tressa Kane, and Frank McDonough who make all the analyses happen, and to Marcia Politovich, Ben Bernstein, Roelof Brintjes, and Greg Thompson, who provide important scientific support for this work.

References

- Benjamin, S.G., K.G. Brundage, P.A. Miller, T.L. Smith, G.A. Grell, D. Kim, J.M. Brown, T.W. Schlatter, and L.L. Morone, 1994: The Rapid Update Cycle at NMC. *Preprints, Tenth Conference on Numerical Weather Prediction*, 17-21 July, Portland, OR, American Meteorological Society (Boston), 566-568.
- Brown, B.G., T.L. Fowler, B.C. Bernstein, and G.S. Forbes, 1993: Use of pilot reports for verification of aircraft icing diagnoses and forecasts. *Preprints, Fifth International Conference on Aviation Weather Systems*, Vienna, VA, 2-6 August, American Meteorological Society (Boston), 277-281.
- Brown, B.G., and A.H. Murphy, 1996: Verification of aircraft icing forecasts: The use of standard measures and meteorological covariates. Paper presented at the 13th AMS Conference on Probability and Statistics in the Atmospheric Sciences, 21-23 February, San Francisco (paper is available from the author).
- Brown, B.G., G. Thompson, R.T. Buintjes, and R. Bullock, 1994: Verification of In-Flight Icing Algorithms: Results of the WISP94 Real-Time Icing Prediction and Evaluation Program (WRIPEP). Report, Research Applications Program, National Center for Atmospheric Research, 90 pp.
- Brown, B.G., R. Bullock, G. Thompson, and R. Buintjes, 1995: WISP94 Real-Time Icing Prediction and Evaluation Program (WRIPEP): Statistical issues and forecast verification results. *Preprints, Sixth International Conference on Aviation Weather Systems*, Dallas, TX, 15-20 January, American Meteorological Society (Boston), 207-212.
- Brown, B.G., G. Thompson, R.T. Buintjes, R. Bullock, and T. Kane, 1996: Intercomparison of in-flight icing algorithms. Part II: Statistical verification results. Submitted to *Weather and Forecasting*.
- Doswell, C.A., III, R. Davies-Jones, and D.L. Keller, 1990: On summary measures of skill in rare event forecasting based on contingency tables. *Weather and Forecasting*, **5**, 576-585.
- Ehrendorfer, M., and A.H. Murphy, 1988: Comparative evaluation of weather forecasting systems: Sufficiency, quality, and accuracy. *Monthly Weather Review*, **116**, 1757-1770.
- Kelsch, M., and L. Wharton, 1996: Comparing PIREPs with NAWAU turbulence and icing forecasts: Issues and results. *Weather and Forecasting*, in press.
- Lee, T.F., and J.R. Cook, 1995: Aircraft icing products from satellite infrared data and model output. *Preprints, Sixth International Conference on Aviation Weather Systems*, Dallas, TX, 15-20 January, American Meteorological Society (Boston), 234-236.
- Reap, R.M., 1996: Probability forecasts of clear-air turbulence for the contiguous U.S. *Preprints, 13th Conference on Probability and Statistics in the Atmospheric Sciences*, 21-23 February, San Francisco, American Meteorological Society (Boston), 66-71.
- Schaefer, J.T., 1990: The critical success index as an indicator of warning skill. *Weather and Forecasting*, **5**, 570-575.
- Schultz, P., and M.K. Politovich, 1992: Toward the improvement of aircraft icing forecasts for the continental United States. *Weather and Forecasting*, **7**, 492-500.
- Schwartz, B., 1996: The quantitative use of PIREPS in developing aviation weather guidance products. *Weather and Forecasting*, in press.
- Stanski, H.R., L.J. Wilson, and W.R. Burrows, 1989: Survey of common verification methods in meteorology. Atmospheric Environment Service Research Report (MSRB) 89-5, Downsview, Ontario, Canada, 114 pp.
- Thompson, G., R.T. Buintjes, and B.G. Brown, 1995: A comprehensive icing prediction and evaluation program. *Preprints, Sixth international Conference on Aviation Weather Systems*, Dallas, 15-20 January, American Meteorological Society (Boston), 243-248.
- Thompson, G., R.T. Buintjes, B.G. Brown, and F. Hage, 1996: Intercomparison of in-flight icing algorithms. Part I: WISP94 real-time icing prediction and evaluation program. Submitted to *Weather and Forecasting*.
- Tremblay, A., S.G. Cober, A. Glazer, and G. Isaac, 1996: An intercomparison of mesoscale forecasts of aircraft icing using SSM/I retrievals. *Weather and Forecasting*, **11**, 66-77.
- Wilks, D.S., 1995: *Statistical Methods in the Atmospheric Sciences*. Academic Press, 467 pp.

DIFFERENTIATION OF FREEZING DRIZZLE FROM ICE HYDROMETEORS AND FREEZING RAIN WITH DUAL-POLARIZATION RADAR

Roger F. Reinking,¹ Sergey Y. Matrosov,² Brooks E. Martner,¹ and Robert A. Kropfli¹

¹NOAA/Environmental Technology Laboratory, Boulder, Colorado

²CIRES, University of Colorado/NOAA, Boulder, Colorado

ABSTRACT. Freezing drizzle (in contrast to ice hydrometeors or freezing rain) has been identified as a primary aircraft in-flight icing hazard. Results from theoretical calculations and verifying field studies demonstrate that freezing drizzle should be detectable and distinguishable from other hydrometeor types in radar measurements of elliptical and linear depolarization ratios (EDR and LDR). A practical procedure is suggested for identifying and monitoring this aviation hazard with polarization radar. This procedure and corresponding potential algorithms for operations require formal field testing. NEXRAD has the potential to add dual-linear polarization to facilitate this method.

1. INTRODUCTION AND CONCLUSIONS

Current evidence indicates that drops the size of freezing drizzle are a primary aircraft icing hazard (Cooper et al. 1984; Politovich 1996). Some means is needed to detect freezing drizzle that may occur below cloud base or in cloud between layers containing ice. Depolarization ratio (DR) measurements were made to distinguish (freezing) drizzle from ice crystals of various growth habits, crystal aggregates, and graupel during the Federal Aviation Administration's (FAA) Winter Icing and Storms Project (WISP; Rasmussen et al. 1992). The K_a-band (8.66 mm) dual-polarization radar from the NOAA Environmental Technology Laboratory (ETL) was used (Kropfli et al. 1995). Measurements of the elliptical depolarization ratio (EDR) and linear depolarization ratio (LDR) backed by scattering calculations and hydrometeor samples indicate that drizzle should be detectable and distinguishable from the other hydrometeor types. The addition of a temperature sounding will establish if the drizzle is freezing or warm. These results suggest a practical procedure for identifying and monitoring this aviation hazard. NEXRAD has the potential to add dual-linear polarization, so given that (freezing) drizzle is detectable in LDR, technology transfer to NEXRAD should be possible without a major capital investment.

2. BACKGROUND

The ETL K_a-band radar has an agile polarization capability provided by a phase-retarding plate (PRP) that resolves the beam into two components, retards the phase of one relative to the other, and then recombines them for transmission (Shurcliff 1962). A 90°-phase-shift PRP produces circular polarization from incident horizontal polarization when its "slow" axis is rotated 45° from horizontal ($\alpha = 45^\circ$). If its phase shift differs from 90°, all the polarizations produced by the PRP will be elliptical except where rotation angle $\alpha = 0^\circ$ and multiples of 90°, for which the polarization will remain linear horizontal. The most nearly circular polarization state possible is then produced at PRP rotations to

$\alpha = 45^\circ \pm n90^\circ$, where n is an integer. In WISP, a 79.5° -phase-shift PRP was used. Measurements of EDR were made with fixed, nearly circular polarization during range-height indicator (RHI) scans. A second observing mode was to rotate the PRP at constant speed with the radar set at a fixed elevation angle (β) to cycle the transmitted polarization through the available continuum of states between linear horizontal and near-circular elliptical. This was repeated at two or three fixed elevation angles (e.g., $\beta = 7.5^\circ$, 45° , and 90°); from this, the limiting depolarization values, LDR and EDR, were used to determine hydrometeor type. With either scanning strategy, data from any specific altitude can be selected for examination.

Ice crystals, drizzle, and rain scatter microwaves according to their aspect ratio (shape), bulk density, orientation, and the polarization state of the incident radiation. Drizzle should not measurably depolarize the incident radiation if it is circular or linear because the scatterers are nearly spherical. Rain is nonspherical and will depolarize the signal. Theoretical calculations to differentiate the depolarizations caused by the various ice crystal types and drizzle were made by Matrosov (1991), and expanded and verified with measurements with the ETL K_a -band radar by Matrosov et al. (1996) and Reinking et al. (1996). The calculated EDR- β relationships for the 79.5° PRP are shown in Fig. 1a, and the LDR- β relationships are shown in Fig. 1b (the details of how these measurements are made make it convenient to reverse the sign of DR from Fig. 1a to Fig. 1b; the sign of LDR is opposite the conventional definition).

The EDR for planar crystals (hexagonal plates, dendrites) is predicted to decrease by about 9 ± 2 dB as β is increased from 0° to 90° . The pattern is the same but the magnitude of change with β is much less for the columnar crystal types. The EDR for the crystals is offset from the -14.8 dB signature for drizzle by 2 – 10 dB at the lowest β . Drizzle should show no variation of DR with elevation angle. An LDR of about $+35$ dB is expected for drizzle; the value is determined by the cross-talk limit between the polarization channels of this radar. In LDR, the offset of drizzle from depolarizations caused by the planar ice crystals is of the same order as that in EDR, and likewise large (8 ± 2 dB) at the low radar elevation angles. The DR- β curve slopes are opposite for columnar and planar crystals in LDR (Fig. 1b) but the same in EDR for a 79.5° PRP (Fig. 1a). When LDR is measured, columnar crystal depolarizations *increase* with increasing β ; the predicted maximum offset from drizzle is much larger (11 – 19 dB) than for EDR and occurs toward zenith rather than toward low β .

These plots show that radar measurements of EDR or LDR as a function of β should differentiate columnar from planar crystal types, and these from drizzle. This differentiation might be easiest in LDR, due to the larger differences in DR among particle types and the opposite slopes of the DR- β curves for columnar versus planar crystals, were it not for the effect of the randomness of crystal orientation (or standard deviation, σ_θ) relative to horizontal settling. The determination of ice particle type is degraded minimally by randomness in crystal orientation when a true circular depolarization ratio (CDR) is measured, and only slightly more using near-circular EDR, but substantially using LDR (Matrosov 1991). The theory in Figs. 1a,b is based on $\sigma_\theta = 3^\circ$; at least this much randomness is expected. Figure 1c shows the effect on LDR of a more random orientation with $\sigma_\theta = 10^\circ$. The effect is to cluster

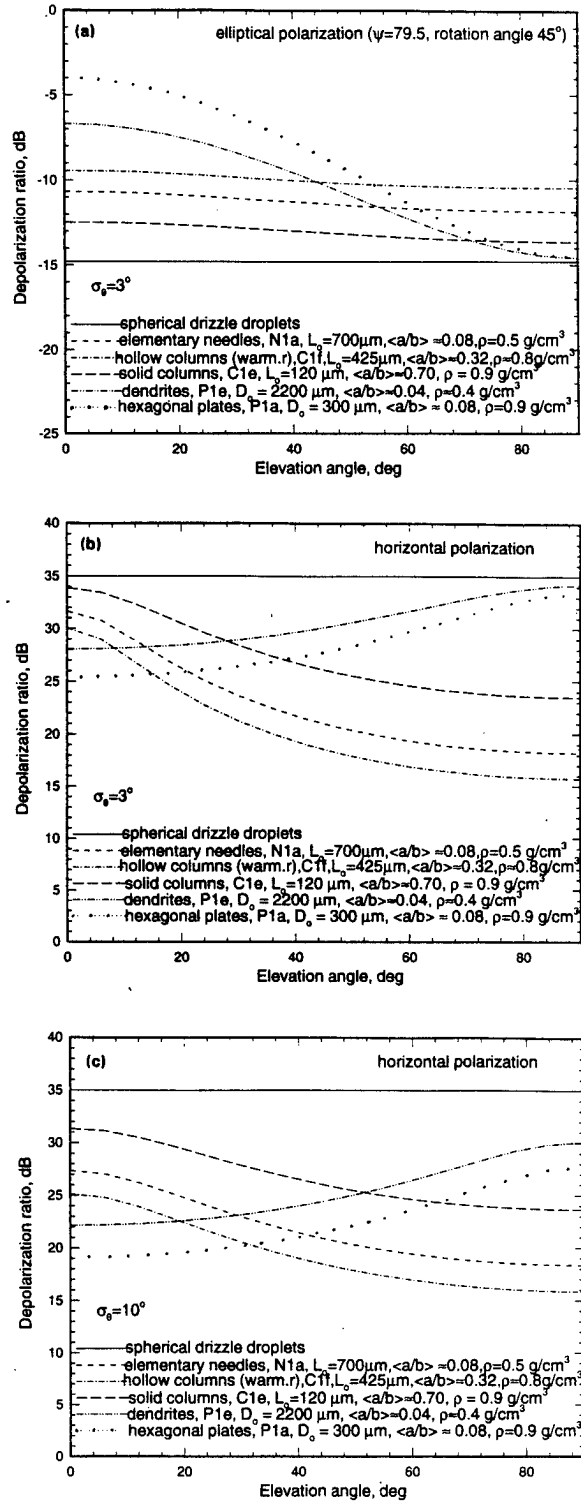


Fig. 1. Calculations of depolarization ratio, DR (dB), as a function of radar elevation angle, $\beta(^{\circ})$: (a) EDR, $\sigma_\theta = 3^\circ$; (b) LDF, $\sigma_\theta = 3^\circ$; (c) LDR, $\sigma_\theta = 10^\circ$. Depolarization increases as the absolute value of DR decreases toward zero.

the LDR- β curves for columnar crystals with those for planar crystals, such that practical differentiation decreases significantly. Measurements confirm that the columnar and planar types are easily differentiated using EDR but more difficult to differentiate using LDR, evidently because of the orientation effect (Reinking et al. 1996). However, the model results in Fig. 1c also predicts that the separability in LDR of both columnar and planar habits from drizzle (+35 dB) will *increase* measurably, by 3–5 dB, with an increase in σ_0 from 3° to 10°. Raindrops are distorted and are expected to be mainly oblate, but internal drop oscillations cause more random shapes and some prolate shapes. In any case, (freezing) rain is not spherical and will produce offsets in depolarizations from the spherical hydrometeor signature of (freezing) drizzle.

To summarize, the scattering calculations show that EDR should provide a very good capability to distinguish among crystals of the various habits and to distinguish these from drizzle, and CDR should be the best. However, if the objective is limited to distinguishing (freezing) drizzle from ice hydrometeors, LDR should offer the better alternative that may be applicable to NEXRAD, which transmits and receives horizontal polarization.

3. MEASUREMENTS

Radar measurements have verified many of the calculations in Figs. 1a–c. The measured EDR from planar crystals provide excellent fits to the theory (Fig. 2), and the differentiation from drizzle is lucid (Figs. 2 and 3). Graupel (Fig. 3) is a type of ice hydrometeor that is most similar in shape to drizzle. Although graupel and freezing drizzle are expected to occur in atmospheres with mutually exclusive temperature soundings, a capability to differentiate them would establish considerable confidence for distinguishing drizzle from other ice hydrometeors. The measurements of EDR in Fig. 3 demonstrate that graupel particles depolarize the signal 1–2 dB more than drizzle for the PRP used in WISP. A PRP at 90° (i.e., circular) would provide greater differences.

During WISP, EDR and LDR were measured concurrently as the extreme values from PRP rotations. For drizzle (Fig. 4a), LDR = $+34.6 \pm 0.9$ dB and EDR = -14.7 ± 0.5 dB; these compare well with calculated values of +35 dB and -14.8 dB, respectively. This PRP rotation was at $\beta = 30^\circ$, but the measured values were independent of elevation angle as expected for drizzle. In contrast, for dendrites, Fig. 4b shows that LDR = $+24 \pm 3$ dB and EDR = -8.6 ± 0.3 dB at $\beta = 30^\circ$, and the depolarizations depended on elevation angle, as in Fig. 2. This is a definitive, theoretically verifiable differentiation from drizzle.

No scattering calculations have been made for graupel. However, in PRP rotations, graupel (Fig. 4c) showed similar EDR values irrespective of elevation angle, and the consistent departure from the EDR for drizzle was similar to that in Fig. 3. However, with LDR = $+32.1 \pm 4.6$ dB and EDR = -13.8 ± 0.3 dB, the average departure from drizzle values was significantly larger in LDR (albeit more variable). Since graupel is expected to be one of the most difficult hydrometeors to distinguish from freezing drizzle, these results are very encouraging for the general application of the depolarization measurements to identify the drizzle.

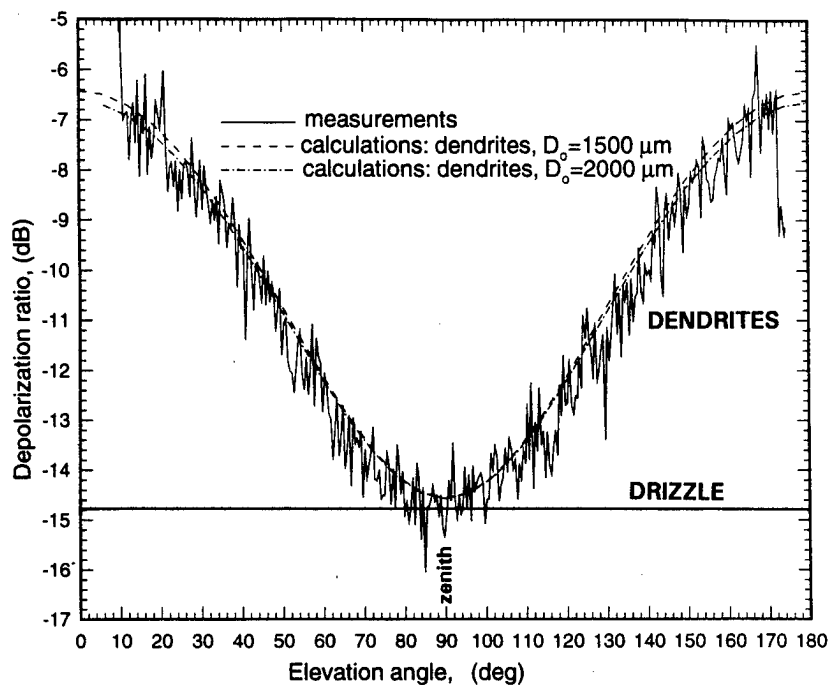


Fig. 2. Over-the-top RHI of EDR (dB) from dendrites (2057 UTC 11 March 1993) and theoretical curves for dendrites and drizzle.

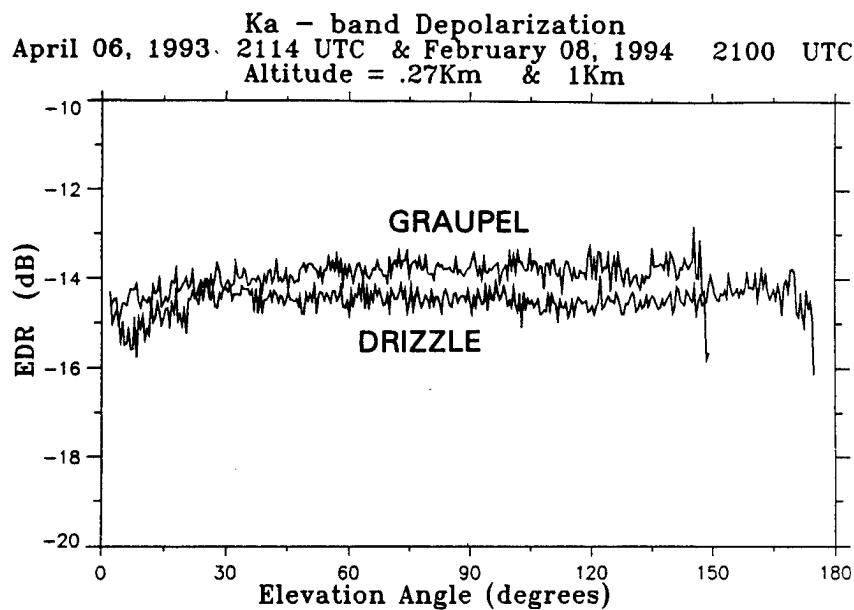


Fig. 3. Over-the-top RHIs of EDR (dB) for drizzle (2114 UTC 6 April 1993) and graupel (2100 UTC 8 February 1994).

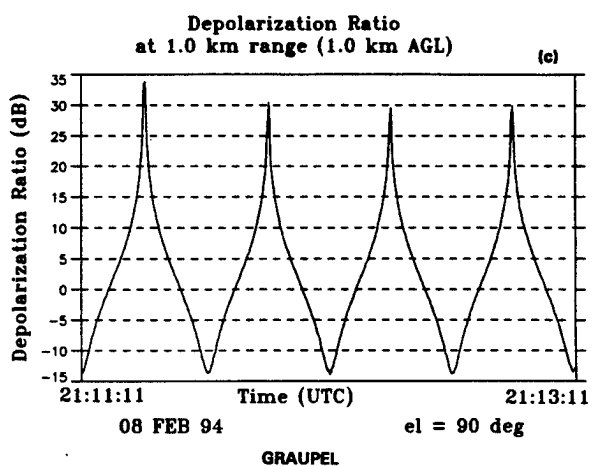
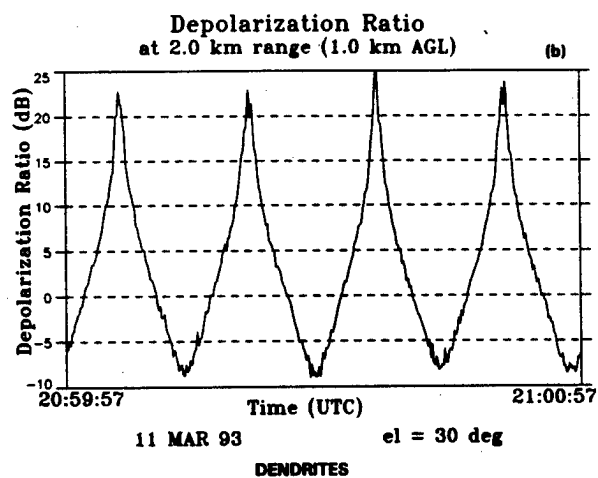
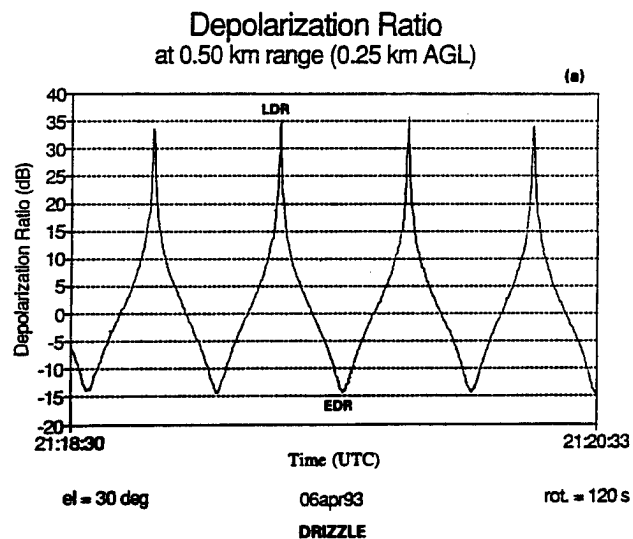


Fig. 4. DR vs. time from a PRP rotation. Positive maxima are LDR; negative minima are the limiting EDR (peak to peak = 90° rotation). (a) In drizzle, $\beta = 30^\circ$, 6 April 1993; (b) in planar crystals (dendrites), $\beta = 30^\circ$, 11 March 1993; (c) in graupel, $\beta = 90^\circ$, 8 February 1994.

4. A HYPOTHEZED PROCEDURE FOR ROUTINE DETECTION OF FREEZING DRIZZLE

The scattering calculations and initial measurements described above suggest that measurements of depolarization versus altitude combined with measurements of depolarization as a function of radar elevation angle can be used to identify cloud layers containing freezing drizzle. In practice, the radar scanning procedure could be refined significantly with the addition of (1) microwave radiometer measurements to establish the absence or presence of liquid (but not the form—drizzle, small cloud drops, or rain—the drizzle being the greater aviation hazard when subcooled), and (2) a temperature sounding to differentiate freezing drizzle from warm drizzle. Radar reflectivity measurements will simply determine cloud boundaries and therefore restrict the altitudes that have any possibility of producing freezing drizzle. The presence of a melting level, easily found in the depolarization signatures, will indicate rain or drizzle below it; however, freezing drizzle can form by drop coalescence rather than melting ice that subsequently subcools, so it is not necessarily accompanied by a melting level. In the cloud layers, the measurements of either LDR or EDR can be obtained from RHI scans or PRP rotations, and either type of measurement should be applicable to achieve the desired drizzle detection. The best separation of the various individual hydrometeor types might be achieved by measuring CDR instead of a near-circular EDR; this is possible with another phase-retarding plate. LDR is expected to be less well behaved in distinguishing among the ice hydrometeor types but is predicted to do well in distinguishing drizzle from the ice hydrometeors. This hypothesis and the envisioned procedure need to be tested with further measurements.

Acknowledgments. This work was funded by WISP, a project of the FAA's Weather Development Program, through a subcontract with the National Center for Atmospheric Research. The views expressed are those of the authors and do not necessarily represent the official position of the U.S. Government.

REFERENCES

- Cooper, W. A., W. R. Sand, M. K. Politovich, and D. L. Veal, 1984: Effects of icing on performance of a research airplane. *J. Aircraft*, **21**, 708–715.
- Kropfli, R. A., S. Y. Matrosov, T. Uttal, B. W. Orr, A. S. Frisch, K. A. Clark, B. W. Bartram, R. F. Reinking, J. B. Snider, and B. E. Martner, 1995: Cloud physics studies with 8-mm-wavelength radar. *Atmos. Res.*, **35**, 299–313.
- Matrosov, S. Y., 1991: Theoretical study of radar polarization parameters obtained from cirrus clouds. *J. Atmos. Sci.*, **48**, 1062–1070.
- Matrosov, S. Y., R. F. Reinking, R. A. Kropfli, and B. W. Bartram, 1996: Estimation of ice hydrometeor types and shapes from radar polarization measurements. *J. Atmos. Ocean. Technol.*, **13**, 85–96.

Politovich, M., 1996: Response of a research aircraft to icing and evaluation of severity indices. *J. Aircraft*, **33**, 291–297.

Rasmussen, R., M. Politovich, J. Marwitz, W. Sand, J. McGinley, J. Smart, R. Pielke, S. Rutledge, D. Wesley, G. Stossmeister, B. Benstein, K. Elmore, N. Powell, E. Westwater, B. B. Stankov, and D. Burrows, 1992: Winter Icing and Storms Project (WISP). *Bull. Amer. Meteor. Soc.*, **73**, 951–974.

Reinking, R. F., S. Y. Matrosov, R. T. Brientjes, and B. E. Martner, 1996: Identification of hydrometeors with elliptical and linear polarization K_a-band radar. *J. Appl. Meteor.* (submitted).

Shurcliff, W. A., 1962: *Polarized Light*. Harvard Univ. Press, 208 pp.

Measurements of Supercooled Liquid Water and Application to Aircraft Inflight Icing

Geoffrey E. Hill
Atek Data Corp. Boulder CO

Abstract

An expendable instrument attached to radiosondes has been developed to measure vertical profiles of supercooled liquid water (SLW). A vibrating wire is exposed to the air as the balloon rises through a cloud. Changes in vibration frequency due to ice collection are used to find SLW concentrations. Comparisons are made with independent SLW measurements by microwave radiometers and by aircraft. It is found that with cold clouds ($T < -10^{\circ}\text{C}$) the vibrating wire yields accurate results, but with warmer clouds the instrument under estimates the SLW by about a factor of two on average. The cause of this problem and the solution are discussed. The structure of SLW clouds is examined with the aid of SLW soundings. It is found that the temperature-humidity-wind profiles appear to relate to the altitude of SLW in a somewhat systematic way. Research to implement improvements and to provide a means for estimating drop sizes in clouds is described.

I. Introduction.

A major hazard to inflight aircraft is the presence of supercooled liquid water (SLW). The hazard is much greater for small propeller-driven aircraft compared to commercial jets. At lower flight altitudes where the temperature is warmer than about -20°C , SLW may be found over wide areas especially during the winter months. Under certain circumstances supercooled droplets may occur at drizzle or raindrop sizes. The supercooled drizzle drops have been found to be particularly hazardous to the aerodynamics of inflight aircraft.

A recent description of the vibrating wire instrument is given by Hill (1994). The method utilizes a vibrating wire exposed to the air as the radiosonde balloon rises through a cloud. As SLW impinges on the wire and freezes, the vibration frequency is reduced in accordance with the added mass of ice. The rate of frequency change is used to find concentrations of SLW as a function of height (or pressure).

On going research is directed at extending this technology in order to retrieve a median volume drop size as a function of height as well. Knowledge of the drop size will be of substantial benefit to aircraft operations. In addition, the drop size information will lead to improved accuracy of the SLW measurement itself.

II. SLW Instrument.

The vibrating wire transducer is 9.0 cm in length and 0.06 cm diameter. When the wire is vibrating there is a total displacement of about 3 cm at the free end of the wire. The wire vibrates in an up-down direction as the radiosonde ascends. This orientation is necessary in order to preserve the airflow characteristics as ice accumulates on the wire. There is a drive coil at the base of the wire and a small sensing ("pickup") coil near the middle of the wire, but away from the airflow. Recently, the small coil has been replaced by an optical system so as to remove interference from the radiosonde transmitter. This revision has been tested in a wind tunnel and has been found to be a substantial improvement.

The vibrating wire device is housed in a specially designed duct, which allows airflow to remain very close to the balloon rise rate even when the radiosonde is swinging and producing added air motion (Figs. 1

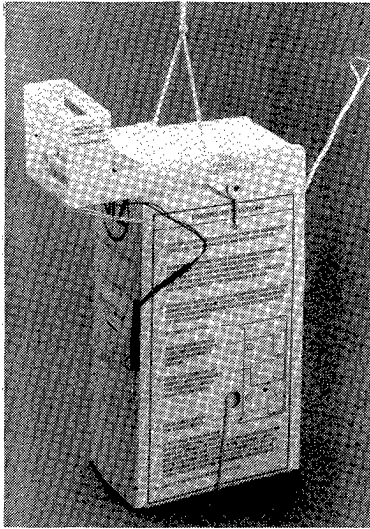


Fig. 1 Radiosonde with vibrating wire unit attached.

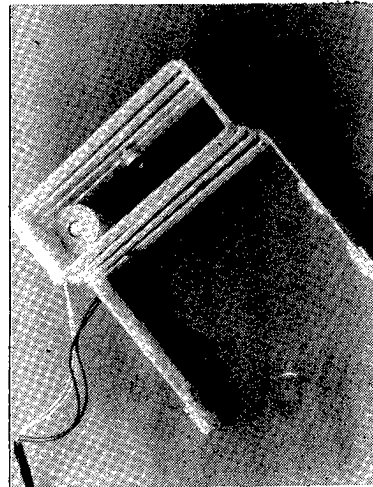


Fig. 2 Closeup of vibrating wire unit.

and 2). Data are collected by using a microcontroller; the period of wire vibration is timed and periodically transmitted to the ground. The transmission is probably the most challenging part of the present system. It is generally required that the SLW data do not interfere with the existing radiosonde data stream. Rather complicated encoding is required to satisfy this requirement. In the future, independent data channels will become available for the SLW data.

III. Comparisons with Independent Measurements.

Microwave radiometer data are used as the primary means of verifying the vibrating wire measurements. NOAA dual frequency and Atek's single frequency radiometers are utilized for SLW control measurements. The vibrating wire measurements are vertically integrated for the comparisons. It is stressed here that whenever the temperature of the air anywhere below cloud top exceeds 0°C, then the radiometer data cannot be relied upon because the presence of wet snow

or water will artificially increase the apparent SLW. Also, large supercooled droplets of several hundred μm will cause the radiometer measured liquid to be substantially overestimated. Additionally, aircraft measurements of SLW are used for comparison.

In Fig. 3 a radiometer sequence measured in Boulder CO in 1992 is shown. During the two broad time periods with high SLW, there were numerous reports of aircraft icing. These include moderate and moderate to severe icing, primarily at 9000 ft (700 mb). In Fig. 4 the temperature-humidity profile is shown. It is observed there is a large temperature inversion between 670 and 650 mb. The vertical profile of SLW is shown in Fig. 5. There is a large amount of SLW at 700 mb. Furthermore, the vertically integrated SLW from this profile is in close agreement with the co-located radiometer measurement. It is also noted that the wind above the SLW layer was from the NNW, whereas below the layer the wind was from the NE and much lighter.

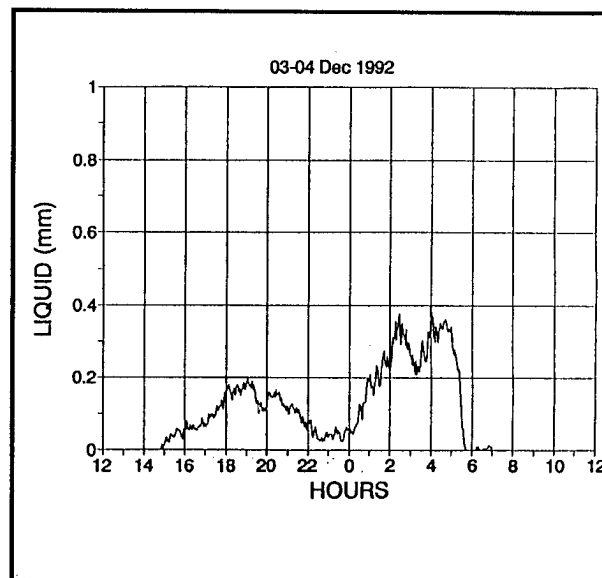


Fig. 3 Radiometer data for Boulder CO.

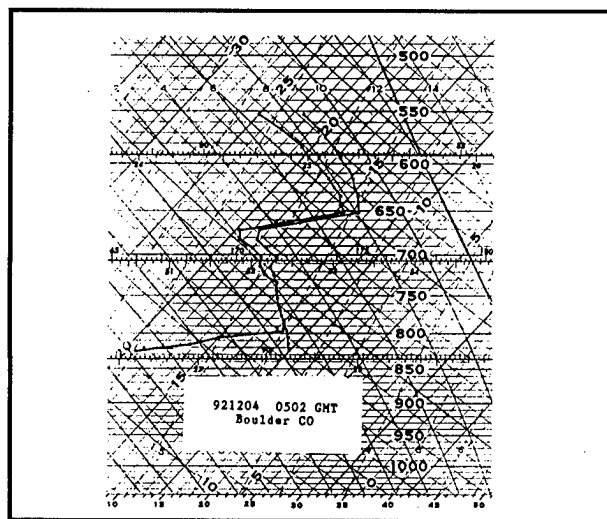


Fig. 4 Temperature-humidity profile Boulder CO 4 Dec. 1992 0502.

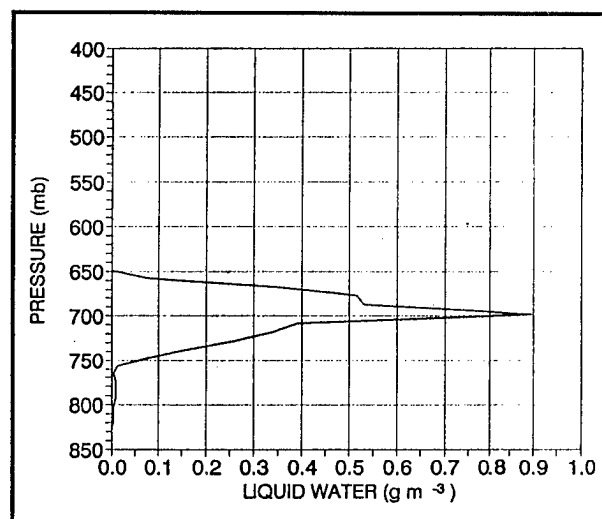


Fig. 5 SLW profile for the sounding of Fig. 4.

A more general comparison between the radiometer and vibrating wire measurements is shown in Fig. 6. Each symbol represents the SLW for one sounding along with the radiometer SLW for the same time and location. There appear to be two categories of soundings, one in which the measurements are in general agreement, the other in which the sounding values are about a factor of two smaller than the radiometer.

In all cases shown here the temperature was below 0°C throughout the sounding. The temperature categories shown on the figure refer to the median liquid temperature. The sounding shown at a sonde liquid of 0.3 mm has a cloud temperature of -10°C, so it is close to being in the cold category. An explanation for the under-estimated SLW in the warm category will be given in section VI of this article. The sounding with a (Sonde) liquid of 0.39 mm is the one described in the previous figures.

IV. Vertical Profiles of SLW.

In this section vertical profiles of SLW along with the temperature, humidity and wind measurements are presented. Some generalizations are offered and possible guidance for predictors are suggested. Nine soundings shown in Fig. 6 (the upper right most) with substantial SLW are presented herein. Also, two other soundings for which the temperature requirement for the radiometer were not met are presented. Table 1 is a listing of these eleven soundings. The soundings are labeled for later reference with an event number not according to date, but according to the median height of the liquid.

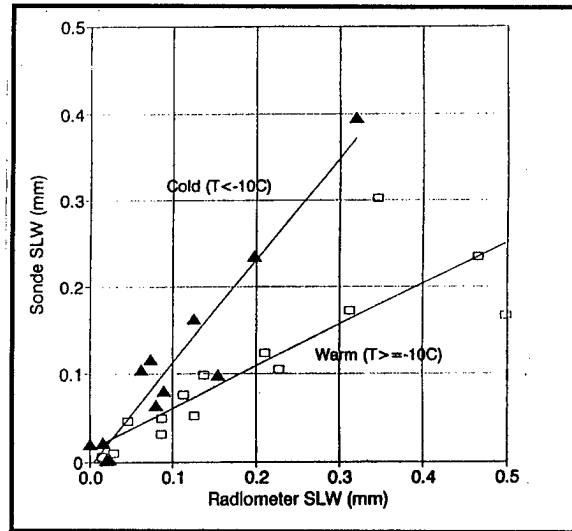
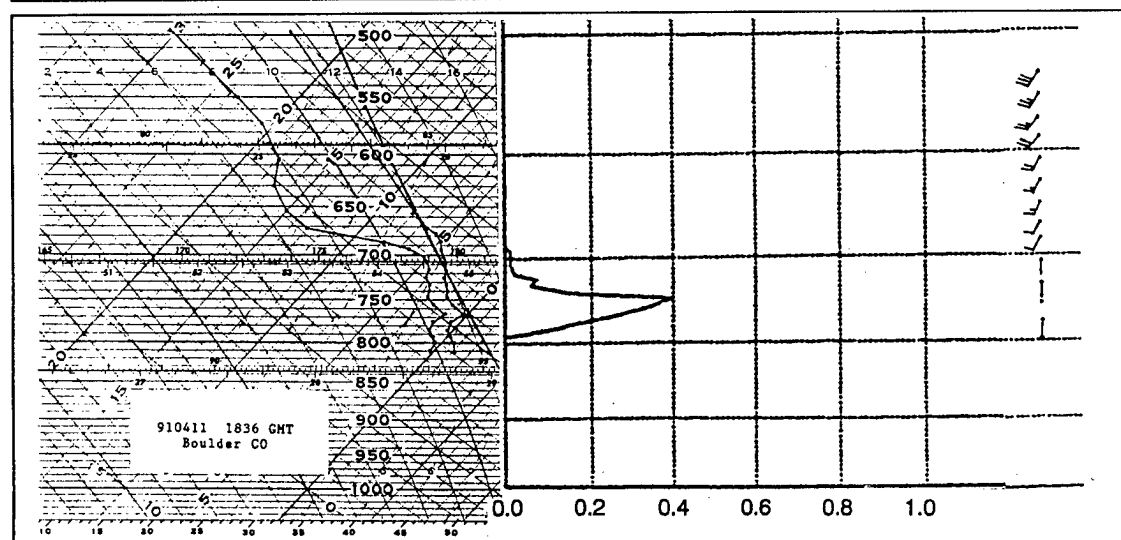
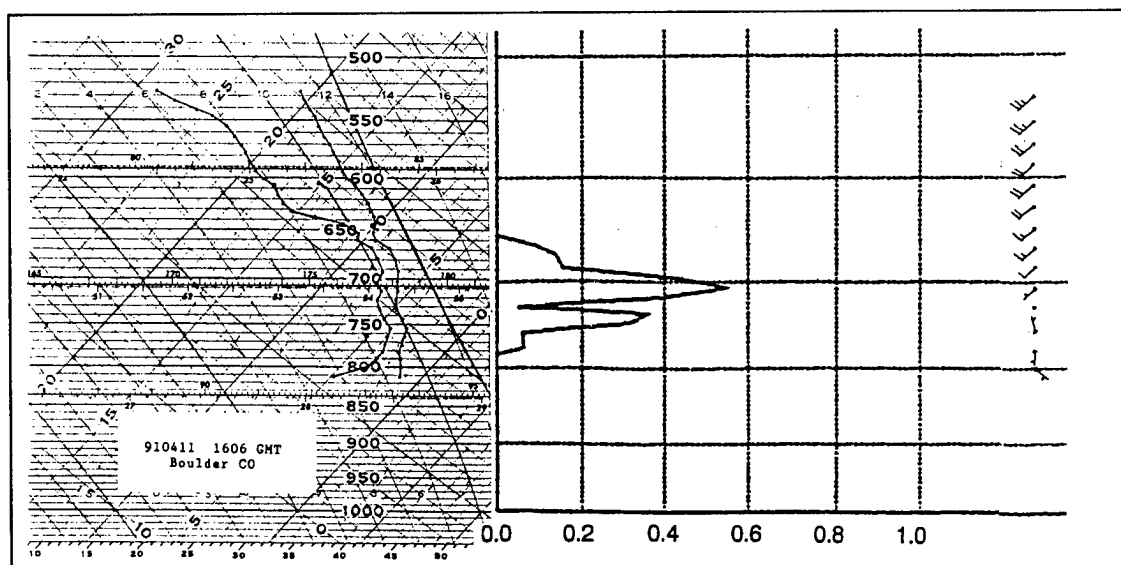
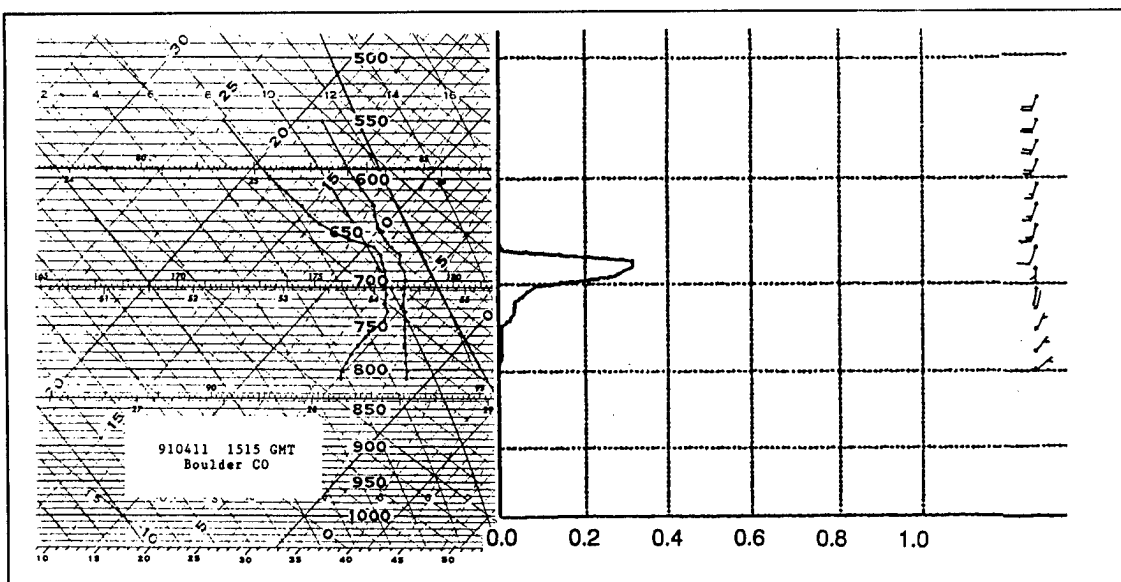


Fig. 6 Radiometer and Sonde SLW comparisons.

Table 1. Soundings with substantial SLW. A * indicates the radiometer SLW is increased by melting precipitation.

Date	Time (GMT)	Event #	RAD SLW	Wire SLW	SLW Temp
910411	1515	8	0.21	0.12	-9
910411	1606	6	0.34	0.30	-10
910411	1836	1	0.36*	0.14	-7
920331	1815	9	0.57*	0.34	-16
921204	0502	7	0.32	0.40	-18
930211	0440	5	0.20	0.24	-17
930312	0152	11	0.13	0.16	-19
940307	2312	4	0.50	0.17	-7
940308	0148	2	0.47	0.24	-7
940308	0323	3	0.23	0.10	-9
940308	1404	10	0.31	0.17	-14

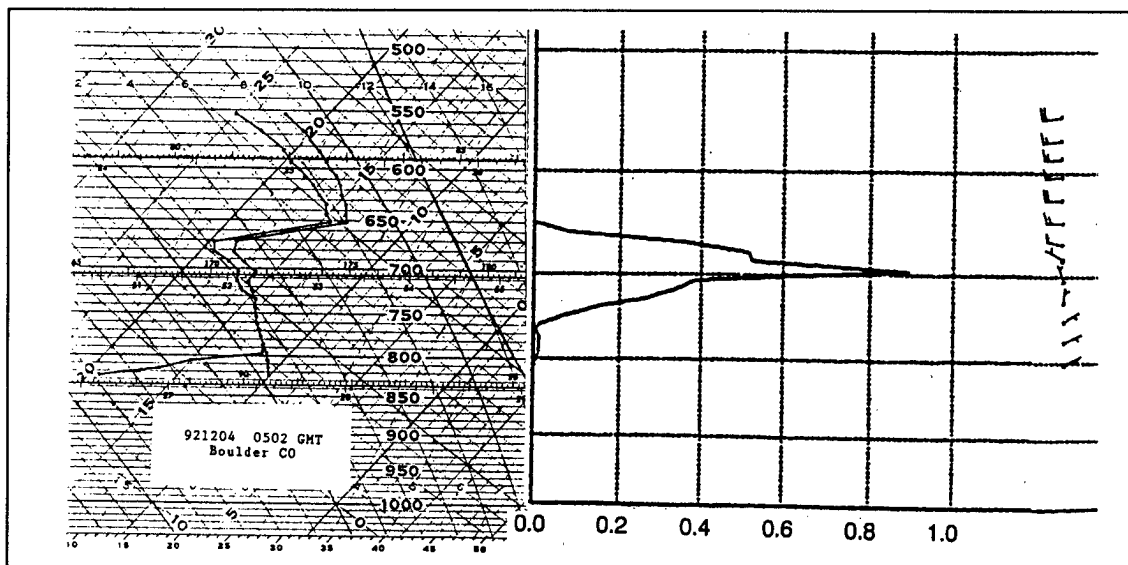
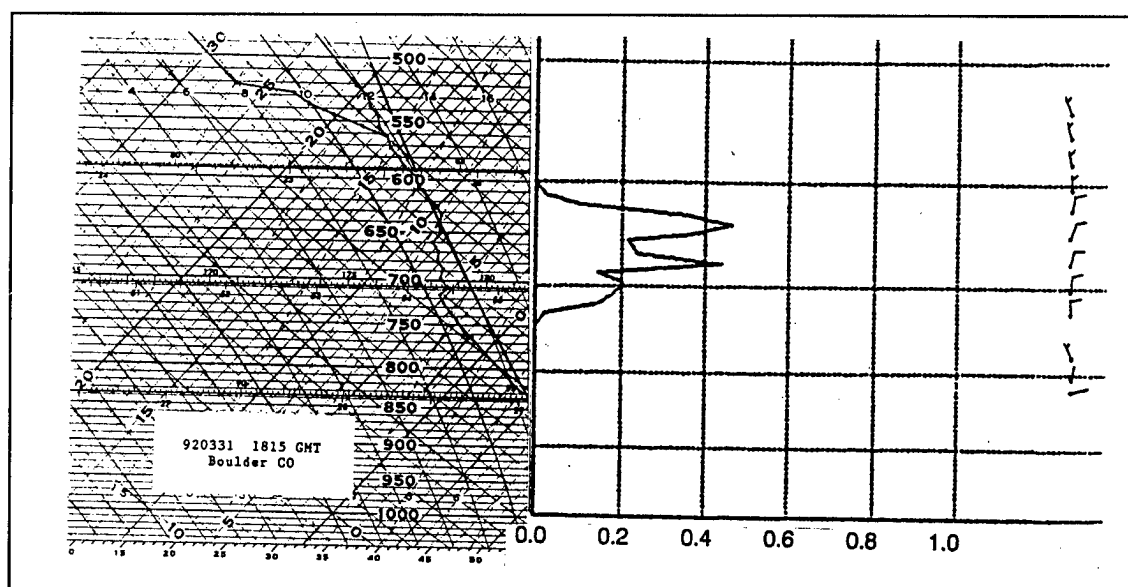
The first three soundings (Figs. 7, 8 and 9) are a sequence taken in Boulder CO on 11 Apr. 1991. The SLW is found to decrease in altitude while reaching a maximum strength at the second sounding. The cloud layer is stable with respect to the moist adiabatic rate. The wind (full barb is 10 m/s) is from the SSW or SW above the SLW layer and weak from various directions below the layer. These soundings are



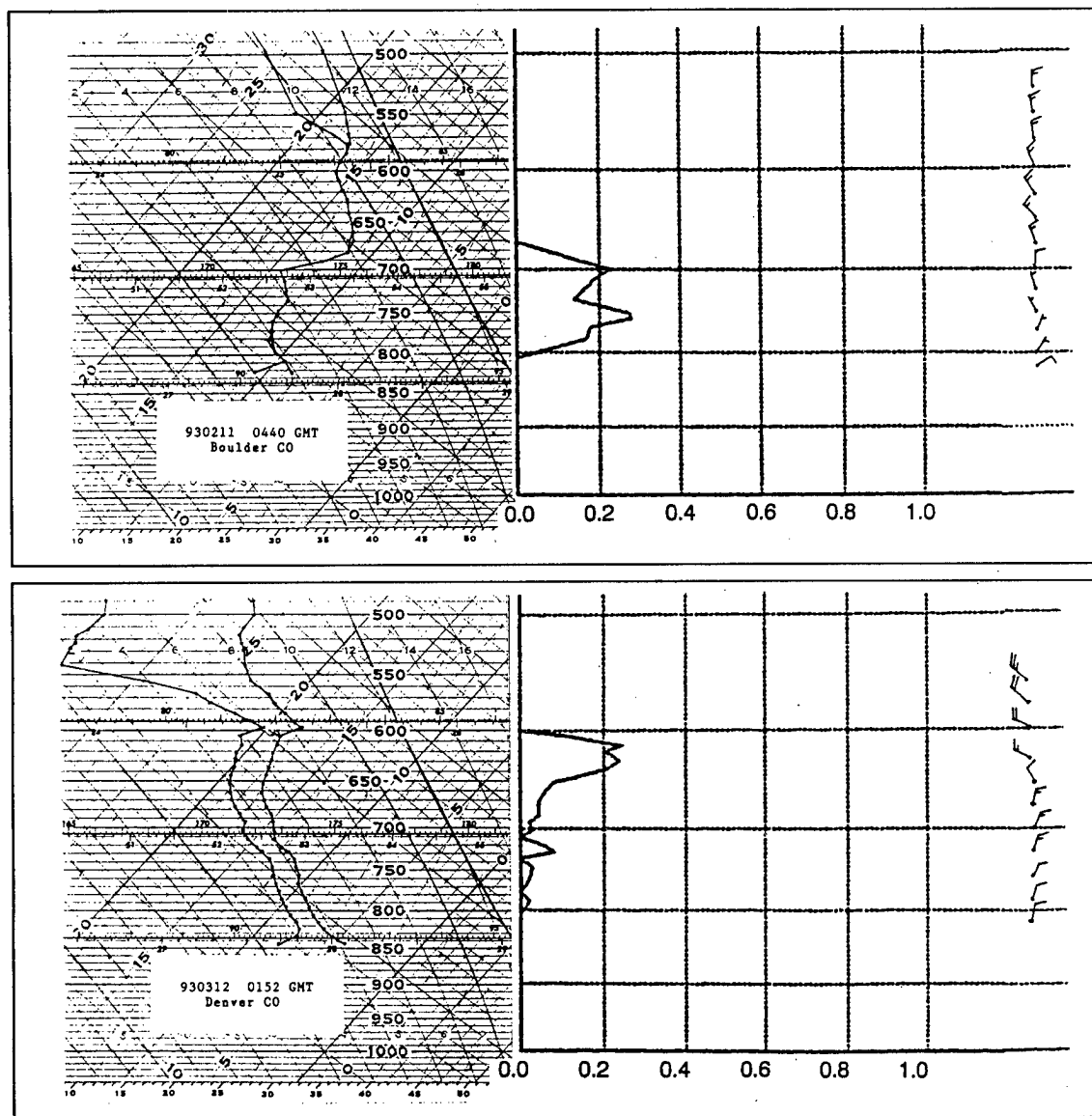
Figs. 7, 8, and 9. SLW soundings at Boulder, CO.

in the warm cloud category and the sounding SLWs are substantially less than the radiometer values. In the last of the three soundings the surface temperature was above freezing and some light but wet snow added an unknown amount of liquid to the radiometer measurement.

In Fig. 10 a sounding at Boulder CO on 31 Mar. 1992 is shown. There is a total liquid of 0.34 mm, while the radiometer measured 0.57 mm. However, this is the other case not included in the comparison because the surface temperature was well above freezing. There was melting snow falling. This case was in the warm cloud temperature category. There was no significant wind shift in the cloud layer. In Fig. 11 the sounding of 4 Dec. 1992 which was previously discussed is shown here for completeness.

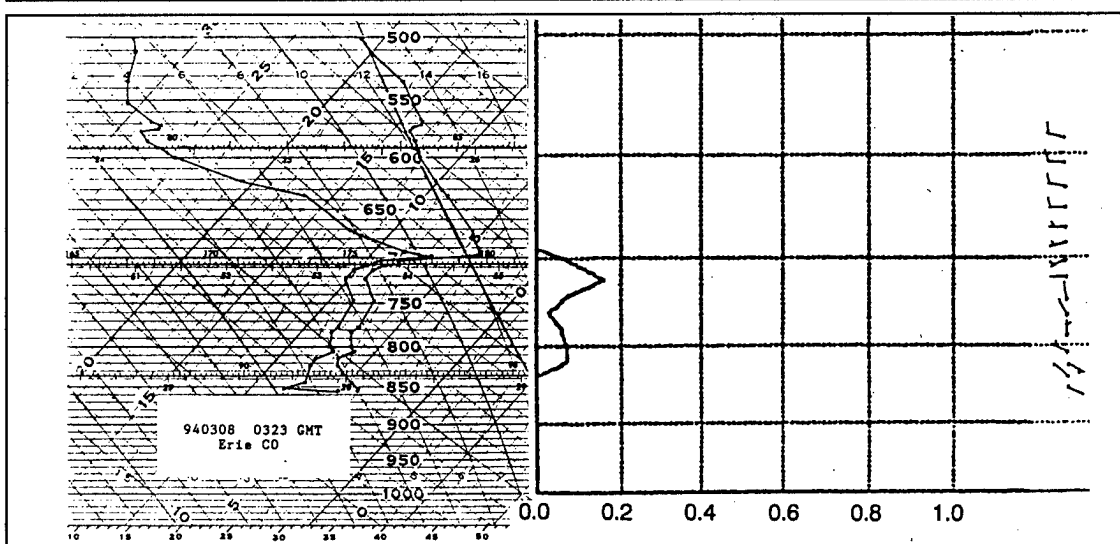
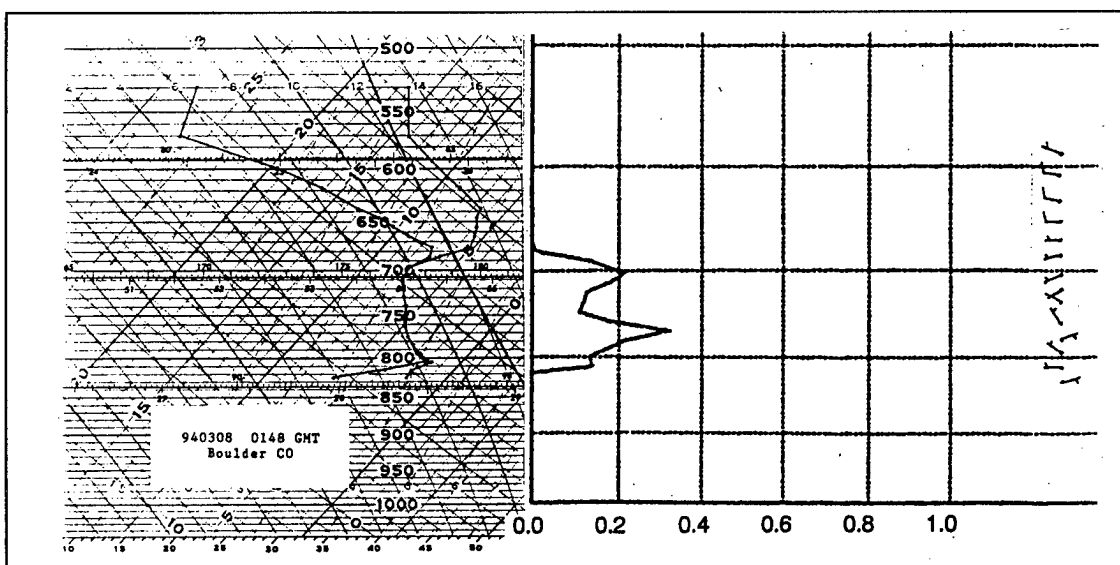
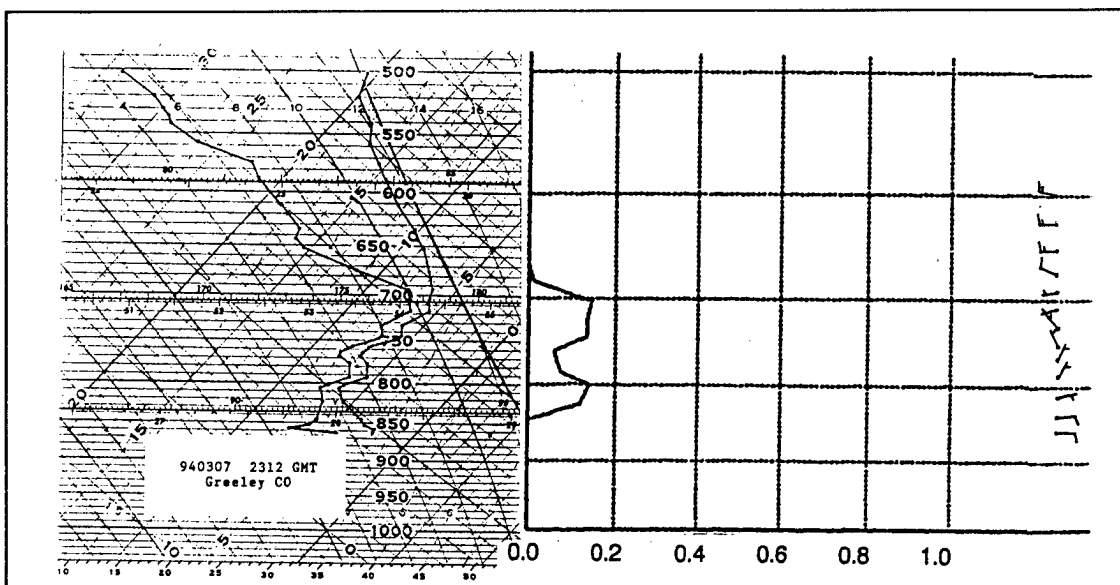


Figs. 10 and 11. SLW soundings at Boulder CO.



Figs. 12 and 13. SLW soundings at Boulder and Denver CO, respectively.

In Fig. 12 a Boulder sounding of 11 Feb. 1993 is shown. There is a strong inversion near the top of the liquid layer. The wind pattern exhibits a shift in direction near the lower portion of the liquid layer. Also, the temperature lapse rate is stable with respect to the moist adiabatic rate. In Fig. 13 the SLW profile for 12 Mar. 1993 at Denver is shown. Here the SLW is located higher than that of the other soundings. Continuous light snow was falling at the sounding time. In the SLW layer the lapse rate is again stable, but underneath, the lapse rate is nearly moist adiabatic.



Figs. 14, 15, and 16. SLW soundings at Greeley, Boulder, and Erie, CO.

Figs. 14, 15 and 16 is a sequence of soundings during a disturbance of 7 and 8 Mar. 1994. Freezing drizzle was present much of the time late on the 7th until about 0600 GMT on the 8th. Thus, these soundings were likely affected by the drizzle. As indicated in Table 1 the SLW in these soundings is substantially underestimated by the vibrating wire in comparison with the NOAA and Atek radiometers. It is possible that the radiometers overestimated the SLW due to the presence of large droplets. Unless the median volume diameter of the droplets approached several hundred μm , this effect would not be dominant. It is believed that the droplets were generally of the size such that the effect on the radiometer was probably about 15 or so per cent. If that is the case then the SLW measured by the vibrating wire is low by a factor of about two for these three soundings.

The SLW in these soundings is found in two distinct layers. There is a strong inversion at the top of the liquid layer, but also other smaller inversions are present at lower altitudes. It appears that two wind shifts were present toward the lower part of the SLW region. It is noted that the cloud temperature is in the range of about -4°C to -8°C . This is well within the warm cloud temperature category. The lapse rate is generally stable in the SLW layer, but some thin moist adiabatic layers are also present within the SLW region.

An important point regarding aircraft operations in SLD conditions is that supercooled drizzle has a significant terminal fall speed. Consequently, it does not take long before freezing drizzle reaches the ground. Therefore, a strategy of changing altitude in icing conditions, in general, should be to increase altitude whenever possible unless there is known to be sufficient airspace below where the temperature is warm enough to prevent further accumulation.

In Fig. 17 a sounding later on the 8th of March is shown. The SLW

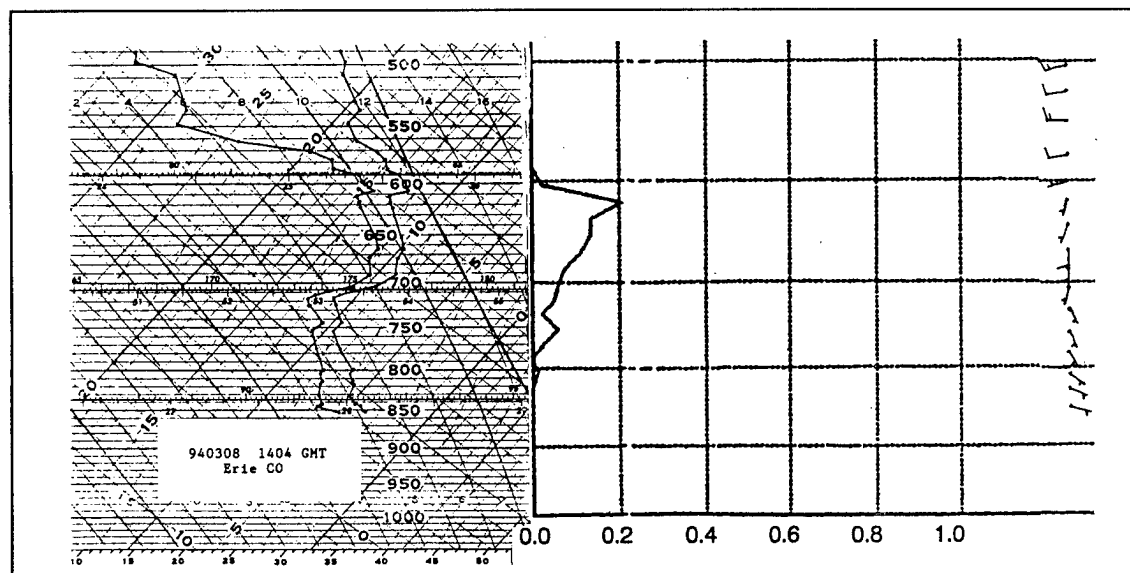


Fig. 17 SLW sounding at Erie CO.

is located somewhat higher than earlier. The cloud temperature is -10°C , marginally in the warm category. The ratio between the radiometer and vibrating wire is 1.8. There are two primary inversions, one located near the top of the liquid, the other near the position of the main inversion of the previous soundings.

V. Preliminary Analysis of the Vertical Profiles of SLW, Temperature, Humidity and Wind.

A preliminary analysis of the data presented herein is provided as a means demonstrating the potential usefulness of the vibrating wire measurements. The eleven soundings analyzed here are ordered according to the median altitude of the SLW as in Table 1. In Event # 1 the median altitude of SLW is at the lowest altitude. Event # 2 has the next highest median altitude and so on. (In Event # 2 two layers are shown. There are two layers in Events # 3, 4 and 5 as well).

In Fig. 18 the pressure level of the SLW maxima are indicated by the X's; the cloud base and top are indicated by the horizontal bars. The cloud top temperature is shown at the location of the cloud top.

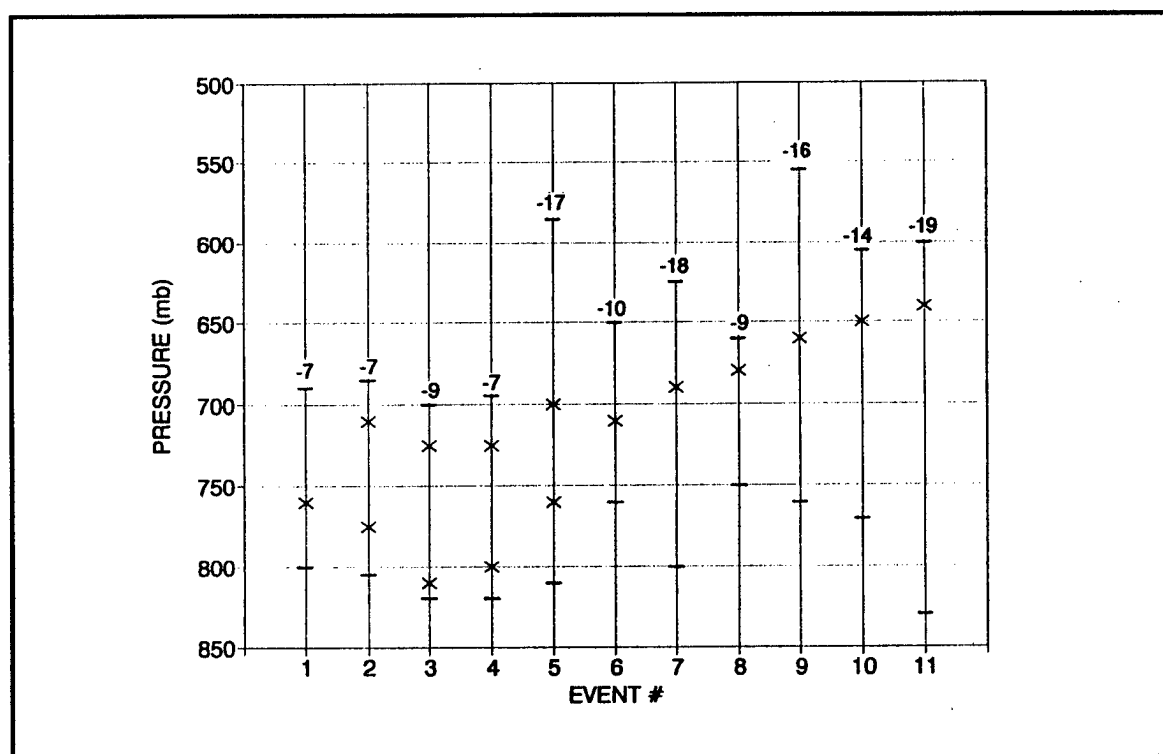


Fig. 18 Pressure levels of the median altitude of SLW for 11 events indicated by crosses. The horizontal bars indicate cloud base and top. The cloud top temperature ($^{\circ}\text{C}$) is shown at the location of the cloud top.

Two questions may be asked regarding the SLW, one: is SLW present within the cloud, and two: where within the cloud will the SLW be found? It is apparent that with these 11 events alone, the first question cannot be answered. Only when other cases without SLW are examined together with these data can that question be addressed. In the future such a study will be proposed using much more data for cases with and without SLW.

For the second question, given that SLW is present, its location may be estimated by other factors. For these 11 events the cloud base shows little relationship to the altitude of SLW. However, there appears to be a modest relationship between the cloud top and the location of SLW, the higher the cloud top, the higher the SLW.

In Fig. 19 the pressure level of temperature inversions are indicated by the horizontal bars; the location of SLW is as in Fig. 18. It is apparent from these data that in the vicinity of Boulder CO the maxima of SLW occur slightly below the temperature inversions, but strong SLW occurs within the inversion layer. In Events # 3 and 5 there were two inversions each with an SLW maximum beneath. In Event # 5 the top inversion had no associated SLW, whereas in Event # 10 the bottom inversion had no associated SLW.

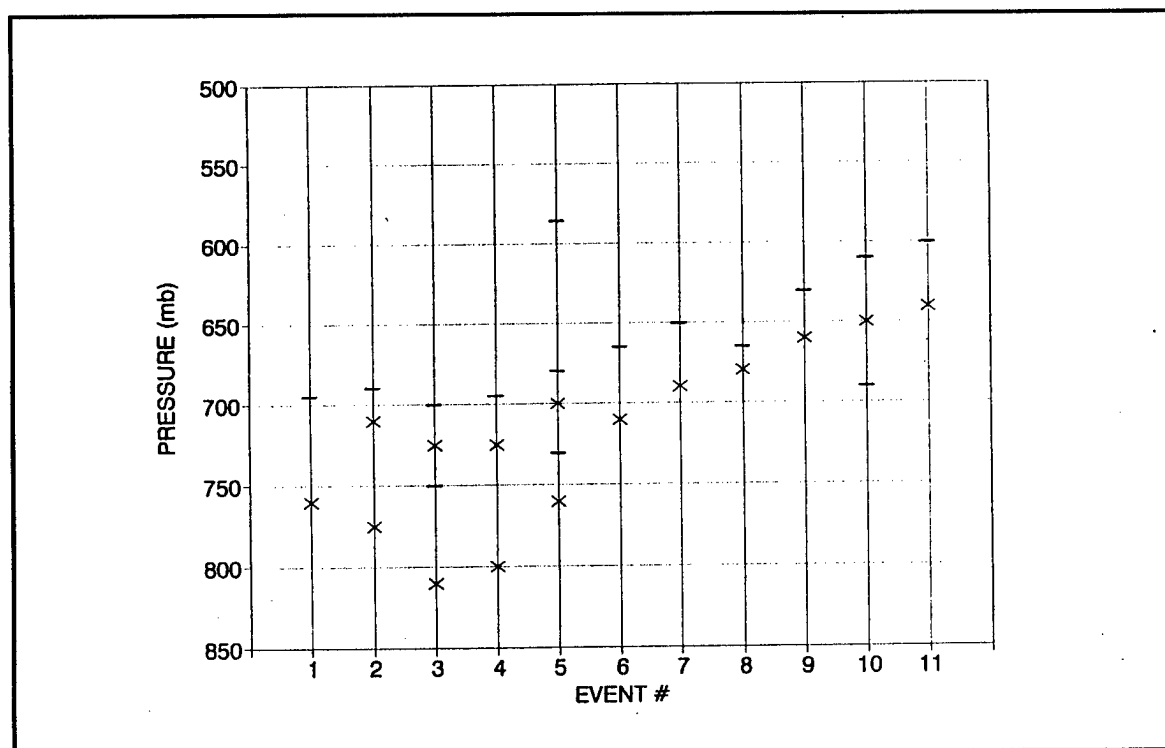


Fig. 19 SLW as in Fig. 18. Inversions and/or the top of stable layers within the clouds are shown by horizontal bars.

In Fig. 20 the pressure level of wind-direction changes are indicated by the horizontal bars; the location of SLW is as in Fig. 18. In most cases the wind shifts are located very close to the SLW maxima. Thus in Event # 5 the lower inversions might be more likely to be associated with SLW than the upper inversion. In contrast in Event # 10 the upper inversion is more likely to be associated with SLW than the lower inversion. (For Event # 9 there is no significant wind shift.)

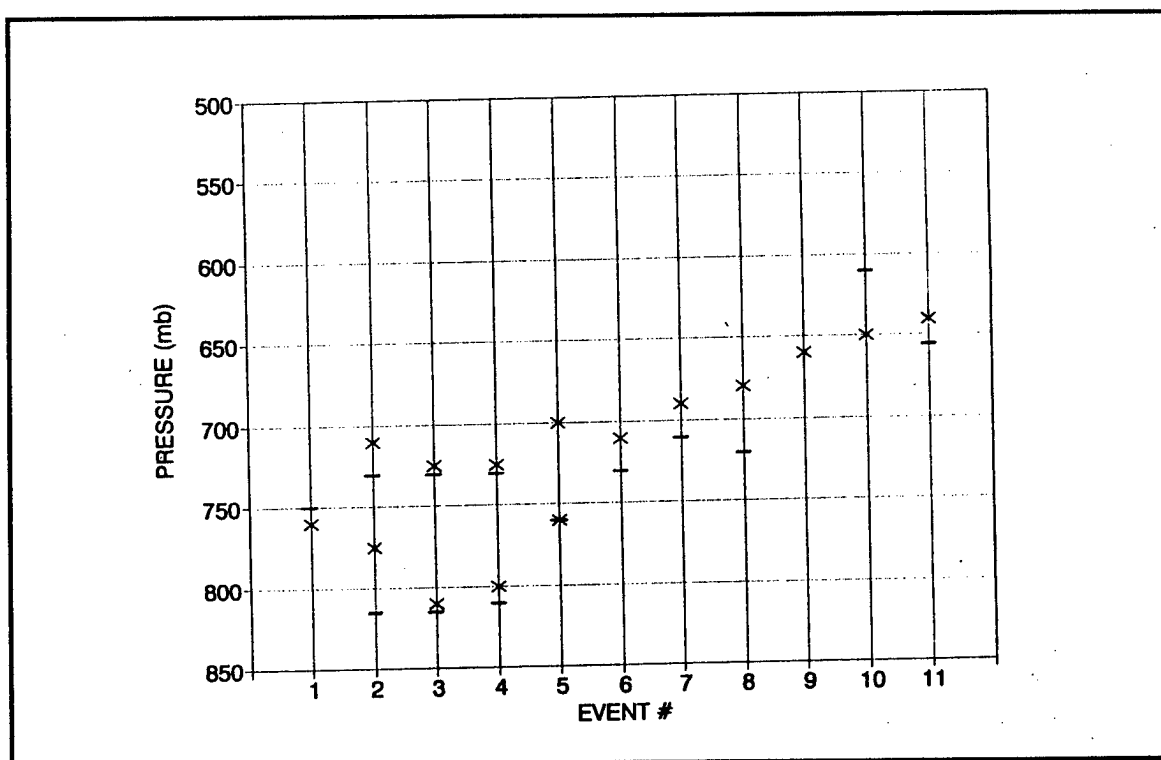


Fig. 20 SLW as in Fig. 18. Wind shifts within the clouds are indicated by horizontal bars.

From the foregoing data it might reasonably be postulated that a combination of the temperature-humidity and wind profiles could be used to estimate the expected altitude of SLW layers. First, the SLW is confined by the saturated layer. Second, the most probable location for an SLW maximum is about 25 mb, or about 250 m below the top of the inversion (or top of stable layer). Third, a substantial change in wind direction is likely to be present near or just below the SLW maximum. With both the inversion and wind direction factors present, the likelihood of a correct estimate appears to be increased.

Whether the results of these data can be applied to other locations remains unknown. It is noted that these data were originally collected mainly to ascertain the usefulness of the instrument and to compare the results with independent measurements. Such SLW soundings may well facilitate the development of suitable predictors of SLW.

Applications of the instrument include: 1) measurement of SLW for use in developing forecast methods; 2) verification of icing forecasts both when icing is forecast and when icing is not forecast; and 3) monitoring of icing conditions, particularly in the vicinity of airports.

VI. Supercooled Large Droplets (SLD) -- Instrument Effects and SLD Measurement.

Wind tunnel experiments have recently been made by Atek to discover why the vibrating wire under estimates SLW in some of the soundings, but not others. In these experiments droplets of 100 μm in an airflow of 5 m/s impinged on a vibrating wire at two different temperatures, one at -11°C the other at -4.5°C . At -11°C the vibration frequency decreased linearly so effects of ice stiffness are not important. The thickness of the ice reached four wire diameters. More importantly the SLW measured by the wire was in very good agreement with an independent measurement of SLW by the multi (two) cylinder method.

On the other hand at -4.5°C the vibrating wire frequency remained unchanged except for an initial slight decrease. Other tests with 20 μm droplets show that ice was collected at temperatures only a fraction of a degree below freezing. Therefore, it is clear that as the droplet size increases (to 100 μm) and the temperature is approximately -5°C , (in the warm category) the collection of SLW on the wire is nil. In the atmosphere apparently only the cloud size droplets are collected in the warm temperature category.

When a vibrating wire with a plastic sleeve of 5 times the wire diameter was used, the 100 μm droplets were collected completely at -4.5°C . This was due apparently to several factors: one, there is a slightly lower vibration frequency; two, the diameter of the cylinder is much larger than the wire; and three, the amplitude of the vibration is somewhat less than that of the plain wire. Only at a temperature near freezing (about -2°C) did the collection of ice on the plastic cylinder begin to diminish.

By utilizing two wires of appropriate diameters it is possible to determine not only the SLW concentration, but the median drop size as well. This result can be achieved by taking into account the collision efficiency which is well known as a function primarily of drop size, other factors being known, and by taking into account the freezing fraction which is primarily a function of the temperature, drop size, SLW concentration and cylinder size. A determination of the freezing fraction will require extensive wind tunnel calibrations under known conditions.

Acknowledgement. Research was supported by the National Center for Atmospheric Research - Research Applications Program and by the U.S. Army Corps of Engineers - Cold Regions Research and Engineering Laboratory.

THE STOVEPIPE ALGORITHM: IDENTIFYING LOCATIONS WHERE SUPERCOOLED LARGE DROPLETS ARE LIKELY TO EXIST

Ben C. Bernstein
Research Applications Program
National Center for Atmospheric Research
Boulder CO 80307

Abstract

The "stovepipe" icing algorithm is based on the combination of surface observations and 3-D computer model output. The algorithm is designed to highlight locations where supercooled large drops are likely to exist and to warn small volumes of airspace while capturing most pilot reports of icing. Background research leading to the development of the algorithm is discussed. An example case and the application of the algorithm to Aviation Weather Center forecasts of supercooled large drops are presented.

1. INTRODUCTION

In recent years, several algorithms have been developed to produce analyses and forecasts of in-flight aircraft icing. The majority of these algorithms were based upon the application of temperature (T) and relative humidity (RH) thresholds to three-dimensional model grids (e.g. Schultz and Politovich 1992). More complicated schemes have recently been developed by Forbes et al (1993) and Thompson et al (1996) which identified several icing categories (stable, unstable, stratiform and freezing rain) based upon the combination of T and RH thresholds with predetermined atmospheric structures. The freezing rain and stratiform scenarios have been shown to analyze and forecast the locations of pilot reports (PIREPs) of icing most efficiently (most PIREPs captured per unit area warned).

Bernstein et al (1996) have shown that icing PIREPs have a very strong relationship with precipitation type and cloud cover reported in National Weather Service (NWS) Surface Airways Observations (SAOs). In particular, freezing precipitation (freezing drizzle, freezing rain and ice pellet) areas, which tended to be rather small in extent, were associated with a disproportionately large number of PIREPs. The PIREPs which occurred near freezing precipitation also occurred within a narrow range of T and RH values. This information, as well as that for other precipitation types has been used to develop the "stovepipe" algorithm, a new icing diagnosis which combines surface observations with 3-D numerical model data to identify locations where large supercooled water drops and general icing are most likely to exist.

2. DATA AND ANALYSIS TECHNIQUES

2.1 PIREP and SAO Datasets

More than 3500 icing PIREPs were compared to surface observations of precipitation type and cloud cover across the continental United States (CONUS). The location of each

PIREP was used to match it to the precipitation type and cloud cover reported by all NWS SAOs within a 75 km radius. A total of six precipitation types (freezing drizzle - ZL, freezing rain - ZR, ice pellets - IP, snow - S, rain - R and drizzle - L) and five cloud cover categories (obscured - XOB, overcast - OVC, broken - BKN, scattered - SCT and clear - CLR) were used. Each PIREP could have been matched to several precipitation type or cloud cover categories. For example, if ZR and S were both reported within 75 km of a PIREP, that PIREP was counted for both precipitation categories. However, a PIREP would only have been counted for a cloud category if it were not matched to any precipitation type. This allowed for the identification of the cloud categories in which icing tended to occur in the absence of precipitation.

PIREPs were categorized by icing severity and type. Icing severities ranged from trace to severe and icing types were rime, mixed and clear. Two combinations of icing severity and type will be discussed in this paper: GENERAL = PIREPs of all severities, all types; WORST = moderate or greater severity PIREPs that were also mixed or clear in type. WORST PIREPs can result from encounters with supercooled large drops, which: 1) tend to form a bumpy glaze, 2) often extend aft of deicing boots, 3) are typically reported as clear or mixed in type, and 4) will often have a significant effect on aircraft performance, causing it to be reported as moderate or greater in severity.

2.2 Observational Statistics

For each precipitation and cloud cover category, the total number of GENERAL and WORST PIREPs were tabulated. Such results indicate where PIREPs occurred most often. However, certain precipitation types and cloud covers may have had higher PIREP counts because they covered larger areas than others. For example, on a typical winter day, S may have been observed across several states, while ZL may have been observed in a narrow band across one or two states. If the area of the S was 10 times larger than that of the ZL, yet each area had 5 PIREPs associated with it, then 10 times more PIREPs occurred *per unit area* of ZL than *per unit area* of S. Thus, the ZL area was the more *efficient* producer of icing conditions.

To ascertain which areas were the most efficient producers of icing conditions, the total areas covered by each precipitation type and cloud cover were calculated. To do this, a regular grid was created over the CONUS. Each grid box was 0.25 degrees latitude by 0.25 degrees longitude, and was assigned the precipitation types and a cloud cover from the SAO closest to the center of the box. A box could have had several precipitation types assigned to it if the SAO reported a mixture of precipitation (e.g. S and R), while only the most intense cloud cover reported would have been assigned. The area of each box was calculated and the areas were summed for all days tested. "Threats" of icing were calculated by dividing the number of PIREPs counted by the summed area for each precipitation type and cloud cover. The highest threats indicate the precipitation types and cloud covers where icing was found most often per unit area covered.

2.3 PIREP-Matched T and RH Statistics

After each PIREP was matched to a precipitation type and cloud cover, it was of interest to find the T and RH present at their locations. To acquire this information, the latitude,

longitude and altitude(s) of each PIREP were used to match it to the closest grid point(s) in 3-D space from the National Center for Environmental Prediction (NCEP) Rapid Update Cycle (RUC) model. Distributions allow us to see the ranges of T and RH at which PIREPs occurred for each precipitation type and cloud cover category. If most of the PIREPs fell within a narrow range of T and RH, then it is easy to identify the altitudes above each precipitation type where the PIREPs ought to occur in the future.

3. RESULTS FOR PIREPS

3.1 Precipitation Type

The discussion of the relationship between PIREPs and either surface precipitation type or cloud cover cannot be conducted in terms of pure percentages. An individual PIREP could be matched to several precipitation and cloud coverages. Thus, only the relative number of PIREP counts matched to and the threats calculated for each precipitation type will be presented. The precipitation types considered were ZL, ZR, IP, S, R and L. All subcategories of these precipitation types were included within them (e.g. snow, snow showers, snow grains and snow pellets were all included in the S category, regardless of their intensity).

Of those used in this study, 58% of GENERAL and 67% of WORST PIREPs were associated with some form of precipitation at the surface. Of the precipitation types, most GENERAL (not shown) and WORST PIREPs (Fig. 1a) were associated with S and R, while about one third as many were associated with L or the individual freezing precipitation types (ZL, ZR and IP). One reason for the high counts for S and R was the large amount of area they covered, relative to the other precipitation types (Fig. 1b). Snow and rain each covered more than $10 \times 10^6 \text{ km}^2$, while all freezing precipitation types combined only covered $2.9 \times 10^6 \text{ km}^2$. The large differences in area covered impacted the threats calculated for each precipitation type. Threats for ZL, ZR and IP were about 2 to 3 times greater than those for R, S and L for GENERAL PIREPs (not shown) and 4 to 7 times greater for WORST PIREPs (Fig. 1c). These ratios were even larger for those PIREPs within 2 km of the surface (not shown, 2-7 times greater for GENERAL and 5-8 times greater for WORST PIREPs).

The dramatically higher threats for the freezing precipitation types make intuitive sense, since their observation at the surface indicates that precipitation-sized supercooled liquid water droplets existed through some depth above the surface. Freezing drizzle droplets, in particular, have recently been shown to be extremely hazardous to aircraft (Sand et al 1984; Politovich 1989). Also, the existence of freezing rain and/or ice pellets at the surface indicates a strong likelihood for the existence of a wide spectrum of droplet sizes aloft, including freezing drizzle.

3.2 Cloud Cover

Approximately 42% of GENERAL PIREPs occurred where no precipitation was falling at the surface. Of those PIREPs not matched to any precipitation, most were matched to SAOs reporting OVC or BKN conditions (Fig. 1a). A gradual decrease in the number of PIREPs was observed with decreasing cloud cover. The exception to this trend was XOB,

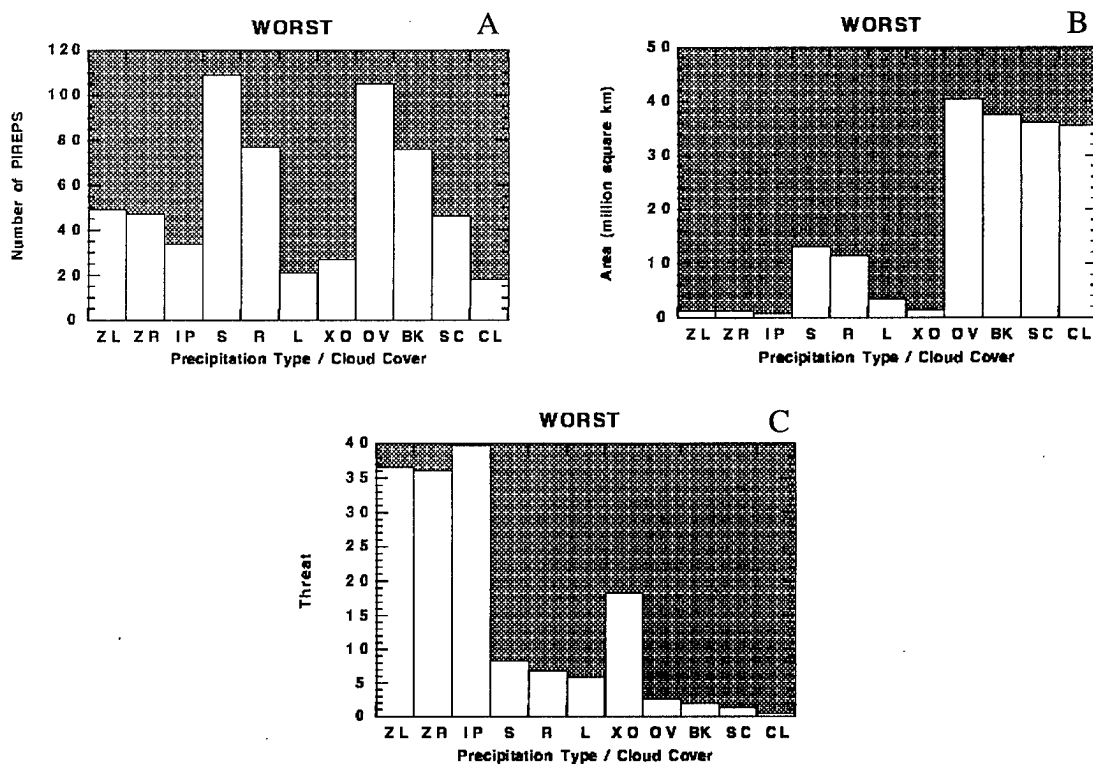


Fig. 1: a) Number of WORST PIREPs matched to, b) areal coverage (10^6 km^2) of and c) threats (# of WORST PIREPs per unit area - $\#/10^6 \text{ km}^2$) calculated for each precipitation type and cloud cover. Cloud cover categories use first 2 letters for each category (e.g. XO instead of XOB for obscured sky cover).

which was matched to the fewest PIREPs. This small percentage is likely attributable to the relatively small areal coverage of XOB conditions when no precipitation was occurring (Fig. 1b). The number of reports matched to XOB conditions was fairly large, however (> 300 GENERAL PIREPs).

Threats for cloud cover (Fig. 1c) overwhelmingly indicated that among non-precipitating areas, those with XOB conditions were by far most likely to contain icing conditions. Threats were more than 6 times greater for XOB than for any other cloud cover, while OVC threats were 20% and 25% greater than those for BKN and SCT sky conditions, respectively. The fact that clear sky conditions had any counts was likely attributable to the inclusion of automated weather station data, which report CLR conditions when cloud cover only existed above ~4 km (12,000 ft) AGL, or errors in pilot reported latitude and/or longitude. This explanation may also apply to a portion of the SCT and possibly BKN observations, but it is possible that discontinuous clouds can cause icing. Also, highly variable sky conditions could have easily existed within 75 km of a PIREP that occurred near a sharp transition zone, such as an Arctic cold front, where even clear skies can precede post-frontal cloudy skies and precipitation.

3.3 T and RH Distributions

To identify the vertical extent of the icing conditions above each precipitation type and cloud cover, the range of T and RH values at which the PIREPs occurred was derived by matching each PIREP to a RUC model grid point (or points if icing was reported through a range of altitudes). The T and RH values from each point were saved, and a distribution of T and RH values was constructed for each precipitation type and cloud cover tested.

The distributions of T and RH (Fig. 2) show that at least 75% of WORST PIREPs matched to ZL, ZR, IP and L occurred at $T > -8^{\circ}\text{C}$ and $\text{RH} > 80\%$. The distributions for S and R were much broader, as at least 75% of PIREPs occurred at $T > -12^{\circ}\text{C}$ and $\text{RH} > 70\%$. Similar results were found for XOB and OVC, and distributions became increasingly broad with decreasing cloud cover (BKN, SCT and CLR). Distributions for GENERAL PIREPs (not shown) were slightly broader than those for WORST PIREPs, but very similar.

4. THE "STOVEPIPE" ALGORITHM

4.1 Description of Algorithm Components

From the above information, an algorithm identifying the most probable locations for icing conditions to exist was created by combining hourly analyses of surface precipitation type and cloud cover with 3-D grids of T and RH. The algorithm consists of two categories of aircraft icing; "supercooled large drops likely" and "general icing."

Observations of ZL, ZR and IP at the surface: 1) indicated that supercooled large drops (SLDs) *must exist through some depth*, 2) were strong indicators of WORST PIREPs aloft, 3) tended to cover small areas, and 4) had rather narrow distributions of T and RH. Combining these attributes allows for the identification of a rather small volume of airspace where SLD icing and WORST PIREPs are expected to occur in the future. This portion of the algorithm is turned on for a particular horizontal (2-D) RUC grid point when ZL, ZR and/or IP are observed at the surface within a 100 km radius. If this condition is met, then

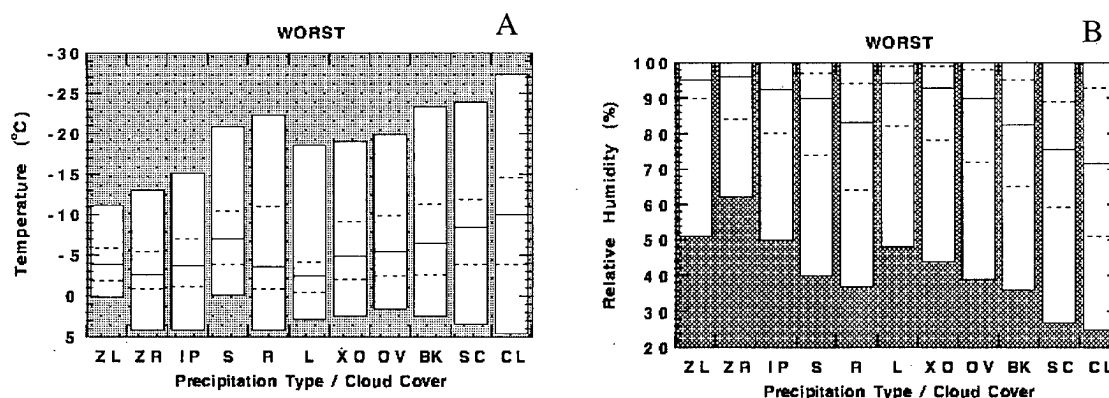


Fig. 2: Distributions of RUC model a) $T (^{\circ}\text{C})$ and b) $\text{RH} (\%)$ values matched to WORST PIREPs for each precipitation type and cloud cover. On each bar, the solid line is the 50th, the dashed lines are the 75th and 25th and the ends of the boxes are the 5th and 95th percentile values in the distributions.

the vertical column, or "stovepipe", of data for that horizontal grid point is checked for layers which have both T between -8 and 0°C and $\text{RH} > 80\%$. If a "warm nose" of air $> 2^{\circ}\text{C}$ is found above a layer of SLD, then SLD conditions are not checked for above the warm nose. Grid points above the warm nose are marked as "general" icing (see next paragraph), if those T/RH criteria are met.

The S, R, L, XOB and OVC areas were not nearly as efficient at identifying icing conditions, but many PIREPs still occurred near surface observations of those conditions. Using the broader T/RH ranges at which most PIREPs occurred, the most probable locations for "general icing" conditions aloft can be identified. This portion of the algorithm is turned on for a particular horizontal (2-D) RUC grid point when S, R, L, XOB and/or OVC are observed within a 100 km radius. If this condition is met, then the vertical column of data for that horizontal grid point is checked for grid points which have both T between -12 and 0°C and $\text{RH} > 70\%$. A 150 km radius is used west of 100° longitude for both algorithms, due to the sparse nature of SAO data in the western CONUS.

Model calculated height values (MSL) for the grid points which meet the above criteria are then used to identify the range of altitudes in each column at which SLD or "general icing" conditions are most likely to exist. A 3-D gridded field of SLD and general icing is then used to graphically depict the horizontal extent and range of altitudes at which icing conditions can be expected. A surface projection of the horizontal extent shows the locations where the SLD and general icing conditions were met at any level in the column, while plots of icing bases and tops show the range of altitudes for SLD and general icing conditions. An example case will be discussed in the next section.

The stovepipe algorithm takes advantage of surface observations to eliminate regions of BKN, SCT or CLR conditions which meet the broad T/RH ranges that other algorithms use to identify probable locations of icing (e.g. RAP "stable" algorithm: T between -16 and 0°C , $\text{RH} > 63\%$; Thompson et al 1995). Without question, some areas where these criteria are met can be completely cloud free. Such cloud free or partly cloudy areas are eliminated by the use of SAO data. Also, the smaller T and RH ranges used in the stovepipe algorithm help to decrease the area/volume flagged as "icing" while most PIREPs are still captured. This helps to maximize the efficiency of the algorithm. An important aspect of the SLD algorithm is that it not only identifies small 3-D volumes where many WORST PIREPs occur, but it is physically based on well-known meteorological principles.

4.2 Statistical Comparisons with the NCAR/RAP Icing Algorithm

Comparisons between stovepipe and the National Center for Atmospheric Research (NCAR) Research Applications Program (RAP) icing algorithm described by Thompson et al (1996) clearly show the advantage of the stovepipe method (Table 1). The statistics shown for the overall stovepipe algorithm (STOVE-total) versus the overall RAP algorithm (RAP-total) are for 46 days. The statistics shown for the stovepipe SLD algorithm (STOVE-SLD) versus the RAP "freezing rain" and "stratiform" algorithms (RAP-ZL and RAP-STRAT) are for subsets of 19 days when at least 1 model grid point of SLD icing was diagnosed and 7 days where at least 1% of the U.S. was diagnosed as SLD icing. The smaller datasets are used because it was most fair to compare those algorithms on days

where they were all active. Algorithm output at 0000 (all times UTC) was compared to PIREPs for 3 hours either side of that time. All statistical values given are the average values calculated for the days tested. Probability of detection (POD) is the number of PIREPs captured divided by the number observed. A perfect POD value is 1.0 (100%), while a POD of 0.0 (0%) means that no PIREPs were captured by the algorithm. Area is the geographic area warned (10^6 km^2) and volume is the 3-D volume warned (10^6 km^3). Area and volume efficiencies are the POD divided by the area and volume warned, respectively.

The STOVE-total algorithm had PODs which were within 6% of those for the RAP-total algorithm for both GENERAL and WORST PIREPs, while the areas and volumes covered by STOVE-total were ~44% smaller than those for RAP-total. This small difference in POD, combined with a large decrease in area and volume, caused the area and volume efficiencies to be ~68% greater for STOVE-total than those for RAP-total. Such improvements are as good or better than those found when the RAP algorithm was masked with satellite data to eliminate "cloud free" areas in icing diagnoses (-11% POD, -40% area, -42% volume, +47% area efficiency; Thompson et al 1996). The satellite screening values were for moderate or greater intensity (MOG) PIREPs of all types and were calculated for 51 cases. Statistical comparisons of the STOVE-total and RAP-total algorithms for MOG PIREPs showed nearly identical results to those calculated for GENERAL PIREPs. The POD values for the RAP-total algorithm were significantly lower than those calculated in earlier tests for MOG PIREPs by Brown et al (1996). This is likely attributable to month-to-month variability in these datasets. Such variability has been noted in further tests of the stovepipe algorithm as well.

Table 1: Statistics for STOVEPIPE and RAP Icing Algorithms

Algorithm	POD (General/ Worst)	Area (10^6 km^2)	Volume (10^6 km^3)	Area Eff. (General/ Worst)	Vol. Eff. (General/ Worst)
STOVEPIPE - Total (46 days)	0.459 / 0.593	1.521	2.880	0.302 / 0.390	0.159 / 0.206
RAP - Total (46 days)	0.488 / 0.607	2.723	5.110	0.179 / 0.223	0.095 / 0.119
STOVEPIPE SLD (19 days)	0.130 / 0.268	0.141	0.186	0.927 / 1.906	0.702 / 1.443
RAP - Stratiform (19 days)	0.174 / 0.225	0.797	0.973	0.218 / 0.282	0.179 / 0.231
RAP - Freezing Rain (19 day)	0.106 / 0.233	0.296	0.168	0.360 / 0.786	0.632 / 1.381
STOVEPIPE SLD (7 days)	0.247 / 0.425	0.290	0.330	0.853 / 1.467	0.748 / 1.287
RAP - Stratiform (7 days)	0.219 / 0.283	0.953	1.059	0.230 / 0.297	0.207 / 0.267
RAP - Freezing Rain (7 days)	0.210 / 0.371	0.529	0.323	0.398 / 0.702	0.651 / 1.148

Results for the STOVE-SLD, RAP-ZR and RAP-STRAT algorithms for the 19-day subset period are also quite interesting. POD values for all three of these algorithms were rather low (< 0.2) for GENERAL PIREPs. This is expected since GENERAL PIREPs can occur in a wide variety of scenarios where the criteria for the algorithms are not met. PODs for WORST PIREPs were markedly better, since these PIREPs have a tendency to

occur in large drop situations, which all 3 algorithms are tuned to identify. POD values for STOVE-SLD algorithm were 15-20% higher than those for RAP-ZR and RAP-STRAT. STOVE-SLD areas and volumes were >80% smaller than those for STRAT and efficiencies for WORST PIREPs were dramatically (325-575%) higher, on average. Area and volume efficiencies for WORST PIREPs were 142% and 4.5% higher for STOVE-SLD than for RAP-ZR. Distributions of area and volume efficiencies (not shown) indicated wide variations in these values, but those calculated for STOVE-SLD were significantly (in a statistical sense) higher than that for RAP-STRAT and RAP-ZR (area efficiency only).

These trends continued for the 7 day subset, but POD values increased dramatically for all three algorithms. In particular, POD of WORST PIREPs increased to .425 for STOVE-SLD, which was 50% and 15% better than the RAP-STRAT and RAP-ZR PODs, respectively. It was on those days, when freezing precipitation covered at least 1% of the CONUS, that the STOVE-SLD algorithm performed best. This is important, since on those days when it warns for the largest areas/volumes, it proves to be most reliable.

4.3 An Example Case - 6 March 1996

To highlight the utility of the stovepipe algorithm, output for an example case is shown. Data for this case can be compared with other icing algorithms presented by Vivekanandan and Thompson (1996) and Politovich and Thompson (1996). On this day, PIREPs of GENERAL icing were widespread across the CONUS, and a swath of WORST PIREPs extended from Oklahoma, through central Illinois and into New England. Many of these WORST PIREPs were associated with spotty freezing precipitation that was occurring northwest of a surface low and stationary front (Fig. 3).

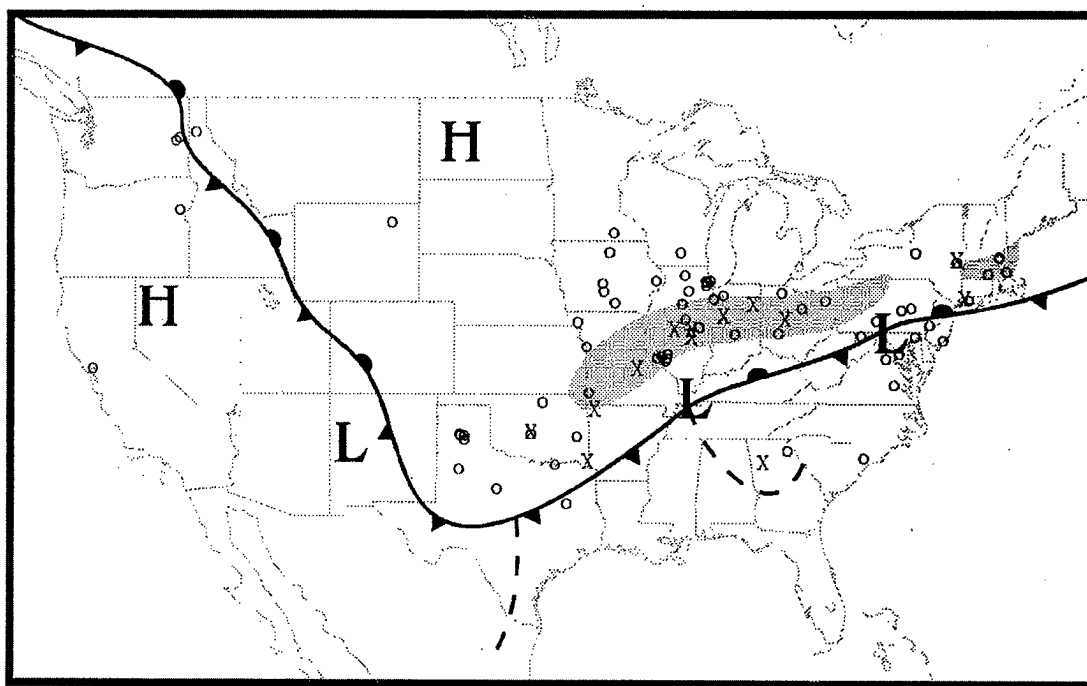


Fig. 3: Locations of surface fronts (barbed solid lines), troughs (dashed lines), pressure centers (L=low, H=high), swath of spotty freezing precipitation (grey shaded areas) and of GENERAL (O) and WORST (X) PIREPs.

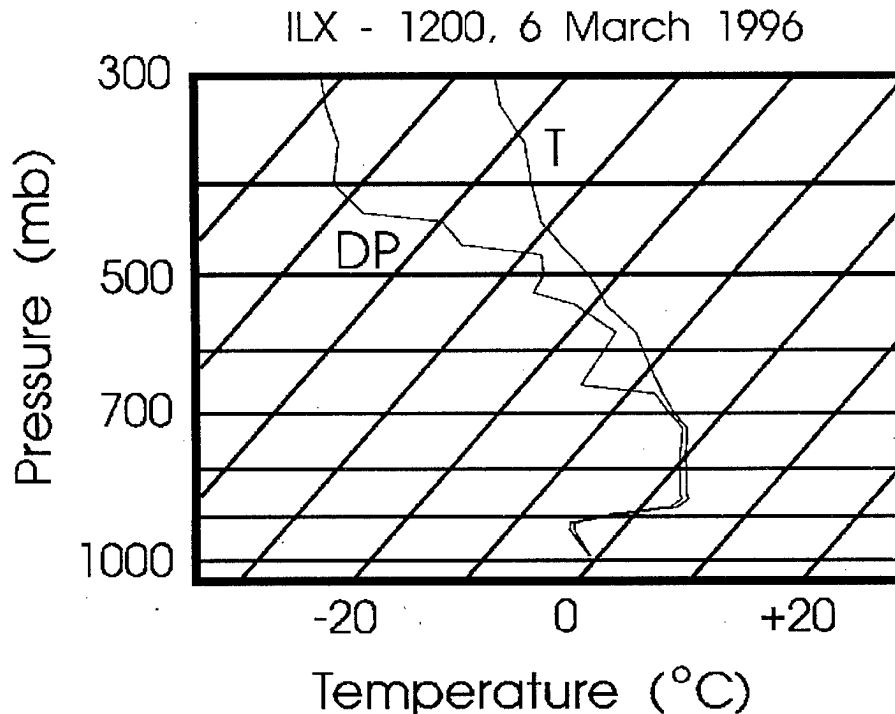


Fig. 4: Skew-T, log-P vertical profile of temperature (T) and dewpoint (DP) for Lincoln, Illinois (ILX) at 1200, 6 March 1996. Note the saturated layer from the surface to ~670 mb with $-8 < T < 0^{\circ}\text{C}$, except for the warm nose centered at 860 mb, where T reached 3°C .

ZL, ZR and IP were observed for many hours near a NWS sounding site at Lincoln, Illinois. The temperature and relative humidity structure observed at this site at 1200 on 6 March (Fig. 4) was indicative of freezing precipitation. A layer of subfreezing temperatures existed from the surface to ~890 mb (1.2 km MSL), with a ~100 mb deep layer of above freezing temperatures (a warm nose) above it, and another ~100 mb deep subfreezing layer above that. These first three layers were all saturated and are indicative of light precipitation (S, ZL or ZR) forming near 3.2 km MSL, falling into the warm nose to become drizzle or rain (not supercooled), and continuing into the subfreezing layer near the ground to become freezing drizzle, freezing rain or ice pellets. Similar structures were common across the freezing precipitation region depicted in Fig. 3.

The freezing precipitation structure described above persisted throughout the afternoon of 6 March. At 1800, temperatures between -8 and 0°C with RH of near 100% were predicted by RUC in a layer just above the surface observations of ZL, ZR and IP caused the SLD algorithm to highlight a discontinuous ~250 km wide swath from northeast Oklahoma to Maine (Fig. 5). Snow, rain, drizzle and solid cloud cover existed across a large portion of the rest of the CONUS, and model temperatures between -12 and 0°C with RH of $>70\%$ caused the “general icing” algorithm to be turned on along most of the east coast, across the midwest and from the Texas panhandle to Washington state (Fig. 5).

The SLD volume had a fairly uniform base between 0 and 0.5 km MSL, but a highly

varied top, with some portions extending above 5 km MSL. This swath covered only ~3.5% of the CONUS, but managed to capture 77% of the WORST PIREPs and 36% of the GENERAL PIREPs which occurred within 2 hours of 1800 UTC. Two of the three WORST PIREPs missed by the SLD algorithm occurred at high altitudes in convective areas southeast of the surface fronts, while the other occurred within the SLD area over Indiana, but had a misreported altitude of 0 m MSL, which put it below ground. The “general icing” algorithm captured one of the remaining WORST PIREPs, giving a POD of 91% for the overall stovepipe algorithm. These results are quite remarkable and well above the average PODs typically found, even on days where SLD covered more than 1% of the CONUS (see Table 1). Several other cases with high PODs have been observed since the algorithm began running in December 1995. The “General Icing” category covered ~33% of the CONUS and captured 86% of the GENERAL PIREPs. In contrast, the overall RAP icing algorithm covered ~51% of the CONUS, and also captured 86% of the GENERAL PIREPs, while the RAP STRAT and ZR algorithms each captured 46% of the WORST PIREPs, while they covered 15% and 4.8% of the CONUS, respectively. As expected, area efficiencies for the STOVE-SLD and STOVE-total algorithms far exceeded those of the corresponding RAP algorithms for this time.

4.4 Freezing Drizzle AIRMETS

The Aviation Weather Center (AWC) in Kansas City produces official forecasts of in-flight aircraft icing every six hours for the CONUS. These forecasts, known as “icing AIRMETS,” indicate the locations where moderate or greater intensity icing is expected. The warned airspace is identified using a series of surface locations and a range of altitudes. The recent attention focussed on SLDs, including freezing drizzle, has prompted the issuance of AIRMETS which specifically address the expected locations of SLD condi-

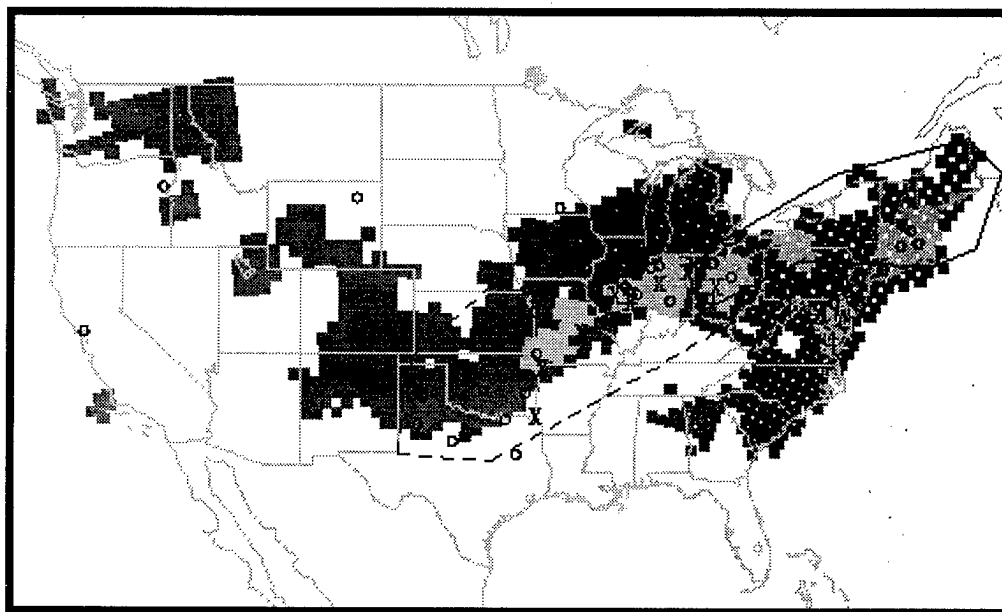


Fig. 5: Stovepipe algorithm output for 1800, 6 March 1996. SLD warned areas in light grey, general icing warned areas in dark grey. Chicago and Boston header AIRMETS valid for 1445-2100 UTC are dashed and solid black polygons, respectively. Locations of GENERAL (O) and WORST (X) PIREPs for 1600-2000 UTC.

tions. These "Freezing Drizzle AIRMETs" are given so that those aircraft which are particularly susceptible to SLD conditions can avoid them.

To assist in the production of ZL AIRMETs, the stovepipe algorithm has been implemented at AWC. AWC icing forecasters use the algorithm in combination with PIREPs, weather observations and numerical model output to produce ZL AIRMETs when they are warranted. ZL AIRMETs are given as part of regular icing AIRMETs, but freezing precipitation and either "clear" or "mixed" icing of moderate or severe intensity (i.e. WORST icing) is typically mentioned. An example of an icing AIRMET with an embedded ZL AIRMET is given below:

```
WAUS1 KCHI 061445
WA3Z
CHIZ WA 061445
AIRMET ZULU UPDT 4 FOR ICG AND FRZLVL VALID UNTIL 062100.
...SEE SIGMET NOVEMBER SERIES FOR SVR ICG CONDS....
AIRMET ICG...NE KS IA MO IL IN MI LM KY OK TX AR TN
FROM GRB TO MBS TO DTW TO FWA TO CVG TO HNN TO MEM TO ACT TO 50W MAF TO
DHT TO 50W LBL TO OMA TO GRB. OCNL MDT RIME/MXD/CLR ICGICIP BLO 100 SLPG TO
LYRS BTWN 100 AND 200 OVR KY TN. ISOLD SVR ICG PSBL SPCLY IN AREAS OF ZL-. MSTLY
RIME ICGIC OVR GRTLKS. MSTLY RIME BLO 50 OVR OK TX PTNS. CONDS CONTG BYD 21Z
SPRDG SWD THRU 03Z.
FRZLVL...AT OR NR SFC PLAINS THRU GRTLKS RGN. MULT LVLS BLO 100 CNTRL IL
CNTRL IN. 80-100 SRN MO THRU OH VLY.
```

This Chicago-header AIRMET, which was valid for 1445-2100 on 6 March, outlined a moderate or greater intensity icing region, which covered a large area, extending from southern Michigan to the Texas panhandle (dashed polygon in Fig. 5). What made this AIRMET unique was the mention of mixed and clear icing and possible severe icing in areas of light freezing drizzle (ZL-), as well as the mention of mostly rime icing in the Great Lakes region, Oklahoma and Texas. The portion of the AIRMET which remained as a likely location of SLD icing extended from southwest Missouri to the Indiana/Ohio border, and correlated well with the SLD flagged area and the locations of every WORST PIREP within the domain of Chicago-header AIRMETs. Forecast altitudes for this area closely matched those diagnosed by the SLD algorithm. The Boston-header AIRMET (solid polygon in Fig. 5), which covered the remainder of the area flagged by the SLD algorithm, did not specifically mention freezing precipitation aloft, but did forecast "occasional mixed/clear icing in clouds and precipitation below 17000 ft" (~5.2 km) over the SLD areas. This range of altitudes closely matched those analyzed by the SLD algorithm and those reported by pilots during the period the AIRMET was valid. The SLD algorithm is a key ingredient in the production of ZL AIRMETs. Forecasters at AWC are able to loop the algorithm diagnoses to follow trends and predict future locations of SLD and general icing (Ron Olson, personal communication). This was likely to have been the case on 6 March 1996, when AWC forecasts of SLD icing conditions aloft closely matched the SLD algorithm output.

5. SUMMARY

The stovepipe icing algorithm is based upon the well known physics of freezing pre-

precipitation processes, combined with statistical relationships drawn between the occurrence of icing conditions and observed precipitation type/cloud cover. The algorithm uses surface observations of precipitation type and cloud cover to indicate the locations where SLD and general icing are most likely to exist. The algorithm warns much smaller areas/volumes of airspace, while capturing essentially the same number of icing PIREPs as the RAP icing algorithm. The stovepipe algorithm is an essential part of the production of freezing drizzle AIRMETS by the Aviation Weather Center. These AIRMETS provide accurate, real-time forecasts of SLD conditions over the CONUS.

REFERENCES

- Bernstein, B.C., T.A. Omeron, F. McDonough and M.K. Politovich, 1996: The relationship between aircraft icing and synoptic-scale weather conditions. Submitted to *Wea. and Fore.*
- Brown, B.G., G. Thompson, R. T. Buintjes, R. Bullock and T. Kane, 1996: Intercomparison of in-flight icing algorithms: Part II. Statistical Verification Results. Submitted to *Wea. and Fore.*
- Forbes, G.S., Y. Hu, B.G. Brown, B.C. Bernstein and M.K. Politovich, 1993: Examination of conditions in the proximity of pilot reports of icing during STORM-FEST. Preprints, Fifth International Conference on Aviation Weather Systems, Vienna, VA, 2-6 August, American Meteorological Society, Boston, 282-286.
- Politovich, M.K., 1989: Aircraft icing caused by large supercooled droplets. *J. Appl. Meteor.*, **28**, 856-868.
- Politovich, M. and G. Thompson, 1996: A meteorologically-based icing severity index. FAA Int'l Conf. on Inflight Icing, Springfield, VA, 6-8 May 1996.
- Sand, W.R., W.A. Cooper, M.K. Politovich and D.L. Veal, 1984: Icing conditions encountered by a research aircraft. *J. Clim. Meteor.*, **23**, 1427-1440.
- Schultz, P. and M.K. Politovich, 1992: Toward the improvement of aircraft icing forecasts for the continental United States. *Wea. and Fore.*, **7**, 492-500.
- Thompson, G., R. Buintjes, B. Brown and F. Hage, 1996: Intercomparison of in-flight icing algorithms: Part I: WISP94 real-time icing prediction and evaluation program. Submitted to *Wea. and Fore.*
- Thompson, G., T.F. Lee and R.T. Buintjes, 1996: Using satellite data to reduce area extent of diagnosed icing. Submitted to *Wea. and Fore.*
- Vivekanandan J. and G. Thompson, 1996: Aircraft icing detection using satellite data and weather forecast model results. FAA Int'l Conf. on Inflight Icing, Springfield, VA, 6-8 May 1996.

ACKNOWLEDGEMENTS

Thanks to Ron Olson of the Aviation Weather Center for his advice on how to make the algorithm as useful as possible. Thanks to Tiffany Omeron of NCAR for her help with figure preparation and data analysis. Thanks to Frank McDonough for his data analysis work and to Marcia Politovich for her support of this project.

This research is sponsored by the National Science Foundation through an Interagency Agreement in response to requirements and funding by the Federal Aviation Administration's Aviation Weather Development Program. The views expressed are those of the authors and do not necessarily represent the official policy or position of the U.S. Government.

AIRCRAFT ICING DETECTION USING SATELLITE DATA AND WEATHER FORECAST MODEL RESULTS

Jothiram Vivekanandan¹, Gregory Thompson¹ and Thomas F. Lee²

¹National Center for Atmospheric Research, Boulder, CO 80307-3000

²Naval Research Laboratory, Monterey, CA 93943-5502

Abstract

Automated diagnostic icing algorithms which use temperature and relative humidity fields from operational weather forecast models have reasonably high probabilities of detection. However, excessive area extent predicted by such algorithms remains a major drawback. That is, the icing regions predicted by the automated algorithms are usually much broader spatially than the actual clouds containing the icing threat. The dependence on relative humidity, alone, to diagnose/predict clouds lies at the root of the problem. Currently, the Research Applications Program of NCAR is investigating a number of techniques for reducing the excessive area coverage or false alarms in icing diagnosis. Two such efforts utilize the new geostationary satellite data from GOES-8/9. Both methods use the multispectral satellite data for generating an icing product. These methods take advantage of the distinct radiative properties of water and ice clouds. For the first method, reflected shortwave IR radiation at 3.9 microns wavelength and cloud top temperature are used as the key parameters. These two parameters, along with additional components, are compared against thresholds to determine regions of supercooled cloud water. The second method also uses these parameters, plus a high resolution surface temperature analysis. This method creates a cloud/no-cloud analysis which is then used to screen regions which are predicted by an algorithm to contain icing but the satellite data indicate that no cloud is present. Basically, this method eliminates forecast icing from the automated algorithms on the basis that a region is cloud-free.

1. INTRODUCTION

The premier weather observing system, Geostationary Operational Environmental Satellites (GOES), is used for monitoring evolution and progression of weather systems. Satellite remote sensing is primarily based on radiometer observations. A radiometer is a passive instrument which senses range cumulative scattering and emission characteristics. The five channel multispectral imagers aboard the GOES-8/9 spacecraft are designed to measure visible (VIS, 0.6 microns), shortwave infrared (3.9 microns), water vapor channel (6.7 microns), and two longwave infrared (IR, 11 and 12 microns) wavelengths. Satellite-based cloud detection makes use of contrasts between the clouds and their backgrounds at these wavelengths. In the visible, this contrast is in terms of differences in reflectance, while in the infrared, this contrast is in terms of brightness temperature. Spatial and temporal resolution of GOES observations are from roughly 1 to 4 km and approximately every 15 minutes respectively. For these reasons, GOES observations are ideally suited for monitoring cloud microphysical properties.

Numerical weather forecast models are routinely used for diagnosis and prediction of atmospheric parameters including temperature, moisture, and winds. More recently, these "state-of-the-atmosphere" variables have been combined with diagnostic/empirical

algorithms to create aircraft icing analyses and predictions (Thompson et al, 1995). A recognized problem with these algorithms is their tendency to overpredict the area extent of the icing threat. This is not unexpected since the determination of icing by these algorithms is based so heavily on relative humidity.

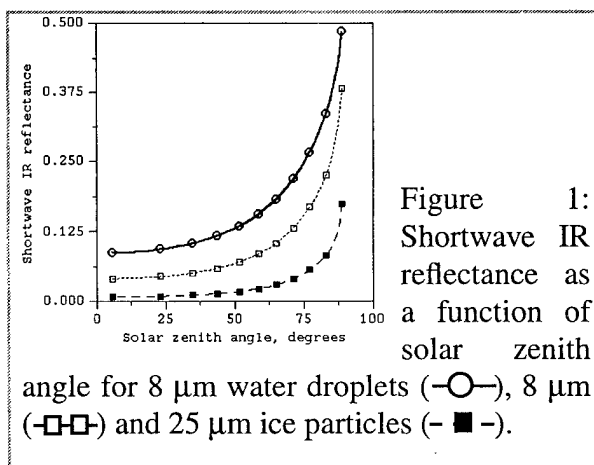
In working towards alleviating this problem of excessive area coverage, the Research Applications Program of the National Center for Atmospheric Research is currently working on combining the aforementioned satellite data with numerical model data to produce an improved aircraft icing product. The research presented in this paper includes two methods for using the satellite data. Each method makes use of the multispectral satellite measurements and shortwave IR reflectance at 3.9 microns wavelength. The first method does not involve weather forecast model data, only the satellite data. Theoretical background for this method is discussed in Section 2. Histograms of the multispectral satellite observations for snow cover, liquid, and ice cloud regions are presented in Section 3. Based on these spectral characteristics, a procedure for icing detection is described. A case study using the technique is also presented. The second method *does* use weather forecast model data in conjunction with the multispectral satellite observations. In this technique, the satellite data are used to create a cloud/no-cloud analysis. This analysis is applied to icing diagnosed from model output to remove regions which are found to be cloud-free. This technique is described, and an example is shown in Section 4. One drawback to both of these methods is that such techniques are only useful to diagnose potential aircraft icing hazards. Because they require satellite data, they cannot be used to predict anticipated icing hazards.

2. THEORETICAL BACKGROUND

A number of studies have dealt with retrieving quantitative microphysical information using multispectral data (Arking and Childs, 1985, Curran and Wu, 1982). Single scattering albedo and optical depth determine the emission and scattering characteristics of clouds. Albedo is a function of refractive index and mean size of a hydrometeor (Stephens, 1994). In visible (VIS) and infrared (IR) spectrums, the refractive indices are such that attenuation by ice particles is greater than the attenuation due to liquid water droplets. Also, as the size of the hydrometeor gets larger compared to the wavelength, the reflectance of the cloud decreases. Visible reflectance is primarily related to optical thickness (total liquid and/or ice water column), while its dependence on effective particle radius is minimal. However, unlike visible reflectance, the shortwave IR (3.9 microns) reflectance *is* sensitive to the average size of the hydrometeor, while its dependence on optical depth is minimal (Nakajima and King, 1990).

The relationship between hydrometeor size and reflectance as well as that between hydrometeor phase (frozen vs. liquid) and reflectance is shown in Figure 1. Figure 1 shows shortwave IR reflectance at 3.9 microns as a function of solar zenith angle, hydrometeor size and state. For a specified mean radius of hydrometeor, reflectance by water droplets is greater than that by ice particles. As the mean radius of ice or water hydrometeor increases, the reflectance dramatically decreases. Thus shortwave IR reflectance can be used to distinguish liquid from ice clouds (Allen et al., 1990) and, to a lesser extent, infer the average size of the hydrometeors in a cloud.

For a specified cloud structure, shortwave IR reflectance can be modeled using radiative transfer computations (Stamnes et al., 1988). Shortwave IR reflectance is defined as the ratio between radiance reflected in a given direction and radiance reflected by a lambertian surface. The essential ingredients for a radiative transfer computation are single scattering albedo, phase function, and extinction and absorption coefficients. We used a Mie scattering program (Evans and Vivekanandan, 1990) for computing these ingredients. Hydrometeor shapes were assumed to be spherical and the size distribution was assumed to be modified gamma with a mean radius of 8 microns.



During the daytime, shortwave IR radiance (which is what the satellite measures) is comprised of both solar reflection and thermal emission at 3.9 microns wavelength. To use the shortwave IR reflectance correctly, we need to isolate the emission and the reflection from the total radiance. The emission and reflection components are separated using concurrent observations from the longwave IR channel (11 microns). The resultant radiance difference is a function of angle between the sun and satellite positions. However, shortwave IR reflectance is independent of sun and satellite positions. To aid the computation of shortwave IR reflectance, bi-directional reflection coefficients are pre-computed for an assumed liquid cloud layer as described earlier.

3. MULTISPECTRAL OBSERVATIONS

Observations from the GOES-8 spacecraft at 1815 UTC 6 March 1996 are shown in Figure 2. Data for the first column of histograms was taken from a region centered in Missouri (see box outline in Fig. 3), whereas data for the second column was taken from a region centered on the Montana-Canada border. The former region is representative of liquid water cloud, while the latter region contains mostly snow cover and some ice cloud. For these two regions, histograms of two of the raw channel data are shown: VIS reflectance and longwave IR brightness temperatures. Then, two derived variables are presented: shortwave IR reflectance, and the difference between the shortwave and longwave IR. As one might expect, there's no obvious difference in visible reflectance (parts a and e) since water clouds, ice clouds and snow covered ground are all highly reflective in the visible. Furthermore, by inspecting the histograms of brightness temperature in the longwave IR (parts b and f), no conclusion as to the state of the hydrometeors can be made. These simply show that most of the two analyzed regions have cloud top temperatures below 0°C.

On the other hand, shortwave IR reflectances (parts c and g) exhibit large differences as theorized. The reflectance in the liquid cloud region is an order of magnitude larger than those found in the ice cloud or snow-covered ground regions. For this reason, the shortwave IR reflectance at 3.9 microns constitutes a major portion of the aircraft icing

algorithm discussed below. Lastly, another good indicator of low and mid-level clouds is the difference between the shortwave IR and longwave IR measurements. Histograms for this difference quantity are shown in parts d and h. Generally, a temperature difference greater than 20°C indicates a good likelihood of low and/or mid-level clouds.

Combining all of these factors, the icing algorithm can be summarized as follows:

- visible reflectance > 20%
- shortwave IR (3.9 μm) reflectance > 8%
- shortwave minus longwave IR > 20°C
- cloud top temps between -20° and 0°C

It is also possible to use this same algorithm for detection of fog by simply including temperatures greater than 0°C in the technique. An example of the icing product is provided in Figure 3. In this figure, the icing regions are represented in white, whereas regions which do not meet the icing criteria are displayed with the visible reflectance. Notice the extensive region of icing from north Texas northeastward into Ohio.

Also shown in Figure 3 are the Pilot Reports (PIREPs) of icing. The PIREPs were collected for one hour prior and one hour after the satellite data time. Only PIREPs of moderate and greater intensity are shown. Most of these PIREPs are located within regions of diagnosed icing. The few PIREPs that are not in the diagnosed icing regions show the limitation of the above-described technique. When high level ice cloud obscures a lower level liquid cloud, the satellite is not able to detect the lower cloud. Satellites generally only sense the first 60 to 300 m deep layer of cloud. The cloudiness along the eastern U.S. coastline may have been a multi-level cloud. Cloud top temperatures in the region of the PIREPs in Virginia and New York were approximately -50°C. This precludes that region from being diagnosed as icing and represents a scenario where other meteorological data sources are needed to correctly diagnose icing. [A ten-hour animated loop of this icing product will be shown at the conference along with the corresponding PIREPs. Images of the icing product are also available on the World Wide Web during the winter months at URL "<http://http.rap.ucar.edu/weather/satellite.html>".]

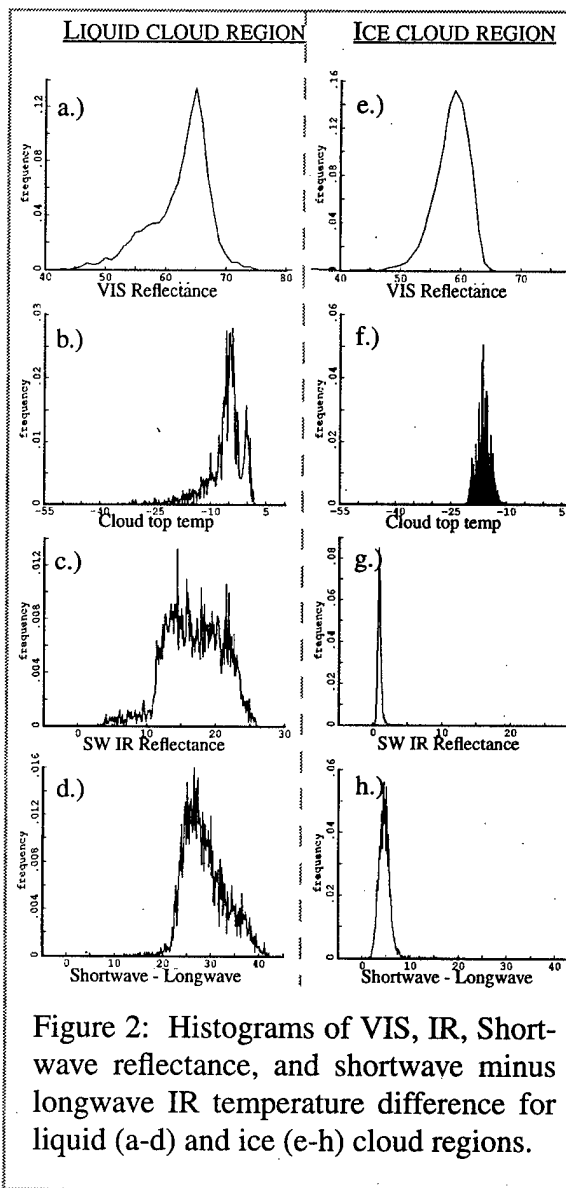


Figure 2: Histograms of VIS, IR, Shortwave reflectance, and shortwave minus longwave IR temperature difference for liquid (a-d) and ice (e-h) cloud regions.

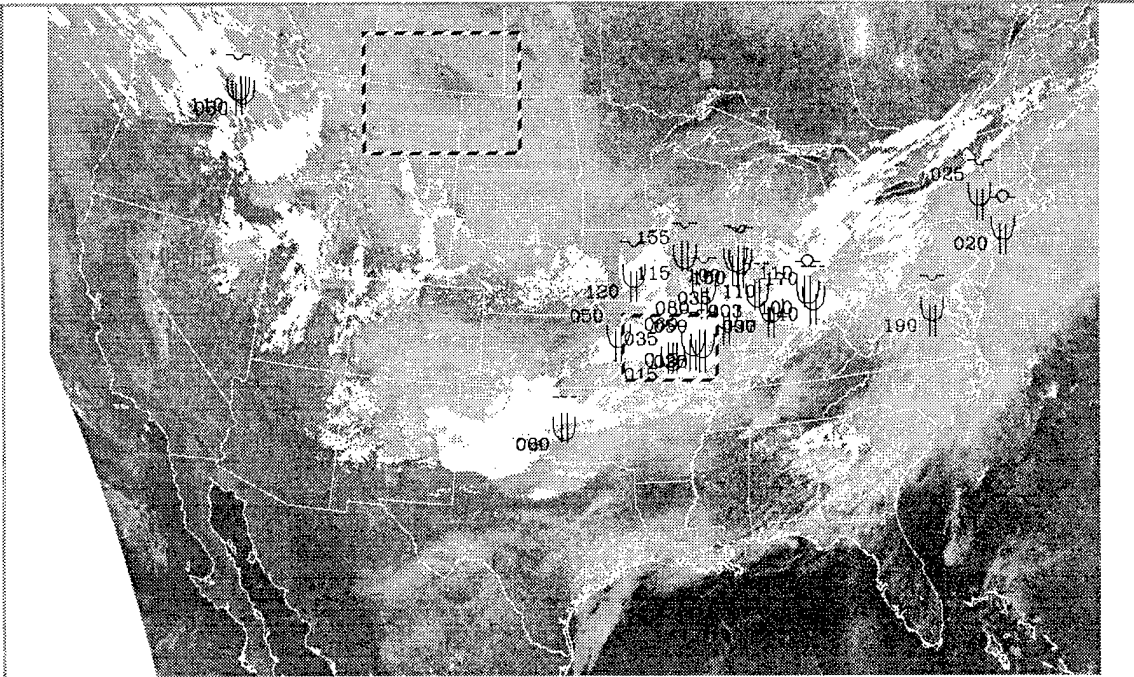


Figure 3: Satellite icing product depiction at 1815 UTC 6 March 1996. Visible imagery is shown in regions that do not meet the icing criteria whereas regions that do meet the criteria are shown as white and represent regions of icing potential. Locations of moderate and greater icing PIREPs are also shown.

During the nighttime, the absence of solar reflectance (VIS or shortwave IR) translates to an absence in two of the portions of the icing technique and lessens the confidence in the resultant icing product. The nighttime icing or fog product is derived using the shortwave minus longwave IR measurements as described in Ellrod (1995). Thus at night, the thresholds for the icing technique are:

- shortwave minus longwave IR between 2.5° and 4.0°C
- cloud top temps between -20° and 0°C

Again, the upper limit on cloud top temperature could be removed to diagnose fog as was mentioned for the daytime technique.

4. USING SATELLITE DATA TO REDUCE ICING COVERAGE BY MODEL-BASED ICING DIAGNOSIS

Recently, aircraft icing diagnosis/prediction has been accomplished with the use of automated diagnostic algorithms (Shultz and Politovich, 1992, Thompson et al., 1995). A recognized drawback of these algorithms is their tendency to overpredict the icing threat. The results of a recent study show this problem can be minimized when the automated icing product is combined with multispectral satellite data. For this study, a simplified version of the icing algorithm reported on by Thompson et al. (1995) was used. For input, the algorithm requires temperature, relative humidity, and geopotential height in the form of a vertical column of data through the depth of the troposphere. These data may be provided by operational numerical models for analysis times (0 hour forecast) or any model forecast times.

For this study, these model data were provided by the Navy Operational Global Atmospheric Prediction System (NOGAPS) numerical model. To obtain the predicted icing field, the NOGAPS analyses were interpolated in time to the time of the NOAA satellite overpass. For example: to obtain a gridded data analysis at 1900 UTC, data were linearly interpolated between the 1200 UTC NOGAPS analysis and the following day's 0000 UTC NOGAPS analysis. For simplicity, only 3 vertical levels of data were used: 850, 700, and 500 mb. For each of these levels, the interpolated "analysis" data were input into the icing algorithm to produce the predicted icing field.

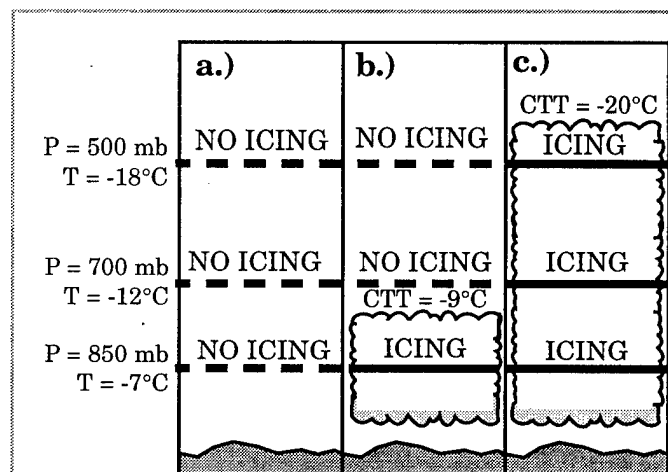


Figure 4: Under the assumption that the model first guess predicts icing at 850, 700 and 500 mb for all three hypothetical regimes, satellite screening results in the following: a) satellite detects no clouds, therefore the icing threat is removed at all three levels; b) satellite infrared temperature indicates cloud top below 700 mb, therefore the threat is removed at 700 and 500 mb and kept at 850 mb; c) satellite infrared temperature indicates cloud top above 500 mb, therefore the threat is kept at all three levels.

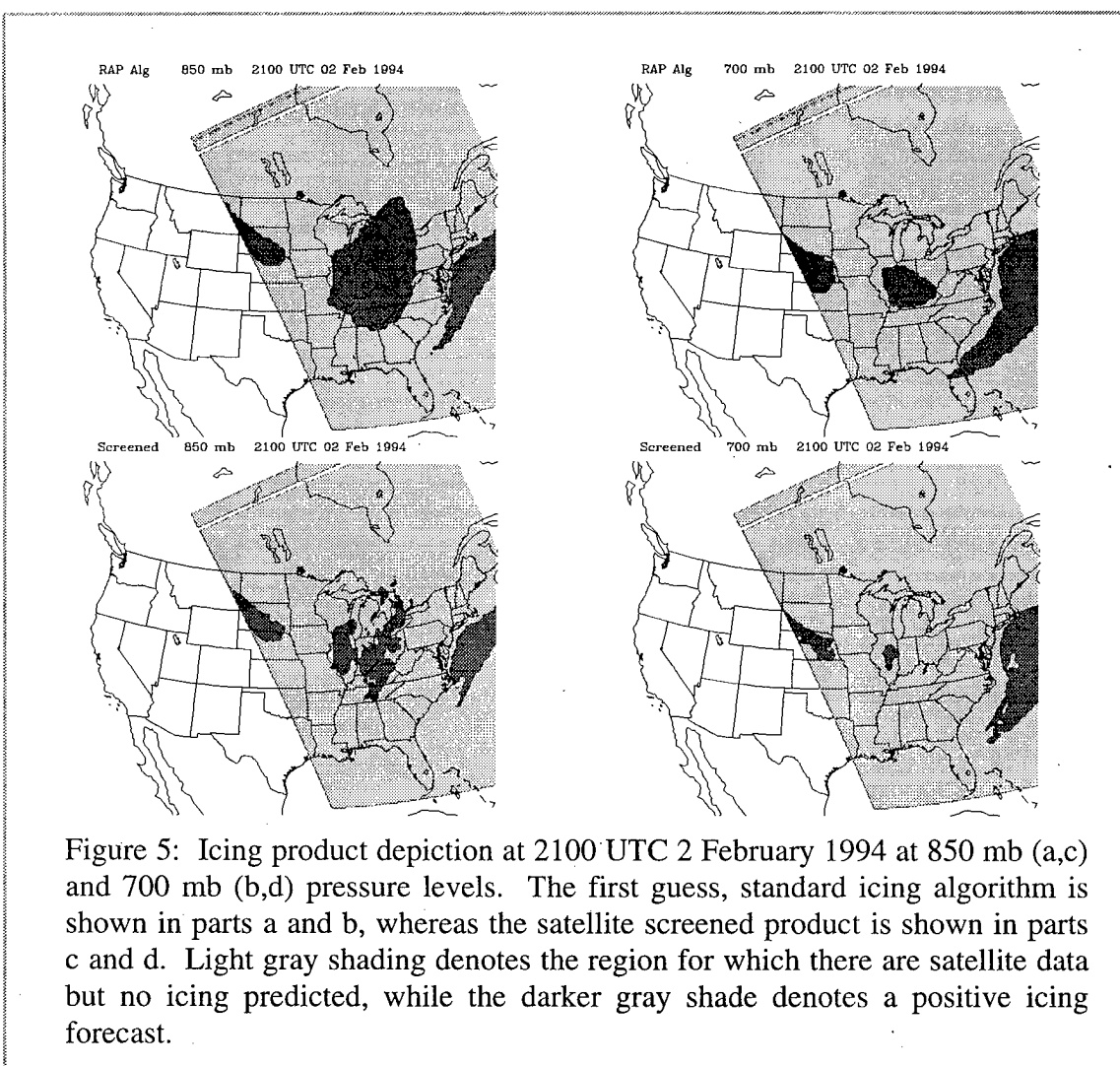
Then, a cloud analysis was performed using the satellite data to distinguish cloudy from clear regions. Satellite data used in this study originated from the Advanced Very High Resolution Radiometer (AVHRR) sensor aboard the NOAA polar orbiting satellites. Two separate cloud screens were created to detect cloud systems. If both checks failed to detect clouds, then a prediction of icing was eliminated from the corresponding model first guess product. The first screen checked for clouds at low temperatures (usually ice clouds) with respect to the surface by subtracting the longwave infrared channel (pixel-by-pixel) (Lee, 1995) from a high resolution (25 km) surface temperature analysis supplied by the Air Force Global Weather Central (Hammil et al. 1992; Kopp et al. 1994). If the temperature difference was less than 20°C then the pixel was assigned a binary "0",

indicating lack of cloud. When the threshold was not satisfied, the pixel was assigned a "1" indicating the presence of cloud. The second screen checked for water clouds at supercooled temperatures using the shortwave IR reflectance and the method outlined in Section 3.

To create the satellite-screened icing prediction, the first guess (model-diagnosed icing) was combined with the satellite analysis in the following manner. If both of the cloud checks outlined above indicated no cloud, then a model first guess of positive icing potential was changed to negative (Fig. 4a). If either cloud check detected cloud, then the infrared cloud top temperature was compared to the temperatures of the three geopotential

levels. If the cloud top temperature was greater than the model's temperature at that level, then the level was assumed to be cloud and icing free (Fig. 4b). Thus, a first guess prediction of icing was changed to negative at that model level. Model levels below the cloud top retain a positive icing prediction provided the first guess contained a positive icing prediction. If the satellite cloud top temperature was less than the model's temperatures at all the levels, then positive icing predictions were retained everywhere (Fig. 4c). In this manner, the screening process could never introduce new regions of predicted icing because temperature or level of the cloud was not known; it could only reduce the area extent of the first guess predicted icing.

Figure 5 presents an illustration of the two icing products. The first, standard icing output by the algorithm, is shown for the 850 (Fig. 5a) and 700 mb (Fig. 5b) levels. The light gray shading denotes the region for which there is satellite data (recall these data are from polar orbiting satellites and therefore appear as "swaths") and no icing predicted, while the darker shading denotes a positive icing forecast. When combined with the satellite cloud/no-cloud analysis, the resultant fields appear similar except some portions of the predicted icing have now been deleted. These "deleted" regions are attributable to the



lack of supercooled liquid cloud in the satellite analysis, thereby creating a "screened" icing prediction. Referring to Figure 5, notice that at 700 mb the standard product depicts icing over most of Illinois and Kentucky (Fig. 5b) whereas the screened product (Fig. 5d) shows that most of this region is not predicted to have icing (i.e. it is cloud-free).

5. CONCLUSIONS

This paper presented icing detection techniques using GOES-8/9 satellite data and weather forecast model results. A satellite-based icing product was generated in near real-time. The icing product showed good agreement with pilot reports of icing. Rigorous statistical evaluation of the icing product will be conducted using PIREPs (currently the only verification data set available). In the airport terminal area, Terminal Doppler Weather Radar (TDWR) and ground-based microwave radiometers could be used for icing detection. The major drawback of the satellite-based icing technique, the obscuration of low-level liquid clouds by higher, ice clouds, may be aided with radar reflectivity. Furthermore, radar and satellite data may be useful for retrieving mean droplet size and liquid water profile (Frisch et al., 1995, Vivekanandan et al. 1996). Thus, a combined remote sensing technique might be useful for estimating an icing severity index (Politovich, 1996).

Acknowledgements

The National Center for Atmospheric Research is sponsored by the National Science Foundation. This research is sponsored by the National Science Foundation through an Interagency Agreement in response to requirements and funding by the Federal Aviation Administration's Aviation Weather Development Program. The views expressed are those of the authors and do not necessarily represent the official policy or position of the U.S. government.

References

- Allen, R. C., P. A. Durkee, and A. H. Wash, 1990: Snow/cloud discrimination with multispectral satellite measurements. *J. Appl. Meteor.*, **29**, 994-1004.
- Arking, A., and J. D. Childs, 1985: Retrieval of cloud cover parameters from multispectral satellite images. *J. Climate and Appl. Meteor.*, **24**, 322-333.
- Curran, R. J., and M. C. Wu, 1982: Skylab near-infrared observations of clouds indicating supercooled liquid water droplets. *J. Atmos. Sci.*, **39**, 635-647.
- Ellrod, G.P., 1995: Advances in the detection and analysis of fog at night using GOES multispectral infrared imagery. *Wea. Forecasting*, **10**, 606-619.
- Evans, F. K., and J. Vivekanandan, 1990: Multiparameter radar and microwave radiative transfer modeling of nonspherical atmospheric ice particles. *IEEE Trans. Geoscience and Remote Sensing*, **28**, 423-437.
- Frisch, A. S., C. W. Fairall and J. B. Snider, 1995: Measurement of stratus cloud and drizzle parameters in ASTEX with a Ka-band Doppler radar and microwave radiometer. *J. Atmos. Sci.*, **52** 2788-2799.
- Hammil, T.M., 1992: A description of the Air Force real-time nephanalysis model. *Wea. Forecasting*, **7**, 288-306.
- Kopp, T.J., T.J. Neu, and J. Lanicci, 1994: A description of the Air Force Global Weather Central's Surface Temperature Model. Preprints, 10th Conf. on Numerical Weather Prediction, Portland, OR, Amer. Meteor. Soc., Boston, 435-437.
- Lee, T.F., 1995: Aircraft icing products from satellite infrared data and model output. Preprints, 6th Conf. on Aviation Weather Systems, 15-20 January, Dallas, TX, Amer. Meteor. Soc., Boston, 234-235.
- Nakajima, T., and M. D. King, 1990: Determination of the optical thickness and effective particle radius of

- clouds from reflected solar radiation measurements. Part I: Theory. *J. Atmos. Sci.*, **47**, 1878-1893.
- Politovich, M. K., 1996: Response of a research aircraft to icing and evaluation of severity indices. *J. Aircraft*, **33** 291-297.
- Schultz, P., and M.K. Politovich, 1992: Toward the improvement of aircraft icing forecasts for the continental United States. *Wea. Forecasting*, **7**, 491-500.
- Stamnes, K., S. C. Tsay, W. Wiscombe, and K. Jayaweera, 1988: A numerically stable algorithm for discrete-ordinate method radiative transfer in multiple scattering and emitting layered media. *Appl. Opt.*, **27**, 2502-2509.
- Stephens, G. L., 1994: Remote sensing of the lower atmosphere: An introduction. Oxford University Press, pp. 523.
- Thompson, G., R. T. Brientjes, and B. G. Brown, 1995: A comprehensive icing prediction and evaluation program. Preprints, 6th Conf. on Aviation Weather Systems, 15-20 January, Dallas, TX, Amer. Meteor. Soc., Boston, 234-235.
- Vivekanandan, J., L. Li, L. Tsang, and C. H. Chan, 1996: Microwave radiometric technique to retrieve vapor, liquid and ice, Part II: Joint studies of radiometer and radar in winter clouds. Submitted to *IEEE Trans. Geoscience and Remote Sens.*

A METEOROLOGICALLY-BASED ICING SEVERITY INDEX

Marcia K. Politovich and Gregory Thompson
National Center for Atmospheric Research
Boulder, CO, USA

Abstract

The development and implementation of an icing severity index based on meteorological parameters is described. Measurements of atmospheric and performance parameters obtained by a Beechcraft King Air 200T are used to construct the index. These measurements suggest that, for this particular aircraft, large droplet icing has a greater effect on flight performance than that resulting from encounters with cloud droplets. The index resulting from this study is intended to be used by forecasters who have available to them numerical weather forecast model output which includes liquid water content. The index builds on previous versions which used liquid water content as the primary variable, with adjustments for temperature and droplet-size effects. An example is shown to illustrate how model-generated liquid water and temperature fields are converted to expected icing severity. No allowance is made for the enhanced severity resulting from large droplet environments since the model used in the example cannot provide this distinction, but suggestions for means of doing so are discussed. It is suggested that a data base of forecast severity and pilot reports of severity be collected and compared to begin calibrating the model-generated index for different types of aircraft.

Introduction

Icing severity is a complex concept. On a very basic level it is quantification of flight degradation due to ice accretion on an airframe during flight. There are different means by which this degradation may be determined, including performance (lift and drag aspects), control and stability. The response of various aircraft to identical environments differs, and even the same aircraft type flown in different configurations (flap settings, attitude, gear up/down, airspeed) can result in different effects.

It may be most suitable to begin with a simple approach. Consider a severity definition based on atmospheric parameters which adversely affect flight in icing. The parameters are compared with performance data from a real aircraft. An index using combinations of the relevant atmospheric parameters is formulated and tested against the data sets from the target aircraft. An increase in the defined severity ought to be reflected by a decrease in our defined performance metric. The index may then have to be modified to accommodate those parameters that can be predicted using numerical weather forecast models. The

result is a map of expected icing severity.

Atmospheric Parameters

There is general agreement that for in-flight icing, three meteorological quantities have the most important influences on flight: liquid water content, temperature and droplet size (as in Hansman 1989). However, there is still not a consensus as to the proper quantification of these meteorological parameters as they affect flight, such as thresholds to describe expected severity. There are several reasons for this. Data sets of both meteorological and aircraft response parameters are relatively scarce, and available for only a few aircraft such as the University of Wyoming King Air and NASA Twin Otter. The transfer of findings from these aircraft to others may be limited.

One of the goals of the Winter Icing and Storms Project (WISP, Rasmussen et al. 1992) is to develop improved methods of forecasting aircraft icing. Quantification of the icing hazard in terms of expected effect on an aircraft is an important component of WISP. Research aircraft were deployed for field experiments to provide in situ measurements of atmospheric conditions. In addition to meteorological data, flight performance parameters were recorded which provide useful information on the response of the aircraft to icing environments.

Data Sets

The target aircraft for this study is the University of Wyoming's King Air. The analysis techniques and data sets are described in detail by Politovich (1996). Data sets were obtained with this research aircraft during two WISP field seasons, conducted in February-March 1990 and January-March 1991, in eastern Colorado. These were supplemented with data from ten encounters with large droplets over the Sierra Nevada mountains in northern California, and over the mountainous area of northern Arizona (Politovich 1989). Note that the large droplet flights were all in visible cloud; encounters with large droplets as freezing drizzle or freezing rain below cloud were not included. Cloud was generally defined as a liquid water content (LWC) $> 0.01 \text{ g m}^{-3}$ and droplet concentration $> 5 \text{ cm}^{-3}$. Median volume diameter (MVD) was used to characterize droplet size.

The aircraft's ability to climb was evaluated by comparing the actual rate of climb (ROC) with that expected for a clean (uniced) aircraft, with the same power settings and angles of pitch and attack, as described by Sand et al. (1984). The resulting difference in climb capability is referred to as ΔROC , where negative values indicate declines in performance. The quantity ΔROC can be calculated continuously along the flight track, and thus provides a means of monitoring aircraft performance capability. Sand et al. (1984) found that this parameter has an accuracy of $\sim 1.2 \text{ m s}^{-1}$.

Flight data were examined and times with local minima in ΔROC were chosen for analysis. These minima may either represent temporary losses in climb capability or instances

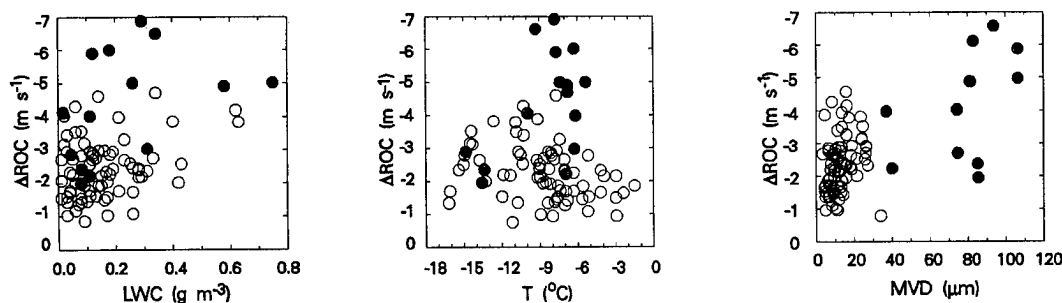


Figure 1. ΔROC plotted against liquid water content (LWC), temperature (T), and median volume diameter (MVD) for King Air data described in the text. Eighty-one WISP (unfilled and grey) and ten California/Arizona (black) points are included. Grey dots are WISP data with $MVD > 40 \mu m$.

when de-icing boots were deployed. However, in general, the pilot did not deploy the boots during cloud penetrations unless absolutely necessary. For comparison with minimum ΔROC values, corresponding 1-min averages of cloud physics measurements were derived. Eighty-two data points were isolated. For the ten data points from California and Arizona, the minimum calculated ΔROC values listed in the reference were used along with the averages of atmospheric parameters from the encounters.

Relation of Atmospheric Parameters to Performance

Figure 1 shows the effects of liquid water content, temperature, droplet size (as the median volume diameter or MVD) on the minimum ΔROC values. For the King Air used in these studies, flight tended to be degraded most under conditions of large ($MVD > \sim 40 \mu m$) droplets with high LWC ($> \sim 0.2 g m^{-3}$). Greatest effects tended to occur in the temperature range ~ -3 to $-12^\circ C$, but there were also cases in this range with no significant degradation. For smaller droplets ($MVD < \sim 40 \mu m$), there was no relation between ΔROC and droplet size. Encounters with larger droplets when liquid water content was low ($< \sim 0.2 g m^{-3}$) resulted in little effect on flight.

For droplet size we have used the MVD as the single size parameterization. This value is most appropriate for monomodal size or mass distributions, which is typical for cloud droplets (diameters $\leq \sim 30\text{--}40 \mu m$). For freezing drizzle and freezing rain size distributions, which are not necessarily monomodal, this may not be a useful parameter. It may be more reasonable to divide icing into "cloud droplet" and "large droplet" categories, and place all liquid water droplets having diameters greater than $40 \mu m$ (including freezing drizzle and freezing rain) into a single category. The data suggest that for "cloud droplet" icing, there is little to be gained by differentiating droplet size.

Table 1: Pilot Reporting Definitions for Icing Severity and Lewis' (1951) LWC Thresholds

Category	LWC	Definition
trace	$<0.1 \text{ g m}^{-3}$	Ice becomes perceptible. Rate of accumulation is slightly greater than rate of sublimation. It is not hazardous even though de-icing/anti-icing equipment is not utilized, unless encountered for an extended period of time (over 1 hour).
light	$0.11\text{-}0.6 \text{ g m}^{-3}$	The rate of accretion may create a problem if flight is prolonged in the environment (over 1 hour). Occasional use of de-icing/anti-icing equipment removes/prevents accretion. It does not present a problem if the de-icing/anti-icing equipment is used.
moderate	$0.61\text{-}1.2 \text{ g m}^{-3}$	The rate of accretion is such that short encounters become potentially hazardous and use of de-icing/anti-icing equipment, or diversion, is necessary.
severe	$> 1.2 \text{ g m}^{-3}$	The rate of accretion is such that de-icing/anti-icing equipment fails to reduce or control the hazard. Immediate diversion is necessary.

Construction of a Severity Index

The definitions of icing severity (listed in Table 1) were derived for use by pilots to report icing during flight, and depend on a pilot's assessment of how well her or his aircraft is coping with the ice accreting on it. The categories, trace-light-moderate-severe, are somewhat subjective, and depend as much on aircraft type and pilot reaction as they do on meteorology. While such an index can be useful for pilots reporting icing during flight, it provides little guidance for forecasters who are called upon to predict such conditions. Lewis (1951) proposed a severity index using the same terminology, based on theoretical accretion of ice on a 3-in diameter cylinder travelling perpendicular to the airstream at 200 kt (89.4 m s^{-1}) for 1 h, for various LWC, assuming a droplet diameter of $15 \text{ }\mu\text{m}$. The actual effect on an aircraft was not evaluated. The Lewis index, as it was intended to be implemented, includes an adjustment to the LWC to account for the difference in collection efficiencies of non- $15 \text{ }\mu\text{m}$ droplets. Jeck (1992) later revisited and revised this index with a temperature-dependent adjustment meant to account for the increased aerodynamic penalty resulting from clear icing at warmer ($> -8^{\circ}\text{C}$) temperatures.

Since most forecasters do not have information about droplet size, an index that requires this information is difficult to implement. Similarly, most forecasters also do not have LWC information, but, several guidelines have been available for its prediction. As an

example, the Air Weather Service Forecasters' Guide on Aircraft Icing, 1980) provides a means to estimate LWC, and recommends a simplified version of the index proposed by Lewis to be used by forecasters to predict icing severity. Droplet size is estimated by using a droplet diameter of 14 μm for stratiform clouds and 17 μm for cumuliform clouds. No temperature adjustment is made.

Even today, operationally-available numerical weather forecast models do not predict droplet size. However, the data from the King Air showed that, at least for this target aircraft, there was little dependence of performance degradation on droplet size for the cloud droplet size range. The presence of large droplets did have an enhanced effect for those cases with LWC and temperature exceeding certain thresholds. So indices are constructed. The first (large droplet index) includes the large droplet effects, and the second (model index) does not. A 15- μm droplet diameter was assumed for the model index, and for the large droplet index where $\text{MVD} < 40 \mu\text{m}$. The assumption of 15 μm is in agreement with data collected in stratiform clouds contained in the FAATC icing database (Jeck, personal communication). For the large droplet index, if $\text{MVD} > 40 \mu\text{m}$, it was assumed all droplets impacted on the airframe (collection efficiency = 1). The large droplet and model indices differ slightly from the index described by Politovich (1996), which includes a cloud droplet size dependence similar to that described by Lewis (1951).

The indices are described in Table 2 and plotted against ΔROC in Fig. 2 with the large droplet encounters from WISP and the California/Arizona data points identified. The WISP large droplet encounters had low LWC, and all were classified as light severity for both indices. The California/Arizona points were light through severe, and had the highest performance degradation. Most of the California/Arizona points had LWC and temperatures enabling the large droplet adjustment, although one point did not meet the $\text{MVD} > 40 \mu\text{m}$ requirement. The model index classified none of these points as severe, and only

Table 2: Large Droplet and Cloud Droplet Severity Indices

Index	LWC	
large droplet	$w(\text{LWC}) + \text{adj}_T + \text{adj}_D$	$w = \epsilon(\text{MVD})/e(15 \mu\text{m})$ where ϵ = collection efficiency as in Lewis (1951) $\text{adj}_T = 0.1 \text{ g m}^{-3}$ if $T > -12^\circ\text{C}$ $= 0$ otherwise $\text{adj}_D = 0.6 \text{ g m}^{-3}$ if $\text{MVD} > 40 \mu\text{m}$, $T > -12^\circ\text{C}$ and $\text{LWC}_m > 0.2 \text{ g m}^{-3}$ $= 0$ otherwise
cloud droplet	$\text{LWC} = \text{adj}_T$	adj_T as for King Air index $\text{LWC} = 0$ if $T > 0^\circ\text{C}$

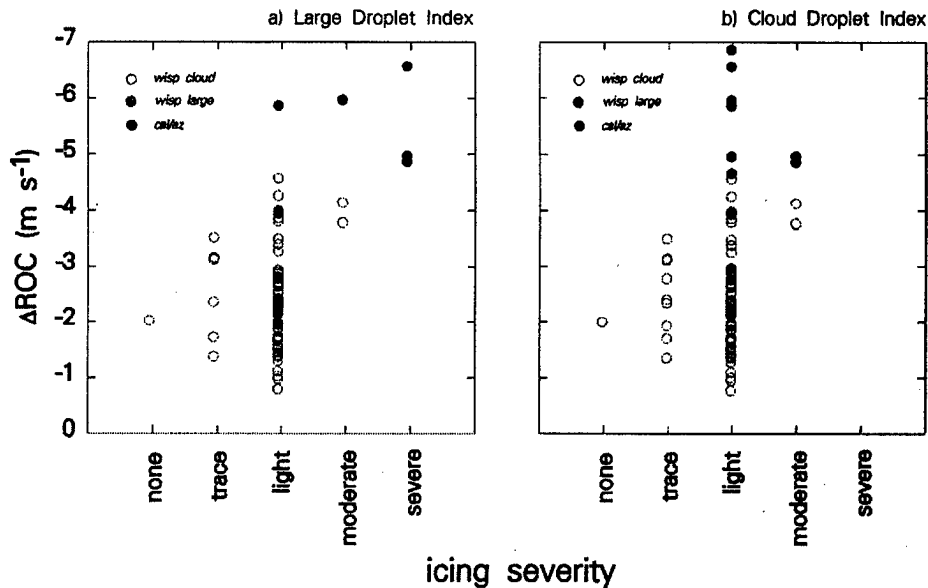


Figure 2 Δ ROC plotted against the large droplet and cloud droplet indices. Data are the same, and shading of data points is the same, as for Fig. 1.

two as moderate. At least for the King Air data set, it appears that the large droplet encounters must be accounted for differently than those areas with only cloud-sized droplets if severity is to be depicted accurately.

The King Air has $7\text{--}10\text{ m s}^{-1}$ reserve climb capability according to Sand et al. (1984). In at least two of the California/Arizona flights shown here, the pilot felt it necessary to leave the icing areas as quickly as possible. During one, a turn was initiated and the pilot felt a buffet as though a wing stall was imminent. He then restored the airplane to a wings-level condition, and made a flat turn using only the rudder. This certainly could be considered a severe icing event; based on comparable decreases in climb capability, most of the other California/Arizona data points probably belong in the severe category.

Implementation

An experimental version of the Eta model, run by the National Center for Environmental Prediction (NCEP), was used for this study. This version has 29-km horizontal grid spacing and 50 vertical levels. It includes cloud liquid water and ice parameterizations (Zhao et al. 1991) and is run every 12 h. Cloud liquid water from this model was combined with the predicted temperature field to produce the model-index severity field. The Eta model does not include an explicit prediction of large droplet environments.

Figure 3a shows Eta model outputs for 1800 UTC, 6 March 1996, at an altitude of ~ 1 km MSL (Eta level 0.878435). The units of LWC shown are in g kg^{-1} , which at this altitude are about 10% higher than the equivalent g m^{-3} units used in the severity indices in Table 2. The main feature is a large, continuous area of LWC that covers the central U.S., with

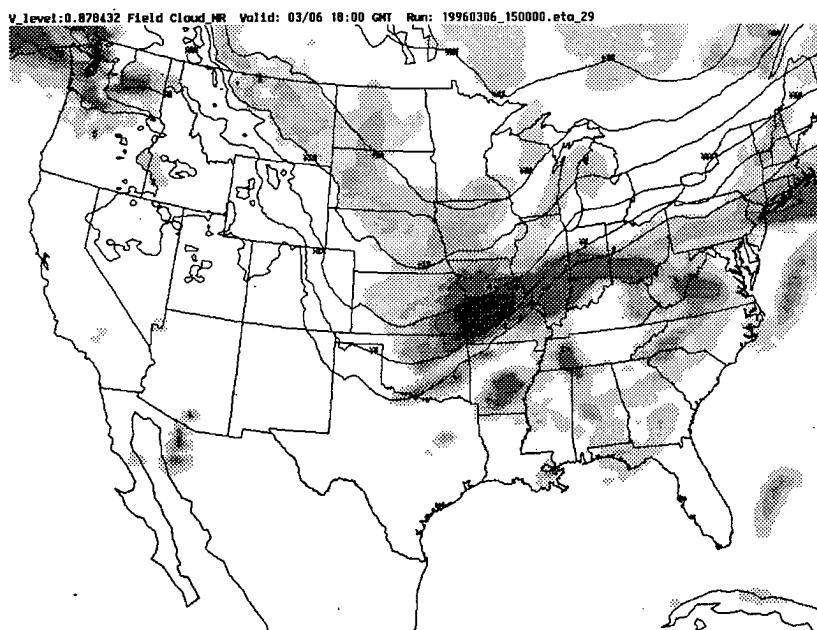


Figure 3a. Eta liquid water for 1800 UTC, 6 March 1996 at ~1000m MSL. Field is contoured starting with 0.2 g kg^{-1} and increasing in 0.2 g kg^{-1} increments. Temperature contours, starting at 0°C and continuing in decreasing 5°C increments to the north, are also shown.

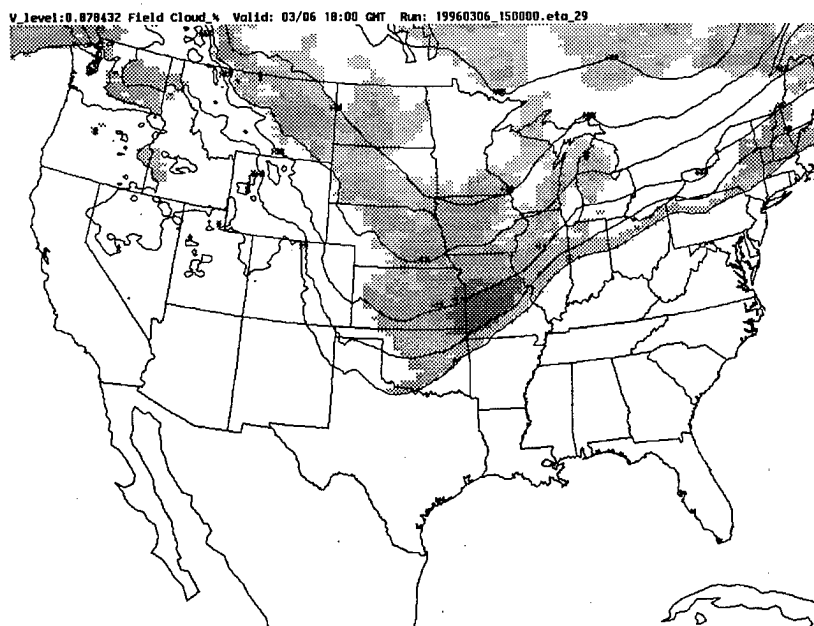


Figure 3b. Model-index severity derived from Eta output for the case shown in Fig. 3a. Shading depicts model index severity: trace is light shading, with light and moderate as darker greys. No severe icing resides at this level and time.

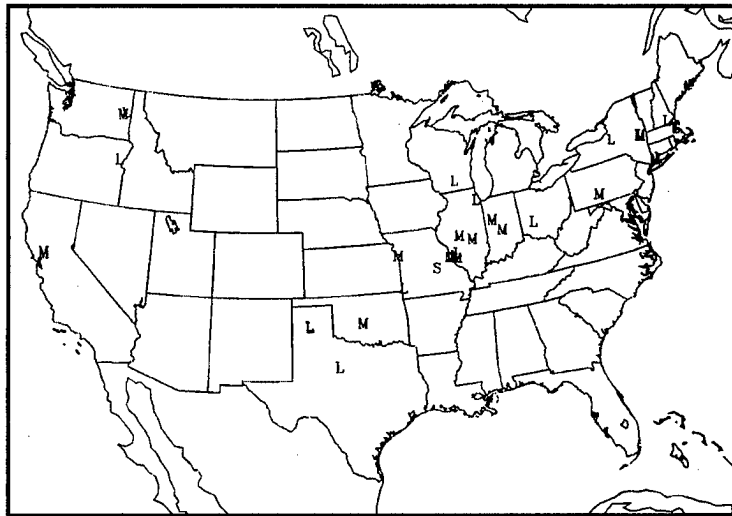


Figure 4. Icing PIREPs 1600-2000 UTC, 6 March 1996, for altitudes 1.5 km MSL and below. T=trace, L=trace-light and light, M=light-moderate and moderate, S=moderate-severe and severe.

values exceeding 0.5 g kg^{-1} . The western edge of the liquid area represents the terrain rising above the 1 km altitude shown. Temperature contours are also shown in the figure; considerable liquid exists at temperatures $> 0^\circ\text{C}$, which is not an icing threat. The model severity index derived from this model output is shown in Figure 3b. Most of the icing is depicted as light, with an isolated area of moderate corresponding with the high LWC and relatively warm temperatures (-5 to -12°C) over Missouri. No severe icing is depicted in this figure.

Figure 4 shows pilot reports (PIREPs) of icing at < 1.5 km MSL for a 4-h window centered on 1800 UTC for this case. The overall pattern of PIREPs, with mostly light and moderate reports, qualitatively matches the predicted severity. It may be useful to use the different interpretations of icing severity -- by the model and by pilots flying airplanes -- to calibrate the model index for different aircraft types, and perhaps adjust the LWC thresholds for severity.

Large Droplet Icing

The severity index as implemented in this example does not account for large droplets. The results from the King Air data set indicated that, for this target aircraft, the large droplet areas should be identified in order to correctly represent the effect on flight. These areas could either be folded into the large droplet severity index described in Table 2, or flagged and warned separately.

The "stovepipe" algorithm (Bernstein, 1996) is one possible solution. At present, this does not provide a forecast product, rather only a current depiction since it uses surface observations of precipitation type for determining where large-droplet icing conditions are

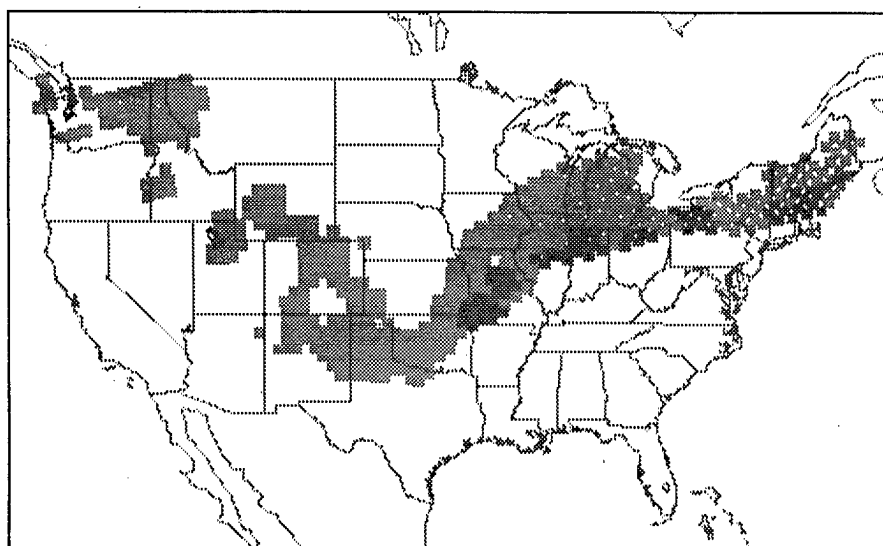


Figure 5. Stovepipe algorithm output for the same time and similar altitude as Fig. 4. Dark shaded areas are those where large droplet icing is likely. Lighter shaded areas are for "general" (non-large droplet) icing.

likely aloft. Figure 5 shows the stovepipe algorithm results for the time and approximate altitude shown in Fig. 3. The largest area of large droplet icing coincides with the moderate icing region shown in Fig. 3b; if we apply the large droplet index criteria described in Table 2, the temperature and LWC are sufficient to move the severity into the severe category.

The current version of the Eta-29 model incorporates a precipitation prediction algorithm (Baldwin et al. 1994) which includes snow, rain, freezing rain and ice pellets at the surface. This could be used to implement the stovepipe algorithm in a forecast mode. The RAP icing algorithm (Thompson et al., 1995) has a freezing rain field which looks for the embedded warm layer structure conducive to producing this type of precipitation. This algorithm can be applied to Eta model output to provide information on freezing rain. Alternatively, it may be possible to use radar and/or satellite information in combination with the model outputs to deduce precipitation type. Thus there are several possibilities for inclusion of large droplet information to enable a better depiction of expected severity; further research in this area is needed.

Summary

The use of an icing severity index, based on meteorological parameters and adjusted for implementation in a current numerical weather forecast model, was demonstrated. The index was developed using three atmospheric parameters considered important to icing severity -- liquid water content, temperature, and droplet size (as median volume diameter). Data from a single target aircraft, a King Air research airplane equipped for both cloud physics and flight performance measurements, was used to test the index to insure

that increasing severity was reflected by decreasing performance. Other effects of icing on stability and control are not included in the index, and the index as developed here has only been tested for the target airplane. More testing, using detailed in situ measurements from other aircraft, as well as comparison with icing PIREPs is needed for further adjustment and to build confidence in this system. An example was presented to demonstrate the implementation of this index using model output, but with no accounting for possible large droplet environments.

Does this mean that the current pilot reporting system for severity should be abandoned? Not at all. For the purposes of pilots assessing the severity of icing on their particular aircraft, that system works, especially when the report includes the aircraft type. That system is appropriate for the type of information the pilot has available, that is, how the aircraft is responding to the icing situation. However, the forecaster is not flying an airplane but rather has a different set of tools to work with, namely, forecasts of relevant meteorological parameters. The index developed in this paper is designed for that application; further work will endeavor to match the two so that differences can be minimized.

Acknowledgments

This research is sponsored by the National Science Foundation through an Interagency Agreement in response to requirements and funding by the Federal Aviation Administration's Aviation Weather Research Program. The views expressed are those of the authors and do not necessarily represent the official policy or position of the U.S. Government. The National Center for Atmospheric Research is base funded by the National Science Foundation. Data from the Wyoming King Air were supplied by the University of Wyoming Department of Atmospheric Science. Ben Bernstein supplied several figures, and Tiffany Omeron formatted the paper.

References

- Air Weather Service, 1980: Forecasters' Guide on Aircraft Icing. U.S. Air Force, Air Weather Service Report Number AWS/TR-80/001, 1980.
- Baldwin, M., R. Treadon and S. Contorno, 1994: Precipitation type prediction using a decision tree approach with NMC's mesoscale Eta model. *Preprints, 10th Conf. Numerical Wea. Pred.*, 17-22 July, Portland. Amer. Meteor. Soc., Boston, 30-31.
- Bernstein, B.C., 1996: The Stovepipe algorithm: Identifying locations where supercooled large droplets are likely to exist. Elsewhere in this volume.
- Hansman, R.J., 1989: The influence of ice accretion physics on the forecasting of aircraft icing conditions. *Preprints, Third Intl. Conf. on Aviation Weather Systems*, Jan. 30-Feb. 3, Anaheim. Amer. Meteor. Soc., Boston, 154-158.
- Jeck, R., 1992: Examination of a numerical icing-severity index. AIAA Paper 92-0164,

- Lewis, W., 1951: Meteorological Aspects of Aircraft Icing. In *Compendium of Meteorology*, Amer. Meteor. Soc., Boston.
- Politovich, M.K., 1989: Aircraft icing caused by large supercooled droplets, *J. Appl. Meteor.*, **28**, 856-868.
- Politovich, M.K., 1996: Response of a research aircraft to icing and evaluation of severity indices. *J. Aircraft*, **33**, 291-297.
- Sand, W.R., W.A. Cooper, M.K. Politovich and D.L. Veal, 1984: Icing conditions encountered by a research aircraft. *J. Clim. Appl. Meteor.*, **23**, 1427-1440.
- Rasmussen, R., M. Politovich, J. Marwitz, W. Sand, J. McGinley, J. Smart, R. Pielke, S. Rutledge, D. Wesley, G. Stossmeister, B. Bernstein, K. Elmore, N. Powell, E. Westwater, B.B. Stankov and D. Burrows, 1992: Winter Icing and Storms Project (WISP). *Bull. Amer. Meteor. Soc.*, **73**, 951-974.
- Thompson, G., R. Brientjes and B. G Brown, 1995: A comprehensive icing prediction and evaluation program. *Preprints, Sixth Conf. on Aviation. Wea. Systems*, 15-20 January, Dallas. Amer. Meteor. Soc., Boston, 243- 248.
- Zhao, Q., F.H. Carr and G.B. Lesins, 1991: Improvement of precipitation forecasts by including cloud water and cloud ice into NMC's Eta model. *Preprints, Ninth Conf. on Numerical Weather Prediction*, 14-18 October, Denver. Amer. Meteor. Soc., Boston, 50-53.

Section IV

Requirements for and Means of Compliance in Icing Conditions (Including Icing Simulation Methods)

Thomas Bond, NASA Co Chair

Eric Parelou, JAA Co-Chair

John P. Dow, Sr., Federal Aviation Administration Co-Chair

AERODYNAMICS OF SUPERCOOLED-LARGE-DROPLET ICE ACCRETIONS AND THE EFFECT ON AIRCRAFT CONTROL

M. B. Bragg*

University of Illinois at Urbana-Champaign

ABSTRACT

The effect of large-droplet ice accretion on aircraft control is examined. Supercooled-large-droplet icing conditions can result in the formation of a ridge of ice aft of the upper surface boot. By comparing this ice shape to data acquired with a spanwise protuberance on an airfoil, it is clear that a ridge of ice aft of the boot can lead to large losses in lift, increases in drag and changes in the pitching moment. This effect is most likely due to the formation of a large separation bubble aft of the ice accretion which grows with angle of attack and eventually fails to reattach, leading to premature airfoil stall. The bubble alters the pressure distribution about the airfoil resulting in a more trailing edge up (negative) hinge moment on the aileron and the resulting change in aileron stick force. This can lead to aileron hinge moment reversal and aileron snatch. The fundamental aerodynamic cause of this lateral control problem is the same as that experienced when elevator control is lost due to horizontal tail stall.

INTRODUCTION

It is well known that ice formation on aircraft surfaces can lead to deterioration of performance and handling characteristics. Loss of aircraft control, where structural ice accretion has been identified as a probable cause, has in some cases been attributed to the presence of supercooled large droplets (SLD) in the atmosphere.

Supercooled large drops (SLD) can form in several ways¹. One way for the SLD to form is through the melting of snow as it falls through a warm layer of air. This can happen when a warm frontal layer penetrates through a cold layer of air, causing a temperature inversion with increasing

altitude. Clouds above the warm layer produce snow which melts while falling through the warm layer and forms drizzle or rain drops. As the drops continue to fall, they enter the colder air layer again and are not likely to freeze again until they impact an object. If the lower cold air layer is at a sufficiently low temperature, the drops may freeze in the air to form ice pellets.

SLD may also form from smaller cloud drops. Droplets falling at different speeds can collide with one another and coalesce to form larger drops. The presence of wind shear and a stable thermodynamic profile near stratiform cloud tops has been attributed to enhanced mixing and increased drop size¹.

On October 31 1994, an ATR-72 commuter aircraft crashed near Roselawn Indiana after loss of control in icing conditions. The meteorological conditions in the region of aircraft's holding pattern just prior to the accident suggested the possibility of the development of supercooled drizzle¹. Supercooled large droplets, in the range of 30-400 μm , have been encountered by research aircraft while collecting data on effects of ice accretion on aircraft performance²⁻⁵. The reduction in the aircraft performance was reported to be unusually large during this encounter. Measured drag increased by as much as a factor of two, while the lift decreased more than 60%⁵. In another flight test in icing conditions, the worst icing encounter was identified as freezing rain⁶. The formation of ice during that encounter was described as ridges downstream of the leading edge on the wing and tails. Other accidents have also occurred due to the loss of aircraft control in conditions where SLD may have been present⁷.

Recent flight tests behind a tanker at Edwards Air Force Base to reproduce large droplet icing conditions caused the formation of ice ridges downstream of the de-icing boots which might have led to an uncommanded roll⁸. Uncommanded roll

* Professor, Department of Aeronautical and Astronautical Engineering.
Copyright © 1996 by Michael B. Bragg.

was identified as the probable cause of three separate An-12 aircraft accidents⁹. The formation of ice upstream of the ailerons was cited as the cause of flow separation on the wing which led to the reversal of aileron hinge moment.

Aircraft designed many years ago experienced aileron control problems with ice, Fig.1. The measurements by Johnson¹⁰ showed lack of aileron control power with leading-edge ice. Brumby¹¹ reports that a relatively small amount of ice on the wing of a commercial transport caused an accident on takeoff due to the loss of roll control. Several other loss of lateral control due to ice anecdotes have appeared in the literature as well.

The phenomenon of ice accretion leading to reduced aircraft control has been observed and documented for over 50 years. This has primarily been for Appendix C type icing clouds, but there is also evidence of large droplet icing also causing control problems. It is the intent of this paper, and its predecessor¹², to identify the underlying aerodynamic causes of reduced aircraft control due to large droplet ice accretions. A recent paper by Ashenden et al.¹³ presents lift and drag data on an airfoil with computer generated large-droplet ice accretion but does not address the control problem. The focus of this paper is aircraft control with large droplet-ice accretion and particularly focusing on aileron control.

DISCUSSION

Ice Accretion

It is well known that as the droplet size increases, the droplet inertia increases, and droplet impingement moves further back on the airfoil surface. The combination of this, with temperatures near freezing, leads to ice accretion shapes which are only now beginning to be studied. As part of the ATR 72 accident investigation, the Air Force icing tanker was modified to produce large droplets in the 100-200 micron range. A typical ice accretion obtained on the ATR-72 test aircraft¹⁴ is shown in Fig. 2. This ice accretion was formed at 180 KIAS, $T = -2^\circ\text{C}$, $MVD = 140$ microns, $LWC = 0.3\text{ g/m}^3$ for 17.5 minutes. Fig. 4a is with the flaps at 0 degrees and Fig. 4b at 15 degrees.

With no flap deflection, the ridge of ice is seen to form aft of the de-icer boot, ahead of the 9 percent chord location on the upper surface with a small ridge also formed on the lower surface. The ridge was found to be jagged in most cases and

discontinuous in the spanwise direction. When ice was accreted with the flaps at 15 degrees, the ice accretion moved back on the airfoil upper surface with a ridge at 9% and accretion to 16%. This occurred due to the reduction in angle of attack required with flaps to maintain the same lift coefficient. Therefore, the result was more exposure of the upper surface to the icing cloud and impingement further back on the upper surface. The maximum ridge height on the upper surface for the conditions tested was 0.75 inches and 0.5 inches on the lower surface. Similar results have been obtained in the Icing Research Tunnel at NASA Lewis¹⁵.

Aerodynamics of Large Droplet Accretions

In 1932 Jacobs¹⁶ conducted wind tunnel tests on an NACA 0012 airfoil to determine the effect of spanwise protuberances on the aerodynamic characteristics. The experiments were conducted at $Re = 3.1 \times 10^6$ with the purpose of documenting the effects of "small projecting objects such as fittings, tubes, wires, rivet heads, lap joints, butt straps, filler caps, inspection plates and many other projections" on the performance of the airfoil. The airfoil with the locations of the spanwise protuberances are shown in Fig. 3. The protuberances were duralumin sheets placed in slots in the wing, one at a time, which acted as forward and aft facing steps. The chordwise width of the protuberance was not reported, but heights of $k/c = 0.0004, 0.001, 0.002, 0.005$ and 0.0125 were tested. For the large droplet case, the ice accretion shown in Fig. 2 occurs between the $x/c=0.05$ and 0.15 protuberances tested by Jacobs. The maximum height of $3/4$ inch seen in the large-droplet tanker test ice accretions has a $k/c = 0.0106$ based on an airfoil chord at the aileron midspan location of 5.9 ft. At the conditions of the tanker test, this section would have been operating at a chord Reynolds number of 8.95×10^6 . The NACA test was conducted at sufficiently high Reynolds number that with these roughness heights, which are very large compared to the local boundary-layer thickness, the simulation should be representative of the behavior of airfoils with large-droplet ice accretions at full-scale commuter aircraft Reynolds numbers.

In Fig. 4 section lift, drag and pitching moment results are shown for the NACA 0012 airfoil with 4 different roughness height protuberances all at $x/c=0.05$ on the airfoil upper surface. For protuberances of $k/c=0.001$ and 0.002 the effect on lift is a slight reduction in lift

curve slope and a sizable reduction in maximum lift. For $k/c=0.005$ the lift curve is further reduced, but here only a local maximum in lift is seen with the lift continuing to increase as angle of attack is increased. This trend is continued for $k/c=0.0125$ with no maximum or local maximum seen in lift. The lift breaks sharply around $\alpha = 6^\circ$, becomes almost constant until $\alpha = 12^\circ$, where it increases again at a reduced, but linear, lift curve slope. The drag polar in Fig. 6 b) shows that this loss in lift is accompanied by a large increase in drag, especially for the 2 largest protuberance sizes. The pitching moment data in Fig. 6 c) shows a much more negative, nose down, pitching moment for the $k/c=0.0125$ case starting at $\alpha = 6^\circ$ where the lift curve breaks. The effect on pitching moment is much less for the smaller roughness cases where the primary effect is a reduced maximum lift at almost the same stall angle. For the large roughness, this change in moment is indicative of a large change in pressure distribution on the airfoil which accompanies the loss in lift. A NACA 0012 airfoil has much of its lift on the forward part of the airfoil. A loss in lift on the forward part of the airfoil along with an increase in lift on the aft part of the airfoil due to the separation would account for the large increase in nose-down moment.

The data of Jacobs¹⁶ can also be used to determine the effect of protuberance location on lift loss. Figure 5 shows the measured lift on the airfoil with the $k/c=0.0125$ protuberance at 5 different surface locations. For angles of attack in the 8 to 16 degree range the largest lift loss is due to the protuberance at the $x/c=0.05$ location on the upper surface. The lift with the protuberance at $x/c=0$ and 0.15 is higher at all angles in this range. With the protuberance at the leading edge, a very gentle stall is seen at a reduced angle from the clean case with a large reduction in maximum lift. The $x/c=0.15$ case behaves much like the $x/c=0.05$ case described earlier where around $\alpha = 6^\circ$ a large reduction in lift curve slope is observed. A protuberance on the lower surface had almost no effect on the airfoil lift. Wenzinger and Bowen¹⁷ tested round and flat spoilers on the upper surface of a 3-D wing in the Langley 19-foot wind tunnel. The effect on lift and drag was very similar to that seen by Jacobs. Wenzinger and Bowen concluded that the largest lift loss came from the spoiler placed on the upper surface between 5 and 20% chord. Therefore, for the large droplet ice accretion case, the observed upper surface ice

accretion locations of between 7 and 9% chord are in the most sensitive region on the airfoil for loss in lift due to a protuberance.

Figure 6 provides some information as to the effect of the shape of the cross-section of the protuberance on the lift loss¹⁶. Jacobs faired some of the protuberances using plaster-of-Paris to make them approximately 1/2 airfoil shape. The effect on the lift for the $k/c=0.005$ protuberance at $x/c=0.05$ on the upper surface is quite dramatic. Here the maximum lift is increased from 0.82 to 1.27 by fairing the protuberance as compared to the clean airfoil maximum lift of 1.52. The reduction in the drag coefficient is also dramatic. These data demonstrate that the shape of the protuberance has a significant effect on the resulting aerodynamic penalty. Again, similar results were reported by Wenzinger and Bowen¹⁷ showing flat spoilers more effective than round spoilers. Jacobs does not report the exact shape of the faired or original protuberance, but the large-droplet ice accretion will most likely fall some place between these two shapes. No data on the effect of a spanwise variation in the protuberance as might be expected on an ice accretion could be found in the literature.

The lift performance of the airfoil with the large protuberance at $x/c=0.05$ and 0.15 as seen in Fig. 6 is very similar to that seen on an airfoil which experiences thin airfoil stall^{18,19}. In thin airfoil stall, a separation bubble forms from the airfoil leading edge and grows in chordwise extent as the angle of attack is increased. When the bubble fails to reattach, or reaches the trailing edge, the airfoil stalls. In most sections a discontinuity can be seen in the lift versus angle of attack curve at the angle of attack where the bubble forms and begins to grow, Fig. 7. In some sections, the discontinuity can be so large due to the sudden and rapid growth of the bubble as to actually cause a local maximum in lift, followed by increased lift as α is increased further. This type of behavior is seen in Fig. 6 in the unfaired protuberance data. The $k/c=0.0125$ protuberance caused a discontinuity in the lift at $\alpha = 6^\circ$ when placed at $x/c=0.05$ or 0.15, Fig. 7. This is probably due to the thin airfoil-like behavior of the separation due to the protuberance. As the angle of attack reaches 6° , the separation bubble caused by the protuberance grows rapidly, causing the abrupt change in lift performance at this angle. Above this angle of attack, the bubble grows more slowly with angle of attack. This slow growth effectively decambers the airfoil reducing the lift curve slope.

The bubble reduces the suction peak pressure and increases the load on the aft airfoil resulting in the more negative, nose down, pitching moment which was measured, Fig. 4.

Thin airfoil stall behavior has been observed before on an airfoil with a simulated leading-edge ice accretion. Bragg et. al.^{20,21,22} tested simulated gaze ice accretions on a NACA 0012 airfoil. The airfoil experienced a large separation bubble aft of the upper surface horn which grew in chordwise extent as the angle of attack was increased, Fig. 8. At 6 degrees and above the flow was very unsteady and the bubble failed to reattach in a time averaged sense. This corresponds to the measured lift coefficient for the clean and iced airfoil shown in Fig. 9. The iced airfoil has a slightly reduced lift curve slope at low angles, but the most dramatic effect is the large break in the lift above 5 degrees. This is where the bubble grows rapidly and eventually failed to reattach to the surface. No measurements were taken above $\alpha = 9^\circ$ due to the large unsteady loads on the model. It is possible that the lift would have increased as α was further increased. This leading-edge ice accretion, simulating a conventional Appendix C cloud encounter, is indeed behaving much like the cases with a large protuberance near the leading edge measured by Jacobs¹⁶. It also has all the characteristics of a very severe thin airfoil stall. The pressure distribution confirms that this is a thin airfoil stall. In Fig. 10 the pressure distribution²⁰ for the clean airfoil is compared to the simulated ice case at three angles of attack. At $\alpha = 4^\circ$ the spike in C_p seen on the leading edge of the clean airfoil is replaced by a region of constant pressure. This constant pressure region is due to the separation bubble aft of the ice horn. As the angle of attack increases, the constant pressure region grows as the bubble grows in length. At $\alpha = 8^\circ$ the separation bubble fails to reattach and the character of the pressure distribution changes. Note the almost constant pressure region extends to $x/c = 0.40$ with only a small amount of pressure recovery occurring from this location to the trailing edge (i.e. the C_p at the trailing edge is much more negative indicating a lower pressure). The effect of this large change in trailing-edge pressure on an aileron will be discussed later. These pressure distributions are very similar to those on an airfoil with thin airfoil stall, such as in Fig. 9.

In this section the aerodynamics of an airfoil with a large-droplet ice accretion have been examined using prior studies on airfoils with

protuberances, thin airfoil stall and a large leading-edge ice accretion. Based on this analysis it is very likely that an airfoil with a large-droplet ice accretion behaves as shown in Fig. 11. The ice accretion causes a separation bubble to form aft of the ice accretion. At low angles of attack the effect is a reduction in lift curve slope and a small change in zero lift angle of attack. In some angle of attack range depending on the size and location of the ice accretion, the separation grows rapidly causing a large change in lift curve slope and maybe a local maximum in lift coefficient. Further increase in α sees the lift increase again, but at a much reduced lift curve slope. Similar aerodynamic effects were seen on an airfoil with a leading-edge ice accretion. There are not enough data at this time to compare the aerodynamic effects of leading-edge and large-droplet ice accretions. In fact, it maybe that for smaller ice accretion and ice roughness the stall mechanism may be enhanced trailing-edge stall and not the thin airfoil or leading-edge stall discussed above. However, based on Jacobs' work, it may be that ice accretions on the upper surface, back slightly from the leading edge produce larger aerodynamic penalties for the same ice accretion height.

Aerodynamic Hinge Moments

Perhaps the most dangerous effect of ice accretion on aircraft is the change in the pilot's ability to control the aircraft. Not only are the effectiveness of the controls crucial, but also the feedback the pilot receives through the hinge moments and ultimately the stick forces. In this section, the basics of control surface hinge moments will be reviewed, followed by a discussion of how ice accretion on the wing can affect the aileron control.

Background

Elevators, ailerons and the rudder are used to provide the pilot with a means to control of the aircraft in pitch, roll and yaw, respectively. These control surfaces are typically plain flaps mounted on the trailing-edge sections of the respective airfoils. A plain flap is simply some portion of the airfoil trailing-edge (typically .15c to .20c) that is hinged about a point within the contour. If no gap is present as a result of the hinge, deflecting the flap essentially changes the camber of the airfoil. For a given section angle of attack, a plain flap of 0.20c is capable of producing increments in sectional lift ranging up to about 1.0.²³ Deflection

of the flap also increases the $C_{l_{max}}$ of the section. When used as ailerons, the plain flaps on each side of the wing are deflected asymmetrically.

The pressure distribution over a control surface creates a moment about the control surface hinge referred to as a hinge moment. If the control surface is free to float, or move without restriction, it will rotate up or down depending upon the pressure distribution over the surface. For most cases, the low pressure created over the upper surface (suction side) of the wing will cause the control surface to want to rotate trailing edge up (toward the suction side).

For a given airfoil, there are two major variables which control the pressure distribution over the control surface. These are the angle of attack of the section and the deflection angle of the flap or control surface. Changes in both the angle of attack of the section and deflection angle of the control surface affect the pressure distribution over the entire airfoil and as a result change the magnitude of the hinge moment. The magnitude of the hinge moment for any combination of sectional angle of attack and control surface deflection angle can be developed from a linear summation of the effects of each. Typical pressure distributions for a section at zero degrees angle of attack, but with varying control surface deflection angles, along with pressure distributions resulting simply from changes in angle of attack are shown in Fig. 12. The suction created over the upper surface of the flap as the flap is deflected downward can be represented as the reaction R acting through the centroid of the pressure area and thereby creating the hinge moment about the hinge line. Stick force is usually considered positive when, in an unpowered system, it opposes an aerodynamically generated positive hinge moment. Stick forces and hinge moment are in reality much more complicated than presented here. Stick force trim, nonlinear effects, dynamic effects, etc. have been ignored here, but are covered in some detail in many books²⁴. In addition, aileron stick force results from the combination of the hinge moment produced by the right and left ailerons which are deflected in opposite directions to produce the desired rolling moment.

Effect of Ice on Hinge Moments

The effect of ice accretion on control effectiveness and control feel can be quite pronounced. These serious effects are the result of flow separation due to the presence of the ice

accretion. When the amount of flow separation is small, usually at low angle of attack or small ice accretions, the effect on aircraft control is also small. However, tests (see Figs. 4, 5, 6 and 9) show that the break in the lift curve, and therefore the onset of large regions of separated flow, begins at lower angles of attack with simulated ice on the airfoil. This early separation leads to a larger suction force on the top of the control surface and therefore a more negative hinge moment than would exist on the uniced airfoil. Compare the pressure distributions shown in Fig. 10 with and without simulated ice. The lift just ahead of the trailing edge is much larger on the iced airfoil due to the separation induced by the ice shape. As a result, there is a large increase in trailing-edge up (negative) hinge moment.

The effect of ice accretion and early flow separation on the horizontal tail was addressed by Ingelman-Sundberg and Trunov²⁵ and later by Trunov and Ingelman-Sundberg²⁶. Figure 13 shows lift and elevator hinge moment for a 3-D horizontal tail tested on a force balance in a wind tunnel. The tail was tested with a hinge moment balance on the elevator. Several different ice accretion simulations were tested as shown. Note that the airfoil leading edge tested was modified from its original shape to increase the leading-edge radius to simulate the NACA 0012 airfoil. The tail was tested at negative angles of attack simulating the download needed at low speed during landing. All the ice simulations tested, even the leading-edge roughness (S5) reduced the maximum lift coefficient significantly. The hinge moment becomes more positive as the iced tail plane stalls. Therefore, at an angle of attack after the iced tail stalls, but before the clean tail stall, the hinge moment is approximately twice as large. This corresponds to a trailing-edge down moment since the tail is at a negative angle of attack. Although the ice simulations are of conventional leading-edge ice, and not large-droplet ice accretions, this effect is similar to what would be expected for large-droplet ice as well.

Trunov and Ingelman-Sundberg²⁶ show the same relationship between the airfoil pressure distribution and control surface hinge moment as discussed earlier. In Fig. 14, taken from their report, the pressure distribution shows the results of an ice induced separation which is apparently of a thin airfoil or leading edge stall type. This can be determined noting the almost constant pressure on the forward lower surface of the airfoil. In this

case the suction side is the airfoil lower surface due to the negative angles of attack.

In Fig. 15 pressure distributions from three airfoils¹⁸ have been integrated to yield the aileron hinge moment for a 20% chord plain flap at zero degrees flap deflection. The NACA 63-018 airfoil has a gradual trailing-edge stall, while the NACA 64A006 and the double diamond airfoil (see also Fig. 7) both have thin airfoil stalls which are thought to be similar to that occurring on iced airfoils. Note that when the leading-edge separation bubble grows rapidly on the diamond airfoil at 6 degrees angle of attack, a large trailing-edge up hinge moment is generated. The trailing-edge stall airfoil which can be thought of as the uniced airfoil, has a much more gentle break in its C_h curve and at much higher angle of attack.

It should be clear now that when the flow about an airfoil begins to separate, the pressure distribution changes, which produces a large change in control surface hinge moment. This occurs whether an ice accretion is present on the airfoil or not. However, with the ice accretion present it will typically occur at lower angle of attack and at lower lift coefficient. The control surface may still be effective at this point, but the maximum lift of the surface is reduced and therefore the maximum force that can be generated by the entire surface is reduced. The change in hinge moment, and therefore control force in an unpowered control system is a even larger potential hazard for the safety of the flight.

Trunov and Ingelman-Sundberg²⁶ cover the effect of ice on the horizontal tail and its effect on elevator effectiveness and hinge moments. Therefore, here a brief analysis of the effect on the aileron will be presented in the context of a recent aircraft accident.

Iced wing roll upset

The digital flight data recorder trace²⁷ of the recent ATR accident which occurred near Roselawn Indiana provides a good example of the effect of ice on aileron control. Ten seconds prior to disengaging the autopilot the aircraft was flying with 15° flaps down, slightly nose down and in a 15° bank to the right. In the 7 seconds before autopilot disconnect, the flaps were retracted from 15° to 0° and as a result the aircraft angle of attack increased from around zero to over 5°. When the autopilot was disengaged, the aircraft ailerons deflected rapidly to over 10 degrees right aileron up, left down and the aircraft rolled to

approximately 70° right wing down. During the roll the aircraft pitched nose down and the angle of attack was reduced. The bank angle reduced momentarily, but as the angle of attack increased again the aircraft rolled further to the right and pitched down drastically. Control was lost and an accident occurred.

Based on the tanker flight tests¹⁴ it is likely that a spanwise ridge of ice existed on the aircraft wing at the 9% wing chord station ahead of the ailerons. At the warm temperatures thought to be present, it is very plausible that the ice accretion was asymmetric due to self shedding. Assume that the ice accretion was more severe on the right wing ahead of the ailerons. At low angle of attack before massive separation occurred on this wing, little change in aileron hinge moment or control effectiveness would result, Fig. 13. However, as the flaps were retracted and the angle of attack was increased, the flow began to separate on the iced right wing and the hinge moment became more trailing edge up on this wing. This resulted in a change in stick force required, and a force to the left being required to maintain the desired roll angle. However, this force was unknown to the pilot since the autopilot was on and supplied this control force.

The autopilot disconnected shortly after the wing flaps reached 0° and slightly before the wing angle of attack reached its maximum value of over 5°. The aileron deflected rapidly to the right (right aileron up and left down) at this time. If the pilot, for what ever reason, does not oppose the separation induced hinge moment with sufficient control force, the ailerons will deflect as described. This self induced roll is referred to as aileron snatch. The reduction in angle of attack which occurred shortly after the initial roll reduced the ice induced separation, reducing the right aileron up hinge moment, and allowing the roll to be temporarily reduced. However, when the angle of attack increased for the second time, the roll increased again due to the same affect on the aileron hinge moment.

So the likely aerodynamic explanation was a significant large-droplet ice accretion on the right wing which caused early flow separation as the angle of attack was increased. This resulted in a trailing-edge up hinge moment on the right wing and an aileron snatch when not accounted for when the autopilot disconnect occurred. The result was a rapid roll to the right and loss of control of the aircraft.

SUMMARY

Large droplet icing conditions can result in the formation of a ridge of ice aft of the upper surface boot. By comparing this ice shape to data acquired with a spanwise protuberance on a different airfoil it is clear that this can lead to large losses in lift, increases in drag and changes in the pitching moment. This effect is most likely due to the formation of a large separation bubble off the ice accretion which grows with angle of attack and eventually fails to reattach leading to premature airfoil stall. This is very similar to the flowfield observed on airfoils with thin airfoil stall and leading-edge ice accretions which have similar lift performance.

The upper surface bubble alters the entire pressure distribution about the airfoil. In particular, it greatly reduces the surface pressure on the upper surface of any trailing edge flap (aileron or elevator). For an airfoil at positive angle of attack this results in a more trailing edge up (negative) hinge moment and a change in stick force. In a severe case on a wing, this could lead to aileron hinge moment reversal and aileron snatch. In aileron snatch the hinge moments are altered to the extent that the aileron is pulled up by the low pressure on the top with sufficient force to induce a rapid roll if a large stick force is not immediately exerted to oppose it. It is possible that this could have occurred in the recent ATR accident.

It has been speculated that this problem may be peculiar to aircraft with "modern" airfoils and only occur with large-droplet ice accretions. However, there is evidence in the literature, some of it reviewed here, which shows that similar lateral control problems are possible with other types of ice accretions and on older designed airfoils. Also, horizontal tail stall control problems due to essentially the same aerodynamic phenomena are not limited to "modern airfoils".

There simply is not enough research to know if some airfoils behave in a significantly different way with ice than other airfoils. Most research on the aerodynamic effect of ice on airfoils has been on older sections. This problem is now being addressed by NASA and more information should be available in the future. What is clear is that all airfoils are in some degree susceptible to a loss in performance due to the accretion of ice and a change in control surface hinge moments and that

this should be considered in the design and operation of the aircraft.

ACKNOWLEDGMENTS

Several people have contributed by providing information and have helped educate me in the area of large-droplet ice and aircraft control. These include: Dr. Abdi Khodadoust and Dr. Mike Kerho, Mr. John Dow and Dr. Jim Riley of the FAA, Mr. Tom Ratvasky, Mr. Tom Bond and Dr. Mark Potopczuk of NASA Lewis, and Dr. Marcia Politovich of NCAR. Also thanks to Mr. Shawn Noe, Mr. Jonathan Reichhold and Mr. Chad Henze of the University of Illinois for their help with the figures.

REFERENCES

- ¹ Politovich et. al., "Meteorological Conditions Associated with the ATR-72 Aircraft Accident Near Roselawn, Indiana on 31 October 1994," *Proceedings of the International Icing Symposium '95*, Montreal, Canada, September 18-21, 1995, pp. 235-243.
- ² Cooper, W.A., Sand, W.R., Politovich, M.K., and Veal, D.L., "Effect of Icing on Performance of a Research Airplane," *Journal of Aircraft*, vol. 21, no. 9, September 1984, pp. 708-715.
- ³ Sand, W.R., Cooper, W.A., Politovich, M.K., and Veal, D.L., "Icing Conditions Encountered by a Research Aircraft," *Journal of Climate and Applied Meteorology*, vol. 23, no. 10, October 1984, pp. 1427-1439.
- ⁴ Politovich, M.K., "Response of Research Aircraft to Icing Conditions and Evaluation of Icing Severity Indices," accepted for publication in *Journal of Aircraft*, April 1995.
- ⁵ Politovich, M.K., "Aircraft Icing Caused by Large Supercooled Drops," *Journal of Applied Meteorology*, vol. 28, no. 9, September 1989, pp. 856-868.
- ⁶ Thoren, R.L., "Icing Flight Tests on the Lockheed P2V," ASME paper no. 48-SA-41, 1948.
- ⁷ "Report on the Accident to Fokker F27 Friendship G-BMAU 2 NM West of East Midlands Airport on

18 January 1987," The Department of Transport, Air Accidents Investigation Branch, Aircraft Accident Report 7/88, HMSO, London, England.

⁸ Dow Sr., John P., "Roll Upset in Severe Icing," Federal Aviation Administration - Aircraft Certification Service, September 1995.

⁹ Teymourazov, R. and Kofman, V., "The Effect of Ice Accretion on the Wing and Stabilizer on Aircraft Performance," Unpublished Report, Interstate Aviation Committee, Moscow, Russia.

¹⁰ Johnson, C.L., "Wing Loading, Icing and Associated Aspects of Modern Transport Design," *Journal of the Aeronautical Sciences*, vol. 8, no. 2, December 1940, pp. 43-54.

¹¹ Brumby, R.E., "The Effect of Wing Contamination on Essential Flight Characteristics", Douglas paper no. 8127, presented at the SAE Aircraft Ground De-Icing Conference, Denver, Set. 20-22, 1988.

¹² Bragg, M.B., "Aircraft Aerodynamic Effects Due to Large-Droplet Ice Accretions" AIAA Paper 96-0932, Jan. 1996.

¹³ Ashenden, R., Lindberg, W. and Marwitz, J., "Two-Dimensional NACA 23012 Airfoil Performance Degradation By Supercooled Cloud, Drizzle, and Rain Drop Icing", AIAA Paper 96-0870, Jan. 1996.

¹⁴ National Transportation Safety Board, "Icing Tanker Test Factual Report", Docket No: SA-512, Exhibit No: 13B, DCA95MA001, Washington D.C., Feb. 16, 1995.

¹⁵ Miller, D., Addy, H. and Ide, R., "A Study of Large Droplet Ice Accretions in the NASA Lewis IRT at Near Freezing Conditions", AIAA Paper 96-0934, Reno, NV, 1996.

¹⁶ Jacobs, E. N., "Airfoil Section Characteristics as Affected by Protuberances", NACA Report No. 446, 1932.

¹⁷ Wenzinger, C.J. and Bowen, J.D., "Tests of Round and Flat Spoilers on a Tapered Wing in the NACA 19-Foot Wind Tunnel", NACA TN 801, March 1941.

¹⁸ McCullough, G.B. and Gault, D.E., "Examples of Three Representative Types of Airfoil-Section Stall at Low Speeds", NACA TN 2502, Sept. 1951.

¹⁹ Hoerner, S.F. and Borst, H.V., "Fluid-Dynamic Lift", Hoerner Fluid Dynamics, 1975, pp. 4-2 to 4-6.

²⁰ Bragg, M.B. and Coirier, W.J., "Aerodynamic Measurements of an Airfoil with Simulated Glaze Ice" AIAA Paper 86-0484, Jan. 1986.

²¹ Bragg, M.B. and Spring, S.A., "An experimental Study of the Flow Field about an Airfoil with Glaze Ice", AIAA Paper 87-0100, Jan. 1987.

²² Bragg, M.B., Khodadoust, A., and Spring, S.A., "Measurements in a Leading-Edge Separation Bubble due to a Simulated Ice Accretion", *AIAA Journal*, Vol. 30, No. 6, June 1992, pp. 1462-1467.

²³ Abbot, I. H., and Von Doenhoff, A. E., *Theory Of Wing Sections*, Dover Publications, Inc., New York, 1959.

²⁴ Perkins, C. D., and Hage, R. E., *Airplane Performance Stability and Control*, John Wiley and Sons, New York, 1949.

²⁵ Ingelman-Sundberg, M. and Trunov, O.K., "Wind Tunnel Investigation of the Hazardous Tail Stall Due to Icing", Swedish Soviet Working Group on Scientific-Technical Cooperation in the Field of Flight Safety, Report No. JR-2, 1979.

²⁶ Trunov, O.K. and Ingelman-Sundberg, M., "On The Problem of Horizontal Tail Stall Due to Ice", Swedish Soviet Working Group on Scientific-Technical Cooperation in the Field of Flight Safety, Report No. JR-3, 1985.

²⁷ "Freezing Drizzle Towards a Better Knowledge and a Better Prediction", published by ATR, Avions de Transport Regional, 1 Allee Piere Nadot, 31712 Blagnac, Cedex, France, Nov. 15, 1995.

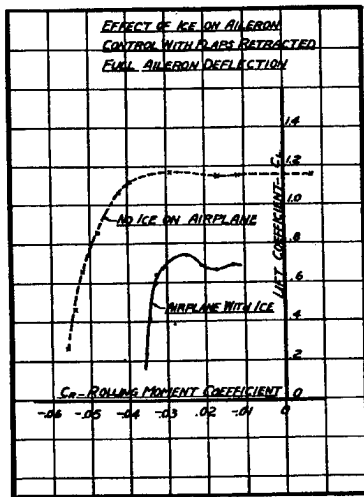
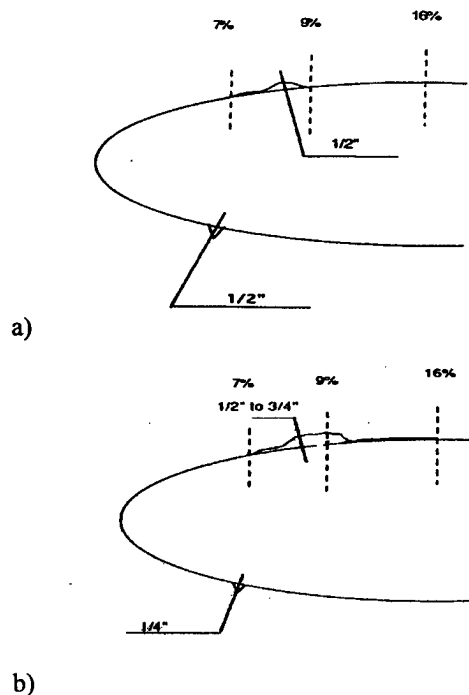


Figure 1. Effect of ice on aileron control¹⁰.



b)

Figure 2. Icing tanker large droplet ice accretion¹⁴. (180 KIAS, $T = -2^\circ\text{C}$, MVD = 140 microns, LWC = 0.3 g/m^3 , 17.5 minutes, with a) $\delta_f = 0^\circ$ and b) $\delta_f = 15^\circ$.)

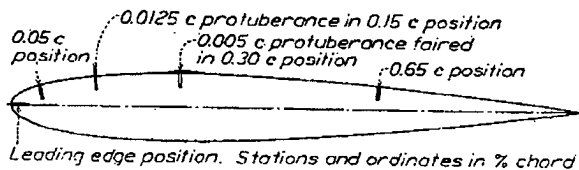


Figure 3. Airfoil and protuberance geometry¹⁶.

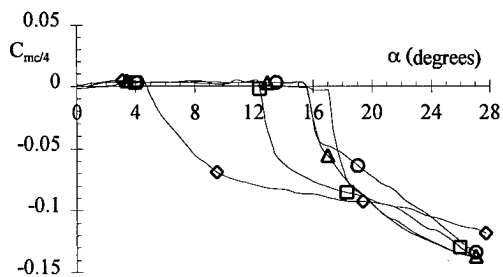
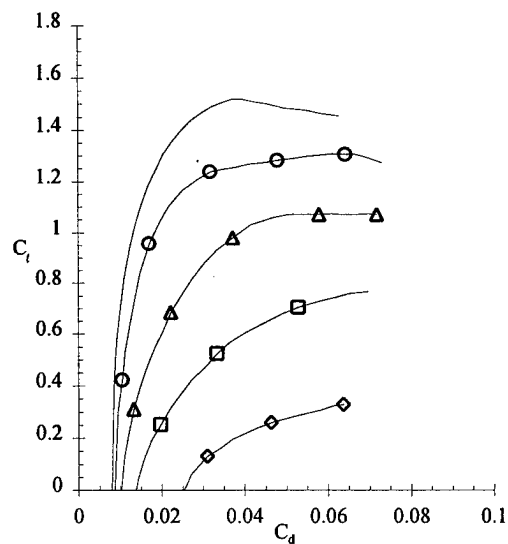
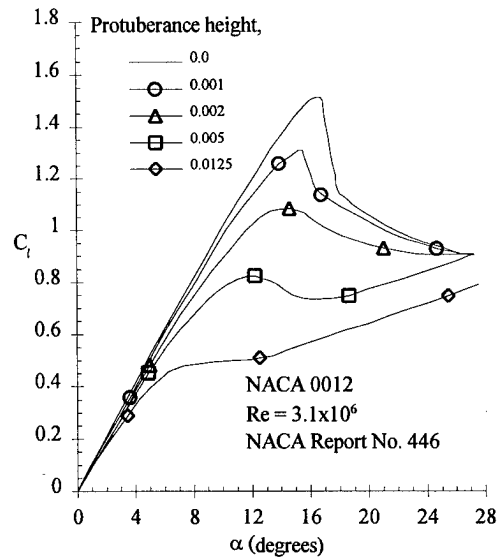


Figure 4. Airfoil performance with protuberance at $x/c=0.05$ on the upper surface¹⁶.

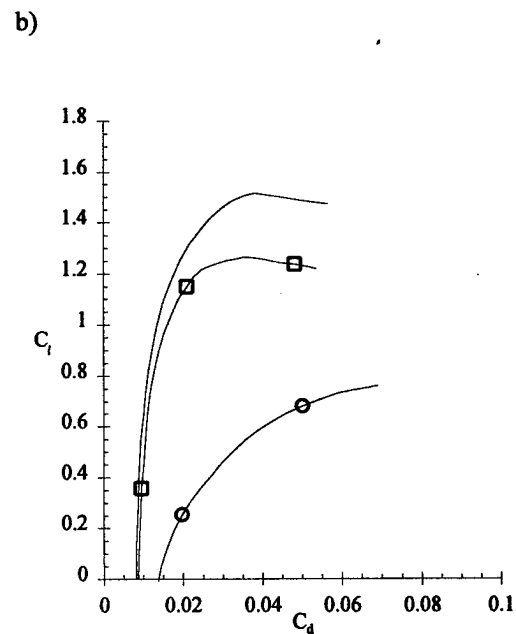
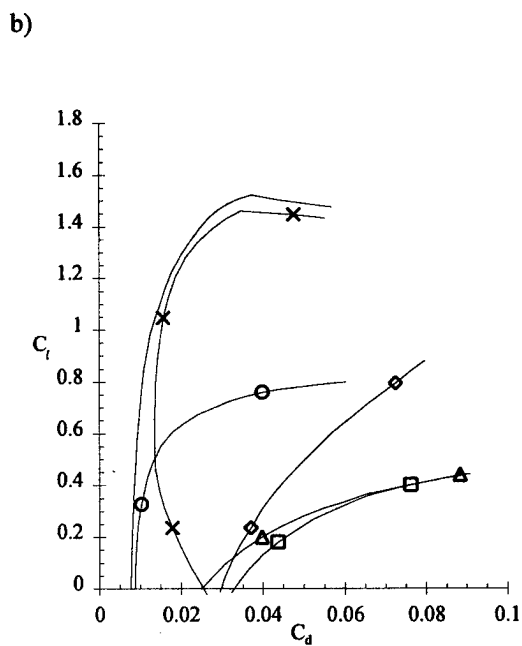
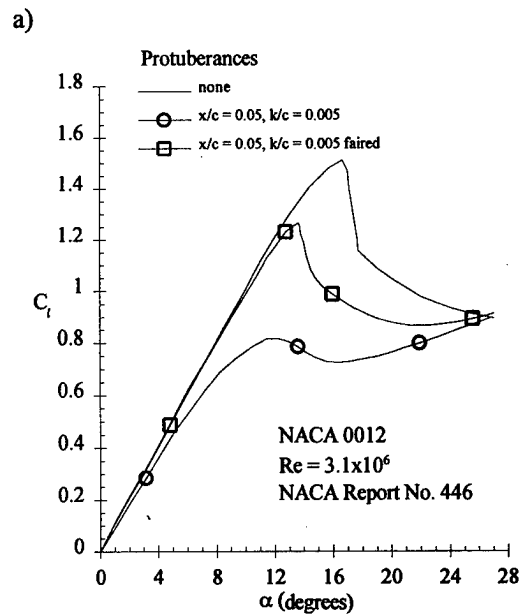
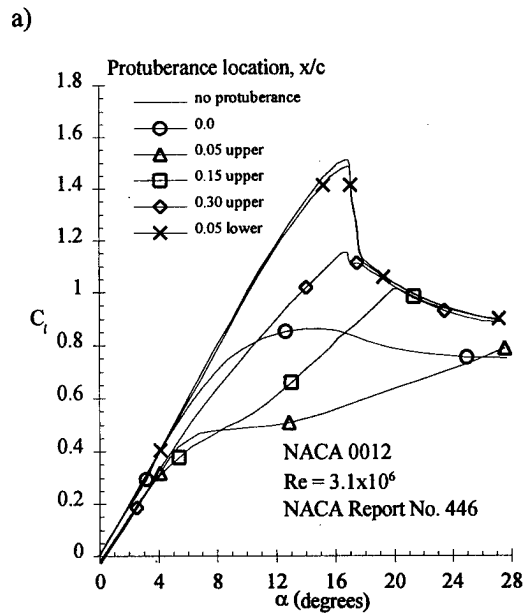


Figure 5. Airfoil performance with 0.0125c protuberance at 5 locations¹⁶.

Figure 6. Effect of fairing the 0.005c protuberance at $x/c=0.05$ ¹⁶.

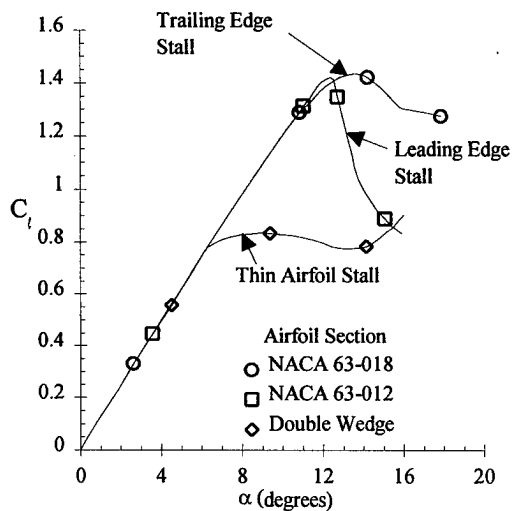
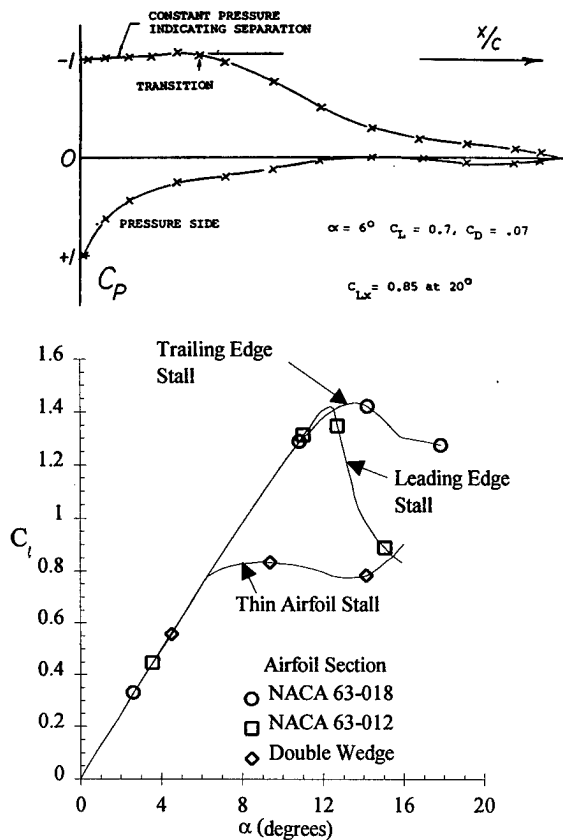
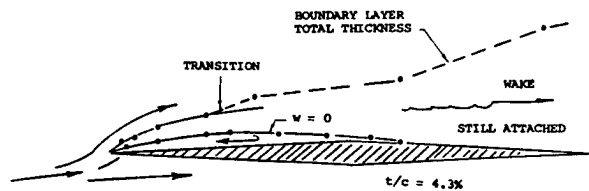


Figure 7. Thin airfoil stall^{18,19}. a) diamond airfoil flowfield at stall, b) diamond airfoil C_p at stall, and c) lift of diamond airfoil and other airfoils.

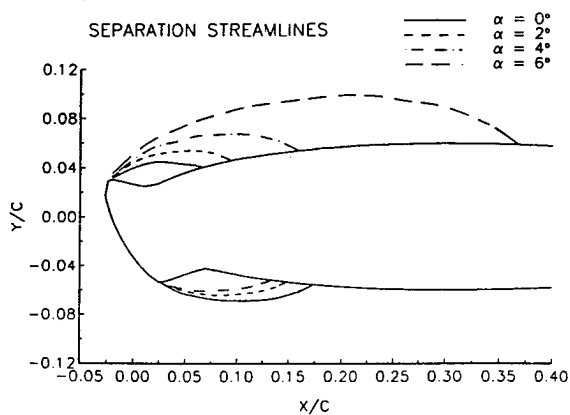


Figure 8. Separation bubble due to a leading-edge ice accretion²².

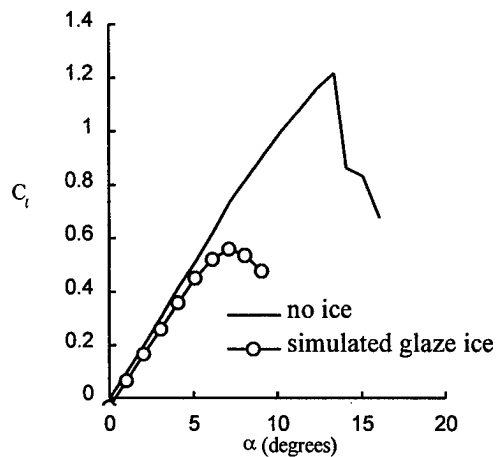


Figure 9. Lift performance of an airfoil with leading-edge ice²¹.

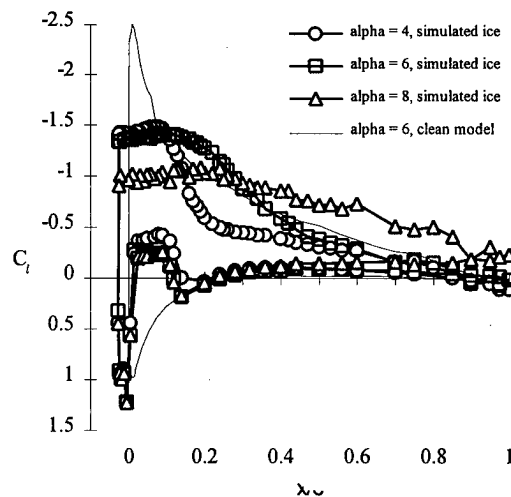


Figure 10. Pressure distribution on an airfoil with leading-edge ice²¹.

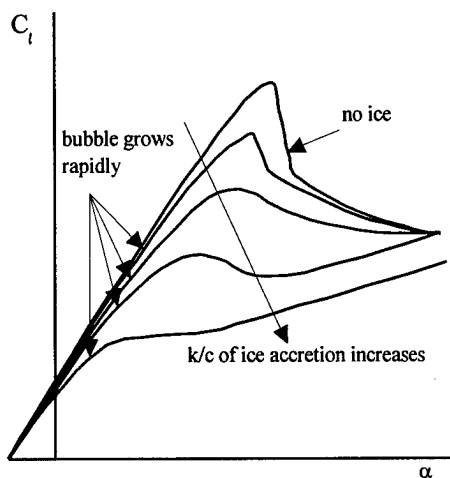


Figure 11. Possible flowfield and lift of an airfoil with a large-droplet ice accretion.

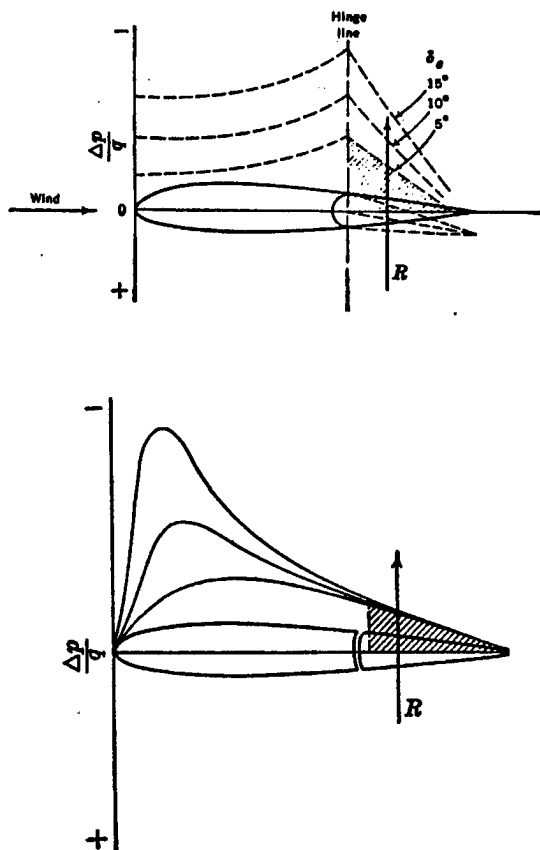


Figure 12. Pressure distribution for an airfoil with control surface deflected (above) and at three angles of attack (below).²⁴

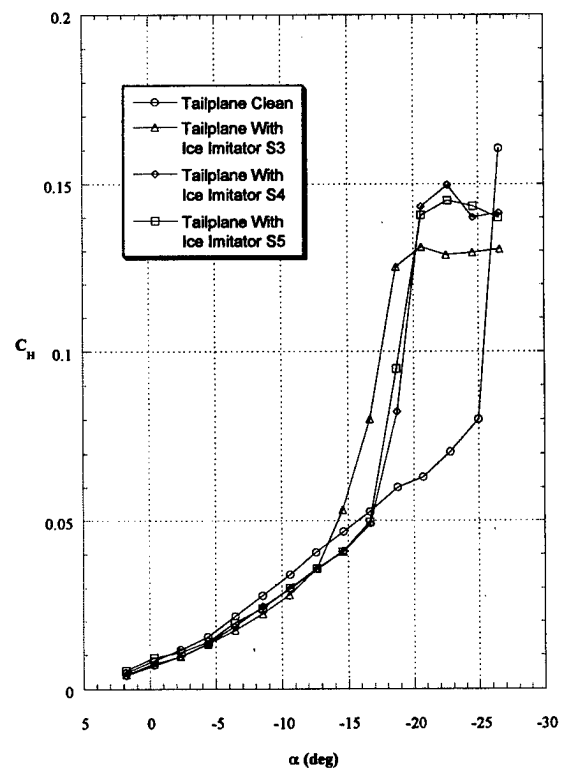
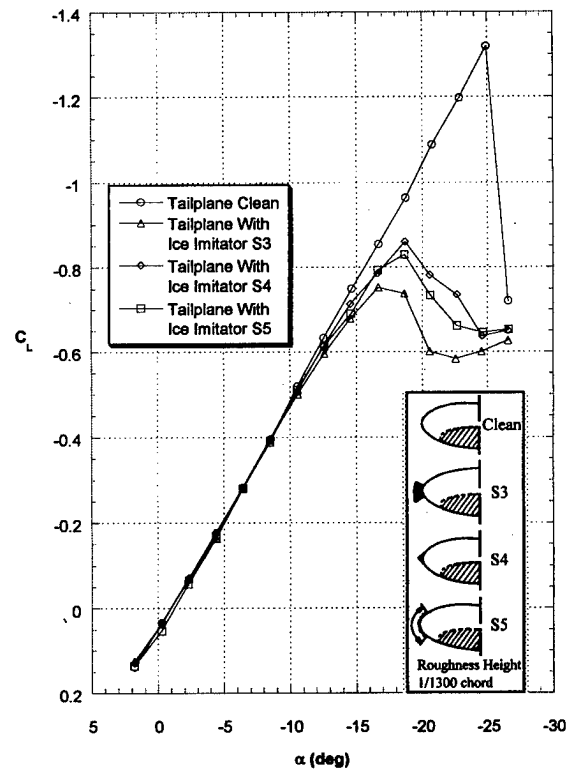


Fig 13. Effect of Icing on Horizontal Tail with Simulated Leading-Edge Thickness Addition²⁶.

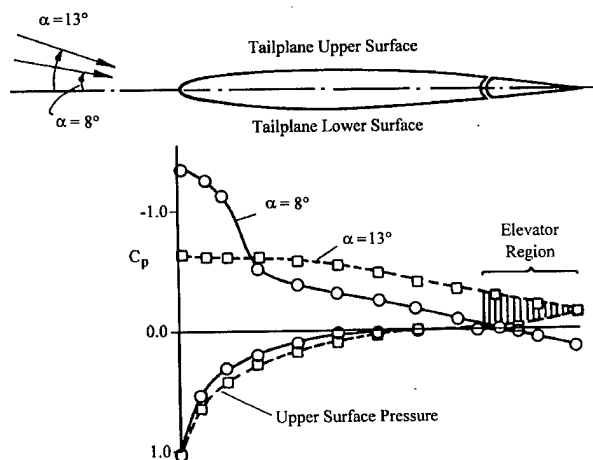


Fig. 14. Change in pressure distribution due to ice induced separation²⁶.

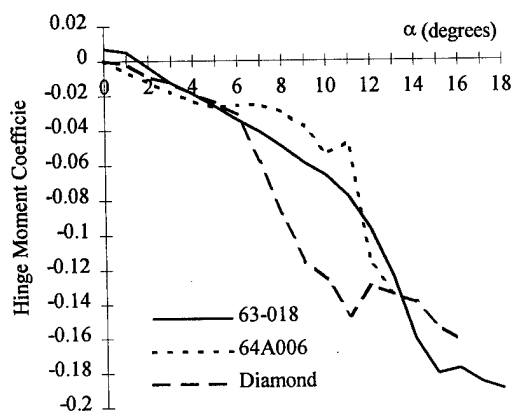


Figure 15. Hinge moments on airfoils with 20% chord plain flaps at $\delta_f=0$. (derived from data in ref. 18)

EFFECT OF ICING ON AERODYNAMIC CHARACTERISTICS OF AIRCRAFT WITH UNSWEPT WINGS AND ENSURING THEIR FLIGHT SAFETY

G.T. Andreev, S.Ya.Naumov, Yu.M.Rogozhkin, Yu.F.Shelyukhin

Ensuring flight safety is an urgent problem of modern aviation. It is well known that when flying in icing conditions the ice accretion formed on the leading edges of the lifting surfaces deteriorates substantially their aerodynamic characteristics. A considerable decrease in maximum lift coefficient and stall angle of attack as well as the degradation of stability and control characteristics take place, especially of the aircraft with unswept wings.

To provide a required flight safety level of aircraft under icing conditions, the effect of ice accretions of lifting surfaces on aircraft aerodynamic characteristics and the peculiarities of aircraft dynamic characteristics should be quantified early in the design process. This will enable developing in advance the requirements for anti-icing systems (AIS) and operational recommendations for automatic equipment incorporated into wheel control systems (WCS). For these problems to be solved, a complex of aerodynamic studies is carried out. Tests of large-scale models with ice-accretion simulators in the TsAGI's full-scale wind tunnel is a constituent of these studies.

Shapes and size of ice-accretion simulators were obtained in natural flight conditions on flying laboratories as well as in testing full-scale wing sections in the refrigerated wind tunnel with a water-atomization setup.

Presented in this paper are some results obtained in testing large-scale models with simulated ice accretion in the TsAGI's T-101 full-scale wind tunnel at Reynolds numbers of $Re=(4-8) \cdot 10^6$.

The shape and size effects of ice simulators attached to unswept wings on aircraft model aerodynamic characteristics are illustrated in Figs.1-3. From the plots shown it follows

that the "wedge like" ice accretion decreases the $C_{y_{\max}}$ by $\Delta \bar{C}_{y_a} \approx 14\%$ at flaps down. The stall angle of attack therewith decreases from $\alpha_{cr} \sim 17^\circ$ to $\alpha_{cr} \sim 14^\circ$. The "barrier-like" ice accretion formed with AIS operative has practically no effect on the values of C_{y_a} and $mz_a = f(\alpha)$, including post-stall angles of attack at flaps both retracted and extended. The "horn-like" ice accretion has the greatest effect on the maximum lift coefficient and critical angle of attack. For example, with 38-degree flaps the value of

$C_{y_{\max}}$ decreases by $\Delta \bar{C}_{y_a} \approx 22\%$ and the stall angle of attack decreases by $\Delta \alpha_{cr} \sim 6^\circ$. The ice roughness simulated with small balls 2-4 mm in diameter has only little effect on the negative increment of ΔC_{y_a} . Fig. 3 shows that both the shape and position of the ice simulator have the grater effect on maximum lift coefficient and stall angle of attack than the ice thickness. The ice simulator with the shape close to elliptic one and the thickness of 3.5% MAC decreases the $C_{y_{\max}}$ by the ΔC_{y_a} which is half as many as that of the "wedge-like" simulator with a height of only 0.5-0.6% MAC positioned on the wing upper surface at an angle of $\varphi_{is} \sim 13^\circ$ to the chord plane. The studies of various ice shapes accreted on unswept wings have shown that the ice formation has practically no substantial effect on pitching moment throughout the operational angle-of-attack range up to α_{cr} . The effect of ice geometry on the hinge moment of the overhang-balanced aileron

of the unswept wing is shown in Fig. 4. As noted above, the presence of the "barrier like" ice accretion has only slight impact on general aerodynamic characteristics of the aircraft model. But the ice formation of this type results in decreasing aileron hinge moment with angle of attack and aileron angle.

The effect of ice simulators, installed on individual model components, on model aerodynamic characteristics is shown in Fig. 5. The ice simulators installed on the wing and horizontal tail affect practically independently the model aerodynamic characteristics up to the stall angle of attack α_{cr} . The ice simulators installed only on the wing cause a decrease in $C_{y_{amax}}$ and, correspondingly, a decrease in stall angle of attack. The effect on pitching moment up to α_{cr} is insignificant.

Ice simulators installed on the horizontal tail affect only slightly the $C_{y_{amax}}$ value for the aircraft but have a significant impact on the nose-down pitching moment growth, especially at small and negative angles of attack. In this case, at these angles of attack as a small negative load factor is produced

($\Delta n_y \sim -0.2$), a sharp pitch-down aircraft motion ("peck") occurs, which is dangerous when flying at low altitudes.

For revealing the peculiarities of iced horizontal tail aerodynamic characteristics, some experiments were carried out on the isolated full-scale tail sections in the TsAGI's T-101 wind tunnel.

Fig. 6 illustrates the effect of the "barrier-like" and "horn-like" ice simulators on the lift coefficient and hinge moment of the elevator. Within the working range of negative angles of attack of the horizontal tail inherent in aircraft of conventional tail-aft configuration, the ice simulators decrease $C_{y_{amax}}$ and α_{cr} values. Over an angle-of-attack range of $\alpha = \pm 6^\circ$ the values of C_{y_a} and m_{he} are practically invariant, whereas at large negative angles of attack a strong decrease in C_{y_a} takes place. Thus, with the

elevator undeflected the $C_{y_{amax}}$ values decrease by $\Delta C_{y_a} \approx 36-46\%$. The stall angle of attack α_{cr} therewith changes from $\alpha_{cr} = -14^\circ$ to $\alpha_{cr} = -9^\circ$ and -7° respectively for the "barrier-like" and "horn-like" accretion shapes. The presence of the ice accretion leads to a sharp increase in the hinge moment coefficient of the elevator with an overhang compensation. Also, this increase in hinge moments of the iced elevator occurs at smaller angles of attack than those with no icing. To improve the run of the pitching moment curve $m_{z_a} = f(\alpha)$ over the region of negative and small positive angles of attack, the critical angle of attack α_{cr} of the horizontal tail should be increased, especially at flaps down. This makes it possible to delay the flow separation on the lower surface of the iced horizontal tail to greater α . For decreasing the effect of the ice accreted on the horizontal tail leading edge on its lifting capability and α_{cr} , the airfoil nose contours have been developed that enable increasing the α_{cr} by $\Delta \alpha_{cr} = 1-4^\circ$ depending of its modifications. The increase of the $C_{y_{amax}}$ and α_{cr} of the iced horizontal tail shifts the angle of attack at which the nose-down "peck" takes place to greater negative values. This increase in the improves the aircraft flight safety in icing conditions. By way of example Figs. 7 and 8 shows the curves $C_{y_a} = f(\alpha)$ for isolated horizontal tail and the curves $m_{z_a} = f(\alpha)$ for the aircraft model with initial and modified airfoil contours of the horizontal tail in the presence of the "horn-like" ice accretion.

In the TsAGI full-size tunnel, investigations were carried out into effects of propeller power plants on aerodynamic characteristics of large-scale aircraft models with unswept wings. The influence of propeller slipstream on the $C_{y_a}=f(\alpha)$ and $mz_a=f(\alpha)$ behavior with ice simulators only on the wing or only on the horizontal tail is shown in Figs. 9-10. "Horn-like" ice simulators on the wing with high-lift devices deflected ($\delta_f=38$ deg) and without propeller slipstream decrease $C_{y_{amax}}$ by $\Delta \overline{C}_{y_a} \approx 22\%$. With engines

operating, the relative values of \overline{C}_{y_a} somewhat decrease, however, α_{cr} in this case remains practically unchanged and equal to $\alpha_{cr} \sim 12$ deg. Ice simulators both in and without slipstream do not influence significantly longitudinal characteristics of the aircraft model. "Horn-like" ice simulators on the horizontal tail in the propeller slipstream greater influence the pitching moment than without slipstream, which degrades the longitudinal characteristics to a greater extent.

The results obtained through testing large-scale models with ice simulators in the TsAGI T-101 wind tunnel well agree with flight test results. Their comparison shows that the linear portions of the $C_y=f(\alpha)$ curves practically coincide, while for high angles of attack of $\alpha > \alpha_{cr}$ the C_{y_a} values obtained in flight tests are somewhat greater than those from wind-tunnel testing, which is attributed to greater Reynolds numbers in the flight tests (see Fig. 11).

Based on the abundant experimental data obtained by testing large scale models with ice simulators on lifting surfaces in the TsAGI wind tunnels and the large amounts of computations of aircraft flight dynamics under icing conditions in various flight regimes, including high incidence ones, a complex engineering methodology was developed. This methodology allows one already at early stages of aircraft design to:

- perform an assessment of the influence of ice accretion with various shapes and thicknesses on aircraft aerodynamic characteristics;
- carry out the mathematical simulation of the aircraft's flight dynamics under icing conditions;
- develop on the basis of computed aerodynamic characteristics recommendations for the rational installation of anti-icing systems, periodicity of their work, and, in some cases, recommendations for the expediency of the anti-icing systems' installation;
- draw out recommendations for the laws of automatic devices in the manual control system and for restrictions on the flight parameters and regimes for providing a necessary flight safety level.

Presented as an example in Figs. 12-13 are the results of computing aerodynamic characteristics of an aircraft with an unswept wing having on its nose ice accretions of various thickness under icing conditions in the cases of the anti-icing system operating and inoperating.

An assessment of the aircraft's aerodynamic characteristics with the selected and normally operating anti-icing system was carried out for the cases when the periodic anti-icing system works when the thickness of the ice on the leading edge become 6mm, which corresponds to turning on the mechanical anti-icing system on the wing. At that moment the ice accretion on the wing results in the decrease in $C_{y_{amax}}$ by

$\Delta \bar{C}_{y_a} \approx 10.5\%$. In this case the critical angle of attack α_{cr} decreases from 17-18 deg to 14-15 deg. The usage of the anti-icing system serving in turn various sections of the wing admits ice accretions of various thicknesses to form on these sections. An analysis of the results of the performed assessment has shown that for the normally operating anti-icing system on the wing the most unfavorable case is the ice accretion of 11 mm thickness on the wing's central sections. The presence of such ice on these sections results in the decrease in the maximum lift for the 50 deg flap deflection by $\Delta \bar{C}_{y_a} \approx 21\%$. In this case the degradation of the maximum lift is practically the same as in the case of a failure of the anti-icing system with the maximum ice layer on the wing ($h=16$ mm). Such icing ($h=16$ mm) decreases $C_{y_{amax}}$, for the flap deflected at 50 deg, by $\Delta \bar{C}_{y_a} \approx 23\%$. The critical angle of attack decreases in this case by $\Delta \alpha_{cr} \sim 6$ deg (see Fig. 13).

Additionally, computations of the aircraft's aerodynamic characteristics allows one at the early design stage not only to select an anti-icing system for providing flight safety but also to consider the problem of designing a stall warning system and automating the control.

As indicated above, for mechanical periodic anti-icing systems an important characteristic is their operating time schedule. It is basically determined by an admissible icing level, i.e. an admissible ice thickness, h_{on} . If the admissible level is set to be corresponding to losses of $0.1 C_{y_{amax}}$, using the relationship $C_{y_{amax}}=f(h)$ one can determine h_{on} and all remaining parameters of the anti-icing system and the stall warning system. In this case we have $V_{sw}=1.13 V_s(h=0)=1.07 V_s(h_{on})$, which meets the requirement of AII and FAR 25.207.

The minimum recommended velocity will be in this case equal to $1.23 V_s(h_{on})=1.3 V_s(h=0)$.

Turning on the anti-icing system is expedient to correspond to the condition $h > h_{on}$, when h_{on} is the acceptable ice thickness based on aerodynamic computations. Control automatization is determined by the behavior of the moment characteristic $mz_a=f(\alpha)$ for the specified ice thickness h_{on} and its choice can be made with traditional means (see Fig. 14).

Thus the methodology of the assessment of the aircraft's aerodynamic characteristics under flight icing conditions allows one still at the design stage not only to rationally select an anti-icing system, but also create a stall warning system and develop an automatization of the aircraft's manual control.

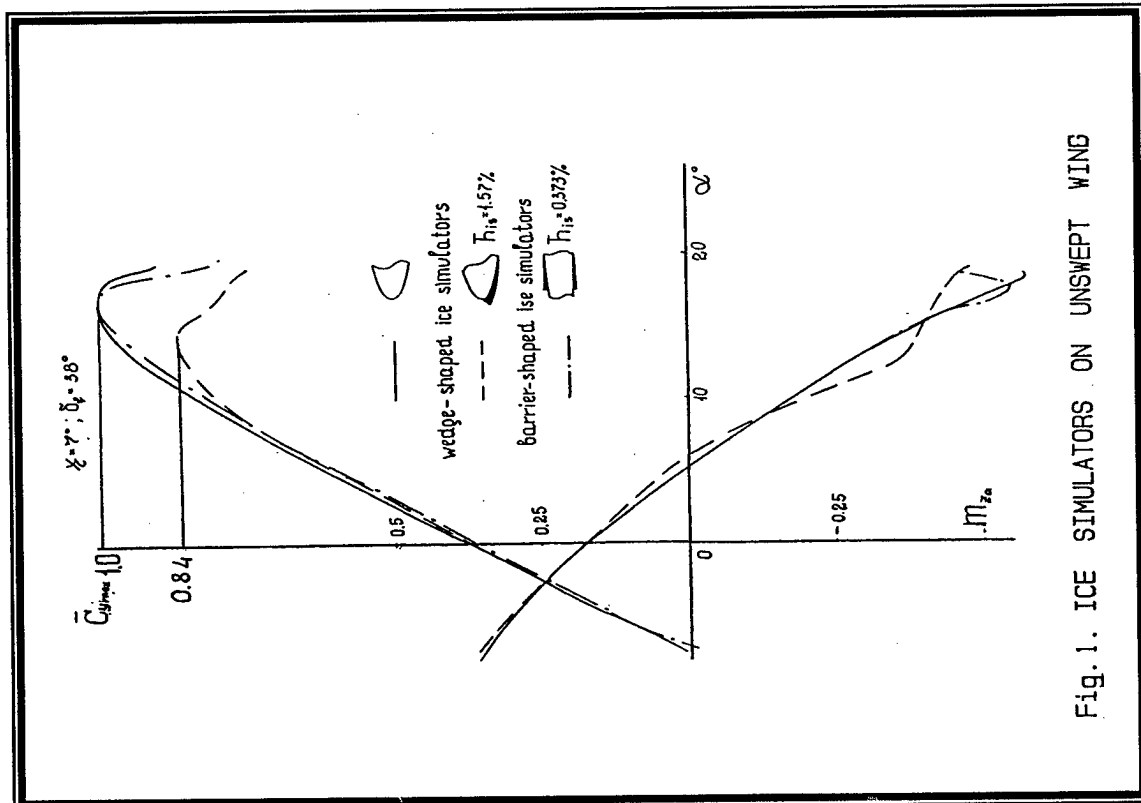


Fig. 1. ICE SIMULATORS ON UNSWEPT WING

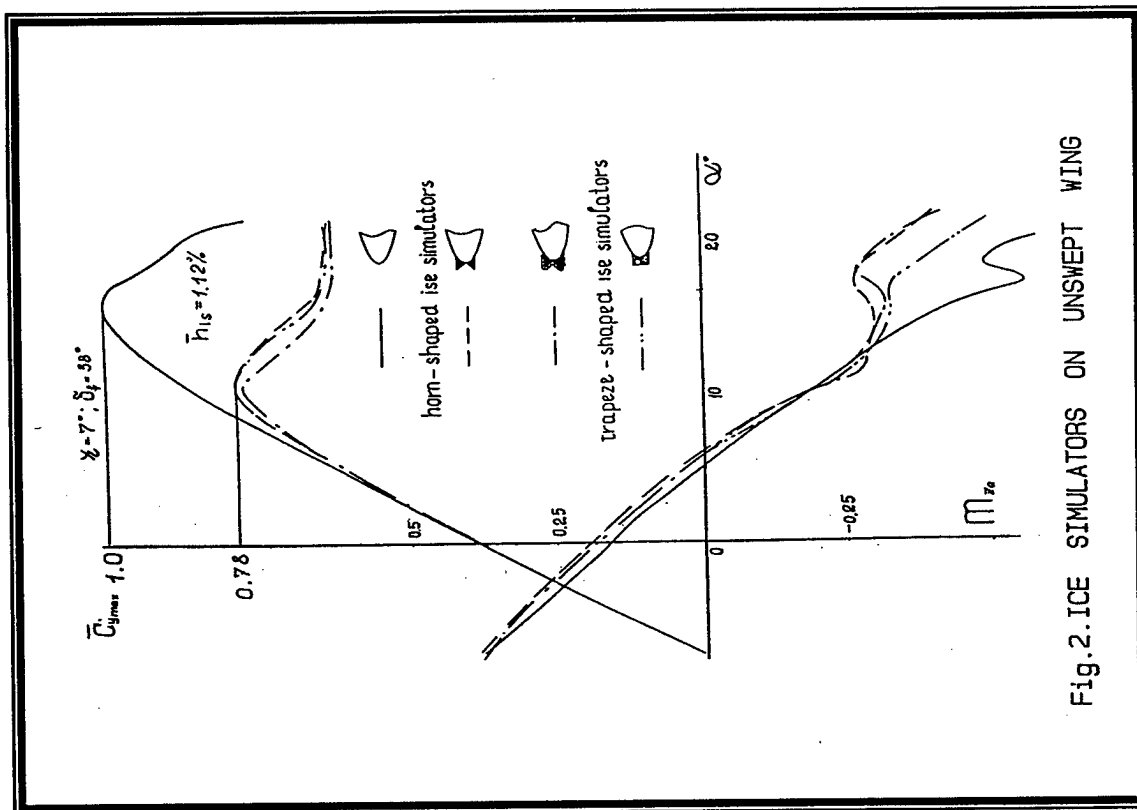


Fig. 2. ICE SIMULATORS ON UNSWEPT WING

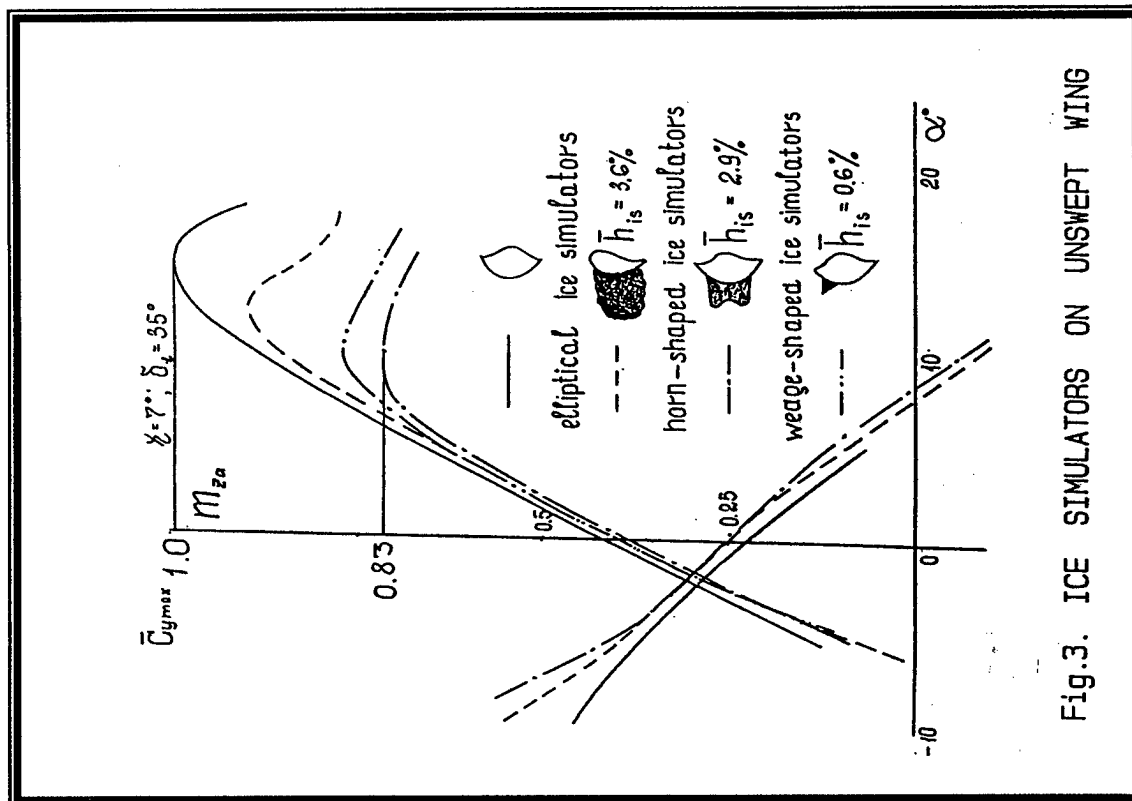


Fig.3. ICE SIMULATORS ON UNSWEPT WING

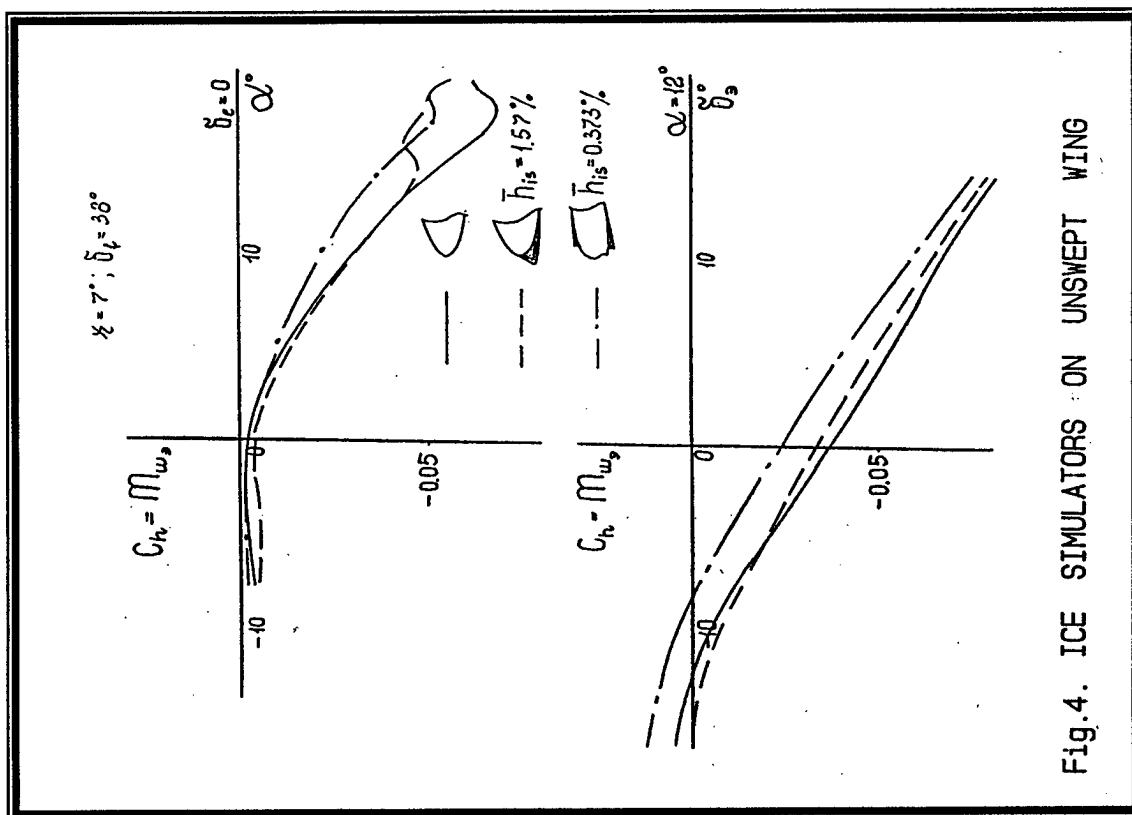


Fig.4. ICE SIMULATORS ON UNSWEPT WING

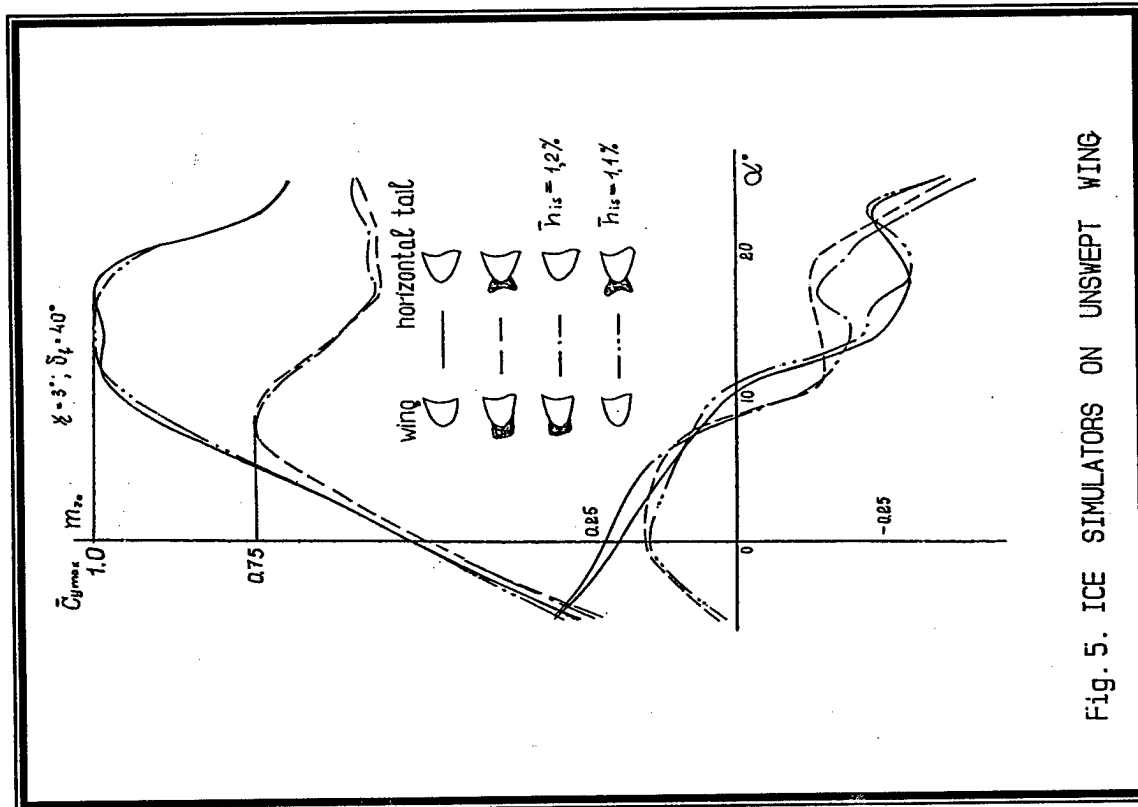


Fig. 5. ICE SIMULATORS ON UNSWEPT WING

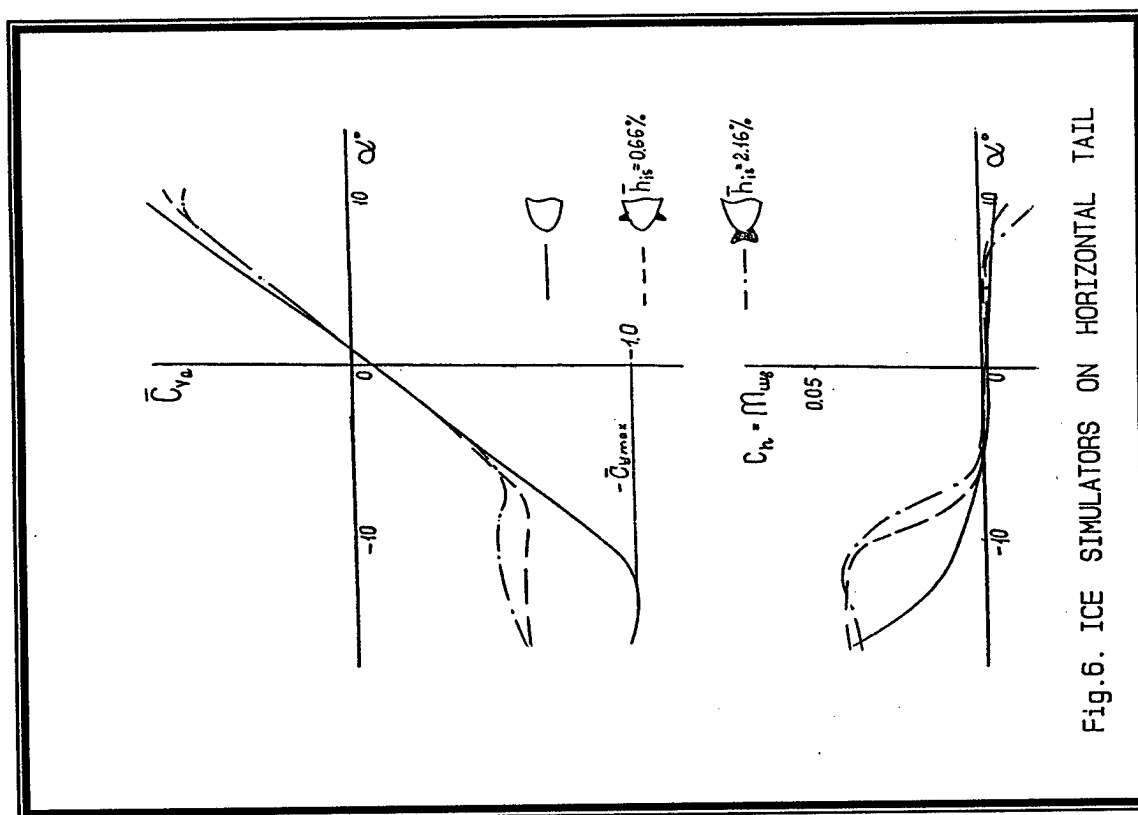


Fig. 6. ICE SIMULATORS ON HORIZONTAL TAIL

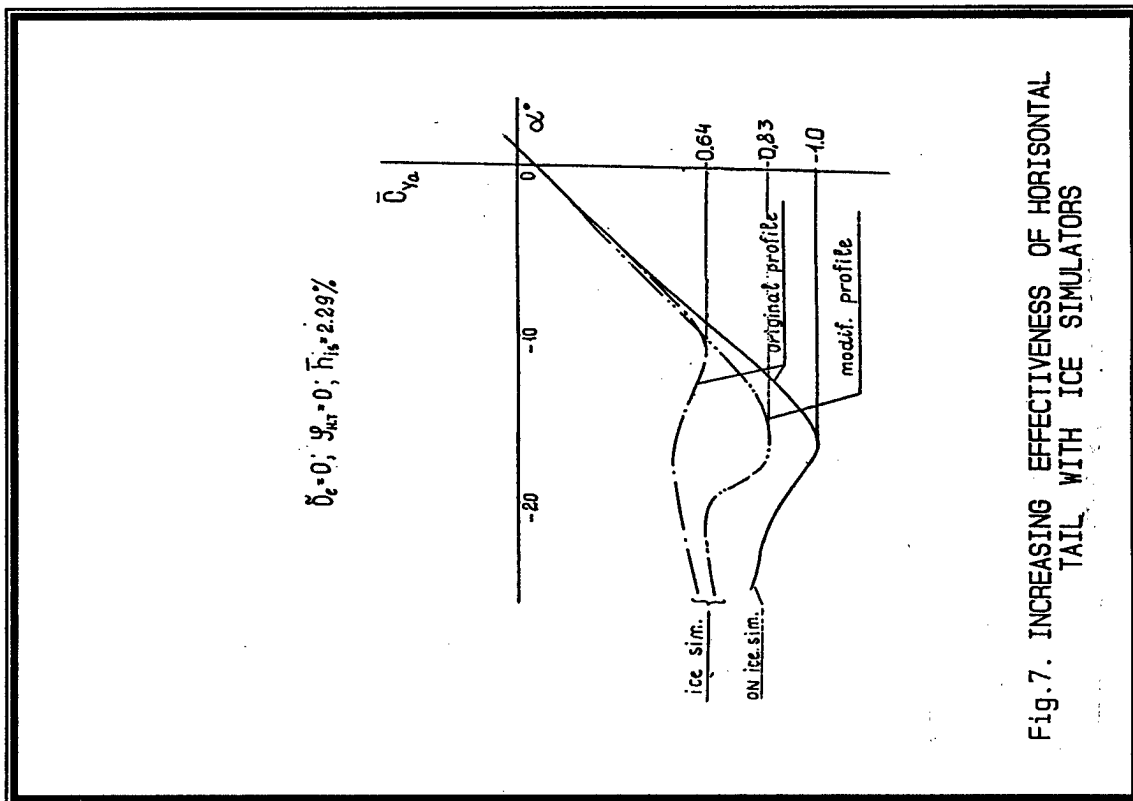


Fig. 7. INCREASING EFFECTIVENESS OF HORIZONTAL TAIL WITH ICE SIMULATORS

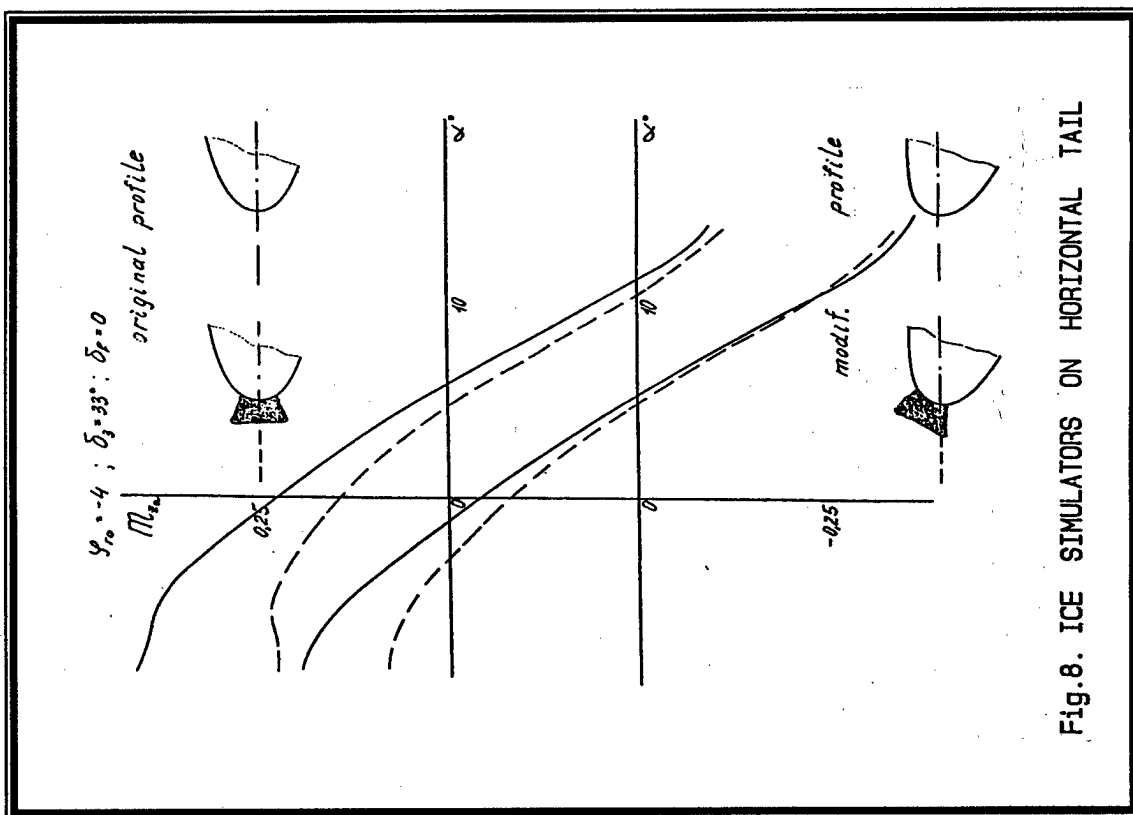


Fig. 8. ICE SIMULATORS ON HORIZONTAL TAIL

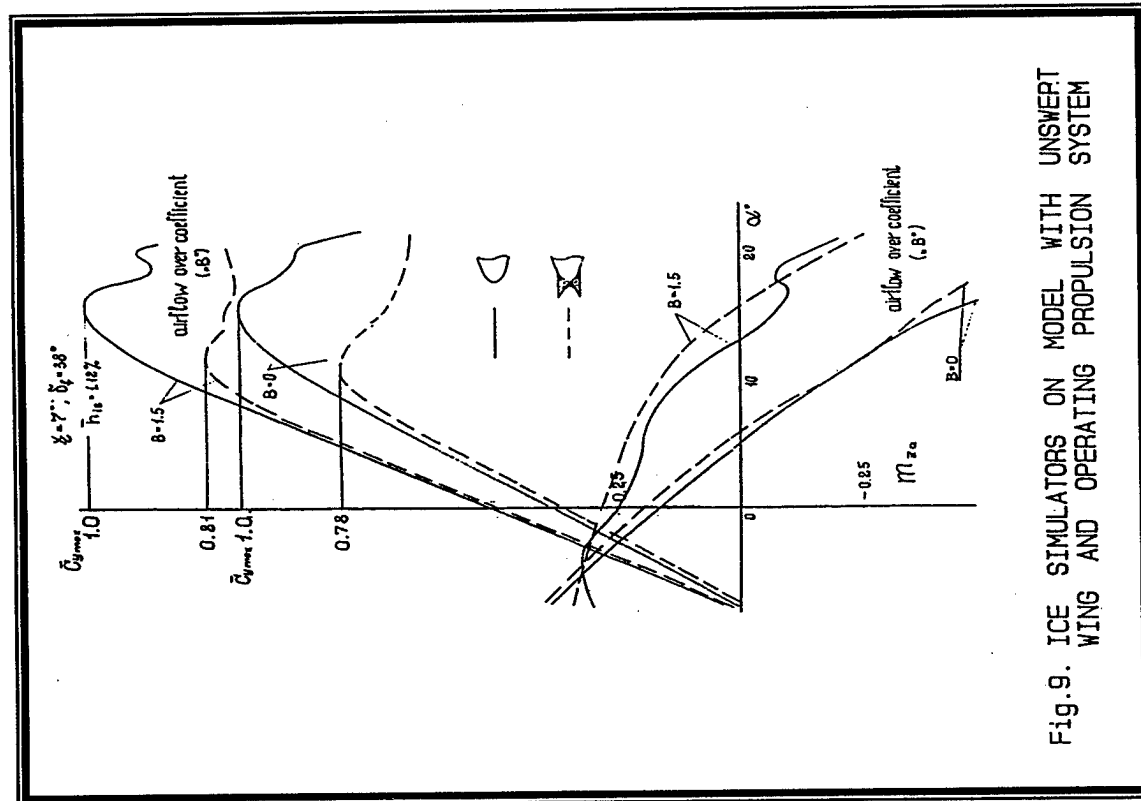


Fig. 9. ICE SIMULATORS ON MODEL WITH UNSWERT WING AND OPERATING PROPULSION SYSTEM

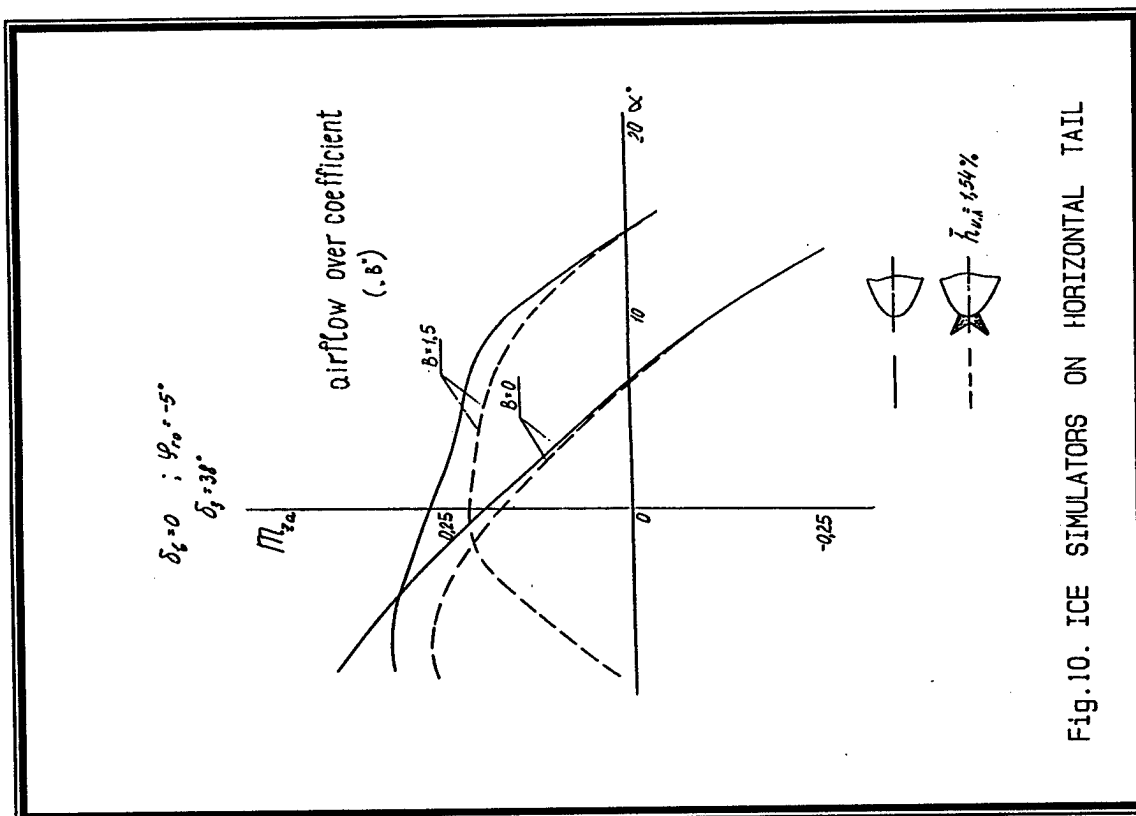


Fig. 10. ICE SIMULATORS ON HORIZONTAL TAIL

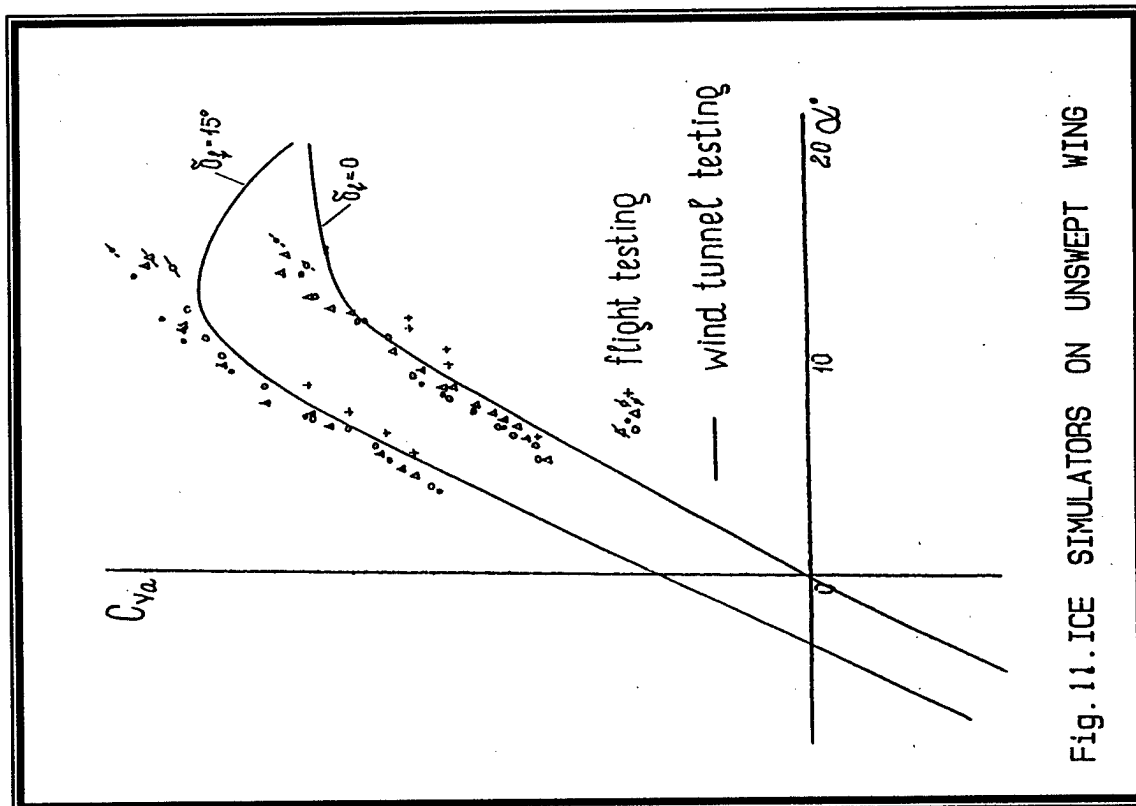


Fig. 11. ICE SIMULATORS ON UNSWEPT WING

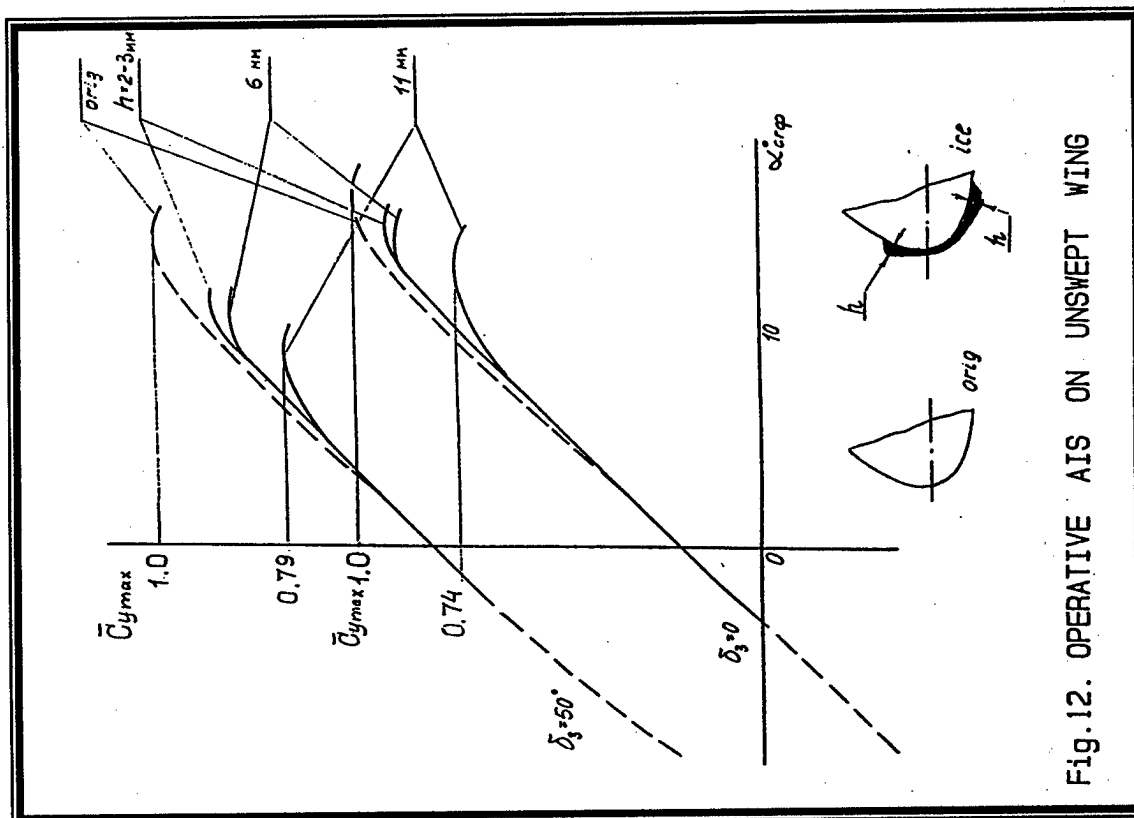


Fig. 12. OPERATIVE AIS ON UNSWEPT WING

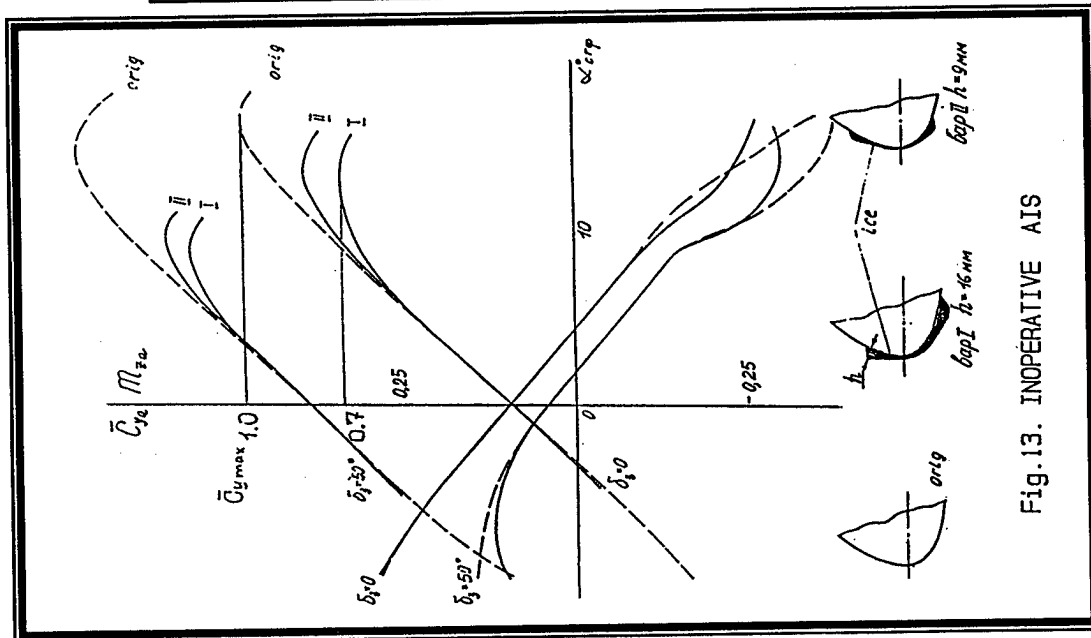


Fig.13. INOPERATIVE AIS

FLYCHT SAFETY IN ICING CONDITION

$$\alpha < 25^\circ$$

Requirements on anti-icing system

$$2. V_{sw} = 1.13V_s (h=0) = 1.07V_s (h_{on})$$

$$C_{L_{sw}}(h_{on}) = 0.78 C_{L_{max}}(h=0)$$

$$C_{L_{max}}(h_{on}) = 0.9 C_{L_{max}}(h=0)$$

determination of the anti-icing system cycle

$$V_{min} hf = 1.23 V_s (h_{on}) = 1.3V_s (h=0)$$

$$\Delta n_2(C_{L_{sw}}) \sim 0.32$$

$$1. V_{sw} > 1.07V_s (h=0) \quad V_{min} hf = 1.3V_s(0)$$

$$C_{L_{sw}} < 0.87C_{L_{max}} \quad C_{L_{min}} = 0.59C_{L_{max}}$$

$$\Delta n_2(\Delta C_{L_{sw}}) > 0.3 (0.47)$$

sw - stall warning, hf - horizontal flight

Fig-14

3. The Airplanes with FBW and Stall Protection Systems

$$V_{min} hf > 1.2V_s (h=0)$$

**JAA CERTIFICATION POLICY
NPA 25F-219 FLIGHT IN ICING CONDITIONS
ACCEPTABLE HANDLING CHARACTERISTICS AND PERFORMANCE
EFFECTS**

**Eric PARELON
Flight Test Engineer, JAA (DGAC-France)
Centre d'Essais en Vol, 13128 Istres Air, France**

ABSTRACT

The JAA Notice of Proposed Amendment NPA 25F-219 is the current Joint Aviation Authorities (JAA) certification policy (large aeroplanes) to deal with the flight characteristics in icing conditions.

This text has been used for some years for JAA and European national certifications and validations to JAR 25.

The intent of this paper is mainly to present the NPA and the current practices in certification activities.

It provides an history of the NPA development, a review of the contents of the NPA with associated certification practices, the limitations of the NPA, the major comments about the NPA made by subscribers, and recommendations for future to improve certification requirements about flight in icing conditions.

Moreover, this paper provides in attachment the text of the regulatory material introduced by the NPA 25F-219.

1 HISTORY

There was concern in the JAA Flight Study Group (FSG) in the mid-80s regarding incidents and accidents to turboprop aeroplanes in icing conditions, typically tailplane stall or stalling and control problems. This service experience has shown the need to provide guidance on flight testing for the investigation of flight characteristics (i.e. performance and handling qualities) in icing conditions.

The FSG agreed that such guidance is necessary and some preliminary papers were discussed.

It was recognized that little material existed addressing satisfactory standards for flight characteristics (performance and handling qualities) for operation in icing conditions for any class of large transport aeroplane. It was considered that JAR 25 Subpart B does not cover clearly the flight in icing conditions.

Flight in icing conditions is in fact currently covered by JAR and ACJ 25.1419. For the most part, this material addresses clearance of ice protection systems and does not give any guidance on acceptable standards of aeroplane handling characteristics and performance. There is, for example, no advice regarding flight characteristics in ACJ 25.1419 on the interpretation of JAR 25.1419(b) "The aeroplane must be able to safely operate in the continuous maximum and intermittent icing conditions determined under Appendix C....."

The FSG decided to provide interpretation to JAR 25.1419(b) for the flight characteristics aspects.

Starting with the special condition prepared by the French Authorities (DGAC) for type certification of turboprop aeroplanes, the FSG issued the NPA 25F-219.

This NPA proposes that an Advisory Material Joint (AMJ) to JAR 25.1419 covering flight characteristics in icing conditions be published in Section 3 of JAR 25 (see attachment). This AMJ would be complementary to the existing ACJ 25.1419.

The NPA 25F-219 is presently used as certification interim policy for large aeroplanes (TGM/25/02) by JAA. It should be used as guidance material for discussions between the Joint Certification Team and the Applicant.

2 NPA SPIRIT

This NPA provides acceptable means of compliance, recommendations, guidelines, and information for the demonstration of flight handling characteristics and performance effects for flight in icing conditions in accordance with JAR 25.1419(b). Other means of compliance may be acceptable.

The basic premises behind the NPA are:

- a/ No credit can be given for the probability of encountering icing conditions if certification for flight in icing conditions is sought, then icing conditions are considered a normal operating environment and the probability of encountering icing conditions must be assumed to be 1 for the purpose of certification.
- b/ The same criteria should be applied to turbojet and turboprop aeroplanes since they operate in the same atmosphere and are subject to the same physical laws.
- c/ Notwithstanding b/, there are clearly differences in the characteristics of aeroplane types, their operating characteristics and the effectiveness of ice protection systems that should be recognized and taken into account in the demonstration of compliance.
- d/ The workload is often higher in the icing environment.

It is the intention of this NPA that JAR 25, Subpart B should be used as a guide to define the appropriate flight conditions to be considered, but it is recognized that all the detailed flight requirements of Sub-Part B cannot be expected to be met in icing conditions. The NPA aims to highlight areas of flight characteristics likely to be critical for safety and to define a common standard for JAA certification.

3 NPA CONTENTS

3.1 General

The NPA could be presented as composed by the following aspects :

- Handling characteristics criteria
- Performance criteria
- Acceptable Means of Compliance
- Ice accretion to be considered
- Airplane Flight Manual

3.2 Handling characteristics criteria (NPA paragraph 4.2)

All flight phases should be addressed and the criteria exposed hereafter should be satisfied with the ice accretion expected for the flight phase concerned.

Note : Excepted when it is clearly specified, the test conditions used to demonstrate the compliance with criteria are elaborated on the bases of team certification engineering judgment. Generally the scope of the test is reduced compared to the Subpart B requirements and focused on operational speeds.

The criteria are the following :

- Adequate stability and control (longitudinal and lateral control capability, static longitudinal and lateral/directional stability, dynamic stability)
- A push stick-force required during push-over maneuver (up to 0g)

The push-over maneuver proposed in NPA paragraph 4.2.2.2 has been developed to reveal any potential for tailplane stall or significant elevator control non-linearity, either following a deliberate or inadvertent pitch-over or associated with the downwash changes following selection of flap in level flight. Longitudinal control problems have been experienced on several types at load factors just below 0.5g absolute and a demonstration of un-reversed stick forces at 0g assures adequate characteristics between 0.5 and 0g. There is evidence from many thousands of hours of flight recorder data which shows, typically, that 0.5g is reached once every 1000 hours due to atmospheric causes and once every 10,000 hours due to pilot induced causes. In addition, 0g is reached once every

100,000 hours from any cause, usually a transient atmospheric event. It is considered, therefore, that a push-over to 0g demonstrates an adequate level of safety.

- Ability to trim

- Acceptable stall characteristics

The stalling characteristics in slow, straight stalls should be investigated. It is considered that restricting stall testing to these types of stall is sufficient to show up any degradation of stalling behavior. Moreover the criteria of acceptability of Subpart B cannot be strictly applied

- Same required Stall warning margin than those required for the clean aeroplane (3kt/3% in case of VS1g "equivalent safety" in certification bases)

- Acceptable maneuvering capability

The demonstration of maneuvering capability in icing conditions contained in NPA paragraph 4.2.2.3 follows that of NPA 25B-215 "Stall and Stall Warning Speeds and Maneuver Capability". It is, however, only applicable to aeroplanes which demonstrate a significant increase in stall speed in icing conditions (defined as a 5% or 5 knots increase in VS1g).

- Free from excessive vibration or buffeting over a range of speeds adequate for normal operations.

3.3 Performance criteria (NPA paragraph. 4.3)

All flight phases should be addressed and the criteria exposed hereafter should be satisfied with the ice accretion expected for the flight phase concerned :

- the effect of ice accretion should be taken into account in performance computations when it is significant.

A significant effect on stall speed is interpreted as a 5% or 5 knot increase in VS1g (whichever is greater) and a significant effect on drag is interpreted as a 5% increase.

For this purpose the NPA requests :

- 1g stall speed determination
- Drag characteristics determination.

In the past, the take-off phase has not been addressed, it being assumed that the airframe is clear of ice at the commencement of the take-off. However, it is apparent that a finite quantity of ice can build-up in this phase of flight. In some case, depending on the sensitivity of the airfoil this accumulation could lead to significant degradation. The accumulation during this phase is not only dependent on ice protection system efficiency but also mainly on the procedures related to the activation of these systems (activation instant : brake release, lift-off, after take-off ?).

3.4 Acceptable Means of Compliance (NPA paragraph. 3)

The compliance may be shown by a combination of methods :

- Flight testing in natural ice
- Flight testing with validated artificial ice shapes
- Icing tunnel test data
- A read across of equivalent results from an earlier version, model or ancestor.

Such means of compliance as Wind tunnel with artificial ice shapes has already been accepted in certification.

Actually the NPA recommends to use Flight testing with artificial shapes in dry air because it is usually not feasible to carry out all handling and performance testing in natural icing. But a complete demonstration with only Flight testing in natural icing conditions could not be rejected.

However, in the case where Flight testing with artificial shapes is retained as basic means, a limited flight testing in natural icing is required for flight characteristics in addition to systems testing.

The objective of these test is :

- to consolidate the results obtained from flight testing with artificial shapes.

It is acceptable that the campaign be limited to general handling evaluation, stall warning/stalls demonstrations and push-over (non-powered flight controls) with limited ice accretions.

- to complete the validation of artificial ice shapes.

3.5 Ice accretion to be considered (NPA paragraph. 2)

The icing conditions of JAR 25 Appendix C, as interpreted by ACJ 25.1419, are to be considered. However, a particular type of ice accumulation is introduced (referred to as "sandpaper ice"). It has become clear that a thin, rough layer of ice has caused handling difficulties on several types of aeroplane.

The ice accumulation shape for performance shall be the one which has the most adverse effect on drag and lift. Similarly the ice accumulation shape for handling characteristics shall be the one which has the most adverse effect on lift and pitch moment. Nevertheless the ice shape having the most adverse effect on flight handling characteristics may be used for performance provided the drag difference can be easily or conservatively taken into account.

In addition, it has been established that the surface roughness of the ice accumulation has an appreciable effect. Guidance on the roughness to be used on artificial ice shapes is therefore offered.

This paragraph details the ice accumulations to be considered for protected parts following failure of the ice protection system. For the ice accumulation appropriate to a failed ice protection system, the NPA follows Transport Canada's AMA525/5-X in allowing half the ice accumulation appropriate to an unprotected surface in the same conditions.

In general, the ice shapes to be considered are those appropriate to the phase of flight. However, if the ice accretion defined by NPA paragraph 2.2 shows a significant increase in stall speed or drag for the take-off configuration, an ice shape which takes account of the duration of the exposure and so determines the performance for the take-off phase is defined in NPA paragraph 4.3.4.

3.6 Artificial ice shapes validation

The methodology for the approval of artificial shapes is not developed by the NPA.

The NPA requests only that the artificial ice shapes be established by a proven technique validated for the type of airfoil geometry used and for aerodynamic parameters such as speed and angle of attack appropriate to the subject aeroplane.

Actually, the certification practice is mainly based on engineering judgment of the authorities icing and flight test specialists.

Until now, the following means of validation have been accepted :

- Analytical predictions methods (computer codes, ...)
- Flight testing in measured natural icing conditions
- Flight testing in measured artificial icing conditions (tanker, ...)
- Icing wind tunnel

3.7 Artificial ice shapes currently used in certification

The artificial ice shapes currently used in certification with application of the NPA are the following :

- Holding / Cruise shape

Thickness : unprotected parts 3"

protected parts - amount depending on ice protection system and activation procedures (could be nothing)

Roughness : 3 mm height, 8-10/cm²

- Shapes representative of system failure cases which necessitate leaving icing conditions

Thickness : unprotected parts 3"

protected parts 1.5" or another value if substantiated

Roughness : 3 mm height, 8-10/cm²

- Take-off shape

Thickness : Ice accretion from brakes release to 400 ft. (generally used for turboprop aeroplanes fitted with de-icing boot)

Roughness : 1 mm height, 8-10/cm²

- Final take-off shape

Thickness : Ice accretion from brakes release to end of take-off path (generally used for turboprop aeroplanes fitted with de-icing boot)

Roughness : 1 mm height, 8-10/cm²

- Critical shape for push-over maneuver ("sand paper", ...)

Roughness : Carborundum paper n°40

Note : generally for a defined flight phase, the same ice shape is used for handling characteristics and for performance.

3.8 Flight Manual (NPA paragraph. 5)

This part indicates that all the appropriate limitations, performance information and procedures for flight in icing conditions, should be established and provided in the Aeroplane Flight Manual.

4 NPA LIMITATIONS

The certification experience in using the NPA has shown the following limitations :

- the present tools are not sufficient to determine the most adverse ice shapes regarding performance, neither regarding handling qualities.
- the NPA is based on Appendix C icing conditions and these conditions do not include such conditions as Supercooled Large Droplets (SLD) which may be insidious and very hazardous.

5 MAJOR COMMENTS ON NPA

During the official phase of consultation of the NPA in 1993, a great number of comments were received.

The major comments were the following :

- Support and Harmonization encouraged
- Rather rulemaking than guidance
- Criteria for handling qualities too vague to ensure consistent certifications

- Performance threshold (5 kt/5% VS1g) too large (proposal for 3kt/3%)
- Unnecessarily demanding for turbo-jets in particular for the take-off phase
- Stall warning margin criteria too severe
- Push-over maneuver not realistic

6 CONCLUSIONS AND RECOMMENDATIONS

During the last ten years European community (Authorities, Industry) has made a large effort to develop regulatory airworthiness material concerning Inflight Icing. The NPA 25F-219 is the result of this effort.

Pending the issue of a more harmonized text it represents at present the certification policy of JAA. In certification, it allows a global approach to the problem in developing discussions and links between systems specialists, aerodynamics specialists and flight test specialists.

JAA is presently working in the Flight Test Harmonization Working Group (Europe, United States, Canada) to continue the effort.

The NPA may be improved by working together with the participation of Authorities, Industry, Research organizations, Airlines and Unions.

In particular research activities about Icing environment characterization, Analytical prediction methods and Ice detection and protection systems represent essential issues for the work progress.

There is no doubt that this International Conference will provide a large positive input for the future work and for the Inflight Icing safety.

ATTACHMENT

NPA 25F-219 Issue 2

22 January 1992

PROPOSALS

Add AMJ 25.1419 in Section 3 of JAR 25

FLIGHT IN ICING CONDITIONS - ACCEPTABLE HANDLING CHARACTERISTICS AND PERFORMANCE EFFECTS

1. PURPOSE

This AMJ provides acceptable means of compliance, recommendations, guidelines, and information for the demonstration of flight handling characteristics and performance effects for flight in icing conditions in accordance with JAR 25.1419(b). Other means of compliance may be acceptable.

JAR 25.1419(b) requires that the aeroplane must be able to operate safely in the continuous maximum and intermittent maximum icing conditions determined under Appendix C. Consequently, the impact on aircraft flight characteristics and performance should be determined for flight in icing conditions.

It is the intention of this AMJ that JAR 25, Subpart B should be used as a guide to define the appropriate flight conditions to be considered.

This AMJ also deals with continued safe flight following a failure or malfunction of the ice protection equipment.

2 CONDITIONS TO BE CONSIDERED

2.1 Types of Artificial Ice

- a) Ambient atmospheric conditions are those defined in JAR 25 Appendix C.

- b) In addition to ACJ 25.1419 for the determination of different ice accumulation shapes, a degree of roughness should be agreed with the Authority as being representative of natural ice accretion.

In the absence of any other approved definition the following may be used:

- i) For small amounts of ice (for example the amount of ice built up during de-icing systems rest time) the roughness should not have characteristics less severe than :
- roughness height : 1 mm, and
 - particle density : 8 to 10/cm²
- ii) For large amounts of ice (for example on an unprotected, exposed surface) the roughness should not have characteristics less severe than:
- roughness height : 3 mm, and
 - particle density : 8 to 10/cm²
- c) Experience has shown that a thin, rough layer of ice can cause handling difficulties. For this "sand paper ice" the roughness should not have characteristics less severe than Carborundum Paper No. 40 (giving a roughness of about 300 microns).

2.2 Ice Accumulation

2.2.1 Unprotected parts

The ice buildup to be considered should be determined in accordance with JAR ACJ 25.1419, para 2.5.4 for unprotected parts. (typically 3 inches/75 mm).

"Unprotected parts" consist of the unprotected airfoil leading edges and all unprotected airframe parts on which ice accretion may develop. The effect of ice accumulation on normal protuberances such as antennae or flap hinge fairings need not be specifically investigated. However aeroplanes which are characterized by unusual unprotected airframe protuberances, e.g. fixed landing gear, large engine pylons or exposed control surface horns or winglets etc., may experience significant additional effects which should therefore be taken into consideration.

2.2.2 Protected Parts With Operative Ice Protection

The ice protection systems are normally assumed to be operative. However the applicant should consider the effect of ice accumulation on the protected surfaces which results from:

- the rest-time of a de-icing cycle or when runback ice occurs

Note: Performance may be established on the basis of the average drag increment over the de-icing cycle.

- a delay in the system activation (for handling characteristics only)

Note: In establishing the maximum icing exposure time prior to crew recognition and system activation, the nature of the detection means and the type of ice protection system should be taken into account. (For example visual cues or ice-warning system).

2.2.3 Protected parts following system failure.

A failure and safety analysis of the ice protection system should be carried out in accordance with JAR 25.1309. Some failures may necessitate leaving icing conditions.

A failure condition which does not require the aeroplane to leave icing conditions is a failure in which there is no further significant deterioration of the aeroplane performance or handling characteristics compared to that established with a fully operative system.

For failure conditions which require the aeroplane to leave icing conditions as soon as possible, it should be shown that the aeroplane is capable of safe continued flight and landing.

For this purpose the ice accumulation on normally protected parts where the ice protection has failed, should be taken as one half of the accumulation specified in para. 2.2.1 above for unprotected parts (i.e. typically 1.5 inches/35 mm) unless another value is substantiated.

The effect on the performance and handling characteristics, if noticeably greater than that established with the systems fully operative, should be stated as part of the Aircraft Flight Manual procedures following failures.

3. DEMONSTRATION OF COMPLIANCE

Compliance with AMJ 25.1419 should be shown by flight testing in natural icing conditions supplemented by a suitable combination of the following methods.

1. Flight testing using ice shapes.
2. Icing tunnel test data.
3. A read across of equivalent results from an earlier version, model or ancestor of the subject aircraft.

It is expected that no one method will provide sole evidence for compliance and any program methods and content must be agreed.

With the exception of the stall warning margin (paragraph 4.2.1(b)) the performance and handling tests required by this AMJ may be based on flight testing in dry air with artificial ice shapes, provided these ice shapes are validated in natural icing conditions with respect to location, general shape and, where possible, thickness.

The artificial ice shapes should be established by a proven technique validated for the type of aerosol geometry used and for aerodynamic parameters such as speed and angle of attack appropriate to the subject aeroplane (see ACJ 25.1419).

The ice accumulation shape for performance shall be the one which has the most adverse effect on drag and lift. Similarly the ice shape for handling characteristics shall be the one which has the most adverse effect on lift and pitching moment. Nevertheless the ice accumulation shape having the most adverse effect on flight handling characteristics may be used for performance provided the drag difference can be easily or conservatively taken into account.

4. FLIGHT TESTING

4.1 General

The certification program for flight in icing conditions should address all phases of flight, including take-off, climb, cruise, holding, descent, landing and go-around.

Power or thrust appropriate to a particular phase of flight should take into account any loss due to:

- bleed air or power extraction as needed for the proper functioning of the ice protection system operated in accordance with AFM procedures, and
- propeller efficiency.

Lift, drag and pitching moment changes due to the most critical ice accumulation shape on the unprotected and protected surfaces should be considered, together with any drag increment due to the ice protection system configuration, for example inflated de-icing boots.

4.2 Handling Flight Tests

4.2.1 Handling Tests With Natural Ice

- a) The objective of certification flight testing to assess handling characteristics in natural icing conditions may be limited to a qualitative assessment for comparison with the results from tests with artificial ice shapes. It is not, therefore, the intention of this AMJ that the handling characteristics be systematically checked through a series of controlled flight tests with natural accretion.
- b) There should be however a specific verification of the stall warning margin (see also par. 4.2.2.6) associated with natural ice shapes, to demonstrate satisfactorily the capability of the stall warning to prevent inadvertent stalling of the aeroplane when operating in icing conditions. This demonstration should be performed in a critical condition in terms of lift loss, that is:
 - with natural glaze ice,
 - with various quantities of ice on the unprotected surfaces (between 0 and 3 inches) and,
 - with a quantity of ice on the protected surfaces, if applicable, dependent on the ice protection system.

The ice accretion on protected parts need not exceed the quantity which is naturally left at the time of the demonstration by the normal functioning of the system.

- c) An investigation should be made to show that flight controls are free of jamming due to ice within the normal flight envelope.

4.2.2 Handling Tests with Artificial Ice Shapes

4.2.2.1 General

Adequate stability and control of the aeroplane with the most critical ice accretion pertinent to each flight phase and related configuration should be demonstrated. This includes longitudinal and lateral control capability, static longitudinal and lateral/directional stability and dynamic stability.

Normal procedures for configuration changes should be demonstrated to be safe.

4.2.2.2 Longitudinal Controllability and Maneuverability

4.2.2.2.1 Background

Elevator hinge moment becomes more sensitive to angle-of-attack as the tailplane stall is approached. This is particularly noticeable with elevators having significant aerodynamic balancing (leading edge and/or horn balance). In flight these effects become apparent by lightening stick pull forces in stall maneuvers and lightening stick push forces in nose down pitching maneuvers. Tailplane leading edge state can also have a significant effect on the available angle-of-attack range and frost and ice can also degrade the tailplane stall margins available. The loss-of-control, transient or sustained, due to flow separation at the tailplane can thus occur with both manually operated and irreversible powered controls.

Experience has shown that aeroplanes with non-powered elevators are most at risk from the phenomenon of large stick-force changes but it is considered that all aeroplanes should be assessed for controllability problems in this respect. For aeroplanes unlikely to be critical in certain icing conditions, it may be possible to show adequate longitudinal controllability by means other than flight test.

All parameters which have an influence on the phenomenon (e.g. aeroplane configuration, change of configuration, speed, weight, c.g., power setting and pitch rate) have to be considered. The maneuver specified in sub-paragraphs 4.2.2.2.2 and 4.2.2.2.3 takes these factors into account.

Longitudinal control problems have been encountered in service and it has been observed that a thin layer of rough ice on the tailplane can have a greater effect than horn ice. The applicant must, therefore, determine the critical icing accretion with regard to location, shape, thickness and texture.

4.2.2.2.2 Demonstration

A push stick-force must be required throughout the following maneuver.

With the aeroplane in trim, or as nearly as possible in trim, at the specified speed, perform a continuous maneuver to reach 0g load factor, or, if limited by elevator power so that 0g cannot be reached, the lowest load factor attainable.

4.2.2.2.3 Conditions

- a) Configuration : with wing flaps and landing gear in all normal positions other than the cruise configuration.
- b) Speeds : all speeds from $1.2 V_S$ or $V_{REF} - 5$ knots, appropriate to the configuration, up to V_{FE} but limited to the extent necessary to accomplish the maneuver and recovery without exceeding V_{FE} or V_{LE} , whichever is applicable.
- c) Power or thrust : from flight idle to maximum take-off power or thrust.
- d) Loading : most critical.
- e) Icing Condition : the applicant should specify the critical ice case(s) to be investigated. The ice case(s) should be defined in terms of location, shape, thickness and texture. The applicant should include allowance for any time delays in the activation of the ice protection system that may reasonably be expected in service. Ice accretion thickness greater than that resulting from application of Appendix C need not be considered.

4.2.2.3 Maneuvering Capability

This paragraph is only applicable to aeroplanes which exhibit a stall speed increment of more than 5 kt or 5% V_{S1G} , whichever is greater. (see 4.3.3.1, below).

There should be no reduction in the maneuvering capability to stall warning in icing conditions from that required of the "clean" aeroplane (see JAR 25.143(g) as introduced by NPA 25B-215).

4.2.2.4 Ability To Trim

The aeroplane should be able to maintain longitudinal, lateral and directional trim or to reduce the corresponding

remaining control forces to a level compatible with safe operation in icing conditions.

4.2.2.5 Stall Handling Characteristics

Any form of wing or aerodynamic surface ice "contamination" increases the stall speed, whilst reducing the stall angle of attack. This effect should be compensated for by either ensuring that the inherent aerodynamic qualities of the aeroplane for the case in question always give an adequate warning, or by providing a change in the artificial stall warning threshold as defined for the "clean" aeroplane.

It is recognized that criteria relevant to acceptable stall characteristics for the "clean" aeroplane cannot be strictly applied with ice accumulation on the airfoils due to the wide range of ice shapes and their subsequent effects on aerodynamic characteristics and stall. The stall warning should therefore, as a compensating factor, have a sufficient margin to prevent an inadvertent stall under any form of ice accretion. Only straight stalls with an entry rate not exceeding -1 kt/sec need be investigated. The action of the aeroplane after the stall should not be so violent or extreme as to make it difficult to effect a prompt recovery and to regain control of the aeroplane using normal piloting skills.

4.2.2.6 Stall Warning

There should be no reduction in the stall warning margin above the stall speed in icing conditions from that required for the "clean" aeroplane. The distinctiveness of the stall warning should be that required for the stall warning of the "clean" aeroplane (see JAR 25.207 as amended by NPA 25B-215).

4.2.2.7 Vibration and Buffeting

The aeroplane should be demonstrated free from excessive vibration or buffeting over a range of speeds adequate for normal operation.

4.3 Performance Flight Tests

4.3.1 General

Aircraft performance information for each flight phase should consider the most critical ice accretions on unprotected surfaces. In addition, consideration should be given to ice accretions accumulating during the rest time of cyclic de-icing systems and to the possibility of runback ice existing with some ice protection systems. Except as described in 4.3.4 for take-off, the performance data should be based on the most critical ice accretion and hence aerodynamic degradation that is expected to occur during a particular flight phase.

In consideration of the margins provided in performance requirements for expected variations of performance, the effect of ice accretion should be considered to be significant if it amounts to more than 5 kt or 5% (V_{S1G}) increase in stall speed, whichever is the greater, or more than 5% increase in drag, as applicable, in the particular flight phase.

4.3.2 Performance Tests with Natural Ice

Given the difficulty of obtaining accurate measurements of performance in a natural icing environment, the validation of performance data by flight tests in natural icing conditions may be limited to the verification that actual performance degradations observed under all encountered icing conditions do not exceed those predicted from the results of flight tests with artificial ice shapes in dry air.

4.3.3 Performance Tests with Artificial Ice Shapes

4.3.3.1 Stall Speeds

One-g stall speeds should be demonstrated in each configuration to be certificated for use in the take-off, en-route, approach and landing phases, with the ice accretion expected for the particular flight phase in accordance with paragraph 2.2.

If the ice accretion in any configuration used during take-off causes a significant increase in stall speed the additional conditions of para. 4.3.4 should be investigated.

4.3.3.2 Drag Characteristics

The drag characteristics in each configuration to be certificated for use in the take-off, en-route, approach and landing phases should be determined with the ice accretion expected for the particular flight phase in accordance with paragraph 2.2.

If the ice accretion in any configuration used during take-off causes a significant increase in drag, the additional conditions of para. 4.3.4 should be investigated.

4.3.4 Additional Performance Tests with Artificial Ice Shapes for Take-off Conditions

If the flight tests conducted with the ice accumulation specified in para. 2.2 show that in any configuration used during take-off the stall speed is increased by more than the greater of 5 kt or 5% V_{S1G} , or that the aeroplane drag is increased by more than 5%, adjustments to the AFM take-off data should be determined and scheduled in the AFM corresponding to:

- a) The increments of stall speed and drag determined in the flight tests conducted in accordance with paragraph 4.3.3, or
- b) At the option of the applicant, the effects on stall speed and drag characteristics determined in additional flight tests with the lesser amounts of ice accumulated during take-off in accordance with paragraphs 4.3.4.1 and 4.3.4.2 below.

4.3.4.1 Ice accumulation

The amount of ice accumulation should be determined by calculation, assuming;

- airfoils, control surfaces and, if applicable, propellers are free from adhering frost, snow or ice at the start of the take-off,

- maximum continuous intensity of atmospheric icing conditions exist throughout the take-off,
- critical ratio of thrust/power - to - weight,
- failure of the critical engine occurs at V_{EF} , and
- no flight crew action to activate the ice protection systems, other than in accordance with AFM procedures, is taken after commencing the take-off roll until the aeroplane achieves a height of 400 ft above the take-off surface.

4.3.4.2 Effect of ice accumulation on aerodynamic characteristics

The effect of ice accumulation on stall speeds and drag should be determined with the ice accumulation existing at the point where the landing gear is fully retracted, at the point where the aeroplane reaches 400 ft height above the take-off surface and at the end of the take-off path in accordance with JAR 25.111(a). At each point, the effect should be considered to be significant if it amounts to more than 5 kt or 5% V_{S1G} in stall speed, whichever is greater, or more than 5% increase in drag, as applicable.

4.3.4.3 Effect of ice accumulation on AFM take-off data

(a) Take-off speeds

If the stall speed in the take-off configuration at the point where the aeroplane achieves 400 ft height above the take-off surface is increased by more than 5 kt or 5% (V_{S1G}), whichever is greater, the minimum take-off safety speed V_{2MIN} should be increased as

necessary to maintain an adequate margin above the stall speed. If the stall speed in the en-route configuration at the end of the take-off path is increased by more than 5 kt or 5 % (V_{S1G}), whichever is greater, the flap retraction speed and the final take-off climb speed V_{FTO} should be increased as necessary to maintain adequate margins above the stall speed.

(b) Minimum distances required for take-off

The effect of any increase in operating speeds (V_R and V_2 , in accordance with (a) above) on the required take-off distance, take-off run and accelerate-stop distance should be determined and scheduled in the AFM. If the operating speeds are not increased, the effect of incremental drag due to ice accretion on these distances may normally be considered to be insignificant.

(c) Take-off flight path and related climb requirements

The effect of ice accretion on the take-off flight path and on the minimum gradients required by JAR 25.121(a), (b) and (c) should be scheduled in the AFM if the incremental drag exceeds 5% or if the operating speeds need to be increased due to an increase in the stall speed of more than 5 kt or 5% V_{S1G} , whichever is greater.

The computation of speed and drag should be based on the ice accretion existing at the following points:

The point where the landing gear is fully retracted, for showing compliance with JAR 25.121(a) and for the determination of the take-off flight path up to the point where the landing gear is fully retracted;

The point where the aeroplane reaches 400 ft height above the take-off surface, for showing compliance with JAR 25.121(b) and for determination of the take-off flight path from the point where the landing gear is fully retracted until the point where the aeroplane reaches a height of 400 ft above the take-off surface; and

The end of the take-off path in accordance with JAR 25.111(a), for showing compliance with JAR 25.121(c) and for determination of the take-off flight path from the point where the aeroplane reaches 400 ft until the end of the take-off path.

5. FLIGHT MANUAL

5.1 General

All the appropriate limitations, performance information and procedures for flight in icing conditions, should be established and provided in the Aeroplane Flight Manual.

5.2 Limitations

Where a specific limitation applies when operating in icing conditions, or observance of a limitation is necessary to ensure continued safe operation in icing conditions, these shall be stated in the AFM.

The AFM should state as a limitation, that an aeroplane should not initiate take-off when the airfoils, control surfaces or propellers are contaminated by frost, snow or ice.

5.3 Procedures

AFM procedures for flight in icing conditions should include both normal operation of the ice protection system and operation of the system taking into account protection system failures and aeroplane system failures.

5.4 Performance

Performance effects for all phases of flight should appear in the AFM. Where performance corrections are used, these should be expressed simply in AFM units and each affected AFM chart should be identified.

5.5 Regulatory Status of AFM Performance Information

AFM performance information produced in accordance with this AMJ should include the following statement:

This performance information has been prepared by the manufacturer and approved by the Authority to assist operators in developing suitable guidance, recommendations or instructions for use by their flight crews when operating in icing conditions.

A REVIEW OF CERTIFICATION FOR FLIGHT IN ICING CONDITIONS AND RECOMMENDATIONS FOR NECESSARY IMPROVEMENTS

Jim Bettcher, Steve Green, Steve
Erickson, Joe Bracken
USA Air Line Pilots Association
Inflight Icing Certification Project Team

ABSTRACT

Current requirements for icing certification are contained in FAR 25.1419 and Appendix C to FAR 25. However, there are no explicit standards for controllability or performance in icing conditions. The FAA Aircraft Icing Handbook and Advisory Circular 20-73 provide some guidance for controllability and performance testing. A European proposal, NPA 25F-219, would improve certification by requiring essentially unchanged controllability and performance in icing conditions, but it fails to address the significant problem of encounters with icing which is more severe than that considered in certification. In order to provide the same safety level that exists in non-icing conditions, essentially unchanged controllability and performance must be insured in Appendix C icing conditions, a specific test to prevent ice contaminated tailplane stall is necessary, and configuration changes in icing conditions must be addressed. Additionally, the tools to deal with inadvertent encounters with conditions that exceed Appendix C (e.g. freezing drizzle and rain) must be provided. Future certifications could employ an icing severity index to allow certification of an aircraft for icing which exceeds Appendix C standards.

INTRODUCTION

Icing conditions are routinely encountered by transport aircraft during at least part of each year in most parts of the world. For this reason, the goal of certification for flight in icing conditions is, and should be, to provide the same safety standard in icing conditions as in other instrument meteorological conditions. Unfortunately, a large number of incidents and accidents have occurred with aircraft whose pilots and certified icing systems were operating "normally" in icing conditions. While many icing problems have involved controllability problems in aircraft with pneumatic deicing boots and reversible flight controls, there are reports of problems with other aircraft in some icing conditions.

A review of certification regulations indicates an inconsistent and incomplete process to insure safety in this routine operating environment. If a consistent, high level of safety is to be maintained in the air transportation industry, aircraft must be certified to 1) insure unchanged handling qualities and performance margins for flight in routine icing conditions, and 2) provide a means of detection and recovery from unintentional flight in exceptional icing conditions.

CURRENT CERTIFICATION GUIDANCE

FAR 25, Section 1419, Ice Protection.

The only specific certification rule for in-flight icing protection of the airframe is located in the equipment subpart of Part 25 (reference 1). It provides criteria for

the certification of airframe ice protection equipment, and does not explicitly address aircraft performance or handling qualities. As such, the rule would appear to envision only immediate and complete removal of all ice by the certified system.

The rule requires that an icing system equipped airplane (icing equipment is optional) be able to "operate safely" within both the continuous and the intermittent maximum icing conditions of Appendix C of Part 25. In order to establish this safe operation, both analysis and flight test in natural atmospheric icing conditions are required. Provisions are also made for dry air or simulated icing tests "as found necessary".

FAR 25, Appendix C.

Appendix C is referenced in paragraph 1419. It specifies two icing environments to be considered for certification. The first is a continuous maximum environment that represents ice accumulation over a relatively long 17.4 nautical mile encounter. The second is an intermittent maximum environment, representing a short, 2.6 nautical mile encounter with a potentially more hazardous environment.

Both environments are defined by the variables of liquid water content, mean effective diameter of the cloud droplets, ambient air temperature, and altitude. However, the size of the droplets and the amount of water in the air are the primary variables of interest. The continuous maximum condition specifies water droplets sized from 15 to 40 microns in diameter, at water densities of 0.05 to 0.80 g/m³. The intermittent maximum condition specifies larger droplets, from 15 to 50

microns, and a significantly larger range of water densities, from 0.02 to 2.8 g/m³. In both conditions the larger droplets are associated with lower water contents.

It should be noted that while the largest droplet size specified by Appendix C is 50 microns, much larger icing droplet sizes are found in nature. The Aircraft Icing Handbook indicates that freezing drizzle droplets range from 200 to 500 microns in size and that freezing rain drops are larger, approximately 1,000 microns. (2:I 1-9)

Aircraft Icing Handbook.

This comprehensive, three volume engineering reference on aircraft icing (reference 2) is the responsibility of the FAA Technical Center in Atlantic City, NJ. It is in effect, the "bible" of ice protection design, analysis, test and certification. In conjunction with Advisory Circular 20-73, Aircraft Ice Protection, discussed below, it forms the detailed guidance available for FAR 25 icing certification.

While the effects of ice accumulations on controllability and performance of aircraft are discussed throughout the handbook, the lack of specific, detailed requirements, and the potential hazards are discussed in the "Evaluations to Demonstrate Adequacy" section as follows:

"No attempt will be made in this section to develop the equations and analysis techniques needed to evaluate ice formation effects on aircraft stability. It is an important area that requires more attention than can be given to the

subject at this time. Its importance is indicated by the icing accidents that occur when pilots are reducing speeds for approach and landing operations. Ice formations affect pitching moments and also the ability of the horizontal and vertical stabilizers to control aircraft attitude...Flight tests at these (*landing*) speeds become quite hazardous, and the effects on stability and control are mainly determined by analysis and by the judgment of experienced flight test pilots.”(2:V 3-5)

Analysis and judgment are not good replacements for explicit standards. When a test pilot detects an effect of ice formations, he then has to decide whether the effect is significant enough to insist that the aircraft be modified. Given the pressures on a company and the authorities during the time critical certification process, this situation should be expected to create an inconsistent standard for handling qualities in icing conditions. Additionally, the flight test hazards referenced in this paragraph are the same hazards that have been encountered in icing conditions in line operations. These hazards must be discovered and eliminated in certification before operational pilots, with cabins full of passengers, encounter them in line operations!

Advisory Circular 20-73, Aircraft Ice Protection.

This advisory circular (AC) was last updated 25 years ago(reference 3). It's stated purpose is "substantiation of ice protection systems on aircraft"(3:i). This purpose illustrates the FAR's overall approach of certifying icing systems for proper operation versus an approach of certifying an aircraft for flight in icing conditions. While the AC does call for dry air and natural icing condition flight tests, and it discusses determination of the effects of ice shapes on flight characteristics and performance, its orientation towards ice system performance leaves it without criteria for the acceptability of any degradations that are found.

Notice of Proposed Amendment 25F-219, Flight Characteristics in Icing Conditions.

This Notice of Proposed Amendment (NPA) was drafted by Europe's JAA Flight Study Group because "Service experience, particularly on turboprop aeroplanes, has shown the need to provide guidance on flight testing for the investigation of flight characteristics (i.e. performance and handling qualities) in icing conditions." (4:1) It was introduced to the Flight Test Harmonization Working Group (FTHWG), an FAA Aviation Rulemaking Advisory Committee (ARAC) working group of North American and European flight testing experts whose task is to harmonize FAA and JAA Part 25 certification requirements, at their October 18, 1994 meeting. Extensive effort has been expended to date on revisions to the NPA as the basis for accomplishment of the FTHWG's task to

“Recommend to the ARAC new or revised requirements and compliance methods related to airplane performance and handling characteristics in icing conditions.”

Joint Aviation Requirement (JAR) 25 differs from its FAR counterpart in paragraph 1419 where it states, “If certification for flight in icing conditions is desired ...”, whereas FAR 25 reads, “If certification with ice protection provisions is desired ...” The JAR certifies the aircraft for flight in icing, but the FAR certifies the icing system for proper operation. This difference, while subtle, is the basis of the NPA’s purpose acknowledging the requirement to safely operate in the Appendix C maximum icing conditions, and determining that, “Consequently, the impact on aircraft flight characteristics and performance should be determined for flight in icing conditions.” (4:1)

To accomplish this end the NPA:

- defines ice shape roughness and requires consideration of accumulations on protected and unprotected parts during normal and failure conditions
- accounts for ice accrued during takeoff and prior to ice system activation
- considers normal configuration changes and all phases of flight
- requires a specific test procedure to insure sufficient longitudinal control margin to prevent ice contaminated tailplane stall (ICTS)
- calls for adjustment of published speeds to maintain maneuver margins if stall

speeds change by the larger of 5 kt or 5% V_{SIG} and directs that stall warning margins not be less than those for the clean airplane

- directs adjustments to bring operational performance data back to clean aircraft requirements if drag increases by more than 5%
- specifies incorporation of “All the appropriate limitations, performance information and procedures for flight in icing conditions ...”(4:12) into operational flight manuals.

While these provisions hardly seem controversial or unreasonable, the FTHWG has yet to reach agreement on the final requirements. What is even more surprising is the fact that these provisions do not already exist, and that most aircraft at this time do not necessarily meet these requirements.

NPA 25F-219 has not yet been harmonized or officially adopted, but it has been applied by special condition to aircraft certified by the JAA for the last five years. Unfortunately, one of the aircraft certified under these more stringent requirements was involved in a fatal accident caused by flight in icing conditions on October 31, 1994 at Roselawn, Indiana. Preliminary accident investigation results indicate the aircraft was unintentionally and unknowingly operated in icing conditions that exceeded the maximum conditions specified in certification and referenced in the NPA (i.e. Part 25, Appendix C). Neither the NPA or the regulations account for the possibility of encountering conditions that exceed

Appendix C. This is their most significant shortcoming.

CERTIFICATION DEFICIENCIES AND NEAR TERM IMPROVEMENTS

The preceding discussion of certification guidance highlights the primary deficiencies in certification for safe flight in icing conditions. The facts of both icing accident and incident histories, and the ever increasing number of aircraft operations in world wide air transportation service, require certification improvements to produce and insure the same level of safety for all operations in instrument meteorological conditions. NPA 25F-219 contains some of these improvements. However, the regulations and advisory material must be further strengthened as follows, to fully accomplish the task for all aircraft.

Performance and Controllability in Nominal Icing Conditions.

The regulations must require essentially unchanged performance and controllability in the most frequently encountered icing conditions. If changes from clean wing characteristics are present in these "every day" icing conditions, the operating envelope and/or performance data must be adjusted to maintain clean wing margins. The maintenance of clean wing margins would provide the same safety level in icing conditions.

Two sections of Part 25, # 25.101 and 25.143, address general performance and handling qualities. Neither section excludes, or specifically includes, aircraft in icing conditions. A requirement that

these sections apply to airplanes operated in Appendix C icing conditions would insure equivalency. Without performance and controllability that is essentially unchanged in icing conditions, these operations will be, by definition, less safe. Unchanged operation and safety in icing is implied by current regulation and guidance, but without a specific requirement, it is not been insured in current certifications.

Performance reductions with normal system operation in icing conditions are particularly insidious. It is well known that even small amounts of ice, approximating sand paper in thickness and roughness, can cause significant drag and lift losses. Also, most FAR 25 performance margins exist to insure safe operation in failure conditions, often conditions of engine failure. Therefore lost performance due to icing would only be "critical" when an engine fails in icing conditions. Engine failures are infrequent; operation at performance limited weights in situations where a limit applies is a very small percentage of overall operations; and icing conditions are only a subset of total operations. Additionally, some aircraft may not have significant performance losses. Combine these small percentages and the lack of an extensive accident history involving icing performance degradations is understandable.

However, engine failure performance margins are small. They are the minimum necessary to provide a reasonable ability to safely recover the airplane in the case of a performance limited engine failure. To operate in icing conditions without this minimum performance margin greatly reduces the capability of a pilot to

safely land if an engine fails at the inopportune time. To not provide this minimum performance, as it is provided for all non-icing operations, is unacceptable. The practical cost in terms of reduced payload is small for the same reasons that the situation is infrequent. No pilot or passenger should ever be intentionally put in a situation where an engine failure will very likely result in a crash. Unfortunately today, because of the lack of this minimum performance requirement in icing, necessary performance is not guaranteed.

Tailplane Stall.

Current controllability requirements of Part 25 do not prevent ice contaminated tailplane stall. This is a known problem and NPA 25F-219 provides a specific test to insure such a stall will not occur. The NPA's provisions for tailplane stall should be adopted as requirements.

Configuration changes.

Icing accumulated in any configuration at one airspeed may have a dramatically different effect in a different configuration and at a different airspeed. Both a system failure condition, and residual ice in normal system operation, must be investigated. All configuration changes must be considered. Configuration changes that result in large controllability or performance changes must be prohibited, until and unless ice accumulations are eliminated by subsequent flight in non-icing conditions.

Exceedance Conditions. As previously mentioned, NPA 25F-219 does not address icing conditions that exceed Appendix C requirements. Such

conditions are well known in nature and are encountered in flight. Droplet sizes that exceed maximum Appendix C size are particularly troublesome since they can produce accumulations aft of areas protected by Appendix C icing systems. Fortunately these exceedance conditions are encountered less frequently than nominal Appendix C conditions. The Icing Handbook estimates an exceedance encounter at one time in every 1000 icing encounters.(2:V 1-3) This chance of exceedance may be accurate as an average, but certain weather patterns produce a much higher possibility of an exceedance encounter. Reported terminal conditions of freezing drizzle or freezing rain guarantee an exceedance encounter! Since exceedance conditions are by definition conditions outside the certification envelope, any effect of these conditions is not discovered through certification. However, these conditions are more severe, and we know that significant degradations are probable. An aircraft must not be operated in these conditions of unknown reduction in controllability and performance if safety is to be maintained. The previously mentioned accident at Roselawn, Indiana is a good example of this maxim.

Exceedance Detection.

Direct visual discrimination of differences in droplet sizes in flight is not possible, although visual observation of ice further aft than normal on aircraft surfaces may indicate larger droplet icing (reference 5). Liquid water contents that exceed certification standards result in larger accumulation rates, so visual detection may be easier. However, thinner airfoils are more efficient collectors of ice and the thinnest airfoils are generally on the

tail. Since the tail is not visible from most cockpits, the aircraft surface that will generally be the first to show excessive accumulation can not be visually monitored. Yet, some method to remain within the certification envelope clearly must be provided if certification safety is to be maintained.

It may be possible to provide an outside-the-cockpit visual reference for exceedance icing. While certification has to consider the human factors elements (delays, work load, etc.) of such a method, it could provide pilot knowledge of exceedance icing.

A better solution would involve installation of ice detectors to monitor ice accretion on critical unprotected surfaces aft of protected surfaces as a method to determine droplet size exceedance. Additional detectors might be required to detect accumulations on the most efficient, protected ice collection surfaces in order to determine excessive accumulation rates. Detectors to accomplish these tasks exist, however they are not widely used. Without certification credit for the quicker, more reliable response that can be expected to the warning provided by such detectors, they will not be widely used. Yet, they could clearly provide more timely and accurate pilot warning of exceedance conditions.

Both of these methods of exceedance detection require flying in conditions which are outside the certification envelope. The best solution for exceedance avoidance would be one that looks forward of the aircraft and warns of exceedance conditions before they are encountered. There is an obvious parallel

with wind shear and thunderstorm avoidance here. The technology for such predictive devices is under development. When it is available, true avoidance of exceedance conditions will be possible.

In any case, some means to detect exceedance conditions must be provided if the safety margins of the certification envelope are to be maintained.

Controllability in Exceedance Icing Conditions.

Some aircraft are known to have critical changes in controllability in exceedance conditions.(6:27) Yet, most aircraft have not been analyzed or tested at all in exceedance icing. Critical changes in controllability can occur with ice accumulations in a specific location on some aircraft. Thus, detection and perhaps elimination of ice in a critical location can be the key to recovery from an exceedance encounter. However, identification of a critical location or any analysis of exceedance icing is not currently required.

Although reliable modeling of such icing is difficult, a determined effort must be made in certification to provide adequate controllability to safely exit exceedance conditions, and to continue flight until the ice has shed or evaporated. When determining the size of an exceedance ice shape, a realistic time for escape from the conditions (based on the detection device and operational factors) must be used. Additionally, any necessary limits on maneuverability, and a maximum exposure time, must be passed to pilots via the airplane flight manual.

An encounter with exceedance icing is an emergency which can only be safely resolved if these steps are taken in certification.

AN IDEAL CERTIFICATION APPROACH

As mentioned earlier, current certification does not address operation in the full known icing environment. We also know that unchanged controllability and performance in all conditions is probably not practical, or even possible for many aircraft. Never-the-less, operational experience certainly indicates that some aircraft are able to handle more severe icing than others.

All aircraft are currently certified to the single standard of Part 25, Appendix C. A more ideal certification procedure would identify the capability of each aircraft, and then certify it for flight in the full environment in which unchanged controllability and performance could be provided. It is obvious that a minimum, nominal environment similar to the current Appendix C would have to be required so that an aircraft would have a reasonable chance of not encountering the emergency condition of exceedance icing on most flights into icing conditions. However, more capable aircraft might be able to takeoff and continue to operate in conditions that clearly exceed current certification criteria, such as freezing drizzle. Thus, more capability would be rewarded with fewer restrictions.

Any certification method needs to be related to the operational environment. The ideal certification approach would require both a parametric, icing severity

index to relate certification to the environment, and sensors to discriminate between severity levels. Such an index does not currently exist, but it has been proposed and studied. With such an index, an aircraft could be certified to the desired level of icing severity. A pilot and dispatcher would refer to icing forecasts and reports to determine safe dispatch of an aircraft. Pilots would report icing encounters in terms of severity level, and subsequent pilots would use forecasts, observations and any pilot reports to avoid conditions that exceeded the capabilities of their particular aircraft.

This certification method awaits only the development of a severity index, and the means to measure it's various levels. Revalidation of Appendix C or determination of a new "nominal" environment might be a byproduct of such an index's development. The recommendations made earlier in this paper would then be applied to the actual capability of the aircraft in relation to the levels of the icing severity index. Appendix C (or any future nominal icing environment) would then be used as a minimum standard, instead of functioning as the single pass/fail criteria as it does today.

CONCLUSION

Certification for flight in icing conditions today suffers from the lack of an explicit requirement for essentially unchanged controllability and performance in these conditions. Yet aircraft are flown in icing conditions with this expectation. Indeed, this controllability and performance standard must be insured if an unchanged level of safety is to be maintained in regularly encountered icing conditions.

An approved means to detect exceedance of the icing certification envelope must be provided to prevent extended exposure to conditions more severe than those investigated in certification. Furthermore, a limited investigation of exceedance effects must be conducted to insure safe escape from those conditions. An ideal change in the approach to certification would replace certification to Appendix C with certification to the level of an icing index that reflects the actual capability of the individual aircraft.

REFERENCES

1. Airworthiness Standards: Transport Category Airplanes, Federal Aviation Regulations, FAR Part 25, Department of Transportation, Federal Aviation Administration, Washington, D.C. 1986.
2. Aircraft Icing Handbook, Volumes 1,2,3, (DOT/FAA/CT-88/8-1,2,3) March 1991, updated 9/93.
3. Advisory Circular 20-73, Aircraft Ice Protection, Department of Transportation, Federal Aviation Administration, 21 Apr 71.
4. Flight Characteristics in Icing Conditions, Joint Aviation Authorities Notice of Proposed Amendment, NPA 25F-219 Issue 2, 22 January 1992.
5. Roll Upset in Severe Icing!, John Dow, Sr., FAA Aircraft Certification Service technical document, September 1995.
6. Special Certification Review Report, ATR Model ATR-42 and ATR-72 Series Airplanes, Federal Aviation Administration / Direction Generale De L'Aviation Civile, September 29, 1995.

EURICE- A European Research on aircraft Ice Certification

A. Amendola and G. Mingione
CIRA Centro Italiano Ricerche Aerospaziali
via Maiorise 81043 - Capua - (Caserta) - ITALY

Abstract

In this paper it is given an overview of a new project that recently started in Europe to study a number of issues around aircraft icing. The project is named 'EURICE: European Research on aircraft Ice Certification' and is partly funded by the European Commission, Directorate DG-VII for Transport, in the frame of the Workprogramme 1994. The project consists of various independent workpackages that are strongly related each other: icing problem sizing, icing atmosphere characterization, atmospheric measurements both with flight testing and remote data acquisition, certification and operation critical reviews. The Project officially started on January the 1st, 1996 (Rome Meeting), and at the present time unfortunately results are not yet available, but they will be the subject of future publications. This paper, as a result of EURICE partner contributions, will illustrate the consortium structure and organization and describe the scenario and basic motivations for this research effort. Then it will go deeply into details about the research objectives and actions.

Introduction

The project EURICE (European Research on aircraft Ice Certification) is partly funded by the European Commission, Directorate DG-VII for Transport, in the frame of the Workprogramme 1994. This workprogramme is part of the Fourth Framework Programme that sets out all the activities of the European Community in the area of research and technological development in the years 1994 to 1998. The Transport workprogramme is also built with contributions from the Joint Aviation Authorities (JAA) and National Aviation Administrations, and therefore it reflects the need to identify any factor that affects the safety of civil aviation and the need to define the possible evolution

of future standards and regulations in the fields of certification and operation. Moreover, one of the main conclusions of International Icing Symposium '95 (Ref. 1) was that there are significant research and development efforts in many countries, mainly US, Canada, France, UK and Russia. Nevertheless there are duplications and poor co-ordination that do not allow the greatest benefits from the available limited resources to be obtained. In this scenario CIRA promoted the creation of the EURICE consortium and submitted a research proposal to the EC for funding. It was done in agreement with the other European research centers in the frame of AEREA (the Aeronautical European Research Establishment Association).

Background

The EC workprogramme relies on some fundamental motivations. It appears from statistics that aviation is the safest means for transportation. This remarkable achievement is the result of dramatic improvements that have been introduced in the last 20 years in many of the fields that affects safety, namely regulation, technology, operation and airport. Therefore the objective of the EC Workprogramme is in general to stimulate *the development of a more efficient, safer and environmental friendly transport system for passengers and goods* (Ref.2). In particular concerning air transport, the workprogramme defines three major areas for future research:

- air traffic management (ATM);
- airports;
- air transport safety and environment.

The last area is specifically addressed to enhance safety and environmental compatibility and it is clearly addressed to *model and assess the airworthiness and operational factors that affects the safety of air transport and environmental issues*.

As a matter of fact even though statistics give such a comfortable feel, it should be also recognized that each aeronautical accident has a much heavier impact on the public opinion due to the larger number of victims per accident generally involved. Therefore significant improvements in aircraft safety standard should be achieved. Unfortunately, given the good level reached by aeronautical standards any little further improvement needs an effort much bigger than what it used to be in the past.

In recent years the aircraft icing issue has been clearly identified as one of the most

critical ones affecting air safety. Recently the JAA Research Committee (JAARC) proposed (Ref. 3) to launch specific research activities on the subject, using both national and international funds. JAARC highlighted also that icing is a complex problem since it involves design, certification, operations and training issues that are all tightly connected each other. All aircraft categories must take care of icing hazard, even though turboprop aircraft and rotorcraft seem to be more sensitive. The sensitivity of turboprop to icing is well understood and it is of particular relevance for European industries that hold the largest share of world market. For these reasons it appeared worthwhile to give emphasis in the current project to turboprop and rotorcraft. These aircraft are aerodynamically more prone to ice accretion since they are by far more exposed to severe icing atmospheres for their operational (cruise, climb, descent) altitudes, for their protection systems based on de-icing and for their reduced power supply and margin from stall if compared to jets.

In order to be more effective the overall problem will be split into separate investigation areas. For example a useful strategy to tackle the problem would be to separate technology from certification and operational aspects. A preliminary analysis highlighted serious doubts concerning both icing certification and operation regulations. More accurate investigations are commonly believed now necessary to establish some fundamental criteria to revise regulations and advisory material. Therefore the main objectives of EURICE is to investigate icing certification and operational problems and as a consequence the icing

atmosphere and its limitations concerning freezing drizzle and rain.

Project overview

The EURICE project is fundamentally aimed to carry out a coordinated effort in Europe to examine current aircraft icing problems and the related certification process, operation procedures and flight standards. In principle the results of this research could be used as a scientific platform by JAA to start a revision process of part of the JAR and the advisory material, or to address further research activities in specific selected areas. An important goal of the project is therefore to establish a positive trend in icing research in Europe where many remarkable efforts on national basis are ongoing (France, UK, Germany) but without a coordinated action.

At the Montreal Symposium six critical areas were clearly identified:

- 1) training/education;
- 2) meteorology;
- 3) ice detection and severity index;
- 4) testing and test facilities;
- 5) theory;
- 6) helicopter protection and certification.

Critical areas identification is only a first step, EURICE wishes to go further, by trying to identify for each area what kind of solution could be envisaged. The project will start with an accurate study of the icing problems in aeronautics by means of a deep analysis of available incident/accident statistics based on reports collected from various sources (FAA, NTSB, TSB, ICAO, CAA). Furthermore the icing atmosphere will be addressed by developing a new data-base for atmospheric data that will be constructed firstly by collecting some data available in Europe from certification

and research flight tests and later on with data measured within the project. EURICE flight test campaign will be carried out using advanced techniques able to measure large droplets, and it will take advantage from remote data acquisition using a Special Sensor Microwave Imager (SSM/I) flown on US Defense Meteorological Satellite Program satellites. Finally a critical analysis and review of certification process and operational procedures will be performed. The consortium is coordinated by CIRA. CIRA will also collect the data and develop the information system for the new icing atmosphere data-base and it will perform atmospheric measurements using a newly designed Phase Doppler Particle Analyzer (PDPA), installed on an aircraft of the consortium. The Partners of the project are industries such as Agusta, the Italian rotorcraft company; Alenia, the Italian aerospace company; Aerospatiale, the most important French aircraft manufacturer and British Aerospace, the leading UK company. Together with industries the European aeronautical research establishments are well represented: DLR, the German aerospace research center; INTA the Spanish center and NLR the Dutch one and the Meteorological Office (Met. Off.) in the United Kingdom. Finally in the consortium there are also two universities, University of Loughborough in UK, that has a long experience in certification and operational studies through previous cooperation with the Civil Aviation Authority (CAA), and University of Pisa in Italy that is also very active in icing issues and that is going to perform the same type of studies. A particular mention should be given to the partnership of RAI (Registro Aeronautico Italiano), RAI is member of the JAARC

and strongly supported the project since its beginning. The workshare is well balanced with partner contributions according to their background and previous experiences. Flight tests will be performed by the flight test departments of DLR, NLR and INTA. DLR will coordinate the flight test and Met.Off. will be the provider of the satellite data. Agusta, Alenia, British Aerospace and Aerospatiale will contribute with new data from certification flights. They will also play an important role in the analysis of certification and operation processes. In particular Aerospatiale will coordinate this task in strong interaction with University of Loughborough and University of Pisa who will be responsible for the surveys and that will act as an independent point of view in the analysis, together with RAI.

Icing Atmosphere

The aeronautic community is today questioning whether the current modelization of icing atmosphere of Appendix C is adequate to describe the actual envelopes of flight conditions. A major concern is that SLD (Supercooled Large Droplets), that includes both freezing drizzle and freezing rain, played or could have played a role in a number of incidents/accidents involving turboprop aircraft. A Met.Off. study commissioned by CAA gave an estimate of up to 5% SLD occurrence in elevated layers due to the classical freezing rain mechanism. Therefore it seems worthwhile to undertake actions to gain a better knowledge of icing atmosphere. An improvement of the knowledge of icing atmosphere physics will have long term benefits that can be summarized as follows:

- developments of advanced icing nowcasting and forecasting techniques;
- enhancements of ice protection system effectiveness;
- improvements in theoretical and experimental tools for icing conditions simulation, namely codes and/or facilities.

In this project we will not consider the influence of snow or ice crystals, since at this stage it seems more critical to understand the possible role of SLD, critical due to recent accidents. As a matter of fact there is no mention of snow and ice in icing certification requirements. The minor importance of such factors was confirmed by a study conducted in 1979 in the North of Spain. In that studies it was remarked that the effect of the presence of ice crystals mixed with supercooled droplets is to reduce the rate of ice accretion through the erosion caused by the ice particles impinging the ice deposit (Ref. 4).

The US Federal Aviation Administration (FAA) and the European Joint Airworthiness Authority (JAA) have adopted the same design criteria for certification in icing conditions. These design envelopes have been in use since 1950 and are based on data collected on an extensive set of clouds research flights conducted by the researchers from the US Weather Bureau and the National Advisory Committee for Aeronautics (NACA) during the winters from 1946 to 1950. These diagrams are grouped in envelopes for convective intermittent clouds, averaged over 2.6 Nm, and in envelopes for stratiform continuous clouds averaged over 17.4 Nm. These distances have no physical meaning but were chosen for convenience because original NACA researchers averaged their

data on distances between 3 and 10 statute miles (2.6 and 17.4 Nm). To account for longer or shorter flight length scaling factors are to be applied. The actual JAA-FAA icing envelopes express a 0.001 probability that all three variables, Liquid Water Content (LWC), Median Volumetric Diameter (MVD), and temperature, represented by a point on the envelopes, will be exceeded simultaneously in natural icing condition. A large number of authors have shown evidence of some deficiencies in the current icing envelopes:

- they are based on data collected only in the USA, for example no European data are included;
- they do not include MVD lower than 15 μm and larger than 50 μm ;
- some authors (Ref. 5) consider that a plot of LWC against the averaging distance is a more convenient way for identifying design icing condition points;
- there are classes of aircraft with altitude limitations for which these conditions are considered too severe (Ref.6);
- there is evidence that conditions exist where the MVD is not enough for simulating the real icing conditions and that the maximum droplet diameter of 50 μm indicated by regulation is exceeded (Freezing drizzle).

During a flight campaign on icing atmosphere characterization, carried out by the University of Wyoming over the past five years with a Super King Aircraft (Ref. 7), some 'non-usual' icing conditions were experienced. These conditions were characterized by LWC and measured MVD not being very large, but the aircraft performance degradation was so sensible to require an aircraft re-routing.

The most impressive problem was that in a previous flight the aircraft had flown in similar LWC, MVD and temperature without showing appreciable performances degradation. Only analyzing the droplet size spectrum by merging the measurements of the 4 probes installed on the aircraft (a Forward Scattering Spectrometer Probe (FSSP) and three Optical Array Probes (OAP): a 1DC OAP, a 2DC OAP and a 2DP OAP) it was possible to demonstrate that the decrease in performances was due to a large number of droplets positioned in the high diameter part of the spectrum.

These conditions, related to the presence of large droplets, up to now were considered a relatively rare event, but recently it has been demonstrated (Ref. 8) that these conditions are far to be considered rare. Through a study conducted over Canada, it has been possible to demonstrate that areas, where these conditions are quite usual, exist. This study is the continuation of the studies conducted under the CASP program (Ref. 9). Since most of the effort in improving icing atmosphere models have been developed up to now in the North America, EURICE represents the occasion to develop a useful and positive contribution to icing research in Europe.

One the first objective of this research is the development of an on-line data-base of icing atmosphere. Even though data-bases of icing atmosphere already exist, the EURICE data-base will have some interesting new features like that of being installed on a relational data-base software easily accessible through the World-Wide-Web protocol which allows connection to everyone who is interested in consulting the data. Moreover in this system the icing atmosphere data will be

completed with digital images, meteorological data including temperature vertical profiles, satellite images and bulletins.

This data-base gather:

- data collected in a past flight campaign (93 flights from 1983 to 1992) with a Do-28 from DLR;
- data collected during certification flights of aircraft such as ATR, AIRBUS, JETSTREAM, ...
- data collected during certification flights of various helicopters (EH101);
- data measured during EURICE flight tests.

In addition the consortium is in favor of cooperation and data exchange between Europe, US and Canada. EURICE-DB will be developed according to a client-server architecture. The server, although centralized and administrated at CIRA, will be widely available by remote access on Internet, to allow clients to retrieve data, upload new data in the data-base, perform statistics and study icing atmosphere models.

The CIRA server will be implemented using a relational Data Base Management System (DBMS) with multimedia and scientific data management extensions. Systems manipulation techniques will be designed and implemented, for easy loading and retrieving of information and for diagram and tabular presentation, documented by report generation and images collected during test flights or satellite and radar data acquisitions.

The data will be grouped as follows:

Flight profile:

- main aircraft characteristics;
- flight profile and location.

Meteorological data:

- weather bulletin;
- temperature profiles, wind situation.

Cloud characteristics:

- cloud physics data;
- atmospheric and microphysical parameters (LWC, MVD, Temperature);
- ice severity and type and amount of accreted ice.

Equipment:

- information on equipment used to collect data (FSSP, OAP, Cylinder).

Output from analysis:

- statistics of severe icing conditions;
- meteorological conditions; associated with the most severe icing conditions;
- correlation of icing conditions with location or season.

New Atmospheric Data

Part of the research will be a flight campaign having the objective of collecting new data, in Europe, on icing atmosphere parameters.

The objectives of the flight campaign are several :

- to revive atmospheric flight testing for icing research in Europe;
- to increase the amount of data collected in Europe in particular in the area of large droplet icing conditions;
- to validate new means for data acquisition, such as satellite;
- to experiment new advanced instrumentation for cloud microphysical measurements.

The flight campaign, will cover three main European area; North Spain, Central Europe and North Sea. We have planned 35 hours with a INTA (C-212) aircraft, 15 hours with a DLR aircraft (Do-228) and 15 hours with a NLR aircraft (FAIRCHILD METRO II). One of the most critical points is to find meteorological conditions potentially leading to supercooled large droplets. An

additional problem is that the number of flight hours is not very large and it is well known how it is difficult to find natural icing conditions. To overcome these problems an attempt will be made to devise a strategy to look for large droplets. We will try to forecast the icing condition using some hypotheses on large droplets formation. A number of candidate regions of SLD will be selected and then the flight will be scheduled according to these forecasting trials.

The aircraft involved in the research are:

INTA C-212: a two engine turboprop aircraft, equipped with pneumatics de-icing boots, with a non-powered lateral axis flight control system, a non pressurized cabin and a fixed landing gear.

DLR Do-228-212: a twin turboprop aircraft with a non-pressurized cabin with two openings in the cabin door.

NLR Fairchild Metro II: a twin turboprop aircraft modified for aerospace research. It has a pressurized cabin with and cargo door.

Each aircraft will be equipped with cloud microphysical instrumentation. Mostly probes from Particle Measuring Systems inc. (PMS), FSSP and OAP, will be used for cloud droplet sizing. The liquid water content will be measured with Johnson-Williams or CSIRO King probes. Details of the instrumentation are not yet fixed.

The use of data from the SSM/I to indicate areas subject to icing conditions and to infer supercooled liquid water contents will be examined. Test flights will be performed in coincidence with SSM/I overpasses. The SSM/I data can be used to infer the Liquid

Water vertical Path (LWP). To retrieve liquid water contents from the LWP, one proposed method to be examined involves the use of a diagnostic cloud microphysics model, the Cox model, which is initialized with data from analyses from the UK global forecast model. The Cox model will be run with various vertical velocities until it produces an LWP in agreement with the SSM/I estimate. Liquid water contents can then be extracted from the model as a function of height and temperature.

In combination with standard instruments a rather new instrument will be installed on one of the aircraft involved in the flight campaign. This instrument is the PDPA, it can perform drop size and velocity measurements using the laser light wavelength as the fundamental scale rather than the scattered light intensity, and as such it is less subject to errors due to beam attenuation.

Certification and Operational Procedures

An important activity of the EURICE project is a critical review and analysis of current certification and operational requirements, procedures and means of compliance. In general terms the objectives are:

- to identify areas where improvements to the current certification and/or operational procedures could be introduced;
- to define these possible improvements;
- to evaluate the economical impact of such modifications.

By improvements it is meant any modification that would have the consequence to enhance the capability of any aircraft to operate safely in an icing environment, even though it would be

characterized by severe conditions.

An other interesting objective is to gain a deep understanding about the status of available tools. Available tools include analytical methods, testing procedures and experimental facilities both ground based and airborne. They play an important role in certification since they allow design, analysis, test, and evaluation of an aircraft and its systems and then to certificate them.

In other world the boundaries of the design and operational envelope that can be explored must be detected, and moreover it should be clarified if such boundaries are adequate. The results of this activity must be a contribution to the discussion about aircraft icing.

The approach that we will follow relies upon a number of contributions in addition to the partners of the EURICE consortium. We will survey a reasonable number of airframe manufactures, aviation authorities and operators in order to have a meaningful sample of views. Airworthiness authorities will be invited to contribute views and comments on the finding of the survey, although the confidentiality of the participating manufactures will be respected. The fundamental steps in our activity are:

- to find a list of certification process and operational procedure topics that in the opinion of the consortium are necessary to be investigated;
- to define a list of questions that if properly designed will allow an analysis of the above topics;
- to select a number of relevant people or institutions that must be interviewed;
- to critically analyze the answers;
- to draw conclusions and suggestions.

An important aspect to notice is that the EURICE consortium is quite heterogeneous since its partners look at the icing problems from different points of view, sometimes even in contrast each other. Far from being a limitation, in our opinion, this characteristic must be considered an advantage since the final results will be already the result of an internal debate with an important role played by the two universities (Loughborough and Pisa) that represent the independent point of view of the problem. From past experience, organizations like universities or research establishments are likely to obtain more valuable information, if compared to companies which may be seen as a commercial rival by the interviewed.

A similar investigation will be conducted for rotorcraft operators. As far as airframe manufactures are concerned the survey will be carried out through a series of meetings. All of the major European manufacturers of aircraft and rotorcraft will be invited to take part in the survey. The meetings will identify the methodology used to demonstrate aircraft compliance with current certification requirements for icing conditions. We wish to have wide ranging discussions even on topics not specifically covered by certification requirements. The topics to be covered will include:

1. Definition of relevant terminology to ensure that the interviewers and manufacturers are using the same set of definitions for icing related phrases and words.
2. Certification requirements used for past and present aircraft, and identification of other publications.
3. Harmonization between operational and certification requirements and procedures (Ref. 10).

4. Methods used to demonstrate compliance and in particular the roles of theoretical analysis, ground based experiments and flight testing.
5. Suitability and accuracy of theoretical methods, with particular emphasis on identifying the perceived limitations.
6. Realism and accuracy of ground based facilities, including identifying any improvements to facilities that are desirable.
7. Flight test techniques used, including the relative merits of simulated ice and natural icing, will be identified. The tests flying techniques used to demonstrate safe handling, and determine aircraft performance decrements will be addressed, as will the success, or otherwise, of identifying suitable icing conditions. Possible improvements to flight testing techniques will be identified.
8. Research and development currently being undertaken by the manufacturer to improve or supplement the methods identified in (4).
9. Methodology used to determine which surfaces need to be provided with ice protection. Having decided on the surfaces, the methods used to choose the type of system will be identified.
10. Need for ice detection, and if required the criteria used to select a suitable detector (ref. 11).
11. Ice onset for tailplane.
12. Maintenance and reliability issues for ice protection and detection equipment. For example, methodology used to demonstrate reliability, use of service records of aircraft operators to assess the reliability and maintainability of the systems, specific limitation of different ice protection systems.
13. Desirable changes to certification requirements and methods used to

demonstrate compliance (e.g. index for ice severity, atmosphere envelope and SLD).

The above list is by no means exhaustive, and additional topics will be added as appropriate. If shown to be desirable, the option is available to extend the survey to cover a limited number of engine manufacturers and ice protection system suppliers.

The survey of operators will be conducted through meetings held with personnel from operators. These personnel will include managers, pilots, and maintenance staff. To ensure detailed and in depth exchange of information, as far as possible, discussions will be held away from the supervisors and managers of the people being interviewed. The topics to be covered in the survey will include:

1. Appropriateness of material from airframe manufacturers, including the aircraft's flight manuals.
2. Operator's winter operations policy, including how the policy is derived and disseminated to air and ground crews.
3. Experience of the aircrew in flying in icing conditions, and how this experience was gained. The use of training, specific to icing, and the measures taken by operators to ensure appropriate levels of experience for aircrew will be considered.
4. Operating procedures used on each type of aircraft in service with an operator will be identified. The survey will then go on to consider the appropriateness of these procedures and how they could be improved.
5. The extent to which turboprop powered aircraft (or rotorcraft) have specific icing issues will be discussed.
6. The perceived effectiveness of ice protection and detection systems will

be investigated. Reliability and maintenance issues for these systems will also be explored.

7. Ground icing, with particular reference to the perceived effectiveness of de-icing procedures and fluids. Possible improvements to the procedures will be considered. For example, possible benefits that may be obtained through the provision of ground ice detectors, or the operational advantages and disadvantages of adopting a clean wing requirement for take-off.

Once again this list of topics is not exhaustive. Past experience from conducting interviews with pilots suggests that many additional topics will be included during the course of each meeting. The choice of operators to be visited has still to be made. A mix of companies will be aimed at. For example, both small companies operating one or two aircraft, and large airlines operating both turbofan and turboprop or fixed wing and rotorcraft, will be included. The choice of operators will be concentrated in areas of Europe where climate and physical geography suggest that operations in icing conditions are common.

Conclusions

A general presentation of the EURICE project has been given. The research recently started in Europe and it is mainly addressed to investigate the most important certification and operational aspects related to aircraft icing, including revision of the icing atmosphere. The research is perhaps one of the first large international cooperative effort to investigate icing related issues. The activities will be focused on supercooled large droplets and they will give a particular emphasis to the aircraft

categories which are more sensitive to icing such as turboprops and helicopters. Atmospheric data-base development, flight tests and survey are among the relevant activities that will be carried out. The research will establish a positive trend for icing research in Europe.

Acknowledgments

The authors wish to thank all their colleagues of EURICE consortium whose contribution was fundamental for the preparation of this paper. In particular Thomas Hauf of DLR (Germany), Peter Render of the Un. Loughborough (UK), M. Cristina Zarpellon of CIRA (Italy), Vittorio Fiorini of RAI (Italy), Malcom Sutton of British Aerospace (UK), Henk Jentink of NLR (The Netherlands), Roderick Brown of the Meteorological Office (UK), Didier Cailhol of Aerospatiale (France), J. Manuel Ezquerro of INTA (Spain). A particular thank to Chris North of the European Commission DG-VII for his valuable suggestions during the proposal preparation and for his continuous support in the future.

References

- 1) Workshop Summary, International Icing Symposium '95, Montreal, Canada
- 2) European Commission, Transport Workprogramme, Edition 1994
- 3) Research Proposal on Aircraft Icing Issues, JAA Research Committee, June 1995
- 4) M. Bain and J.F. Gayet, 'Aircraft Measurements of Icing in Supercooled and Water Droplet/Ice Crystal Clouds', Journal of Applied Meteorology. vol. 21, No. 5, May 1982

- 5) R.K. Jeck, 'Other ways to Characterize the Icing Atmosphere' AIAA-94-0482, 32nd Aerospace Sciences Meeting Reno Jan. 10-13, 1994
- 6) R. K. Jeck 1983 'A New Data Base of Supercooled Cloud Variables for Altitudes up to 10000 Feet AG and the Implications for Low Altitude Aircraft Icing' Report DOT/FAA/CT-83/21
- 7) W.R. Sand, W.A. Cooper, M. K. Politovich and D.L. Veal 'Icing Conditions Encountered by a Research Aircraft', Journal of Climate and Applied Meteorology vol. 23, No. 10, October 1984"
- 8) J.G. Cober, G. A. Isaac, J.W. Strapp, D. Marcotte 'Icing Environments Associated with Supercooled Drizzle' International Icing Symposium, Montreal Canada, September 18, 21 1995, American Helicopter Society
- 9) S.G. Cober, G.A. Isaac, J.W. Strapp, 'Aircraft Icing Measurements in East Coast Winter Storms' J. Appl. Meteor. Vol. 34 pp. 88-100
- 10) S. Green, 'Inflight certification working paper', International Icing Symposium '95, Montreal, Canada
- 11) P.M. Render, L.R. Jenkinson, R.E. Caves, D. E. Pitfield ' Ice detection for turboprop aircraft', CAA Paper 95007

FLIGHT IN ICING CONDITIONS
INTERNATIONAL STANDARDIZATION OF CERTIFICATION
REQUIREMENTS FOR TRANSPORT CATEGORY AIRPLANES

FAA International Conference on Aircraft Inflight Icing
Springfield, Virginia
May 6-8, 1996

Colin S. Fender
FAA Transport Airplane Directorate
Renton, Washington

David J. Kotker
Boeing Commercial Airplane Group
Seattle, Washington

ABSTRACT

This paper presents an overview of an international project to harmonize flight test requirements and methods to gain certification for flight in icing conditions. The goal of the project is to develop standardized airworthiness regulations and advisory material, as required, to assure safe flight in the icing conditions of Appendix C to Part 25 of the Federal Aviation Regulations (FAR) and European Joint Aviation Regulations (JAR) 25.

The starting point for the flight in icing harmonization project was provided in the form of advisory material published in the European Joint Aviation Authorities' (JAA) Notice of Proposed Amendment (NPA) 25F-219, "Flight in Icing Conditions - Acceptable Handling Characteristics and Performance Effects," and draft advisory material published by the Federal Aviation Administration (FAA) for inclusion in the revision to Advisory Circular 25-7, "Flight Test Guide for Certification of Transport Category Airplanes."

The flight in icing harmonization project is being worked by the Flight Test Harmonization Working Group (FTHWG), a body that is composed of an international field of technical specialists from the aerospace industry and airworthiness authorities. Considerable discussion has been held with regard to the obligation of the industry to comply with the tests described in NPA 25F-219. The result of these discussions has been the separation of criteria into one group for which full FAR/JAR 25 regulatory compliance will be required, and another group for which advisory material will be provided.

The major technical issues identified by the FTHWG, and discussed in this paper, are: 1) What stall warning and maneuver margins should exist for an airplane that is contaminated with ice accumulations? 2) What type of test maneuver should be

executed, and what should the pass/fail criteria be for showing an airplane is not susceptible to tailplane stall? 3) What amount of performance degradation, relative to FAR/JAR 25 minimum standards, should be permitted before performance adjustments are required? 4) What flight regimes (i.e., takeoff, cruise, etc.) should be investigated for performance degradation due to ice accumulation? and 5) What other aspects related to operations in icing conditions, such as ice detection systems, ice protection system design, and the characterization of the icing atmosphere, should be considered in the formulation of requirements and advisory material for demonstrating the ability to safely operate in icing conditions?

INTRODUCTION

Certification of transport category airplanes for flight in icing conditions has historically been addressed in fairly general terms, with no standardized specific guidance available. As part of the proposed revision to the Federal Aviation Administration's (FAA's) Advisory Circular (AC) 25-7, "Flight Test Guide for Certification of Transport Category Airplanes," an attempt was made to remedy this situation by including guidance related to airplane performance and handling characteristics evaluations in icing conditions.

Coincidental with the revision of AC 25-7, the European Joint Aviation Authorities (JAA) was developing Notice of Proposed Amendment (NPA) 25F-219, "Flight in Icing Conditions - Acceptable Handling Characteristics and Performance Effects." This NPA traces its origins back to work started by the JAA Flight Study Group (FSG) approximately 10 years ago and represents a coordinated effort by European airworthiness authorities and industry. NPA 25F-219 was issued for public comment in April 1993. The NPA provided a considerable amount of detailed guidance for showing compliance with the requirement of Joint Aviation Regulation (JAR) 25.1419 that the airplane ". . . must be able to safely operate. . ." in the icing conditions described in Appendix C to JAR 25. Means of compliance were described that included tests with artificial ice shapes installed and tests in natural icing conditions.

Since 1990 the FAA, the JAA, and Transport Canada Aviation (TCA) have been officially involved in an effort to harmonize their airworthiness regulations and guidance material. As a part of this harmonization process, the proposed revision to AC 25-7 has been highly coordinated with the JAA and TCA, the goal being adoption of the eventual AC 25-7 revision as the standard flight test guide for all three airworthiness authorities. Included in these flight test guide harmonization discussions were methods for demonstrating the ability to safely operate in icing conditions. Due to the considerable differences between the FAA and JAA approaches, and the desire by both authorities to produce a comprehensive guidance package for flight in icing conditions, it was decided to defer harmonization on this issue to be worked as a separate project.

In the interim, the FAA and American aerospace industries implemented the Aviation Rulemaking Advisory Committee (ARAC) in an attempt to streamline the rulemaking process. The ARAC system includes industry representatives throughout the rulemaking process in an attempt to improve the useability of the end product. The ARAC, which includes representatives from approximately 65 domestic and foreign organizations, also became the FAA's official venue for harmonization. Under the ARAC system, "working groups" are established to resolve the technical issues and draft proposed rule changes and guidance material.

In late 1993, aerospace industries from Europe and North America proposed a harmonization project that would use NPA 25F-219 as a starting point, and following a review of the public comments received, modify that advisory material to produce an internationally accepted "harmonized" document. This proposed harmonization project was officially tasked to the Flight Test Harmonization Working Group (FTHWG) in June 1994 and provided an allowance for regulatory changes, if deemed necessary, in addition to revising the guidance material of NPA 25F-219. (The FTHWG is the forum for discussing the harmonization technical issues and is composed of flight test specialists representing an international group of aerospace manufacturers and operators.)

This paper presents a summary of the proceedings of the FTHWG's efforts related to producing harmonized material for demonstrating transport category airplane performance and handling characteristics in icing conditions.

RULEMAKING VS. GUIDANCE

Though some minor wording differences exist, Part 25 of the U.S. Federal Aviation Regulations (FAR) and the European JAR-25 both require that airplanes ". . . must be able to safely operate. . ." in the icing conditions of Appendix C (ref.: FAR/JAR 25.1419). The stated purpose of JAA NPA 25F-219 is to provide an acceptable means of compliance with this requirement in terms of airplane performance and handling characteristics.

A significant number of comments against NPA 25F-219 proclaimed many elements of it to be rulemaking. This became the primary topic of discussion between industry and the airworthiness authorities at the first three FTHWG meetings on this subject. Though the NPA has been applied in full to several European airplane types, it describes more testing than has typically been done in FAA certification programs. Industry viewed this new (or additional) testing as rulemaking without due process. The FAA's position was that because it is new does not necessarily make it rulemaking if it is possible to get from the referenced rule to the guidance material. The FAA believes that, as used in FAR 25.1419, the term "safely operate" must be interpreted within Part 25, i.e., the flight requirements of Subpart B of FAR 25 for airplane performance and handling characteristics. This position generated strong opposition from industry members of the FTHWG who maintained it was inappropriate to apply

Subpart B criteria to interpret a rule contained in Subpart F (dealing with systems and equipment) of FAR/JAR 25.

At the third meeting the JAA members were tasked with an action item to establish a position relative to the applicability of Subpart B requirements to testing conducted to gain certification approval for flight in icing conditions. The result was the JAA agreed with the FAA's position. The FAA and JAA further honed this position by limiting their intent for full Subpart B compliance to specific aspects of handling characteristics.

At the last meeting of the FTHWG, the airworthiness authorities presented an "authorities' statement," which proposed regulatory changes to Subparts B and F of FAR 25 and JAR 25. The current FAR/JAR 25.1419 (Ice Protection) rules make the ability to safely operate in icing conditions contingent upon having an ice protection system (FAR 25) or seeking certification for flight in icing conditions (JAR 25). Since all of today's transport category airplanes will be exposed to icing conditions, and since the flying public does not expect those airplanes to have a different minimum level of safety in icing conditions, it was proposed that the existing optional nature of showing an airplane's ability to safely operate in icing conditions be removed from FAR/JAR 25.1419. With regard to Subpart B flight characteristics, the airworthiness authorities proposed adding a paragraph to FAR/JAR 25.21 (Proof of Compliance) that would require full compliance with specific FAR/JAR 25 handling characteristics regulations in the icing conditions described in Appendix C; other aspects of airplane performance and handling characteristics would be addressed by advisory material using Subpart B regulations as a guideline. This proposal was well received by the aerospace industry representatives and should play a significant role in reaching consensus on the remaining technical issues.

The remainder of this paper provides some insight into the technical issues that have been the primary subjects of discussion in the four FTHWG meetings on this subject.

STALL WARNING AND MANEUVER MARGINS

Over the last ten years the FAA and other airworthiness authorities have formulated rule changes that would revise the way stall speeds are defined; rather than defining the stall speed as the minimum speed in the maneuver, as prescribed by the current regulations, a 1g stall speed (V_{SI-G}) would be defined as the speed at which wing lift alone can support the weight of the airplane in 1g flight. Another element of these proposed rule changes is the addition of a requirement to demonstrate adequate low speed maneuver margins without encountering stall warning; this demonstration consists of executing constant speed turns at specified bank angles in four standard terminal area airplane configurations (i.e., flap setting, landing gear position, and thrust/power setting). (NOTE: The proposed 1g stall regulatory changes were published for public comment as Notice of Proposed Rulemaking 95-17/Docket No. 28404 on January 18, 1996. The comment period closes May 16, 1996.)

Nearly all of today's transport category airplanes employ some type of artificial stall warning system, generally a "stick shaker" to simulate the vibrations the flight crew would sense in an airplane with well-defined aerodynamic stall warning (i.e., airframe buffet). These artificial stall warning systems are activated when the airplane reaches the angle of attack (AOA) that is scheduled for the particular configuration of the airplane high lift devices. Most artificial stall warning systems will use a single AOA value to provide stall warning for more than one airplane configuration, thus providing more than adequate margin for some configurations, while providing minimal warning margins for other configurations. The impact of any ice contamination on the wing will be to reduce the AOA at which flow separation begins and the wing subsequently stalls. The reduced stall AOA will equate to an increase in the stall speed, whereas the stall warning will still occur at the AOA and speed scheduled for the clean (i.e., uncontaminated) airplane. The net result of this is a reduction in the margin between stall warning and stall.

The philosophy employed by the JAA in NPA 25F-219 is to maintain the minimum stall warning margins specified by the regulations when ice accumulations are present on the unprotected surfaces. In application this has resulted in several airplanes having their stall warning AOAs reset to lower values (higher speeds) when the ice protection system is turned on. The increased stall warning speeds can also lead to increased operating speeds to maintain maneuver margins. If the clean airplane has more than the regulatory minimum stall warning margin, it may be possible to maintain that minimum margin above the 1g stall speed with ice using the clean airplane stall warning AOA settings. Alternative approaches that have been discussed include retaining the clean airplane AOA settings and implementing time delays before pilot action is taken to reduce the AOA; the pass/fail criteria would be no indication of stall (e.g., uncommanded nose down pitch) before recovery. Proposals have included one and three knot per second entry rates with varying delay times.

One proposal would not require any adjustment to the stall warning system until the stall speeds with ice had increased by more than a specified minimum above their clean airplane counterparts. After this threshold was exceeded, the stall warning system would be reset to maintain the minimum stall warning margin, and clean airplane operating speeds would be retained by allowing a five degree decrease in the bank angle for the constant speed turn maneuver margin demonstrations.

Another proposal would not require any adjustments to stall warning or operating speeds if the increase in the 1g stall speed due to ice was not greater than a defined threshold value; if the threshold value was exceeded, an assessment of flight characteristics would be made over the range of clean airplane operating speeds. If the results of this flight characteristics assessment were found acceptable, no changes to clean airplane performance would be required. If the results were not found acceptable, full performance accountability would be required, thus maintaining the minimum regulatory stall warning and operating speed margins.

The airworthiness authorities are amenable to allowing an increase in stall speeds up to a certain threshold value without full performance accountability being required. However, above that threshold, the authorities favor full performance accountability and no reduction in clean airplane maneuver margin capability.

As of this writing, consensus has not been reached on a method to address stall warning and maneuver margins with ice.

ICE CONTAMINATED TAILPLANE STALL INVESTIGATION

NPA 25F-219 describes a zero-g pushover maneuver that was originally designed to investigate susceptibility to elevator autodeflection (overbalance) for airplanes that do not have powered irreversible control systems. The test maneuver is equally applicable for investigating the susceptibility of airplanes that do have such control systems to stalling of the horizontal tailplane. The term tailplane stall is used to describe both phenomenon in this paper.

Tailplane stall has been responsible for several incidents and accidents when the leading edge of the horizontal stabilizer has been contaminated with ice. It has been found that even small levels of contamination that may be characterized as "sandpaper" ice, such as those that may accumulate before activation of an ice protection system, can make an airplane susceptible to tailplane stall. Initiating circumstances include vertical gusts, aggressive pushovers to capture the glideslope, and flap deflection; all of these contribute to an increased negative angle of attack on the horizontal tailplane, and may, in combination or singly, increase the tailplane AOA to the point of separation when contamination is present. The classic case for an airplane with a reversible unpowered control system and a fixed horizontal stabilizer would be applying a nose down elevator input following selection of landing flaps at high speed, the type of maneuver that would be executed if an airplane was making an instrument approach too fast and above the glide slope. The tailplane AOA, which is already toward the negative range due to high airspeed, is further increased to the point of stall by the increased downwash angle from flap deployment, resulting in a trailing edge down autodeflection of the elevators that often times results in control forces to recover that are beyond the flight crews' capabilities.

Accident data showed that most of the departures occurred between 0.5g and 0g with pitch rates on the order of 10 degrees per second. The zero-g pushover maneuver was devised as a simple test procedure to obtain the necessary results without need for sophisticated test equipment.

The FAA published a memorandum in 1992 that prescribed the zero-g pushover maneuver for investigating airplanes' susceptibility to tailplane stall. Additionally, the FAA memorandum added a requirement for a sideslip maneuver, resulting from lessons learned from airplanes where disturbed flow emanating from the contaminated vertical

stabilizer interacted with the flow over the contaminated horizontal stabilizer culminating in an uncommanded nose down pitching moment.

The majority of discussions in the FTHWG have centered on the need to demonstrate stability to 0g. The aerospace manufacturers have presented several proposals that were based on flight test results for some existing types that were stable to a certain g-level after which they exhibit stick force lightening with an eventual force reversal before reaching the 0g condition; these airplanes were deemed controllable throughout the maneuver by the manufacturers' test pilots. The manufacturers' proposal would require a flight test pushover maneuver to 0g with a push force to some g-level below unity, after which the control force would be permitted to reverse provided the airplane remained controllable.

The airworthiness authorities have maintained a desire to have a push force to 0g, the concern being for an operational pilot of average skill in less than desirable atmospheric conditions (the typical tailplane stall environment). One of the problems the airworthiness authorities have cited with a criteria that requires stability to some g-level below unity, and then controllability from that point on, is the element of subjectivity that would be introduced in determining what is "controllable."

The latest proposal being considered by the FTHWG is an extension of the manufacturers' proposal; it would require a push force to a load factor at least as low as 0.5 with control force reversals permitted below that load factor provided they were gradual and the airplane easily controllable. This proposal also includes a requirement that it is possible to execute a recovery without exceeding 1.5g (total) and without requiring a control force of more than 50 pounds.

PERFORMANCE THRESHOLDS

Prior to the implementation of NPA 25F-219 by the JAA as interim policy for the certification of transport category airplanes for flight in icing, there was no written requirement to account for the effects of ice accretion on performance in the FAR/JAR, or by TCA. FAA policy was to require the effects of ice drag on approach and landing climb performance to be included in the Airplane Flight Manual (AFM), but there was no requirement to account for the effects of ice on takeoff performance. Recent attempts to determine the original rationale for including the effects of ice drag on approach and landing climb have been unsuccessful, but there are indications that the low all engine thrust-to-weight ratios of early four engine jet transports was a consideration

The first known instance of an authority requiring performance accountability during the takeoff phase was in conjunction with ATR 72 Special Condition B6. Its requirements for the takeoff phase were essentially the same as the NPA's and included, (1) critical engine failure at V_{EF} , (2) most critical thrust-to-weight ratio, (3)

maximum continuous intensity of atmospheric icing throughout the takeoff, and (4) airplane assumed to be free of ice at brake release.

A major difference between the NPA and the Special Condition was that the NPA introduced the concept of performance thresholds, in order to allow for an acceptable level of degradation from the Subpart B performance requirements in icing conditions. The performance threshold during the takeoff (for any configuration used during takeoff) was defined as a stall speed increase due to ice accumulation of not more than the greater of 5 kts. or 5% V_{S1-G} , or an airplane drag increase of no more than 5%. Per the NPA, exceeding either the stall speed or drag threshold would necessitate appropriate AFM performance adjustments.

In their opening remarks at the first FTHWG meeting to address flight in icing, the JAA stated that the "basic premises behind the NPA were (1) the probability of encountering icing conditions must be assumed to be 1 for the purpose of certification, and, (2) the same criteria should apply to all types of aeroplanes, although it was recognized that differences in operation and the effectiveness of ice protection should be taken into account in the methods used to demonstrate compliance." The FAA stated that "some leeway in terms of reduced margins is possible, but the FAA considers that the NPA accountability threshold of 5%/5 kts. is too large." Transport Canada stated that in the past their "primary concern had been safe handling characteristics, and the performance accountability proposed in the NPA went beyond their past practice." These remarks set the stage for the discussion of takeoff performance at this and the next two meetings.

The positions of the participants during these discussions are summarized as follows:

- The authorities' positions were essentially as described above, but they recognized that there were design features of certain airplanes that compensated for the effects of ice accumulation.
- The Airline Pilots Association of America (ALPA) considered that any performance degradation that could be anticipated should be accounted for.
- The European aerospace manufacturers had been a party to the development of the NPA and generally agreed with its premises, but argued that some relief from the Appendix C icing envelope at ground level was in order. They also recognized that certain airplanes might have design features that compensated for the effects of ice accumulation.
- The American aerospace manufacturers, as represented by the Aerospace Industries Association of America (AIA), considered the requirement for AFM takeoff performance adjustments based on ice accumulation to be rulemaking, and suggested that those sections of the NPA that were rulemaking be addressed as such. AIA also: (1) presented the jet transport safety record to show that there

was no safety reason to require takeoff performance accountability, (2) enumerated the design features that could compensate for the effects of ice accretion, and (3) presented data to show that if the Appendix C icing envelope were extended to ground level, visibility would be below takeoff minimums for most operators.

At the fourth flight in icing meeting of the FTHWG, the authorities presented their "authorities' statement" that recognized the rulemaking aspects of the NPA, and also presented a harmonized proposal to establish the performance threshold to be 3 kts. or 3% increase in stall speed (the drag threshold is to be addressed in further work). The AIA presented additional data on the low visibility associated with Appendix C clouds at ground level (fog), that supported their restricted visibility thesis introduced in the previous meeting. The AIA also stated that the ice accumulation for takeoff should be assumed to start at liftoff instead of at brake release and that the liquid water content to be assumed should be reduced from the maximum value contained in Appendix C. This was because: (1) if icing conditions exist at ground level, the airplane will be protected by deicing/anti-icing fluid that has a transitory effect on performance, and (2) data for fog show that it has a reduced liquid water content. The AIA has an action item to present additional data in support of their proposal at the next FTHWG meeting.

RELATED HARMONIZATION ACTIVITY

At the second FTHWG meeting several presentations were made that related to the subject of large supercooled droplets. The FAA made a presentation regarding "other FAA plans and activities" related to flight in icing conditions. Two of the planned activities were closely related to the guidance material contained in NPA 25F-219. The first was the proposed formation of another ARAC group that would harmonize FAR/JAR 25.1419 and review the Appendix C icing envelope. The second was a proposed R&D project to recharacterize the Appendix C envelope as well as consider application of the freezing rain/drizzle environment to certification and operation. The French airworthiness authorities presented a draft of a paper that requested consideration of freezing drizzle by the working group. Although these presentations were of considerable interest, no action was taken or assigned because the large supercooled droplet environment was considered by some to be outside the terms of reference for this FTHWG project.

At the third FTHWG flight in icing meeting, the FAA reported that the terms of reference of the "other" working group had been drafted and was in the review process. The JAA reported on discussions between the Flight Study Group chairperson and JAA management about the need to maintain close coordination between the various icing-related harmonization activities. This concern was also shared by members of the harmonization working group, and it was agreed that the FTHWG should be involved in the "other" group's activities. During the meeting, the French airworthiness authorities presented a revision to their paper on freezing rain/drizzle that

proposed prohibiting flight through such conditions; considerable discussion was held on this subject.

During the fourth FTHWG flight in icing meeting, the FAA and JAA formally introduced their "Authorities' Statement." This statement included a proposal to harmonize the wording of FAR 25.1419 and JAR 25.1419. Although this was a task proposed to be assigned to the "other" working group, the authorities had reached a harmonized position on this issue that industry generally agreed with. This left the "other" working group with the task of reviewing the Appendix C icing environment with respect to the inclusion of freezing rain/drizzle droplet sizes. Industry members of the FTHWG proposed that the review of the icing environment be conducted by a group of appropriate specialists, and that the review of airplane certification for flight in this environment be taken up by the FTHWG. It was also proposed that the FTHWG provide oversight of the Appendix C review activity.

CONCLUSION

The regulatory changes proposed by the airworthiness authorities, together with agreement of industry, presented a breakthrough in the harmonization process. Work is now expected to continue at a rapid pace to develop the specific regulatory requirements and advisory material for demonstrating the ability of transport category airplanes to safely operate in icing conditions. FTHWG members who are technical specialists have volunteered to coordinate a resolution of the technical issues identified in this paper.

Extension of the regulatory requirements to include flight in freezing rain/drizzle is closely related to the current task of the FTHWG, and its members are active participants in the FAA International Conference on Aircraft Inflight Icing. It is expected that the FTHWG will also actively participate in harmonization of the recommendations of the conference related to characterization of, and flight in, the icing environment.

THE NASA LEWIS ICING RESEARCH TUNNEL: TESTING AND DATA ACQUISITION

Thomas B. Irvine
David N. Anderson, Ph.D.
NASA Lewis Research Center
Cleveland, OH

ABSTRACT

The Icing Research Tunnel is the world's largest refrigerated icing wind tunnel, capable of duplicating the icing conditions encountered by aircraft by controlling liquid water content, droplet size, and air temperature within the tunnel. The purpose of this paper is to document the tunnels existing capabilities including recent and planned improvements especially with regard to simulating supercooled large droplet conditions. Methods to scale for large droplet testing are evaluated. The IRT provides a valid experimental simulation facility with coverage of large portions of the FAR 25 Appendix C icing criteria envelopes. Based upon results of airfoils tested to date, the IRT is also a viable test facility for assessing aircraft icing and for instrumentation development in simulated large droplet icing conditions.

INTRODUCTION

The purpose of this paper is to highlight the NASA Lewis Research Center's Icing Research Tunnel's capability to reproduce, in the icing wind tunnel environment, repeatable and predictable supercooled large droplet icing encounters. The Icing Research Tunnel (IRT) is the world's largest refrigerated wind tunnel capable of duplicating icing conditions encountered in-flight by aircraft¹. This is accomplished by controlling water content, water droplet size, air temperature, air speed, and spray duration. The purpose of the IRT is to simulate the natural icing environment under controlled test conditions.

The crash of American Eagle ATR 72-210, Flight 4184, on October 31, 1994 has been attributed to aircraft icing in the supercooled large droplet (SLD) environment. Since then, experimental simulation methods have been used to study SLD encounters including flight testing behind aircraft spray tankers, testing with replicated ice shapes and icing wind tunnel tests².

The Icing Research Tunnel is a versatile tool for experimental simulation of aircraft in-flight icing for the entire range of icing encounters including FAR 25 Appendix C criteria and SLD. Icing wind tunnels as a class of test facility offer low cost, high productivity and low safety risk relative to flight testing. NASA Lewis Research Center has conducted icing wind tunnel tests in the IRT for purposes of documenting the capability of the facility to produce icing clouds of supercooled large droplets, to further understanding of ice accretion on airfoils similar to that of the ATR 72-210 in support of the NTSB accident investigation, to investigate several ice protection systems and sensors with specific applications to SLD encounters, and to perform parametric studies of commuter-class wing sections to quantify

the effects of various parameters on ice accretion and ice shapes. These tests have shown that for testing of 2D or 3D airfoils of full scale chord or for development of instrumentation and sensors, the IRT is a viable test facility for assessing aircraft icing in simulated large droplet icing conditions.

The test matrix for a typical icing test includes the variables of airspeed, temperature, altitude, cloud LWC, cloud droplet size distribution and model size or scale. Certain combinations of variables will be unattainable in the wind tunnel environment. Therefore, scaling is used to produce desired results, for example, geometrically similar ice shapes. Other objectives for a scaled test have been previously noted³. Here, the ability to simulate the supercooled large droplet environment by scaling droplet size is addressed. At present, no verified method exists for performing tests with scaled models and "small" droplets ($\sim 40\mu\text{m}$) such that large droplet spray could be simulated.

I. TUNNEL OVERVIEW & CAPABILITIES

Icing Research Tunnel Systems

A schematic of the Icing Research Tunnel is shown in figure 1. Three systems combine to make the IRT a unique icing simulation facility. The low speed wind tunnel system, the refrigeration system, and the spray bar system. The IRT is a closed-return, atmospheric type wind tunnel which supports year round operation made possible by the refrigeration system and 7400 kW (2100 ton) heat exchanger. The spray bar system consist of a set of eight (8) bars mounted horizontally in the settling chamber upstream of the test section. Approximately 90 atomizing air-assist type water spray nozzles, attached to the 8 bars, inject the cloud of microscopic droplets into the air stream. The test chamber is 1.8 m (6 ft) high by 2.7 m (9 ft) wide by 6.1 m (20 ft) long. The uniform icing cloud in the test section is strongly a function of cloud MVD and tunnel airspeed. On average the uniform cloud measures 0.8 m (2.5 ft) high by 1.4 m (4.5 ft) wide at the turntable (typical model mounting location) vertical centerline. The turntable has automated $\pm 20^\circ$ angle-of-attack capability for vertically mounted models. Types of test articles which can be tested in the IRT include 2D and 3D airfoils, aspirated and non-aspirated inlets, subscale models of both fixed wing aircraft and rotorcraft, and instrumentation and sensors.

Calibrated Parameters

The IRT aerothermodynamic and icing cloud properties have been fully calibrated^{4,5}. The calibrated parameters of the tunnel are given in Table 1.

The airspeed given in this table is for an empty test section. Model blockage and model assembly drag coefficient affect maximum test section airspeed. For example, the maximum airspeed for 10% model blockage with 0.5% drag coefficient is approximately 325 knots. Turbulence intensity is measured with the spray bar air and water systems turned off. The introduction of spray bar air increases turbulence in the test section but no reliable measurement is available for this condition³.

The icing cloud calibration procedures employed at the IRT are discussed in a later section. Note from table 1 that full icing cloud calibrations are available for only the nominal FAR 25 Appendix C criteria. For icing clouds with median volume diameters less than 15 μm and greater than 40 μm , point calibrations at single liquid water content values are available. Other calibrated parameters, such as cloud uniformity and droplet distribution are available for the FAR 25 Appendix C criteria⁵.

Recent/Planned Improvement

Two recently implemented enhancements, a five component force balance and a sheet laser flow visualization capability, and a planned new spray bar system, add to the IRT's capability to assess aircraft icing in both the nominal FAR 25 Appendix C and the SLD environments.

The force balance measures aerodynamic loads on test models. A lower platform balance which is mounted in the test section turntable (fig. 2) measures two forces, a) parallel to the turntable centerline to 4448 N (1000 lbs), and b) normal to the turntable horizontal centerline to 44480 N (10000 lbs) and one moment about the turntable vertical centerline to 13558 N*m (10000 ft-lbs). The upper bearing balance mounted in the ceiling of the test section measures the force parallel to the turntable centerline to 4448 N (1000 lbs) and the force normal to the turntable centerline to 44480 N (10000 lbs). Loads transmitted to the lower and upper balances are measured and recorded independently, allowing users to analyze load reactions separately when a model is supported at both its upper and lower ends. As the turntable is rotated to vary angle-of-attack, the directions of the measured loads also rotate, remaining parallel to and normal to the turntable centerline. Because of the tunnel aerodynamic characteristics as noted in table 1, force balance measurements can be used to understand trends and evaluate the gross effectiveness of ice protection systems. Experimental measurements of the effects of ice accretion on airfoil aerodynamics should be performed in a dry air low speed wind tunnel with replicated or simulated ice shapes, acquired during an IRT icing test, attached to the wind leading edge.

A sheet laser flow visualization system was successfully used to illuminate organized flow patterns around a 3D wing tip model, using the icing cloud as the seeding material. The laser sheet is produced with a 15W argon-ion laser connected to a laser sheet generating optic head via a fiber optic cable. This system proved very useful in observing and measuring flow pattern changes during the ice accretion process and for visualizing before and after changes in tip and leading edge vortices occurring due to the ice accretion process. A possible future use for the sheet laser is gross screening of icing cloud uniformity via measurement of the laser sheet light intensity.

The description and capabilities of the planned new spray bar system for the IRT are found in table 2. Capabilities of note are a) step function type changes in the icing cloud liquid water content, made possible by the introduction of a second water supply header to the water spray nozzles and b) a decrease in time from less than 1 minute in the present system to approximately 2 seconds in the new system to achieve steady-state water flow rates at the spray nozzles, made possible by solenoid valve control at each nozzle. This latter capability

is manifested as the time to achieve a uniform icing cloud in the test section on the order of seconds as opposed to the present tens of seconds. The new system is scheduled to be on-line by April 1997.

II. SUPERCOOLED LARGE DROPLET TESTING

Icing Wind Tunnel Advantages & Challenges

The advantages of aircraft icing testing in an icing wind tunnel and the disadvantages / challenges have been documented previously⁶. The advantages of icing wind tunnel testing include icing cloud and temperature repeatability and controllability to within acceptable tolerances, demonstrated repeatability in ice accretions, the ability to closely observe the ice accretion process via a variety of imaging technologies⁷, and direct measurement of ice shapes via hand or laser tracing. The challenges associated with wind tunnel testing include achieving cloud uniformity covering much of the test section's cross sectional area, reproducing nature's wide range of LWC, droplet size spectra and MVD, accurate measurement of the icing cloud properties, and the requirement to conduct scaled testing if desired test variables are not achievable. The challenges associated with icing wind tunnel testing are exacerbated in creating a simulated supercooled large droplet icing cloud.

Icing Cloud Calibration

The IRT is fully calibrated for large portions of the FAR 25 Appendix C criteria where droplet MVDs range from 15 to 40 μm . For large droplet work to date, the calibration was extended at single liquid water contents for five discrete median volumetric diameters between 56 and 192 μm . Further calibrations in the SLD range will be planned and performed as necessary.

Calibration of the IRT includes five components⁵. The water spray nozzle flow coefficient (C_f) is established for all nozzles installed in the spray bar system. At the IRT, only those nozzles with a C_f within $\pm 5\%$ of the average C_f for all nozzles are selected for use. Tests are then performed in the IRT to establish icing cloud liquid water content, cloud uniformity, droplet median volume diameter, and droplet distributions or spectra.

LWC is measured directly by placing an icing blade at the center of the test section and measuring the ice accretion. Based on the accretion thickness (ΔS) and other variables including ice density (ρ_{ice}), collection efficiency of the blade (E_b), free stream velocity (V) and exposure time (t), and a unit conversion constant (C), the LWC can be calculated using the equation:

$$LWC = \frac{C \rho_{ice} \Delta S}{E_b V t} \quad (1)$$

Liquid water content uniformity is measured by ice accretion on 0.04 m (1½ in.) rotating cylinders. The cylinders are mounted vertically at 9 evenly spaced test section width-wise locations. Uniformity at discrete spatial (x,y) locations is stated as a percent of the central liquid water content and is determined by the following:

$$\frac{LWC(x,y)}{LWC_c} = \frac{C(x,y) - C_{pipe}}{C_c - C_{pipe}} \quad (2)$$

where C_{pipe} = circumference of the pipe, $C(x,y)$ = circumference of the iced pipe at location x,y, and C_c = circumference of the iced pipe at the test section central location.

To determine droplet size and spectra, two Particle Measuring System, Inc. aircraft type instruments are inserted in the tunnel. The Forward Scattering Spectrometer Probe (FSSP) measures droplets from 2 to 47 µm. The Optical Array Probe (OAP) measures droplets from 15 to 450 µm. From the measurements, particle count histograms and percent volume histograms are calculated. A data analysis computer program is used to calculate the Median Volume Diameter (MVD) from a combination of the droplet distributions from each of the two probes.

The point calibrations for the large droplet settings are shown graphically in figure 4. The only difference in measurement methodology from that described above for the reported values of LWC and MVD in this figure was the use of the rotating cylinders instead of the icing blade to measure LWC. In this case, the time constant from equation (1) is divided by 2. Figure 4 also depicts graphically the existing Appendix C criteria and the reported Roselawn conditions at the time of the ATR 72 accident. Because the water nozzles in the IRT spray bar system are set, in terms of number and locations, for Appendix C criteria, the relatively low LWCs associated with an SLD encounter is difficult to achieve. Figure 4 displays the challenge of simulating a wide range of icing conditions (MVDs from 15 to > 400 µm) in an icing wind tunnel.

Large Droplet Supercooling

Analysis and a controlled experiment confirmed that large droplets in the IRT are supercooled by the time they impinge on a test article installed in the test section⁸. A droplet trajectory/temperature prediction capability developed at Arnold Engineering Development Center was used to determine the effect of spray bar water temperature on droplet cooling. The results of this analysis indicated that initial spray bar water temperature has negligible effect on droplet temperature and that the droplets in the IRT do become supercooled.

An experiment using a Twin Otter 2D airfoil was conducted where spray bar water temperature was parametrically varied between 22 °C and 85 °C (72° F and 185° F). Ice shapes were traced (figure 5) and leading edge temperatures were measured via a leading edge thermocouple. As seen in the figure, repeatable ice shapes indicate an insensitivity to

initial spray bar water temperature. From the thermocouples, the spray was measured to cool the airfoil leading edge upon impingement, thus proving that the water droplets were at or approaching the static air temperature in the tunnel.

SLD Test Programs

NASA Lewis Research Center has conducted icing wind tunnel tests in the IRT for purposes of documenting the capability of the facility to produce icing clouds of supercooled large droplets, to further the understanding of ice accretion on airfoils similar to that of the ATR 72-210 in support of the National Transportation Safety Board (NTSB) accident investigation, to investigate several ice protection systems and sensors with specific applications to SLD encounters, and to perform parametric studies on commuter-class wing sections to quantify the effects of various parameters on ice accretion and ice shapes.

Several entries of note include the MS-317 airfoil tests and the NACA 23012 airfoil test. An MS-317 model, similar in shape to the ATR-72 wing, was tested in support of that accident investigation. A 2D model with 0.9 m (3 ft) chord and 1.8 m (6 ft) span (fig. 6) was tested and the effect of temperature and MVD on ice accretion and shape were determined by measuring ice accretion repeatability. The results were presented in a briefing to the NTSB in January 1995 and at the FAA Supercooled Large Droplet Icing (Phase II) Meeting in June 1995.

The NACA 23012 airfoil test objective was to conduct a parametric study of large droplets at near-freezing temperatures by varying temperature, droplet size, airspeed, angle-of-attack, flap setting and de-icer cycle time. The model was a full scale 2D wing section with a nominal 1.7 m (68 in.) chord at half span (fig. 7). Previously, a Twin Otter airfoil SLD entry had been completed with the identical test objective⁸. By testing the NACA 23012 2D model, airfoil specific effects on ice accretion could be measured and evaluated. Results from both entries indicate the sensitivity of ice accretion (ice ridge aft of the active ice protection system), to the above listed parameters, especially temperature.

Other SLD related tests conducted in the IRT included a Twin Otter airfoil with an Aerospace Safety Technologies, Inc. Thermion No-IceTM electrothermal ice protection system⁹ and a BF Goodrich impedance type detector for SLD ice detection. The results of the latter test entry are to be presented at the FAA International Conference on Aircraft In-flight Icing.

Prospects for Simulation of Large-Droplet Test Conditions by Scaling

As noted previously, icing tunnels have been designed to provide simulation of natural clouds which fall within the FAR 25 Appendix C envelope. Until recently, there was little interest in being able to simulate clouds with drops larger than 40 μ m median volume diameter; thus, the ability of existing tunnel spray systems to produce drops of around 200 μ m needs further calibration and study. One possible approach to obtaining test data in a tunnel for large-drop conditions might be to test with drops of, say, 40 μ m but with the model and conditions appropriately scaled to simulate the large-drop situation. This section will evaluate some

methods to scale for large-droplet tests.

Icing researchers have been faced with the problem of how to test models of reduced scale in icing tunnels since the 1940's. Through the years a number of methods have been developed which rely on matching the scale and full-size (or reference) values of various parameters deemed to be important to the ice accretion process. The objective of these scaling laws has always been to provide scaled test conditions such that tests with the sub-scale model would yield ice shapes geometrically similar to those which would have accreted if the full-size model were exposed to the desired icing conditions. The most complete analyses have been made by Charpin and Fasso¹⁰ and by Ruff¹¹. The Charpin and Fasso method was evaluated by Anderson¹². Ruff's method, also known as the AEDC method, has been tested by Ruff¹¹, by Bilanin and Anderson¹³ and by Anderson¹⁴ and has been widely used. A new method which requires that the Weber number be matched in addition to the parameters traditionally considered was proposed by Bilanin and Anderson⁴ in 1995. This method appears to provide more accurate simulation of ice shapes than the traditional methods, but it requires that the scale airspeed be greater than the speed to be simulated. The discussion here will use the AEDC method and the constant-Weber-number method to assess the reasonableness of simulating large-droplet icing encounters by performing scaled tests with small droplets.

The physical effect of changing droplet size is a change in the droplet trajectory. The trajectory is a function primarily of airspeed, model size and droplet size. Thus, to maintain the droplet trajectory while reducing droplet size it is necessary to change the model size or the airspeed. The approximate relationship which relates droplet size to the other parameters such that the droplet trajectory is matched is

$$\frac{\delta_S}{\delta_R} = \left(\frac{c_S}{c_R} \right)^{.62} \left(\frac{p_S}{p_R} \right)^{.24} \left(\frac{V_S}{V_R} \right)^{.38} \quad (3)$$

In this equation, δ is the droplet median volume diameter, c is a characteristic dimension such as the model chord, p is the static pressure, and V is the airspeed. The subscript S refers to scale and R to the reference conditions to be simulated. Equation (3) shows that to simulate an encounter with droplets of 200 μ m median volume diameter by testing with 40 μ m droplets, the model size must be reduced to $(40/200)^{1/.62} = .075$ of the reference model size if pressure and airspeed are matched to the reference conditions. Besides the fact that such extreme scaling of size has never been verified, very small models pose difficulties in making accurate ice-shape measurements. This example illustrates the basic difficulty of using a scaling approach to supercooled large droplet testing. It is evident from equation (3), however, that if the scale airspeed, V_S , is increased over the reference value, V_R , the model size scale need not be so extreme. In the following discussion, specific examples of scaling using the AEDC and the constant-Weber-number methods will be presented to explore the feasibility of scaling with reasonable model sizes.

Two scaling scenarios were chosen for study based on one reference condition. The reference condition included an airspeed of 200 mph, a droplet median volume diameter of 200 μ m and a liquid-water content of .5 g/m³. In the first, the scale tests were to be conducted with a droplet median volume diameter of 40 μ m, in the second, 50 μ m. Each scaling method was applied twice; the first calculations used the normal application of the method, then a modified approach was tried with the objective of producing a more reasonable (i.e, larger) required model scale.

Both scaling methods require that the scale and reference droplet trajectories, accumulation parameters and energy balance terms be matched. In additions, the constant-Weber-number method matches the Weber number. The Weber number is the ratio of the aerodynamic inertia forces to the surface-tension forces acting on droplets or on liquid water on the surface of the ice accretion:

$$We = \frac{\delta \rho V^2}{\sigma} \quad (4)$$

Here ρ is the water density and σ is the water-air surface tension. This equation shows that a reduction in the size of the droplet median volume diameter, δ , must be accompanied by an increase in airspeed, V , to maintain Weber number constant. However, by adding surfactant to the water spray the surface tension, σ , can be reduced for the scale tests, and the scale airspeed, V , need not be as large as for the scale case with unaltered water surface tension. Scaling results are given in Table 3 for the constant-Weber-number method both for unaltered water and for added surfactant.

Table 3 (a) gives the scaling results for the case of a 40 μ m scaled droplet size. The first column of numbers lists the reference conditions. The next two are the scaled conditions for the constant-Weber-number method first with an untreated water spray and then with surfactant added to the spray. Without the surfactant, the required scale airspeed is 447 mph and the scale total temperature is 44°F. Clearly, these results are unacceptable. When surfactant is added, the scale airspeed becomes a reasonable 304 mph and the total temperature 29°F. The scale model size with surfactant needs to be about 1/9th the reference size. Because the constant-Weber-number method has been validated with scales of no smaller than 1/3, it would be extremely risky to use this method to simulate large droplets without thorough testing and validation. In addition to the model size concern, there are the practical problems of the extremely short spray time (.8 min) and the inconvenience of adding surfactant to the spray.

Tests in the IRT have been performed with surfactant added in two ways¹³. In the first, a commercial liquid soap was added to the spray-bar supply tank so that the entire cloud had a reduced surface tension. However, some personnel entering the tunnel test section after such sprays complained of difficulty breathing, and the spray-bar system required extensive flushing to resume testing in a normal (untreated-water) mode. For tests in which

measurements were needed only in a local region, a single spray nozzle was set up with a water supply separate from the spray-bar system. Surfactant was added to this single-nozzle supply. The local ice shape which resulted from both methods was compared in reference 13 and found to be the same within normal repeatability variations. The single-nozzle approach requires no system flushing and does not fill the tunnel air with irritating vapor.

Two sets of results using the AEDC scaling method are also given in Table 3 (a). Unlike the constant-Weber-number method, the AEDC method permits the user to specify the scale airspeed. Two situations were considered: In the first, the scale airspeed was chosen to match the reference, and in the second, the scale airspeed was specified as 50% greater than the reference. The matched-airspeed approach was shown in reference 5 to result in scaled ice shapes which matched reference shapes fairly well if the scale model size was no smaller than half the reference. To simulate supercooled large droplets with a 40 μ m MVD, Table 3 (a) shows that the scale model size must be reduced to less than 1/10 the reference. In addition, the scale liquid water content required is more than three times the reference value. It is extremely unlikely that valid scaled tests can be conducted with conditions so different from the reference conditions.

For the second set of results for the AEDC method, the scale airspeed was specified as 50% greater than the reference. The higher airspeed permitted the model to be 30% larger than the constant-airspeed case, and the liquid-water content was now only about 50% higher than the reference. However, the scale model size required is still only 1/9 the reference, and these results are not acceptable scaling conditions.

The calculations were repeated with the scale droplet size relaxed to 50 μ m droplet median volume diameter. Table 3 (b) gives results for this scaling scenario; again, a 200 μ m MVD is to be simulated, and the other reference conditions from Table 3 (a) are the same. The larger scale droplet size permits testing with scale model sizes which are significantly larger than those shown in Table 3 (a), but models still need to be smaller than 1/6 reference size. This is still a much greater size reduction than has been found effective for either scaling method. Further tests with the constant-Weber-number method with surfactant addition are needed to resolve if this method can achieve the needed model size reductions.

At the present, no verified method exists to permit scale tests to be performed with small models and 40 μ m MVD sprays such that large-droplet (200 μ m MVD) sprays could be simulated. The very large model size reductions required make the results from any scaling approach extremely uncertain. Furthermore, the near-freezing temperatures sometimes associated with large-droplet icing cannot be scaled. Thus, to properly simulate encounters of large-droplet conditions in icing tunnels, calibrated sprays of supercooled large drops are essential.

III. SUMMARY

Several airfoils have been tested in the Icing Research Tunnel in simulated Supercooled Large Droplet conditions for the purposes of documenting facility capabilities and for performing

studies to determine the effect of various parameters on ice accretion and ice shape. The IRT reproduces ice shapes believed to occur in nature during SLD encounters. An ice ridge aft of the active ice protection system has been formed on all airfoils tested to date. This empirical data along with results of the limited calibrations for for icing clouds with droplet MVDs from 40 μm to 200 μm leads to the conclusion that the IRT is a viable test facility for assessing aircraft icing and for instrumentation/sensor development in simulated SLD icing conditions. At present, there is no verified method for performing tests with scaled models and "small" droplets ($\sim 40 \mu\text{m}$) such that large droplet spray could be simulated.

References

- 1) Soeder, Ronald H. and Charles R. Andracchio, "NASA Lewis' Icing Research Tunnel User Manual," NASA TM 102319, 1990
- 2) Private Correspondance, J. Dow letter to K. Yoeman, dated July 7, 1995
- 3) Reinmann, John J. and Robert J. Shaw, Richard J. Ranaudo, "NASA's Program on Icing Research & Technology," NASA TM 101989, 1989
- 4) Arrington, E. Allen and Mark T. Pickett, David W. Sheldon, "Flow Quality Studies of the NASA Lewis Resarch Center Icing Research Tunnel," NASA TM 106545, 1994
- 5) Ide, Robert F., "Liquid Water Content and Droplet Size Calibration of the NASA Lewis Resarch Tunnel," AIAA-90-0669, 1990
- 6) Reinmann John J. and Mark Potapczuk, "Icing Simulation: A Survey of Computer Models and Experimental Facilities"
- 7) Slater, Howard and Jay Owens, Jaiwon Shin, "Applied High-Speed Imaging for the Icing Research Program at NASA Lewis Resarch Center," NASA TM 104415, 1991
- 8) Miller, Dean R. and Gene Addy, Robert Ide, "A Study of Large Droplet Ice Accretions in the NASA Lewis IRT at Near-Freezing Conditions," AIAA-96-0934, 1996
- 9) Perkins, Porter and O. Hastings, William Rieke, "Thin, Lightweight, Electrothermal Ice Protection - New Technology Supplementing Existing Ice Protection," AIAA 96-0391, 1996
- 10) Charpin, Francois and Fasso, Guy, "Icing Testing in the Large Modane Wind Tunnel on Full Scale and Reduced Scale Models," L'Aeronautique et l'Astronautique, no.38, 1972. English Translation published as NASA TM-75373.
- 11) Ruff, Gary A., "Analysis and Verification of the Icing Scaling Equations," AEDC-TR-85-30, Vol 1 (Rev), March, 1986.
- 12) Anderson, David N., "Rime-, Mixed- and Glaze-Ice Evaluations of Three Scaling Laws," AIAA 94-0718, January, 1994.
- 13) Bilanin, Alan J. and Anderson, David N., "Ice Accretion With Varying Surface Tension," AIAA 95-0538, January, 1995
- 14) Anderson, David N., "Further Evaluation of Traditional Icing Scaling Methods," AIAA 96-0633, January, 1996

Table 1: IRT Calibrated Parameters

AEROTHERMO-DYNAMICS	MIN	MAX	VARIATION
Airspeed	22 m/s (43 knots)	192 m/s (373 knots)	0.002 to 0.011 Mach No. Variation
Flow Ang. (Pitch)		$\pm 1.5^\circ$	
Flow Ang. (Yaw)		$\pm 2.0^\circ$	
Turb. (Spray Off)	0.5%	1.0%	
Total Air Temp.	-30 °C (-22 °F)	4 °C (40 °F)	0.6 °C to 1.7 °C (1 °F to 3 °F)
ICING CLOUD			
LWC	0.2 g/m ³	>3.0 g/m ³	
MVD (Full Cal.)*	15 μ m	40 μ m	

(*) Point calibrations (single LWCs) for MVDs <15 μ m or >40 μ m

Table 2: IRT New and Existing Spray Bar System Comparison

CHARACTERISTIC / CAPABILITY	EXISTING SPRAY BAR SYSTEM	NEW SPRAY BAR SYSTEM
Number of Spray Bars	8 (Full Width)	10 (Full Width)
Water Spray Nozzles	Air-Assist Atomizing (IRT Standard & Mod 1 Nozzles)	Air-Assist Atomizing (IRT Standard & Mod 1 Nozzles)
Water Headers	1	2 Independent: Capability to do step change in LWC
Nozzle Flow Control	Via Supply Valve @ Water Header	Via Solenoid Valve @ Each Nozzle
Steady-State Water Flow Rate/Pressure Set Point	In < 60 sec. via Supply Valve @ Water Header	± 6895 N/m ² (± 1 psi) in 2 sec.
Spray Bar Trailing Edge	Faired/Fixed	Faired/Removable
Air Pressure	$6.9 (10)^4$ to $55.2 (10)^4$ N/m ² (10 to 80 psig)	$3.4 (10)^4$ to $55.2 (10)^4$ N/m ² (5 to 80 psig)
Air Flow	0.1 to 14.7 kg/min/bar (0.25 to 32.5 lbm/min/bar)	0.1 to 12.7 kg/min/bar (0.25 to 32.5 lbm/min/bar)
Water Pressure	$6.9 (10)^4$ to $227.5 (10)^4$ N/m ² (10 to 330 psig)	$6.9 (10)^4$ to $227.5 (10)^4$ N/m ² 10 to 330 psig
Water Flow Rate	$3.0 (10)^{-4}$ to $1.0 (10)^{-2}$ m ³ /min/bar (0.08 to 2.64 gal/min/bar)	$3.0 (10)^{-4}$ to $1.0 (10)^{-2}$ m ³ /min/bar 0.08 to 2.64 gal/min/bar

Table 3. Assessment of Scaling for SLD

(a) 40 μ m Scaled Drop Size

Parameter	Reference Conditions	Scale Conditions			
		Constant- <i>We</i> Method		AEDC Method	
		Untreated Water	Surfactant Added	$V_s = V_r$	$V_s = 1.5 V_r$
chord, in	36	5.5	4.2	3.1	4.0
static temperature, °F	15	8.2	12.8	15	12.9
total temperature, °F	22.2	44.0	29.3	22.2	29
airspeed, mph	200	447	304	200	300
MVD, μ m	200	40	40	40	40
LWC, g/m ³	.5	.314	.954	1.702	.796
spray time, min	18.4	2.00	.75	.46	.86
spray surface tension, dyne/cm	65	65	30	65	65

(b) 50 μ m Scaled Drop Size

Parameter	Reference Conditions	Scale Conditions			
		Constant- <i>We</i> Method		AEDC Method	
		Untreated Water	Surfactant Added	$V_s = V_r$	$V_s = 1.5 V_r$
chord, in	36	7.1	5.6	4.4	5.7
static temperature, °F	15	9.9	13.6	15	12.9
total temperature, °F	22.2	38.6	26.8	22.2	29.0
airspeed, mph	200	400	272	200	300
MVD, μ m	200	50	50	50	50
LWC, g/m ³	.5	.413	.965	1.43	.669
spray time, min	18.4	2.20	1.09	.78	1.44
spray surface tension, dyne/cm	65	65	30	65	65

Icing Research Wind Tunnel

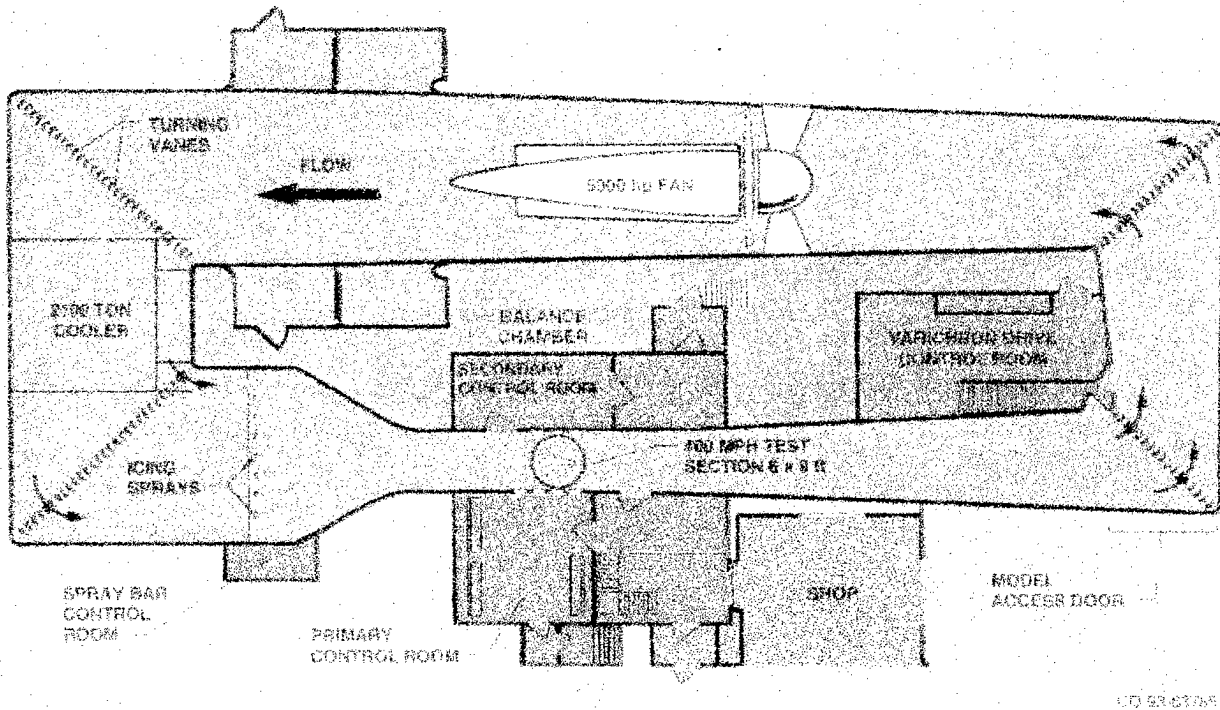


Figure 1: Icing Research Tunnel Schematic

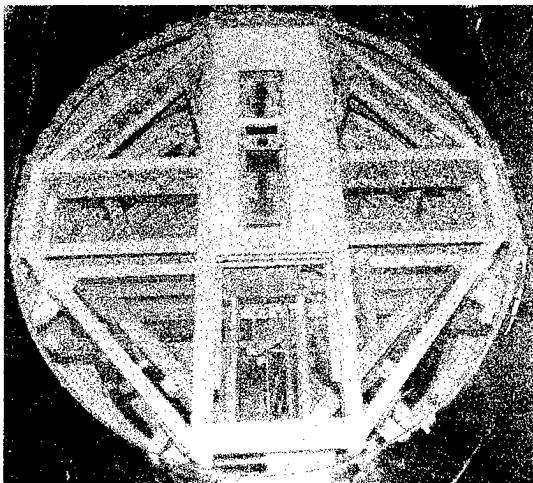


Figure 2: IRT Force Balance Internal Mechanism; Lower Balance Only



Figure 3: Sheet Laser image of tip vortex from 3D model

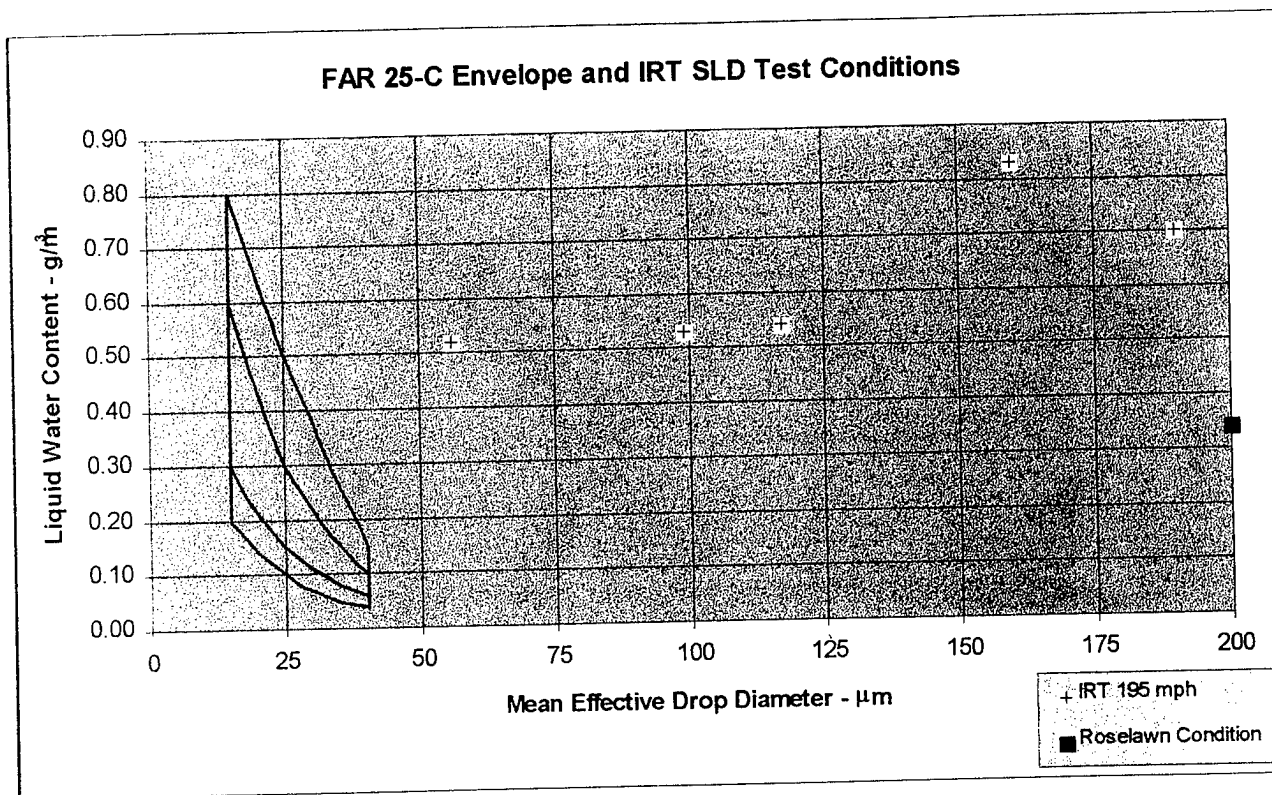


Figure 4: IRT Supercooled Large Droplet "Point" calibrations from 56 to 192 μm

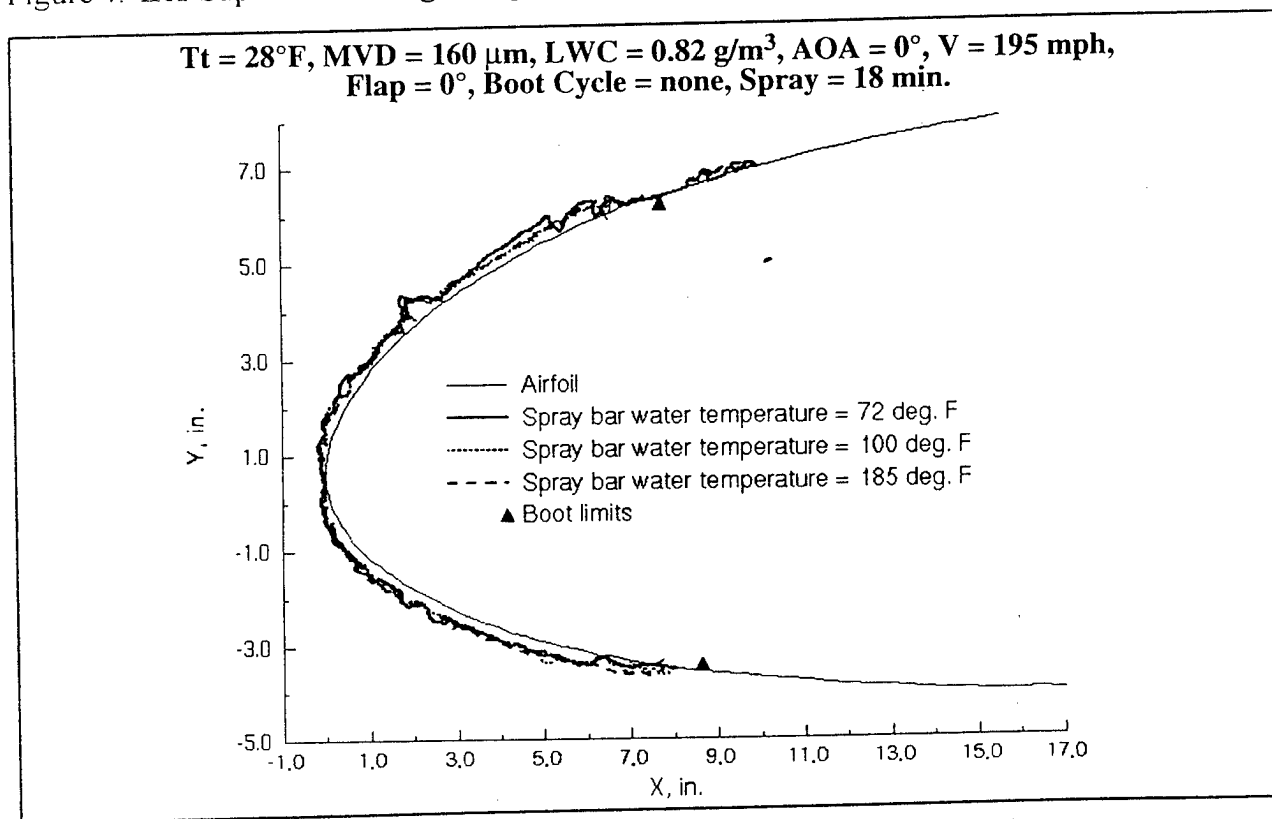


Figure 5: Supercooled Large Droplet Ice Shape Comparison Showing Ice Accretion Repeatability of the Icing Research Tunnel

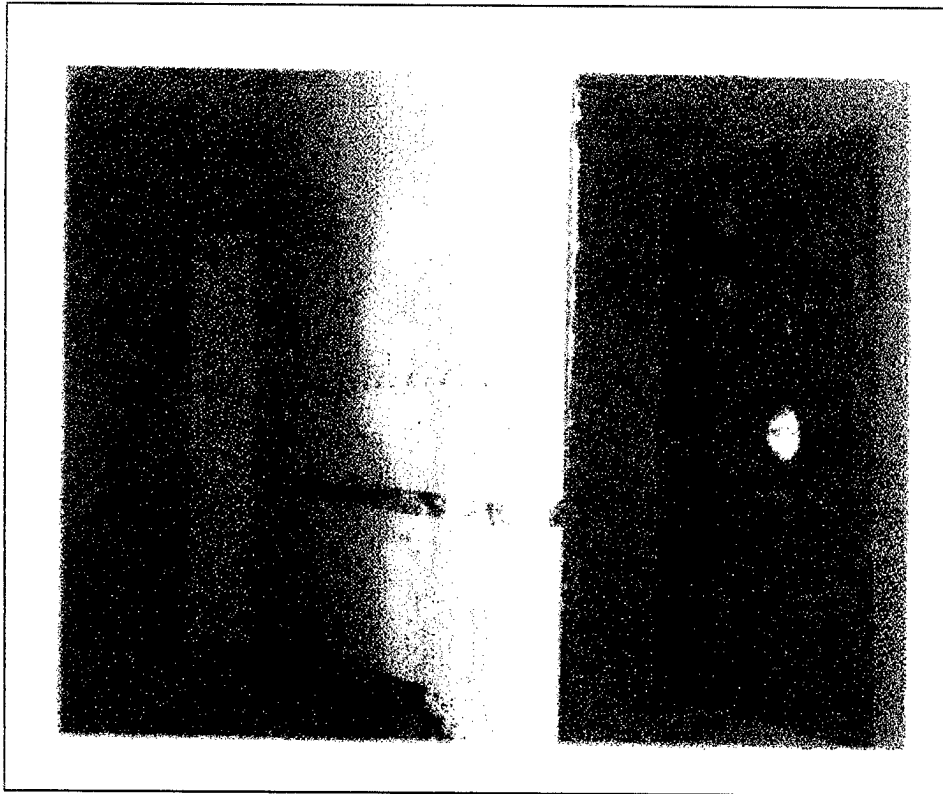


Figure 6: The MS 317 Airfoil in the IRT Test Section for Ice Accretion Repeatability Investigations

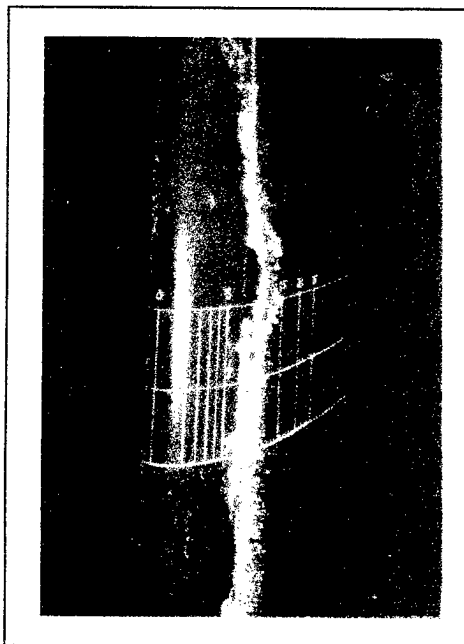


Figure 7: The NACA 23012 Airfoil with a representative ice ridge aft of the active ice protection system

A STUDY OF LARGE DROPLET ICE ACCRETION IN THE NASA LEWIS IRT AT NEAR-FREEZING CONDITIONS; PART 2

Harold E. Addy, Jr.
Dean R. Miller
NASA Lewis Research Center

Robert F. Ide
Army Research Laboratories
Vehicle Propulsion Directorate
NASA Lewis Research Center

Abstract

Results of experiments designed to determine the effects of large droplet ice accretion on a NACA 23012 wing section are presented. Using primarily an icing condition with a median volumetric diameter droplet size of $160\mu\text{m}$ and a liquid water content of 0.82 grams per cubic meter, the effects of various air temperatures, angles of attack, and de-icer boot cycle interval times on ice accretion were studied. Measurements of aerodynamic performance penalties due to the ice accretions were made. Results were also compared with similar tests conducted with a Twin Otter wing section in Part 1 of this study. The form of the ice from the large droplet cloud varied as a function of air total temperature; particularly at the near-freezing temperatures of 28°F to 34°F . Changing boot cycle interval time did not prevent formation of an ice ridge. The most detrimental aerodynamic effects occurred at an air total temperature of 28°F .

Introduction

This investigation is part of a series of experimental large droplet icing tests conducted in NASA Lewis' Icing Research Tunnel (IRT) since late 1994¹. Large droplet icing conditions are defined as icing clouds composed of water droplets which have a distribution of droplet sizes ranging from 40 to $400\mu\text{m}$ in terms of Median Volumetric Diameter (MVD). The more common icing clouds consist of droplet distributions in the 15 to $40\mu\text{m}$ MVD range. These IRT tests constitute the first comprehensive effort to study the effects of large droplet ice accretions on aircraft at near-freezing temperatures.

The atmospheric conditions which result in the creation of large droplet icing clouds are relatively rare. However, there is growing evidence that the frequency of aircraft encounters with large droplet icing clouds is higher than expected. This is of particular concern since the hazard to an aircraft flying in these conditions is also greater than what has been anticipated and is potentially catastrophic.²

Earlier portions of this study found that aircraft ice formed from large droplet icing clouds accretes further aft on aircraft surfaces than that formed from the more common 15- $40\mu\text{m}$ droplet icing clouds.¹ This is primarily due to the fact that large droplets impinge further aft on the airfoil surfaces than do small droplets. A significant amount of runback and secondary impingement has also been observed in these tests. Secondary impingement is a term used to describe the action of unfrozen water droplets blowing off

the accreted ice, then impinging on the model further downstream. Whether this is characteristic of the large droplets or is due to high water loading has not been determined at this time.

In Part 1 of this study,¹ it was found that a significant amount of ice from a large droplet icing cloud can accrete aft of conventional ice protection equipment on an airfoil. If the ice protection equipment is activated during the icing encounter, only the ice on the protected portion of the airfoil is removed leaving a forward facing ridge of ice aft of the protected area. When the ice protection system is not activated during the encounter and the air is at a near-freezing temperature, ice will accrete until a large portion of it is blown off the leading edge by aerodynamic forces. The residual ice aft of the leading edge, again, has a forward facing ridge. These scenarios were studied in Part 1 of this investigation. In that part of the study, a Twin Otter wing section was mounted in the IRT and subjected to an array of large droplet icing conditions including variations in temperature, airspeed, droplet size, angle of attack, pneumatic deicing boot cycle interval, and flap setting. Specific findings were:

- ◇ An ice ridge formed aft of the active portion of the deicer boot for every experimental test run in which ice was accreted. The location, height, and spanwise extent of the ridge varied considerably. This variability was caused by random shedding of the ice.
- ◇ Large droplet ice accretions were found to be sensitive to changes in total temperature. As the temperature was varied, the ice ridge reached a relative maximum at a total temperature of 28°F for 125 mph and of 30°F for 195 mph.
- ◇ An increase in droplet size moved the impingement limits further aft on the airfoil. In addition, runback and secondary impingement accreted ice aft of the impingement limits on the airfoil.
- ◇ Increasing the angle of attack caused more ice to accumulate on the pressure surface and less ice on the suction surface.
- ◇ As flap setting was increased, the extent and amount of ice accretion on the suction surface decreased.
- ◇ Variation in the boot cycling time did not appear to have a significant effect on the residual ice accretion.

Part 2 of this investigation is described herein. Tests similar to those conducted with the Twin Otter in Part 1 were carried out using a NACA 23012 airfoil to expand the knowledge base about large droplet ice accretion and to help identify airfoil specific effects.

Facility and Model Description

Icing Research Tunnel

The NASA IRT is a closed loop refrigerated wind tunnel.³ The test section is 6 feet high and 9 feet wide and contains a turntable assembly which allows for model angle of attack changes. A 5000 hp fan provides airspeeds up to 400 mph (empty test section). The refrigeration heat exchanger can control the air temperature from -40°F to +40°F.

Icing Cloud Spray System

The spray system that generates the icing cloud in the IRT is composed of eight spray bars containing a total of ninety-five spray nozzles. The spray bars are located in the settling chamber upstream of the test section. The spray nozzles used are air-assist type atomizers.³ Two different sets of nozzles are currently used in the IRT spray system and are designated Standard and Mod-1. The Mod-1 nozzles were used for the large droplet tests described in this report because they produce liquid water content(LWC) levels closer to those expected for large droplet icing clouds found in nature.

A droplet size of 160 μ m MVD was used to simulate a large droplet icing cloud during most of the test runs in this part of the study. This droplet size is outside the normal operating envelope of 10-40 μ m MVD for the IRT. In order to simulate a large droplet icing cloud, special tests were run in the tunnel to calibrate the cloud for droplet size distribution and for cloud uniformity. Results of these tests indicated that the 160 μ m cloud generated in the IRT would be the best to simulate large droplet icing condition.¹ However, time did not permit calibration of the 160 μ m MVD cloud at various LWC's at a given airspeed. Therefore, the effect of varying LWC was not investigated in this study.

Model

The test model was a 6 foot span, single element, NACA 23012 wing section which was mounted vertically in the IRT test section. It had a chord length which varied from 73.8 inches at the floor to 65.2 inches at the ceiling of the tunnel and was 68.6 inches at the model centerline. The leading edge of the model was outfitted with a full span pneumatic de-icer boot extending to approximately 6% chord on the suction surface and to 11% chord on the pressure surface. A photograph of the test model is shown in Fig. 1 while Fig. 2 shows the airfoil's cross section.

Parametric Investigation

As in Part 1, a primary objective of these tests was to study how parameters such as air temperature, droplet size, angle of attack, airspeed, and pneumatic deicer boot cycle time affect large droplet ice accretions. Table I lists the parameter values which were investigated.

Not all possible combinations of parameters were tested. To make more effective use of the test time, a particular value for each parameter was selected and designated as an anchor point value. The anchor point values were selected based upon representative flight operating conditions as well as knowledge of large droplet ice accretions which formed at near-freezing conditions. While the effects of one parameter were being investigated by varying it, the other parameters were held constant at their anchor point values. The anchor point values are given in Table I.

The parameter array values vary slightly from those for the Twin Otter test matrix as reported in Ref. 1. However, many identical conditions were used with the NACA 23012 so that direct comparisons could be made. Several different values (24, 26, 35, 37°F) were added to the air total temperature array because it was found to be the dominant

parameter in determining the characteristics of the ice accretion. This allowed the problem to be more thoroughly bounded. Two values (1.3° , 3.9°) were added to the angle of attack array to examine conditions typical of flight for this type airfoil. The value of 163 mph was dropped from the airspeed array because speed was found to have little effect on the ice accretion. The values for the droplet size and for the boot cycle interval time arrays remained the same as in the Twin Otter tests.

Ice Shape Repeatability

Since an important aspect of these tests is to document the ice shapes formed under the various parameters in this study, the repeatability of the ice shapes is significant. The capability of the IRT to accurately reproduce icing clouds is well established. Previous studies, including Part 1 of this effort, have documented this capability.¹⁴

Even though the icing cloud in the IRT remains generally consistent and repeatable from test run to test run, it was discovered in Part 1 of this work that the ice shape formed due to a large droplet icing cloud at near freezing conditions is random and not repeatable in a quantitative way. The chordwise location, height, and spanwise extent and position of the ridge varied from run to run under icing cloud conditions intended to be the same. This was found to be primarily due to the random manner in which residual ice remained on the model after activation of the ice protection system or after an aerodynamically induced self shed. Random ice shedding can also be expected for small droplet ice accretions at near-freezing conditions, however, because very little small droplet ice forms aft of the ice protection system, the residual ice left after boot activation is negligible.

This random shedding was observed during Part 2 of this work. At the same icing cloud conditions, the height, chordwise location, and spanwise extent and position of the ridge varied considerably for five separate test runs at the anchor point conditions. Figure 3 shows profiles of the ice remaining on the model for these test runs. All of these profiles were traced at the centerline of the model. It should be noted that there was more variability in the ice shape on the suction(upper) surface than on the pressure(lower) surface. On the pressure surface, the ridge usually began at the edge of the active portion of the boot (10% chord) and extended aft to 15% chord where the composite leading edge of the model intersected with the aluminum skin. The aluminum skin covered the aft 85% chord of the model. Some ice accreted on the model just aft of this intersection, most likely due to secondary impingement. On the suction surface, the ridge begins at some random point between 6% and 9% chord. The active portion of the boot ended at approximately 5% chord. Also, the ridge height can be seen to have varied considerably from run to run.

Temperature Effect

As in the previous large droplet study with the Twin Otter wing section, the total temperature of the air was found to have a very strong effect on the NACA 23012 ice accretion. For this large droplet investigation, tests were run at total temperatures from 5°F to 37°F while holding the other parameters constant at their anchor point values. The temperature of 37°F was chosen to isolate the upper limit where no ice accretion formed,

while the 5°F temperature represented the lowest temperature at which the large droplet icing condition is believed to exist in nature.⁵

The effect of total temperature on NACA 23012 ice accretions was essentially the same as that observed with the Twin Otter wing section. At 37°F, all the impinging water ran back to the trailing edge and was blown off the model. At 34°F, less runback was noted and ice formed. When the ice formed, there was a distinct ridge just after the active portion of the boot on both the suction and pressure surfaces. The ice protection system was activated at three minute intervals for all of these test runs.

The effect of temperature on NACA 23012 large droplet ice accretions is illustrated in Fig. 4. Photographs of suction surface ice accretions are presented for total temperatures ranging from 34°F to 5°F. These photographs were taken at the conclusion of the eighteen minute icing spray. The ice protection system had last been activated at fifteen minutes into the spray, therefore, the photos show the condition of the ice accretion just prior to another pneumatic boot activation. The markings on the model indicate percent chord of the airfoil. The boot ends at 6% chord.

Perusal of Fig. 4 reveals that at the warmer temperatures (30°F to 34°F), the ice ridge behind the active portion of the boot had a tendency to randomly self shed. However, as the total temperature was decreased below 30°F, the ice ridge appeared to "harden" and become more resistant to self shedding. Also, these photos show that as the temperature was successively decreased more ice froze on the boot surface. At 34°F, a layer of ice is evident beginning at the 5% chord line, while at 28°F, the ice layer appears to have moved forward to the stagnation line. This trend suggests that as the temperature was decreased more water froze forward on the boot, thereby reducing the amount of runback water available to "feed" the development of the ice ridge. Ice thickness measurements at the stagnation line corroborated this trend, because the thickness of ice on the boot increased as the temperature decreased.

Based on the above result, one would surmise that the ice ridge height would lessen as the temperature was decreased. This was not the case. In fact, for temperatures below 30°F, substantial ice ridges developed aft of the active portion of the boot. The largest ice ridges occurred at the colder temperatures of 24°F through 28°F. Ice ridge heights of over 1 inch were observed on the suction and pressure surfaces at these temperatures. Clearly, runback is not the only mechanism affecting the development of the ridge. It is possible that increased structural strength at the colder temperatures facilitates the ice ridges growth farther into the flow, which then has the effect of increasing the collection efficiency of the ridge. Table II lists ice ridge heights and ice thickness at the stagnation point as well as calculated freezing fraction for the above temperatures.

Angle of Attack Effect

Tests were run at AOA's of -2°, 0°, 1.3°, 2°, and 3.9° while the other parameters were held at their anchor point values. As the AOA increased, the extent of ice aft of the boot on the pressure surface increased significantly. The front of the ridge on this surface was

usually located at the end of the active boot, although there were some variations due to random shedding.

On the suction surface, as the AOA increased, the aft edge of the ice accretion moved forward and the total amount of ice decreased. Inspection of the photographs and tracings showed that there can be a high ridge at a high AOA condition, but that it is due to a random lump of ice stuck to the surface as opposed to a ridge with some spanwise extent. In general, a ridge is less likely to form because less ice accumulates. These trends were similar to those observed in the Twin Otter tests.

Boot Cycle Effect

The time interval between pneumatic boot activation was referred to as boot cycle. Three different boot cycle times were used: forty-two seconds, three minutes, and six minutes. For comparison purposes, a full, eighteen minute spray was run with no boot activation. As was found in the Twin Otter model portion of the study, the total air temperature of 32°F allows ice to form which is relatively weak and is prone to self shedding. A ridge formed on both the pressure and suction surfaces for all the boot cycle cases at 32°F. For the cases with boot activation, the ridges formed in the vicinity of the edge of the active portion of the boot. In the no boot cycle run, the ridges were very random in location due to the random self shedding of the ice. No further correlation between ridge and boot cycle was observed at this temperature.

To more thoroughly investigate the effects of various boot cycle times, the above tests were repeated at air total temperatures of 28°F and 5°F. At these temperatures, no self shedding of the ice was observed. Photos of the ice at 28°F are shown in Fig. 5a and the corresponding centerline ice tracings are shown in Fig. 5b. These photos and tracings were taken after eighteen minutes of icing just before the next boot activation was to occur. At 28°F, the ridges on the suction surface were similar for all three time intervals. However, on the pressure surface, no distinct ridge formed for the forty-two second interval run although significant ice did accrete aft of the boot. For the three and six minute intervals, a relatively high ridge formed on the pressure surface at the edge of the active portion of the boot. At 5°F, as the boot cycle interval increased, it was observed that the amount of residual ice left on the boot also increased. The forty-two second interval run left very little residual ice on the protected area. Both the three and six minute intervals left considerable residual ice. A photo of the three minute boot cycle case at 5°F was shown in Fig. 4h.

Aerodynamic Performance

In addition to documenting the characteristics of the ice formation on the model during an icing encounter, measurements of the change in lift and drag for the wing section due to the ice were also made. These changes in lift and drag were made using an external force balance system which had a significant limitation when used in this application. It measures aerodynamic effects over the entire wing section while the IRT's large droplet icing cloud does not uniformly cover the entire span of the model. In fact, the cloud has a uniform liquid water content at an MVD of 160µm for about a one foot span at the

model's center. The cloud tapers off in LWC over a significant length at each end of the wing section. Definitive, absolute measurements are difficult to make under these circumstances.

Despite this limitation, the aerodynamic performance data can be helpful if it is interpreted cautiously. Figure 6a shows the change in lift coefficient for the wing section as a function of air total temperature. All of the data points shown as diamonds were run using a three minute boot cycle interval with the model set at a 0° angle of attack. These data suggested that air total temperature had a large effect on the ice accretion and the resulting decrease in aerodynamic performance. The highest lift loss was observed at an air total temperature of 28°F . Figure 6b shows the change in drag coefficient for the same set of test runs; also plotted as a function of air total temperature. Here too, air total temperature is shown to have a significant effect on the resulting aerodynamic performance with the highest drag increase also occurring at an air total temperature of 28°F .

The square in Fig. 6a indicates the highest measured lift loss. This resulted from the large droplet ice accretion at 28°F with no boot cycle. The drag increase measured for this ice shape is shown in Fig. 6b, also with a square. It is of interest to note that the large droplet ice accretion which results in the highest measured lift loss does not also result in the highest drag increase.

Summary of Results

A parametric study of large droplet ice accretions at near freezing temperatures was conducted in the NASA Lewis IRT using a single element NACA 23012 wing section. Parameters studied were air total temperature, angle of attack, and boot cycle interval. In summary, the results of this portion of the study were:

- ◆ Similar to the Twin Otter wing section tests, an ice ridge formed aft of the active portion of the de-icer boot for nearly every test run. The location, height, and spanwise extent of the ridge varied due to random shedding of the accreted ice.
- ◆ Again, similar to the Twin Otter results, the large droplet ice accretions were found to be sensitive to changes in total temperature. At temperatures of 30°F to 34°F , the ice aft of the active boot self shed regularly. At temperatures of 24°F to 28°F , the ice aft of the active boot did not shed as readily and resulted in the highest ridges.
- ◆ Increasing the angle of attack caused more ice to accumulate on the pressure surface and less on the suction surface. This was also found during the Twin Otter tests.
- ◆ Variation in boot cycling time did not have an effect on the residual ice at a total air temperature of 32°F . At 28°F and 5°F , the forty two second boot cycle interval was more effective at removing ice, especially on the pressure surface. However, a ridge still formed on the suction surface for all temperatures and boot cycle intervals. Boot cycling was investigated only at 32°F with the Twin Otter model and was found to have no effect on the ridge.
- ◆ The effect of large droplet ice accretion on aerodynamic performance was measured for a number of test runs with the NACA 23012 model. The air total temperature of 28°F produced both the greatest lift loss and drag increase. However, the greatest lift

loss was observed for a 28°F case for which the boot was not cycled, while the greatest increase in drag occurred for a 28°F, three minute boot cycled case.

References

1. Miller, D.R., Addy, H.E., and Ide, R.F., "A Study of Large Droplet Ice Accretions in the NASA Lewis IRT at Near-Freezing Conditions", AIAA Paper No. 96-0934, Jan. '96.
2. Ashenden, R., Lindberg, W., and Marwitz, J., "Two-Dimensional NACA 23012 Airfoil Performance Degradation By Super Cooled Cloud, Drizzle, and Rain Drop Icing", AIAA Paper No. 96-0870, Jan. 1996.
3. Soeder, R.H., and Andracchio, C.R., "NASA Lewis Icing Research Tunnel User Manual", NASA Tech. Memorandum 102319, June 1990.
4. Shin, J. And Bond, T.H., "Repeatability of Ice Shapes in the NASA Lewis Icing Research Tunnel", Journal of Aircraft, Vol. 31 No. 5 pp. 1057-1063, Sept.-Oct. 1994.
5. Jeck, R., "Representative Values of Icing Related Variables Aloft in Freezing Rain and Freezing Drizzle", AIAA Paper No. 96-0930, Jan. 1996.

Table I. Parameter Values for Large Droplet Study

Total Temperature, °F	0, 5, 24, 26, 28, 30, 32, 34, 35, 37
Droplet Size, μm (MVD)	40, 99, 160
Airspeed, mph	125, 195
Angle of Attack, degrees	-2, 0, 1.3, 2, 3.9
Boot Cycle Interval, min.	none, .7, 3, 6
Anchor Point Conditions	32°F, 160 μm , 195 mph, 0° AOA, 3 min. Boot cycle, 18 min. spray

Table II. - Measured Ice Thickness And Calculated Freezing Fraction on NACA 23012 Wing Section

		Ice Thickness, (inches)						
Run #	Total Temp. (°F)	Pressure Surface Ridge		Leading Edge		Suction Surface Ridge		Freezing Fraction
		max	min	max	min	max	min	
403	34	0.04	0.03	0.0	0.01	0.0	0.03	
404	33	0.25	0.08	0.05	0.56	0.04	0.59	
405	32	0.50	0.43	0.06	0.41	0.05	0.47	.07
406	30	0.91	0.84	0.12	0.46	0.07	0.95	.10
407	28	1.48	1.12	0.14	0.83	0.13	1.07	.14
408	26	0.53	0.38	0.19	0.64	0.14	1.14	.17
409	24	1.31	0.81	0.17	1.3	0.15	1.9	.20

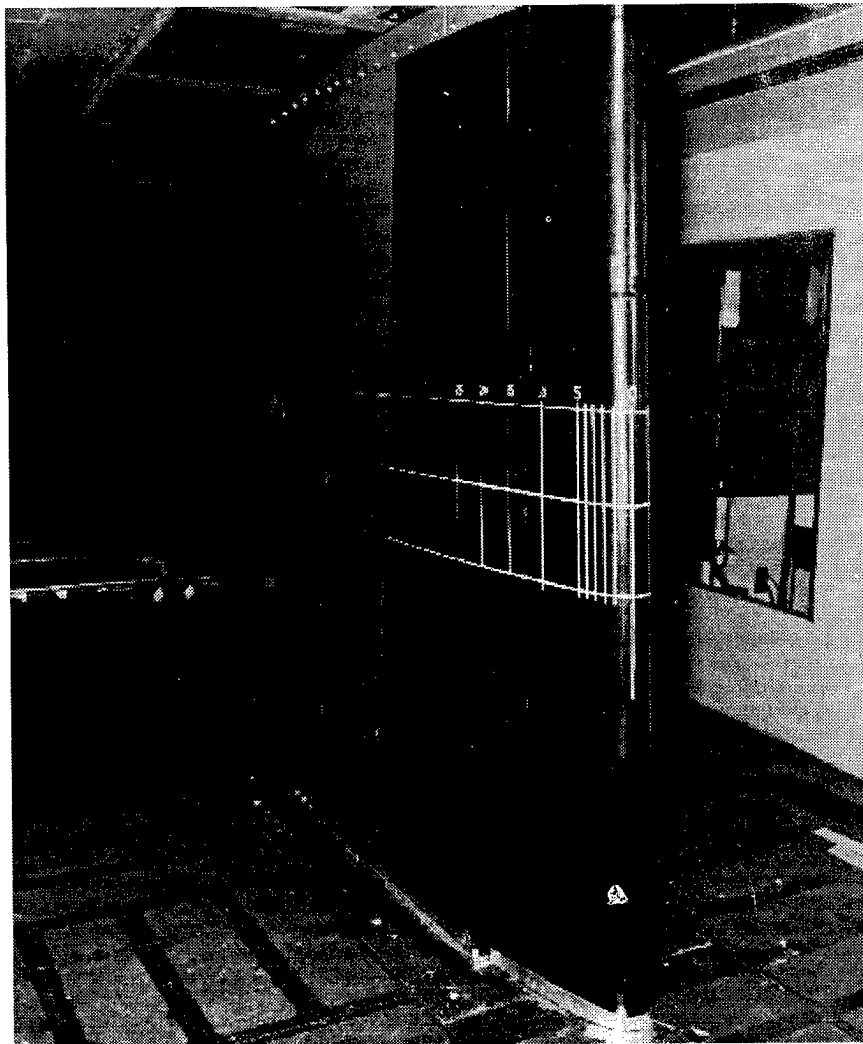


Figure 1 – NACA 23012 wing section installed in Icing Research Tunnel.

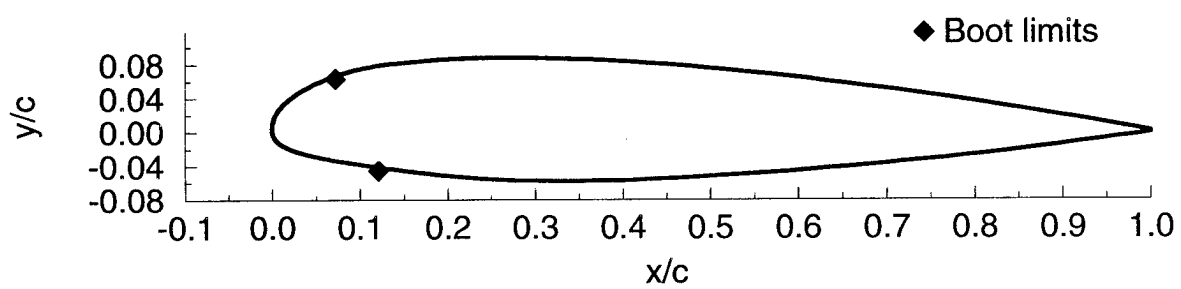


Figure 2 – NACA 23012 airfoil.

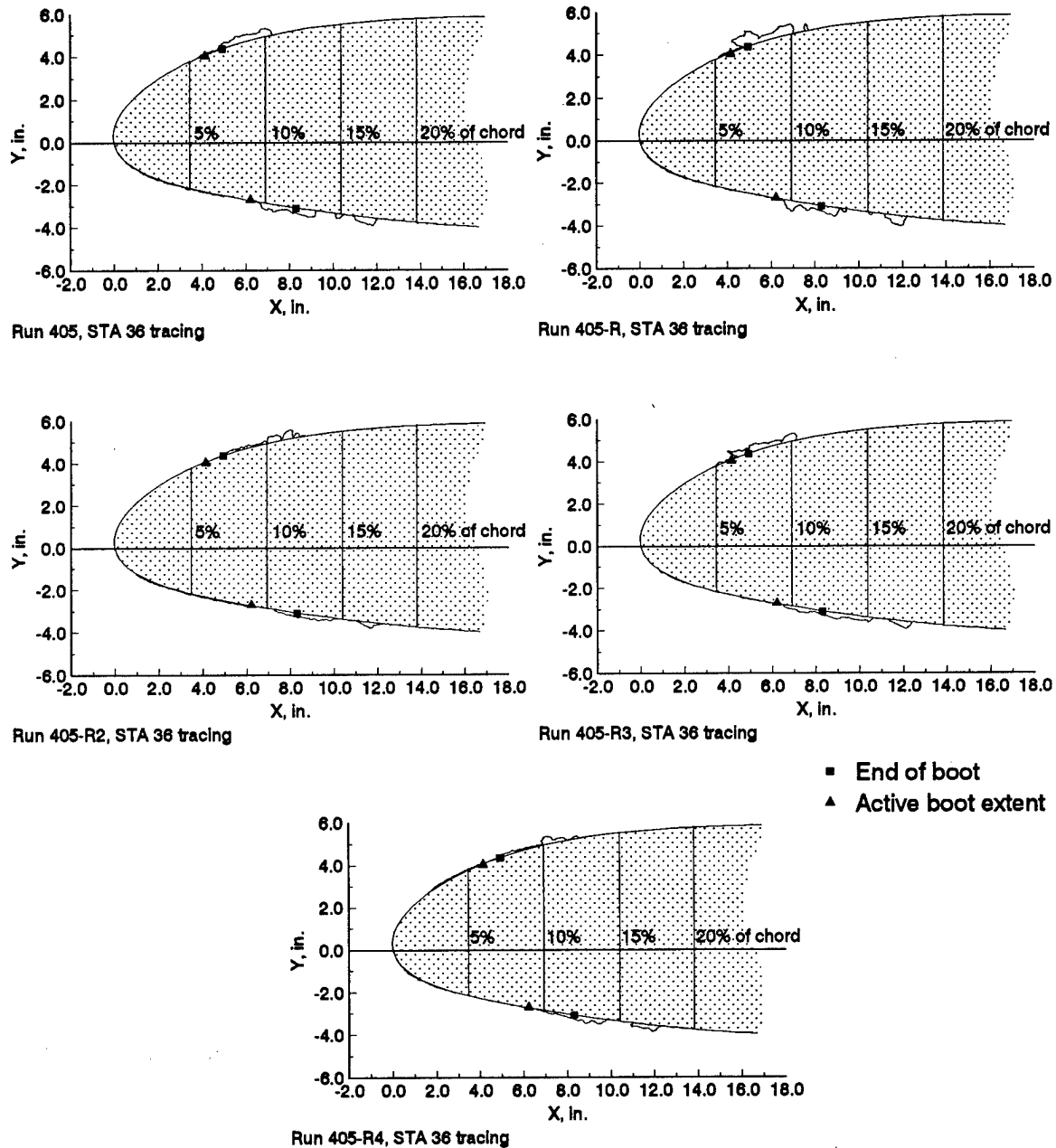
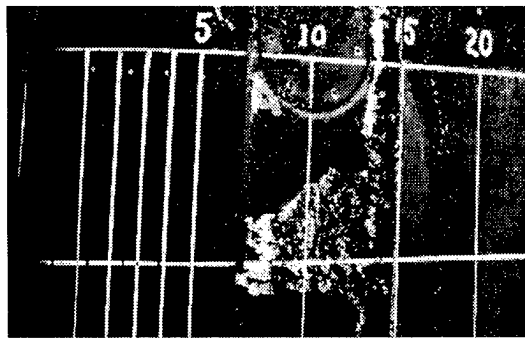
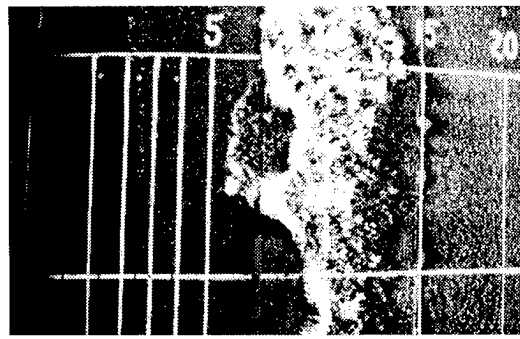


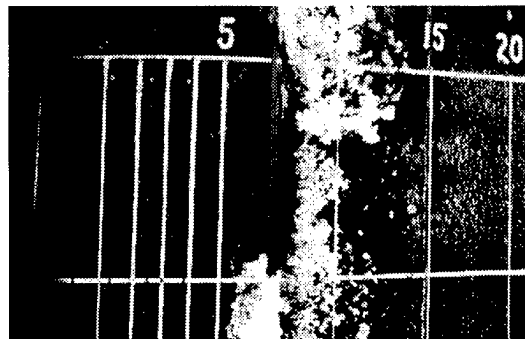
Figure 3 - Run-to-run repeatability of large droplet ice accretions.
 ($T_t = 32^\circ\text{F}$ (0°C), $MVD = 160 \mu\text{m}$, $LWC = 0.82 \text{ g/m}^3$, $AOA = 0^\circ$,
 $V = 195 \text{ mph}$ (170 kts), Boot Cycle = 3 min., Spray = 3 min.)



a). Run 403, $T_t = 34^\circ\text{F}$ (1.1°C)



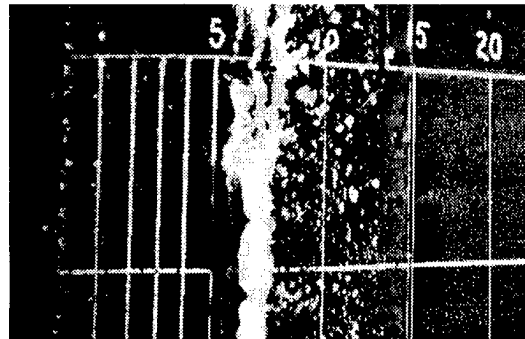
b). Run 404, $T_t = 33^\circ\text{F}$ (0.6°C)



c). Run 405, $T_t = 32^\circ\text{F}$ (0°C)



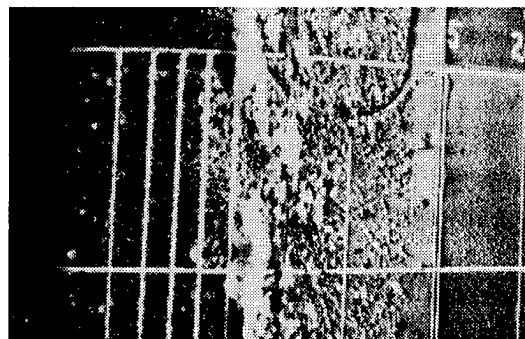
d). Run 406, $T_t = 30^\circ\text{F}$ (-1.1°C)



e). Run 407, $T_t = 28^\circ\text{F}$ (-2.2°C)



f). Run 408, $T_t = 26^\circ\text{F}$ (-3.3°C)

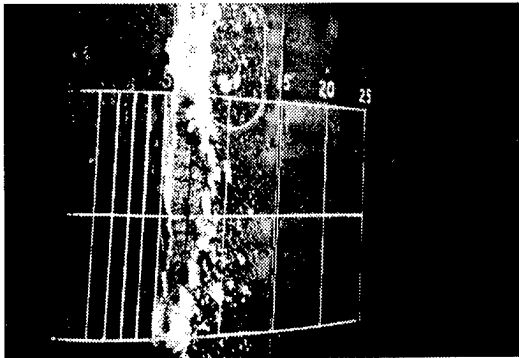


g). Run 409, $T_t = 24^\circ\text{F}$ (-4.4°C)

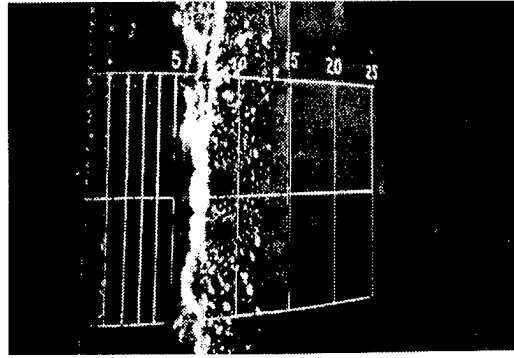


h). Run 417, $T_t = 5^\circ\text{F}$ (-15°C)

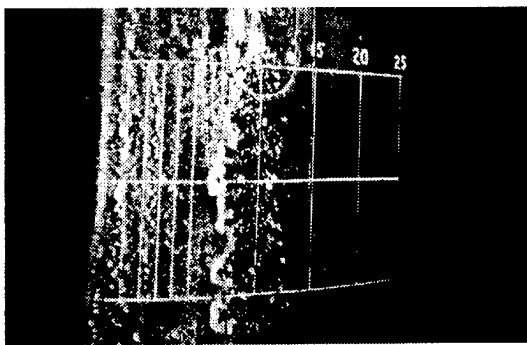
Figure 4 – Effect of total temperature on large droplet ice accretion.
 ($V = 195$ mph (170 kts), $MVD = 160\ \mu\text{m}$, $LWC = 0.82\ \text{g/m}^3$, $AOA = 0^\circ$,
 Boot Cycle = 3 min., Spray = 18 min.)



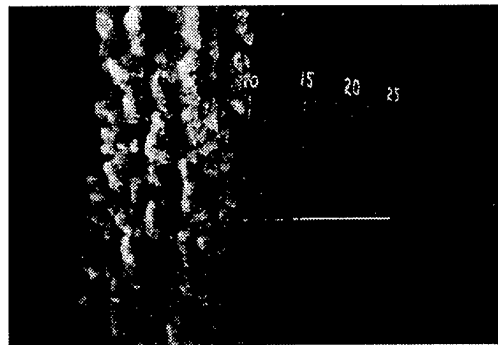
Run 413, Boot Cycle = 42 sec.



Run 407, Boot Cycle = 3 min..

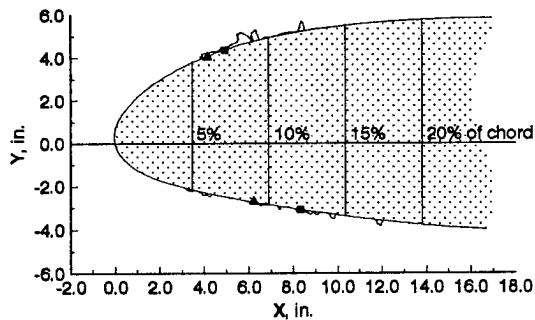


Run 414, Boot Cycle = 6 min..

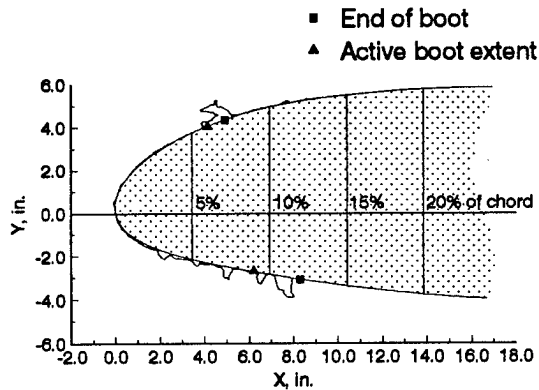


Run 416, No Boot Cycle

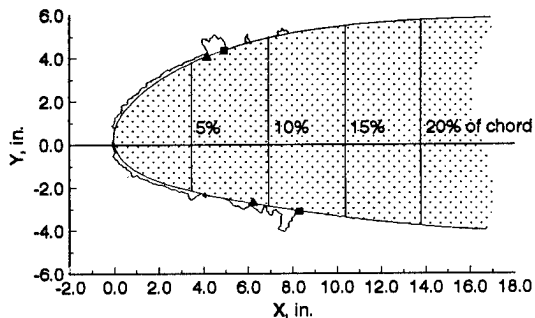
a). Photos



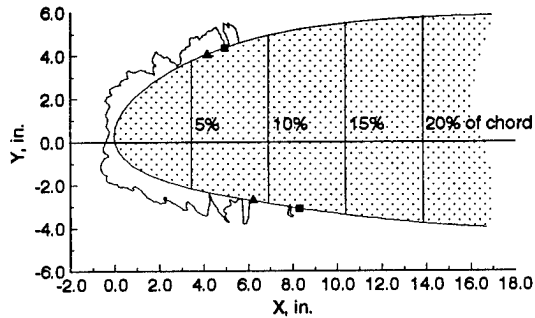
Run 413, Boot Cycle = 42 sec.



Run 407, Boot Cycle = 3 min.



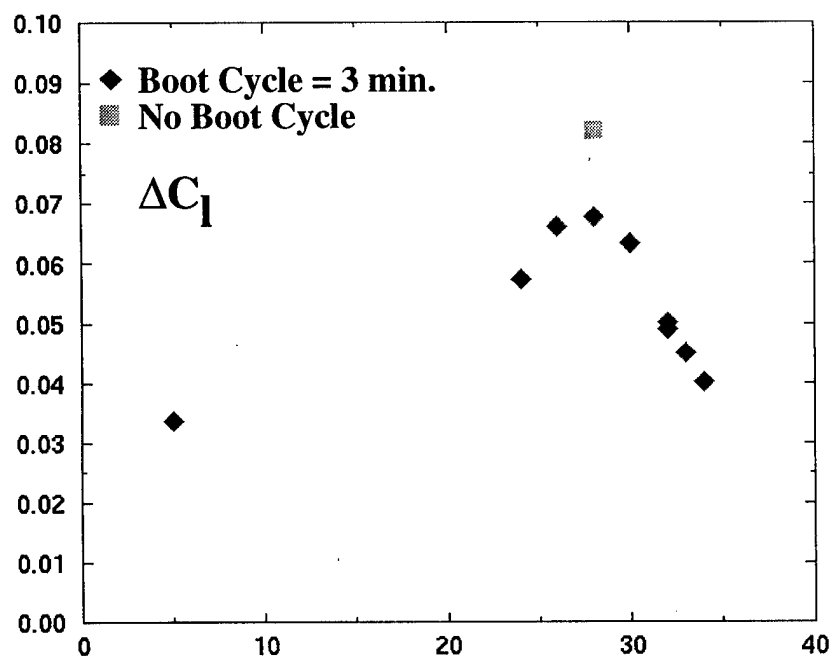
Run 414, Boot Cycle = 6 min.



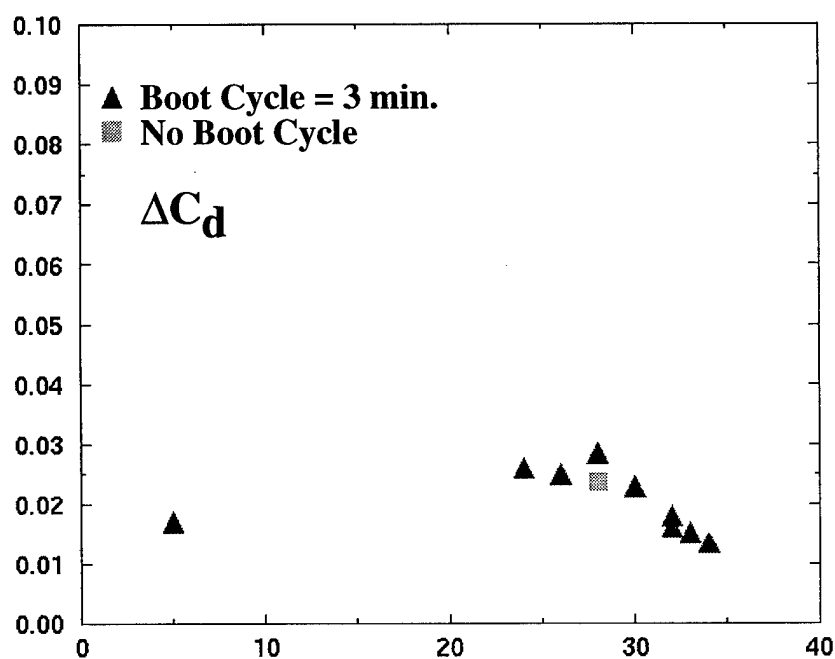
Run 416, No Boot Cycle

b). Ice shape tracings

Figure 5 - Boot cycle effect. ($T_t = 28^\circ\text{F} (-2.2^\circ\text{C})$, $\text{MVD} = 160 \mu\text{m}$, $\text{LWC} = 0.82 \text{ g/m}^3$, $\text{AOA} = 0^\circ$, $V = 195 \text{ mph} (170 \text{ kts})$, $\text{Spray} = 18 \text{ min.}$)



a). Change in lift coefficient.



b). Change in drag coefficient.

Figure 6 – Aerodynamic effects of large droplet ice accretion on NACA 23012 wing section. ($T_t = 28^\circ\text{F}$ (-2.2°C), $MVD = 160\ \mu\text{m}$, $LWC = 0.82\ \text{g/m}^3$, $AOA = 0^\circ$, $V = 195\ \text{mph}$ (170 kts), Spray = 18 min.)

LARGE SCALE ICING TESTS IN THE ONERA S1MA WINDTUNNEL

CURRENT CAPABILITIES AND NEW STUDIES TO GENERATE LARGE SUPERCOOLED DROPLETS

F. Charpin

O.N.E.R.A. Modane-Avrieux Test Center
73500 Modane - France

J. Prieur

O.N.E.R.A. Châtillon Center
B.P. 72 - F 92322 CHATILLON CEDEX - France

Abstract

Since the early 60s, ONERA has been performing icing tests in its Modane S1MA windtunnel on full scale aircraft or helicopter components as well as on scaled models. Examples of such tests include Concorde at scale 1/6, Airbus at scale 1/12, helicopter rotor at scale 1/4, full size Corvette, to quote only a few.

At the end of 1994, ONERA was invited to perform icing tests at conditions beyond the certification requirement (median volume diameter of 200 microns and liquid water content as low as 0.3 g/m³) on models of a turboprop regional transport. In order to generate the required freezing drizzle, a special spray nozzle was developed by ONERA. The performances of the nozzle grid in terms of droplet sizes were measured in situ by a Phase Doppler Particle Analyser developed at ONERA.CERT. The transverse drizzle distribution was checked by laser sheet.

Tests were performed in February/March 1995 on a full span scaled model and a full size real outer wing of 5.2 m span equipped with pneumatic de-icers.

Although the control of the freezing drizzle conditions proved to be somewhat less than ideal under these new testing circumstances, the tests performed provided the expected information on ice accretion for these extended icing conditions.

In order to consolidate its capabilities, after these encouraging results, ONERA intends to undertake the development of spray nozzles in order to extend the droplet size range beyond 200 microns. The implementation of the method for in situ determination of drizzle conditions (droplet size, velocity, spectrum) is to be improved. The effect on the drizzle of parameters such as temperature or phenomena such as droplet break up will also be studied.

Some results of the 1995 campaign are briefly presented. Finally the current efforts to consolidate and extend the ONERA S1MA icing test capabilities are also addressed.

Nomenclature

d_g	Droplet diameter	m
$L.W.C.$	Liquid Water Content	g/m ³
$M.V.D.$	Median volume diameter	μm
ρ_a	Air density	kg/m ³
σ_g	Surface tension of water against air	65.10 ⁻³ N/m
t_s or $O.A.T.$	Ambient static temperature	°C
t_t	Ambient total temperature	°C
V	Airspeed	m/s
V_g	Droplet velocity	m/s
Weber	Weber number = $\frac{\rho_a (V - V_g)^2 \times d_g}{\sigma_g}$	dimensionless

Introduction

Since the early 60s, ONERA has been using its large closed circuit S1MA windtunnel facility to perform icing tests. It has therefore been necessary to generate in the tunnel icing conditions representative of those encountered in flight. On the basis of statistical meteorological data, the Certification Authorities have

defined the sizing parameters for icing clouds likely to be encountered in flight and the requirements to obtain the Certification for flying under icing conditions. The relevant basic documents are FAR 25 Appendix C for transport aircraft and FAR 29 Appendix C for helicopters. Over the years the requirements have evolved; the current specification of the icing cloud features to be achieved in order to obtain certification are shown on fig. 1, from FAR 25 Appendix C.

The icing rig of the S1MA tunnel has been originally designed to meet the above requirements, including their translation into specification for icing tests on scaled models (down to 1/12 scale).

At the end of 1994, ONERA was requested by one of its clients to extend the icing capability domain shown on fig. 1 towards larger droplet sizes. This request was later confirmed by the French Certification Authorities. Typically, the new requirements are :

- MVD about 200 microns,
- LWC = 0.3 g/m^3 ,
- $t_t = 0^\circ\text{C}$ (32°F).

These requirements (shown in figure 1), far from the original specification, mainly for the MVD, may even be further extended up to MVD of 400 microns. This lead to a reconsideration of the icing rig, especially the injection nozzles.

The first part of the paper describes the testing techniques and the tests performed within the FAR 25 framework. The second part covers the work performed since the beginning of 1995 in order to achieve icing conditions with a MVD of about 200 microns and a LWC close to 0.3 g/m^3 .

Icing on full size or scaled down models performed within the FAR 25 framework

The early icing tests were performed on full scale models, and still are for tests on deicer efficiency. Although the S1MA test section is large (8 m in diameter) full size models consist usually of aircraft parts. Tests are valid only when the effect of the aerodynamic flow field due to the rest of the aircraft is small compared to the flow field generated by the tested part itself.

When the above condition is not fulfilled, as it happened for icing tests on Concorde or helicopter rotors, it is then necessary to perform the tests on scaled models of the complete aircraft. ONERA have therefore investigated the physical icing phenomena in order to establish, with the assistance of BAe (then British Aircraft Corporation) ^{1,2} the scaling rules to

be used to achieve representative icing conditions on scaled models³. The major work areas are :

- the study of the mechanics of droplet capture in the aerodynamic flowfield of the tested component, based on a study of the General Electric Company⁴;
- the study of water and ice distributions on profiles, taking into account the LWC, the icing exposure time and the convective heat transfer coefficients on the basis of the work reported in ⁵;
- the study of the difficult question of thermal equilibrium of a wall under icing conditions, based on ⁶;
- the compilation of above studies in order to derive icing scaling rules on the basis of work reported in ^{7,8}.

The scaling rules were validated during windtunnel icing tests, first on simple cylindrical shapes, then on delta wings and on transport aircraft wing profiles. Reproduction of ice deposits was considered valid for model scales down to 1/12.

More recently, David N. Anderson of NASA Lewis⁹ has performed checks of the scaling rules on cylindrical shapes and confirmed their validity.

However, to our knowledge, care should be exercised as these scaling rules have not yet been validated for an extended icing domain with static temperatures close to 0°C and droplet sizes close to 200 microns.

Test facility

The icing tests are performed in the continuous closed circuit S1MA windtunnel of the Modane-Avrieux test center of ONERA. The tunnel is cooled by air exchange with outside air (about 20 % of the test section flow rate) and icing tests are generally possible between mid November and mid March.

The 8 m diameter test section allows testing of large models with a small obstruction.

Icing rig

The upstream part of the test section is fitted with a spray grid equipped with 444 nozzles. The nozzles are supplied with compressed air providing an homogeneous droplet cloud with MVD adjustable between 10 and 25 microns over an area of 4 m^2 . Depending upon the test model shape, the grid can be configured as a $2 \times 2 \text{ m}^2$ square or a $4 \times 1 \text{ m}^2$ rectangle. The LWC of the cloud is adjustable between 0.3 and 10 g/m^3 for airflow velocities up to 100 m/sec (fig. 2).

The air supply to the nozzles can reach up to 8 bar and is preheated in order to counterbalance the temperature drop resulting from the expansion at the nozzle exit. Without preheating, a significant amount of water can be directly transformed into ice at the nozzle (fig. 2).

The air and water supply to the nozzle grid can be automatically controlled in order to alternate various icing conditions (maximum intermittent, maximum continuous, clear sky, in accordance with the specification of the official regulations) while keeping the droplet MVD fairly constant. The cycle durations are adjustable from a few seconds to a few tens of seconds.

Test section air flow saturation

Preliminary tests have demonstrated that droplets turn into vapor if the test section airflow is not saturated with moisture. This water vaporization changes the droplet diameter and LWC in the icing cloud, thus resulting in non representative ice deposits for the nominal set point. In order to remedy this, the tunnel has been equipped with a moisture saturation system made of 8 spray nozzles with a flow rate of 900 l/hour each, capable of achieving close to 100 % humidity in the test section. The control of the moisture level in the test section is performed by an automatic dew point measurement system with permanent sampling of the air flow (fig. 2).

Airflow downstream of the grid

Depending on the model shape and location, the grid position can be changed within the test section. The aerodynamic flow quality behind the grid has been extensively investigated.

Total pressure and angular probe rakes have been used to determine the grid pressure loss (or gain, depending on the nozzle air supply pressure) and possible flow angularity. The effect of the nozzle air supply pressure decreases when the test section air speed increases : at 100 m/sec, this effect is insignificant and the pressure loss is 3 %.

Test results

The large test section size (8 m in diameter) allows, not only the introduction of large test models, but also easy access to the various iced model parts within about 5 minutes after stopping the icing tests. This easy access allows determination of ice deposit shape and extent by photographic records or direct measurement of ice accretions. Photograph

interpretation can be facilitated by using either plates with a given dimensional pattern or by markings painted directly on the model surface to identify chordwise or angular positions.

For ice accretions with a significant size, ice molding can be performed after removing carefully ice samples from the model.

The test section walls have windows which can be equipped with lighting, photographic or video equipment to monitor and record on line ice build up throughout the test. This type of information is very important for tests where pneumatic, electric or electromagnetic deicer efficiency is being investigated as well as for icing tests at temperatures close to 0°C (+ 32°F) where natural ice breakage can be significant. The study of ice piece trajectories, for natural or forced breakage from the leading edge of models, is performed with high speed cameras (1 200 pictures/sec). This is very important to assess the risks of ice ingestion in the engine intakes or ice piece impingement and impact on the rear part of the aircraft.

For icing tests on rotors, the observation of ice build up is performed using a stroboscopic lighting system. For this type of test, ice breakage due to centrifugal loads is frequent.

For icing tests on scaled full span or half models, six component balances and torquemeters (for rotors) can be used to determine the effect of icing on the aerodynamic coefficients and rotor power requirements throughout the ice build up period or afterwards.

Icing tests for non standard conditions

Extension of the operating capability of the S1MA icing rig for testing beyond standard conditions

As already stated, new demands from the Certification Authorities relate to icing tests at temperatures close to 0°C (32°F) with large droplets. Typical required parameters are :

- t_t = 0°C (32°F)
- MVD = 200 microns
- LWC = 0.3 g/m³
- V = 100 m/sec (i.e. M = 0.3)

The above conditions result in a static flow temperature of about - 5°C and a model wall temperature of 0°C at the stagnation points.

The main problems encountered to achieve the required conditions are :

- generation and control of droplets with the required MVD ;
- droplet cooldown along their trajectories from the nozzle to the model.

Generation and control of droplet M.V.D.

For liquid droplets injected into a gas flow, the risk of droplet shattering (break up into smaller size droplets) is determined from the Weber number. The non dimensional Weber number takes into account the relative velocity of the droplet with respect to the air flow.

$$\text{Weber} = \frac{\rho_a (V - V_g)^2 \times d_g}{\sigma_g}$$

where ρ_a : air density (kg/m³)
 V : air velocity (m/sec)
 V_g : droplet velocity (m/sec)
 d_g : droplet diameter (m)
 σ_g : water surface tension : 65 10⁻³ N/m

To avoid droplet shattering, the Weber number should be below 10.

Within the frame of the current regulations, for droplet sizes below 50 microns injected with zero speed into an airflow having a velocity of 100 m/sec, the Weber number is :

$$\text{Weber} = \frac{1.2 (100 - 0)^2 \times 50 \times 10^{-6}}{65 \times 10^{-3}} = 9.23 < 10$$

In the above case, the Weber number is below 10 and there is no risk of droplet shattering ; the droplets are strong enough to withstand the acceleration due to the external airflow.

For droplet sizes of 200 microns, the Weber number is about 37, thus leading to droplet shattering.

The conclusions of the above are that for droplets injected at zero speed into a 100 m/sec airflow, their diameters will end up being smaller than 50 microns. In order to achieve large size droplets into a 100 m/sec airflow, it is necessary to inject them with a velocity close to the airflow velocity.

Obviously, the Weber number calculation with a zero droplet speed is very conservative. The Weber number is very sensitive to droplet velocity ; as an example, with a droplet initial speed of 50 m/sec into a

100 m/sec airflow, the Weber number drops down to 9.23 for 200 micron droplets. On the other hand, during icing tests the droplet size spectrum is rather large : droplets with sizes of 400 or even 600 microns are encountered into a cloud with a MVD of 200 microns. For these large droplet diameters the Weber number may exceed 100.

In view of the above, the Large Test Facilities Department of ONERA with the assistance of the Centre d'Etudes et de Recherches (CERT) of Toulouse, have performed a quick modification of the existing nozzle in order to generate large droplets with an average nozzle exit velocity of 50 m/sec.

On the basis of the work performed by J.R. Oldenberg¹⁰ and by L.G. Dodge and C.A. Martin¹¹, ONERA decided to measure the droplet velocities and sizes, using a Phase Doppler Particle Analyser (PDPA).

This device, developed and adapted at CERT, was used for the development of the modified nozzle as well as for on line MVD measurement in the tunnel during icing tests.

Within the framework of studies to define a nozzle capable of generating large droplets, measurements have been performed using simultaneously two systems surveying the same fog sample :

- at the upstream position, the Phase Doppler Particle Analyser (PDPA) with a size range capability between 11 and 400 microns, divided into 50 classes,
- at the downstream position, the Knollenberg Optical Array Probe (OAP) with a measurement range from 14 to 310 microns, divided into 15 classes.

Although the two systems do not cover the same range, especially for large diameters, the comparison of droplet spectra and the MVD changes measured by each system may give more confidence in the test result interpretation.

Fig. 3 shows the comparative results of both systems for 16 test cases : ideally, all results should fall on the straight line (slope 1). Beyond a diameter of 150 microns, the OAP provides a diameter measurement smaller than the PDPA, due to the fact that droplets with sizes above 310 microns are ignored by the OAP; In view of this limitation, the results of both systems are relatively good and in fair agreement with each other.

Twelve sequential measurements over a 3 minute time period provide an MVD of 213 to 236 microns. This indicates a fairly good steadiness of the icing cloud.

Three measurements were performed with the PDPA measurement point moving by 200 mm in a plane perpendicular to the airstream velocity, while maintaining the spray nozzle conditions constant (as controlled by the OAP which was left in one single position). The measurements were performed over 9 minutes. The results are as follows (MVD) ;

OAP : 138 μm , 136 μm , 139 μm ;

PDPA : Position 1 : 169 μm ,
 Position 2 : Position 1 + 200 mm : 186 μm ,
 Position 3 : Position 1 - 200 mm : 177 μm .

These results confirm the deviation between the PDPA and OAP measurements (due to large droplets being ignored by the OAP) and the good icing cloud uniformity, reflected by the small scatter in the PDPA results.

Fig. 4 shows a typical calibration result obtained with the PDPA for a 50 m/sec airflow, at a distance of 10.5 m downstream of the nozzle grid. The sample is made of 5 638 droplets surveyed over a period of 176 sec. Fig. 4-a shows the velocity spectrum of the droplets with an average velocity of 48 m/sec (for an airflow velocity of 50 m/sec). Fig. 4-b show the droplet diameter spectrum. Fig. 4-c gives the water volume for each droplet size band as well as the overall cumulative amount of water which is used to calculate the MVD. As can be seen on fig. 4-b, there are many droplets with a diameter ranging from 10 to 100 microns ; however these represent only a minor volume fraction (fig. 4-c). Although there are very few droplets with a diameter above 300 microns, these alone represent 50 % of the water volume. The cumulative volume curve near 400 microns exhibits a non horizontal asymptotic behaviour ; this reflects the fact that by limiting the spectrum at 400 microns, there is probably a significant amount of droplets with sizes above 400 microns which have been ignored in the sampling. The calculated MVD of 283 microns is therefore probably underestimated.

Fig. 5 shows the same type of results for the same nozzle conditions (air pressure and water flow) as for fig. 4 but with an airflow velocity of 100 m/sec instead of 50 m/sec. The sample, observed over 120 sec, consist of 8 836 droplets.

The velocity spectrum shown on fig. 5-a indicates an average velocity of 94.2 m/sec (for an airflow at 100 m/sec). Fig. 5-b and 5-c show the droplet diameter and water volume spectra respectively. The cumulated volume curve has a clear horizontal asymptotic value for diameters above 220 microns thus indicating that in this example, the spectrum has covered all droplet sizes ; therefore the calculated

MVD of 129 micron is considered as a correct representative value for the icing cloud.

As the only difference between the two cases presented in fig. 4 and 5 is the airflow velocity (50 m/sec for fig. 4 and 100 m/sec for fig. 5), it can be concluded that the reduction of the MVD from 283 microns (under estimated value) down to 129 microns is due to the droplet shattering under the effect of the airflow velocity. As a result, it appears that the generation of icing clouds with MVD of about 200 microns is not only determined by the injection nozzle parameters (air supply pressure and water mass flow). It is therefore prudent to control and measure the MVD value just in front of the test object. This is why the PDPA system implemented by ONERA in the SIMA tunnel can measure MVD, in front of the model, at distances between 2.5 to 4 m from the tunnel wall and control the uniformity and steadiness of this MVD.

Cooling of water droplet along their trajectories

Theoretical as well as experimental studies have been performed years ago showing that droplets with an MVD not exceeding 50 microns, into an airflow at temperatures below 0°C, become very quickly supercooled. For droplets with an MVD of 200 μm , as the mass to surface ratio increases like the droplet diameter, clearly the time constant of the cooling process will be much longer. A study was performed based on the work of P. Creismeas (C.E.Pr) reported in 12,13. Fig. 6, extracted from additional work of P. Creismeas with MAGIC code, shows the droplet temperature versus the distance from the nozzle for a droplet of 200 microns, with an initial temperature of 5°C and an initial zero speed, injected into a saturated airflow (100 % relative humidity) at 100 m/sec and having a temperature of - 5°C. Supercooling starts at about 2 m from the nozzle and the droplet temperature is within 1 degree from the air flow static temperature after about 10 m.

Following these estimates, the model was positioned at about 12 m from the grid and the water supply temperature was controlled close to the nozzles. Controlling this temperature between 2 and 5° for a set of 444 nozzles appears as a challenging task due to the need of avoiding frost formation for the nozzles at the far end of the water circuit.

Icing test results for non standard icing conditions

Early in 1995, Aerospatiale, Aeronautical Branch, placed a contract with ONERA for the performance of an icing test campaign for non standard icing conditions on an ATR 72 model. These "abnormal"

icing conditions are representative of an icing cloud with small LWC and an MVD of about 200 microns (current regulations are limited to MVD ranging from 15 to 50 microns).

The model is a full scale outer wing of the ATR 72 with a 5.2 m span, equipped with pneumatic deicers and located at about 12 m from the nozzle grid (fig. 7).

The tests were conducted at $M = 0.3$ (about 100 m/sec and static temperatures from -5°C to -1°C . LWC was 0.3 g/m^3 and MVDs ranged from 100 to 200 microns. The MVD was measured on line in the test section with the PDPA system and the cloud uniformity was checked with a laser sheet. Preliminary aerodynamic tests were performed in order to determine, from pressure measurements, the exact stagnation point position on the wing leading edge.

Fig. 8 shows the ice deposits obtained for a reference case (deicers not in operation). For this particular case, with an icing duration of about 30 minutes, the leading edge deposit is about 45 mm thick on average. The photograph clearly shows in the ice deposit a crevasse down to the model skin. This crevasse appears in the stagnation point area where, for this particular test case, the temperature is above 0°C .

For other test cases with similar icing conditions except for the temperature which is 1 to 2 degrees above the previous test case temperature, liquid water has been observed during the test at the bottom of the crevasse; this liquid water may run between the ice and the skin; this leads to large chunks of ice (30 to 60 cm) departing from the model. After this natural ice removal, ice starts to build up again and the phenomenon may become a cyclic process. Obviously, at the end of the test, the ice deposit shape (fig. 9) is very different from the one shown on fig. 8 for the previous case. For these test conditions close to 0°C , the ice accretion shapes are extremely sensitive to minor flow temperature variations (1 to 2°C).

Fig. 10 shows the ice deposit obtained at conditions close to the above described reference case but with the pneumatic deicers in operation. The leading edge is completely clear from ice with only a small frost barrier developing on the upper side of the wing at the downstream boundary of the deicer area. This discontinuous barrier develops throughout the test by successive accumulations on residual deposits existing beyond the deicer active area.

Some of these accumulations disappear naturally, which contributes to the discontinuous appearance of the barrier. In some cases, the barrier height may reach 20 mm as shown on fig. 11.

Such results have been encountered, in similar icing conditions, by Th. M. Bond of NASA Lewis¹⁴ as well as during flight icing tests behind a tanker (fig. 12).

The downstream extension of ice deposits for icing at near 0°C temperature with large droplets (MVD \approx 200 microns) may be due to the combination of two effects :

- with increased droplet sizes, the ratio of the inertia forces and aerodynamic forces acting on the droplets will increase, and the large droplets will impinge on the model further downstream, as compared to small droplets ;
- when the droplet temperature comes closer to 0°C (32°F), the "icing fraction" coefficient⁶, i.e. the fraction of the amount of water which turns immediately into ice when impacting on the profile, becomes smaller. The remaining liquid volume, becoming larger, tends to follow the airstream and to freeze further downstream of the impact point on the profile.

Automatic ice shape recording

Ice shape records are one of the major results of icing tests. Measurement techniques such as viewing through a marked plate, photograph and blade rakes generally produce good results but suffer from being long to be implemented. Further, these methods do not produce numerical outputs. In order to save time and to obtain rapidly a computerized output, ONERA developed and tested in an industrial environment, an automatic ice shape recording system.

The system sensor is a laser telemeter having a 100 mm dynamic range with a 50 micron accuracy. The sensor is mounted on a motorized mobile support, the position of which is measured via a potentiometer. The contour of the profile is recorded before the icing tests and numerical data are stored into a file. At the end of the test, the ice contour is recorded in the same manner and the numerical results stored into another file. Computerized data processing is used to generate quickly ice deposit shapes as well as numerical files in order to manufacture ice contour blocks which can later be used for flight or windtunnel aerodynamic testing.

Currently, the experience is limited to ice shape recording on cylindrical samples. An example of result is given of fig. 13. The duration to perform such a record is one minute. This year, it is intended to extend the application of this method for ice shape measurements on full scale wing leading edges.

Future developments

The droplet shattering phenomenon as well as the problem of minimum distance for obtaining supercooled droplets will necessitate a complete reconsideration of the current icing test techniques if the test domain is to be extended towards droplet sizes up to 600 micron MVD. In such a case, the injection nozzles to be used may have to be of the same type as those used for transonic rain erosion tests i.e. delivering a single size of droplets. As far as the droplet cooldown is concerned, the distance between the nozzle grid and the model may have to be considerably increased. In order to increase the distance between the grid and the model up to 30 m it has been considered to install the grid in the tunnel settling chamber. This would enable droplets with MVD of 600 microns to be properly cooled down. However, such a consideration requires an accurate estimate of droplet trajectories between the settling chamber and the test section, taking into account gravity and segregation effects in the contraction. It may also become necessary to perform icing tests under controlled non saturated airflow conditions in order to take advantage of the cooling effects due to partial droplet vaporisation.

Fig. 14 shows the potential large effect of the moisture level on the droplet cooling distance. Indeed, in a non saturated flow, droplets tend to cooldown while being partly vaporized. It is therefore conceivable to save 5 to 10 m of cooling distance by injecting the droplets into a non saturated airstream, due to the droplet vaporisation process. The theoretical calculations (made by C.E.Pr) show that after 25 m, into an airstream with a 100 m/s velocity and 50 % relative humidity, a 400 micron droplet reduces in size by a negligible amount to 399 microns. However droplets with an original size of 10 to 20 microns would be fully vaporized. It is therefore important to measure the MVD just in front of the model under tests.

Conclusions

Many icing test campaigns have been performed in the ONERA S1MA facility in the Modane-Avrieux test center, in order to meet the requirements of Appendix C of FAR 25, using full size or scaled models or model parts.

The scaling laws used for icing tests on scaled models have been validated.

At the initiative of the French Certification Authorities or at the request of aircraft manufacturers, in cooperation with the French Propulsion Test Center (C.E.Pr.), the S1MA operating domain for icing tests has been extended : the injection nozzles have been adapted to generate icing clouds with droplets having an MVD of 200 microns for LWC of 0.3 g/m^3 (non standard icing).

The droplet spectra (size and velocity) have been measured on line using a Phase Doppler Particle Analyser (PDPA) system implemented by the Measurement Department of the ONERA-CERT. The cloud uniformity has been checked by laser sheet.

The shape and extent of ice deposits obtained under icing conditions with large droplet sizes (100 to 200 microns) at temperatures close to 0°C are in fair agreement with those obtained under similar conditions in other facilities or during flight testing behind a tanker.

If the need to extend the test domain towards large droplet sizes up to an MVD of 600 microns was to be confirmed, the rig used to generate the corresponding icing conditions, especially the nozzles, should be entirely reconsidered.

Acknowledgement

The permission by Aerospatiale, Aeronautical Branch, to present in this paper some results of the 1995 icing test wind tunnel campaign as well as some flight test results are greatly appreciated.

REFERENCES

- [1] Googan R. et Jackson E.T.
Development Study "the use of scale models in an icing tunnel to determine the ice catch on a prototype aircraft, with particular reference to the Concord". Issued by B.A.C. (operating) Ltd, Filton Division -
Aircraft Engineering Dept.
SST/B75T/RMMoL/242 - Issue 1 -
24th July 1967.
- [2] Googan R. et Hubbard J.A.
Concorde de-icing "icing tests on a 1/6th scale model (G14) at Modane".
Preliminary test/programme SST/B72T -
51/5027 - Issue 1 - 7th August 1968.
- [3] Charpin François et Fasso Guy
Icing testing in the large Modane wind tunnel on full scale and reduced scale models.
L'Aéronautique et l'Astronautique no. 38, 1972.
English translation published as NASA
TM-75373.
- [4] Langmuir Irving et Blodgett Katharine B.
A mathematical investigation of water droplet trajectories.
Army Air Forces technical report no. 5418,
February 1946.
- [5] Gelder T.F. et Lewis J.P.
Comparison of heat transfer from airfoil in natural and simulated icing conditions.
NACA T.N. 2480 - Septembre 1951.
- [6] Messinger B.L.
Equilibrium temperature of an unheated icing surface as a function of airspeed
I.A.S. preprint no. 342. Presented at annual summer meeting, June 1951.
- [7] Hauger H.H., Englar K.G. et Reaser W.W.
Analysis of model testing in an icing wind tunnel.
Douglas Aircraft Company Inc.
Report no. SM 14993 - May 1954.
- [8] Brun E.A.
Icing problems and recommended solutions.
Agardograph 16. November 1957.
- [9] Anderson D.N.
Rime-, mixed- and glaze-ice evaluations on three scaling laws.
AIAA 94-0718. 32nd Aerospace Sciences Meeting and Exhibit.
January 10-13 1994/Reno, NV
- [10] Oldenburg J.R.
Comparison of two droplet sizing systems in an icing wind tunnel
AIAA-90 0668 - 28th Aerospace Sciences Meeting - January 8-11-1990/Reno, Nevada
- [11] Dodge L.G., Martin C.A.
Evaluation of drop-sizing instrumentation for wind tunnels with icing capabilities.
AIAA-91.0559 - 29th Aerospace Sciences Meeting - January 7-10, 1991/Reno, Nevada
- [12] Feuillebois F., Lasek A., Creismas P., Pigeonneau F. et Szaniawski A.
Freezing of a subcooled liquid droplet.
Journal of colloid and interface science 169,90-102 (1995).
- [13] Creismas P
A Eulerian/Lagrangian model to calculate the evolution of a water droplet spray.
International journal for numerical methods in fluid. Vol. 20, 135-155 (1995)
- [14] Bond Th. H.
Video of near freezing/large droplet icing research tunnel test case.
Note and video tape. Ref. 2720 -
May 31st, 1995

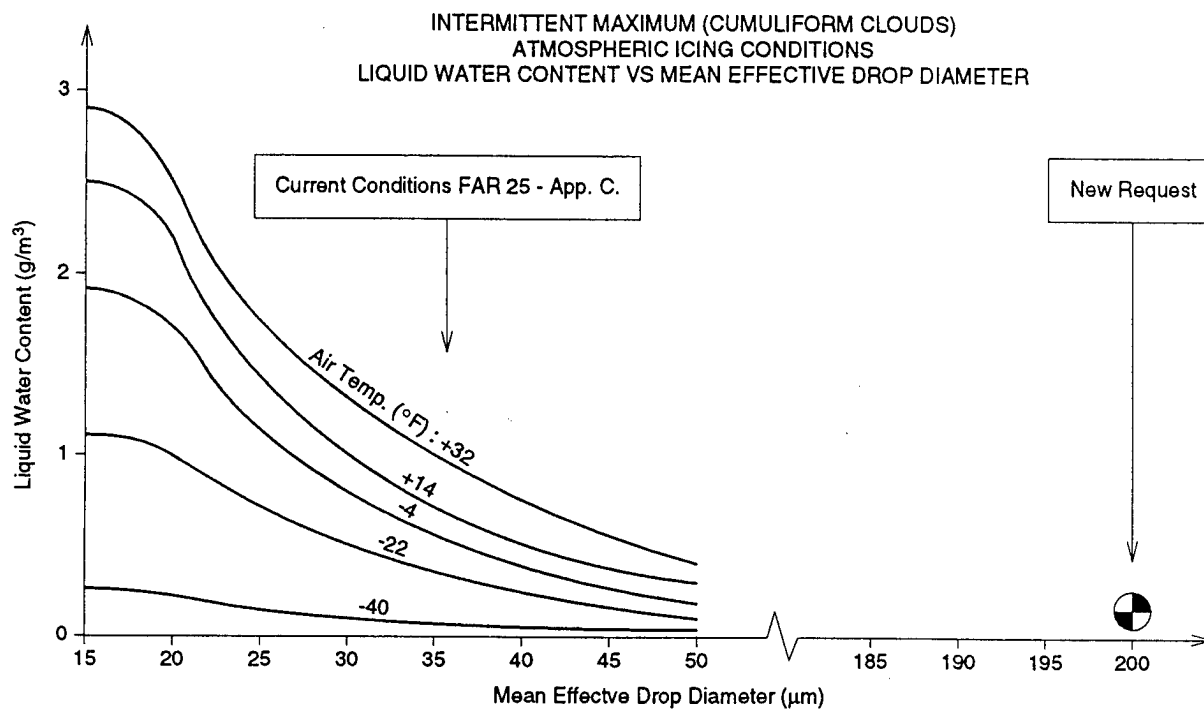


Figure 1 : Atmospheric icing conditions

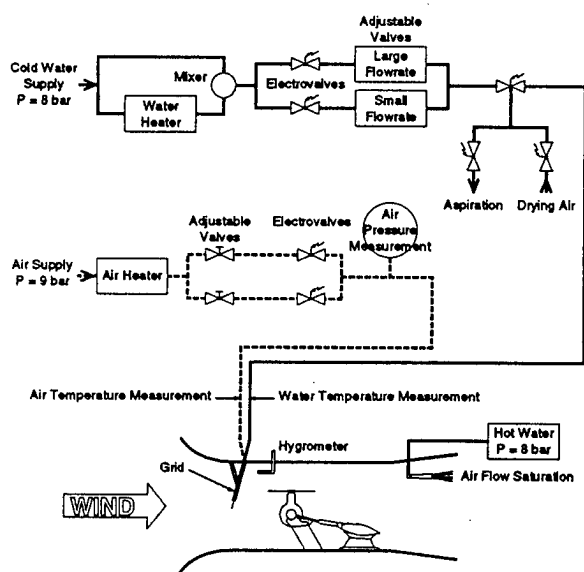


Figure 2 : Icing rig

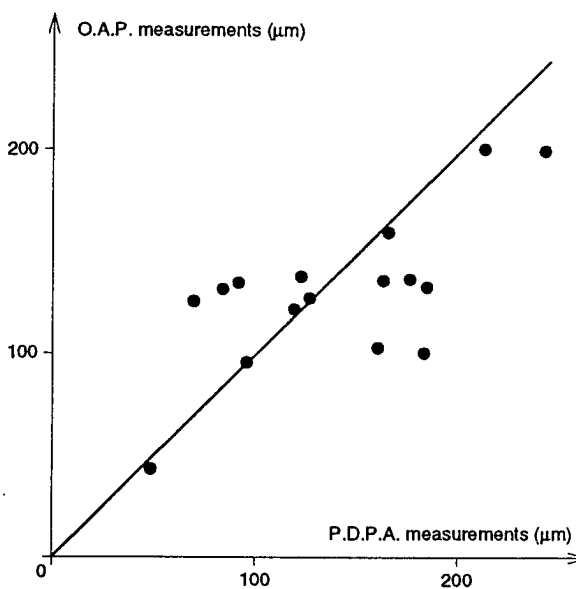


Figure 3 : O.A.P. measurements VS P.D.P.A. measurements

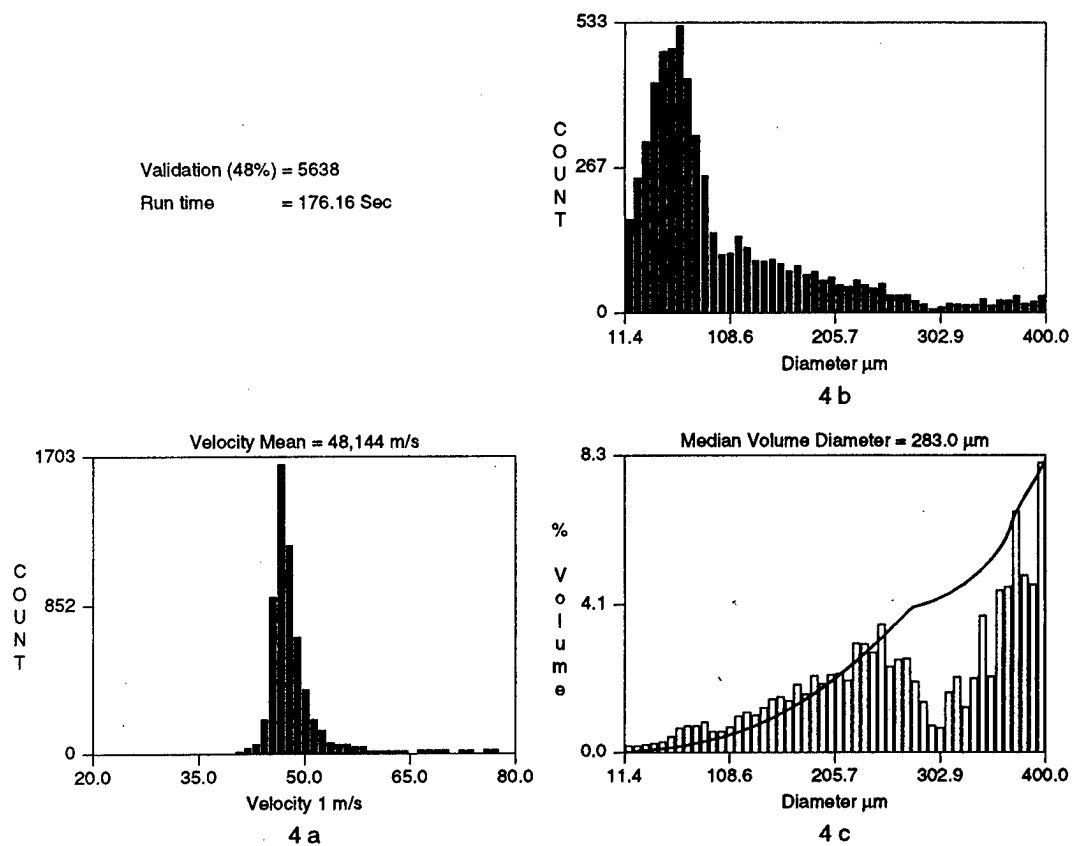


Figure 4 : Velocity and diameter spectrum at $V_0 = 50 \text{ m/s}$

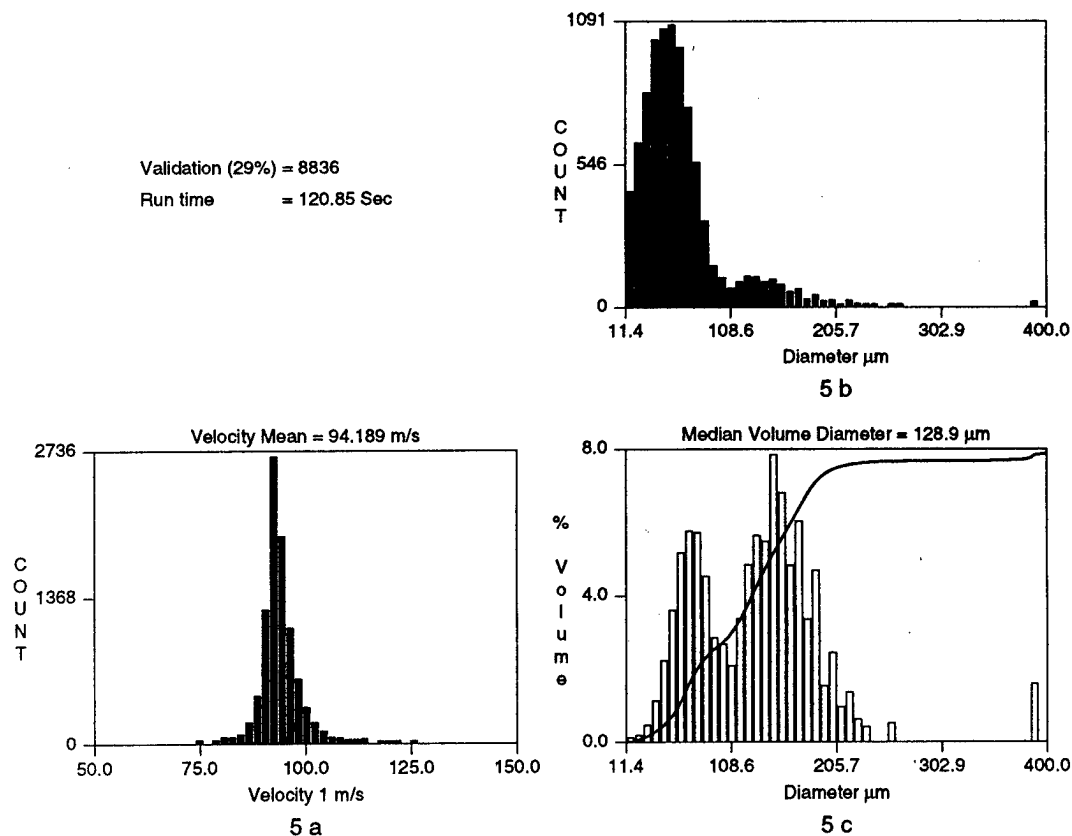


Figure 5 : Velocity and diameter spectrum at $V_0 = 100 \text{ m/s}$

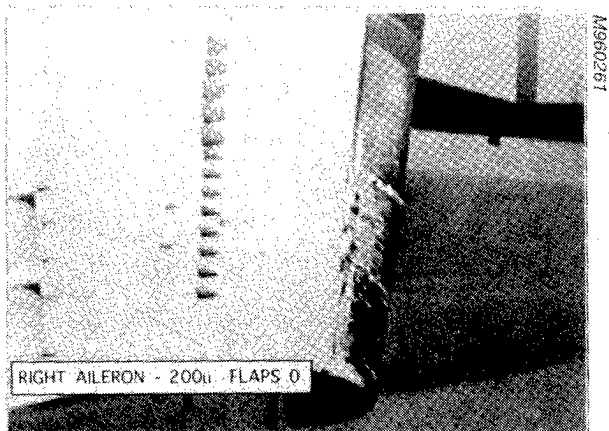


Figure 12 : Icing tanker testing of the ATR-72 at Edwards AFB

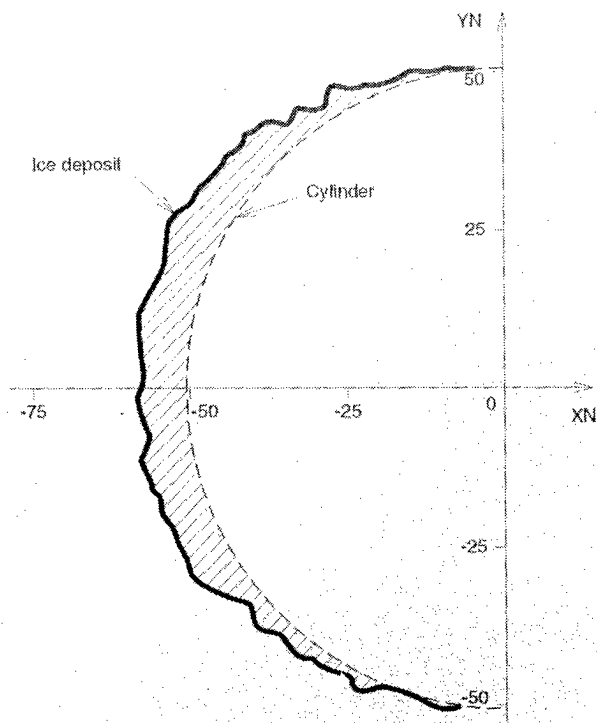


Figure 13 : Fast recording of ice deposit shape

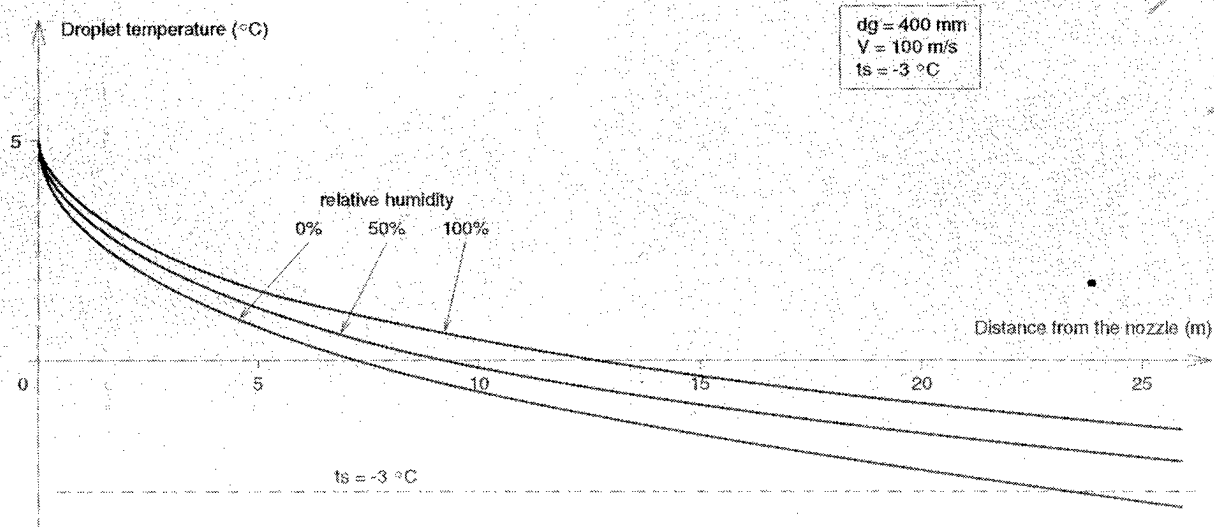


Figure 14 : Droplet temperature VS Distance from the nozzle

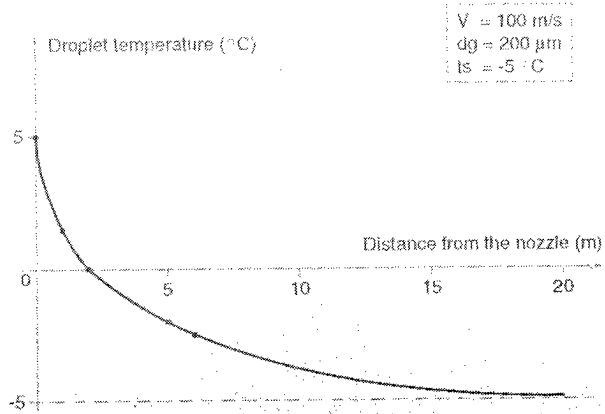


Figure 6 : Droplet temperature
VS Distance from the nozzle

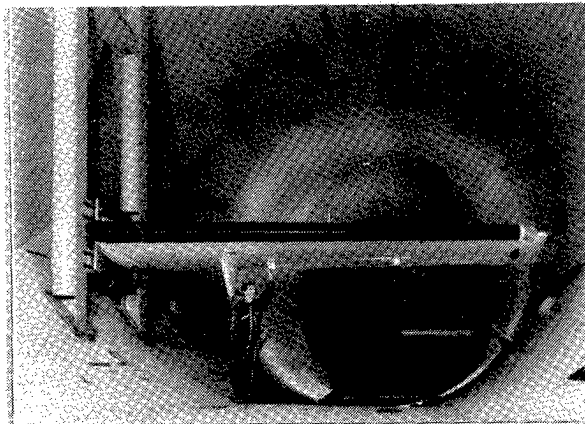


Figure 7 : ATR 72 wing tip assembly

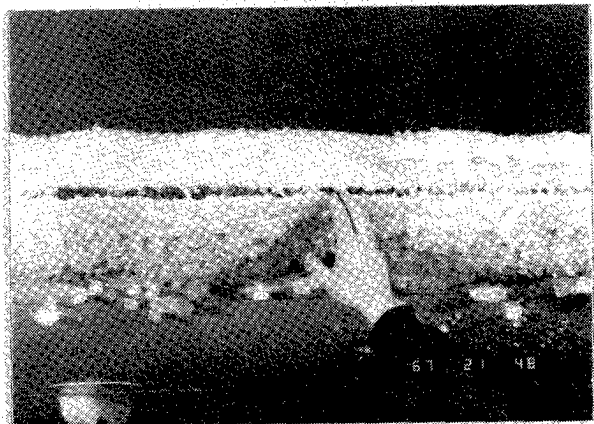


Figure 8 : Ice deposit on leading edge
De icer "off"

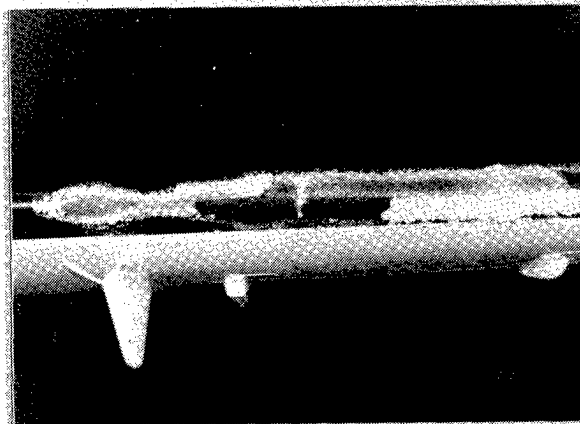


Figure 9 : Ice sheddings on a leading edge
De icer "off"

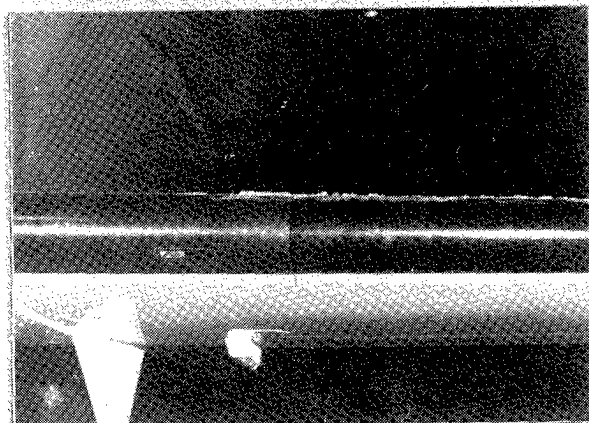


Figure 10 : Ice deposit on leading edge
De icer "on"



Figure 11 : Close-up on leading edge deposit
De icer "on"

THE EFFECT OF ALTITUDE ON ICING TUNNEL AIRFOIL ICING SIMULATION

Myron M. Oleskiw, National Research Council, Canada
Fabrizio De Gregorio, Biagio Esposito, CIRA Wind Tunnel Department, Italy

Abstract

While icing scaling laws have been developed which predict the changes required in icing simulation parameters to compensate for a difference in air pressure between natural and simulated environments, recent studies have shown that these scaling laws need further refinement and can require conditions which are difficult or impossible to achieve in an icing wind tunnel. A series of experiments were performed in NRC's Altitude Icing Wind Tunnel focused on determining the effects upon ice accretion profiles of changing altitude while the other simulation parameters were held constant. While relatively small changes were noted in the forward-facing portion of the profiles, the extent of the ice accretion along the airfoil surface increased consistently as the altitude increased. It is possible that such additional accretions could have a significant aerodynamic impact, particularly when the leading edge of the airfoil is de- or anti-iced.

Introduction

A number of tools in addition to in-situ testing are available to research scientists or engineers for simulating in-flight icing on aircraft or their components. These tools range from physical simulation tools: spray tankers, spray rigs and icing wind tunnels; through to computational models. While it is optimal for all of the conditions which contribute to the size and shape of icing to be replicated when using one of these tools, in the case of the physical simulation tools, facility limitations may prevent this. One possible limitation could be the size of the object upon which the accretion is to occur. For many tests performed at ground level, the static pressure of the original conditions cannot be replicated.

A number of scaling laws have been developed to determine the relationship between the various physical parameters affecting the ice accretion under full flight conditions and in a simulated environment (hereafter referred to as the scaled environment). For this purpose, two categories of laws exist which correspond to the two major categories of icing. Rime icing occurs where supercooled water droplets freeze immediately upon impact, retaining much of their shape on impact and producing a relatively low density ice. Glaze icing forms when only a part of the accreting supercooled water freezes upon impact, with the remainder running back along the surface of the accretion before freezing.

For the study of rime icing, provided that the droplets freeze on impact, the correct scaling of the supercooled droplet trajectories and the scaling of the flow field about the object upon which the accretion is occurring are sufficient to ensure the accuracy of the simulation. A major work leading to droplet trajectory scaling was that of Langmuir and Blodgett (Ref. 1). Their work has been modified more recently by, amongst others, Bragg (Ref. 2).

In the case of glaze icing, scaling of the thermodynamics of the ice accretion process must also occur. One of the first to provide a comprehensive study of the factors affecting this type of ice accretion was Messinger (Ref. 3). His work was expanded to provide the scaling laws (Ref. 4), which were used in the ONERA icing tunnel at Modane. More recent analyses of the factors influencing this type of icing (Refs. 5 through 8) have led to the inclusion of more scaling equations. Since not all of the equations believed to influence the accretion process can be satisfied concurrently for a given test, some effort has been

undertaken to optimize the accuracy of the scaling by formulating laws which satisfy combinations of scaling equations involving those terms which most influence the results. Thus while these "optimized" scaling laws may result in better agreement between the reference and scaled conditions, the application of the laws within the limitations of the test conditions available in a given simulation facility suggest that tests are required to first validate and then determine the utility of any given law.

Recently, the Italian Center for Aerospace Research (CIRA) has commenced the development of an Icing Wind Tunnel (IWT) suitable for testing both aircraft structures and engine inlets. During the preliminary design process, CIRA realized that since most current icing tunnels do not have the capability of varying static pressure, little was known about the effects of a lack of correctly duplicating altitude during icing tests. One of the few test facilities capable of studying the problem is the National Research Council's (NRC's) Altitude Icing Wind Tunnel (AIWT), and so CIRA and NRC commenced a joint research program with the following objectives:

1. to perform tests to determine the effect of changes in static pressure (altitude) upon ice accretions;
2. to attempt to validate numerical icing simulation models which are under development; and

3. to determine if CIRA's IWT should have the capability of varying static pressure.

This paper will present the results of some of tests performed as a part of the joint research program.

Altitude Icing Wind Tunnel

All of the experiments reported below were performed in NRC's AIWT. Its primary characteristics are shown in Fig. 1.

All of the icing tests were performed on a NACA 0015 airfoil of 35.4 cm chord which horizontally spanned the entire cross section of the tunnel. The model was constructed of extruded aluminum. At the velocity used for the tests, the Reynolds number based on the airfoil chord was of the order of 2.9×10^6 .

Tunnel data acquisition was performed on a personal computer which recorded total and static pressures, total air temperature, fan speed, and other parameters at a 1 Hz rate. Two droplet-size spectrum measuring devices were employed to determine the characteristics of the icing spray prior to the tests. A Malvern diffraction device was installed across the test section upstream of the airfoil. A forward scattering spectrometer probe (FSSP) was also inserted into the airstream in place of the airfoil. For the tests presented here, the results from the Malvern instrument will be reported. The LWC was determined prior to the

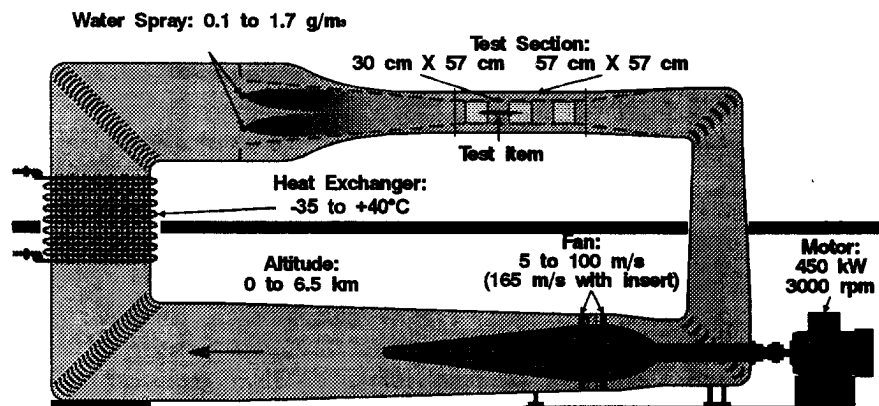


Fig. 1. Characteristics of the NRC Altitude Icing Wind Tunnel.

experiments through the use of a CSIRO King probe, a hot wire device. The King probe was calibrated using a small rotating cylinder (Ref. 9).

The AIWT spray system uses distilled water that can be heated prior to reaching the spray nozzles. The external mix spray nozzles used in the tunnel permit a large range of LWC values to be achieved at various tunnel airspeeds by varying the flowrate (pressure) of the water supply without requiring a large variation in air pressure. As a result, the spray droplet size distribution and its median volume diameter (MVD) can be adjusted to remain constant with only small changes in air pressure despite the large range of LWC values. In this exploratory set of experiments, only one spray nozzle was used. While this allowed improved test repeatability, the ice which accreted on the airfoil was not uniform in the spanwise direction. As a result, there exists the possibility that the accretion profile observed along the tunnel centerline during some of the glaze ice accretion tests might have been influenced by slightly thicker ice accretions on both sides where the liquid water content was lower but the freezing fraction higher.

Ice Profiling Technique

Traditionally, ice accretion profiles have been measured through the use of either a casting of

the ice in place, or the measurement of ice thickness using a hot knife technique. In both of these cases, the ice accretion is disturbed, and the experiment must recommence. For this study, another technique was attempted. A 20 mW helium-neon laser beam was directed through a cylindrical lens with a horizontal principal axis. This created a vertically oriented laser light sheet. This light sheet passed through one of the tunnel's viewing windows and was aligned to intersect the airfoil along the centerline of the tunnel. A schematic diagram of this illumination technique is shown in Fig. 2. A 35 mm camera was mounted outside the test section viewing almost parallel to the leading edge of the airfoil. With the tunnel room darkened, the camera could record either the profile of the clean airfoil, or of the ice accretion. Two miniature light sources were located on the opposite wall of the tunnel and were used to ensure proper registration and thus comparison between photographs of the clean and accreted airfoil. Any possible distortion due to misalignment, i.e. camera not sighted precisely parallel to the leading edge, was removed in the post-processing of the images.

The 35 mm images were scanned and the digital images which resulted were superimposed to determine the shape and thickness of the ice accretion. The leading edge of the airfoil and of the ice accretion were obtained by tracing the outlines of these shapes

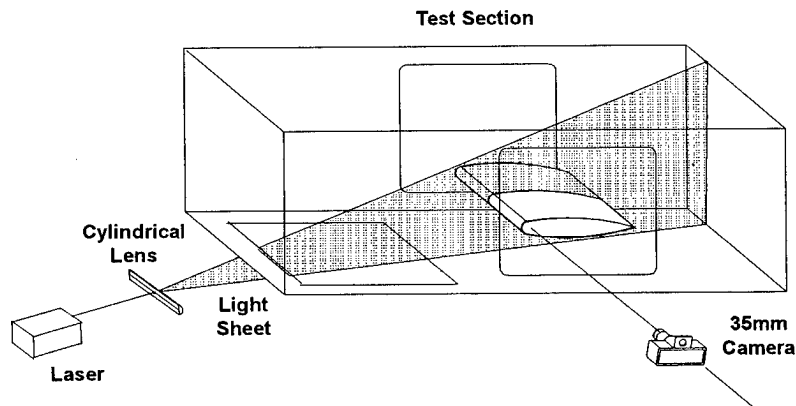


Fig. 2. Schematic diagram of the laser light sheet illuminating a cross-section of the airfoil with ice accretion.

through the use of commercial image manipulation software. In the future, an effort will be made to provide for the automatic tracing of the edge of the accretion. An example of the results obtained through this technique, a reproducibility test, is shown in Fig. 3.

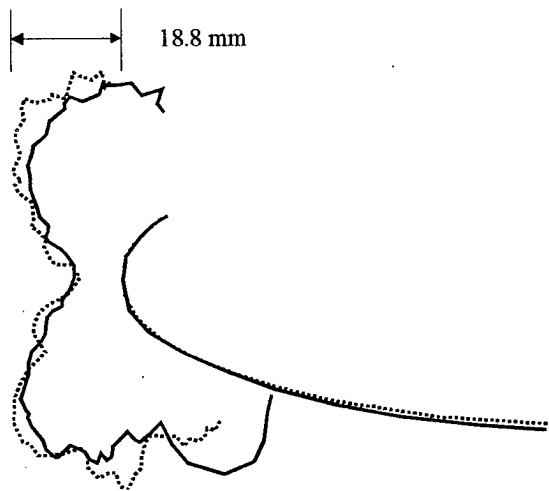


Fig. 3. Reproducibility of Test 23. (P:101 kPa; T: -5C; MVD: 23 μm ; LWC: 1 g/m^3 ; Time: 600 s; V: 95 m/s)

One of the advantages of this non-intrusive method of obtaining ice profiles is that experiments do not have to be interrupted in order to obtain an interim measurement of ice accretion. Since ice accretion can vary from

one experiment to another even with identical initial conditions (because of the stochastic growth of rime feathers, for example), the shape of a thin layer of ice depends upon the shape of the preceding thin layer. Thus, once an accretion has been interrupted, subsequent accretion may not be exactly the same as it would otherwise have been. Also, since this technique does not necessitate stopping the accretion process, there is no disturbance to the thermodynamic balance at the ice accretion surface. Two examples of successive two-minute time interval accretions are displayed in Fig. 4. In all of the cases presented in this paper, only the lower half of the airfoil and accretion profiles are displayed in their entirety due to the lighting limitations discussed above. In future, a beam splitter and two cylindrical lenses will be incorporated, which will permit the airfoil to be illuminated from both above and below.

Numerical Ice Profile Prediction

In order to evaluate the comparative importance of some of the physical processes influencing the ice accretion experiments to be described in the following section, a comparatively simple numerical ice accretion model developed by Lozowski et al. (Ref. 10) was implemented for use on a personal

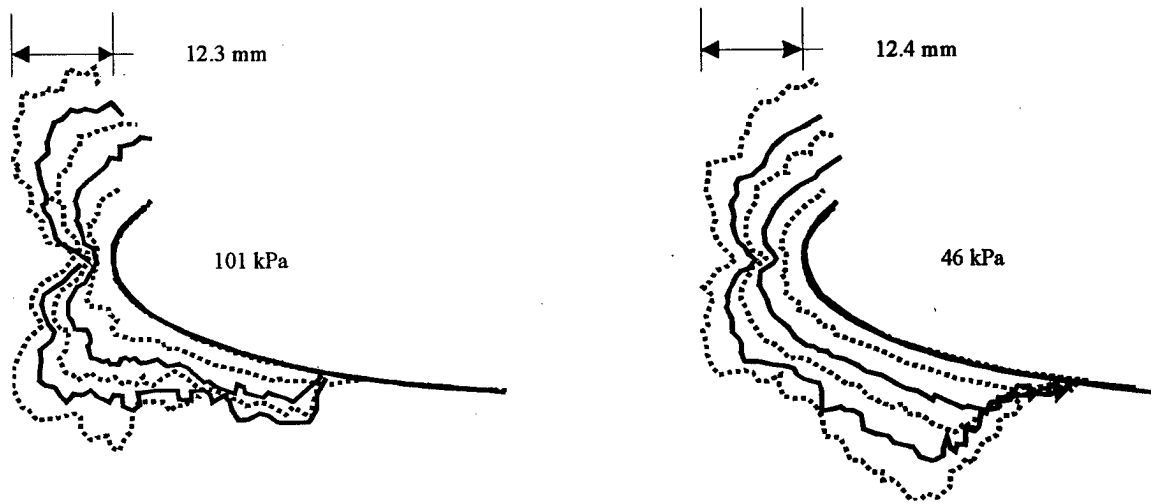


Fig. 4. Two examples of ice accretion time history as obtained from the laser light sheet image analysis technique.

computer. This model utilizes the potential flow solution for the windward half of a non-rotating cylinder, and then computes the thermodynamic balance on this surface following the control volume method first proposed in Ref. 3. It then estimates the ice thickness as a function of angle from the stagnation line. More sophisticated models have been developed during the last 13 years (e.g. Refs. 11 through 14) which allow for multi-step ice accretion with recalculation of the flow field about an arbitrary shape. Some models have incorporated more sophisticated calculation of the boundary layer or have even used Navier-Stokes flow solvers. The goal here, however, was simply to solve the heat balance equations to determine a first-order approximation for the changes in accretion profile to be expected as a result of changes in air pressure. The cylinder radius which best matches the radius of curvature of the leading edge of the airfoil has been used in the comparisons.

The present implementation of the model was verified against the results presented in the original paper (Ref. 10). In addition, the model was used to study the scaling law developed by Ruff (Ref. 5) and presented by Bartlett (Ref. 15). Table 1 indicates some of the results of the application of this model to the

conditions presented in Table 13 of Ref. 15. With the change in altitude from 1000 ft to 20,000 ft, the Ruff scaling law suggests changes to the air temperature, the velocity, LWC, MVD and accretion time to maintain equivalent conditions. The results from running the model show that important characteristics of the predicted accretion such as the initial freezing fraction and rate of ice growth over a cylinder are well represented. It is important to note, however, that had the test been performed in the AIWT, the required increase in velocity to $125 \text{ m}\cdot\text{s}^{-1}$ could only have been accomplished through the use of a test section insert and the reduction of MVD from 15 to $9.7 \mu\text{m}$ would have pushed this requirement to the lower limit of the MVD range for the AIWT.

The limitations of the application of this scaling law are well demonstrated in Table 2 which is a subset of Table 16 of Ref. 15. It shows that as the altitude decreases, the scaling law requires a decrease in velocity to near zero values. In addition, the liquid water content jumps to very high values as the altitude decreases. Clearly, other scaling methodologies are required if air pressure cannot be simulated correctly in icing wind tunnels.

Table 1. Application of the cylinder icing model to a scaled icing simulation.

Parameter	Units	Value at sea-level	Value at altitude
Altitude	ft	1,000	20,000
Pressure	kPa	98	47
Temp.	°C	-20	-21.3
Velocity	$\text{m}\cdot\text{s}^{-1}$	61	125
LWC	$\text{g}\cdot\text{m}^{-3}$	1.00	0.48
MVD	μm	15.0	9.7
Time interval	s	100	101
Stagnation collision efficiency		0.79	0.80
Stagnation surface temp.	°C	-3.2	-3.9
Stagnation freezing fraction		1.0	1.0
Stagnation ice thickness	mm	5.28	5.25

Table 2. Variation of scaling law predicted parameters between altitude and sea level conditions.

Parameter	Units	Altitude 1	Altitude 2	Altitude 3
Altitude	ft	20,000	18,500	14,000
Pressure	kPa	46.9	51.7	58.6
Temp.	°C	-5	-4.8	-4.6
Velocity	m·s ⁻¹	61.0	44.2	9.2
LWC	g·m ⁻³	2.00	2.47	5.79
MVD	μm	25.0	29.0	56.8
Time interval	s	100	112	230

Experimental Results

A number of experiments were performed in NRC's AIWT to investigate the effects of changing several parameters (air temperature, droplet MVD, spray LWC and air pressure) on the ice accretion. The conditions utilized for a subset of these tests are presented in Table 3.

This table indicates that several tests were repeated to determine the degree of ice profile reproducibility (as previously indicated in Fig. 3). Several of the tests needed to be repeated when it was discovered that even

though the LWC had been measured at sea-level pressure, the additional cooling of the air and water exiting the spray nozzles at higher altitudes resulted in the freezing of some proportion of the total number of supercooled water droplets prior to their impact with the airfoil model. This partial freeze out reduced the LWC while maintaining the total water content. This problem was overcome in most cases by additionally heating the water supplied to the spray nozzles.

The first three pairs of experiments to be described were performed to quantify the result

Table 3. Summary of experimental conditions.

Test #	Air Temp. (°C)	Droplet MVD (μm)	LWC (g·m ⁻³)	Pressure (kPa)	Water Temp. (°C)	Comments
10	-10	15	0.3	101		
11	-10	15	0.3	53		
13	-5	19	0.75	101		
14	-10	19	0.75	101		
15	-20	19	0.75	101		
16	-30	19	0.75	101		
23A	-5	23	1.0	101	35	
23B	-5	23	1.0	101	35	Repeatability
24A	-10	23	1.0	101	Rising to 50	
24B	-10	23	1.0	101	50	Correction
28A	-5	23	1.0	46	Rising to 35	
28B	-5	23	1.0	46	35	Correction
29A	-10	23	1.0	46	Rising to 45	
29B	-10	23	1.0	46	50	Correction

of changing the altitude while attempting to maintain all of the other test conditions. In all of these tests, the air velocity in the tunnel was $95 \text{ m}\cdot\text{s}^{-1}$, the ice accretion interval was 10 min, and the angle of attack was 0 deg.

In the first of these sets of experiments, the static air temperature was -5°C , the liquid water content was $1.0 \text{ g}\cdot\text{m}^{-3}$ and the median volume diameter of the droplet distribution was $23 \mu\text{m}$. The observed ice profiles obtained at sea level and at 46 kPa are displayed at the left in Fig. 5. In comparing the profiles obtained at the two pressures, it appears that the ice grown at the lower pressure is slightly thicker at the stagnation point, then becomes somewhat thinner away from the stagnation line. The extent of droplet impingement and/or fluid runback is greater for the higher altitude case since the ice profile extends further rearward in this case.

The results from the cylinder icing model are shown at the right in Fig. 5. The 2.5 cm diameter cylinder upon which the accretion is predicted to occur is shown in comparison to the 35.4 cm chord NACA 0015 airfoil upon

which the ice accretion actually occurred in the experiments. The code predicts that the increased collision efficiency at the higher altitude (e.g. 0.85 versus 0.81 along the stagnation line) would result in an increased ice thickness (7.3 versus 6.0 mm on the stagnation line). The freezing fraction in this region is predicted to increase slightly from 0.12 to 0.14. Thus the model correctly predicts the slight increase in ice thickness at the stagnation line as the altitude increases.

The next pair of experiments is shown in Fig. 6. Here, the conditions are identical to those above except that the air temperature has been decreased from -5°C to -10°C . Once again the ice thickness is observed to be greater on the stagnation line at the higher altitude, but decreases near the horns of the accretion. As for the previous case, the extent of the accretion along the length of the airfoil is greater at the higher altitude. The predicted collision efficiencies for this case are virtually identical to the previous case, but the freezing fractions are computed to be higher at about 0.32 at both pressures.

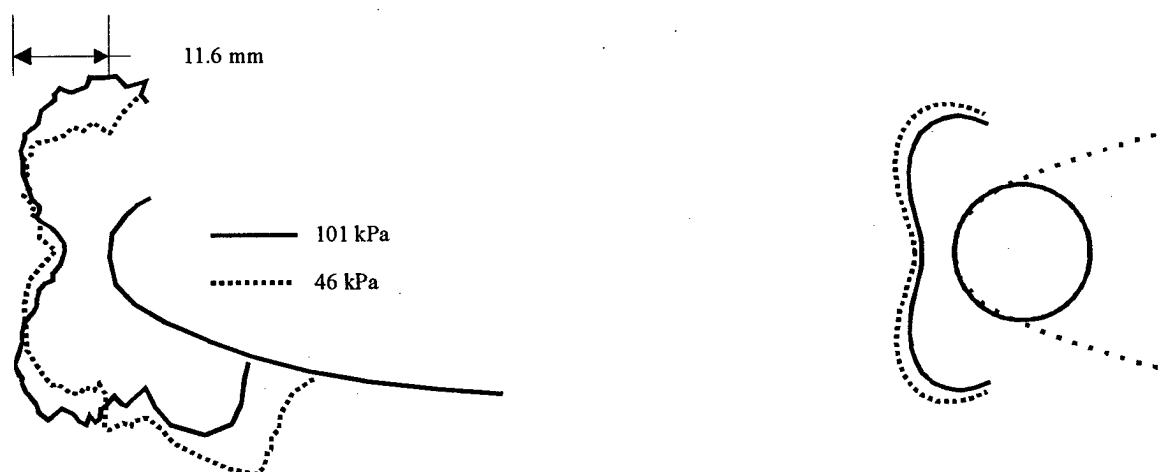


Fig. 5. Experimental results at left (Tests 23 & 28); cylinder icing model at right. (T: -5°C ; MVD: $23 \mu\text{m}$; LWC: $1 \text{ g}/\text{m}^3$; Time: 600 s; V: 95 m/s)

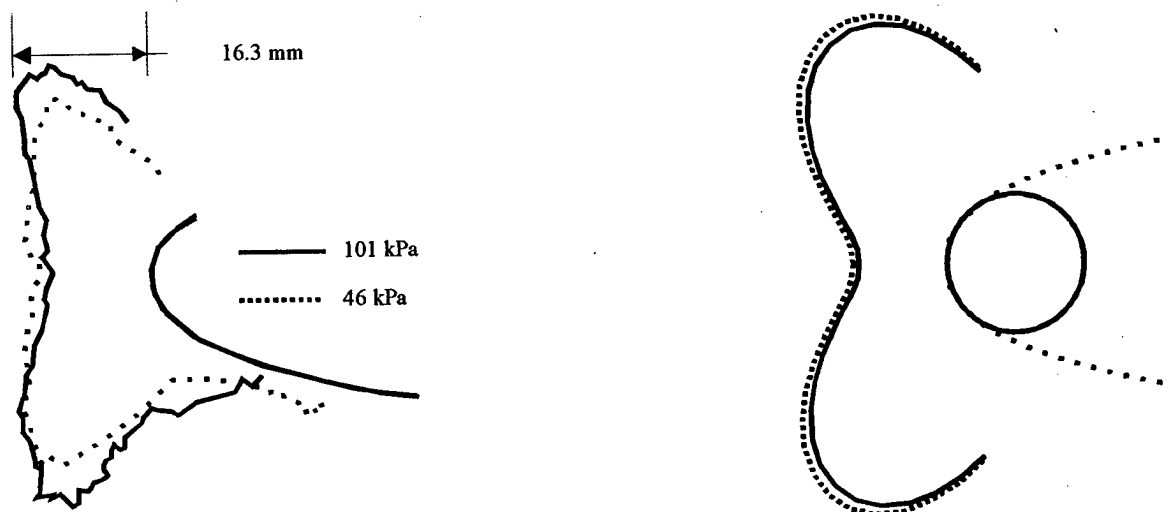


Fig. 6. Experimental results at left (Tests 24 & 29); cylinder icing model at right. (T: -10°C ; MVD: $23\text{ }\mu\text{m}$; LWC: 1 g/m^3 ; Time: 600 s; V: 95 m/s)

Finally, Fig. 7 gives the experimental and numerical results for a case with a static air temperature of -10°C , a liquid water content of 0.3 g/m^3 and a median volume diameter of $15\text{ }\mu\text{m}$. In this case, the observed ice thickness along the entire forward-facing section of the accretion decreases with increased altitude, but the extent of the accretion along the airfoil surface once again increases. The model predicts very little change in ice thickness as a result of the change in altitude, but suggests that the freezing fraction should be much higher (0.89) in this case than for the two previous cases.

As a basis for comparison, a series of tests

were performed over a range of air temperatures but at a constant pressure (101 kPa). Here the MVD was $19\text{ }\mu\text{m}$ and the LWC was 0.75 g/m^3 . The results of this series of tests are given in Fig. 8. Clearly, the changes in ice profile over this temperature range (-5°C to -30°C) are greater than those due to the variation in altitude given in the three previous figures.

The relatively small changes in ice profile shape with changes in altitude in comparison to the changes experienced with variations in air temperature noted here are in agreement with those noted in Ref. 16.



Fig. 7. Experimental results at left (Tests 10 & 11); cylinder icing model at right. (T: -10°C ; MVD: $15\text{ }\mu\text{m}$; LWC: 0.3 g/m^3 ; Time: 600 s; V: 95 m/s)

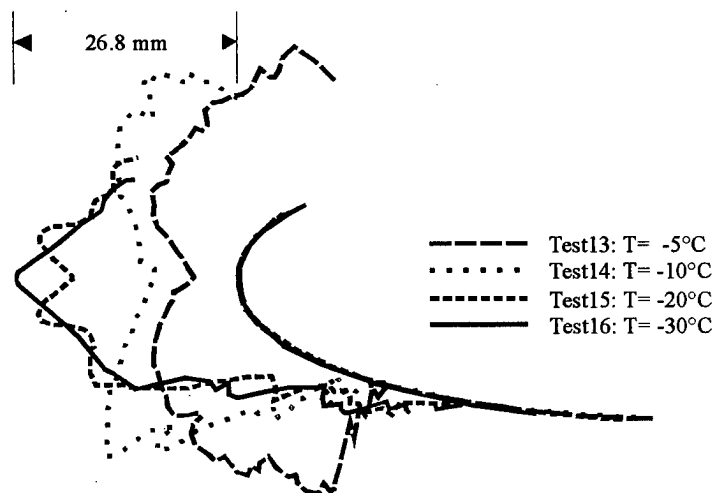


Fig. 8. An example of the effect of varying temperature.
(P: 101 kPa; MVD: 19 μm ; LWC: 0.75 g/m³; Time: 600 s; V: 95 m/s.

Conclusions and Recommendations

A series of tests performed in NRC's Altitude Icing Wind Tunnel have shed light on the effect that altitude can have on ice accretions formed on a NACA 0015 airfoil. The laser light sheet illumination and analysis technique, which was developed for determining the ice accretion profiles without disturbing the ice accretion process, provided high quality, reproducible profile shapes. The following conclusions can be drawn from the experiments:

1. Pairs of experiments in which only the air pressure changed showed that only relatively small changes in the forward-facing ice thickness occurred.
2. The extent of the ice accretion rearward along the airfoil surface increased consistently as the air pressure decreased. This could be due to the higher collision efficiency of droplet impingement at the lower pressure causing more runback and freezing of water further rearward, the greater extent of impingement along the upper and lower airfoil surfaces, or a combination of the two. Had the leading edge of the airfoil been de- or anti-iced, it is possible that the increased air accretions rearward on the airfoil surface at the lower

pressures could have had significant additional aerodynamic impact.

3. A simple numerical model utilized for predicting single-step ice accretion on a non-rotating cylinder provided good first-order approximations for the changes in ice accretion shape and thickness on the NACA 0015 airfoil when the cylinder radius matched the radius of curvature of the leading edge of the airfoil.

As a result of this study, it is recommended that:

1. Further experiments of this type be performed to better determine the effect of transitions between rime, mixed and glaze accretion types as air pressure varies.
2. Improvements to the spray system in the AIWT be completed which will ensure a more uniform LWC over the test section cross-section. In addition, the illumination of the upper airfoil surface by a second laser light sheet would permit a more accurate and complete profiling of the upper half of the airfoil ice accretion.
3. Further work should be performed on icing scaling laws to determine if a new law can be formulated which improves upon the compromises incorporated in the currently formulated laws while at the same time

allowing for more flexibility in the choice of scaled test conditions.

4. Because of the limitations of current scaling laws, the CIRA Icing Wind Tunnel should be constructed with an altitude capability. Not only would this allow for the direct simulation of conditions which exist at normal flight altitudes, but the additional degree of freedom permitted by the addition of variable air pressure would enhance the ability of the tunnel to perform accurately scaled icing experiments in those cases where some other simulation parameter (e.g. model size) cannot replicate the full-scale condition.

Acknowledgments

The authors wish to acknowledge the valuable contributions made to the success of this study by: Giuseppe Mingione, a numerical simulation specialist at CIRA who assisted with the selection of test conditions; Fred Hyde, a Technical Officer at NRC who was responsible for the operation of the tunnel and who made many improvements to the test setup and operating procedures; and Ryan Aebig, a high school student who very capably performed many of the ice accretion profile analyses during a work term at NRC.

References

1. Langmuir, I. and Blodgett, K.B., "A mathematical investigation of water droplet trajectories", *Collected Works of Irving Langmuir*, Vol. 10, Pergamon Press, 348-393, 1946.
2. Bragg, M.B., "A similarity analysis of the droplet trajectory equation", *AIAA Journal*, Vol. 20, 1681-1686, 1982.
3. Messinger, B.L. "Equilibrium temperature of an unheated icing surface as a function of airspeed", *J. Aero. Sci.*, 23-42, Jan. 1953.
4. Armand, C., Charpin, F., Fasso, G. and LeClere, G., "Techniques and facilities used at the ONERA Modane Centre for icing tests", North Atlantic Treaty Organization Advisory Group for Aerospace Research and Development, AGARD-AF-127, Nov. 1978.
5. Ruff, G.A., "Analysis and verification of the icing scaling equations, Vol. I", AEDC-TR-85-30, (AD-A162226), Nov. 1985.
6. Bilanin, A.J., "Proposed modifications to ice accretion/icing scaling theory", *J. Aircraft.*, Vol. 28, 353-359, 1991.
7. Bilanin, A.J. and Anderson, D.N., "Ice accretion with varying surface tension", AIAA 95-0538 and NASA TM 106826, Jan. 1995.
8. Anderson, D.N., "Methods for scaling icing test conditions", AIAA 95-0540, Jan. 1995.
9. Stallabrass, J.R., "An appraisal of the single rotating cylinder method of liquid water content measurement", NRC DME Report LTR-LT-92, Nov. 1978.
10. Lozowski, E.P., Stallabrass, J.R. and Hearty, P.F., "The icing of an unheated, nonrotating cylinder. Part I: A simulation model", *J. Clim. Appl. Meteor.*, Vol. 22, 2053-2062, Dec. 1983.
11. Ruff, G.A. and Berkowitz, B.M., "Users manual for the NASA Lewis ice accretion prediction code (LEWICE)", NASA CR-185129, May 1990.
12. Gent, R.W., "TRAJICE2 - A combined water droplet trajectory and ice accretion prediction program for aerofoils", DRA Technical Report TR90054, Nov. 1990.
13. Guffond, D. and Hedde, T., "Prediction of ice accretion: Comparison between the 2-D and 3-D codes", *Proc. First Bombardier Int'l. Workshop*, Sep. 1993.
14. Tran, P., Brahimi, M.T., Paraschivoiu, I., Pueyo, A., Tezok, F., "Ice accretion on aircraft wings with thermodynamic effects", AIAA 94-0605, Jan. 1994.
15. Bartlett, C.S., "An analytical study of icing similitude for aircraft engine testing", DOT/FAA/CT-86/35, AEDC-TR-86-26, Oct. 1986.
16. Bartlett, C.S., "An empirical look at tolerances in setting icing test conditions with particular application to icing similitude", AEDC-TR-87-23, DOT/FAA/CT-87/31, Aug. 1988.

SURVEY OF ICE ACCRETIONS FORMED
IN FREEZING DRIZZLE UNDER NATURAL ICING
AND SIMULATED ICING BEHIND THE UNITED STATES AIR FORCE TANKER
AND IN THE NASA-LEWIS ICING RESEARCH TUNNEL

BY

PORTER J. PERKINS
CONSULTANT, AIRCRAFT ICING
ROCKY RIVER, OH

JOHN P. DOW, SR.
FAA ACE-112
KANSAS CITY, MO

DAVE SWEET
BFGOODRICH AEROSPACE
ICE PROTECTION SYSTEMS DIVISION
UNIONTOWN, OH

ABSTRACT

Observations of ice formations in freezing drizzle on the same type airfoil obtained in natural icing, and simulated behind the Air Force Icing Tanker and in the NASA Icing Research Tunnel (IRT) are presented under similar measured icing parameters, including air temperature (near freezing), droplet sizes, and liquid water content. Photographs show the characteristics and locations of the ice around the leading edge of a wing as observed from both facilities. These parameters are important in evaluating the performance of aircraft components. Less costs are involved in tunnel testing which allows freedom of varying the icing parameters. On the other hand, if the effects of ice accretions on the aerodynamic performance and/or control of the aircraft are of prime importance, testing behind the tanker offers immediate and direct results. However, whether using icing tunnel or icing tanker to obtain ice shapes, dry wind tunnel testing or flight tests with artificial ice shapes are recommended for subsequent aerodynamic evaluation. Thus, the characteristics of the ice accretions formed from each test facility and their relation to natural icing need to be considered. No recommendations are given for testing in either facility. Effects of the ice accretions on the aerodynamic performance of the airfoil, if any, are not presented.

INTRODUCTION

Shortly after the October 31, 1994 accident of the ATR-72-212 aircraft in Roselawn, Indiana, information from various sources suggested the presence of freezing drizzle aloft, also known as supercooled drizzle drops (SCDD). Freezing drizzle (ZL) is a form of icing which is outside that defined in the 14 Code of Federal Regulation (CFR) part 25 Appendix C icing envelope. Freezing drizzle is characterized by droplets ranging from 200 to 500 microns in diameter. The mean volumetric diameter (MVD) of icing clouds defined by Appendix C is on the order of 10 to 50 microns.

The presence of freezing drizzle or freezing rain (ZR) is often associated with a temperature inversion, i.e., the air is warmer aloft than near the ground. According to FAA Report ADS-4 freezing rain most often exists from ground level up to an altitude of 5000 feet. SCDD, which was discovered during meteorological research flights, can exist at higher altitudes and is not associated with a temperature inversion.

Airborne de-icing systems used on transport category aircraft have been designed and certified to the requirements of Appendix C. Since the de-icing devices are located primarily in the vicinity of the airfoil leading edge, icing conditions which exist outside Appendix C may render these inadequate. In the case of the ATR-72 it is believed that the presence of drizzle size droplets in combination with near freezing temperature caused a spanwise ridge of ice to form chordwise aft of the area protected by the de-icing devices. It is also believed that the height of the ridge led to a separation of airflow such that it did not reattach ahead of the ailerons. A change of hinge moment was thus experienced which forced the ailerons to the right wing down position after the autopilot self-disconnected.

One of the recommendations of the National Transportation Safety Board to the FAA was to examine the hinge moment characteristics of the ATR-72 in the freezing drizzle icing environment. The manufacturer and the FAA were faced with a dilemma. There were few means available that could be used to develop realistic ice shapes to perform a reliable evaluation. The options were natural icing conditions, ice shape prediction codes, icing tunnels and icing tankers.

Ruled out first were ice shape prediction codes for several reasons. They had not been validated for droplets in the freezing drizzle size range nor were they sufficiently accurate at temperatures near freezing which was the thermal environment at the time of the accident. Additionally, assumptions inherent in the models used within the codes that made them sufficiently representative for droplets in the Appendix C icing envelope were obviously inappropriate for freezing drizzle or freezing rain size droplets (supercooled large droplets or SLD) such as assumption of spherical shape for droplets, no droplet breakup, no splashing, etc. Most problematic were thermodynamics and energy balance problems associated with glaze ice formation, that were daunting for large ice shape prediction. To modify or develop a code for these conditions would require careful comparison of theoretical models to measured icing. This process was estimated to require much longer than the time scale demands for the accident investigation.

Similarly, few icing tunnel experiments with SLD up to that time seemed to suggest that the resulting ice formations had substantial chordwise accretion -- far greater than limited natural observations but not as much height. Since height was one critical variable in the effect of the ice shape on the aerodynamic response of the airfoils, use of icing tunnels did not appear to offer the most representative results. Further scaling and other artifacts of the tunnel in this droplet size range might not be understood or interpreted easily. Finally, it would also be impractical to test various parts of the airplane as the engine, propeller, nose, and various wing sections without elaborate wind tunnel models.

Natural freezing drizzle conditions were infrequent and would therefore be difficult to locate, however, the key elimination factor for use of natural freezing drizzle conditions was the potential for an unsafe condition. After all, the goal of the evaluation was to attempt to determine how an airplane might experience an anomaly in the roll axis. A successful experiment may well result in another airplane accident.

FAA carefully weighed the benefits and the drawbacks of each method and finally requested that testing be accomplished using the United States Air Force icing tanker. The icing tanker (NKC-135A) was a modified refueling airplane similar to a Boeing 707. The tanker had been used for various in-flight icing tests. Tankers as a class were generally known to produce icing clouds containing droplets larger than Appendix C conditions. Up to the time of the SLD testing, the large droplet distribution characteristic considered undesirable, would now be an asset. Further adjustments to the water flow and air pressure settings would shift the distribution of droplets toward the freezing drizzle range.

On December 13, the test program commenced and the droplet cloud was measured by a chase airplane with instruments capable of sampling the parameters of the cloud. The tanker cloud droplet distribution characteristics compared favorably to natural icing cloud, and the resulting ice shapes appeared comparable to that described in anecdotal reports by operational pilots and by research pilots. The physics of the Tanker cloud were measured and the liquid water content (LWC) was higher than that obtained in natural icing conditions. However, the resulting ice characteristics appear to correspond favorably with ice accreted in the natural environment. Several factors, not totally understood, may account for such differences.

It was the first time the USAF Icing Tanker would generate an SLD icing cloud. Other benefits of the tanker were that various surfaces of the airplane could be tested in the cloud at full scale and representative flight conditions without, scale, or tunnel effects. This included the effects of propeller wash. Of course, there were tradeoffs. The icing cloud was approximately 9 feet in diameter at the test distance and maintaining a precise spatial relationship with the tanker was tedious. Due to the downwash from the tanker, water and fuel weight were important criteria in order to maintain an optimum flap setting at a given speed.

Through several tests, variations in the ice accretions led to the examination of the measured variables and how they might affect the outcome of the testing.

Further experiments and development at NASA's Lewis Research Center (LeRC) Icing Research Tunnel in SLD similarly progressed. Finally, separate testing was conducted on similar airfoils behind the icing tanker and the icing tunnel. The airfoil tested was also similar to that on an airplane used in instrumented research of SLD conditions. While not exhaustive, these three means provide some measure of gross comparability of the simulated icing conditions with each other and with the freezing drizzle size range of the natural SLD icing environment.

DISCUSSION

Table 1 of this report is a comparison of the Air Force icing tanker and NASA IRT simulations with what is currently known about the natural icing environment for SCDD. Specific benefits can be derived from testing in each environment.

Testing in the natural icing environment is preferred. However, the condition was believed to be fairly rare. FAA Report ADS-4 shows that of all icing encounters experienced in the 1948 icing season, only about 1% were large droplet or freezing rain encounters. There were no statistics for SCDD. Since the aircraft only experienced icing for a total of about 10% of the flight time, this means large droplet icing was only experienced about 0.01% of the total flight time. SCDD conditions are an even more rare occurrence. However, later statistics suggest that freezing precipitation may occur more frequently than previously thought, especially in certain geographical areas. If the aircraft has not been tested in SCDD conditions, the effects of potentially dangerous ice shapes on aircraft handling will not have been analyzed.

The icing tanker affords the user an opportunity to evaluate different surfaces on the aircraft to determine the effects of SCDD ice shapes on performance. After ice shapes are formed on limited areas, effects of these on handling and roll control can be readily evaluated.

However, control of environmental conditions may not be as precise as desired. An example is the effect of relative humidity when using the tanker. If the air is relatively dry many of the smaller droplets in the icing plume may evaporate prior to impinging on the surface being tested. Dry air may lead to significant differences in the resulting ice shape. Evaporation may freeze out ice in a short time altering the shape and sublimation may reduce the dimensions of the ice features. Temperature stability is important for large drop testing at temperatures near freezing where runback naturally contributes to ice formation. Selection of test areas to minimize temperature and humidity variations is an important consideration.

It is believed from flight recorder evidence recovered from the ATR-72 accident aircraft, that the outside air temperature environment was within a few degrees of the freezing point. As shown by Miller and Addy (Ref. 3), the formation of an ice ridge aft of the protected zone is greatly influenced by the temperature of the airfoil surface. If the outside temperature is very near the freezing point, the airfoil in the vicinity of the stagnation line will remain above freezing due to aerodynamic heating effects. This will cause the water to runback and freeze on aft areas. This

runback freeze phenomena is thus a major contributor to the initial site and growth rate of ridge formation. Control of temperature within a few degrees of freezing while flying behind the icing tanker is dependent upon the air mass and the underlying terrain. Flight over water or early in the day can enhance temperature stability.

The icing tunnel offers an environment in which temperature can be controlled to within one degree Centigrade. The tunnel also offers the user an opportunity to easily evaluate other factors leading to ridge formation. These include the height and location of surface anomalies, effects of extended protection, and performance of surface mounted ice detection sensors.

Table 1			
Survey of Natural Freezing Drizzle Conditions, Icing Tanker (Ref. 1, 2), and Icing Tunnel (Ref. 3)			
Parameter	Natural Conditions	Icing Tanker ⁽¹⁾	NASA Icing Tunnel
Droplet Distribution	40 to 400 μm Diam. ⁽²⁾	100 to 140 μm MVD	99 and 160 μm MVD
Liquid Water Content	0.15 to 0.50 g/m^3	0.60 to 0.90 g/m^3 ⁽³⁾	0.50 and 0.80 g/m^3 ⁽⁴⁾
Static Air Temperature (SAT)	0° to -18°C	Controlled by altitude	Calculated
Total Air Temperature (TAT)	Determined by aircraft velocity, SAT, PA	Determined by aircraft velocity and SAT, PA	1.0° and -15°C
Temperature Stability	N/A	$\pm 0.5^\circ\text{C}$ ⁽⁵⁾	$\pm 0.5^\circ\text{C}$
Relative Humidity	$\leq 100\%$	12 to 90% ⁽⁵⁾	$> 80\%$
Angle-of-Attack	Variable	Variable by Speed	Variable
Speed Range	Variable	150 to 350 KTAS	109 to 169 KTAS
Test Section	Unlimited	$< 6'$ to $8'$ Diameter	$6'$ by $9'$
Typical Effective Cloud Width	Unlimited	$4'$ to $5'$	$1'$
Ice Shape Determination and Location	Photographic	Photographic	Photographic & Direct Measurement
Altitude	Variable	Variable ⁽⁶⁾	3000' PA
Other	Effects of engine/propeller wash or other features can be directly observed	Effects of engine propeller wash or other features can be directly observed. Dye enhances the ability to visualize the icing process: Yellow indicates ice; green indicates water.	Ability to mold ice shape and determine roughness. Dye can be added to tunnel water.
References	R. Ashendon	R. Hobbs	G. Addy/D. Miller

(1) Based on testing to date with standard configuration. Does not reflect the potential for increased range by changes to the nozzle design.

(2) For natural icing conditions the range of diameters is given. For others it is the median volumetric diameter (MVD) is used. MVD means that 50% of the liquid water of the icing cloud is found in droplets larger, and 50% of the liquid water in droplets smaller than the theoretical MVD). However, due to the small number of larger droplets, a more representative measurement is 80 VD where 80% of the liquid water would be found in droplets smaller and 20% in droplets larger than the 80 VD. An alternate expression of MVD could be 50 VD. For example, in a natural icing encounter of freezing drizzle, the MVD was 112 μm while the 80 VD was 147 μm .

(3) The values shown are those that have been used for tests and are not intended to suggest limiting values of the system.

(4) Relationship of LWC is a fixed function of droplet distribution.

(5) Subject to the test environment

(6) Minimum altitudes are prescribed for test safety reasons.

Comparison of ice formations behind the tanker and in the IRT with natural conditions.

As part of the FAA program last fall to evaluate turboprop aircraft for susceptibility to large droplet conditions, the Embraer Model EMB-120 was flown in simulated conditions behind the icing tanker at Edwards Air Force Base. At the same time the wing airfoil was also tested within the NASA Lewis IRT. Both tanker and tunnel ice formations on this 230XX airfoil could thus be compared.

Wing Icing Behind the Tanker

Results of icing at TAT of +2.7 to +3.7°C is observed in Figure 1 (a)* extending to 2 inches aft of the last active tube. Ice is seen around the leading edge prior to boot activation. A narrow zone of no ice exists at the stagnation line on the leading edge.

Figure 1 (b & c) show ice formations after 20 minutes exposure to the spray cloud. Ice ridges were on the inactive part of the top surface of the boot. Partial periodic self shedding was noted. Figure 1(c) is a close-up photo which points out the jagged nature of the ice ridge with separate large lumps of ice. Chunks of ice estimated at 3/4" high can be seen at random areas along the span. For the most part, a clean surface exists in the active area of the boot. Conditions were: TAT +2.6 to 2.7°C (SAT -3.0°C); Rel. Hum. 32 to 30%; airspeed 175 KIAS; altitude 14,550 ft; MVD 104-135 microns; and LWC 0.59-0.86 g/cu m.

A large ice ridge aft of the boot is shown in line with the prop wash on the wing between the fuselage and nacelle in Figure 1(e).

Wing Icing in the NASA Icing Research Tunnel

With the precise temperature control in the tunnel, temperature effects are readily visible. Figures 2(a & b) show an ice formation on the suction side of the airfoil when the total air temperature was set at 34°F (195 mph). The angle of attack was zero degrees and the de-icer was cycled every 3 minutes.

Results after 18 minutes of icing are shown. Most of the surface of the airfoil remains at a temperature above freezing. Impinging water runs back and freezes at the chordwise aft limits of the de-icer. It is believed that the surface discontinuity at this point becomes a collecting point for the runback, and thus a site for ridge formation. Partial self shedding of the ice ridge occurs at this temperature as evidenced by the missing section of ridge above the center of the effective SLD cloud.

Figures 2(c & d) show the pressure side of the airfoil during the same test. Some ridge formation is seen at the chordwise aft edge of the de-icer. However, all of the water within the effective SLD cloud (as denoted by the chordwise painted lines) has runback and frozen at > 20% chord.

* For Figures 1(a) through 3(b), refer to pages 202-214

Figures 2(e & f) show the ice formation on the pressure side of the airfoil when the total air temperature has been reduced to 28°F (only test parameter changed). Figure 2(f) specifically shows a much smaller area in the vicinity of the stagnation line which remains free of ice. The de-icer has been cycled every 3 minutes up to 15 minutes and the test shut down after 18 minutes total icing. The ridge height is jagged and with peaks as high as 1.45 inches. Effects of de-icer cycling are readily apparent as the site of the primary ice ridge is at the aft limit of the de-icer tubes.

Figure 2(g) shows the pressure surface of the airfoil at 28°F. Again a ridge has formed at the chordwise aft limit of the de-icer tubes. This ridge has prevented droplet impingement beyond.

Experiments were run in which the de-icers were not cycled for the duration of the test. Figure 2(h) shows the ice shape that resulted.

The test conditions were 28° (total) air temperature, angle of attack of 1.3 degrees, a 21 minutes encounter at 195 mph. Figure 2(j) is a close-up of the jagged rough ice shape. At this temperature, all of the ice was contained within the chordwise limits of the de-icer.

All of the figures shown used a cloud of 160 μm MVD and LWC of 0.82 g/m^3 . An impingement test of this cloud was run at 0 degrees angle of attack. The duration of the run was 3 minutes. The tunnel total temperature was set at 0°F. This was done so that all of the water would freeze upon impact. Figures 2(k) and (l) show the ice formation of the suction side of the airfoil. Impingement limit is judged at 13% chord. Figures 2(m) and (n) show the ice on the pressure side of the airfoil. Impingement was judged to be at 21% chord.

Wing Icing In Natural Conditions

Encounters with drizzle droplet icing have been reported by research meteorologists. The University of Wyoming using an instrumented King Air 200 have reported on about 30 encounters since 1982 (Reference 4). In one encounter, the pilot (George Bershinsky) described a build-up of a one inch high ridge of jagged ice on top of the wing behind the de-icer (Reference 5). An immediate departure from the icing condition was required.

Photographs provided by another University of Wyoming pilot (Dr. Wayne Sand) are shown as Figures 3(a) and 3(b). Ridges of ice characteristic of the simulated ice accretions behind the tanker and in the icing tunnel are seen. The aircraft has the same type airfoil as was tested in the tunnel and behind the tanker.

Figure 7.21 reprinted from Reference 6 shows a significant loss of climb rate during a natural drizzle droplet encounter (not associated with Figures 3(a) and 3(b)). Figure 7.26 also reprinted from Reference 6 shows droplet data taken at the time of maximum performance loss. According to Sand, images of droplets in the 200 to 300 micron diameter range were clearly visible.

* For Figures 1(a) through 3(b), refer to pages 202-214

CONCLUSIONS

Our conclusions from the comparisons of the simulation methods with natural SCDD icing are limited due to the short time in which this phenomena has been studied. However, we believe that the icing clouds produced by both the tanker and the icing tunnel are reasonable representations of nature by their droplet size distributions and as they produce similar ice shapes. **We also believe that whatever facility is used to simulate the natural environment, careful attention to the variables presented in this paper and the referenced works is critical.** We also appreciate that much work has been done in a relatively short timeframe by some very competent icing and aircraft professionals.

REFERENCES

- 1.) Ashenden, R. And Marwitz, J. D.: "Supercooled Large Droplet Distributions in the Natural Environment and Comparison to Artificial Drizzle from the Air Force Water Spray Tanker." To be presented at the FAA International Icing Conference, Springfield, VA, May 1996. This paper revised from AIAA 96-0632.
- 2.) Ashenden, R.: "The Air Force Flight Test Center Artificial Icing and Rain Testing Capability Upgrade Program." Presented at the 31st Aerospace Sciences Meeting & Exhibit, Reno, NV, Jan. 11-14, 1993. AIAA 93-0295.
- 3.) Miller, Dean R.; Addy, Harold E, Jr.; and Ide, Robert F.: "A Study of Large Droplet Ice Accretions in the NASA-Lewis IRT at Near-Freezing Conditions." Prepared for the 34th Aerospace Sciences Meeting and Exhibit, sponsored by AIAA, Reno, NV, Jan. 15-18, 1996.
- 4.) Bershinsky, George, Ashenden, Russel and Marwitz, John D.: "Recognition of Drizzle Induced Icing and Recommended Escape Procedures." Department of Atmospheric Sciences, University of Wyoming, Laramie, WY 82071.
- 5.) Bershinsky, George: "My First Time".
- 6.) Sand, Cooper, Politovich, Veal, "Icing Conditions Encountered by a Research Aircraft" **Journal of Climatic and Applied Meteorology**, Volume 23, Number 10, October 1984.

ACKNOWLEDGEMENTS

Contributions to this document by the following individuals are greatly appreciated by the authors:

Mr. Harold Addy, Jr.; NASA-Lewis Research Center.

Mr. Russell Ashenden; University of Wyoming

Mr. George Bershinsky; Pilot.

Mr. Rene Landman; Aerodynamicist, Embraer

Dr. John Marwitz; University of Wyoming

Mr. Dean Miller; NASA-Lewis Research Center

Mr. Decio Pullium; Chief Aerodynamicist, Embraer

Dr. Wayne Sand, Consultant

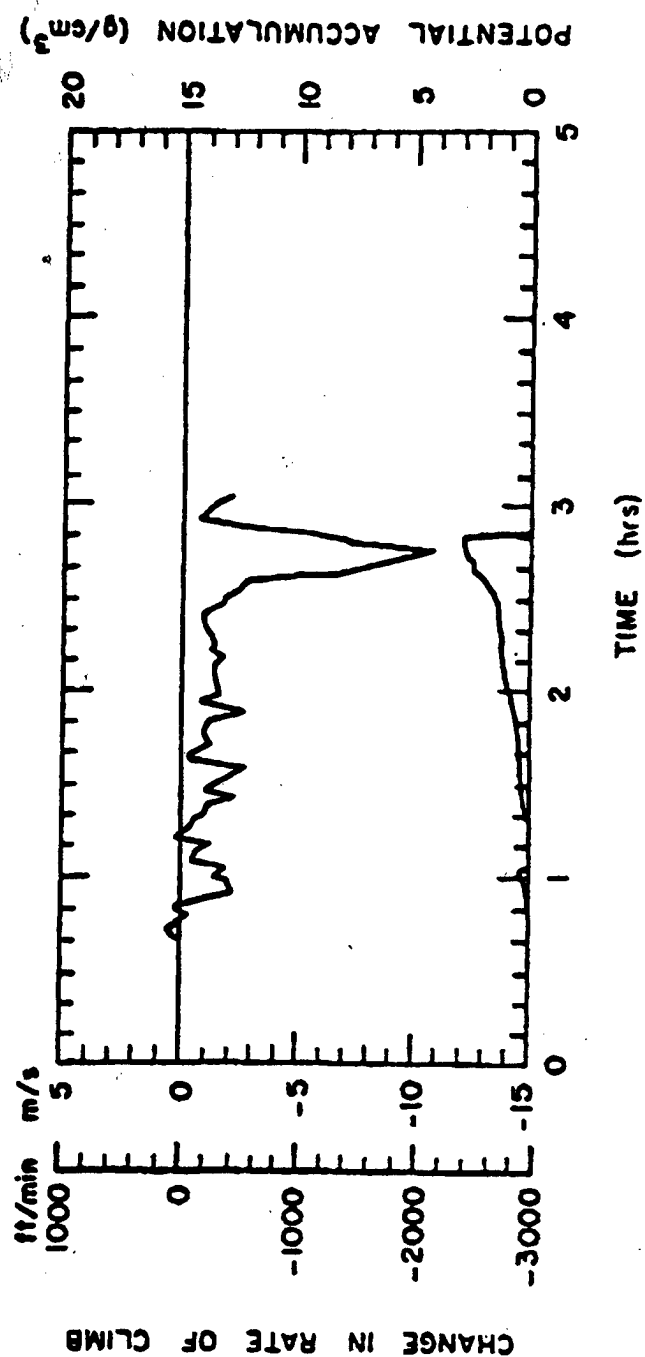


Figure 7.21: The potential accumulation (lower curve) and the difference between the expected and actual rates of climb (upper curve) for the 26 February 1982 flight. The expected rate of climb was calculated from the recorded power setting and airspeed, via use of the performance coefficients CL and CD for the clean aircraft. The time starts at 1800Z.

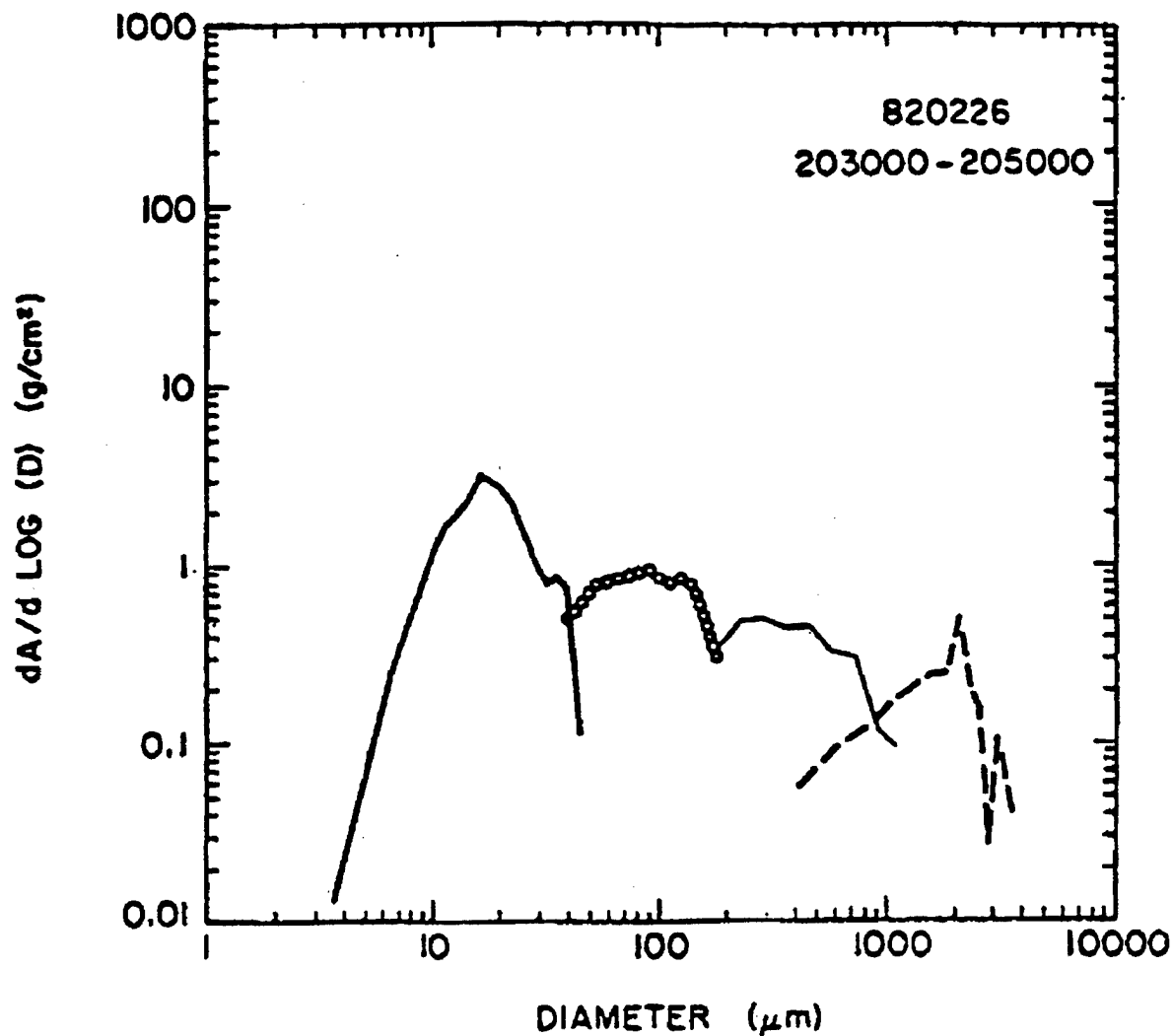


Figure 7.26 Contributions of different parts of the hydrometeor spectrum to the potential accumulation (A) of 26 February 1982, for the interval 2030-2050Z when the maximum performance degradation occurred. All objects were assumed spherical water drops in this calculation, but in this case the 2D images verified that this assumption was valid for most of the hydrometeors.

AIRCRAFT ICING DUE TO SUPERCOOLED LARGE DROPLETS

M.T. Brahimi* P. Tran† F. Tezok‡ I. Paraschivoiu§

*Department of Mechanical Engineering, École Polytechnique de Montréal
C.P. 6079, Succ. Centre-Ville, Montréal, P.Q., Canada, H3C 3A7*

*‡Advanced Aerodynamics, Bombardier Inc./Canadair
400 Côte-Vertu, Dorval, P.Q., Canada, H4S 1Y9*

ABSTRACT

In recent years, many theoretical and experimental studies have been conducted to investigate ice accretion observed on aircraft components. However, most of these studies were concerned with the case of ice accretion in moderate meteorological conditions. The objective of this paper is to study the magnitude of the effects of supercooled large droplets (SLD) on aircraft operating in natural icing conditions. Results are presented in terms of impingement limits, local and global collection efficiencies and, finally ice accretion shapes. The numerical model used in the present study is based on *CANICE* icing code developed by the J.-A. Bombardier Aeronautical Chair with the collaboration of Bombardier Inc./Canadair. This code has the capability to predict ice accretion on supercritical and multi-element airfoils, and on wings using the equivalent angle of attack method. The numerical model is based on iterative process with a time-stepping procedure where successive thin ice layers are formed on the surface and followed by flowfield and droplet impingement recalculations.

NOMENCLATURE

c	: chord length, m	\vec{r}	: droplet position, m
C_D	: drag coefficient	Re	: Reynolds number
C_L	: lift coefficient	s	: impingement position, m
D	: droplet diameter, m	T	: temperature, $^{\circ}C$
E	: global catch efficiency	\vec{V}_{∞}	: freestream velocity, m/s
E_{hw}	: ratio of mean height to width	\vec{V}_a	: air velocity, m/s
\vec{F}_b	: buoyancy force, N	\vec{V}_r	: relative velocity, m/s
\vec{F}_D	: drag force, N	\vec{V}_T	: terminal fall velocity, m/s
\vec{F}_g	: gravitational force, N	x	: horizontal coordinate, m
\vec{g}	: gravitational acceleration, m/s^2	y	: vertical coordinate, m
Ga	: Galileo number	y_0	: release position, m
h	: airfoil project height, m	α	: angle of attack, deg
h_c	: convective heat transfer, $W/(m^2^{\circ}C)$	β	: local catch efficiency
k_s	: roughness height, m	β_{max}	: maximum local catch efficiency
LWC	: liquid water content, kg/m^3	Δy_0	: effective height, $(\Delta y_0 = Eh)$, m
N_D	: Best number	μ_a	: air dynamic viscosity, kg/ms
		ρ_a	: air density, kg/m^3
		ρ_d	: droplet density, kg/m^3

*Research Associate, École Polytechnique

†Ph.D. Student, École Polytechnique

‡Staff Specialist, Bombardier Inc./Canadair

§Aeronautical Chair Professor, École Polytechnique

1. INTRODUCTION

Investigation of aircraft crashes due to wing contamination indicates that for the safe operation of an aircraft, current regulations applicable to ice, frost or snow accumulation might not be effective in preventing aircraft icing accidents [1, 2]. Particularly, for aircraft operating outside the certification envelope of the Federal Aviation Regulation (FAR) as in icing environment where supercooled large drops (SLD) exist. This has been identified as a possible cause of the ATR-72 crash in 1994 [3] and has served to focus the attention on icing due to SLD and other icing conditions outside the FAR-part 25. In addition, the development and design of new aircraft incorporating advanced and modified control and lifting surfaces have presented the Federal Aviation Administration with new certification and flight safety assessment issues.

Many theoretical and experimental studies have been conducted to investigate ice accretion observed on aircraft components. However, most of these studies were concerned with the case of ice accretion in moderate meteorological conditions where droplets size do not exceed $40\text{ }\mu\text{m}$ which is the upper limit of the FAA certification envelope. Currently, more work is being undertaken to investigate ice accretion due to supercooled large droplet such as the simulation of SLD behind the Air Force KC-135 Tanker [4] or as the simulation of SLD on a full scale Twin-Otter wing section at the NASA-Lewis Icing Research Tunnel (IRT) [5]. The objective of the present work is to investigate the effects of supercooled large droplets (SLD) on ice accretion. Results are presented in terms of impingement limits, local and global collection efficiencies, and ice shapes. The numerical model used in the present study is based on *CANICE* icing code which has the capability to predict ice accretion on supercritical and multi-element airfoils, and on wings by using the equivalent angle of attack method [6, 7].

2. MECHANISM OF ICE FORMATION

Icing on aircraft components such as wings, control surfaces and engine intakes occurs when the aircraft flies at a level where the temperature is at, or slightly below the freezing point and the atmosphere contains supercooled water droplets. When a droplet hits aircraft surfaces it begins to freeze immediately. As the water

freezes, heat is released so that its temperature rises until it reaches 0°C . As this temperature is reached, freezing stops while the remaining liquid fraction of the droplets starts to run back along the surface of the aircraft or along existing ice. The rate of heat loss from the aircraft surfaces is such that some or all of the droplets are frozen before they can run off the body. Two basic types of ice can be formed, rime ice, if all the impinging water droplets freeze upon impact, or glaze ice if only a fraction of the water droplets freezes while the remainder runs back along the body surface.

The amount and the shape of ice collected depend mainly on liquid water content, temperature, airspeed, droplet size and surface roughness. The droplets formed in the cloud are not all of the same size. Due to their inertia and different fall velocities these droplets may collide and often coalesce to form large drops. Another way for large drops to form is through the melting of snow while falling in a warm layer of air [3]. The most dangerous icing develops when the ambient temperature is at or slightly below freezing point and the aircraft flies through a region where the liquid water content is high and droplets are large.

Results from wind tunnel and flight icing tests indicate that ice accretion on aircraft components can lead to a number of aerodynamic degradation problems and consequently is a major safety problem [8, 9]. The most severe penalties encountered are decreased maximum lift, increased drag, decreased stall angle, changes in the pressure distribution, early boundary-layer transition, increased stall speed and reduced controllability. The droplet size influences the rate of icing through the increase of collection efficiency and the change of the upper and lower impingement limits which move further downstream. The drops also form an irregular shape of ice ridge beyond the airfoil protection systems [5]. A reduction of wing lift by as much as 60% and an increase of drag by 100% have been observed due to ice contamination as a consequence of supercooled large droplets [10]. This observation is less severe in the case of ice accretion due to small droplets where lift is reduced by 30% and drag is increased by 40% [11].

3. BACKGROUND

Despite the advances made in theoretical and experimental techniques to investigate ice accretion on aircraft operating in natural icing conditions [8, 12] and the existence in many countries of regulations regarding flight in icing conditions, we are still faced with icing-related accidents. Presently, one of the most important part in the investigation of aircraft icing is to understand the micro-physical processes of ice accretion such roughness, boundary-layer transition, separated flow, local heat transfer, effect of large drops exceeding the upper limit of the FAA certification envelope and de-icing/anti-icing fluid behaviour. Several researchers [8, 13] have developed 2-D and 3-D models to predict aircraft icing in moderate meteorological conditions and calculate the aerodynamic characteristics of lifting and non-lifting surfaces with ice, NASA [14], DRA (England) [15], ONERA (France) [16] and Bombardier Chair (Canada) [6]. These significant studies started with the work of Bragg [17], Lozowski and Oleskiw [18], Frost *et al.* [19], and Cansdale and Gent [20]. In the light of these developments, more experimental and theoretical investigations of icing have been performed by many researchers such as Flemming and Lednicer [21], Cebeci [22, 23], and Bragg and Khodadoust [24]. Other important studies involving experimental observations of ice accretion mechanisms has been conducted by Hansman [25]. ONERA has also initiated a research program to predict ice accretion, work is being conducted by Guffond [26] for the 2-D case and by Hedde and Guffond [27] for the 3-D case. Presently, researchers are concerned with the improvement of actual icing codes by developing models for physical icing parameters such as drop size, roughness height, ice density, droplet drag coefficient, drop breakup and drop splashing. Since the crash of ATR-72 near Roselawn, Indiana, on October 31, 1994 now more attention is actually focused on icing due to SLD [4, 5, 10, 28] since it is believed that it represents a probable cause of the crash.

4. CALCULATION APPROACH

Simulation of ice accretion is divided into four basic calculation modules: flowfield calculation, trajectory calculation and impingement characteristics, thermodynamic analysis and geometry

update. The accuracy of any ice prediction will depend on the accuracy of each parts involved in the calculation. The main objective of ice simulation is the calculation of the impingement of the particles on the airfoil which determines the droplet impingement regions as well as the mass of liquid on the body surface. The main applications are for use as input to ice accretion calculation, to predict aerodynamic performance degradations, and for use in the design of de-/anti-icing systems. The computational procedure is an iterative process with a time-stepping procedure where successive thin ice layers are formed on the surface and followed by flowfield and droplet impingement recalculations. This procedure is performed for each time step to calculate a new ice layer.

Flowfield Calculation

The flowfield calculation provides the velocity field at the airfoil surface as well as at any point in the field away from the surface. In the present study, a 2-D flowfield calculation module, based on the panel method of Hess & Smith [29] has been developed and implemented in the ice accretion calculation code to obtain ice shape on airfoil surface. Other authors have suggested to solve Navier-Stokes equations to obtain flowfield velocities, however, it is believed that no additional accuracy is provided [30]. This is due to the use of empirical models within the energy balance and to the limited understanding of surface roughness with ice. As a consequence, it is more convenient to use a simple model, such as panel method, to calculate the flowfield velocities and then perform droplet trajectories calculation. In the case of multi-element airfoils, an extension of the Hess & Smith panel to multiple element configurations has been incorporated into *CANICE-ME* code [7]. Once the flowfield for a given geometry has been determined, the trajectory module uses this information to compute droplet trajectories from release points upstream of the airfoil leading edge.

Droplet Trajectory Calculation

Droplet trajectories are determined by solving the equation of motion to obtain the entire path for each droplet moving in the flowfield and hitting the airfoil. Once the trajectory paths are known, the droplet impingement limits as well as the global and local collection efficiencies can be calculated using an efficient scan procedure

of the airfoil frontal surface. The calculation of the water flux impinging on each panel forming the airfoil surface is performed, then the ice accretion is calculated and the geometry is modified defining the ice shape for the first time step. This procedure is performed for another time step to calculate a new ice layer.

The forces acting on a droplet moving in a steady airflow are aerodynamic drag \vec{F}_D , buoyancy \vec{F}_b and gravitational forces \vec{F}_g .

$$m \frac{d^2 \vec{r}}{dt^2} = \vec{F}_D + \vec{F}_g + \vec{F}_b \quad (1)$$

The drag force, which depends on air density, projected frontal area, drag coefficient and local relative velocity, tends to keep the droplets on streamlines, while the inertial force, which depends on the droplet mass and its rate of velocity change, forces the droplets to continue in a straight line. Since the mass of droplets is proportional to density times the cube of the diameter and projected frontal area is proportional to the square of the diameter, changes in droplet size will have larger effects on its inertia than on drag. Consequently, large drops are deflected less than smaller ones. This deflection is well expressed by the collection efficiency number, β , which is defined as the ratio of the surface mass flux to the freestream mass flux. The higher the droplet size the higher the collection efficiency is.

At each integration step, the local velocity needed to solve the droplet equation of motion is obtained from the flowfield solution while the integration is continued following droplets until they impinge on the airfoil surface or pass downstream of the airfoil. The droplet equation of motion is given by

$$\frac{d^2 \vec{r}}{dt^2} + \frac{C_D Re}{24} \frac{1}{K_A} \frac{d \vec{r}}{dt} = \vec{K}_G + \frac{C_D Re}{24} \frac{1}{K_A} \vec{V}_r \quad (2)$$

where $\vec{K}_G = (\rho_d - \rho_a) \vec{g} / \rho_d$, $K_A = \rho_a D^2 / (18 \mu_a)$ and droplet Reynolds number $Re = \rho_a D V_r / \mu_a$. The droplet trajectory equation represents a second order differential equation which can be solved using classical difference methods.

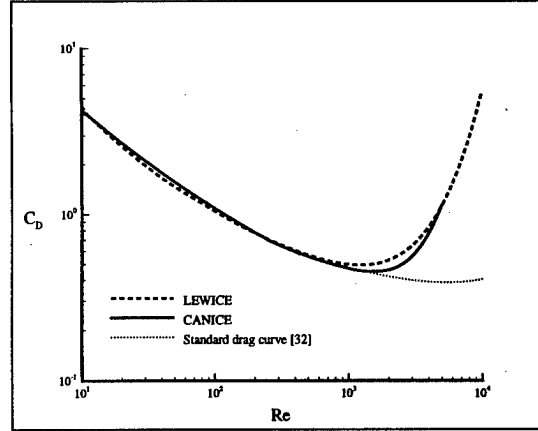


Fig. 1. Drag coefficient as function of Reynolds number

Droplet Drag Coefficient

The coefficient $C_D Re / 24$ in Eq. 2 is a function of Reynolds number and can be determined using a steady-state drag coefficient for a sphere. Many empirical and semi-empirical equations have been proposed to determine drag coefficient as a function of Reynolds number [31, 32]. Most of these relations have been reviewed and critically evaluated by Clift *et al.* [32] and by Khan and Richardson [33]. In the present study, the recommendation of Clift *et al.* for calculating the value of C_D embracing the complete standard drag curve (from $Re = 0.01$ to $Re = 10^6$) has been adopted. The whole range of Reynolds number is divided into 10 subintervals with a distinct correlation for each interval although Khan and Richardson [33] suggested only one equation for $0.01 < Re < 3 \cdot 10^5$

$$C_D = (2.25 Re^{-0.31} + 0.36 Re^{0.06})^{3.45} \quad (3)$$

Figure 1 shows the variation of drag coefficient for a sphere as a function of Reynolds numbers as used by LEWICE and CANICE compared to the standard drag curve [32]. It is important to note that drops larger than 1 mm in diameter are significantly non spherical, in this case the ratio of mean height to width is approximated, by [32]

$$E_{hw} = 1.030 - 0.0062D \quad (4)$$

where D is in mm ($1 < D < 9$ mm), Fig. 2. This deformation increases the drag coefficient

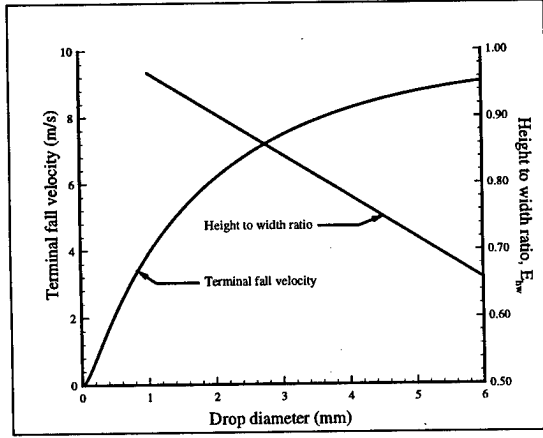


Fig. 2. Terminal fall velocity and drop ratio E_{hw} as function of droplet diameter

above the standard drag curve (Fig. 1, *CANICE* curve). In the present study an empirical correlation has been calculated based on the curve (C_D vs Re) given by Clift *et al.* [32]. For $Re \leq 1200$ the correlation for the standard curve is adopted while for $Re > 1200$ the following equation is used

$$C_D = a + bRe^3 + c \frac{\ln Re}{Re} \quad (5)$$

where $a = 0.35219227$, $b = 6.11571126 \cdot 10^{-12}$ and $c = 15.96227280$.

Free Fall Velocity

To start the droplet trajectory calculation, it is necessary to determine the initial position from where the droplet is released, hence the falling velocity must be calculated. To predict particles terminal falling velocities the forms of correlation of Re vs C_D are not convenient since the unknown velocity appears in both parameters. However, we can evaluate the value of $C_D Re^2$ only as a function of physical properties of the particle and fluid and the acceleration due to gravity. A new dimensionless parameter known as Galileo number is defined as

$$C_D Re^2 = \frac{4 g \rho_a (\rho_d - \rho_a) D^3}{3 \mu_a^2} = \frac{4}{3} Ga \quad (6)$$

where the dynamic viscosity of air is given by

$$\mu_a = 2.6936 \cdot 10^{-6} \frac{T^{3/2}}{1.8 T + 216} \quad (7)$$

Based on the large number of experiments, Clift *et al.* [32] derived an expression of Reynolds number as a function of Best number, N_D ($N_D = 4/3Ga$). More recently, Khan and Richardson [33] derived an expression of Reynolds number as a function of Galileo number by minimizing the difference between calculated and measured values. The general equation for Reynolds number, $10^{-2} < Re < 3 \cdot 10^5$, is given by

$$Re = (2.33Ga^{0.018} - 1.53Ga^{-0.016})^{13.3} \quad (8)$$

Once the Reynolds number is known it is possible to calculate the terminal falling velocity of the droplets. Figure 2 gives the distribution of the terminal velocity as a function of droplet diameter. This curve is approximated using curve-fitting by

$$\ln V_T = a + b(\ln D)^2 + c \ln D \quad (9)$$

where $a = 1.35643444$, $b = 0.17207999$ and $c = 0.78122037$. The terminal fall velocity is used to determine the initial droplet velocity where the horizontal component is equal to the air velocity and the vertical component is taken as the sum of free fall and air velocities.

5. HEAT TRANSFER ANALYSIS

Thermodynamic analysis of ice process on the iced surface is based on the first law of thermodynamics which states that the mass and energy must be balanced in a control volume on the surface. The model is based on work by Messinger [34]. The heat transfer coefficient, h_c , is computed from two empirical relations, one for the laminar region and one for turbulent region. The laminar-turbulent transition is determined using Von Doenhoff criterion [35]. The convective heat transfer model requires the specification of the equivalent sand grain roughness, k_s . This parameter is either uniform or function of liquid water content, static air temperature and droplet diameter as given by Shin *et al.* [9]. The correlation was used by assuming that the roughness parameter for V_∞ is constant as it was demonstrate by experimental study [36]. The empirical relation is given by

$$k_s = 0.6839 \left[\frac{k_s/c}{(k_s/c)_{base}} \right]_{LWC} \left[\frac{k_s/c}{(k_s/c)_{base}} \right]_T \left[\frac{k_s/c}{(k_s/c)_{base}} \right]_D \left(\frac{k_s}{c} \right)_{base} c \quad (10)$$

6. RESULTS AND DISCUSSION

Effects of airfoil geometry

The effects of the most influencing parameters have been investigated using *CANICE* code and confirmed the observations of several authors [8, 9, 13, 37]. Ice shape is influenced by ambient temperature, liquid water content, accretion time, angle of attack, freestream velocity, drop size, roughness height and chord length. An extensive analysis has also been done by Bragg and Gregorek [38] to study the droplet impingement characteristics and analyze the icing properties of 30 low and medium speed airfoils. It was found that new airfoils such as NASA MS(1)-0317, NASA GA(W)-2, OSU NLF-0315, FX-67-K170/17 have no significant differences in icing characteristics compared to NACA airfoils. In Figure 3, the distribution of global catch efficiency is plotted as a function of maximum airfoil thickness for 0 deg angle of attack. Airfoils from 9% to 20% thickness show that the global catch efficiency decreases with increasing thickness. However, the total mass accumulated on each airfoil increases with increasing thickness due to the increase of effective height as shown in Fig. 4. Figure 5 illustrates to show the effect of camber on resulting ice shapes at ambient temperature of -12.6°C , velocity of 129.46 m/s , liquid water content of 0.5 g/m^3 , droplet diameter of $20 \mu\text{m}$, angle of attack of 0 deg, chord length of 0.3 m and accretion time t of 120 s . The general shape for both NACA 0012 and NACA 4412 airfoils is similar although the impingements limits are slightly different. The ice shape near the nose is almost identical. The distribution of local catch efficiency, β , for both airfoils is presented in Fig. 6. As expected from ice shapes, the maximum β is similar but the impingements limits for the cambered airfoil are shifted towards the upper surface. Other effects on icing characteristics, such as leading edge radius and maximum camber, are given in reference [38].

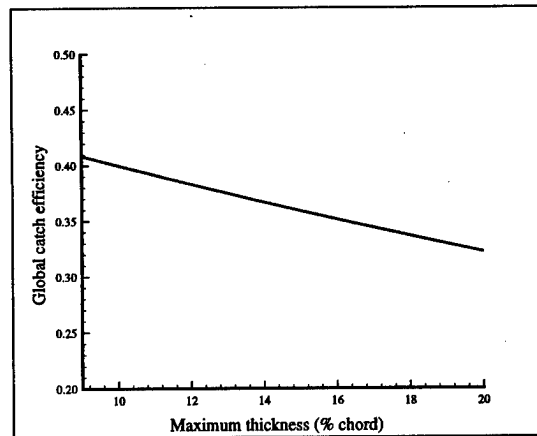


Fig. 3. Global catch efficiency as function of maximum thickness

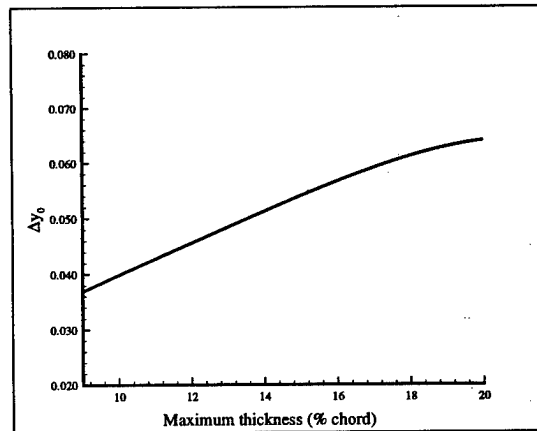


Fig. 4. Effect of maximum thickness on effective height

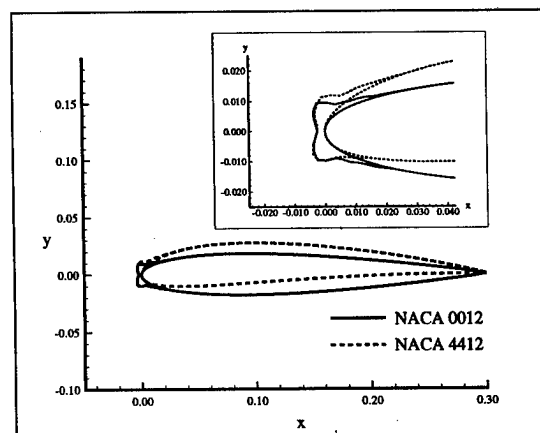


Fig. 5. Effect of camber on glaze ice shapes

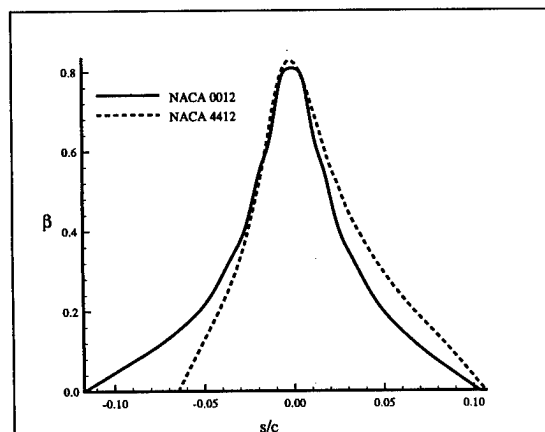


Fig. 6. Local catch efficiency for symmetrical and cambered airfoils

Effects of supercooled large droplets

To study the magnitude of the effects of supercooled large droplets (SLD) on ice accretion, *CANICE* code has been adapted to handle SLD simulation. Predictions of global and local catch efficiencies, droplet trajectories and ice shapes are presented. Differences between small and large drops reside in the very large inertial force of SLD and their non negligible free fall velocity. These effects may be seen in Fig. 7 where two droplets starting from the same point are released. The smaller droplet avoids the airfoil whereas the larger droplet impinges on it. To impact on the airfoil, large drops are released at higher y coordinate compared to small droplets as shown in Fig. 7 where y_0 denotes the release point of impacting droplets and s , the impingement position. To study the effect of droplet diameter on catch efficiency, the beta curves are plotted in Fig. 8 for NACA 0012 airfoil at zero incidence. As it was expected, the droplet size influences the rate of icing through the increase of catch efficiency and the change of the upper and lower impingements limits which move further downstream. For larger drops, 50 μm to 2000 μm , Fig. 9, the catch efficiency has the same tendency up to 250 μm , higher sized drops show that the lower impingement limit moves upstream while the upper limit continues to move downstream. This is believed to be a consequence of geometrical considerations since larger drops approach the airfoil at a higher angle. Figure 10 is plotted to show how the droplet size affects the maximum and global catch efficiencies. As a consequence, airfoils subjected to large drops collect more ice than smaller droplets. This curve illustrates also the rapid increase in global catch efficiency

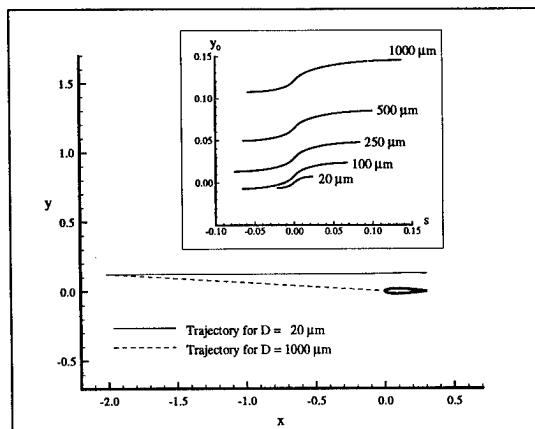


Fig. 7. Particle trajectories for two droplet diameters and release position as function of drop size

up to drop size of 250 μm then E approaches 1.0 showing that deflection is small. Resulting ice shapes for the above cases are presented in Figs. 11 and 12. As shown in the beta curves, ice shapes change drastically from 5 μm to 40 μm . For larger drops, Fig. 12, while the ice shape is similar, the ice thickness increases further downstream.

The distribution of local catch efficiency, β , as function of airfoil surface length for two angles of attack, 0 deg and 4 deg , is presented in Fig. 13 for drop size of 250 μm . As expected, increasing angle of attack moves ice accretion towards the lower surface and greatly affects the impingement limits.

To ascertain if other types of airfoils have similar icing characteristics in the presence of SLD, a test case was conducted using the MS-317 airfoil at an angle of attack of 0 deg , temperature of -12.6°C, liquid water content of 0.5 g/m^3 and velocity of 64.73 m/s . These conditions are identical to the case of NACA 0012. The catch efficiency of drops size ranging from 15 μm to 40 μm is shown in Fig. 14. As in the case of NACA 0012, the tendency that maximum catch efficiency increases with drop size and impingement limits move further downstream is maintained. For larger droplets, the maximum catch efficiency shows large variations compared to small drop size as shown in Fig. 15. However, for drops larger than 250 μm , the beta peak (β_{max}) changes slowly reaching almost the same value for very large drops. From these figures, we can see that the trends for catch efficiency is similar for both airfoils although it is necessary to have additional comparisons by changing icing conditions.

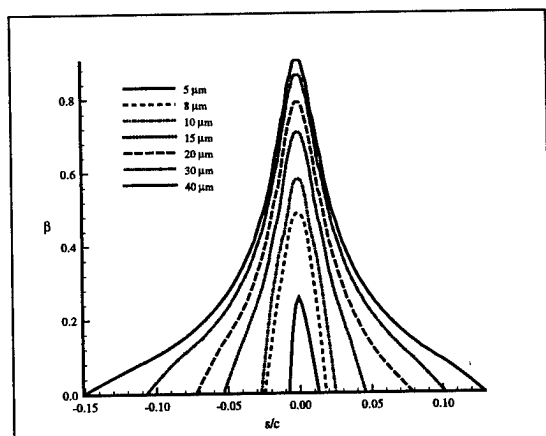


Fig. 8. Local catch efficiency for small droplets on NACA 0012 at $\alpha = 0 \text{ deg}$

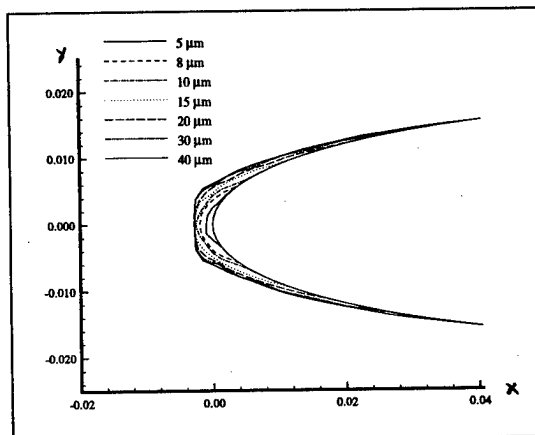


Fig. 11. Ice shapes for small droplets on NACA 0012 at $\alpha = 0 \text{ deg}$ and $T = -12.6^\circ\text{C}$

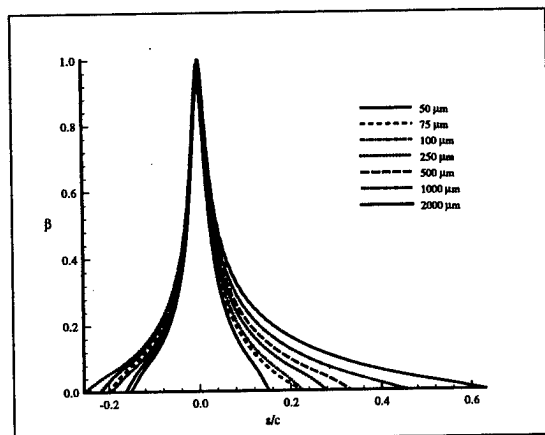


Fig. 9. Local catch efficiency for large drops on NACA 0012 at $\alpha = 0 \text{ deg}$

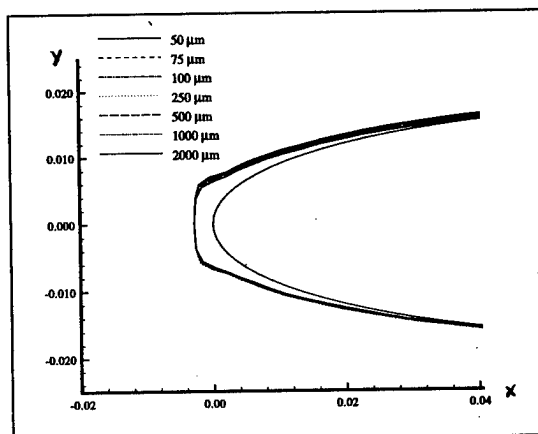


Fig. 12. Ice shapes for large drops on NACA 0012 at $\alpha = 0 \text{ deg}$ and $T = -12.6^\circ\text{C}$

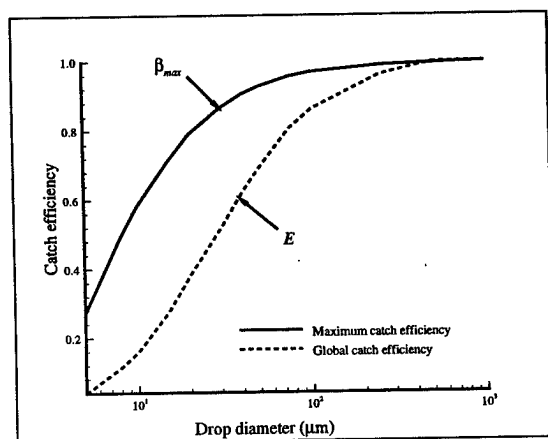


Fig. 10. Distribution of global and maximum catch efficiencies as function of drop diameter

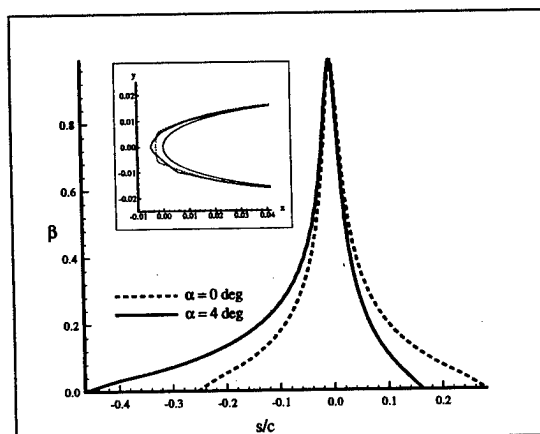


Fig. 13. Local catch efficiency and ice shapes for $D = 250 \text{ micrometers}$ and two angles of attack at $T = -12.6^\circ\text{C}$

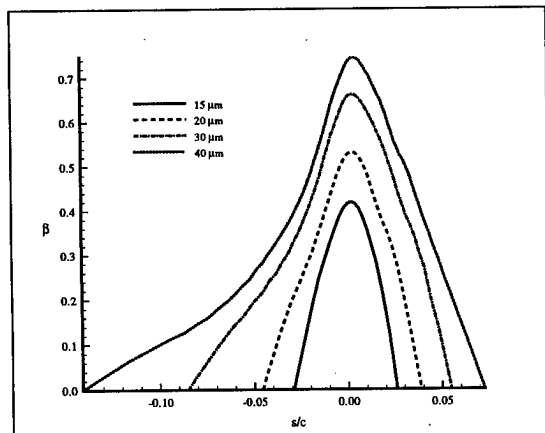


Fig. 14. Local catch efficiency for small droplets on MS-317 at $\alpha = 0$ deg

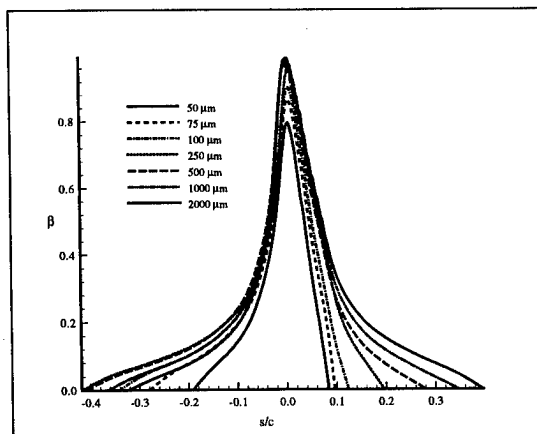


Fig. 15. Local catch efficiency for large drops on MS-317 at $\alpha = 0$ deg

7. CONCLUSIONS

An extensive study on icing characteristics due to supercooled large droplets has been conducted using *CANICE* icing code. This work was aimed at investigating the magnitude of the effects of SLD on icing by analyzing local and global catch efficiencies, drop limit trajectories, ice shapes as well as meteorological and aerodynamic conditions. Results from this investigation show that drop size greatly affects both upper and lower impingement limits, catch efficiencies and ice shapes. Increasing drop size moves the impingement limits further downstream of the airfoil and mostly ice will accrete beyond icing protection systems as shown by some experimental studies [5]. It was also shown that increasing angle of attack will shift significantly droplet impingement limits. A rapid increase in global catch efficiency has also been observed for SLD up to 250 μm . These general trends have been found for both NACA 0012 and MS-317 airfoils.

The present study showed the capability of *CANICE* to investigate ice characteristics under different meteorological and aerodynamic conditions. Results presented will improve our understanding of the effects of SLD on icing. Additional comparisons and parametric studies will be conducted on multi-element airfoils.

ACKNOWLEDGEMENTS

This work was prepared in the context of J.-A. Bombardier Aeronautical Chair. The authors gratefully acknowledge the support provided by Bombardier Inc./Canadair.

REFERENCES

- [1] Green, S. "In-Flight Icing Certification Working Paper", International Icing Symposium '95, Montréal, Canada, September 18-21, 1995, pp. 401-411.
- [2] Mavriplis, F., "Icing and Contamination of Aircraft Surfaces: Industry's Concerns", Proceedings of the First Bombardier International Workshop on Aircraft Icing and Boundary-Layer Stability and Transition, Montréal, Sept. 20-21, 1993, pp. 51-55.
- [3] Politovich, M.K., Bemstein, B.C., Rakph, F.M., Newman, P.J., Marwitz, J.D. and Ashenden, R. "Meteorological Conditions Associated with the ATR-72 Aircraft Accident Near Roselawn, Indiana on 31 October 1994", Proceedings of the International Icing Symposium '95, Montreal, September 18-21, 1995, pp. 235-243.
- [4] National Transportation Safety Board, "Icing Tanker Test Factual Report", SA-512, Exhibit 13b, DCA95MA001, Washington D.C., February 16, 1995.
- [5] Miller, D.R., Addy, H.E. and Ide, R.F. "A Study of Large Droplet Ice Accretion in the NASA-Lewis IRT at Near-Freezing Condition", AIAA Paper 96-0934.
- [6] Brahim, M.T., Tran, P. and Paraschivoiu, I., "Numerical Simulation and Thermodynamic Analysis of Ice Accretion on Aircraft Wings", Centre de Développement Technologique de l'École Polytechnique de Montréal, C.D.T. Project C159, Final Report prepared for Canadair, May, 1994.
- [7] Tran, P., Brahim, M.T., Tezok, F. and Paraschivoiu, I., "Numerical Simulation of Ice Accretion on Multi-Element Configurations", AIAA Paper 96-0869.

- [8] "Effects of Adverse Weather on Aerodynamics", AGARD Conference Proceedings CP-496, December 1991.
- [9] Shin, J., Berkowitz, B., Chen, H. and Cebeci, T., "Prediction of Ice Shapes and their Effect on Airfoil Performance", Journal of Aircraft, Vol 31, No 2, March-April, 1994, pp. 263-270, (also AIAA Paper 91-0264).
- [10] Politovich, M.K., "Aircraft Icing Caused by Large Supercooled Drops", Journal of Applied Meteorology, Vol 28, No 9, September, 1989, pp. 856-868.
- [11] Bergun, N., "Warming Trend for Icing Research", Aerospace America, August 1995, pp 22-27.
- [12] Potapczuk, M.G. and Reinmann, J.J., "Icing Simulation: A Survey of Computer Models and Experimental Facilities", AGARD-CP-496, North Atlantic Treaty Organization, Toulouse, France, April 29th-May 1st, 1991, pp. 5.1-5.27.
- [13] Proceedings of the First Bombardier International Workshop on Aircraft Icing and Boundary-Layer Stability and Transition, Edited by I. Paraschivoiu, Montréal, Canada, September 20-21, 1993.
- [14] Reinmann, J.J., "NASA Aircraft Icing technology Program", NASA TM-104518, December 1991.
- [15] Gent, R.W., "Ice Accretion Prediction on Aerofoils", Proceedings of the First Bombardier International Workshop on Aircraft Icing and Boundary-Layer Stability and Transition, Montréal, Canada, September 20-21, 1993, pp. 113-138.
- [16] Hedde, T., "Modélisation tridimensionnelle des dépôts de givre sur les voilures d'aéronefs", Thèse de doctorat de l'Université Blaise Pascal, Clermont-Ferrand II, France, No d'ordre: D.U. 462, Décembre 1992.
- [17] Bragg, M.B., "Rime Ice Accretion and its Effects of Airfoil Performance", Ph.D. Dissertation, The Ohio State University, 1981 (also NASA CR 165599, March 1982).
- [18] Lozowski, E.P. and Oleskiw, M.M., "Computer Simulation of Airfoil Icing Without Runback", AIAA Paper 81-0402, January 1981.
- [19] Frost, W., Chang, H.P. and Kimble, K.R., "Particle Trajectory Computer Program for Icing Analysis", Final Report for NASA Lewis Research Center, Contract NAS3-22448, FWG Associates Inc., April 1982.
- [20] Cansdale, J.T. and Gent, R.W., "Ice Accretion on Airfoils in Two-Dimensional Compressible Flow - A Theoretical Model", Royal Aircraft Establishment, Technical Report 82128, 1983.
- [21] Flemming, R.J. and Lednicer, D.A., "High Speed Ice Accretion on Rotorcraft Airfoils", NASA CR-3910, August 1985.
- [22] Cebeci, T., "Effect of Environmentally Imposed Roughness on Airfoil Performance", NASA CR-179639, June 1987.
- [23] Cebeci, T., "Calculation of Flow Over Iced Airfoils", AIAA Journal, Vol. 27, No. 7, July 1989, pp. 853-861.
- [24] Bragg, M.B. and Khodadoust, A., "Effect of Simulated Glaze Ice on a Rectangular Wing", AIAA Paper 89-0750.
- [25] Hansman, R.J., "Microphysical Factors Which Influence Ice Accretion", Proceedings of the First Bombardier International Workshop on Aircraft Icing and Boundary-Layer Stability and Transition, Montréal, Canada, September 20-21, 1993, pp. 86-103.
- [26] Guffond, D., "Validation du programme bidimensionnel de captation", ONERA RT 20/5146 SY, May 1988.
- [27] Hedde, T. and Guffond, D., "Improvement of the ONERA 3D Icing Code, Comparison with 3D Experimental Shapes", AIAA Paper 93-0169.
- [28] Bragg, M.B., "Aircraft Aerodynamic Due to Large Droplet Ice Accretions", AIAA Paper 96-0932.
- [29] Hess, J.L., Smith, A.M.O., "Calculation of Potential Flow About Arbitrary Bodies", Progress in Aeronautics Sciences, Vol. 8, pp.1-138, 1966.
- [30] Cebeci, T. and Besnard, E., "Progress Towards the Prediction of the Aerodynamic Performance Degradation of an Aircraft in Natural Icing Conditions", Proceedings of the First Bombardier International Workshop, Montréal, September 20-21, pp. 56-85 (also AIAA Paper 94-0292).
- [31] Chhabra, R.P., "Bubbles, Drops, and Particles in Non-Newtonian Fluids", CRC Press, 1992.
- [32] Clift, R., Grace, J.R., and Weber, M.E., "Bubbles, Drops, and Particles", Academic, New York, 1978.

- [33] Khan, A.R. and Richardson, J.F. "*The Resistance to Motion of a Solid Sphere in a Fluid*", Chemical Eng. Communication, Vol 62, 1987, pp. 135-150.
- [34] Messinger, B.L., "*Equilibrium Temperature of an Unheated Icing Surface as a Function of Air Speed*", Journal of the Aeronautical Sciences, January 1953, pp. 29-42.
- [35] Von Doenhoff, A.E. and Horton, E.A., "*A Low Speed Experimental Investigation of the Effect of Sandpaper Type of Roughness on Boundary-Layer Transition*", NACA TN 3858, 1956.
- [36] Shin, J., "*Characteristics of Surface Roughness Associated with Leading-Edge Ice Accretion*", Journal of Aircraft, Vol 33, No 2, March-April, 1996, pp. 316-321.
- [37] Olsen, W., Shaw, R. and Newton, J., "*Ice Shapes and the Resulting Increase for NACA 0012 Airfoil*", NASA TM 83556, 1984.
- [38] Bragg, M.B. and Gregorek, G.M., "*Analytical Evaluation of the Icing Properties of Several Low and Medium Speed Airfoils*", AIAA Paper 82-0582.

COMPUTATIONAL SIMULATION OF LARGE DROPLET ICING

William B. Wright
NYMA, Inc.
Brook Park, OH

Mark G. Potapczuk
NASA Lewis Research Center
Cleveland, OH

Abstract

Certification for flight into known icing remains one of the more challenging goals for aircraft manufacturers. This activity has been further complicated by the current interest in large droplet icing. Due to the lack of data available on the meteorology of this phenomena, there is currently an incomplete picture of the nature of the condition and even less information on its impact on aerodynamic performance. This paper describes current simulation tools available at NASA Lewis Research Center, their capabilities, and future development goals with respect to large droplet icing simulation.

Introduction

Computational simulation of the ice accretion process and its effects on aircraft performance has been undertaken by various researchers¹⁻⁸ in recent years. Results have indicated that simulation of rime ice accretions, for the range of icing conditions required for compliance with FAR 25 guidelines, can be done with a high degree of confidence in the accurate reproduction of experimentally produced ice shapes, whether they were produced in-flight or in a ground based facility. On the other hand, the accurate reproduction of glaze ice accretions remains an elusive goal due to

the complexity of the process and the lack of a complete understanding of some of the underlying physics. In the area of computational simulation of aerodynamics associated with iced airfoil geometries, there is a similar degree of fidelity available from current methods. Previous researchers⁶⁻⁸ have shown that the current computational methods can provide information on integrated parameters such as lift and drag but a complete reproduction of the details surrounding the boundary layer characteristics on the rough ice surface has yet to be completed.

Currently, there is a desire to be able to extend the use of these simulation methods to include the so-called large droplet regime (i.e. 40 μm to 400 μm diameters). In this paper we will indicate the current capability available for computational simulation of large droplet icing conditions by presenting results from the NASA ice accretion code LEWICE and a NASA Navier-Stokes aerodynamics code, ARC2D.

Ice Accretion Simulation

A theoretical evaluation is performed to ascertain the capabilities of LEWICE, the NASA Lewis ice accretion simulation code, for large drops. Then, a parameter study is performed to show typical results

in this regime. A Twin Otter airfoil was selected for these runs, as large droplet ice shapes were generated on this model in the IRT. A range of drop sizes from 10 micron to 1000 micron was selected. These limits were chosen so as to fill out a log scale plot. Local and total collection efficiencies, impingement limits, and maximum local collection efficiency are presented.

This paper will also present the assumptions used in the droplet trajectory code in LEWICE and will evaluate their applicability for large drops. A large drop in this context applies to any drop size larger than 40 μm , the current upper limit in the FAA certification envelope. LEWICE currently uses the following assumptions:

- solid particles
- spherical particles
- drops do not breakup due to acceleration
- particles do not rotate
- particles have no lift
- particles have no moment
- drag for a stationary sphere applies
- no transient effects due to changing drag
- evaporation of the drop is negligible
- turbulence effects are neglected
- flow is incompressible
- drops do not interact with each other
- continuum flow around drop
- all drops which strike the airfoil impinge

Drop Size Study

In a previous report¹, an analysis was performed on the droplet physics in LEWICE² to estimate the potential effect of different phenomena for drops beyond the current FAA certification envelope. That analysis used a MS-317 airfoil and showed that droplet splashing was the major factor

which needed to be accounted for in any code modification. Since then, tests have been performed in the NASA Icing Research Tunnel (IRT) on a NACA23012 airfoil and a Twin Otter Airfoil. The first part of this report will repeat some of the earlier analysis using the Twin Otter airfoil. It was chosen since the large majority of ice accretions used this airfoil.

LEWICE assumes that all drops which strike the surface impinge, thus neglecting splashing and/or bouncing of drops. A recent experimental study by Mundo, Sommerfeld and Tropea⁹ using a two-component phase doppler anemometer categorized droplet-wall collisions and correlated splashing in terms of Reynolds number and Ohnesorge number ($Oh = \sqrt{We/Re} = \mu / \sqrt{(\rho \sigma d)}$). These numbers are based on the liquid properties and the component of the impact velocity normal to the surface. Based on the results of their experiment, splashing occurs if the factor $K = Oh \cdot Re^{1.25}$ is greater than 57.7. A plot of this parameter for a drop size of 160 microns is shown in Fig. 1.

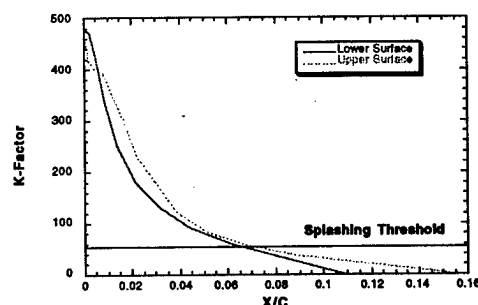


FIGURE 1. K-factor for droplet splash

A 160 micron drop size was chosen since this was the drop size used in the IRT experiment. This figure shows that, according to their research, droplet splashing is a significant factor for this drop size. The Mundo paper also provides a characterization of the size, velocity and direction of

the splashed particles. By knowing these parameters, a feature could be added to LEWICE to track the trajectories of the splashed particles and the trajectories of particles after breakup. As this modification has not yet been made, a more qualitative approach is taken by analyzing the current trends as drop size increases. This approach will now be presented.

Parameter Study

The capabilities of LEWICE in the large drop regime were evaluated by means of a parameter study on drop size. Twenty cases were evaluated using drop sizes ranging from 10 microns to 1000 microns. The airfoil used for these runs was a 6 foot chord Twin Otter airfoil. The meteorological conditions ran were:

$$\alpha = 0^\circ$$

$$\text{LWC} = 0.82 \text{ g/m}^3$$

$$V = 195 \text{ mph}$$

$$T = 28^\circ\text{F}$$

$$\text{MVD} = 10 \text{ } \mu\text{m} \text{ to } 1000 \text{ } \mu\text{m}$$

Figures 2-4 show the local collection efficiency, β , of each drop size ran in this study. The maximum local collection efficiency increases with drop size, both the upper and lower limits are further downstream with increasing drop size and the total collection efficiency increases with drop size. All of these trends are expected and intuitive. Figure 2 shows a large variation over the initial drop size range while in Fig. 3 this trend slows somewhat and finally, collection efficiency is nearly the same for the very large drop size range. This occurs because the larger drops have so much inertia that their trajectory is nearly ballistic.

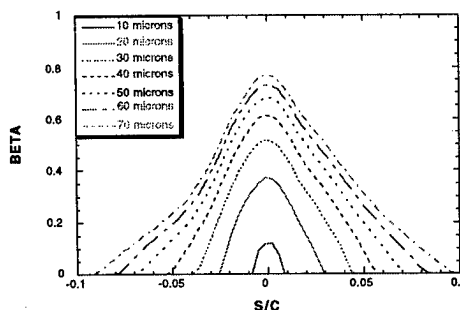


FIGURE 2. Collection efficiencies for MVD from 10 to 70

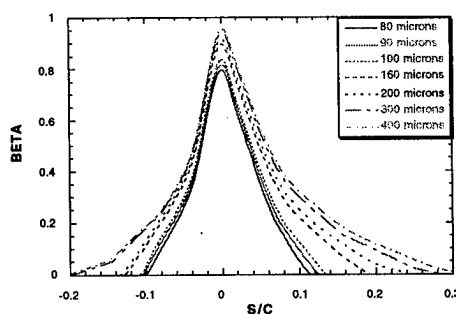


FIGURE 3. Collection efficiency for MVD from 80 to 400

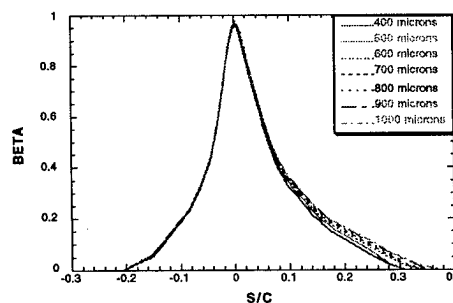


FIGURE 4. Collection efficiency for MVD from 80 to 400

Since this analysis focuses on the major characteristics, maximum collection efficiency, impingement limit and total collection efficiency, these parameters are also plotted in Figs. 5-7.

These plots reveal the reasons why there is an upper limit to the local collection effi-

ciencies shown earlier. The larger a drop gets, the more ballistic its trajectory will be and the local collection efficiency becomes simply a reflection of the curvature of the airfoil geometry.

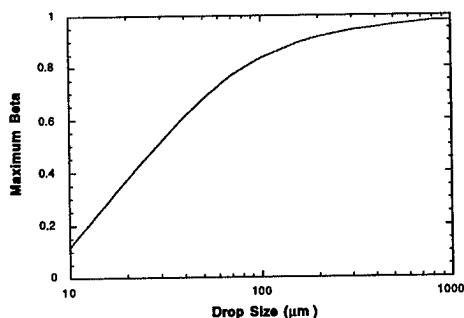


FIGURE 5. Maximum beta as a function of drop size.

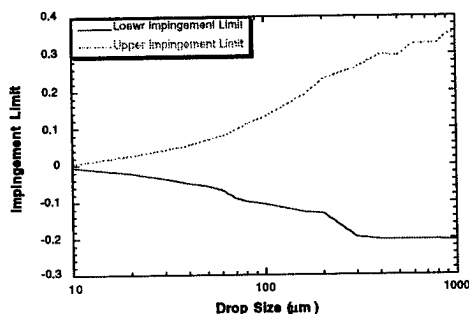


FIGURE 6. Impingement limit as a function of drop size.

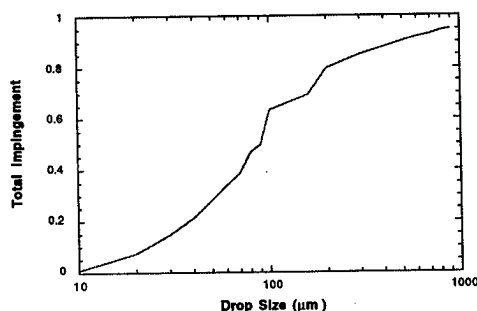


FIGURE 7. Total collection efficiency as a function of drop size.

Figure 5 shows the maximum local collection efficiency. Since this cannot, by definition, be greater than one for a Twin Otter airfoil, β_{\max} provides one limitation with drop size. Figure 6 shows the upper and lower impingement limits. The theoretical limit are the maximum and minimum thickness of the airfoil. The 1000 μm drop size impingement limit is very close to this value.

The theoretical limitations are best shown in Fig. 7. The total collection efficiency is the integral of the local values normalized to the airfoil thickness. This shows the degree to which the drops are deflected by the airfoil. If the drops come in with no deflection, the total collection efficiency is one. This curve shows a rapid increase in total collection efficiency up to 100-200 micron range, then gradually approaching a value of one at 1000 microns.

Comparison with IRT Data

In order to quantify the effect of droplet splash and other phenomena due to large drops, a comparison is made between LEWICE and experimental data taken in the IRT. The results of the IRT entry are presented in another paper at this conference.¹⁰ The first set of comparisons required no adjustments in LEWICE to account for the behavior of large drops. Discrepancies, if any, between predicted and experimental shapes are presumed to be due solely to the effects of droplet splash. Then, an empirical splashing model is created to model the case where LEWICE did not accurately predict the ice shape.

The first case, Fig. 8, is an 18 minute ice shape generated on a NACA 23012 airfoil at the following conditions: $T_o = 28^\circ\text{F}$, $V =$

195 mph, $LWC = 0.82 \text{ g/m}^3$, $MVD = 160 \text{ }\mu\text{m}$, $\alpha = 0^\circ$.

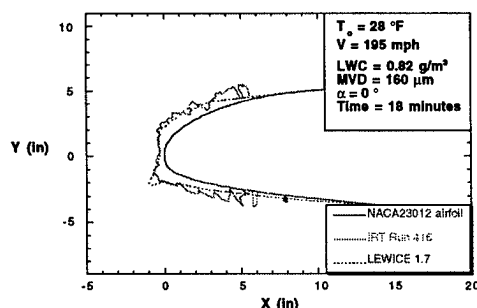


FIGURE 8. LEWICE comparison with IRT Run 416.

This is an excellent comparison for LEWICE. It should be noted that LEWICE outputs only the smooth ice shape and does not display the roughness which is predicted within the code. Due in part to the high LWC and large drop size, the predicted roughness for this case is extremely high. A maximum roughness of 2.5 mm (0.1 in) was predicted for this case, with an average roughness of 0.9 mm. It is also possible that the large feathers on the back of the IRT shape are due to droplets which splashed and reimpinged at that location.

The second case, Fig. 9, is an 18 minute ice shape generated on a Twin Otter airfoil at the same conditions as those for Fig. 8.

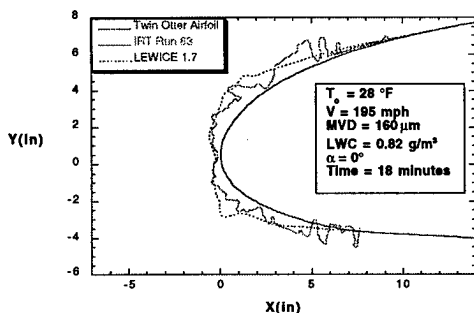


FIGURE 9. LEWICE comparison with IRT Run 83.

This case also shows excellent comparison with the IRT ice shape. Other ice shape

comparisons at warm temperatures are provided in an Appendix at the end of the report. The good comparison shown in these figures is confusing at first, since the previous analysis showed that droplet splashing is a major factor for large drop conditions and LEWICE does not account for it. A possible explanation for this discrepancy can be implied from the comparison shown in Fig. 10, which shows a comparison for a Twin Otter airfoil at a lower ambient temperature, $T_o = 5^\circ\text{F}$.

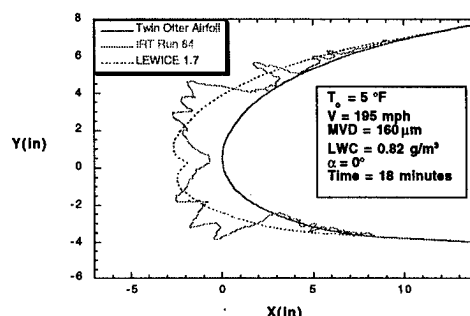


FIGURE 10. LEWICE comparison with IRT Run 84.

This comparison shows more ice in the stagnation zone and less at the horns for the predicted ice shape versus that for the IRT shape, with the overall mass being approximately the same. Normally, this would be attributed to a possible deficiency in the predicted heat transfer coefficient. However, since the predictions for warmer conditions are very good, an alternate theory will be presented which will incorporate the effects of droplet splashing.

A prediction of the change in results once droplet breakup and droplet splash are considered can now be estimated. The suggestion is that neither of these factors result in a loss of mass to the surface. The IRT ice shapes show the same amount of ice as predicted by LEWICE, even though LEWICE does not account for these effects and close up videos taken during the IRT

entry show some splashing of water. Therefore, the splashed drops may not reenter the airstream, but may actually reimpinge on the surface downstream of the initial impact location. This is illustrated in Fig. 11.

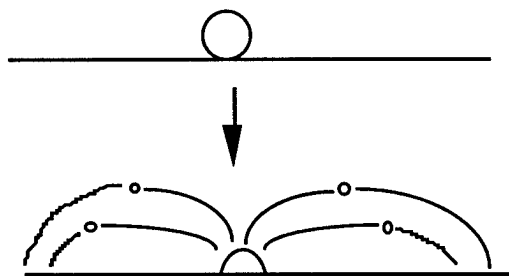


FIGURE 11. Representation of Droplet Splash

Using this model, a drop which splashes at the stagnation point will redistribute its mass to downstream regions of the airfoil. In effect, the splashed droplets behave very much like surface runback water. Thus, for high temperature conditions where much of the impinging water does not freeze, there is no difference in the ice shape generated by LEWICE, which moves the water downstream via runback, and the IRT case, which moves some of the water downstream via runback and some via splashing. For the colder temperature case however, much of the impinging water freezes and LEWICE predicts little runback. In reality, some of the water which freezes in LEWICE is splashed downstream causing more apparent 'runback' which was demonstrated in Fig. 10.

An empirical model is planned to account for this effect. The model will take part of the water which would have impinged and moves it to the next downstream location. The exact amount moved at each location will be computed from the K-factor described earlier.

Airfoil Performance Simulation

Simulation methods are also available for assessment of the aerodynamic impact of large droplet ice formations. These methods can be used in conjunction with wind tunnel tests to identify ice formation features that play a critical role in performance losses for a given airfoil geometry.

These calculations were performed using a 2D, Reynolds averaged, Navier-Stokes code (ARC2D)¹¹ coupled with an algebraic turbulence model¹² modified for use with ice shape geometries. The grid code used is a hyperbolic grid generator developed by Barth.¹³

Results from the current study indicate possible mechanisms for performance loss due to large droplet ice formations. This was accomplished by calculating flow solutions for airfoils with and without ice shapes on the leading edge regions. The ice shapes examined were tracings of actual ice shapes generated in the NASA Lewis Icing Research Tunnel (IRT), an artificial shape used to simulate ice for a flight test, and a LEWICE generated ice shape. The results are used to gain understanding of the aerodynamics associated with iced airfoils and to compare the aerodynamics of the real ice shape to that of an artificial ice shape.

Figures 12 and 13 show the results from a calculation of the flowfield surrounding an MS-317 airfoil with an ice shape generated in the NASA IRT. The ice shape profiles was generated for the conditions of LWC = 0.5 g/m³, a median volume diameter of 190 μ m, and a total temperature of 34°F. The calculations were performed for a free stream Mach number of 0.28, a Reynolds

number of 9 million, and an angle of attack of 4 degrees.

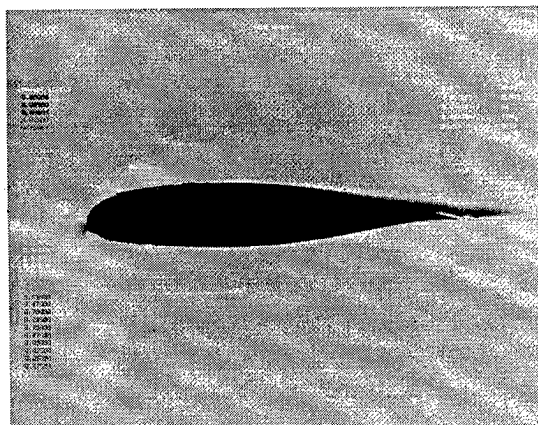


FIGURE 12. Regional transport wing section with large droplet ice accretion. $M = 0.28$, $Re = 9 \times 10^6$, $\alpha = 4$

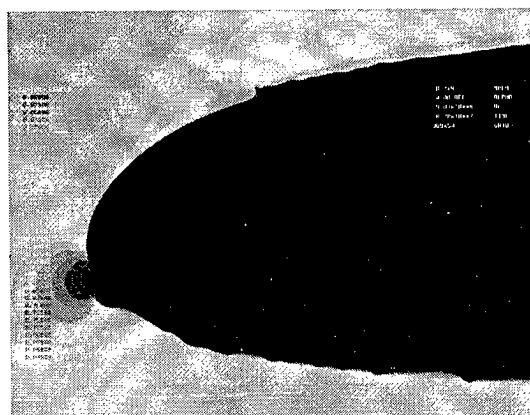


FIGURE 13. Regional transport wing section with large droplet ice accretion. $M = 0.28$, $Re = 9 \times 10^6$, $\alpha = 4$

In Fig. 12, the Mach number contour plots show a large low flow region near the trailing edge, indicated by the dark contour region. This region corresponds to a separation bubble that forms due to the momentum loss suffered by the boundary layer as it passes over the rough ice region. The roughness itself is better illustrated in Fig. 13, where the dark contour lines indicate additional regions of low flow between ice roughness elements.

The second airfoil examined was a representative regional transport wing section with a quarter round obstruction applied to the upper surface. The quarter round was 0.5 inches in height and was located at 6 percent chord.

This was done to simulate some earlier pre-flight tests performed on a runway. In those tests, the airplane wings were fitted with quarter round strips along the span of the wing and the aircraft performed a run-up to takeoff. The aircraft was actually taken to the rotation condition in order to safely determine aerodynamic performance for a wing with ice ridges aft of the protected region.

Figures 14 and 15 show the Mach number contours for the regional transport both in a clean condition and with the artificial ice shape near the leading edge.

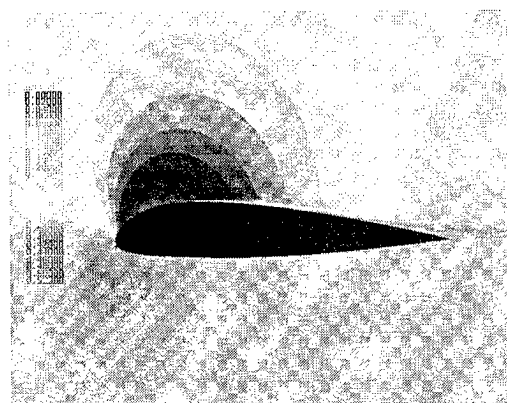


FIGURE 14. Regional transport wing section without ice accretion. $M = 0.28$, $Re = 9 \times 10^6$, $\alpha = 6$

Figure 14 shows the clean airfoil Mach number contours which indicate a normal flow pattern for an airfoil of this type. In Fig. 15, the same airfoil, except with the quarter round protuberance, displays a much different flow field. The flow is unsteady and there is considerable vortex shedding occurring aft of the airfoil. In this case, however, the shedding is not associ-

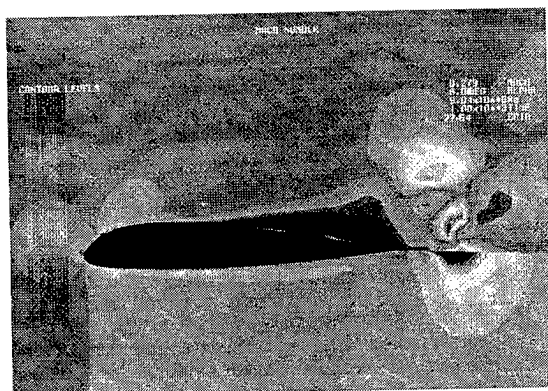


FIGURE 15. Regional transport wing section with quarter round simulated ice accretion. $M = 0.28$, $Re = 9 \times 10^6$, $\alpha = 6$ ated with a premature tail stall but is actually precipitated by the behavior just aft of the protuberance itself. This is illustrated in Fig. 16, which shows the flow field pattern in the vicinity of the artificial ice shape.

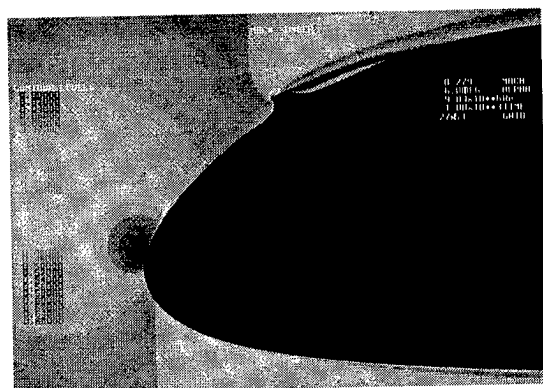


FIGURE 16. Regional transport wing section leading edge with quarter round simulated ice accretion. $M = 0.28$, $Re = 9 \times 10^6$, $\alpha = 6$

The final series of calculations were for a NACA 23012 airfoil geometry. In this case, ice shapes were obtained from a LEWICE calculation as well as from ice shape tracings obtained in the NASA IRT. The two shapes used are those from Fig. 8. The icing conditions used to generate those shapes were mentioned during the discussion of the ice shape comparisons.

Figures 17-19 show the Mach number contours calculated for those shapes and illustrate one of the difficulties in reproducing ice shapes for the purpose of aerodynamic

performance assessment, regardless of whether that assessment is experimental or computational in nature.

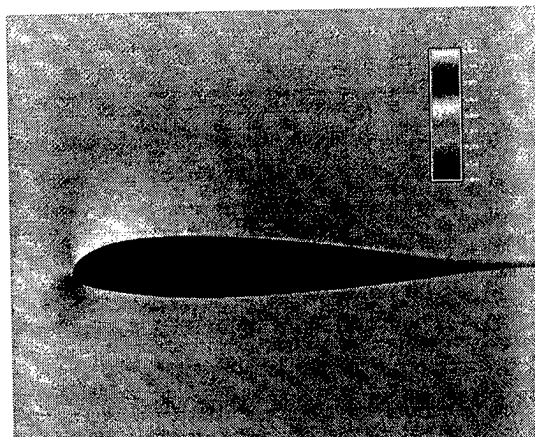


FIGURE 17. Mach No. contours for a clean NACA 23012 airfoil. $M = 0.28$, $Re = 9 \times 10^6$, $\alpha = 6$

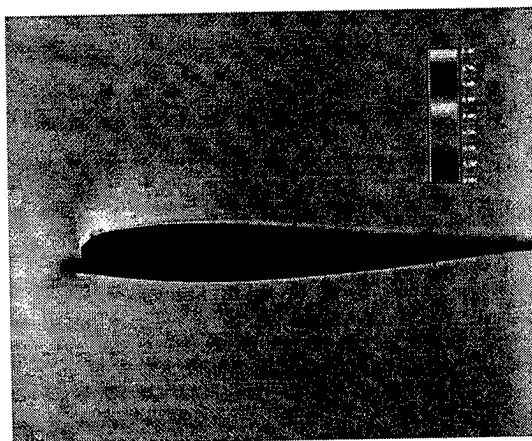


FIGURE 18. Mach No. contours for a NACA 23012 airfoil with a LEWICE generated ice shape. $M = 0.28$, $Re = 9 \times 10^6$, $\alpha = 6$

Figure 17 shows the clean airfoil results. Once again, the computation shows a well behaved flow field solution similar to results available for other airfoils of this type. In Fig. 18, the LEWICE generated ice shape has been added to the leading edge. The flow code results indicate that this ice shape has caused a premature trailing edge separation, similar to that from

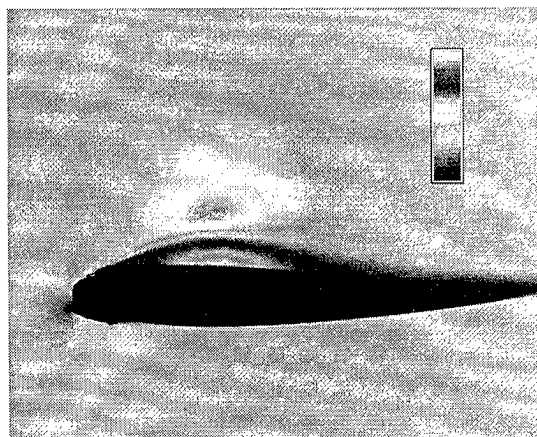


FIGURE 19. Mach No. contours for a NACA 23012 airfoil with an IRT generated ice shape.
 $M = 0.28$, $Re = 9 \times 10^6$, $\alpha = 6$

the MS-317 calculation, which had an IRT ice shape.

As described earlier, this LEWICE ice shape compares quite well with the ice shape obtained from the IRT under the same conditions. The ice mass, the overall thickness and the icing limits are all reproduced by the calculation. However, the flow code results for the LEWICE shape are quite different from those for the IRT ice shape, as shown in Fig. 19.

The IRT ice shape produces an unsteady leading edge stall condition with vortex shedding from the upper surface of the airfoil. Figure 19 shows only one moment in time from that shedding process. Thus, the ice shapes from LEWICE and from the IRT, although similar in shape, could produce very different performance results if tested in a dry air wind tunnel. This suggests that some additional criteria must be considered when evaluating the acceptability of ice shape simulation methods.

The desire to evaluate airfoil geometries for susceptibility to large droplet icing performance effects suggests a need for a reinvigorated code development program. A significant amount of work has been per-

formed on ice shape geometries resulting from icing conditions within the FAR-25 envelope. This work could be extended to large droplet ice shapes. It should also be tied to an aerodynamic analysis method in order to insure that the desired characteristics are included in any simulation method. If this approach is followed, it could result in a computational method for simple evaluation of large droplet icing aerodynamic impact.

Conclusions

A parameter study was performed to show the predicted collection efficiencies for large droplets and to estimate the effect of droplet splash, which is the major change which will occur in this regime. The LEWICE user is cautioned that the splashing estimates depend not only on drop size, but on velocity as well. The key parameter is the Weber number, which is proportional to drop size but is proportional to velocity squared. Therefore, velocity will play a large factor in the determination of splashing effects.

A comparison is then made with data generated in the IRT. For high temperature cases, LEWICE predicts the ice shapes extremely well. For a colder condition, LEWICE predicts more mass at stagnation and less elsewhere. It is theorized that drops which splash at stagnation reimpinge downstream.

LEWICE has been shown to be a very robust code for predicting droplet trajectories and ice accretion for numerous different conditions. Research is continuing on improving the physical models within the code in order to produce a code which can accurately predict ice shapes for any condition.

Performance evaluation using computational methods can provide an inexpensive and timely means for evaluating aircraft susceptibility to large droplet icing conditions. Results indicate that large droplet ice shapes can result in premature stall conditions and that the cause can be due to a leading edge or a trailing edge separation. The reason for stall will be dependent on the ice shape size, location, and roughness level and on the geometry of the airfoil itself.

Determination of the correct ice simulation shape to use in aerodynamic testing or analysis must include a consideration of the tremendous variation in actual ice shape profiles and roughness levels and the resulting variation in aerodynamics associated with those geometries. Some form of analytical analysis should be performed to determine the range of conditions that are to be expected from a wind tunnel test program designed to evaluate performance degradation due to large droplet ice accretions.

References

- 1) Wright, W. B., "Capabilities of LEWICE 1.6 and Comparison with Experimental Data," presented at the AHS International Icing Symposium, Montreal, Canada, Sept. 1995.
- 2) Wright, W.B., "Users Manual for the Improved NASA Lewis Ice Accretion Code LEWICE 1.6," NASA CR198355, June 1995.
- 3) Hedde T., Guffond D., "Improvement of the ONERA 3D icing code, comparison with 3D experimental shapes," AIAA 93-0169
- 4) Gent, R.W., "TRAJICE2 - A combined water droplet and ice accretion prediction code for aerofoils," Royal Aerospace Establishment TR 90054, 1990.
- 5) Brahimi, M.T., Tran, P., and Paraschivoiu, I., "Numerical Simulation and Thermodynamic Analysis of Ice Accretion on Aircraft Wings," Centre de Développement Technologique de l'École Polytechnique de Montréal, C.D.T. Project C159, Final Report prepared for Canadair, 1994.
- 6) Potapczuk, M.G., Al-Khalil, K.M., Velazquez, M.T., "Ice Accretion and Performance Degradation Calculations with LEWICE/NS," NASA TM-105972, AIAA-93-0173, Jan. 1993.
- 7) Shin, J., Berkowitz, B., Chen, H., and Cebeci, T., "Prediction of Ice Shapes and Their Effect on Airfoil Performance," AIAA Paper 91-0264, Jan. 1991.
- 8) Kwon, O.J. and Sankar, L.N., "Numerical Study of the Effects of Icing on Finite Wing Aerodynamics," AIAA Paper 90-0757, Jan. 1990.
- 9) Mundo, C., Sommerfeld, M., and Tropea, C., "Droplet-Wall Collisions: Experimental Studies of the Deformation and Breakup Process," Int. J. Multiphase Flow, v. 21, No. 2, pp. 151-173, 1995.
- 10) Addy, G. and Miller, D., "A Study of Large Droplet Ice Accretions in the NASA-Lewis IRT at Near-Freezing Conditions; Part 2," FAA International Conference on Icing, May 1996.
- 11) Pulliam, T.H., "Euler and Thin Layer Navier-Stokes Codes: ARC2D,

ARC3D," UTSI E02-4005-023-84,
March 1984.

12) Potapczuk, M.G., "Navier-Stokes
Analysis of Airfoils with Leading Edge
Ice Accretions," NASA CR 191008,
February 1993.

13) Barth, T., Pulliam, T.H., and Buning,
P.G., "Navier-Stokes Computations for
Exotic Airfoils," AIAA Paper 85-0109,
Jan. 1985.

Appendix

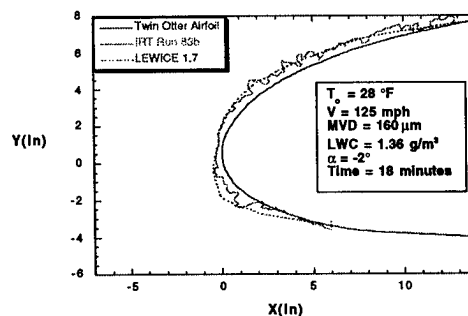


FIGURE 22. LEWICE comparison with IRT Run 83b

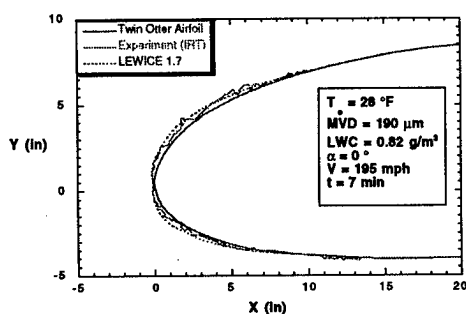


FIGURE 20. LEWICE comparison with IRT Run DC2

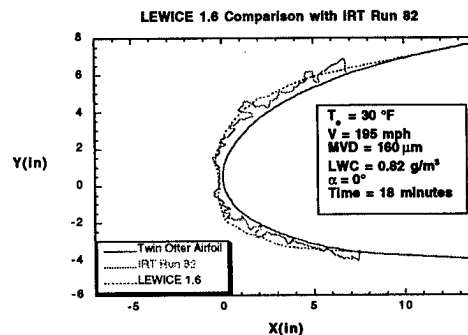


FIGURE 23. LEWICE comparison with IRT Run 82

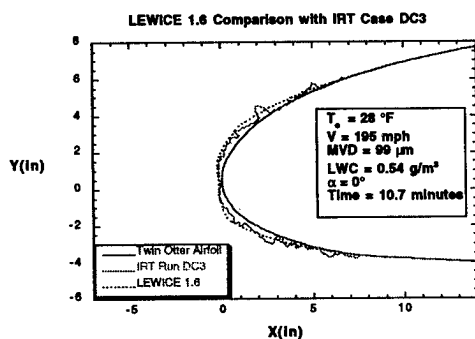


FIGURE 21. LEWICE comparison with IRT Run DC3

Section V

Operational Regulations and Training Requirements

Robert Brayton, Industry Co-Chair

Katherine Hakala, Federal Aviation Administration Co-Chair

FLIGHT INTO FREEZING RAIN/DRIZZLE: A GENERAL AVIATION/BUSINESS JET MANUFACTURER'S PERSPECTIVE

**S. Heathman, R. Rice, D. Wariner, S. Woodson
Cessna Aircraft Company, Wichita, Kansas**

Abstract

Expansion of Appendix C to include supercooled large droplets (SLD) is believed to be premature at this time. Poor icing characteristics displayed by certain designs should not be used to set a precedent for all certifications. Some airfoils in use today, when compared to the widely used 23000 series, can be shown to have unique pressure distributions and collection efficiencies. Additional testing and analysis is being requested for droplet sizes greater than 200 microns. Serious limitations exist for creating and measuring large droplets. Safety issues associated with flight evaluation of these conditions is a major concern. The NASA Lewis Research Center's Icing Research Tunnel (IRT) is limited to 190 MVD micron droplet sizes. It is not believed that computer codes developed to predict icing trajectory and accretion have been validated at the droplet sizes for which foreseen regulations will force its use. Limited IRT data is available for the airfoil families in contemporary and anticipated use. Freezing drizzle (ZL) and freezing rain (ZR) are flight conditions to be avoided instead of knowingly penetrated with reliance on protection from de-ice and anti-ice systems. Meteorological prediction capabilities must continue to be improved to identify the small percentage of ZR/ZL environments. Methods for inflight detection of critical icing must be developed and implemented. Pilot education must be targeted at identification of icing encounters, and operational procedures and handling characteristics associated with exiting these events. Criteria are described which are believed to be more appropriate for ZR/ZL: controllability, and immediate exit.

I Introduction

This conference is part of the third phase of the FAA's response to an accident of an ATR-72 in Roselawn, Indiana in October 1994. Flight 4184 was in a holding pattern in severe icing conditions for an extended period, with autopilot engaged and flaps extended. When the flaps were retracted, the airplane suffered a roll upset and crashed killing all 68 people on board. An outcome of this accident was a formation of a Special Certification Review (SCR) team. This team's charter was to review the design and certification issues associated with the operation of ATR airplanes in icing conditions, and determine if the current regulations in FAR Part 25 are adequate. It was concluded that the ATR-42 and ATR-72 were certificated properly in accordance with their certification basis and the Bilateral Airworthiness Agreement between France and the USA, and that the Roselawn accident occurred in icing conditions more severe than those described in Appendix C of FAR/JAR 25. The focus of attention has shifted to the

operation of aircraft in icing conditions outside the FAA icing certification envelope described in Appendix C, specifically the Supercooled Large Droplet (SLD) environment. One of the objectives of this conference is to make recommendations for operations and rulemaking concerning this SLD environment. The adequacy of the current Part 25 Appendix C envelopes is under examination. It needs to be determined whether safe operation of aircraft should include avoidance and immediate exit from the SLD environment, or expansion of the FAR/JAR 25 Appendix C envelope for design and certification of aircraft for flight into this severe environment. Cessna is a proponent of the policy of avoidance of severe icing conditions and for providing a means for a safe and immediate exit from this environment, once encountered.

II Investigation of the Current FAR/JAR Part 25 Appendix C Envelope

The FAR Part 25 Appendix C envelope provides a quantitative description of icing conditions used as design criteria for aircraft ice protection equipment for certificated flight into known icing. This certification criteria has satisfactorily served for 30 years, but is currently undergoing investigation for its adequacy. Technological capabilities have changed, including inflight data measuring techniques, analytical methods, updated facilities, and weather forecasting and analysis. However, it has yet to be demonstrated that any of these technological improvements can be brought to bear to provide safe operation of aircraft in the SLD environment. Issues that have been discussed in examining the present certification envelopes include parameters used to describe the droplet size distribution, the complication of the magnitude of Liquid Water Content (LWC) and droplet size variation with horizontal distance, and the limitation of measurement devices and techniques to accurately evaluate the icing environment.

Both MED (Mean Effective Diameter) and MVD (Mean Volumetric Diameter) are statistical functions which represent the droplet diameter that divides the total water volume in the cloud in half. Half the sample consists of drops larger than the quoted value, half containing drops smaller. Measurement techniques used to characterize droplet distributions at the time the icing certification envelopes were developed included rotating multicylinder devices. These devices required a monomodal, or single bell curve assumption (the Langmuir-Blodgett distribution curve) regarding the droplet size distribution to calculate a MED value. Improved particle measuring probes measure droplet sizes directly, providing a MVD value obtained by actual drop size measurements. Current research suggests that both bimodal and monomodal distributions can be present in the icing atmosphere, depending on the droplet formation processes involved. Studies show the bimodal distribution to include a minor population of larger droplet sizes under a second smaller bell curve in addition to the major peak concentration of smaller droplet sizes typically represented by the single bell curve (Ashenden, 1996). The effect of this variation in the icing environment has not been evaluated.

Jeck (1994) discusses new ways to characterize the icing environment, using LWC as a function of cloud Horizontal Extent (HE) for a given Mean Volumetric Diameter (MVD) and temperature. The Appendix C envelopes characterize LWC and MVD for a fixed

average distance, and then provide a correction factor for adjusting the LWC limits for other distances. Jeck's convention would allow wind tunnel, tanker flights, and natural icing flight conditions to be plotted directly, and eliminate the discrepancy of test exposure compatibility to the fixed reference distances of the envelopes. This report suggests alternate and interesting formats to characterize icing conditions, which would simplify evaluating icing exposures, but it does not demonstrate a statistical requirement for expanding the current envelopes to include the relatively rare and severe SLD environment.

The limitations of particle measurement devices to characterize the SLD environment also must be carefully considered. Different measuring probes are accurate for different particle size ranges. It has been reported that the measurement techniques used by the early NACA researchers were unable to accurately measure droplets larger than roughly 40 microns. Jeck's icing characterization study is based on a computerized database of approximately 28,000 nautical miles of inflight measurements of icing conditions assembled over the past few years by the FAA Technical Center. Jeck reports statistically only 2% of the recorded MVD's exceed 30 microns, and the longest recorded exposure to 30 micron MVD droplets is only a little more than 20 nautical miles.

Cober, et al (1995) conducted research flights in regions of North Atlantic winter storms to understand the physics of the formation of supercooled drizzle droplets. The Freezing Drizzle Experiment (FDE) flew eighty periods where drizzle was observed. Only forty-one percent of these cases had MVD's larger than 30 microns, including regions below cloud bases where freezing precipitation was falling, where MVD's of 200 to 800 microns were measured. The most noticeable effect of icing associated with freezing drizzle was the coating of the cockpit front and side windows, a phenomena not generally observed with icing from cloud droplets. This difference provides a means for the pilot to identify icing caused by drizzle sized droplets. The presence of large diameter droplets in freezing drizzle does not create an argument to include it in design and certification criteria for flight into known icing. Freezing drizzle and freezing rain are hazardous and relatively isolated conditions. Flight into the SLD regime should be considered similar to flight through thunderstorms. It should be avoided and immediately exited if inadvertently encountered.

Appendix C design and certification standards have met the test of time. Aircraft designed and tested to meet these requirements have been proven safe for routine flight encounters with icing for the past thirty years. The investigation of the adequacy of the present certification standards has resulted from a response to the Roselawn incident involving the ATR-72, holding in conditions in which freezing drizzle was most likely evident. A review of current icing criteria investigations suggest that the Appendix C envelopes are reasonable standards for safe flight into known icing. The key issue that is to be addressed is whether the certification criteria should be expanded to assure safe operation in all possible icing conditions, including the severe freezing drizzle/ freezing rain environment.

III Envelope expansion Issues

Some in the airline community are asking for a re-evaluation of the certification envelopes to include larger droplets, since many commuters feel pressured to penetrate such severe conditions. Increased demand to meet expected schedules has increased the volume of operations in icing conditions, as a normal operation for aircraft. The Air Line Pilots Association (Green, 1995) has suggested a redefinition of the icing characterization envelopes based on acceptable exceedance probabilities resulting from critical icing environmental studies.

The primary area of concern is icing due to the SLD environment, which is outside of the current certification envelopes. Cloud droplets are defined as those with diameters up to 200 microns, freezing drizzle consists of droplets up to 500 microns, and freezing rain is defined as droplet sizes up to approximately 1000 microns. There is some ambiguity between the definition of cloud and drizzle drops. The term SuperCooled Drizzle Drops (SCDD) has been coined to describe diameters from 40 to 400 micron droplets. It is questioned what droplet size would be an acceptable exceedance probability in the critical icing environment; 200 microns, 500 microns, or 1000 microns.

Many issues need to be addressed relative to aircraft design, evaluation, certification, product cost, and liability to provide aircraft operations into this relatively rare icing environment.

Aircraft are designed to demonstrate safe operation in the Appendix C envelopes through analysis and testing. Analytical ice accretion codes used today for system development and certification efforts are well utilized and documented for the current icing environment characterization. Limitations exist in utilizing these analytical tools for the SLD environment. Current codes that predict ice impingement limits and ice accretions, do not accurately account for the physics of SLD environment such as droplet splashing, coalescing, and breakup effects associated with the larger droplets. Heat transfer and turbulence modeling codes need to be developed to analyze airflow over growing ice shapes, with transition and roughness modeling. Such technological developments require expensive computational platforms to run these Navier-Stokes solvers. Analytical codes that predict droplet trajectory and accretion are currently validated on a limited representation of airfoils, and have not yet been validated for SLD due to current testing facilities limitations. Utilization of unvalidated computational analysis tools should be cautioned.

A test program is required to evaluate the aircraft ice protection systems and flight characteristics to obtain certification for flight into known icing. This program usually involves wind tunnel tests, dry air ground and flight tests, tanker icing simulation, and flight into natural icing conditions to complement and confirm analysis. Wind tunnel facilities are needed to test larger droplet sizes if Appendix C is expanded to include SLD. NASA Lewis has improved and expanded their testing capabilities of the Icing Research Tunnel (IRT) to provide up to 190 MVD droplets. It is questioned whether this

is sufficient for investigating the effects of freezing drizzle and freezing rain which can include up to 1000 micron droplet sizes. Tanker availability to simulate icing conditions is presently limited. The NKC-135A tanker at Edwards Airforce Base provides a 9 foot plume sprayed from the tail boom, which has recently been used to produce drizzle size drops up to 200 microns, and MVD's in excess of 70 microns. Cessna utilizes an existing test aircraft article modified for tanker flight testing to simulate icing conditions. Modification of existing company tankers for SLD evaluation and certification would require spray nozzles that could provide a range of MVD droplets, and the tanker-spray systems would require re-calibration for the SLD environment.

In addition to tanker simulation, certification procedures include flight into natural icing conditions to demonstrate safe operation in icing conditions. Flight evaluation in natural icing conditions to include the severe SLD environment would not only require capability to locate and identify such conditions, but would increase the element of risk for both the aircraft manufacturer and FAA test pilots. Instrumentation to accurately measure droplet particles in the SLD environment is an additional limitation. Currently, a combination of several particle measuring probes must be utilized to measure droplet sizes from 3 to 800 microns. The FSSP probe is capable of measuring 3 to 45 micron droplet sizes, the 1D-C probe has a 80 to 300 micron droplet capability, and the 2D-C probe particle size range is 100 to 800 microns (Hobbs, 1995). To measure the droplet distribution in the SLD environment, a combination of particle measuring probes would be required to be carefully placed and aligned in undisturbed flow for accurate measurements. Ideally, the probes should be located in the same proximity to accurately reflect the sampled environment, which creates structural and flow alignment challenges.

The requirement of the aircraft to provide safe flight into the SLD environment would have a great impact on aircraft design, complexity, and cost. Large droplets impinge further aft on the airframe surfaces, splash and run back before completely freezing. Protection in this environment would require a greatly increased surface coverage of protected surfaces. Designing for safe flight operation in the SLD environment would substantially increase aircraft weight and complexity due to these modifications. The final result for the customer would be decreased aircraft product performance, increased product maintenance, and increased product cost in efforts to provide safe flight in a relatively rare and hazardous environment.

It is questionable whether the expansion of the certification envelope to provide flight into known severe icing provides enhanced safety to the consumer. A positive element that has come out of the tragedy at Roselawn is the awareness of the hazards associated with flight into known icing. Unfortunately, the level of danger associated with severe icing is not generally considered as hazardous as that of thunderstorms, and the presence of the SLD environment is much more difficult to forecast. Currently, known-icing approval does not extend to flight in SLD conditions. It should be emphasized that it is unsafe for a pilot to fly in this condition any longer than it would take to get out of it.

IV Recommendations

There are many improvements that should be pursued prior to setting a precedent of expanding the icing certification envelopes to include a more severe environment. These improvements must be pursued by the Federal Aviation authorities, aircraft manufactures, ice protection system manufacturers, meteorological communities, operators, and training organizations.

Involvement from the FAA should include developing or funding research to validate an accepted system for measuring the droplet size distribution that would lead to an accurate characterization of this environment. Advisory Circulars should be issued that stress crew compliance with identification of and immediate exit from the SLD environment. Airport and ATC procedures should be developed to limit holding at low altitude where severe icing conditions may exist during the approach phase of flight.

The aircraft manufacturers response should include efforts to assure adequate flight characteristics for landing with flap limitations as required. Re-calibration on stick shaker or other stall warning devices for ice accretion effects should be explored. Airplane specific procedures in the AFM should be published for early identification of SLD ice accretions and procedures for immediate exit from this environment. AFM publications should include any additional airplane limitations specific to SLD icing encounters, including procedures for use of autopilot and high lift devices when in icing conditions. It should be clarified by the manufacturers that the AFM limitation for flight into known icing conditions does not include extended operation in freezing rain/ freezing drizzle environments. Manufacturers need to improve and implement reliable and accurate methods for inflight detection of airframe icing.

The ability to identify the small percentage of SLD icing environment through forecasting is needed to help pilots avoid flight into this regime. Technological developments have helped improve forecasting algorithms to provide increased accuracy and reliability in icing hazard warnings. Research needs to be pursued to provide droplet size estimates in efforts to forecast large droplet icing (Politovich, 1996).

Operators need to assure a company wide understanding of the critical nature of severe icing encounters. Flight crews should be provided recurrent training for early recognition of SLD, and procedures for a safe and immediate exit from that environment. Training programs should be developed to help the pilot identify and safely exit a SLD encounter.

The manufacturer cannot design and build aircraft for every possible icing environment. It is our responsibility, as an industry, to emphasize, and more clearly articulate, the hazards of the freezing drizzle/freezing rain environment and to explain what it means to be certified for flight into known icing. Key issues that are believed to be more appropriate for flight into this regime are identification, and safe and immediate exit from this severe environment.

V References

Ashenden, R., Marwitz, J.D., "A Comparison of the Air Force Water Spray Tanker Artificial Drizzle Cloud Distributions to the Natural Environment", AIAA-96-0632, 34th Aerospace Sciences Meeting & Exhibit, Reno, NV, January 1996.

Cober, S., Isaac, G., Strapp, J.W., "Icing Environments Associated with Supercooled Drizzle", International Icing Symposium Proceedings, Montreal, Canada, September 1995.

Green, S., "Inflight Icing Certification Project", IFALPA Aircraft Design and Operation (ADO) and Airport and Ground Environment (AGE) Joint Committees Meeting, Geneva, Switzerland, October 1995.

Hobbs, R., Morrison, B., "Processing Data from Particle Measuring Probes for Icing Certification", International Icing Symposium Proceedings, Montreal, Canada, September 1995.

Jeck, R., "Other Ways to Characterize the Icing Atmosphere", AIAA-94-0482, 32nd Aerospace Sciences Meeting & Exhibit, Reno, NV, January 1994.

Politovich, M.K., Brown, B.G., Thompson, G., Brintjes, R., Bernstein, B.C., "Toward Improved Aviation Forecasts for Icing", AIAA-96-0137, 34th Aerospace Sciences Meeting & Exhibit, Reno, NV, January 1996.

SOME OBSERVATIONS on DESIGN,
CERTIFICATION, and TRAINING
for
OPERATION OF AIRCRAFT IN ICING SITUATIONS

C. P. (Pete) Hellsten
Aeronautical and Marine Consultant

Abstract

It is apparent that there is a significant disconnect between engineering, certification, training and operation of modern aircraft in icing situations. During the engineering design phase, a major goal is to achieve icing certification with the least impact to the design in terms of cost weight and performance. The certification process, in a similar manner, goes about showing compliance with appropriate regulations. Because of this philosophy and the breakdown in communication brought about by the current trend toward ultra-specialization, the engineering and certification process does not always represent current experience or the "state-of-the-art" of the real operational world. Training builds on the same data base developed during the design and certification processes and again does not address fully, if at all, what might be expected during icing encounters, be they in or out of the "envelope," inadvertent or otherwise. Aircraft operations proceed on the basis of approved data from engineering, certification and training and a well-developed network of information within the operational community to address the real needs of that group. Unfortunately the lessons learned in operation do not feed back in a timely manner to the design, certification and training cycles. From the perspective of a designer and independent consultant, with broad exposure to the aircraft industry in the US, and abroad, this paper presents some observations, examines several of the problems, and proposes a few quick, inexpensive, and timely recommendations to be considered for safer operations in the icing environment.

Introduction

Over the past several years I have had the opportunity to spend a considerable time analyzing and reviewing the operation of commuter aircraft in icing situations. With a background as performance engineer, aerodynamicist and designer this experience has proven to be very enlightening. In reflecting on the development procedure from the drawing board to full operational capability, one begins to question the judgment that is exercised during design and certification. The process is characterized by specialization, engineers with relatively limited exposure to the total system and poor communication between the various elements. These attributes lead to some questionable positions that directly reflect on the safety of daily operations.

In a very limited way I have attempted to summarize some of experiences that may provide insight to improve the safety of aircraft operations in icing conditions. As an independent consultant I have no allegiances to any manufacturer, airline operator or certification agency. I have worked for all three and so my comments hopefully reflect a position that cuts to the heart of problem and is not biased by allegiance to any particular segment of the process.

The Design Process

The development of any aircraft design requires a series of compromises to balance the numerous conflicting requirements imposed by the customer, operator or ultimate user of the vehicle. The success of a design hinges on establishing the proper balance between the conflicting demands for reliability, maintainability, cost (both initial and operational) and performance. A design that can not meet its performance objectives won't get off the drawing board. If performance shortfalls are discovered during flight development, the resulting economic problems caused by expensive rework or contract penalty clauses will mean short production runs and, in extreme situations, program cancellation. Clearly the demand for performance dominates the design process.

The need for performance is so great that many systems and other requirements are relegated to a secondary roll in the development process. In the era of ultra specialization, off design considerations often slip between the cracks. Engineers have become so specialized they do not understand the repercussions their area of responsibility may have on other parts of the design. The ice protection system is a good example. Aerodynamicists working to achieve the ultimate in lift and drag are primarily concerned with uncontaminated characteristics. Competitive pressures leave no design margin to accommodate for aerodynamic deterioration of the airframe. The result is unreasonable constraints on the design and performance of the ice protection systems. This coupled with schedule constraints and a lack of good aerodynamic design data means the evaluation for the impact of contamination comes late in the design process, if at all. Typically, the problems appear during flight test or even later, during normal revenue flight operations.

In a recent paper* Render and Jenkinson point out that "*in-flight icing is a frequent occurrence in the United Kingdom and Europe, even during the summer months*" and that "*80% of the flights each year need activation of the ice protection system.*" They further point out the certified performance characteristics of only two turboprop commuter aircraft are rescheduled for operation in icing conditions. The information presented in the Aircraft Flight Manual (AFM) for operations at elevated temperatures compared to that for icing conditions makes one wonder why there isn't more consideration for aircraft operations on a sub-standard day. Reflecting on my own career, as a performance engineer, aerodynamicist and designer it is clear why so much effort is being expended working the

* AIAA Paper 95-0751 presented at the AIAA 33rd Aerospace Sciences Meeting And Exhibit, Reno NV, Jan 9-12, 1995

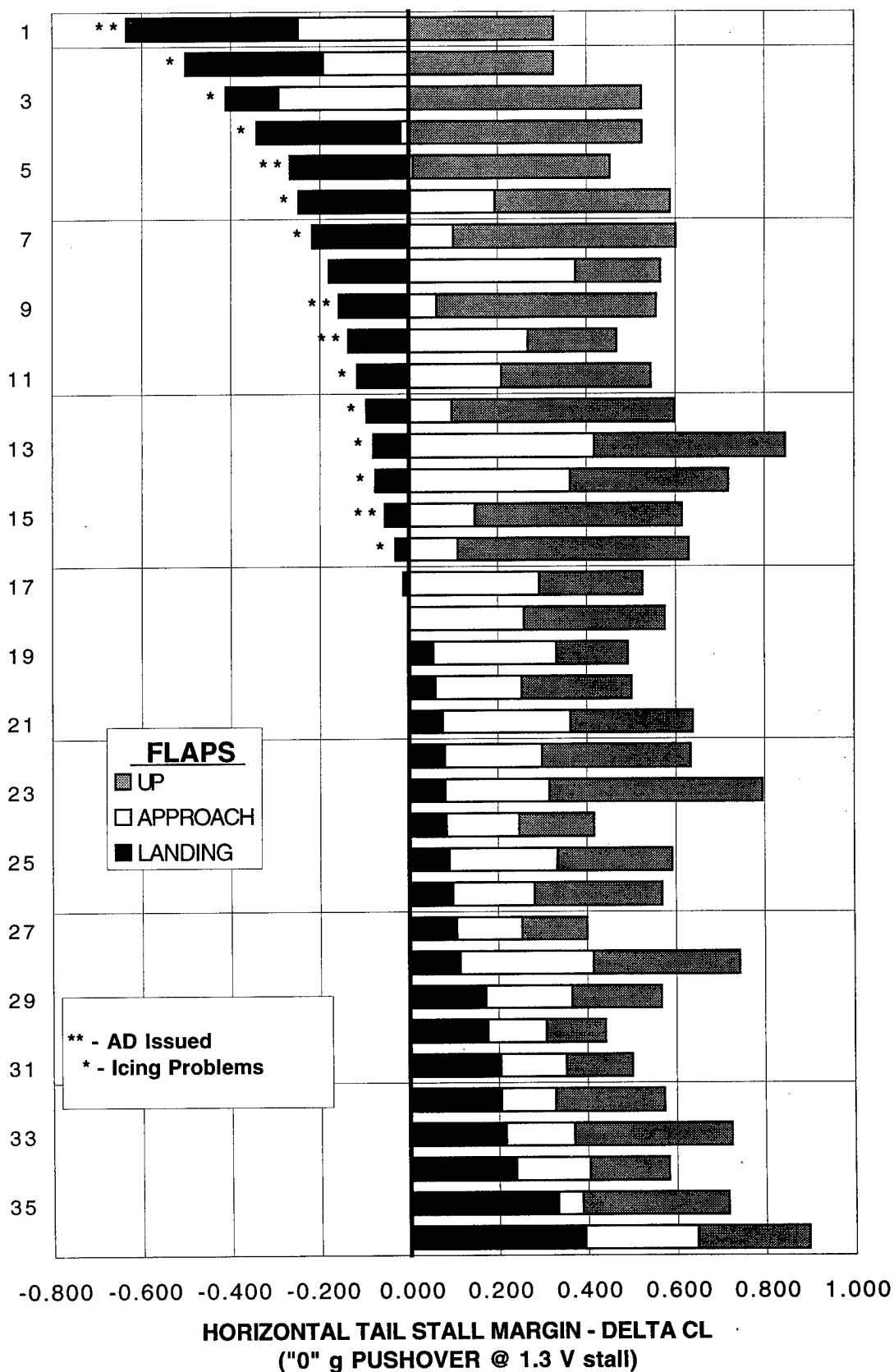
problems arising from this lack of attention during the design process. Would we be meeting this week if the designers, aerodynamicists and systems engineers spent more time evaluating operations in a more realistic environment?

In the era of specialization the problem of communication needs careful attention. The lines of communication between designers, certification authorities, trainers and the operators need a major overhaul. The time between the identification of problems and their solutions is extraordinarily long. As an example, look at ICTS (Ice Contaminated Tail-Plane Stall). The first documented tail-plane stall occurred in 1958. Only now, with a full understanding of the causes is the aircraft industry taking steps to prevent its occurrence. Unfortunately, there is a whole generation of aircraft in operation that have had or may be susceptible to tail-plane stall problems. Figure 1 gives a summary of the tail-plane stall margins for 36 designs that are currently operational in the turboprop commuter fleets today. Of this group nearly half have reported icing related tail-plane stall problems and five models have had airworthiness directives issued. Only now, almost 40 years later, are we proposing flight demonstrations to show satisfactory operation. The problem, in retrospect, is a simple one. Why have we, in the aviation community, taken so long to address it?

The answer appears to be communication. A proposal to stretch a very successful twin turboprop conversion was under consideration. Recent concern about ICTS prompted the FAA to request the applicant demonstrate satisfactory characteristics. Because of a long and very successful operating history there was no concern. Analysis predicted an ICTS and flight testing proved the analysis to be correct. Looking back on this very successful design; why had there been no hint of a possible tail-plane stall? The answer was simple. A query of the pilots who had been operating the aircraft successfully and safely for years revealed they never used full flaps in icing conditions. The word spread through the piloting community, but did it get to a place where corrective action could avoid the same mistake in future designs and certifications? Maybe, but proprietary interests and the current litigious nature of our society (particularly in the US) make it virtually impossible to expose or correct such a problem. In our zeal to "fix the problem" and write regulations an important message should not be lost. This airplane operated successfully for over 40 years without incident because the piloting community was aware of the problem and took the necessary measures to avoid it. No rule was necessary to insure safe operation, but it must be noted there was no severe performance penalty for using a reduced flap setting.

FIGURE 1

ICE CONTAMINATED TAIL-PLANE STALL MARGIN SUMMARY



Certification

Certification of a modern aircraft is a lengthy and expensive process with the objective of providing the flying public with a safe, economical means of transportation. Without question this objective is being met; the level of safety in today's aircraft is truly exceptional. A recent TV tabloid on aviation safety alluded 60% of aviation accidents are related to "human error." If accurate, this suggests certification requirements are not adequately addressing the human operator in the loop, nor the true operational environment. In recent years the bureaucracy in the US has reduced the FAA to the position of a watch dog, rather than a leader in the promotion of safety. The loss of technical expertise has meant the work needed to address the increasingly complex operational and human factors issues is not happening. The allegation that a large percentage of accidents are caused by "human error" leads quickly to a critical evaluation of training procedures and the environmental definitions for which we certify operation. Training will be dealt with later in this paper; the question of environmental requirements is currently getting long over due scrutiny.

FAR Part 25, Appendix C describes the operational environment to which you must certify anti-ice and deicing systems. It has been known for many years that the environment can be more severe than described in Appendix C but, it was thought, for very short periods of time. The design of an anti/deicing system for this more severe environment is impractical; flight in these situations, however, is a real possibility. Most importantly, an aircraft must be able to deal with these encounters long enough for the flight crew to recognize the situation and take corrective action. The perception that large droplet encounters is a rare event, may be true for some operations. On the other hand, modern turboprop/commuter operations encounter these "out of the envelope" situations almost routinely; certainly more frequently than anyone previously thought. I recently had the opportunity to meet with a group of flight crews that had ice accumulations on areas of their aircraft that could not be cleared by the deicing system; that is, large droplet encounters. In each case there was a significant ice buildup in a matter of just minutes. Appropriate action, by these alert, professional pilots promptly corrected the situation.

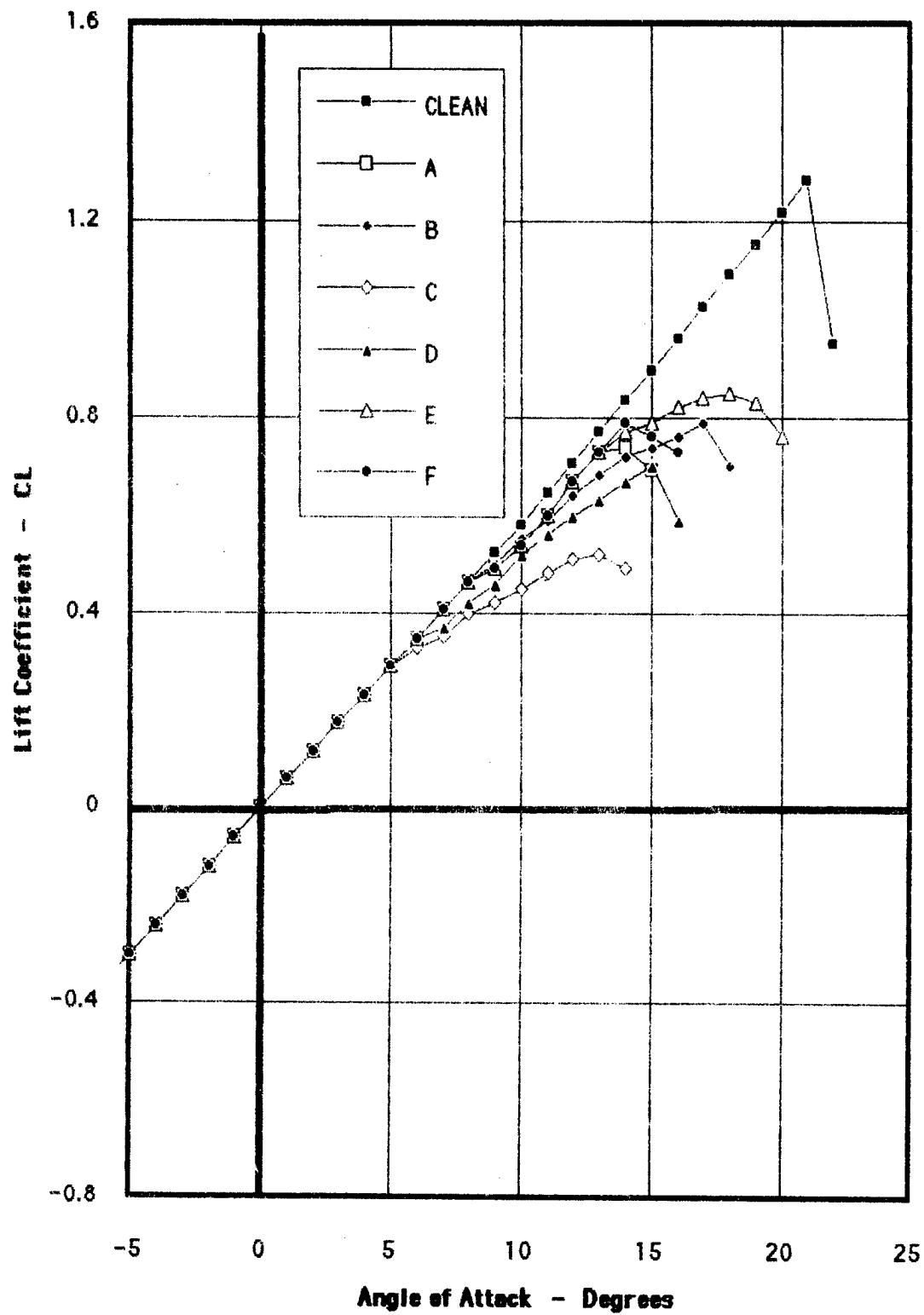
If there had not been an awareness of the situation, this ice accretion could have had much more serious consequences. It is my belief virtually every icing related incident/accident can be prevented. The technology is available for more tolerant designs. Flight crews are aware their aircraft, though certified for flight in known icing, have limitations, but they need a much clearer definition those limitations. The much greater frequency of icing encounters worse than Appendix C needs immediate attention. That flight crews from one airline reported five occurrences in a matter of a few months is proof. More tolerant designs will provide solutions for the future, but what answers are there for the certified aircraft all ready in operation? No amount of rule making will ever solve that problem. The alternative is education and training.

In the quest for safe operation in icing conditions an extensive effort has focused on the problem of defining ice shapes. I would suggest more effort be spent understanding the macro effects of contamination. A small amount of ice may be far more insidious than large accumulations. The

latter will quickly get your attention but the effect of frost and leading edge roughness can be equally as dangerous and far more devious because it builds up quickly and often is not easily seen. Figure 2 presents wind tunnel data showing the effect of various ice shapes on a full scale horizontal tail. Configurations B, C, D, and E were several sharp or ramped edged shapes that would typically occur aft of the active boot area. Configuration A was simply roughness over the first 50% of the airfoil and configuration F was roughness over just the leading edge area. It is not untypical for leading edge roughness to cause a 30% loss in maximum lifting capability of a wing. In addition the roughness may trigger a leading edge type stall that spreads rapidly and manifests itself in an abrupt roll-off.

To further emphasize this point, is an experience that occurred during flight tests on a production jet aircraft that experienced a wing stall prior to stick push. We were at a loss to explain the problem on this particular aircraft. Before the problem developed, the aircraft received with a new leading edge to correct for structural damage. After two flights without any progress, the project pilot suggested that we grit the wing to insure a turbulent boundary layer on the new leading edge. The stall on the next flight, characterized by a 90 degree snap roll, occurred even sooner. Small disturbances on the leading edge of a wing can have disastrous effects on its characteristics. It should be noted that the aircraft had flown extensively with large double horned ice shapes during certification. This characteristic never surfaced during that evaluation. Even today, cost and schedule constraints permit only cursory evaluations of a design in some parts of the environment it will operate.

Figure2
EFFECT OF ICE CONTAMINATION



Training

During the design and certification process of an aircraft there is so much pressure on technical goals and requirements that the ultimate operation of the aircraft gets lost in the shuffle. Of course there are cockpit design reviews so that the controls, displays and other functional requirements are properly integrated. Consideration for operation in a non-spec environment, of necessity, comes much later in the process. During a time I was involved in the development and certification of several business aircraft, the design group was co-located with the training and simulation operation. This was a unique situation. When operators were in for initial or recurrent training any questions they couldn't get answers to, from the training folks, usually wound up in the design office. It was a very tight loop but the interesting part was that training focused primarily on systems knowledge and to a lesser degree on piloting skills. Strangely the things we considered critical to design and certification were only lightly touched upon in the training syllabus.

An example that comes to mind is the demonstration of critical field length that, of course, great pains were taken to get as short as possible. I was explaining this to a customer one afternoon before his scheduled simulator session and suggested that he request a critical field demonstration. After two tries he succeeded in bringing the aircraft to a stop before going through the fence. The point is; we talk about the procedures necessary for safe operation, but fail to demonstrate and drive them home. In this case the data were all available; in the case for operation in icing conditions more effort is required.

Spreading the word about the hazards of tail-plane stall has been a major effort over the past several years by the FAA. It is not getting the attention required at the training operations. I recently met, on a flight from Fort Worth to Atlanta, a young Army pilot who just finished his recurrent training at a civil school. He was enroute for nine months of intense cold weather flight operations in Korea. I asked about icing operations, particularly what he had been taught about tail-plane icing. To my dismay, the subject was not covered and he was operating one of the aircraft that was identified with a reported tail-plane icing problem.

In another conversation recently, a private pilot intensely interested in the subject of tail-plane icing, complained he could get no information other than that published in the general literature. He was looking for details on the aircraft he was operating and came up dry. I suspect that because of the fear of litigation subjects as these are not getting the exposure they should from the manufacturers, particularly those in the US. Here again there is a shortfall in the area of training.

Another subject that falls under the heading of training is procedures. They need critical review and update, considering the most current information. A prime candidate would be the landing check list. Render and Jenkenson pointed out in their paper that *"there is no evidence to suggest that ice bridging occurs on turboprop aircraft. If ice bridging does not occur, this fact should be communicated to pilots, and consideration should be given to revising the operating instructions for pneumatic boots."*

On a flight between Cleveland and Indianapolis on a small twin turboprop we began to pick up some light ice. Of course I had some concern because of my close involvement with the FAA ICTS Screening Study. We landed without ever attempting to clear the ice either on the wing or the tail. I thought about this for some time and finally realized that the pilot was going by the book. He was waiting for the normal 1/4 to 1/2 inch of ice to build up before activating the boots, thus avoiding the possibility of bridging. The point is; the tail-plane stall problem is critical only in the landing configuration. It would then seem prudent that before deployment of the landing flaps that the boots be activated to clear any ice that may have accumulated, be it large or small. This procedure would dispose of any undetected ice that may have built up, particularly on the tail. Bridging should not be a concern since landing is imminent.

Conclusions

The design process for modern aircraft focuses on achieving some very ambitious performance goals and leaves very little flexibility for off design performance considerations. With the increasing frequency of operations in icing conditions beyond those identified in FAR 25, Appendix C it is time to evaluate what performance margins are required to permit safe operation in brief and unrecognized ice encounters. The philosophy of "either get rid of it or get out of it" is safe but also unrealistic in a very competitive market.

There should be encouragement for the development of a family of airfoils, applicable to the commuter, that are tolerant to some reasonable accumulation of ice. NASA was very successful in developing a laminar flow airfoil that was tolerant to the effects of rain. An extension of this work for the effects of ice contamination would be an invaluable addition to the aerodynamic designer. Additionally programs to develop reliable ice detectors, energy conservative anti/deicing systems as well as performance monitoring systems should be supported to the greatest extent possible.

The above recommendations will have their biggest pay off in future designs and maybe some retrofit applications, but will have little impact on current operations. The biggest short term pay off will come from the increased understanding that can come from improved communication and training. Because of cost and time constraints during flight test and certification only a limited icing data base is established. If the lines of communication between operational flight crews, certification authorities and manufacturers could be improved, in a non confrontational way, this data base could be greatly expanded. With that knowledge, procedures could be reviewed and updated to reflect more realistically current operations. Areas that need to be addressed are things such as ice bridging - fact or fiction, operational margins with small accumulations of undetected ice and boot operation prior to deployment of landing flaps, to name a few. There will also be a host of detailed questions related to individual airframes that could be answered in such a forum. With a dedicated effort to provide the pilots with an expanded understanding of their aircraft and improved training, safer operation of aircraft in icing situations can be achieved, quickly!

DIFFICULTIES IN THE OPERATION OF AIRCRAFT IN ICING CONDITIONS

Steve Erickson, Steve Green, Jim Bettcher,
Joe Bracken
USA Air Line Pilots Association
Inflight Icing Certification Project Team

ABSTRACT

There are no clear guidelines for operating aircraft in and around areas of hazardous Icing. Aircraft that are certificated for flight in icing conditions do not have restrictions in their operating manual which are based on the environment specified for icing certification. Unfortunately this does not relieve pilots of their responsibility under FAR 121.629 to ascertain what is hazardous icing and to then avoid it. The tools available to help a pilot comply with this responsibility are totally inadequate. Since no ice protection equipment can deal with every possible type of icing, significant emphasis has been placed on avoidance of hazardous icing. The avoidance strategy which is based on current and forecast meteorology and pilot reports of actual icing does not work. In addition, the ambiguity, subjectivity, and lack of information surrounding the guidelines and tools for operating in icing condition detracts from effective icing training for pilots and dispatchers.

INTRODUCTION

In October of 1994 an American Eagle ATR-72 crashed near Roselawn, Indiana. The aircraft was holding in an area of what meteorologists believe were supercooled drizzle drops (SCDD). SCDD represents a subset of supercooled large droplets (SLD), which are not considered in certification for

flight in icing conditions. SLD is part of what could be referred to as the exceedance environment, or the environment which exceeds FAR 25, Appendix C. It can impinge and freeze on aerodynamically critical surfaces which are unprotected. For this reason it can be hazardous to an aircraft whose ice protection equipment appears to be working effectively. Although the cockpit voice recorder transcript reveals that the experienced crew knew they were accreting ice on the aircraft they made no statements suggesting a concern about the ability of the ice protection equipment to manage the accretion. At this time the NTSB has not issued a report citing probable causes and contributing factors for this accident. However, the FAA has since focused on the certification and operating standards for flight in icing conditions because of the accident.

While no manufacturer makes the claim that their aircraft can fly in any type of icing, restrictions on flight in conditions which are not a part of the certification environment are curiously absent from most aircraft operating manuals. The correlation between certification and operation standards has diverged so much among operators that many have manuals that allow or approve flight in freezing drizzle (ZL) and light freezing rain (-ZR). This in spite of the fact that no aircraft is certified for flight in ZL or ZR of any kind.

The lack of regulatory restrictions on flight in certain types of icing conditions is surely a competitive issue for manufacturers. Listing specific icing restrictions for a certain aircraft type when other similar aircraft do not have those same restrictions puts that aircraft at a disadvantage in the marketplace. No manufacturer can afford to have their aircraft grounded when other

aircraft types are flying. It seems obvious though that no aircraft should be intentionally operated in environmental conditions for which it was not designed, tested or certificated. However, many operators and at least some within the FAA feel that flights conducted outside of the icing certification envelope are acceptable.

Unfortunately this makes the pilot's task of determining what is and isn't hazardous icing that much more difficult. If it is acceptable to fly in ZL or ZR during the most critical phases of flight (takeoff and landing) than why should a pilot be compelled to avoid it in flight at all? How many pilots would take off in these conditions if they were told that not even the manufacturers test pilot has explored them? The fact that pilots are required to safely operate their aircraft in and around hazardous icing without adequate information and tools seems very clear. As the Air Line Pilots Association has stated in their position paper on inflight icing,

"The rule (FAR 121.629) may actually be the precise embodiment of the disharmony between certification and operating rules.... There is an absence of any certification consideration of conditions which exceed Appendix C. There is an absence of any means to discriminate exceedance conditions from Appendix C conditions while in flight. There are regulatory exceptions which infer approval to operate in severe icing. There is AFM limitations language that does not reflect the actual limitations used in certification. There are FAA issued documents, approved training and approved operation programs which state that operations in know freezing precipitation are elective. All of these factors unite to form a disjointed body of knowledge and rules regarding structural

icing which bars from the pilot access to any consistent and knowledgeable approach to forming the opinion required by (FAR) 121.629(a). The industry has virtually guaranteed that this opinion will be a blind one."¹

OPERATION IN ICING CONDITIONS

Current Guidelines

FAA guidelines for operating aircraft in icing conditions are anything but clear. FAR 91.527(c) states:

"Except for an airplane that has ice protection provisions that meet section 34 of appendix A, or those for transport category airplane type certification, no pilot may fly an aircraft into known or forecast severe icing conditions."²

This would seem to imply that some aircraft are certified for flight into severe icing even though no certification program considers severe icing. The definition of severe icing contained in the Airmen's information Manual (AIM) states,

"The rate of accumulation is such that deicing/anti-icing equipment fails to reduce or control the hazard. Immediate flight diversion is necessary"³

FAA published holdover time tables for Type II ground deicing fluid contain a column for light freezing rain and freezing drizzle. Without an accompanying statement clarifying that aircraft are not certified for flight in ZL or ZR a pilot might be led to believe that if he can taxi out to a runway in these conditions without dangerous ice accretion then he can also depart in them. In fact, many operators allow just that. Recently, an article in

Aviation International News on the Regional Airline Association's position on proposed restrictions for turboprops on flight in ZL and ZR stated that,

"the RAA contends,... (that) 'light freezing drizzle' ... often exist during the winter months and with appropriate ground de-icing precautions prior to takeoff, do not pose a hazard to aircraft operations."⁴

Of course it is well established that ground deicing procedures and fluids are not intended to provide inflight protection for aircraft.

The operating manuals of aircraft that have been certified for flight in icing conditions simply state that the aircraft is "certified for flight in icing conditions." Usually no qualifiers on what type or quantity of icing the aircraft can safely handle are given. Wording that is used to provide guidance often requires subjective interpretation. One major U.S. operator of the Boeing 727 advises that compressor speed be increased when the TAT is below 7 degrees C and "moderate or heavy icing conditions are encountered." While the term "moderate" is defined in the AIM; the term "Heavy" is not defined. It is representative of the disjointed approach to the issue when one parameter, temperature, can be specified to an accuracy of 1 degree C, yet the quantification of icing is left to terms which are at best subjective and at worst undefined. In addition, the FAA has approved operation manuals and specifications which actually authorize flight in light freezing rain and drizzle. One particular manual from a major airline in the U. S. states,

"When light freezing rain, light or moderate freezing drizzle, or light,

moderate or heavy snow is falling, the airplane may take off....."

"When light freezing rain, light or moderate freezing drizzle, or light, moderate or heavy snow is falling, the airplane may land."

A memo sent to pilot's at the operator of flight 4184 prior to the accident even went so far as to state that the operator's aircraft were,

".. certified for flight into freezing drizzle and light freezing rain .."⁵

Operational guidelines like these have been allowed even though the FAA has specifically stated that aircraft icing certification does not consider flight in ZL or ZR. A recent series of NPRM's by the FAA on proposed airworthiness directives restricting flight in these conditions specifically states,

"... no airplane is certificated for operation in freezing drizzle conditions,.."⁶

John Dow of the FAA also states,

"No aircraft is certified for flight in SLD conditions "(Supercooled Large Droplets)"⁷

Pilots are being allowed and even encouraged to operate their aircraft in conditions for which they have not been designed, tested, or certificated. Specific data on what icing conditions are limiting for his aircraft and how his aircraft might respond to conditions beyond that are not made available him. When available, information on what hazardous ice accretions might look like are very general in nature and often not aircraft specific at all.

This plethora of misinformation combined with poor communication of currently available information leaves the pilot in a difficult position. The FAA has stated,

"... in general, flight crews are not currently provided with adequate information necessary to determine when the airplane is operating in icing conditions for which the airplane is not certificated .."6

Unfortunately this lack of information does not relieve the pilot of his responsibility to safely operate his aircraft in and around these conditions. FAR 121.629 (a) states,

"No person may dispatch or release an aircraft, continue to operate an aircraft enroute, or land an aircraft when in the opinion of the pilot in command or aircraft dispatcher (domestic and flag carriers only) icing conditions are expected or met that might adversely affect the safety of flight."2

The person who is ultimately responsible for the safe operation of a flight, the pilot, is not given the necessary information to make the very best operational decisions regarding flight in icing. Questions which a pilot must have answered before he can be expected to operate safely around hazardous icing include , What type of icing is my aircraft designed and certificated to handle? How will I recognize icing beyond those limits on my specific aircraft type? If I do accrete ice beyond those limits how will my airplane react? Most pilots who fly in icing conditions have not been provided the answer to even one of these questions.

Lacking this information the pilot must depend on his experience in icing conditions in the specific model of aircraft he is flying. Unfortunately icing experience between

different pilots varies significantly. As the Air Florida crash in the early 1980s showed us, pilots can have significant flight experience without having gained a proportional level of winter and icing operations experience. A pilot who has been principally operating in warmer climates where icing is not generally encountered cannot be expected to have the same knowledge about icing that a pilot flying in the Great Lakes area of the U.S. might have.

In addition this experience is principally gained by penetrating areas of icing which are beyond the capabilities of his equipment and which the manufacturer has not explored. The successful result of several trials of this sort of ad hoc test flying, with passengers or cargo on board, may lead pilots to a level of false confidence. A recent study in the U.K. by the CAA on turboprop ice detection published in November of 1995 suggests that,

"Pilots of turboprop aircraft are confident in their ability to detect the onset of inflight icing condition through the use of visual cues."

and also,

"Having identified the onset of icing all pilots felt that they could continue to fly their aircraft safely." 8

Unfortunately confidence cannot make up for a lack of knowledge about what hazardous icing looks like and how it might affect the performance and controllability of an aircraft in these conditions. Information of this nature which the aircraft manufacturers do have is limited but often even this limited information is not passed along freely to the pilot in the cockpit.

Pilots do not even know if the icing conditions they are flying in have ever been explored before.

Operational Tools

In an airline environment placing restrictions on flight around areas of hazardous icing can leave many flights stranded. Competitive pressures and the expectations of the traveling public mean that aircraft in commercial service must be able to fly in a majority of weather environments. To allow continued operation when the hazard of inflight icing exists the aviation industry relies on ice protection equipment and avoidance of icing environments.

ICE PROTECTION EQUIPMENT

Ice protection equipment falls into the categories of anti-icing, which prevents ice from accreting and deicing, which removes ice once it has accreted. Only certain parts of the aircraft are protected. Areas that are protected are designed, tested, and certified for the environment specified in FAR 25 Appendix C. This environment does not include all icing conditions, in particular SLD. Pilots are usually not given specific training on what type of icing their particular aircraft equipment was designed or certificated for. Because of the limited power available in turboprop aircraft pneumatic deicing boots are used to protect wing and empennage leading edges rather than the bleed air powered, fully evaporative anti-ice system used in most turbojets. Aircraft that utilize boots have a higher pilot workload associated with their use and require the pilot to estimate icing thickness for proper operation. Confirmation of equipment effectiveness is accomplished by visual means on all

systems. This of course makes a check of deicing effectiveness on areas such as the tailplane impossible.

ICING AVOIDANCE TOOLS

While improvements in aircraft icing equipment can improve safety no one has proposed building an aircraft which can fly in all possible icing conditions. This means that the avoidance of hazardous icing becomes extremely important. The conventional wisdom about any type of icing is "Don't fly in it". Unfortunately this advice cannot always be followed. A short flight at a low altitude from South Bend, Indiana to Chicago, Illinois might mean that the flight will be operated in ice accretion conditions for most of the flight. The shortest escape route may be the flight to the destination. Nevertheless pilots need to have good avoidance tools so that they can make routing and altitude changes which will minimize the risk of continued ice accretion. The tools available for icing avoidance include current and forecast meteorology as well as direct pilot observation and PIREPS.

Meteorology

Current weather observations of exceedance environment icing have in the past been limited to surface observations (SAs) of freezing precipitation. There has not generally been a problem with this type of terminal weather information. (although operators continue to conduct flights in these conditions because of the previously mentioned confusion surrounding operating guidelines). Work on the area of freezing drizzle or super cooled drizzle drops (SCDD) has been going on for some time at the University of Wyoming. Their work in conjunction with the National Center for

Atmospheric Research in the U.S. (NCAR) has shown that ZL and ZR conditions can exist without the presence of an overrunning warm front. Although some work has been accomplished in the meteorology community to develop better icing forecasts more work needs to be done. Helping pilots to accurately understand where hazardous icing exists is crucial to their ability to lower the flight's risk of exposure. The Research Applications Program at the National Center for Atmospheric Research (NCAR RAP) has led an ongoing project to improve inflight icing forecasts since 1989. Their work has been through the FAA's Aviation Weather Development Program (AWDP). The use of newly available satellite data may mean that operationally reliable forecast of inflight icing may soon be a reality. It may also mean that at some point in the future real time data on areas of hazardous inflight icing will be available to pilots on the ground and in flight.

The current operational usefulness of icing forecasts at enroute altitudes is poor at best. They tend to be general in nature and if followed by operators with respect to severe icing can shut down an entire hub unnecessarily. This lack of reliability leads operators and pilots to place little confidence in the forecasts and so defeats the purpose for their existence. The work being conducted by organizations such as NCAR and the Canadian weather services to improve icing forecast reliability is very important to the future of the avoidance strategy. NCAR has recently used new algorithms to provide an improving icing forecast product to a commercial vendor of weather services. Improvements to icing forecast meteorology appear to be one of the quickest roads to a more effective response to inflight icing.

Pilot Reports

For these reasons the icing avoidance system is left with a heavy dependence on PIREPs. Pilot reports of inflight icing are made using a severity index which is based on the reporter aircraft's ability to deal with the icing encounter. This system is open to much subjectivity and reduces the usefulness of the report.

As the Green, et al have noted in their paper, Operational Management of Inflight Icing in the Twenty-First Century,

"... there is no clear figure for the temporal or geographic validity of a PIREP. When a new report is given a previous PIREP in the same area is dropped out of the system. For these reasons many pilots give limited weight to PIREPS in avoiding hazardous icing conditions."⁹

The lack of meaningful and useful icing severity index makes the reporting and interpretation of PIREPs very difficult. As Green, et al also states,

"It can become literally impossible for one pilot to extrapolate the severity of any particular icing report or forecast to his specific aircraft, at his specific location, at one specific time."⁹

Those who design, certify, and operate aircraft in icing conditions must have a common language which they all can relate their work to. As John Dow says,

"To avoid ambiguity, meaningful terminology must be well-defined"⁷

An objective icing severity index can and must be created and implemented. It is obvious that the current icing PIREP

system does not merit the dependence which our airspace system has placed on it.

Identification of Hazardous icing

Current methods of identifying the type and amount of ice accretion on an aircraft range from watching a fastener head visible from the cockpit to electronic ice detection probes which give the pilot an aural or visual alert in the cockpit. Specific airframe locations such as the tailplane and upper flight surfaces are usually not monitored. Tailplane monitoring is especially important in view of the fact that their thinner profile airfoils are usually more efficient collectors of ice. Since the primary means of ice detection is visual observation from the cockpit it involves a subjective interpretation by the observer. Because pilots are not generally given pictorial training on the appearance of hazardous versus nonhazardous ice formations they are left to draw upon their own experiences in ice to evaluate what they see. Unfortunately the experience of pilots vary and how the icing experience gained in one aircraft relates to another aircraft is not clear.

When initially entering SLD conditions it is difficult to determine whether the aircraft is accreting clear ice or if it is just wet. The NRC in Canada noted that during tests of Type II ground deicing fluid in the wind tunnel an observer could not accurately tell when the fluid changed states from a liquid to a solid. And that was while observing a wing from just a few feet away. (Oleskiw et. al 1995)¹⁰ [Although this observation occurred during research for the referenced paper it is not directly mention there. M. Oleskiw of the NRC confirmed this

observation at the 1995 International Icing Symposium in Montreal]¹

In addition many pilots may not feel the need to identify SLD icing. A recent study in the United Kingdom sponsored by the CAA stated that,

"... most pilots do not worry about identifying different types of icing.."8

Indeed, most manufacturers have not identified a clear visual cue for inflight SLD accretion for their particular aircraft. Therefore the pilot usually has no specific and clear guideline with which to evaluate what he sees. At this time the ATR series of aircraft are the only aircraft in the world with a verified method of identifying SLD accretion. To understand the difficulties in visual evaluation of icing the reader has only to imagine night time visual observation of clear ice on light colored wing surfaces while flying in a thick cloud.

This illustrates the need for cockpit instrumentation which can objectively alert the crew to the presence of ice on critical aircraft surfaces. New methods of ice detection are being developed and should be incorporated on new and existing aircraft. Since droplet size cannot currently be detected from the cockpit the location of freezing precipitation becomes especially critical in the detection of SLD. Because SLD freezes further aft than smaller droplets the location of detection probes could be used to differentiate between

¹. Although this observation occurred during research for the referenced paper it is not directly mention there. M. Oleskiw of the NRC confirmed this observation at the 1995 International Icing Symposium in Montreal.

appendix C and SLD environments . Flush mounted detectors which can evaluate the quantity and quality of ice and aerodynamic performance monitoring are two new technologies which hold some promise.

TRAINING

Pilot training is crucial to any effective response to the icing issue. Although new information on severe icing may become available in the near future currently available information is not being passed along. Ambiguous operating guidelines, an absence of meteorology training, and equipment limitations training have produced pilots who do not understand the risks associated with hazardous icing.

Operators today depend on new hire pilots and dispatchers to have a strong understanding of meteorology. This is evidenced by the fact that initial and recurrent training usually includes very little information on weather. When weather information is presented to pilots it is usually in the form of company policies and procedures and FAA regulations. Information on how to use ice protection equipment is given but what the limitations of that equipment are or what will happen if they are exceeded is not passed along. General information about research and new findings in the meteorological community are seldom communicated. Work on the area of SCDD has been going on for several years at the University of Wyoming and NCAR but much of their research has not made it to the pilot community.

A 1989 paper by Marcia Politovich discusses test flight conducted by the University of Wyoming's King Air in SLD

conditions. It was noted that a short exposure to large droplets ,

" ..can result in a serious deterioration of the airfoil when only a small amount of airframe ice is actually accreted."10

Could this information if passed along in regular operator training have heightened the awareness of the crew of American Eagle 4184? We'll never know.

In addition, because of competitive pressures, operators and manufacturers are reticent about discussing difficulties which their aircraft have experienced in icing conditions. Previous to the Roselawn accident many of the pilots flying the ATR series of aircraft were not aware of the series of icing incidents and the accident which the aircraft had experienced. While this may not have prevented this particular accident, knowledge of an aircraft type's incident/accident history by the pilot is essential to good risk management in the operation of that aircraft type. The capabilities and limitations of each aircraft varies and the pilot must be made aware of all of them.

Clear, consistent training throughout the entire pilot community on identifying and reporting different types of icing does not exist. The previously mentioned study in the UK seems to suggest that many pilots appear to be unconcerned about ice accretion on their aircraft. This may be due to a lack of information being made available to them and to their own successful experiences in icing conditions. Of course, successful encounters with environmental conditions of undetermined hazard should never reduce a pilot's respect for them. A free exchange of information on the icing certification process, new

weather information related to icing and the specific icing capabilities of specific aircraft types can all be accomplished through training.

RECOMMENDATIONS

- Clear unambiguous guideline on operations in icing conditions must be made available to pilots. Guidelines must be based on design, testing, and certification limits and not just on operational experience. Perhaps the FAA could adopt JAR-OPS 1.345 (c) which states,

"A commander shall not commence a flight under known or expected icing conditions unless the aeroplane is certificated and equipped to cope with such conditions."¹³

- A graduated parametric method of describing icing severity which is meaningful to the meteorological, aircraft design, regulatory and operator communities must be developed.

- Operationally useful and reliable icing forecasts must be developed to reduce the risk of hazardous icing exposure.

- Reliable onboard reactive or predictive detection must be developed and required for all aircraft operating in icing conditions.

- Training for pilots and dispatchers should include the certification process and limitations of aircraft specific ice protection equipment, current icing meteorology, and effective recognition and reporting of hazardous icing.

REFERENCES

1 Green, S., Bettcher, J., Erickson, S., Bracken, J., 1996 Air Line Pilots

Association, Inflight Structural Icing, An Operational Analysis and Global Approach

2 Federal Aviation Regulations, U.S. Government, Parts 91, 121

3 The Airman's Information Manual, 1996, U.S. Government

4 RAA contests icing ADs; fears for turboprop image, April 1, 1996 Page 65 and 67 Aviation International News

5 American Eagle 4184 NTSB Public Hearing Exhibits 1995, Indianapolis, Indiana

6 Department of Transportation NPRM Docket No. 95-NM-146-AD

7 Dow, J. P. Sr., 1996, Pilots Can Minimize the Likelihood of Aircraft Roll Upset in Severe Icing. Flight Safety Digest, January 1996

8 Render, P.M., Jenkinson, L.R., Caves, R.E., Pittfield, D.E., 1995: Ice Detection For Turboprop Aircraft. Loughborough University of Technology, Flight Safety Digest November 1195 Page iii and 5.

9 Green, S.D., Bettcher, J., Bracken, J., Erickson, S. 1996: Tools For the Operational Management of Inflight Icing in the Twenty-First Century. Air Line Pilots Association, AIAA - 96-0136

10 Oleskiw, M., Penna, P., Crabbe, R., and Beyers, M. 1995: Full Scale Wind Tunnel Simulation of Takeoff Performance Degradation with Contaminated Fluid Runback. International Icing Symposium Montreal, Canada Proceedings Pages 177-190.

11 Politovich, Marcia K. 1989 : Aircraft Icing Caused by Large Supercooled Droplets. Journal of Applied Meteorology Vol 28 Pages 856 - 868

12 Politovich, M.K., Brown, G. , Thompson, R., Ruintjes, R., Bernstein, B.C. 1996: Toward Improved Aviation Forecasts for Icing AIAA 96-0137

13 JAR-OPS 1 Subpart D - Operation Procedures paragraph 1.345 (C)

**AIRCRAFT ICING
THE DISPATCHER'S ROLL IN FORECASTING AND AVOIDANCE**

**PREPARED FOR
FAA INTERNATIONAL CONFERENCE ON AIRCRAFT INFLIGHT ICING**

BY: STEVEN K. HORTON

OVERVIEW

The widespread acceptance of turbojets at the larger airlines for the past several years has lulled us into a comfortable, almost lackadaisical attitude about en route aircraft icing. Since turbojets, with their good climb and descent profiles, coupled with compressibility temperature rise, spend such little time at lower levels, en route icing has become a manageable issue in the overall scheme of airline operations. Those of us who were around before the widespread use of turbojets will remember a time when en route icing was much more of a consideration in day-to-day operations. The piston powered airliners introduced after World War II were well equipped to handle moderate airframe and engine ice through a variety of de-ice and anti-ice systems. As the turbine engine became more accepted, we were introduced to a higher level of anti-ice protection by using hot air for airframe anti-ice systems. Because of the turbojet advantages mentioned earlier, it is not necessary to anti-ice a turbojet to the extent that we were accustomed to with the piston powered aircraft. Even the Air Traffic Control System has cooperated through the reduction in holding at major terminals at low and mid altitudes.

COMMUTER AIRLINES

Commuter airlines are proliferating in size and numbers at a rate we never dreamed possible. Because of route structure and passenger demand, the turboprop airliner has become an economical, comfortable ingredient in the safe completion of commuter airline operations. Since it is very often necessary to operate these commuter flights at lower altitudes, we are quite often right back to the 1950s with regard to operating in en route icing conditions.

SYSTEMS

Today's commuter airliners have the best de-ice and anti-ice systems available. Proper use of these systems by the flight crews (sometimes anticipating icing conditions) is of course paramount in allowing safe operations in icing conditions. No system can replace proper training of the flight crews.

PLANNING

Although a vigilant attitude by the flight crew to allow early detection of serious icing conditions prompting appropriate action to combat or escape from these conditions, the Aircraft Dispatcher can contribute a great deal to help avoid problems by proper planning prior to the start of the trip and proper monitoring while en route.

TOOLS

Since areas of really serious icing conditions are generally quite small vertically and laterally, forecasting is very difficult. Weather Bureau Area Forecasts cover such a large area, they can do little to pinpoint areas of icing of lethal consequence. Since few if any commuter airlines have a Meteorology Department, the Dispatcher is pretty much on his/her own to get the information needed. A few vendors have made icing forecasts available that do pinpoint areas of icing with suspected severity. These forecasts provide a good service at a modest cost, but remember that we are still talking forecast. Much more up-to-the-minute information is needed, and is available in pilot reports. Interpretation of PIREPS is important. One pilot's severe is always another pilot's moderate. Still, remember that in the case of icing reports, the pilot is probably well qualified for the mission. The most accurate, and therefore the most valuable PIREPS are those that come from your own airline. Since these pilots get the same training, and fly the same or similar equipment, the PIREPS will carry a greater degree of credibility. All commuter airlines should have a system in place that gets PIREPS to the Dispatcher and encourages reports from en route crews.

DISSEMINATION

If the system recommended in the previous paragraph is in place, the Dispatcher will get the PIREPS as needed for planning purposes. Great! Now for the en route flights: It is the responsibility of the Dispatcher to provide information to the crew en route. This is what Operational Control is all about. Communicate.

SUMMARY

Several commuter accidents in recent years have pointed out that there is work to be done in the area of en route icing. The aircraft we are operating are technically state-of-the-art. We can do something to improve safety, however. An increased awareness of icing conditions, along with increased respect for icing situations will allow safer operations with the equipment we have.

FAA INTERNATIONAL CONFERENCE ON AIRCRAFT INFLIGHT ICING

**PRESENTATION BY
JACK SQUIRES
VICE PRESIDENT, FLIGHT OPERATIONS
AIR TRANSPORT ASSOCIATION OF CANADA**

**WORKING GROUP 5
OPERATIONAL REGULATIONS & TRAINING REQUIREMENTS**

**How A Canadian Air Carrier
(for example)
Informs, Trains and Provides Instructions
For Its Crews
On Operations Where Severe Icing Conditions
May Be Encountered**

CONTENT

- 1) Information and Knowledge On Severe Icing Conditions
 - 2) Training On How To Recognize and Avoid/Exit Severe Icing Conditions
 - 3) Operating Experience In Areas Where Severe Icing Conditions Prevail
 - 4) Regulatory Issues - Operations
-

DEFINITIONS OF ICING

- **MODERATE -** The rate of accumulation is such that even short encounters become potentially hazardous, and use of de-icing/anti-icing equipment or diversion is necessary.
- **SEVERE -** The rate of accumulation is such that de-icing/anti icing equipment fails to reduce or control the hazard. Immediate diversion is necessary.

NOTE

In each case, the flight crew members' full attention to the environmental conditions affecting the aeroplane is mandatory.

CARRIER'S OPERATING RESTRICTIONS

- **Take-off will not be made with ice, snow or frost adhering to the wings, control surfaces or propeller of the aeroplane.**
- **Take-off will not be made in freezing precipitation or moderate wet snow except in accordance with the restrictions and procedures in the ground icing operations program.**
- **Flights will not be cleared to operate or be intentionally operated in known severe icing conditions.**
- **Aircraft equipped with suitable de-icing equipment may be planned to take-off through known moderate icing conditions provided the airport of departure has landing limits or better and runway conditions are suitable for the aircraft to return and land safely.**
- **Flights shall not depart cruising altitude to attempt landing at a station reporting heavy freezing precipitation.**
- **Under instrument conditions, final approach will not be continued in icing of such intensity that instrument flight cannot be carried out with adequate precision and safety.**
- **Notwithstanding the foregoing, it is company policy that a flight shall not commence nor continue into known or expected icing conditions in which the formation of ice on the aeroplane may adversely affect the safety of the flight.**

ENROUTE ICING CONDITIONS

- **Propeller and Engine Anti-Ice on prior to its requirement.**
- **Auto ignition must be considered.**
- **Appropriate airframe ice accumulation required prior to cycling airframe de-ice.**

HOLDING

- **Do not hold in severe icing conditions.**
- **Where minimum icing conditions are expected, use 0° flap and appropriate airspeed for clean configuration and autopilot disengaged.**
- **Avoid icing conditions with engine out situation.**
- **If severe icing is encountered, request immediate altitude change.**

APPROACH AND LANDING

- **Plan descent to minimize exposure time in icing conditions.**
- **If MAP is possible and freezing drizzle is being experienced, note the altitude at which the temperature is above 0° so as to request this level from ATC.**
- **Allow extra speed when operating in icing conditions but be cognizant of runway length and conditions.**
- **If landing flap selection is accompanied by stick force lightening, or other such force irregularities, retract flap to approach setting immediately. Cycle wing/tail de-icer boots and land using a smaller/lesser flap setting.**

GENERAL INFORMATION ON ICING

- **During descent, the pilot must remember that the probability of encountering supercooled clouds at low altitudes can contribute to an increased potential for ice accumulation. The probability of increased exposure time in holding patterns at high density airports can accentuate the problem.**
- **The most severe icing conditions can occur at temperatures between 0°C and -10°C in cumuliform clouds and freezing precipitation. At temperatures below -10°C, either continuous ice or mixed rime and clear might occur.**

GENERAL INFORMATION ON ICING (Cont'd)

- **Frontal weather situations cause almost all severe icing conditions in terminal areas.**
- **Of particular note is the stratocumulus cloud layer which forms in a cold air mass that has moved over a warmer surface.**

As the low levels of the air mass gain heat and moisture very rapidly, the stratocumulus layer is formed.

Icing is often moderate or severe in the tops of these clouds.

In summary, air carriers should:

- **Provide information on severe icing conditions in Company Operations Manual (COM).**
- **Provide annual and recurrent training on how to recognize and avoid or exit severe icing conditions.**
- **Present operating procedures and restrictions involving severe icing conditions in COM.**
- **Emphasize value of operating experience as applied to severe icing conditions, and**
- **Highlight any Regulatory Provisions regarding operations in severe icing conditions.**

Section VI

Appendix of Additional Papers Submitted at the Conference

DEVELOPMENT OF AN ICE ACCRETION MONITOR FOR AIRCRAFT

R. Lowell Smith
Texas Research Institute
9063 Bee Caves Road
Austin, TX 78733-6201

ABSTRACT

This paper addresses the development of a mass-loaded piezoelectric oscillator sensor which should be suitable for attachment behind exterior aircraft control/lift surfaces for the purpose of monitoring inflight icing. The operation of this instrumentation depends very simply on observing changes in the resonant frequency of a structure induced as a result of the added mass or altered stiffness associated with ice accumulation. Piezoelectric sensors are well understood and historically have been applied to a wide variety of subtle measurement problems. Established applications include sonar, medical ultrasound, and nondestructive testing. Texas Research Institute has applied this technology to rubber/metal debond detection, monitoring aircraft corrosion, and measuring accumulated rainfall. Development of an ice accretion monitor for aircraft appears to represent a natural extension of the general approach. Details concerning measurement philosophy, sensor design, control and interrogation provisions, and experience with breadboard prototypes are presented.

INTRODUCTION

Following the crash of the ATR-72 aircraft near Roselawn, Indiana on Oct. 31, 1994, there has been a great deal of research interest in the formation of super-cooled large droplets (SLD) in the atmosphere and their potential impact on aviation. Means to detect and monitor SLD conditions are the subject of current research initiatives. The implications of flying through SLD conditions are being studied in icing tunnel facilities and by means of tests conducted using the Air Force KC-135 tanker. Typically, SLD icing results in the formation of a ridge of ice just behind the wing or tailplane surfaces normally protected with pneumatic deicing boots. This artifact disrupts streamlined flow over the airfoil, leading to degraded performance of the wing and ailerons. Obviously, development and qualification of appropriate means to detect and/or remove accumulated aircraft ice buildup represents a significant step toward mitigating the SLD icing hazard.

A number of papers and presentations at this conference address these concerns, and a vigorous competition to develop preferred methods is in progress. This paper considers only the remote or non-visual ice detection issue. The reader is referred to other papers in these proceedings to develop a more general perspective of the range of preferred ice detection methodologies considered to be feasible. A brief comparison of some of these approaches is shown in Table 1. The aircraft ice accretion problem is

rendered difficult by a number of confounding influences, such as, ice-water mixtures, the presence of deicing fluid or other contaminants, morphological variability including dendritic formations, and variation of physical properties with temperature.

Table 1. Comparison of Basic Approaches to Inflight Ice Detection

Type of Approach (measurement parameter)	Typical Sensor Configuration	Features/Constraints
Capacitance	Flat format, surface mounted	Sharp threshold, early saturation. Range controlled by overall size.
Electrical Conductivity	Flat format, surface mounted	Variable threshold. Range and saturation depend on conductivity.
Electromechanical	Modular, flush or sub-surface mounted	Sensitive, good range, potentially vulnerable to wide range of effective modulus for different icing morphologies.
Ultrasonic	Modular, sub-surface	Good discrimination between air, water, and ice phases.
Optical	Modular, flush mounted	Sensitive, robust, range characteristics unspecified.
Heat-of-fusion	Flat format, surface mounted	Heating profile is interpreted. Sensitive to mass of ice melted. Cycle repeated for cumulative measurement.

IMPEDANCE SPECTROSCOPY APPROACH

Impedance spectroscopy [1] is a very sensitive established method for characterizing broad classes of electrical networks. Several approaches to ice detection presented at this conference incorporate measurements of electrical impedance. Parkins and Edmonds [2] discuss how the interelectrode capacitance of foil electrodes is affected by the buildup of ice over them. The electrical conductivity of ice and ice-water systems is addressed by Sweet and Reich [3]. Both approaches represent purely electrical measurements. The commercial ice accretion detector manufactured by Vibro-Meter SA [4] incorporates piezoelectric elements. Thus electrical artifacts associated with the mechanical characteristics of an attached ice layer can be observed and interpreted. The Vibro-Meter sensor is flush-mounted, which involves cutting a hole in the aircraft skin. This paper addresses a non-invasive alternative in which piezoelectric elements are bonded to the underside of the structure where the ice accretion measurement is made.

Often when one speaks of impedance spectroscopy as opposed simply to impedance measurement, availability of mathematical models to permit more global interpretations of the measurement data is implied. This point will be addressed in greater detail shortly. There are other reasons why electromechanical impedance methods are attractive. Mass-loaded oscillators are very stable and lend themselves to a variety of specialized measurement applications. They can be configured as disks for which the bulk stiffness is controlled by modifying the thickness of the structure. In this way evaporated coatings can be monitored by how they raise a characteristic resonant frequency of the disk. Such a structure is also very sensitive to the loss of material and can be calibrated to monitor corrosion. Piezoelectric oscillators can equally well be configured in ways such that changes in resonant frequencies are dominated by added mass rather than altered stiffness [5]. Piezoelectric oscillators perturbed by interaction with external structures have also been applied to the detection of debonds [6] and for the purpose of measuring the viscoelastic properties of materials in bulk [7]. The proposed ice accretion monitor for aircraft has many features in common with these established methods.

PROPOSED ICE ACCRETION SENSOR

Figure 1 shows the laboratory test fixture that was assembled to evaluate the proposed ice accretion monitor operational concept. Four rings of piezoelectric material, 1 cm in diameter and 0.5 cm high were bonded to the underside of an aluminum plate 0.032 inch thick as indicated. A light-weight barrier was attached to the other side of the plate so that a shallow pool of water could be isolated and frozen in the region opposite the location of the piezoelectric ceramic. The ceramic was configured such that it could be monitored using a Hewlett-Packard 4192A impedance analyzer. The data were acquired in a stepped frequency mode, giving rise to files which could be plotted as impedance magnitude and phase as functions of frequency. The piezoelectric ceramic elements can be connected in series or parallel such that the axial strain in the primary oscillator structures is out-of-phase or in-phase as desired. These two configurations emphasize coupling of the oscillators predominantly via stiffness or mass-loading respectively.

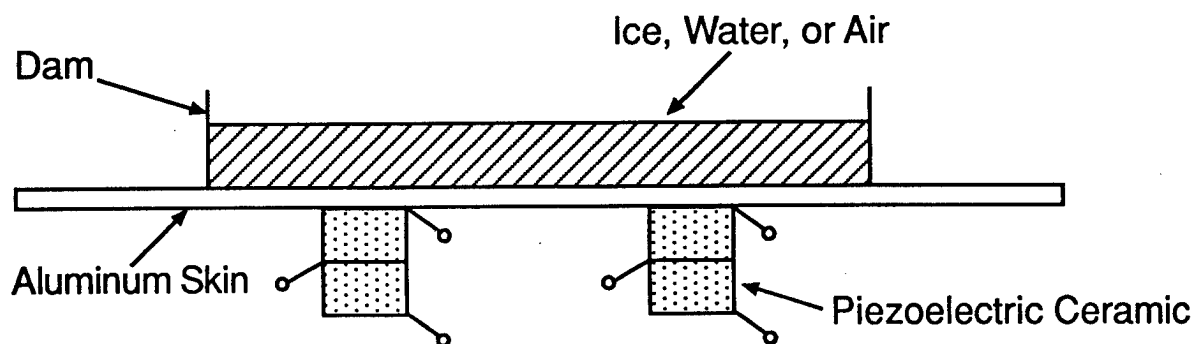


Figure 1. Laboratory Test Fixture for Monitoring Ice Accretion

One can visualize the operation of the ice accretion monitor by referring to Figure 2, which shows a lumped distribution of mass, stiffness, and damping representing the gross performance of the coupled oscillator system. If there is no ice or water present, then the two pairs of ceramic rings are coupled only by the thin aluminum plate representing the aircraft skin. This is the baseline or reference state of the system. If water or ice is present, then the mass, stiffness, and damping parameters of the ice-water coupling region indicated in the figure are altered. Electrically driving the ceramics in phase implies a sensitivity predominantly to added mass. In contrast, out-of-phase operation emphasizes changes in coupling stiffness. Data representing the latter situation are presented in Figure 3.

In order to develop a robust measurement tool, it is desirable to monitor several physical attributes of accumulated ice. The reason for this is that ice buildup can exhibit a high degree of variability [3]. Thus, in this preliminary study the coupled oscillators were driven both in-phase and out-of-phase. In the case of water loading, damping effects are also apparent, especially in the slushy, semi-frozen state. Future work might include more systematic ways of cataloging and reporting damping data. Currently, it appears that a piezoelectric ice accretion monitor is most conveniently interrogated by tracking frequency shifts associated with ice accumulation. This can be automated using standard phase-locked-loop technology as indicated in Figure 4. A local oscillator drives the piezoelectric elements, and feedback is provided via the phase comparator as indicated. The control loop alters the drive frequency such that the voltage and current are in phase (resonance). This frequency is measured using a standard counter and appropriate time gating, and interpreted in terms of the underlying ice accretion.

PERFORMANCE MODELING

Electrical equivalent circuit modeling methods are well developed for piezoelectric oscillators [1,8], and may be used for design optimization and data analysis. Using the well-known impedance analogy [1], the lumped-element equivalent circuit corresponding to Figure 2 is presented as Figure 5. The negative capacitances seen in the figure are familiar artifacts associated with longitudinally polarized ceramic. They do not complicate the practical use of Figure 5. Operationally, one can replace the series combination of C_m and $-C_e$ by a single capacitor with a capacitance of $C_m C_e / (C_e - C_m)$. Equivalent circuit models are useful because they provide a computational basis for interpreting measurement data. This has not yet been implemented for the proposed ice accretion monitor, but constitutes a useful tool for design and performance optimization of developmental sensor technology.

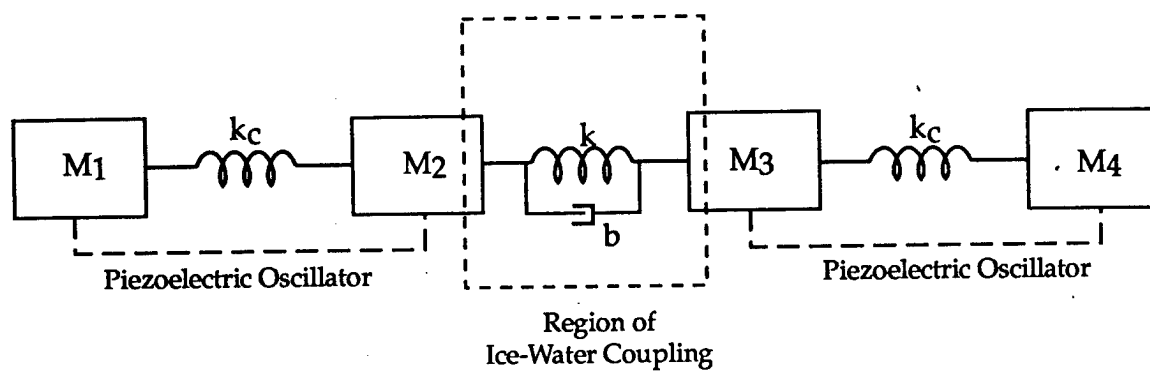


Figure 2. Mass-Spring-Dashpot Functional Analog

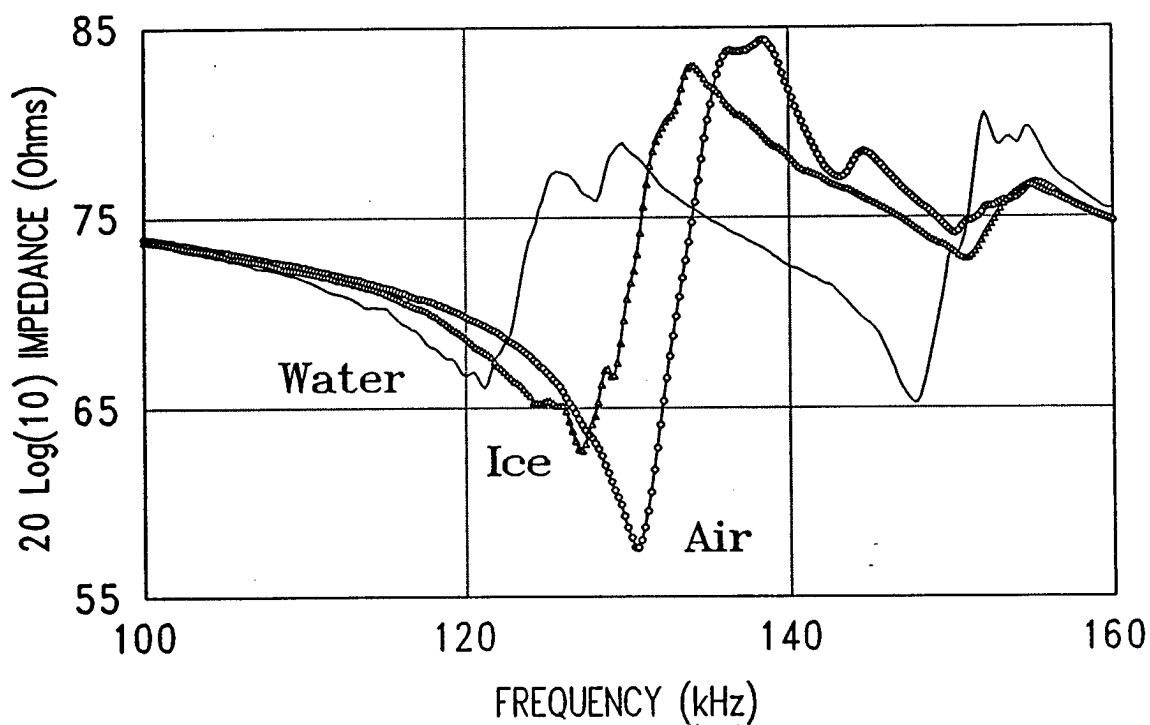


Figure 3. Data Comparison for Compound Oscillator Test Fixture (water/ice 3 mm thick)

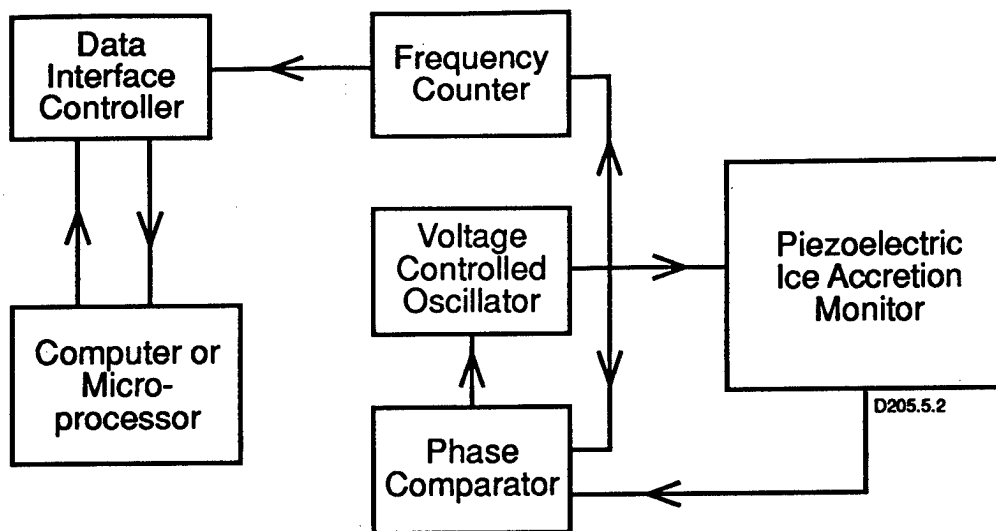


Figure 4. Proposed Driver/Interface for Interrogating a Piezoelectric Ice Accretion Monitor

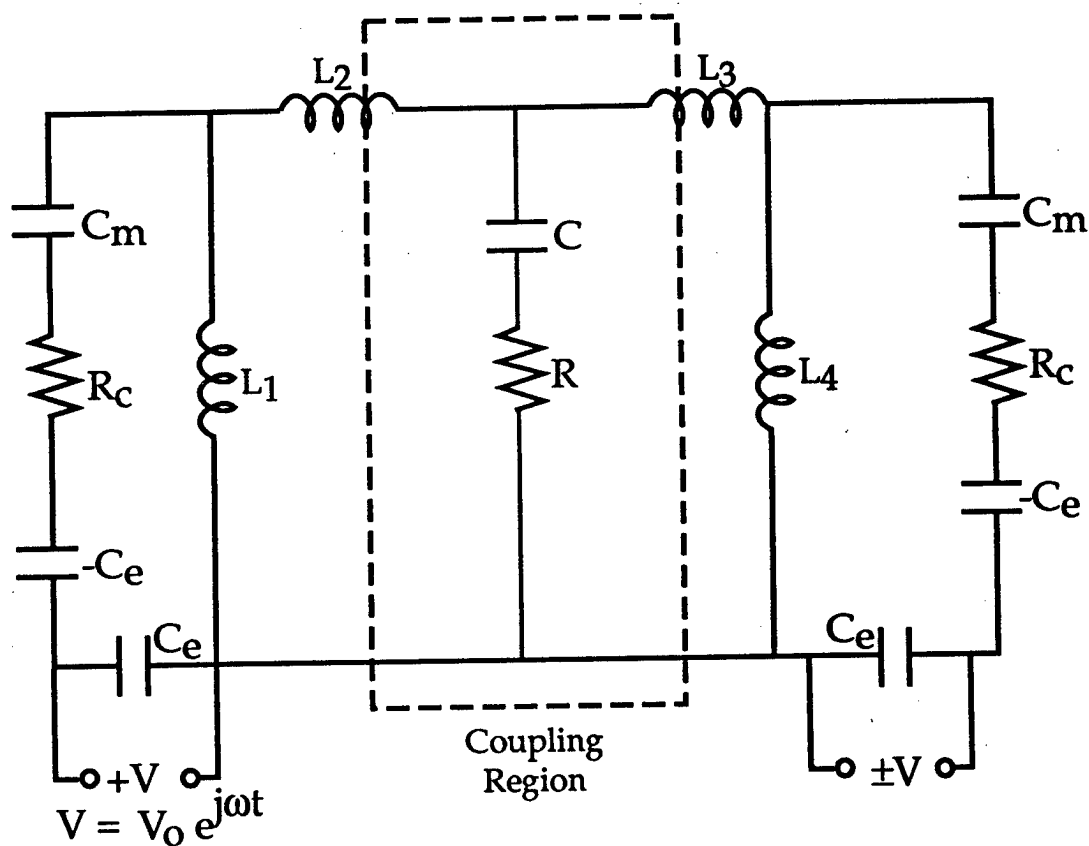


Figure 5. Electrical Equivalent Circuit Analog for the Proposed Ice Accretion Monitor

CONCLUSIONS

Based on the preliminary study reported here, it appears that development of an ice accretion monitor for use to observe inflight icing conditions is feasible. One expects this type of detector to be small, lightweight, and have very minimal power requirements. More specifically, the sensor volume is estimated to fall in the range of 2 to 10 cubic centimeters. The mass of the structure is expected to be from 5 to 20 grams. In the laboratory study the interrogation power requirement was less than one microwatt. The sensitivity, range, and preferred physical configurations of a practical piezoelectric ice accretion monitor remain to be established. However, it appears that resolution on the order of 0.1 mm with an accuracy of 0.1 to 0.2 mm should be achievable. The working range is expected to be up to an ice thickness of 2 cm or more, depending on the overall scale of the sensor.

REFERENCES

1. R.L. Smith, "Impedance Spectroscopy and Resonance Methods for Nondestructive Testing," Nondestructive Testing Handbook, 2nd edition, Vol. 7, Section 10, Part 4, published by The American Society for Nondestructive Testing, Columbus, OH, 1991.
2. D.C. Parkins and J. Edmonds, "An Impedance-Based Sensor Technology for Assessing Airframe Icing," these proceedings.
3. D.B. Sweet and A.D. Reich, "Super-Cooled Large Drop (SLD) Ice Formation Detection," these proceedings.
4. P. Zollinger, "Use of Flush Mounted Smart Skin Ice Sensors for the Detection/Exit Criteria," these proceedings.
5. R.L. Smith, "Development of a Mass-Loaded Oscillator Rain Gauge," TRI Proposal A3061:RLS to the U. S. Dept. of Commerce, 17 Jan 1994.
6. R.L. Smith, A.V. Bray, and C.M. Teller, "Development of a Resonant Probe for Evaluating the Integrity of Rubber-to-Metal Bonded Joints," Proceedings of the 17th Symposium on Nondestructive Evaluation, San Antonio, TX, April 17-20, 1989.
7. R.L. Smith, "Inverse Acoustic Modeling as a Technique for Monitoring Aging Effects in Transducers," J. Underwater Acoust. (USN), 35, 87 (1985).
8. W.P. Mason, Electromechanical Transducers and Wave Filters, second edition, New York, NY, Van Nostrand, 1948.

Airfoil Performance Monitoring using the Turbulence Intensity Parameter

A Paper Presented to the
Ice Protection and Detection Working Group
FAA International Conference on Aircraft Inflight Icing
Springfield, Virginia, May 6-8, 1996

J.M. Maris, Consulting Engineering Test Pilot
Marinvent Corporation, Montreal, Canada

Disclosure: The author is the originator of the Turbulence Intensity Parameter concept for airfoil performance monitoring. This paper is based on information provided by Aerospatiale, Fokker Aircraft, and, in particular, by Mr. Paul Catlin of B.F. Goodrich. These contributions are gratefully acknowledged, but it must be stressed that the views expressed herein are the author's, and should not be interpreted as representing the position of the other parties.

OUTLINE

1. Contamination Effects: Background
2. The Turbulence Intensity Parameter
3. Test History
4. The B.F. Goodrich Stall Warning Plus™ System
5. F100, ATR 42 Case Study Findings
6. Conclusions and Recommendations

Contamination Effects Background

Airfoil contamination (including ice accretion) can cause:

- Significantly increased stall speeds
- Reduced maximum lift coefficient
- Adverse controllability effects
- Critical-configuration effects
- Tailplane stalls
- Reduced takeoff performance

Icing contamination effects are unpredictable functions of (among others):

- Ice shape, thickness, and roughness
- Ice location
- Airfoil characteristics
- Aircraft configuration

The effects of ice accretion are highly unpredictable. Pilots therefore cannot rely on simple ice-detection techniques to determine:

- Minimum safe operating airspeeds
- Safe aircraft configuration management
- Safe aircraft maneuvering limits
- Takeoff go/no-go criteria

These operational limitations led to the examination of the Turbulence Intensity Parameter for airfoil performance monitoring and contamination detection.

Test History

The following evaluations have been conducted:
(not an exhaustive list)

- 1979 Imperial College low speed wind tunnel
- 1984 Raspet Flight Research Lab (Grumman AA5)
- 1987 Tracor Flight Test Systems (Lockheed T33)
- 1989 USAF Test Pilot School (Piper PA 30)
- 1990 Avtel Flight Test Inc. (Lockheed Sabreliner)
- 1990 OSU 7x10 low speed wind tunnel*
- 1990 NASA Heavy Rain Facility (L1011 wing)
- 1991 B.F. Goodrich (Cessna 421)
- 1993 B.F. Goodrich (Fokker 100)
- 1994 B.F. Goodrich (ATR 42)

* SAE Technical Paper #922010 "Stall Warning Using Contamination Detection Aerodynamics" written and presented by Mr. Paul Catlin of B.F. Goodrich at Aerotech '92; 5 October 1992.

The Turbulence Intensity Parameter

- The Turbulence Intensity Parameter (R) is a normalised measure of boundary layer turbulence and separation.
- The state of the boundary layer airflow is a direct measure of the aerodynamic "stress" experienced by an airfoil.
- Turbulence intensity can be computed from high frequency RMS velocity or pressure measurements.
- R is typically measured adjacent to the "suction" surface of an airfoil; sensor location is dependent on the airfoil stall and contamination characteristics.

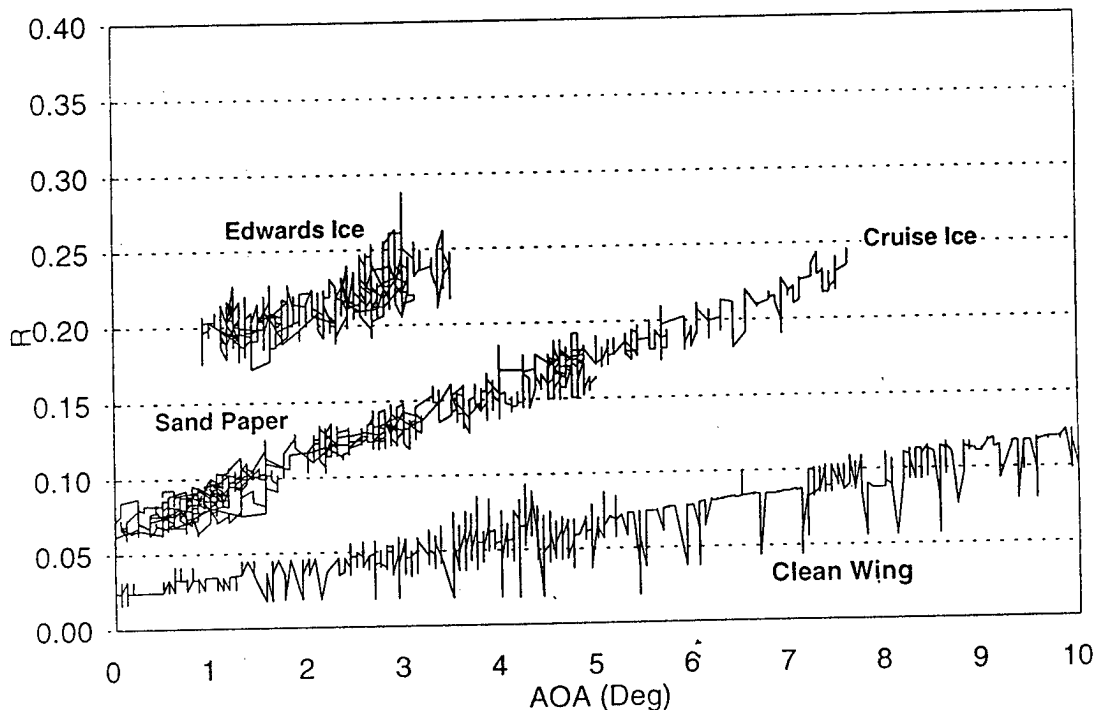
The B.F. Goodrich Stall Warning Plus™ System

- SW+ is an implementation of a Turbulence Intensity-based aerodynamic performance monitor, using high-frequency solid-state pressure sensors.
- SW+ has been evaluated during Fokker F100 and Aerospatiale ATR 42 icing trials.

General Findings

- The Turbulence Intensity Parameter (R) exhibited a high positive correlation with available airfoil lift coefficient for both contaminated and clean airfoils.
- A preset R limit was usable for take-off contamination detection at approximately 20 - 50% of the liftoff velocity, depending on the aircraft type.
- The R parameter was usable at all aircraft flap settings.

ATR 42-500 (Flaps = 15 Deg)

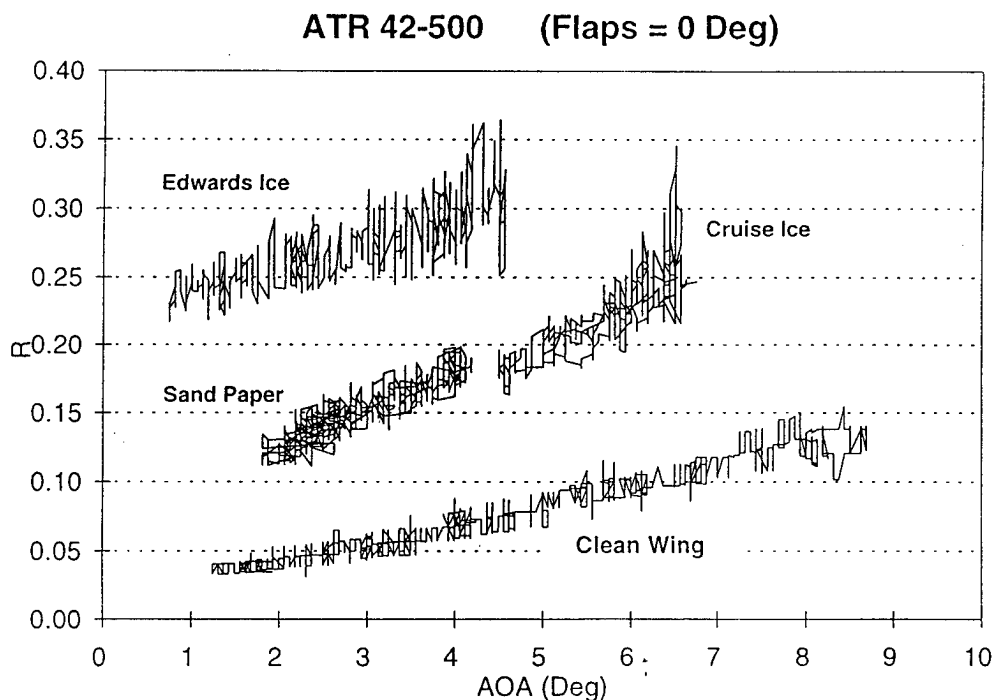


Fokker F100 Findings

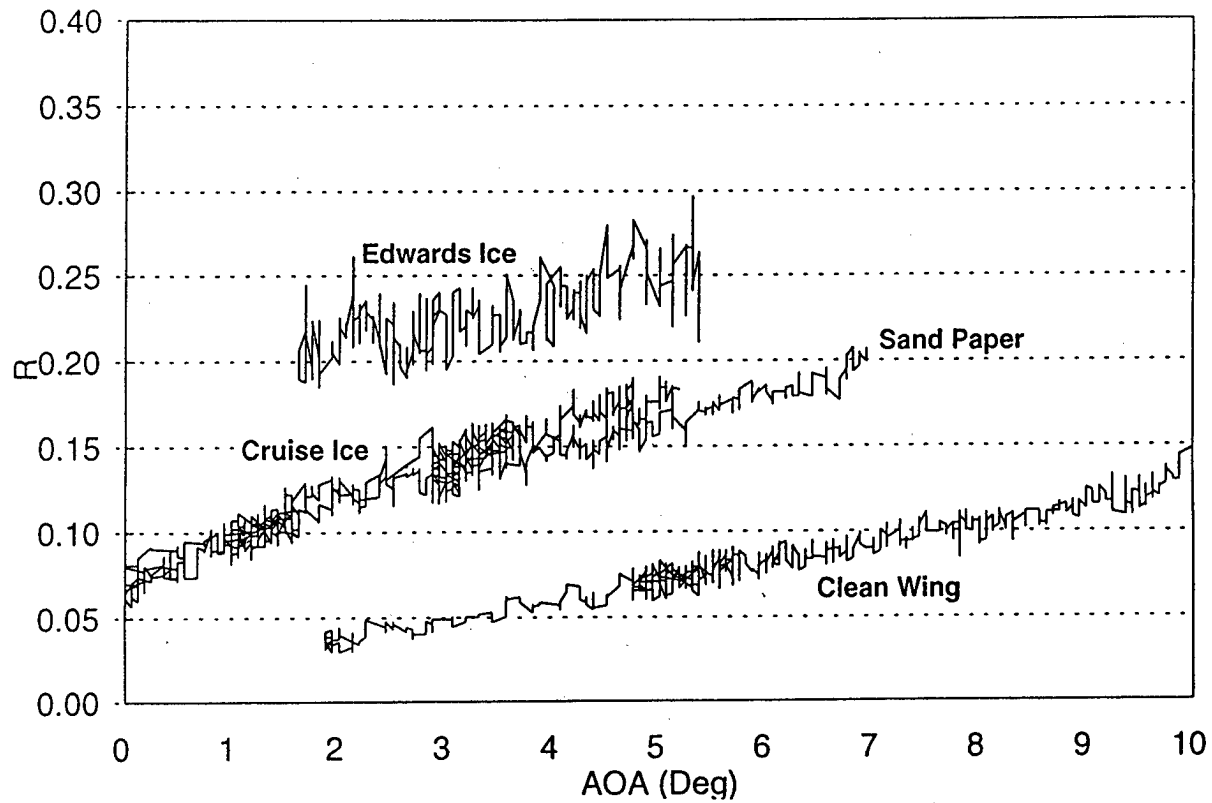
- The R parameter was sensitive to the ice forms tested.
- R was usable for take-off contamination alerting, commencing at approximately 30 knots in the takeoff roll.
- R correctly responded to high altitude compressibility effects.

ATR 42 Findings

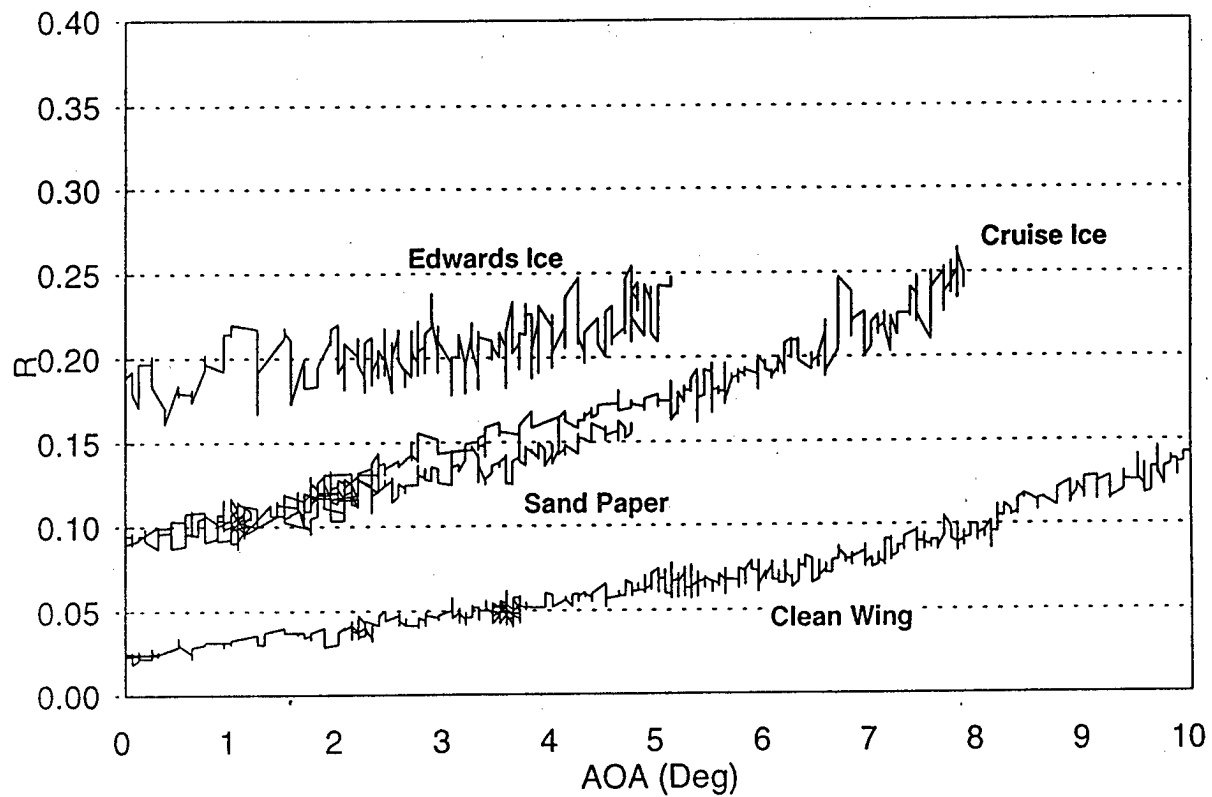
- The R parameter was extremely sensitive to the “Edwards” ice and “sandpaper” ice forms.
- R was usable for airfoil performance monitoring at all tested flap settings: 0, 15, 25, and 38 degrees.
- Optimum response and coverage would dictate a minimum of two probes per wing on the ATR 42.



ATR 42-500 (Flaps = 25 Deg)



ATR 42-500 (Flaps = 38 Deg)



Conclusions and Recommendations

The Turbulence Intensity Parameter gives aircrew a clear indication of the airfoil performance margin in icing conditions, which is not available from dedicated ice sensors or angle-of-attack indicating systems.

In order to optimise the sensor location(s) for specific aircraft types, the following points should be considered:

- Where possible, turbulence intensity measurements should be recorded during future wind-tunnel and in-flight icing investigations.
- CFD modelling should be performed to determine the optimum sensor location for representative airfoil sections.
- Manufacturers should be encouraged to disseminate information regarding airfoil idiosyncrasies and stall characteristics when ice accretion or other contamination is present.

GOES Experimental Aircraft Icing Risk Product

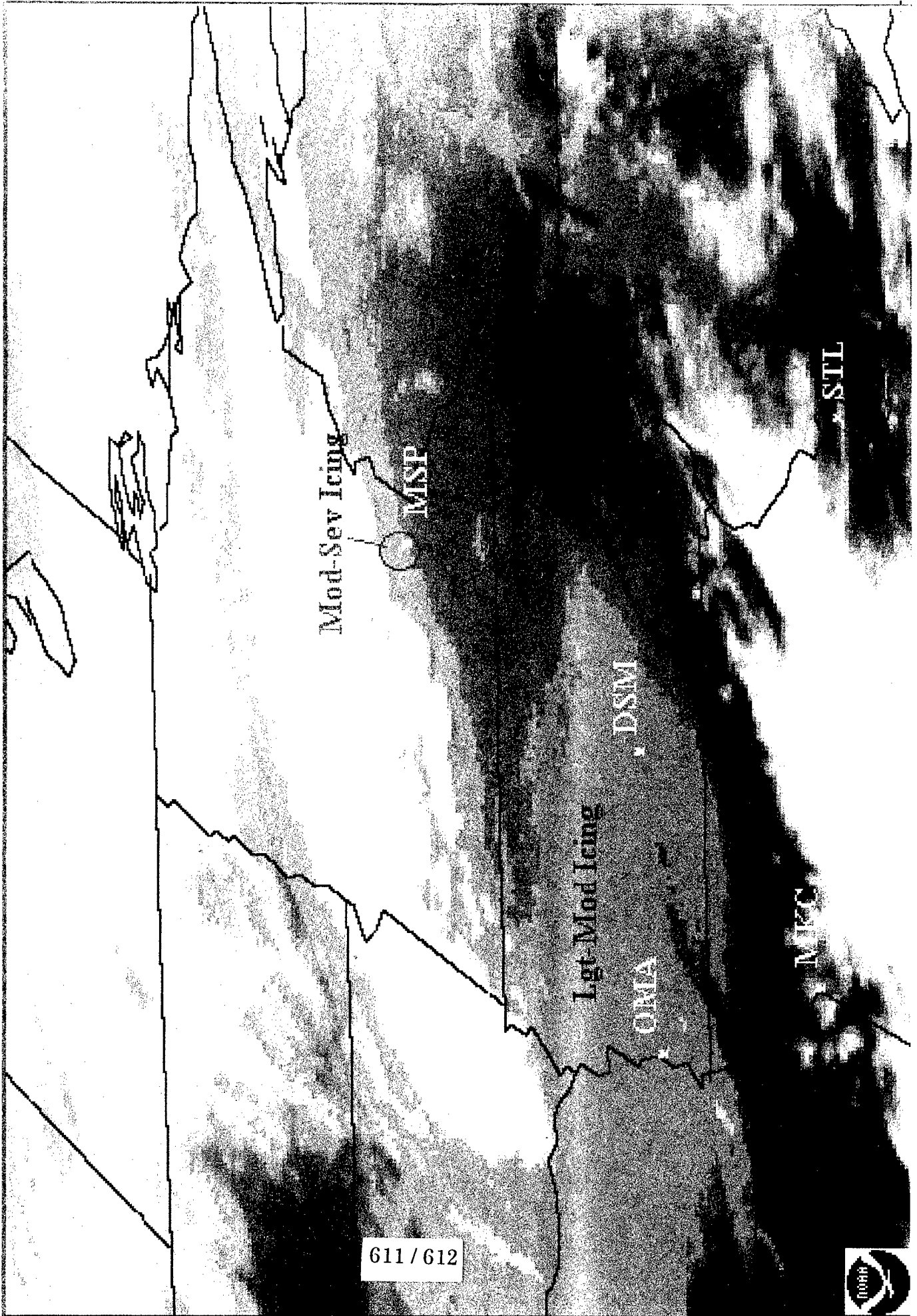
Gary Ellrod
SAL/ORA (NOAA/NESDIS)

GOES Experimental Aircraft Icing Risk Product:

- ◆ Highlights areas of supercooled stratiform clouds
- ◆ Uses GOES-8 imager data:
 - Daytime - 4 channels
 - ◆ Visible, 3 IR (3.9, 10.7, 12 micron)
 - Night - 2 channels
 - ◆ Infrared (3.9, 10.7 micron)
- ◆ Program uses thresholds/ranges of:
 - IR Temperature
 - Dual Channel temperature difference
 - Visible brightness
- ◆ Program runs five times/day (10 sec CPU)
on HP-755 workstation in McIDAS-X

- ◆ Thresholds/ranges used by program:
 - $T(10.7) = -2$ to -17°C (cloud top temps)
 - $B(\text{Vis}) > 40$ counts (day vs night)
 - $T(10.7) - T(3.9) > 2^{\circ}\text{C}$ (water clouds at night)
 - $T(3.9) - T(10.7) > 0.16B - 6$ (water clouds during day)
 - $T(10.7) - T(12) > 2^{\circ}\text{C}$ (thin cirrus filter)

Aircraft Icing Experimental Product - 12 April 96/1915Z



611/612



EMB-120 SUSCEPTIBILITY TO SLD ICING ENVIRONMENT DEMONSTRATION

Decio Pullin - Aerodynamic Group Manager - EMBRAER

EMBRAER APPROACH

- Two dimensional wind tunnel test to measure the aileron hinge moment change with quarter round shapes
- Flight simulator utilization introducing the results from the wind tunnel test and creating an asymmetric condition
- High speed taxies and flight test with the EMB-120 prototype installing wooden quarter round shapes in front of the ailerons
- Icing Tanker tests to obtain actual shapes and visual cues
- NASA Lewis icing tunnel test to investigate the SLD ice shape and chord position location in a 2D EMB-120 airfoil

Two-dimensional wind tunnel test

- Quarter round shapes of 1 in. and 0.5 in. (pic. 01)
- Chord position of 6% (End of boot), 10%, 12.5% and 15%.
- Internal balance to measure the aileron hinge moment.
- Angle of attack variation from -2 to +18 deg.
- Aileron deflection from -25 to +15 deg in 5 deg steps
- Results showed an hinge moment coefficient offset of -0.05 corresponding an upfloat of approx. 10 deg TEU. (graph 01)
- The offset is constant with the angle of attack and start at an AOA that is function of shape size and position.
- The 6% chord position was chosen as most representative because is the end of the boot and is as critical as others.

Flight simulator utilization

- Hinge moment offset from wind tunnel and theoretical lift loss and drag increase introduced on the left wing (most critical)
- Take-offs and landings performed with asymmetric ice in preparation for the actual flight
- Holding condition, flaps up, 160 Kias, auto-pilot on. The asymmetric ice effect is suddenly introduced and a delay of 3 sec in pilot reaction is simulated after the A/P disengage
- Same as above but with 1 sec. delay only
- Same as above but in manual flight
- Results showed aileron forces above 60 lbs during transient but it was always possible to control the airplane and return to level flight
- Results were considered satisfactory and a decision to go for the actual flight test was made

Flight tests with quarter round shapes

- One inch quarter round shapes attached to both wings in front of ailerons at 6% chord position
- Ice shapes could be released in flight with a mechanical device and were divided in three segments per wing (pic. 02)
- High speed tests with up to 120 kias and 5 deg nose up attitude were performed and an aileron force of about 7 Kgf was obtained
- A progressive sequence of flights were performed with one third, two thirds and full aileron coverage with the ice shapes
- A moderate to heavy buffet was noticed when flying with two or more ice shapes on each wing, flaps up and airspeed of 160 Kias. With flaps 25 and 150 Kias, there was no buffet.
- Landings were performed with flaps 25 and in an asymmetric condition after ice shapes release on the right wing

Flight tests with quarter round shapes (Cont.)

- The airplane was trimmed at 160 Kias, flaps up (holding condition in ice) and the ice shapes on the right wing were released creating an asymmetric condition
- Tests were performed with auto-pilot on and off
- With auto-pilot on, after the ice shapes release, the A/P was able to hold the aileron force up to its servo torque limit with a small roll rate. The A/P did not disengage and after 3 sec and a roll angle of about 15 deg, the A/P was disconnected and a maximum roll of about 40 deg was reached with an aileron transient force of about 40 to 60 Kgf
- The aileron force to maintain wings level, flaps up and 160 Kias was about 36 Kgf
- The aileron force to maintain wings level, flaps 25 and 150 Kias was zero

Dry Air Tests after Icing Tanker

- After discussions with the FAA, the following artificial ice shapes were agreed to be flown in dry air to check the EMB-120 controllability:
- A density of 46% span coverage of one inch high ridges with 1/4 inch high irregular shapes between (twice the density observed during Tanker tests to introduce conservatism) (pic. 06)
- The ice shape would cover the wing span from the propeller tip outboard extension to the wing tip at a 6% chord position
- The ice shape would be installed in one wing only (left)
- An additional flight with a continuous 1/2 inch high irregular shape attached to the same position was also agreed (pic. 06)

Dry Air Tests after Icing Tanker (Cont.)

- Dry Air test results:
- No controllability degradation was observed
- No buffeting and/or tendencies
- Aileron forces to maintain wing level in holding condition (160 Kias) are less than 2 Kgf
- Auto-Pilot characteristics are not affected by the ice shapes

Flight tests with quarter round shapes (Cont.)

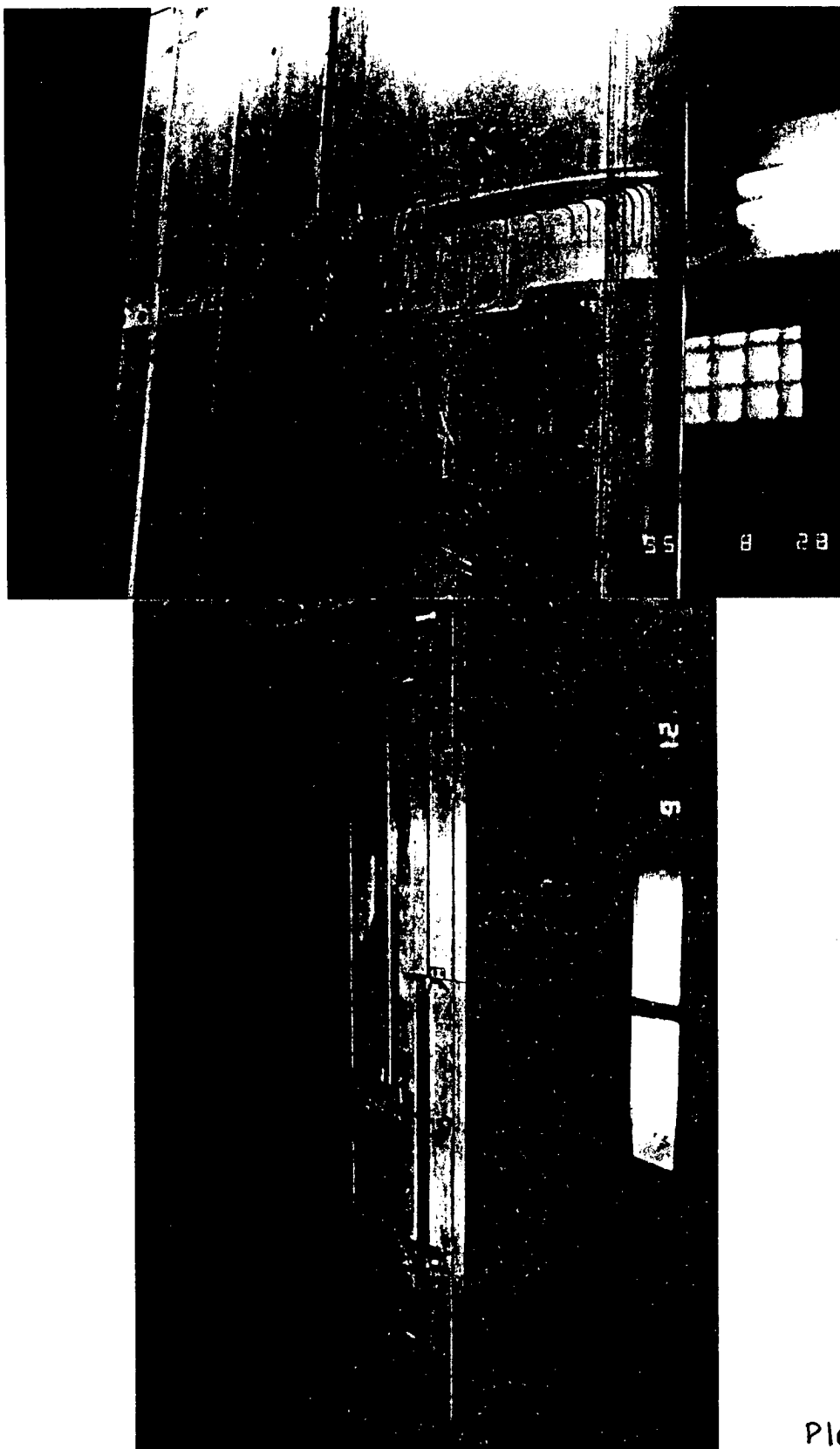
- Aileron efficiency remained constant in all conditions
- Aircraft response was always immediate to control wheel inputs
- In manual flight, after a delay of 1 second, the airplane reached about 25 deg of roll and after control inputs the roll angle reached a maximum of about 68 deg and the aileron force stayed around 20 to 40 Kgf with a peak of 55 Kgf momentarily
- After selection of flaps 25 and airspeed of 150 Kias, the aileron force was zero and a normal approach and landing was performed.

Icing Tanker Tests

- Performed in Dec/95 with a representative EMB-120 (S/N 038) flying behind the USAF NKC-135 Icing Tanker at Edwards AFB (pic. 03)
- Two flights and 5:30 flight hours simulating normal (40μ and 0.5 g/m^3) icing conditions and SLD (170μ and 0.65 g/m^3) conditions.
- Visual cues were obtained from wings and propeller spinner (pic. 04)
- Ice protection system was able to remove ice from all protected areas
- Ice shapes obtained on the wing were much less severe than the one inch quarter round (23% span coverage of 1 inch high ridges) (pic. 05)
- During the tests no change to the airplane controllability was noticed
- Accurate representation of the observed ice shapes during the Tanker Tests to be used in dry air controllability checks were obtained

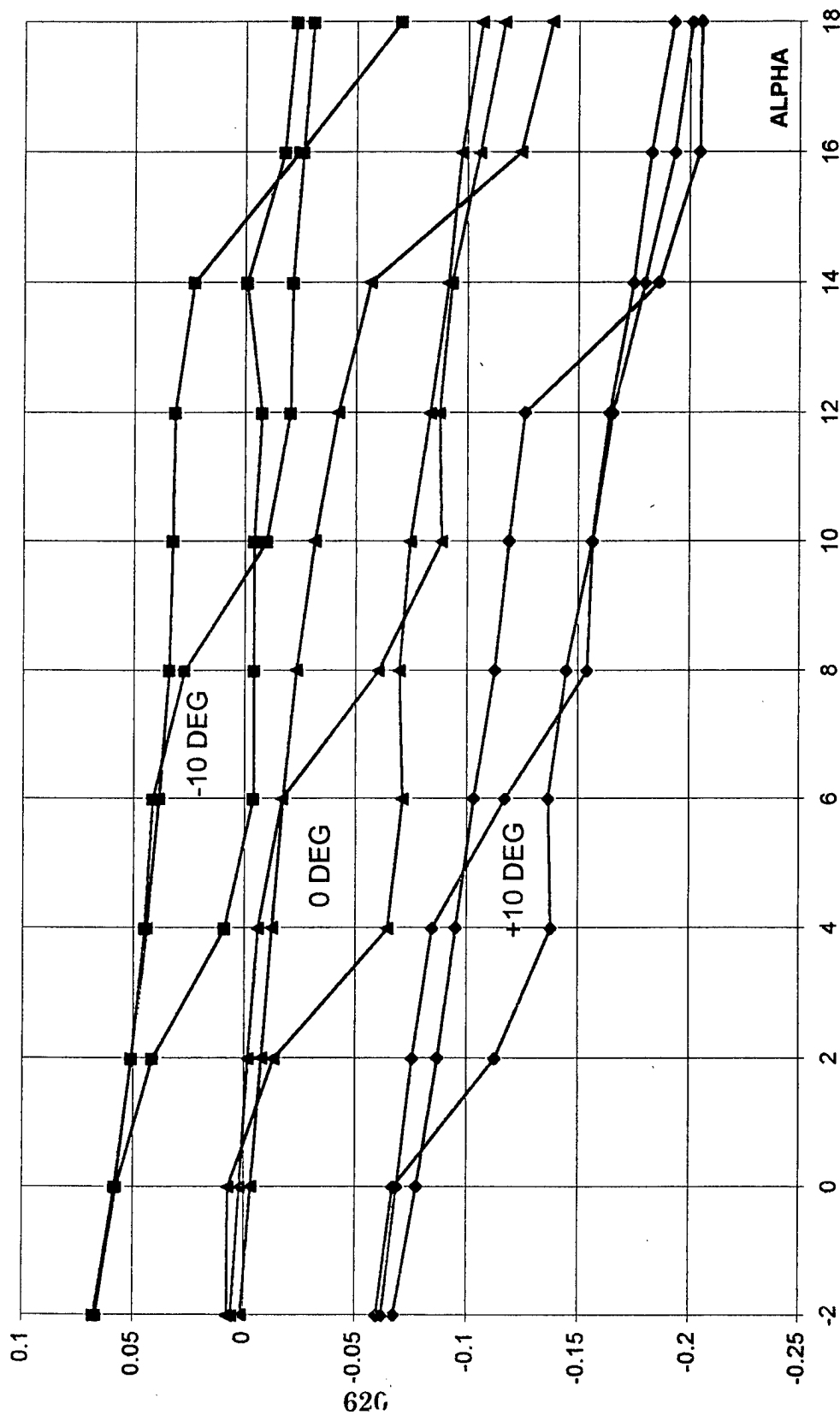
Final Comments

- One Inch Quarter Round shapes are too conservative
- High speed taxies may be not fully representative
- Tanker results interpretation due to test limitations are questionable (Conservatism must be included ?)

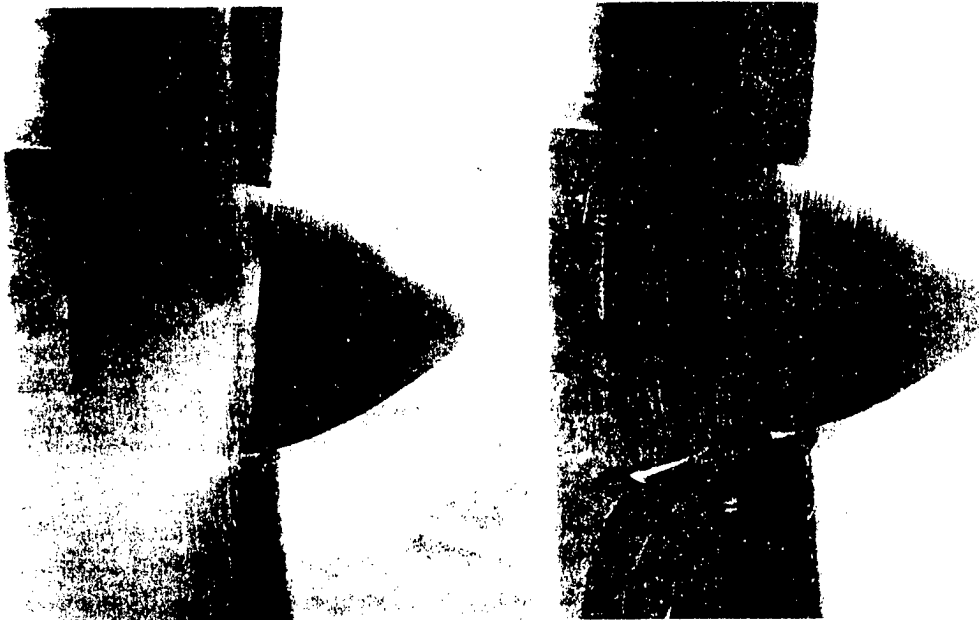


PIC.01

EMB-120 AILERON HINGE MMT - G10 C6 / G05 C6

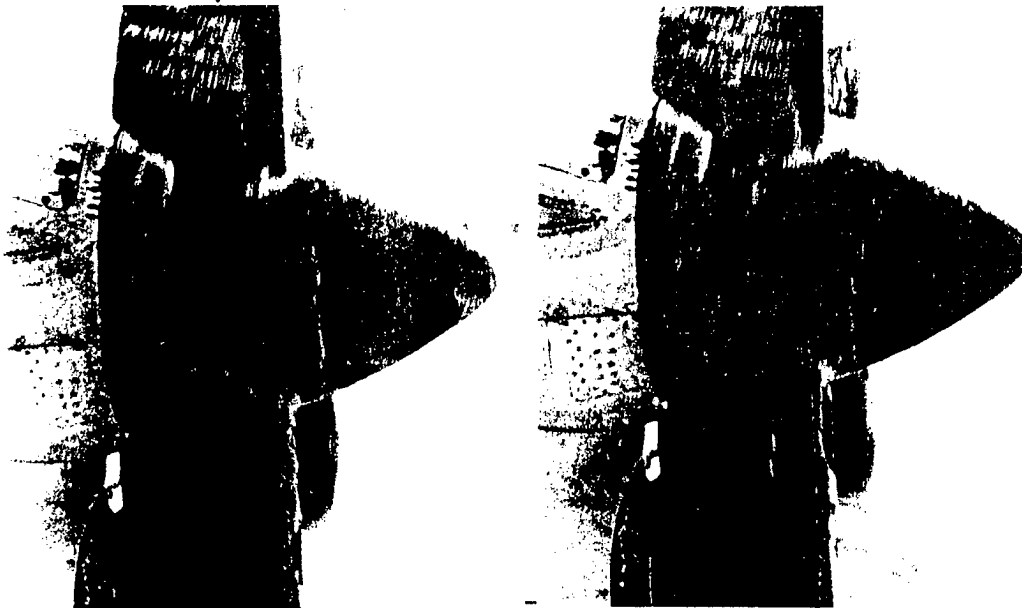


40 μ SPRAY ON THE SPINNER

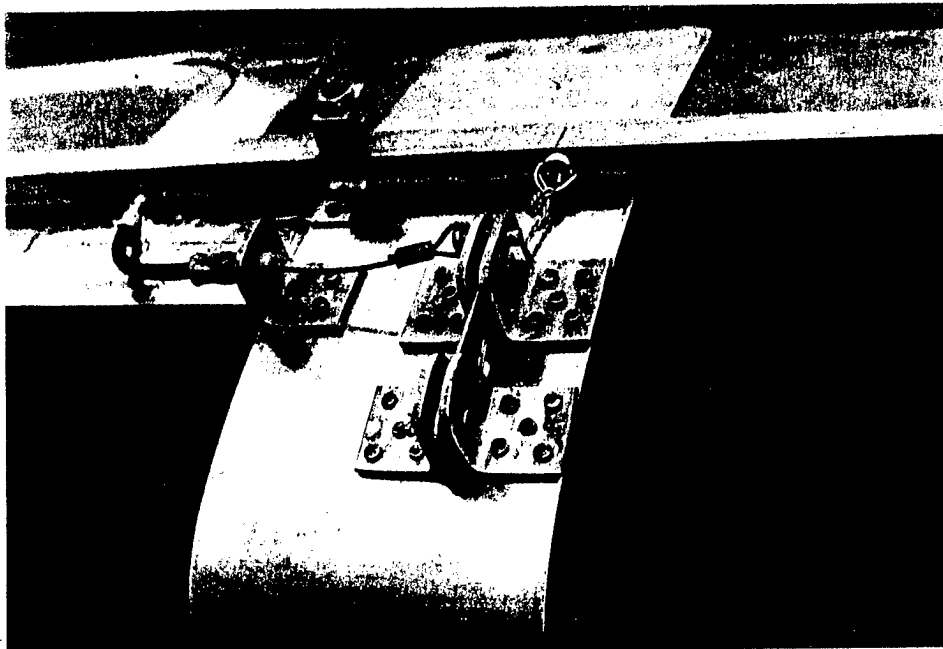


Normal ice spray on the spinner shows ice accumulation concentrated on forward half.

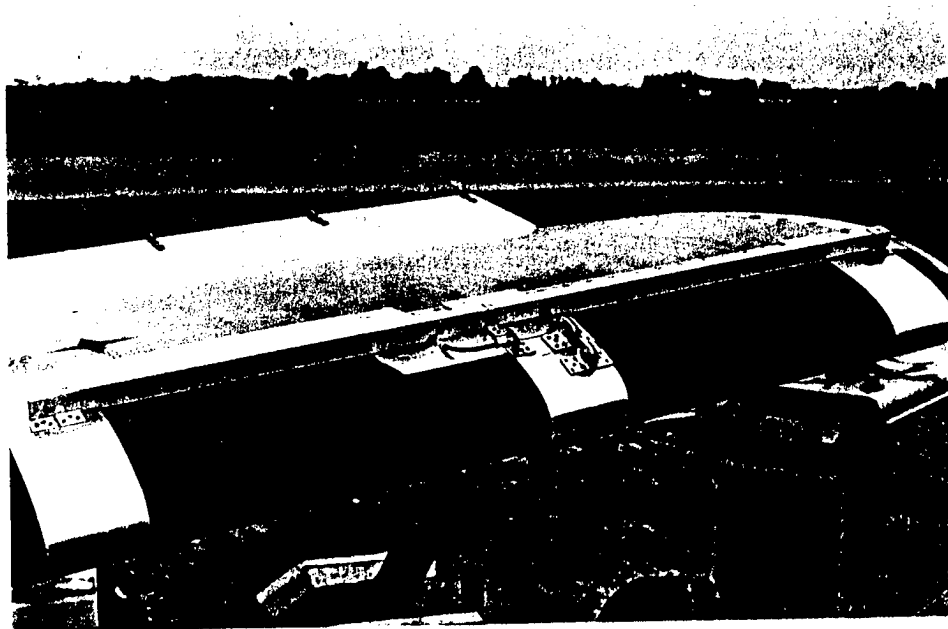
170 μ SPRAY ON THE SPINNER



SLD icing concentrated on the aft half of the spinner.



3 - ICE SHAPE RELEASE TRIGGER



4 - LEFT WING OUTBOARD ICE SHAPE (FRONT VIEW)

EMIÇÃO: REVISÃO:

AIRBUS POSITION ON ICING CERTIFICATION ISSUES

**prepared for the
FAA INTERNATIONAL CONFERENCE ON AIRCRAFT
IN-FLIGHT ICING**

May 6-8, 1996

by Claudius LA BURTHE, Flight Test Engineer

- 1 - DETERMINATION OF ICE SHAPES FOR HQ CERTIFICATION**
- 2 - REQUIREMENTS FOR HANDLING QUALITIES CERTIFICATION**
- 3 - REQUIREMENTS FOR ICING IN ETOPS**

DETERMINATION OF ICE SHAPES FOR HQ CERTIFICATION

- * CURRENTLY DONE BY "APPROVED" COMPUTER CODES**
- * RESULTS DO NOT CONFORM TO REALITY**
- * EXCESSIVE USE OF THE ENVELOPE-SHAPE CONCEPT**
- * POSSIBLE "HISTORICAL" MISTAKE:
TO-DAY'S CODES MAY HAVE BEEN VALIDATED
WITH EXCESSIVE CONFIDENCE IN DOUBLE HORN SHAPE**
- * QUITE SIGNIFICANT RESEARCH ISSUE**

REQUIREMENTS FOR HANDLING QUALITIES CERTIFICATION

- * CL MAX HAS TO BE MEASURED
WITH ICE ON UNPROTECTED SURFACES**
- * A320 AND A319 HAVE EXACTLY THE SAME WING**
- * BUT ADDITIONAL REQUIREMENT
COVERING THE CASE OF WING ANTI-ICE FAILURE
WAS INTRODUCED FOR THE A319**
- * RESULT IS TO INTRODUCE USELESS DOUBTS IN
PILOT'S' MINDS ON SIMILARITY OF BOTH TYPES**

REQUIREMENTS FOR ICING IN ETOPS

- * PROBLEM IS TO DETERMINE REALISTIC ICE SHAPES
TO BE USED IN A 3 HOUR DIVERSION AT FL100, 300KT**
- * CURRENT METHODS (AGREED CODES) FAIL**
- * 3 INCHES IS TOTALLY IRREALISTIC**
- * CASPII RESULTS SHOWED
VERY RAPID EVOLUTION OF THE ICE SHAPE**
- * DOUBLE HORN RIME ICE
BECOMES MOON SHAPED GLAZE ICE
IN LESS THAN 30 MINUTES**

ICING IN ETOPS CONSEQUENCES OF FINDINGS

- * ACCRETION PROCESS NOW APPEARS AS RESULTING
FROM A DIFFERENCE IN BIG NUMBERS (RIME ICE ONLY?)**
- * ACCRETION LOOKS SPONGY, WITH SIGNIFICANT INSIDE
WATER FLOW AND HEAT EXCHANGE**
- * ONCE OUT OF THE CLOUD, IN ETOPS CONDITIONS,
PROCESS CONTINUES AND LEADS TO RIME ICE**
- * AGREED CODES ARE VERY FAR FROM THAT**

CONCLUSION

- * DO NOT CHANGE THE RULES FOR LARGE AIRCRAFT**
- * TODAY'S RULES ARE ALREADY EXCESSIVE, IN
COMPARISON TO THE MILLIONS OF HOURS FLOWN**
- * RESEARCH HAS TO BE PURSUED ON UNDERSTANDING
AND SIMULATING THE ICE ACCRETION PROCESS**
- * WE NOW UNDERSTAND WHY WWII PILOTS REPORTED
SO OFTEN ON GLAZE ICE AS OPPOSED TO RIME AND
RARELY MENTIONED THE DOUBLE HORN**

DNE TECHNOLOGIES, INC.
Flush Mount Ice Detector

1.1 Scope

DNE Technologies, Inc. (DNE) is pleased to offer its Integrated Planer Ice Detector / Accretion Rate System. The unit offered is based on DNE's patented heat of fusion technology, that includes over twelve years of production experience and over ten thousand delivered, qualified, highly reliable, aircraft ice detectors. It should be noted that the warranty return rate of all units delivered over the past 12 years is less than 1%; an excellent indication of the reliability and quality of DNE ice detector products.

DNE Technologies, Inc. manufactures a unique and patented line of ice detectors which make use of the latent heat of fusion of ice in order to detect and report ice. These ice detectors are currently installed on the C-130, F-16, B-1, F-117A, B-2, F/A-18E/F and the Advanced Cruise Missile. This ice detector was also qualified for installation on the A-12 aircraft. All of these ice detectors operate in a similar manner: the final physical configuration changes to accommodate the particular installation.

DNE's pulsed ice detector method was granted a patent in June 1982 (Patent 4,333,004). The method has been successfully applied to a variety of shapes and sizes of ice detectors. Among the varieties delivered to customers are cylindrical probes, curved conformal sensors and flat thin sensors. DNE ice detectors have performed well finding turbine engine inlet ice, radome ice, piston engine carburetor ice, and meteorological ice on Mount Washington.

DNE has recently completed qualifying a microprocessor controlled ice detector with an MTBF of greater than 90,000 hours, a BIT capability of 98%, and software designed, documented and qualified to MIL-STD-2167 requirements. The controller for this system occupies less than 50 cubic inches and weights less than 2.0 pounds.

2.1 Principles of Operation

Only a few proven principles have been successfully applied to sensing ice on aircraft surfaces. DNE uses the heat of fusion of ice when it turns to water to measure the presence of ice on its probe. The virtue of using this property is the large signal to noise ratio that it provides. When one gram of ice is heated from -1°C to 0°C , approximately 1 Calorie of energy must be added to it. When one gram of water is heated from 0°C to $+1^{\circ}\text{C}$, approximately 1 Calorie of energy must be added to it. To change that same gram of ice to 1 gram of water at 0°C , 80 Calories must be added. This large difference is called the heat of fusion. DNE's patented ice detectors use this principle to measure the presence of accreted ice.

The flat sensor uses nickel bonded at the molecular level to a non-conductive substrate. The nickel is etched forming a bonded thin, strong wire (typically 0.002 " diameter, hardened nickel). This design provides a number of vital performance characteristics that permit the supplier to take advantage of the heat of fusion principle.

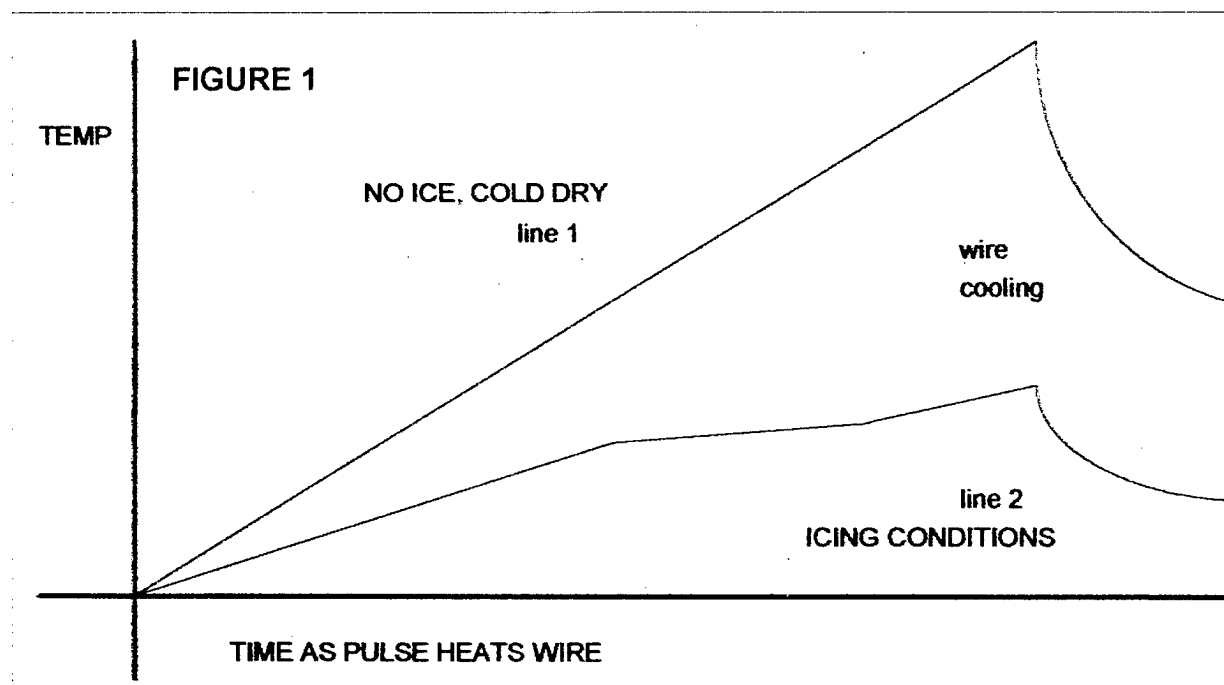
The sensor has two major components; a dual redundant bonded element (nickel bonded to the substrate at the molecular level) to determine temperature and detect ice, and a heater (nickel bonded to the substrate on the reverse side) to deice the sensor after reporting an ice event. This combined sensor / heater configuration also permits electronic interpolation of icing rate using recent changes in accreted ice thickness as a function of time by utilizing a rapid thermal time constant / turn around time due to the proximity and nature of the heating element.

In operation, a trickle sense current is passed through the nickel element to determine the temperature of the sensor. When the temperature is in the range that will permit ice accretion, the controller starts ice detection mode. In this mode, a pulse is passed through the sense element, and the response of the wire to this pulse is measured by the controller electronics. The pulse is generated every second (once for each element), and after two consecutive ice detects the electronic controller will report ice detection to the air vehicle. Concurrently with reporting ice detection, an electrical heater is activated to deice the assembly. The temperature of the sensor is measured during heater

operation, and the heater is turned off after it reaches a few degrees beyond freezing. Upon cooling, the sequence then starts over again.

The sensor / heater is of extremely low mass and is thermally isolated from any external heat conducting surfaces. This allows for a rapid detect / deice cycle. This rapid cycle, combined with the highly sensitive and stable (micro controlled) threshold, creates an accretion sensing ability that is inversely proportional to the number of detects. In other words, the unit would count the number of detects between aircraft deicings, and provide an analog or digital output representative of the correlated ice thickness. When the unit is implemented as an "accretion rate ice detector", the unit is substantially more accurate than currently available rate ice detectors.

The nickel that is bonded to the substrate is connected electrically to a source of current. When sufficient current is passed through the nickel wire it heats up rapidly. In the supplier design, it heats so rapidly that velocity of air going by the

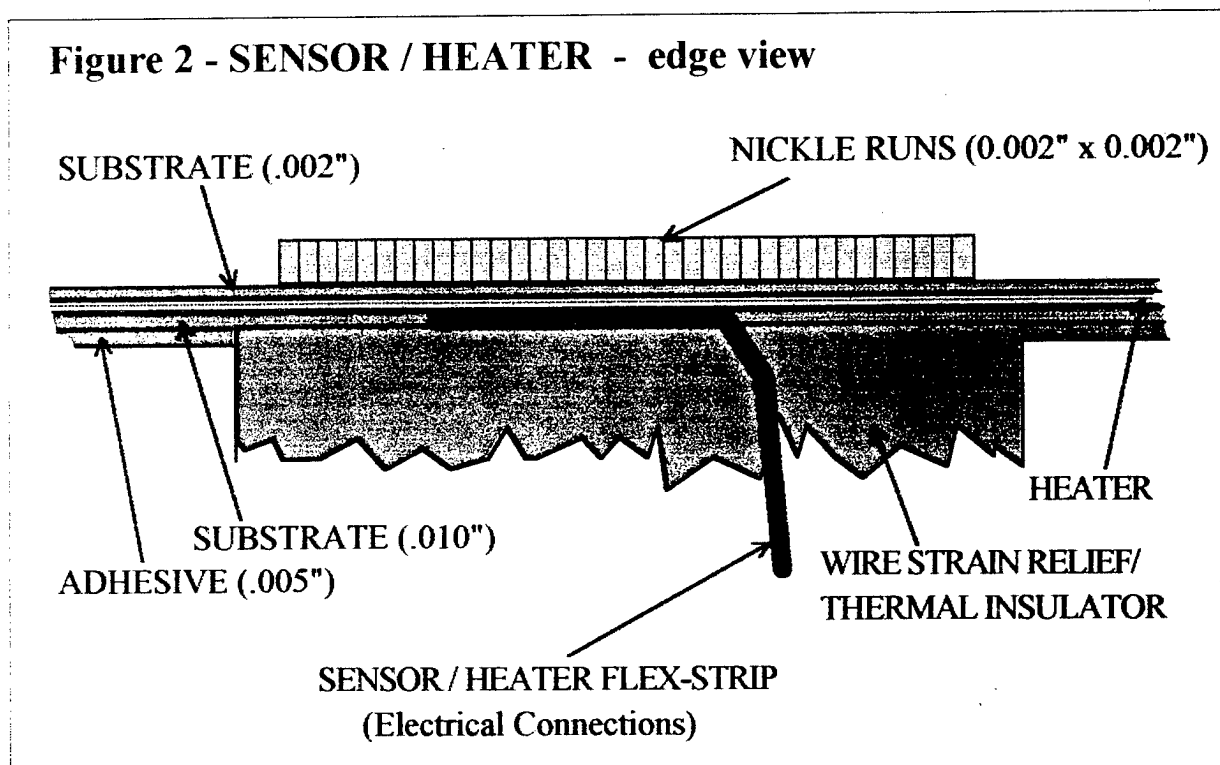


sensor has a negligible effect (over the velocities of interest) on the rate of change of temperature.

Ice which accretes on the surface of the wire has a strong effect on the temperature of the wire as the pulse current changes the wire temperature. Thus for cold dry air the wire will change temperature as shown in Figure 1, line 1 and for ice the temperature change will approximate line 2.

The break in line 2 as it heats corresponds to the ice which has adhered to the surface of the wire melting at constant temperature to water. Following the pulse the wire cools and returns rapidly to ambient temperature. By monitoring the distinctively different shapes of the temperature rise, DNE's ice detectors readily distinguish the "ice" from the "no-ice" condition.

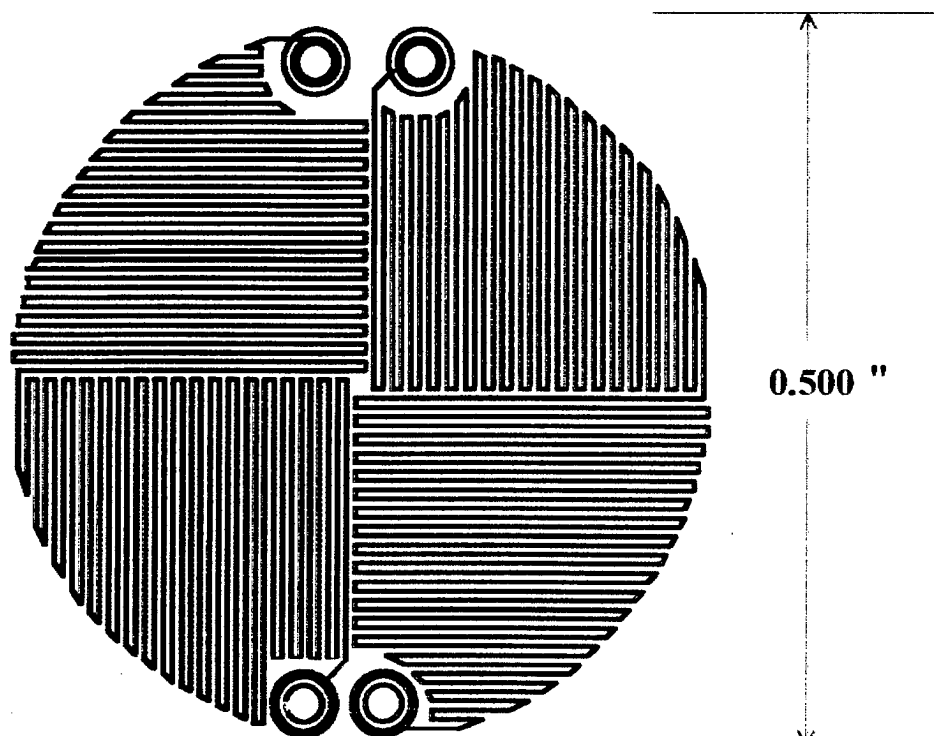
3.1 Construction



The Integrated Planer Ice Detector / Accretion Rate System sensor contains **two** independent etched sensing elements and redundant parallel heaters. When coupled with the dual sense and pulse drive channels and Built In Test of the controller, a system is created that will detect **all** failures that will prevent ice detection. Also, to minimize the possibility of overdriving the heater, **two**

independently controlled series heater drivers are included in the controller. The sketch of Figure 2 shows an edge view configuration of a typical flat sensor / heater.

Figure 3 - TYPICAL SENSOR ELEMENT LAYOUT



A variety of materials, patterns and configurations can be used to detect ice. The models for this invention utilize a polyimide substrate, nickel elements and a nickel heater. The sketch in Figure 3 illustrates a typical etched pattern used for the Integrated Planer Ice Detector Sensor.

The nickel element is constructed by depositing nickel on the substrate in such a manner as to cause as close to a square wire geometry as possible. This is necessary in order to maintain a reasonable signal to noise (a square allows ice to accrete on three quarters of the sensor element surface).

Of equal importance to the Integrated Planer Ice Detector is maintaining adequate space between the element runs for the ice to build. The models use 0.003 inches of space between runs.

The heater element is bonded directly on the reverse side of the sensor, with as direct and as short a thermal path to the sensor as practical. By proportionally heating the sensor and raising the temperature of the sensor always to the same temperature in the same amount of time, the Integrated Planer Ice Detector becomes repeatable enough to be used as an accurate accretion sensor.

4.1 Generalizations Of The Invention

The sensor has been drawn as a flat surface. It will function equally well on a simple or compound curved surface. The substrate material chosen for the models were polyimide. Any nonconductive structural material can be used. Nickel was chosen as the sensor element due to its familiar conductivity, temperature coefficient and corrosion resistant properties.

Note that the ultimate capabilities still need to be evaluated in a calibrated icing wind tunnel capable of simulating all expected icing encounter profiles.

Ice Detection

Dana P. Hemmingsen
Vice President
Marketing & Sales

TDG Background

- Founded in 1991
- Product development & engineering
- Specialize in ice protection
- Well versed in certification process

NOFOD™

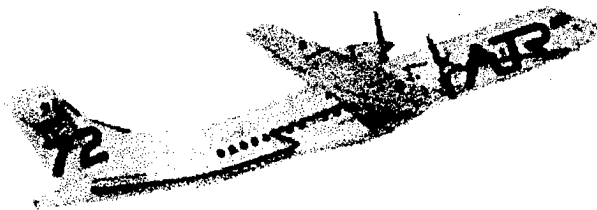
- Overwing ice protection system
- MD-80 clear ice
- Alternate means of compliance
- American Airlines operational
- Alaska airlines installing
- Delta & USAir conducting ISE

Ice Detection

- Optical sensing technology
- Developed over the last 2 years
- Tested at NRC wind tunnel
- Next step: in-service evaluation
- -100F flush mounted sensor
- Rugged housing & simple controller
- Annunciation tailored to aircraft
- Reliable, responsive & accurate

Applications

- Aft of leading edge
- Tail planes
- Engine inlets
- "Blind" spots



Beyond

- Assess environmental icing conditions
- Determine rate of ice accumulation
- Measure particle size

SOLA - ASDIS System Proof of Concept and Technical Overview

Steven D. Palmer and Michael G. Lamb

ABSTRACT

The SOLA-ASDIS system performance monitor can monitor aircraft wing performance from the taxiway, through takeoff, flight, landing, and back to the taxiway. In so doing, SOLA can be shown to serve as an effective ice detection system for both on ground and in flight usage.

Aers, Inc.

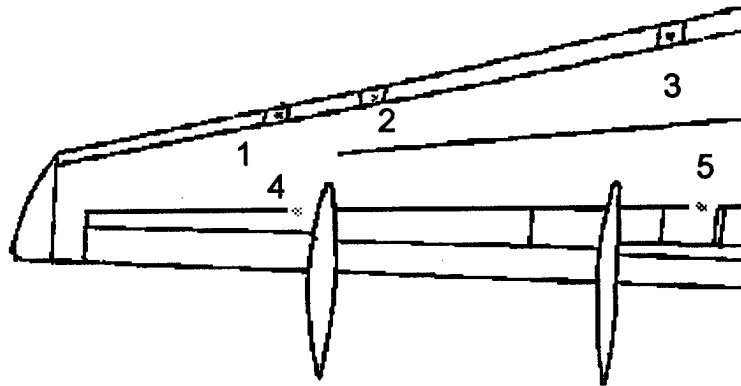
presents the

**System for Onboard Lift Analysis
(SOLA)
and the**

**Coming Revolution in Advanced Flight Management,
Control, Flight Safety and Airline Earnings**

SOLA COMMERCIAL WING PROOF OF CONCEPT TEST AND TECHNICAL OVERVIEW

PARTIAL SYSTEM WING INSTALLATION DIAGRAM



The above diagram shows the locations of the SOLA port groups installed on the commercial wing proof of concept test aircraft. A total of five SOLA port pairs were installed at the locations numbered 1 - 5. Three ASDIS ports were installed at locations 1 - 3 on the wing. For analysis purposes SOLA ports 4 and 5 were paired with ASDIS ports 1 and 3. The ports were flush mounted so as to fit wing contours and be able to operate within the boundary layer. The ports themselves are designed to replace / resemble existing aircraft fasteners and be virtually unnoticeable to the casual observer. (a detailed design overview is provided elsewhere).

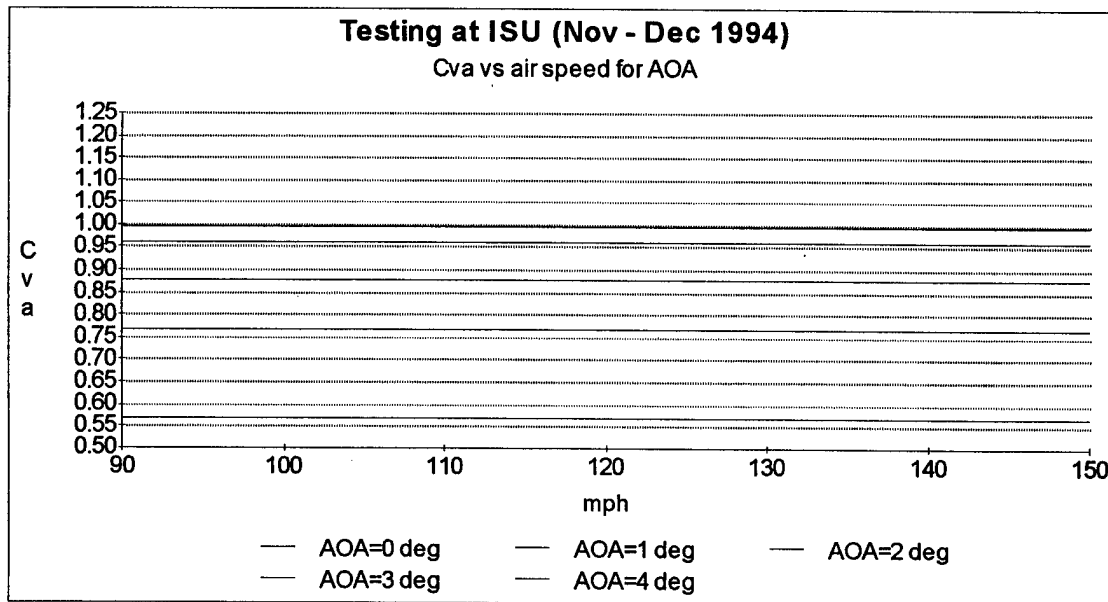
In its normal system format, SOLA utilizes an array of ports along the leading edges of the aircraft's wings, horizontal stabilizers and either replaces or is tapped into the wing pitot system. Such an installation allows SOLA to operate as a real time, highly sophisticated aerodynamic performance monitor and analysis system's technology, not unlike taking a wind tunnel facility aloft with the aircraft.

In order to accomplish the analysis functions involved, SOLA had to be able to successfully integrate not only the C_p of its various airfoil placements, but also had to be able to successfully identify the precise airspeeds and correct angles of attack that the airfoils were operating in.

SOLA has shown these required capabilities are well in hand. Air speed was relatively easy to obtain, since SOLA's sensitivity and its array structure allow it to operate effectively from zero knots through maximum aircraft speeds with previously unattainable levels of accuracy.

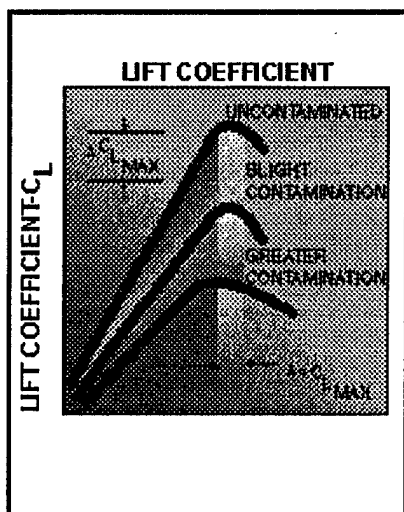
SOLA likewise is able to establish the wings precise angle of attack by utilizing this V_{pitot} and ASDIS (or other) reference C_p Values. This reference value C_{va} , in a real sense, eliminates the variables from determining how well the airfoil is performing aerodynamically.

The most basic fundamentals of aerodynamic studies include the following information, if a given wing's design is known, its airspeed is known, and two wing based pressures are available, then it is possible to determine the wing's Angle Of Attack. In the case of SOLA as shown in the following graphic, a relationship exists between the indicated air speed (IAS) and certain selected port location pressures. The ratio developed between the IAS and this pressure reading yields an easy method for accurately determining an airfoils AOA. The graphic shows how irrespective of the IAS the ratio between the IAS and these ASDIS pressures stays constant at any given AOA. The AOA can thus be calculated very accurately by referencing the wings Cva ratios. The graphic clearly shows the ratios that the tested wing develops at several selected angles of attack (0, 1, 2, 3, and 4 degrees AOA). These ratios held constant irrespective of the nominal V_{pitot} . The graph here represents the constant as measured at airspeeds of from 90 to 140 knots in the wind tunnel tests for reference purposes although the number remains constant at all air speeds.

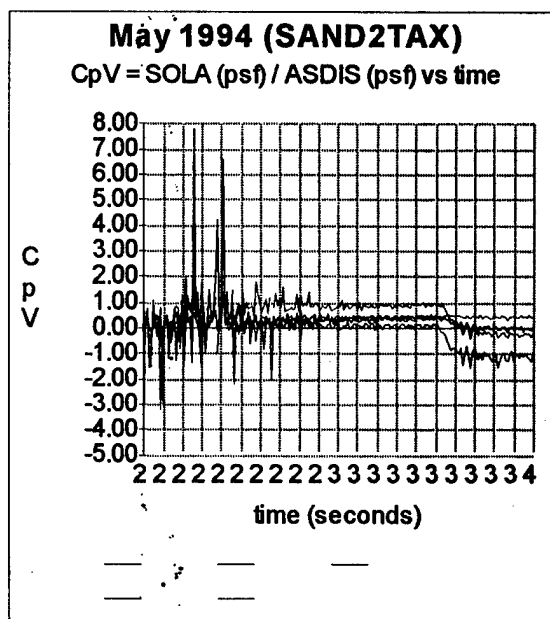
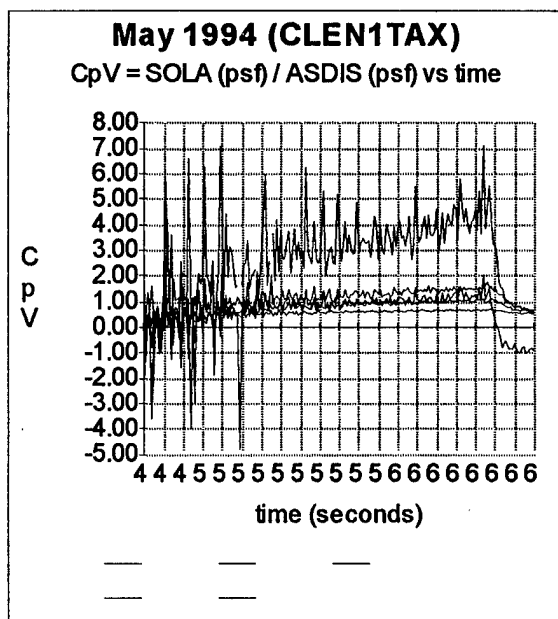


This allows SOLA to establish a single Wing Performance Reference Constant for each port location group. Any deviation from the WPRC has to have a specific cause. Flaps and other control surface operation are easily corrected for, thus it is now possible in real time to judge how well the airfoil is performing. This ability is further enhanced in that the SOLA ports operate within the wings boundary layer, an area far less subject to turbulence, yet an area that precisely and far more accurately reflects the state of the airfoils performance. A change in the WPRC at any port location shows up at all port locations (see following graphs on contamination detection as an example).

SOLA is thus able for the very first time in history of aviation to provide a very precise analysis of how the wing is performing aerodynamically and to do it in real time and real world operating conditions.



The chart on the right shows how the Coefficient of Lift is affected by the presence of contamination. SOLA Systems Technologies effectively measures this in real time in real world flight conditions. Owing to its innovative design and remarkable sensitivity SOLA is capable of operating at the very low end of the scale. This not only serves well as an ice detection device, but also is capable of functioning as a TOPM and a myriad of other in flight avionics systems.



The two charts above show the effect that contamination has on a wings performance. The displayed raw data is taken from a series of test runs done on cross wind runways, using a partial SOLA System installed in the pilot's side wing, actual placement of the port groups is depicted on the preceding page (see Wing Port Locations diagram).

While numerous runs were conducted involving take-off runs in each direction on the cross wind runway, it is worth noting that those charts taken from actual take-offs are identical to those of the cross wind clean wing configuration depicted here in the left hand graph, despite the fact that actual take-offs occurred in a normal head wind configuration. SOLA is not affected by crosswinds.

While SOLA only did a direct S/A analysis of the wings performance it is still easy to determine that the wing readings shown in the right hand chart are from a contaminated wing. This SOLA analysis shows that from brake release on SOLA is capable of determining if a wing is clean or contaminated.

It is also worth noting that SOLA ports groups 4 and 5 detected the presence of the leading edge contamination, despite the fact they were 4 and 12 feet from the nearest contamination. The level of contamination was equal to 0.01 inch of rime ice interspersed along the wing's leading edge.

Over wing icing is just as easily detected by SOLA, Aers ran literally thousands of tests without a single failure or false alarm occurring in any of them. SOLA was used in conducting research for the Dryden Commission of Transport Canada which measured the aerodynamic effects of Type II fluids as well as being part of testing to determine the sheared droplet size of the fluid.

Utilization of a complete SOLA System produces a much smoother graph. Brake release points on the two runs depicted above were 51 seconds for the clean wing run and 22 seconds for the contaminated run. As you can clearly see that the difference in the S/A readings for all the port groups from clean to contaminated is substantial and remains constant throughout the entire take-off run. Speed ranges for the clean wing were from 0 to 120 knots (90% Vr) and from 0 to 100 knots contaminated, acceleration was identical on both runs.

SOLA can accurately figure the correct angle of attack within a few minutes of a degree at any operational air speed as the following graphs show. The charts provided are simple ones taken from some of Aers wind tunnel test programs as part of our early POC (Proof Of Concept) testing.

A commercial wing section was installed in the wind tunnel and was subjected to several different air speeds at each of several angles of attack. Note that the Asdis readings are constant for any given AOA at each of the air speeds indicated.

SOLA System's Technologies measure an assortment of differential readings from the airfoil combines them with its highly accurate IAS output and then provides a highly accurate analysis of various airfoil functions in real time.

SOLA System's Technologies are about to undergo primary safety system PSS/ MEL Certification by the FAA onboard a corporate jet aircraft and initial commercial certification is now scheduled to begin early this summer. SOLA will be certified as:

1. TOPM (take-Off Performance Monitor)
2. AOA Indicator
3. Stall Warning Device
4. In Air Ice Detector (also as a trigger for de-icing systems onboard the aircraft)
5. Side Slip Monitor (and later as a Side Slip Correction Device)
6. Indicated Air Speed Monitor
7. Aerodynamic Configuration Verification Device

Due to its unique capabilities both as a stand alone system and later as an integrated component of Advanced Flight Management and Control Systems, SOLA will offer to make flight far safer and far more profitable. SOLA can allow an aircraft to operate with shorter Balanced Field Lengths, have reduced approach speeds, greatly assist in making both Cat III and standard landings smoother and safer, allow the aircraft to more efficiently climb to altitude, reduce its specific flight fuel burn, increase its allowable MGTOW and many other things. SOLA can accomplish these many tasks because, the "**REAL AERODYNAMIC PERFORMANCE**" of the aircraft is known for the very first time in the history of aviation.

Heretofore inviolable "set in concrete" thumb nail rules for setting safety margins are now open for reassessment. Transport Canada offered to reduce the approach speed of one aircraft by from 7 to 10 knots if the aircraft had our system onboard. This results in a 15% reduction in the amount of energy to be dissipated during the landing. This means, not only reduced fuel burn and maintenance costs, but also means that the aircraft at its MGLW can now service far shorter runways successfully. Similarly the required runway length for MGTOW take-offs is also reduced significantly. This equates directly into huge revenue enhancements to the airline industry.

Further, SOLA can replace several other on board avionics instruments and can often be a weight saving device as well as offering a noticeable improvement in performance over the system it replaces.

Payback time for a stand alone SOLA System onboard a commercial aircraft is typically pegged at between 3 and 8 months depending on the type of service and the specific aircraft model. Few, if any, devices currently available can make anywhere near the same claims to performance earning enhancements that SOLA can. SOLA can be retrofitted to existing aircraft and is also easily adapted for installation in new production units as well.